NAS 1.55: 3106/v.1

NASA Conference Publication 3106, Vol. I

1991 International Aerospace and Ground Conference on Lightning and Static Electricity

Proceedings of a conference held at
Cocoa Beach, Florida
April 16–19, 1991

NASA

NASA Conference Publication 3106, Vol. I

1991 International Aerospace and Ground Conference on Lightning and Static Electricity

John F. Kennedy Space Center
Kennedy Space Center, Florida

Proceedings of a conference sponsored
by the National Aeronautics and Space
Administration, the National Interagency
Coordination Group (NICG), and Florida
Institute of Technology and held at
Cocoa Beach, Florida
April 16–19, 1991

NASA
National Aeronautics and
Space Administration
Office of Management
Scientific and Technical
Information Program
1991

E

NICG

COMMITTEE CHAIRPERSONS

Chairman	W. Jafferis NASA, KSC, Florida (407) 867-3185 or 3529 (407) 867-4079 (FAX)
NICG Secretary	M. Glynn FAA Technical Center (609) 484-4134
Financial Coordinator	Dr. A. Revay Florida Institute of Technology (407) 768-8020
Conference Coordinator	Eric Smith NASA, KSC, Florida (407) 867-3185
European Coordinator	J. L. Boulay ONERA, France

NICG STEERING COMMITTEE

F. Pitts	NASA Langley Research Center
V. Mazur	U. S. Department of Commerce
D. Albright	U. S. Army Aviation Systems Command
L. Runke	Naval Research Laboratory
W. Walker	Naval Air Development Center
L. Walko	Wright Research and Development Center
M. Whittaker	Naval Air Test Center
B. Burrows	Culham Laboratory, England

LAUNCHING INTO SPACE

The National Interagency Coordination Group (NICG) extends you a cordial invitation to attend the 1991 International Aerospace and Ground Conference on Lightning and Static Electricity.

Kennedy Space Center and Cape Canaveral Air Force Station are frequently called America's Spaceport. This title is earned through the integration of many skills in a wide variety of technical fields and successful implementation throughout labor and management levels that enables America to reach into space. Among the many challenges confronting the country's primary launch site are lightning protection, detection, and forecasting. This conference focuses on studies that attempt to solve these problems by presenting papers on active research on many appropriate topics.

The technical program for this year's conference consists of 119 papers and posters presented by investigators from fifteen countries making this a truly international effort. The conference is divided into twenty-six sessions based on research in lightning, static electricity, modeling, and mapping. These sessions span the spectrum from basic science to engineering, concentrating on lightning prediction and detection and on safety for ground facilities, aircraft, and aerospace vehicles. There is something for everyone, whether student or veteran to the field. I invite you to come to the conference and participate with us, sharing what you have learned and your concerns.

William Jafferis
Conference Chairman

TABLE OF CONTENTS

Volume I of II

SESSION I

Lightning Threat to Aircraft: Do We Know All We Need To Know? 1-1
V. Mazur

SESSION 2A

Description and Interpretation of Aircraft Lightning Attachment Electric and Magnetic Fields Measurements and Video Observation 2-1
J. Moreau and S. Larigaldie

Intracloud Development of Lightning Strikes to Aircraft 3-1
V. Mazur

Current Waveform Observed During Lightning Strikes on Aircraft 4-1
J. Boulay

SESSION 2B

Lightning Current Rate of Rise in the New Lightning Flash Model for the Space Shuttle Program 5-1
N. Bankston

Modeling of Electrically Thick Materials. Theoretical and Experimental Aspects 6-1
V. Gobin, F. Issac, and F. Jaillot

Sparking Characteristics of Carbon Fiber Composite Fastened Joints With Various Waveforms 7-1
D. Heidlebaugh and J. Carter

Investigations Into the Damage for Various Types of Unprotected Carbon Fibre Composites With a Variety of Lightning Type Arc Attachments ... 8-1
G. Reid

TABLE OF CONTENTS (cont)

SESSION 3A

Characteristics of Winter Lightning Currents Struck an Isolated Tower . 9-1
Y. Goto, K. Narita, and H. Komuro

Thunderstorm Detection and Warning System Atmospheric Potential Monitor 10-1
R. Markson and R. Wojtasinski

Electrical Emissions of Airplanes Flying in Electrified Clouds and Their Effect on Airplane Measurements of Cloud Electric Fields 11-1
J. Jones

E and dE/dT Waveshapes for Narrow Bipolar Pulses in Intracloud Lightning 12-1
P. Medelius

SESSION 3B

The Performance of Cable Braids and Terminations to Lightning Induced Transients 13-1
D. Crofts

Lightning Protection of the Fokker 100 CFRP Rudder 14-1
A. Ruiter

Protection of Electrical and Electronic Equipment Against Lightning Indirect Effects on the Airbus A340 Wing 15-1
O. Spiller

First and Subsequent Return Stroke Properties of Cloud-to-Ground Lightning 16-1
S. Namasivayam and S. Lundquist

TABLE OF CONTENTS (cont)

SESSION 4A

Characteristics of Return Stroke Electric Fields Produced by Lightning Flashes at Distances of 1 to 15 Kilometers 17-1
Ch. Hopf

Electromagnetic Radiation Field of Multiple Return Stroke Lightning 18-1
S. Gupta

Airborne Observations of Electric Fields Around Growing and Decaying Cumulus Clouds 19-1
K. Giori and J. Nanevicz

SESSION 4B

Lightning Location System Supervising Swedish Power Transmission Network 20-1
S. Melin

Range Estimation Techniques in Single-Station Thunderstorm Warning Sensors Based Upon Gated, Wideband, Magnetic Direction Finder Technology 21-1
A. Pifer, W. Hiscox, K. Cummins, and W. Neumann

Thunderstorm Monitoring and Lightning Warning, Operational Applications of the SAFIR System 22-1
P. Richard

VHF Discharge in Storm Cells Producing Microbursts 22A-1
P. Laroche, C. Malherbe, A. Bondiou, M. Weber, C. Engholm, and V. Coel

SESSION 5A

The QT Interval in Lightning Injury With Implications for the "Cessation of Metabolism" Hypothesis 23-1
C. Andrews, M. Darveniza, and D. Colquhoun

TABLE OF CONTENTS (cont)

Further Identification and Treatment Modalities in Telephone Mediated Lightning Strike 24-1
C. Andrews and M. Darveniza

Step Voltage Analysis for the Catenoid Lightning Protection System 25-1
J. Chai, D. Barker, R. Briet, and H. Eley

Hardening Communication Ports for Survival in Electrical Overstress Environments 26-1
O. Clark

SESSION 5B

P-Static Interference to Aircraft RF Receivers 27-1
W. Devereux

Evaluation of the Observability of Electrostatically Charged Rotocraft . . . 28-1
P. McKenna, R. Dalke, R. Perala, and D. Steffen

Charge Control Experiments on a CH-53E Helicopter in a Dusty Environment 29-1
C. Moore, J. Jones, and S. Hunyady

Results of Recent Precipitation Static Flight Test Program on the Navy P-3B Antisubmarine Aircraft 30-1
M. Whitaker

SESSION 6A

Launch Pad Lightning Protection Effectiveness 31-1
J. Stahmann

Activation of the Navy's Indirect Effects Lightning Simulation Laboratory 32-1
M. Whitaker

Characteristics of Vertical Electrical Fields and Associated Voltages Induced on an Overhead Power Line From Close Artificially Initiated Lightning 33-1
M. Rubinstein

TABLE OF CONTENTS (cont)

Lightning Protection for Shuttle Propulsion Elements 34-1
C. Goodloe and R. Giudici

SESSION 6B

Photographic Spark Detection Sensitivity With Various Film Types and Utilizing Multiple Spark Sources 35-1
D. Dodrill and D. Heidlebaugh

Lightning Transient Monitoring on the Titan IV 36-1
D. Downs

Influence of Configuration Effects on "Multiple Burst" Simulation Testing 37-1
J. Emanuely and M. Cantaloube

Evaluation of the Damage Caused by Lightning Current Flowing Through Bearings 38-1
E. Garbagnati, O. Celi, and A. Pigini

SESSION 7A

A Transportable 50 KA Dual Mode Lightning Simulator 39-1
K. Salisbury, S. Lloyd, and Y. Chen

Mathematical Models for Determining the Protected Spaces of the Vertical Lightning Rod 40-1
I. Mladenovic and A. Vorgucic

Designs for Surge Immunity in Critical Electronic Facilities 41-1
E. Roberts

The Sandia Transportable Triggered Lightning Instrumentation Facility 42-1
G. Schnetzer and R. Fisher

TABLE OF CONTENTS (cont)

SESSION 7B

FD-TD Calculation With Composite Materials. Application to C160 Aircraft Measurements 43-1
J. Alliot, J. Grando, F. Issac, and X. Ferrieres

Time Dependant Behavior of a Carbon Composite Case to Simulated Lightning 44-1
M. Taylor

The Electromagnetic Environment in CFC Structures 45-1
C. Hardwick and S. Haigh

A New Approach to Equipment Testing 46-1
C. Hardwick, V. Dunkley, B. Burrows, and I. Darney

SESSION 8A

Damage to Metallic Samples Produced by Measured Lightning Currents . 47-1
R. Fisher and G. Schnetzer

An Assessment of Tailoring of Lightning Protection Design Requirements for a Composite Wing Structure on a Metallic Aircraft 48-1
T. Hardwood

Lightning Protection Design and Testing of an All Composite Wet Wing for the Egrett 49-1
B. Burrows, S. Haigh, C. Chessum, and V. Dunkley

SESSION 8B

Lightning Protection of Full Authority Digital Electronic Systems 50-1
D. Crofts

Simulation and Measurement of Melting Effects on Metal Sheets Caused by Direct Lightning Strikes 51-1
A. Kern

TABLE OF CONTENTS (cont)

Application of Designed Experiments Statistical Approach to Lightning Testing of Carbon Fiber Composites 52-1
J. Ward and A. Booker

SESSION 9A

A Survey of Laser Lightning Rod Techniques 53-1
A. Barnes

Predicting Cloud-to-Ground Lightning With Neural Networks 54-1
A. Barnes, D. Frankel, and J. Draper

The Electric Field Change Caused By a Ground Flash With Multiple Channels 55-1
Z. Kawasaki

SESSION 9B

FD-TD Numerical Simulation of an Entire Lightning Strike on the C160 Aircraft 56-1
J. Alliot, J. Grando, J. Muller, and X. Ferrieres

Observations of Bidirectional Leader Development in Triggered Lightning Flash 57-1
P. Laroche, V. Idone, A. Eybert-Beard, and L. Barret

Application of Surface Electrical Discharges to the Study of Lightning Strikes on Aircraft 58-1
J. Boulay and S. Larigaldie

The Scale-Model Charge-Transfer Technique for Measuring Enhancement Factors 59-1
J. Kositsky and J. Nanevicz

TABLE OF CONTENTS (cont)

SESSION 10A

The Electric Field Changes and UHF Radiations Caused By the Triggered Lightning in Japan 60-1
Z. Kawasaki, T. Kanao, K. Matsuura, M. Nakano, K. Horii, and K. Nakamura

The Detection of the Electric Field Vertical Distribution Underneath Thundercloud: Principle and Applications 61-1
S. Soula and S. Chauzy

Discussions on a Long Gap Discharge to a Transmission Tower by a Rocket Triggered Lightning Experiment 62-1
K. Nakamura, A. Wade, and K. Horii

Correlation Between Some Current Parameters and Optical Radiation Generated by 280 mm Long Laboratory Sparks 63-1
D. Windmar, V. Cooray, and V. Scuka

SESSION 10B

Modeling Structural Joint Lightning Currents for Direct Effects Evaluation 64-1
J. Carter and J. Sutton

The Effects of the Exhaust Plume on the Lightning Triggering Conditions for Launch Vehicles 65-1
F. Eriksen, T. Rudolph, and R. Perala

Power and Energy Dissipation in Subsequent Return Strokes as Predicted by a New Return Stroke Model 66-1
V. Cooray

Horizontal Fields Generated by Return Strokes 67-1
V. Cooray

TABLE OF CONTENTS (cont)

Volume II of II

SESSION 11A

Lightning Induced Currents in Aircraft Wiring Using Low Level Injection Techniques 68-1
E. Stevens and D. Jordan

Observations of Lightning Processes Using VHF Radio Interferometry 68A-1
X. Shao, C. Rhodes, P. Krehbiel, and R. Thomas

The Physics of the Oscillating Lightning 69-1
P. Storebo

A System for Mapping Sources of VHF and Electric Field Pulses From In-Cloud Lightning at KSC 70-1
E. Thomson and P. Medelius

A New Approach to the Determination of the Striking Distance From the Lightning Channel Photos 71-1
A. Vorgucic and I. Mladenovic

SESSION 11B

Electromagnetic Topology: Characterization of Internal Electromagnetic Coupling 72-1
J. Parmantier, J. Aparicio, and F. Faure

A Real Scale Simulator for High Frequency Lemp 73-1
D. Gauthier and D. Serafin

A Theoretical Analysis of the Electromagnetic Environment of the AS330 Super Puma Helicopter External and Internal Coupling 74-1
M. Gauthier, D. Serafin, F. Flourens, and T. Morel

TABLE OF CONTENTS (cont)

SESSION 12A

Three-Dimensional Time Domain Model of Lightning, Including Corona Effects 75-1
A. Podgorski

Surface Wind Convergence as a Short-Term Predictor of Cloud-to-Ground Lightning at Kennedy Space Center: A Four Year Summary and Evaluation 76-1
A. Watson, R. Holle, R. Lopez, and J. Nicholson

Assessment and Forecasing of Lightning Potential and its Effect on Launch Operations at Cape Canaveral Air Force Station and John F. Kennedy Space Center 77-1
N. Wyse, T. Graziano, M. Secrist, J. Weems, and C. Pinder

SESSION 12B

Basic Studies on Sparks in Composite Carbone Fuel Tanks 78-1
P. Gondot, J. Avenet, S. Larigaldie, G. Hartmann, R. Haug, O. Farish, and M. Aked

Protection of Graphite Composite Fuel Tanks From Lightning Strike Damage and Fuel Vapor Ignition 79-1
R. Schmidt

Measurements of Some Parameters of Thermal Sparks With Respect to Their Ability To Ignite Aviation Fuel/Air Mixtures 80-1
S. Haigh, C. Hardwick, and R. Baldwin

SESSION 13A

The Effect of the Earth's Oblate Spheroid Shape on the Accuracy of a Time-of-Arrival Lightning Ground Strike Locating System 81-1
R. Bent and P. Casper

Experience Gained in Operation of the VLF ATD Lightning Location System 82-1
A. Lee

TABLE OF CONTENTS (cont)

Extension of and Improvements to the ERDC Low Frequency Magnetic Direction Finding System 83-1
M. Lees

An Interactive Method for Obtaining the Optimum Lightning Location on a Spherical Surface 84-1
G. Chao and M. Qiming

SESSION 13B

Comparison of Lightning Location Data and Polarisation Radar Observations of Clouds 85-1
A. Illingworth and M. Lees

The Spatial Variations of Lightning During Small Florida Thunderstorms 86-1
E. Krider and T. Oram

Weak Positive Cloud-to-Ground Flashes in Northeastern Colorado 87-1
R. Lopez, M. Maier, R. Holle, and J. Garcia-Miguel

Predicting the Onset and Cessation of Natural Lightning Hazards: Capabilities of Existing Sensor Systems as Illustrated by Two Case Studies 88-1
M. Maier and L. Maier

SESSION 14A

Lightning Mapping System 89-1
C. Lennon and L. Maier

Lightning Testing at the Subsystem Level 90-1
F. Luteran

Cloud-To-Ground Lightning Surveillance Capabilities at the U.S. Air Force Eastern Space and Missile Center 91-1
M. Maier and R. White

TABLE OF CONTENTS (cont)

A Continually Recording Method for Lightning Stroke Waveform 92-1
X. Lingen, G. Chao, and L. Xinkang

SESSION 14B

Implementation of the FAA Research and Development Electromagnetic Database 93-1
D. Grush, D. Cook, R. McDowall, and M. Glynn

The New Section 23 of DO160C/ED14C Lightning Testing of Externally Mounted Electrical Equipment 94-1
B. Burrows

Design of Lightning Protection for a Full-Authority Digital Engine Control 95-1
M. Dargi, E. Rupke, and K. Wiles

Certification of Lightning Protection for a Full-Authority Digital Engine Control 96-1
M. Dargi, E. Rupke, and K. Wiles

POSTER PAPERS (MEASUREMENTS)

On Error Sources During Airborne Measurements of the Ambient Electric Field 97-1
B. Evteev

Lightning to Upper Atmosphere: A Vertical Light Pulse From the Top of a Thunderstorm As Seen by a Payload Bay TV Camera of the Space Shuttle 98-1
O. Vaughan, W. Boeck, R. Blakeslee, B. Vonnegut, M. Brooks, and J. McKune

A Study of Point Discharge Current Observations in the Thunderstorm Environment at a Tropical Station During the Years 1987 and 1988 99-1
G. Manohar, S. Kandalgaonker, and S. Sholapurkar

TABLE OF CONTENTS (cont)

Portable Combined Optical and Electric Field Change Intracloud Lightning Detector 100-1
R. Markson

Errors in Electric Field Measurements Using Instrumented Aircraft 101-1
B. Evteev

Characteristic Features of Small, Average, and Large Ion Concentrations in Different Mobility Ranges, During Thunderstorms at Poona, India . . . 102-1
G. Srivastava

The Feedback Vibrating Capacitor Fieldmeter 103-1
J. Vosteen and W. Vosteen

Optimal Parameters of Leader Development in Lightning 104-1
N. Petrov and G. Petrova

POSTER PAPERS (METEOROLOGY)

On Charging of Snow Particles in Blizzard 105-1
H. Shio

On the Interactions of Positive Streamers With Hydrometeors 106-1
T. Verma

POSTER PAPERS (P-STATIC)

Development of a Portable P-Static Simulation Test Set 107-1
W. Devereux

POSTER PAPERS (AEROSPACE VEHICLES, TEST CRITERIA AND TECHNIQUES)

A Simulated Lightning Effects Test Facility for Testing Live and Inert Missles and Components 108-1
J. Craven, J. Knaur, T. Moore, and T. Shumpert

TABLE OF CONTENTS (cont)

POSTER PAPERS (MODELING)

Electron Distribution Functions in Electric Field Environments* 109-1
T. Rudolph

Charge Transfer During Individual Collisions in Ice Growing by Riming 109A-1
E. Avila and G. Caranti

How to Create Ball Lightning 110-1
R. Golka

Experimental Modeling of Lightning Interaction Phenomena With Free Potential Conducting Objects 111-1
C. Chernov, A. Lupeiko, and N. Petrov

POSTER PAPERS (GROUND PROTECTION)

Diffuse Dispersive Delay and the Time Convolution/Attenuation of Transients 112-1
B. Bittner

Advances in Lightning Protection That Satisfies Contemporary Standards 113-1
R. Carpenter

Circuit Protection Devices for Transient Suppression 114-1
R. Childers

Evaluating Lightning Hazards to Building Environments Using Explicit Numerical Solutions of Maxwell's Equations* 115-1
R. Collier and P. McKenna

Voltages Induced on a Power Distribution Line By Overhead Cloud Lightning 116-1
Z. Yacoub, M. Rubinstein, M. Uman, E. Thomson, and P. Medelius

Lightning Protection, Risk and Management Responsibility (Guidelines for a Proposed Lightning Protection Policy of a Golf Association or Tournament Sponsor) 117-1
C. Hillyer

TABLE OF CONTENTS (cont)

Influence of Channel Base Current and Varying Return Stroke Speed on the Calculated Fields of Three Important Return Stroke Models **118-1**
R. Thottappillil, G. Diendorfer, and M. Uman

High Current Pulse Testing for Ground Rod Integrity **119-1**
L. Walko

ATTENDEES LIST

NAME		AFFILIATION	ADDRESS	CITY	STATE	ZIP	COUNTRY	TELEPHONE
Abboud	Gaby F.	GE/MD34039	1000 Western Ave.	Lynn	MA	01910	USA	617-594-4365
Adams	Richard C.	SRI International	333 Ravenswood Ave 402-19	Menlo Park	CA	94025	USA	(415) 859-2370
Albright	David L.	U.S.A Aviation Sys Com	4300 Goodfellow Bl AMSAV	St. Louis	Missouri	63120-1798	USA	(314) 263-1634
Alliot	Jean-Claude	ONERA	8 Rue Vertugadins	Meudon		92190	France	33-1-4534-7501
Andrews	Dr. Chris	Univ. of Queensland	148 Jesmond Rd.	Indooroopilly	Qld	4068	Australia	61-7-878-2451
Armstrong	W. Thomas	Los Alamos National	SST-7, MS D466	Los Alamos	NM	87545	USA	(505) 667-9517
Bankston	Nathaniel	Rockwell International	10241 Lakewood Blvd.	Downey	CA	90241	USA	213-922-2456
Barker	Don L.	The Aerospace Corp	P.O. Box 21205	KSC	FL	32815	USA	(407) 853-6666
Barnes	Arnold	USAF	PL/GP/LYA	Hanscom AFB	MA	01731-5000	USA	617-377-2939
Baseley	Dennis	USAF ASD/ENACE	Wright-Patterson AFB	Dayton	OH	45431-6503	USA	513-255-5070
Becker	Perry L.	NASA/KSC	TE-FAC	KSC	FL	32899	USA	407-861-2771
Beens	Kagan	LBA	Roborweg 8	Braunschweig		D-3300	Germany	0531-23550
Boetti	Ron	NASA/KSC	TV-VPD-1	KSC	FL	32899	USA	407-867-4735
Berger	Gerard	CNRS	ESE Plateau Du Moulon	GIF		91120	France	33-1-69-41-80-40
Bergman	Carl	Carl Bergman & Assoc.	12741 159th Lane, SE	Rainier	WA	98576	USA	206-446-7750
Bisford	Ronald C.	Mission Instruments Co	5937 E. Pima St.	Tucson	AZ	85712-4353	USA	602-795-0949
Bittner	Burt J.	Harris Corp.	2500 Clinton Dr. NE	Palm Bay	FL	32905	USA	407-727-6440
Boeck	William	Niagara University	DePaul Hall	Niagra Univ.	NY	14109	USA	(205) 544-1538
Bootsma	Peter	Boeing Canada/ Havil.	Garratt Blvd	Toronto	Ontario	M3K1Y5	Canada	416 375 4305
Boulay	Jean-Louis	ONERA	8 Rue des Vertugadins	Meudon		92190	France	33-1-45347501
Brohm	E. H.	ABB Germany	7 Scheresberg	Birkenau		D-6943	Germany	011-49-6201-31466
Brewer	Ronald W.	Instrument Specialties	P.O. Box A	Delwater Gap	PA	18327	USA	717-424-8510x113
Briet	Richard	The Aerospace Corp.	P.O. Box 92957, MS M4-934		CA	90009	USA	213-336-1912
Burrows	Brian	UKAEA-Culham Laboratory	Abingdon	Oxon		OX143DB	England	44-235-464243
Burtzlaff	Richard J.	Martin Marietta Corp.	PO Box 179	Denver	CO	80201	USA	303-977-1064
Busse	Heinrich	Bundesakademie fur	Seckenheimer Landstr 8-10	Mannheim		D-6800	Germany	0621-418091
Canniff	John	US DOT/VNTSC	Kendall Square	Cambridge	MA	02142	USA	617-494-2501
Castaleube	Maurice	Centre Essais Aero. de	23 Ave Henri Guillaumet	Toulouse	31054		France	61-58-7320
Caranti	Georgio M.	Nat. Univ. of Cordoba	Laprida 854	5000 Cordoba			Argentina	5451-40669
Carpenter	Roy	Lightning Eliminators	6687 Arapahoe Rd	Boulder	CO	80303	USA	303-447-2828
Casper	Paul	Atmospheric Research	23 Commerce Park Dr.	Palm Bay	FL	32905	USA	(407) 725-8001
Catani	Jean-Pierre	Centre National	18 Avenue Edouard Belin	Toulouse		31450	France	(33) 61 273677
Coli	Ornella	CESI	Via Rubattino 54	Milano		20134	Italy	02-2125423
Chai	Jason	The Aerospace Corp.	P.O.Box 92957, MS M4-934	Los Angeles,	CA	90009	USA	213-336-8341
Chen	Dr. Y.G.	Maxwell Laboratories I	8888 Balboa Ave.	San Diego	CA	92123	USA	(619) 576-7852
Childers	Richard	Electromer Corp.	290 Harbor Blvd.	Belmont	CA	94002	USA	(415) 637-1030
Clark	Mel	General Semiconductor,	2001 W. Tenth Place	Tempe	AZ	85281	USA	
Cline	Jay D.	Dayton Granger, Inc.	2605 Castilla Isle	Ft.Lauderdale	FL	33301	USA	(305) 463-3451
Cohen	Richard L.	Panamax	150 Mitchell Blvd.	San Rafael	CA	94903	USA	415-499-3900 x3918
Collier	Richard S.	Electro Magnetic Appl	12567 W. Cedar Drive,	Lakewood	CO	80228	USA	(303) 980-0070

ATTENDEES LIST

NAME		AFFILIATION	ADDRESS	CITY	STATE	ZIP	COUNTRY	TELEPHONE
Conover	Don	NASA/KSC	DL-ESS-23	KSC	FL	32899	USA	(407) 867-3404
Cooray	Vernon	Inst of High Voltage R	Husbyborg	Uppsala		75592	Sweden	46 18 533636
Craven	Jeffrey D.	U.S. Army	Redstone Technical Test	Redstone	AL	35898	USA	(205) 842-2952
Crofts	David	Raychem	Eddison Road	Swindon			U.K.	0793-482307
Currlin	Waldemar A.	Electronique 2000	8 Rue Rene-Camphin	Fontaine		38600	France	(33) 76264327
Davis	Jim	Bendix Engine Controls	717 N. Bendix Dr.	South Bend	IN	46620	USA	(219)231-4464
Dellera	Luigi	CESI	Via Rubattino, 54	Milano		20134	Italy	02-2125348
Demers	Patrick	Pratt & Whitney Canada	235 Sherbrooke W. #1204	Montreal	Quebec	H2X 1X8	Canada	(514) 281-8405
Dhooge	Ted	Panamax	1870 Lodgepole Dr.	Milton	FL	32583	USA	904-626-0690
Dress	William M.	USBI	PO Box 1900	Huntsville	AL	35807	USA	205-721-2262
Dye	Anita F.	Peterson AFB	4WX/DOOS	Colorado	CO	80914	USA	(719) 554-4269
Eberhardt	Peggy	NASA/KSC	DL-DSD-23	KSC	FL	32899	USA	407-867-3185
Eckhoff	Anthony	Boeing Aerospace Ops.	Mail Stop: FA-55	KSC	FL	32899	USA	(407) 867-2281
Eilts	Michael	Nat'l Severe Storm L.	1313 Halley Cr.	Norman	OK	73071	USA	405-366-0414
Eisenberger	Ephriam	Navy Sea System Comm	Code 6650	Washington	DC		USA	703-602-2080
Eley	R.E.	The Aerospace Corp	P.O. Box 21205	KSC	FL	32815	USA	407-853-5501
Elkins	David B.	U.S. Army	STERT-Te-E-EM	Redstone	AL	35898	USA	(205) 876-3415
Emmanuely	Jean-Luc	Centre D'Essais Aero.	23 Av H. Guillaumet	Toulouse		31056	France	61587322
Engle	David C.	Grumman Melbourne Sys	2000 NASA Blvd.	Melbourne	FL	32902	USA	(407) 751-5042
Eriksen	Dr. Fred J.	Electro Magnetic Appl.	P.O. Box 260263	Denver	CO	80226	USA	303 980 0070
Eybert-Bera	Andre	CEA	BP 85X 38041	Grenoble			France	33-76-88-30-87
Fanio	Eric	Aerospatiale	316 Route de Bayonne	Toulouse		31060	France	33 61 93 79 28
Feit	David M.	Office of Fed	6010 Executive Blvd.	Rockville	MD	20852	USA	301-443-8704
Fisher	Richard J.	Sandia National Labs	P.O. Box 5800	Albuquerque	NM	87185	USA	(505) 846-2419
Floret	Nicolas	Hellite	16 Rue Bertin-Poiree	Paris		75001	France	33-1-45084747
Free	Dwayne L.	USAF	2542 Mobility Ave.	Melbourne	FL	32934	USA	407-242-7878
Fransberg	Hans	Saab-Scania AB A/C Div	S-581 88 Linkoping	Linkoping			Sweden	46-13-181211
Frick	Sam E.	F.A.A.	3229 E. Spring Street	Long Beach	CA	90806	USA	213-988-5250
Garry	John B.	FAA	FAATC, ACN-270	Atlantic City	NJ	08405	USA	(609) 484-6734
Gauthier		DGA/DRET/CEG		Gramat			France	65 105435
Gerlach	John	NASA/GSFC	E108	Wallops	VA	23337	USA	804-824-1188
Giori	Kathy	SRI International	333 Ravenswood Ave 408-30	Menlo Park	CA	94025	USA	415-859-3138
Glynn	Michael S.	FAA Technical Center	ACD 230	Atlantic City	NJ	08405	USA	609-484-4138
Gobin	Vincent	ONERA	8 Rue Vertugadins	Meudon		92190	France	33-1-4534-7501x4445
Golka	Robert K.,	Golka Associates	Box 676	Brockton	MA	02403	USA	(508) 586-7320
Gondot		Aerospatiale	12 Rue Pasteur	Suresnes		92152	France	
Goodloe	Carolyn C.	MSFC	EL54	MSFC	AL	35812	USA	205-544-2363
Goto	Kenichi	Mississippi State Univ	114 Airport Rd.	Starkville	MS	39759	USA	(601) 325-8859
Goto	Yukihiro	Tohoku Gakuin Univ.	1-13-1 Tagajo	Miyagi		985	Japan	22-368-1115
Grachan	Kenneth	Bendix/King, m/s 37	400 N. Rogers Rd.	Olathe	KS	66062	USA	(913) 782-0400

ATTENDEES LIST

NAME		AFFILIATION	ADDRESS	CITY	STATE	ZIP	COUNTRY	TELEPHONE
Grauby		GERAC	BP 505 31674	Labege Cede			France	33-61-39-93-75
Grush	Donna J.	EG&G Idaho, Inc.	P.O. Box 1625, MS 2408	Idaho Falls	Idaho	83415-2408	USA	(208) 526-9406
Gumley	Rick	Int'l Protection Cons.	Technopark	Hobart	Tasmainia	7010	Australia	61-02-730066
Haigh	Stephen	LTT - Culham Lab.	Abingdon	Oxon		OX143DB	England	235-464243
Haines	Joel D.	Naval Air Test CenterX	Code SY84	Patuxent	MD	20670	USA	(301) 863-3872
Hardwick	C.J.	LTT - Culham Lab.	Abingdon	Oxon		OX143DB	England	235-464243
Harger	Thomas R.	Harger Lightning Prot	1066 Campus Drive	Mundelein	IL	60060	USA	(708) 362-4848
Harwood	Ted	Arc Inc.	2711 Jefferson Davis Hwy	Arlington	VA	22202	USA	704-418-6415
Hasbrouck	Richard T.	LLNL	P.O. Box 808, L-154	Livermore	CA	94550	USA	(415) 422-1256
Heidlebaugh	Diane L.	The Boeing Co.	PO Box 3707, m/s 4A-11	Seattle	WA	98124	USA	206-655-6111
Heistand	Ralph W.	Florida Power & Light	P.O. Box 1565	Homestead	FL	33090-1565	USA	305-246-6598
Herhold	Charles E.	Elite Electronic Eng	4309 N. Banana River	Cocoa Beach	FL	32931	USA	(407) 783-2360
Herring	Harold C.	Comptr Sciences	P.O. Box 4127 CSR 4600	Patrick AFB	FL	32925-0127	USA	(407) 853-5205
Hess	Richard	Honeywell, Inc	P.O. Box 21111	Phoenix	AZ	85036	USA	(602) 436-1285
Hillyer	Dr. Charles	CAWRF	4700 Ortega Blvd	Jacksonville	FL	32110	USA	
Hohl	Axel	Lockheed Space Ops	1100 Lockheed Way	Titusville	FL	32951	USA	(407) 867-6330
Holden	Daniel	Los Alamos National	Group SST-7, MS D466	Los Alamos	NM	87545	USA	(505) 667-3406
Holle	Ron	NOAA-NSSL	325 Broadway	Boulder	CO	80302	USA	303-497-6637
Holmes, Jr.	Everett D.	Los Alamos National	713 Kris Court	Los Alamos	NM	87545	USA	(505) 662-2973
Hondl	Kurt	Nat'l Severe Storms	1313 Halley Cr.	Norman	OK	73069	USA	405-366-0433
Hopf	Christian	University of Federal	W. Heisenberg - Weg 39	Neubiberg		8014	Germany	0049-89-6004-372
Jackson	John	Kaman Sciences	1500 Garden of Gods Rd.	Colo. Spgs.	CO	80818	USA	(719) 599-1961
Jafferis	William	NASA/KSC	DL-ESS-23	KSC	FL	32899	USA	(407) 867-3529
Janischewsk	Wasyl	University of Toronto	Dept. of Electrical Eng.	Toronto	Ontario	M5S 1A4	Canada	416-978-3116
Jenkins	Harry G.	Los Alamos National	P.O. Box 0 MS J900	Mercury	NV		USA	702-295-4589
Jolly	Jon B.	Jon B. Jolly, Inc.	5416 California Ave., SW	Seattle	WA	98136	USA	206-938-4166
Jones	James J.	New Mexico Tech	Langmuir Laboratory	Socorro	NM	87801	USA	505-835-5751
Jones	Christopher	British Aerospace	Warton Aerodrome (W7G)	Preston	Lancs	PR4-1AX	England	UK 772-854799
Kapryan	Dr. Walter	Retired NASA/KSC	316 10th Terr	Indialantic	FL	32903	USA	407-727-1813
Karpinchik	Karin	CREOL UCF	12424 Research Parkway	Orlando	FL	32826	USA	(407) 658-6830
Kawasaki	Zen	Osaka University	Yamadaoka 2-1	Suita	Osaka	565	Japan	81-6-877-5111
Kern	Dr. Alexander	Univ. of the Federal	W. - Heisenberg - Weg 39	Neubiberg		8014	Germany	49-89-60043721
Khandani	Moody	Boeing Aerospace	Mail Stop: FA-55	KSC	FL	32899	USA	(407) 867-7426
King	Charles K.	Boeing Commercial	PO Box 3707, M/S 9R-39	Seattle	WA	98124	USA	
Klouda	Thomas	Elite Electronic	1516 Centre Circle	Downers Grove	IL	60515	USA	(708) 495-9770
Krider	E. Philip	University of Arizona		Tucson	AZ	85721	USA	(602) 621-6831
Kuhlman	Brian	McDonnell Douglas	3855 Lakewood Blvd.	Long Beach	CA		USA	(213) 593-9514
Laroche		ONERA	8 Rue Vertugadins	Meudon		92190	France	33-1-4534-7501
Lebourg	Serge	Dassault	BP24	Merignac		33701	France	33-56-55-2649
Lee	A.C.L.	Meteorological Office	Bldg. Y70, Royal	Farnborough	Hants	GU14 6TD	U.K.	(252) 24461 x 5730

ATTENDEES LIST

NAME		AFFILIATION	ADDRESS	CITY	STATE	ZIP	COUNTRY	TELEPHONE
Lees	Dr. M.I.	Electricity Res & Dev	Centre, Capenhurst	Chester			U.K.	44-51-347-2309
Lehmann	Monty R.	K-Tech Corp.	P.O. Box 70	Lexington	MD	20653	USA	301-863-8607
Lennon	Carl L.	NASA/KSC	TE-CID-3	KSC	FL	32899	USA	(407) 867-4020
Lehninger	Axel W.	U.S. Army	Picatinny Arsenal, Bldg	Dover	NJ	07806-5000	USA	201-724-3209
Lopez	Raul E.	NOAA-NSSL	325 Broadway	Boulder	CO	80303	USA	303-497-6699
Luteran	Frank	R & B Enterprises	20 Clipper Road	W.Conshohocken	PA	19428	USA	215-825-1960
Lyle	John	USAF	ASD/YSEF	WPAFB	Ohio	43433	USA	(513) 255-9526
Madura	John T.	USAF	ESMC/WE	Patrick AFB	FL	32425	USA	(407) 494-5915
Magyar	Ernest A.	G&R Tech. Corp.	10169 New Hampshire Ave.	Silver Spring	MD	20903	USA	(301) 431-3246
Maier	Launa M.	NASA	TE-CIQ-3	KSC	FL	32899	USA	(407) 867-4409
Maier	Michael W.	Computer Sciences/Rath	CSR 3220, P.O. Box 4127	Patrick AFB	FL	32925-0127	USA	407-494-4252/2012
Markson	Ralph	Airborne ResearchAssoc	46 Kendal Common Rd.	Weston	MA	02193	USA	(617) 899-1834
Mayer	William J.	Los Alamos Nat. Lab	P.O. Box 1662, Mail	Los Alamos	NM	87545	USA	(505) 667-4246
Maytrott	Craig	Fl Solar Energy Center	300 S.R. 401	CapeCanaveral	FL	32920	USA	407-783-0300 x 153
Mazur	Dr. Vladislav	Nat'l Severe Storms L.	1313 Halley Circle	Norman	OK	73069	USA	(405) 366-0406
McCartney	Gen. F.	NASA/KSC	Center Director	KSC	FL	32899	USA	
McDowall	Rosemarie	Computer Resource Mgt	200 Scarborough Dr.,	Pleasantville	NJ		USA	(609) 383-8300
McRae	Steve	AeroJet	1 NASA dr	Iuka	MS	35630	USA	601-423-0672
Medelius	Pedro	University of Florida	311 Benton Hall	Gainesville	FL	32611	USA	(904) 392-4241
Mladenovic	Ilija	Prof.ElectronicFaculty	Skopska 8	Leskovac		16000	Yugoslavia	Y0016-41-69655-642
Moreau	Jean-Patrick	Dassault Aviation/DGT/	78 Quai Marcel Dassault,	Saint Cloud		92552	France	33-1-47114194
Mulvehill	Alice	The MITRE Corporation	Burlington Road	Bedford	MA	01730	USA	(617) 271-3130
Nakamura	Koichi	Nagoya Institute Tech	Gokiso Showa	Nagoya		466	Japan	52-732-2111
Nakano	Minoru	Toyota College ofTech.	Eisei-Cho	Toyota		471	Japan	565-32-3463
Namasivayam	S.	Inst of High Voltage R	Husbyborg	Uppsala		75244	Sweden	46 18 531293
Nanevicz	J. E.	SRI	333 Ravenswood	Menlo Park	CA	94025	USA	415-859-2609
Neiman	Norman	Nyma, Inc.	1980 N. Atlantic Ste 630	Cocoa Beach	FL	32931	USA	407-799-2489
Nguyen	Cuong C.	NASA, KSC	DF-FED-21	KSC	FL	32899	USA	407-867-4564
Nial, Jr.	John A.	U.S. Navy (DOD)	Naval Ord. Sta Code 6720	Indian Head	MD	20640-5000	USA	(301)743-4130/4466
Nicholson	James R.	NASA/KSC	PT-AST	KSC	FL	32899	USA	407-867-2780
O'Neill	Mike	Meas. Technology, Ltd.	Power Court	Luton	Beds.	LU1 3JJ	England	(+44) 582-450-042
Olson	Glenn O.	Boeing Mil. Airplanes	P.O. Box 3707, M/S 4C-69	Seattle	WA	98124-2207	USA	(206) 662-0121
Oram	Timothy D.	Univ of Ariz (PAS 522)	Inst of Atmospheric Phy.	Tucson	AZ	85721	USA	(602) 621-6831
Owens	John K.	Mississippi State Univ	P.O. Drawer EE	Miss. State	MS	39762	USA	(601) 325-3623
Owens	Paula	Ministry of Defense		Liverpool			England	
Page	George D.	NAV PMO SSP DET	P. O. Box 157	Magna	Utah	84044-0157	USA	(801) 251-4137
Parmantier	Jean-P	Dassault Aviation/DGT/	78 Quai Marcel Dassault,	Saint Cloud		92552	France	(33) 1-37-11-41-94
Patterson	Stephen D.	HQ Air Weather Service		Scott AFB	IL	62225	USA	618-256-4858
Perala	Dr. Rodney A.	Electro Magnetic Appl	12567 W. Cedar Dr., #250	Lakewood	CO	80228	USA	303-980-0070
Phelps	Chris. T.	Embry-Riddle Aero.	Dept. of Math & Phys Sci	Daytona Beach	FL	32114	USA	(904) 239-6708

ATTENDEES LIST

NAME		AFFILIATION	ADDRESS	CITY	STATE	ZIP	COUNTRY	TELEPHONE
Pifer	Alburt E.	Lightning Locat &	2705-E. Medina Rd	Tucson	AZ	85706	USA	602-741-2838
Pitts	Felix L.	NASA-Langley	MS130	Hampton	VA	23665	USA	804-864-6186
Plumer	Andy	Lightning	10 Downing Parkway	Pittsfield	MA	01201	USA	413-499-2135
Podgorski	Elizabeth	Transport Canada	Pl de Ville Twr C 9th Fl	Ottawa	Ontario	K1A 0N8	Canada	613-957-6947
Podgorski	Dr. A.S.	NRC - Canada		Ottawa		K1A 0R6	Canada	613-993-4198
Pratt	Greg	LMSC	1 NASA Drive W3-02	Iuka	MS	38852	USA	601-423-0596
Reid	G.W.	LTT - Culham	Abingdon	Oxon		OX143DB	England	235-464243
Revay	Dr. Andrew	FIT	150 W. University Blvd.	Melbourne	FL	32901	USA	407-723-0189
Richard	Philippe		Parc des Algorithmes	St Aubin		91194	France	1-69-41-27-01
Roberts	Ed	FAA, Airway Facil. Div	3400 Norman Berry Drive	East Point	GA	30344	USA	(404) 763-7417
Robinson	Randy	Beech Aircraft Corp.	9709 E. Central Avenue	Wichita	KS	67201-0085	USA	(316) 676-7933
Ross	Fred L.	Lockheed Aer Systems	86 S. Cobb Drive	Marietta	GA	30063	USA	404-494-1406
Roth	Jan-Uwe	Dornier Luftfahrt GmbH	PO Box 1303	Friedrichshaf		7990	Germany	7545-84897
Rubinstein	M.	University of Florida	Dept. Electrical Eng	Gainesville	FL	32611	USA	(904) 392-4930
Ruhnke	Lothar H.	NRL	Code 4006	Washington	DC	20375	USA	202-767-2951
Ruiter	A.M.	Fokker Space & Systems	P.O. Box 12222	Amsterdam		1100AE	Holland	011-31-20-6056255
Rupke	Ed	Lightning Technologies	10 Downing Parkway	Pittsfield	MA	01201	USA	(413) 499-2135
Rustan	Pete	SDIO/TNI	12500 Cassonora Ct.	Woodbridge	VA	22192	USA	(703) 693-1671
Salaun	Michal	Dassault	78 Quai M. Dlt. CEDEX 300	St. Cloud		92552	France	
Salisbury	Kenton	Maxwell	8888 Balboa Ave.	San Diego	CA	92123	USA	619-576-7866
Sanders	Gary	Sandia National Labs	POBox 5800	Albuquerque	NM	87185	USA	505-846-0085
Sannicandro	Rocco	Boeing Aerospace Ops	FA-55	KSC	FL	32899	USA	867-2281
Scheps	Richard D.	Rockwell International	3371 Miraloma Ave.,HB-13	Anaheim	CA	92803-3170	USA	(714) 762-3738
Schnetzer	George H.	Sandia National Labs	P.O. Box 5800	Albuquerque	NM	87185	USA	505-844-6185
Schroeder	Jack	Lightning Diversion Sy	17851 Jamestown Lane	Huntington	CA	92647	USA	714-841-1080
Serafin	Dominique	Centre d'Etude Granat		Gramat		46500	France	(33) 65105446
Shaheen	George	Honeywell	5353 West Bell Rd.	Glendale	AR	85030	USA	602-436-7237
Shao	Xuan-min	New Mexico Tech	Physics Department	Socorro	NM	87801	USA	(505) 835-5137
Shio	Dr. Hisashi	Hokkaido Univ.	Dept. of Physics	Iwamizawa	Hokkaido		Japan	0126-22-1470-336
Shrier	Karen	Electromer		Belmont	CA	94002	USA	(415) 637-1830
Smith	Eric	NASA/KSC	DL-ESS-23	KSC	FL	32899	USA	407-867-3185
Soula	Serge	L. Aerologie	118 Route de Narbonne	Toulouse		31062	France	61-55-60-02
Spalding	Richard E.	Sandia National Labs	PO Box 5800, Dept. 9290	Albuquerque	NM	87185	USA	(505) 844-5934
Spiller	Olaf	Deutsche Airbus	Hunefeld St. 1-5	2800 Bremen			Germany	421-538-4423
St. Jean	Paul	Thiokol	5614 S. Meadow Lane #21P	Ogden	VT	84403	USA	(801) 863-3500
Stahmann	James R.	Beoing Aerospace Ops	FA-48	KSC	FL	32899	USA	407-867-7507
Stevens	E.G.	ERA Technology Ltd.	Cleeve Road	Leatherhead	Surry	KT22 7SA	England	372-374151
Stobie	James G.	AF Office of Sci Res	AFOSR, Inc.	Bolling AFB	DC	20332	USA	(202) 767-4960
Storebo	Per B.	Norwegian Def ResEstab	P.O. Box 25	Kjeller		N-2007	Norway	47-6-807855
Taylor	Nathan	NASA/KSC	TE-FAC-3	KSC	FL	23899	USA	407-861-2779

ATTENDEES LIST

NAME		AFFILIATION	ADDRESS	CITY	STATE	ZIP	COUNTRY	TELEPHONE
Thomas	Garland L.	NASA, KSC	RT-ENG-1	KSC	FL	32901	USA	(407) 867-4493
Thompson	Paul J.	Lawrence Livermore Nat	P.O. Box 45	Mercury	NV	89023	USA	(702) 295-2411
Thomson	Ewen	University of Florida	Dept. Electrical Eng.	Gainesville	FL	32611	USA	904-392-4041
Thottappill	Rajeev	University of Florida	Dept. Electrical Eng.	Gainesville	FL	32611	USA	(904) 392-4930
Travis	Joshua	NASA/KSC	DL-DSD-1	KSC	FL	32899	USA	
Uesugi	Masato	NASDA	Sengen 2-1-1	Tsukuba	Ibaraki	300	Japan	81-298-52-2293
Uman	M.	University of Florida	Dept. Electrical Eng.	Gainesville	FL	32611	USA	
Veazey	Don R.	US Army Atmos Sci	ATTN: SLCAS-DP	WSMR	NM	88002-5501	USA	(505) 678-5232
Vislocky	Tim	NASA/KSC	3571 S. Atlantic Ave.	Cocoa Beach	FL	23931	USA	
Vorgucic	Aleksandar	Prof.Electronic Fac.	T. Roksaudica 3	NIS		18000	Yugoslavia	38-18-46466
Vosteen	James	Monroe Electronics Inc	100 Housel Ave.	Lyndonville	NY	14098	USA	(716) 765-2254
Wakefield	Charles T.	U.S. Navy	Naval Ordnance Station	Indian Head	MD	20640-5000	USA	(301) 743-4130/4466
Walker	William	Naval Air Devel. Ctr.	Code 7021	Warminster	PA	18974	USA	215-441-2906
Walko	Lawrence C.	USAF Aero Propulsion L	WL/PooX-3, WPAFB	Dayton	OH	45429-6563	USA	513-255-9634
Ward	John M.	The Boeing Co.	PO Box 3707, M/S 4A-11	Seattle	WA	98124	USA	206-655-6111
Watson	Andrew I.	NOAA/NSSL	325 Broadway R/E/NS1	Boulder	CO	80303	USA	303-497-6630
Weber	R.	Aerospatiale	22 Rue Pasteur	Suresnes		92150	France	
Wheeler	Mark M.	Comptr Sciences/Rayth	P.O. Box 4127	Patrick AFB	FL	32925	USA	(407) 853-5151
Whitaker	Mike	U.S. Navy	NATC (SY84)	Pax River	MD	20670	USA	301-863-3868
Whitworth	Daniel	NASA, KSC	SI-FSD-4	KSC	FL	32899	USA	407-867-7157
Wiedmann	Dr. Juergen	Dornier	P.O. Box 7303	Friedrichshaf			Germany	7541-4961
Willett	John C.	AFGL	105 Drummer Road	Acton	MA	01720	USA	(508) 263-1857
Wilson	Michael J.	Lawrence Livermore N L	P.O. Box 808, L-153	Livermore	CA	94550	USA	415-294-4011
Windmar	Dan	Inst of High Voltage R	Husbyborg	Uppsala		75592	Sweden	
Wyse	Neil R.	USAF	ESMC/WE	PAFB	FL	32925	USA	(407) 853-8492
Yokoyama	Kiyoaki	Mississippi State Univ	114 Airport Road	Starkville	MS	39759	USA	(601) 325-8859
Zimbalatti	Anthony	Consultant	294 Crowell St.	Hempstead	NY	11550	USA	(516) 483-4742
Zischank	Dr. Wolfgang	Fed. Armed Forces	Werner-Heisenberg - Weg	Neubiberg		D-8014	Germany	089-60043721

# ATTENDEES 228

# COUNTRIES 14

T cont,

Be Stroke
at m Stroke
.... 118-1

Session 1, Tuesday 9:00

Opening Session

Tes 119-1

LIGHTNING THREAT TO AIRCRAFT: DO WE KNOW ALL WE NEED TO KNOW?

Vladislav Mazur
NOAA/National Severe Storms Laboratory, Norman OK 73069

The problem of lightning threat to aircraft has two aspects: strike avoidance and aircraft protection. Let us address these two issues separately.

LIGHTNING STRIKES, WEATHER CONDITIONS AND NATURAL LIGHTNING RATE

For strike avoidance we need to know where in electrified clouds strikes to aircraft may take place and with what probability. This information is useful to pilots, aviation meteorologists and possibly to air-traffic controllers.

Three major research programs studying lightning-aircraft interaction: NASA Storm Hazards Program (1980-1986), USAF/FAA Lightning Characterization Program (1984-85, 1987) and French Transall Program (1984, 1988) although focusing on in-flight measurements of strike parameters also produced significant new data about environmental conditions conducive to lightning strikes to aircraft in summer thunderstorms. Thunderstorms were the obvious choice to conduct such measurements because of the belief that lightning hazards occur where lightning activity naturally exists.

The important thing about lightning-aircraft interaction we learned from this experience was that all lightning strikes in storms at flight altitudes above 7 km (high altitudes) and about 90 % of strikes at altitudes below 7 km (low altitudes) are triggered by the aircraft itself [1, 2, 3]. Thus, the main factor contributing to lightning strike to aircraft is not a presence of natural lightning activity, but a presence of a sufficient ambient electric field to initiate a discharge on an aircraft of given size, configuration and speed. It was also shown that only about 10 % of strikes at low flight altitudes are actually intercepted natural lightning flashes [2, 3].

The previous beliefs that lightning strikes to aircraft somehow relate to the presence of turbulence were dismissed. Most lightning strikes in summer storms occur in light rain and light turbulence conditions [2]. We also learned, from data obtained with the NASA F-106B instrumented airplane during high altitude storm penetrations, that the probability of triggering lightning decreases with the increasing rate of natural lightning [1]. A similar conclusion was made in rocket-triggered lightning experiments: the probability of triggering lightning is very low when the rate of natural lightning is high and vice versa [personal communications with J.L. Boulay, P. Laroche, and W. Jefferies]. This seemingly paradoxical phenomenon may be understood if we consider a natural triggering mechanism in storms and compare it with an artificial triggering by aircraft. When the natural triggering mechanism is active, it works like a firing electrode for a large gap discharge (lightning flash) starting it each time when an ambient electric field inside the cloud is ready to support propagation of this discharge. In such a case, an additional source of triggering (aircraft or rocket with a wire) does not produce lightning initiation being out of phase with the big gap (cloud) electric field.

In line with this explanation are observations showing that the decaying stage of the storm is the most dangerous for penetrating aircraft: the probability of aircraft-triggered lightning as well as chances to succeed with a rocket-triggered lightning are the highest at this time [2]. Although the cloud is still electrified during the decaying stage, the natural triggering mechanism there is very weak, evidence of which is lack of natural lightning activity. Thus, an aircraft or a rocket with a trailing wire becomes a likely source of lightning initiation due to its conductivity and size.

As far as the safest place for aircraft penetration, we learned from the experience of the NASA Langley Storm Hazards and FAA/USAF programs that the longest flight time needed to obtain a lightning strike to aircraft is at altitudes near and below cloud base. The question of whether these altitudes may be considered the safest for aircraft in relation to lightning hazards remains to be proven.

While storm penetrations with instrumented aircraft provided scientific data on environmental conditions conducive to lightning hazards, the same kind of data on lightning hazards to aircraft in winter storms, marginally electrified stratiform and mixed phase clouds are totally lacking. What is known from pilots' surveys is that the majority of reported strikes to civil aircraft and space vehicles in the U.S. occurred in marginally electrified and mixed-phase clouds [4], and in Japan the majority of reported strikes occurred in winter storms [5].

Marginally electrified and mixed phase clouds do not produce natural lightning. Furthermore, we presently do not know how to evaluate the magnitude and structure of the electric field inside these clouds remotely without entering them. Therefore the study of electric hazards in these clouds should be more comprehensive than in thunderstorms and should include in-situ and remote sensing for electrical and microphysical parameters, kinematic modeling of electrification processes and in-situ measurements of electric discharges to aircraft. The objective of such a study would be to identify the cloud electrical condition (field intensity and structure) by its association with microphysical parameters and cloud kinematics from radar observations with Doppler and polarization diversity radars. Such a scientific approach could be utilized during the CAPE-91 research program scheduled for summer 1991 in central Florida.

Unfortunately, after the last in-flight program conducted by the FAA in 1987 there is no further commitment from U.S. government agencies to in-situ measurements of lightning-aircraft interaction. The FAA has decided not to support the combined U.S.-France program that was designed partly to investigate electrical hazards to aircraft in the marginally electrified clouds. The USAF was unable to support the proposed exploratory study of electrification mechanisms in stratiform clouds utilizing opportunities of the CAPE-91 program. The NASA Airborne Electric Field program presently underway with a single objective to evaluate the electric field inside "non-thunderstorm" clouds is an example of an engineering rather than a scientific approach to solving this problem.

Since the problem of lightning hazards to aircraft in most common weather conditions of marginally electrified clouds remains unsolved, the Atlas-Centaur accident of 1987 [6] should be a constant reminder to us that this could happen again.

AIRCRAFT PROTECTION (ENGINEERING VS. SCIENTIFIC APPROACH)

In simple terms, an engineering approach to the evaluation of the lightning threat to aircraft consists of flying an instrumented airplane in thunderstorms in order to encounter lightning strikes, to measure some of their parameters and to apply results to aircraft testing and certification. A scientific approach is based on the comprehension of the entire lightning strike process to the degree that affects the aircraft, to measure and evaluate all components of the process, and to synthesize results for applications. Let us review what we did measure during past in-flight programs, how well we did measure it, and how well our measurements represent the lightning threat to aircraft.

Most quantitative measurements of lightning strikes were made during the initial attachment of the lightning channel to the aircraft [7, 8, 9]. With a maximum frequency range up to 80 MHz in digital recording systems, the short (minimum duration of a few μs) records were obtained to characterize individual pulses during the initiation stage [10]. Continuous records of electromagnetic waveforms for the entire strike duration (hundreds of ms) were made at frequency ranges up to 2 MHz [3, 11, 12]. The peak detector used during the NASA Storm Hazards Program, although having a wide frequency band, produced records that were random (one record per flight) and therefore could not be identified with any of the lightning processes.

Measurements described above produced a population of statistically compounded pulses (their amplitudes, rise times, and durations) that characterize strike initiation with an acceptable accuracy [13]. Measurements of other processes involved in strike development following the initiation are less precise because of the limited frequency band width of recorders and the sometimes small number of samples.

The scientific interpretation of airborne measurements advanced the hypothesis that a lightning strike starts at the aircraft as a bidirectional leader with positive and negative leaders exiting from the aircraft's extremities that have maximum charges of opposite signs [14]. This hypothesis was verified in numerous laboratory studies [15, 16] and most recent airborne measurements [personal communication with J.P. Moreau].

After initiation on the aircraft, the lightning strike develops inside the cloud similarly to natural lightning discharge and may become either an intracloud or cloud-to-ground flash, depending on the environmental electrical conditions and flight altitude. During such development, the aircraft remains part of the lightning channel for most of flash duration (hundreds of ms). Thus, the similarity between processes in triggered and natural lightning especially for processes following the initiation is rather obvious [17]. This means that we can apply definitions of natural lightning processes to the aircraft-triggered lightning.

We learned from the scientific analysis of lightning strike development that:

1. All lightning strikes to aircraft at high altitudes (> 7 km) develop after their initiation similar to intracloud flashes [1].

2. At altitudes of 7 km and below, about 25% of lightning strikes develop into CG flashes [18].

3. The intracloud development of lightning strikes is characterized by a continuing current flow of positive leaders and intermittently occurring negative recoil streamers [14].

4. The amplitudes of return strokes reaching the aircraft are much smaller that those measured at the ground level. They are comparable to or less than the amplitudes of both the recoil streamers intercepting the aircraft during the intracloud development of the strike and the negative leader pulses during the initiation process [11, 19].

5. New initiation processes may take place during the intracloud lightning development of the strike [11].

This new knowledge is not reflected yet in the technical document, the SAE AE4L committee report (Orange book) [20], that defines technical criteria for lightning strike protection of the aircraft systems in the U.S. The latest version of this document revised in January 1989 still equates a lightning strike to aircraft to a cloud-to-ground flash and uses the reference book [21] as a source of data. The analysis of airborne lightning data obtained during the past decade, however, clearly identifies a typical lightning strike as similar to an intracloud rather than to a cloud-to-ground natural flash. Therefore the present zonal application of current waveforms on the aircraft's surface described in the Orange Book should be corrected. The correction may require (1) a review of airborne data already obtained with zones and waveforms attached to them identified, and possibly (2) new airborne measurements of current waveforms and video images of strikes for assisting in zone identification.

The direct strike environment as presently seen from scientific analysis of airborne data includes the following elements:

4

1. Component A. Series of current pulses during the lightning initiation process on aircraft. Peak amplitude of at least 20 kA (possibly 55 kA), pulse duration of a fraction of μs to less than 2 μs, series duration of maximum 20 ms, and pulse rate of up to 20 ms^{-1} [14], peak rate of rise is 4.0×10^{11} A s^{-1} [13]. Component A is present in 90% of all lightning strikes to aircraft. Measurements listed are obtained with sufficient frequency band width and from a statistically significant population of samples. The maximum value of 55 kA was measured by the peak detector on the NASA F-106B airplane during a non-cloud-to-ground strike [13]. Because of the ambiguity of the measurement, this peak value can be attributed either to Component A or B pulses.

2. Component B. Single pulse of negative recoil streamer or dart leader. Duration from tens of μs to a few hundreds of μs, peak amplitude of several kA, possibly up to 55 kA (see comment about Component A), rise time of hundreds of ns [11, 12]. Measurements of amplitudes and rise times are, however, frequency limited. Component B is present in all lightning strikes to aircraft inside thunderstorms, although the number of pulses per strike varies.

3. Component C. Continuing current lasting for hundreds of ms with low frequency variations of higher amplitudes and of tens of ms long. An average amplitude is a few tens of Amperes, maximum amplitudes of hundreds of Amperes [14]. The Component C is present in all aircraft-triggered strikes. Measurements are statistically sufficient.

4. Component D. Return stroke pulses with duration of several hundreds of μs, peak amplitude up to 26-30 kA, rates of rise of less than 1.6×10^{11} A s^{-1} [18]. The Component D is present in about 25 % of lightning strikes at altitudes below 7 km. The unambiguous measurements of peak amplitudes with a wide frequency band are lacking. More in-flight measurements are needed to obtain a statistically sufficient population of samples.

The SAE AE4L report needs to be upgraded to include the testing and certification criteria that reflect the characterization of lightning strike processes obtained from the analyses of airborne measurements during the last decade. Although some estimates of lightning parameters are not supported by a statistically significant number of samples, e. g. in cloud-to-ground strikes to aircraft, they nevertheless represent a realistic picture of lightning-aircraft interaction and with this reservation should be mentioned in the SAE AE4L report.

LIGHTNING THREAT TO AIRCRAFT: WHAT ELSE DO WE NEED TO KNOW?

In-flight research programs during the last decade were conducted only in summer thunderstorms, where lightning strikes to aircraft are very much similar to natural lightning flashes. Although there is a strong indication that the physics of strike initiation in winter thunderstorms, stratiform and mixed-phase clouds would be the same as in thunderstorms, we lack scientific data on the characteristics of electrical discharges under these conditions. Presently we project our knowledge of lightning strikes to aircraft in summer thunderstorms on those experienced in other environmental conditions. This assumption is not justified yet and therefore misleading or possibly erroneous. By conducting in-flight measurements we need to determine the characteristics of strikes to aircraft in winter storms and marginally electrified non-thunderstorm clouds to find out how much they are the same or different from those in summer thunderstorms. It is expected that owing to the different strength, spatial extension and distribution of electric fields inside winter storms and non-thunderstorm clouds, the strikes there may differ from those in summer storms. By the same reasons, the cloud regions with the highest probability of lightning strikes to aircraft may be quite different from those in summer storms. The long term goal of this investigation would be to gain the ability, using remote sensing techniques, to evaluate a threat of aircraft-triggered lightning prior to penetration of a given cloud by a given space vehicle.

In spite of significant progress made in the evaluation of lightning hazards to aircraft in summer thunderstorms this task is not completed yet. Additional airborne measurements with a wide frequency band are needed for the statistical evaluation of current waveforms for processes during intracloud and cloud-to-ground development of lightning strikes following initiation (recoil streamers, dart leaders, return strokes, new initiations).

REFERENCES

1. Mazur, V., B.D. Fisher, and J.C. Gerlach, Lightning strikes to an airplane in a thunderstorm, J. Aircraft, 21, 607-611, 1984.

2. Mazur, V., B.D. Fisher, and J.C. Gerlach, Lightning strikes to a NASA airplane penetrating thunderstorms at low altitudes, J. Aircraft, 23, 499-505, 1986.

3. Reazer, J.S., A.V. Serrano, L.C. Walko, and H.D. Burket, Analysis of correlated electromagnetic fields and current pulses during airborne lightning attachments, Electromagnetics, 7, 509-539, 1987.

4. Plumer, J.A., N.O. Rasch, M.S. Glynn, Recent data from the airlines lightning strike reporting project, J. Aircraft, 22, 429-433, 1985.

5. Goto, Y. and K. Narita, Lightning interaction with aircraft and winter lightning in Japan, Res. Letters on Atmos. Electricity, 6, 27-34, 1986.

6. Christian, H.J., V. Mazur, B.D. Fisher, L.H. Ruhnke, K. Crouch, and R.A. Perala, The Atlas/Centaur lightning strike incident, J. Geophys. Res., 94, 13,169-13,177, 1989.

7. Pitts, F. L., Electromagnetic measurements of lightning strikes to aircraft, J. Aircraft, 19, 246-250, 1982.

8. Rustan, P. L., B. Kuhlman, J. Showalter, and J. Reazer, Electromagnetic measurements

of lightning attachment to aircraft, Proc., 8th International Aerospace and Ground Conference on Lightning and Static Electricity, Fort Worth, Tex., June 21-13, 1983, pp. 45.1 - 45.8, 1983.

9. Moreau, J. P., and J. C. Alliot, E and H fields measurements on the Transall C160 aircraft during lightning flashes, Proc., 10th International Aerospace and Ground Conference on Lightning and Static Electricity, Paris, France, June 10-13, 1985, 281-287, 1985.

10. Thomas, M. E., and H. K. Carney, 1984 direct strike lightning data, NASA Tech-Memo., NASA-TM-87690, 1986.

11. Mazur, V., Intracloud development of lightning strikes to aircraft (present Proceedings).

12. Moreau, J.P. and S. Larigaldie, Description and interpretation of aircraft lightning attachment-electric and magnetic field measurements and video observations (present Proceedings).

13. Pitts, F.L., L.D. Lee, R.A. Perala and T.H. Rudolph, New methods and results for quantification of lightning-aircraft electromagnetics, NASA Tech. Paper 2737, 63p., 1987.

14. Mazur, V., A physical model of lightning initiation on aircraft in thunderstorms, J. Geophys. Res., 94, 3326-3340, 1989.

15. Bicknell, T. A., and B. M. Humood, Bipolar corona and aircraft triggering discharges, Proc. 9th Intl. Aerospace and Ground Conf. on Lightning and Static Electricity, Orlando, Florida, June 26-28, 1984, pp. 4.1-4.4, 1984.

16. Labaune, G., J.P. Moreau, J.C. Alliot, V. Cobin, B. Hutzler, G. Riguel, and R. Garbedian, Experimental study of the interaction between an arc and an electrically floating structure, Proc. 11th Intl. Aerospace and ground Conf. on Lightning and Static Electricity, Dayton, Ohio, June 24-26, 1086, pp. 27.1-27.9, 1986.

17. Mazur, V., Triggered lightning strikes to aircraft and natural intracloud discharges, J. Geophys. Res.,94, 3311-3325, 1989.

18. Mazur, V. and B.D. Fisher, Cloud-to-ground strikes to the NASA F-106 airplane, J. Aircraft, 27, 466-468, 1990.

19. Mazur, V., B.D. Fisher and P.W. Brown, Multiple cloud-to-ground strike to the NASA F-106B airplane, J. Geophys. Res., 95, 5471-5484, 1990.

20. SAE Committee AE4L, "Recommended Draft Advisory Circular: Protection of Aircraft Electrical/Electronic Systems Against Indirect Effects of Lightning", Society of

Automotive Engineers Committee Rept. AE4L-87-3, Feb. 1987.

21. Uman, M.A., The lightning discharge, Academic Press, Inc., New York, 1987.

Session 2A, Tuesday 10:15

Lightning Phenomenology Measurements 1

Krider, Chairman

DESCRIPTION AND INTERPRETATION OF AIRCRAFT LIGHTNING ATTACHMENT ELECTRIC AND MAGNETIC FIELD MEASUREMENTS AND VIDEO OBSERVATION

J. P. Moreau and S. Larigaldie

Office National d'Etudes et de Recherches Aérospatiales
B.P. 72, 92322 CHATILLON CEDEX, FRANCE

ABSTRACT

In 1988, ONERA carried out a complete airborne lightning characterization program. Among other features, the program has provided a significant amount of data from analog records of electric and magnetic field sensors to give a description of all stages of the lightning process. The initiation phase has been described in the past, so the objective of the present paper is to give a description of the other stages of the discharge, based on the observation of analog electromagnetic waveforms and of fast video (200f/s) image processed pictures. During lightning attachment, the aircraft remains electrically connected to the lightning channel where a large variety of physical processes occurs. These physical processes include recoil streamers, return strokes, and even other initiation processes of secondary discharges. The paper shows and comments typical records of analog electromagnetic field along with relative luminosity variation of the channel, which shows that there is no extinction of the continuous current throughout the discharge process. A computation of current and potential waveforms using the transmission line formalism is presented and gives satisfactory results for the representation of two of the typical waveforms observed in the recoil streamer processes..

1. INTRODUCTION

In the past, data reduction of airborne lightning characterization programs has been logically focused on quantitative characteristics of the threat [Pitts, 1982; Rustan et al., 1983; Moreau and Alliot, 1985; Raezer et al., 1987; Moreau et al., 1989]. Meanwhile the interpretation and the description of physical processes was dedicated to the beginning of the attachment, where the triggering aspect was addressed, and where the bi-Leader concept was formulated and confirmed [Rustan and Moreau, 1985; Moreau and Alliot, 1986; Moreau et al., 1989; Mazur, 1989]. Observation of the data related to the total discharge shows that, as in the beginning phase, there are recognizable types of electric field variations, and that the largest current pulses occur during the later development of the discharge.

This intracloud process then affects aircraft directly, and therefore deserves to be understood and considered in the description of the threat for lightning hazard certification of aircraft [SAE, 1987]. In addition the flying aircraft provides a unique access to direct measurements of intracloud processes which have only been studied from electric field measurements above the ground [Brook and Kitagawa, JGR 1960]. The junction phases J and the K changes (Recoil-streamers) are also well identified on aircraft recordings.

The main objective of this paper is to present and interpret the lightning processes during the total development of a strike. For the analysis we used the airborne records of electromagnetic waveforms of lightning strikes to the DRET, CEV, ONERA instrumented airplane along with the 200 frames/s video

10

images, obtained during the Transall-88 program. After a presentation of typical recordings where the different types of waveforms are identified, the analysis of the channel luminosity will be presented.
In the interpretation paragraph, a brief description of the beginning process will be recalled, followed by a more extensive analysis of the junction phases and recoil-streamers. A computational model is then exposed using the transmission line formalism to represent the two typical waveforms observed during a recoil-streamer phase.

2. DATA PRESENTATION

We will use the analog recordings (DC - 500 Mhz) of the capacitive antenna and of the magnetic field sensor network to give the description of the event. Figure 1 presents the waveforms obtained for event number 12, lasting about 350 ms. This figure shows from bottom to top: two signals from capacitive antennas (Track A, B), one fast electric field record (Track C), and one magnetic field (Track D). Before going further, we can notice that most important pulses occur during the progression of the discharge and are not concentrated during the beginning of the attachment. It is also immediatly seen that the signals from different capacitive antennas (A and B) are quite identical, although they are located at different places on the aircraft structure. This is a first indication that the aircraft sustains potential variations, and that it is totally connected to the lightning channel throughout the process.
The potential variations have been computed. In the configuration of a lightning attachment for a similar variation of electric field on all sensors of 300 kV/m there is a decrease of potential of 1MV.
The potential variations observed are due to the differential current between the entry point and the exit point of the lightning channel, which charges the aircraft capacitance.
On figure 1 we can mark different phases which we will describe later on. These phases are labelled 1 for the beginning (triggering process), 2 from the end of 1 and including junction phases (J) and recoil-streamers (K). This phase corresponds to the development of the discharge. Phase 3 is not always present and corresponds to a secondary discharge.

WAVEFORM DESCRIPTION

Figure 2 is a close view of the triggering phase showing the evolution of the surface electric field (figure 2a), and the synchronized current recording (figure 2b). During the "AB" phase the aircraft potential is decreasing. Then it increases during the "BC" phase while current pulses can reach 10 kA (a higher value has never been observed during this phase). Point "C" corresponds to a new potential decrease which will be discussed later on.

Further development of the discharge shows three typical processes that are identified by letters as described in figure 3:

- Phases "DE1" and "F12E2" that are typical of junction phases.
- Type "E" pulses (E1,E2) characterized by a step variation of the electric field.
- Type "F" pulses (F11,F12,F21,F22,F23,F24) that are typical of recoil streamers.

11

All these processes will be dealt with in the discussion part.
During the junction phase, the aircraft remains connected to the lightning and a continuous current keeps flowing in the channel.
"E" pulses correspond to a global positive potential variation of the channel and consequently of the aircraft. A current pulse of hundreds of amperes corresponds to this potential variation, as shown on figure 4.
"F" pulses are separated by some milliseconds and correspond to a surge of negative potential which remains at its previous value after the pulse. This indicates a propagating pulse of current along the channel. F pulses are typical recoil-streamers and produce high current pulses on the aircraft as shown in figure 5.

CHANNEL LUMINOSITY OBSERVATION

Channel luminosity has been computed by integrating the light of the channel in every image. The value obtained is then plotted versus the time when the picture was actually taken by the 200 F/s camera. In the following figure 6, plots of corresponding electric field are made on the same time base. On this figure the luminosity of the channel may be interpreted as a continuous current record. This shows that the aircraft remains totally connected since the luminosity never goes to zero except just before a secondary discharge. It is not possible because of the 5ms resolution of the video frames to exatly correlate pulses of recoil-streamers with spikes of luminosity. Nevertheless recoil-streamer stages are more luminous than junction phases.

3. INTERPRETATION

From the recordings of E(t) and I(t) shown on figures 1, 2, 3, we will now attempt to reconstruct the whole history of the intracloud lightning flash related to event number 12.

3.1. LIGHTNING FORMATION

Taking into account the fact that the triggering phase "ABC" seems similar for most of the recorded lightning events, our starting hypothesis will be that the lightning flash would be triggered by the airplane when crossing a fictive area located very near (some 100 m) the boundary of the negative charge region in the storm cloud. Indeed, at this location: a) the external field is expected to reach a high value, b) the charged area is close to the triggering airplane.

Following [Mazur, 1988], it is then assumed that the flash begins by the inception of a faint positive leader from the airplane (figure 7a) (current $\leq$ 1 A; velocity $\approx$ 10^4 m/s [Groupe des Renardières, 1977]). This causes the negative increase of the aircraft electrical potential observed during "AB" phase. While this potential reaches high negative values, aborted negative leaders slow down the charging process and may induce fast current pulses (as probably recorded on the Nasa F106B airplane [Pitts et al., 1987]).
Next to instant "B", a negative-stepped leader starts to propagate away from the airplane (figure 7b). It removes part of the express negative charges from the aircraft structure, leading to the positive increase of the airplane potential observed on phase "BC" of the recordings...

We believe that the new negative increase of the airplane potential which follows instant "C" is due to the arrival of the free extremity of the positive leader inside the negative space charge region (figure 7c). Indeed, in order to neutralize a volumic space charge, the positive leader is likely to develop numerous branches when growing inside the charged media. Obviously, two different effects are to be expected from this tree like propagation:

- due to the ability of each individual expanding branch to generate electrical current, the overall intensity which travels along the lightning leader system will strongly increase;
- the expansion of the conductive filament network increases the capacitance between the leader and the external media, so the mean potential of the electrically floating leader system (including the airplane) will become more and more negative.

As shown on the close view figure 2, the expected E(t) and I(t) developments are actually those recorded during the 3.5 ms "CD" region.

Then, the 30 ms duration phase "DE1" exhibits a rather slow potential evolution, with only a low continuous current ($I < 100$ A) flowing across the aircraft. This probably corresponds to the expansion of the stepped-leader from the airplane neighbourhood up to the positively charged upper region of the storm cloud (figure 7d). Assuming the typical mean stepped-leader velocity to be ≈ 2.10^5 m/s - as measured on cloud-to-ground lightning, while the typical gap between the opposite charged areas is ≈ 5 km [Krehbiel, 1987], the stepped-leader travel duration should be ≈ 25 ms. This value is comparable to the time interval which separates instants "D" and "E1" on recordings (figure 3). Within this hypothesis, the mean current along the stepped-leader should be ≈ 50 A. [Uman, 1969].

3.2. INTRACLOUD PROCESSES

From this point of view, the electrical field and current pulses that occur at instant "E1" translate the connection of the free extremity of the stepped-leader with the positive charge region. Logically, one would now expect a phenomenology almost similar to the 3.5 ms duration "CD" phase, when the positive leader entered the negative region. However, the short rise time (≈ 60 μs) of the recorded impulses proves, on the contrary, that the connection now occurs much more suddenly.
As shown on figure 8a, it seems rather likely that a spatial bidirectional leader could be triggered, inside the positively charged region, by the electric field from the incoming stepped-leader. The sudden connection of this spatial leader with the free extremity of the stepped-leader generates a large (some tenth of MV) positive pulse, which, in turn, propagates along the stepped-leader channel. This pulse reaches the airplane some kilometers further, while being almost completely attenuated by the resistance per unit length of the line (figure 8b).

Then, the string of negative potential pulses F11, F12... may be attributed to the same physical process, but now occurring ahead of each main branch of the positive leader, at the base of the storm cloud (figures 8c and 8d). As we postulate that the triggering of the intracloud lightning occurs when the airplane flies very near the negative charge boundary, the "F" negative pulses would be less attenuated that the positive "E" ones when they reach the aircraft. This explain why "F" pulses generally exhibit shorter rise times (≈ 1 µs) and higher current amplitudes (some 10^3 A) than the "E" ones (typically 60 µs, 300 A - figure 4).

In number 12 event, the whole intracloud process repeats twice with an increasing mean pulse amplitude (figure 1). In fact, assuming the leader channel to be conductive enough, the electric field in front of the leader branches is expected to increase as the lightning channels expand further into the charged regions. So the impulse process will be more and more energetic, until the whole space-charge of the storm cloud is neutralised and the lightning flash ends.

6. COMPUTATION OF POTENTIAL AND CURRENT PULSES WAVEFORMS

From the physical picture built-up in the preceding paragraph, we shall now attempt to compute the potential and current waveforms for the "E" and "F" pulses linked to the intracloud processes.
For numerical discretisation, the stepped-leader channel is viewed as a RLC transmission line which follows the differential relationships:

$$\delta V/\delta x = - R.I - L.\delta I/\delta t \qquad (1)$$

$$\delta I/\delta x = -C.\delta V/\delta t \qquad (2)$$

where:

$$C = 2\Pi\varepsilon_0/\mathrm{Ln}(2D/r) \qquad (3)$$

$$L = (\mu_0/\Pi).\mathrm{Ln}(2D/r) \qquad (4)$$

are the capacitance and inductance per unit length of the ionised channel of radius r. Due to the logarithmic variation, the length D from the channel to its electrical image does not require a precise determination. D is then a characteristic length of the problem, in the range of 10^4 m.

The resistance per unit length R and the channel radius r are assumed to be those of a 50 A free burning arc in air at atmospheric pressure; i.e: R = 20 Ω/m and r = 1.5 mm [Vacquié, 1984]. Moreover, as the characteristic evolution time for thermal processes in electrical arc is longer than ≈ 1 ms [Dow, 1952], electrical properties of the ionised channel are assumed to remain unchanged during the pulse propagation.
The airplane, with electrical parameters $R_a = 10^{-3}$ Ω, $C_a = 10^{-9}$F, and $L_a = 10^{-4}$ H, is inserted into the propagation line, 4500 m distant from the connection. The computed waveform of the current which flows through the airplane is displayed on figure 9, together with the airplane electrical potential. Comparison with the experimental results on figure 4 shows a fair agreement for the "E" pulse numerical simulation.
Concerning the "F" pulses, we assumed that - besides the voltage polarity- the main difference with the "E" pulses lies in the leader length between the connection point and the aircraft. Under the same conditions, figure 10 presents the computed waveforms for current and potential pulses on the aircraft, this one now being inserted on the line only 500 m distant from the connection point.
The current pulse appears very similar to the typical recorded "F" ones (figure 5). The computed potential pulse however seems too wide as compared to the measured one. Nevertheless, this may be due to an experimental

artifact: indeed, as the airplane voltage suddenly suffers several Megavolt amplitude rises, shielding of the field sensors by impulse corona discharges is likely to occur.

7. CONCLUSION

Lightning flashes triggered by aircraft probably resemble natural intracloud flashes more closely than any other natural discharge in controlled environments. Among many other recorded airplane strikes, event number 12, related to the instrumented "Transall" inflight measurements of June 1988 in the south of France, has provided us an excellent opportunity for an interpretation of the complete development of a typical intracloud flash.

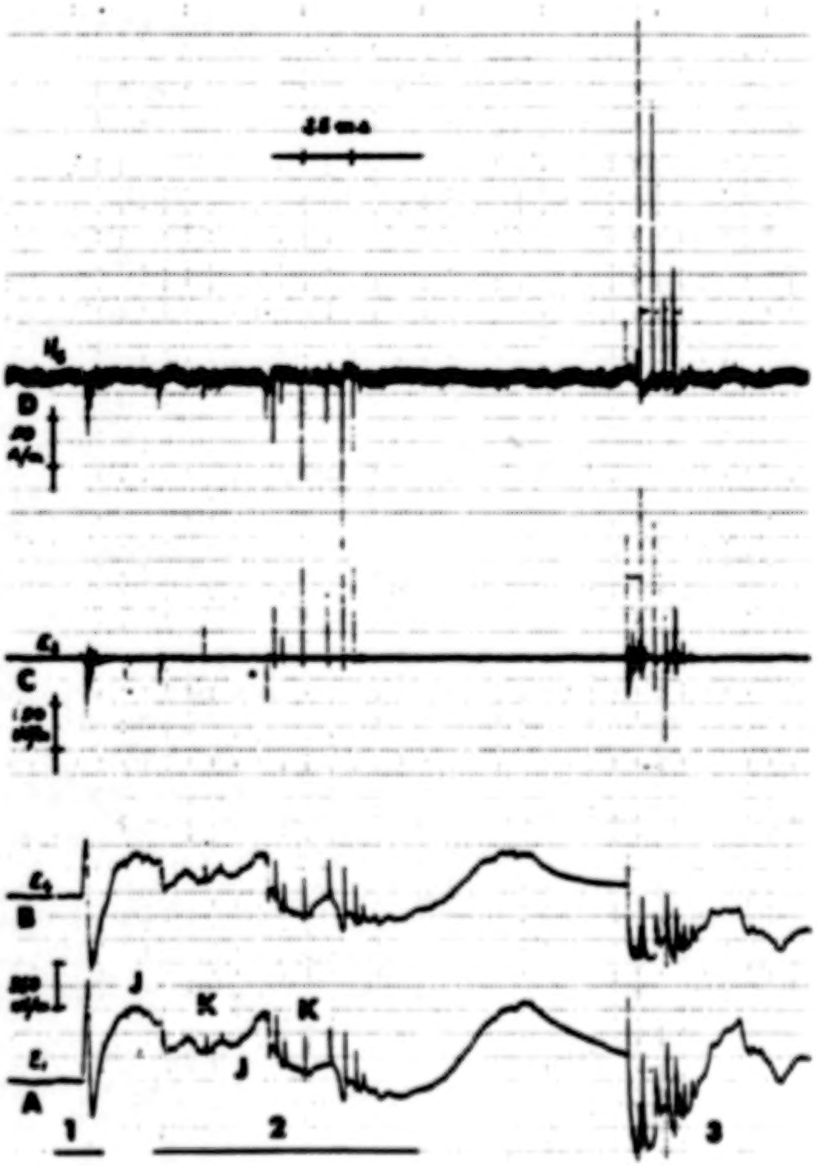

Fig. 1 – Total record of a lightning strike: a) and b) Slow electric field variation; c) Fast electric field variation; d) Magnetic field.

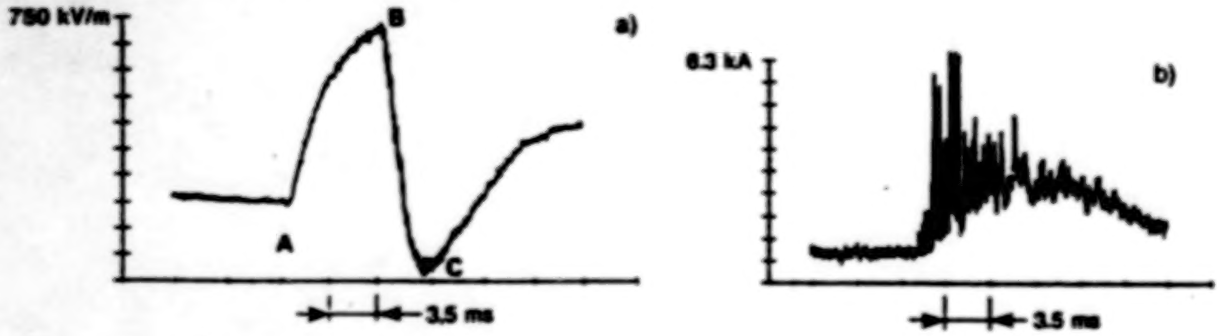

Fig. 2 – First milliseconds of attachment: a) Electric field; b) Current.

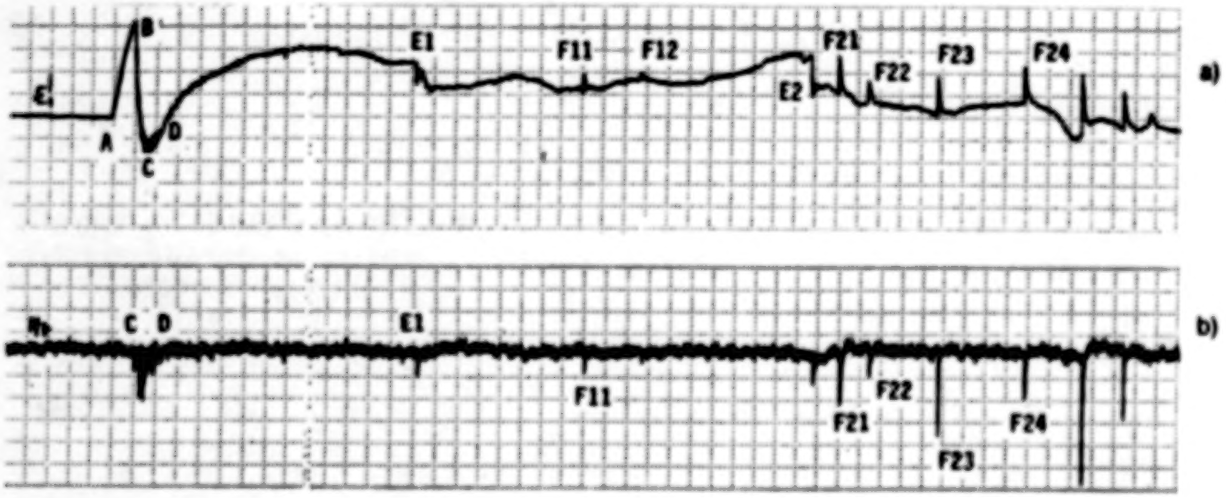

Fig. 3 – Beginning and Recoil streamer phase: a) Electric field; b) Current.

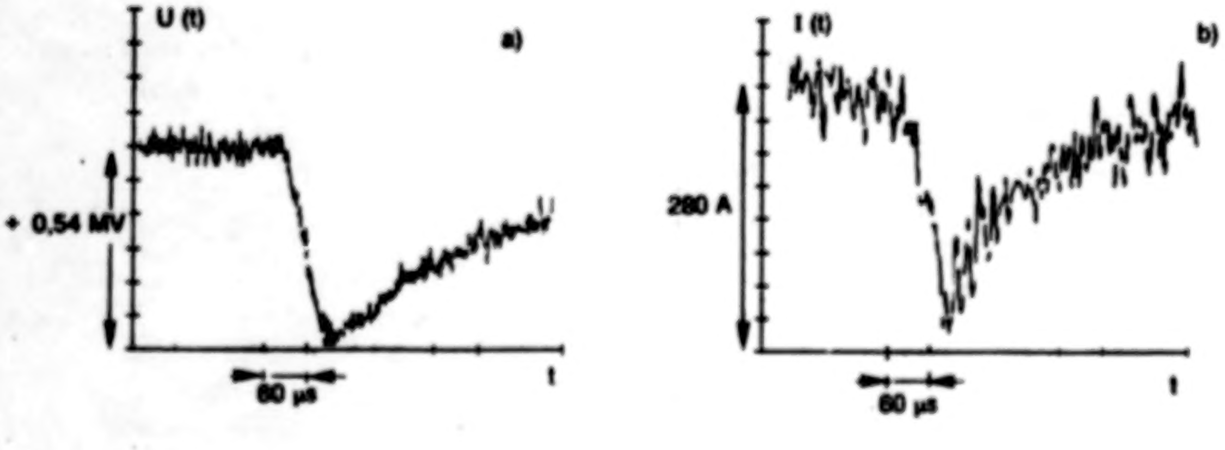

Fig. 4 – Type E Pulse: a) Potential ; b) Current.

16

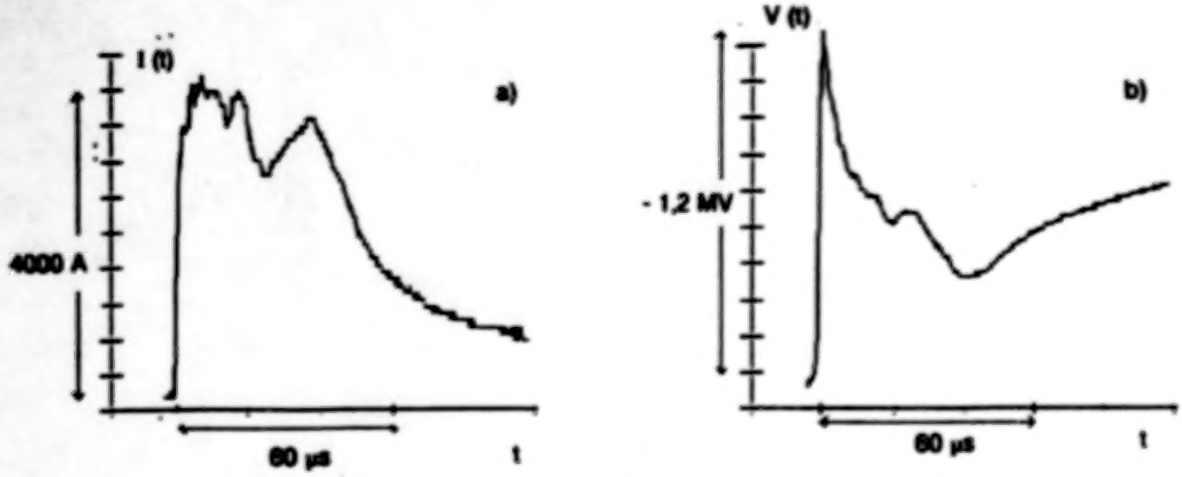

Fig. 5 – Type F Pulse: a) Current, b) Potential.

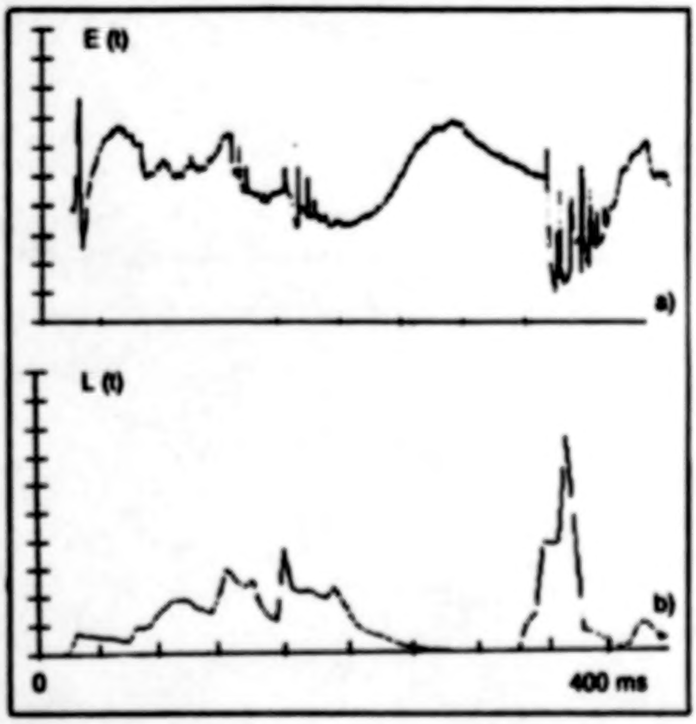

◄ Fig. 6 – Channel luminosity variation versus electric field measurements.
a) Field, b) Light.

Fig. 7 – Lightning initiation scenario (a, b).
▼

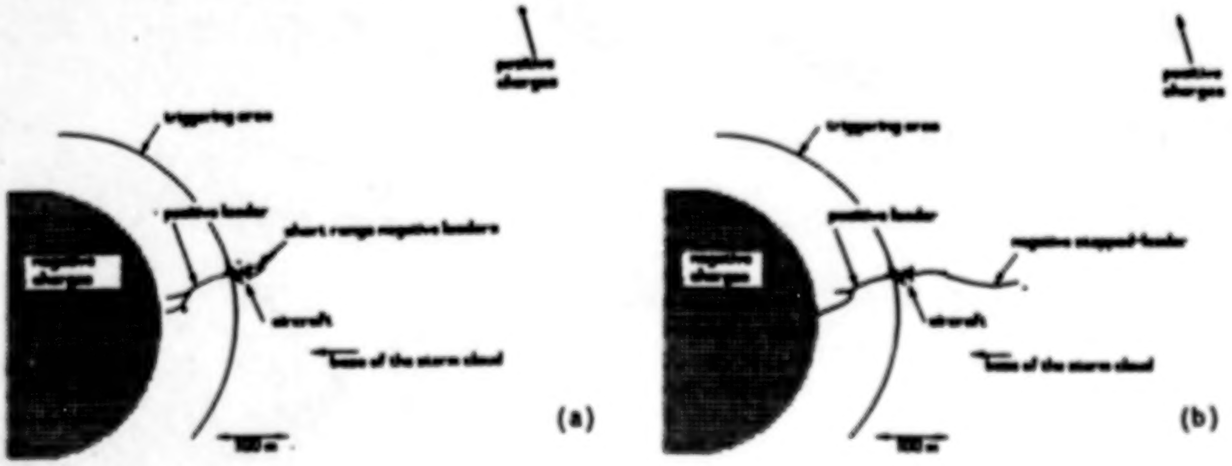
positive charges
triggering area
positive leader
short range negative leaders
negative charges
aircraft
base of the storm cloud
100 m
(a)
positive charges
triggering area
positive leader
negative stepped leader
negative charges
aircraft
base of the storm cloud
100 m
(b)

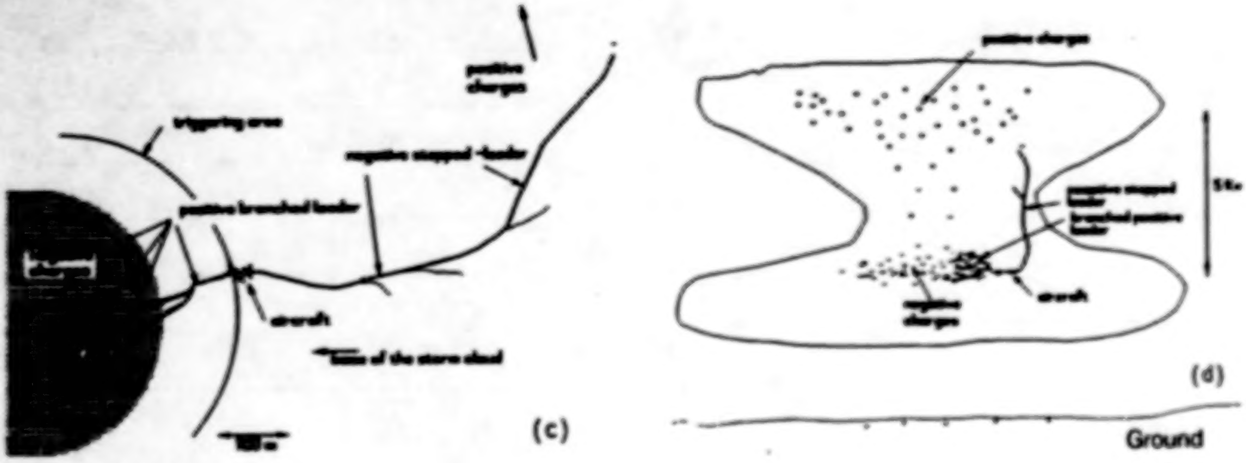
positive charges
triggering area
negative stepped leader
positive branched leader
aircraft
base of the storm cloud
(c)
positive charges
negative stepped leader
branched positive leader
aircraft
negative charges
5 km
(d)
Ground

Fig. 7 – Lightning initiation scenario (c, d).

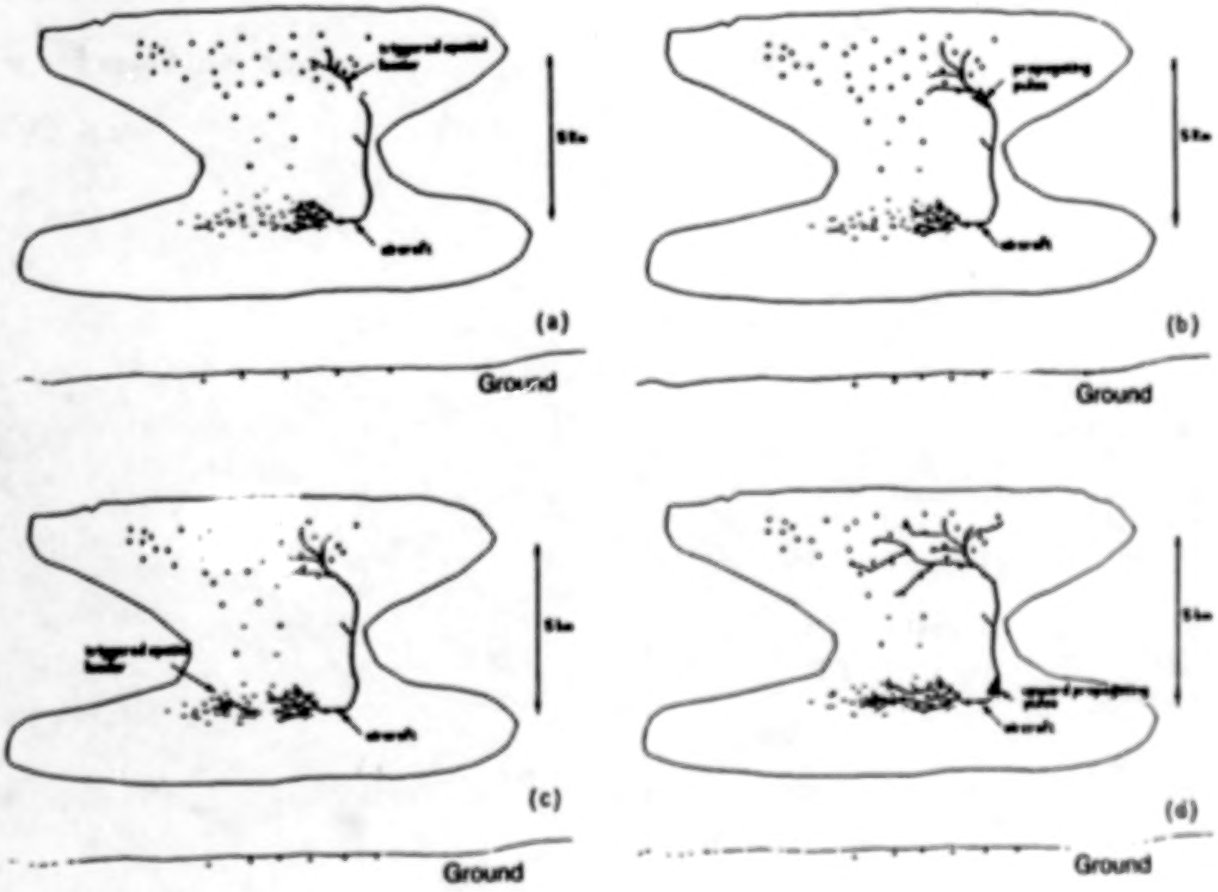
triggered spatial leader
aircraft
5 km
(a)
Ground
propagating pulse
aircraft
5 km
(b)
Ground
triggered spatial leader
aircraft
5 km
(c)
Ground
aircraft
5 km
(d)
Ground

Fig. 8 – Intracloud lightning discharge development scenario.

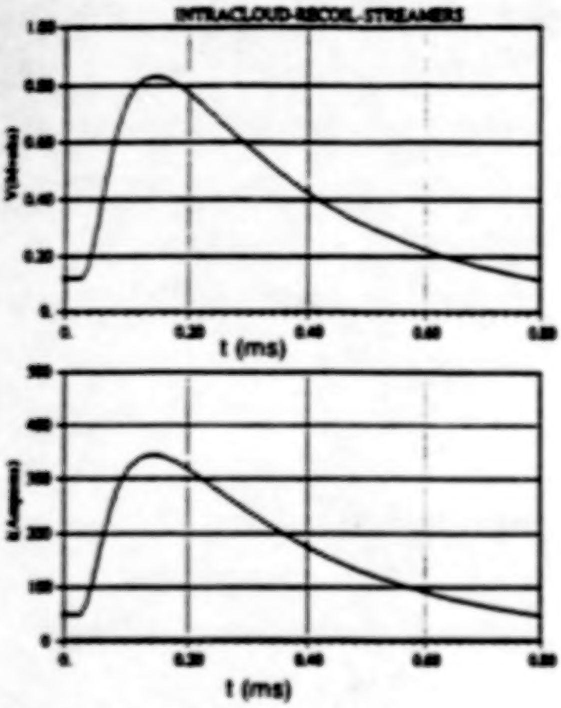

Fig. 9 – Computed waveform of potential and current for an E pulse.

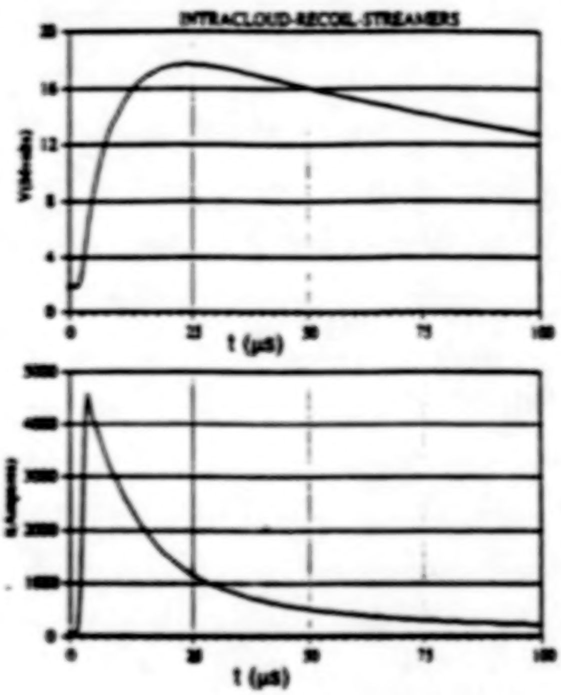

Fig. 10 – Computed waveform of potential and current for an F pulse.

REFERENCES

Brook M., Kitagawa N.,
Comparison of intracloud and cloud to ground lightning discharges. J.G.R, 65, 1189-1201, 1960.

Dow W.G.,
Fundamentals of Engineering Electronics. Wiley edit. p. 524, 1952.

Groupe des Renardières,
L'Amorçage en Polarite Positive des Grands Intervalles d'Air.
Electra n°53, 1977.

Krehbiel P.R.,
The Earth's Environment. National Academy Press, Washington D.C., 1987.

Mazur V.,
A Physical Model for Lightning Initiation on Aircraft in Thunderstorms. J. Geophys. Res., 94, 1989.

Moreau J.P., Alliot J.C.,
E and H field measurements on the Transall C160 aircraft, ICOLSE 1985.

Moreau J.P., Alliot J.C.,
Analysis of the first milliseconds of aircraft lightning attachment. ICOLSE 1986.

Moreau J.P., Raezer J., Rustan P.L.,
Summary of inflight data on lightning currents and fields. ICOLSE 1989.

Moreau J.P., Mazur V.,
Lightning initiation on aircraft from in situ electric measurements and fast video observations. Submitted to J.G.R., 1991.

Pitts F.L.,
Electromagnetic measurements of lightning strikes to aircraft. J. of Aircraft,19, 246-250, 1982.

Pitts F.L., Perala R.A., Rudolph T.H., Lee L.D.,
New Results for Quantification of Lightning /Aircraft electrodynamics. Electromagnetics, Vol 7, n° 3-4, 1987.

Raezer J., Serrano A., Walko J.C.,
Analysis of correlated electromagnetic fields and current pulses during airborne lightning attachments. Electromagnetics, 7, 509-539, 1987.

Rustan P.L., Kuhlman B., Showalter J., Raezer J.,
Electromagnetic measurements of lightning attachment to aircraft. ICOLSE 1983.

Uman M.A.,
Lightning. Mc. Graw-Hill, New York, 1969.

Vacquié S.,
L'Arc Electrique et ses Applications. Edition du CNRS, Tome 1, chap. 5, p. 175, 1984.

INTRACLOUD DEVELOPMENT OF LIGHTNING STRIKES TO AIRCRAFT

Vladislav Mazur
NOAA/National Severe Storms Lab., Norman OK 73069

ABSTRACT

The analysis of airborne electromagnetic records of seven lightning strikes to the FAA CV-580 instrumented airplane during the 1987 field campaign was aimed at revealing and interpreting processes taken place during the intracloud propagation of lightning strikes initiated on or intercepted by the airplane. It is shown that intracloud development of the strike may consist of recoil streamers, dart leader/return stroke sequences, and the secondary initiations of new discharges. These processes, with their high current pulse amplitudes, may present greater threat to aircraft than current pulses during strike initiation. The latter are presently considered by the technical community to be the primary lightning treat to aircraft.

INTRODUCTION

Most previous investigations of lightning strikes to aircraft with in-situ measurements, have focused on interpretation of lightning interaction with aircraft [1, 2, 3], as well as on quantitative measurements of lightning strike characteristics during the initial period of lightning attachment [4, 5, 6, 7]. The initial encounter of aircraft with lightning (usually several ms long) is believed to produce the most severe electromagnetic impact resulting from high current amplitudes and fast current rise times. Such a view is not, however, verified by experimental measurements. The processes following strike initiation and associated with its intracloud development (junction stage) for hundreds of ms have not been investigated, with the exception of Reazer et al.[7] and Mazur et al.[8]. Meanwhile, these processes may affect aircraft in a most direct way and need therefore to be evaluated, considered, and included in the definition of the lightning threat to aircraft in the current SAE document [9].

The primary objective of this paper is to characterize and interpret lightning processes during the junction stage of strikes. We analyzed the airborne records of electromagnetic waveforms of seven lightning strikes to the instrumented FAA CV-580 airplane at altitudes below 6 km during storm penetrations in the 1987 field campaign.

No comments are made regarding quantitative measurements of electromagnetic waveforms, because of the frequency-limited recording and an insufficient dynamic range which often produces signal saturation.

DEFINITIONS OF LIGHTNING PROCESSES INVOLVED AIRCRAFT

Interpretations of lightning strikes to aircraft are based on the following four definitions of the processes that compose a lightning flash. They are known from the literature on lightning [10] and are also verified for lightning-aircraft interaction [3].

(1) A positive leader is a continuously propagating ionized channel, current of which increases with length. Its speed of propagation is about 10^4 m s^{-1}. When initiated on aircraft, the positive leader is followed by a decrease in the aircraft's electrical potential, noticed as a negative change of the local E-field.

(2) A negative stepped leader is a series of current pulses with pulse duration of a fraction of a microsecond, pulse amplitude of hundreds to thousands of Amperes, and pulse rate of several pulses per ms. The average speed of the negative stepped leader propagation is 10^5 m s^{-1}. When initiated on aircraft, the negative stepped leader is followed by an increase in the aircraft's electrical potential, noticed as a positive change of the local E-field.

(3) A recoil streamer is a negative current pulse originating in a cloud, possibly near the tip of the positive leader and traversing the ionized channel of the positive leader toward the region of flash initiation. Recoil streamers occur later in the flash, usually during the junction stage of the discharge. Recoil streamers deposit a negative charge to the aircraft; their speed of propagation is about 10^7 m s^{-1}.

(4) A dart leader/return stroke sequence characterizes multistroke cloud-to-ground strikes (CG). Like a recoil streamer, a dart leader is a negative current pulse originating in the cloud, having all the other features of recoil streamers but terminating on the ground rather than in the cloud. A return stroke in a negative CG flash is a positive current pulse originating from the ground, thus depositing a positive charge to the aircraft. A dart leader/return stroke sequence may be recognized in airborne records by a different polarity of charges deposited to the aircraft by two pulses and by the short (a few ms) interval between them. With the propagation speed of both dart leaders and return strokes changing with the distance from the source [11], the average speed is assumed here to be at least half of their maximum speed near the ground, i.e., $0.5\text{x}10^6$ m s^{-1} and $0.5\text{x}10^7$ m s^{-1} for dart leaders and return strokes, respectively.

Positive leaders are recognized by slow negative variation of the E-field, produced by continuous current, while negative leaders and streamers are recognized by a single current pulse or a series of pulses. The only current pulses that produce positive changes in the E-field record are from return strokes.

DATA PRESENTATION

The sign convention for currents is shown in Fig. A. In the records of the three current shunts included in the analysis, both the positive charge flowing into the boom and onto the aircraft and the negative charge flowing off the boom and off the aircraft produce a positive output. The sign convention for the E-field is as follows: the positive sign corresponds to the positive aircraft electrical potential; the positive E-field change corresponds to the positive polarity D-dot pulse,and visa-versa.

Signal ranges of the data recorders are:

Currents: Range 10 A - 1.6 kA, frequency range DC-500 kHz,
E-field: Range 2.25 kV m^{-1} - 2.25 MV m^{-1}, frequency range 0.5 Hz-500 kHz,
Electric field derivative (D-dot): Range $3.54\text{x}10^{-8}$ -$8.85\text{x}10^{-6}$ C m^{-2}, frequency range 400 Hz- 2 MHz.

The current pulses initiated on the aircraft and those traversing it have distinctly different signatures in the E-field record. For the former, the E-field value makes a step to a new level during the duration of the pulse and remains there until the next pulse. For the latter, the E-field bounces back to the pre-pulse value after the pulse exits the airplane, so that the variation looks like a pulse.

Following are several examples of processes during the intracloud development of a lightning strike. The time reference in the descriptions is given in ms of absolute time.

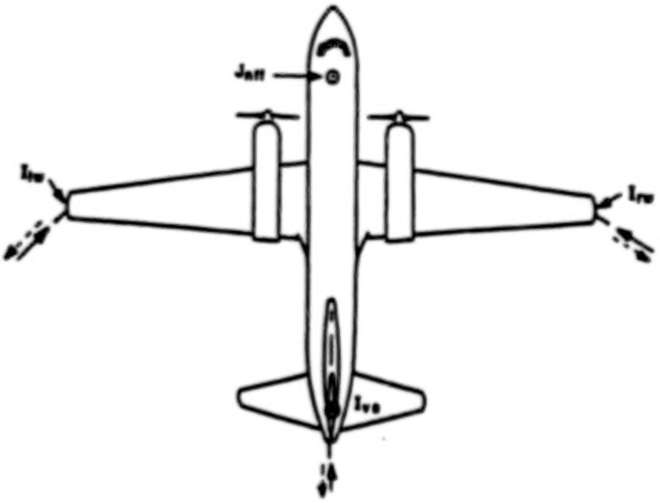

Figure A. Sign convention of current producing a positive response in the current shunt records. Solid and dashed lines indicate positive and negative charge flows, respectively.

CLOUD-TO-GROUND FLASHES INITIATED ON THE AIRCRAFT

Strike 1 (day 87197, start time 1444:02.068) is initiated on the CV-580 at 68.85 ms (mark 2, Fig. 1). The initiation process is depicted in the waveforms shown in Figure 2. Decrease of the aircraft electrical potential during period T1, 1.6 ms prior to the first negative leader pulse, corresponds to the emergence of the positive leader from an aircraft extremity [3]. A negative stepped leader is seen as a series of current pulses superimposed on the continuous current of the positive leader. Negative change of the E-field during period T2 results from the growing continuous current.

The current pulse at about 59 ms after initiation (at 127.9 ms, mark 3 in Fig. 1) produces a positive change in the local E-field (Fig. 3). The presence of continuous current at the left wing prior to the pulse (Fig. 1) is evidence of the continuous attachment of the lightning channel to the aircraft after initiation. With this in mind, the only possible interpretation of the current pulse, which deposits

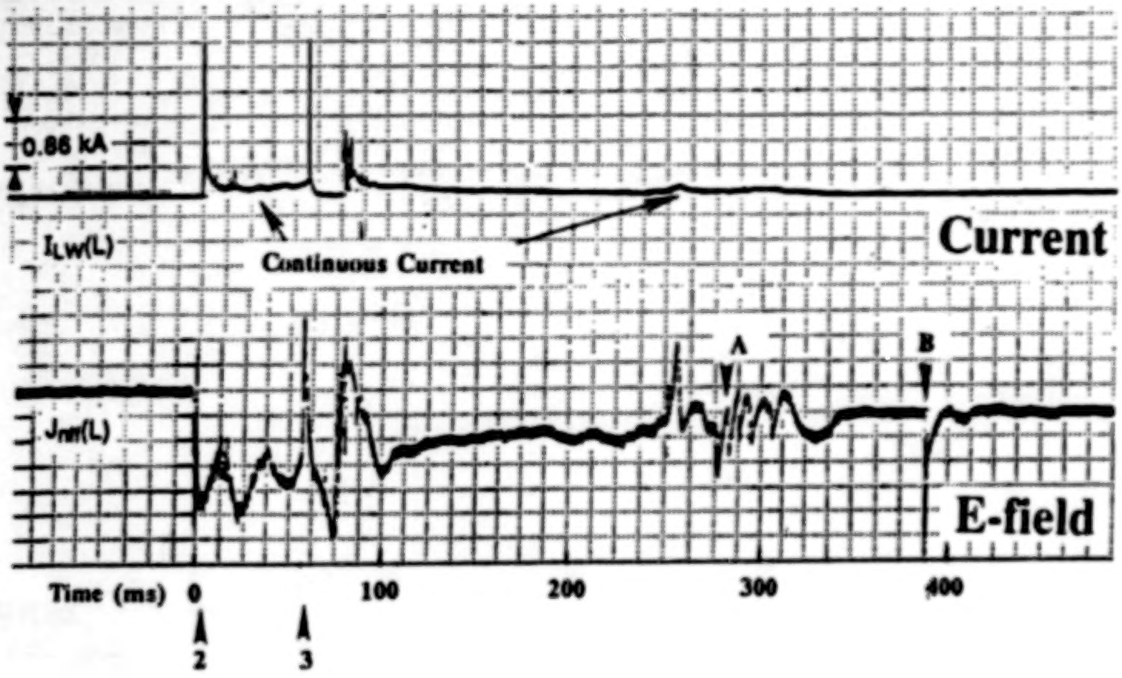

Figure 1. Strike 1, day 87197, start time 1444:02.068, duration 388 ms: E-field and current record on the left wing of the CV-580.

a positive charge to the aircraft, is that it is a return stroke of a CG flash. Assuming this, it takes about 60 ms for the stepped leader to reach the ground from a flight altitude of 6 km, and less than 1 ms for the return stroke that traverses the stepped leader channel to reach the aircraft. Notice that the magnitude of the return stroke is greater than that of the negative stepped leader.

For strike 4 (day 87216, start time 2253:01.074), the E-field and D-dot records at 75 ms are typical of the lightning initiation process on the aircraft and are similar to those in Fig. 2. At 326 ms (251 ms after the initiation), there is a pair of current pulses intercepting the aircraft. The first pulse deposits a negative charge and the second one deposits a positive charge as indicated by both the E-field changes and the polarity of D-dot pulses (Figs. 4). The pair of pulses matches the dart leader/return stroke sequence both in terms of the order of pulses (first negative, then positive) and the 3 ms interval; this interval is sufficient to cover the distance from the aircraft to the ground twice, with respective propagation speeds. Thus, the CG flash developed following intracloud propagation of the lightning strike initiated on the aircraft. For this CG flash, the dart leader amplitude is greater than that of the return stroke.

RECOIL STREAMERS

Recoil streamers take place usually tens of ms after strike initiation. During strike 4, mentioned earlier, the series of current pulses deposited a negative charge (see polarity of D-dot pulses, Fig. 5) on the aircraft, starting at 147 ms (73 ms after the initiation). The rate of these pulses (about 0.46 per ms) is considerably lower than that in negative stepped leaders (n per ms)[3]. The pulse-like E-field changes indicate that recoil streamers intercepted the aircraft. The largest of these recoil streamers, at 191 ms, has an amplitude greater than 1.5 kA (record saturation level). Continuous current accompanies the pulse series for about 38 ms, starting at 155 ms. The duration of the individual recoil streamers is measured in hundreds of μs, usually not exceeding 500 μs.

Later in the same strike, at 213 ms, a new series of pulses carrying negative charges exits the right wing tip (Fig. 6). The rate of pulses is about 3 per ms, which is a rate typical of stepped leaders. However, the pulse-type of E-field variation suggests that pulses intercepted the aircraft. A surge of continuous current during this series, seen as a low frequency envelope in the current record, is at least of 400 A maximum value, and lasts for about 7 ms. This series of negative current pulses may be a series of rapidly branching recoil streamers or a negative stepped leader initiated somewhere in a cloud. The durations of individual pulses are, however, much greater that those in negative stepped leader and correspond to recoil streamers. Unfortunately, a definite distinction between these two processes cannot be made with airborne records alone.

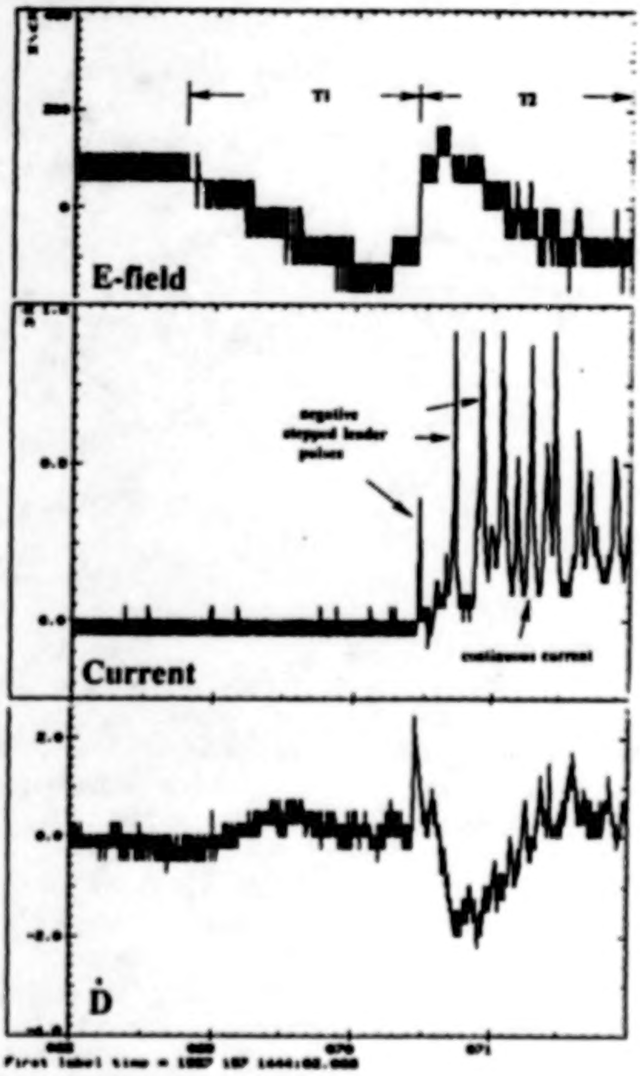

Figure 2. Strike initiation process on the aircraft. T1- period of positive leader development prior to occurrence of the negative stepped leader. T2- part of the negative stepped leader process. Notice the correspondence of current pulses and D-dot pulses in the negative stepped leader. Their rate is about 10 per ms. Continuous current (about 160 A) seen in the record produces the negative E-field change.

Strike 5 (day 87216, start time 2254:00.082) is also triggered by the aircraft. The two recoil streamers that intercepted the aircraft at about 227 ms are separated by less than a 1 ms interval (Fig. 7), and the amplitude of one of them is above 1.5 kA. Such a short interval between recoil streamers is frequently observed.

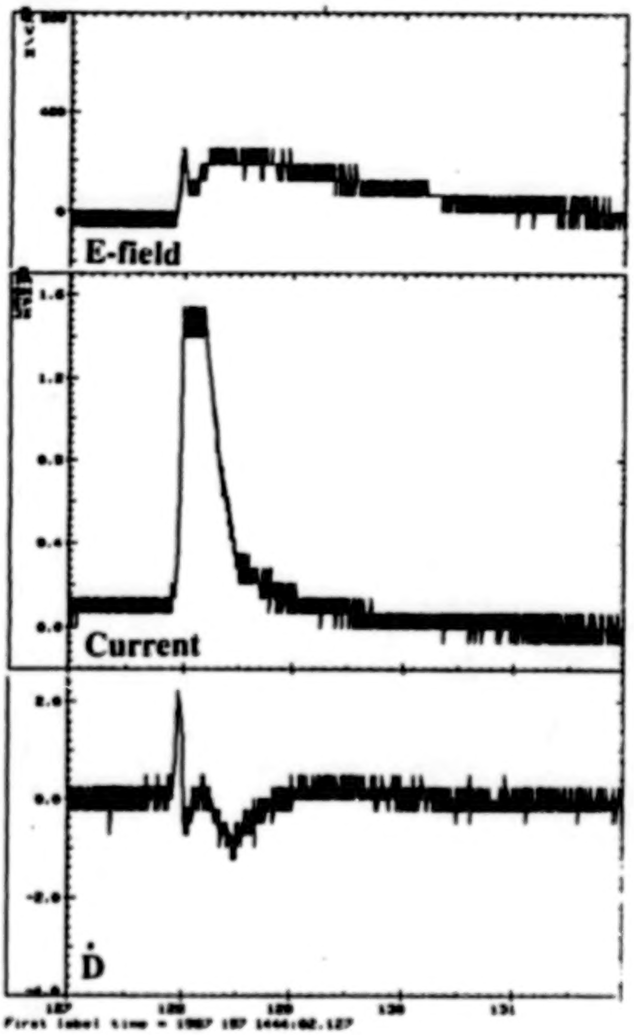

Figure 3. Return stroke intercepting the aircraft, after traversing the channel from to ground.

NEW LIGHTNING INITIATION PROCESSES

Strike 3 (day 87211, start time 1925:00.045) is a classic case of lightning initiation on aircraft. At about 165 ms (120 ms after initiation), there is a negative E-field change (lasting 0.5 ms) (marked 3, 4 in Fig. 8) which is not accompanied by current pulses (Fig. 9). The entire process resembles the initiation of lightning on aircraft (Fig. 2), but with (1) a shorter than usual decrease of the aircraft's potential prior the first negative leader pulse, and (2) a fewer than usual negative pulses. Notice the step-like E-field changes during the occurrence of pulses 1 and 2, which suggests their emergence from the aircraft. Three recoil streamers intercepted the aircraft (pulses 3, 4, and 5) immediately following the new initiation process. The evidence supporting such an interpretation are the negative D-dot pulses and the pulse-type changes in the E-field record, both of which characterize an interception. A group of recoil streamers separated by

24

intervals of 2, 4, and 6 ms (Fig. 10) conclude the process. A continuous current surge associated with development of the positive leader (Fig. 8, mark 3,4; and Fig. 10) lasts for at least 25 ms. The gradual negative change of the aircraft's potential (the local E-field) during this period is explained by the positive continuous current emerging from the aircraft.

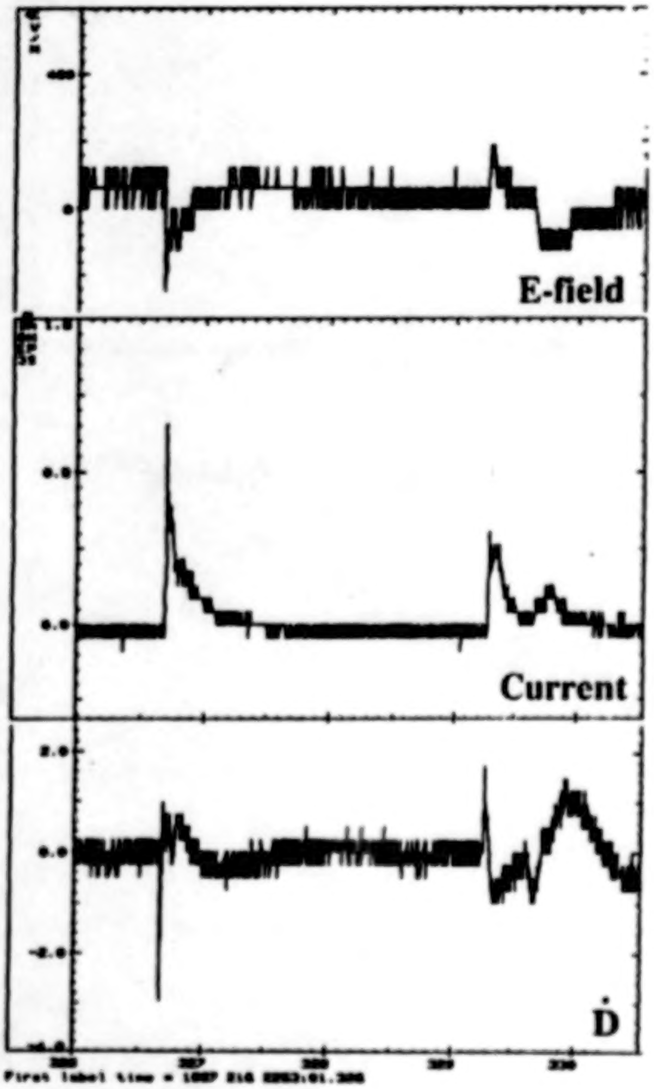

Figure 4. Sequence of a dart leader/return stroke intercepting the aircraft. Notice pulse-type E-changes and D-dot pulses of opposite polarity indicating interception rather than initiation of pulses.

Strike 6 (day 87223, start time 1934:00.058) is an example of intercepted natural lightning (Fig. 11). At 252 ms (mark 4, Fig.11), a new initiation process begins (Fig. 12), with positive leader development (negative E-field change) preceding the occurrence of the negative stepped leader at the right wing tip. This process is similar to the one in strike 3 (Fig. 9) and to the lightning initiation process in strike 1 (see the resemblance between the bracketed part in the D-dot and current record of Fig. 12, and those in Fig. 2). Two recoil streamers follow shortly (Fig. 12).

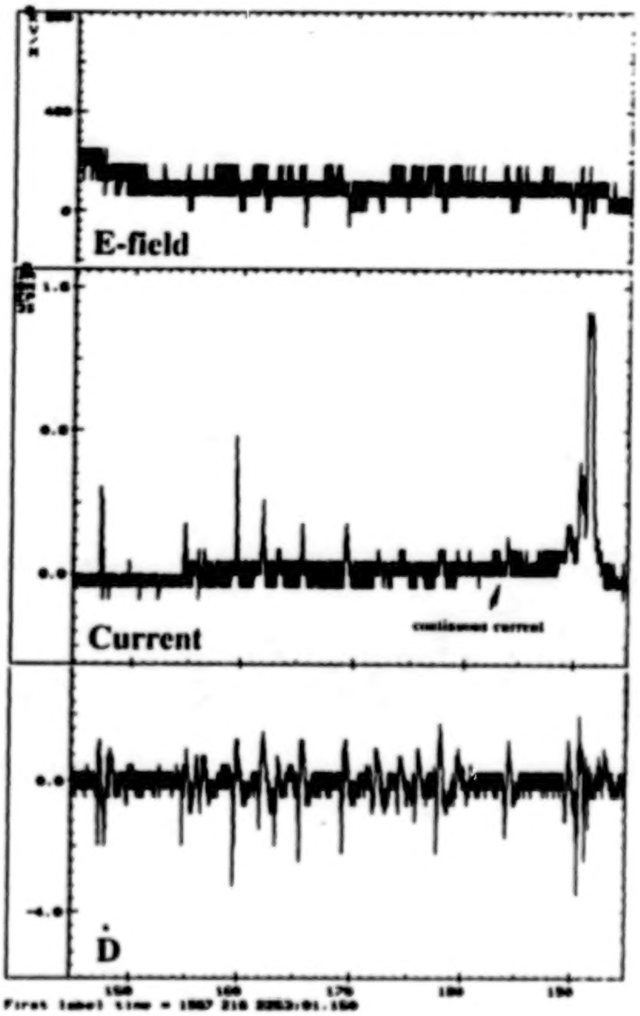

Figure 5. Series of recoil streamers intercepting the aircraft. Notice presence of continuous current and correspondence of current pulses to negative D-dot pulses and pulse-like changes in the E-field record.

DISCUSSION AND CONCLUSIONS

Several novel observations have resulted from the analysis of the entire airborne electromagnetic records of lightning flashes which were either triggered or intercepted by the CV-580 aircraft. For example, evidence was obtained that recoil streamers occur both as a single pulse and as a series of pulses separated by less than 1 ms intervals. The idea of recoil streamers presently accepted considers them as single pulses [12]. The hypothesis is advanced that "bunches" of recoil streamers are associated with rapidly branching channels. This suggestion may be tested with simultaneous high-speed video and electromagnetic measurements.

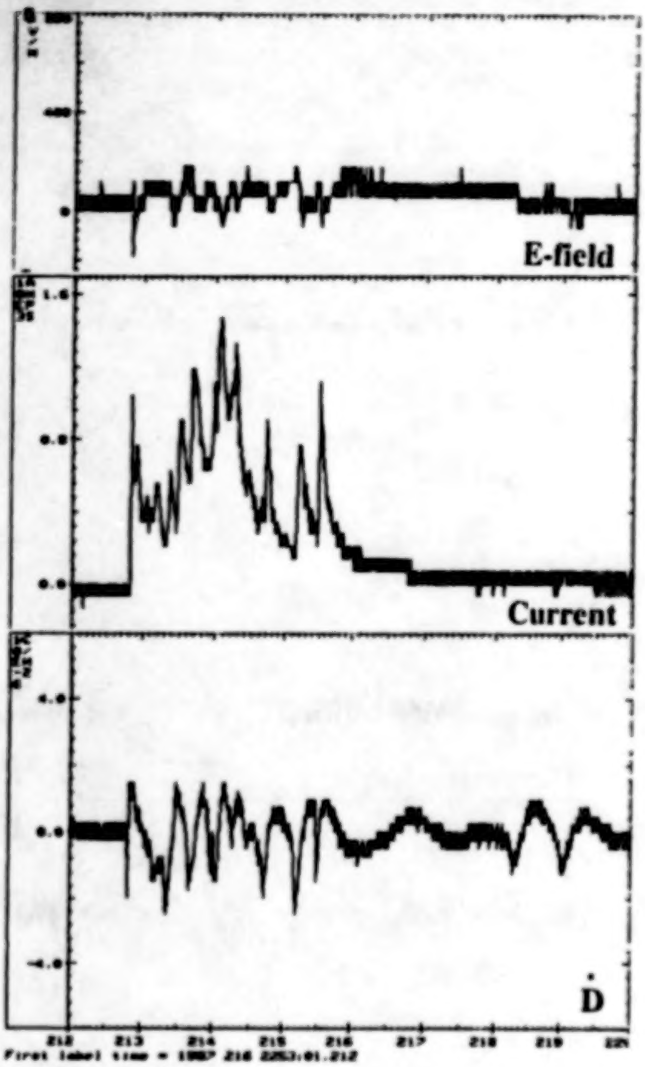

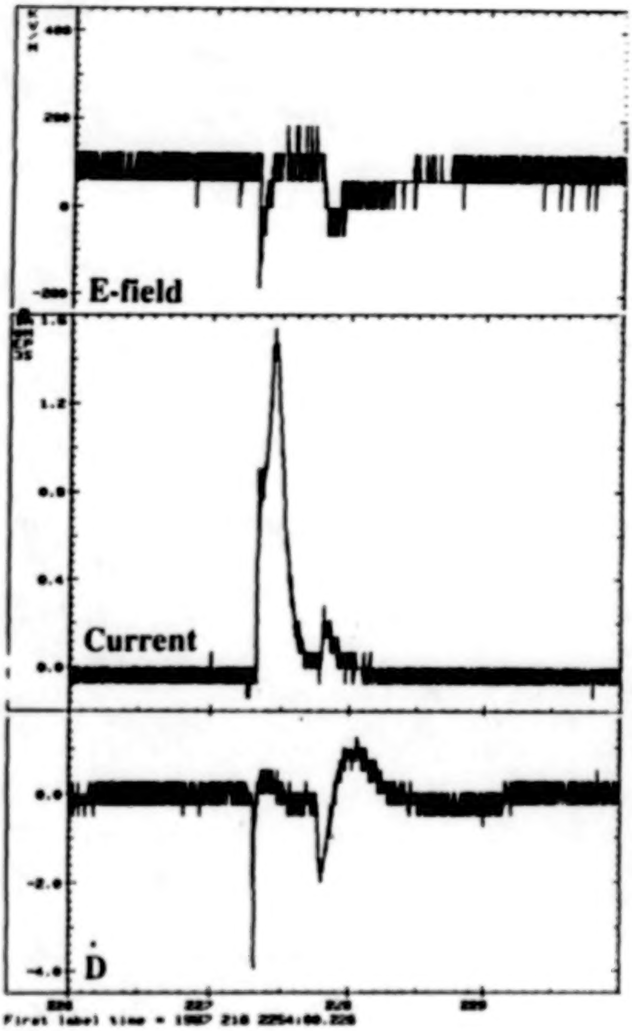

Figure 6. Group of negative pulses (branching recoil streamers or a stepped leader) intercepting the aircraft. Notice continuous current present between 213 and 219 ms.

Figure 7. Two recoil streamers intercepting the aircraft.

Another observation is that the amplitudes of recoil streamers are usually much larger than those of negative stepped leaders during the initiation process. This conclusion should be taken into consideration for a new definition of the lightning threat to aircraft. A comparison of stepped leaders in natural lightning flashes with those in strikes to aircraft should not be made, however; this is because of the possible dependence of the stepped leader in an aircraft-triggered flash on a given aircraft's size and shape. Recoil streamers, on the other hand, being less influenced by aircraft, are similar to those of natural lightning flashes. This means that recoil streamers may be measured unambiguously by an instrumented airplane.

It is also shown in this study that lightning strike development following its initiation on the aircraft (in cases of low altitude storm penetrations) frequently turns into a cloud-to-ground flash. In three cases of strikes out of seven, a CG flash developed after the strike initiation on the aircraft, and in one case, after the aircraft was intercepted by a natural flash. As previously observed by Mazur [8] in a case of multistroke CG flash to NASA F-106B, and also demonstrated by this study, return stroke currents at flight altitudes are much smaller in amplitude than those measured on the ground, and are usually smaller than current pulses of dart leaders and recoil streamers. This observation strongly indicate the need for re-examining the threat to aircraft from the return strokes.

During the intracloud development of a lightning strike, processes resembling a new initiation process of a secondary discharge on the aircraft were discovered. These processes have much shorter durations of both positive and negative leaders than those observed during initiation of the original flash. Initiation of the secondary discharges on the

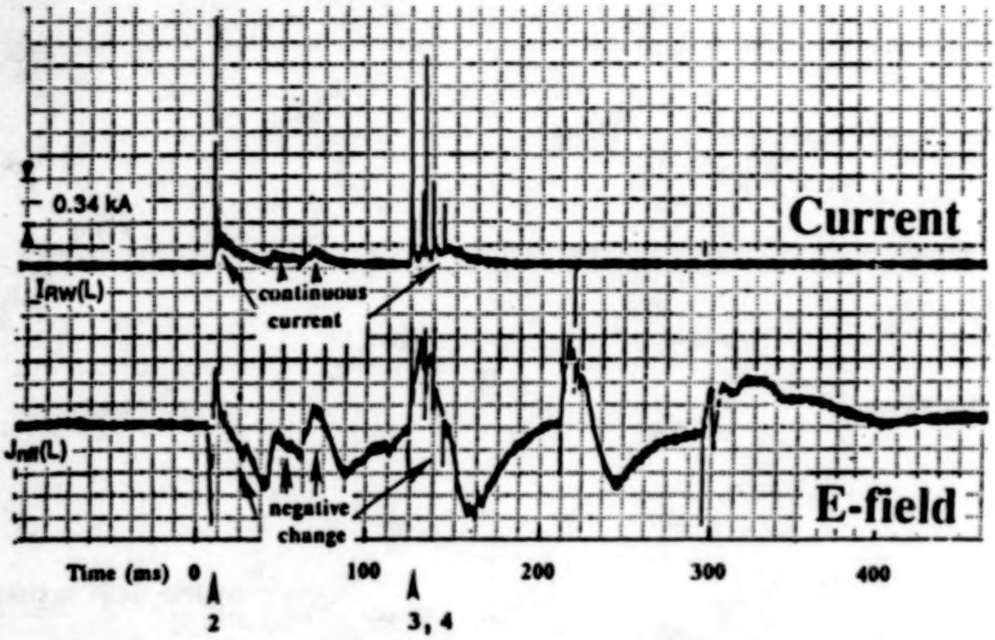

Figure 8. Strike 3, day 87211, start time 1925:00.045, duration 406 ms: E-field and current sensor record on the right wing of the CV-580. Notice time correspondence between periods of continuous current flow and periods of negative E-field changes. At the end of these periods, the aircraft's potential reaches its highest negative value, after which the positive change begins.

aircraft was observed to take place more than once during the course of a strike. We speculate that re-initiation occurs when intracloud development of the flash stops, continuous current flow ceases, but the aircraft is still in the high ambient electric field that produced the strike in the first place.

ACKNOWLEDGEMENTS

The author is grateful to Jim Elliott and Hank Weigel of EMA, Inc. for their assistance in data reduction and to Donna Crider for her help with data processing. This work was supported in part by the Federal Aviation Administration grant DTFA03-87-A-00021.

REFERENCES

1. Rustan, P. L., Jr., and J. P. Moreau, Aircraft lightning attachment at low altitudes, Proc., 10th International Aerospace and Ground Conference on Lightning and Static Electricity, Paris, France, June 10-13, 1985, 259-265, 1985.
2. Moreau, J. P., and J. C. Alliot, Analysis of the first milliseconds of aircraft lightning attachment, Proc., 11th International Aerospace and Ground Conference on Lightning and Static Electricity, Dayton, Ohio, June 24-26, 1986, pp. 18.1 -18.6, 1986.
3. Mazur, V., A physical model of lightning initiation on aircraft in thunderstorms, J. Geophys. Res., 94, 3326-3340, 1989.
4. Pitts, F. L., Electromagnetic measurements of lightning strikes to aircraft, J. Aircraft, 19, 246-250, 1982.
5. Rustan, P. L., B. Kuhlman, J. Showalter, and J. Reazer, Electromagnetic measurements of lightning attachment to aircraft, Proc., 8th International Aerospace and Ground Conference on Lightning and Static Electricity, Fort Worth, Tex., June 21-13, 1983, pp. 45.1 - 45.8, 1983.
6. Moreau, J. P., and J. C. Alliot, E and H fields measurements on the Transall C160 aircraft during lightning flashes, Proc., 10th International Aerospace and Ground Conference on Lightning and Static Electricity, Paris, France, June 10-13, 1985, 281-287, 1985.
7. Reazer, J. S., A. V. Serrano, L. C. Walko, and H. D. Burket, Analysis of correlated electromagnetic fields and current pulses during airborne lightning attachments, Electromagnetics, 7, 509-539, 1987.
8. Mazur, V., B.D. Fisher, and P.W. Brown, Multistroke cloud-to-ground strike to the NASA F-106B airplane, J. Geophys. Res., 95, 5471-5484, 1990.
9. SAE Committee AE4L, "Recommended Draft Advisory Circular: Protection of Aircraft Electrical/Electronic Systems Against Indirect

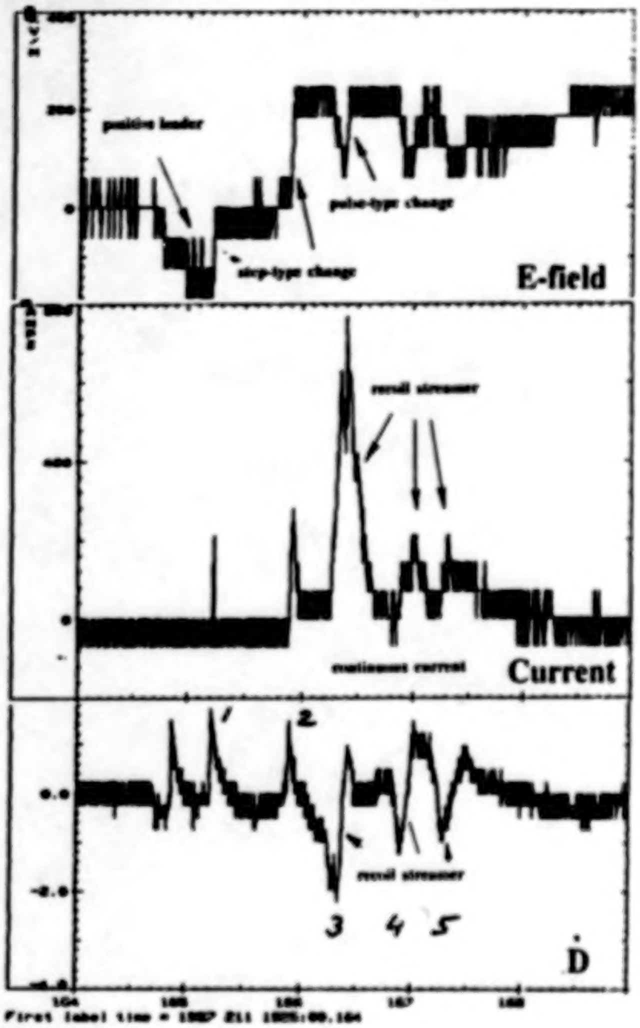

Figure 9. New initiation process on the aircraft, followed by a series of recoil streamers. Notice negative E-field change corresponding to positive leader development, then step-type positive changes corresponding to stepped-leader pulses emitted from aircraft, and pulse-type changes from intercepted recoil streamers.

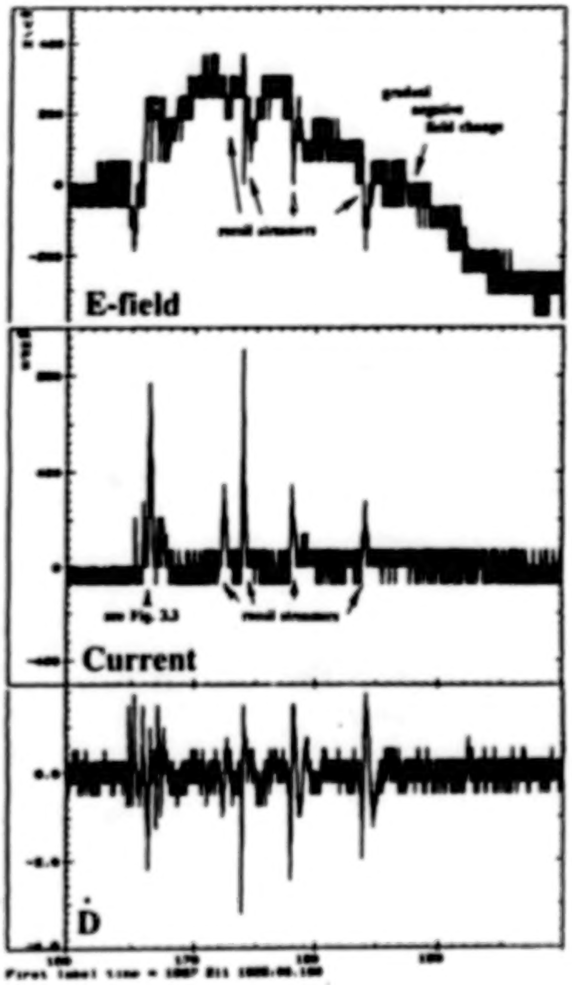

Figure 10. Series of recoil streamers followed the new initiation depicted in Fig. 9. Recoil streamers occur during the gradual negative E-field change. This period corresponds to the period of continuous current, seen in Fig. 8.

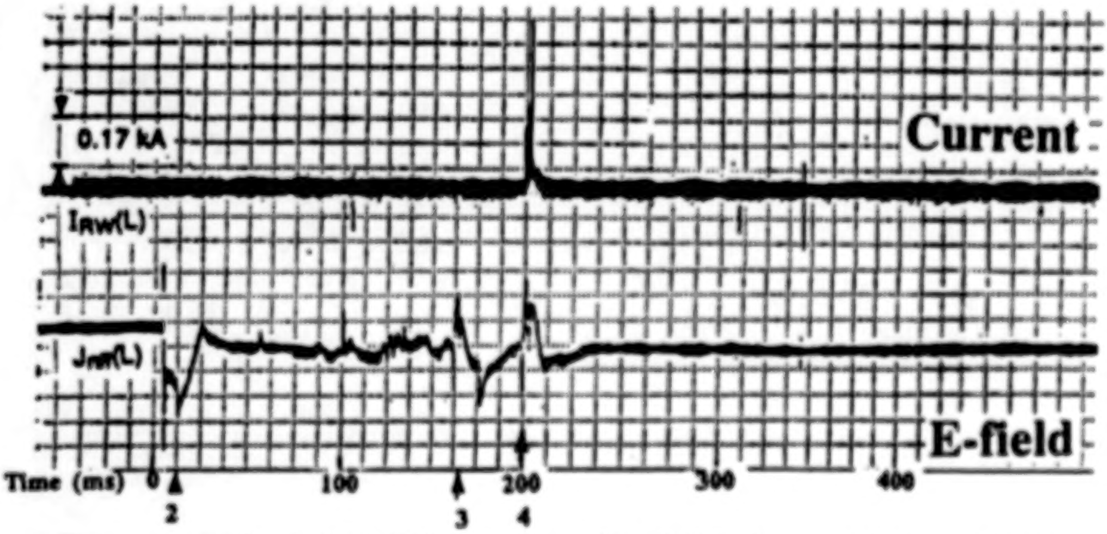

Figure 11. Strike 6, day 87223, start time 1934:00.058, duration 210 ms: E-field and current sensor records.

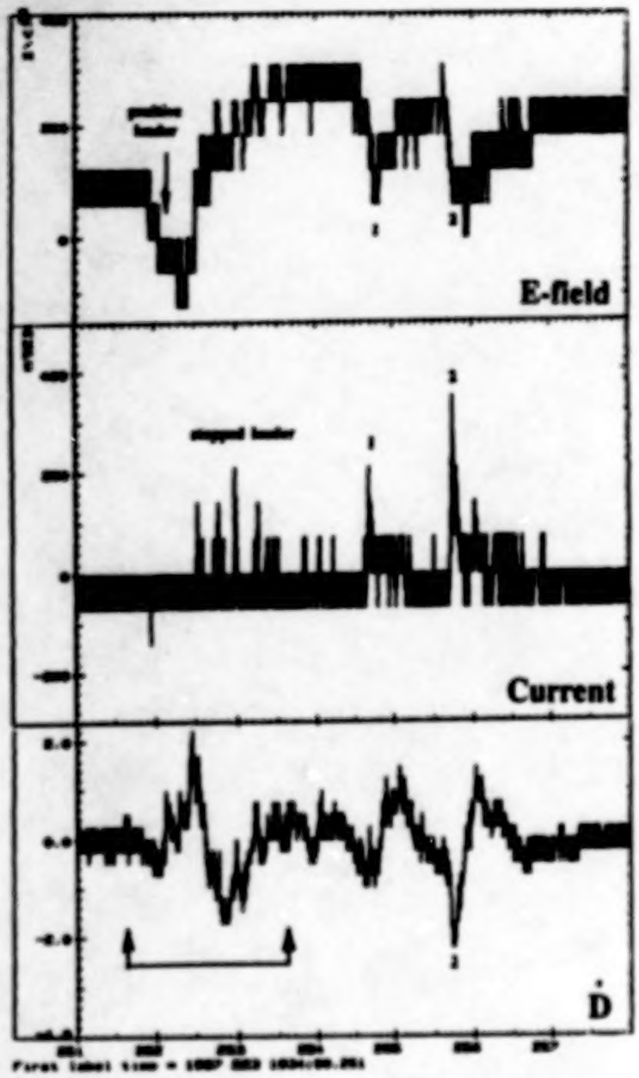

Figure 12. New initiation process of a secondary discharge. Notice features typical of a positive leader and a stepped leader. This initiation process is followed by recoil streamers, marked 1 and 2.

Effects of Lightning", Society of Automotive Engineers Committee Rept. AE4L-87-3, Feb. 1987.

10. Uman, M., The Lightning Discharge, Academic Press, Inc., New York, 1987.
11. Jordan, D.M., and Uman, M.A., Variation in light intensity with height and time from subsequent lightning return strokes, J. Geophys. Res., 88, 6555-6562, 1983.
12. Kitagawa, N., and M. Brook, Comparison of intracloud and cloud-to-ground lightning discharges, J. Geophys. Res., 65, 1189-1201, 1960.

CURRENT WAVE-FORM OBSERVED DURING LIGHTNING STRIKES ON AIRCRAFT

J.L. Boulay

OFFICE NATIONAL D'ETUDES ET DE RECHERCHES AEROSPATIALES
B.P. 72 - 92322 CHATILLON CEDEX - FRANCE

1. INTRODUCTION

Since 1980, several experimental programmes have been carried out to study lightning strikes on aircraft ; the first was the NASA programme, which began in 1980 on an F106 type aircraft. This programme continued through to 1986 [1]. A second program was initiated in the United States in 1985, by the Air Force. This programme was carried out on a Convair CV580 aircraft, and several test campaigns were run between 1985 and 1987 [2]. A third programme was initiated in France, in 1981, using a Transall 04 type aircraft. Three major measurement campaigns were run, respectively in 1984, 1986 and 1988 [3] [4].

One fact that is already certain is that all these programmes yielded practically identical results. One of the most important points derived from a first analysis of the data is that we have now accepted the fact that it is the aircraft itself that initiates the process of the lightning strike. We also know that a lightning strike on an aircraft occurs in several phases :

- a preparation phase
- an electric arc attachment phase
- a connection phase, and
- a re-light phase

The important thing to note is that for both the attachment phase and the re-light phase, the pulse rating has now been demonstrated in measurements of both current and magnetic field, and the pulses obtained have very high peak values, and most of all extremely short rise times. These pulses are quite obviously responsible for the disturbances in on-board electronic systems.

Whether the objective is to assess these electromagnetic disturbances in the equipment, or to define aircraft qualification type test standards with a view to preventing these disturbances, it is important that we obtain a perfect knowledge of the essential characteristics of these pulses. This global knowledge will therefore be the result of a complete theoretical model of all the physical processes involved in a lightning strike on an aircraft.

Before obtaining this complete model, the present task consists in providing a preliminary validation of a certain number of mechanisms that

30

can be associated with various phases encountered during in-flight lightning strikes.

This validation can be obtained in several ways :

- By repeating the experiments on aircraft using instruments adapted to each of the phases being examined. It is quite clear that these aircraft programmes are costly, and are very often difficult to implement.
- By using the surface discharge technique. This enables several of the discharge phases found on aircraft to be demonstrated, such as the leader phase, the recoil streamer phase, and even the return-stroke phase. [5] [6]
- There is also the technique of studying long arcs under laboratory conditions, using pulse generators with a sufficiently high voltage rating. [7]
- And there is also the possibility of using techniques to artificially trigger lightning strikes, by launching rockets towing conductive wires. [8]
- Finally, the study of natural lightning strikes, using appropriate examination facilities such as the VHF electromagnetic interferometer, provides valuable information on the mechanisms associated with the different phases of discharges. [9]

In this document, we will confine our analysis to the study of the readings obtained during the attachment phase, and to the experiments carried out in order to validate the scenarios that we are currently able to grasp, with the objective of explaining this attachment phase. Finally, we will very briefly review the experiments that are currently being carried out in an attempt to understand the re-light phase.

2. EXAMINATION OF IN-FLIGHT DATA

As an example, Figure 1 shows a dual recording of an electric field and a magnetic field observed during a lightning strike obtained on the Transall aircraft. This typical recording enables us to show up the different phases of the process. To begin with, there is a preliminary phase that is not shown on this figure, and which corresponds to the lightning strike preparation phase.
This preliminary phase shows the action of a high external field, generating corona currents on the structure of the aircraft. The global balance of these corona currents causes an increase in the global charge of the aircraft, and therefore an increase in its potential with respect to infinity ; it concentrates electric field lines at particular points of the aircraft.
During this preliminary preparation phase, no noticeable current can be detected since the order of magnitude of the corona currents does not exceed one milliampere. Furthermore, the electric field variations are much too slow to be detectable by the E-sensors located on the skin of the aircraft.
The lightning strike process therefore begins with an attachment phase, and the example given in Figure 1 shows the typical electric field E1 signature

obtained. This signature is repeated on all lightning strikes observed with the Transall aircraft and with the US Air Force's CV580 aircraft.
This attachment phase is followed by a continuous phase (or connection phase), during which a permanent current can pass through the structure of the aircraft. The value of this permanent current can be in the region of a few hundred amps.
During this DC phase, we can also see intermittent superimposed "re-light" phases in which pulses occur at intervals which are very often in the region of 10 milliseconds. Generally speaking, and considering the results obtained on the Transall aircraft, there are two or three re-light zones.

2.1 ATTACHMENT PHASE

Figure 2 shows the discharge current readings during this attachment phase, corresponding to the three types of aircraft fitted with instruments. The upper curve corresponds to a series of current pulses measured on the front probe of the NASA F106 aircraft. A pulse repetition phenomenon can be clearly seen, as well as the emergence of a continuous current component from the fourth pulse onwards. Exactly the same phenomenon can be observed on the intermediate curve corresponding to the US Air Force CV580 aircraft. Thus, after a phase during which the current is practically null, the first restricted-value pulses clearly begin to appear ; a permanent current is added after the fourth pulse, and reaches a peak value of 1500 amperes in this particular case. The example also shows a relatively constant period between pulses.
The lower curve shows the pulses observed during two simultaneous readings obtained on the front and rear probes of the Transall aircraft, during the experiment carried out in 1988. The curves show that these pulses are strictly synchronous for both pairs of readings and, just as for the two previous examples, we can distinguish two phases in this pulse process : phase 1, during which there is a first set of pulses with a limited peak value, followed by phase 2 which starts with a permanent current, over which the repeated pulses are still superimposed.
For all three types of aircraft, there are periods of repetition between pulses that can last between 100 and 300 microseconds. It should be recalled that the total duration of the attachment phase is approximately 10 milliseconds.

Typically, an isolated pulse can reach a peak value of several thousand amps with very variable rise times, which can be anything between a few tens of nanoseconds and a few microseconds. The electromagnetic interference created by these pulses will therefore be particularly dependent on this rise time.

2.2 RE-LIGHT PHASE

We have already seen that during the "connection" phase when a permanent current is flowing through the structure, there are periods during which there is a very high pulse activity corresponding to the re-lighting of the discharge channels on the aircraft.

As an example, Figure 3 shows two curves which indicate, for the same period, variations of the electric field E observed in two separate points of the structure ; these variations can be as high as 10^5 volts/metre. We also now know that these pulses can have two typical characteristics ; one corresponds to the pulse marked A in Figure 3, which is a permanent step in the electric field, followed by type B pulses shown on the same figure, which correspond to a bipolar electric field pulse.

The high speed photographic recordings obtained with the wing video camera enabled us to associate each of these electromagnetic field current pulses with a violent re-lighting of the lightning channel. An example of this re-lighting is shown in Figure 4, where we see a very important increase in the illumination of the channel around the cockpit of the aircraft, corresponding to one of the electric field pulses shown in the upper diagram (note that the second channel of the discharge cannot be seen on the camera recording, due to the fact that the corresponding electric arc was located on the other wing of the aircraft, outside the camera's field of view). This high speed camera has also made it possible to show that the re-lighting also coincides with the sweeping of the electrical arc over the structure of the aircraft.

When the discharge current readings are appropriate (lightning channels connected to the measurement probes), it is possible to associate current waveforms such as those shown in Figure 5. This pulse was recorded on the NASA F106 aircraft, and shows both a very high peak current value (24 000 amperes), and an extremely short rise time (about one hundred nanoseconds), thus producing resonance excitation of the aircraft structure. It should also be noted that the duration of the pulse is in the region of a few microseconds. It should be recalled that when a train of pulses is observed on an aircraft, the mean period between these pulses is approximately 10 milliseconds. We will now describe, in the following paragraph, the physical model which enables us to explain, or at least begin to explain, the physical mechanisms involved in the process.

3. MODELS CURRENTLY BEING ANALYSED

In the current state of the interpretation of the readings obtained on aircraft, we can examine all of the mechanisms that could, at least at a primary level, explain these readings. To visualise this phenomenology, refer to the functional diagrams in Figure 6.

3.1. LIGHTNING PREPARATION PHASE

As mentioned in the previous paragraph, this lightning preparation phase consists in accepting that the aircraft initially has a null potential and a null global charge, and moves into an atmospheric configuration in which there is a high electric field E_0. We know that when the aircraft is inside this electric field E_0, and due to its geometry, it will provide amplification for the field in such a way that corona discharges will appear in different areas of the aircraft, with either a positive or a negative polarity depending on the orientation of the aircraft with respect to the electric field.

The differential current between positive and negative corona will therefore increase the potential V_S of the aircraft in proportion to its basic capacitance ; this will consequently increase the corresponding field E_S. This preparation period can last between a few seconds and a few tens of seconds.
The actual lightning initiation threshold will correspond to the beginning of a strong discharge, when a positive electric field E_S appears in a given point of the structure. It should be recalled that during this phase, the currents exchanged on the aircraft are too small to have been detected by the measurement equipment normally used on the aircraft. We furthermore now know, after creating models of these lightning preparation phenomena, that the critical external initiation field is in the region of 40 to 50,000 volts/metre.

3.2. ATTACHMENT PHASE [10] [11]

The initiation of this attachment phase is clearly understood through an observation of the variation of the electric field in points of the structure. From a starting point A, a slow evolution of the electric field can be seen over a period of 3 to 4 milliseconds, shown by diagram AB in Figure 6.

We now know that this phase AB corresponds to the start of a streamer leader discharge (S+/L+), which starts from a preferential point on the line. During this phase, the discharge currents observed are still too small to be detected. When, at a particular point on the aircraft, the negative field exceeds a critical value, a negative streamer situation occurs.
This phase is marked BC on the third diagram in Figure 6. This phase BC corresponds to the first three or four pulses that are detectable by airborne measurement equipment. These first pulses are therefore apparently the result of the emergence of bursts of negative streamers. The final point to note is that this phase BC has a typical duration of around one millisecond.
When point C is reached, a continuous current appears on the measurement sensors and the repeated pulses are superimposed over it. In our opinion, this period, defined by CD on the fourth diagram of Figure 6, corresponds to the establishment of a self-propagating streamer leader system (L-/S-). Then, the two streamer leader systems (S+/L+ and S-/L-) continue to propagate in order to reach the zones in space where the respective positive and negative charges are sustained.

3.3. CONNECTION PHASE

At this time, we are in a situation where the aircraft is effectively connected to two charged regions by two conductors constituted by two electric arcs. A permanent current can therefore circulate between the two terminals of the "power supply", and pass through the structure of the aircraft. This connection phase can last several hundred milliseconds, with permanent currents that can reach several hundred amperes.

3.4. RE-LIGHT PHASE

We also know that "re-light" phases can occur during this connection phase, that very high current pulses are detected at this time, and that the intrinsic properties of the plasma corresponding to the two discharge channels will be very considerably modified. A theoretical approach of the mechanism associated to this re-light phase is proposed in a companion paper [11].

4. EXPERIMENTAL VALIDATION OF THE PULSE PHASES

In order to validate, or at least begin to validate, the mechanisms that have just been described, we have attempted a number of validation tests on these mechanisms. Several techniques were used for this purpose :

- long arc tests in a laboratory environment,
- triggered lightning tests at an altitude,
- observation of natural lightning strikes, using an electromagnetic interferometer.

In parallel with these experimental operations, we have approached the creation of theoretical models : both two-directional leader phases and re-light phase are currently being studied.

4.1. LABORATORY VALIDATION OF TWO-DIRECTIONAL PROPAGATION [7]

This validation was carried out in cooperation with EDF, in the Renardières High Voltage Laboratory. The principle of the experimentation is defined by the diagram in Figure 7. A high voltage pulse generator, with a peak value of 5 megavolts, was used to create a very high voltage pulsating electric field across an interval of approximately 15 metres. A cylindrical object, with a length of approximately 4 metres, was placed between the polarised electrode and the ground. The object was maintained in a floating position, like the aircraft in flight. In order to obtain the most homogeneous electric field possible, the 5 megavolt electrode was a metal plate of about 20 metres in width. In addition to the electric field and current readings taken on the high voltage electrode itself, the experiment mainly consisted in following the propagations with an image converter camera used in streak mode.

August 1989 saw the first propagation of a two-directional discharge under laboratory conditions. This discharge is shown in the photograph in Figure 7. It clearly shows, on the upper part of the cylinder, the propagation of a positive leader with the emergence of a positive streamer at its end, corresponding to the continuous white light that can be seen.

At the bottom of the cylinder, we can clearly see the opposite L-/S- system in which the characteristic light of the negative streamer appears in a pulsating manner, which is a good representation of the stepped characteristic of the negative discharge. The positive and negative system continued to propagate in this way for several hundred microseconds ; there were typical periods of about 20 microseconds between the different re-lights of the L-/S- system, and a complete re-light appeared in the air gap of the experiment when the positive streamer system reached the high voltage electrode.

4.2 VALIDATION BY MEANS OF LIGHTNING STRIKES TRIGGERED IN ALTITUDE [8]

Triggered lightning experiments have been in progress for several years, in cooperation with the NASA Kennedy Space Center. The principle of these experiments consists in launching a small rocket towing an electric wire.
In order to attempt to trigger a lightning strike comparable to those which occur on aircraft, the experimental principle has been modified by using a rocket with a conductor wire which is not connected to the ground. The principle consists in releasing, at an altitude and in an environment where the atmospheric electric field is considerable, a conductive body consisting of an conductive wire several hundred metres long ; if the electric field conditions are sufficiently strong, a lightning strike can be initiated.
As an example, Figure 8 shows the static image of a first bi-leader type discharge initiated in altitude. This static photograph, taken by the University of New York, corresponds to the triggering obtained with a 450 metre conductor, with its highest point at 650 metres. This photograph clearly shows the streamer leader system starting at the top of the rocket and propagating towards the clouds, and the S-/L- conductor coming out of the bottom of the rocket and connecting itself to the ground.

This is the first event obtained under these conditions, thus making it possible to validate a scenario showing the start of a lightning strike by emergence of a dual positive and negative propagation.

4.3. VALIDATION OF THE TWO-DIRECTIONAL LEADER SYSTEM BY STUDYING NATURAL LIGHTNING [12]

In view of the results recorded on aircraft, we took greater interest in the results of the readings taken several years ago using a VHF interferometer. The system used has a detection capacity of approximately 10 microseconds, and provides spatial localisation data with a precision of approximately one hundred metres. This instrument enabled us to follow the evolution of all inter-cloud discharges as a function of time. [9] [illegible]

Figure 9 is an example of the recordings obtained using [illegible] VHF interferometer. The first figure shows the ground projection [illegible] the localisation points. The results clearly show two main phases :

- A first phase, with a duration of approximately 100 mil[illegible]nds, corresponds to a mean localisation propagation with speeds of be[illegible] 10^5 and 10^6 metres/second, the mean emission level being around [illegible] pulse every 10 microseconds.
- Next we observe a second phase, a few hundred milliseconds after the first, and which also lasts approximately 100 milliseconds. Very high speed propagations then appear, the mean velocities being in the region of $2x10^7$ metres/second, the mean duration of each of these propagations being approximately one pulse per microsecond.

The particularity of this second phase is that all the propagations recorded by the interferometer follow trajectories which appear to converge on the same point in space, this point itself being the point of initiation of the propagation corresponding to the first phase.
We can therefore demonstrate, as shown in the first diagram of Figure 10, the initiation of an inter-cloud lightning strike through the establishment of a two-directional process consisting of a negative and a positive propagation. It is now clear that the work we have put into the definition of models has enabled us to carry out this validation, that only the negative propagation phase of the discharge is observable by interferometry, and that positive type discharges (which pulsate far less than negative discharges) cannot be detected by the equipment. The process nevertheless consists of the propagation of two systems starting from the same region of space and extending on either side of the region with dual polarity propagations.

4.4. VALIDATION OF THE RECOIL-STREAMER PHASE

We do not, as yet, have even a preliminary validation to provide a correct interpretation of the recoil-streamer phase. However, in view of the results obtained by electromagnetic interferometry, and particularly if we refer to the results given in Figure 9 above, a basic idea of the behaviour of recoil-streamers can be examined.
We have therefore shown the establishment of a two-directional discharge with a positive and negative polarity. We know that this phase is followed by a second phase, in which propagations appear with a tendency to converge towards the same single region of space. Therefore, using the two-directional discharge diagram as a basis, it is possible to reconstitute the trajectories of the initial positive discharge by attempting to superimpose the trajectories corresponding to the re-light phases.
It can therefore be clearly seen, as shown by the readings obtained on aircraft, that a connection phase can, from time to time, be disturbed by a re-light phase corresponding to very high speed propagations using the initial channels created by the positive discharges, enabling currents and therefore electrical charges to travel from a negatively charged zone in space towards the initial point of convergence.

5. CONCLUSION

The different programmes for measuring lightning strikes on aircraft in flight have shown a very high level of similarity between the readings obtained, and have also defined two major pulse zones or phases.
There is a very great need to achieve a model representation that is as complete as possible, showing these different pulse phases, in order to be able to correctly interpret the peak values of the pulses involved, as well as their rise times and their mean repetition period. It is necessary for these intrinsic parameters to be related to influencing parameters such as, for example, the ambient electric field, the configuration of the aircraft (and therefore its capacitance), etc.

This work should lead to the creation of a simulation model that is as complete as possible, enabling any type or shape of aircraft to be studied in the future.

We have been able to show that these different events, or these different phases in a lightning strike, can be simulated and therefore validated by means of experiments that are more easily accessible than in-flight experiments. To do this, we have carried out laboratory studies on surface discharges, and we have validated the principle of the two-directional discharge in two ways: firstly by producing long arcs under laboratory conditions, using very high voltage generators, and secondly by using the altitude triggered lightning technique.

We now know that these two pulse phases must be correctly simulated for qualification tests on aircraft equipment.

This problem is currently being discussed. A large amount of work remains to be done in the future, and it is particularly necessary to continue with:

- the altitude triggering experiments, in order to completely validate the bi-leader model,
- work on recoil-streamers, by using surface discharges (or other techniques),
- work on the observation of inter-cloud discharges, using electromagnetic interferometry facilities,
- and finally, it will be necessary to converge all of these experimental data into a complete theoretical model capable of completely simulating the in-flight lightning strike phenomenon.

REFERENCES

[1] F.L. Pitts et al. - F106 data summary and model results relative to threat criteria and protection design analysis - 11th ICOLSE, Dayton, June 1986.

[2] P.L. Rustan and J.P. Moreau - Aircraft lightning attachment at low altitudes - 10th ICOLSE, Paris, June 1985.

[3] J.P. Moreau and J.C. Alliot - E and H field measurements on the Transall C160 aircraft during lightning flashes - 10th ICOLSE, Paris, June 1985.

[4] J.L. Boulay et al. - Analysis of recent in flight lightning measurements on different aircraft, ICOLSE 88, Oklahoma city 19, 21 Avril 1988.

[5] S. Larigaldie - "The spark propagation mechanism in ambient air at the surface of a charged dielectric: I - Experimental: the main stages of the discharge" - J. Appl. Phys., 61, 90, 1987a.

[6] J.L. Boulay, S. Larigaldie - Application of surface electrical discharges to the study of lightning strikes on aircraft. at this conference

[7] B. Hutzler, I. Taudière - Attachment process of lightning on aircraft in the light of laboratory simulations. ICOLSE 89, bath, 26-28 september 1989.

[8] P. Laroche, A. Eybert-Berard, L. Barret and J.P. Berlandis, "Observations of preliminary discharges initiating flashes triggered by the rocket and wire technique", 8th Int. Conf. on Atmospheric Electricity. Uppsala, june 1988.

[9] P. Richard, A. Delannoy, G. Labaune, and P. Laroche: "Results of spatial and temporal characterisation of the VHF-UHF radiation of lightning", J. Geophys, Res., Vol. 91, No. D1, January 20 (1986).

[10] V. Mazur, "A physical model of lightning initiation on aircraft in thunderstorms", J.G.R., Vol. 94, n°D3, March 1989.

[11] J.P. Moreau, S. Larigaldie - at this conference.

[12] A. Bondiou, P. Richard, I. Taudière, F. Helloco: "Preliminary correlation between 3-dimensional lightning discharge mapping and radar measurements", International Conference on lightning and static electricity, Day electricity, Dayton, USA, June 24-26, 1986, ONERA - Reprint No. 1986-161.

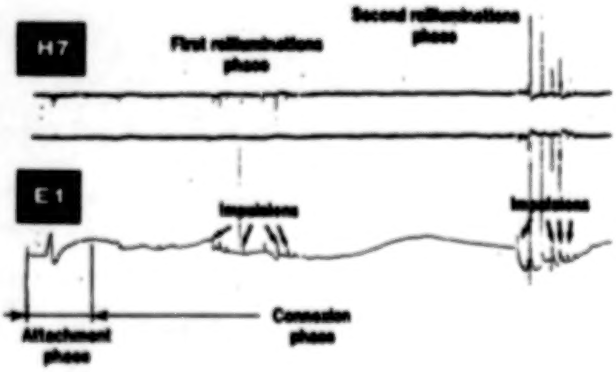

Figure 1
Different phases of the lightning event.

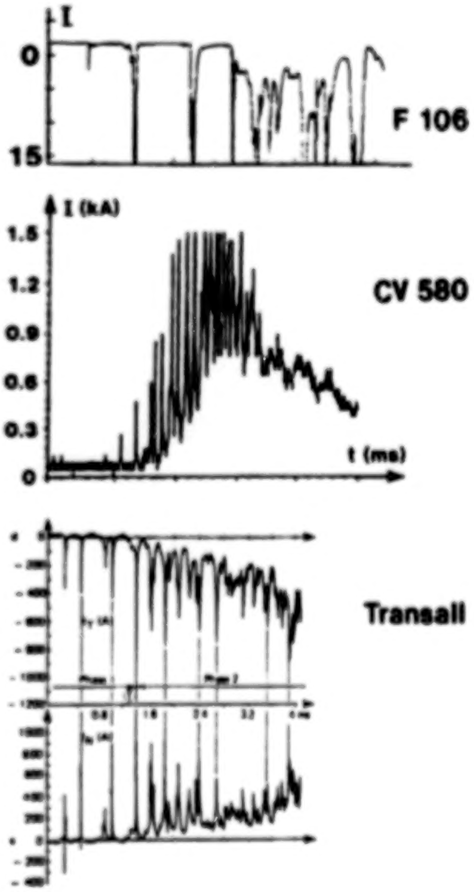

Figure 2
Attachment phase.

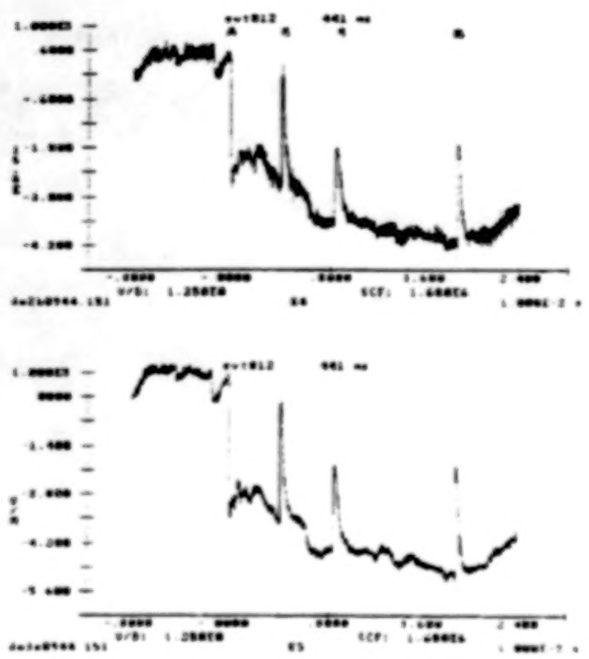

Figure 3
E field measurements associated to recoil-streamers.

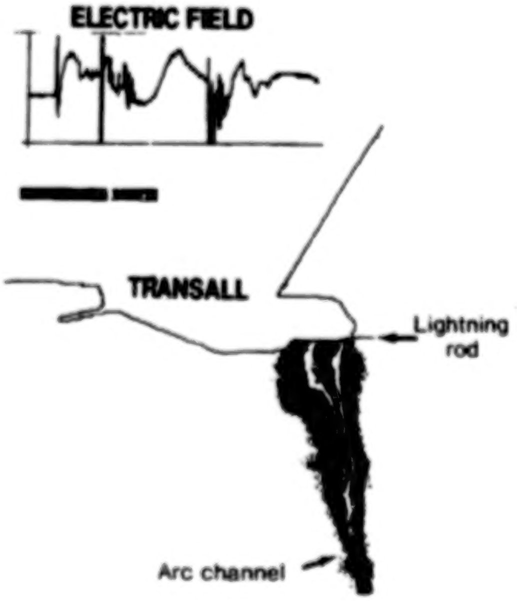
ELECTRIC FIELD
TRANSALL
Lightning rod
Arc channel

Figure 4
Re-light phase on the Transall aircraft.

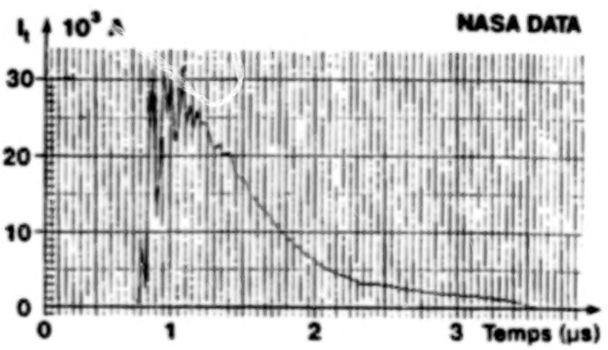

Figure 5
Current pulse associated to channel re-light on the aircraft.

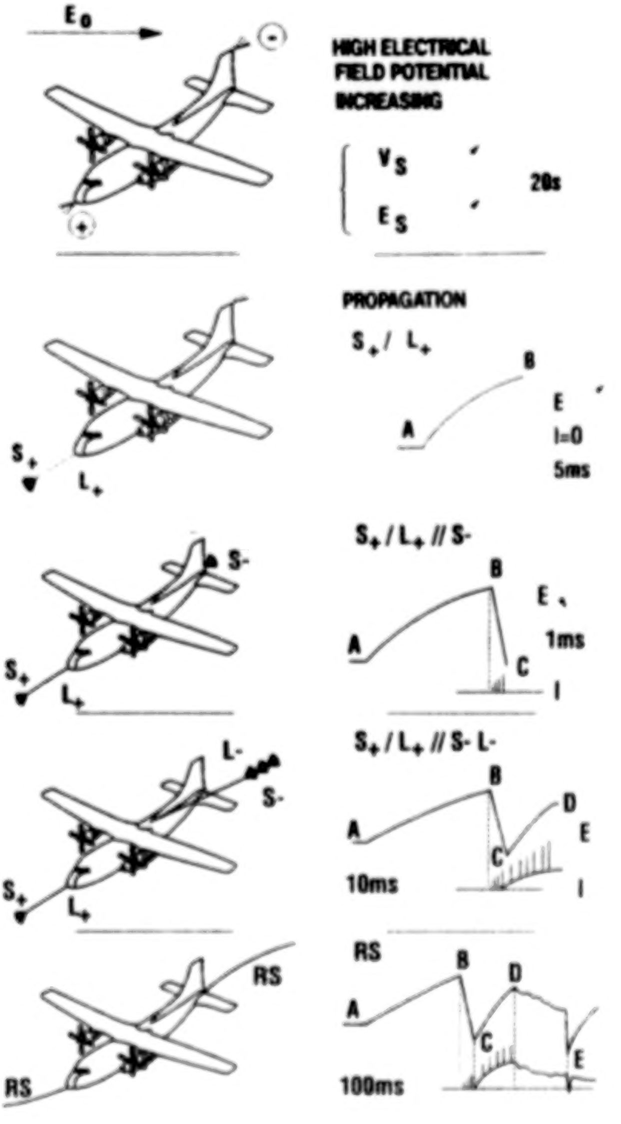
E0
HIGH ELECTRICAL FIELD POTENTIAL INCREASING
VS
ES
20s
PROPAGATION
S+ / L+
A
B
E
I=0
5ms
S+
L+
S+ / L+ // S-
S-
A
B
C
E
1ms
I
S+ / L+ // S- L-
L-
S-
A
B
C
D
E
10ms
I
RS
A
B
C
D
E
100ms

Figure 6
Lightning phenomenology on aircraft.
Attachment phase.

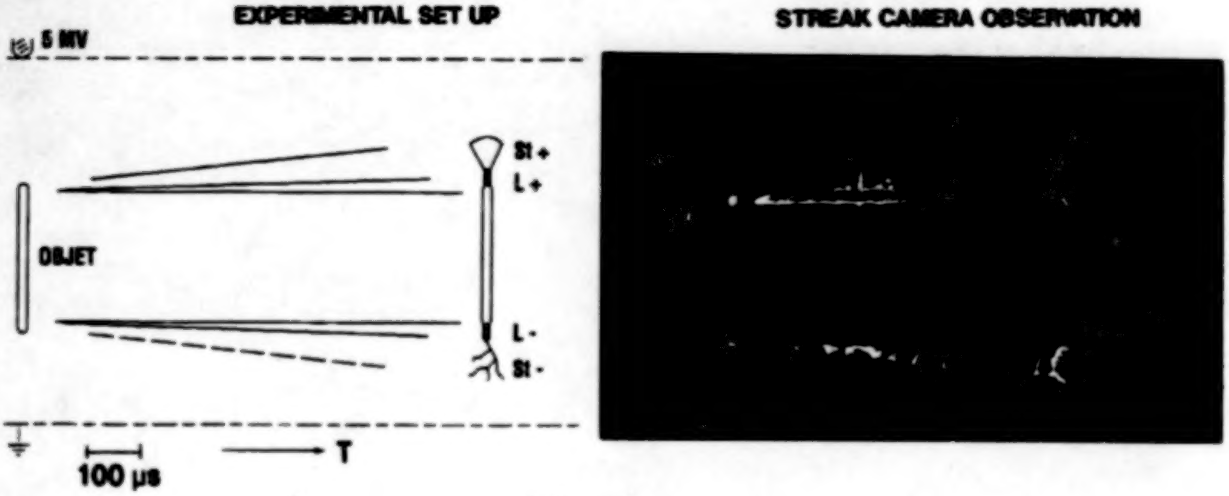

Figure 7
Bidirectionnal leader in laboratory.

Figure 9 →
Intracloud lightning discharge observed by VHF interferometry.

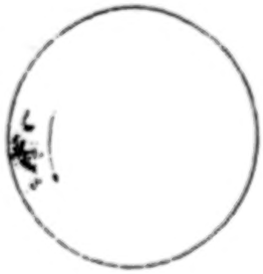

PRE-BREAKDOWN AND LEADER PHASE

= The 300 MHz interferometer only detects the negative stepped leader phase.
(cf.laboratory studies)

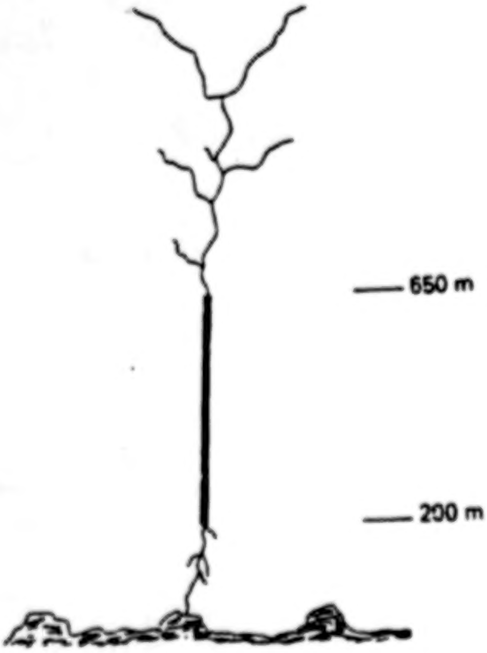

Figure 8
Flash triggered in altitude.
Video picture from SUNYA.

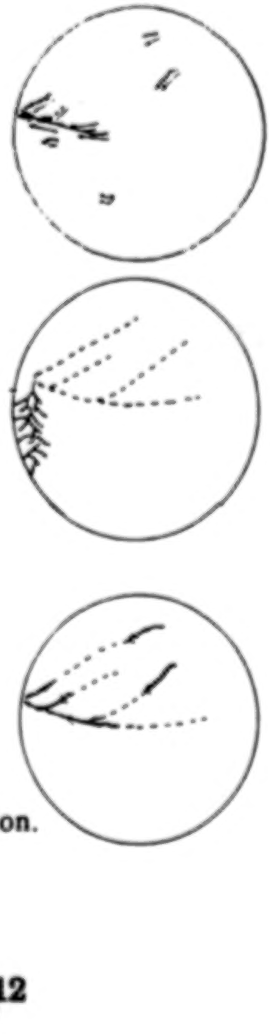

RECOIL STREAMERS PHASE

= Propagations along the positive leader channels.
(back from the leader tip)

1ST PHASE

duration :several 100 ms
emission rate:1 pulse/ 10 µs
velocities ranging from 10^5 m/s to several 10^8 m/s (in the most filamentary parts)

2ND PHASE

duration :several 100ms
velocities~2.10^7 m/s
time interval between 2 propagations: 10 ms
several propagations in the same channel.
emission rate :1 pulse/ µs

Figure 10
VHF measurements interpretation.

Session 2B, Tuesday 10:15
Aerospace Vehicles
Structures and Materials 1
Perala, Chairman

LIGHTNING CURRENT RATE OF RISE IN THE NEW LIGHTNING FLASH MODEL FOR THE SPACE SHUTTLE PROGRAM

Nathaniel G. Bankston
Space Systems Division of Rockwell International
Downey, California

ABSTRACT

In this paper the recently baselined Space Shuttle lightning effects flash model is discussed. The discussion is limited to the current rate(s) of rise. A review of some of the recent data is presented, as well as a discussion of how interaction processes affect the induced voltages and currents which arise from a lightning strike. It is concluded that the multiple pulse components of the new flash model present a more severe threat to complex avionic systems, than is presented by a single pulse having an extremely fast rate of rise.

INTRODUCTION

On July 26, 1990 the National Aeronautics and Space Administration (NASA) baselined a new lighting requirements document [1] for the Space Shuttle Program. This represented the culmination of two and one-half years of effort. The new requirements document contains waveforms which represent the lightning environment and waveforms which can be used for test and analysis. The document also discusses the relationship between the swept strokes which occur during a lightning flash, and the zoning of vehicle surfaces to define the applicable threat parameters. Other topics included are definitions of equipment safety margins, and guidelines to achieve adequate lightning protection through the use of shields, grounds, and bonds.

This paper illustrates the process which was used to recommend that the NASA should baseline these requirements. The lightning stroke parameter which has been chosen to illustrate this process is the current rate of rise.

The use of the current rate of rise should not be taken as an assertion that this is the most important parameter of a lightning flash for engineering applications. In fact, Cianos and Pierce [2] stated that the peak current and charge transferred during a lightning flash are the two most important parameters to be considered in engineering applications.

The current rate of rise has been selected for two reasons: a) recent research has demonstrated that the current rate of rise may be faster than older (pre 1970) data indicates, and b) it is one of the parameters of a lightning flash which directly determines the indirect effects to aerospace systems operation. These indirect effects are especially important for computer controlled avionics

43

systems where even temporary malfunction may cause loss of life or vehicle, or both.

The new criteria are based on three factors which Clifford [3] stated should be considered whenever an engineering flash model is designed: a) the best understanding of the natural lightning environment as it impacts the operation of systems, b) the physics of the interaction of the natural environment with aerospace systems, and c) the ability to use the criteria for test and analysis.

THE CURRENT RATE OF RISE

The current rate of rise data which was reviewed was taken from four principal areas of lightning research: a) natural cloud-to-ground flashes measured using instrumented towers, b) in-flight triggered and intra-cloud flashes measured using instrumented aircraft, c) triggered flashes using small rockets, d) simultaneous two station measurements of the electromagnetic fields radiated by natural cloud-to-ground flashes.

It is not the purpose of this paper to critically review all of these areas. The data is discussed for the purpose of illustrating the extent of the effort that was conducted prior to recommending the new requirements document to the NASA. All parameters of a lightning flash having an engineering application were subjected to this type of review.

a. CLOUD-TO-GROUND TOWER DATA

One of the more extensive data bases is that of Berger, et al [4] obtained with instrumented towers located on mountain tops in Switzerland. Table I gives the front duration and maximum current rate of rise as compiled from this data. The current rate of rise is greater for subsequent strokes than first return strokes: 120 kA/usec to 32 kA/usec, respectively. Berger's data has been criticized as being biased toward positive flashes which increase with height, and by the mechanisms associated with the propagation of upward streamers from tall structures which could increase the front time, and consequently result in lower derived values of the current rate of rise.

Table II shows similar instrumented tower data recorded by Garbagnati [5]. His data also shows that subsequent strokes have faster current rates of rise and much shorter front times than first return strokes.

None of Garbagnati's plotted data for the maximum current rate of rise in subsequent strokes extended beyond about 110 kA/usec. This is in complete agreement with Berger's results. Garbagnati's data can be criticized for all of the same reasons as given in the criticism of Berger's results.

Eriksson using an instrumented tower on relatively flat terrain in South Africa reported a measured current rate of rise of 180 kA/usec [6]. For natural cloud-to-ground flashes, this is one of the fastest rates ever recorded. Subsequently, Anderson and Eriksson [7] published new results based on Berger's original data. Using this data, they published a revised concept of the front waveshapes of both first and subsequent strokes. Figure 1. shows their analysis of the front shape of a lightning stroke. Their analysis shows two slopes are present: 1) an initial slowly rising rate of change labeled TAN 10, and 2) near the current peak a fast rising rate of change labeled TANG.

Table III presents a summary of their results. Note that the current rate of rise value exceeded by 5% of the subsequent strokes is shown as 161.5 kA/usec. This should be compared to the 120 kA/usec value for the same 5% level as previously indicated in both the Berger and Garbagnati data.

b. IN-FLIGHT TRIGGERED DATA

Table IV is a summary of the peak rates of rise recorded by the NASA F106 in flight lightning study [8]. The flashes encountered are most likely due to intra-cloud discharges and triggered flashes initiated by the F-106. The values shown in the table are the fastest recorded rates of rise for a given flight. The fastest rate of rise recorded was 380 kA/usec. None of the peak rates of rise were time tagged in a particular lightning flash, so no attempt was made to locate where in a particular flash the peak rate occurred. Some of these peak rates could possibly be the result of leader attachment processes. The groups of burst pulses observed in many of the recorded waveforms was interpreted as additional evidence that lightning flashes presented multiple pulse threats to aircraft. Many of these pulses have faster current rates of rise than any of the previously reported cloud-to-ground data.

c. ROCKET TRIGGERED FLASHES

The Rocket Triggered Lightning Program (RTLP) is a joint research program (U.S. and French) that has been the source of some of the most recent data on lightning current rates of rise. Table V is a summary of the results for the years 1985, 1986, and 1987. The 1985 and 1987 data was obtained in Florida at the NASA Kennedy Space Center. One 1987 multiple stroke flash is of particular interest as it had a recorded rate of rise of 411 kA/usec during the ninth stroke. Data for this flash, No. 8717B, is shown in Table VI.

Unlike the two slope front waveshapes of cloud-to-ground flashes shown by Anderson and Eriksson, the RTLP waveshapes do not show evidence of a slow ramp portion during the front time.

The RTLP flash data does not show any of the classical characteristics of a first return stroke followed by one or more subsequent strokes [5], but the data does indicate that very fast current rates of rise do occur when a lightning flash is initiated.

d) TWO STATION FIELD DATA

For many years Uman, Krider, Lin, McLain, et al [5], [9], have measured the radiated fields from lightning flashes and analytically derived from this data the shape of lightning current pulses. From this type of data, Krider and Uman derived a current rate of rise of 360 kA/usec. Figure 2 shows a model of the field front waveshape as derived from the measured field data. The front shape, like the Anderson and Eriksson analysis, shows two slopes, with the faster slope occurring near the crest value. It is from this type of data that Krider, et al, have asserted the existence of sub-microsecond rise times in the field front times [10]. By inference, these sub-microsecond rise times may also be present in the current rise time.

THE INTERACTION PROCESS

As noted above in the statements made by Clifford, equal importance must be given to the interaction that takes place when a lightning strike occurs to an aerospace vehicle. The NASA model as baselined is an interaction or effects model. The various components of the model have been synthesized to produce effects within an aerospace vehicle at the avionics box level which are representative of the effects of natural and triggered lightning. The effects that are most closely associated with the current rate of rise are the induced voltages and currents which appear on the internal wires and cables.

These induced voltages and currents cannot be considered apart from understanding how they are the result of interaction processes which occur externally and internally.

The interaction is best described as a three part process: a) the first involves the appearance of surface currents and charges on the external surface of the aircraft which gives rise to normally directed electric fields and tangentially directed magnetic fields, b) the second is the penetration and diffusion of these fields through apertures and the aircraft skin, c) the third is the internal propagation on cables, metallic fluid lines, and the conductors inside cables of currents and voltages induced by the penetration and diffusion of the lightning induced fields [11].

The whole interaction process is subject to non-linear perturbations as a result of external processes like corona and streamering. Non-linearities can also arise from internal processes like arcing and sparking. Ultimately, it is this complex interaction between the vehicle and the lightning currents and voltages that determine the magnitude of the induced currents and voltages. The values of the parameters that are given in any flash model are important, but only to the extent to which they have been

%

constructed with some understanding of the role played by the interaction process.

The effects due to rise time have been shown to be dependent on the duration of the rise time [12]: a) for rise times greater than 5 usec, vehicle responses can generally be analyzed using simple lumped parameter circuit theory, without the need to use transmission line theory, b) for rise times between 1 and 5 usec, the responses can be obtained by treating the vehicle as a transmission line having a single surge impedance. This allows the use of simple equations for reflection and transmission coefficients of current and voltage to be used to compute values of voltage and current [13], c) for rise times less than 1 usec but approaching 0.5 usec, the vehicle appears as a set of connected transmission lines having different surge impedances. This results in multiple reflections and refractions at each interface. It has been postulated that pulses with rise times near 0.1 usec would not be capable of traversing the length of an aircraft without being greatly attenuated as a result of these multiple reflections and refractions. It is known that transmission lines tend to act as low pass filters and fast rising pulses are attenuated along the length of the line. The rate of rise of a lightning stroke current pulse is greatly affected by these differing surge impedances, as well as being reduced by the delays which result from penetration and diffusion effects [13].

The skin effect at the surface of the vehicle also acts to prevent high frequency components of the lightning current from instantaneously appearing on the inner surface of the skin. Travelling wave reflections and refractions may well superimpose some fast early time oscillatory voltages and currents on the lightning induced voltages and currents. If these early time oscillations occur, the rate of rise of these oscillations usually exceeds the rate of rise of the stimulus pulse. So even if the worse case rate of rise which has been measured is not made a part of a flash model, the real effect of any rate of rise is to be increased when oscillatory currents are excited by the model pulse.

The recent data which has been reviewed also shows that the fast current pulses are also narrow. Being narrow, they may induce a large inductive voltage spike, but they cannot act as efficient energy couplers. The hardware of an aircraft (wires, cable bundles, etc.) is not an efficient energy absorbing antenna. Any test or analysis performed with a specified current rate of rise must address the duration over which that rate of rise is applied. Experience has shown that application of a pulse at a fixed rate of rise for less than 0.5 usec does not result in sufficient coupling. A current pulse rising at 1000 kA/usec for only a few nanoseconds will result in less short circuit current than a pulse rising at 100 kA/usec which lasts for 0.5 to 1.0 usec.

Phenomena such as the skin effect, field penetration induced eddy currents (which are oppositely directed with respect to the stimulus current [13]), inductive and capacitive attenuation which

47

arises as a consequence of current and voltage pulses propagating through an airframe must be considered with respect to how they reshape any applied transient pulse. These considerations are present in the new baselined requirements document.

THE NEW BASELINED ENVIRONMENT MODEL

The environment model as baselined consists of several different waveforms. They should all be used in assessing lightning induced effects. It is the total criteria in application that provides the confidence that the Space Shuttle Vehicle (SSV) is sufficiently protected or requires some additional effort to provide adequate protection.

The model adopted is variously referred to as an effects model, a conducted current model, or an interaction model. This model has been adopted by both the Federal Aviation Administration [14] and the Department of Defense [15]. The waveforms are synthesized components of a severe cloud-to-ground flash, and one component which represents the short duration rapidly changing pulses of current associated with leader attachment and intra-cloud processes. The model components are described by practical mathematical waveshapes which can be used for analysis and test. The model is designed to simulate the effects of natural lightning. The waveforms are not intended to be replicas of any naturally occurring lightning pulses. The baselined model includes multiple stroke and multiple burst arrangements of lightning stroke current pulses. These repetitive pulses are intended to be used to evaluate the system upset potential of induced transients in avionic systems. This upset potential is known to depend on the multiplicity of induced pulses in addition to their rate of rise and amplitude.

SELECTED MODEL COMPONENTS

The model components which are representative of faster current rates of rise and that are used to make up the multiple pulse patterns are A, D, and H: (1) Component A has a peak amplitude of 200 kA and a rate-of-rise of 100 kA/usec at t=0.5 us. It has a peak rate of rise of 140 kA/usec at t=0+. The waveform is shown in Figure 3. (2) Component D has a peak amplitude of 100 kA and a rate-of-rise of 100 kA/usec at t=0.25 us. It has a peak rate of rise of 140 kA/usec at t=0+. The waveform is shown in Figure 3. (3) Component H has a peak current of 10 kA and a peak rate of rise of 200 ka/usec at t=0+. The waveform is shown in Figure 4. Component H represents a high rate of rise pulse whose amplitude and time duration are much less than those of a first return stroke. Such pulses have been found to occur randomly throughout a lightning flash, interspersed with the other current components. While not likely to cause physical damage to the SSV or any electronic components, the random and repetitive nature of these pulses may cause interference or upset to certain systems. The model components which are made up of multiple arrangements of components A, D, and H are the multiple burst and multiple stroke: (1) The multiple burst waveform comprises repetitive Component H waveforms in 24 sets of 20 pulses each, distributed over a period of up to two seconds, as shown in the multiple burst waveform in Figure 4.

(2) The multiple stroke flash is defined using as a basis the definitions of Component A (first return stroke) and D (restrike). The multiple stroke waveform is defined as an A current component followed by 23 restrikes having a peak amplitude of 50,000 amperes each (D/2), as shown in Figure 5.

The new requirements document also includes several indirect effects waveforms specifically tailored to represent the interaction effects known to result from a lightning strike to an aerospace vehicle. Two of these are discussed for illustrative purposes only. They are a damped sinusoid and a long duration current waveform.

The damped sinusoidal waveform is one of the responses to Component A. It will be the only response to very short duration pulses such as Component H. The waveform normally appears in the early time portion of a cable response. It may also appear later if sparking occurs in the airframe.

The long duration current waveform arises from diffusion coupling and may have slower rise times and longer durations than those of the external currents. This waveform is especially important in assessing induced effects in vehicles which use non-metallic materials.

CONCLUSION

As lightning data accumulates from a variety of sources, it is evident that current rates of rise have gone up. But for an effects model, the relevant question is still one of utility: is the model sufficient to uncover marginal situations and enable the user to reduce the probability of a lightning strike resulting in serious damage or loss.

The real objective in defining a flash model is to be able to use the model parameters in the assessment of lightning susceptibility/vulnerability, and as an aid in the design of protection schemes for critical flight equipment. To achieve these goals it is not necessary to use values for the parameters which describe a lightning flash that are the absolute worse case values which have been recorded. Some reasons for such a conclusion are:

1. Single instance worse case values are usually measured in worse case environments.
2. These worse case values are subject to some experimental errors.
3. No one single naturally occurring flash should be expected to reproduce all of the aspects of a severe engineering flash model.

4. Interaction processes will modify current pulses having very fast rates of rise.

The 200 kA/usec rate of rise of component H and the multiple pulse components of the baselined model are considered sufficient, when properly applied, to uncover any circuit problems which are the result of induced effects.

List of References

[1] "Lightning Protection Test and Analysis Requirements", National Aeronautics and Space Administration NSTS 07636 Rev. E, September 27, 1990

[2] N. Cianos and E. T. Pierce, "A Ground-Lightning Environment for Engineering Usage", Stanford Research Institute Technical Report, No. 1 Project 1834, August 1972

[3] Don W. Clifford, "Lightning Test Criteria for Aircraft Avionics Systems", AGARD Lecture Series No. 110, Atmospheric Electricity Aircraft Interaction

[4] K. Berger, R. B. Anderson, and H. Kroninger, "Parameters of Lightning Flashes", Electra, Vol. 80, pp 23-37, 1975

[5] M.A. Uman, "The Lightning Discharge," International Geophysics Series, Vol. 39, 1987

[6] A.J. Eriksson, "Lightning and Tall Structures", Transactions: The SA Institute of Electrical Engineers, August 1978

[7] R.B. Anderson, A.J. Eriksson, "A Summary of Lightning Parameters for Engineering Applications", International Conference on Large High Voltage Electric Systems 1980 Session, August 27-September 4

[8] F. L. Pitts, L. D. Lee, R. A. Perala, T. H. Rudolph, "New Methods and Results for Quantification of Lightning - Aircraft Electrodynamics", NASA Technical Paper 2737, June 1987

[9] M. A. Uman, E. P. Krider, "A Review of Natural Lightning: Experimental Data and Modeling", IEEE Transactions on Electromagnetic Compatibility, May 1982, Vol EMC-24, Number 2

[10] D.W. Clifford, E.P. Krider, M.A. Uman, "A Case for Submicrosecond Rise-Time Lightning Current Pulses for Use in Aircraft Induced-Coupling Studies" IEEE 1979 International Symposium on Electromagnetic Compatibility" San Diego, CA, October 9-11, 1979

[11] R.A. Perala, T. Rudolph, and F. Eriksen, "Electromagnetic Interaction of Lightning with aircraft, IEEE Transactions on Electromagnetic Compatibility," May 1982, Vol. EMC-24, No. 2

[12] K.E. Crouch, "Aircraft Lightning - Induced Voltage Test Technique Developments," NASA Contractor Report 170403, June 1983

[13] F.A. Fisher, J.A. Plumer, and R.A. Perala, "Aircraft Lightning Protection Handbook," DOT/FAA/CT-89/22, September 1989

[14] U.S. Depart of Transportation Federal Aviation Administration Advisory Circular AC No. 20-136, March 5, 1990

[15] Department of Defense MIL-STD-1795A, 20 June 1989

TABLE I

Selected Lightning Current Parameters

Number of events	Parameters	Unit	Percentage of cases exceeding tabulated value 95%	50%	5%
	Front duration (2 kA to peak)				
89	Negative first strokes	usec	1.8	5.5	18.0
118	Negative subsequent strokes	usec	0.22	1.1	4.5
19	Positive first strokes	usec	2.0	16	150
	Maximum *di/dt*				
92	Negative first strokes	kA/usec	5.5	12	32
122	Negative subsequent strokes	kA/usec	12	40	120
21	Positive first strokes	kA/usec	0.20	2.4	32

TABLE II

Current Parameters Reported by Garbagnati and Co-Workers in Italy for Discharges Lowering Negative Charge [a]

	First strokes	Subsequent strokes
Number of strokes	42	33
Peak value (kA)	33 (0.25)	18 (0.22)
Maximum rate of rise (kA/usec)	14 (0.36)	33 (0.39)
Time to crest (usec) (3 kA to peak)	9 (0.40)	1.1 (0.33)
Time to half-value (usec)	56 (0.32)	28 (0.50)
Impulse charge (C) (to end of impulse or 500 usec)	2.8 (0.35)	1.4 (0.31)

[a] The values given are geometric means; the standard deviations in parentheses are expressed in logarithmic units consistent with the existence of a log normal parent distribution.

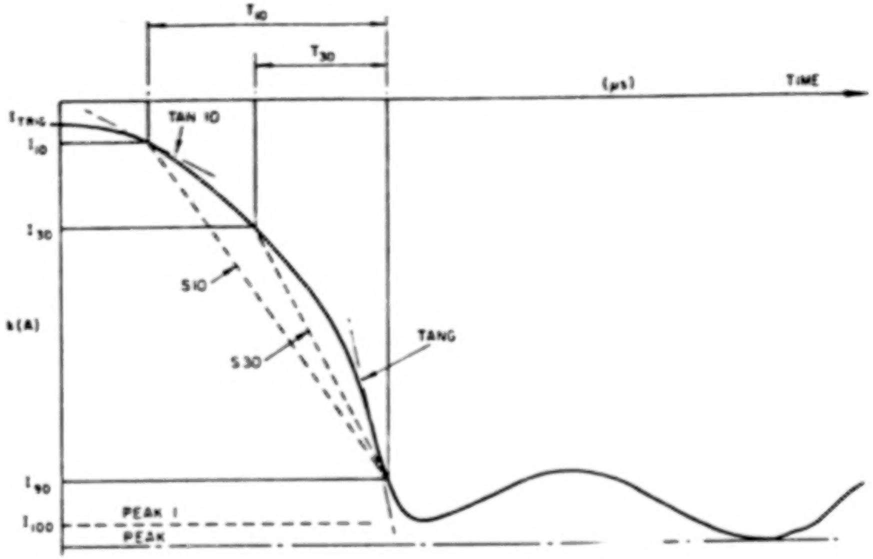

Figure 1 - Definition Of Impulse Front Parameters

TABLE III

Summary of Front Shape Parameters Defined by Anderson and Eriksson

Parameter	*N*	Units	Approximations by log-normal distribution[a] Mean	SD	Percent of cases exceeding tabulated value 95%	50%	5%
First stroke							
TAN - 10	75	kA/us	2.6	0.40	0.6	2.6	11.8
S - 10	75	kA/us	5.0	0.28	1.7	5.0	14.1
TAN - G	75	kA/us	24.3	0.26	9.1	24.3	65.0
PEAK - 1	75	kA	27.7	0.20	12.9	27.7	59.5
PEAK	80	kA	31.1	0.21	14.1	31.1	68.5
Subsequent strokes							
TAN - 10	108	kA/us	18.9	0.61	1.9	18.9	187.4
S - 10	114	kA/us	15.4	0.41	3.3	15.4	72.0
TAN - G	113	kA/us	39.9	0.37	9.9	39.9	161.5
PEAK - 1	114	kA	11.8	0.23	4.9	11.8	28.6
PEAK	114	kA	12.3	0.23	5.2	12.3	29.2

[a] The values given are geometric means; the standard deviations are expressed in logarithmic units consistent with the existence of a log normal parent distribution.

TABLE IV

Largest Peak Rates of Change of Current for 60 Flights of the F-106 Aircraft[a]

Number of strikes	Largest peak rates, kA/us
1	1.90, 7.6, 9.6, 10, 20, 20, 42, 54, 78, 82, 96, 134, 136
2	7.6, 11.4, 24, 28, 34, 40, 84, 88
3	1.91, 1.91, 20, 78, 88, 300
4	7.6, 42
5	5.8, 11.4, 44, 48, 60, 68, 198
6	3.8, 15.2, 22, 50, 110, 162
7	5.8, 22, 30, 76, 98
8	86, 134, 240
9	194, 380
11	44
14	86
19	17.2
12	42
20	260
27	174
40	240
72	54

[a] Maximum current over all flights was 54 kA

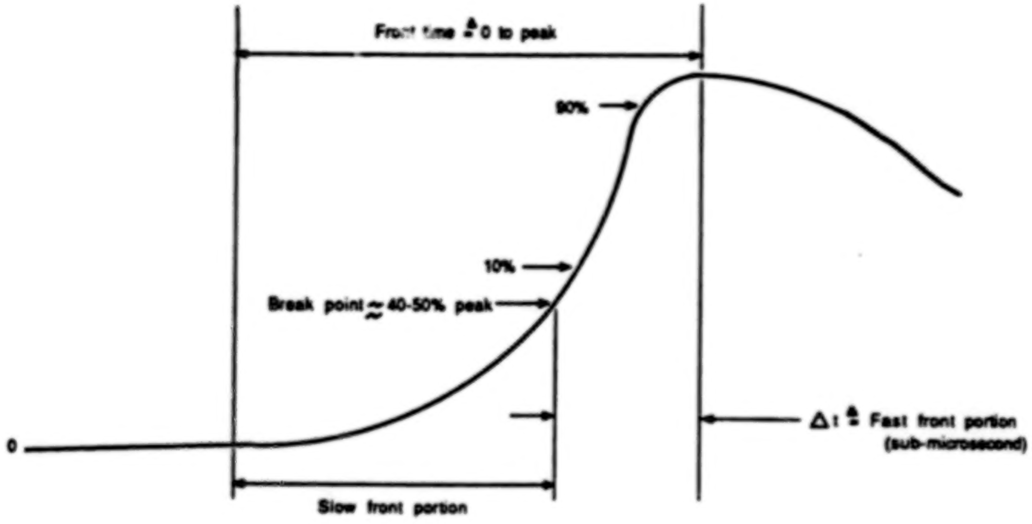
Front time ≜ 0 to peak
90%
10%
Break point ≈ 40-50% peak
0
Δt ≜ Fast front portion (sub-microsecond)
Slow front portion

Figure 2 - Front Shape Parameters Defined By Krider, et al.

TABLE V

RTLP Data[a]

	N	Peak Current (kA)		Rise time (kA/usec)	
		Mean	SD	Mean	SD
Florida - 1985	31	13.5	9	112	48
France - 1986	9	17.0	12	68	40
Florida - 1987	44	16	11	125	72
Totals	84	15	10	114	63

[a] Three papers presented by French and American Researchers in 1988 at the International Aerospace and Ground Conference on Lightning, April 19-22, Oklahoma City and 8th International Conference on Atmospheric Electricity, June 13-16, Uppsala, Sweden.

TABLE VI

RTLP 1987 General Results

DAY	HOUR (TU)	I MAX (kA)	DI/DT (kA/uS)	ALTITUDE OF TRIGGERING	REF. NUMBERS
212 (07/31)	19:45:08:856	4	38	650	
	:880	7	97		8717 B
	:890	6	124		
	:907	12	252		
	:925	8	162		
	:955	8	54		
	:970	11	76		
		12	59		
	:150 09:002	60	411		

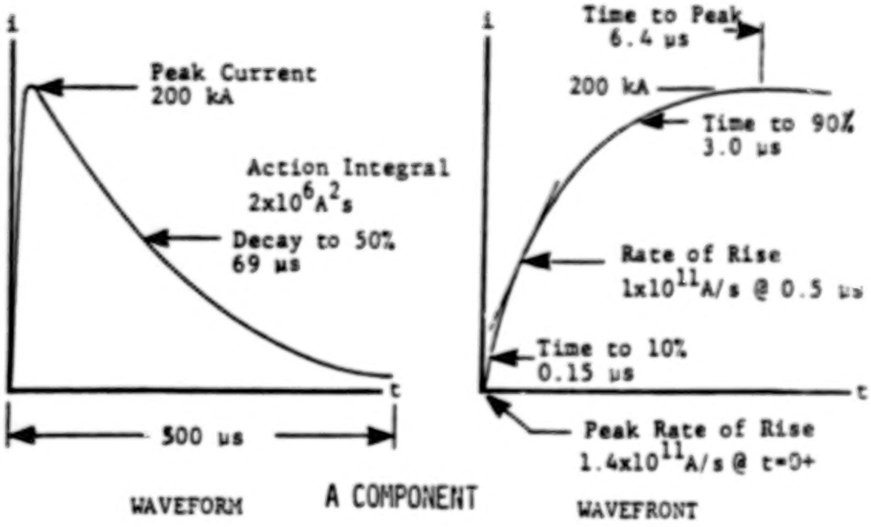
i
Peak Current
200 kA
Action Integral
2x10⁶A²s
Decay to 50%
69 µs
t
500 µs
WAVEFORM
A COMPONENT
WAVEFRONT
i
Time to Peak
6.4 µs
200 kA
Time to 90%
3.0 µs
Rate of Rise
1x10¹¹A/s @ 0.5 µs
Time to 10%
0.15 µs
t
Peak Rate of Rise
1.4x10¹¹A/s @ t=0+

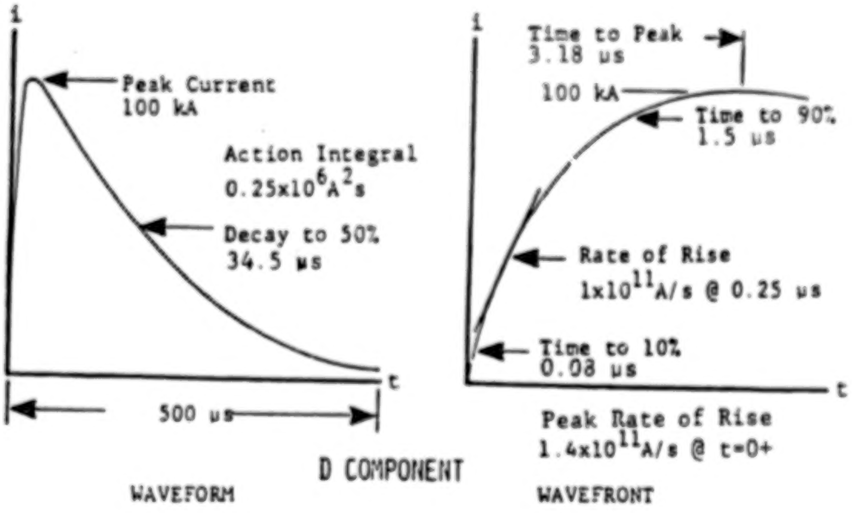
i
Peak Current
100 kA
Action Integral
0.25x10⁶A²s
Decay to 50%
34.5 µs
t
500 µs
WAVEFORM
D COMPONENT
WAVEFRONT
i
Time to Peak
3.18 µs
100 kA
Time to 90%
1.5 µs
Rate of Rise
1x10¹¹A/s @ 0.25 µs
Time to 10%
0.08 µs
t
Peak Rate of Rise
1.4x10¹¹A/s @ t=0+

Figure 3 - Components A and D

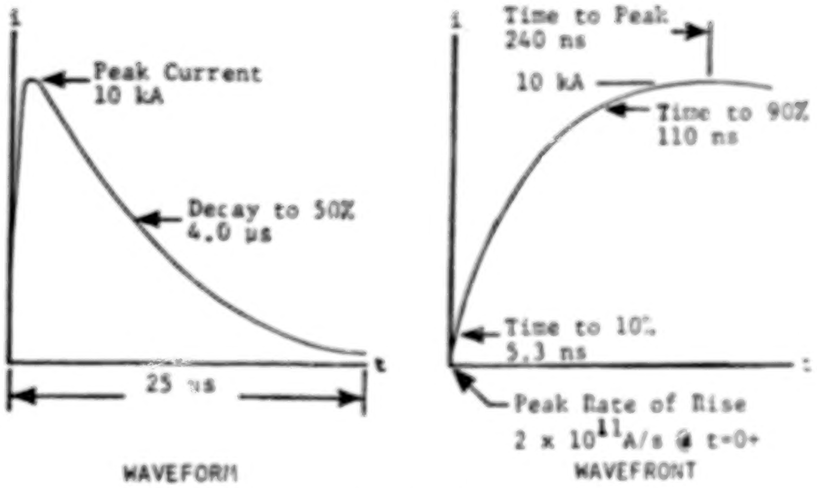

H COMPONENT

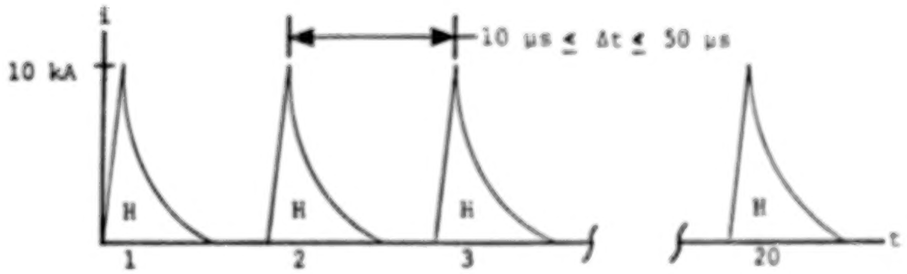

One burst is 20 pulses in 1 millisecond

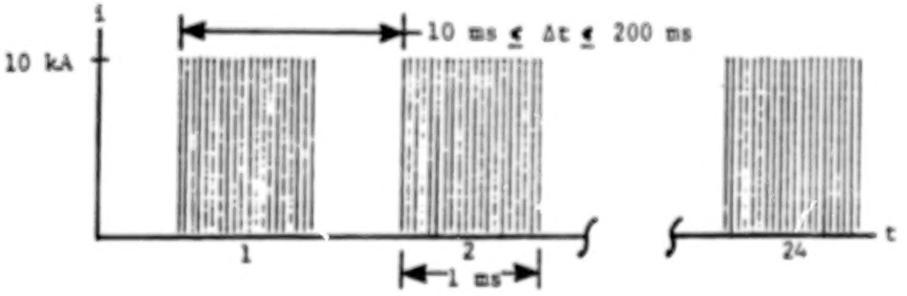

Twenty-four bursts distributed over a period of up to 2 seconds

Figure 4 - Multiple Burst Waveform and Component H

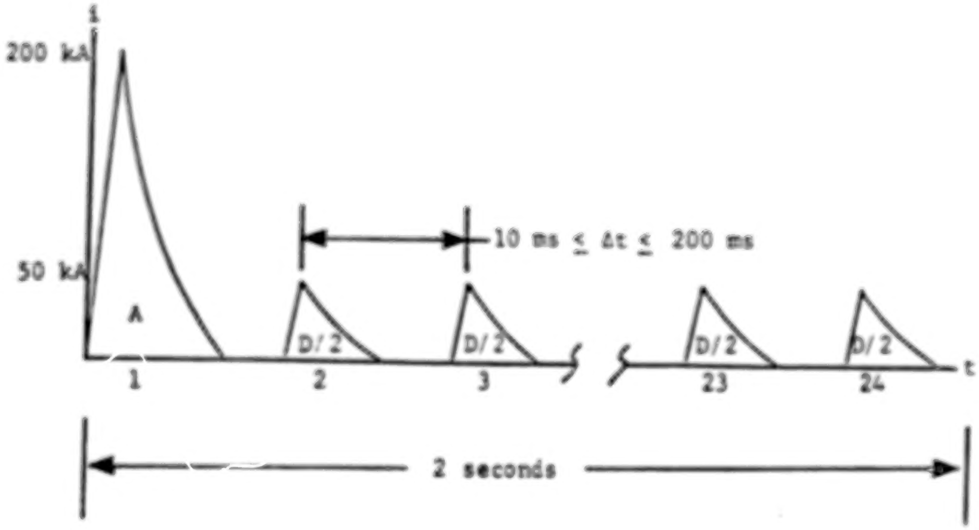
i
200 kA
50 kA
A
D/2
D/2
D/2
D/2
1
2
3
23
24
t
10 ms ≤ Δt ≤ 200 ms
2 seconds

Figure 5 - Multiple Stroke Waveform

MODELING OF ELECTRICALLY THICK MATERIALS
THEORETICAL AND EXPERIMENTAL ASPECTS

V. Gobin, F. Issac and F. Jaillot

Office National d'Etudes et de Recherches Aérospatiales
B.P. 72, 92322 CHATILLON CEDEX, FRANCE

ABSTRACT

The shielding effectiveness of modern aircraft depends upon the nature and the electromagnetic properties of the materials used. It has been shown that thin materials are modeled well by a sheet surface impedance. Unfortunately, this formalism fails in the high frequency domain (when skin effect occurs), and when the materials are physically thick. The purpose of this paper is to propose a general formalism that renders the skin effect and can be used with multilayered samples. These electrically thick materials are studied using symmetrical boundary conditions applied to tangential fields. The domain of validity of the method is discussed and experimental validations are presented.

1. INTRODUCTION

With the increasing use of composite materials on modern aircraft, the scattering of electromagnetic energy through the skin of structures has to be taken into account in evaluating electromagnetic coupling on internal wires and cables. In the low frequency range, many modern materials (CFC for example) can be represented accurately by a sheet surface impedance. The objective of this paper is to delimit the validity of such a model and to discuss a formalism that is valid for electrically thick materials. The formalism is based on the electrical characteristics of a homogeneous material having a permittivity ε, an electrical conductivity σ and a magnetic permeability μ.

Introducing a complex permittivity ε^*, it is possible to determine the intrinsic wave impedance Z_1 of the material and the constant of propagation γ that characterizes a locally plane wave:

$$\varepsilon^* = \varepsilon - j \frac{\sigma}{\omega} \qquad (1)$$

$$Z_1 = \sqrt{\frac{\mu}{\varepsilon^*}} \qquad (2)$$

$$\gamma = j\omega \sqrt{\varepsilon^* \mu} \qquad (3)$$

For good conductors, the influence of the permittivity ε can be neglected ($\varepsilon \ll j \frac{\sigma}{\omega}$) and Z_1 or γ reduce to:

$$Z_1 = \frac{(j+1)}{\delta\sigma} \tag{4}$$

$$Y = \frac{(j+1)}{\delta} \tag{5}$$

where δ is the parameter generally called "skin depth", which is defined by:

$$\delta = \frac{1}{\sqrt{\pi\mu\sigma f}} \tag{6}$$

In EMC studies, we are generally interested in the shielding effectiveness of a given structure of an arbitrary shape. Numerical codes can be efficient tools for calculating electromagnetic fields, provided that a proper formalism is introduced to take into account the properties of the materials. It is also best to analyse a few simple shapes for which analytical results exist because this way it is possible to separate the effect of the shape and dimensions of the shields from that of the materials themselves. We will begin by summarizing some representative results found in the literature:

SPHERICAL SHIELD

We are interested in a spherical shield of radius a, made of a material characterized by its thickness d and conductivity σ, under a uniform magnetic field H_o. The magnetic field H inside the shield cavity is given by [1]:

$$\frac{H}{H_o} = \left[ChYd + j\omega\mu \frac{a}{3} \frac{ShYd}{Z_1}\right]^{-1} \tag{7}$$

The low frequency limit of this expression is:

$$\frac{H}{H_o} = \left[1 + jf \frac{2\pi}{3} \mu_o a\sigma d\right]^{-1} \tag{8}$$

It is important to observe that the effect of the local characteristics of the material in the low frequency domain depends only on the product of σ and d.

LOADED APERTURE

We are interested now in a circular aperture of radius a, cut in a perfectly conductive plane and submitted to a local uniform incident magnetic field. At a chosen point, the scattered field H_o can be calculated using the equivalent dipole formalism. If we load the aperture with a thin panel (thickness d, conductivity σ) perfectly joined to the metal wall, the scattered magnetic field can be approximated by [2]:

$$\frac{H}{H_o} = \left[1 + jf \frac{8}{3} \mu_o a\sigma d\right]^{-1} \tag{9}$$

Once again, provided that the panel is electrically thin, the effect of the material appears only in the σd term.
The interest of the loaded aperture configuration is that these results can be verified experimentally using a TEM cell and samples of various thickness and conductivity.

PARALLEL CIRCULAR LOOPS

We now consider a conductive loop of radius a, carrying a current I and creating a magnetic field H_o. We choose to measure this field with a second open loop placed on the axis of the first loop at a distance a. If a thin sample is placed between the two loops, the field H measured with the second loop is modified in a ratio that can be expressed approximately by [3]:

$$\frac{H}{H_o} = \left[1 + jf\,\frac{\pi}{1.4}\,\mu_o a\sigma d\right]^{-1} \qquad (10)$$

This confirms that, at low frequency, the product σd is a pertinent parameter that represents the material behavior. This parallel loop configuration is easy to study experimentally [4] and furthermore the position of the sample between the loops has no influence, facilitating the experimental measurements.

The three above examples illustrate the interest of separating the influence of the shield geometry from the nature of the material. We will now study the material itself for both electrically thick and thin samples.

2. MODELING OF A HOMOGENEOUS MATERIAL

Before studying a one-layer homogeneous material, we must first investigate what happens at the interface between air and a good conductive material, assuming an incident plane wave propagating from the air side, at an arbitrary angle of incidence θ_i (θ_i being referenced to the direction perdendicular to the interface). The angle of incidence θ_t of the transmitted wave within the material is classically given by the expression:

$$\sin \theta_i = \sqrt{\varepsilon^*} \sin \theta t \qquad (11)$$

For any good conductive material, it is easy to verify that $\sqrt{\varepsilon^*}$ is larger than unity. Thus, whatever θ_i may be, the direction of propagation of the transmitted wave is always more or less perpendicular to the interface. Because moreover a non-uniform incident wave can be broken down into an infinite sum of plane waves at various angles of incidence, we will consider in this paper, that the energy propagates inside the materials perpendicular to the interface, provided that they are good conductors.
Thus we consider now a locally plane material of thickness d, characterized by σ, ε and μ. We suppose that the tangential fields of unspecified value at both interfaces are (E_1, H_1) and (E_2, H_2). In light of the previous remark, we consider that the fields inside the material are the sum of two plane waves

travelling perpendicular to the interfaces, in opposite directions (see figure 1).
Assuming only that the fields on both interfaces are continuous, one can calculate the expression for the volumic current density in the material and demonstrate boundary conditions between the tangential fields:

$$\vec{J}(z) = \sigma\vec{E}(z) = \frac{\sigma Z_1}{\mathrm{ShYd}}\left(\mathrm{ChY}\,(z_2 - z)\,\overrightarrow{n_1}\wedge\overrightarrow{H_1} + \mathrm{ChY}\,(z - z_1)\,\overrightarrow{n_2}\wedge\overrightarrow{H_2}\right) \tag{12}$$

$$\begin{bmatrix}\overrightarrow{E_1}\\ \overrightarrow{E_2}\end{bmatrix} = \begin{bmatrix} Z_s & Z_T \\ Z_T & Z_s\end{bmatrix}\begin{bmatrix}\overrightarrow{n_1}\wedge\overleftrightarrow{H_1}\\ \overrightarrow{n_2}\wedge\overrightarrow{H_2}\end{bmatrix} \tag{13}$$

with

$$Z_s = \frac{Z_1}{\mathrm{thYd}} \tag{14}$$

$$Z_T = \frac{Z_1}{\mathrm{ShYd}} \tag{15}$$

We have introduced here an impedance matrix [Z] that models the proper boundary conditions for the fields both sides of the wall. The relations mean that the electric field on one side of the wall is the sum of a term proportional to the magnetic field on that same side (Z_s term) and a term proportional to the magnetic field on the opposite side (Z_T term).
The expression for [Z] can be specified for any good materials that are within the scope of this paper, and for which (4) and (5) are available. We can now introduce an arbitrary characteristic frequency f_δ defined as the frequency for which the skin depth δ is equal to the physical thickness d of the material being studied. We can thus write:

$$f_\delta = f|_{\delta=d} = \frac{1}{\mu\pi f\sigma d^2} \tag{16}$$

and

$$Yd = (j+1)\cdot\frac{d}{\delta} = (j+1)\sqrt{\frac{f}{f_\delta}} \tag{17}$$

LOW FREQUENCY APPROXIMATION OF [Z]

When $Yd \ll 1$ or $d \ll \delta$ or $f \ll f_\delta$, the expression for [Z] is simplified and depends only on the "sheet surface impedance" Z_{so}.

$$Z_s = Z_T = Z_{so} = \frac{1}{\sigma d} \tag{18}$$

We recognize here the expression that appeared in (8), (9) and (10). In addition, the boundary conditions lead to:

$$\overrightarrow{E_1} = \overrightarrow{E_2} = Z_{so}\,\overrightarrow{n_1}\wedge\left(\overrightarrow{H_1} - \overrightarrow{H_2}\right) = Z_{so}\cdot\overrightarrow{J_s} \tag{19}$$

where $\vec{J}_s$ is the current surface density (equal to the integral of the density through the wall).

HIGH FREQUENCY APPROXIMATION OF [Z]

When $Yd \gg 1$ or $d \gg \delta$ or $f \gg f_\delta$, it is easy to show that the Z_T term reduces to zero. This means that the attenuation through the material is so great that both sides may be considered as independent of each other. At the same time, Z_s becomes equal to the intrinsic wave impedance Z_1 of the material. This means that from each side the material is seen as a half space having the same intrinsic properties.

DOMAIN OF VALIDITY OF THE LOW FREQUENCY APPROXIMATION

It is interesting to determine the frequency up to which the sheet impedance formalism is sufficient for estimating shielding properties of structures. Figure 2 represents the variation of the various impedances: Z_{so} (cf (18)), Z_s (cf (14)), Z_T (cf (15)) and Z_1 (cf (4)). All these impedances have been normalized to Z_{so}, and the frequency axis is normalized to f_δ so that the curves are valid for any material.

In figure 3, we compare the graphs of the ratio H/H_o as calculated with the exact (7) and with approximate formulas (8), for a sphere of radius $a = 0.1$ m and thickness $d = 1$ mm.

To quantify the domain of validity of the low frequency formulas, the relative errors have been plotted in figure 4. In each case, the difference between the exact and approximate values is normalized to the low frequency result and is expressed as a percentage.

These curves show one interesting feature: although a 10% error is made on Z_s for $f/f_\delta = 0.6$, the same error on H/H_o is reached only for $f/f_\delta = 2$. This means that even if the elements of the matrix [Z] do begin to differ from their low frequency limit, the shielding effectiveness is less affected by the approximation. If we remark that an alternative expression for (7) versus Z_s and Z_T is:

$$\frac{H}{H_o} = \left[\frac{Z_s}{Z_T} \left(1 + jf \; \frac{2\pi \, \mu_o a}{3 \, Z_s} \right) \right]^{-1} \qquad (20)$$

then we can see that Z_s begins to increase when Z_T decreases, so that H/H_o is still quite correctly calculated with (8). Let us remember that, for a sphere, a 10% error is obtained for $f/f_\delta = 2$ and a 50% error for $f/f_\delta = 5$.

COMMENTS ON THE FORMALISM

The low and high frequency limits of the impedance matrix indicate the generality of the formalism. Moreover, we have made no assumptions concerning the fields on either side of the material, and the expression of the boundary conditions (13) is perfectly symmetrical. In some cases, further approximation can be derived but one has to keep in mind the domain of

61

validity of the simplification. The two following examples illustrate this point.

Symmetrical structure

We consider here a plane sample, carrying a current I. The return path of I is perfectly symmetrical. In that case, $\vec{n_1} \wedge \vec{H_1} = \vec{n_2} \wedge \vec{H_2}$ and the surface current J_s is given by:

$$\vec{J_s} = \vec{n_1} \wedge \vec{H_1} + \vec{n_2} \wedge \vec{H_2} = 2 \left(\vec{n_1} \wedge \vec{H_1} \right) = 2 \left(\vec{n_2} \wedge \vec{H_2} \right) \qquad (21)$$

It is possible to introduce these expressions in (12) and thus calculate the current density J(z) within the material. Figure 5 represents the variation of J(z) (normalized to the average value J_s/d) for various frequencies. As expected, the current concentrates symmetrically close to the two interfaces with increasing frequency. In addition, the general boundary conditions (13) lead to a direct relation between the tangential electric fields and J_s:

$$\vec{E_1} = \vec{E_2} = \frac{Z_s + Z_T}{2} \vec{J_s} \qquad (22)$$

Shielding enclosure

A closed shield may be considered as a rather common structure in EMC studies. As illustrated by the example at the beginning of this paper, the fields inside such a shield (say H_2, E_2) rapidly become smaller than the outside fields (say H_1, E_1) and the general boundary conditions may be simplified. Because $\vec{n_1} \wedge \vec{H_1} \gg \vec{n_2} \wedge \vec{H_2}$, for high frequencies it can be said that:

$$\vec{J_s} = \vec{n_1} \wedge \vec{H_1} \qquad (23)$$

$$\vec{E_1} = Z_s \vec{J_s} \qquad (24)$$

$$\vec{E_2} = Z_T \vec{J_s} \qquad (25)$$

We have now asymmetrical relations, because the internal volume has been distinguished from the external. Equations (23) to (25) are sometimes presented in the literature as general assumptions. We prefer to use our symmetrical boundary conditions, chiefly for eventual use in 3D numerical codes.

To conclude this discussion, we have given in figure 6 the current distribution in the wall of a sphere, for various frequencies. The internal field H_2 introduced in (12) has been assumed to verify (7). It can be observed that, at high frequency, the entire current concentrates at the outside interface of the sphere.

3. MODELING OF A MULTILAYERED MATERIAL

The boundary conditions introduced to model a one-layer homogeneous material can be generalized to include multilayered materials. Each layer surface impedance matrix $[Z]_i$ has to be calculated and transformed into a $[T]_i$ matrix (giving the relation between (E_1,H_1) and (E_2,H_2)). The $[T]_i$ matrices are then multiplied by each other to give the resulting [T] matrix which is converted back into [Z] form. Further calculations show that the impedance matrix of any multilayered material is characterized by three different terms.

$$[Z] = \begin{bmatrix} Z_{s1} & Z_T \\ Z_T & Z_{s2} \end{bmatrix} \tag{26}$$

For a material that is symmetrical about the medium plane, Z_{s1} is equal to Z_{s2}. In the last part of this paper, we will discuss only the case of a particular multilayered material type of practical interest that we will call double sheet material: we consider a sample of two identical thin conductive sheets (characterized by their common sheet impedance Z_{so}) and separated by a dielectric medium (characterized by the constant of propagation $\gamma = j\beta$, the intrinsic impedance Z_1 and the thickness d). The point of interest of such a sample is that it is representative of certain thick materials used in aeronautics.
The result of our matrix calculation leads to:

$$Z_s = \frac{(Z_{so}\cos\beta d + Z_1 \sin\beta d)\, Z_{so} Z_1}{2\, Z_{so} Z_1 \cos\beta d + \left(Z_{so}^2 + Z_1^2\right)\sin\beta d} \tag{27}$$

$$Z_T = \frac{(\cos^2\beta d - \sin^2\beta d)\, Z_1 Z_{so}^2}{2\, Z_{so} Z_1 \cos\beta d + \left(Z_{so}^2 + Z_1^2\right)\sin\beta d} \tag{28}$$

The low frequency limit of Z_s and Z_T is $Z_{so}/2$, which is consistent with the behavior of two parallel resistive plans. It may be remarked that this limit is independent of the distance d between the sheets. The high frequency limit of Z_s is Z_{so}, meaning that only one sheet is seen from each side at high frequency. Figure 7 represents the variation of Z_s and Z_T (normalized to their low frequency limit) versus βd.

EXPERIMENTAL VERIFICATION OF THE FORMALISM

We will now present some experimental results to confirm our model. As pointed out in the introduction, two different experimental setups have been used. The first one is based on a TEM cell [5], in which a square 0.2x0.2 m aperture has been cut and loaded with material under test. The behavior of the sheet impedance shielding effectiveness has been calculated (see (9)) and represents the thin material approximation. The second measurement is based upon the two parallel loop (radius 3,4 cm) setup described previously [4] and the expected low-frequency results are given by (10).

Figure 8 represents the shielding ratio H/H_o measured with both methods, the material under test being a double sheet sample. As expected, the first part of the two curves is given by (9) and (10), the difference between the 3 dB characteristic frequency being explained by the geometrical dimensions of the two setups. At high frequencies, the attenuations differ from the 20 dB/decade curves at the same value of the frequency.

In figure 9, we have plotted the experimental results obtained with various double sheet samples. In each case, the characteristics of both sheets are identical, the only difference between the samples being the distance d between the sheets. As previously suggested, the low-frequency part of the data is independant of the distance d between the sheets. On the other hand, at high frequency, the larger d, the greater the shielding effectiveness.

4. CONCLUSION

We have discussed a boundary condition formalism that is valid for representing electrically thick materials (skin effect is taken into account and multilayered sample may be studied). Our initial experimental results have shown the advantage of the method, and further experimental study is now needed to confirm all the aspects of the theory. The advantage of the symmetry of the boundary conditions (which illustrates the generality of the concepts) is that they can be introduced in a 3D numerical code. Our first step in this area will be to introduce the impedance boundary conditions in a frequency domain 3D method based on an integral equation solved by the Method of Moments.

REFERENCES

[1] H. Kaden,
Wirbelströme und Schirmung in der Nachrichtentechnik, 2. Auflage, Springer Verlag Berlin, Göttingen, Heidelberg, 1959.

[2] K.F. Casey,
Low frequency electromagnetic penetration of loaded apertures. IEEE Trans. on Electromagnetic Compatibility, EMC-23, 1981, pp. 367-377.

[3] V. Gobin,
Diffraction par des ouvertures et par des objets tri-dimensionnels. Thèse de doctorat, Université des Sciences et Techniques de Lille Flandres Artois, 3 juillet 1990).

[4] V. Gobin, G. Labaune et F. Issac,
Conductive materials surface impedance measurements. ICOLSE, Bath (G.B), September 26-28, 1989.

[5] V. Gobin, G. Labaune and F. Issac,
Electromagnetic coupling through composite materials, ICOLSE, Oklahoma, April 19-21, 1988, pp. 370-377.

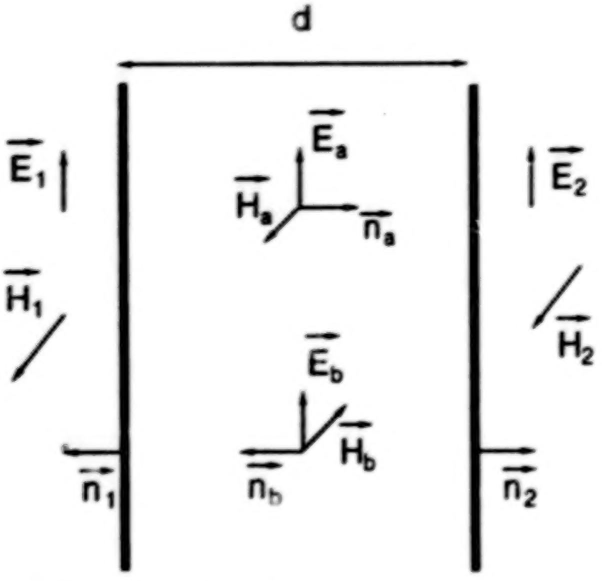
d
$\vec{E}_1$
$\vec{H}_1$
$\vec{n}_1$
$\vec{E}_a$
$\vec{H}_a$
$\vec{n}_a$
$\vec{E}_b$
$\vec{H}_b$
$\vec{n}_b$
$\vec{E}_2$
$\vec{H}_2$
$\vec{n}_2$

Figure 1 : Fields in a homogeneous layer.

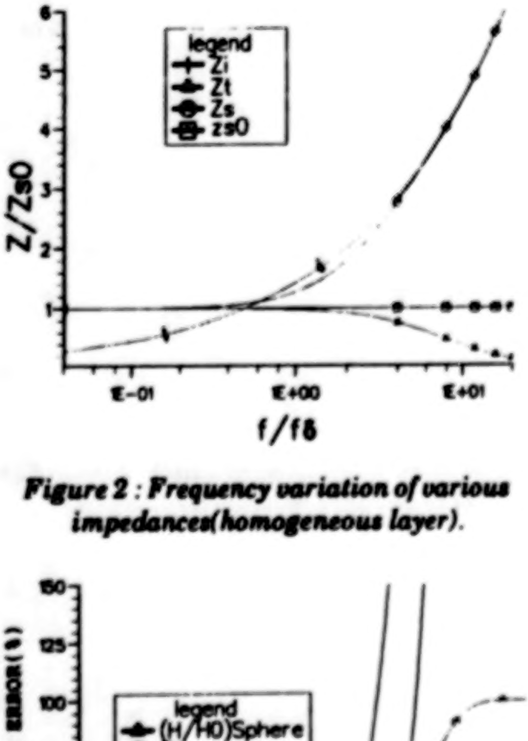

Figure 2 : Frequency variation of various impedances(homogeneous layer).

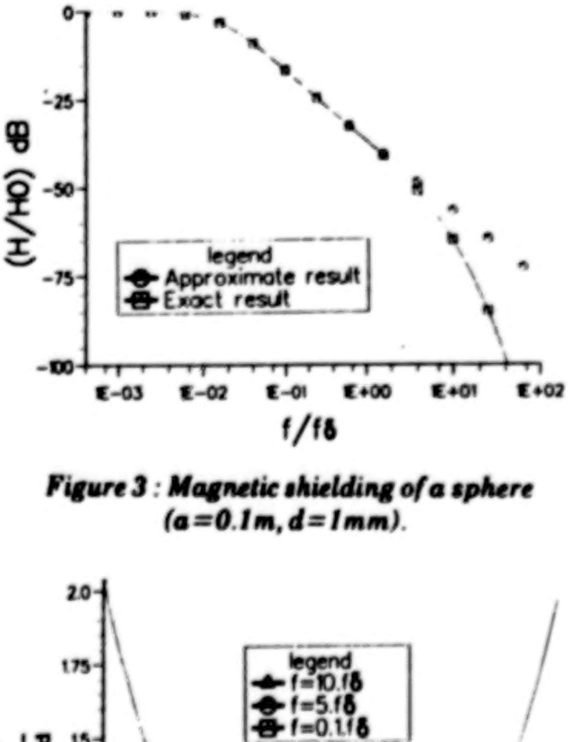

Figure 3 : Magnetic shielding of a sphere (a=0.1m, d=1mm).

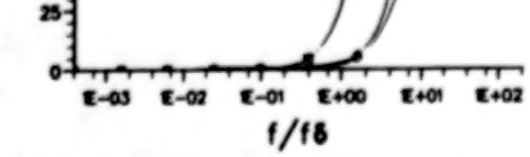

Figure 4 : Relative errors between the exact expressions and their low frequency limit.

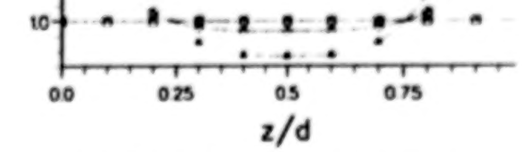

Figure 5 : Volume distribution of current in the symmetrical case.

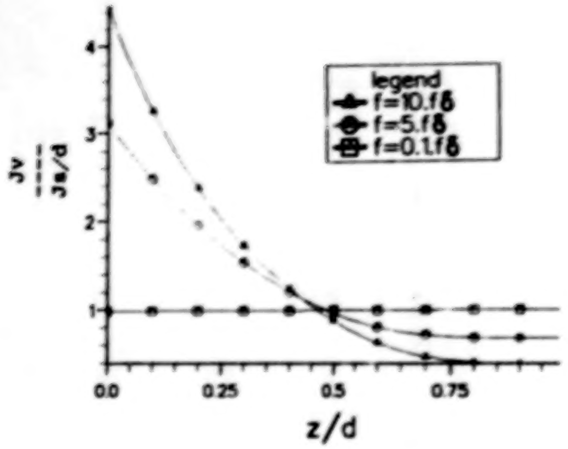

Figure 6 : Volume distribution of current in the wall of a sphere.

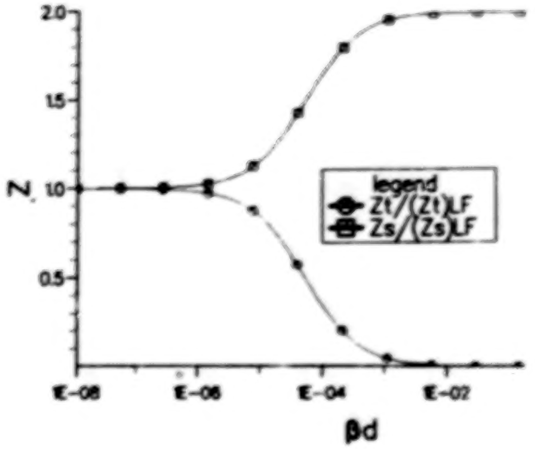

Figure 7 : Frequency variation of Z_S and Z_T (double sheet material).

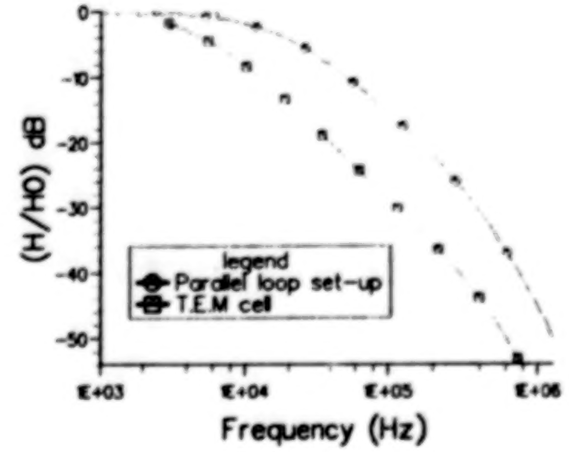

Figure 8 : Magnetic attenuation for a double sheet sample with two experimental setups.

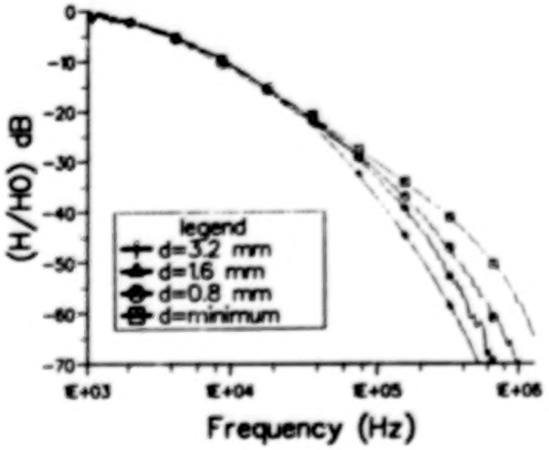

Figure 9 : Experimental verification of the influence of the distance between the two sheets.

Sparking Characteristics of Carbon Fiber Composite Fastened Joints With Various Waveforms

by D. Heidlebaugh and J. Carter

No paper available.

INVESTIGATIONS INTO THE DAMAGE FOR VARIOUS TYPES OF UNPROTECTED CARBON FIBRE COMPOSITES WITH A VARIETY OF LIGHTNING ARC ATTACHMENTS

G W Reid
Lightning Test and Technology, Culham Laboratory,
Abingdon, Oxford, OX14 3DB, UK

ABSTRACT

Very little quantitative information exists on the extent and nature of damage caused to unprotected carbon fibre composite (CFC) due to lightning arc attachment. This paper describes an initial investigation into the arc damage to three different types and various thickness of CFC from Components 'A' and 'C' type lightning discharges. The difference in damage which the two types of waveform produced and the way the area of damage varies with different levels of action integral and charge transfer is compared.

In some cases the temperature rise at the rear of the panels has been recorded for various levels of action integral and charge transfer.

A comparison has been made of the area of damage from visual inspection and soft 'X' ray photograph using a suitable penetrant in the damaged area. It is concluded there is a need for a more detailed analysis of the damage. It is proposed to do this in conjunction with RAE Farnborough in the near future.

1 INTRODUCTION

Very little quantitative information exists on the damage to unprotected carbon fibre composite (CFC) from the effects of lightning strike arc attachment. Substantial damage can be caused and in consequence most of the information covers various methods of protection using conductive surface layers. The object of the present investigation was to establish the degree and nature of the damage caused by various types of lightning arc currents.

It was proposed the following factors would be investigated:

1. The effect of varying peak current.
2. Effect of varying the action integral $\int i^2\,dt$.
3. Effect of varying the slow components B and C with different charge transfers.
4. Effect of different testing techniques such as size and shape of the electrode and sample/electrode spacing.
5. Different types, thicknesses and construction of materials.
6. Temperature measurements at the rear of the panels.

The work is at present proceeding and this paper describes some of the initial results which have been obtained.

2 PREVIOUS WORK

We know of only two early sources of work on these topics, the first of which was reported by Fisher and Plumer in Reference 1. This Report only considers the effect of action integral. It is known that the depth of damage can mainly depend on the charge transfer and this is discussed by Schneider et al in Reference 2. There is only limited agreement between the two sets of results but details of the tests methods and construction of

68

the material are not available and could readily account for the differences. It therefore seemed desirable to investigate the damage effects in more detail.

3 DETAILS OF THE TESTS

Only a limited amount of CFC material was available for these tests, the panels being of the order of 400mm x 400mm. A number of shots were therefore made to each panel especially at the lower levels in order to obtain as much data as possible.

The panels were mounted in the standard LTT co-axial arc test rig. A 100mm fine fuse wire initiated arc was used with a variety of different electrodes. The panels were clamped at their edges to the test rig after the surplus resin had been cleared off. Some early tests using a metal surround and self tapping screws had been tried to obtain better contact to the inner plies but this did not seem to affect the arc root damage.

The panels were not masked other than at the connecting edges to prevent possible arc attachments to the rig. As there were a number of tests to each panel the damage caused by previous tests was screened before further testing.

The object of the tests was to obtain some form of scaling factor of damage with increasing levels of lightning current. For Component 'A' the current and action integral were scaled as for 200kA and $2 \times 10^6 A^2s$, ie, 100kA $0.5 \times 10^6 A^2s$ 50kA $0.125 \times 10^6 A^2s$, etc. Component 'C' used a charge transfer up to 200C.

4 GENERATORS AND DIAGNOSTICS

The standard LTT slow and fast bank generators were used for these tests as shown in Figure 1. The currents were measured for the fast bank using Rogowski coils and a co-axial shunt for the slow bank. These signals were recorded using a 10 Mega-samples per second transient digitiser which could also calculate the action integral and charge transfer of the various waveforms. The fast bank waveforms used both ringing and clamped (crowbarred) shots for the higher action integrals and the slow bank used clamp waveforms. Typical test waveforms are shown in Figure 2.

5 DAMAGE ASSESSMENT

A major problem is the damage assessment resulting from the arc attachment. For this report we have only been able to do a visual inspection and in some cases a few samples have been measured using soft 'X' rays as described below. The damage area is not of course rectangular and the figures quoted for the area is a rough equivalent. It is expected to do a more detailed examination at the Materials and Structures Division of RAE Farnborough and this information should be available at a later date.

For a number of panels soft 'X' ray pictures at 20kV were taken using a penetrant of Trichlorethane in the damage areas. The film used was Kodak M x 4 and the exposure time was about 1 to 1½ minutes. The films were developed in Perceptol for 8 minutes.

6 TEMPERATURE MEASUREMENTS

It was decided it would be very useful to try to obtain a temperature measurement at the rear of the panels during the arc attachment. Ideally the use of a thermal imaging camera would be the more suitable way of doing this but unfortunately an instrument was not available. We have however used the surface temperature measuring device, the Kane-May Infratrace 1000, which averaged the surface temperature over a 30mm dia circle of the material and recorded the peak value which occurred in the test.

7 MATERIALS TESTED

The first set of material tested was kindly supplied by Westland Helicopters consisting of ± 45° lay up, 2mm thick panels the details of construction being as follows:

"The six cross-ply laminates consist of 16 plies giving a nominal thickness of 2.0mm laid in an unbalanced ± 45° manner. The preimpregnate was manufactured by Fiberite (HYE 1682W) consisting of Fiberite 982 epoxy resin and Enka Besfight HTA/12K carbon fibre. The details of the cure cycle was essentially a 120°C cure."

The second set of material tested had been specially manufactured by the Materials and Structures Section at RAE Farnborough details of which are as follows.

Two thicknesses of woven cloth laminates 0.5mm and 1.0mm. XAS/913.

Two thickness of Quasi-Isotropic laminates (0, ± 45°, 90°) 2.0mm and 4.0mm XAS/914.

8 DETAILS OF TESTS

The present series of tests have mainly been concerned with applying Component 'A' and Component 'C' type waveforms separately to the various types of panels at different levels to identify the type and degree of damage that they produce. A few combined waveforms have been used but it is expected to extend the investigation into combined waveforms at a later date.

The results of the tests are summarised in the Tables 1-7 and are designated as follows:

Westland material ± 45° lay up 2mm thick.	
Table 1	Tests with Component 'A' waveforms.
Table 2	Tests with Component 'C' waveforms.
Table 3	Tests with combined 'A' and 'C' waveforms.
RAE	0.5 and 1.0mm woven material.
Table 4	Tests with Component 'A' waveforms.
Table 5	Tests with Component 'C' waveforms.
RAE	2.0mm and 4.0mm Quasi-Isotropic Laminates.
Table 6	Tests with Component 'A' waveforms.
Table 7	Tests with Component 'C' waveforms.

The results from these tests are somewhat limited but it is expected to obtain more results in the near future. At the moment they have been plotted graphically in Figures 3 to 8 though in some cases there are very few points available. In most cases the area of visible damage and estimated number of plies deep has been used but a number of estimates of damage area from the soft 'X' ray pictures was available for Westland material.

9 RESULTS

The area of visible damage from the results is plotted in Figures 3 to 8. Figures 3 and 4 shows the damage from A and C components separately for the ± 45° material and the limited number of results give a reasonable linear correlation between the damage and action integral and charge transfer. It is interesting to note in relation to the maximum threat of an action integral of $2 \times 10^6 A^2s$ and charge transfer of 200C the damage area would be greater for the 'C' Component, 15,000mm^2 as compared with 11,000mm^2 for Component 'A'.

Typical 'X' ray damage pictures are shown in Figure 9 and these indicate a substantial increase over the visual assessment of the order of 70-80%.

The results of the RAE Farnborough material are shown in Figures 5, 6, 7 and 8. Very few test shots were made with the 0.5mm thick material as this failed at comparatively low test levels mainly from blowing apart the 2 separate woven layers and damage at the supporting edges due to the shock wave. It was felt more consideration should be given to the methods of support before continuing with the testing. In the case of the woven material the damage from Component 'A' mainly resulted from the burning away of the resin with comparatively little damage to the plies. The layers of woven ply also tend to blow apart. The low current Component 'C' produces some tufting of the plies but over a comparatively limited area.

The damage to the multi-directional ply material see Figure 10 appears considerably less than that for the ± 45° and the variation in damage between the 2 and 4mm thicknesses looks to be small.

For Component 'C' the visual damage again appears considerably less than for the ± 45°, see Figures 3 and 4 and it is interesting to note the woven material appears to have suffered less damage than the multi-directional ply for these types of pulses.

The results of temperature measurements at the rear of the panels with the Kane-May Infratrace 1000 as described in Section 6 and are shown in Figures 7 and 8. It is important to note that this temperature measurement is an average peak value over a circular area of about 30mm dia. There are only a very limited number of points available for the results but they seem to scale reasonably with action integral and charge transfer and also thickness of material.

10 COMMENTS AND CONCLUSIONS

The results so far obtained from these tests clearly indicate the damage is very dependent on the material construction, ie, ply lay-up or woven, etc, so it would not be practical to predict damage without some knowledge of this.

The degree of damage would appear to be directly dependent on the action integral or charge transfer, however more results are required to confirm this and there may well be a threshold and level where catostrophic damage is reached. This information is however very useful as often in testing CFC it is not easy to predict the exact levels of action integral or charge transfer for a specific test and this will allow some extrapolation of the damage to the required level to be made.

It is interesting to note the different types of damage produced by Components A and C. The difference in the damage caused by these components is quite noticeable by visual inspection alone. The action integral of the Component 'A' of the lightning current produces splitting and fractures of the carbon fibres with little burning of the resin bonding, whereas the charge transfer of the Component 'C' results in burning of the resin and deeper penetration of the CFC, and generally the damage is spread over a wider area, see Figure 10.

It is obviously necessary to do a more detailed assessment of the damage than the visual inspection reported here and it is planned to do this in conjunction with the NDT Section at RAE Farnborough.

11 ACKNOWLEDGEMENTS

We would like to acknowledge the help given by Mr D Mead of Materials and Structures Section, RAE Farnborough for their advice and preparation of some of the test samples, and to Dr M Cann for obtaining the test material from Westland Helicopters. Also to Messrs J G Talboys and R W Butler for their assistance in the testing and measurements.

This work was commissioned by MoD(PE)AES 23b from whom permission was obtained to publish these results.

12 REFERENCES

1. F A Fisher, J A Plumer "Lightning Protection of Aircraft" NASA Reference Publication 1008 October 1977.
2. Schneider, Hendricks and Olson "Vulnerability/Survivability of Composite Structures to Lightning Strike" Report AFFDL-tr-77-127, 1978.

TABLE 1

TESTS TO INVESTIGATE DAMAGE CAUSED BY COMPONENT 'A' 'ACTION INTEGRAL' 2mm WESTLAND ± 45° MATERIAL

TEST NO	I kA	$\int i^2 dt$ $\times 10^6 A^2 s$	AREA OF DAMAGE (mm)	NO. OF PLIES PENETRATED	COMMENTS	'X' RAY DAMAGE AREA (mm)
1	84.7	0.18	35 x 55	1		55 x 50
2	75.6	0.18	25 x 70	1		60 x 50
3	88.7	0.33	40 x 100	2		70 x 80
4	38.3	0.052	15 x 30	1		30 x 60
5	97.8	0.39	30 x 60	2	Main damage area	75 x 60
6	95.7	0.55	80 x 15 100 x 100	2	With small tufts	70 x 80
7	147	0.88	120 x 40 100 x 110	3	Main damage area With small tufts	80 x 100
8	174.7	0.82	100 x 40 100 x 90	3	Main damage area With tufts	85 x 100
15	238	1.53	140 x 50	4/5	Panel clamp with screws	90 x 90
16	96	0.4	100 x 30	2	Panel clamp with screws	
23	177	1.68	50 x 120	3/4	Results a bit confused due to possible damage from Shot 24	105 x 80

TABLE 2

TESTS TO INVESTIGATE DAMAGE CAUSED BY COMPONENT 'C' 'CHARGE PASSED Q' 2mm WESTLAND ± 45° MATERIAL

TEST NO	I kA	Q COULOMBS	AREA OF DAMAGE (mm)	NO. OF PLIES PENETRATED	COMMENTS
10	0.92	65.7	100 x 30	3	
11	1.36	146	160 x 60	3	
12	1.9	206	200 x 80	4	
13	0.94	60	90 x 30	3	
14	0.47	20	20 x 10	2	

TABLE 3

TESTS TO INVESTIGATE DAMAGE CAUSED BY COMBINED COMPONENTS A AND C. WESTLAND ±45° MATERIAL

COMPONENT 'A'			COMPONENT 'B'					
TEST NO	I kA	$\int i^2 dt$ $\times 10^6 A^2 s$	I kA	Q Coulombs	AREA OF DAMAGE (mm)	NO. OF PLIES PENETRATED	COMMENTS	'X' RAY DAMAGE AREA (mm)
17	98	0.42	0.43	14.6	100 x 30	2	It looks as if Slow Bank damage occurred in different areas to fast.	60 x 80
24	222	0.946	1.88	206	200 x 180 At least	4	Sample was not large enough for this level of pulse damage was completely over area to sample edges.	200 x 100 At least

72

TABLE 4
TESTS TO INVESTIGATE DAMAGE CAUSED BY COMPONENT 'A' ACTION INTEGRAL.
RAE WOVEN MATERIAL

TEST NO.	DETAILS OF PANEL	I kA	$\int i^2dt$ $\times 10^6 A^2s$	AREA OF DAMAGE (mm)	NO. OF PLIES PENETRATED	TEMPERATURE RISE AT REAR OF PANEL °C	COMMENTS
25	0.5mm thick	79	0.26	30 x 30	Only top plies	212	Surface damage over 150x140mm
26	0.5mm thick	131	0.87	-	-	476	Specimen caught fire and laminate split over area 140 x 150mm. Flame burnt up the panel causing burn out of resin
27	1.0mm thick	79	0.28	40 x 50	Top woven layer	61	It looks as if 2 woven sections have delaminated internally over 40 x 50mm. Top fibres broken of 30 x 30mm. Surface area damage 100 x 100mm

TABLE 5
TESTS TO INVESTIGATE DAMAGE CAUSED BY COMPONENT 'C' CHARGE PASSED.
RAE WOVEN MATERIAL

TEST NO.	DETAILS OF PANEL	I kA	Q COULOMBS	AREA OF DAMAGE (mm)	NO. OF PLIES PENETRATED	TEMPERATURE RISE AT REAR OF PANEL °C	COMMENTS
36	1.0mm thick	0.64	62	25 x 30	2	48	Matrix removed 50 x 50mm. 10mm dia at back.
38	1.0mm thick	0.9	106	25 x 30 +15 x 20	2-3	134	Matrix removed 90 x 90mm. 35mm dia at back.
37	1.0mm thick	1.16	171	40 x 40	3-4	211	Sample on fire,

TABLE 6
TESTS TO INVESTIGATE DAMAGE CAUSED BY COMPONENT 'A' ACTION INTEGRAL.
RAE QUASI-ISOTROPIC MATERIAL

TEST NO.	DETAILS OF PANEL	I kA	$\int i^2dt$ $\times 10^6 A^2s$	AREA OF DAMAGE (mm)	NO. OF PLIES PENETRATED	TEMPERATURE RISE AT REAR OF PANEL °C	COMMENTS
28	2mm thick	80	0.29	20 x 30	2-3	13	Tufting in on places 80 x 80mm
41	2mm thick	141	0.68	45 x 30	2-3	35	Tufting over area 110 x 110mm
29	2mm thick	131	0.97	70 x 20 +20 x 25	4-5	89	Tufting over 130 x 150mm in odd places
42	2mm thick	141	1.6	60 x 60	2-3	110	Surface tufting over area 170 x 170mm
31	4mm thick	78	0.28	20 x 30	1-2	22	Tufting in odd places over area 100 x 100mm
30	4mm thick	131	0.7	60 x 20	2-3	26	Tufting in odd places over area 100 x 100mm

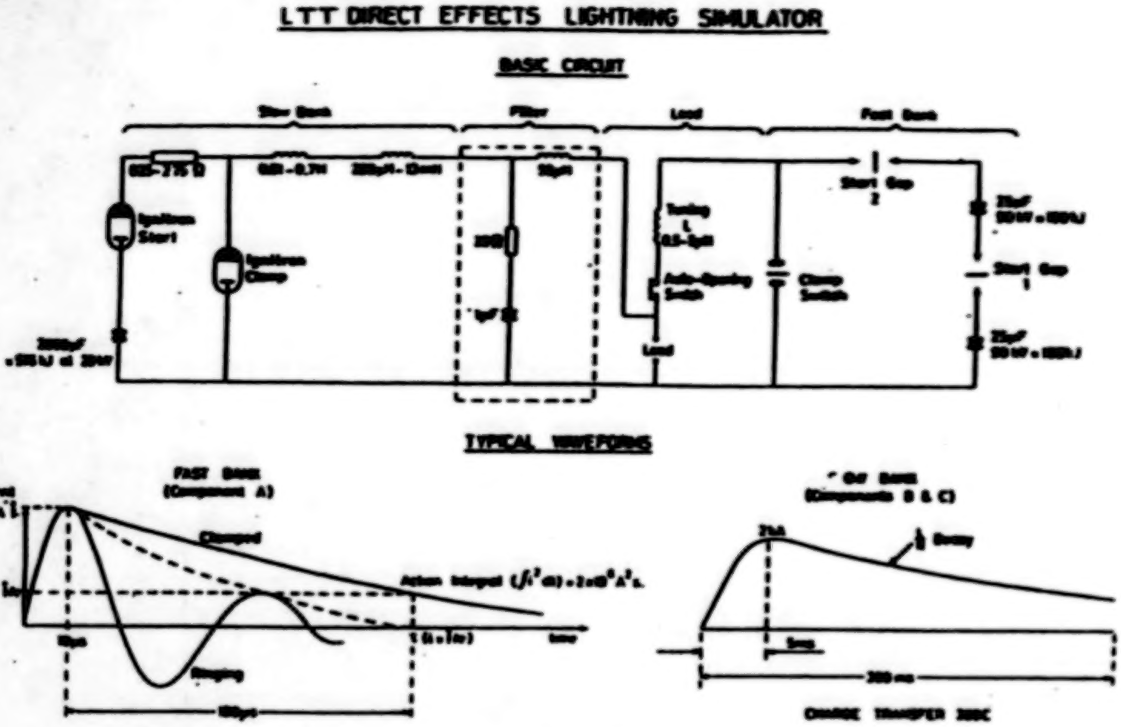
LTT DIRECT EFFECTS LIGHTNING SIMULATOR
BASIC CIRCUIT
Slow Bank
Filter
Load
Fast Bank
Ignitron Start
Ignitron Clamp
Tuning L
Auto-Opening Switch
Clamp Switch
Start Gap 2
Start Gap 1
Load
TYPICAL WAVEFORMS
FAST BANK (Component A)
Current
200kA
Clamped
Ringing
Action Integral
time
(Components B & C)
2kA
Decay
CHARGE TRANSFER 200C

COMBINED OPERATION
The fast pulse can be applied with the slow at any time during the slow pulse.

COMPONENTS A, B & C are defined in CLM-R163 Fig A11

FIGURE 1 Details of Test Current Generators

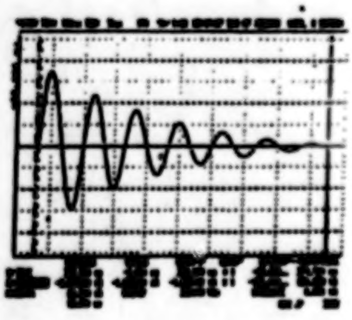

25kA/DIV
40µs/DIV

Low Level Component 'A' Ringing

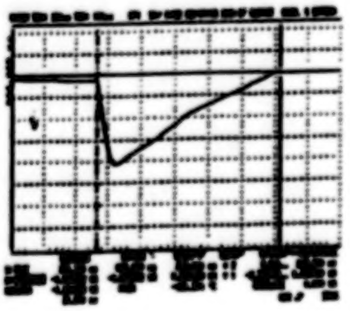

300 A/DIV
40ms/DIV

Component C

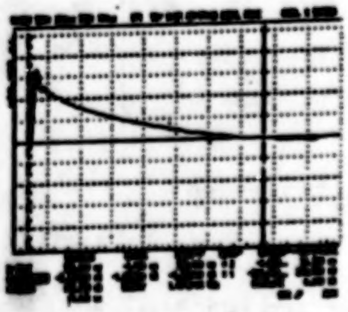

45kA/DIV
80µs/DIV

FIGURE 2 Typical Test Current Waveforms

High Level Component 'A' Clamped (Condensed)

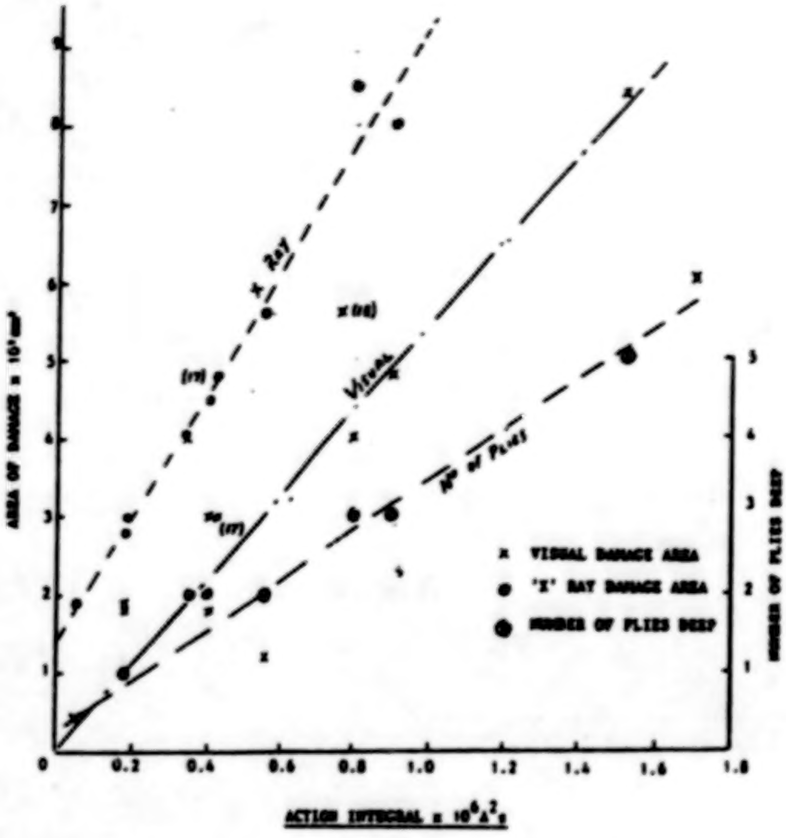

FIGURE 3 Damage Caused by Component 'A' 2mm Westland ±45° Material

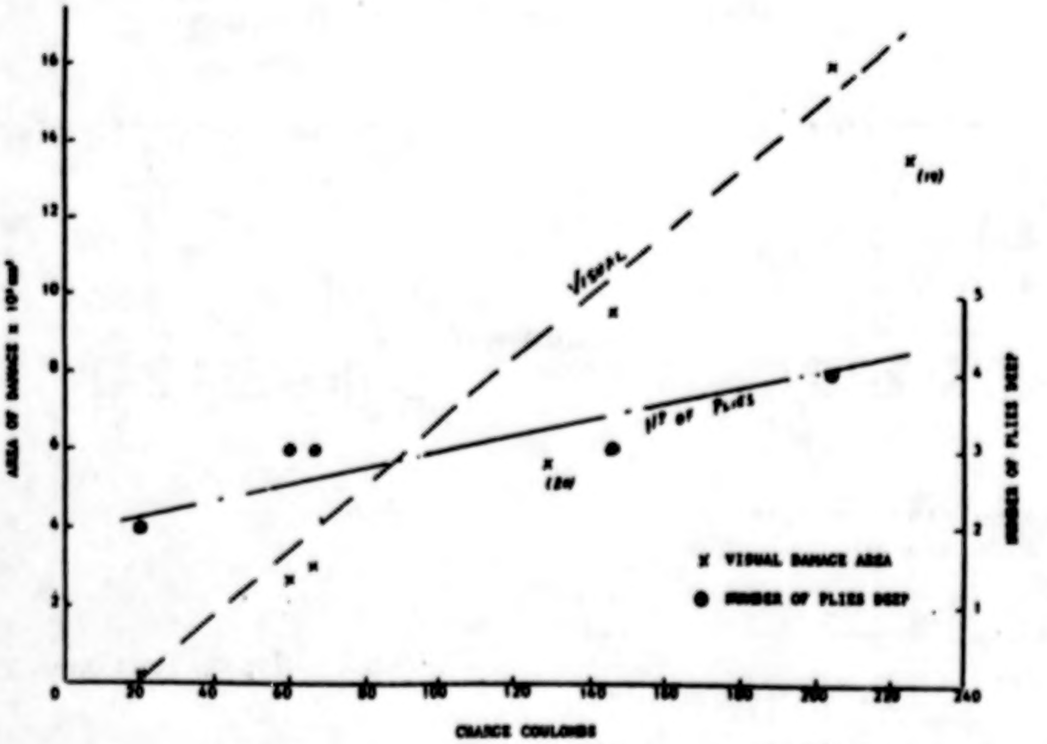

FIGURE 4 Damage Caused by Component 'C' 2mm Westland ±45° Material

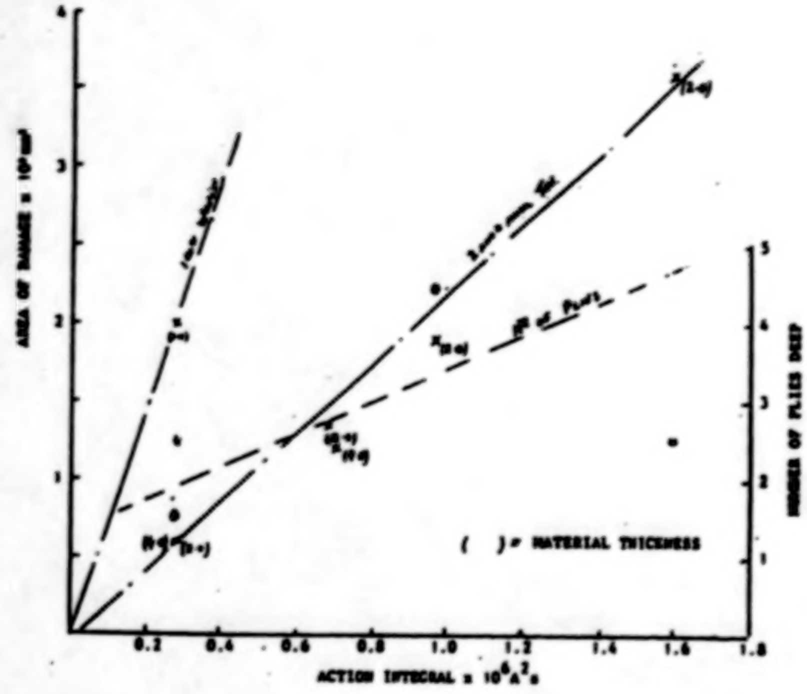

FIGURE 5 Damage Caused by Component 'A' RAE Material

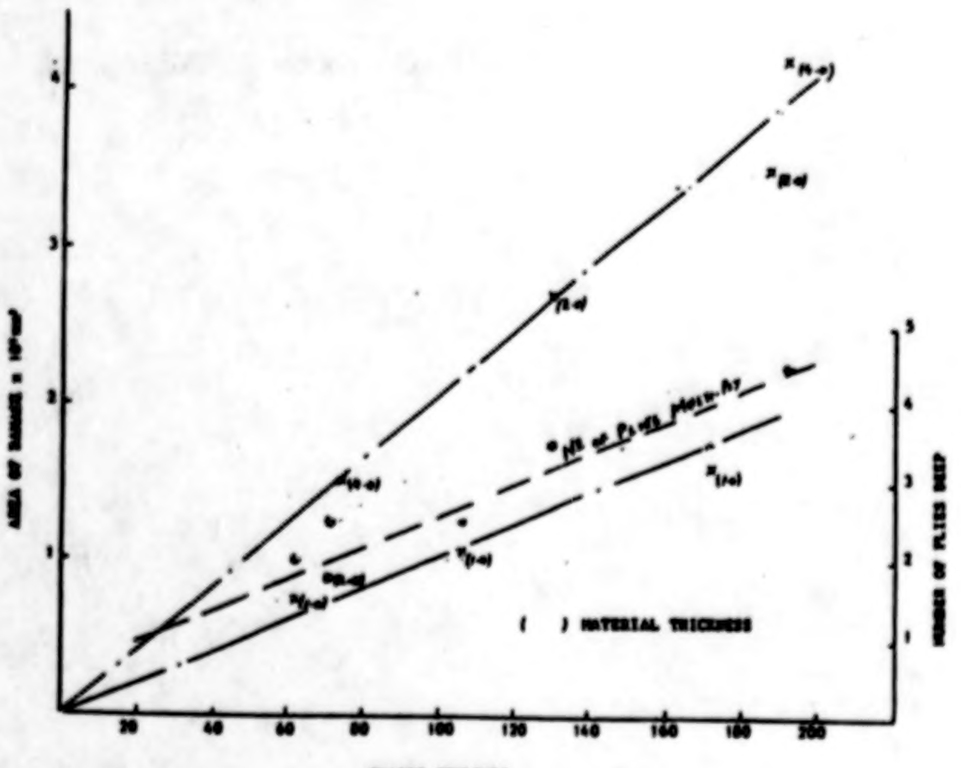

FIGURE 6 Damage Caused by Component 'C' RAE Material

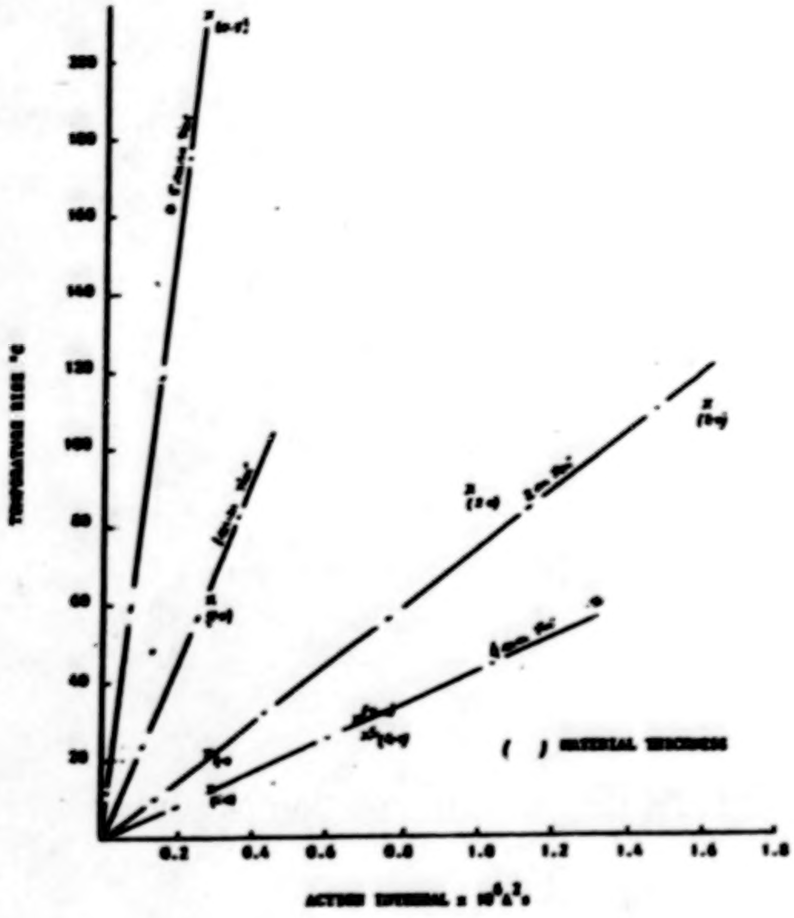

FIGURE 7 Temperature Rise at Rear of Panel for Component 'A' RAE Material

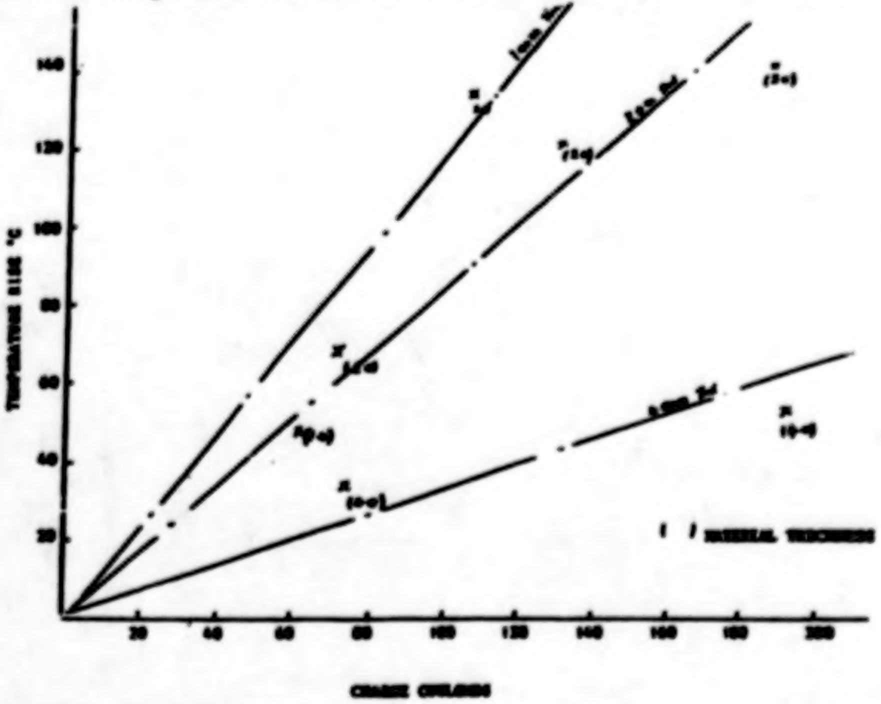

FIGURE 8 Temperature Rise at Rear of Panel for Component 'C' RAE Material

FIGURE 9 'X' Ray Damage Photographs (Test 23)

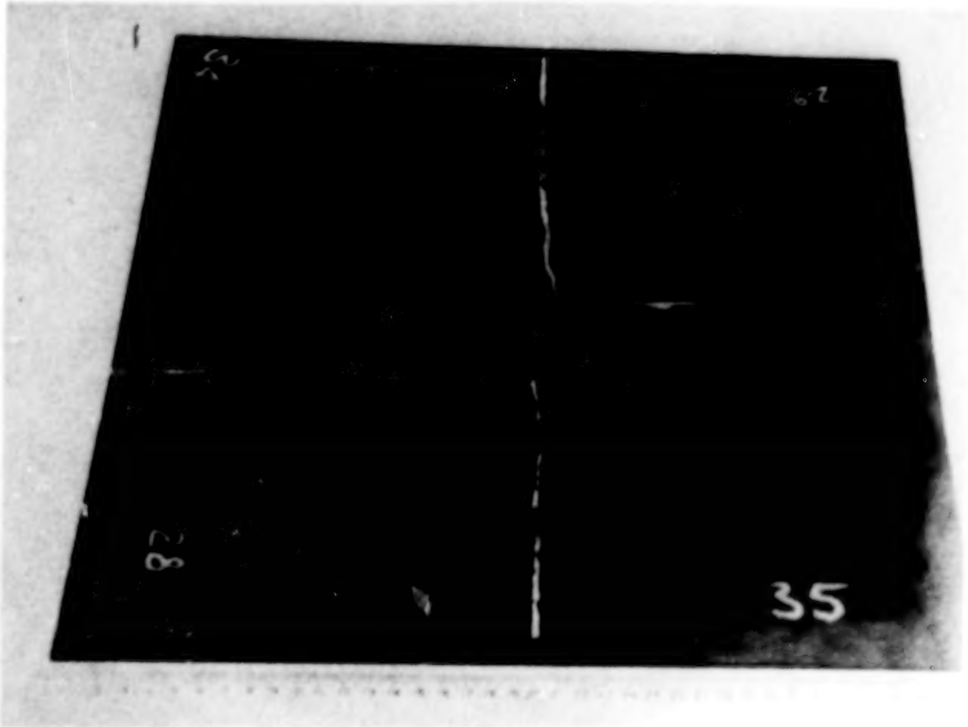

FIGURE 10 Picture of Different Types of Damage

Session 3A, Tuesday 1:30
Lightning Phenomenology Measurements 2
L. Maier, Chairman

CHARACTERISTICS OF WINTER LIGHTNING CURRENTS STRUCK AN ISOLATED TOWER

Yukihiro GOTO
Department of Electrical Engineering, Tohoku University,
Aoba, Aramaki, Aoba-ku, Sendai, 980, JAPAN

Ken'Ichi NARITA
Miyagi Polytechnic College, Tsukidate, Miyagi, 987-22, JAPAN

Hiroshi KOMURO
Electricity Technology Research and Development Center,
Tohoku Electric Power Company, Inc., Nakayama, Aoba-ku, Sendai, 981, JAPAN

ABSTRACT

To make clear the characteristics of winter lightning flashes, the current waveforms of winter lightning flashes have been measured by using of two resistive shunts which were connected two lightning rods since the winter of 1981, and another measurement has started using a set of five Rogowsky type coils since the winter of 1982. They have been recorded by computer controlled digital recording systems.

Up to date, 145 current waveforms of the winter lightning flashes, which have the current amplitude over 1kA, have been obtained by the shunt systems and/or the coils system. They show that winter lightning flashes often have a very long duration or continuing current and sometimes have a very large amplitude over 200kA in positive flashes. For example measured at Jan. 9, 1987, the current parameters were the maximum current amplitude +280kA, maximum current derivative $1.0\text{x}10^{10}$ A/s, total charge +400C and action integral $1.5\text{x}10^{7}$ $A^{2}s$.

The statistical evaluation leads that medium peak values of winter lightning flashes (50% values) were about 5kA for negative and 10kA for positive, and 5% values were about 30kA for negative and 170kA for positive.

The winter lightning current waveforms are classified into three types, that is, single stroke flashes, mono-polar multi-stroke flashes, and bi-polar flashes. Moreover each flash is subdivided into positive or negative, single peak or multi peak, and with or without continuing current.

1. INTRODUCTION

In the winter season, many thunderstorms occur on the north-west coast of Honshu Island facing the Sea of Japan. It has been reported that the nature of winter lightning is rather anomalous[1].

The currents for the lightning threat definition are based on the tower current measurements of lightning strokes performed primarily by Berger[2], Garbagnati[3], and Eriksson[4]. But those lightning current data are almost for the summer lightning. So, it is very important for designing protective measures in electric power facilities and equipments to make clear the characteristics of winter lightning currents.

The observation of winter lightning struck an isolated meteorological observing tower has been made since the winter of 1976. The tower is constructed on the ridge of 125m above the sea level and about 400m apart from the seaside and it's height is about 150m [5],[6],[7].

The current waveforms of winter lightning flashes have been measured by the two resistive shunts connected to two lightning rods and tower structure respectively since the winter of 1981, although in the early stage, they were measured by the loop coil and oscilloscope system with a recording camera at the point of 50m apart from the tower base. As the lightning hitting points were not only the lightning rods but also several other extruding portions of the tower top such as the top of main poles or the edge of shield ring, the current measurement using the Rogowsky type coils set for the current pickup sensor has been done since the winter of 1982.

This report describes the aspects of these measuring systems and the characteristics of winter lightning current obtained by the measurement of current waveforms.

2. MEASURING SYSTEMS FOR LIGHTNING CURRENT WAVEFORMS

Two measuring systems have been prepared to record the waveforms of the lightning current. Figure 1 shows the tower top configuration and the positions of two co-axial resistive shunts and five Rogowsky type coils.

The first system has been equipped with co-axial shunts as current sensors for automatically observing lightning current waveforms by Tohoku Electric Power Co., Inc. since 1981. It consists of two co-axial shunts of 2milli-ohm for the lightning rod installed on the tower top and 4milli-ohm for the lightning rod installed on the shield ring, E/O and O/E converters, optical fiber cable and transient recorders controlled by a computer. Figure 2 shows a block diagram of this system. In this system, three transient recorders are used. They have memory capacities of 32, 32 and 64k words, 8 bits per word and their minimum sampling time are 100ns. The memories in the first and second recorder are divided into five parts operated at a sampling time of 100ns with the minimum delimited period of 0.5ms, therefore five strokes are stored separately in one flash. The third recorder is prepared for a multiple strokes flash or continuing current struck the lightning rod of the tower top and operated mainly at a sampling time of $2\mu s$. Obtained digital data are transferred to dual 8" floppy disks by a micro-computer.

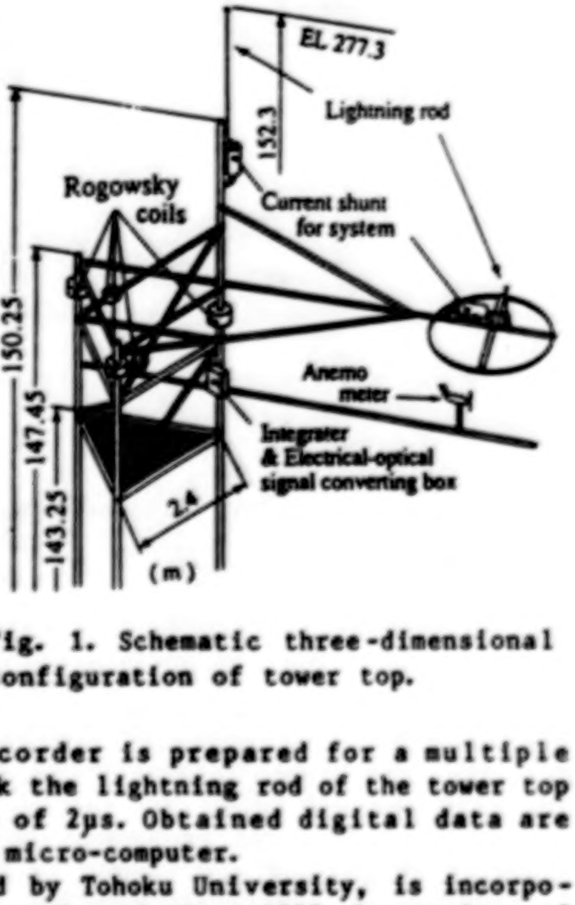

Fig. 1. Schematic three-dimensional configuration of tower top.

The other system, which was developed by Tohoku University, is incorporated with Rogowsky type coils as sensors and used since 1982. It consists of five Rogowsky type coils, passive R-C integrator (time constant is 75ms), optical converters, optical fiber cable and transient recorders controlled by a computer. The coils are installed at five positions as shown in Fig. 1, on three main poles and two braces underneath the tower top. These coils are connected in series to obtain a total lightning current struck the tower.

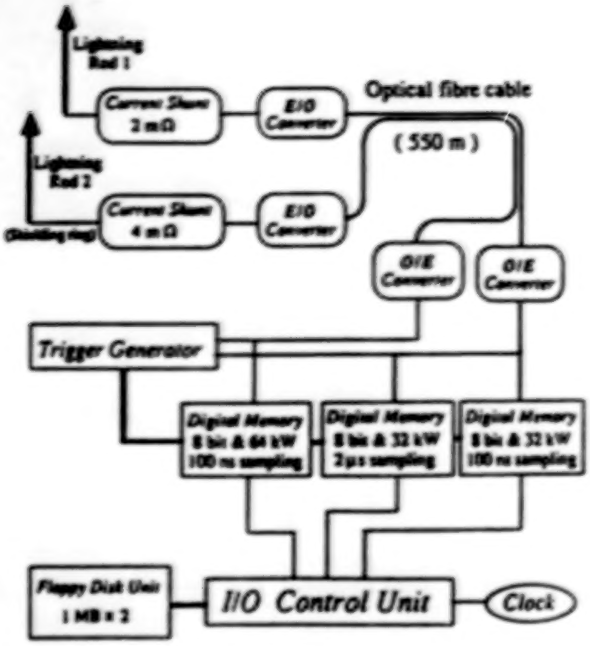
Lightning Rod 1
Lightning Rod 2
(Shielding ring)
Current Shunt 2 mΩ
Current Shunt 4 mΩ
E/O Converter
E/O Converter
Optical fibre cable
(550 m)
O/E Converter
O/E Converter
Trigger Generator
Digital Memory 8 bit & 64 kW 100 ns sampling
Digital Memory 8 bit & 32 kW 2 µs sampling
Digital Memory 8 bit & 32 kW 100 ns sampling
Floppy Disk Unit 1 MB × 2
I/O Control Unit
Clock

Fig. 2. Block diagram of digital recording system for lightning current waveform using two coaxial shunts.

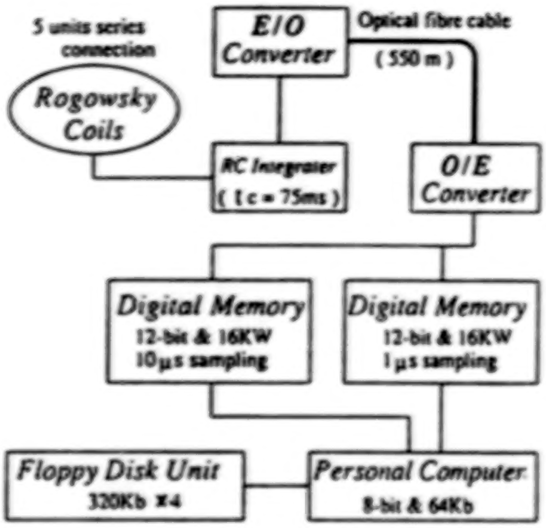
5 units series connection
Rogowsky Coils
E/O Converter
Optical fibre cable
(550 m)
RC Integrater
(I c = 75ms)
O/E Converter
Digital Memory
12-bit & 16KW
10µs sampling
Digital Memory
12-bit & 16KW
1µs sampling
Floppy Disk Unit
320Kb ×4
Personal Computer
8-bit & 64Kb

Fig. 3. Block diagram of digital recording system for lightning current waveform using five Rogowsky coils set.

Figure 3 shows a block diagram of this system. In this system, two kinds of transient recorders were used. They had memory capacities of 4 and 8k word in early stage, each 8 bit per word and their minimum sampling time are 50ns and 1us respectively. Since 1986, these recorders were replaced to that which have memory capacities of 16k word, 12 bit per word and minimum sampling time of 1µs. And they were operated with sampling time 1µs and 10µs respectively. Now, the digital memory of the recorder operated as sampling time 10µs was improved the memory capacity to 64k word, therefore measuring range is 640ms.

3. RESULTS OF LIGHTNING CURRENT MEASUREMENT

Up to date, 121 current records of winter lightning flashes by the co-axial resistive shunt system and 71 records by the Rogowsky coils system were obtained. 145 current waveforms, which the maximum current amplitude exceeded 1 kA, were obtained by the shunt system and/or the coils system and evaluated statistically. It might be thought that the systems recorded the greater part of winter lightning flashes struck the tower. However all waveforms could not be obtained owing to various trouble with measuring instruments, the program error of a computer, the mistakes

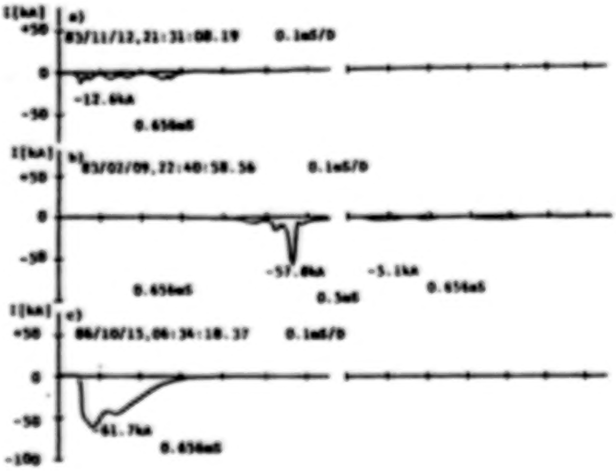

Fig. 4. Example of current oscillogram from negative flashes with single stroke obtained by the shunt system.

in setting the trigger level and the limitation on the recording time.

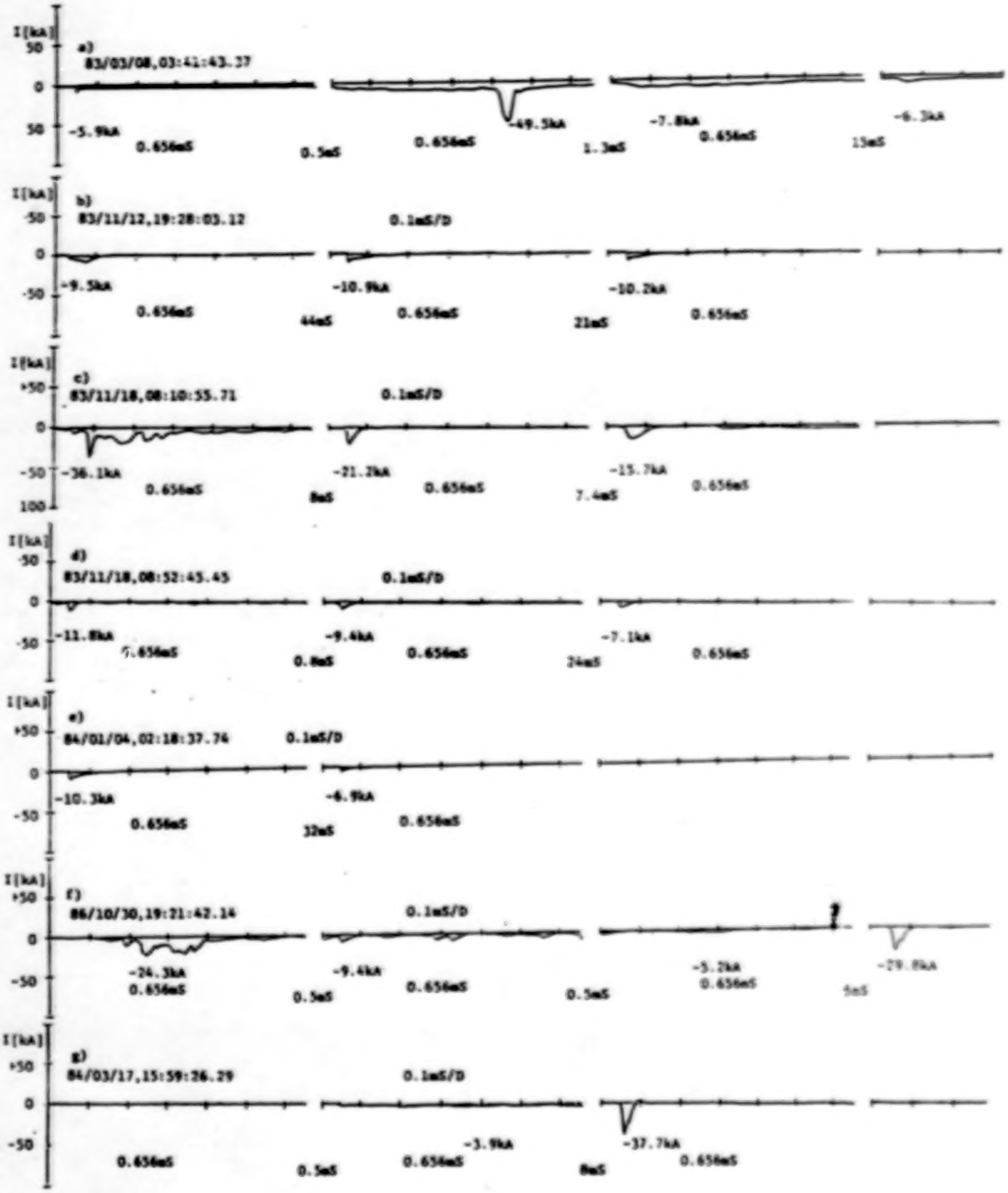

Fig. 5. Example of current oscillogram from negative flashes with multiple strokes obtained by the shunt system.

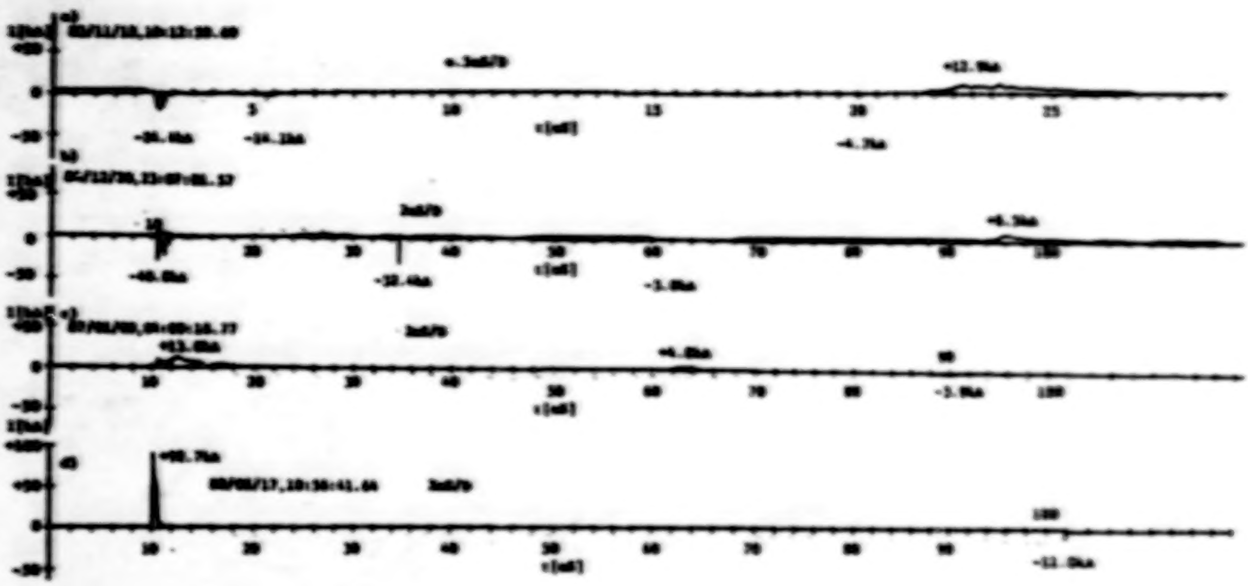

Fig. 6. Example of current oscillogram from positive flashes with multiple strokes obtained by the shunt system.

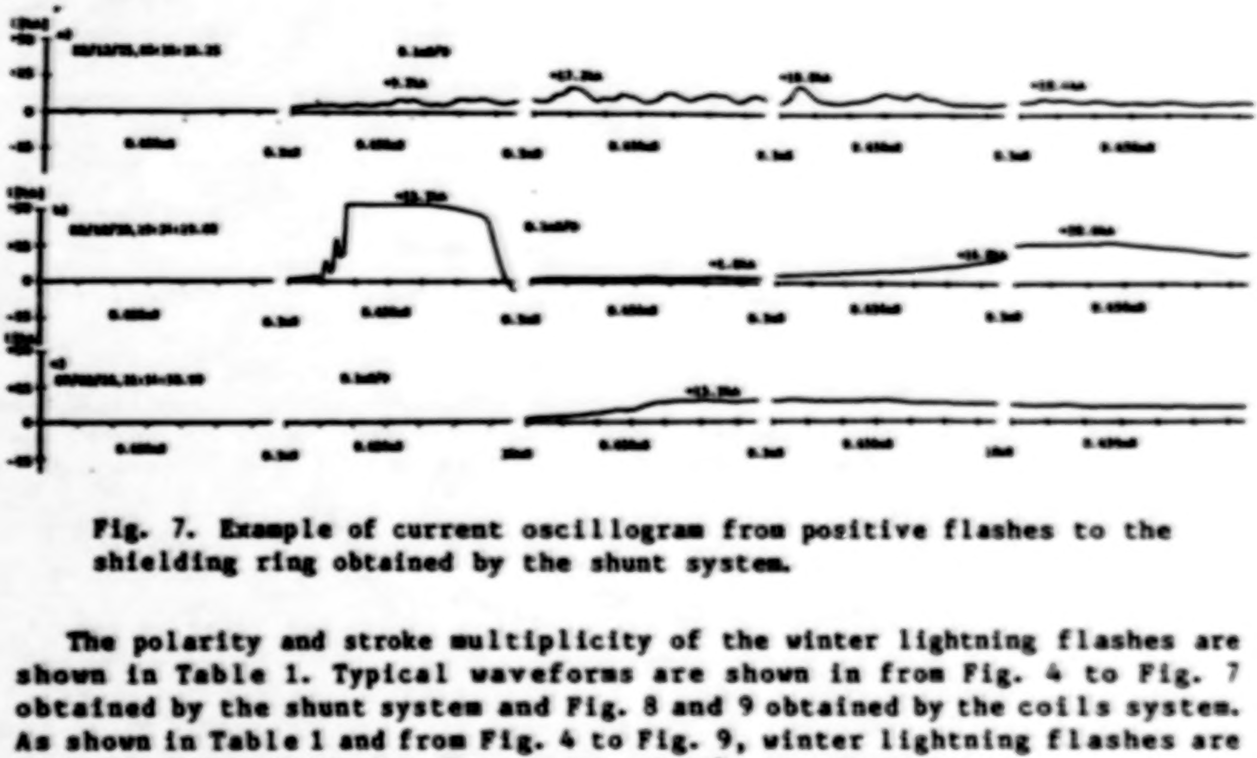

Fig. 7. Example of current oscillogram from positive flashes to the shielding ring obtained by the shunt system.

The polarity and stroke multiplicity of the winter lightning flashes are shown in Table 1. Typical waveforms are shown in from Fig. 4 to Fig. 7 obtained by the shunt system and Fig. 8 and 9 obtained by the coils system. As shown in Table 1 and from Fig. 4 to Fig. 9, winter lightning flashes are classified into following five types and it's percentage is;

(a) negative flash with single stroke (Fig.4)........35.9%
(b) positive flash with single stroke (Fig.9-b)...... 9.7%
(c) negative flash with multiple strokes (Fig.5).....26.9%
(d) positive flash with multiple strokes (Fig.8-a).. 7.6%
(e) bipolar flash with multiple strokes (Fig.6)......20.0%

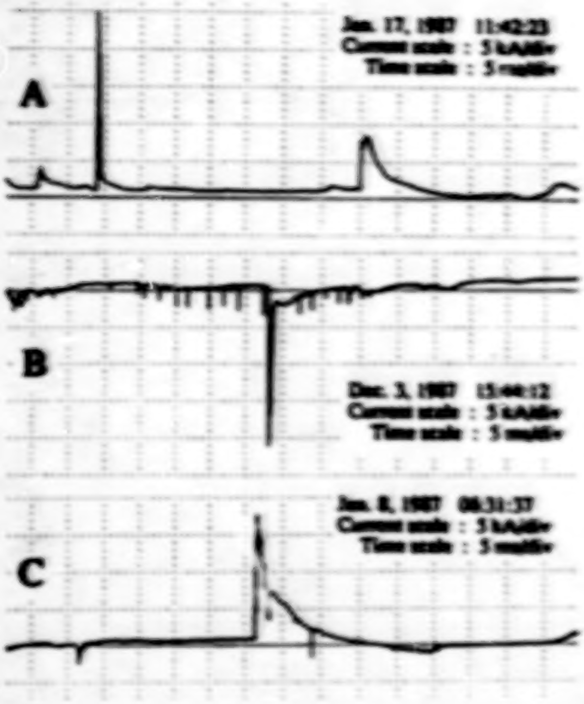

Fig. 8. Example of current oscillogram from multiple stroke flashes obtained by the coils system.

Although the rate of negative flashes is about 63% for winter lightning, it is very lower than that for summer lightning (over 90%). The other hand, the rates of positive flashes and bi-polar flashes are 17.2% and 20% respectively. They are very higher than that of summer lightning.

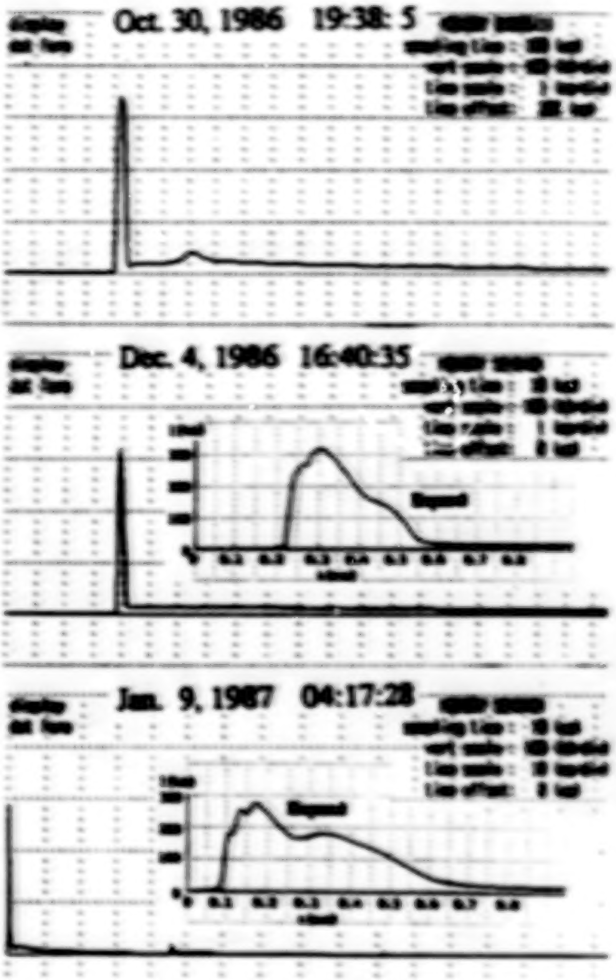

Fig. 9. Example of current oscillogram for superbolt lightning obtained by the coils system.

Figure 7 shows the typical current waveforms flowed through the lightning rod installed on the shield ring. Figure 8 shows some examples of current oscillogram for multiple stroke flashes obtained by the coils system. As

Table 1 Polarity and multiplicity of winter lightning flashes

		Number of Multiple stroke							
		1	2	3	4	5	6	7& >7	Total
Mono-polar Flash	+	14	7	3	0	1	0	0	25
	-	52	6	9	10	9	2	3	91
Bi-polar Flash	+ - -	*	2	5	0	0	0	0	7
	- - +	*	6	4	4	5	1	2	22
Total		66	21	21	14	15	3	5	145
Percentage[%]		45.5	14.5	14.5	9.7	10.3	2.1	3.4	100

known from Fig. 4 to Fig. 9, the current waveforms of each stroke are divided into three types; single peak stroke, double peak stroke and multiple peak stroke. The ratio of the winter lightning flashes with multiple peak stroke as the first stroke is 55.9%. These multiple peak strokes are like those of cloud discharges which have been measured by airplanes[8]. The current begins with small current pulses (hundreds of ampere) which amplitude gradually increases, these pulses are separated by periods of and are superimposed in a continuing current.

Figure 9 shows the current waveforms of very large amplitude lightning flashes obtained by the coils system. This flashes could be the superbolt lightning which were named by Turmann[9]. Those current parameters of superbolt lightning are shown in Table 2.

Table 2 The current parameters of superbolt lightning

Date	I_p[kA]	Q[C]	Action Int.[A^2-s]	dI/dt[A/s]
Oct. 30, 1986	+ 340	+ 330	3.6×10^7	3×10^9
Dec. 04, 1986	+ 320	+ 180	1.5×10^7	1×10^{10}
Jan. 09, 1987	+ 280	- 400	1.5×10^7	1×10^{10}

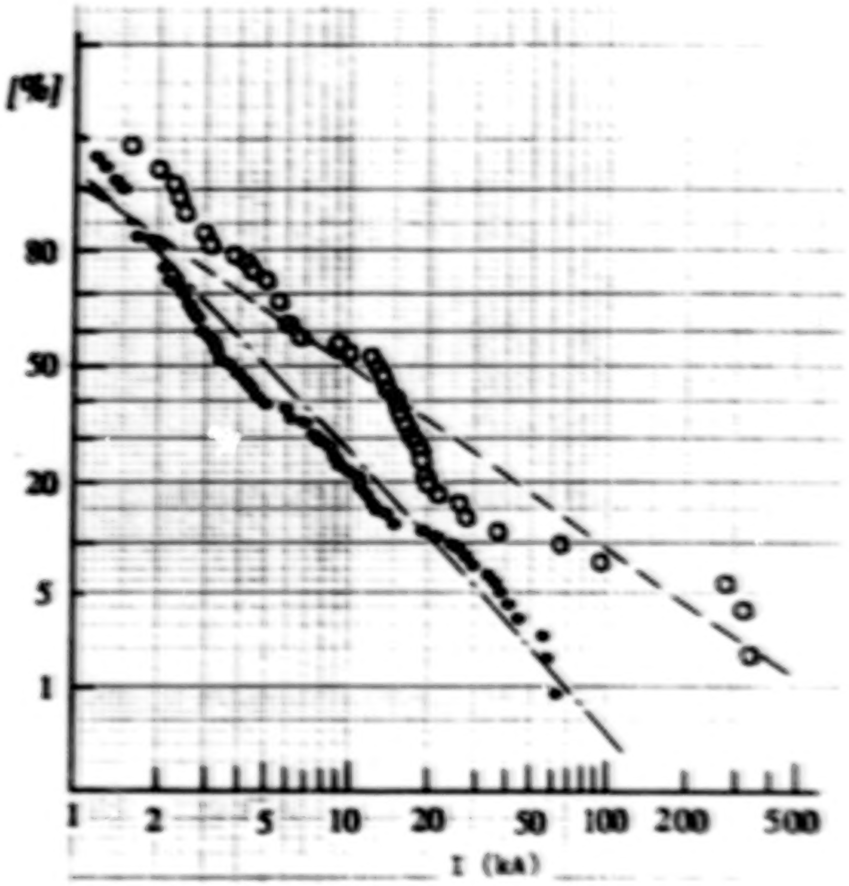

Fig. 10. Cumulative frequency distribution of lightning peak currents.

In observed winter lightning flashes, the maximum peaks of current amplitude are present in successive strokes of 43 flashes out of 79 multiple stroke flashes (54.4%). This is a special feature of winter lightning. Sometimes the strokes with very long duration have been recorded. The current flow last over from several milli second to several ten milli second. Figure 10 shows the cumulative frequency distributions of the positive and negative maximum current amplitudes for winter lightning flashes. From this figure, median peak values of winter lightning flashes are about 5kA for negative flashes and about 10kA for positive flashes. Those values are lower than that of summer flashes. However the 5% values are about 30kA for negative flashes and 170kA for positive flashes, it is higher values significantly.

4. CONCLUSION

Up to date, our measuring systems recorded many current waveforms of winter lightning flashes struck the tower. There are 145 flashes with the amplitude over 1kA obtained by the resistive shunt system and/or by the Rogowsky coils system. From the obtained results for current waveforms, following items as the characteristics of winter lightning current are pointed out;

(1) Winter lightning flashes are classified into five types: both negative and positive flash with single stroke, both negative and positive flash with multiple strokes, and bipolar flash with multiple strokes.

(2) Of 145 flash records, 91 flashes (62.8%) were negative, 25 flashes (17.2%) were positive and 29 flashes (20%) were bipolar. The ratio of positive and bipolar flashes were very higher than those of summer lightning.

(3) Three flashes with very large amplitude exceeding 200kA were recorded.

(4) In the winter lightning flashes, the maximum peaks of lightning currents are present in successive strokes of about a half measured multiple stroke flashes (54.4%).

(5) Sometimes the strokes had very long duration. The current flow last over several milli seconds to several ten milli seconds.

(6) The ratio of winter lightning flashes having multiple peak strokes as the first stroke is 55.9%. These stroks are like those of cloud discharges measured by airplanes.

(7) Median peak values of winter lightning flash are about 5kA for negative flash and 10kA for positive flash. Although those values are lower than that of summer lightning, the 5% values are 30kA for negative and 170kA for positive.

REFERENCE

[1] K.Nakahori, T.Egawa and H.Mitani: Characteristics of winter lightning currents in Hokuriku District, IEEE Trans. Power Apr. Sys., **PAS-101**, 4407-4412 (1982).

[2] K.Berger, R.B.Anderson and H.Kroninger: Parameters of lightning Flashes, Electra, **80**, 23-37 (1975).

[3] E.Garbagnati and G.P.Lo Piparo: Parameter von Blitzstroemen, Electrotech. Z. ETZ-A, **103**, 61-65 (1982).

[4] A.J.Eriksson: Lightning and Tall Structures, Trans. South Africa. IEE, **69** (Pt.8), 238-252 (1978).

[5] Y.Goto, K.Narita and F.Naito: The digital recording system for lightning currents and some results obtained for winter thunderstorms, Res. Lett.

Atmos. Electr. Jpn., 3, 27-32 (1982).

[6] S.Sawada, H.Komuro, Y.Goto and K.Narita: Current measurement of lightning superbolt at the Japan Sea coast, ICOLSE, Oklahoma City, U.S.A., 4B-1, 103-110 (1988).

[7] K.Narita, Y.Goto, H.Komuro and S.Sawada: Bipolar lightning in winter at Maki, Japan, J. Geophys. Res., 94, 13191-13195 (1989).

[8] J.P.Moreau, J.Y.Jouan and F.Issac: Transall 88 Lightning Characterization Program, ICOLSE, Bath, UK, 7A-2 (1989).

[9] B.N.Turmann: Detection of Lightning Superbolt, J. Geophys. Res., 82, 2566 (1977).

Airborne Research Associates
46 Kendal Common Road
Weston, MA 02193
617-899-1834

THUNDERSTORM DETECTION AND WARNING SYSTEM

ATMOSPHERIC POTENTIAL MONITOR

Because thunderclouds must have intense electric fields to produce lightning, it is always possible to obtain advanced warning of lightning by monitoring electric fields or electric potentials. When a thunderstorm approaches a location its electric field, which is 10 to more than 100 times larger than the normally present fair-weather field, causes the ambient field magnitude near the ground to rise from the normal fair-weather value of about 100 V/m to several 1000 V/m in a short period of time depending on the speed of the storm's movement and/or rate of development. In addition, because the atmosphere is always positively charged in fair-weather, but the bottom of thunderclouds are negatively charged, there is a characteristic reversal of field polarity associated with the approach of a thundercloud. The anomalous field reversal and increase in field intensity occurs initially when the storm is about 5 miles away. Similarly, for a storm developing over a location, the field intensity increases and reverses polarity before there is any lightning. These two characteristics of the dc-electric field, which are only caused by thunderstorms, can be identified easily by an observer looking at a display and in addition the system can be set to automatically sound an alarm. A yellow "alert" can be set when the field exceeds 750 V/m and the recommended setting for the red "danger" signal is 1500 V/m. Typical advanced warning of lightning danger varies from a few minutes to tens of minutes.

Another feature of electric field records identifies thunderstorms. If lightning is occurring in the approaching or developing thundercloud it causes abrupt changes in electric field intensity followed by a recovery period of about 10 seconds. The increase in frequency and amplitude of these characteristic discontinuities in the electric field record provides additional evidence of an approaching thundercloud. Thus, monitoring of the electric field provides warning of lightning danger from three different types of variation which are only caused by local thunderclouds. The end of the storm can be identified by the field returning to fair-weather intensity and the lightning spikes no longer occurring. These features are illustrated in the attached figure.

A new type of electric field instrumentation has been developed over the last 3 years for lightning prediction at NASA/Kennedy Space Center. Currently it is being installed at several government laboratories and now is being made available to the public. It has important advantages over the previous method for measuring electric fields with motor driven field mills:

1. It has no moving parts and requires little maintenance compared to rotating machinery.

2. It is unaffected by rain, snow, sand or insects, all of which can influence field mills.

3. The lightweight sensor can be mounted easily on a tall mast; this puts it above much of the blanket of point discharge ions that are emitted from objects on the ground during thunderstorms. This space charge limits the ability of any ground based electric field sensor to accurately measure cloud electric fields which produce lightning. The elevated mounting has been demonstrated to significantly improve monitoring of thunderstorm electric fields.

This new instrumentation measures the atmospheric potential relative to earth at a corona needle sensor on top of a mast which normally is mounted on a tower or roof. The needle is kept in corona at all times by a low power high voltage powersupply. This produces a small cloud of ions around the needle allowing a current to flow. Measurement of the current provides the atmospheric potential. The potential divided by the height of the needle above the ground is proportional to the average electric field between the needle and earth. The potential on top of a tall pole or above a rooftop is more representative of the intensity of cloud electrification than electric field measurements made at ground level.

The accompanying photographs depict the computer terminal and video display of a 2-sensor system and the individual components installed on a tower.

ADVANTAGES OF CORONA INSTRUMENTATION WITH POINTS AT 20 METERS HEIGHT COMPARED TO FIELD MILLS ON THE GROUND

1. NO MOVING PARTS AND SIMPLE CIRCUITRY PROVIDE HIGH RELIABILITY
2. LOWER COST
3. LOWER MAINTENANCE
4. LITTLE OR NO SITE PREPARATION
5. DATA MORE REPRESENTATIVE OF CLOUD ELECTRIFICATION
6. INTERNAL CALIBRATION CONSISTENCY OF CALIBRATION WITHIN AN ARRAY
    - not sensitive to topographic and vegitation differences between sites
    - not as sensitive to form factor variations caused by space charge

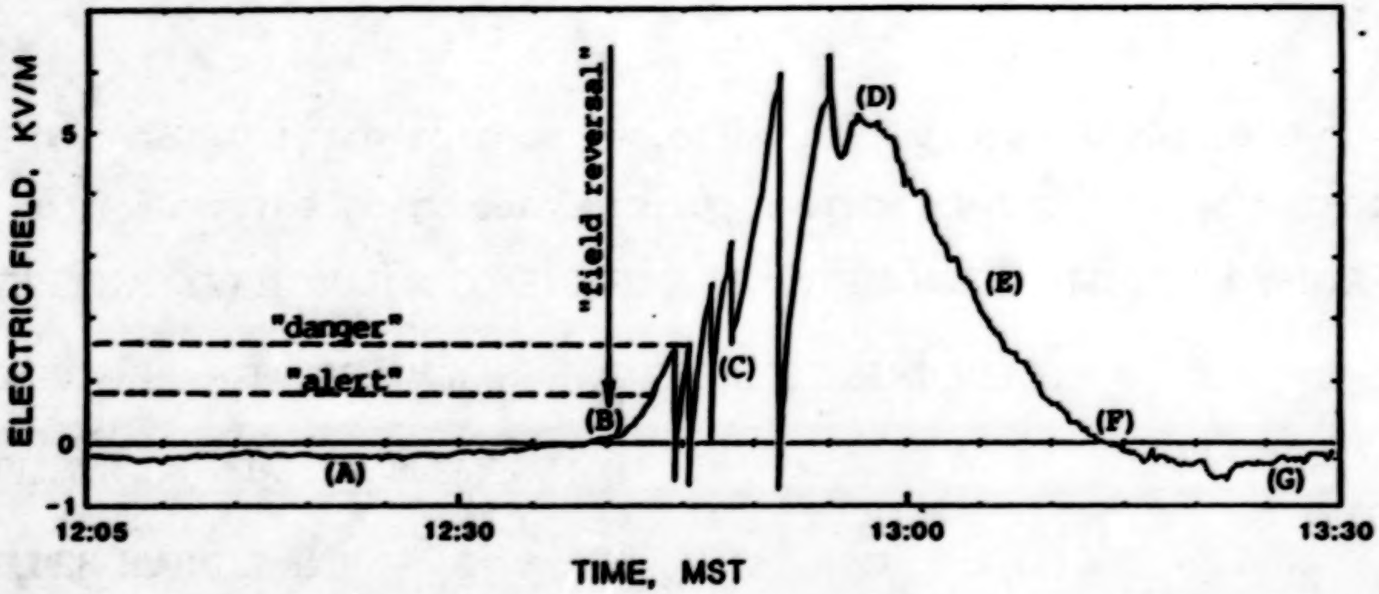

Electric field record made 3 miles from a thunderstorm. Initially there is the relatively smooth typical fair-weather field in the range 100-200 V/m (A). As the storm develops there is a "field reversal" of polarity at (B). Lightning spikes (C) are seen in the developing phase which maximizes at a typical value of about 5 kV/m (D) for ground based sensors. During the rise in field intensity the "alert" and "danger" levels are passed. The declining phase (E) is characterized by no lightning in this instance although this is not always true. At (F) the field crosses zero and reverts to fair-weather polarity and intensity (G).

Atmospheric Potential Components on Tower

Installation at the Nevada Test Site. The sensor mast assembly is on top of a 15 meter fold down tower. The high voltage powersupply unit is below the mast and the electronics unit is at the base of the tower. Landlines carry the signal to the data acquisition system in a nearby building which can be controlled and monitored locally as well as at Lawrence Livermore Laboratory in California via modem and telephone lines.

Electronics Unit

The system electronics (other than the high voltage section) are housed in a weatherproof box at the bottom of the tower. This unit contains an amplifier, powersupplies and differential line driver capable of transmitting the signal tens of miles with minimal noise pickup. Diagnostic test points are within the box for servicing.

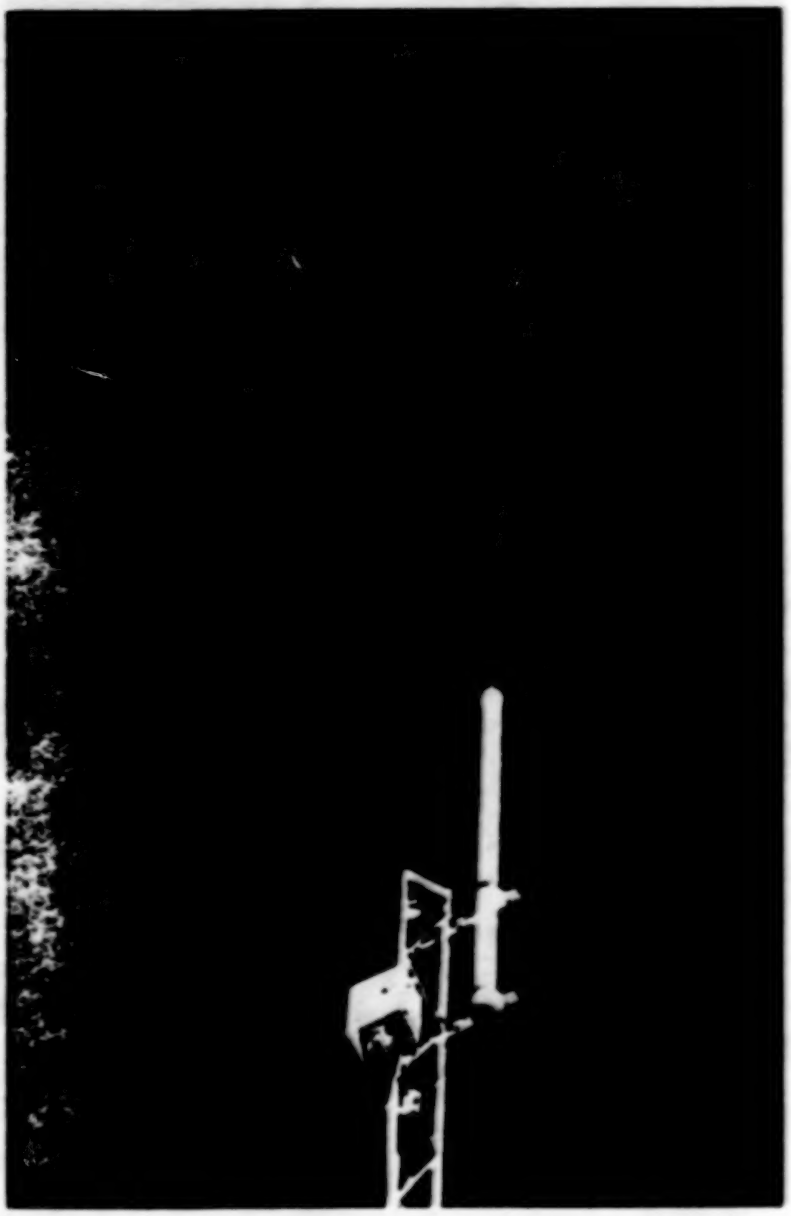

Sensor Mast Assembly

This component consists from top to bottom of a stainless steel corona needle in a removable holder on top of a 2.5 meter long aluminum rod. The base of the removable rod is connected to the top of a high ohm resistor and high voltage coupling capacitor array which is potted inside a 1.5 meter long acrylic tube. The signal comes out the bottom of the array and goes to the electronics unit at the base of the tower. The high voltage powersupply, which keeps the needle active at all times, is housed in a weatherproof container at the base of the mast. This assembly can be mounted on towers of any height or the top of a building.

Thunderstorm Detection and Warning System

Atmospheric Potential Monitor

Display and Control Station

Control and display station for a 2-sensor system developed for Sandia National Laboratories, Tonopah Test Range, Nevada. Alternately, a single potential sensing unit may be mounted on the roof of the building with the control station. An AT computer controls the system and display and stores up to one year's data on hard disc for review and analysis, if desired. The menu controlled software can handle a network with many sensors all of which can be monitored on the CRT. The interval displayed can be adjusted from 1 minute to several days. Modems (shown right of computer) are installed at each sensor and one is at the computer terminal when the signal is carried by wires from sensors that can be more than 10 miles away. The operator selects "alert" and "danger" electric field levels, which might typically be 750 and 1500 V/m respectively; the other warning criterion is a "reversal" of electric field polarity from that existing in fair-weather. The screen changes colors for "alert" and "danger" conditions and associated signals are transmitted to warning devices such as lights and/or buzzers. In case of a power failure, the system restarts automatically or it can be restarted by pushing a button.

ELECTRICAL EMISSIONS OF AIRPLANES FLYING IN ELECTRIFIED CLOUDS AND THEIR EFFECT ON AIRPLANE MEASUREMENTS OF CLOUD ELECTRIC FIELDS

James J. Jones
Langmuir Laboratory for Atmospheric Research
New Mexico Institute of Mining and Technology
Socorro, NM 87801

ABSTRACT

The signature of the cloud electric field components deduced from measurements made with electric field meters carried on airplanes penetrating electrified clouds is often complex, especially when the airplane experiences strong electrical charging. However, simple electric field variations were obtained for penetrations involving severe charging of the airplane on flights over Kennedy Space Center, Florida, on August 19, 1988. During these episodes of severe electrical charging, the airplane typically became negatively charged as it approached a region of negative cloud charge and then became positively charged as it receded from the cloud charge. The charge acquired by the airplane within the cloud was so large that the electric fields at the faces of the mills mounted on the fuselage were as large as for an ambient electric field of 60 to 80 kV m^{-1}. However, the deduced electric field components perpendicular to the direction of flight, to which these mills respond, were only about 5 to 10 kV m^{-1}. The variation of the deduced ambient field component in the direction of flight was anti-symmetric about the charge region for these penetrations.

Analysis of these results suggests that intense plumes of electric charge were emitted from the airplane and that the electric field associated with these plumes overcame the electric field due to the cloud charge at the tail-mounted field mill. As a consequence, the deduced component of the ambient electric field in the direction of flight was severely distorted. These findings emphasize the need for careful evaluation of airplane electric field measurements and of the need for further work on techniques for improving the measurements.

INTRODUCTION

Although Benjamin Franklin demonstrated the electric nature of lightning some 200 years ago, the mechanisms whereby clouds become electrified and lightning is produced are as yet not satisfactorily understood. Despite a fairly clear picture of the large-scale distribution of electric charge in thunderclouds, we have yet to resolve reliably the small-scale structure of charge distributions. In order to differentiate between electrification mechanisms currently advocated, it is important to know where charge first begins to accumulate in a cloud and how it develops and moves within the cloud as electrification progresses. Direct measurement of the free charge on individual precipitation particles has been possible for some years. However, it has not been possible to measure the charge, if any, that resides on cloud particles due to their much smaller size and the consequent smaller maximum charge that an individual particle can carry. Consequently, much effort has been devoted to detecting regions of charge indirectly by measuring their associated electric fields near and within thunderclouds. Since electric field strength varies as the inverse square of the distance from the source charge to the observing site, measurements made outside the clouds do not well resolve small-scale details of charge distributions. Thus it is necessary to make measurements inside clouds in order to gain better resolution of charge distributions.

Over the past five or more decades balloons, rockets and airplanes have been used to measure electric fields outside and inside electrified clouds. Even with perfect measurement of the electric field within clouds, the desired goal of determining charge distributions would be far from accomplished since the variation of $\vec{E}$ along the airborne probe's path is most dependent on charges near the path and in any case does not provide a unique solution for the locations and magnitudes of charges near the path, much less those farther away. Unfortunately, although reliable electric field measurements can be made in clear air, measurements made inside clouds are prone to serious error. This paper addresses a serious limitation, of which researchers need to be especially aware when they use airplanes to measure electric fields inside clouds.

97

OBSERVATIONS

METHOD

Airplanes used for measuring atmospheric electric fields are instrumented with electric field transducers, typically electric field meters of the rotating-shutter variety commonly known as electric field mills, or "field mills," although other devices have been used as well. There are two solvable problems which arise when measuring electric fields with airplanes. The first is that the airplane typically becomes electrically charged, resulting in the electric field of the airplane charge being superimposed on the ambient atmospheric field to be measured. The second is that the airplane itself distorts the ambient field. By artificially charging the airplane when the ambient field is very small it is possible to determine the response of the transducers to the electric field of the charged airplane. The second problem imposes the need to correct for the distortion of the electric field components deduced from the field mill data. Several methods have been devised to calibrate the transducer response so that the undistorted ambient field may be deduced. It has been shown that when the calibration has been done correctly the electric fields deduced from measurements made in clear air are consistent with those of the field sources within nearby clouds [1]. The reliability of measurements made inside clouds is not so easily demonstrated and indeed the deduced electric fields may be seriously in error as will be demonstrated by this paper.

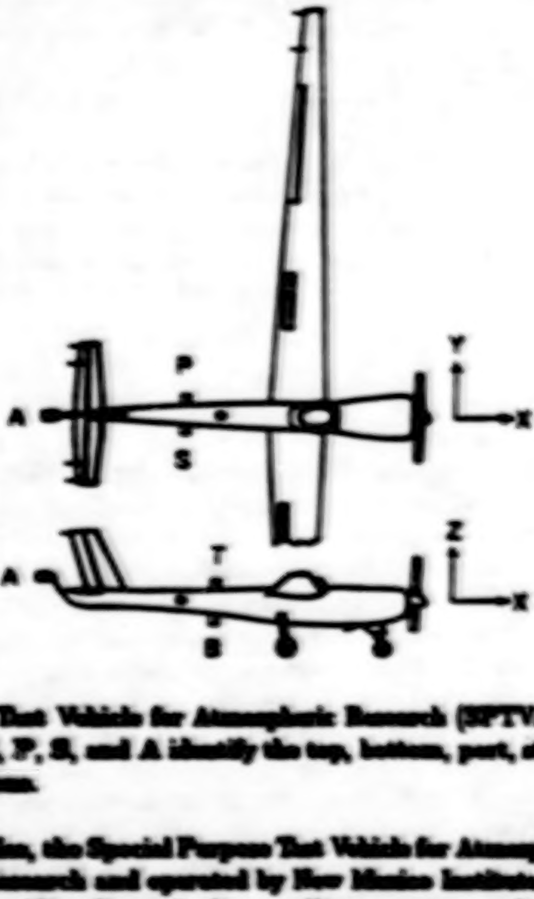

Figure 1: The Special Purpose Test Vehicle for Atmospheric Research (SPTVAR) and the airplane coordinate system. The letters T, B, P, S, and A identify the top, bottom, port, starboard, and aft field mills which face in coordinate directions.

The airplane used in our studies, the Special Purpose Test Vehicle for Atmospheric Research (SPTVAR), owned by The Office of Naval Research and operated by New Mexico Institute of Mining and Technology (NMIMT), is shown in Fig. 1. Also shown is the coordinate system used to define the electric field component directions relative to the airplane. Our convention for the sign of the electric field is that the tip of the electric field vector points toward negative charge. Often the component of the electric field most important for locating charge regions, especially if the airplane flies directly through the charge region, is the component along the airplane fuselage, E_X.

Figure 2 shows the variation of E_X as SPTVAR flew through a small initial charge high in a cloud over the Magdalena Mountains in central New Mexico on August 3, 1984, just as the cloud began to electrify. The bipolar variation shown in this figure is consistent with SPTVAR having passed through a spherical

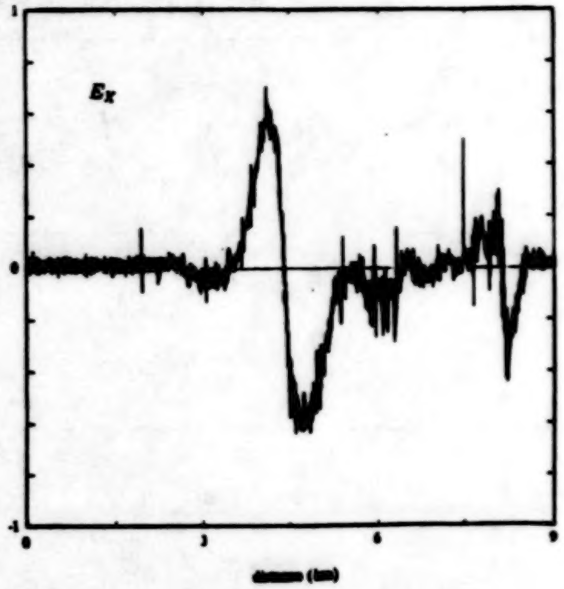

Figure 2: E_X deduced for penetration of small region of negative charge in a cloud over central New Mexico on August 3, 1984.

region about 400 m across containing some 0.01 C of negative charge. Although SPTVAR was somewhat charged by collisions with cloud particles during this penetration of the cloud, the net charge acquired was small compared to charges often acquired when flying through clouds in the presence of strong electric fields.

EXAMPLE CLOUD PENETRATION: AUGUST 19, 1989

Let us next consider the E_X variation deduced along the flight path from field mill measurements made when SPTVAR flew through a cloud over Kennedy Space Center on August 19, 1989. The E_X variation shown in Fig. 3 was deduced for the third of four passes through the cloud base at an altitude of 3.7 km (12,000 ft) during the 13-minute interval 1648–1701 UT.

The variation of E_X over the first 4 km of flight path shown in Fig. 3 closely resembles that for the first 4.5 km of Fig. 2, while the final 2.5 km resembles the last 5 km of Fig. 2. We might infer from this that SPTVAR passed through a negative charge early in the penetration (at the 3.4-km point in the plot) and another one late in the pass (at 6.7 km). The variation of E_X between about 5 and 5.75 km in Fig. 3 suggests another region of negative charge through which SPTVAR passed. This interpretation may be tested by assuming three uniform negatively charged spherical regions along the flight path, the diameter and total charge of each chosen to simulate the negative slope portions of the E_X curve in Fig. 3. Figure 4 shows E_X calculated from such a triple-charge arrangement plotted together with the deduced cloud E_X on the same graph. This comparison shows that both the first negative and last positive peak of the measured E_X are inconsistent with such a charge distribution.

Another parameter that may be deduced from the field mill data is the strength of the electric field due to charge on the airplane. Since all the field mills respond to the superposition of this field and the ambient atmospheric field, determining the ambient field components amounts in part to separating the two contributions. In Fig. 5 the average electric field at the mills on the top and bottom of SPTVAR, E_q, is shown plotted on the same graph as E_X. The magnitude of E_q has been multiplied by 0.64 in order to emphasize the great similarity between the shape of the two E_q peaks and the corresponding peaks in E_X. This similarity suggests some relation between E_X and E_q. Although the separation of the contributions to the field mill measurements due to airplane charge from those due to the ambient field is determined from airplane charges smaller than those acquired by SPTVAR during this penetration, the linearity of the field mills as electric field transducers and the linear nature of electrostatic fields give us confidence that the two largest peaks in E_X are not due to incomplete separation of E_X and E_q.

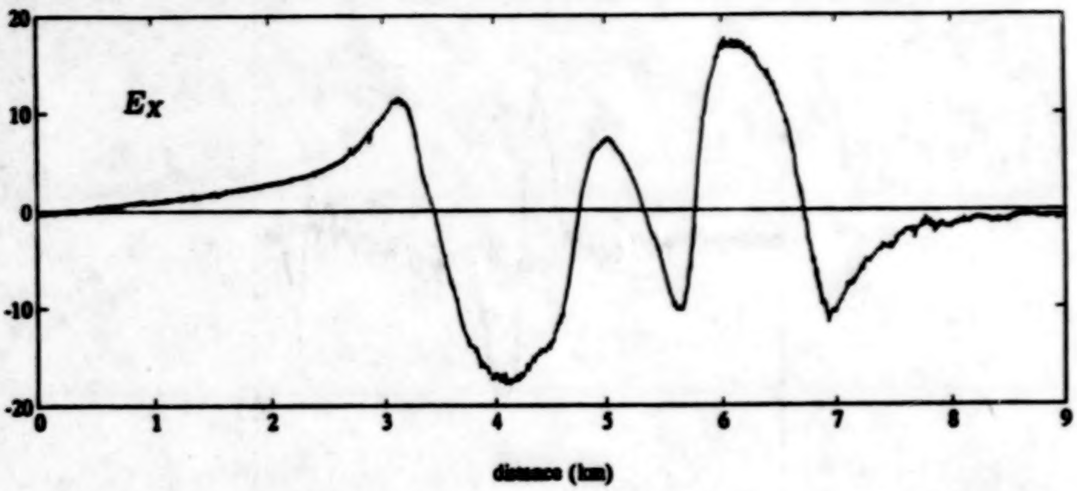

Figure 3: E_X deduced for a pass through the base of a cloud over Kennedy Space Center on August 19, 1989.

Typically, charging of SPTVAR results from interaction with cloud particles [2]. During this penetration, measurements with a liquid cloud water probe (of the type described by King *et al.* [3]) indicate a lack of significant cloud water droplets while data from the ice particle detector on SPTVAR [4] show that ice was also not present along the SPTVAR path through the cloud. What then explains the large airplane charge responsible for such a large E_q, much larger than normally experienced during flight through large liquid water concentrations? During the four penetrations between 1648 and 1701 UT the pilot reported rain from the cloud. At 1658 UT he reported that the lower part of the cloud (through which he had just flown) had mostly fallen away as rain. This indicates that rain was probably present when the large charging of SPTVAR occurred, although there are no direct measurements (other than sporadic noise in the liquid water signal) that show the extent of the rain shaft along the SPTVAR flight path. In the absence of electric fields SPTVAR does not become significantly charged during flight through rain. However, when the X component of the ambient field is strong it is possible that an induction process acting during collisions with rain drops could be responsible for the charging of the airplane.

Proposed correction of the distortions in E_Y and E_X. In order to investigate this possibility we consider the lateral or Y component of the deduced ambient field. Figure 6 is a plot of E_Y with E_q, reduced to a similar scale, shown for comparison. Two segments of the E_Y curve depart abruptly from what otherwise would be a single negative peak. Such sudden variations in E_Y are not realistic for diffuse cloud-charge distributions. Furthermore these two segments are coincident with the two peaks in E_q. Since we are confident of the deduced field components when the airplane is in clear air and carrying little or no charge, we place more confidence in the value of E_Y deduced before, between and after the occurrences of strong airplane charging. The dashed lines connecting the E_Y values during these time intervals indicate a more probable single peak variation of E_Y during this penetration. If this conclusion is correct, the deduced E_Y indicates a single region of charge, and does not support a triplet of charge regions.

If indeed there were only one region of charge, the deduced E_X should resemble Fig. 1. Since E_Y was apparently incorrectly deduced during the periods of strong airplane charging, the deduced E_X was probably also incorrect for those times. Figure 7 shows how we may connect the portions of the E_X curve for the periods that the airplane charge was small to obtain an E_X variation similar to Fig. 1, consistent with a single region of negative charge.

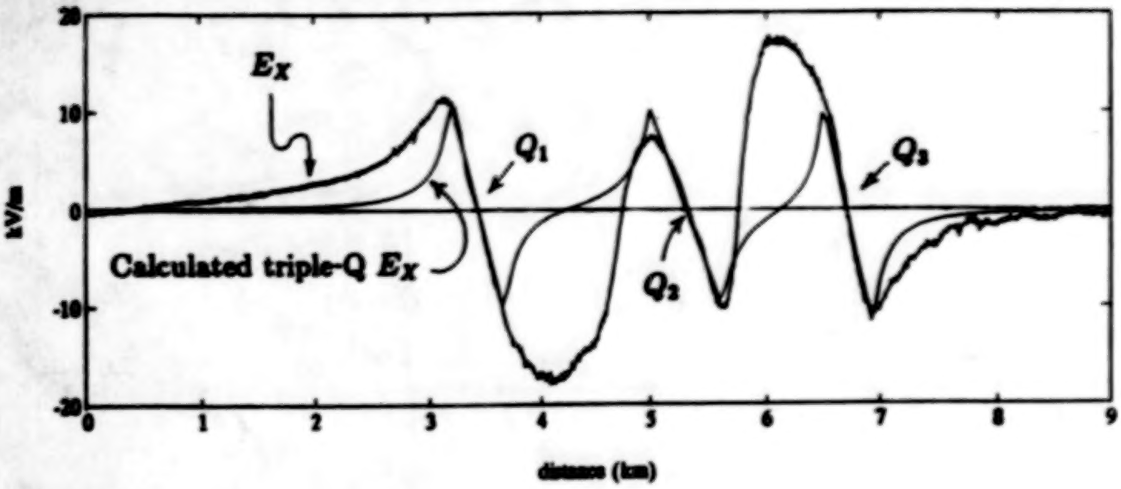

Figure 4: E_X of Fig. 3 and E_X calculated for a series of three negative charges chosen to simulate the cloud E_X. Charges used were $Q_1 = -7$C, $Q_2 = -10.8$C, and $Q_3 = -5.9$C.

DISCUSSION

MODEL OF AIRPLANE CHARGING PROCESS

The resulting simple bipolar E_X variation for the August 19, 1989 example, if correct, provides a way to understand the airplane charging events during this penetration. The modified E_X curve indicates a region of negative charge extending for about 1.5 km along the SPTVAR path. Both E_X and E_q are anti-symmetric about the midpoint of the charge region, the 5.7-km point in the plot. The magnitude of E_q is proportional to that of E_X, although of opposite polarity, suggesting still that E_q and E_X were somehow directly related.

For the following discussion the dashed line in Fig. 7 will be assumed to be a good representation of the actual ambient E_X due to the charge in the cloud. Furthermore, the discussion will be confined to the first 5.7 km of the flight path shown in Fig. 1, that is, up until SPTVAR was at or near the center of the charge region at which point E_X first became negative.

Consider a small surface area, A, on the leading edge of the SPTVAR wing and a falling raindrop, D, just in front of and about to be impacted by area A. Since E_X was positive, a positive surface charge was induced on A while the raindrop, although having zero net charge, was polarized with excess positive charge on the side away from SPTVAR and excess negative charge on the side facing SPTVAR. At the instant of impact the negative charge on the near side of the raindrop was absorbed by SPTVAR while the excess positive charge on the far side was repelled by the excess positive surface charge on A. It is likely that some of the excess positive charge on the far side of D remained with any splash that was carried away in the air stream. In this way SPTVAR began to acquire a net negative charge. The process is shown diagrammatically in Fig. 8.

Once SPTVAR became negatively charged, the field experienced by subsequent raindrops about to be impacted by area A was modified due to the presence of the net charge on SPTVAR. The field at the rain drop may be separated into the locally distorted E_X of the cloud charge and a local field E_q due to the net excess charge residing on SPTVAR. Whereas E_X was positive, E_q due to the negative airplane charge was negative, so that the total field at the raindrop, $E_D = E_X + E_q$, was less than E_X. Had E_X increased from zero in a single step and then remained constant, the rate at which negative charge was acquired by area A would have begun at some appropriate value and then decayed as the surface charge on A asymptotically approached the value for which the magnitude of E_q was the same as that of E_X so that E_D was zero. However, E_X increased steadily until it peaked at about 35 kV m^{-1}. Thus, although E_q was increasing, E_X remained always larger in magnitude so that E_D was always positive and SPTVAR continued to acquire yet more negative charge.

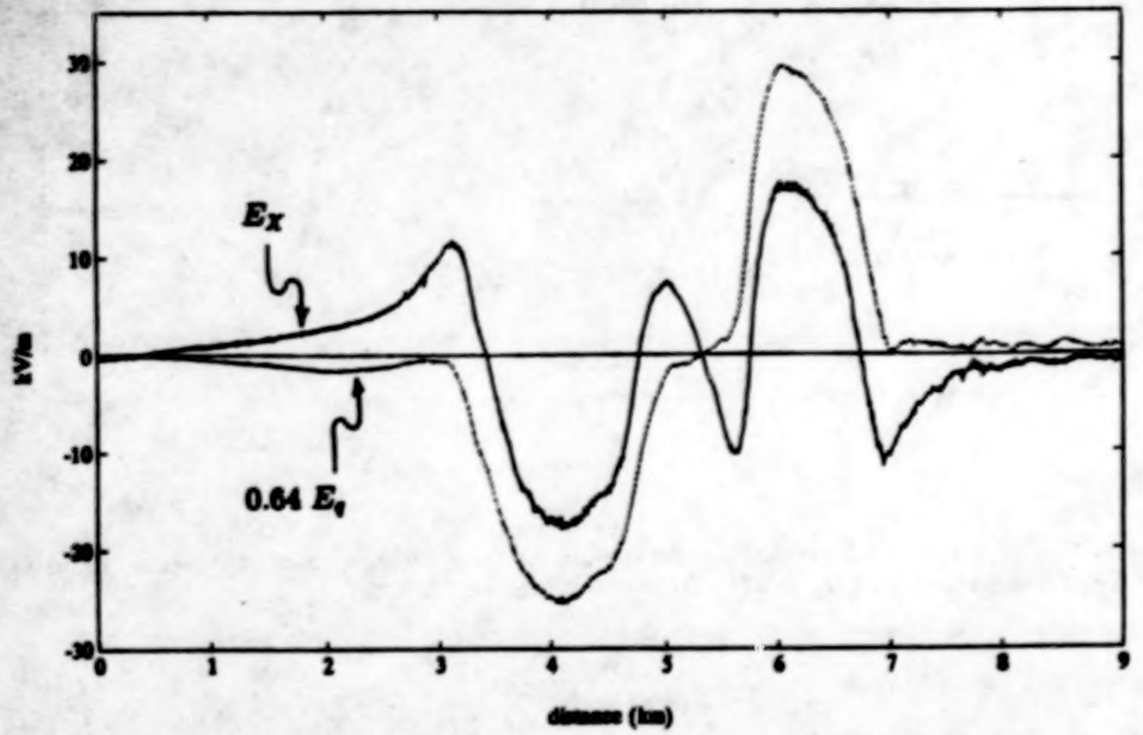

Figure 5: E_q, the mean electric field due to airplane charge at the top and bottom mills on SPTVAR, scaled by 0.64, and plotted with the cloud E_X of Fig. 3.

Once E_X had peaked at 35 kV m^{-1} and had begun to decrease, however, $|E_X|$ became less than $|E_q|$ so that E_D changed sign, becoming negative. Positive charge was then on the near side of the polarized raindrops about to be impacted by area A and SPTVAR acquired positive charge due to raindrop impacts. This reduced the negative airplane charge so that the airplane charge declined along with E_X as SPTVAR neared the center of the charge region.

The charging of SPTVAR was not as simple as described above. It has been demonstrated that once an aircraft has acquired sufficient charge it begins to shed some of that charge due to the strong electric fields that develop at sharp points on the airplane surface [2]. Corona develops at the sharp points and plumes of charge are thereby released into the air stream behind the airplane. For the first part of the penetration being discussed here, E_X and E_q were both positive at rear-facing points on SPTVAR so that E_X enhanced the field, E_q, due to the airplane charge. The resulting charge plumes, emitted mostly from rear-facing edges and corners of the tail assembly and wings, removed negative charge from the negatively charged SPTVAR thereby damping the rate at which the airplane charge increased due to the inductive raindrop process occurring on the leading surfaces of SPTVAR as E_X increased. Once E_X began to decrease, however, the raindrop process caused SPTVAR to acquire positive charge as described above so that it aided the plumes in removing the excess negative charge on SPTVAR, and the airplane charge rapidly decreased toward zero as seen in Fig. 7. Since E_q continued to increase as long as E_X was increasing, it appears that the raindrop charging process was able to generate a charging current that was consistently greater than the current carried into in the airstream behind SPTVAR by the charge plumes.

DISTORTION OF E_X DUE TO FIELD OF CHARGE PLUMES

In addition to providing an explanation for the charging of SPTVAR that occurred, the model developed above can also account for the distortion of E_X deduced from the field mill measurements. Since charge plumes were probably emitted from discharge wicks and sharp corners of the tail assembly near the aft mill, the field measured by that mill is likely to have included a contribution from the electric field associated with the plumes. Thus the electric field at the aft mill may be considered to have been the combination of E_X due to the cloud, E_q due to the airplane charge, and a field, E_P, due to the plumes. Thus

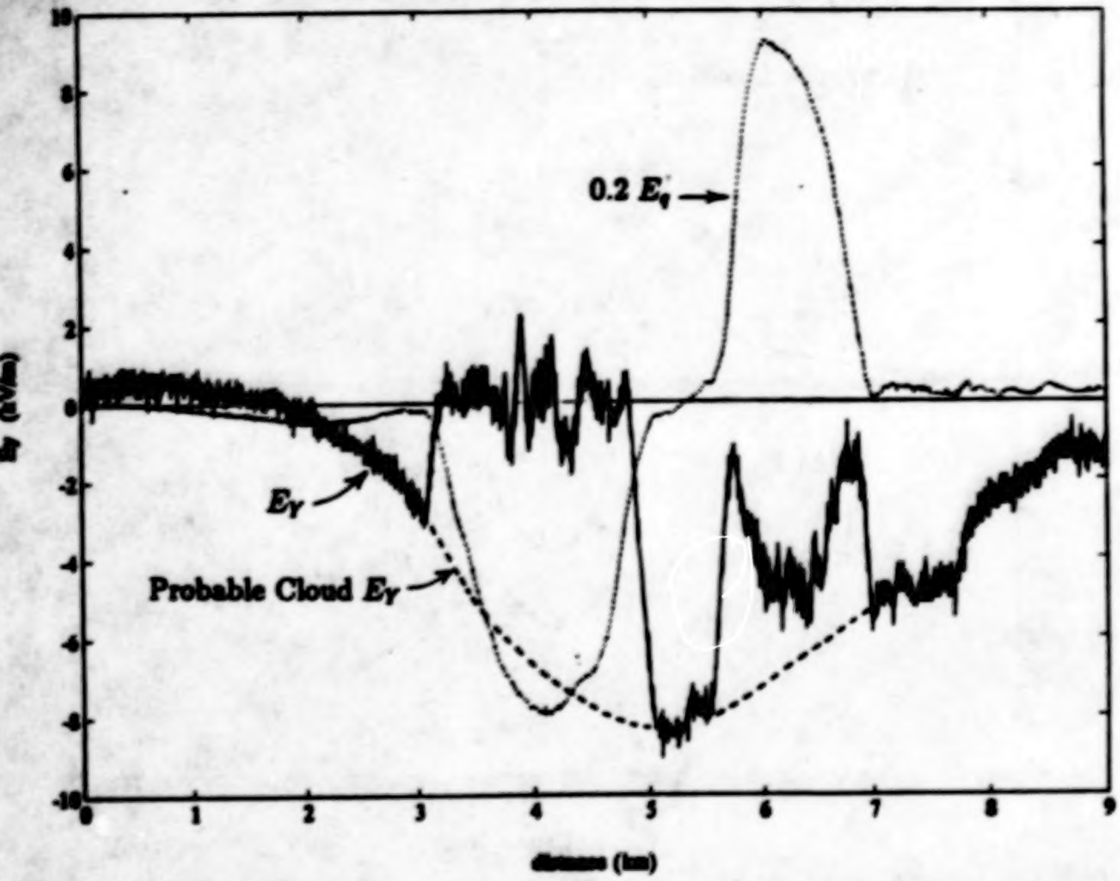

Figure 8: E_Y deduced for the Aug. 19, 1989 pass and E_q plotted together. The dashed line spanning the sudden depressed regions of E_Y are believed to better represent the ambient E_Y of the cloud during the periods of large SPTVAR charge.

$E_{\text{aft mill}} \simeq E_{X(\text{aft mill})} + E_{Q(\text{aft mill})} + E_{P(\text{aft mill})}$. The determination of E_X amounts to subtracting $E_{q(\text{aft mill})}$ from $E_{\text{aft mill}}$ so that the result is independent of the charge on SPTVAR. Consequently the value determined for E_X is actually $E_X \simeq E_{X(\text{aft mill})} + E_{P(\text{aft mill})}$. Since $E_{P(\text{aft mill})}$ was negative whereas $E_{X(\text{aft mill})}$ was positive, the sudden reversal in slope of E_X just past the 3-km point in Figs. 3 and 7 and the subsequent negative peak suggest that, once plumes began to be emitted, the near proximity of at least some of the plumes to the aft mill allowed the magnitude of $E_{P(\text{aft mill})}$ to exceed that of $E_{X(\text{aft mill})}$.

THE SECOND PART OF THE PENETRATION

E_X and E_q were both anti-symmetric about the midpoint of the charge region at 5.7 km in Fig. 5. Furthermore, SPTVAR's direction of flight relative to the charge region changed after it passed the midpoint of the charge region. Thus the behavior of all the parameters of the model developed here was similar before and after the midpoint, except for a reversal of sign. Under these conditions all the same processes acted with reversed polarity during the period of strong positive charging that occurred as SPTVAR flew out of and away from the charge region. Thus all the features of the measurements made with SPTVAR during this penetration can be explained by the model developed above.

QUANTITATIVE ASSESSENT

Since the arguments presented have been of a qualitative nature rather than quantitative it is useful to make some numerical estimates to assess the reasonableness of the model. The methods developed by Jones [2] allow the actual charge on SPTVAR to be estimated for the time when E_q reached its maximum negative value of -30 kV m^{-1}. The value determined is about -420 μC. According to the model, the difference between the positive peak shown as a dashed line in Fig. 7 and the negative peak in E_X actually

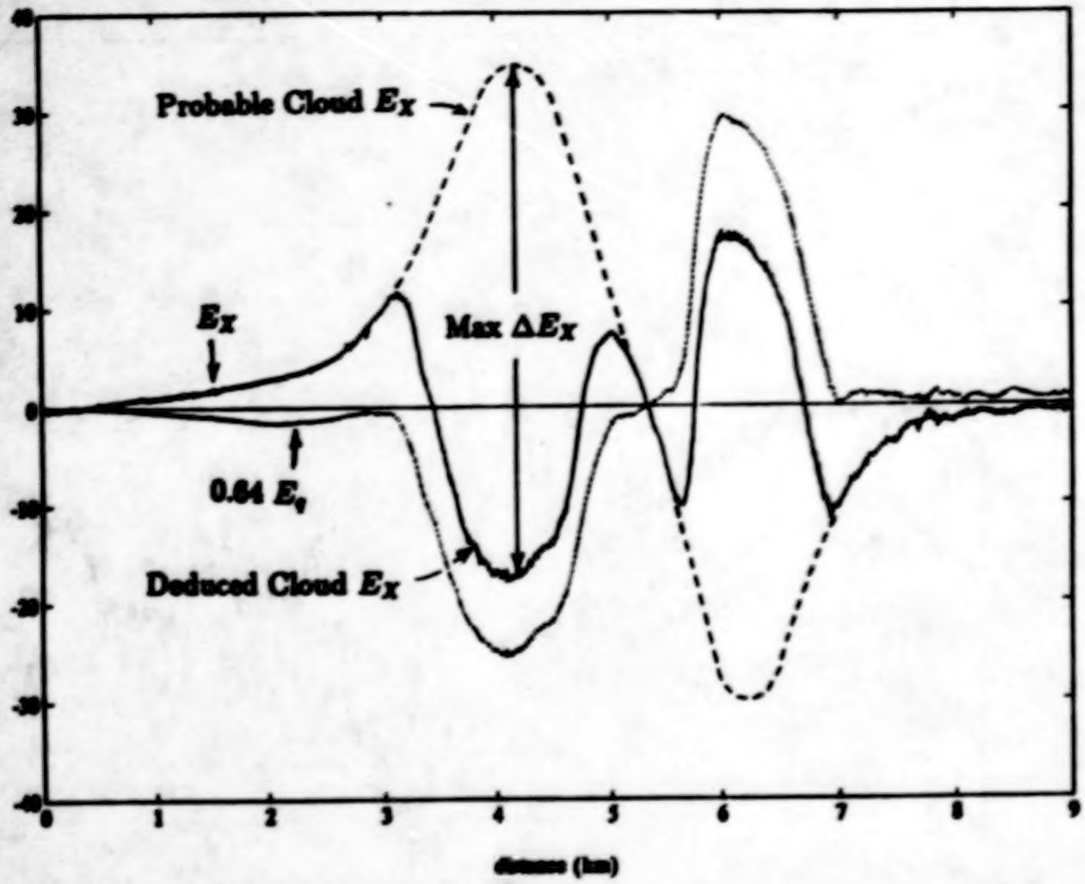

Figure 7: Fig. 5 with a dashed line which is believed to better represent the true ambient cloud E_X during the periods of large SPTVAR charge.

deduced directly from the field mill measurements is just the electric field of the charge plumes at the aft mill. The difference, ΔE_X, shown in Fig. 7, is $\simeq$ 50 kV m^{-1}. The tips of the vertical and horizontal control surfaces are all about 1.5 m from the aft mill. Three semi-infinite line charges beginning at these points would have to have a total charge density of about 90 μC m^{-1} to produce the estimated ΔE_X at the time of the E_X peak. Since SPTVAR's airspeed was about 53 m s^{-1} at that time, the plumes were carrying a current of about 48 μA. Subsequent to the peak in E_q most of the -420 μC charge on SPTVAR was dissipated in about 10 s. Since the charge declined approximately linearly, the charge removed by the plumes may be estimated as a mean current of about 24 μA lasting about 10 s, or about 240 μC. During this time the raindrop process was also reducing the airplane charge since it was causing SPTVAR to acquire positive charge. Thus the remaining approximately -180 μC was apparently neutralized by raindrop collisions.

CONCLUSIONS AND RECOMMENDATIONS

The X component of the ambient electric field determined for this cloud penetration was severely distorted due to the large charge on the airplane and the resultant emission of intense plumes of charge behind the airplane. The effect of the field due to the plumes on the aft mill was not corrected for, thereby causing the deduced E_X to be distorted. Since the field due to plumes may not be easily determined independently, measurements made inside clouds must be considered suspect when an airplane is strongly charged, especially if field-mill locations on the airplane are near sources of such plumes. In the future, airplanes instrumented with field mills should have the mills mounted well forward of any probable charge plume sources. It would also be of interest to measure the currents flowing from the various extremities of the aircraft.

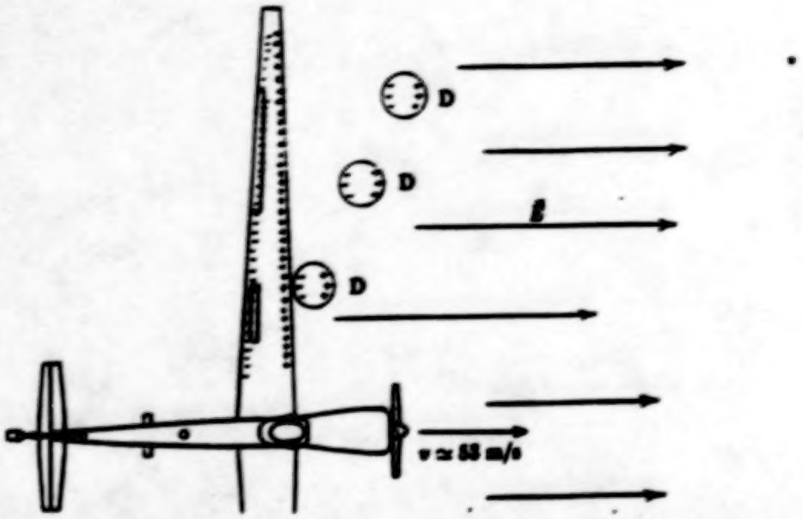

Figure 8: The inductive raindrop process believed to have charged SPTVAR during the 19 August 1989 cloud base pass. Rain drops, *D*, are polarized by the electric field, as is the airplane. Upon impact the drops deposit an excess negative charge on SPTVAR.

ACKNOWLEDGMENTS

I wish to thank all the people who have participated in the work involving the SPTVAR, especially my colleagues W. P. Winn and C. B. Moore for all they have done to make the SPTVAR program possible; pilots J. W. Bullock and P. Fleischhacker; and Langmuir Laboratory Coordinator Sandy Kieft. Many NASA and USAF personnel contributed to the success of the research flight operations in Florida. I especially thank Hugh Christian; Col. John Madura; Captain Tom Strange and the forecasters of the 2nd Weather Squadron, Launa Maier and Mark Wheeler, for their enthusiastic help. Various other personnel at Patrick AFB and Kennedy Space Center contributed to the success of the project. I thank the Federal Aviation Administration Air Route Traffic Control Center controllers in Miami, Florida, and Albuquerque, New Mexico, for coordinating airplane activities. I thank NASA and the Space Division of the U. S. Air Force for support of the work in Florida under NASA grant NAG8-751. Thanks also to James Hughes and the Office of Naval Research and Ronald Taylor and William Beasley of the U. S. National Science Foundation for their sincere interest and support. Some of the work was supported by NSF funds which came from grants ATM-8205468, 8218621, 8600526 and 8919697.

REFERENCES

1. Winn, W. P., F. Han, J. J. Jones, D. J. Raymond, and T. C. Marshall, Thunderstorm with anomalous charge, *Proceedings, Eighth International Conference on Atmospheric Electricity*, Uppsala, Sweden, 1988.

2. Jones, J. J. Electric charge acquired by airplanes penetrating thunderstorms. *J. Geophys. Research - Atmospheres 95*, 16589–16599, 1990.

3. King, W. D., D. A. Parkin and R. J. Handsworth. A hot-wire liquid water device having fully calculable response characteristics, *J. Appl. Met. 17(12)*, 1978.

4. Jones, J. J., C. Grotbeck and B. Vonnegut. Airplane instrument to detect ice particles. *J. Atmos. Oceanic Tech. 6*, 545–551, 1989.

E AND DE/DT WAVESHAPES FOR NARROW BIPOLAR PULSES IN INTRACLOUD LIGHTNING

P.J. Medelius, E.M. Thomson and J.S. Pierce

Department of Electrical Engineering
University of Florida, Gainesville, Florida 32611

ABSTRACT

Wideband electric field and dE/dt waveforms were recorded and digitized at a 100 MS/s rate at Kennedy Space Center during the summer and fall of 1989. These waveforms have been combined to produce composite electric fields with an effective bandwidth of 3 Hz to 50 MHz. Bipolar electric field pulses are characterized in terms of their E and dE/dt waveshapes. Half width mean durations were found to be 1.83 and 3.64 microseconds for negative and positive bipolar pulses respectively. 20 of 30 of these pulses were found to occur independently of any other lightning activity. Analysis of the frequency content of these pulses as a function of time shows that radiation at different frequencies peak at different times. In addition to the initial peak and subsequent overshoot in the composite E waveshape, secondary humps following the initial peak are characterized according to their time of occurrence within the pulse. 156 narrow negative bipolar pulses and 10 positive narrow bipolar pulses are analyzed. dE/dt signatures range from impulsive variations lasting several microseconds both before and after the initial peak of the electric field pulse, to smoother variations closely associated with peak.

INTRODUCTION

Submicrosecond-scale pulses have been previously reported and characterized by several researchers. Krider et al. [1] and Weidman and Krider [2] recorded large-amplitude intracloud lightning pulses along with HF radiation at different frequencies. They found that the shape of the pulses tends to be bipolar, superimposed with very fast unipolar pulses. They noted that large pulses can occur either as a precursor in a cloud-to-ground flash, or in the initial part of an isolated cloud discharge. The initial polarity of the pulses tended to be positive when they were precursors of a cloud-to-ground discharge, and negative when they were a part of an intracloud discharge. Their electric field antenna system had a 500 Hz to 2 MHz bandwidth and electric fields were digitized at a 10 MS/s rate. Le Vine [3] identified bipolar pulses that produced strong HF radiation. They found that these cloud pulses produced stronger RF radiation than return strokes. Their recorded pulses consisted of an initial negative-going pulse followed by a positive-going overshoot. The duration of the negative part was in the order of ten microseconds, while the total duration was 20 microseconds. These fast pulses appeared to be relatively isolated and infrequent. They concluded that this type of pulse could be an occasional, very fast (~10^8m/s) K change. Cooray and Lundquist [4] presented statistical data on cloud pulses similar to those observed by Le Vine [3]. These pulses had a smooth rise to peak and a half-width of about ten microseconds and their initial polarity was opposite to that of return strokes that lower negative charge, that is, with the same initial polarity as the negative pulses reported by Krider et al. [1] and Le Vine [3]. The total duration of the pulses was about 70 microseconds. The mean risetime from zero to peak in the order of 4 microseconds. Bils et al. [5] presented electric field cloud pulses recorded on analog magnetic tape with an upper 3 dB response of 500 kHz. Because of the reduced bandwidth, pulses shorter than a microsecond were significantly attenuated. Only negative-polarity pulses were reported. Since the analog tape records were relatively noisy, only pulses 50% larger than the 4 V/m noise level of the tape recorder were analyzed. These pulses had a median 30-90% risetime of 1 microsecond with a half width of 2.7 microseconds. All the pulses were superimposed on a negative going field change and most (84%) occurred in the first third of the overall field change. Large cloud pulses of several microseconds width were observed to occur early in the field record and they appeared to be related to the initiation of the cloud discharge. Willet et al. [6] recorded 18 narrow bipolar pulses, with initial polarity opposite to that of a typical return stroke. They found that these pulses had an average full width at half maximum of about 2 microseconds, with the peak followed by a small overshoot. Their dE/dt records showed large amplitude, high frequency noise superimposed on the slower variation that could be expected from the shape of the E-field record. Their data were recorded using transient waveform recorders sampling at 100 MS/s and triggered by a HF receiver. The location of the thunderstorm cell was 45 miles away from the recording station with propagation path over salt water.

In the present work, we show statistics on 156 narrow negative bipolar pulses and on 10 narrow positive bipolar pulses. We have found that these pulses, which are of the type described by Willet et al. (1989), are much more common than earlier studies indicate. In a single thunderstorm, we identified 153 narrow bipolar pulses, whereas Willet et al. found 18 pulses in one thunderstorm. Their triggering technique involved using a narrowband signal in the 3 to 18 MHz range while we employed as trigger sources a 225 MHz receiver with 10 MHz bandwidth, the electric field, and the electric field derivative signal.

EXPERIMENT

The electric field, dE/dt and narrowband VHF measurements were performed using the setup shown in Figure 1. The wideband electric field recordings consisted of an electronically integrated "slow-decay" E-field sensor with a bandwidth of 3 Hz to 7 MHz, a "fast-decay" E-field sensor with a bandwidth of 16 kHz to 7 MHz, and a dE/dt sensor with an upper frequency response of about 100 MHz. The narrowband receivers had a 10 MHz bandwidth and were centered at 50 and 225 MHz. Flat-plate antennas were used for the E-field and dE/dt measurements, and quarter-wavelength vertically polarized antennas were used for the VHF receivers. The recording station was situated about 150 meters away from the antennas. Four sets of wideband (50 Hz to 150 MHz) fiber optic links were used to transmit the data from the sensing location to the recording station. At the recording station, the incoming signals were simultaneously digitized at a 100 MS/s rate using a 5-channel LeCroy TR-8818 series digitizer. Signals were also recorded on a Honeywell 101 analog magnetic tape recorder. Three sources were simultaneously used to trigger the digitizing system: (I) The electronically-integrated E-field, (II) The dE/dt waveform, and (III) the output of the 225 MHz

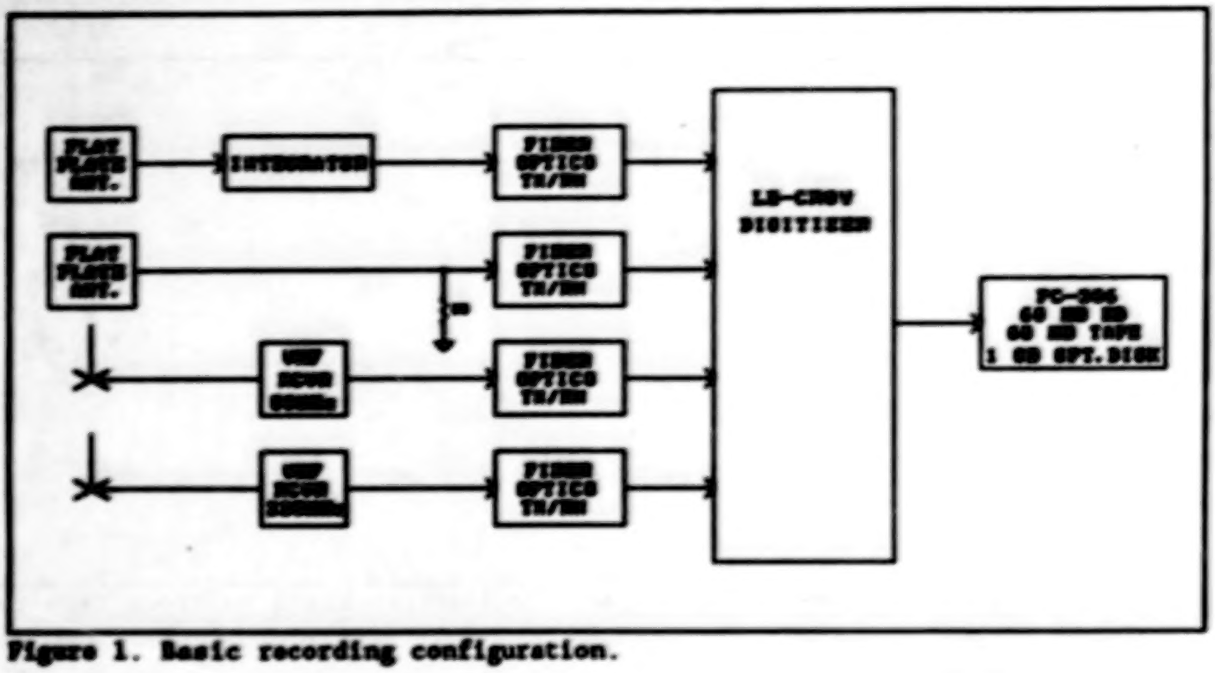

Figure 1. Basic recording configuration.

VHF receiver. The digitizers were operated with a 41 microsecond pretrigger. Each digitized record contained 16,384 points, thus allowing for 163.84 microseconds of continuous data. The digitized data were transferred to a 80386-based microcomputer through a GPIB bus at a rate close to 400 KB/s, allowing the system to be re-armed and ready to digitize again 200 milliseconds after a trigger. These data were first stored in a 60 MB hard disk. When the hard disk capacity was reached, the information was transferred to digital magnetic tapes and later recorded on optical disks for permanent storage.

RESULTS AND DISCUSSION

Data

Data were collected from overhead lightning during days 266 (Sept. 23), 268 (Sept. 25) and 269 (Sept. 26). The advantage on studying overhead lightning is that the attenuation of high frequencies resulting from propagation over non perfect conductors such as land, and to a lesser extend, salt water is avoided. Only records corresponding to intracloud pulses are analyzed and presented in this paper.

In order to increase the effective bandwidth of the E-field recordings, the digitized E-field signal and the dE/dt signal were combined using digital signal processing techniques to obtain a composite waveform with frequency components from 3 Hz to 50 MHz as shown in Figure 2. A set of digital filters were designed for this purpose. This procedure involved filtering the dE/dt signal through a digital highpass filter with a cutoff frequency of 3 MHz, thus removing frequency components below this frequency. In a similar way, the E-field signal was filtered through a digital lowpass filter with the same cutoff frequency of 3 MHz, removing this way the frequency components above this frequency. The filtered signals were then scaled and digitally added together to produce the composite E-field waveform. The actual frequency and phase response of both filters were tested by applying a square wave at the input of each filter and

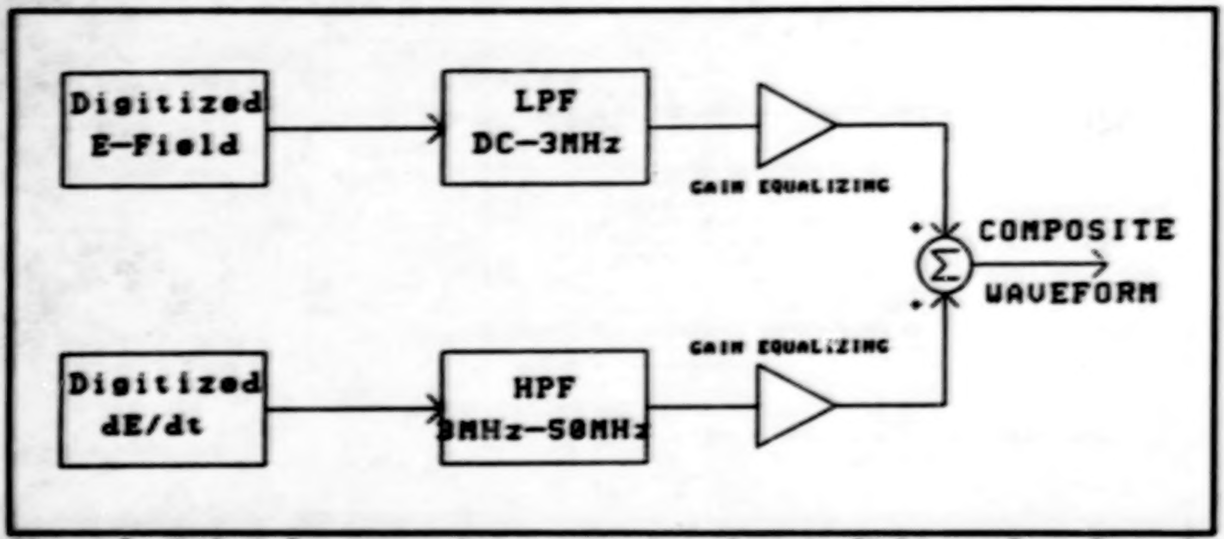
Digitized
E-Field
LPF
DC-3MHz
GAIN EQUALIZING
+
Σ
+
COMPOSITE
WAVEFORM
GAIN EQUALIZING
Digitized
dE/dt
HPF
3MHz-50MHz

Figure 2. Method for generating a composite electric field waveform from the dE/dt and E-field signals.

adding the outputs to produce a composite waveform. The resulting composite waveform was a square wave with exactly the same amplitude as the input signal.

The sequence shown in Figure 3 illustrates the procedure described in the previous paragraph. An actual dE/dt waveform is shown in Figure 3(a). A

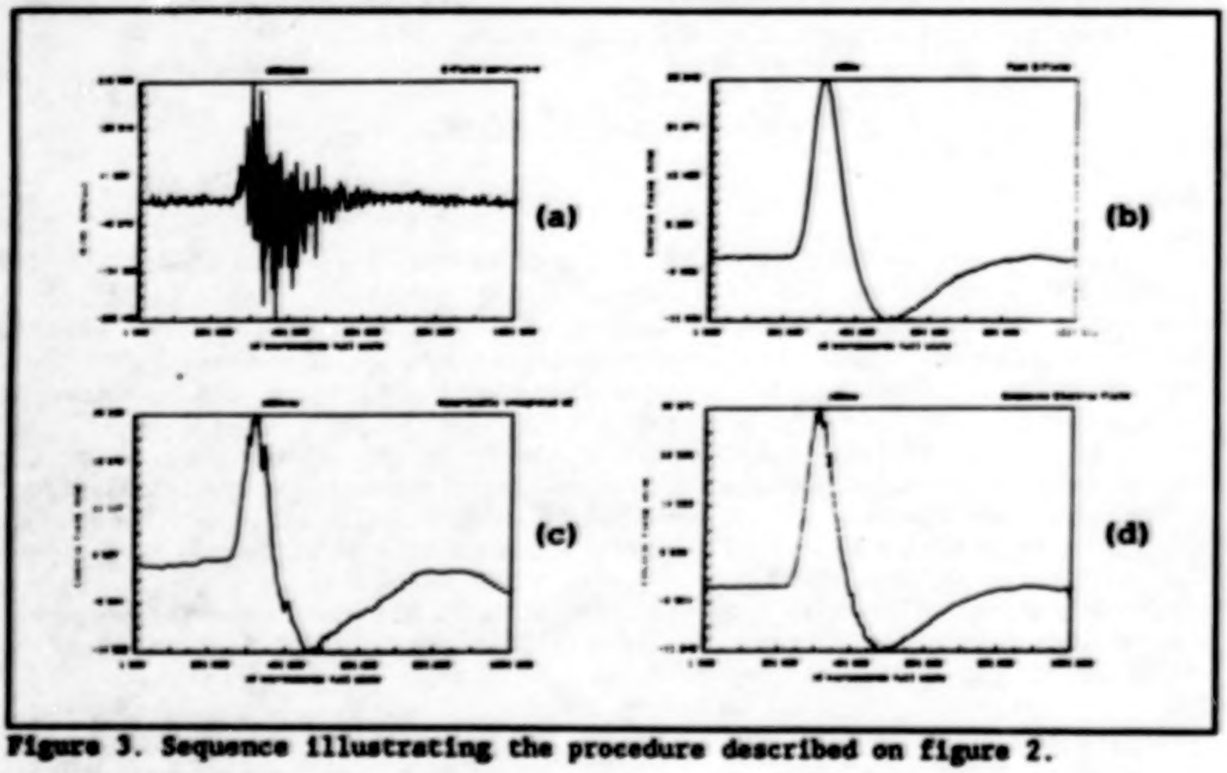

Figure 3. Sequence illustrating the procedure described on figure 2.

simultaneously recorded electronically integrated E-field waveform is shown in Figure 3(b). Figure 3(c) presents the result of numerically integrating the dE/dt waveform shown in Figure 3(a). The composite signal, obtained after filtering, scaling and adding together both E-field waveforms is presented in Figure 3(d). Recordings of the envelope of the narrowband VHF radiation at 50 and 225 MHz for the same cloud pulse are presented in Figure 4 (a) and (b) respectively.

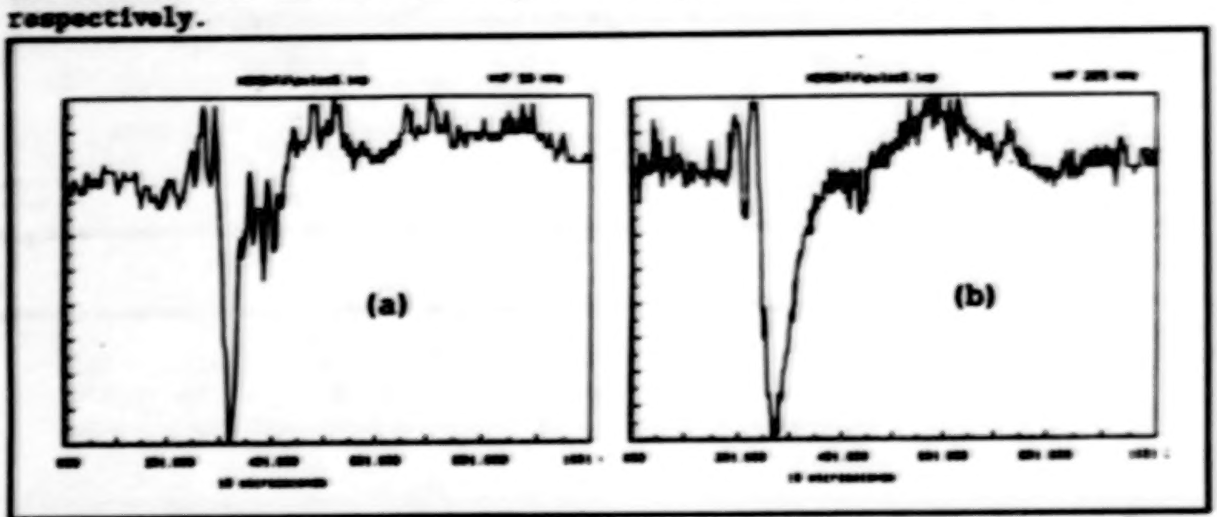

Figure 4. VHF pulses recorded simultaneously with the waveforms shown in figure 3.

Waveform characteristics

A wide variety of cloud pulses were recorded during the course of the 1989 experiment. Pulses with 10 to 90 percent risetimes faster than 0.5 microseconds were commonly observed. The fastest observed was a pulse with a 10 to 90% risetime of 0.3 microseconds. The waveforms were characterized according to several parameters, as shown in Figure 5. Some cloud pulses contained a hump before or after the negative overshoot. Examples of pulses are shown in Figure 6 as follows: (a) Bipolar pulse with overshoot without hump, (b) Bipolar pulse with hump before the overshoot, (c) Bipolar pulse with hump during the overshoot, and (d) Bipolar pulse with hump after the overshoot. The frequency of the occurrence of humps is presented in Table I. Different parameters were measured on each waveform. The main characteristics of the E-field and the electric field derivative waveforms are shown in Table II.

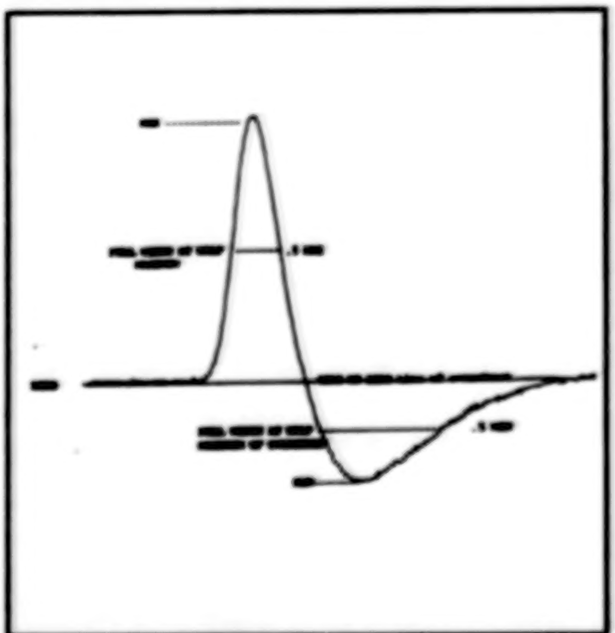

Figure 5. Description of the parameters used in the characterization of the cloud pulses.

Other researchers have normalized their E-field readings to a

Table I

Table I. Frequency of occurrence of bumps

	156 Negative pulses	10 Positive pulses
Bump before overshoot	16	2
Bump during overshoot	40	4
Bump after overshoot	35	1
No bump	65	3

Table II

TABLE II. Average and Standard Deviations of Cloud Pulse Characteristics data collected during days 266, 268 and 269. Times are in microseconds.

	156 Neg. Pulses	10 Pos. Pulses
Composite Electric Field		
Ratio of initial peak to overshoot peak	4.57 +/- 2.14	4.19 +/- 1.51
Time between initial and overshoot peaks	6.45 +/- 5.68	7.44 +/- 3.99
10-90% risetime	1.54 +/- 1.04	1.82 +/- 0.87
10% to peak time	1.83 +/- 1.08	3.64 +/- 2.23
Peak to zero time	2.90 +/- 2.24	4.05 +/- 2.84
Total overshoot width	8.53 +/- 7.23	14.09 +/- 7.94
Width of initial peak at half-maximum	1.83 +/- 0.63	1.60 +/- 0.87
Time from initial peak to bump peak	7.06 +/- 2.13	4.74 +/- 2.20
Time between dE/dt peak to E-field peak	9.15 +/- 3.78	6.04 +/- 2.39
Electric Field Derivative (dE/dt)		
Ratio of dE/dt maximum to dE/dt minimum	0.66 +/- 0.57	-1.60 +/- 0.59
Time between dE/dt maximum and dE/dt minimum	0.80 +/- 0.21	

given distance. In the case of Willet et al (1989), their statistics on narrow bipolar pulses included E-field and dE/dt records normalized to a distance of 100 km. This normalization was done assuming that all of the bipolar pulses came from a range of 45 km, based on the locations given by a lightning location system. Since in our case the lightning activity was mainly overhead, the closest possible distance for the source is probably the cloud base at 1.5 km. However, recorded pulses could have originated as far as 20 km. Since we have no means to find the exact location in space of the cloud flashes, E and dE/dt waveforms shown in this paper are presented with the actual readings in V/m and V/m/us respectively, without any attempt to normalizing at a particular distance.

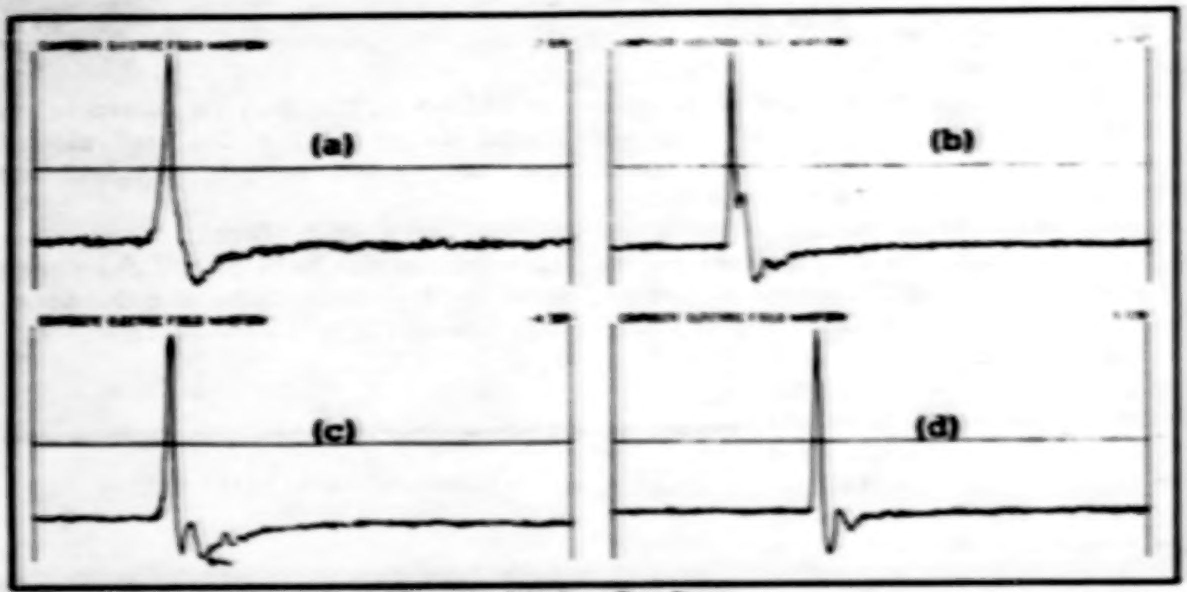

Figure 6. Examples of different kinds of pulses.
(a) Bipolar pulse with positive overshoot and no hump.
(b) Bipolar pulse with hump before the overshoot.
(c) Bipolar pulse with hump during the overshoot.
(d) Bipolar pulse with hump after the overshoot.

The dE/dt records sometimes exhibited large variations for several microseconds before and after the main peak of the E-field pulse, as shown in Figure 7 (a). On some occasions, the electric field derivative waveform was monotonically varying and closely associated with the E-field pulse fast rise to peak as seen in Figure 7 (b). Several cloud pulses consisted of a monotonically varying dE/dt waveform coincidental with the rise of the E-field pulse, followed

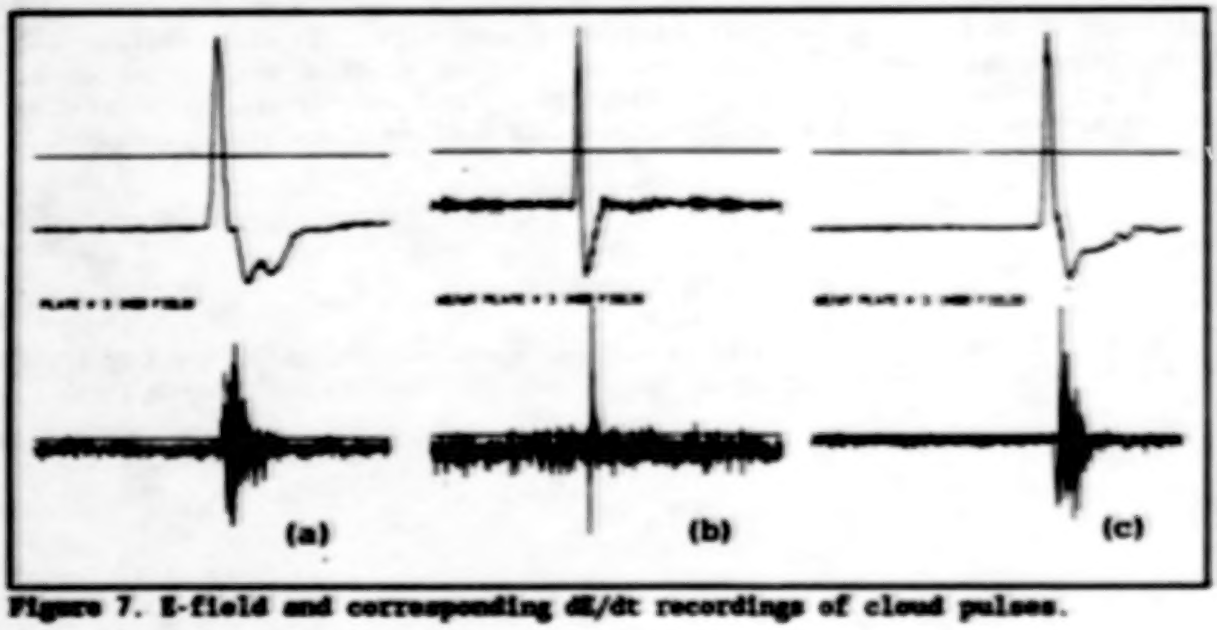

Figure 7. E-field and corresponding dE/dt recordings of cloud pulses.

by large variations with a duration of about ten microseconds. This case is shown in Figure 7 (c). On others, there was little correlation between the dE/dt and the E waveshapes.

Thirty negative bipolar pulses were identified on the E-field recording on analog magnetic tape. 21 of them were found to be single isolated pulses occurring more than one second apart from any burst activity typical of lightning, as presented in Table III.

In order to investigate how HF and VHF receivers at different frequencies might have responded during these pulses, time-domain analysis of the frequency components of the dE/dt waveforms was performed by digitally filtering the data. Twelve digital finite-impulse-response (FIR) bandpass filters were designed. All bandpass filters were designed to have a 5 MHz bandwidth and 30dB/octave rolloff. The filters had identical characteristics, the only difference being their center frequency. Each of the twelve digitally filtered waveforms was rectified and lowpass filtered. This operation simulated the signals that would have been obtained from the output of envelope detector receivers. Figure 8 shows the result of performing this operation on an actual dE/dt recording. Note that the total duration of the radiation for all different bands was about the same and coincidental with the duration of the initial pulse. However, peaks in the radiation on different bands typically developed at different times within the duration of the received dE/dt waveform. This suggests that different portions of the cloud pulse spectrum may occur at different times during the ten microseconds or so of the cloud pulse duration. A possible explanation of different frequencies being received at different times is that the sources of different frequencies are spatially separated, although it is also possible that all frequencies have collocated sources but the sources are turned on at different times. In either case our findings are highly relevant to the mapping of VHF sources in space and time. This point is further discussed in Thomson and Medelius [7].

Table III

TABLE III. Occurrence of bipolar pulses

Isolated	21
Less than 1s before burst activity	5
During burst activity	3
Less than 1s after burst activity	1

ACKNOWLEDGEMENTS

This research was sponsored in part by NASA Grant NAL-10-0049 and by AFOSR Grant 91-0093. We specially thank Mr. W. Jafferis for his continuous support.

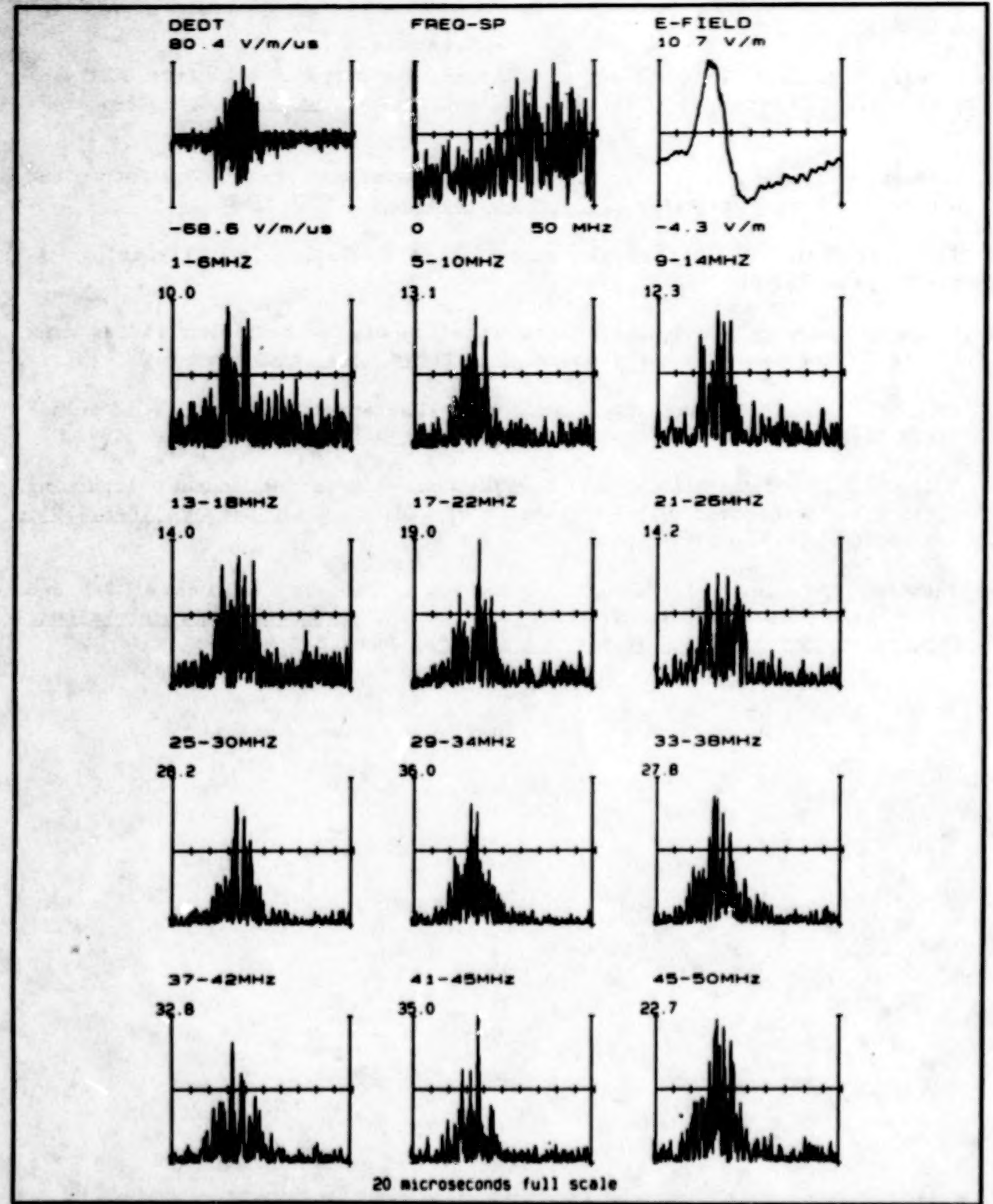

Figure 8. **Time-domain analysis of the frequency contents of an actual dE/dt waveform. Frequency bands are indicated on each plot. Time varying signals are 20 microseconds full scale. Frequency spctrum "FREQ SP" is from 50 kHz to 50 MHz.**

BIBLIOGRAPHY

1. Krider, E.P., C.D. Weidman, and D.M. LeVine, The temporal structure of the HF and VHF radiation produced by intracloud discharges, J. Geophys. Res., 84, 5760-5762, 1979.

2. Weidman, C.D. and E.P. Krider, The radiation waveforms produced by intracloud lightning discharge processes, J. Geophys. Res., 84, 3157-3164, 1979.

3. Le Vine, D.M., Sources of the strongest RF radiation from lightning, J. Geophys. Res., 85, 4091-4095, 1980.

4. Cooray, V. and S. Lundquist, Characteristics of the radiation fields from lightning in Sri Lanka in the tropics, J. Geophys. Res., 90, 6099-6109, 1985.

5. Bils, J.R., E.M. Thomson, M.A. Uman, and D. Mackerras, Electric field pulses in close lightning cloud pulses, J. Geophys. Res., 93, 15,933-15,940, 1988.

6. Willet, J.C., J.C. Bailey, and E.P. Krider, A class of unusual lightning electric field waveforms with very strong HF radiation, J. Geophys. Res., 94, 16,255-16,267, 1989.

7. Thomson, E.M. and P.J. Medelius, A system for mapping sources of VHF and electric field pulses from in-cloud lightning at KSC, Proceedings, International Conference on Lightning and Static Electricity, Cocoa Beach, 1991.

Session 3B, Tuesday 1:30

Aerospace Vehicles Structures and Materials 2

Whitaker, Chairman

THE PERFORMANCE OF CABLE BRAIDS AND TERMINATIONS TO LIGHTNING INDUCED TRANSIENTS

David Crofts
Raychem Ltd., Swindon, UK

ABSTRACT

The latest specifications detailing the test waveforms for indirect lightning transients as applied to aircraft wiring systems specify very high voltages and currents. Although considerable data exists for measuring cable screen leakage using such methods as Surface Transfer Impedance and Bulk cable Injection there is little data on the likely core transient level that is likely to be induced from these threats. In particular the new Waveform 5 at very high current levels (10kA) is reputed to cause severe cable damage.

A range of representative cables were made with various screen termination techniques and screening levels. These were tested first to determine their relative screening performance and then they were subjected to lightning transient testing to all the specified waveforms. Core voltages were measured for each test.

Tests were also performed on bundles with fewer wires to determine the failure criteria with waveform 5 and these tests also included Flat Conductor Cables.

The test showed that correctly terminated cable bundles performed well in all the tests and would provide a high level of protection to the electronic systems. The use of overbraides, provided the individual screens are well terminated appears to be un-necessary.

INTRODUCTION

Cable screens are widely used to achieve EMC within aircraft and they can be extremely efficient if properly terminated. Most test used to evaluate their performance, however, use CW techniques over a very wide frequency range, at low amplitude and measure cable screen leakage. Values for the screening efficiency are then determined at various frequencies and these are used for quality assurance and design purposes. The tests are usually performed on short samples (1m) of the cable and results are quoted below resonance frequencies where in reality most leakage would occur.

The situation with a lightning transient is more complicated since the performance of the cable screen is known in frequency domain but not in time domain. It is, of course, relatively easy to calculate the core current waveforms produced by an external pulse of current on the screen using the techniques described by Vance [1]. However, many of the required parameters have to be estimated and are difficult to accurately measure in the real situation. This is certainly true when dealing with a typical aircraft wiring loom that consists of a number of individual screened wires such as twisted pairs. This bundle could then have an outer braid and the termination of all the braids to ground is another significant variable.

The latest indirect lightning transients as detailed in SAE AE4L-87-3 Rev B, DO160C and ABD0007 and describe three basic waveforms which have been well described by Wiles [2]. Although it would be possible to estimate the core current from these waveforms the errors could be very large. The effects of high currents causing local heating and high voltages causing breakdown would of course not be known. It should be remembered that peak currents can now be 10 kAmps with peak voltages of 3.2 kVolts. Further with the oscillatory wave shapes the maximum leakage would occur at resonance frequencies and to evaluate a cable screen it would be essential to determine this frequency.

The lack of any real understanding of the performance of cable braids with these transient levels has resulted in a safety first approach with additional braids being added to cables. It has always been our design aim to produce an optimized design, i.e. a terminated system that adequately meets the threat but at the lowest weight and size. To achieve this one has to build up a library of basic cable and termination performance levels which will also allow one to validate the theoretical calculations.

To this end a series of tests have been carried out on a wide range of cable assemblies with different termination systems. The screening effectiveness of each system was determined using both Surface Transfer Impedance (Zt) and Bulk Cable Injection (BCI) techniques. Each cable was then tested with the specified transients from the SAE AE4L document, waveforms 2,3,4 & 5 at level 5. Additional tests were carried out at the resonance frequencies of each cable, as determined by BCI, with the oscillatory waveform 3. The core voltage was measured in each case and the system examined for physical damage.

A sample using Flat Conductor Cable (FCC) was also added to the trial since there have been a number of doubts over the current carrying capacity of these film bonded copper foil shields.

A final trial was to determine the damage threshold of bundles of screened twisted pairs where each screen was separately terminated to a connector. The number of screened twisted pairs being progressively reduced and the waveform 5 transient injected down the braids. This has the effect of concentrating the current in fewer terminations and will lead to eventual failure.

TEST SAMPLES

The samples were divided into three basic groups, the first was based on screened twisted pair bundles with various termination techniques and the second on screened wire bundles with flat connectors and the third on a Flat Conductor Cable (FCC) structure. The samples in the first group were all 3m long whilst the other groups were 1 m. These groups were also fitted with connectors. The other group whilst having termination fittings where fitted with dummy brass inserts instead of connectors.

The types of termination for the screens of the twisted pairs within the first group where considered essential and three systems were used, first standard pigtails, second an iris cone clamp and thirdly individual ferrules for each twisted pair mounted into a retaining plate (Hexashield). These are illustrated.

Screened Twisted Pair Bundles.. This consisted of 20 screened 24 awg twisted pairs machined laid to make a harness. The following samples were made:-

STP/0B/P	Cable with no outer screen, wire screens, terminated by pigtail
STP/0B/I	Cable with no outer screen, wire screens, terminated by Iris clamp.
STP/0B/H	Cable with no outer screen, wire screens, terminated by Hexashield.
STP/1B/P	Cable with single outer screen, wire screens, terminated by pigtails.
STP/2B/P	Cable with double outer screen, wire screens, terminated by pigtails.

Flat Connector System. This consisted 24 awg Screened Twisted Pairs and the numbers in each harness were 20, 15 and 10. The normal number for such a connector is 20 wires and hence the current level per termination was increased by 33% and 50% above the specified levels. Termination was by a bus-bar that commoned all the screens.

20STP/0B	Cable with 20 STP terminated separately, into MTC Connector.
15STP/0B	As above but 15 wires.
10STP/0B	As above but 10 wires.

Flat Conductor System. Screens consist of film bonded mylar/copper foils. The basic cable consisted of two flat conductor cables with a mylar/copper foil bonded to each and a second foil between the two layers. This gave a total of three screening copper foils and an overall mylar/copper foil was used to screen the complete harness.

FCC/3F/1B/MTC	FCC with three copper foil screens and an outer wrap around foil screen, grounded to MTC connector.

SCREENING PERFORMANCE

There have been many papers presented that overview methods of measuring Surface Transfer Impedance (Zt) [3,4 & 5] and also Bulk Cable Injection (BCI) [6] and space does not permit detailed description of the techniques. Zt was measured by driving a current down the cable braid (over a ground plane) and measuring the resultant voltage on the central conductors. BCI used an injection coil to generate the screen current and in our tests the resultant voltage on the central conductors recorded. The test set up is, however, unmatched and the upper frequency where the results are still valid for this length of cable is about 10 MHz.

SCREENED TWISTED PAIR TERMINATION TECHNIQUES

BRAID STRAP OR PIG-TAIL. Each braid of the screened twisted pair is terminated to the overall cable screen.

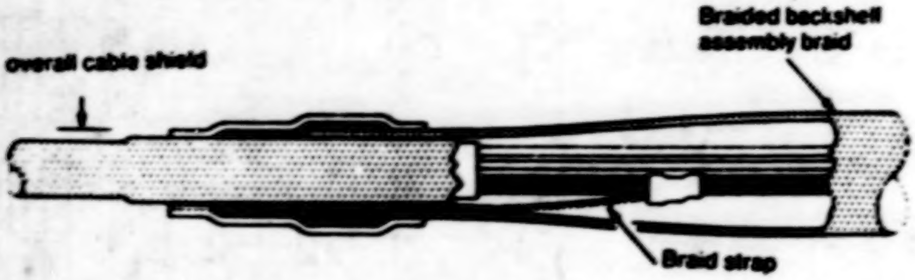
Braided backshell assembly braid
overall cable shield
Braid strap

IRIS CLAMP. Each screened twisted pairs braid is combed out and trapped under a spring IRIS and the connector backfitting.

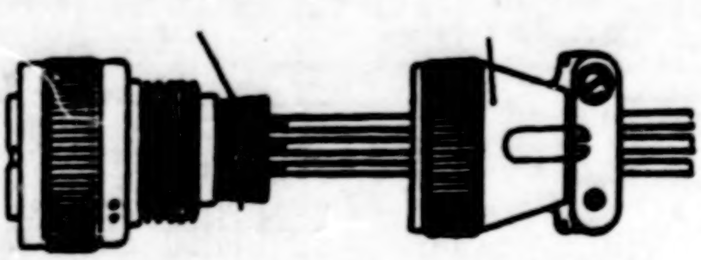

HEXASHIELD TERMINATION. Onto each screened twisted pair braid a metal ferule is terminated with a solder sleeve. Each ferule fits into a metal retaing plate and is secured by a clamp nut.

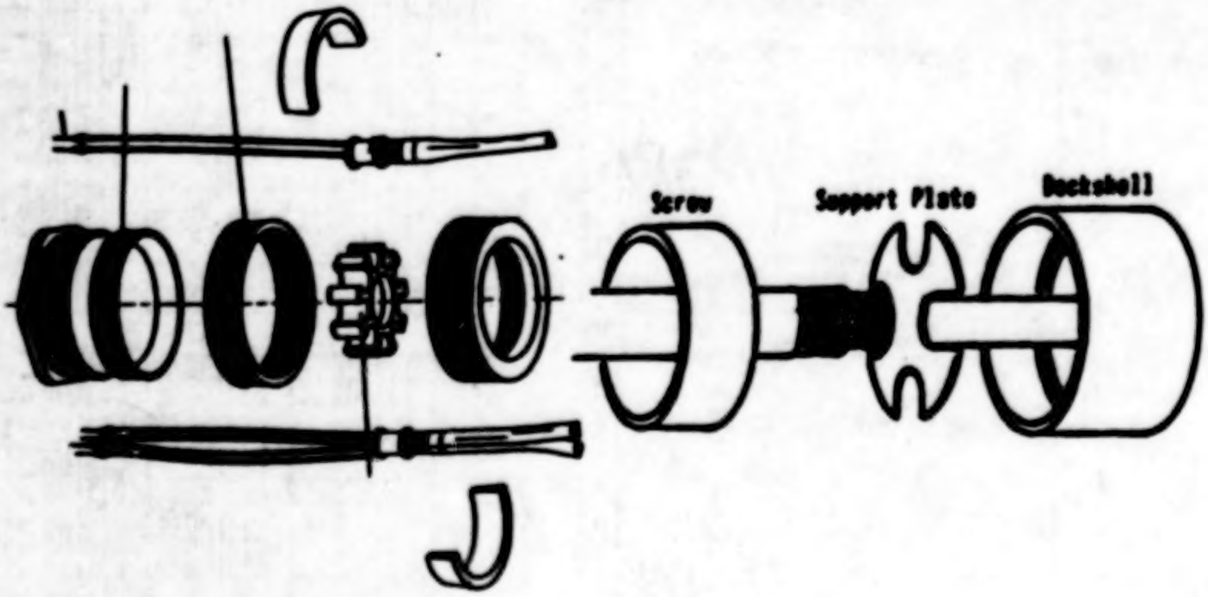
Screw
Support Plate
Backshell

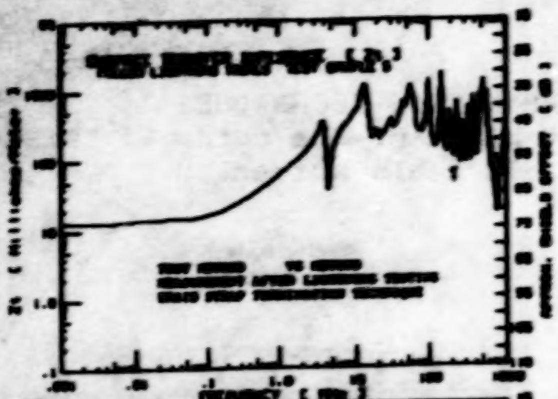
Zt (Milliohms/Meter)
FREQUENCY (MHz)
OVERALL SHIELD EFFECT (dB)

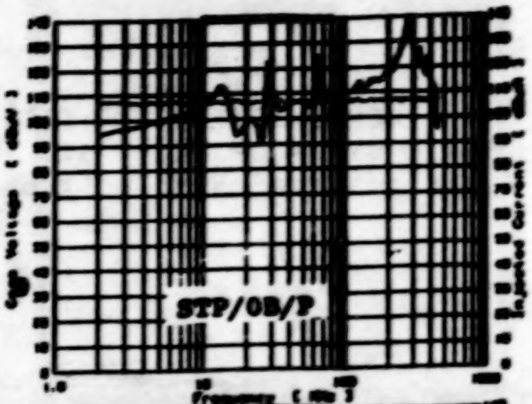
STP/0B/P
Core Voltage (dBuV)
Frequency (MHz)
Injected Current

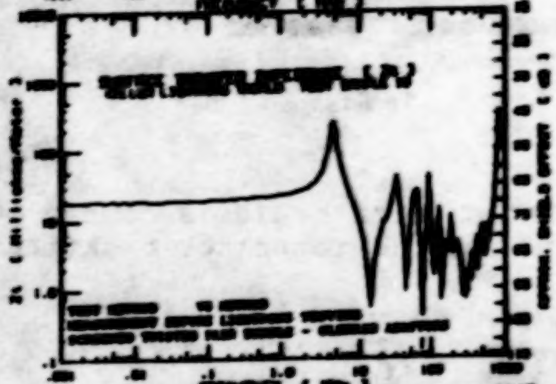
Zt (Milliohms/Meter)
FREQUENCY (MHz)
OVERALL SHIELD EFFECT (dB)

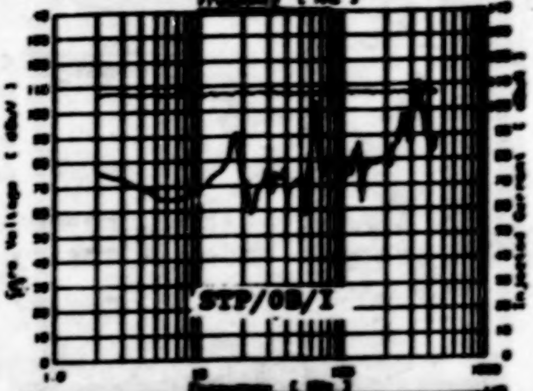
STP/0B/I
Core Voltage (dBuV)
Frequency (MHz)
Injected Current

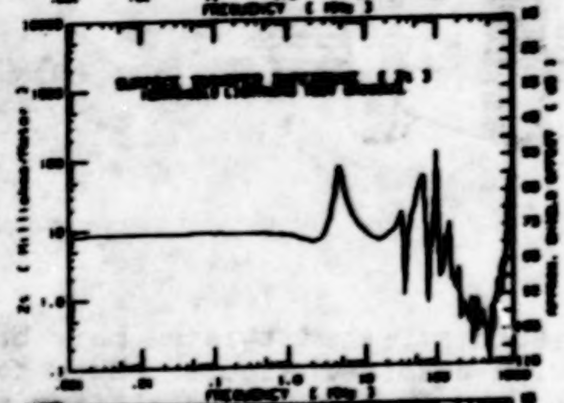
Zt (Milliohms/Meter)
FREQUENCY (MHz)
OVERALL SHIELD EFFECT (dB)

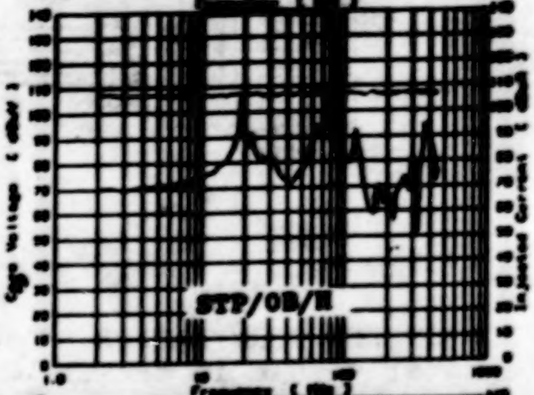
STP/0B/H
Core Voltage (dBuV)
Frequency (MHz)
Injected Current

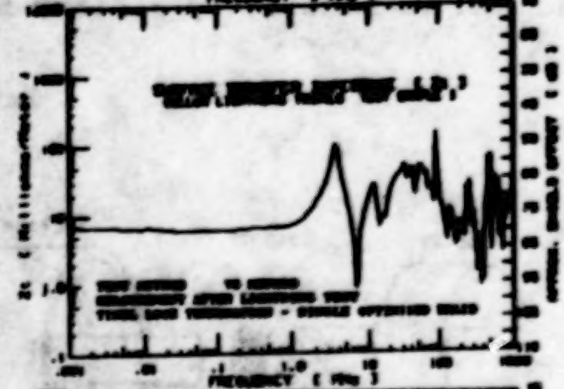
Zt (Milliohms/Meter)
FREQUENCY (MHz)
OVERALL SHIELD EFFECT (dB)

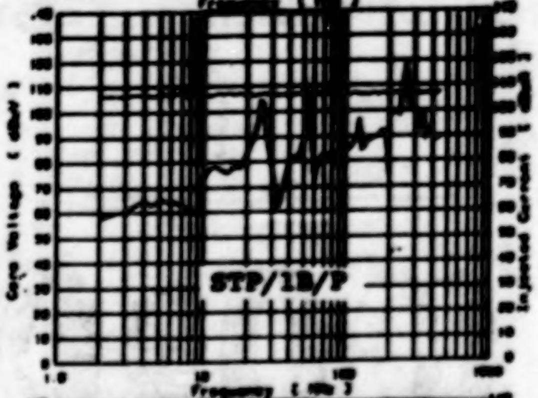
STP/1B/P
Core Voltage (dBuV)
Frequency (MHz)
Injected Current

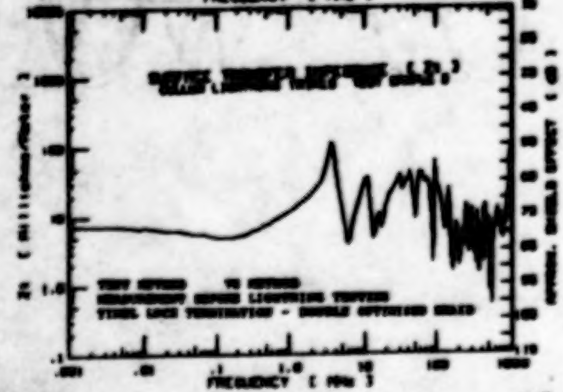
Zt (Milliohms/Meter)
FREQUENCY (MHz)
OVERALL SHIELD EFFECT (dB)

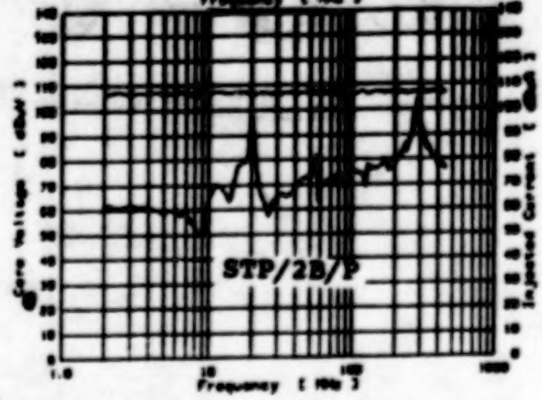
STP/2B/P
Core Voltage (dBuV)
Frequency (MHz)
Injected Current

LIGHTNING TESTING

Screened Twisted Pairs (Group 1). The lightning transients were applied to the cables using two techniques as described in the reference [2] and these were Bulk Cable for waveforms 2 and 3 and Ground Injection for waveforms 4 and 5. The number of pulses applied was 5 of each polarity. The test configuration is shown.

Level 5 was used for each transient. The higher frequency waveform 3 oscillatory waveform was tested at 1, 10, 30 and 50MHz as well as the resonant frequency. The first cable resonance as determined from the BCI test was included as this is the frequency of maximum cable leakage.

We were interested in any possible damage that could occur with the very high powered waveform 5 at 10 kAmps and we remeasured the basic screening performance after these tests using both Zt and BCI.

The voltage waveform on the central conductor was recorded. All the central conductors were commoned together in these trials. The termination resistance was 50 Ohms.

The test conditions used were those described in the SAE AE4L-87-3 Rev B 1989 document.

Screened Twisted Pairs with MTC Connectors (Group 2). This trial was intended to determine the number of individual screened wires can be used and still carry the full threat of waveform 5. The test was applied to each of the harnesses until either a total of 10 shots were passed or damage occurred to the sample.

Flat Conductor Cable with MTC Connector (Group 3). This trial was carried out using waveform 5 at 10 kAmps. A total of 10 shots were made and the sample examined for any damage.

Level	Waveforms			
	2 Vp/Ip	3 Vp/Ip	4 Vp/Ip	5 Vp/Ip
1	50/10	100/4	50/10	N/A
2	125/25	250/10	125/25	N/A
3	300/60	600/24	300/60	300/100
4	750/150	1500/60	750/150	750/1000
5	1600/320	3200/128	1600/320	1600/3000 to 20,000

Vp – Peak Open Circuit Voltage Line-to-Ground
Ip – Peak Short Circuit Current On A Line

Suggested ETDL Voltage and Current Levels

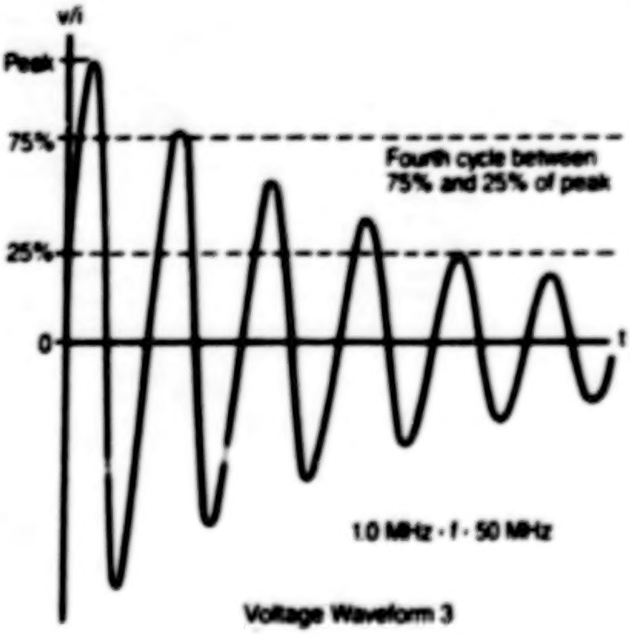

Voltage Waveform 3

Idealised induced voltage and current waveforms

/21

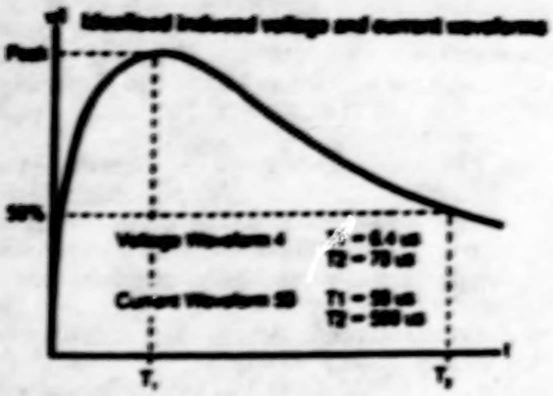

WAVEFORM 2 SHORT PULSE
BULKCABLE INJECTION 320 Amps/6usecs
CABLE CORE VOLTAGE

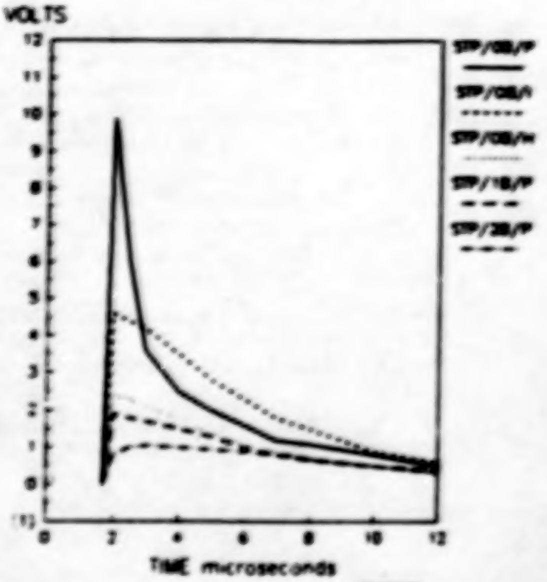

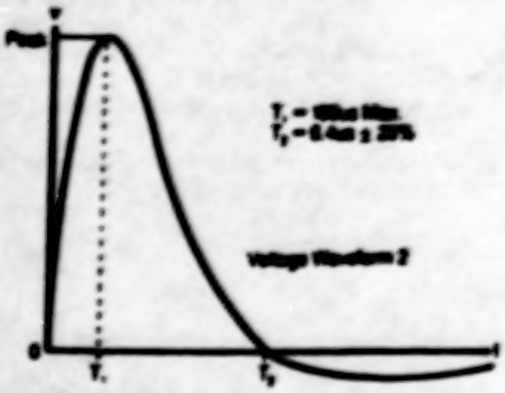

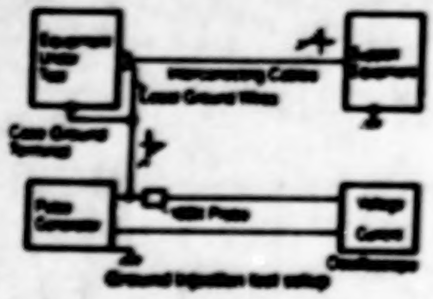
Equipment Under Test
Interconnecting Cable
Load Equipment
Case Ground Wire
Case Ground Terminal
Pulse Generator
Voltage Probe
Oscilloscope
Ground injection test setup

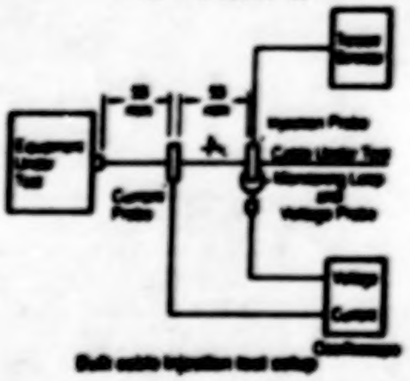
Transient Generator
Equipment Under Test
Injection Probe
Cable Under Test
Current Probe
Monitoring Loop and Voltage Probe
Oscilloscope
Bulk cable injection test setup

WAVEFORM 4
GROUND POINT INJECTION 320 Amps/70 usecs
CABLE CORE VOLTAGE

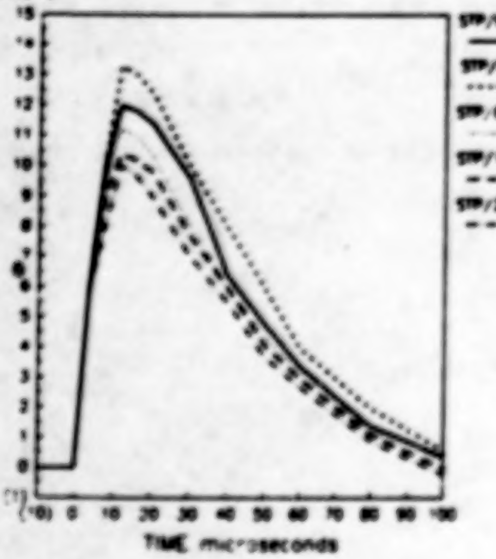

WAVEFORM 5 TEST (LONG PULSE)
GROUND POINT INJECTION 10kAmps/500us
CABLE CORE VOLTAGE

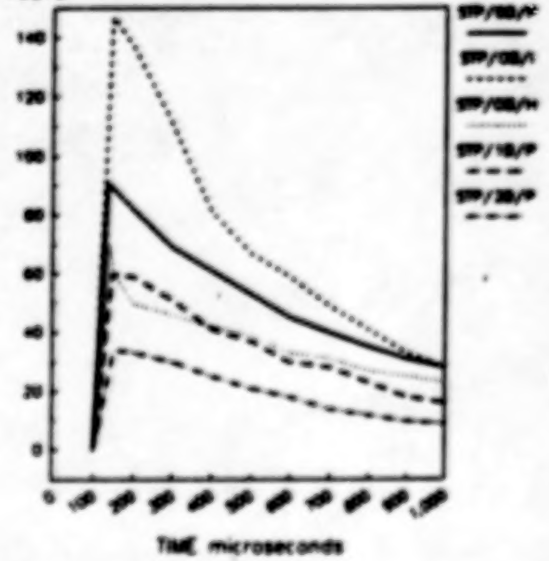

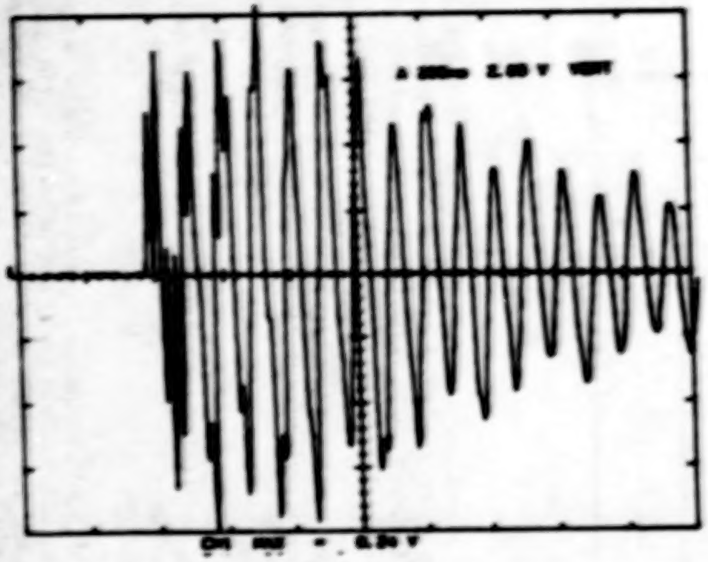

STP/OB/P

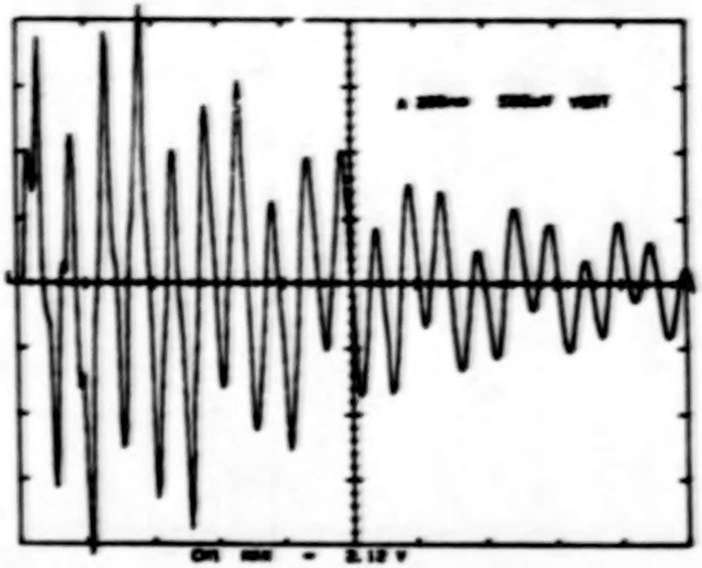

STP/OB/I

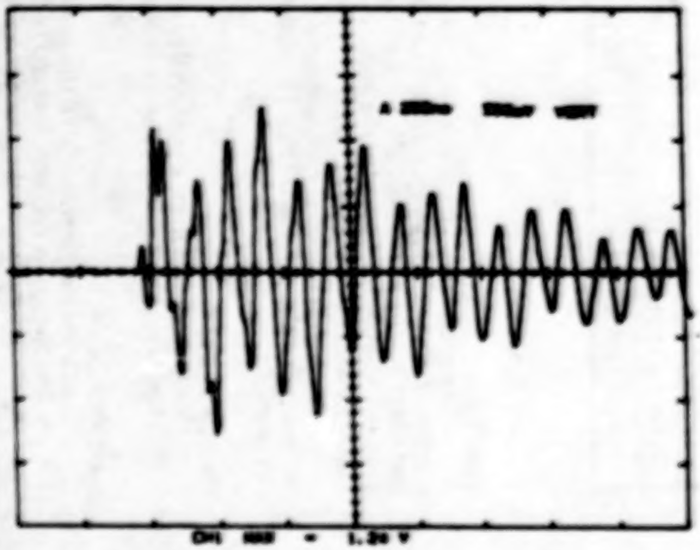

STP/OB/H

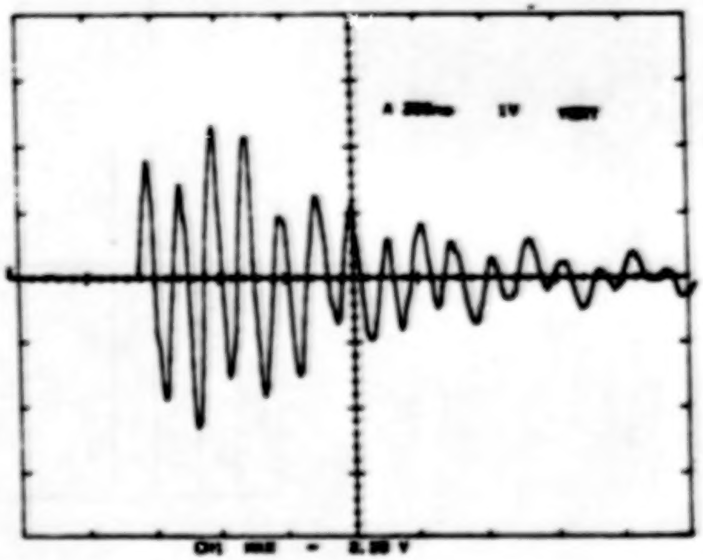

STP/1B/P

TEST RESULTS

Screened Twisted pair Cables (Group 1 Samples).
Cable Leakage. There were two techniques used and these were Surface Transfer Impedance (Zt) and Bulk Cable Injection (BCI) and the test results for both these tests for the Screened Twisted Pair Bundles of the first group of test samples are shown. The BCI current was 250 ma.

Lightning Transient Testing. The waveforms for the voltage waveforms 2,3 and 5 are shown for the first group of samples i.e. the screened twisted pair cables.
The number of waveforms tested of the oscillatory form (Wfm. 3) are too numerous to reproduce and the table gives the peak values, examples are given.

Screened Twisted Pairs with MTC Connectors (Group 2). Each sample was tested a number of times until failure. Samples with 20 and 15 wires passed and that with 10 failed catastrophically after 2 shots. An explosion destroyed the connector backshell and the terminations. The connector termination failing when the current stress level was twice the specified level. Failure was not in the connector or the screened twisted pair but in their interconnection.

Flat Conductor Cable with MTC Connectors. The sample passed the trial and the peak voltage was 57 volts.

PEAK VOLTAGE TRANSIENT DURING PULSE TESTING

WAVEFORM	STP/0B/P	STP/0B/I	STP/0B/H	STP.1B/P	STP/2B/P
DC Rest mohms	8.7	9.3	6.1	8.0	3.4
Wfm 2 (320A)	9.9	4.4	2.3	2.0	0.8
Wfm 3 (128A)					
1 MHz	3.8	3.8	1.4	1.6	0.6
10 MHz	8.2	2.1	1.2	2.3	0.7
30 MHz	19.2	15.4	7.1	25.2	11.4
50 MHz	104.0	39.2	5.6	8.6	3.9
Resonance	81.7	33.0	17.9	20.2	19.5
Wfm 4 (320A)	11.7	13.0	10.9	10.2	9.5
Wfm 5 (10kA)	91.0	147.0	70.0	60.0	33.0

CONCLUSIONS

Waveform 5 Tests.

The waveform 5 transient does not appear to pose a threat to aircraft wiring looms. The threat current of 10 kAmps can be carried by both bundles of screened twisted pairs (with as few as 10 wires) and Flat Conductor Cables. Connectors of the MTC design can carry the full threat current without damage. Connector fittings, if the current is localised by having only a few current carrying wires can be damaged with this waveform.

The induced central core voltage can be simply calculated from the DC resistance of the cable and assuming the current is DC. This induced voltage is certainly capable of upsetting or damaging electronics.

Waveform 2 & 4.

Both these waveforms produced double exponential voltage transients of similar but low magnitude. They would be capable of upset in certain signal lines.

Waveform 3.

This transient demonstrated the importance of braid termination. It is well known how bad pigtails are and the effect on cable leakage is clearly seen in the results for Zt and BCI. The cable STP/0B/P, the one where the screens were terminated with pigtails shows very poor performance at high frequency. The termination of the same cable with an "IRIS" type clamp reduces the voltage dramatically whilst the soldered ferule clamped into the metal housing of the HEXASHIELD termination provides outstanding performance.

It can be seen from samples STP/1B/P and STP/2B/P where the pigtail samples have had over-braides put over the cable bundles that the performance is still not as good as a cable with no overall cable screen but good 360° individual screen termination.

General Comment.

The voltage transients were not as severe as first predicted and the effect of the high current waveform 5 did not cause the problems that we had been warned against. In general most screened cable bundles with proper screen termination should provide a high level of protection.
The use of techniques such as Surface Transfer Impedance and Bulk Cable Injection provides useful indications of likely performance but given the inaccuracy of these methods when applied to an unmatched system estimated performance should be treated with caution.

REFERENCES

1 Vance, "Coupling to Shielded Cables" . J. Wiley & Sons.
2 Wiles, 1989 Int. Conf. on Lightning and Static Electricity, Bath.
3 Martin, 5th Int Zurich Symposium on EMC 1983.
4 Fowler, 9th Int Zurich EMC Conf on EMC 1991.
5 Carter, Int EMC Conference York University 1990.
6 British Defence Standard Def-Stan 59-41 1989.

ACKNOWLEDGEMENT

To the staff at the Culham Lightning Studies Unit for their help in performing the Waveform 5 tests and for their technical advice.

LIGHTNING PROTECTION OF THE FOKKER 100 CFRP RUDDER.

A.J.M. Ruiter,
Fokker Space & Systems B.V.,
(formerly of Fokker Aircraft Corporation),
Amsterdam,
Holland.

ABSTRACT

This paper describes the construction of the structural parts of the Fokker 100 CFRP rudder with respect to the requirements for electrical bonding and lightning protection. Futhermore the philosophy for the selection of a consumable trailing edge is given. A description of possible alternative designs for trailing edges and their advantages and disadvantages with respect to damage after lightning impact will also be reviewed.

An overview of the tests performed on test samples and the rudder construction will be presented and discussed. The effectiveness of both the selected structural provisions and trailing edge will be described (and proven) by reporting the results of the simulated lightning tests performed at the High Voltage Laboratory of the N.V. KEMA, Arnhem, Holland. Proof will be presented that the trailing edge construction and its bonding through the structural parts of the rudder to the main aircraft structure is a solution which results in minor damage to the rudder after lightning impact. Furthermore it will be shown that the selected trailing edge construction is less favoured by the structural designers due to the weight penalty.

INTRODUCTION

Since the Fokker 100 empennage has a top mounted horizontal stabiliser which acts as a shield, the change of swept strokes or a direct lightning strike on the rudder's surface seems to be very small, but can not however be entirely excluded. In this case the rudder might become a part of the current path and would have to conduct a substantial current. The point of exit on the rudder of the lightning strike may either be at one of the bonding jumpers over the hinges at the trailing edge or at the static discharger.

Previous simulated lightning tests were based on direct impact damage in order to investigate the effectiveness of the protective layer on glass, aramid or carbon fibre reinforced test panels. The sample panels were positioned under a rod. The rod was positioned at a distance of about 1 cm above the test panel's surface. Futhermore, in these tests the effectiveness of several edge constructions was also tested. The latter was established by grounding the test panels at the aluminum supports at the edges (representing the aircraft's structure). The degree of damage to unprotected test panels was also established.

126

1. DESIGN CONSIDERATIONS

Due to the geometric shape and location of flight control surfaces like flaps, ailerons and rudders etc., the attachment or exit points of the lightning strikes will be localised at the trailing edge. The use of CFRP shall result in damage of the trailing edge after lightning impact. The degree of damage will strongly depend on the construction of the trailing edge used. After impact the current will be divided over the upper and lower skin panels of the affected flight control surface. This action will result in two effects:

- electromagnetic forces (causing delamination),
- resistive heating (causing vaporisation of the adhesive and/or resin, resulting in delamination).

Both effects will occur in cases where the upper and lower skins are terminated at the trailing edge and are connected by means of an adhesive layer (figure 1). In the case of a construction as shown in figure 2, the electromagnetic forces will dominate.

The degree of damage will be minimized by using a construction in which the trailing edge consists of a massive material (without resistivity change at the attachment point). Futhermore, this trailing edge must be connected to the upper and lower skins by means of rivets at a certain distance away from its extremity. In order to obtain the same degree of resistivity as the upper and lower skin panels the trailing edge has to be made from the same material (figure 3). Due to the absence of an adhesive layer the occurrance of an explosive expansion of this layer as a result of resistive heating is prevented. In addition, the degree of electromagnetic forces will be less at the connecting rivets of the skins to the trailing edge. This is because of the greater distance between the (skin) rivets and the lower current density in both skins (i.e. not concentrated at the trailing edge) compared to figures 1 and 2. The result will be that the actual electromagnetic force in the trailing edge will be les severe. So the degree of damage will only be dominated by the resistive heat build-up at the attachment point of the trailing edge.

Based on the above mentioned considerations it was decided to evaluate a trailing edge construction as shown in figure 3.

2. PURPOSE

Simulated lightning tests were carried out to investigate and verify the adequacy of the selected trailing edge and its fastening method. During the same tests the interfaces at the bonding jumper connection were subjected to the same test currents. For other reasons, it was decided at a later stage to mount a static discharger on the rudder. The method of fastening the static discharger base was also subjected to simulated lightning tests. The simulated lightning tests were performed at the High Voltage Laboratory of the N.V. KEMA, Arnhem, Holland and were in accordance with "Aerospace recommended practice: Lightning effect tests for aerospace vehicles and hardware" [1]. The test currents were based on zone 2 requirements [1]. Futhermore, the tests were mainly performed to determine the effects on the electrical bonding methods after being submitted to simulated lightning tests; this in accordance with MIL-STD-1757A [2].

3. TEST SET UP

During the tests the lightning current generator was connected either to one of the bonding jumpers and the trailing edge or between two bonding jumpers. This in order to simulate a possible current path through the rudder. After the aircraft has been hit by a lightning flash the lightning currents may flow through one bonding jumper (or enter at the trailing edge). These currents may enter the rudder either at the rudder construction at one of the bonding jumpers or at the trailing edge. Conductive tests were carried out in order to determine the capability of the structure to conduct the currents to which it will be subjected. For these tests the high current source was solidly connected to the test sample at one of the bonding jumpers or at the (for this reason extended) trailing edge. A rod was only necessary in order to create an attachment at the trailing edge. However the applied test current wave forms were the same.

All test specimens were subjected to a current impulse consisting of two components in accordance with reference 1 for zone 2. The first component was a current wave with a maximum amplitude of 100 kA and a duration of 2 µs. After 100 µs from the start of the first component a second component consisting of a current wave with an amplitude of 1,8 kA and a virtual duration (the time during which the amplitude of the impulse is greater than 10% of its peak value) of 3,5 ms was applied [1].

4. TEST SPECIMEN DESCRIPTION

4.1. Test specimen 1.

Test specimen 1 consisted of two CFRP sandwich skin panels connected at the trailing edge by means of a CFRP trailing edge member (figure 3). The specimen dimensions are representive for the Fokker 100 CFRP rudder at the location between the middle and upper hinge (figure 4). Due to the weight penalty caused by rivetting, the design office preferred to adhesively bond the trailing edge to both skin panels. In order to compare the effects of adhesive bonding and rivetting, the trailing edge of the test specimen was split into two sections. The upper section was adhesively bonded while the other section was rivetted (figure 5). The trailing edge was also extended for some distance in order to be able to make a connnection to the lightning current generator. Futhermore the sandwich skin panels were fixed in the correct position by means of two dummy (PU) ribs.

4.2. Test specimen 2 and 3.

4.2.1. First test series configuration.

Both test specimens consisted of CFRP sandwich panels representing a skin of the Fokker 100 rudder. Both test specimen cross sections were the same as for test specimen 1, but one of the corners was made representative for the spigot area. So both panels were equipped with two bonding jumpers: one for the middle hinge and one for the spigot area. Compared with test specimen 1 the construction was modified as follows:

1. bonding jumpers (greater cross section for the previous selected one had failed),
2. electrical bonding provisions at the bonding jumpers (e.g. a CFRP insert at the attachement area),
3. totally rivetted trailing edge,
4. additional CFRP layer at the outer surface of the outer skin, orientated perpendicular to the trailing edge (mainly for strength reasons, but the fibre direction will be beneficial by influencing the desired direction of current flow in the surface layer of the outer skin).

Futhermore the test specimens were equipped with dummy front-spar flanges and rib-flanges (spigot area). See figure 6.

4.2.2. Second test series configuration.

The (delaminated) front-spar flanges of both test specimens were replaced by a representative part of a production spar (complete). The (delaminated) dummy-rib flanges of both test specimens were replaced by another dummy. At test specimen 2 two monel rivets were mounted at the "ends" of the spar-rib flanges and at the "end" of the dummy rib (at the trailing edge location). Futhermore the number of rivets at the bonding strip of the middle hinge area was doubled.

4.2.3. Third tests series.

The delaminated production front spar of test specimen 2 was removed and replaced by another one. Futhermore the delaminated dummy-rib flange was also replaced. At the ends of the front spar flange and of the dummy-rib flanges metal strips were rivetted (figure 7). This is in order to simulate the (heavy) metal parts at the hinges and in the spigot area.

5. TEST RESULTS

5.1 Test specimen 1.

5.1.1. Test performed over the bonded trailing edge.

Before testing it was decided to add four rivets to one side of the adhesively bonded trailing edge (lower part of figure 8A). This was done at the request of the design office. They estimated that four rivets at the adhesively bonded trailing edge would be sufficient to conduct the simulated lightning currents. This in order to obtain a configuration with the lowest possible weight penalty. After being submitted to the simulated lightning current wave form, the adhesively bonded trailing edge was delaminated. In-house investigations revealed later that the trailing edge was delaminated over more than 75% of the cross section of its connection to the skin panel (upper part of figure 8A).

The trailing edge connection provided by four rivets was also delaminated, although to a much lesser extent. Furthermore, the outer skin plies of the trailing edge at all rivets was also heavily delaminated.

5.1.2. Tests performed over the rivetted trailing edge.

The rivetted trailing edge showed minor damage after the simulated lightning test. The damage was limited to small delaminations of the outer plies at some rivets. After this test the simulated lightning tests were repeated a further three times.

The damage to the trailing edge after the simulation of an attachment was limited to local burning of the resin (see figure 9A and 9B). The damage shown is the result after two subsequent tests.

After completion of these two tests a dummy static discharger base was mounted on the rivetted trailing edge. The subsequent simulated lightning tests showed that the fastening of the base by means of three rivets is sufficient to preclude structural damage after lightning attachment.

5.1.3. General.

At the bonding jumper area (representing the middle hinge) the CFRP skins of both skin panels were delaminated. Futhermore one of the bonding jumpers was broken during the simulated lightning tests.

5.2. Test specimen 2 and 3.

5.2.1. First test series.

5.2.1.1. Bonding jumper area.

At the bonding jumper connection of the middle hinge for both test specimens some arching and delamination of the outer CFRP plies (at the inner side of the rudder) occurred after the tests. This was considered to be unacceptable for the following reasons. In the event that the aircraft is struck in actual service it is difficult to establish damage inside the rudder. Furthermore, this was not acceptable in view of maintenance considerations.

No damage was detected on either of the two test specimens at the bonding jumper connection at the spigot area and at the trailing edge.

5.2.1.2. Flanges.

The dummy front-spar flanges of both test specimens were delaminated at both ends after the tests (figure 10A and 10B). The dummy rib flange of both test specimens was also delaminated at the end situated at the trailing edge area. The ends of the dummy rib flanges of both test specimens at the bonding jumper connection of the spigot area did not suffer any damage.

5.2.2. Second test series.

5.2.2.1. Test specimen 2.

Two simulated lightning tests were performed between the bonding jumper of the middle hinge and the trailing edge. Despite the two rivets installed at the ends of the front spar flanges, both areas suffered from delamination of the outer CFRP plies at the rivets.

5.2.2.2. Test specimen 3.

After the simulated lightning tests between the bonding jumpers of the middle hinge and the spigot area the end of the front-spar flange was heavily delaminated (figure 12A). At the end of the flange the resin in its "neck" had been vaporized blowing away carbon fibres (figure 11A and 11B). Futhermore, the inner and outer skin of the test specimen was delaminated at the honeycomb connection. This occurred in the region from the inner skin via the CFRP insert at the middle hinge area to the outer skin (figure 12B).

5.2.3. Third test series.

After two simulated lightning tests minor delamination occurred at the middle hinge bonding jumper attachment area of the inner skin (figure 13). This delamination occurred after the seventh simulated lightning test applied to this test specimen. The test specimen was subjected to a further three simulated lightning tests. No sign had been found to indicate that the delamination had grown after each single test. Futhermore no delamination occurred at the ends of the front-spar flange and at the end of the dummy rib flange (in the trailing edge area).

6. DISCUSSIONS.

For the actual Fokker 100 rudder design a rivetted trailing edge had been selected. This despite the weight penalty. Futhermore, the bonding jumper areas of the middle and upper hinge were designed simular to the configuration tested as described in chapter 5.2.3. Futhermore the ends of the front spar flanges of the rudder are well protected against damage by the heavy metal parts at the upper hinge and the spigot area. No metal parts at the ends of the top and bottom ribs have been applied. This decision is justified by the number of rivets and fasteners installed over the length of both ribs.
This had been a requirement from the Dutch Airworthiness Authorities. For strengthreasons the design could not be permitted to rely solely on the quality of the adhesively bonded ribs. The same observation had been made for all the other ribs and the front spar. On the other hand this requirement was favourable for the electrical bonding of the structural parts of the rudder. Futhermore it would be very difficult, if not impossible, to apply a metal strip at the ends of both the top and bottom rib in the trailing edge area.

7. CONCLUSION.

Although the tests were not performed on a full scale rudder, the simulated lightning current was not reduced. So the skin current density and the current through the rivets and the bonding jumpers had a magnitude which is above the design requirements, resulting in worst case conditions.

The simulated lightning tests have resulted in a rudder design which is capable of conducting lightning currents. The result will be minor damage at the trailing edge.

Futhermore it is believed that:

1. the damage after (a possible) attachment to the trailing edge can be temporarily repaired, if necessary, by means of a so called high speed tape. The required cosmic repair can be performed later at the home base of the airliner.
2. No inspection of the (inner) rudder construction is necessary after the aircraft has been struck by a lightning flash.

8. REFERENCES

1. SAE Committee AE4L, Special Task F: Aerospace recommended practice "Lightning effects tests on Aerospace vehicles and hardware.
2. MIL-STD-1757A: Lightning Qualification Test Techniques For Aerospace Vehicles and Hardware.

9. ACKNOWLEDGEMENT

The author wishes to thank Fokker Aircraft Corporation for allowing him to present this paper. Futhermore the author wishes to thank Mr. W. Scholten of Fokker Aircraft Corporation for his cooperation during the tests and for his comments on this paper.

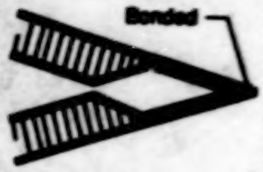

Figure 1.

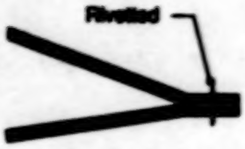

Figure 2.

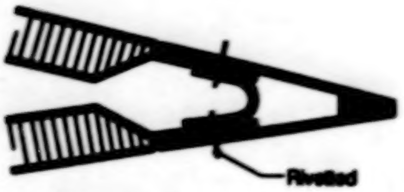

Figure 3.

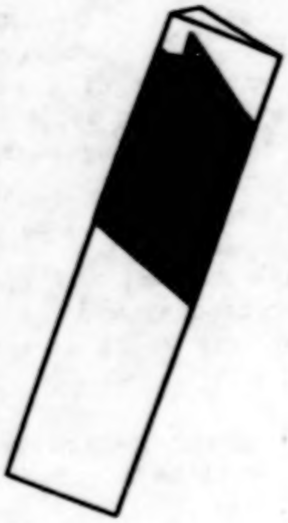

Figure 4.

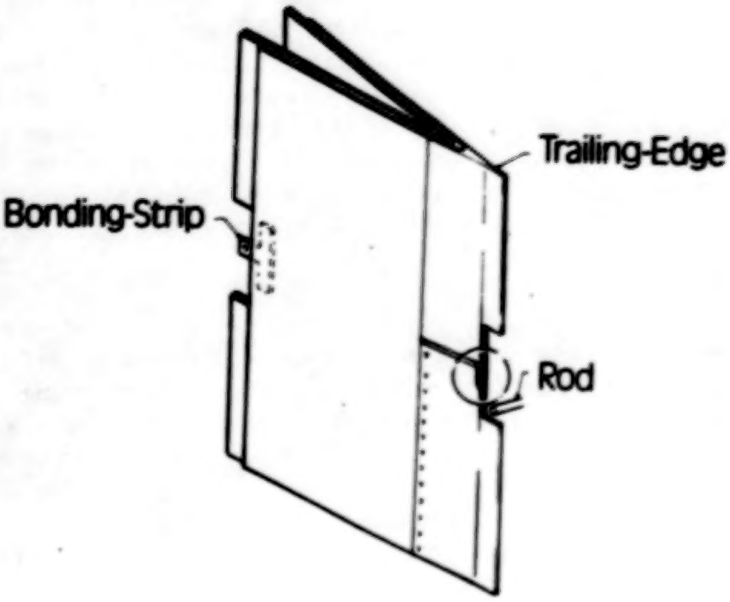
Trailing-Edge
Bonding-Strip
Rod

Figure 5.

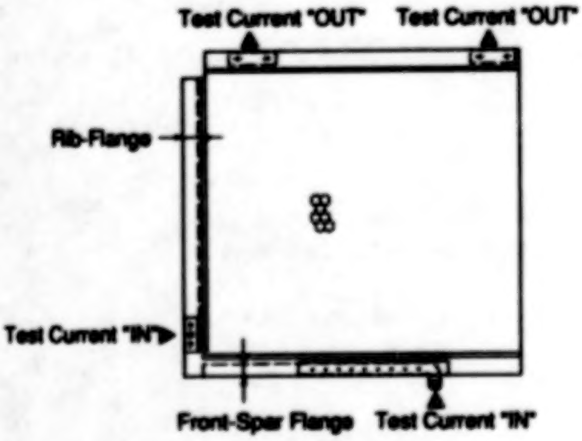
Test Current "OUT"
Test Current "OUT"
Rib-Flange
Test Current "IN"
Front-Spar Flange
Test Current "IN"

Figure 6.

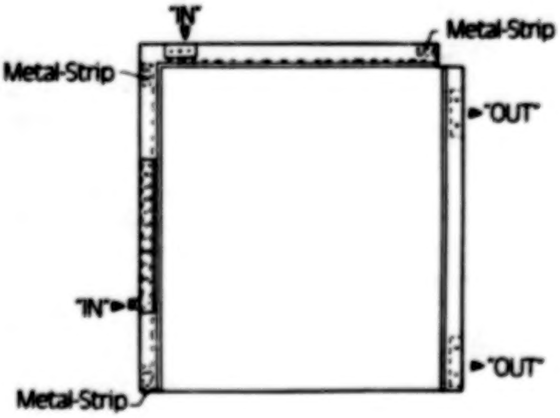
"IN"
Metal-Strip
Metal-Strip
"OUT"
"IN"
"OUT"
Metal-Strip

Figure 7.

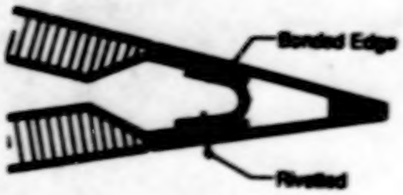
Bonded Edge
Rivetted

Figure 8A.

Figure 8B.

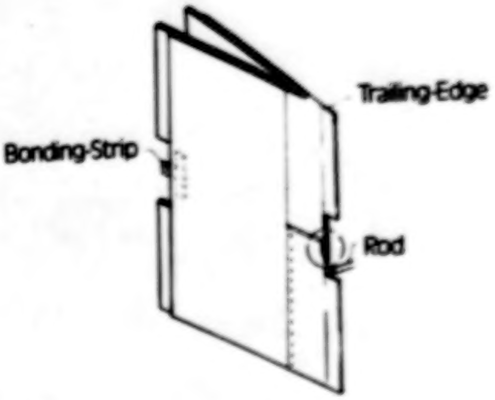
Trailing-Edge
Bonding-Strip
Rod

Figure 9A.

Figure 9B.

Figure 10A.

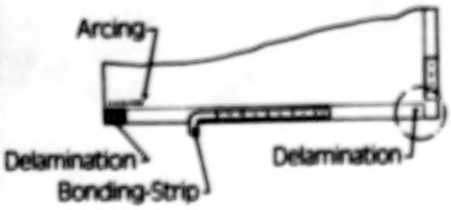
Arcing
Delamination
Bonding-Strip
Delamination

Figure 10B.

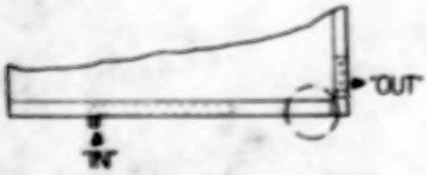

Figure 11A.

Figure 11B.

Figure 12A.

Figure 12B.

Figure 13.

PROTECTION OF ELECTRICAL AND ELECTRONIC EQUIPMENT AGAINST LIGHTNING INDIRECT EFFECTS ON THE AIRBUS A340 WING

Olaf Spiller
Deutsche Airbus GmbH, Bremen, Germany

ABSTRACT

This paper deals with the provisions applied to the Airbus A340 wing wiring against lightning indirect effects. The construction and installation of the wiring's shielding systems are described, and it takes a look at the analysis and tests performed to determine the effectiveness of the measures taken. A first evaluation of the results of the theoretical analysis together with the provisional results of tests indicate a sufficient safety margin between required and achieved protection level.

1. INTRODUCTION

Airbus Industrie's newly developed aircraft A330 and A340 have, as the already flying A320, a complex fly-by-wire system. Failure of, or errors in, such a system may be hazardous. Therefore, the need to ensure that these systems are not affected by a lightning strike is paramount. The increased use of non-metallic materials, like carbon or glass fibre in the construction of the aircraft also means that the inherent screening against the magnetic field of the lightning current is reduced [1].

The protection of electrical and electronic equipment against this effect can be achieved either by filter/protection devices, shielding of the dedicated wiring or both. To apply any method alone would probably be too expensive or just not practicable. Further, any protection method must allow easy maintenance and cater for future modifications without any degradation in the protection performance.

2. LIGHTNING ENVIRONMENT

2.1 EXTERNAL ENVIRONMENT

Lightning strike to an aircraft does in fact happen often enough to consider it as something that with a high probability will occur at some stage in an aircraft's lifetime.

The analysis of, and research into, the nature of lightning is reflected in numerous publications. They give a physical model of the lightning, which is needed for threat assessment and other theoretical evaluations (e.g. [2],[3] and [4]). The model used for the analysis described in this paper is specified in the Advisory Circular 20-136 [4]. It also forms a basis for the certification of the aircraft. Its parameters for a severe single strike are a peak current of 200 kA, an action integral of $2 \cdot 10^6$ A^2s and a rate of rise of $1,4 \cdot 10^{11}$ A/s with a double exponential waveform (component A).

2.2 INTERNAL ENVIRONMENT

Equipment not exposed to a direct lightning attachment will be subjected to the indirect effects of the lightning strike. These indirect effects are described as the "internal environment". The aircraft's internal environment is the result of the lightning current flowing through the aircraft and electromagnetic fields penetrating the skin or existing in open areas and therefore are determined by the external environment. These transient fields induce voltages in the aircraft's wiring. Typical lightning induced voltages and currents on interconnecting wiring are defined in the Advisory Circular AC 20-136 [4]. They are used to specify the equipment transient design level (ETDL), giving the maximum voltage and current amplitudes allowed at the equipment interfaces as well as their waveforms.

Equipment and wiring associated with the A340 wing (Figure 1) have been regarded as being in a severe electromagnetic environment and the equipment has been specified accordingly. Since experience showed that these voltages induced would be harmful, one approach to compatibility is through shielding of the interconnecting wiring.

For the certification of the aircraft, analysis and tests have to show that actual transient levels on the wing wiring are lower than the transient control level (TCL), which is the ETDL minus a safety margin, and therefore the maximum level of lightning induced voltage appearing at equipment interfaces.

3. SHIELDING SYSTEMS

3.1 CONSTRUCTION

Any type of shield for the use in modern aircraft has to fulfill many requirements, a number of which are not related to their shielding effectiveness directly. Their properties are not independent from each other, and an optimum solution for a mechanical requirement could cause a degradation of the shielding performance.

Some restrictions for all kinds of systems in the aerospace industry are due to a lack of space for the installation and the requirement for a minimum of weight. On the other hand, the design shall be mechanically robust and immune to all environmental influences (hydraulic fluids, salt water, etc.). It must also be taken into account that the shield cannot be installed in a straight run, but usually has to go around equipment or pipes (Figure 2). The wires must be kept in place in the harness under all conditions without the danger of chaffing. Additionally, the need for maintenance work should be kept to a minimum and it should allow for modifications to, or addition of, cables.

3.2 THE A340 WING

The above mentioned and to some degree conflicting requirements, led to a solution for the A340 wing, where two different shields have been used.

The main cable looms from the fuselage on the front and rear spar to the wingtip are mainly routed in open ducts with four separate channels, known within Airbus Industrie as "raceways" (Figure 3). These are made of an aluminium alloy and have a protective coating. They come in three different sizes to cater for the growing size of the looms closer to the wing root. The channels are filled up to approx. 65% of their height. Over the wing span, the raceways are mounted on brackets as segments of a length between 150 and 700 mm, depending on the constructional needs. Two neighboring raceways share one bracket. The gaps between two segments are usually 4 mm or less.

The second type of shield used is that of a braided conduit made of nickel plated copper. They are used for the short breakouts where wires run from a raceway to a piece of equipment or where the routing around corners or many bends over a short distance prohibit the use of raceways. This harness system can be equipped with a range of special conducting adaptors and connectors. These allow an electrically low resistance connection to equally furnished equipment housings and to the aircraft structure, thus providing 360° circumference bonding.

When cables are led from raceways into a conduit, the end fittings of the conduits are mounted on brackets as close as possible to the raceway, so that the cables run only over a very short distance outside of a shield.

4. ANALYSIS OF THE SHIELDING EFFECTIVENESS

4.1 UNPROTECTED WIRING

As already mentioned, the use of wiring routed outside of the shielding systems in the wing has been avoided as far as possible. In that sense, the wires are only routed unshielded in the gaps between raceways or conduits and raceways. Over the wing span the accumulated length of gaps has been limited to some 140cm in the leading edge and 70cm in the trailing edge. The greater length allowed in the leading edge is the result of the better inherent shielding by the metal skin, whereas the trailing edge is a more or less open area, which provides little or no attenuation of the lightning current's electromagnetic field.

4.2 BRAIDED CONDUITS

The decisive parameter for the shielding effectiveness of the braided conduits is the transfer impedance (Z_t). In the frequency domain, Z_t is dominated by the resistance in the range below 1 MHz and by the transfer inductance above those frequencies [2]. Figure 4 shows the transfer impedance as a function of the frequency.

The DC-resistance depends on the volume of metal of the shield. A low resistance calls for a dense, but heavy and less flexible shield. Other decisive factors are the optical coverage and the weave angle of the braid. A high optical coverage and a small weave angle improve the shielding effectiveness, but also decrease the flexibility.

The braided conduits in the A340 wing have an optical coverage of about 90% and a DC-resistance of less than 10mΩ/meter. The transfer impedance, as given in the manufacturers data sheet, is 5 to 10mΩ/meter up to a few MHz with a significant increase in Z_t beyond 10MHz. The low transfer impedance at the bottom of the frequency range is more important. Though the lightning energy is spread over a broad spectrum, the peak energies in the case of induced voltages are in the 50kHz to 100kHz band [1].

The overall performance of a shield also depends on the low resistance connection of the conduits to the back shells of adaptors and connectors, of the sockets to the equipment and the shielding effectiveness of those elements themselves. A table with the transfer impedance of typical aerospace cable connectors is given in [2].

4.3 RACEWAYS

4.3.1 Theoretical Analysis

The purpose of the calculations is, to assess the into the wiring induced transient voltages appearing at equipment interfaces. They are compared with the protection measures to give a first indication of the possibility of over- or undersized protection.

The calculations are based on the distribution of the lightning current in the wing. With certain assumptions it is possible to represent the three-dimensional wing structure as an array of parallel wires [2]. Since there are different materials, resistance values and a corresponding diameter have been assigned to each wire. Those cuts through the wing were made at four points (ribs), each representing a section of the wing (Figure 1).

With the self-inductance of each conductor and the mutual inductance between any two, a system of differential equations can be set up by Kirchhoff's law. These differential equations were solved by a computer code especially developed for lightning assessment purposes by Deutsche Airbus in Hamburg. The code gives the current and its time derivative versus time in each conductor. It then calculates the time derivative of the magnetic flux in a specified wire loop, giving the induced voltage. The way in which the current changes within a given time depends on the change of the lightning current during that time, as well as the geometry and material of the wing in the chosen cross-section. For the wing assessment, a model consisting of up to 585 parallel wires, leading to 584 coupled differential equations was used.

To calculate the voltage induced into cables, a diagnostic wire grounded at one end is assumed to run parallel to the structure within the cross-section of the wing at the position of the shielding system . The calculations were done considering that the wires run in- and outside of a shielding system.

The magnetically coupled voltage into this wire is the result of the time-dependant rate of change of the magnetic flux through the plane between a wire representing the structure and the diagnostic wire. The total induced voltage also contains a fraction generated by the voltage drop U_r along the structure. The worst case calculation for this is to multiply the lightning current $I_L(t)$ by the resistance R_L of the wire representing the wing. This voltage is added to the magnetically induced voltage. The reduction of the resistive fraction by the skin-effect for highly conductive materials has not been considered here. Since U_r is negligible compared to the inductive coupled voltage, a change in that fraction is negligible, too.

4.3.2 Results of Analysis

For the purpose of the comparison between the results of the analysis and the equipment protection level, braided conduits, where they have been installed, have been assumed to have the same shielding effectiveness as the raceway system. For the wing structure, the computations were done for several configurations (e.g. flaps/slats extended or retracted). Examples of these are shown in Figure 5.

The results of the calculations are the induced common-mode voltage in a diagnostic wire and the current flowing through the raceways. Table I showes these values for the examples above at the four cross-sections of the wing. For 1m of exposed wiring, the calculated voltages for wires outside of a shielding system usually range from approx. 130V in the leading edge up to 480V in the trailing edge. This confirms the need to put a more stringent limit on the accumulated length of gaps between raceways in the trailing edge.(see chapter 4.1) For cables routed in raceways, these induced voltages are reduced to less than 10V per meter of wire for all areas. Therefore, it can be said that the transient amplitude on a wire is mainly determined by the length over which it is running outside of a conduit or raceway.

The results of the computations were used to draw up a list of the transient voltages appearing on each wire of the electrical systems related to the wing, according to the theoretical analysis. For this list, the length of each wire in different areas of the wing was determined and the voltages induced in each area were added up, as shown in Table II.

4.3.3 Tests

For the raceway system, not enough data about the shielding performance (i.e. the transfer impedance) were available. Therefore, tests were carried out at the University of Hannover, Germany, where the transfer impedance was to be determined from measuring voltages induced into the wires when a current of a known value flows through a raceway segment.

The induced voltages were picked off wires put into each type of raceway. Two wires were fixed in each of two chosen channels at 65% and 80% of the height of the respective channel. Pulse currents of ca. 25kA with a damped sine waveform with frequencies of ca. 16kHz and 114kHz were injected into the segments. The tests were carried out on a single raceway with a length of about 1m and on two raceways with a combined length of about 1m, separated by a gap typical for the actual installation in the wing. The segments were mounted on brackets with fasteners in accordance with the original assembly.

Though the measurements have not been completely assessed, the first results indicate an excellent shielding effectiveness of the design. For each type of raceway and for wires running at up to 65% of the channel's height, the values for the transfer impedance are much less than 10mΩ/m in the tested frequency range. The coupling proved to be mainly inductive, as di/dt*L is the main portion of the induced voltage (0,07mΩ/m plus 0,71nH/m inductance).

140

Comparing the results of the calculation and the tests on a raceway gives an estimate of the value of the computer model. The induced voltages, in relation to the current flowing through the raceway, in either case give a difference between calculation and tests of approx. 10%. The voltages therefore expected at the equipment interfaces are usually ca. 320V or less.

5. PRODUCTION AND QUALITY CONTROL

5.1 INSTALLATION

While the shielding effectiveness of the shield itself is the result of its design, the performance of the in the aircraft fitted system depends very much on the design of the installation and its low bonding resistance. It must ensure that the shields can be fitted well during production process and that the assembly does not degrade beyond a limit during its life-span.

5.2 QUALITY CONTROL

To function as a shield against lightning current magnetic fields, raceway segments and braided conduits have to be bonded well on both ends to the aircraft structure [5][6]. The problem is to guarantee this low resistance passage after the systems have been built in.

Electrically, the installed shield bonding resistances act as a parallel connection in a conventional bonding measurement (Figure 6). Therefore, a low reading on an ohm meter would not give the true values.

The solution is to induce a current of up to 100A into the loop formed by the shield and the aircraft structure, where the joints form a serial connection (Figure 7). A measurement of the voltage drop across one joint would,together with the current, allow to calculate its bonding resistance. In reality, the whole procedure is more complicated, because it was required that the measurement device should not touch the surfaces of the raceway or brackets.

At the Deutsche Airbus factory in Bremen, a tool is now used that has been developed by a company in Germany, on the initiative of the Deutsche Airbus lightning protection specialists. It allows to measure the bonding resistance of the complete loop, where each joint has a specified maximum value of 2mΩ. The resistances of the metallic aircraft structure and shield in this loop have been regarded as insignificant for this measurement. Though it has been especially designed to measure the bonding resistance of raceways, it also can be used for braided conduits connected to brackets or equipment.

6. DISCUSSION

The installation and theoretical evaluation of the protection measures applied to the A340 wing wiring have been described. This is not a complete review of the protection scheme of the aircraft and its systems, but concentrates on how the induction of damaging transients into the wiring has been countered. The assessments use some simplifications. The interaction between lightning current and aircraft structure has been reduced from a three- to a two-dimensional model. All wires are assumed to be routed at the maximum allowed height in a channel. Possible shielding effects by hydraulic pipes and other metal framework have not been considered.

The induced voltages obtained from analysis and tests are common-mode voltages. When compiling the list of induced voltages for each wire at the equipment interface, the wires have always been considered to be single and without an individual shield. The voltages induced between the wires of a twisted two or multiple wire circuit (differential-mode) are assumed to be lower by a factor of 10 or more.

Together with the first test results, it can be said that the protection looks adequate. A final judgement about the value of the theoretical work can only be given after full aircraft tests have been performed and evaluated at a later stage in the program.

7. ACKNOWLEDGEMENTS

The author gratefully acknowledges the work on the A340 wing lightning protection of Mr.M.Kaste and Mr.H.-W.Krüger from Deutsche Airbus Hamburg and Mr.G.Holste from Deutsche Airbus Bremen, as described in chapter 4.3.

8. REFERENCES

[1] B.J.C.Burrows,
"Designers Guide to the Installation of Electrical Wiring and Equipment to Minimise Lightning Effects"
Culham Laboratory CLM-R212, 1981

[2] F.A.Fisher, J.A.Plumer et.al.,
"Lightning Protection of Aircraft"
Lightning Technologies, Pittsfield 1990

[3] W.C.Hart, E.W.Malone,
"Lightning and Lightning Protection"
Don White Consultants, Inc., 1979

[4] DoT/FAA Advisory Circular AC 20-136,
"Protection of Aircraft Electrical/Electronic Systems Against the Indirect Effects of Lightning"
DoT/FAA, 1990

[5] A.J.Schwab,
"Elektromagnetische Verträglichkeit"
Springer Verlag, Berlin 1990

[6] I.P.MacDiarmid,
"Shielding Against Lightning Induced Currents and Voltages"
in: AGARD Lecture Series No.144, 1986

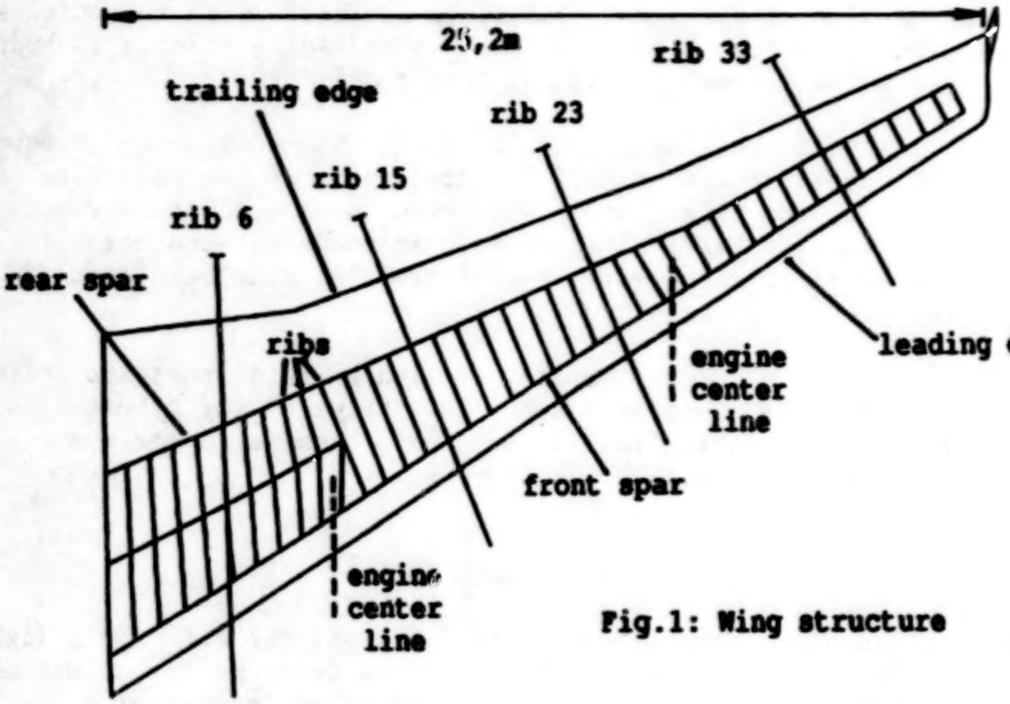
26,2m
rib 33
trailing edge
rib 23
rib 15
rib 6
rear spar
ribs
engine
center
line
leading edge
front spar
engine
center
line

Fig.1: Wing structure

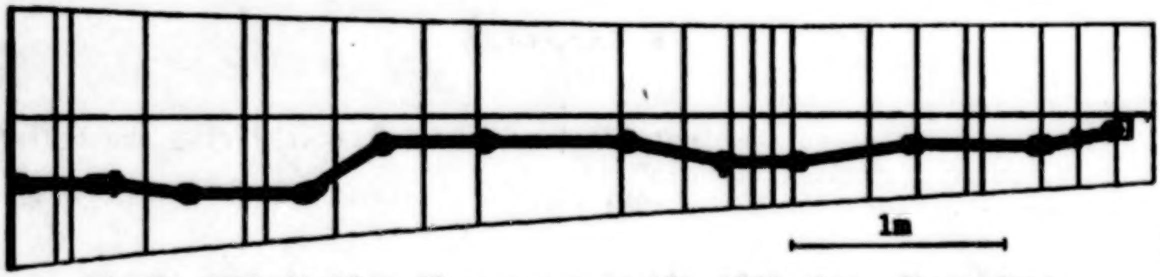

Fig.2: Installation of raceways on the A340 wing, front spar

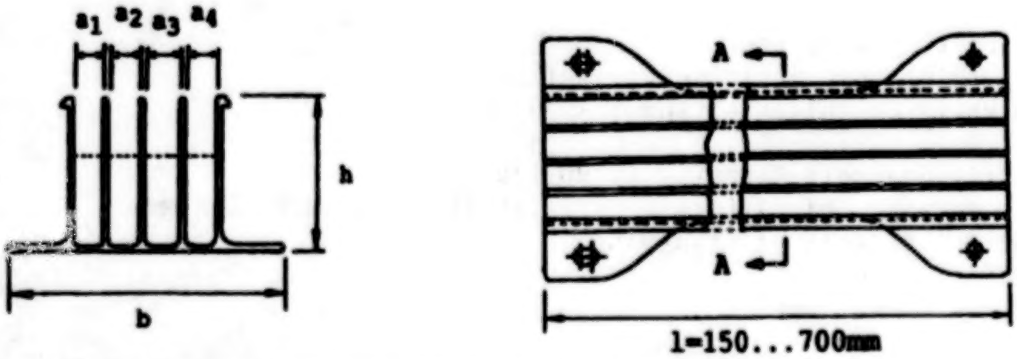
a1
a2
a3
a4
h
b
A
A
l=150...700mm

view A-A

raceway type	in millimeters					
	b	h	a_1	a_2	a_3	a_4
II	89	33	9,25	8,5	20,75	9,25
V	76	23	8,5	8,5	9,25	8,5
VII	79	43	8,5	8,5	9,25	8,5

Fig.3: raceway segment

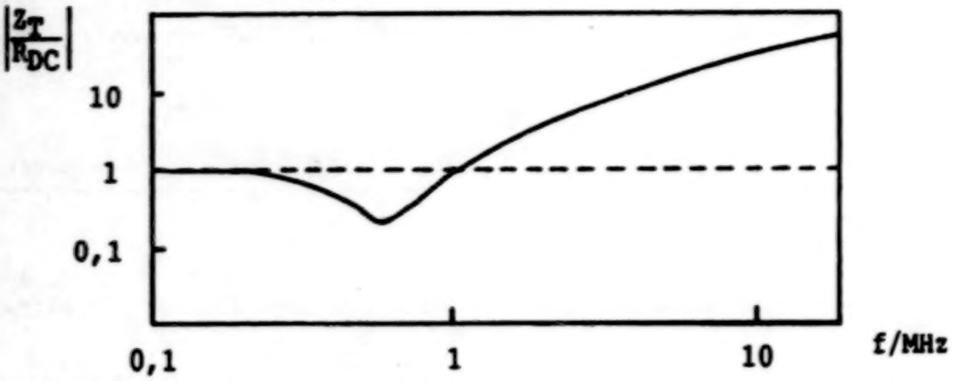

Fig.4: Braided conduit transfer impedance Z_T as a function of the frequency

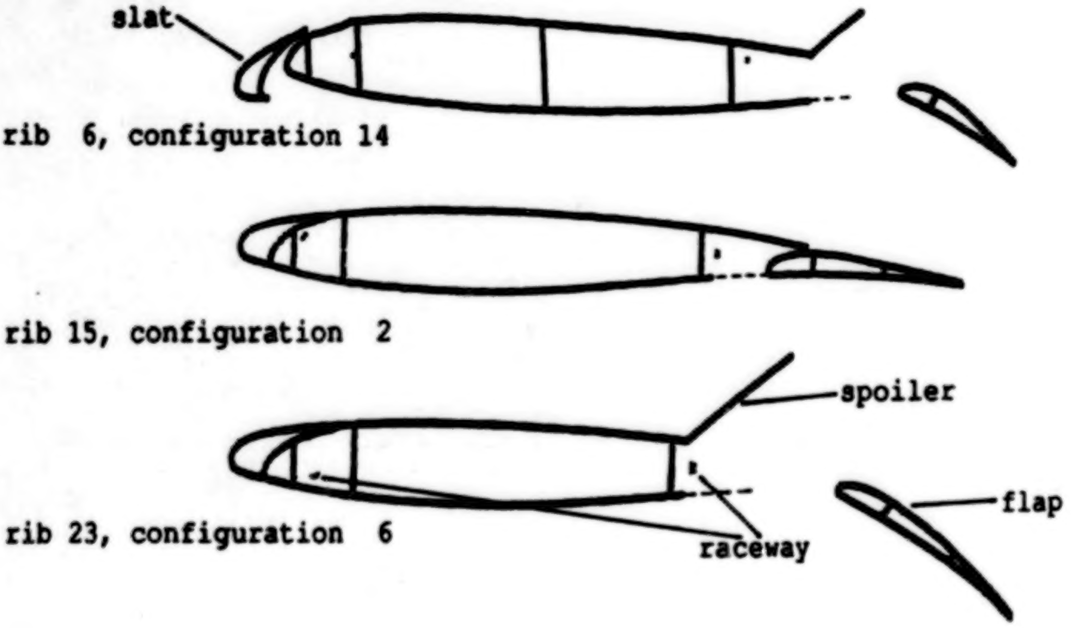
slat
rib 6, configuration 14
rib 15, configuration 2
spoiler
flap
rib 23, configuration 6
raceway

Fig.5: Parallel wire model of different wing configurations

Table I: Induced voltages and raceway currents

Config.	Induced Voltage (V/m)								Current through raceway (kA)							
	rib 6		rib 15		rib 23		rib 33		rib 6		rib 15		rib 23		rib 33	
	L/E	T/E	L/E	T/E	L/E	T/E	L/E	T/E	L/E	T/E	L/E	T/E	L/E	T/E	L/E	T/E
14	<.1	.4	.49	6.8	<.1	9.3	.11	1.7	.11	-.07	.52	2.6	.42	3.5	.63	4.7
2	<.1	.42	0.1	3.6	0.1	5.3	0.2	1.8	.06	-.09	.07	2.2	0.6	3.1	0.8	5.2
6	<.1	.31	0.1	7.1	0.1	9.8	0.2	1.8	.06	-.07	.06	2.7	0.6	3.7	0.8	5.2
5	2.7	19	3.4	353	31	487	43	231	configuration as 6, but no raceway							

L/E - leading edge
T/E - trailing edge

Table II: Calculation of induced voltage at equipment interface

Subject/Component	signal	wire type	length [m]	area	voltage induced (calc.)	remarks
RH flap wing tip brake wire no. 1						
1-wire cable	DC	CF18	0.32	32	4.5	in conduit
			0.98	32	13.8	in raceway
			8.65	28	89.1	"
			2.77	24	1.3	"
			2.07	24	0.9	in conduit
			0.33	22	0.1	junction box
			0.56	24	0.3	in conduit
			0.2	22	0.1	box
					110.1 V	total voltage

$$R_g = \frac{R_1 \cdot R_2}{R_1 + R_2}$$

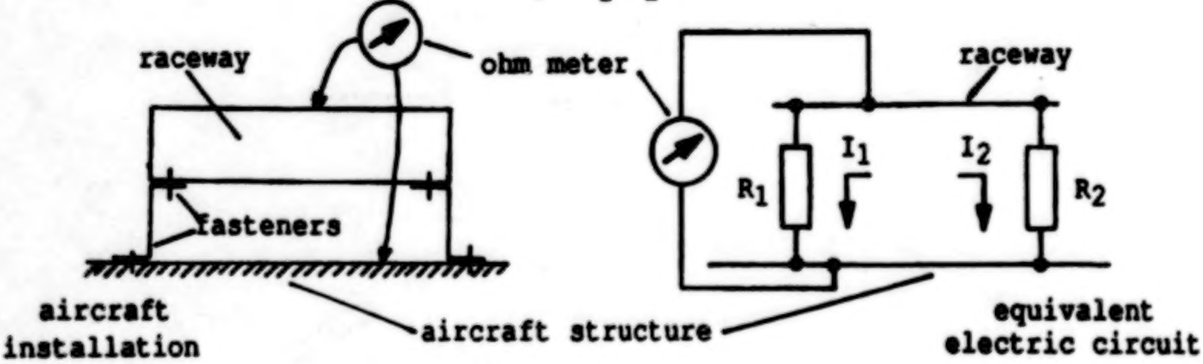
raceway
ohm meter
fasteners
aircraft installation
aircraft structure
raceway
I_1
I_2
R_1
R_2
equivalent electric circuit

Fig.6: Bonding measurement with ohm meter

$$R_g = R_1 + R_2$$

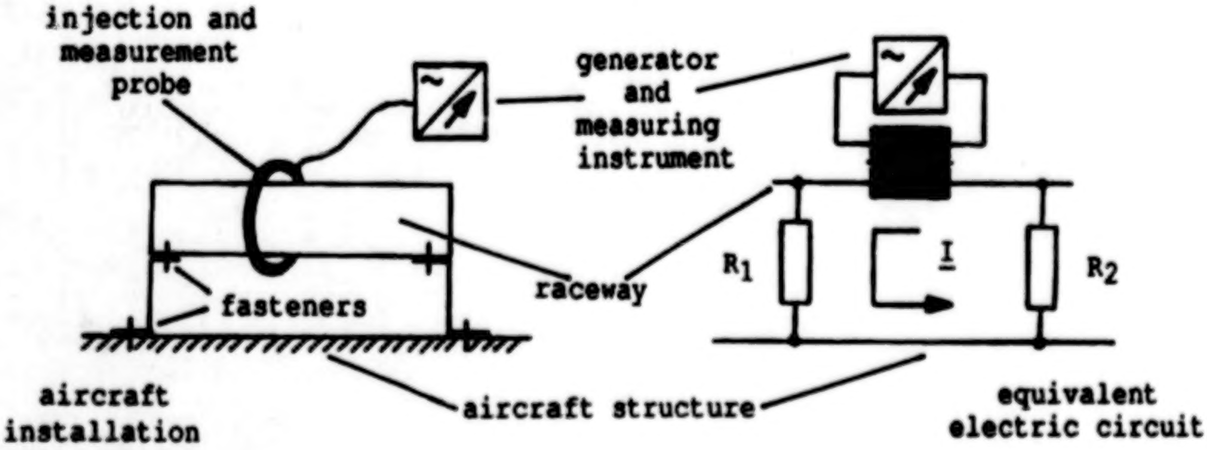
injection and measurement probe
generator and measuring instrument
fasteners
raceway
R_1
I
R_2
aircraft installation
aircraft structure
equivalent electric circuit

Fig.7: Bonding measurement with special tool

First and subsequent return stroke properties of cloud-to-ground lightning

by

S.Namasivayam and Stig Lundquist
Institute of High Voltage Research
A Department at Uppsala University
S-755 92 Uppsala
Sweden

Abstract

Lightning properties obtained by a network of magnetic direction finders and by electric field measurements for distances from 50 to 500 km are compared for three summer thunderstorms in Sweden. The data from direct field recordings indicate 31%, 17% and 26% of negative subsequent return strokes with peak current (as inferred from the peak electric field) higher than the first. Electric fields from first strokes are compared with normalised amplitudes registered by the magnetic direction finding system. The efficiency of detection by the magnetic direction finding system is discussed in terms of the percentage of of lightning flashes observed by electric field measurements that are not localised. Statistics of the number of strokes per flash and the interstroke time intervals are presented.

Introduction

In Scandinavia, cloud to ground lightning is monitored by a ground based commercial lightning location and registration system (LL&R) which provides information about the coordinates of the striking point, the amplitude of the first stroke field transition, the total number of strokes in each flash (multiplicity) and the time of occurrence of each flash. In the summer of 1988, the vertical electric field of natural lightning was measured (by one of us, S.N) during several thunderstorms and compared with the data collected by the LL&R system.

Experiment

The electric field sensor was a flat plate antenna oriented parallel to the ground. The instrumentation consists of a transient recorder capable of storing waveforms spaced a millisecond apart with a date and time tag on diskettes [1]. The data consists of time waveforms of 600 µs duration at a sampling spacing of 1.14µs. The decay time constant of the antenna system was chosen to be longer than the duration of the recorded waveforms. A preamplifier at the antenna provided impedance matching and the output of the preamplifier was connected to the transient recorder by a 20m long coaxial cable terminated with the characteristic impedance.

Results and discussion

From the data stored on diskettes, the characteristic signature of the return stroke field transitions can be easily identified. For a return stroke waveform, with a corresponding registration from the LL&R, the distance to the point of strike could be obtained. There were instances when more than one LL&R localisation data matched the time tag of the return stroke waveform within a set selection limit of one second. If this was in the case of flashes with more than one stroke, then a visual check of the waveforms was performed to verify that no subsequent stroke has been classified as a first stroke. First stroke waveforms are characterised by several subsidiary peaks following the initial rise to peak of the wavefront [2]. Further if two or more multiple stroke flashes were registered within the selection limit then these were not used in the analysis of data since the particular sequence of recorded waveforms could have been from different flashes which would lead to error for e.g. in the estimation of interstroke interval. First strokes whose initial peaks exceeded the full scale voltage range of the transient recorder were excluded from the analysis of amplitude distributions but were included in estimating interstroke intervals. As will be discussed later in this paper, there were also several cases of recorded return stroke waveforms with no matching registration from the LL&R.

Figure 1a, 1b and 1c show the comparison of the registered LL&R network amplitude units to the recorded initial peak electric field in V/m of negative, positive and both negative and positive first strokes together respectively. Approximately 90% correlation coefficient is observed in the cases of positive and both positive and negative first strokes together. For 100 LL&R amplitude units the measured electric field is approximately 3.0 V/m which is in fair agreement with an earlier estimate of 3.6 V/m [3]. Since the spread of data around the line of best fit was larger for negative first strokes, for a selected number of cases, the measured peak electric field was compared to the registered LL&R network amplitude units and to the Uppsala DF station field strength units and the results are shown in figures 1d and 1e respectively. Although a slightly better correlation coefficient is observed in the latter (comparing figure 1d to figure 1e), similar values of DF field strength units are observed for several different measured peak electric fields between 2 and 2.5 V/m. A possible explanation could be that the resolution at the lower end of the voltage range of the DF unit is limited due to the fewer number of bits used to represent the voltage signal in digitised form. This would not contribute to errors in localisation as only the angles from DF stations are utilised to compute the point of strike (except in the case of baseline calculation) but would result in an incorrect estimation of the normalised amplitude units as calculated by the LL&R network. Localisation errors of the LL&R network could however be attributed to the difference in the spread of data between figure 1d and 1e around the line of best fit.

The amplitude distribution (normalised to 100 km) of the electric fields of single stroke flashes is shown in figure 2 and of the first stroke from flashes with multiple strokes in figure 3. The geometic means of the initial peak electric field amplitude distributions for single stroke flashes and for multiple stroke flashes do not show any significant difference and are in good agreement with earlier observations in Sweden [3]. Measurements from Florida have shown a lower geometic mean initial electric field for single stroke flashes than first strokes in multiple stroke flashes [4].

From measurents by Krider et al in Florida [5], we infer that at least 10% of the electric fields from subsequent strokes preceded by dart-stepped leader processes were higher than the first stroke. In Sweden, measurements indicate a significantly larger fraction of subsequent strokes with the highest electric field peak in a multiple stroke flash. For three thunderstorms observed during the periods 7-8th June 1988, 27-30th June 1988 and 15-16th July 1988, from multiple stroke flashes, the percentages of subsequent strokes with electric field peak amplitudes higher than the first stroke were 31%, 17% and 26%. The ratio of the peak amplitude of the largest stroke in a flash to the peak amplitude of the first stroke in the same flash for the data from 7-8th June 1988, is shown in figure 4. The results show a significant number of subsequent strokes with higher field peaks for flashes with weak first strokes. The return stroke peak current is strongly correlated with initial peak electric field [6]. If this correlation is applied to derive the peak current from the initial peak electric field data then the peak current for a significant number of subsequent strokes are larger than for first return strokes. This can have several practical implications. Assuming the relationship $d_s=10\ I^{0.65}$, where d_s is the striking distance [7] the protection zone e.g. by a lightning conductor over an electrical installation is reduced by a weaker first stroke and a more vulnerable point can be struck. Worse damage could result if followed by a subsequent stroke possibly having larger derivative of current and a larger current. Further, the mean time between failures (MTBF) for the performance of metal varistor oxide (MOV) used as current surge protective devices is strongly dependent on temperature, a critical number of current surges and the time derivative of the current density [8]. If a transient current surge in a powerline either by a direct strike or induced by a nearby strike is suppressed by the MOV device, it would be heated by the energy absorbed. In the event of a subsequent stroke with higher energy, the deterioration effects on the device could be expected to be higher.

Measurements of the current of direct strikes to instrumented towers show, however, that the peak current for first return strokes are significantly larger than for all subsequent strokes [9]. Since the initial peak electric field depends not only on the peak current but the velocity of propagation of the wavefront along the return stroke channel it is possible that a smaller current travelling faster upwards along the channel could still produce higher electric fields. Another explanation could be that the return stroke channel previously traversed by the first stroke has cooled sufficiently to be non conducting some hundred metres close to the ground. Calculations of the time necessary for a previously established return stroke channel of 2.5 cm diameter to cool sufficiently to a temperature for which the channel becomes non-conducting, indicate a value close to 100 milliseconds[10]. If this is the case then a stepped dart leader could establish a spacially separate channel linking the lowest point of the conducting part of the channel to the ground for a subsequent stroke. A return stroke current flowing in a channel some 50-100 metres from the ground level would be sufficient to produce an electric field with risetimes of the initial peak of the order of a few microseconds. A consistent feature observed in many of the subsequent stroke waveforms with larger amplitudes than the first stroke was either the very pronounced pulse characteristics of leader steps or a very disturbed field preceding the abrupt transition to peak (see figure 8b and 9c). If the decrease of the speed of descent when a dart leader transforms into a dart-stepped leader, would lead to an accumulation of the hitherto smooth flow of charge brought down by the dart leader then it is reasonable to expect larger currents if the return stroke neutralises a major portion of this charge. From simultaneous measurements of optical and electric fields in Florida, [11] the peak optical output from a subsequent stroke preceded by dart-stepped leader is less than for the first stroke (figure 4 of their paper) with the electric field of the subsequent stroke higher than the first stroke. Since the peak light intensity is correlated to stroke peak current, the current in the dart-stepped subsequent strokes may be expected to be less than in the first stroke. If a dart-stepped leader forges a spacially separate channel, then the point of strike could be different for the first stroke and the subsequent stroke and the arguments presented earlier regarding the vulnerablity of an electric installation to multiple strikes may not be valid.

Figure 5 depicts the interstroke interval of the subsequent strokes as a histogram and it follows that a large percentage of subsequent strokes with an interstroke interval of more than 100 ms are present. The most probable interval is between 30-90 millisconds, and the geometric mean inter-stroke interval is 0.89 secs in good agreement with measurements in Florida [12,13].

The amplitude of the large subsidiary peaks as a fraction of the initial peak for first return stroke waveforms have been reported from measurements in Florida [2] and Sri Lanka [14]. From the data given, the mean amplitude ratios of the second subsidiary peak to the initial peak are 0.8 ± 0.1, 0.7 ± 0.2 (two storms in Florida) and 0.82 ± 0.14 (Sri Lanka). Using the number of observations given, at most 4 of 72, 2 of 36 and 3 of 53 would have the second subsidiary peak larger than the initial peak. However, in Sweden, from the 7-8th June 1988 data, of 379 single return strokes which were localised between 90-200 km, 108 had larger subsidiary peak amplitudes than the initial peak amplitude of the waveforms. Of all first return stroke waveforms analysed, 6% had ratios greater than 1.3 and were not localised by the LL&R probably due to the requirements imposed by the DF electronics that no subsidiary peak can exceed the first peak amplitude by more than 20%. From the 7-8th June 1988 data, for distances of the location of strike between 100 and 300 km, the amplitude of the large subsidiary peaks as a fraction of the initial peak of localised strokes are depicted in figure 6. The highest number of peaks recorded was seven and the separation between the initial peak and subsidiary peaks is summarized in figure 7. Of 420 waveforms 44%, 20%and 12% had the separations between the first and second, second and third, third and fourth subsidiary peaks within 10µs from each other but only 4% had all three subsidiary peaks within 10µs from each other. These fractions of waveforms represent a higher value than in Florida and lower than the data from Sri Lanka indicate. The small peak following the initial peak reported by [2] was sometimes observed on both first and subsequent strokes. We have not attempted to analyse these due to the limited resolution of the recording instrument. However, the time separations were at least 2-5µs from the initial peak. Since the second subsidiary peak in most cases were large it was difficult to discern whether these small peaks were always present. The mean separation of the second subsidiary peak from the initial peak is probably biased towards a lower value due to the presence of the small peaks. A noticeable feature when comparing the waveforms of return strokes localised at more than 100 km (figure 9) with a return stroke within 50 km (figure 8) is the width of the subsidiary peaks are very narrow and more closely spaced for the closer return stroke waveform. The amplitudes of the subsidiary peaks are probably attenuated and their widths are broadened by propagation over finitely conducting ground. If the DF station electronics reject the stroke on the criteria that the amplitude of subsidiary peaks for the closer strokes are more pronounced, then the subsequent stroke may be accepted as a first stroke. In the case of a strong return stroke it is possible that the next DF station would accept the waveform after subjection to propagation. In the case of first strokes with small peak amplitudes probably a lower multiplicity would be registered by the LL&R network.

Typical first and subsequent return stroke waveforms have been recorded by direct field measurements that were not localised by the LL&R network. The waveforms not localised by the LL&R due to high subsidiary peaks formed only a fraction of the total. Since distance is unknown, we could only guess whether these were strong or weak strokes. We therefore present the data as a percentage of the total data used in this study. Of a total of 1419 consisting of both first and subsequent strokes, 206 first and subsequent return stroke waveforms were not localised giving a detection efficiency of less than 85%. Further for flashes localised within 150 km from the measurement location, a higher number of subsequent strokes were recorded than the multiplicity registered by the LL&R. Therefore the number of return strokes in a flash are calculated using the electric field record for distances upto 150 km and compared to the data for multiplicity given by the LL&R network. From the 7-8th June 1988 data, the average number of return strokes in a flash obtained from electric field records is 2.1 with a standard deviation of 1.4 and from the LL&R network is 2.7 with a standard deviation of 1.9.

In this report we have tried to evaluate the data given by the LL&R network by measured electric fields. The results obtained in this study show that the data obtained using a LL&R network must be interpreted with caution. It may be necessary that in order to obtain better results the selection criteria must be appropriately set to the signature of lightning electromagnetic radiation fields for a particular region.

List of References

[1] Namasivayam, S., Jokanovic', N., Scuka,V., Israelsson.,S., and Lundquist,S., "The design of an instrument for the continuous recording of transient waveforms utilising high time resolution", 19th International Conference in Lightning Protection, 5.6, April 25-29,1988.

[2] Weidman, C.,D., and Krider, E.,P.,; "The fine structure of lightning return stroke waveforms", Journal of Geophysical Research, Vol 83, No. C12., Dec 20, 1978.

[3] Cooray, V., and Lundquist, S.,"On the characteristics of some radiation fields from lightning and their possible origin in positive ground flashes", J. Geophysical Research, Vol 87, No C13 , 1982.

[4] Rakov, V., A., and Uman, M.,A., "Some properties of negative cloud to ground lightning", 20th International Conference in Lightning Protection, 6.4, Sept 24-28, 1990.

[5] Krider, E.,P., Weidman ,C.,D., and Noggle, R.,C.,"The electric fields produced by lightning return stepped leaders" J. Geophysical Research, Vol 82, No. 6., 1977

[6] Willet, J.,C., Bailey, J.,C., Idone, V.,P., Eybert-Berard, A., and Barret, L., "Submicrosecond intercomparison of radiation fields and currents in triggered lightning return strokes based on the transmission line model", J.Geophysical.Research., Vol 94, pp.13275-13286, 1989.

[7] "The lightning conductor", Chap 4 in the book 'Lightning protection' by Golde, R., H., published by Edward Arnold (publishers) Ltd.,1973

[8] Workshop organised by URSI commission E during the 1983 EMC Symposium and exibition, Zurich, edited by V.Scuka,"Lasting effects of transients on equipment performance", UURIE 147-83, Institute of High Voltage Research, Uppsala University, Sweden.

[9] Berger , K., Anderson, R., B.,and Kroninger, H.,"Parameters of lightning flashes", Electra 80, pp. 23-37,1975.

[10] Uman, M.,A., and Voshall, R.,E., "The time interval between lightning strokes and the initiation of dart leaders", J.Geophysical. Research, Vol 73, pp.497-506, 1968.

[11] Changming Guo, and Krider, E.,P., "The optical and radiation field signatures produced by lightning return strokes", J. Geophysical Research, Vol 87,No. C11, 1982.

[12] Brantley,R.D., Tiller, T.,A., and Uman, M.,A.; "Lightning properties in Florida thunderstorms from video tape records", J. Geophysical Research., Vol 80, No.24. 1975.

[13] Thomson,E.,M., Galib, M., A., Uman, M.,A.,Beasley, W., H., and Master, M., A., "Some features of stroke occurrence in Florida lightning flashes.",J. Geophysical. Research., Vol 89, No. 24., 1984.

[14] Cooray, V., and Lundquist, S.,"Characteristics of the radiation fields from lightning in Sri Lanka in the tropics", J. Geophysical. Research, Vol 90, No D4 , 1985.

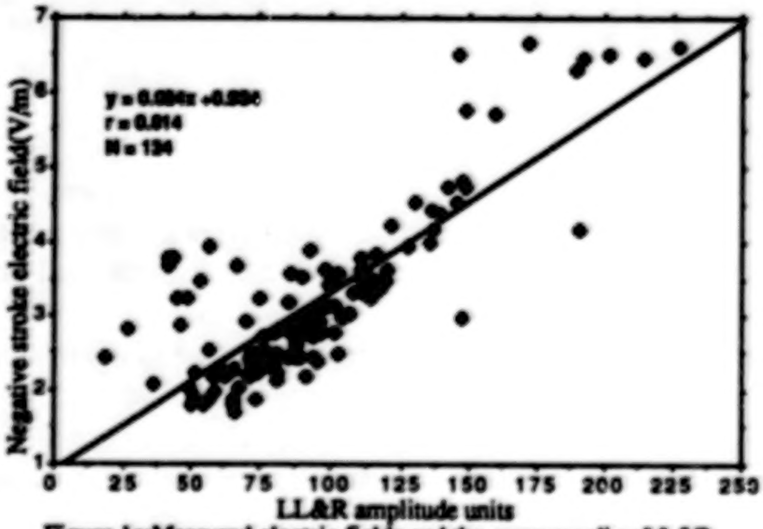

Figure 1a:Measured electric fields and the corresponding LL&R amplitude units

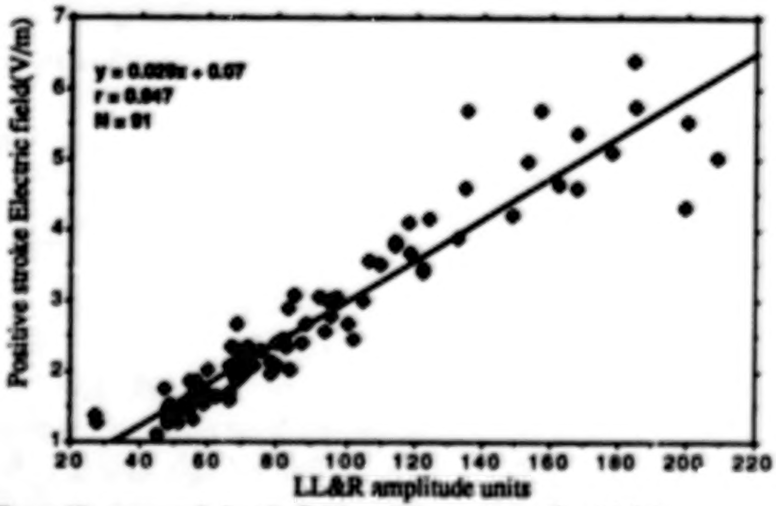

Figure 1b: measured electric fields and the corresponding LL&R amplitude units

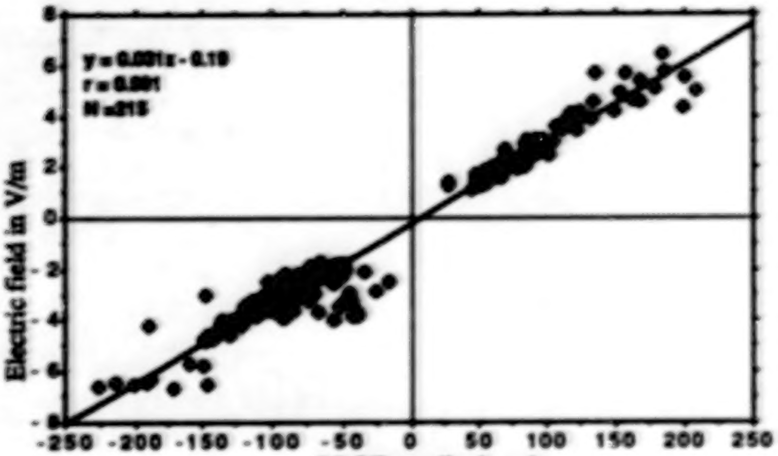

Figure 1c: Measured electric field and corresponding LL&R amplitude units

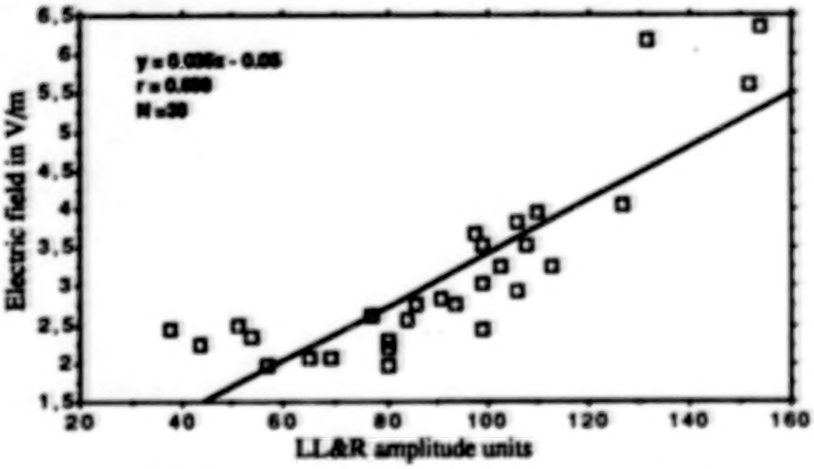

Figure 1d: Measured electric field and corresponding LL&R amplitude units

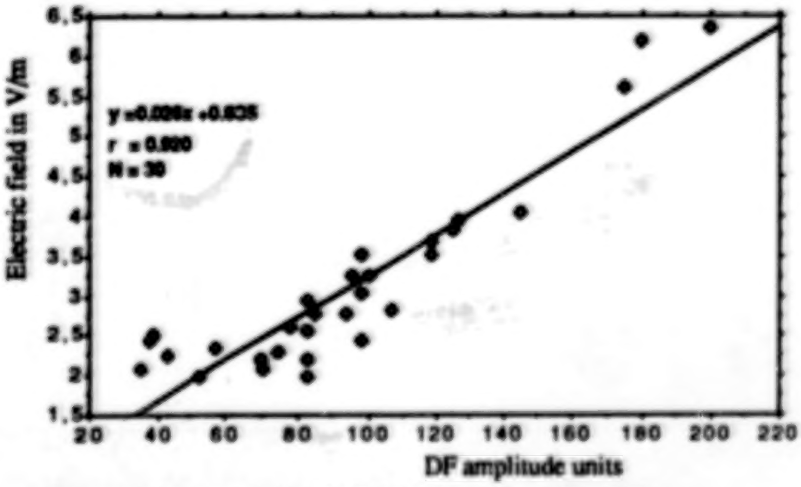

Figure 1e: Measured electric field and corresponding DF amplitude units

152

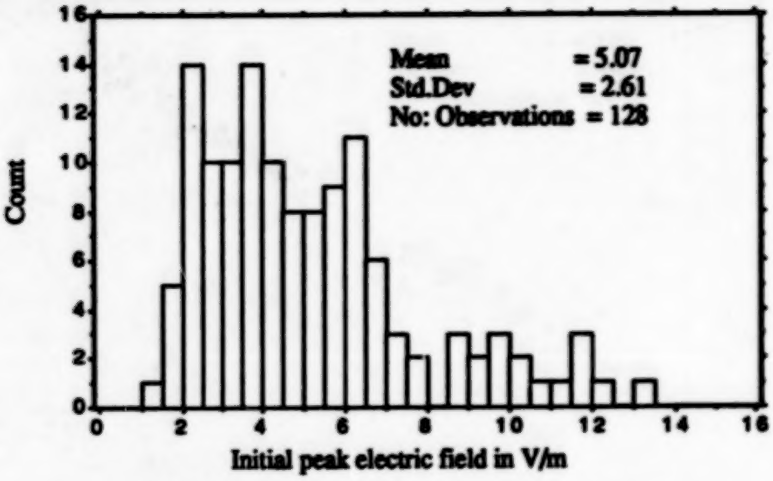

Figure 2: Distribution of normalised (to 100 km) amplitudes of negative single strokes

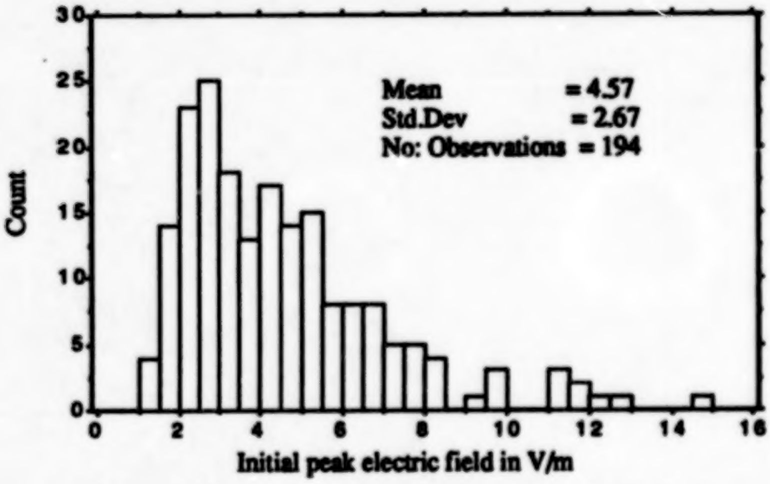

Figure 3: Distribution of normalised (to 100 km) amplitudes of negative first strokes in multiple stroke flashes

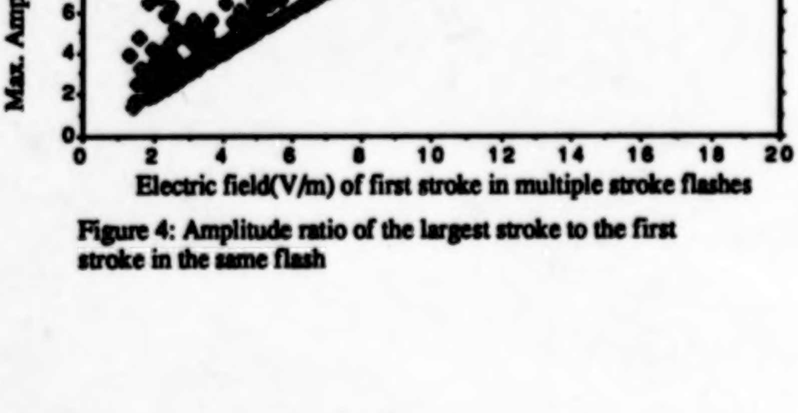

Figure 4: Amplitude ratio of the largest stroke to the first stroke in the same flash

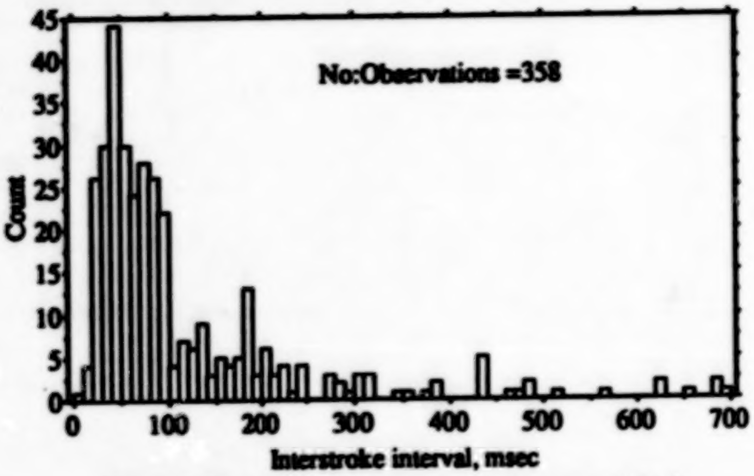

Figure 5: Histogram of subsequent stroke separations in milliseconds

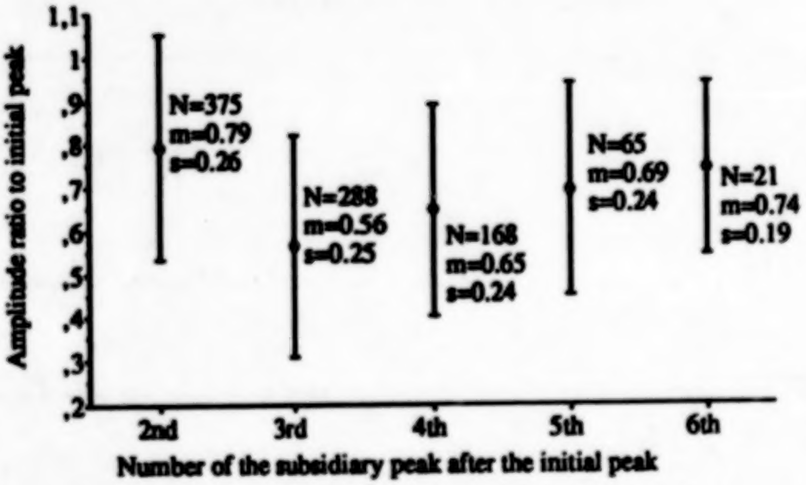

Figure 6: Amplitude ratio of secondary peaks to initial peak

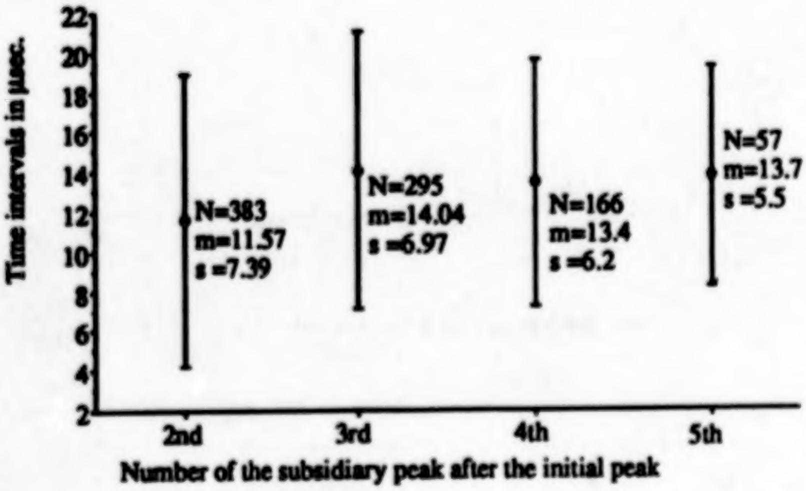

Figure 7: Time separations between subsidiary peaks in µseconds

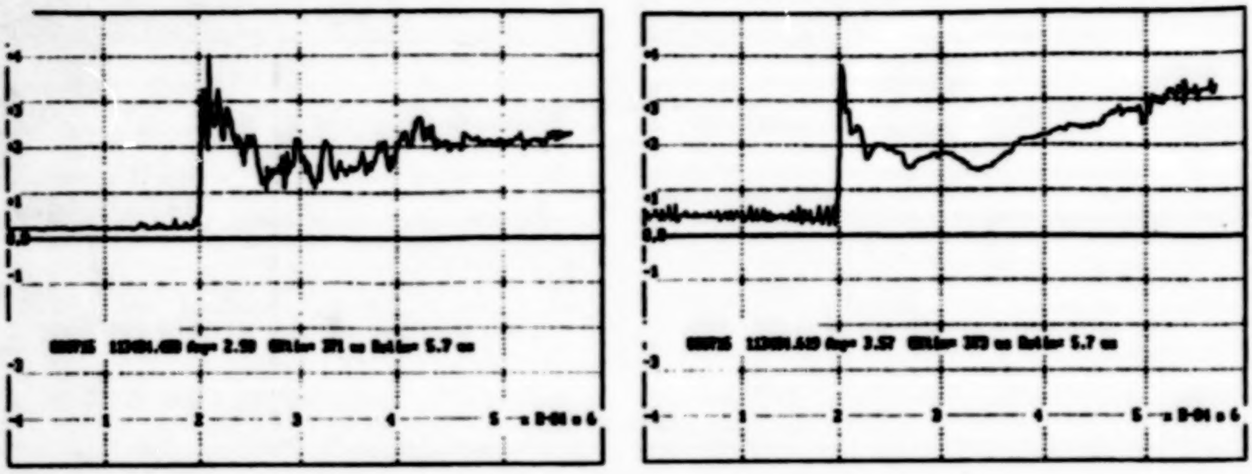

Figure 8a and 8b: The electric field waveforms of the first and subsequent strokes of a close flash within 50 km distance.

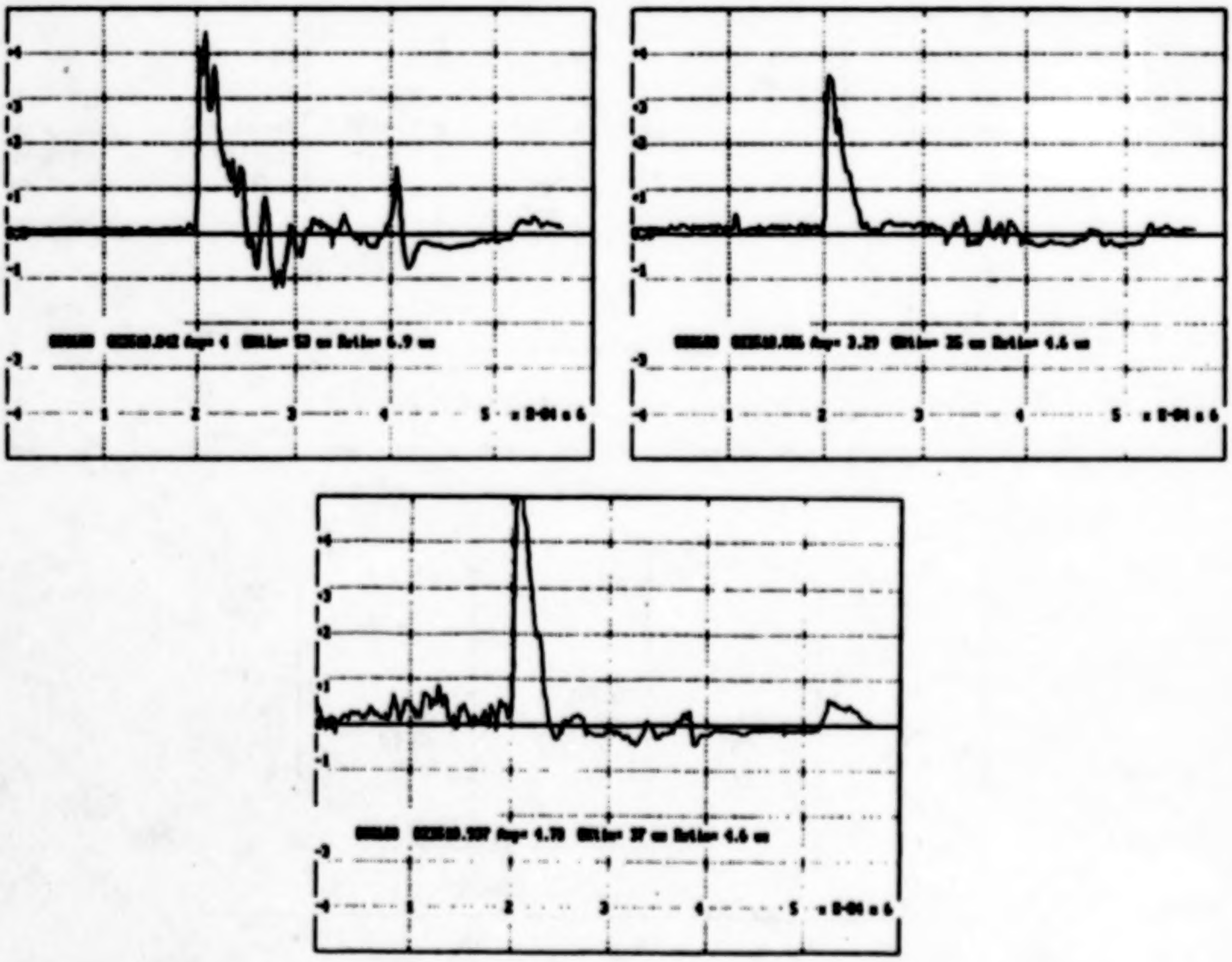

Figure 9a, 9b and 9c: The electric field waveforms of the first and the next two subsequent strokes in a flash at more than 100 km distance.

Session 4A, Tuesday 3:45

Lightning Phenomenology Measurements 3

Rhunke, Chairman

Characteristics of return stroke electric fields produced by lightning flashes at distances of 1 to 15 kilometers

Ch. Hopf
University of the Federal Armed Forces
Munich, Germany

$\dot{E}$-signals from single and multiple lightning strokes measured at the lightning research station of the University of the Federal Armed Forces near Munich in 1989 are presented. For about 25% of all acquired waveforms, produced by return strokes, stepped leaders or intracloud discharges, type and distance of the signal source are known from the observations by an all sky video camera system.

The analysis of the $\dot{E}$-waveforms in the time domain shows a significant difference in the impulse width between return stroke signals and those of stepped leaders and intracloud discharges. In addition the computed amplitude density spectrum of return stroke waveforms lies by a factor of 10 above that of stepped leaders and intracloud discharges in the frequency range from 50 kHz to 500 kHz.

Introduction

In the past a lot of electric field derivative measurements of return strokes, stepped leaders and intracloud discharges in the near distance range were made [e.g. 1, 2]. However often difficulties remain in determining distance and type of the signal source. Hence in the case of single station measurements the recording of optical and acustical lightning signals by using various video cameras [3] or a so called all sky video camera system is necessary.

Only if type and distance of the signal source are certainly established criterions can be worked out derived from the measured electric data to discriminate signals from return strokes from other signals. To achieve this aim analysis in the time domain, as well as in the frequency domain down to low frequencies of 50 kHz, are performed.

Experiment

The fully automatically working measuring station consists of two components, firstly the measuring devices for obtaining the electrical signals of a lightning discharge and secondly the so called all sky video camera system. Figure 1 shows a overview of the measuring station with the HP 9836 computer as the controller.

The electric field derivative $\dot{E}$ is registered by a capacitive 0.5 m rod antenna with a spherical termination at the top. Combined to a coaxial cable with a surge resistance of 50 Ω it leads to a bandwith of at least 50 MHz. Using a digital storage oscilloscope LeCroy 9450 with a sample rate of 10 ns it is possible to record at maximum 20 $\dot{E}$-waveforms of 20 µs duration, which are separately to be triggered, within one lightning event.

As it is reported from near field measurements [1, 2, 4, 5] the interesting $\dot{E}$-signals of return strokes which are of main interest show a typical bipolar impulse with dominant frequencies up to a few MHz. To avoid triggering on very fast impulses, e.g. produced by stepped leaders, an external trigger generator in combination with a separate similar rod antenna is used. It works as a bipolar trigger with an upper cutoff frequency of 5 MHz.

A DSO GOULD 4072 samples at a rate of 1 ms both the electrostatic field measured by a slow field mill (bandwidth = 10 Hz) and the maximum $\dot{E}$-signals using peak detection during 1 sec. A positive change of the electrostatic field points at a negative flash, a negative change at a positive flash, if it is produced by a cloud-to-ground flash. The peak detection of the $\dot{E}$-signal over a time period of 1 sec gives informations about the duration of one whole event and the maximum amplitudes of the electric field derivative.

The second essential part of the station is represented by the all sky video camera system. The simultaneous storing of the video camera output together with the mixed in date and time signal of a video timer and the signals of two thunder microphones enables the operator to estimate the distance to the striking point by the time difference between thunder and optical signal. Similar to the photoelectric detector described by Uman [6] a video camera is mounted in vertical position below a convex mirror in a height of about 6 m above ground (Fig. 2). The rotationally symmetrical aluminium mirror (Fig. 3) is optimized to wavelengths of 380 nm to 780 nm. A distance of about 350 mm between mirror and camera objective results in an elevation angle of 60° and an asimuth angle of 360°. According to the weather conditions lightning flashes in a range up to 15 km are recognizable as cloud-to-ground (Fig. 4a), resp.

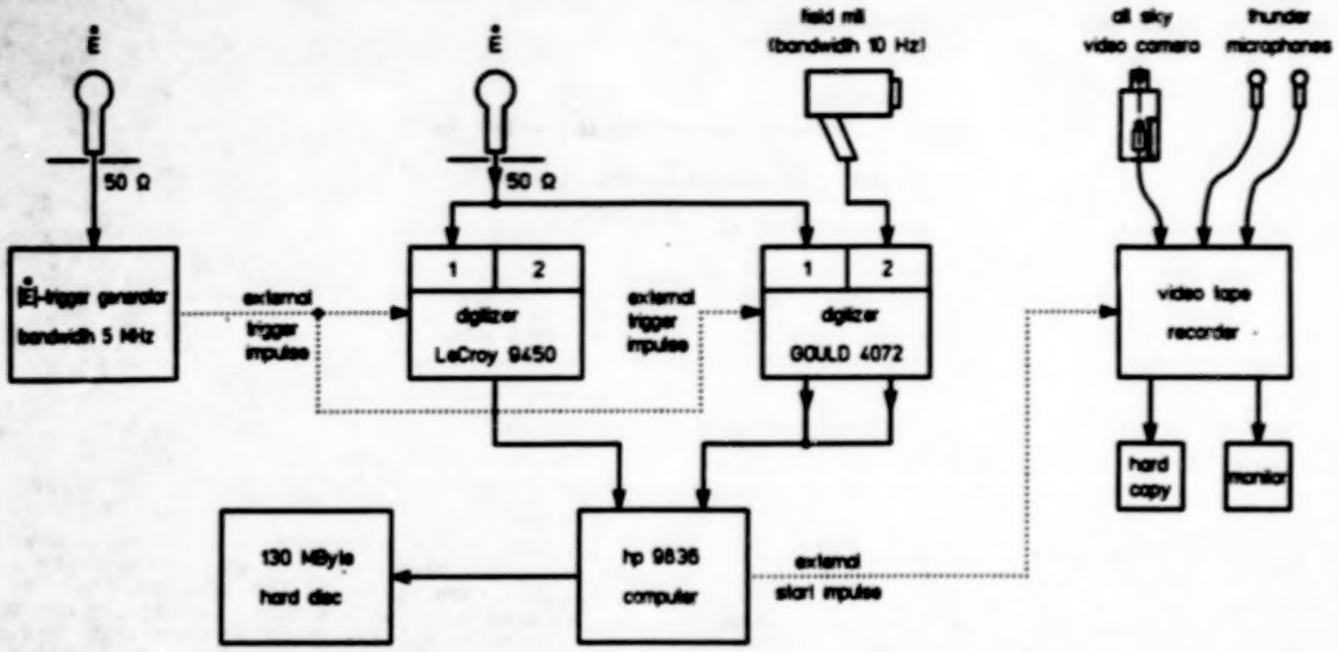
$\dot{E}$
$\dot{E}$
field mill
(bandwidth 10 Hz)
all sky
video camera
thunder
microphones
50 Ω
50 Ω
$|\dot{E}|$-trigger generator
bandwidth 5 MHz
external
trigger
impulse
1
2
digitizer
LeCroy 9450
external
trigger
impulse
1
2
digitizer
GOULD 4072
video tape
recorder
hard
copy
monitor
130 MByte
hard disc
hp 9836
computer
external
start impulse

Fig 1: Block diagram of the automatically working electric field measuring station used in 1989.

cloud-to-cloud discharges (Fig. 4b). Thereby the horison appears as the inner circular disk surrounded by the sky as an englightened annular ring. With the video image repetition rate of 40 ms it is possible to resolve even subsequent strokes. During the automatic operation the computer starts the video recorder after the first trigger impulse and stops it 7,5 min after the last trigger impulse in order to make the most of the video tape with a recording time of 180 min.

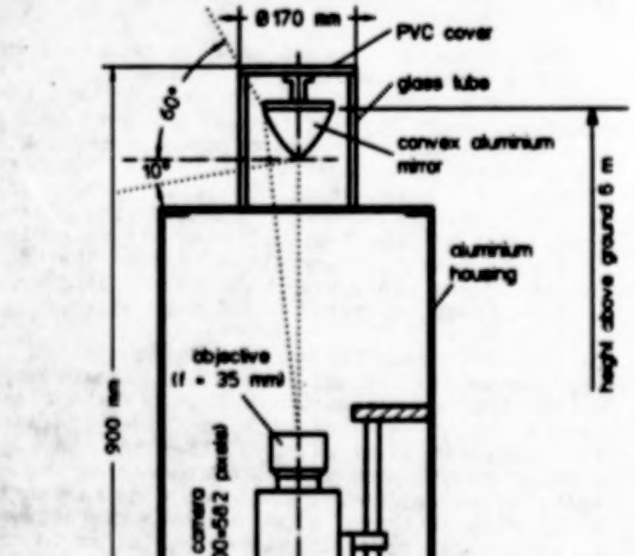
Ø170 mm
PVC cover
glass tube
60°
10°
convex aluminium mirror
aluminium housing
height above ground 6 m
objective
(f = 35 mm)
900 mm
video camera
(resolution 500×582 pixels)

Fig. 2: All sky video camera system with an azimuth angle of 360° and an elevation angle of 60°

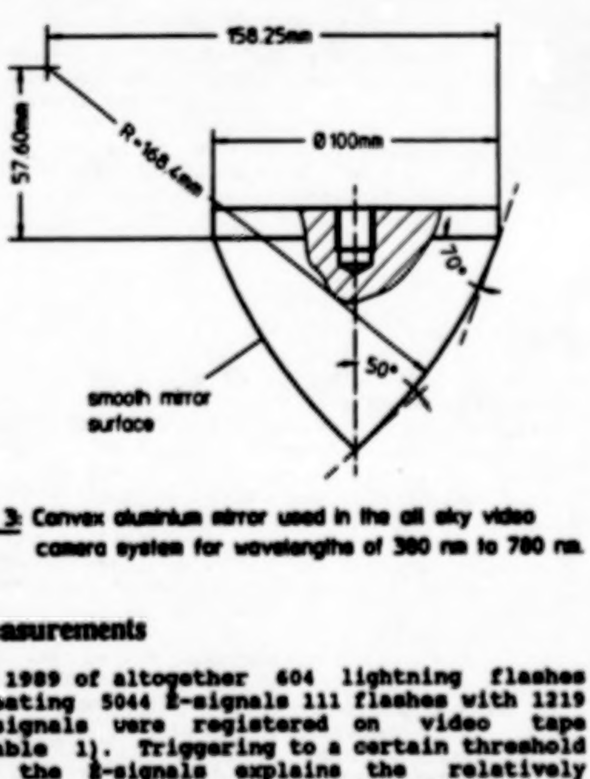
158.25mm
57.60mm
R=168.4mm
Ø100mm
70°
50°
smooth mirror
surface

Fig. 3: Convex aluminium mirror used in the all sky video camera system for wavelengths of 380 nm to 780 nm.

Measurements

In 1989 of altogether 604 lightning flashes creating 5044 $\dot{E}$-signals 111 flashes with 1219 $\dot{E}$-signals were registered on video tape (Table 1). Triggering to a certain threshold of the $\dot{E}$-signals explains the relatively small number of 54 obtained return stroke waveforms compared to 2165 single impulse waveforms produced by stepped leaders and intracloud discharges. In the following $\dot{E}$-signals are examined with a single characteristic impulse within 20 µs. Figure 5 shows the interesting parameters, that is the impulse width (T_{50}) and the maximum peak of the $\dot{E}$-signals ($\dot{E}_{max}$), resp. the initial peak of the computed electric field (E_{max}). 2813 $\dot{E}$-waveforms without a regular structure or with multiple characteristic impulses within 20 µs are ignored.

a) Cloud-to-ground lightning channel

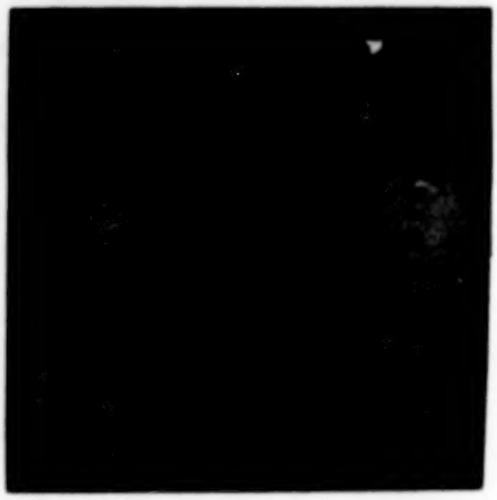

b) Cloud-to-cloud lightning channel

Fig. 4: Video images of a cloud-to-ground (a), resp. cloud-to-cloud (b) lightning channel observed by the all sky video camera system.

	All measured data	Data with determined distances
Multiple characteristic impulses or amorphous signals	2825	704
Negative single impulses of stepped leaders and intracloud discharges	973	233
Positive single impulses of stepped leaders and intracloud discharges	1192	271
Neg. impulses of return strokes	7	3
Pos. impulses of return strokes	47	8
Σ	5044	1219

Table 1: Overview of 5044 $\dot{E}$-signals (20 μs, 10 ns sample interval) in 604 flashes, resp. 1219 $\dot{E}$-signals in 111 flashes with determined distances measured in 1989.

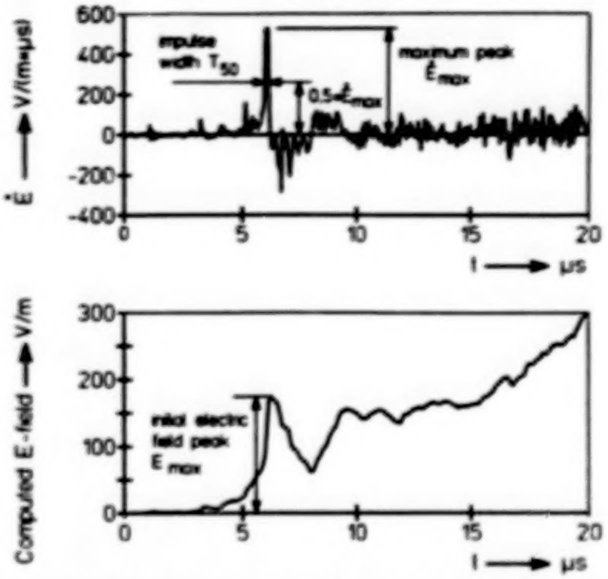

Fig. 5: Example of field derivative $\dot{E}$ and computed E-field waveforms of a return stroke in a distance of 2 km. The impulse width T_{50}, the maximum $\dot{E}$-peak $\dot{E}_{max}$ and the electric field initial peak E_{max} as the interesting parameters are shown.

Results

In agreement with former measurements [1] the maximum peaks of the electric field derivative $\dot{E}_{max}$ with a mean value of 128 (V/m)/μs for all measured data of stepped leaders and intracloud discharges, resp. 7.59 (V/m)/μs for determined distances normalized to 100 km by the inverse distance relationship, lie in the same order as those of return strokes with a mean value of 109 (V/m)/μs for all data, resp. 5.53 (V/m)/μs for determined distances normalized to 100 km (Fig. 6).

Against that the electric field initial peaks E_{max} differ with a mean value of 4.82 V/m for all measured stepped leaders and intracloud discharges, resp. 0.247 V/m for determined distances normalized to 100 km, from return strokes electric field initial peaks with a mean value of 88.6 V/m for all data, resp. 3.95 V/m for determined distances normalized to 100 km (Fig. 7). The mean value of 3.95 V/m for Emax of return stroke waveforms normalized to 100 km is also found in [3] and [7].

The comparison of T_{50} shows the most obvious difference between stepped leaders and intracloud discharges on the one hand with a mean value of 26.2 ns for all acquired data, resp. 23.1 ns for determined distances, and return stroke signals on the other hand with a mean value of 606 ns for all data, resp. 564 ns for determined distances (Fig. 8).

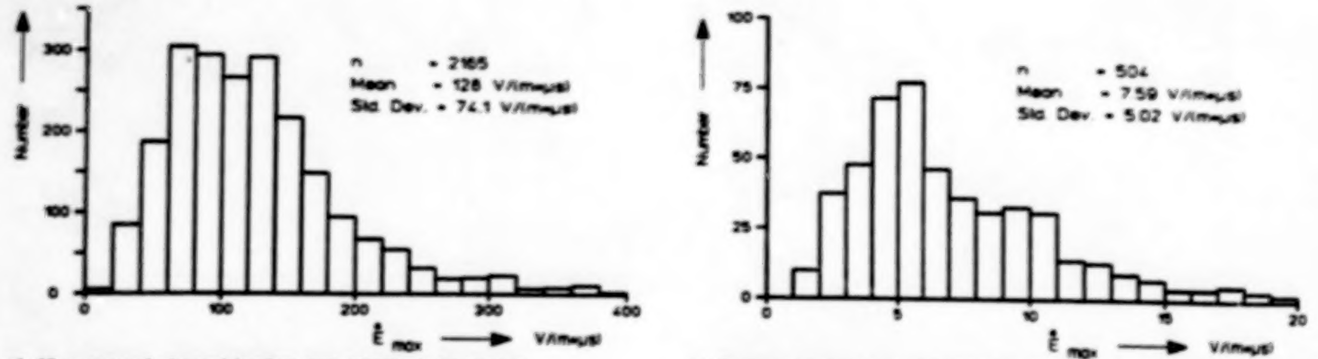

a) All measured stepped leaders and intracloud discharges

b) Stepped leaders and intracloud discharges with determined distances normalized to 100 km range

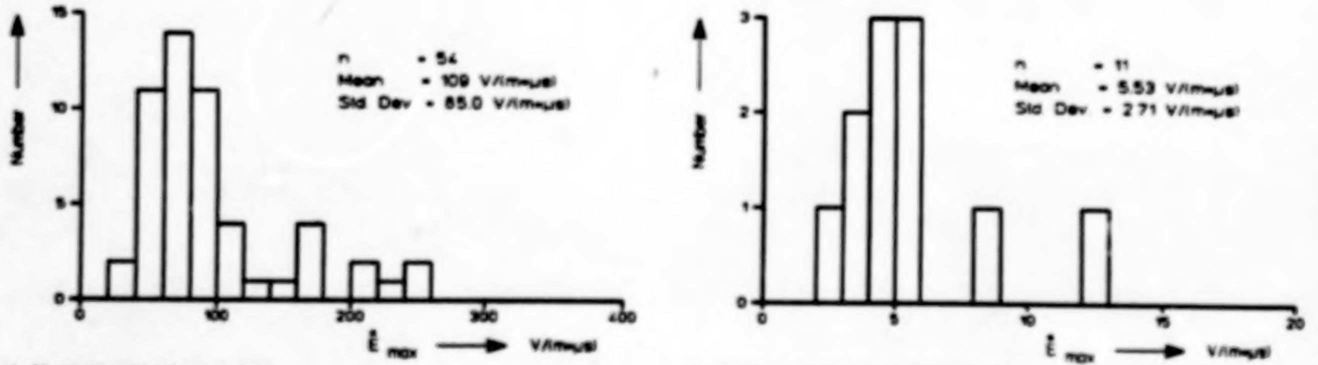

c) All measured return strokes

d) Return strokes with determined distances normalized to 100 km range

Fig. 6: Histograms of maximum peaks $\hat{E}_{max}$ (pos. and neg.)

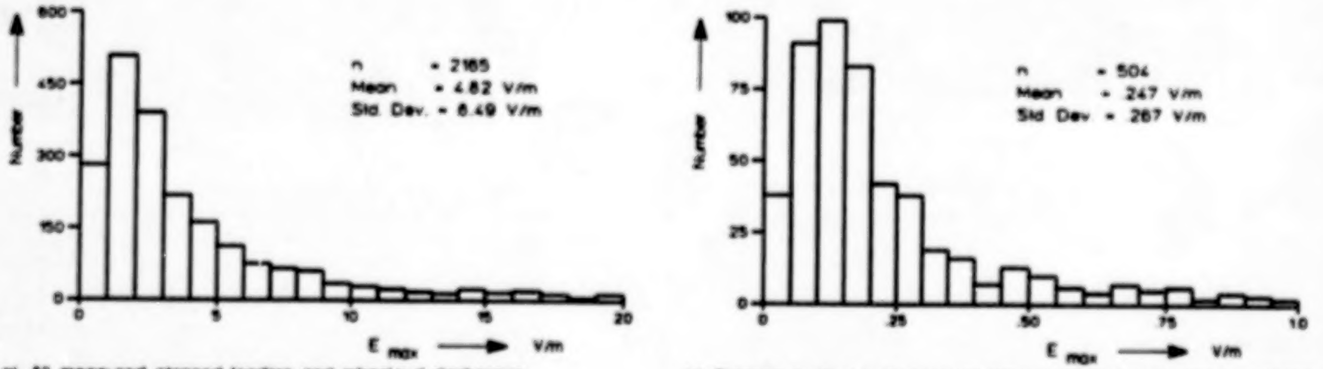

a) All measured stepped leaders and intracloud discharges

b) Stepped leaders and intracloud discharges with determined distances normalized to 100 km range

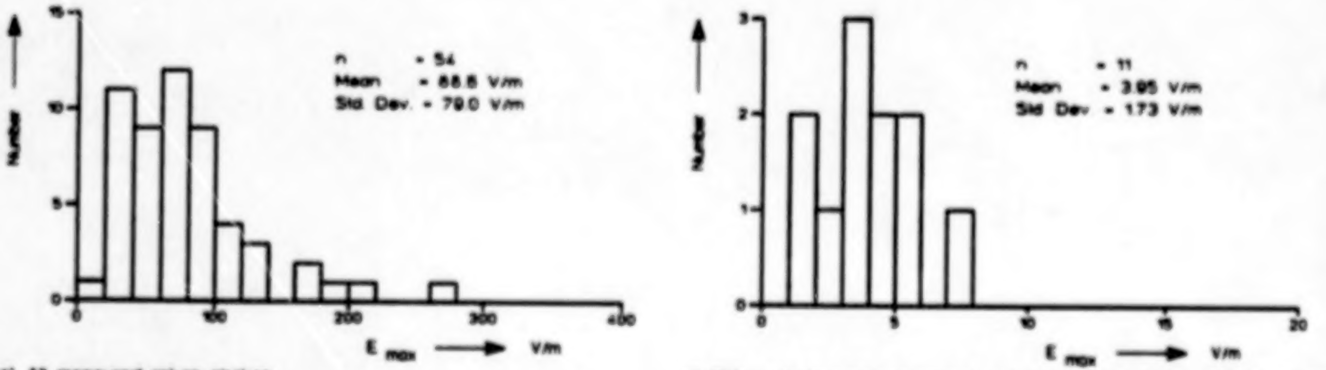

c) All measured return strokes

d) Return strokes with determined distances normalized to 100 km range

Fig. 7: Histograms of electric field initial peaks E_{max} (pos. and neg.)

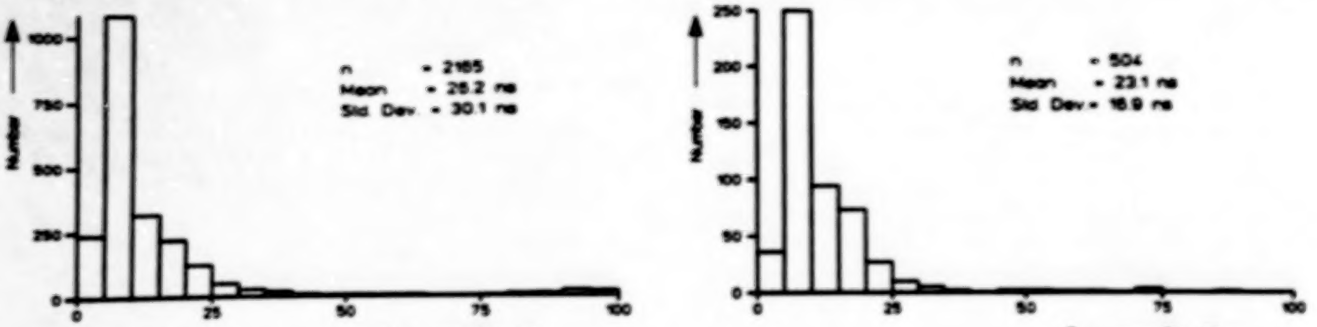

a) All measured stepped leaders and intracloud discharges.

b) Stepped leaders and intracloud discharges with determined distances.

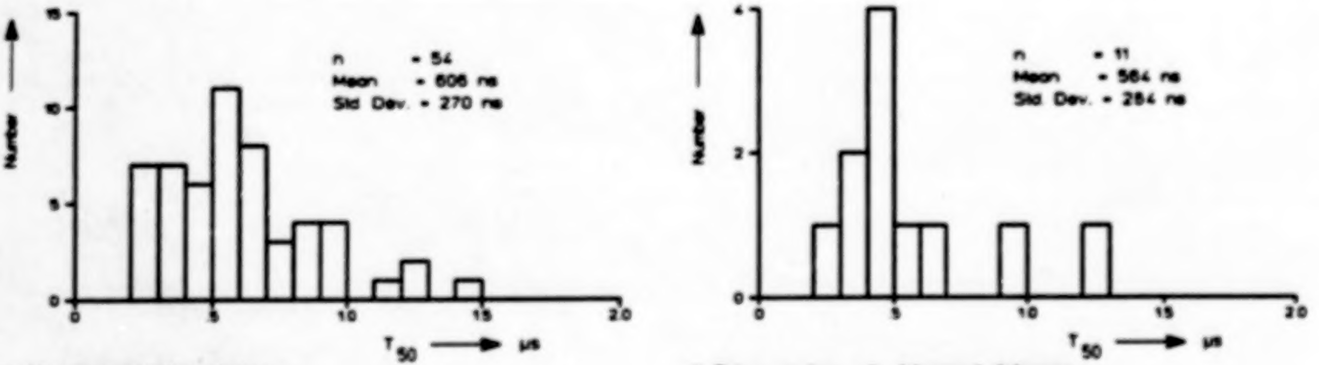

c) All measured return strokes.

d) Return strokes with determined distances.

Fig. 8: Histograms of impulse widths T_{50}

Discussion

The results show, that for the discrimination of electric field derivative signals of the return strokes from those of stepped leaders and intracloud discharges in the range to 15 km both the impulse width and the electric field initial peak by a factor of 15 seem to be appropriate criterions. The evident difference of T_{50} in the time domain points at a significant difference also in the frequency domain.

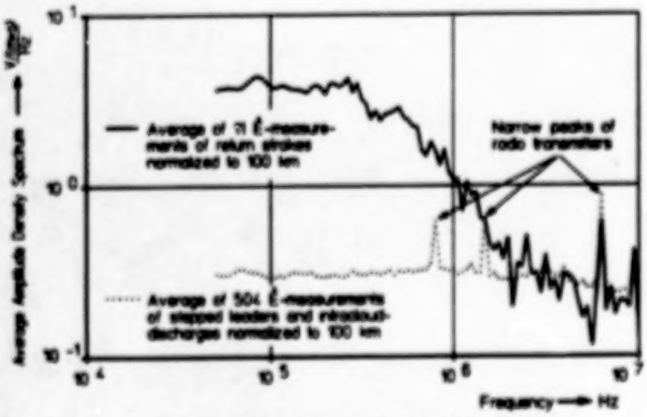

Fig 9: The means of amplitude density spectra for return strokes, resp. stepped leaders and intracloud discharges both normalized to 100 km, recorded at distances up to 15 km.

In Fig. 9 the two average amplitude density spectra of the Ė-waveforms produced by return strokes (solid) resp. stepped leader and intracloud discharges (dotted) are presented [8]. Before computation of the Discrete Fourier Transform in the frequency range from 50 kHz to 10 MHz is performed the data are normalized to 100 km. Up to frequencies of 500 kHz the average amplitude density spectrum of 11 Ė-signals originating from return strokes lies by a factor of 10 above that of 504 Ė-signals produced by stepped leaders and intracloud discharges. For frequencies higher than 2 MHz no such difference is recognizable as also reported in [9]. This correponds to the relatively long T_{50} of return strokes, which is caused by the massive removal of charge from the lightning channel at the beginning of the return stroke phase.

Deduced from Fig. 9 a bandwidth limitation of the Ė-measuring system, that means of the trigger device, by a lowpass filter with a cutoff frequency of 500 kHz leads to an appropriate discriminator for return stroke signals produced by cloud-to-ground flashes in the 15 km range.

In order to eleminate strong stepped leader pulses of near cloud-to-ground discharges or signals of cloud-to-cloud discharges the Ė-signals filtered by a 4th order Butterworth lowpass filter with a 3 dB cutoff frequency of 500 kHz is compared to the unfiltered Ė-signals. Fig. 10 shows the ratios of the maximum peaks within the 20 µs time window of the filtered and unfiltered Ė-signals

($\hat{E}_{max/500kHz}/\hat{E}_{max}$) produced by return strokes. The 4th order Butterworth lowpass filter was simulated by a digital recursive filter using the bilinear transform. For all return stroke signals the ratio is greater than 25% with a mean value of 61.2%, resp. 57.8% for signals with determined distances. Against that the ratio for all other acquired signals lies under 35%.

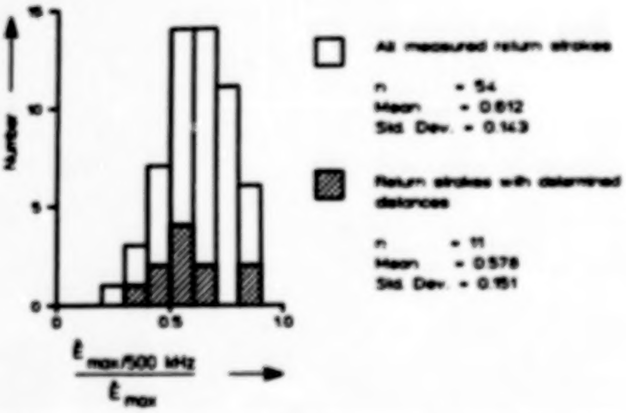

Fig. 10: Histograms of ratios of maximum peaks of filtered $\hat{E}$-signals $\hat{E}_{max/500\,kHz}$ (4th order butterworth lowpass-filter with a 3 dB cutoff frequency of 500 kHz) and of corresponding unfiltered $\hat{E}$-signals $\hat{E}_{max}$.

Conclusion

The comparison of $\hat{E}$-signals with determined distances by the use of the all sky video camera system results in significant differences both in the time and the frequency domain for return strokes on the one hand and all other signal sources on the other hand.

To achieve the discrimination of return stroke signals in the 15 km range two criterions have to be fullfilled. First the $\hat{E}$-signal filtered by a 4th order lowpass filter with a cutoff frequency of 500 kHz must exceed a certain level, which affects the effective range of the measuring system. Second the ratio of the maximum peaks of the filtered and unfiltered $\hat{E}$-signal ($\hat{E}_{max/500kHz}/\hat{E}_{max}$) has to be greater than 35% in order to register at least 90% of the return stroke $\hat{E}$-signals (first and subsequent) in the 15 km range and to exclude predischarges, stepped leader and cloud-to-cloud pulses.

References

[1] Heidler, F.: Lightning Electromagnetic Impulse, Theorie und Messungen. Dissertation, Univ. of Fed. Armed Forces, Munich, 1987.

[2] Weidman, C.D.; Krider, E.P.: The Fine Structure of Lightning Return Stroke Wave Forms. JGR, Vol. 83, 1978.

[3] Master, M.J.; Uman, M.A.; Beasley, W.; Darveniza, M.: Lightning Induced Voltages on Power Lines: Experiment. IEEE Transactions on Power Apparatus and Systems, Vol. PAS-103, 1984.

[4] Krider, E.P.; Weidman, C.D.; Noggle, R.C.: The Electric Fields Produced by Lightning Stepped Leaders. JGR, Vol. 82, 1977.

[5] Weidman, C.D.; Krider, E.P.: The Radiation Field Wave Forms Produced by Intracloud Lightning Discharge Processes. JGR, Vol. 83, 1979.

[6] Uman, M.A.: The Lightning Discharge. Academic Press Inc., Orlando, 1987.

[7] Lin, Y.T.; Uman, M.A.; Tiller, J.A.; Brantley, R.D.; Krider, E.P.; Weidman, C.D.: Characterization of Lightning Return Stroke Electric and Magnetic Fields From Simultaneous Two-Station Measurements. JGR, Vol. 84, 1979.

[8] Hopf, Ch.; dE/dt Measurements and Simultaneous All Sky Camera Observations. 9. EMC-Symposium (1991), Zurich, Paper H3.

[9] Weidman, C.D.; Krider, E.P.; Uman, M.A.: Lightning Amplitude Spectra in the Interval from 100 kHz to 20 MHz. Geophysical Research Letters, Vol. 8, 1981.

Adress of author:

Ch. Hopf
Universität der Bundeswehr München
ET / 7
Werner-Heisenberg-Weg 39
D-8014 Neubiberg, Germany

Electromagnetic Radiation Field of Multiple Return Stroke Lightning

by S. Gupta

No paper available.

AIRBORNE OBSERVATIONS OF ELECTRIC FIELDS AROUND GROWING AND DECAYING CUMULUS CLOUDS

K.L. Giori and J.E. Nanevicz
SRI International, Menlo Park, California

ABSTRACT

Airborne electric-field data were gathered in an SRI International study of atmospheric electrification during the summer of 1989 near Cape Canaveral, Florida. A Learjet 36A operated by Aeromet, Inc., was instrumented with eight electric-field meters (mills) and five different particle probes. The local electric-field enhancements at each field mill site were determined under laboratory conditions and verified using in-flight data. The overdetermined system of eight equations (one for each field mill) was solved using a weighted least-squares algorithm to compute the magnitude and direction of the ambient electric field. The signal-processing system allowed the measured data to be expressed in terms of earth coordinates, regardless of the attitude of the aircraft. Thus, it was possible to take maximum advantage of the Learjet's speed and maneuverability in studying the electric-field structure in the vicinity of clouds.

Data gathered while circling just outside the boundary of a growing cumulus cloud show a nonsymmetric pattern of electric-field strength. Field intensity grew rapidly over a period of less than 10 minutes. The observed direction of the ambient electric-field vector can be explained by an ascending motion of the charge centers of a classic tripole model of a thunderstorm. A mature and decaying cumulus cloud was orbited four times. The electric-field strength again showed a nonsymmetric pattern similar to the growing cumulus. The direction of the field, however, followed a descending motion of classic tripole charge centers.

INTRODUCTION

Lightning discharge is a powerful audio and visual display of just part of the potential energy developed in convective storms. The complex nature of atmospheric electrification that can lead to the lightning discharge is related to cloud size, type, and nature of growth or decay. Understanding these relations is important to the launch community at Cape Canaveral, where the frequent thunderstorms and lightning can delay launches, can damage susceptible electronics, and pose hazards to ground personnel.

AIRBORNE PLATFORM

The platform used to gather data for this study was a Learjet 36A aircraft operated by Aeromet, Inc., of Tulsa, Oklahoma. This aircraft had been instrumented with various particle probes to measure the microphysical characteristics of clouds for previous weather reconnaisance missions over the Pacific Ocean (**Figure 1**). Eight electric-field mills were mounted with the sensor heads flush to the skin of the aircraft at locations also shown in Figure 1. The field meter amplifier electronics and computer processing systems for all sensors were located in the main cabin of the aircraft. Data from the particle probes, forward-looking video, and other sensors were stored

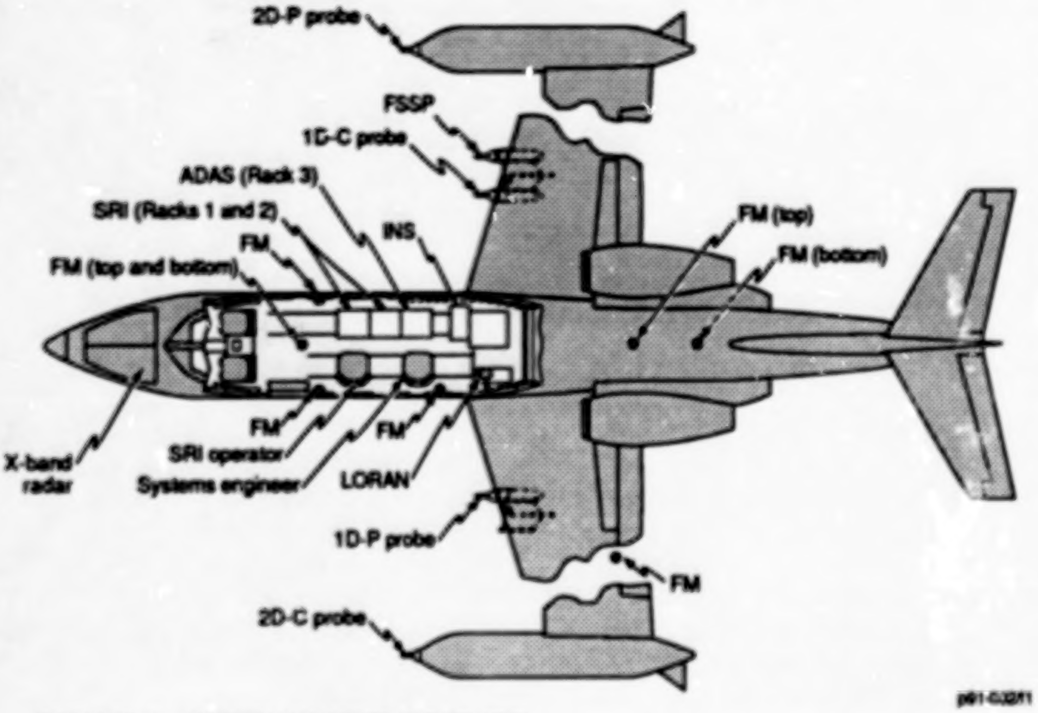

FIGURE 1. INSTRUMENTED LEARJET
The instruments include eight electric field mills (FM), five particle measuring probes (e.g., 2D-C), LORAN and INS navigation systems, and data acquisition systems (e.g., ADAS).

for comparative analysis with the stored electric-field measurements. All data could be displayed in real time, both aboard the Learjet and at a ground station.

MEASUREMENT OF ATMOSPHERIC ELECTRIC FIELD

Airborne measurements using electric-field meters of various types have been performed since the 1940s, but solving the problem of properly extracting an accurate measure of the atmospheric electric field independent of the perturbing probe has sometimes eluded researchers. The most difficult problems have been (a) to accurately determine the local electric-field perturbation due to the introduction of the airborne platform, and (b) to resolve the ambient field even in the presence of space charge about the platform. As noted by Vonnegut et al. [1], space charge around aircraft platforms can result from various mechanisms, such as (a) the electrification of aircraft exhaust, (b) triboelectric or induction charging of cloud particles that contact the aircraft during cloud penetrations, and (c) ion plumes that trail from aircraft extremities in corona. Local enhancement factors at electric-field meter sites on an airborne platform can be accurately determined using an experimental technique discussed by Kositsky and Nanevicz [2] in a companion paper. However, the three listed space charge effects, though negligible in clear air, are still a significant problem for aircraft platforms during cloud penetrations [3,4].

In the absence of space charge effects, the local electric field measured at each field mill site is a linear combination of the aircraft-perturbed ambient electric field **E** and the field resulting from nonzero aircraft potential V. The local electric fields measured at each mill site can then be expressed as

$$F_i = a_{ix}E_x + a_{iy}E_y + a_{iz}E_z + a_{iv}V \tag{1}$$

where

i = Mill number from 1 to 8
F_i = Measured electric field of Mill i
$a_{ix}, a_{iy}, a_{iz}, a_{iv}$ = Local field enhancement factors of Mill i
E_x, E_y, E_z = Vector components of the ambient electric field E
V = Potential of the aircraft with respect to ground.

In vector notation, the system of equations can be written F = AE. The enhancement matrix A contains the a_i terms, called enhancement factors, that are determined experimentally and verified using in-flight data [2]. The solution to the four unknown terms, E_x, E_y, E_z, and V, requires a minimum of four measurements, F_i. Since the described airborne system uses eight field meters, the solution to the set of eight equations is overdetermined. The additional information provided by the overdetermined system of equations can be solved using a weighted least-squares algorithm that is considerably more accurate than a system of only four equations. The general solution used for real-time computation, in matrix notation, is:

$$E = (A^T CA)^{-1} A^T CF \tag{2}$$

where

A = Enhancement matrix
C = Weighting matrix
F = Field meter measurements $F_1, F_2, \ldots F_n$
E = Vector (E_x, E_y, E_z, V).

The extra information from redundant field mills also allows for a real-time error-analysis algorithm to estimate the point-by-point uncertainty in the computed ambient electric field. Details and testing of the error-analysis and above algorithms is described in a comprehensive report by Kositsky et al. [4]. Finally, signal processing allows the atmospheric electric field to be expressed in fixed earth coordinates, regardless of aircraft orientation, as long as the orientation is known.

Case of a Rapidly Growing Cumulus

Figure 2 shows the southern region of a towering cumulus cloud taken a few minutes before the Learjet circuited just outside the cloud boundary. By flying in clear air, the measured fields are known to accurately represent the ambient electric field. The paragraphs below show that data gathered while circling a cloud with a jet aircraft can provide valuable insights into the dynamics of cloud growth and decay and can identify the internal cloud regions that have the highest electrical intensity.

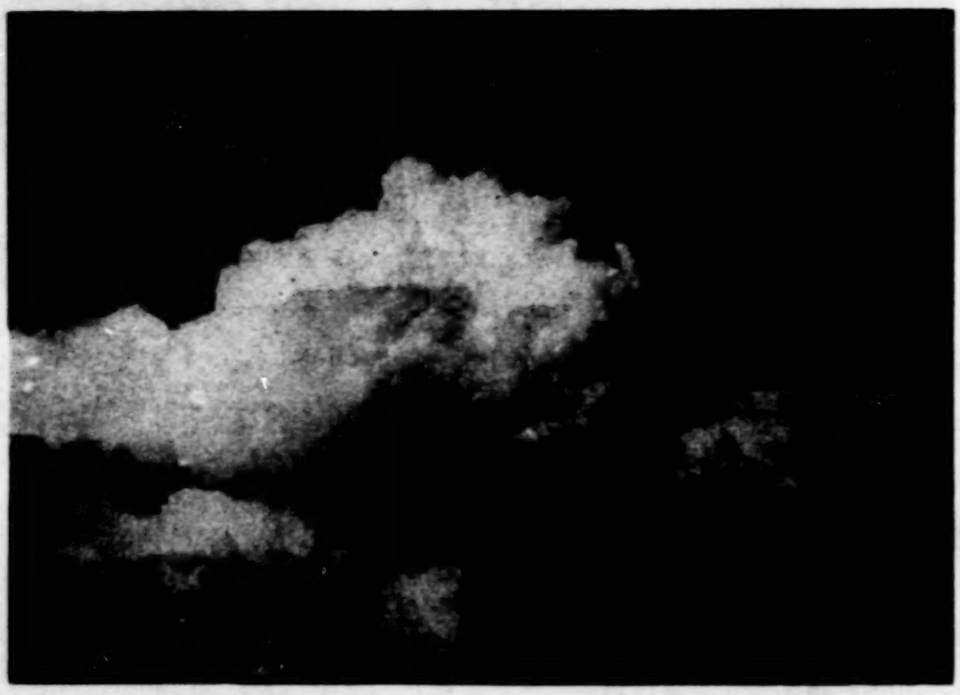

FIGURE 2. TOWERING CUMULUS
This photo was taken looking to the north at 19:10:17 UT,
1 September 1989.

The first loop around the cloud occurred at an altitude of about 5500 m. The magnitude and direction of the computed ambient electric field is plotted as a vector along the aircraft flight track in a three-dimensional perspective (Figure 3a). A two-dimensional (2D) top view showing the horizontal field component of the same data set (time period) is shown in Figure 3b. The open ends of the plotted electric-field vectors are defined as the ends where an arrow would point to show the direction of motion of a positive test charge inserted into the field. The peak electric field encountered during the first pass was 0.5 kV/m along the cloud's southern boundary.

During the second pass, a peak field of 5 kV/m was measured along the southern edge (Figures 3c and 3d). The electric-field strength increased an order of magnitude between the first two passes over a time period of 3.75 minutes. During the third pass, which occurred about 5.5 minutes after the second pass, the peak field at the southern edge was 20 kV/m (Figures 3e and 3f). A summary of all three passes is shown in Table I.

The rapid increase in electric-field strength indicates that the cloud was indeed growing. Such growth can also be noted by following the change in the direction of the peak electric field. The direction change is interpreted to be caused by the upward motion of the charge centers in a classic tripole model of an electrified cloud. The field pattern from a generic tripole model is shown in Figure 4. The model consists of a large positive charge at greatest altitude, a large negative charge at some middle altitude, and a small positive charge at the lowest altitude. The three darkened vectors, labeled 1, 2, and 3, represent the peak electric-field direction vectors of the respective aircraft passes. They are mapped to the cloud model vectors

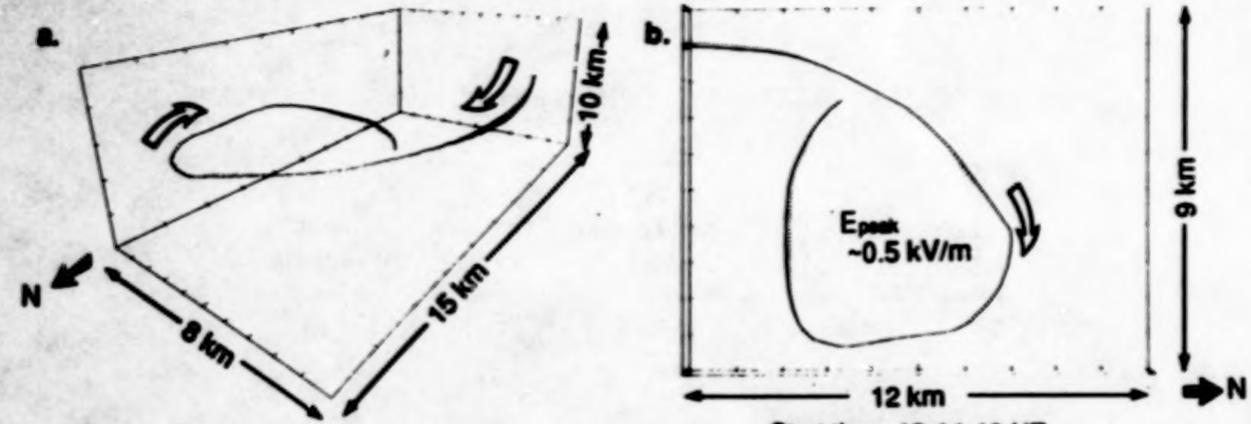

Start time: 19:11:10 UT
Stop time: 19:15:20 UT
Orbit 1

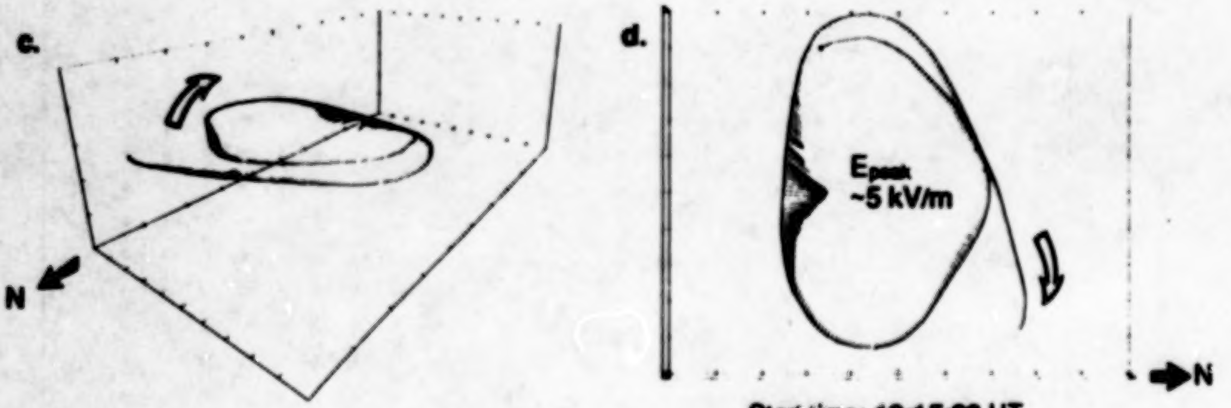

Start time: 19:15:28 UT
Stop time: 19:21:12 UT
Orbit 2

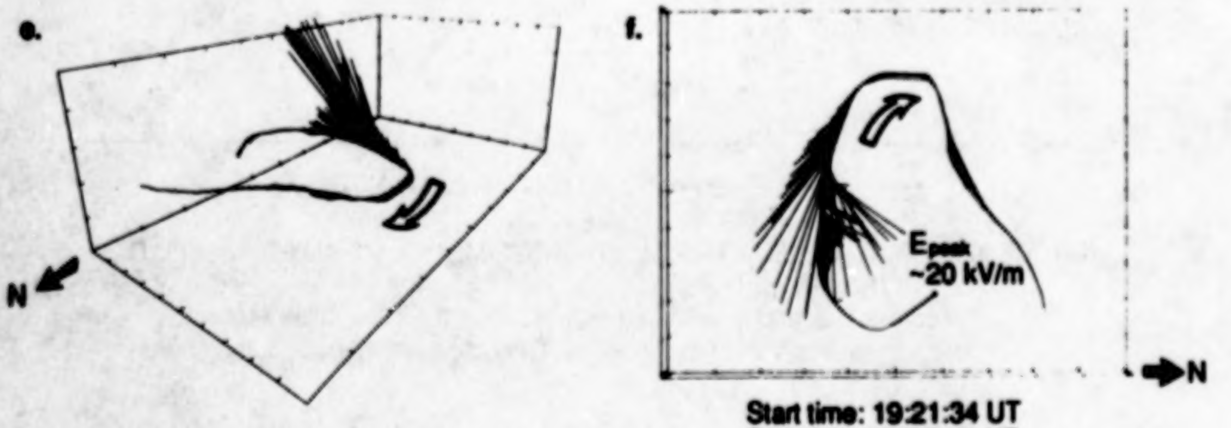

Start time: 19:21:34 UT
Stop time: 19:26:41 UT
Orbit 3

p91-002/f3

FIGURE 3. ELECTRIC-FIELD VECTOR MAPPED TO FLIGHT TRACK
These data were gathered 1 September 1989 while encircling a growing towering cumulus cloud. The peak electric field occurred on the south side of the cloud.

Table I

SUMMARY OF PEAK ELECTRIC FIELD: GROWING TOWERING CUMULUS

Orbit	Time (UT)	Flight Altitude (m)	E_{peak} (kV/m)	E_{peak} Direction
1	19:14:45	5500	0.5	N 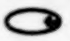 S
2	19:18:30	5200	5	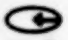
3	19:24:10	4600	20	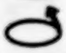

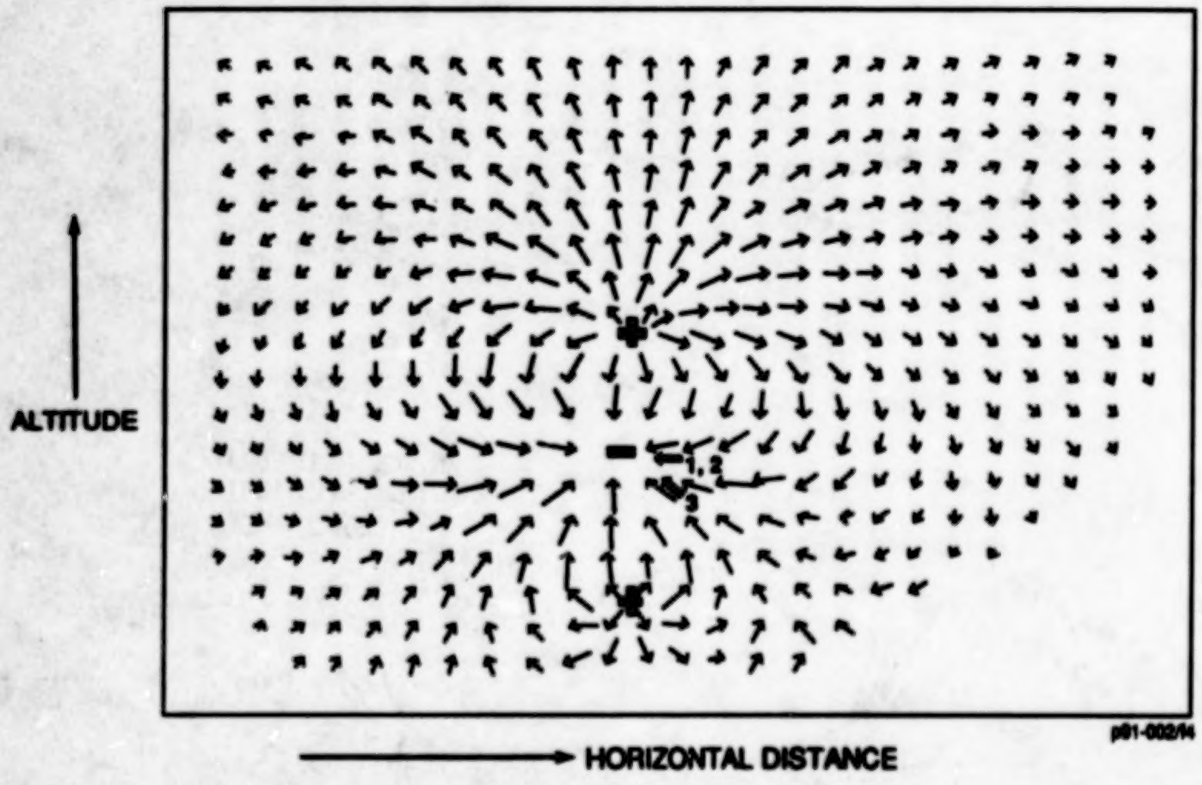

FIGURE 4. ELECTRIC-FIELD TRIPOLE CHARGE MODEL OF AN ELECTRIFIED CONVECTIVE CLOUD
Vectors 1, 2, and 3 point in the direction of the peak fields associated with the orbits shown in Figure 3. The ratio of magnitude of the charges is +20: -20: +3

according to their direction, not altitude. Although the Learjet lost some altitude while circling the cloud, which would slightly change the peak direction, the major change in the field direction is likely caused from a significant physical growth of the cloud that would carry charged particles upward and probably create many newly charged particles. For observations at constant altitude, an upward shift in the location of the top positive modeled charge would account for the increasingly upward-pointing field vector for each aircraft pass. An increase in the amount of charge at each of the modeled charge centers would account for the increasing magnitude of stored electrical potential energy.

The southern region of the cloud in Figure 3 shows vastly greater electric-field strength than the other sides. This nonsymmetry suggests that the cloud drew most of its electrical energy from the vigorous motion of air currents on one particular side of the cloud. That particular side probably caused the continuing cloud growth by drawing in a channel of moist air from below.

Case of a Mature, Decaying Cumulus

Figure 5 shows the southern region of a mature, decaying cumulus cloud. The cloud top had already exceeded 40 kft (12,000 m) before data sampling around the cloud began. The photograph suggests that the southern edge of the cloud had entrained somewhat into an anvil.

Again, the Learjet circled the cloud without penetrating it. During the first pass, performed at an altitude of 8000 m (Figures 6a and 6b), the northern region of the cloud was most strongly electrified. Abrupt discontinuities in the magnitude and direction of the field typically result from nearby lightning. The peak field was 7.5 kV/m. The two-dimensional perspective shows that the small portion of the horizontal components pointing away from the cloud occurred for the peak field region, as if a larger population of positive charge were present on that side of the cloud boundary. The remaining vectors point slightly inward and down, as if there were a distribution of predominantly positive charge above and predominantly negative charge in closer proximity below.

On the second pass (Figures 6c and 6d), the peak field had increased to 11 kV/m. The direction of the peak region field was now horizontal, as if predominantly positive charge was distributed at the level of the northern boundary of the Learjet flight track.

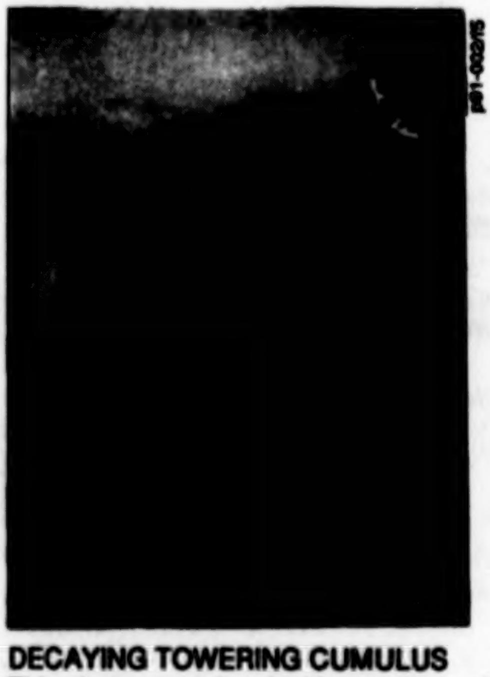

FIGURE 5. DECAYING TOWERING CUMULUS
This photo was taken looking to the north
at 19:38:01 UT, 3 September 1989.

On the third pass (Figures 6e and 6f), the ambient electric field peaked to a lesser value of 4 kV/m. The direction of the peak region field now pointed somewhat upward, as if the positive charge distribution level responsible for the horizontal peak of the second pass had now dropped below the altitude of the Learjet.

On the fourth pass (Figures 6g and 6h), the peak field had increased slightly to 6 kV/m. The peak field direction again continued its upward trend as though the positive charge distribution continued to drop.

The 2D plots (Figures 6b, 6d, 6f, and 6h) show that, on each successive pass, more and more of the field vectors pointed outward around the northern peak-field region. The horizontal component direction change is consistent with the successive upward shift of the peak field direction. That is, a downward motion of the predominant positive charge distribution occurs with the physical decay of the cloud. The negative charge distribution that would be located below the upper positive region, according to the tripole model described earlier, may also be moving downward as the cloud decays. A summary of the peak field activity is shown in Table II.

Table II

SUMMARY OF PEAK ELECTRIC FIELD: DECAYING CUMULUS

Orbit	Time (UT)	Flight Altitude (m)	E_{peak} (kV/m)	E_{peak} Direction
1	19:42	8000	7.5	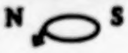
1	19:46	8200	11	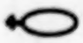
3	19:50	8300	4.5	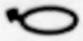
4	19:54	7800	6.5	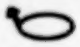

The peak-field direction change is noted for each successive rotation about the cloud as a darkened vector, labeled 1, 2, 3, and 4 on the generic tripole cloud model of Figure 7. The motion of the charge centers would be downward to explain the peak field direction changes, which is opposite to the case of the growing cumulus. Since the cloud photo taken just prior to data gathering showed that the cloud was already quite mature, it is not unreasonable to propose that the cloud was decaying. Although the peak field direction change clearly indicates decay, the variation of the peak field magnitude would not have been a good indicator as it had been for the cloud growth case.

CONCLUSIONS

A Learjet 36A equipped with eight electric-field meters was used to measure the atmospheric electric field. The overdetermined system of eight equations was solved using a weighted least-squares algorithm that is considerably more accurate than a system of only four equations. The field

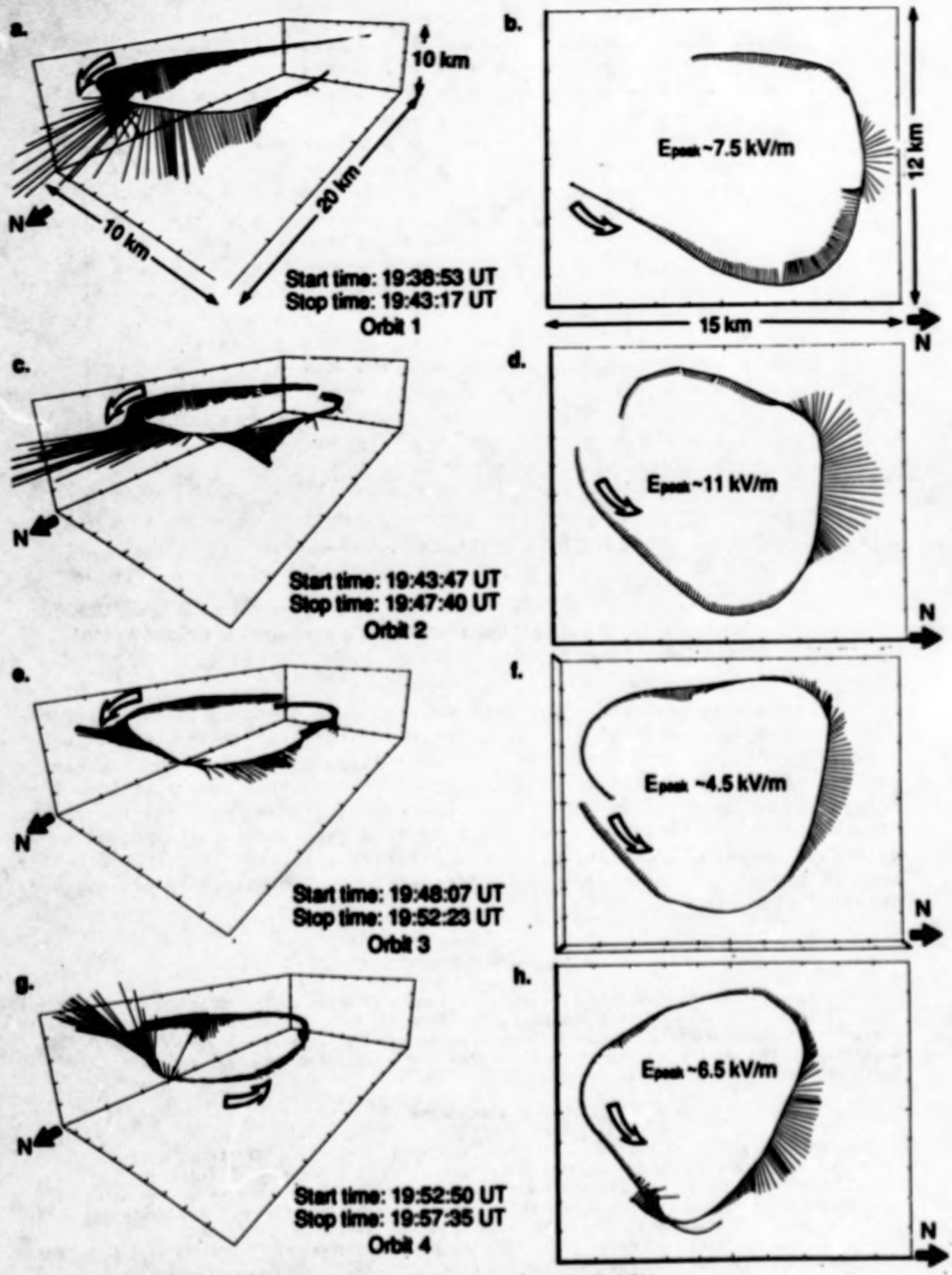

FIGURE 6. ELECTRIC-FIELD VECTOR MAPPED TO FLIGHT TRACK
These data were gathered 3 September 1989 while encircling a decaying towering cumulus cloud. The peak electric field occurred on the north side of the cloud.

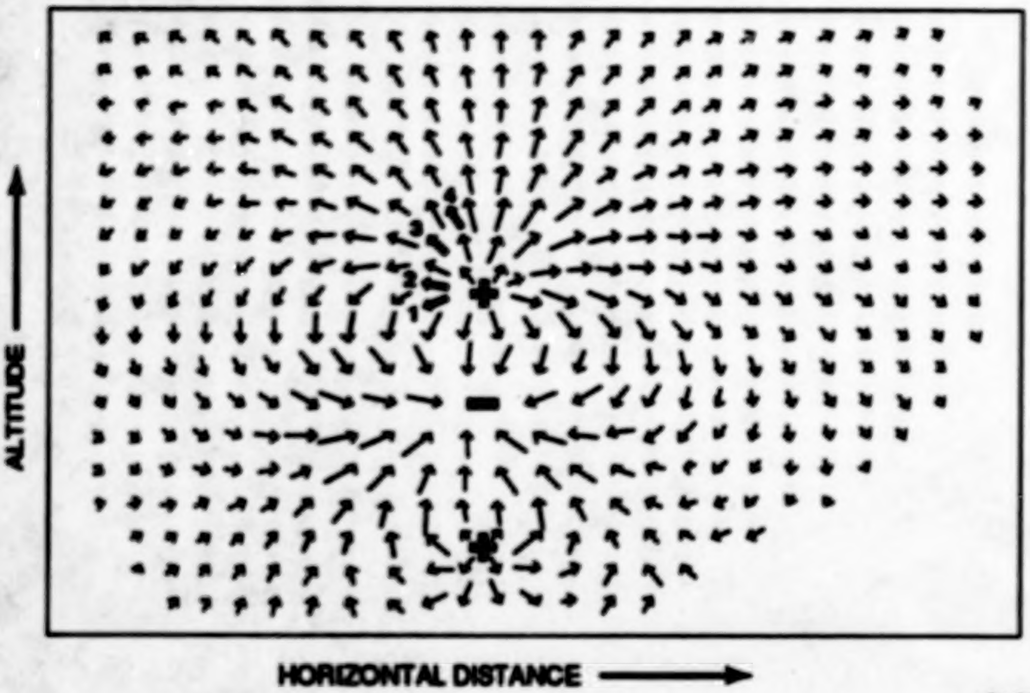

p91-002/f7

FIGURE 7. ELECTRIC-FIELD VECTORS RESULTING FROM A TRIPOLE CHARGE MODEL
Vectors 1, 2, 3, and 4 point in the direction of the peak fields associated with the orbits shown in Figure 6.

measurements were performed just outside the cloud boundary to avoid the problem of space charge effects that occur during cloud penetrations. Data gathered while circling clouds at constant altitude showed a nonsymmetric pattern of electric-field strength, which is interpreted to result from a nonsymmetric distribution of internal charge. The changing direction of the observed peak electric field was found to be a good indicator of cloud growth or decay, assuming a classic tripole model electric-field distribution. The Learjet's speed and maneuverability were effective for sampling growing and decaying cloud systems.

ACKNOWLEDGMENTS

The airborne data-gathering activity during summer 1989 was supported by the U.S. Air Force Space Systems Division. We thank the group from Aeromet, Inc., led by co-pilot Dr. Ray Harris-Hobbs, for their tremendous experimental contributions and professional support. We also sincerely appreciate the efforts of many SRI personnel, including Joel Kositsky, Robert Maffione, Paolo Bochi, and Cora Taylor.

REFERENCES

1. B. Vonnegut, C. B. Moore, R. P. Espinola, and H. H. Blau, Jr., "Electric Potential Gradients Above Thunderstorms," J. Atmos. Sci., Vol. 23, November 1966.
2. J. Kositsky and J. E. Nanevicz, "Scale-Model Charge-Transfer Technique for Measuring Enhancement Factors," paper (p91-003) presented at 1991 International Conference on Lightning and Static Electricity, Florida, February 1991.
3. J. J. Jones, "Electric Charge Acquired by Airplanes Penetrating Thunderstorms," J. Geophy. Res., Vol. 94, No. D10, pp. 16589-16600, September 1990.
4. J. Kositsky, E. L. Ciori, R. A. Maffione, D. H. Cronin, and J. E. Nanevicz, "Airborne Field Mill (ABFM) System Calibration Report," Task A Final Report, SRI Project 1449fr, SRI International, Menlo Park, California, January 1991.

Session 4B, Tuesday 3:45
Lightning Mapping Systems 1
M. Maier, Chairman

LIGHTNING LOCATION SYSTEM SUPERVISING SWEDISH POWER TRANSMISSION NETWORK

Stefan A. Melin
Swedish State Power Board (Vattenfall)
Vällingby, Stockholm, Sweden

ABSTRACT

For electric utilities the ability to prevent or minimise lightning damage on personnel and power system is of greatest importance. For these reasons Vattenfall, the Swedish State Power Board, has been utilising data since 1983 from a nation-wide lightning location system (LLS) for accurately locating lightning strikes to ground.

Lightning data is distributed and presented on colour graphic displays at regional power network control centres as well as at the national power system control centre for optimal data utilisation.

Main objectives for Vattenfall's utilisation of LLS are:
- **Supervising of the power system for optimal and safe utilisation of the transmission and generating capacity during periods of thunderstorms.**
- **Warning service to maintenance and service crews at power lines and sub-stations to terminate operations hazardous when lightning.**
- **Rapid positioning of emergency crews to locate network damage at areas of detected lightning.**
- **Post-analysis of power outages and transmission faults in relation to lightning using archived lightning data for determination of appropriate design and insulation levels of equipment.**

Staff at the supervisory control centres have found LLS extremely useful and economically justified since the availability of the power system has increased as well as the level of personnel safety. Comprehensive experience has been obtained regarding integration of LLS lightning data and LLS system to ordinary operations routines and standard equipment at control centres.

INTRODUCTION

In recent years, considerable progress has been made in the field of lightning research, the practical results being reflected by today's highly-developed protection and warning systems. However, the rapid pace of modern technological development constantly produces new demands for protection against lightning which, in combination with demands for higher safety, necessitates further development work in several fields. An automatic lightning location system (LLS) may be of major importance in various areas of industry, commerce, and municipal activities in reducing the incidence of lightning damage to property and plant, and in minimising human injury.

Electrical transients associated with lightning represent a major injury hazard to personnel working on high-tension lines and sub-stations. Accidents of this nature (some with fatal results) are reported every year. Reliable lightning warning systems would greatly increase personal safety and reduce maintenance costs.

The main transmission network can be made less vulnerable by modifying the pattern of generation so as to increase the tolerance of the system to line outages such as occur during thunderstorms. However, since this implies that the grid is not used in the optimum manner, this type of rescheduling should be carried out only when the risk of lightning is present. High-tension subscribers, such as process industries, who are particularly

n5

susceptible to power failure can use their own (albeit expensive) in-house facilities to supply sensitive, high-priority loads at periods of high risk. Reliable advance warning of electrical storms by lightning detection systems would be of major financial benefit in both of these cases.

More detailed information received by lightning location systems regarding current and approaching thunderstorms would enable plant operations and power production to be scheduled in a manner which might enable loss of supply to be avoided.

Lightning striking an inadequately protected electrical installation will usually cause a power interruption of a lesser or greater duration, due to disruption of the remote control system or because of damage to a plant component. The consequences of such faults are often difficult to evaluate, the cost of a power failure being dependent both on the category of subscriber and of the duration of the interruption. Improved thunderstorm and lightning statistics collected by lightning location systems can be used to develop a financially optimised system of lightning protection, enabling the period of disruption to be reduced by adopting precautionary measures during the most hazardous weather conditions.

As example, transformers used in power distribution networks are particularly vulnerable to lightning. In Sweden, a large number of transformers is destroyed annually, adding considerably to the costs incurred by the utilities. Further damage is suffered by other electrical installations, high-tension and low-tension cabling, insulators, circuit breakers etc., causing major financial losses. The resultant disruption of power supplies also causes financial loss in terms of lost production etc. Accurate and reliable lightning data from LLS for investigating correlation with statistics of faults and outages in the power systems would probably result in better and safer insulation standards and coordination for improved protection.

Other areas in which lightning detection systems may provide valuable information include the public meteorological service, telecommunications, national air forces, civil aviation, forest fire protection, process industries, the maintenance of high masts, blasting operations, offshore drilling operations, oil platforms etc.

REQUIREMENTS

Information regarding thunderstorms and lightning discharges is of vital importance to Vattenfall in the following main areas:

- For day-to-day system operations and the reporting of imminent thunderstorms.
- To ensure the safety of personnel engaged in work on transmission lines and sub-stations.
- To locate damage caused by lightning in transmission and distribution power networks.
- For the retrospective investigation of grid faults and disturbances.

Prior to the utilisation of the LLS network, information on current and approaching thunderstorms was generally obtained as follows:

Firstly, the national power system control centre received forecasts from the Swedish Meteorological Institute (SMI) by telephone. During the thunderstorm season (May to September inclusive), forecasts were supplied every morning followed, if the weather situation is changing, by a new forecast during the day. At other times of year, forecasts were supplied only as required by the weather situation. The National Control Centre transmitted the forecasts to the local and regional power network control centres.

Secondly, manned power and transformer stations supplied information to the local and regional control centres regarding the presence of thunderstorms and their passage through the particular area. The local and regional control centres, in turn, informed the National Control Centre and other control centres in areas which may conceivably be affected by the weather system.

These information channels suffered from obvious defects, both individually and as a combination. For instance, forecasts were and still are based on analysis of meteorological data f.i. from weather radar and satellite pictures, which gives good information on clouds and precipitation but cannot display or locate lightning. However, the most disturbing aspects from the Vattenfall's viewpoint was the trend from manually-operated to automated, remotely-controlled power and transformer stations, a development which had greatly reduced the number of manned installations in recent years.

Furthermore, both the Vattenfall's own regions and those of other power utilities reported that the centralisation of personnal resources brought about by the commissioning of regional operations monitoring systems and other such facilities is such that it will not be possible, in future, to undertake the reporting of electrical storms in the manner required.

The workers unions had strongly commented on the hazards involved in transmission line and switching station work resulting from the fact that the reporting system no longer provided countrywide coverage and that the system was not as accurate as in previous years. Reports dealing with this aspect had emphasized the need to provide replacements for the existing manual reporting procedures.

Although SMI forecasts usually provided indications as to the likelihood of lightning, information regarding current electrical storms was the type mainly used as a basis for determining whether or not to commence or to terminate transmission line and switching station work; for assessing the need for modifying the pattern of generation in a major network and, in the case of large, vulnerable subscribers such as process industries, etc., for deciding whether or not to switch high-priority systems to independent supplies. However, unexpected events may occur in view of the inherent uncertainty and susceptibility to error or forecasts. Since thunder and lightning may occur despite an optimistic forecast, correct information regarding current or imminent thunderstorms is of particular importance.

Furthermore, the frequently incomplete and inexact type of information available made it extremely difficult to establish in which cases lightning had been the true cause of operational disturbances and plant faults. In most cases, it was possible only to state whether or not this may have been the likely cause.

In view of the foregoing, it was natural to try to supplement existing systems and, in the long term, also to provide a replacement for at least the manual reporting procedures.

LLS NETWORK DEVELOPMENT

Vattenfall has been supporting research and development of a nation-wide lightning location system (LLS) network for locating lightning strikes to ground. A joint project was commenced in 1983 in cooperation with the Institute for High Voltage Research (IfH) at Uppsala, Sweden. IfH had been running a network of LLS in the southern part of Sweden since the end of the 1970's for research purposes with interestingly good results.

LLS is a computerised data aquisition system that employs electro-magnetic pulses from lightning for real-time calculation and determination of the position of cloud-to-ground lightning strokes. The ground strike point is plotted on a map on a multi-colour graphic display for accurate visual presentation. Information includes lightning polarity, amplitude and multiplicity.

The LLS manufactured by Lightning Location & Protection (LLP) Inc. has been commercially available on the market for more than a decade so no detailed technical presentation of the system will be given in this paper. The schematic system function is described in a block diagram in *Figure 1*.

The LLS equipment consisted at that time of four Direction Finders (DF) and a central computer, the Position Analyzer (PA), real-time processing the lightning data received from the DF's. Lightning data from the LLS network was presented in real-time on multi-colour displays and multi-colour hard-copy units at Vattenfall's National Control Centre for the power system. All data communication were established via dedicated telephone lines. On the map in *Figure 2* the locations of the original DF's can be noted.

Identical LLS network was operated in Norway and in Finland and Denmark there were plans to install similar systems. In these countries the electric utilities had been playing a major role in supporting and funding development of national LLS. Integration of the systems in all four Nordic countries into one large systems would probably lead to several advantages, f. i. cost reduction, larger geographical area of system coverage, etc. Increased system availability will also be the result of an integrations since a large number of DF's provide for a high level of mutual redundancy.

After the first couple of years of utilization of lightning data at Vattenfall it became quite clear that the number of DF's was much too small to give an altogether appropriate geographical coverage by the LLS. Engineers at the power network control centres wanted such a LLS coverage so all the main 400 kV transmission lines could be supervised during thunder and lightning. This called for an expansion of the system to seven DF's which was completed in 1986. Another expansion including one extra DF station was made in 1988. DF sites of today in Sweden and in the other Nordic countries are presented in *Figure 3*.

During the same period communication links were set up with the Norwegian system, the completed Finnish system and later the Danish system for real-time integration of the systems when desired. A special committee worked out recommendations for a total integration of the Nordic systems which called for a large-scale substitution to a new generation of equipment designed for packet-switching data communication in order to reduce the data transmission costs. Using data transmission via packet-switching data network instead of dedicated telephone lines will reduce the transmission cost in the inter-Nordic LLS network by 50 to 80 percent depending on country. Due to the high costs of a total substitution of equipment it was decided that each country would care for its own time schedule for system up-grading regarding data communication development and economical aspects.

The last couple of years the Nordic LLS network have been partly interconnected i.e. the Swedish LLS network has been able to utilise real-time data from some Norwegian and some Finnish DF stations and the LLS systems in Norway and Finland have been connected to certain Swedish DF stations. This test-integration has proven successful and has provided interesting results and will probably be made permanent during 1990 or 1991. These integration tests were carried out using dedicated telephone lines or dial-up telephone connections. When integration is going to be permanent a packet-switching data communication network will be utilised.

In Norway a technique was developed for presentation of real-time lightning data on ordinary personal computers with multi-colour graphic displays. This was a major contribution for low-cost distribution of lightning data to several locations within the organisation and to companies with limited financial resources. Vattenfall sponsored this development since experiences of the the original display units were not satisfactory mainly because of lacking in proper handling routines for control centre environment.

Basic demands for data presentation equipment to be used in power system control centres are that all information displayed on monitors should be quite clear and easy to understand. The equipment has to be extremely simple to use. In a situation where a major outage or disturbance in the power system has occurred there are no time for misunderstandings or mistakes in equipment management. Everything has to run smoothly in order to carry out the major task to rearrange the power network as fast as possible. The system must provide clear, unambiguous indications which preclude the possibility of misinterpretation and should require a minimum of operation. Instrumentation must be kept to the absolute minimum. Of these reasons it is of great importance to be able to customise presentation and handling routines on ordinary personal computers suitable for specific needs and utilisation.

UTILISATION AND EXPERIENCE

The Vattenfall personnel have long been aware of the limitations of the old manual lightning reporting system. As a result, the development of automatic detection systems has been followed with intense interest by Vattenfall.

A simple test link with the LLS system was established and evaluation of the test showed that the results were excellent. The LLS system was greatly superior to the Vattenfall's existing reporting system in terms of coverage, accuracy and efficiency. The LLS tests indicated that the old manual system of observation stations was inadequate.

Access to lightning information supplied by the LLS system in real time is considered by the National Control Centre to be extremely valuable, especially in view of the opportunities which this would afford in terms of issuing sufficient advance warning to service crews working on the grid, and of the facility of rescheduling operations to minimise the incidence of system faults.

Presentation units and associated multi-colour video displays and hard-copy units were purchased and installed immediately adjacent to the normal control operators work stations at the National Control Centre to enable the operators to observe the lightning information displayed on the VDU's with complete ease and to minimise the problems of operating the equipment as far as possible. The equipment was connected to the LLS network by a dedicated telephone link. During the first couple of years the presentation equipment was the old type of original Remote Display Processors from LLP Inc, so called RDP's. Nowadays Vattenfall is using ordinary personal computers with multi-colour graphic displays as presentation units. This solution calls for qualified soft-ware development but is still favourable economically.

When a lightning discharge is recorded by the system, the presentation unit emits a high-pitched audible alarm and a red lamp commences to flash. The strike point is indicated on the screen by a cross or square depending on the polarity, and the coordinates of the point are displayed simultaneously at the bottom of the screen. Typical displays are shown in *Figure 4*. The operator records the area in which the discharge has taken place, and can use the controls to select a more detailed map to identify the strike point more accurately. The operator is then in a position to inform the local control centres in question of the electrical storm and to correlate simultaneous power system faults directly with the strike. This procedure greatly facilitates and accelerates the implementation of corrective measures such as the restoration of supplies, rescheduling of operations, fault tracing, starting of stand-by generation plant, etc.

The provision of the presentation unit with a memory for storing lightning data facilitates the subsequent investigation of whether or not lightning has been the cause of system disturbances. This is done by redisplaying the lightning data for the particular period on the screen and studying the thunderstorm activity, if any in the particular area.

Having been in service for some years the general impression among operating personnel following the utilisation of LLS data and the display systems is that the equipment is a valuable addition to the other monitoring systems installed in the National Control Centre and local and regional control centres, and that more detailed and reliable information than hitherto regarding thunderstorms and lightning discharges would be of major benefit.

It has been established that the LLS system has provided the National Control Centre with considerable more information regarding lightning phenomena than the earlier manual reporting procedures. On occasions, having observed and reported lightning strikes to the local control centres in the areas affected, the National Control Centre system supervisor has found that staff at these centres have been unaware of the presence of thunderstorms in their areas. These situations may have been due to the deficiencies of the existing manual reporting system as already described.

The inevitable degree of uncertainty inherent in the SMI lightning forecasts, as demonstrated by the occasions on which the LLS system unit has recorded lightning in areas assigned a forecast of low lightning risk, may also be noted. There are several examples on occasions where LLS system monitors have reported lightning discharges along transmission lines, the strikes being accompanied by earth fault indications on the lines. No lightning reports were received from the field, while the forecasts for the areas indicated low risk of lightning.

The fact that the presentation unit displays lightning information in real-time is a major advantage which allows the operator to follow the course of an electrical storm across the country enabling him to predict the areas which will be affected. On such occasions, operators have been able to issue advance warnings to the various districts, thereby allowing line work to be deferred, unsuitable operations schedules to be revised, standby plant to be started or kept in service, etc. Operators have stated that they now work in a somewhat different manner than heretofore now that the lightning information is available in an easily comprehensible manner. "Being continuously aware of the lightning information, we are now more careful to avoid certain operating decisions which we would take under normal circumstances, but which appear less appropriate when thunderstorms are in the offing."

The following example illustrates the favourable economic consequences of utilising data from the LLS network and how control centre personnel make use of the data presented. From time to time the transmission network is scheduled for transmitting power generated by hydro power stations in the north of Sweden to the south of Sweden and to Denmark. For safety reasons power transmission is accepted only up to a certain level in case of lightning striking one of the transmitting lines causing extreme transmission load on the intact lines which might lead to severe network instability and a major outage with far-reaching consequences. At these occasions the engineers and supervisors at the National Control Centre have been able to increase the transmitted power considerably since they can keep track of existing and imminent lightning by using data from the LLS network making sure there is no risk of lightning approaching the vulnerable transmitting section. If the LLS network records lightning in the vicinity of the transmission lines the control centre supervisors immediately order a rapid decrease in the level of power transmission according to the safety standards. If the transmission had not taken place the power would normally have been generated locally by oil-fired power plants. Since producing electric power in oil condense power plants is much more expensive than producing the power in hydro power plants, it is of great economical interest to transmit as much low-cost hydro power as possible substituting power using oil. At one specific time, transmission at a higher level of 1000 MW could continue for 24 hours since the power network was supervised by utilising lightning data thus during this short period creating a profit exceeding US$ 100 000 compared to the alternative of producing the power locally by using expensive fuel.

CONCLUSIONS

In summary, it may be said that the installation of presentation units and display systems at the National Control Centre and at other control centres and their connection to the lightning location system has proved to be a valuable aid to improved and more reliable operations management and supervision. The equipment is also appreciated by the personnel, although it has naturally suffered from the invariable teething troubles in the early days. However, it would appear that since the change to the PC based display systems the operators and the control centre supervisors are very much in favour of the equipment and the utilisation of lightning data in transmission network operation and supervision.

Vattenfall is aware that the system has not yet achieved its optimum accuracy and efficiency. However, it is not until in this present situation when Vattenfall has acquired an sufficient insight into the potential of the system, it would be of interest to undertake a careful expansion of the LLS network so that the deficiencies of the system might be studied in closer detail and, hopefully, eliminated. Discussions with the users have indicated that there is considerable interest in expanding the existing LLS network by the installation of further units, provided that new equipment should be installed in a way and by a schedule which will meet the requirements of the users to the greatest possible extent.

To conclude, the LLS has proven to have a high degree of availability, to have increased the level for personnel safety and to have been quite profitable.

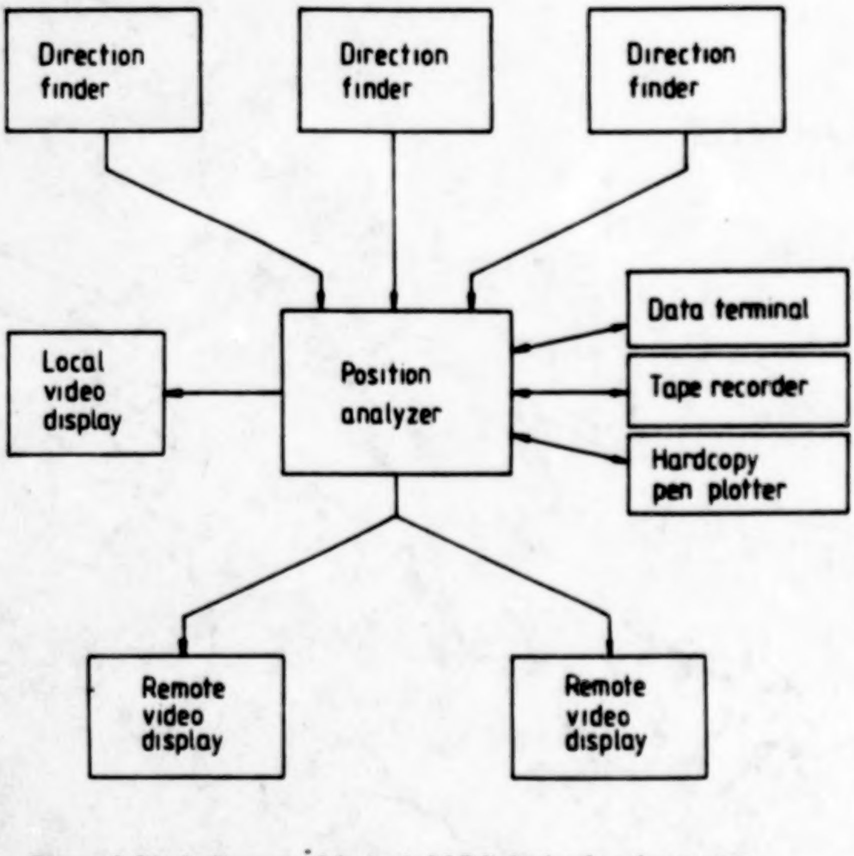
Direction finder
Direction finder
Direction finder
Data terminal
Local video display
Position analyzer
Tape recorder
Hardcopy pen plotter
Remote video display
Remote video display

Figure 1. Block diagram of the basic LLP lightning location system

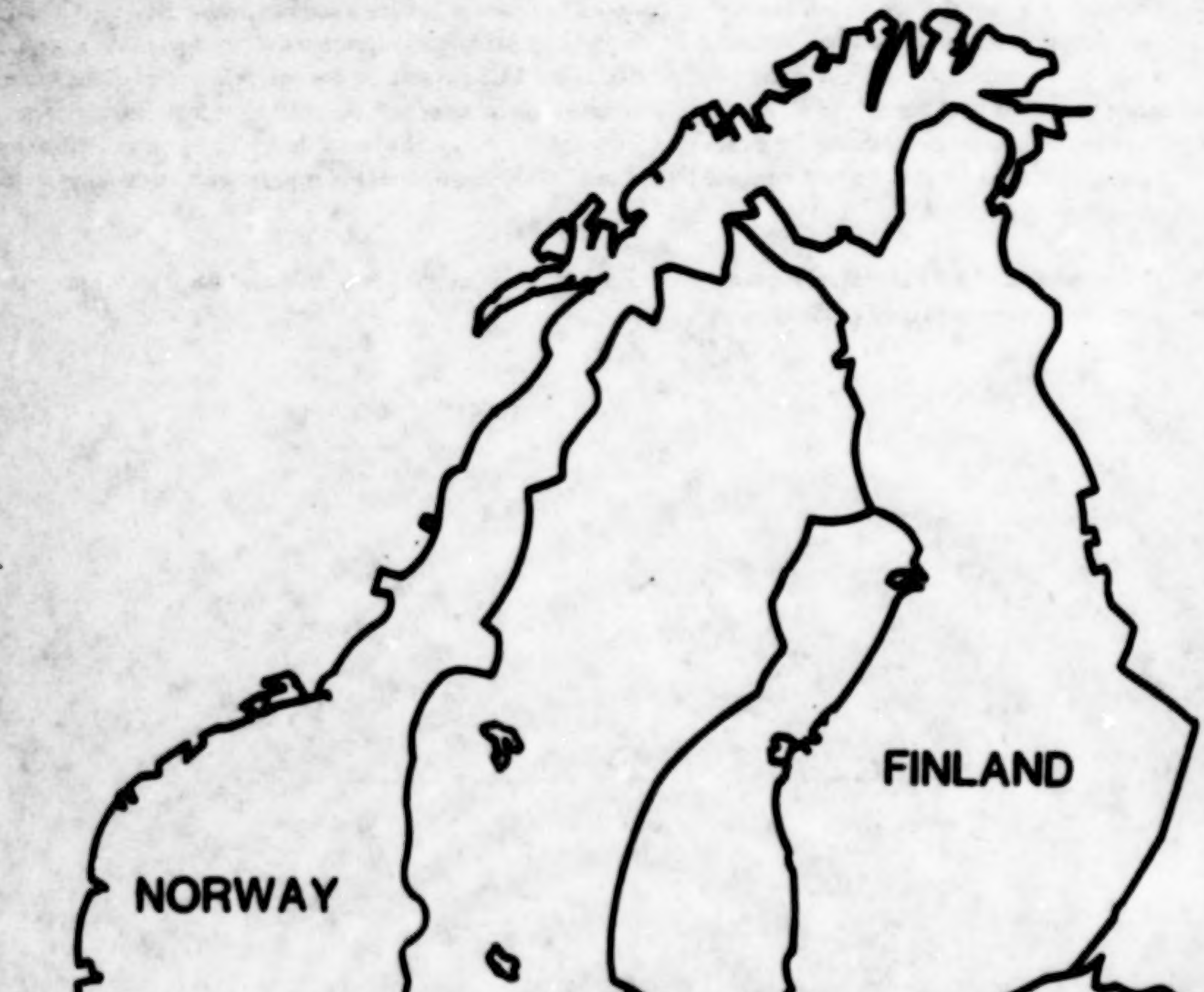
NORWAY
FINLAND
SWEDEN
90 km
320 km
505 km
DENMARK
U.S.S.R.

Figure 2. DF-sites in Sweden 1983

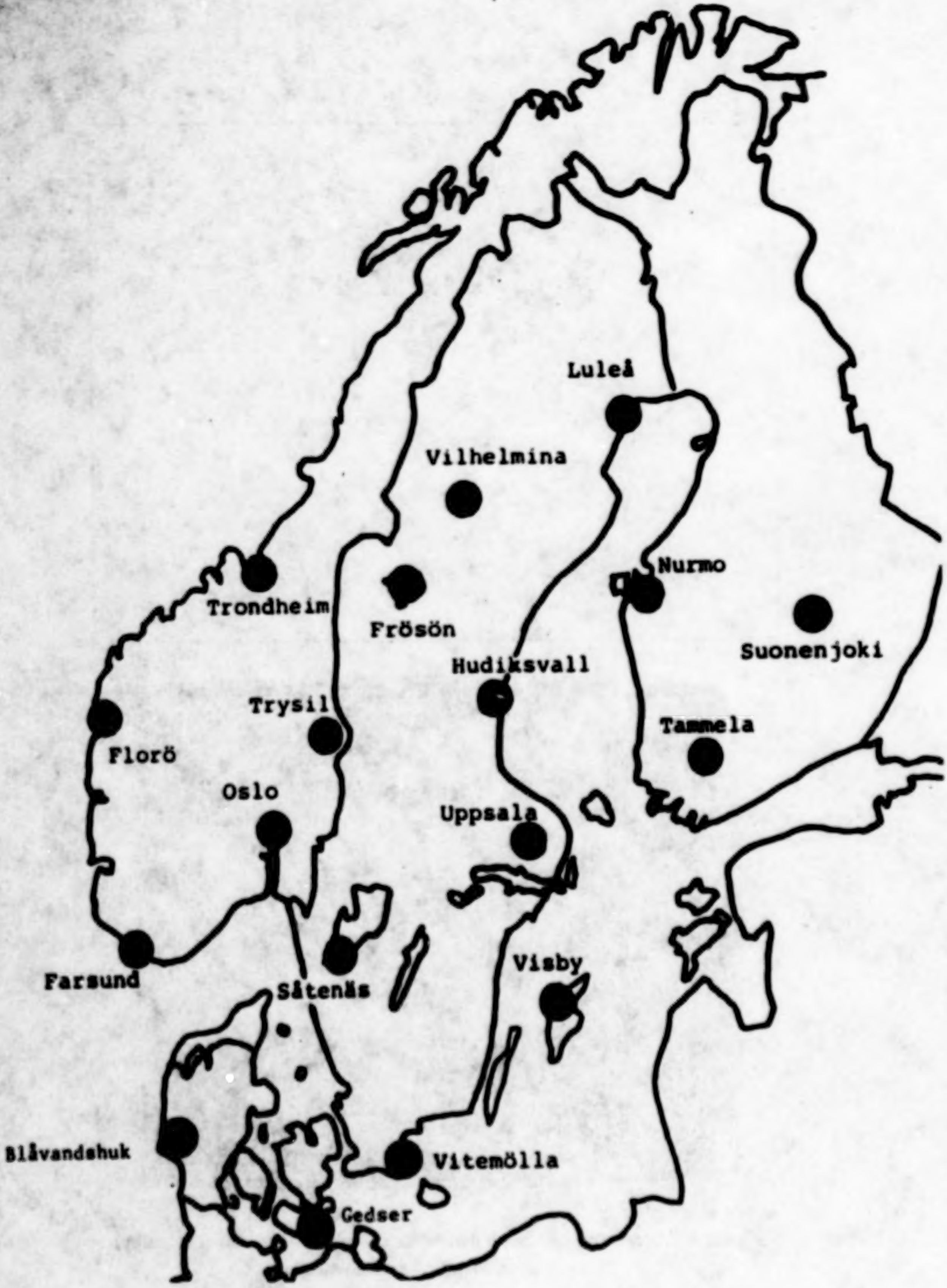
Luleå
Vilhelmina
Nurmo
Trondheim
Frösön
Suonenjoki
Hudiksvall
Trysil
Tammela
Florö
Oslo
Uppsala
Farsund
Såtenäs
Visby
Blåvandshuk
Vitemölla
Gedser

Figure 3. DF-sites 1989 in Sweden, Norway, Finland and Denmark

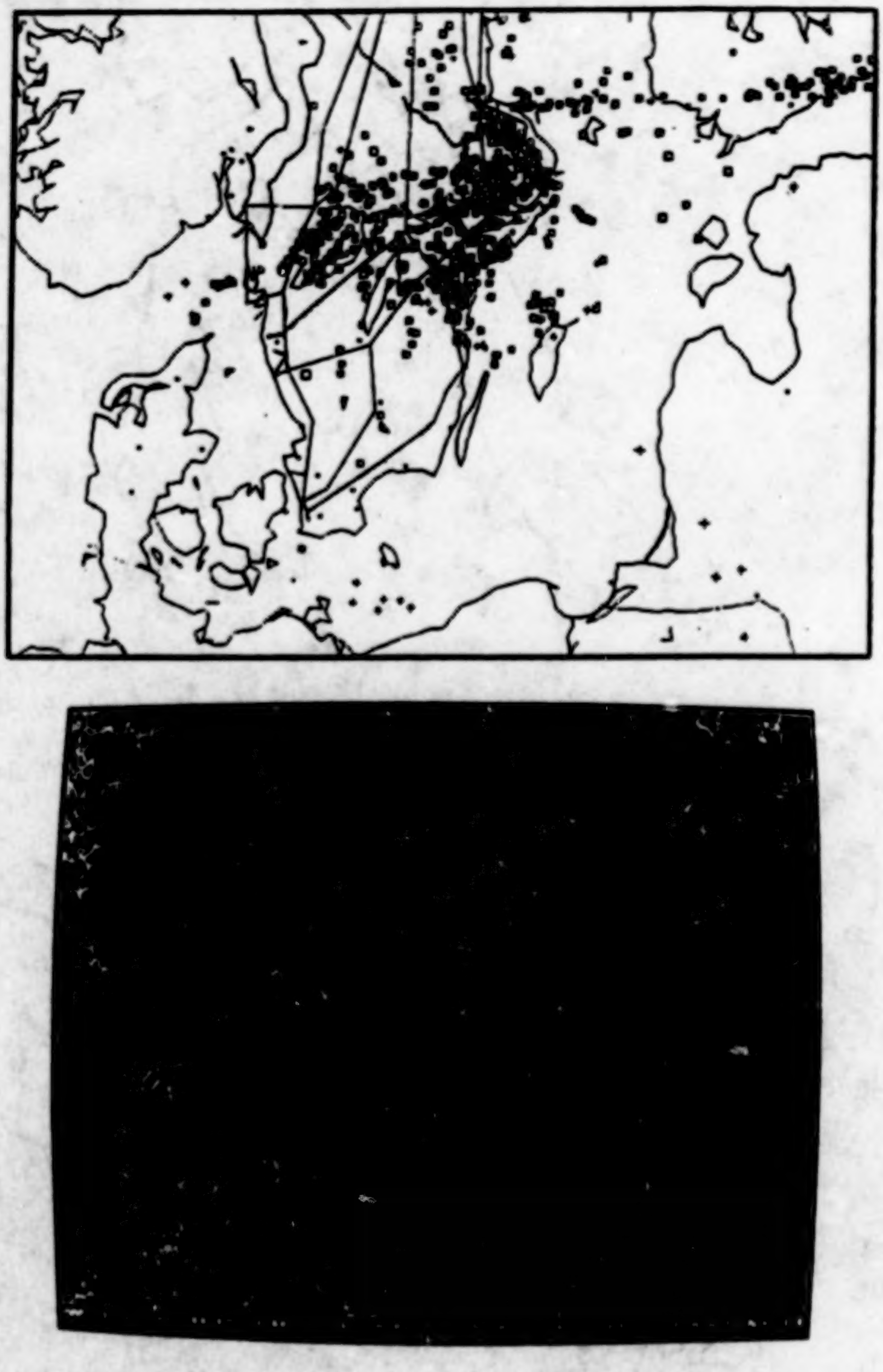

Figure 4. Examples of real-time lightning data displays (multi-colour in reality). Please note the indicated transmission lines.

RANGE ESTIMATION TECHNIQUES IN SINGLE-STATION THUNDERSTORM WARNING SENSORS BASED UPON GATED, WIDEBAND, MAGNETIC DIRECTION FINDER TECHNOLOGY

Alburt E. Pifer, William L. Hiscox, Kenneth L. Cummins, and William T. Neumann
Lightning Location and Protection, Inc.
Tucson, Arizona
U.S.A.

ABSTRACT

Gated, wideband, magnetic direction finders (DFs) were originally designed to measure the bearing of cloud-to-ground lightning relative to the sensor. A recent addition to this device uses proprietary waveform discrimination logic to select return stroke signatures and certain range dependent features in the waveform to provide an estimate of range of flashes within 50 kilometers. In this paper, we will discuss the enhanced ranging techniques designed and developed by Lightning Location and Protection, Inc, for use in its single-station thunderstorm warning sensor. Included in the paper will be the results of on-going evaluations being conducted under a variety of meteorological and geographic conditions.

INTRODUCTION

The LLP thunderstorm sensor (TSS) is a single-station thunderstorm warning system that provides real-time information about the occurrence of cloud-to-ground lightning in and around an area of concern. This information is used in a variety of ways to improve safety and effect cost savings. Typically, the TSS warnings are used to clear personnel from exposed areas, to shut down hazardous operations, and to switch sensitive equipment over to backup power. The TSS indicates the approach and the direction of approach of a thunderstorm to the area of concern as well as warning of the occurrence of cloud-to-ground lightning within the area of concern. When the storm has passed and no cloud-to-ground lightning has been detected within the area of concern for a certain time period (usually 15 minutes), the warning is lifted, indicating it is safe to resume normal operations. Some typical applications are entertainment parks, airport operations, construction projects, and sensitive manufacturing plants.

The TSS is a major improvement over any thunderstorm warning device previously available because it incorporates the same patented technology that is used in the LLP lightning locating networks [1-4]. The sensor detects the presence of thunderstorms by detecting cloud-to-ground lightning on a flash-by-flash basis. For each stroke in the flash the sensor determines the time, the direction, the signal strength, the polarity, and the change in the electrostatic field associated with the stroke. The detected waveforms must pass some fairly restrictive waveform criteria tests to be considered valid return strokes. These tests eliminate background interference and cloud lightning (cloud-to-cloud, intra-cloud etc.).

The location of the thunderstorms is inferred from flash data that have the following performance properties:

- The flash identification is very good. For a properly sited sensor the false rate due to background noise is essentially zero. The only false flashes are due to cloud lightning that is misidentified as cloud-to-ground. Fewer than 1% of the waveforms accepted by the sensor are due to non-cloud-to-ground lightning. These do not cause a problem because they only occur during a thunderstorm, and they are such a small fraction of the events that they do not appreciably influence the thunderstorm algorithm.

- The flash direction is very accurate (+/- 1 degree).

- The flash time measured relative to the TSS clock is precise (+/- 1 millisecond).

- The sensor is a long-range instrument. Storms can be sensed as far away as 100 nm.

Given the difficulty of determining range with a single-station sensor, one might recommend using location information from a lightning locating system to calculate the range. This would certainly be a viable alternative, but a single-station sensor offers a number of important advantages:

Cost	A locating system requires at least two sensors and a central analyzer to calculate the location. In addition, remote sites must be located and communication between the sensors and the central analyzer set up.
Installation	Since a single-station sensor is located at the facility of concern , siting and communication issues can usually be performed by local personnel.
Accuracy	Since a single-station sensor is located at the area of concern, its systematic errors are relative to the area of concern, and are guaranteed to have a relatively minor effect.
Control	Since the entire warning system is under direct control of those most concerned with its proper operation, maintenance and operational priorities can be tailored to meet the needs of the facility.
Performance	Since the warning systen is tuned for optimal performance in the immediate vicinity of the sensor, a single-station sensor is frequently able to offer higher short-range detection efficiency and directional accuracy than a wide-area locating network.

Studies of the spatial distributions of cloud-to-ground strike points has shown, that for small cells the mean distance between successive flashes is from 3.2 to 4.2 km (Krider [5]). This means that, if any lightning is detected within this distance, it is time to issue a thunderstorm warning.

Since the function of the TSS is to detect the presence of thunderstorms, as opposed to locating individual flashes, the sensor classifies each flash as one of 4 ranges: 0-3, 3-10, 10-30, and beyond 30 nautical miles. The number of flashes in each classification during the last 15 minutes are used to determine the presence and position of thunderstorms. The range classification is not precise in that a flash near the edge of one classification has a finite probability of being assigned to the adjacent classification. The effectiveness of the range classification is completely characterized by the probability, as a function of range, of a flash being assigned to each of the four range classifications.

In this paper, we present the results of an experiment that was made to determine these four probability distributions. We also present the results of a number of experiments that test how well the TSS agrees with human observers and with radar.

THE RANGE ALGORITHM

The sensor has 3 receiver channels, each with a bandwidth of 1 kHz to 350 kHz, that detect the north-south and east-west components of the horizontal magnetic field and the vertical component of the electric field. Figure 1 shows typical waveforms for cloud-to-ground return strokes at 2, 5, 10, and 50 kilometers. The initial sharp rise to a peak is the radiation field due to rapid turn-on of the return stroke current when a leader has approached close enough to ground to initiate a discharge. This radiation field returns to zero over a period of 50 μsec as the current slowly turns off as charge in the cloud is neutralized. This can be seen in the 50 kilometer waveforms of Fig. 1 which are essentially pure radiation fields. Note that the magnetic and electric waveforms at 50 kilometers are quite similar to each other as they should be for the radiation fields. The electric and magnetic waveforms for 2, 5, and 10 kilometers differ from each other considerably after the initial radiation peak. The electric field waveform has a ramp due to the change in the vertical component of the electrostatic field. This is primarily a dipole effect due to transporting charge between the cloud and ground, and it should be inversely proportional to the range cubed. Likewise, the magnetic waveforms have a hump due to induction fields, and are inversely proportional to the range squared. In each case the waveform for the first stroke (solid line) is significantly larger than that of the second stroke (dashed line). The theoretical basis for these assertions is contained in Uman [6].

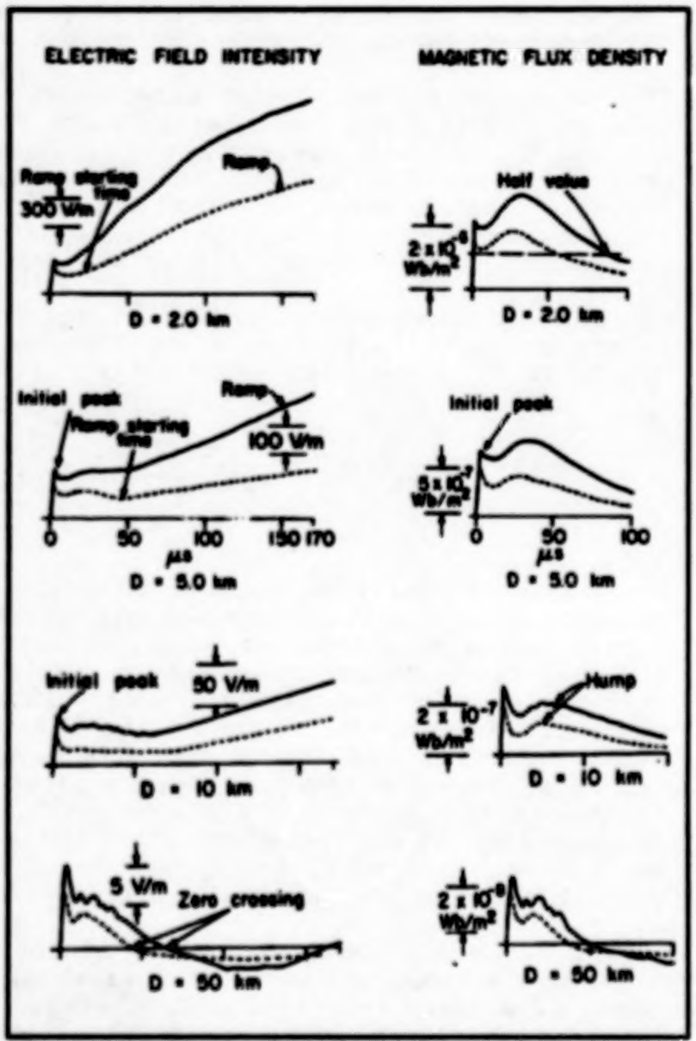

Figure 1 Typical electric and magnetic waveforms for cloud-to-ground return strokes at ranges of 2, 5, 10, and 50 km (adapted from Lin et al. [7]). The solid lines are the first stroke, the dashed curves are subsequent strokes.

The sensor samples all 3 channels simultaneously at the radiation field peak and then resamples the electric field channel at 170 μsec after the peak. The electric field is sampled at 170 μsec to be consistent with Lin et al. [7]. This time is fairly arbitrary. It could be any time that gives a measure of the ramp. The magnetic field components are used to calculate the direction to the stroke and the magnitude of the radiated field peak (the signal strength). The magnetic field components are used to calculate the signal strength because the gain of the magnetic field antennas is nearly independent of siting, whereas the electric field antenna gain depends strongly on siting. The signal strength is approximately proportional to the peak current in the return stroke and inversely proportional the range as shown in Eq. 1.

$$SIGNAL = CONSTANT \times \frac{CURRENT}{RANGE} \qquad (1)$$

The inverse range dependence arises due to conservation of energy, as the radiated energy is spread out over a spherical shell with a radius equal to the range. The "constant" is empirically determined for the sensor from the signal strengths of flashes at known ranges. In order to do this, it is assumed that the median of the range-normalized signal strength distribution corresponds to the median of measured current distributions.

If the return stroke current were known for each flash, then Eq. 1 could be used to calculate the flash range. Since the current is not known for a single-station sensor, the range can be estimated by assuming that the current is equal to the median current. Due to the large variation in the return stroke currents, this is not a very good estimate of the range. However, it is useful for distinguishing close lightning from distant lightning, where the range variation is large enough that it dominates the uncertainty in the current.

The primary quantity used by the LLP sensor to determine the range is the ratio of the electric field sampled at 170 µsec to radiation peak in the electric field, which is referred to as the relative electric field change (REFC):

$$REFC = \frac{ELECRIC\ FIELD\ AT\ 170\ \mu SEC}{ELECTRIC\ FIELD\ RADIATION\ PEAK} \qquad (2)$$

The value of the REFC depends mainly on the range. This is because both quantities in the ratio are roughly proportional to the total charge transferred by the return stroke, which allows the charge dependence to cancel out. The electric field at 170 µsec is a measure of the electrostatic field change, which, in a simple dipole model, is proportional to the total charge transferred times the height of the charge center. The value of the electric field radiation peak is proportional to the peak current, and given that all return stroke waveforms have approximately the same shape, and that the total charge is the integral of the current, the total charge is approximately proportional to the peak current. The dependence on total charge for both quantities is somewhat rough because of the large variations in the spatial distributions of the charges involved.

Fig. 2 shows the combined data of Lin et al. [7] and Tiller et al.[8]. These data show a large scatter of the value of the REFC at a particular range, but there is a clear correlation with range. Fig. 2 also shows that the REFC for first strokes tends to be larger than that for subsequent strokes. Presumably this is an effect of the side channels of the first stroke.

The range-dependence of the REFC is approximately the reciprocal of the range squared. This is because the radiated field is inversely proportional to the range, and a dipole field, which dominates the field at 170 µsec, is inversely proportional to the range cubed. This strong range-dependence means the REFC is useful only for ranges of 20 km or less.

An important fact to note is that since both quantities in the REFC ratio are measured on the electric field channel, the antenna gain cancels out, resulting in REFC being insensitive to sensor siting.

As mentioned above, the TSS assigns each flash to one of four ranges: 0-3, 3-10, 10-30, and beyond 30 nm. For flashes within 3 and 10 nm, range is determined on the basis of the REFC and signal strength of the first stroke. The remaining flashes are assigned to 10-30 or beyond 30 on the basis of signal strength alone. If the signal strength of a given flash exceeds the dynamic range of the instrument (over-range), it will be automatically considered to be within 3 nm. The thresholds for the REFC at 3 nm criteria have been selected so that any flash with an REFC greater than the threshold has a probability of 0.9 of being within 3 nm.

The TSS maintains a running total of the number of flashes in each range region for a given interval, which is typically the last 15 minutes. The 3-10, 10-30, and beyond-30 regions are divided into octants. A red warning is issued whenever one or more flashes have occurred in the 0-3 region, or whenever 6 or more of the 3-10 octants have 1 or more flashes.

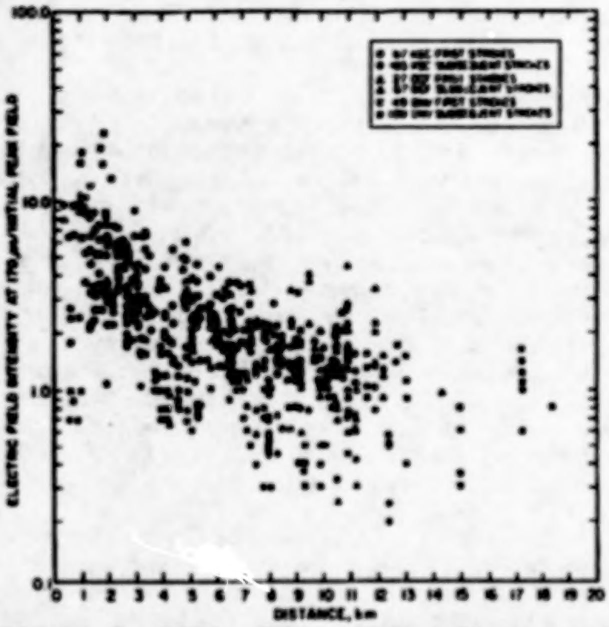

Figure 2 REFC for close first and subsequent return strokes (combined data from Tiller et al. [8] and Lin et al. [7]).

EVALUATION OF THE RANGE ALGORITHM

Over the course of the last several years, LLP has invested considerable effort in the characterization, design, and execution of formal tests to evaluate the effectiveness of single-station thunderstorm sensors. Initially, LLP experimented with location techniques that were based exclusively on averaging the measured signal strengths of groups of flashes. In this early testing, human observers and radar records were the primary points of comparison. Although this ranging technique showed some promise, it was determined that the overall performance had to be improved if single-station technology was to provide an effective warning system.

With the addition of the REFC enhancement to the ranging algorithm in 1986, a substantial improvement was made in single-station ranging. However, it was realized that in order to properly measure this improvement, a standardized method must be established to characterize the operation of a single-station warning device. The first step in this process was a careful analysis of the factors affecting both the reporting instrument and the measuring instrumentation, as described in Neumann, et al. (1988) [9]. From this work, an initial test was undertaken during the summer and fall of 1988 in Tucson, using local facilities including a locating network and National Weather Service (NWS) observer reports. This initial work, which included ranging information based on REFC techniques, was reported in Neumann, et al. (1989) [10]. In addition to the observations related directly to the performance of the sensor, this experiment also provided an important opportunity to analyze the methodology and design of the test itself, and served as an important milestone for subsequent work.

In conjunction with the experiment to formally characterize REFC, described later in this paper, a carefully formulated test of the performance of the Thunderstorm Sensor (TSS) was undertaken in Tucson. In this test, the two TSS instruments were co-located inside a region of highly accurate performance of the LLP Tucson Research Network. In addition, data were collected from on-site human observers, NWS records from a manned weather station in the area, and NWS weather radar. The purpose of this test was not to characterize the sensor's performance on individual flashes, but rather on properly monitoring the development, movement, and dissipation of thunderstorms in the vicinity.

The results of this experiment clearly indicated the benefit of an automated thunderstorm warning system. Not only did the sensor agree with the human observers in this test, the TSS was able to provide the warning earlier, since its measurements were not limited by line-of-sight or other local distractions. In addition, the TSS also provided a significant enhancement to the interpretation of NWS radar images by differentiating areas of highly convective activity from that of rain shafts from precipitation. The TSS also showed good agreement with the LLP locating network. Although, as one might expect, precise locations could not be obtained from the TSS, the approximate distance and direction reported by the TSS were consistently in agreement with the locations provided by the network. Moreover, the lack of erroneous reports from the TSS also indicates the important benefit of waveform discrimination for identifying lightning events. Incorrectly reporting the presence of lightning has been a chronic problem of many single-station warning devices, and no such events were identified in this field experiment.

In addition to this carefully instrumented and monitored test, there have also been other field experiments and operational commercial installations that have reported similar findings. In two instances, Thunderstorm Sensors have been placed near NWS field offices on the east and southeast United States coastlines for data collection. When NWS observers have had access to the data reported by the TSS, they have reported being able to detect thunderstorms at an earlier point in their development, and to better differentiate thunderstorm activity from heavy precipitation. In addition, commercial installations of the TSS at heavily used airfields in the upper mid-west, mid-south, and desert southwest have also returned anecdotal information of earlier and more accurate warning of thunderstorm activity based on using the TSS independently or in conjunction with other weather sources, such as radar, which has directly improved their operational efficiency.

To further quantify performance, in the summer of 1990 LLP performed a explicit test of the ranging algorithm. In this test, the Tucson LLP research lightning locating network was used to determine the flash range. The LLP network consists of 3 low-gain DF's with baseline distances of 36.1, 37.5, and 51.7 km, as shown in Fig. 3 (along with some sample flash data). The test took advantage of the fact that, since the DF's have comparable hardware to the TSS, the DF's can also measure the quantities necessary to calculate the REFC. During the test the DF's ran a special version of firmware that transmitted the electric field radiation peak and the electric field at 170 μsec along with the data normally send the central site. This data was recorded along with the flash location. The data was reprocessed off-line to calculate the REFC as a function of range. The network was run in this mode during the summer of 1990. The data presented below are all the negative flashes from 4 days at the peak of the monsoon (August 3, 11, 12, and 16) where a "good" location was calculated. A "good" location required that the range from one DF was less than 40 nm, that the time reported by the DF's be within 5 milliseconds, that the semi-major axis of one standard deviation error ellipse be less than 0.5 nm, and, if all 3 DF's reported so that an optimized location could be calculated, that the χ^2 per degree of freedom be less than 5. A standard error of 1 degree was used in calculating the χ^2.

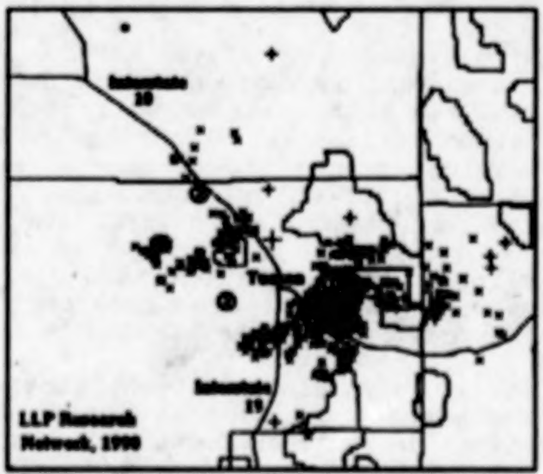

Figure 3 LLP Research Network, 1990

A total of 10,591 flashes were detected by the network in the 4-day sample. Most of these were too distant from the DF's to meet the requirements of a "good" flash. The final data sample consisted of 895 flashes with 2339 DF reports with a range less than 40 nm. The range distribution of the final data sample is shown in Fig. 4. If the flashes were distributed uniformly over the area of the network, this distribution would increase linearly with range starting at zero. The first three bins have been depopulated due to over-ranges, and due to being rejected by a waveform criterion that requires that any subsequent peak in magnetic field be smaller than the initial radiation peak. This criterion, which helps reject cloud discharges, is normally enabled in a DF, but it is disabled in a TSS because the induction hump in the magnetic waveforms (see Fig. 1) is larger than the radiation peak for return strokes close to the sensor. Ideally, this criterion should have been disabled for this test since the DF's were being used to simulate TSS's, but this could not be done due to other operational requirements of the network. The fall-off at distances greater than 20 nm is primarily due to the strict accuracy requirement and the short baseline of the network.

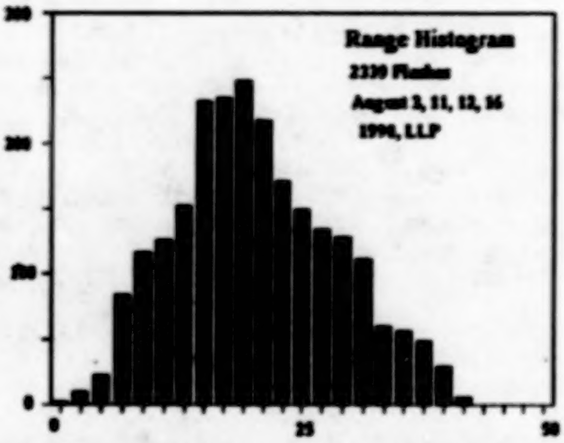

Figure 4 Combined range distribution for all DF's.

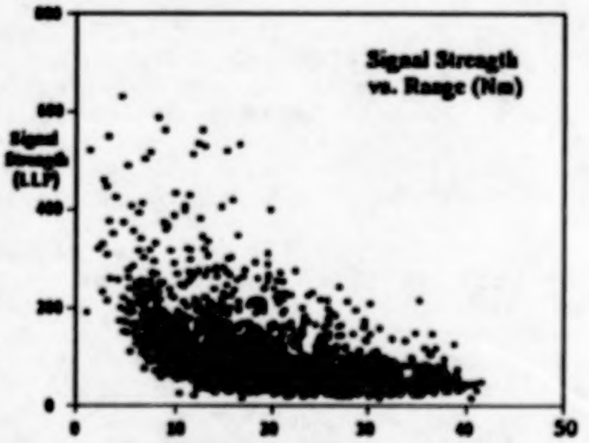

Figure 5 Scatter plot of signal strength vs. range for all DF reports.

A scatter plot of the signal strength vs. range for this same sample of DF reports is shown in Fig. 5. The large scatter is due to wide log-normal distribution of return stroke currents. The signal strength is the only criterion used to classify flashes as beyond 30 nm or within 30 nm. This results in a rather slow fall-off of the probability at 30 nm for the 10-30 and beyond 30 classifications.

A scatter plot of the REFC vs. range for the data set is shown in Fig. 6. The scatter of the data in this plot is significantly less than in the signal strength scatter plot (Fig. 5). With the exception of eight or so (< 0.5%) outliers, the data falls in a fairly tight band with clear range dependence. This range dependence is consistent with the expected reciprocal range squared dependence as discussed above. Much of the data within 5 nm was not available due to the use of the second peak waveform criterion. If the data within 5 nm had been available, it is believed that much larger values of REFC would have been plotted, and the range dependence would be even more dramatic.

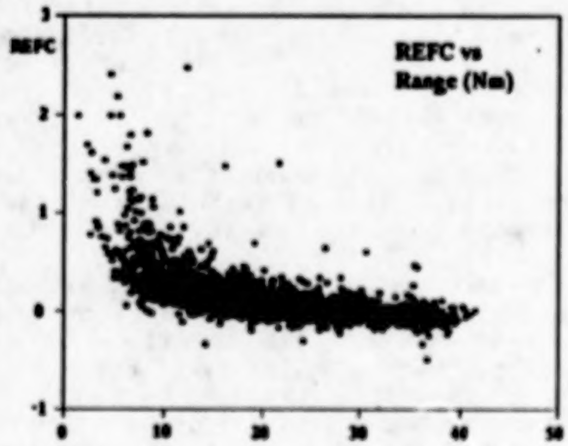

Figure 6 Scatter plot of REFC vs. range for all DF reports.

For this analysis, any flash with a first stroke signal strength less than 41.25 LLP signal strength units was classified as beyond 30 nm. The probability of a flash being classified as beyond 30 nm as a function of range is shown in Fig. 7. Each bin is the percentage of DF reports of the corresponding bin in Fig. 4 that had a signal strength less than 41.25 LLP units. This distribution would rise to 100% for large ranges if the data set included data beyond 40 nm. The value 41.25 was picked so that this distribution would have a value of approximately 50% at 30 nm. Note that the distribution does not go to zero until a range of 10 nm. This is due to return strokes with small peak currents.

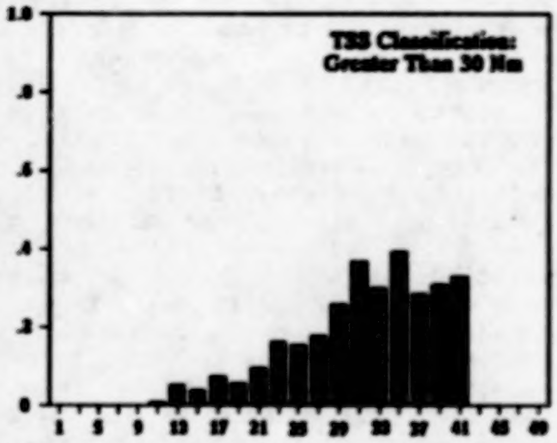

Figure 7 Probability of a flash being classified as beyond 30 nm.

A return stroke was classified as 10-30 nm: 1) if the signal is between 41.25 and 75, or 2) the signal is greater than 41.25 and the REFC is less than 0.5. The probability of a flash being classified as 10-30 as a function of range is shown in Fig. 8. The cutoff at 10 nm is fairly sharp due the combined effect of the REFC and the signal strength criteria. The cutoff at 30 nm is very slow since it is due to the signal strength criteria alone. The effect of the signal strength criteria at 10 nm is much sharper than the effect at 30 nm because the slope of the inverse range dependence of the signal strength is 9 times greater at 10 nm than at 3 nm.

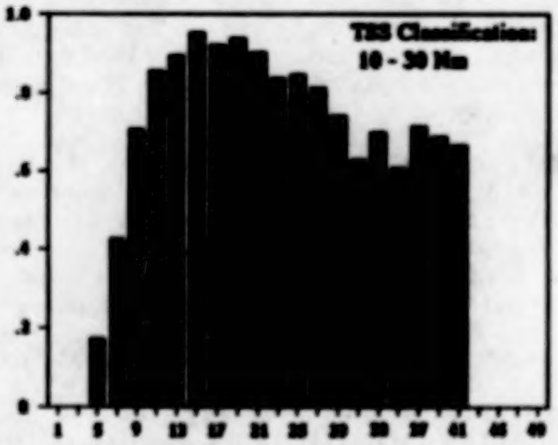

Figure 8 Probability of a flash being classified as between 10 and 30 nm.

The criteria for 10-30 were picked so that the distribution is just starting to fall as the range is decreased from 10 nm. This tends to pull flashes from the 3-10 classification, but also prevents return strokes from outside 10 nm from being classified as within 10 nm. This is to prevent false alarms due to return strokes with large peak currents that are outside 10 nm.

A return stroke was classified as 3-10 nm: 1) if the signal strength is between 75 and 125 and the REFC is greater than 0.5 , or 2) if the signal is greater than 125 and the REFC is between 0.5 and 1.5. The probability of a flash being classified as 3-10 nm as a function of range is shown in Fig. 9.

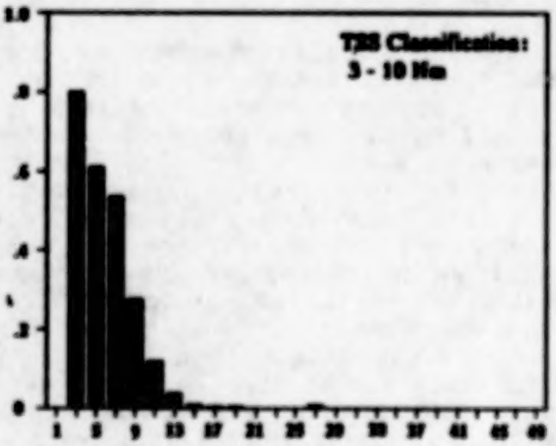

Figure 9 Probability of a flash being classified as between 3 and 10 nm.

A return stroke was classified as 0-3 nm if the signal is greater than 125 and the REFC is greater than 1.5. The probability of a flash being classified as 0-3 nm as a function of range is shown in Fig. 10.

For this analysis, the same REFC thresholds were used for positive flashes as for negatives, but the signal strength thresholds were increased by a factor of 2 because median peak current for positive flashes is approximately twice as large as that for negatives. However, the positive flashes were not analyzed because of the very small data set from the monsoon thunderstorms used in this test.

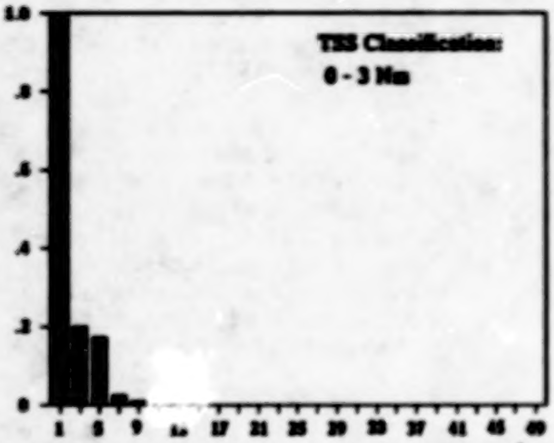

Figure 10 Probability of flash being classified as between 0 and 3 nm.

CONCLUSIONS

The LLP Thunderstorm Sensor provides better thunderstorm warning than any previous single-station device, with performance comparable to, if not better than, that of a multi-station lightning locating system. A number of tests have shown good correspondence with human observers and radar, and an explicit test of the ranging algorithm has demonstrated excellent performance within 10 nm. The combination of signal strength and REFC (relative electric field change - see Eq. 1) provides sufficient range information to determine storm location and issue timely thunderstorm warnings. The instrument has been shown to have good correspondence with theory and previous experiments (see Figs. 5 and 6).

REFERENCES

1. Krider, E. P., R. C. Noggle and M. A. Uman, "A Gated Wideband Magnetic Direction Finder for Lightning Return Strokes," *J. Appl. Meteorology*, 15, 402-405, 1976.

2. Krider, E. P., A. E. Pifer and M. A. Uman, "An Automatic Locating System for Cloud-to-Ground Lightning," *Lightning Technology*, Proc. of Technical Symposium held at NASA Langley Research Center, Hampton, VA, April 22-24, 1980, NASA CP-2128, FAA-RD-80-30.

3. Binford, R. C., L. G. Byerley, E. P. Krider, M. W. Maier, A. E. Pifer and M. A. Uman, "Wideband Magnetic Direction Finder Networks for Locating Cloud-to-Ground Lightning," *Proc. Eighth International Aerospace and Ground Conference on Lightning and Static Electricity*, Fort Worth, TX, June 21-23, 1983.

4. Maier, M. W., L. G. Byerley, R. C. Binford, W. L. Hiscox, E. P. Krider, A. E. Pifer and M. A. Uman, "Gated Wideband Magnetic Direction Finders for Locating Cloud-to-Ground Lightning, *Proc. International Conference on Atmospheric Electricity*, p. 305-310, Albany, NY, June 3-8, 1984.

5. Krider, E. P., "Spatial Distribution of Lightning Strikes to Ground During Small Thunderstorms in Florida," *Proc. 1988 International Aerospace and Ground Conference on Lightning and Static Electricity*, Oklahoma City, April 19-22, 1988.

6. Uman, M. A., *The Lightning Discharge*, New York:Academic Press, 1987.

7. Lin, Y. T., M. A. Uman, J. A. Tiller, R. D. Brantley and W. H. Beasley, "Characterization of Lightning Return Stroke Electric and Magnetic Fields from Simultaneous Two-Station Measurements," *J. Geophysical Res.*, 84, 6307-6314, 1979.

8. Tiller, J. A., M. A. Uman, Y. T. Lin, R. D. Brantley and E. P. Krider, "Electric Field Statistics for Close Lightning Return Strokes Near Gainesville, Florida," *J. Geophysical Res.*, 81, 4430-4434, 1976.

9. Neumann, W. T., L. G. Byerley, A. E. Pifer, W. Hiscox, "Considerations for Using Lightning Locating Systems in Performance Evaluations of Single-Station Lightning Detection Sensors," *Proc. 1988 International Aerospace and Ground Conference on Lightning and Static Electricity*, Oklahoma City, April 19-22, 1988.

10. Neumann, W. T., W. L. Hiscox, D. W. Howard, A. E. Pifer and E. P. Krider, "A Single-Station Thunderstorm Warning Sensor Using Gated, Wideband, Magnetic Direction-Finding Technology," European Geophysical Society, XIV General Assembly, Barcelona, March 13-17, 1989.

THUNDERSTORMS MONITORING AND LIGHTNING WARNING,

OPERATIONAL APPLICATIONS OF THE SAFIR SYSTEM

Philippe Richard

DIMENSIONS, Parc des Algorithmes, 91194 St Aubin Cedex,
France

A INTRODUCTION

During the past years a new range of investigation has been opened by the application of electromagnetic localization techniques to the field of thunderstorm remote sensing. VHF localisation techniques were used in particular for the analysis of lightning discharges and gave for the first time access to time resolved 3D images of lightning discharges within thunderclouds.
The French national agency for aerospace research (ONERA) has been active for more than ten years in this domain. It developped systems based on the principle of VHF interferometry for research in lightning physics and thunderstorm phenomenology. Today these techniques are used for operational applications. The DIMENSIONS company, a spin-off of ONERA, develops thunderstorms monitoring and lightning warning systems for use in fields such as aerospace, industry, military activities and meteorology.

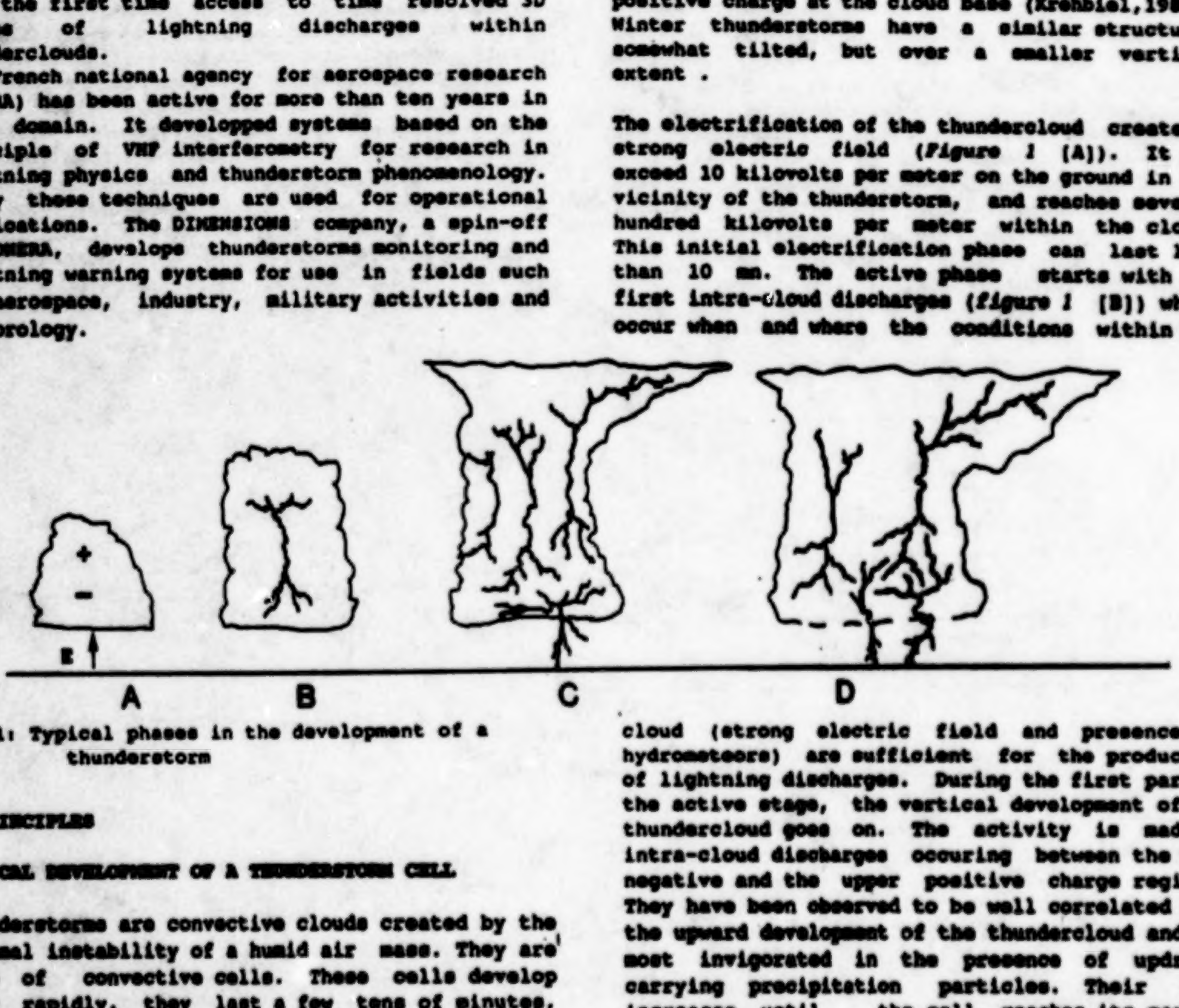

Fig 1: Typical phases in the development of a thunderstorm

B PRINCIPLES

TYPICAL DEVELOPMENT OF A THUNDERSTORM CELL

Thunderstorms are convective clouds created by the thermal instability of a humid air mass. They are made of convective cells. These cells develop very rapidly, they last a few tens of minutes, grow up to altitudes of 10 to 15 km and have a diameter of about 10 km. Thunderstorms are frequently multicellular, they can extend over tens or hundreds of kilometers and last several hours.

During its development a thunderstorm cell presents very strong updrafts (up to 50 m/s) carrying up precipitation particles such as ice crystals, supercooled droplets and graupels.

The main electrification process of the thundercloud during its development is due to the charging of graupels and ice crystals by collisions and to their separation by differential vertical motions within the cloud. These processes result in a tripole electrical structure with a main negative charge around 6 km at the -15°C level, a positive charge in the upper part of the cloud from 8 to 12 kilometers and a small positive charge at the cloud base (Krehbiel,1986). Winter thunderstorms have a similar structure, somewhat tilted, but over a smaller vertical extent .

The electrification of the thundercloud creates a strong electric field (*Figure 1* (A)). It can exceed 10 kilovolts per meter on the ground in the vicinity of the thunderstorm, and reaches several hundred kilovolts per meter within the cloud. This initial electrification phase can last less than 10 mn. The active phase starts with the first intra-cloud discharges (*figure 1* (B)) which occur when and where the conditions within the cloud (strong electric field and presence of hydrometeors) are sufficient for the production of lightning discharges. During the first part of the active stage, the vertical development of the thundercloud goes on. The activity is made of intra-cloud discharges occuring between the main negative and the upper positive charge regions. They have been observed to be well correlated with the upward development of the thundercloud and are most invigorated in the presence of updrafts carrying precipitation particles. Their rate increases until the cell reaches its maximum vertical development (*Figure 1* (C)).

Intra-cloud lightnings are thus the principal electrical manifestation of these charged and convective zones. They radiate electromagnetic waves over a very wide frequency spectrum and can be detected and located at long range.
In multicellular thunderstorms, intra-cloud lightnings can extend over very large distances (several tens of kilometers) between cells, within the anvil or in the dissipating part of the thundercloud. Intra-cloud lightnings are much more frequent than cloud to ground lightnings, they

typically represent 70 to 90% of the total lightning activity of a thunderstorm.

First cloud to ground lightnings are usually observed 5 to 30 minutes after the first intra-cloud lightnings, during or after the thundercloud maximum development. They are due to the subsequent descent of precipitation particles below the main negative charge layer. At this moment the intra-cloud activity rate begins to decrease and the cloud to ground rate increases (*Figure 1 [D]*). Cloud to ground lightning activity culminates during the decay of the thunderstorm cell, it is accompanied in severe thunderstorms by strong downdrafts and intense precipitations at ground level; these severe phenomena have been observed to follow the peak intra-cloud activity with a delay of 5 to 10 minutes (Williams et al, 1988).

ELECTROMAGNETIC RADIATION FROM LIGHTNING

Lightning discharges produce electromagnetic radiation over a very large frequency spectrum. The overall spectrum of lightning peaks at a few hundred kHz and extends up to the Ghz with a 1/f dependance. The electromagnetic emissions are due to the occurence of intense and rapidly varying currents within the lightning channels.

The most powerfull radiation is the pulse produced by the return stroke wave during cloud to ground flashes. This wave typically occurs when a pre-ionised leader channel, progressing downward from the thundercloud, reaches the ground. At this moment an intense current propagates upward within the lightning channel at about 1/3 the velocity of light. The current waveform has a typical risetime of a few μs and a peak value of several tens of kA. This phenomena radiates at low frequency, mainly below 1 MHz. This radiation is used principaly for the measurement of the characteristics of the cloud to ground return stroke current (peak value, polarity, energy...) and for the long range localization of lightning strokes to ground.

But lightning discharges radiate much more frequently at higher frequencies. The radiation is made of very short pulses of a few ns risetime, they cover the whole HF-VHF-UHF spectrum. These radiation pulses come from all along the lightning channels during their formation, or during the rapid propagation of a current wave within an existing pre-ionised channel . They are mainly due to fast transitions occuring between low and high conductivity phases of the lightning channel plasma in negative polarity breakdowns. They are observed in all types of lightning flashes (intra-cloud and cloud to ground), and in most phases of a discharge (preliminary breakdowns, stopped leader, dart leader, recoil streamer and return stroke). These pulses usually occur in bursts lasting from a few hundred μs to several ms; the pulse rate can range from a pulse every 50 μs up to several tens per μs.

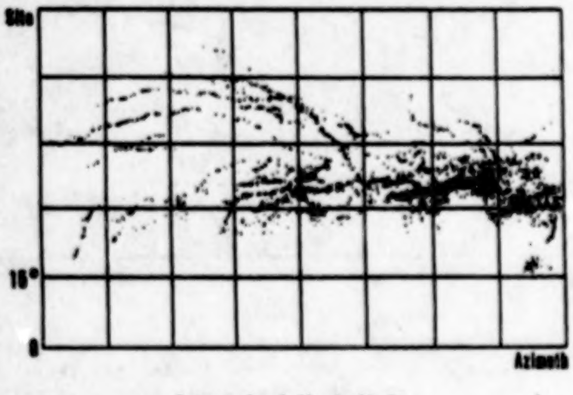

Intra-cloud flash (2-D)

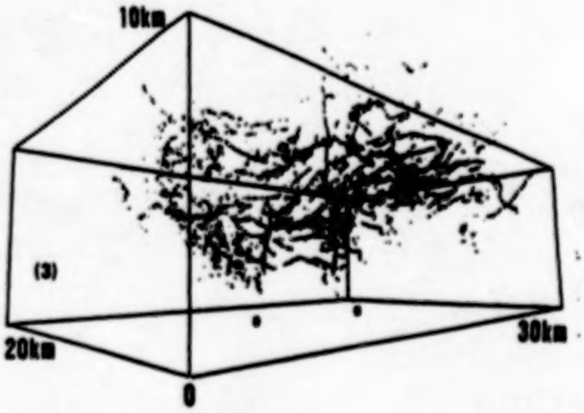

3-D imaging of propagating discharges during 20 minutes of storm activity

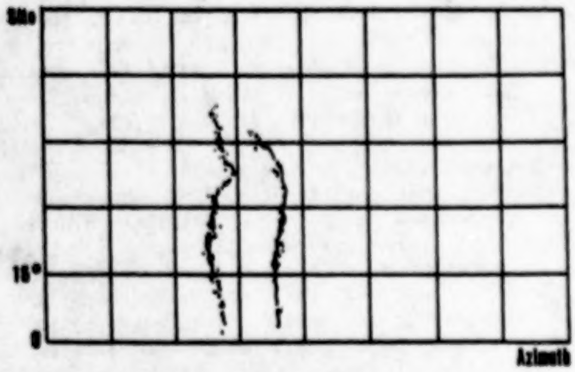

Cloud to ground return strokes (2-D)

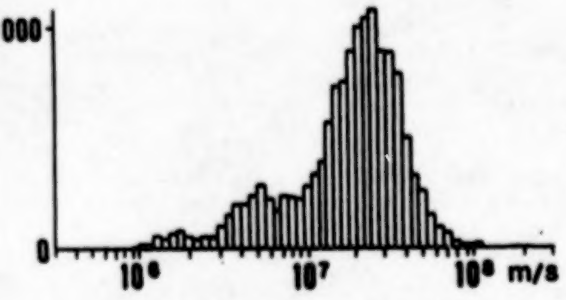

Histogram of discharge propagation velocities

Fig 2: Examples of results obtained with 3D VHF interferometry

196

VHF detection and location techniques have been of great interest for the analysis of lightning discharges properties, in particular within the thundercloud, where previous optical techniques were ineffectives, and which contain the large majority of lightning discharges phenomena. Figure 2 presents some of the results obtained at ONERA with a 3D interferometer, it illustrates some of the main characteristics of lightning discharges.

THE INTERFEROMETRIC TECHNIQUE

Measurement principles - Interferometry is based on the measurement of phase differences between signals received on different antennas of an antenna array. These phase differences are directly related to the direction of arrival of the signal and are used to calculate the angular position of the source in azimuth and elevation. 2D or 3D spatial location can then be obtained by the combination, through triangulation, of angular data given by at least two different interferometric stations.

Characteristics and advantages

The main advantage of this type of measurement is that it is independent of the signal wave form since measurement is only made on the electromagnetic wave phase. This is to be opposed to other modes of radio localisation using amplitude measurements and wave form identification. Interferometric localisation is thus not tributary to the identification of a typical wave form and can be made on any type of radiation from lightning phenomena. In addition the use of the VHF frequency range allows the localisation of a large variety of atmospheric discharges phenomena in this band and the fine reconstruction of the spatial structure of lightning discharges in its different phases of development.

C APPLICATIONS TO THUNDERSTORM MONITORING AND LIGHTNING WARNING

Detection and localisation techniques developped at ONERA during lightning research programs have been applied to the design of the SAFIR system. This development had for main objective the design of an operational system capable to assess and warn in real-time for lightning hazards and potential thunderstorm hazards.

The basic principle is that all along the development of a thunderstorm cell, the electrical activity (production of lightning discharges and generation of an electrostatic field) is closely related to the different stages of evolution of the cell and to the thunderstorm severity. The electrical activity of a thunderstorm can in consequence be used for achieving thunderstorm early detection and lightning hazard early warning, and for evaluation of potential thunderstorm hazards.

The SAFIR system main detection technique is the long range interferometric localization of thunderstorm electromagnetic activity; the system performs the localisation of intra-cloud and cloud to ground lightning discharges and the analysis of the characteristics of the activity.

Applications and capabilities of the SAFIR technique in the field of thunderstorm monitoring and lightning warning can be summarized as follow:

High efficiency detection and monitoring capabilities - SAFIR can locate VHF sources present in all types of lightning discharges (intra-cloud and cloud-to-ground), and can therefore locate and monitor the total lightning activity of a thundercloud. The additional detection of intra-cloud activity usually represents a three-fold to ten-fold improvement in monitoring efficiency, it has been observed to reach a hundred fold in some cases of severe thunderstorm.

early lightning warning capability - Detectable at long range, intracloud discharges are the first signs of the electrical development of a thunderstorm.
By localising these discharges SAFIR can provide early warning of thunderstorm developments and lightning hazards before the first cloud to ground discharges. Warning delays between first IC and first CG range from 5 to 30 minutes.

mapping and monitoring of electrically active hazard areas - Lightning discharges can extend over distances of several tens of kilometers, the localization and monitoring of these discharges enables the system to delimit the real extension of electrically active areas and to estimate the potential lightning hazard levels on the ground and in the air. In conjonction with previous capabilities the system is able to precisely analyse the stage of development of the thunderstorm and can project at short term its evolutions in space and time to give a previsionnal mapping of lightning hazard areas.

potential for the assessment of severe thunderstorm hazards - A close correlation exists between the convective state and severity of the thunderstorm and the characteristics of its lightning activity. Maximum vertical development of the thundercloud coincides with the maximum in total flash rate. The severe phenomena occuring at ground level during the thunderstorm decay such as maximum cloud to ground flash rate, intense precipitations, strong downbursts, have been observed to occur 5 to 10 minutes after the peak in IC flash rate (Williams et. al., 1988). Real-time localization and monitoring of total thunderstorm activity is thus a potential tool for the assessment of weather hazards produced by thunderstorms.

SAFIR SYSTEM ARCHITECTURE

A SAFIR system basic configuration is made of 3 detection stations and a central processing station (*figure 3*). Each detection station performs the interferometric angular localization of lightning discharges. Data are transmitted to the central station where the spatial locations of discharges are calculated by triangulation technique.

The central station performs the real-time monitoring and analysis of the activity and displays the hazard maps and warning informations. These informations can then be transmitted automatically or on request to remote display terminals.

Fig 3: SAFIR system typical configuration

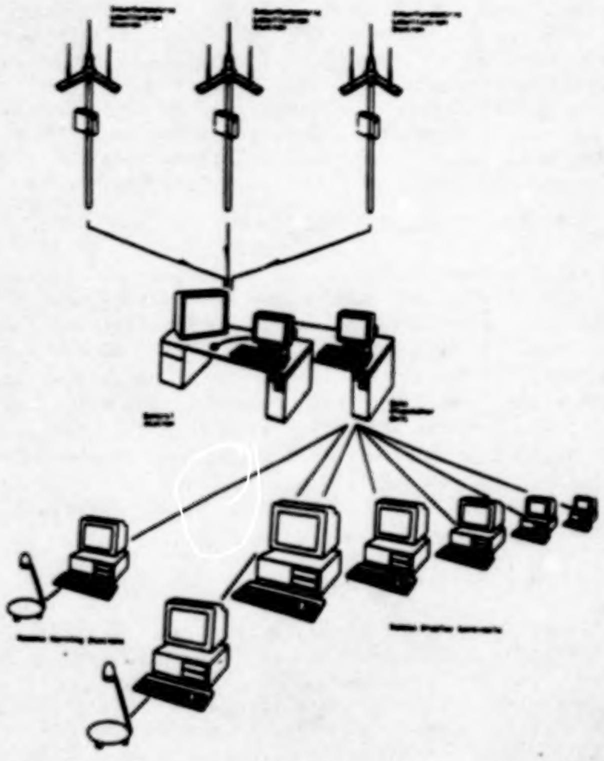

Fig 4: Real time Display

Real time functions are displayed in full scale in the 3 secondary windows

- A: location of lightning flashes
- B: present mapping of electrically active hazard areas
- C: previsional mapping of hazard areas

Each function can be displayed in the main window (D) here is an enlargement of the previsional mapping of hazard areas; present contours of cells are displayed as well as short term previsional positions. Present and previsional activity levels are color coded for each cell

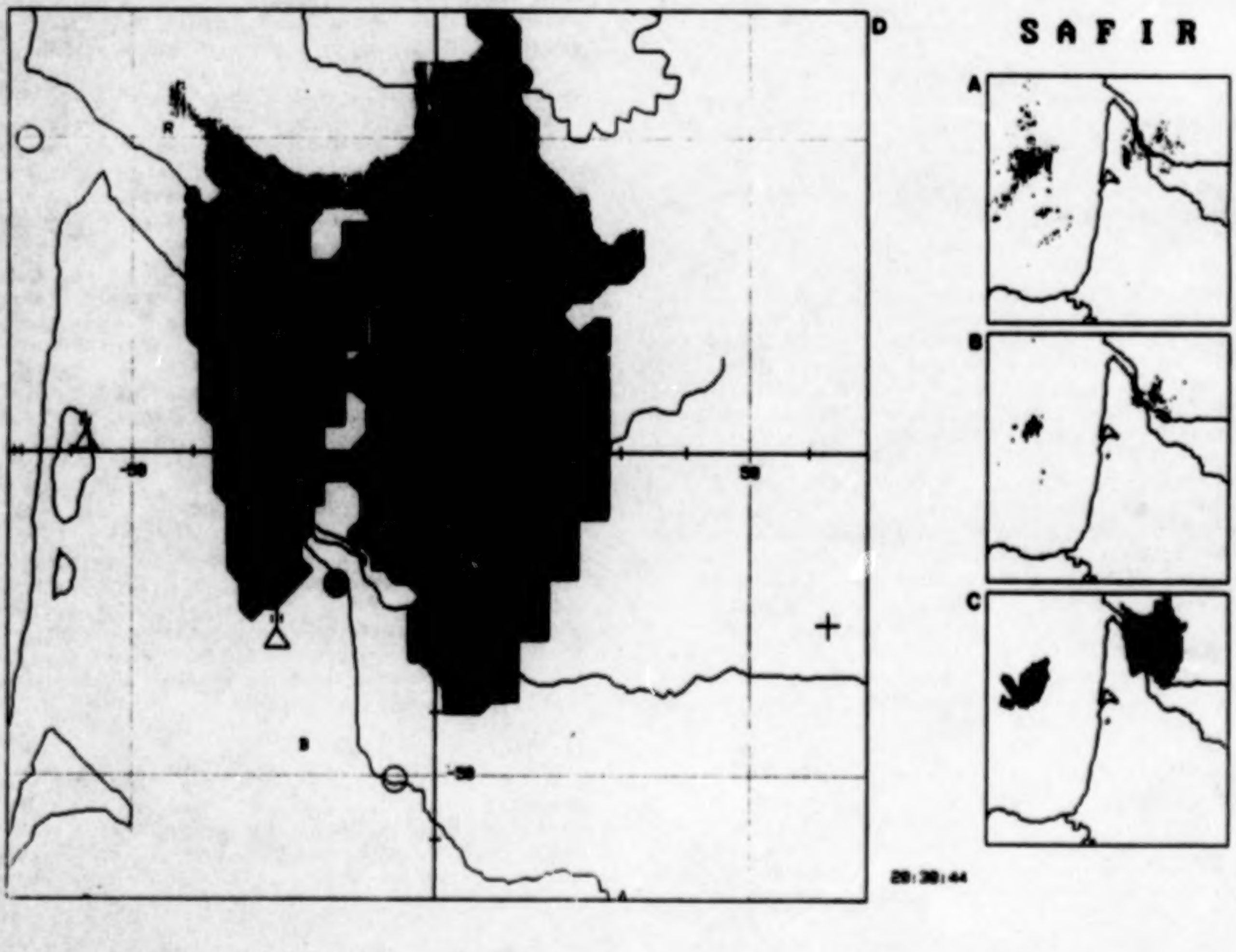

Typically, the coverage of the system is 300 by 300 km, the distances between stations can range from 20 to 100 km according to applications, and the locating accuracy is between a few hundred meters and five kilometers depending on the system configuration and the lightning location.

OPERATIONAL FUNCTIONS

The main real time operational functions of the SAFIR system are presented on a graphic display (fig 4), they include:

-localisation of lightning discharges;
discharges are displayed on background maps with color coding of their characteristics and time of occurence

-mapping of electrically active hazard areas;
the activity level is color-coded within pixels of 2x2 km, evaluation is based on the real time analysis of the spatial and temporal characteristics of lightning activity.

-provisional mapping of electrically active hazard areas and automatic warning ; the real time processing function detects and tracks electrically active cells, the activity is analysed within each cell and a mapping of short term projections of thunderstorm position and intensity is provided (typically up to 30 min). For sensitive sites, the system calculates warning informations and can warn automatically the user of an approaching danger.

All data are stored for analysis. Post processing enables the user to perform statistical analysis on the electrical activity in order to characterise lightning hazards on a site or over a whole region.

EXAMPLES OF THUNDERSTORM SITUATIONS.

These examples illustrate the functions and performances of the system.
The first situation (*figure* 5) is a thunderstorm which occured in the SW of France in july 1989.
The local meteorological situation is characterised by a strong convective activity and a violent advection to the North/North-East high altitude. On the wind profile we can note very high wind velocities above 3000m up to 85 knots at 7000m.
This thunderstorm propagates over a distance of 140 km at an average speed of 100km/hour. It produces a total number of 867 ligtning flashes among which 13 are cloud-to-ground strokes. The time delay between the first intra-cloud lightning and the first cloud-to-ground lightning is 28 minutes.

This particular example illustrates two of the principal features of the SAFIR system :
The early lightning warning function before cloud-to-ground activity, and the monitoring capability mainly based on the location of intra-cloud activity.
An additional application is the assessment of severe weather hazards associated to a thunderstorm. This particular thunderstorm, though giving only a small number of cloud to ground discharges, produced heavy precipitations and caused important destructions on the ground. The plot of its lightning flash rate is presented in *figure 5B* together with its maximum radar reflectivity and its total radar reflectivity. Peaks in maximum radar reflectivity occur,5 to 10 minutes after the peaks in the flash rate, and the total precipitation reaches its maximum 35 minutes after the time of maximum flash rate.

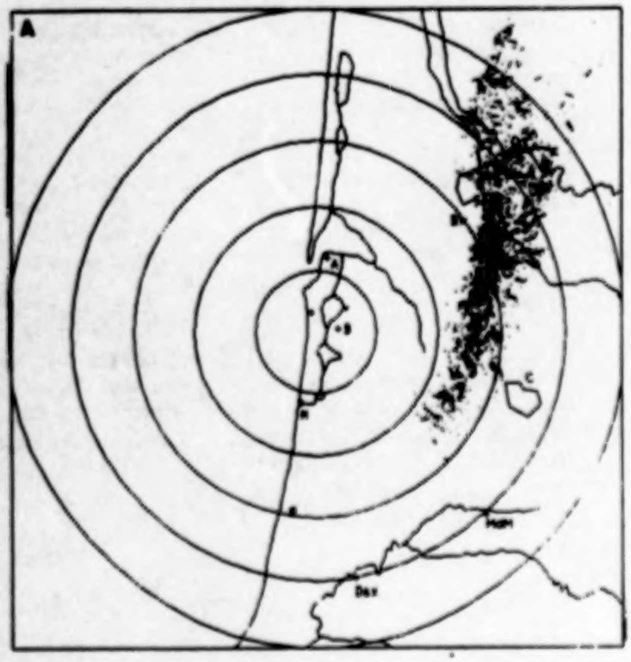

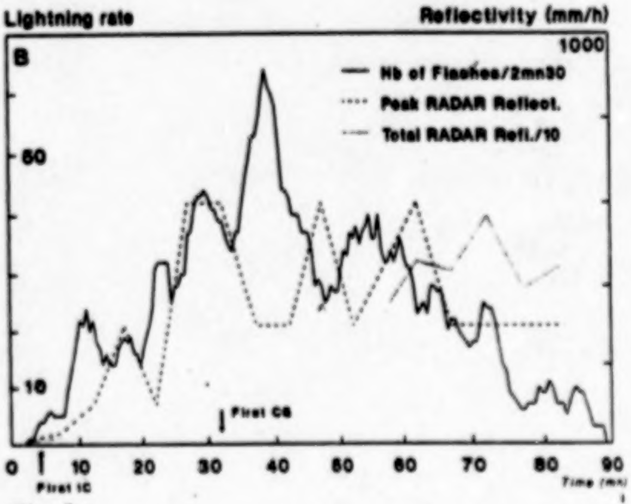

Fig 5:

A - Location of lightning discharges
B - Evolution versus time of the total flash rate, the peak radar relectivity and the total radar relectivity of the thunderstorm

The second situation was observed in april 1989 in the South-West of France.
The thunderstorm presented in *figure 6A* lasted for 1H30mn and moved slowly to the North over a distance of about 40 km. It produced 105 lightning flashes with 39 cloud to ground strokes.
Figure 6B presents separately the temporal evolutions of intra-cloud and cloud-to-ground flash rates. We can note that the warning delay is 27 mn between first IC and first CG; equaly remarkable is the 5 mn time delay between peaks in IC activity and peaks in CG activity which again appear in good agreement with the typical thunderstorm phenomenology. Both results confirm the IC activity as an effective solution for CG flashes warning.

Several thunderstorms were observed on the same day in the same meteorological situation. Time delays between first IC and first CG ranged between 8 minutes to 31 minutes.

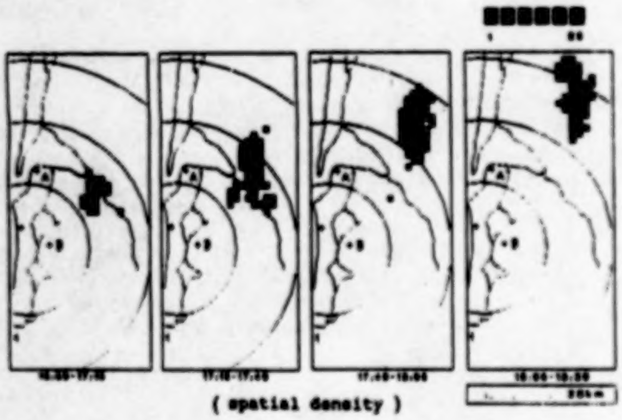
(spatial density)

fig 6A: Location of lightning discharges

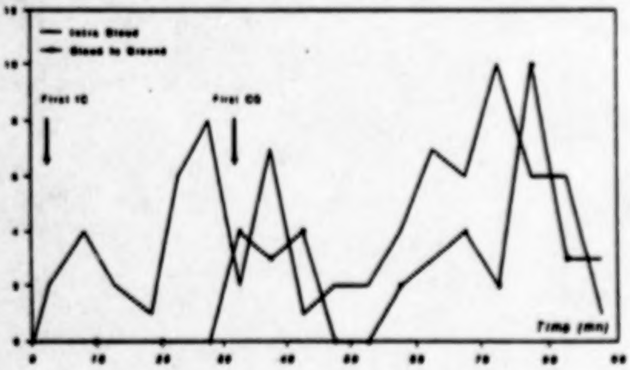

fig 6B: Evolution versus time of CG and IC flash rates

OPERATIONAL APPLICATIONS

Safir is already in operation at the European Space Center in Kourou, French Guiana. A second system is in use at the "Centre d'essais des Landes", a flight test center in the southwest of France.

Early lightning warning and thunderstorm monitoring functions have applications for the safety and efficiency of ground and airborne operations. Applications on the ground range from the management, protection and maintenance of telecommunication and power networks to decision making and active lightning protection for industrial and military sites.

For civil and military aerospace activities, the system in an important component in ensuring in-flight safety of launch vehicles and aircrafts; principal applications are for space centers, test ranges, and airports, where its lightning warning and thunderstorm monitoring capabilities aids in terms of air-traffic control and safety.

References

KREHBIEL (P.);
"The electrical structure of thunderstorms ", Studies in Geophysics, The Earth Electrical Environment, National Academy Press, 1986.

LABAUNE (G.), RICHARD (P.) and BONDIOU (A.);
"Electromagnetic properties of lightning channels formation and propagation " , Electromagnetics, Special issue on Ligntning, 1988.

RICHARD (P.), DELANNOY (A.), LABAUNE (G.) and LAROCHE (P.);
" Results of spatial and temporal characterisation of the VHF-UHF radiation of lightning ", J. Geophys. Res., 91, D1, January 20, 1986.

WILLIAMS (E.R.), WEBER (M.E.) and ORVILLE (R.E.);
"The relationship between lightning type and convective state of thunderclouds", 8th International Conference on Atmospheric Electricity, Uppsala, Sweden, june 1988.

VHF DISCHARGES IN STORM CELLS PRODUCING MICROBURSTS

P. Laroche, C. Malherbe and A. Bondiou
Office National d'Etudes et de Recherches Aerospatiales
BP 72 92322 Chatillon, Cedex, France

M. Weber, C. Engholm, and V. Coel
Massachusetts Institute of Technology Lincoln Laboratory
Lexington, Massachusetts 02173 USA

1. INTRODUCTION

In the last twenty years, several fatal aircraft accidents have been attributed to encounters with low altitude thunderstorm outflows termed microbursts -- outflows which exceed 10 m/s differential velocity over a distance of less than 4 km [1]. The FAA has addressed this issue by establishing the Terminal Doppler Weather Radar (TDWR) program. Under this program, MIT Lincoln Laboratory is sponsored to build a testbed TDWR and test it at various locations in the United States. In the summer of 1990 the testbed TDWR was operationally demonstrated in Orlando, Florida.Research has shown that microbursts are usually associated with convective clouds having high surface rain rates and electrical activity. Williams, et al.,[2] and Goodman, et al.,[3] have studied these phenomena, both finding that in many cases the peak intra-cloud (IC) lightning flash rate is in phase with the maximum vertical development of the cloud, and that this peak precedes the maximum differential velocity of the microburst by a few minutes. They also found that, in general, IC activity dominates in the early stages of the storm and cloud-to-ground (CG) activity peaks later. In order to confirm and enlarge upon these results, ONERA joined Lincoln Laboratory in Orlando to obtain simultaneous multiple-Doppler and VHF lightning measurements. This paper presents a description and some preliminary results of this joint experiment, including our comparisons of microburst strength and location with the related VHF activity caused by lightning.

2. DESCRIPTION OF THE EXPERIMENT

2.1 The VHF Interferometer

The eventual objective of the joint experiment will be to compare three-dimensional mapping of VHF sources to a three-dimensional description of the reflectivity and dynamics of the associated cloud cells observed by the radar network. Because of scheduling restrictions, we were limited to the use of a two-dimensional interferometer in 1990. The lightning detection equipment installed was a new version of a Systeme d'Alerte Foudre par Interferometrie Radioelectrique (SAFIR) system, designed and marketed by the French firm DIMENSIONS[4]. A SAFIR station is an interferometer with an aerial antenna system which detects a VHF signal, the phase of which is proportional to the azimuth of the emitting source (see figure 1). The VHF signal is processed, digitized, and transmitted by the electronic network installed in a 0.1 m3 box attached to the base of a 17 m high mast supporting the antenna. Data and control signals are transmitted to a central station by a dedicated 9600 baud phone line. VHF locations are displayed in real time at the central station where raw data are stored for off-line analysis. The interferometer is tunable within the international radio navigation band, 110 MHz - 118 MHz. The time resolution of each location is 100 μs; the acquisition capacity is 100 locations per second. The system used in Orlando consisted of two stations installed 5 km south and 11 km east and west of the TDWR, respectively (see figure 2). The horizontal position of each VHF source is determined by triangulation, yielding an accuracy of better than 1 km within the shaded zone indicated in figure 2. This region encloses the operational area of the TDWR, which includes the airport and its vicinity. For the 1990 experiment, we added an identification device which delivers information on the CG or IC nature of the lightning flash corresponding to the points localized by the interferometer. It is a prototype apparatus based on a wide band measurement of the radiated electric field at ground (5 MHz).

201

2.2 The 1990 Orlando Radar Network

Detection of microbursts was accomplished using the FAA/Lincoln Laboratory's testbed TDWR [5].The TDWR is a narrow-beam (0.5°) 5 cm radar. Its signals are processed by algorithms which provide detection of surface outflows of microburst strength, with predictions obtained by utilizing recognition of features aloft. The scan strategy is designed to maximize the algorithms' capabilities, obtaining greater resolution near the surface than aloft. The final output of the algorithms is simple alert information displayed to the air traffic controller (ATC) at the control tower or directly telemetered to the aircraft on a special display installed in the cockpit. Off-line analysis of the radar data is supported by simultaneous 5 cm radar observations taken by the MIT Department of Earth, Atmospheric, and Planetary Sciences radar and the University of North Dakota (UND) radar. These measurements are used for dual- and triple-Doppler analysis to calculate the vertical component of the wind. The update rate is approximately one volume scan every 2.5 minutes, with a surface scan every minute.

3. COMPARISON BETWEEN VHF ACTIVITY AND MICROBURST OCCURRENCE

3.1 Summary of Events Detected by the TDWR

More than 500 microbursts were detected by the TDWR within a range of 70 km of the airport during its operation from early June to mid-September 1990. Most of these microbursts were produced by high reflectivity cells, with precipitation at the ground in excess of 45 dBZ. Figure 3 gives the distribution of the maximum outflow velocity and surface reflectivity. The most frequent value is between 10 and 15 m/s.

3.2 Comparison with VHF Activity

The SAFIR system was in operation from mid-July to mid-September, during which time 123 microbursts were detected within a range of 30 km from the TDWR. The equipment worked well until August 25, but it experienced minor technical problems after that date. The data set of events with both radar and interferometer observations consists of 61 microbursts, most of which were associated with lightning activity. Only two of the events cannot be related to electrical activity: one which gave a weak outflow and another which was produced by a cell with little precipitation (maximum reflectivity of 24 dBZ at the surface). During this same time, 38 large zones of VHF activity were observed, each of which may include several storm cells. Five of these zones exhibited little activity and were not associated with any microbursts. Their activity levels were equivalent to the least active zone which could be associated with a microburst. For this preliminary study, we compared the relative timing and magnitudes of the microburst outflows and the lightning activity. Statistical information about the VHF activity and microburst comparisons are indicated in figure 4. We have considered here only that VHF activity beginning 10 minutes prior to microburst onset or later. This implies that the mean time lags computed are lower than their actual value. From this analysis we note that:

For 93 percent of events, lightning occurred before the onset of the outflow on the ground. For 65 percent of the cases, the delay exceeds 10 min.

For 77 percent of the events, the first peak in VHF activity occurred up to 10 min before the outflow onset (the mean delay is about 5 min).

For 91 percent of the microbursts, we observed the first peak in activity before the maximum outflow – the mean delay is 9 min.

4. DETAILED ANALYSIS OF MICROBURSTS

In this effort, we wanted not only to confirm past work but also to use the interferometer data to expand in the direction of a more detailed analysis of the structure of individual flashes. We have done this for three different days in August. First we present a review of how flash structure can be inferred from interferometric observations. Following that are an outline of how we define a single flash and its components from a set of VHF sources, a look at the data from the three different days, and two microburst case studies.

4.1 Information Available from the VHF Location System

A lightning flash is composed of a sequence of elementary atmospheric discharge processes. Two different flashes will create different discharge channels. The development of one flash may be directly influenced or initiated by a preceding one (in which case, the two flashes can propagate simultaneously)). In general, the time difference between two successive flashes in the same cloud cell is between a few tenths of a second and two seconds. This delay depends on the intensity of the charge separation process. Electromagnetic radiation due to a lightning flash has been measured by several experimenters. Narrow-band measurements were gathered by Pierce [6] and presented on a graph showing normalized magnitude (versus distance and bandwidth) as a function of frequency (figure 5). The form of the resulting curve indicates that the magnitude of the overall radiation is something on the order of 1/f. The return stroke process involved in the CG flash is mainly responsible for radiation in the low-frequency (LF) and high-frequency (HF) ranges (1 kHz - more than 10 MHz). The VHF radiation, to which our interfero- meter is sensitive, is mainly due to the pre-breakdown and leader discharges encountered in both CG and IC flashes.The overall duration of a flash is, in general, less than one second. During that time the following phases may be observed:

Pre-breakdown activity occurs up to 200 ms before the onset of a downward negative stepped leader involved in an IC discharge or preceding a return stroke in a CG process. Pre-breakdown activity radiates in HF and VHF ranges[7],[8].

A **stepped leader** is a negative discharge process. It propagates at greater than 10^6 m/s, by steps a few tenths of a meter long. It radiates in the HF and VHF range; steps are fast rise time current pulses of a few kA, which have a repetition rate between 10 μs and 100 μs.10 The typical duration of the propagation of the stepped leader is shorter than 10 ms [9].

A **positive leader** propagates at greater than 10^5 m/s. It constitutes, with the stepped leader (which propagates simultaneously), a neutral and bi-directional discharge process. Its propagation is pulsed,[10] but its current magnitude is low and therefore the radiated energy is very much smaller than that due to the negative stepped leader. The duration of the propagation may be a few hundred ms.

Recoil streamers are high-current IC junction discharges which are hypothesized to propagate within the channel traced by the preceding positive leaders. The velocity of recoil streamers is in excess of 10^7 m/s;[11] peak current measured on an instrumented aircraft may reach 10's of kA. This discharge corresponds to the K-change in the electric field [12] which radiates mainly in the VHF range. The duration of a recoil streamer may be as long as 800 μs, but the mean duration calculated from a 30-minutes storm observed in southwest France was 150 μs.[11]

A **dart leader** initiates the subsequent stroke in a CG flash. It propagates within the channel of the preceding stroke with a velocity of more than 107 m/s. Its duration is a few milliseconds and it radiates in the VHF range.[13]

A **return stroke** occurs when a leader connects to ground. It consists of a high-current pulse propagating in the leader channel. Its velocity is up to 10^8 m/s; its magnitude may exceed 100 kA, and its typical duration is less than 100 μs.

To understand what kind of analyses are possible with a two-dimensional interferometer system, one must take into account how each of the individual discharge components described above are localized by the apparatus.

Pre-breakdown activity radiates pulsed energy at a rate of one pulse or more each 10 μs over several hundred ms. This activity might not be detected by the system due to the low mean level of emission within a 100 μs time window, or it can be measured as a set of isolated points.

A stepped leader has a low pulse rate emission at the beginning of its propagation (typical stepping rate is 50 μs) and again, initially might not be detected by the system. As its propagation continues, the branching of the discharge grows and the mean rate of pulses increases to the point that it becomes detected by the interferometer. Figure 6 shows a plan view of such an event; propagation is detected continuously for 7 ms. Each point might be randomly positioned on the X-Y projection of the propagating front of the discharge. The horizontal extension of the negative stepped leader is small, about 3 km by 3 km for 80 percent of the associated localized points.

Based on results obtained previously with a high-resolution interferometer and on the physical properties of the process, we infer that the radiation due to the positive leader is not normally detected by this kind of equipment.

Recoil streamer and dart leader processes may be associated with the same basic physical process. The associated radiation consists of pulses emitted at a rate of close to or greater than 1 μs. With

100 μs resolution equipment, we observed continuous propagation for a recoil streamer, the duration of which exceeded 100 μs. Figure 7 shows the horizontal projection of a flash exhibiting several recoil streamers.

VHF radiation emitted by return strokes is weaker than its LF counterpart. We know from previous measurements that the magnitude of the VHF radiation is great enough to be localized by our equipment.

4.2 Criteria Applied for the Analysis of Lightning Phenomenology

We have used the understanding related above to formulate automated algorithms for identifying flashes, recoil streamer or dart leaders, and negative leaders. The following two criteria were used to determine if a set of points belong to
a single flash:

1) The overall duration of a flash must be less than or equal to one second.

2) Two successive points in a flash are separated by a horizontal distance of no more than 25 km, or a distance equivalent to a horizontal velocity of no more than $5. 10^7$ m/s.

Within a single flash, a recoil streamer or dart leader processes is identified as a burst of points with the following two characteristics:

1) We require a burst to be composed of at least two locations, even though previous measurements demonstrate that the mean recoil streamer duration may be less than 200 μs.

2) The points within a burst may not be separated by more than 200 μs (two successive samples where VHF activity is below threshold). This allows for any lack of sensitivity in the VHF receiver.

A negative leader is identified by a burst of at least 10 points. We note that our data indicate that the burst associated with a negative leader exhibits small horizontal extent.

4.3 General Activity Associated with Three Different Storm Days

Having identified flashes and their components, we chose three days with microburst activity on which to concentrate our analysis. We analyzed the VHF locations observed within an area limited to about 70 km east and west and up to 80 km north of the TDWR. The beginning and ending times of the period processed were approximately 10 minutes before the first surface outflow differential velocity reached 10 m/s and 10 minutes after the last outflow fell below 10 m/s. In table 1 below we indicate the overall number of locations, flashes, bursts, and leaders for time periods from August 16, 18, and 22. Due to a technical problem, August 18th is divided into in two sequences, separated by 7 minutes without VHF information.

Table 1.Analysis of VHF activity for three storm days.

Date	Time (min)	Num. of points		Num. of Flashes		Num. of Bursts		Num. of Leaders	Bursts/ Flash	% Flashes with a Leader
		total	per min	total	per min	total	per min			
8-16	87	9162	105	811	9.3	1557	17.9	84	1.90	10.3
8-18 I	36	2920	81	756	21.0	514	14.3	4	0.68	0.5
II	59	6375	108	600	10.2	1017	17.2	77	1.69	12.8
total	95	9295	97	1356	14.3	1531	16.1	81	1.13	6.0
8-22	88	9222	105	1421	16.1	1739	19.8	59	1.22	4.2

For August 16, we observed a mean flash rate of 9.3 flashes per minute, with 10.3 percent of these flashes containing a recognizable leader. This is the lowest flash rate for any of the three sequences, but a relatively large percentage of flashes with negative leader detection.

The first part of the sequence from August 18 corresponds to the onset of general activity. We observed a high mean flash rate (21 flashes per minute) and the lowest percentage of flashes with leader detections (0.53 percent); it must be pointed out that a large number of these flashes are identified by a single point. It should also be noted that past work (e.g. Williams, et al.[2]) suggests that the onset of activity is likely to contain fewer CG flashes, i.e., fewer negative leaders. The second part of the sequence is similar to August 16: 10.2 flashes per minute and 12.8 percent of which contain a recognizable leader. Combining the two sequences we see flash rate and leader detection percentages that lie between the values computed for the other two storm days.

For the sequence from August 22, we observed a higher mean flash rate (16.1 flashes per minute) and a lower rate of leader detection (4.15 percent of the flashes) compared to the other two storm days. To summarize, we note that:

1) The mean detection rate is basically the same for the hour and a half duration of the sequences (105 locations per minute), except for the first part of August 18 during which the rate is lower (81 locations per minute).

2) The mean rate of burst identification is consistent between three of the sequences (about 18 bursts per minute). The exception is the first sequence of August 18, whose identifica-tion rate is lower in the same proportion as the mean location rate (about 14 bursts per minute; that is, 30 percent less than that observed in the other cases).

3) The three similar sequences (August 16, August 18 II, and August 22) exhibit different flash rates and different percentages of flashes with a negative leader detection.

4.4 Case of Microburst #6 (MB6) of August 16

Six outflows were identified by the TDWR on August 16, 1990. Each outflow is identified by its type (e.g., microburst (MB)) and an event number. The outflow corresponding to MB6 was first identified by the TDWR at 22h57. A maximum outflow differential velocity of 24 m/s was reached at 23h06, and the differential velocity dropped back below the 10 m/s threshold at 23h19. During the 22 minutes of the outflow, its location changed less than 3 km east-west from its mean position of 29 km north and 11 km east of the radar.

This microburst position corresponded to the large area of VHF activity represented in figure 8a. The overall evaluation of the activity in this electrical cell between 22h45 and 23h11, which is the time interval corresponding to the most active phase, is characterized by the following:

4720 VHF sources detected (181 sources/min)

463 flashes (17.8 flashes/min)

826 bursts (31.7 bursts/min)

36 negative leader detections (7.8 percent of all flashes had a leader detected)

This activity was much greater than the mean general activity observed on the same day (described in table 1 above). This one cell contained over half of all the VHF detections, flashes, and burst detections of that day. The percentage of flashes with leader detections was slightly less than the mean – 7.8 compared to 10.3 percent.

The boundary of the electrical cell associated with this microburst is stationary. The 40 dBZ surface reflectivity contour, which was used to define the cloud cell, moves slightly northward. At the beginning of the outflow, the precipitation was south of the electrical activity, although the correlation between both phenomena is quite good at the end of the life of the microburst.

A comparison of the electrical and cloud cells indicates that the VHF activity clearly preceded the collapse of the cloud cell.

The relative evolutions of the electrical and cloud activity can also be seen through a comparison between flash rates and outflow strength. Figure 8b indicates the temporal evolution of the total flash rate, leader detection rate, and CG flash rate indicated by the flash identification algorithm. We have also drawn the time evolution of the outflow on the same figure. We note a rather good qualitative correlation between leader rate detection and CG flash rate. This supports the idea that negative

leaders may be involved in a CG process.
Peak IC activity was reached at 22h54; peak CG activity was reached one minute later. Absolute peak activity happened at 22h58, with a value of 34 flashes/min. This very high flash rate is evidence that this electrical activity is not associated with a single dynamic cell, but more likely with a set of several active centers. A peak flash rate of 10 flashes per minute is what is commonly observed at other sites.
We observe a regular increase in the number of bursts per flash and of the mean burst duration (up to 8 per flash and 600 µs duration around 23h). The distribution of the mean horizontal velocity of each burst indicates a peak frequency between 2 and 5. 10^7 m/s. The distribution of time intervals between successive bursts shows three peaks of frequency:

1.8 percent between 1 and 3 ms;

12.0 percent between 10 and 30 ms; and

13.3 percent between 100 and 300 ms.

The overall peak frequency is 10.2 percent for the 100-200 ms interval. This point is discussed more fully in Section 5.
There is one further interesting point to note about the negative leaders and their relationship to the microburst outflow. The leader horizontal development is limited to a region which is approximately 5 km in diameter, and the mean position of leaders remains close to the microburst location (see figure 8a).

4.5 Case of Microburst #5 (MB5) of August 16

The outflow corresponding to MB5 develops southwest of MB6, from 23h12 to 23h31. A maximum outflow velocity of 20 m/s is reached at 23h17. VHF activity is observed in the vicinity of MB5 between 22h31 to 23h28. This activity was very much weaker than the mean general activity observed:

1402 locations (24.6 locations/min – 1/4 the mean rate)

101 flashes (1.8 flashes/min – 1/5 the mean rate)

239 bursts (4.2 bursts/min – 1/4 the mean rate)

12 negative leaders observed by the interferometer (11.9 percent of all the flashes – similar to the mean rate)

A heavy precipitation area at the surface corresponded to an area of horizontal VHF activity, but the relative maximum of both phenomena are not coincident. Still, the development of the negative leaders are mainly in the vicinity of the outflow (see figure 9).
The first peak in IC activity is reached at 23h05 (7 minutes before the onset of the outflow). The peak CG activity is reached at 23h13 (figure 9). The number of bursts per flash, the mean burst duration, and the mean flash duration increase regularly up to the end of the life of the electrical cell (with maximums of 4 bursts per flash, [illegible]00 µs burst duration, and 0.9 s flash duration). The distribution of the mean horizontal velocity of the bursts shows a maximum frequency between 5.10^6 and 10^7 m/s. The distribution of time intervals between successive bursts presents the same characteristics as for the case of MB6 – i.e., three local maxima of frequency are observed:

6.7 percent between 1 and 3 ms;

15.5 percent between 10 and 30 ms; and

11.3 percent between 100 and 300 ms.

The overall peak frequency is 10 percent between 100 and 200 ms. Except for intervals 1-3 ms, these values are close to those obtained for MB6, and are discussed below.

5. DISCUSSION

A preliminary overview of the data available for 61 cases of microbursts shows clearly, in 93 percent of the cases, that the electrical activity precedes the development of outflow. Our results strongly confirm the results of Williams, et al.,[2] and Goodman, et al.,[3] that the peak in IC activity precedes the maximum value of the outflow. We find this same result in 91 percent of the events. For several cases, we observed a correlation between the onset of the IC electrical activity and the development of slantwise divergence at mid and upper levels (i.e., divergence along PPI's at altitudes of 7 km and above). The presence of this signature may suggest an updraft at these levels, but both the interpretation of this feature and its relationship to electrical activity has yet to be confirmed by more extensive analysis.

We have not yet found any direct relationships between the magnitude of the outflow and the intensity of the corresponding electrical activity. The two examples presented above illustrate this point clearly. We are continuing our work in this area.

The analysis of VHF activity due to atmospheric discharges derived from a limited time resolution two-dimensional interferometer (100 μs - 100 locations per second) give valuable information on the behavior of the lightning flash.The interferometer detected the strongest and closest negative stepped leader processes. We have verified that the ratio of flashes with leader detection increases when the storms are closer to the measuring stations. Temporal comparison with a return stroke identification system confirms that these leaders are associated with CG processes preceding return strokes. This comparison is, up to now, qualitative due to some technical problems which can be resolved by a more elaborate data reduction process.

Observed burst propagations are known to be due to recoil streamers or dart leader processes [9]. The distribution of velocity of such phenomena obtained with a high-resolution three-dimensional interferometer indicated a mean velocity of 2.10^7 m/s for a set of 800 bursts detected during 20 minutes of a storm in southwest France. These results are consistent with those presented here for Florida storms. Even if the actual distribution may be centered on a slightly lower velocity (for example, 10^7 m/s for MB5), this means that the propagations are mainly horizontal. This supports the results by Krehbiel [14] which indicated that the propagation of positive leaders (in channels in which recoil streamers are supposed to propagate) has an important horizontal component.

The distribution of time intervals between successive bursts contains, for most of the cases we observed, three peaks. The first one (1 to 3 ms) is typical of that observed for M-changes and, in that case, can be associated with a continuing process (which corresponds to the propagation of a positive discharge) [15]. The second one (10 to 30 ms) corresponds to the mean interval between successive recoil streamers[16]. The third peak (100- 200 ms) might correspond to a dart leader preceding the return stroke process. This point may be inferred from statistical results showing that in the vicinity of Kennedy Space Center (KSC), the mean interval between strokes of natural flashes is 86 ms,[17] the same as for all the flashes triggered at KSC by the wire and rocket technique between 1984 and 1989. For those two experiments, it has been shown that the mean number of strokes per flash is between two and three. The ratio between the number of leaders and bursts of this last category is quite consistent with that point.

The objectives of our work are to find, within the temporal and spatial characteristics of IC and CG lightning activity, information to predict, with good reliability, the place and time of microburst events. In order to achieve this goal, we will be continuing our analyses by:

1) Extensively comparing the VHF activity with information on cloud features present in the radar data above the surface layer, and
2) Conducting a similar experiment with a three-dimensional interferometer to relate the electrical activity to the vertical development of the cell.

ACKNOWLEDGMENTS

This work has been done under contracts of DRET (French DOD) and DGAC (French civil aviation authority). Collaborative experiments involving MIT and ONERA have been organized via a DEA between the FAA and DGAC. The work of MIT Lincoln Laboratory is sponsored by the FAA.

References

[1] T.T. Fujita and F. Caracena, An analysis of the weather related aircraft accidents, Bull. Amer. Met. Soc., 1977, vol. 58, pp 1164-1181.

[2] E. Williams, M.E. Weber, and R. Orville, The relationship between lightning type and convective state of thunderclouds, Int. Conf. on Atmos. Elec., Uppsala, Sweden, 1988.

[3] S. Goodman, E. Buechler, and D. Wright, Lightning and precipitation history of a microburst producing storm, GR Letter, vol. 15 no. 11, pp. 1185-1188.

[4] P. Richard, SAFIR system, an application of real time VHF lightning location to thunderstorm monitoring, Sixth Conf. on Severe Local Storms, American Meteorological Society, Canada, October 1990.

[5] M. Merritt, D. Klingle, J.W. Wilson, and S.D. Campbell, Windshear detection with pencil beam radars, Lincoln Laboratory Journal, vol. 2, no. 3, pp. 483-510.

[6] E.T. Pierce, Atmospheric and radio noise, in lighting, edited by R.H. Golde Academic Press Inc., London, 1977.

[7] P. Richard, A. Delannoy, G. Labaune, et P. Laroche, Results of spatial and temporal characterization of the VHF-UHF radiation of lightning, JGR, vol. 91, no. D1, January 20, 1986.

[8] W.H Beasley,M.A Uman and P.L. Rustan, Electric fields preceeding cloud to ground lightning flashes, JGR, vol. 86,1982

[9] E.P. Krider and G. J. Radda, Radiation field wave forms produced by lightning stepped leaders, JGR, vol. 80, no. 18, June 1975.

[10] P. Laroche, A. Eybert-Berard, L. Barret, and J.P. Berlandis, Observations of preliminary discharges initiating flashes triggered by the rocket and wire technique, Eighth Int. Conf. on Atmos. Electricity, Uppsala, Sweden, June 1988.

[11] A. Bondiou, I. Taudiere, P. Richard, and F. Helloco, Analyse spatio-temporelle du rayonnement VHF-UHF associe a l'eclair, Revue de Physique Appliquee, no. 25, February 1990, pp. 147-157.

[12] N. Kitagawa and M. Kobayashi, Field changes and variations of luminosity due to lightning flashes, in Recent Advances in Atmospheric Electricity, L.G. Smith Pergamon Press, 1959.

[13] P. Richard, A. Delannoy, G. Labaune, et P. Laroche, Results of spatial and temporal characterization of the VHF-UHF radiation of lightning, JGR, vol. 91, no. D1, January 20, 1986.

[14] P. Krehbiel, M. Brook, and R.A. McCrory, An analysis of charge structure of lightning discharges to ground, JGR vol. 84, pp. 2432-2456, 1979.

[15] R. Thottappillil, V.A. Rakov, and M.A. Uman, K and M changes in close lightning ground flashes in Florida, JGR, vol. 95, no. D11, October 1990.

[16] N. Kitagawa and M. Kobayashi, Field changes and variations of luminosity due to lightning flashes, in Recent Advances in Atmospheric Electricity, L.G. Smith Pergamon Press, 1959.

[17] R.D. Brantley, J.A. Tiller, and M.A. Uman, Lightning properties in Florida thunderstorms from video tape records, JGR, vol. 80, no. 24, August 1975.

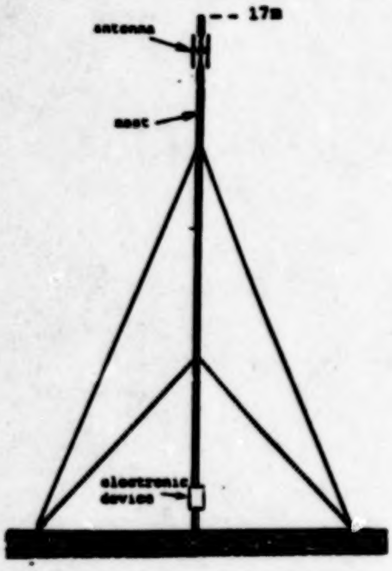
17m
antenna
mast
electronic device

Figure 1: VHF interferometer measuring station.

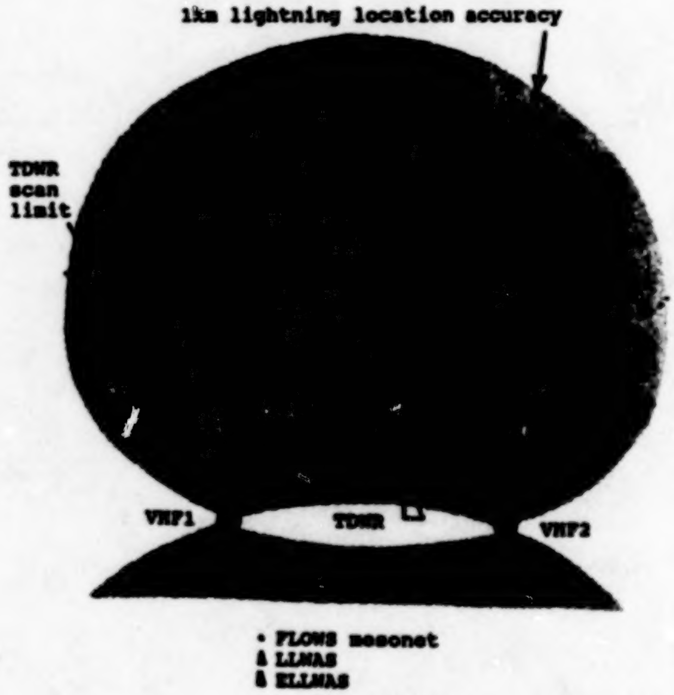
1km lightning location accuracy
TDWR scan limit
VHF1
TDWR
VHF2
• FLOWS mesonet
▲ LLWAS
▲ ELLWAS

Figure 2: Orlando 90 network.

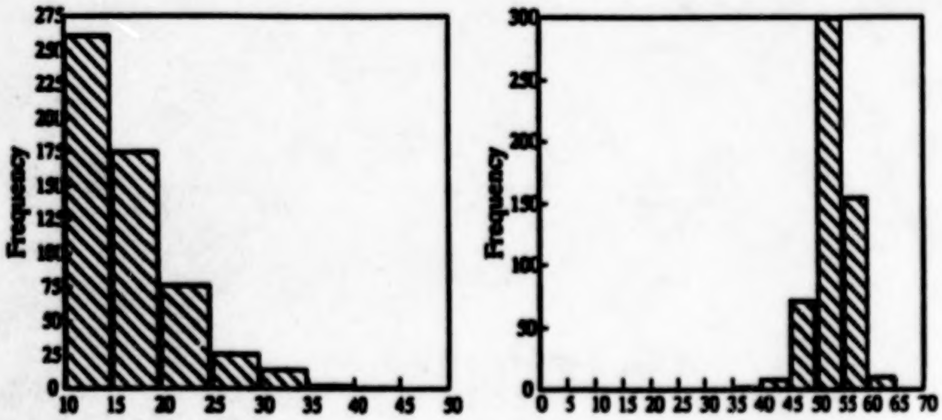

Figure 3: Distribution of outflow strength and surface precipitation for the more than 500 microburst cases detected during operations in Orlando, Florida.

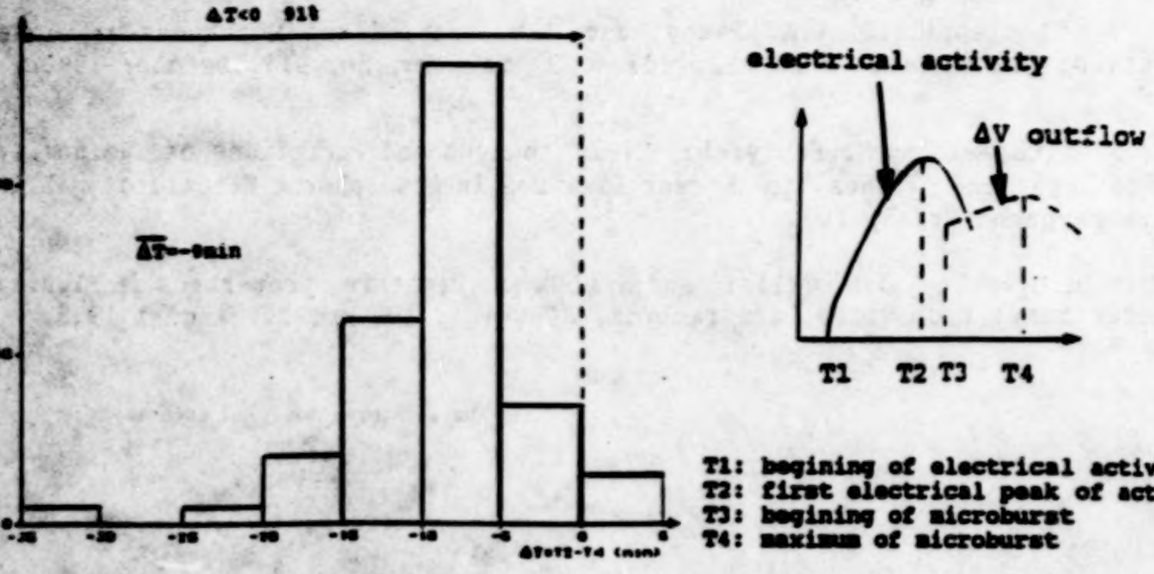

T1: begining of electrical activity
T2: first electrical peak of activity
T3: begining of microburst
T4: maximum of microburst

Figure 4: Statistical comparisons between VHF activity and microburst development.

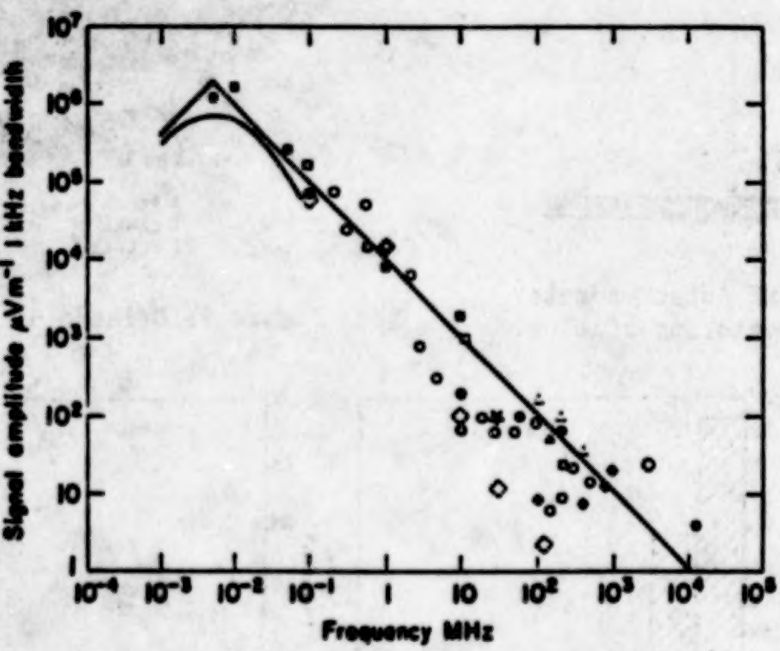

Figure 5: Peak received amplitude at 10 km for signals radiated by lightning (E.T. Pierce).

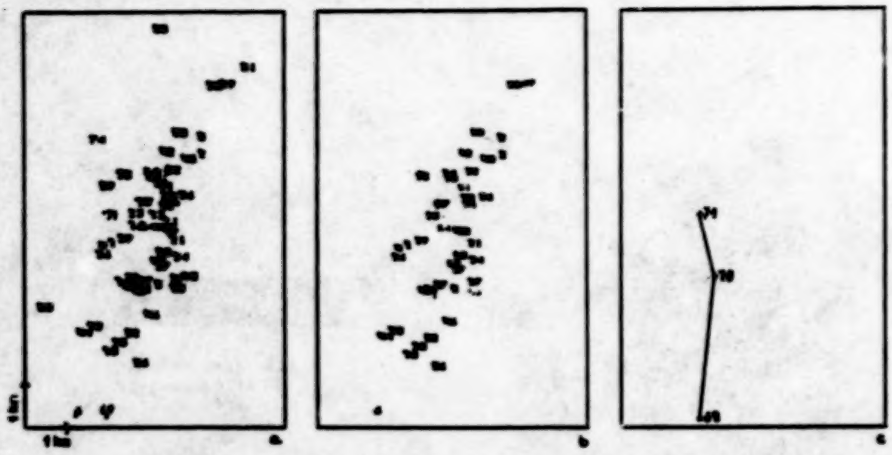

Figure 6: Flash initiated by a negative step leader. The overall horizontal flash extension is 8,7km x 5km but, 80% of the locations are included in a 2,8km x 3,3km. This event is made of 74 locations, it lasts 137,5 ms (a). The first event is a negative leader of about 7 ms duration (b) which is followed by 5 bursts (recoil-streamer or dart leader) at time intervals betwenn 14 ms and 60 ms. One of those bursts is presented on figure c. It lasts 300 µs.

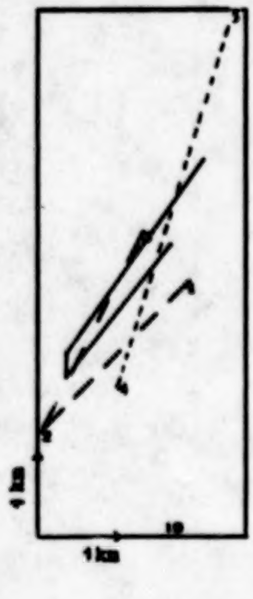

Figure 7: Intra-cloud flash with 3 bursts. The flash is made of 10 locations. Its duration is 345,3 ms. Its overall extension is 2,5km by 6km.

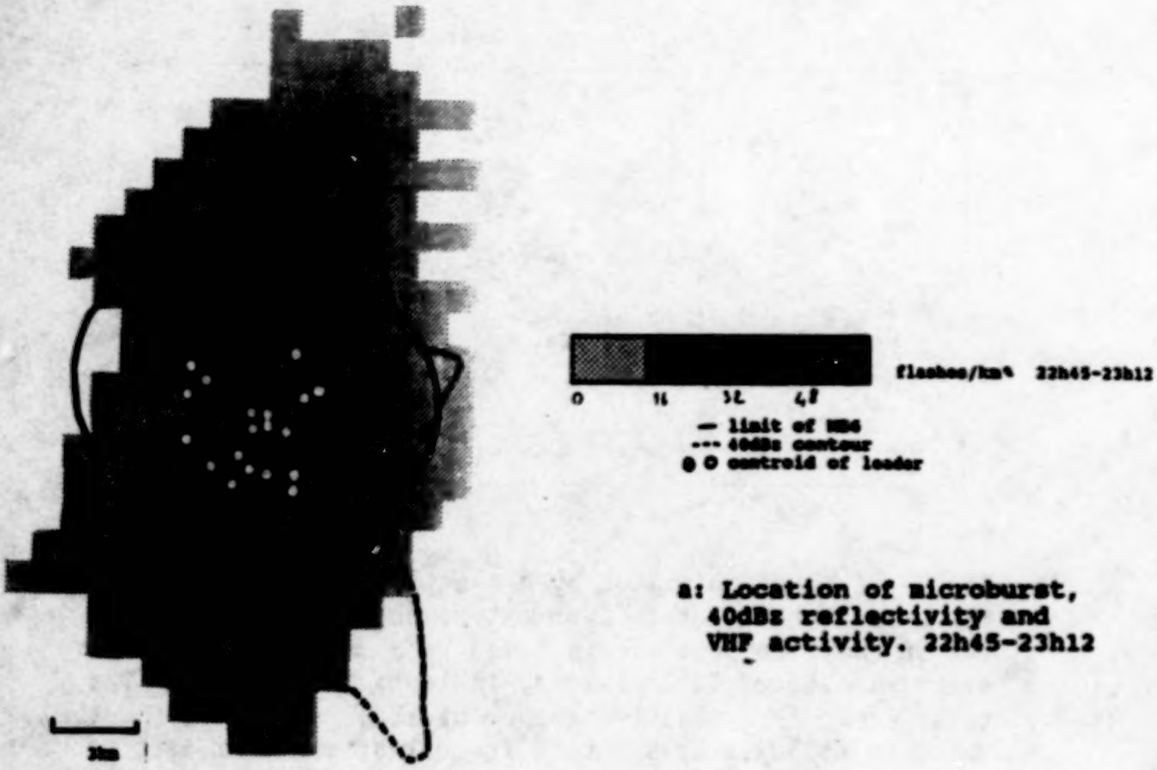
flashes/km² 22h45-23h12
0
16
32
48
— limit of MB6
--- 40dBz contour
● ○ centroid of leader
3km

a: Location of microburst, 40dBz reflectivity and VHF activity. 22h45-23h12

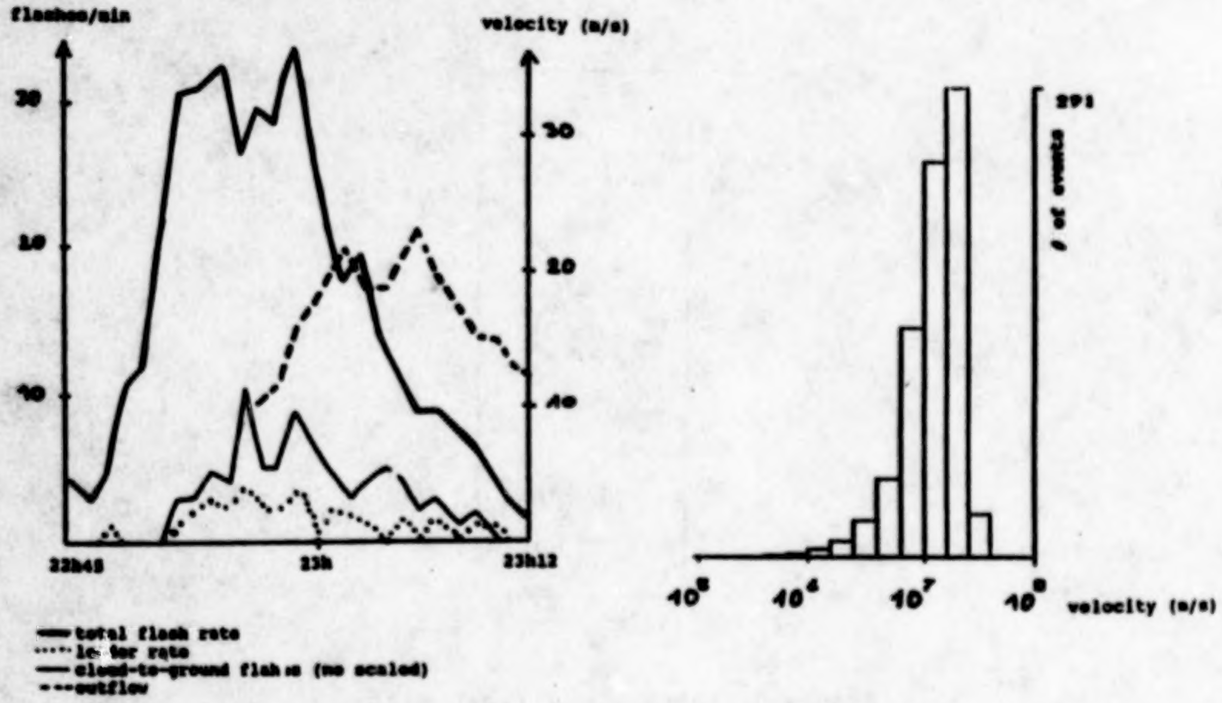

b: Temporal evolution of flashes rate and microburst development

c: Bursts mean velocity distribution

Figure 8: Case of microburst #6 of August 16.

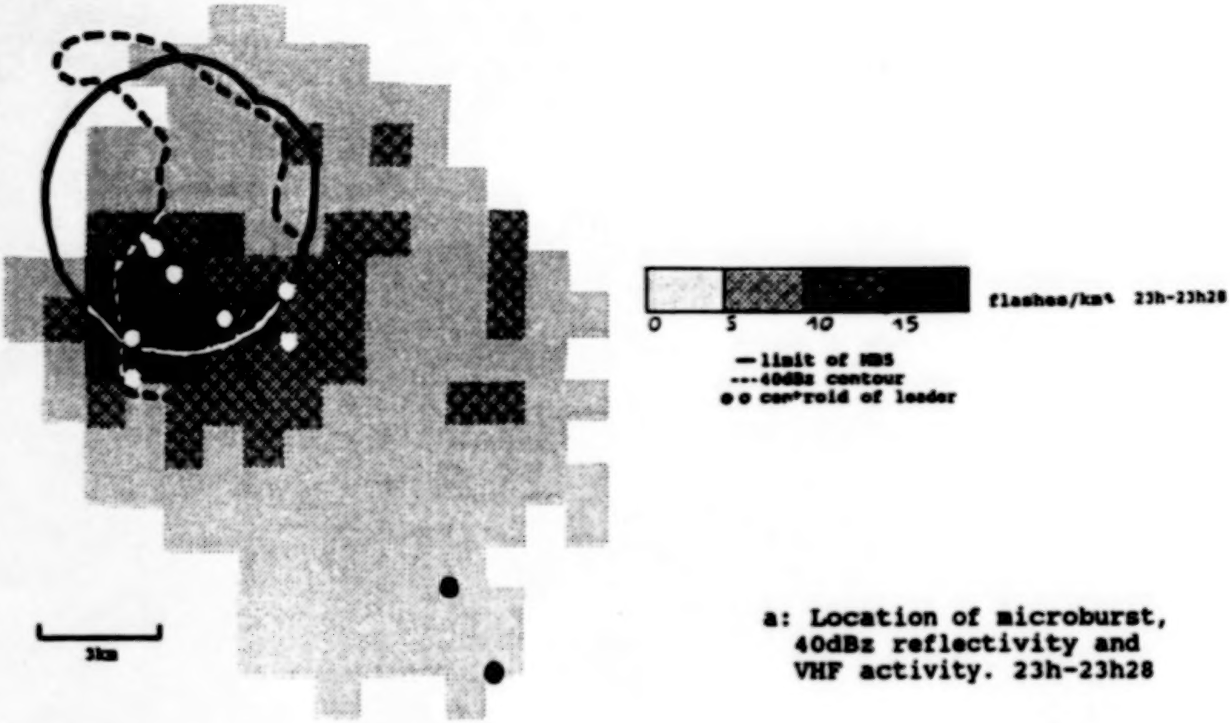
flashes/km² 23h-23h28
0
5
10
15
— limit of MBS
--- 40dBz contour
● o centroid of leader
3km

a: Location of microburst, 40dBz reflectivity and VHF activity. 23h-23h28

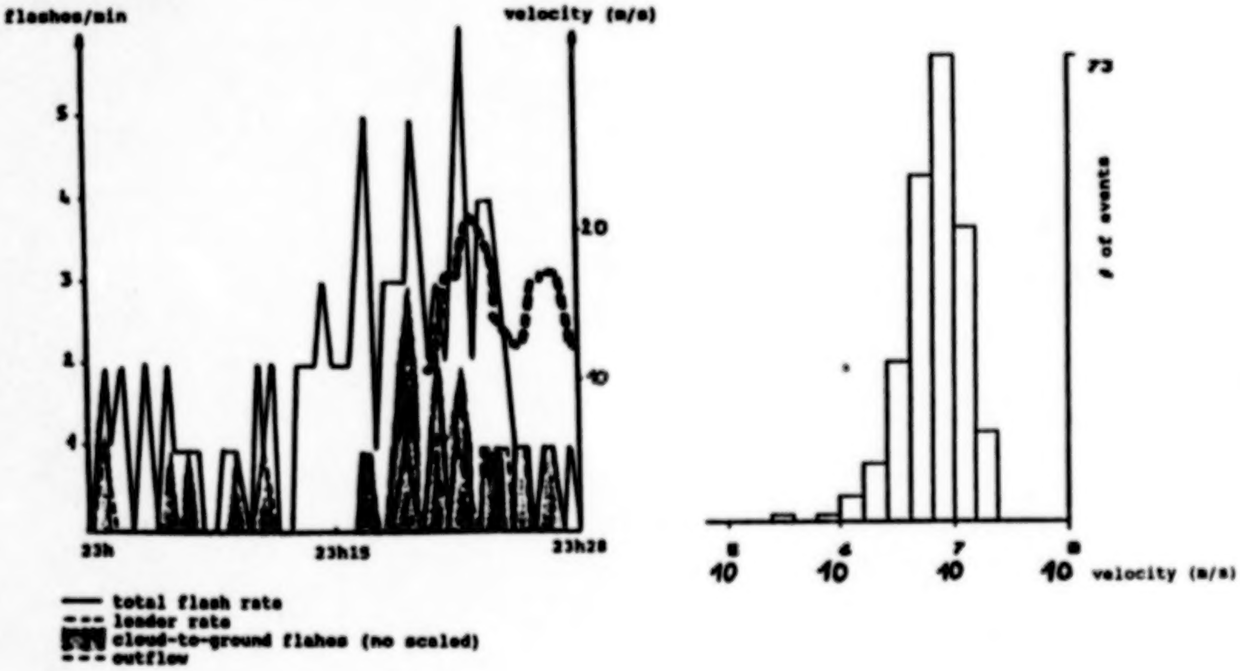

b: Temporal evolution of flashes rate and microburst development

c: Bursts mean velocity distribution

Figure 9: Case of microburst #5 of August 16.

Session 5A, Wednesday 8:00
Ground Protection 1
Fisher, Chairman

The QT Interval in Lightning Injury with Implications for the 'Cessation of Metabolism' Hypothesis

by

Dr. Christopher J. Andrews[12] BE MEngSc DipCompSc MBBS MACS SMIEEE SMIREE
Dr. David M. Colquhoun[1] MBBS FRACP
Prof. Mat Darveniza[2] BE PhD DEng FIEAust FIEEE FTS

[1]The Wesley Hospital, Brisbane, Australia
[2]University of Queensland, St Lucia, Brisbane, Australia

ABSTRACT

An hypothesis is presented to provide an alternative explanation to the 'Cessation of Metabolism' hypothesis often invoked in lightning injury. 'Cessation of Metabolism' has been proposed to explain the observation of good recovery after a prolonged period in cardiac arrest in some lightning injured patients. Re-evaluation of ECGs from lightning injured patients which demonstrates a high incidence of QT prolongation. Re-examination of the cases used to support 'Cessation of Metabolism' also reveals little evidence to justify the hypothesis.

The finding of QT prolongation coupled with the hyperadrenergic state said to exist in lightning injury, may promote a state of episodic induction of and recovery from Torsade de Pointes Ventricular Tachycardia (VT). Histological examination of the myocardium supports the new hypothesis.

This is the first concerted description of lightning injury as one of the general causes of QT prolongation. It appears to occur frequently after lightning injury, is a prerequisite of and predisposes to episodes of Torsade de Pointes VT. These electrocardiographic abnormalities explain 'Cessation of Metabolism' and recognition may change management and lead to greater survival.

1.0 Introduction

Reported survival after lightning strike following prolonged periods of unresuscitated cardiac arrest remains enigmatic.

In re-appraising the literature containing these reports, the authors have noted that a large number of electrocardiograms in reports of lightning injury demonstrate a prolonged QT interval. This prolongation has only been noted in passing previously and/or in isolated cases (e.g. Divakov (1966), Palmer (1987)). The authors draw together the literature on electrocardiograms of lightning injured patients and provide the first unified collation of QT prolongation.

There is general consensus in the cardiology literature that a prolonged QT interval is a prerequisite for the development of Torsade de Pointe ventricular tachycardia (VT). In this paper, the implication of this fact for lightning injury is explored, and it is proposed that it is possible that longer than normal periods of *apparent* arrest are explicable using a Torsade model.

In acute hyperadrenergic states reversible severe cardiac failure resulting in acute pulmonary oedema can occur. This is seen, for example, in Scorpion, jelly-fish an Irukandji stings (Guerow (1980), Williamson (1988)). In the chronic hyperadrenergic state such as exists in phaeochromocytoma, a reversible cardiomyopathy may occur (Velasques (1984)). Myocardial biopsy shows patchy myocardial necrosis. In lightning injury pulmonary oedema may occur, patchy myocardial necrosis has been documented, and a hyperadrenergic state is probably the norm, though likely of severe intensity but brief duration.

Lastly, it is noted that Torsade VT may occur as a paroxysmal entity and during its process an individual may appear to be in cardiac arrest.

These issues are expanded in succeeding sections and a final hypothesis is proposed.

2.0 Elements from the Literature

One of the major enigmas of lightning injury is the widely claimed phenomenon of documented survival with minimal deficit after prolonged unresuscitated cardiac arrest. This contention appears untenable, and flies in the face of accepted findings where it is agreed that cerebral anoxia leads to permanent damage after four minutes of lost perfusion.

To explain this it has been proposed that, after a strike, all metabolism ceases and that the lack of metabolic demand means lack of perfusion is immaterial. This proposition receives most currency due to its espousal by Taussig (1968). Since then it has often been repeated (e.g. Nesmith (1971), Bartholome, et al., (1975), Msonge, et al., (1976), Kleiner, et al.,(1978)). Although the notion is widely attributed to Taussig, in fact it predates her widely quoted paper though not in such definite form. Former reports include those of Critchley(1934), Jellinek(1942), and Ravitch, et al.,(1961).

Jex–Blake(1913) provides a fascinating account of the history of views on lightning injury which include views on resuscitation. Many are obviously speculative, but an equivalent of cessation of metabolism does not seem to have been mentioned to that stage. The first time that the proposal is made is attributed by Critchley(1934) to Jellinek(1932a and 1932b). The effect is described in this initial work as 'suspended animation'. The notion that respiration and circulation were intimately involved with survival had long been current (see Jex–Blake), and the necessity to re–establish both was known. Critchley(1934) was the first to suggest that resuscitation after 'several hours' of demonstrated cessation of respiration and circulation was possible, based not on personal experience but on other reports. The reason for the resucitability was said to be that the victim was in 'suspended animation'. Lynch and Shorthouse(1949) provide a similar reference to Jellinek and Critchley, and are perhaps the first to pronounce scepticism over the phenomenon saying that a certain German expert Alvensleben was sceptical over resuscitation after more than half an hours 'suspended animation'. Nonetheless they recognise that reports of long term suspended animation being reversed exist – but more often after technical electrical injury than lightning injury.

Ravitch, et al.,(1961), also summarised earlier by Morikawa, et al.,(1960), provide a report of such a case. A child was struck and immediately after the strike was questionably thought to demonstrate a pulse, but no respiratory effort. He was given manual respiration for about 10 minutes, and this was then ceased though a pulse was still thought possibly to be present. Seven minutes later he arrived at hospital by ambulance with no successful pulmonary inflation for all that time and was found to be pulseless. An open thoracotomy indicated an asystolic heart with no bleeding from the wound. After a further three minutes – 20 minutes from the strike – cardiac action was restored, and ultimately successful restoration of function was achieved.

This sequence of events was later cited by Taussig(1968) as her only support for the hypothesis of immediate 'cessation of metabolism' in lightning strike thus allowing prolonged arrest with successful later resuscitation. The example is therefore not a good one in this connection. It would seem more to fit the sequence of events described by Andrews et al.,(1989a) in which experimental data supported the hypothesis of primary cardiac arrest and respiratory arrest, followed by cardiac recovery and secondary hypoxic arrest.

Based only on the case above, Taussig strongly asserts that all body metabolism ceases after a lightning strike. The assertion has then been repeated by several authors in a form giving it status as accepted theory.

There is no experimental evidence to support the contention of cessation of metabolism and it is seriously questioned by those with any experience in tzeating such patients (Cooper (1989), ten Duis (1989), Andrews, et al., (1989b)).

Several reports commonly regarded as supporting the notion of such recovery (see e.g. Kleiner, et al.,(1978) who state that at least 6 published cases support the contention) bear further examination, e.g. Kravitz, et al.,(1977), Kleinot, et al.,(1966), Yost, et al.,(1974), Burda(1966), Hanson, et al.,(1973). In each of these cases there was certainly a prolonged period of cardiac arrest, but early resuscitation was also attempted to greater or lesser degree within the knowledge of the day. Most often this was respiratory support only. In the given reports, there was no documented period of prolonged hypoperfusion that would require the induction of an hypothesis to suggest low metabolic demand. The fact that recovery was achieved, at least temporarily, indicates more the success of the resuscitation attempted. It may be that such resuscitation was ineffective, given more recent knowledge of techniques of emergency first aid, and, if so, one must look for further explanation for the documented survival, but the reports concerned are not couched in this light. That another explanation is required is only necessary if it is presumed that ineffective attempted resuscitation occurred, and certainly not as a result of documented prolonged unresuscitated arrest. There is no evidence to support recovery from lightning injury after the accepted period of a small number of minutes of unresuscitated arrest has passed, and it is on this misconception that many of the claims for a state of metabolic standstill have been made.

Indeed, one of the present authors (Andrews, et al. 1989b) has stated that the 'cessation of metabolism' hypothesis though implausible has not been supplanted by anything better if indeed one accepts that the phenomenon occurs at all. Though evidence is at best questionnable, as above, for recovery after a documented prolonged unresuscitated arrest, the dogma is still widely held. At best, survival after prolonged unconsciousness with attempted resuscitation, is supported by the literature. It is the aim of the following discussion to propose a more plausible alternative than the currently held version of 'cessation of metabolism' on the assumption that resuscitation was less than effective – given it was generally non–cardiac, and using techniques of respiratory support that have been supplanted.

2.1 Torsade de Pointe Ventricular Tachycardia

In developing a new hypothesis, we first discuss a recent strand of the cardiological literature.

Dessertenne (1966) identified a 'new' morphological form of ventricular tachycardia (VT). The initial recognition was based on morphological grounds alone. Cokkinos, et al., (1978), state that its characteristics are a changing pattern of ventricular complexes, spontaneous onset and offset, refractoriness to defibrillation and a number of antiarrhythmic drugs, especially quinidine and other Type I agents. They state that prior to induction of a paroxysm, QT prolongation is almost universally seen. They note distinct differences between the new form and classical VT:

i. The complexes are almost identical to each other rather than polymorphous, with undulation of the QRS axis over a series of 5–20 beats with concomitant alternation of size

ii. Classical VT (and indeed ventricular fibrillation (VF)) are seldom self limited, while spontaneous onset and offset is a hallmark of the new form

iii. Electroversion is of no help in the new form, and antiarrhythmic medication often exacerbates the arrhythmia.

Thus the morphological appearance of the arrhythmia is of an undulant series of similar appearance ventricular complexes twisting in axis around the electrical baseline giving the appearance of a modulated sine wave. The descriptive term 'Les Torsade de Pointes', or roughly translated, 'the twisting of the points', was coined by the French writers initially describing the arrhythmia. Other descriptive terms have been applied, with varying degrees of correctness – 'cardiac ballet', 'paroxysmal ventricular fibrillation', 'transient recurrent ventricular fibrillation', and 'polymorphic ventricular tachytachycardia'.

Clinical features of Torsade include an episodic course with dramatic drop in (but not absence of) cardiac output during an episode, and consequent syncope. Historical features may include, among others, antiarrhythmic drug ingestion (especially Type I), phenothiazine ingestion (especially thioridazine), a family history of one of the hereditory QT prolongation syndromes, an associated hypokalaemia, and usually QT prolongation. Thus impaired repolarisation, for one of many reasons, is a cardinal feature of the arrhythmia. It is specifically predisposed, also, in situations of bradycardia or high grade AV block, and can degenerate into VF or VT or remain episodic.

The onset of Torsade seems to be due to an extrasystole occurring *late* in the T wave, as opposed to classical VT or VF where the extrasystole occurs early in the critical interval. Krikler, et al., (1976) use this observation, and the fact that they have seen Torsade induced in several cases by electrical stimulation, to suppose that it is due to a re-entry mechanism in a setting of impaired repolarisation.

The underlying pathophysiology is only postulated at this stage but a consensus view seems to be that it represents two (or more) ectopic foci operating slightly out of synchrony with the ventricles attempting to synchronise first with one, and then the other, focus. The synchronicity is thought to be variable in extent, and gradually changing between the two foci. Other explanations have been given, and Kossman, (1978), for example, provides a good summary of these and an attempt to place Torsade into a classification of atypical ventricular arrhythmias.

For our purpose it is noted that a lightning strike could indeed represent the electrical stimulation required as above, and that the cardiac insult suffered could indeed impair repolarisation by disruption of membrane pores and pumps. Thus a situation predisposing to episodic arrhythmiae could indeed be set up.

The next section examines evidence for impaired repolarisation after lightning strike.

2.2 The QT Interval in Lightning Strike

Palmer(1987) has noted a prolonged QT interval in the ECG of a patient following lightning strike. In this patient QT prolongation was initially slight, and increased over several days and then resolved over a period up to one month. Cheng(1988) contends this may have been pseudo–prolongation, but admits that the consequences for possible arrythmias are the same. Kleiner, et al.,(1978) note QT prolongation in passing in a short review, and Divakov(1966) is said to note similar prolongation, though a translation of that work is not available to the present authors. Generally QT prolongation has passed unrecognised.

A re-examination of ECG tracings in published literature known to the authors (that is in the bibliography in Andrews, et al., (1989b), supplemented to date) has been undertaken and the QT interval in each tracing has been measured. This is presented in Table 1 where rate corrected QT intervals are then compared with the 'normal' value of 440mS.

When those cases in which a definite QT_c can be determined are examined, it will be seen that 64% demonstrate a prolonged QT_c. Only 33% show a normal QT_c, and of these the shortening is relatively little, compared with a dramatic degree of lengthening in the other cases. The only problem with a compilation such as this is that in a percentage of reported cases, a full tracing is not given (only isolated complexes are shown), and thus heart rate is not able to be found.

In an attempt to include those cases where a heart rate was not obtainable, the QT_c has been determined assuming a heart rate of $50min^{-1}$. This is highly conservative, and if the QT interval is long at this rate, it will certainly be long at a (more likely) higher rate. For those with assumed heart of $50min^{-1}$, 59% demonstrate a long QT_c, and only 37% are normal. Again the same observation as above regarding the shorter intervals holds. Of course, no account has been taken of a normal range of QT_c, with the above figures derived on a strict application of a normal value of 440mS.

It may be seen, then, that the vast majority of tracings show QT prolongation,. and the general tendency is for QT interval to extend during a recovery phase after injury. Often a period of some months elapses before normality returns. The time course of QT_c prolongation is shown when the results are graphically presented against their time course in Fig. 1. In this figure both stated rate and assumed rate ($50min^{-1}$) measurements are shown and a distinct appreciation of the time course of recovery can be seen. This reinforces the view that in lightning injury cardiovascular followup should extend for a substantial period after recovery is otherwise thought to have been effected.

2.3 Myocardial Necrosis and Hyperadrenergia in Lightning Strike

The next theme to be taken up is that of the histopathological findings in lightning injury within the myocardium. The picture is somewhat variable, and only those victims actually succumbing to their injuries have histological study of their myocardium performed. Necrosis in some form is however the rule. No myocardial biopsies have been done on survivors of lightning strike.

Hanson, et al.,(1973) present two cases where defined localised areas of necrosis of the posterior wall of the myocardium was found. Increased serum catecholamine levels ante-mortem (dominantly adrenaline) were also demonstrated. The findings in the case reported by Ekoe, et al.,(1985) were of a larger inferior area of necrosis and in both these reports, the picture was of a coagulative necrosis with diffuse (patchy) inflammatory infiltration. Myers, et al.,(1977) report a localised large inferior infarction but with no comment on histology.

Kotogal, et al.,(1982), however, report a different picture. After treatment for seven days in which there were also several periods of ventricular tachycardia, the patient died and myocardial histology showed diffuse varying stages of myocardial necrosis. Wakasugi, et al.,(1986) report a similar picture. Kravits, et al.,(1977) describe a case in which diffuse myocardial necrosis was found, and also a hyperadrenergic state was demonstrated. It was commented that "the most prominent findings were the focal myocardial necrosis, myocardial degeneration, and early reorganisation of myocardial loss with fibroblastic replacement".

The case reported by Chia(1981) is of interest. It is a case demonstrating pulmonary oedema (see below), and unfortunately no comment is made regarding measurement of catecholamines or QT prolongation.

McCrady-Kahn, et al.,(1981) report the transient hypertension and tachycardia often seen and note normal urinary catecholamines. No other cause for the signs could be found, and serum catecholamines were not measured.

While not a universal picture, it may be said that there is a body of reports which notes patchy myocardial necrosis, and elevated serum catecholamines. Pulmonary oedema is also seen (Buechner, et al.,(1961), Kleiner, et al.,(1978)), and the author's personal evaluation of local post-mortem reports (Andrews, unpublished data) shows a 70% incidence of pulmonary congestion in the 10 victims examined.

2.4 Pulmonary Oedema and Myocardial Necrosis in Phaeochromocytoma

A recent report of cases of otherwise unexplained cardiac failure (Sardesai, et al.,(1990)) draws attention to the fact that phaeochromocytoma can produce a cardiomyopathy, and this can lead to pulmonary oedema and cardiac failure. As it may not readily come to mind, they argue for its inclusion on any differential diagnosis of otherwise unexplained pulmonary oedema. Further it is argued that normal urinary catecholamine levels do not exclude the diagnosis. The histological picture seen is one of patchy myocardial necrosis. It is stated by the authors that this picture is "consistent and predominant".

3.0 An Alternative Hypothesis to Cessation of Metabolism

A synthesis of the above elements is possible. Admittedly this synthesis is speculative, however it is believed plausibly so – more so than alternatives. The wide currency of the questionnable 'cessation of metabolism' alternative requires a more plausible alternative explanation, even though there is slight evidence to encourage one to delay resuscitation as a desirable course. Indeed the opposite. The hypothesis detailed below is thought to be operative also where pulmonary resuscitation alone is given in a state of prolonged arrest. The occurrence of this state *does* have support from the literature (indeed, wide support), and demands examination.

It is first noted that Andrews et al. (1989a) have given credence to a form of the secondary arrest dogma. They showed that the initial arrest after lightning injury is likely to be asystolic, and that the heart restarts in a brief period of bradycardia. After two to three bradycardic beats, an intense tachycardia is evidenced, and the heart proceeds to secondary hypoxic arrest as a result of continuing respiratory arrest. The tachycardia was taken as indication of hyper-adrenergia, though this is not always demonstrated in reported cases. Thus adrenergic stimulation must be regarded, at best, as variable in the injury.

A hypothesis of subsequent cardiac behaviour is now outlined especially where some form of respiratory support has been given.

It is first noted that QT prolongation highly predisposes to Torsade de Pointe VT and that QT prolongation is a strong feature of lightning injury. In that state, pulses will be absent. A victim will therefore *appear* to be in cardiac arrest. Nonetheless it is known that cardiac output may still be just present in this or indeed other forms of VT, though not of course compatible with anywhere near full function.

Subsequent events, it is postulated depend on catecholamine levels in the individual case.

If it is assumed that a hyperadrenergic state exists, then Torsade VT may well terminate in cardiac recovery, at least initially. Sufficient catecholamine may arrive at the heart to stimulate recovery, and a good rhythm and output may occur and be maintained. If sufficient catecholamine levels persist the heart may proceed to secondary hypoxic arrest as outlined above. It is concievable that if catecholamine levels fall subsequent to this degree of recovery, further episodes of Torsade VT may then occur and the process may cycle.

Alternatively, if catecholamine levels are not high, the heart may again lapse into bradycardia and/or episodic Torsade VT, since QT prolongation will still exist. Episodes of Torsade VT and bradycardia may be sufficient to maintain perfusion just sufficient to maintain viability.

In either case, and the balance may depend on catecholamine levels in individual cases, and a period relatively longer than the classically allowed few minutes in cardiac arrest will appear to have occurred. The victim may appear pulseless and lifeless as if cardiac arrest due to ventricular fibrillation has occurred. If ventilation without cardiac support occurs, as has been reported in the literature especially in days prior to external cardiac compression, then the state may persist for some time giving an illusion of recovery after prolonged arrest.

Further support for the presence of circulating catecholamines is gained from the histological picture of the myocardium at autopsy mirroring that in phaeochromocytoma. While not at all the only explanation for patchy necrosis, at least it may be one factor.

Recent experimental work (Factor et al. (1985)) has demonstrated that high levels of catecholamines may precipitate vascular spasm and medial smooth muscle contraction bands (MSC) (Ming, et al., (1976), Van Citters, et al. (1962), Joris, et al. (1981)). Histological examination of coronary arteries of patients who had premorbid conditions associated with high levels of catecholamines showed a high frequencies of MSC. This suggests coronary artery spasm may be frequent in hyperadrenergic states. The subsequent myocardial ischaemia predisposes to ventricular arrhythmias including Torsades de Pointes. Catecholamine release can be a cause or trigger for the development of Torsades de Pointes VT.

Thus an alternative hypothesis to 'Cessation of Metabolism' has been proposed, its operation depending on catecholamine levels, and enhanced by varying degrees of artificial ventilation.

4.0 References

Andrews, C.J., and Darveniza, M., (1989a), *"Effects of Lightning on Mammalian Tissue"*, Proc. Third Int. Conf. Lightn. Stat. Elec., Bath Sept. 1989, ERA Tech., Leatherhead, Surrey.

Andrews,C.J., Darveniza,M., and Mackerras,D., (1989b) *"Lightning Injury: A Review of Clinical Aspects, Pathophysiology, and Treatment"*, Adv. Trauma, 4:241–288, 1989.

Bartholome, C.W., Jacoby, D., and Ramchand, S., *"Cutaneous Manifestations of Lightning Injury"*, Arch. Dermatol, 111:1466–8, 1975.

Buechner, H.A., and Rothbaum, J.C., *"Lightning Stroke Injury – A Report of Multiple Casualties from a Single Lightning Bolt"*, Milit.Med., 126:775, 1961.

Burda, C.A., *"Electrocardiographic Changes in Lightning Stroke"*, Am.Heart.J., 72:521, 1966.

Cheng,T.O.,*"Lightning Injury Causing Prolongation of the QT Interval"*, Postgrad. Med. J., 64:335,1988.

Chia, B.L., *"Electrocardiographic Abnormalities and Congestive Cardiac Failure due to Lightning Stroke"*, Cardiol., 68:49–53, 1981.

Clore, E.R., and House, M.A., *"Prevention and Treatment of Lightning Injuries"*, Nurs. Pract., 12(12):37–45, 1987.

Cokkinos,D.V., Mallios,C., Philias,N., and Vorides,E.M., *" 'Torsade de Pointe': A Distinct Entity of Ventricular Arrhytmia?"*, Acta Cardiol., XXXIII(3):167–84, 1978.

Cooper, M.A., Personal Communication.

Craig, S.R. *"When lightning strikes. Pathophysiology and treatment of lightning injuries"*, Postgrad Med, 79(4):109–12, 121–4, 1986.

Critchley, M., *"Neurological Effects of Lightning and of Electricity"*, Lancet, 1:68, 1934.

Dessertenne,F., *"La Tachycardie Ventriculaire a Deux Foyers Oppose Variables"*, Arch. des Mal. du Coeur, 59(2): 263–72, 1966

Divakov, G.M., *"ECG Changes in Persons Struck by Lightning (title trans from Russian)"*, Klin. Meditsima (Mosc.), 1966, 95.

du Pasquier,G., and Freeman,J., *"Le foudroiement"*, Ann. Fr. Anesth. Reanim., 5:601–4,1986.

du Toit, J.S., "A Case of Bilateral Cataract Caused by Lightning", J. Med. Soc. S. Afr., 1:503, 1927.

Eber,B., Himmel,G., Schubert,B., et al., *"Myokardiale Schaedigung nach Blitzschlag"*, Z. Kardiol., 78:402–4, 1989.

Ekoe, J.M., Cunningham, M., Jacques, O., et al., *"Disseminated Intravascular Coagulation and Acute Myocardial Necrosis caused by Lightning"*, Int.Care.Med., 11:160, 1985.

Factor, S.M., and Cho, S., *"Smooth Muscle Contraction Bands in th Media of Coronary Arteries: A Posmortem Marker of Antemortem Coronary Spasm"*, JACC, 6(6):1329–37, 1985.

Funiak,S., Hendrich,F., Drimal,J., Markuljak,I., and Funiakova, S., *"Srdcovy Infarkt Pri Poraneni Bleskom"*, Vnitrni lekarstvi, 30(11):1118–21,1984.

Guerow, M., Grupp, R.J., Gabel, M., Grupp,G., *"Hemodynamic and Myocardial consequences of Scorpion Venom"*, Am. J. Cardiol., 45:979, 1980.

Gupta,G.B., Gupta,S.R., Somani,P.N., and Agrawal,B.V., *"Atrial Fibrillation with Inferior Wall Myocardial Ischaemia Following Lightning"*, J. Assoc. Phys. India, 36(5):354–5,1988.

Hansen, G.C., and McIlwraith, G.R., *"Lightning Injury: Two Case Histories and a Review of Management"*, Brit. Med J., 4:271, 1973.

Jackson, S.H.D., and Parry, D.J., *"Lightning and the Heart"*, Br. Heart. J., 43:454, 1980.

Jellinek,S., Wien Klin Wschr., 45:37, 1932a, quoted in Lynch, et al., op cit.

Jellinek,S., Electrische Verletzungen, Leipzig, 1932b, quoted in Lynch, et al., op cit.

Jellinek, S., *"Death by Lightning (Letter)"*, Brit. Med. J., Dec. 12, 1942, p714.

Jex–Blake, A.J., *"Goulstonian Lectures : Death by Electric Currents and by Lightning"*, Brit. Med. J, pp 425–430, 492–498, 548–552, 601–603; Mar. 1, 8, 15, 22, 1913.

Joris, I., and Majno, G., *"Medial Changes in Arterial Spasm Induced by L–Norepinephrine"*, Am. J. Pathol., 105:212–22, 1981.

Kleiner, J.P. and Wilkin, J.H., *"Cardiac Effects of Lightning Stroke"*, JAMA, 240:2757, 1978.

Kleinot, S., Klachki, D.M., and Keeley, K.J., *"The Cardiac Effects of Lightning Injury"*, S.Afr.Med.J., 40:1141, 1966.

Kossman,C.E., *"Torsade de Pointes: An Addition to the Nosography of Ventricular Tachycardia"*, editorial, Am.J.Cardiol., 42:1054–6, 1978.

Kotogal, S., Rawlings, C. A., Chen, S., Burris, G., and Nouri, S., *"Neurologic, Psychiatric and Cardiovascular Complications in Children Struck by Lightning"*, Paed., 70(2): 190, 1982.

Kravitz, H., Wasserman, M.J., Valaitis, J., et al., *"Lightning Injury"*, Am. J. Dis. Child., 131:413, 1977.

Krikler,D.M., and Curry,P.V.L., *"Torsade de Pointes, an Atypical Ventricular Tachycardia"*, Br. Heart J., 38:117–20, 1976.

Kroob, M.J., and Cram, A.E., *"Lightning Injuries: A Multisystem Trauma"*, J. Iowa. Med. Soc., 73(6): 221, 1983.

Lynch, M., and Shorthouse, P.H., *"Injuries and Death from Lightning"*, Lancet, 1:473, 1949.

Morikawa, S., and Steichen, F., *"Successful Resuscitation after 'Death' from Lightning"*. Anesthesiol., 21(2):222–4, 1960.

Ming, S–C, McNiff, J., *"Acute Ischemic Changes in Intestinal Muscularisis"*, Am. J. Pathol., 82:315–26, 1976

Msonge, B., and Evans, R.L., *"Lightning Stroke on Ukerewe Island"*, East Afr. Med. J., 53(6):350–1. 1976.

Myers, G.J., Colgan, M.T., and van Dyke, D.H., *"Lightning Disaster Among Children"*, JAMA, 238:1045, 1977.

Nesmith, M.A., *"A Case of Lightning Stroke"*, J. Fla. Med. Assn., 58:36, 1971, quoted in Hanson, et al.,(1973).

Palmer, A.B.D., *"Lightning Injury causing prolongation of the Q–T interval"*, Post. Med. J., 63–891–4, 1987.

Ravitch, M.M., Lane, R., Safar, P., Steichen, F., and Knowles, P., *"Lightning Stroke"*, NEJM, 264(1): 36, 1961.

Read, J.M. *"Man Struck by Lightning Reveals Marked ECG Changes Hours Later"*, Med. Trib., March 28, 1966, p3.

Sardesai,S.H., Mourant,A.J., Sivathandon,Y., Farrow,R., Gibbons,D.O., *"Cardiomyopathy Presenting as Heart Failure"*, Brit. Med J., 1990.

Schmidt,W., Gruetzner,A., and Schoen,H.R., *"Beobachtungen bei Blitzschlagverletzungen unter Beruecksichtigung von EKG and EEG"*, Deutsches Arch. Klin. Med., 204:307–24, 1957.

Sinha, A.K., *"Lightning Induced Myocardial Injury – A Case Report With Management"*, Angiol., 36(5):327, 1985.

Taussig, H., *"'Death' from lightning and the Possibility of Living Again"*, Ann.Int.Med., 68:1345, 1968.

ten Duis,H.J., Personal Communication.

Terranova,S., *"Su un Caso di Infarto Miocardico da Elettrocuzione Atmosferica"*, Rif. Med., 71(4):93–96,1957.

Van Citters, R.L., Wagner, B.M., Rushmer, R.F., *"Architecture of Small Arteries During Vasoconstriction"*, Circ. Res., 10:668–75, 1962.

Velasquez,G., O'Sousa,V.J., Hackshaw, B.T., Glass, T.A., et al.,
"Phaeochromocytoma and cardiomyopathy", Br. J. Radiol., 57:89, 1984.

Wakasugi, C., and Masui,M., *"Secondary Brain Hemorrhages Associated with Lightning Stroke: Report of a Case"*, Jpn. J. Legal Med., 40(1):42–6, 1986.

Williamson,J.A., Burnett, J.W., Colquhoun, D., et al., *"The 'Irukandji Syndrome' and Acute Pulmonary Oedema"*, Med. J. Aust., 149:150–156, 1988.

Yost, J.W., and Holmes, F.F., *"Myoglobinuria Following Lightning Stroke"*, JAMA, 228:1147, 1974.

Zeana, C.D., *"Acute Transient Myocardial Ischaemia After Lightning Injury"*, Int.J.Cardiol., 5:207, 1984.

TABLE 1 QT Interval measurements derived from the Lightning Literature

AUTHOR	ECG REFCE	RATE beats/second	ACTUAL QT ms	QTc (ms) notes 2,3	Relation to 440ms (1,3)
Sinha	Fig 2 30h	136	320	482	+
	Fig 3 3.5d	75	440	492	+
	Fig 4 8.5d	100	360	464	+
Zeana	7 days	83	480	565	+
	7 mths		640	(584)	(+)
Burda	Fig 1,2 36h	60	600	600	+
	Fig 1,2 1w		280	(292)	
	Fig 1,2 4m		360	(328)	
	Fig 1,2 1y		400	(365)	
Palmer	imm.			460	+
	Fig 1 2d			680	+
	Fig 2 4d			500	+
	1m			410	−
Hansen	Case 1 30mn	140	320	489	+
	Case 2 30mn	110	300	406	−
	3d	125	300	433	−
Schmidt,et al	Case 1 1d	100	640	826	+
	2d		680	(620)	(+)
	3d		680	(620)	(+)
	4d		640	(584)	(+)
	11d		680	(657)	(+)
	17d		760	(694)	(+)
	23d		760	(694)	(+)
	Case 2 1d	90	600	734	+
	27d		640	(584)	(+)
Kleinot,et al	Case 1 imm	72	360	394	−
	unst		320	(292)	(−)
	Case 2 imm	100	440	568	+
Chia	3h		440	(401)	(−)
	6m		400	(365)	(−)
Read	1d	100	360	464	+
	2d	86	400	478	+
	7d	66	400	419	−
	35d	62	360	365	−
Jackson,et al	Case 1 1h		740	(675)	(+)
	72h		570	(520)	(+)
	9d		550	(502)	(+)
	Case 2 1h		630	(575)	(+)
Kleiner,et al	imm		360	(329)	(−)
	2d		440	(401)	(−)
	7d		440	(401)	(−)
	12d		480	(438)	(o)
Kroob, et al		85	360	428	−
Craig	1d		360	(328)	(−)
	3d		420	(383)	(−)
	7d		440	(401)	(−)
	43d		420	(383)	(−)
du Pasquier, et al.	1d	125	340	491	+
	14d	115	360	498	+
	32d	100	340	439	o
Funiak, et al		150	240	379	−
Terranova	1d	73	400	463	+
	32d	75	400	447	+
	50d	65	360	375	−

Gupta, et al	1d	76	420	473	+
	3d	70	360	385	−
Eber, et al	1d		680	(621)	(+)
	2d		760	(693)	(+)
	5d		800	(730)	(+)
	49d		840	(767)	(+)
Clore, et al.		136	300	452	+
Subramanian et al.	11d	95	400	503	+
	35d	60	420	420	−

Note: 1. + Prolonged QT interval Total: 21 of 33 (64%)
− Shortened QT interval Total: 11 of 33 (33%)
o Expected QT interval Total: 1 of 33 (3%)

2. Formula of Bassett $QT_c = QT_{measured} / \sqrt{RR \text{ interval}}$

3. Figures in parentheses represent QT_c based on a rate of 50min^{-1}, where no rate was given in text. This is a conservative assumption. If QT_c is long at this rate, it will certainly be long at a higher rate
(+) Possibly long QT_c Total: 16 of 27 (59%)
(−) Short QT_c Total: 10 of 27 (37%)
(o) Expected QT_c Total: 1 of 27 (4%)

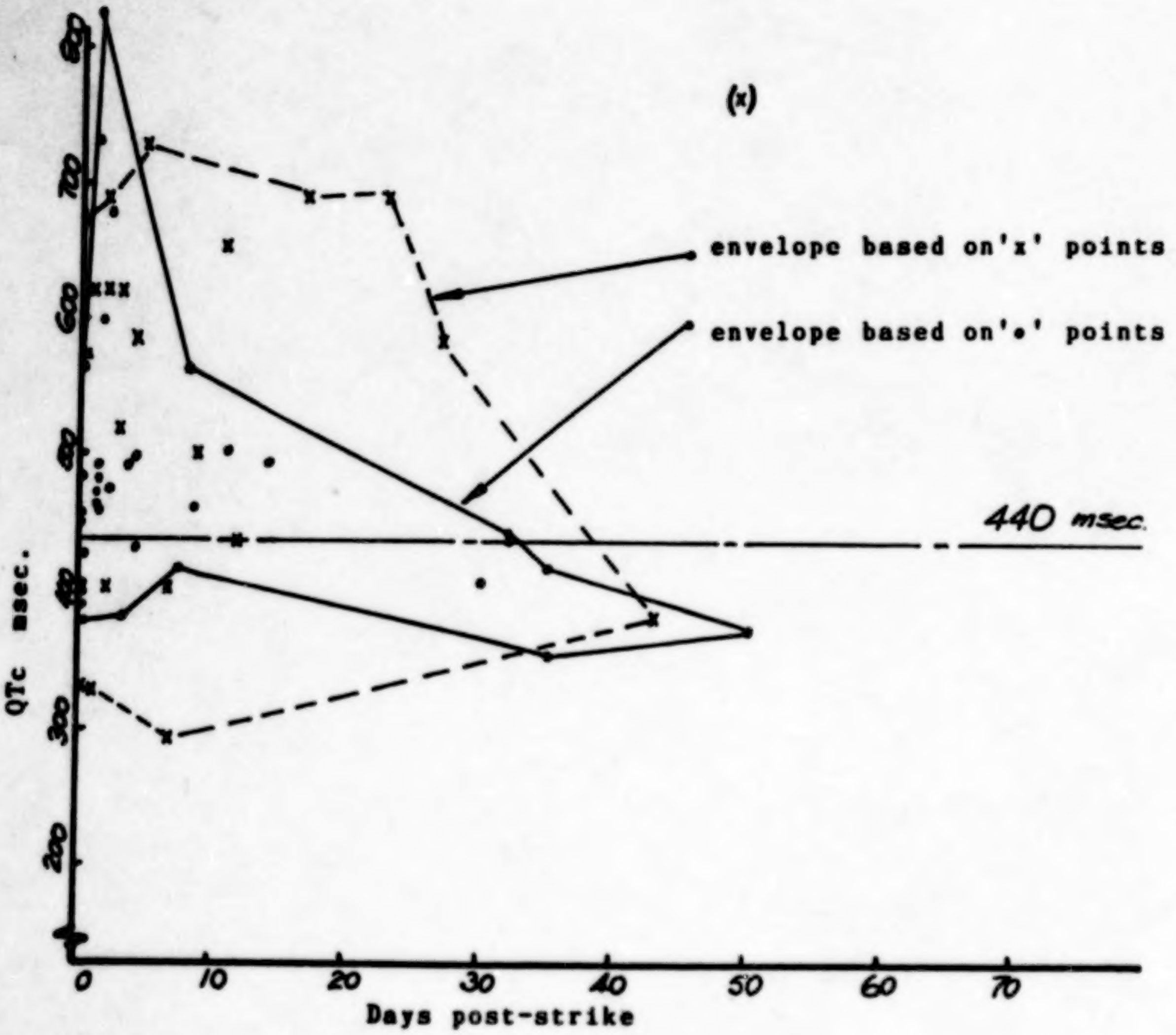

Fig.1. QTc vs time for lightning injured patients.
(• based on rate derived from report
(x based on conservatively assumed rate of 50/min)

FURTHER IDENTIFICATION AND TREATMENT MODALITIES IN TELEPHONE MEDIATED LIGHTNING STRIKE

by

Dr. Christopher J. Andrews[1,2] BE MEngSc DipCompSc MBBS MACS SMIEEE SMIREE
Prof. Mat Darveniza[2] BE PhD DEng HonDSc(Eng) FIEAust FIEEE FTS

[1]The Wesley Hospital, Brisbane, Australia
[2]University of Queensland, St Lucia, Brisbane, Australia

ABSTRACT

This paper reports the results of a prospective survey of people injured by lightning impulses transmitted by the public telephone system. The results are compared with those of a previous retrospective survey. Various deficiencis in the methodology of the latter survey have been addressed.

A division into a population with severe injury and a population with mild injury is made based on medical history and examination taken immediately after a strike. The best predictors of severe injury were found to be the presence of symptoms beyond one week after the strike, and also the initial presence of musculoskeletal injuries. Psychological upset is also seen to be a significant factor in severe injury.

The only physical parameter of strike which could be used as a predictor of severe injury was the presence of concomitant power system damage. The importance of earth bonding between power and telephone system is thus supported in a protection strategy.

The first author finally draws on experience in treating patients with these injuries to propose a treatment regimen for those with ongoing symptoms. The importance of evaluating and treating psychological and physical aspects is stressed.

I. INTRODUCTION

At a previous meeting, the authors (Andrews, et al., 1988) reported the results of a retrospective study of people who had been subjected to lightning strike delivered via their telephone lines. At that stage it was pointed out that this phenomenon had been very little studied and represented a significant source of morbidity and mortality in the Australian environment. Since that time, further study has been undertaken and the object of this paper is to report the results of the new work.

The dearth of literature on the subject was alluded to in the previous study and very little new literature has come to light since that time. Most writers regard the "telephone mediated" circumstance as only being an extension of "in the field" lightning strike. The injuries are therefore presented merely as a further mechanism of more general field lightning injuries. Little attention is paid to the circumstance in its own right, and it has already been stated (Andrews, et al., 1988) that significant differences exist both in the magnitude of the insult and the method of delivery of the injuring agent.

Eriksson, et al., (1988), report results of post mortem examinations for lightning victims in Sweden. They cite two cases where victims died when subject to a lightning surge while using the telephone. Notable in this report is the immediate localisation of all manifestations of injury to the face, head and neck. This is strikingly in consonance with the findings of the present study and will be alluded to later. It is also in consonance with the previous study.

Frayne, et al., (1988), also report a case of a man struck while using the telephone and again the localisation of his symptoms were to the head and neck with a marked bias to neurological disability. A significant finding of the previous study (Andrews, et al., 1988) was that the injuries were locally mediated rather than centrally mediated, although some personality change was noted indicating a certain global element of cerebral damage.

The previous study was conducted in a retrospective fashion and therefore suffered from certain deficiencies. Marked among these deficiencies was the need for subjects to recall their injuries after a substantial period, and therefore firstly a degree of selective recall, and secondly a degree of inaccurate recall, existed in the reporting process. There was also a degree of biased sample selection and these problems were alluded to at the time.

The current research aimed to rectify some of these deficiencies.

II. AIM OF RESEARCH

Bearing in mind the deficiencies of the previous sampling method, it was decided to gain access as quickly as possible to all persons who had recently been subjected to such an injury immediately the injury occurred. The aim was thus to provide recent sampling of the complete spectrum of injury. It was felt that less bias would be introduced into the sampling process in terms of the tendency for more severely injured people to respond to retrospective study, and less recall problem in the reporting process would be evidenced. Also when those injured were examined immediately, a more objective view of the injuries could be obtained by an external observer.

During three lightning seasons from 1988 to 1990 in the immediate regional vicinity of the authors' institution, 18 people reported lightning injuries to Telecom Australia. Twelve of these were examined and ten provided data suitable for inclusion in this study.

An immediate comment is made on these numbers. Firstly, the total number receiving injuries over three lightning seasons is markedly decreased over the incidence discussed in the previous paper (approximately 30/year). Reasons for this need to be advanced. It is felt that Telecom monitoring of this problem has now been active for at least ten years and in that time, those people in areas of maximum risk have been supplied with protection for their telephone apparatus. Therefore the remaining population is a relatively low risk population. Further a substantial public education programme has been undertaken in that time, and, as well, substantial publicity has been given to the authors' research. Public behaviour with regard to telephone usage during thunderstorms has been substantially modified. For these reasons it is reasonable to expect the incidence of telephone mediated lightning injury to have decreased markedly.

III. METHODOLOGY

This research relied heavily on the co-operation of Telecom Australia, and that was willingly and readily forthcoming. Telecom Australia and the research team were at pains to be sensitive to issues of confidentiality. The participants in this prospective study were therefore guaranteed that their access to the research team was entirely confidential to the team and the result of any examination was not made available to Telecom Australia. The mechanism for recognising individual injured patients therefore took this into account.

During the period of the study every person who reported an injury to Telecom had their incident investigated by Telecom Australia. At the time of this investigation they were given a letter and verbal encouragement to contact the research team. The letter they received invited them to contact the research team as soon as possible to arrange an interview and examination with regard to their injuries. Co-operation was earnestly sought and verbal encouragement to do so was provided by the Telecom investigator. Whether a person subsequently made contact with the research team or not, however, was a matter of individual initiative and the Telecom officers in fact had no knowledge as to whether subsequent contact was made or not. Confidentiality was thus assured.

All respondents who made contact with the research team were visited and examined immediately by a medical member of the team (CJA). They were asked to consent to a medical examination which included electrocardiography and audiometry. In each case consent as given. The two excluded patients came to the authors' notice outside this mechanism and for the sake of consistency were excluded from the study.

The response to the invitation in this study was double that of the previous study and although the numbers are small, represent a consistent cross-section of the injured population.

The mechanism was however, was not without minor criticism and the major disappointment was the delay occasioned in some cases by some respondents in returning the form and making contact with the research team after the visit of the Telecom investigator. This was remedied part way through the study by allowing the respondent the option, at their own initiative, of returning the form to the research team via the Telecom investigator, should they so desire. The sacrifice in confidentiality was not considered by the majority to be of any moment.

The analysis to which the data were subjected aimed at identifying a particular risk group within the injured population. Cluster analysis was used in the previous study and three lightning strike syndromes were identified. Data was accumulated in two ways. Firstly on the examination visit, information regarding the circumstance of the strike, (physical details), was collected, as was comprehensive medical details of injuries sustained. Subsequent to that, with the respondent's consent, a copy of the Telecom report of technical matters surrounding the strike was obtained and used to supplement the physical details referred to above. As these were more comprehensive than the author's own assessment of the physical circumstances, the Telecom report was relied on heavily for the physical details.

Cluster analysis was applied to the subjects based purely on the medical details of their examination. This initial clustering allowed the grouping of individuals into categories of severity of injury. In this first analysis the physical variables derived from the Telecom report were then added to the data. Statistical analysis was applied to them to see if there were significant differences in the physical surroundings of particular strikes given that the categories of severity of injury had already been fixed. It was thus hoped to identify particularly risky circumstances based on the severity of injury sustained during the strike.

A second analysis was conducted for comparison in which clustering was applied to the whole data set, just as in the previous study, with all the physical data included in the clustering process. This was done as a check on data consistency and for a wider view of the significant factors participating in the clustering process.

The results were then compared.

IV. RESULTS AND DISCUSSION

IV.1 Numbers

A gratifyingly high response was obtained to this methodology, of the order of 60% of total strikees. This is roughly double the response obtained in the retrospective survey and was felt to be an adequate response.

Comments have already been made regarding the absolute size of this sample.

IV.2 Presentation of Data

An examination was made of the data in raw form and this is presented in Table 1, which has been ordered to reflect the groupings later derived from the cluster analysis. The absolute symptoms that were seen mirror those that were seen in the previous study. Symptomatology was divided as before, into short term and long term symptomatology. The natural break point for this, was approximately one week for short term injuries, versus greater than one week for long term symptoms. The break point for the previous study was in fact into three groups, one day, one week and longer. However, examination of the data for this study showed the above to be a more natural division.

It was quite noticeable that the number of both short term and also long term symptoms that were reported were smaller than in the retrospective study. This is regarded as confirmation of the bias by which individuals magnify over a period of time the symptomatology that they had experienced a long time previously. The current set of symptoms, as found in this study, would seem to be a more realistic indication of the symptomatology of the injury.

The symptomatology in the short term centres around three or four major areas.

Firstly, there is a group of ear symptoms appearing in three of the respondees, where pain, tinnitus and altered sensation were noted. Secondly, a group of burns were seen, however, only in two of the respondees. Facial, neck, and arm pain, including alteration in sensation, were seen in three of the respondees, however psychiatric symptoms, largely centring around anxiety, were seen in six of the respondees, often to a marked degree.

Cardiovascular findings were evidenced in only three respondees, and consisted of tachycardia, which may well have been a manifestation of an anxiety state. Other minor symptoms, the largest one of which was generalised musculoskeletal pain in three cases, was also seen. The duration of these initial injuries ranged from one to five days, with the majority less than three.

Long term symptoms were seen in only three of the ten subjects. This represents a larger percentage of the total than found in the previous study wher approximately 10% were found to have significant ongoing symptoms. Two of these three indicated marked psychological disturbance and problems have continued to date. The remaining symptoms centred entirely around continuing musculoskeletal pain, particularly in the arm, face and neck.

Thus a first conclusion is that the major long term sequelae of this sort of lightning strike are pain (particularly musculoskeletal) and psychological disturbance.

IV.3 Cluster Analysis

The first analysis divided the subjects cleanly into two groups (Fig.1.).

Subjects six and ten formed a separate cluster from the remainder of the subjects. Examination of these subjects' data indicates that they are in fact two of the three subjects who demonstrated long term and continuing upset. Thus a predictor for severity of injury would seem to be duration of symptoms. It is interesting that subject nine was left out of this cluster by the clustering process. However, examination of that subject's data shows that his continuing symptoms were mild and the other two subjects were in fact quite debilitated. Once again the major continuing problem was psychological upset and pain. In the case of subject nine, psychological upset was not as prominent.

Each of the data items contributing to the cluster analysis were then examined for statistical significance between the two groups seen. All the variables representing long term symptomatology were significantly different ($P<.05$) between the two groups. Further the only variables in the short term symptomatology that were significantly different between the groups were those representing arm pain and altered arm sensation. In this study these particular variables could be used as discriminators for long term injury and thus severity of injury. It was noticeable that none of the physical circumstances discriminated between the particular groups, (initially based on the physical data collected by the author.)

When the physical data collected by Telecom Australia was added to the study, only two reached significance. Those two were the variables relating to associated power system damage with the given strike. Particularly there was no significance to variables like storm intensity, storm history, phone line construction, housing construction or terrain. The fact that these variables did not reach significance may be a reflection of the small sample size. However, consistent significance with associated power system damage adds credence to the stated Telecom Australia view that entry into a dwelling via associated power system strike, is a highly important means of entry of the injuring impulse. Further comments on this matter will be made later.

The second analysis, (Fig.2.), allowed the clustering to proceed on the basis of all variables including Telecom physical data. The clustering in this process showed an almost identical division into two cluster classes. This time however, subjects six, nine and ten were clustered into a group of greater severity than the first analysis. In retrospect it may be seen that subject nine only joined with the lightly injured group at a very late stage in the clustering process in the previous analysis and so may be regarded as "a floater". Once again the division on severity of injury is made on the basis of long term symptomatology alone and these are the only medical variables which reached statistical significance.

In the second case the physical data of significance also included whether the victim was wearing shoes or not. This may well represent a chance association. However the analysis shows that severity of injury is statistically positively associated with the wearing of shoes. This may represent a tendency to capacitive coupling to the impulse rather than direct conductive coupling. One author, (MD), has previously drawn attention to the phenomenon of a "capacitive spark", as opposed to a "conductive spark".

The only other variable shown to be of significance in this second analysis was whether the victim was thrown or not by the impulse. This would seem naturally a correlate with severity of injury and could well indicate a degree of musculoskeletal trauma which could give rise to long term musculoskeletal disability.

V. IMPRESSIONS FOR THERAPY

It is noticeable in this study, as in the previous study, that injuries, and particularly injuries of severe degree, are local to the passage of electric current and are not derived from a central causation for continuing symptomatology.

Subsequent to this study, the author has been called upon to treat a number of these victims, something which was specifically precluded in the previous research methodology. Having completed the study, it was felt by the first author that he was ethically able to undertake such treatment.

The major features of injury are psychological and musculoskeletal. And this finding of the study has been borne out as an impression of the presentation of these people clinically. Further clinical impressions are now described.

The pain which the victims present with is very local to the line of the strike. It is felt to have been neuritic in origin, that is, derived from direct peripheral nerve cell damage. This is borne out by the clinical nature of the pain and secondly, by a plausible connection with the passage of electric current. That is, the electric current specifically and selectively damages the sensory nerve terminals and peripheral sensory neural conducting pathways which are traversed by the current. This is further borne out by success that the first author has had in treating these injuries with carbemasepine and/or clonasepam. These are agents known to be of particular use in neuritic pain. A standard dose regimen has been used gradually decreasing the dosage until the minimum to achieve control is found. Although the symptoms lasting greater than 1 week have been classified as long term, in fact they appear to improve gradually over six to eight months and the need for medication is finally removed.

Psychological factors are seen to be prominent when these people present and it is a clinical impression of the first author that the majority of people having continuing problems are of the more obsessional type of personality. This is not necessarily derived from the current data. It represents a clinical impression and is a plausible extension of the anxiety states seen in this study. The obsessional personality finds it difficult to cope with situations beyond immediate control. Issues of control of destiny and control of health are very strong in the obsessional. Many of the patients report frustration at having continuing problems they don't understand and that are foreign to their experience. In their perception the loss of control is made worse because "no-one else seems to understand" the syndrome either. They feel that the good health of which they had been totally in control previously had now been independently snatched from them and this created anxiety in itself, and particularly anxiety generated by being subject to the unknown. All this plausibly connects with psychological feelings of ongoing anxiety and mixed anxiety depression. The author has therefore found it useful to add a degree of tricyclic anti-depressant medication (particularly clomipramine) to the above pain relief. The basis for doing this is to provide relief from the obsessional features of the psychological disturbance as well as to provide primary anti-depressant action. Tricyclics also are known to be useful adjuncts to pain relief modalities.

Thus the regimen of anti-neuritic pain relief and anti-depressant therapy has become close to the author's standard.

VI. IMPLICATIONS FOR PROTECTION STRATEGIES

It was hoped that this study would indicate clearly particular groups of subjects that were at risk of injury due to their physical circumstances, and thus to allow the authorities to concentrate on protecting those particular individuals. This has not turned out to be the case. The only positive association which could be drawn from the study was the association with power system strikes and the severity of cross coupling between the power system and the telephone system. This is something that is not altogether unknown already. Perhaps the study can be regarded as providing positive reinforcement for the insistence on earth bonding between the telephone system and power supply system by Telecom as a matter of priority in service protection.

Particularly, no geographical or terrain feature, or feature of storm intensity has been found to be significant in this study even though the numbers were small. The only formal parameter not measured has been earth resistivity. Otherwise the study is felt to be have been comprehensive.

VII. CONCLUSIONS

This study has provided the first prospective detailed examination of people struck by lightning which was mediated via the public telephone system. It has had a gratifyingly high response and in the currently Australian climate, represents a comprehensive examination of the injuries. The broad findings of the previous retrospective study have been confirmed in that the majority of injuries seen, and particularly those of severe degree, are local to the line of current and not mediated centrally. The best predictors of severity of injuries and their duration are the presence of musculoskeletal pain and the presence of symptoms lasting longer than possibly three days, and at least one week. The major physical parameter found to be of significance in predicting injury severity has been the presence of power system damage and this provides a measure of reinforcement for the current policy of regarding earth bonding as a significant step in system protection. Impressions of treatment have also been given particularly recommending the use of anti-neuritic pain relief, and anti-depressant therapy.

VIII. REFERENCES

Andrews, C.J., Darveniza, M., *Telephone Mediated Lighting Injury; An Australian Survey*, Proceedings 3rd International Conference Lightning Static Electricity, National Severe Storms Lab, Norman Oklahoma, 1988.

Eriksson, A., Ornehult, L., *Death by Lightning*, American Journal of Forensic Medicine and Pathology Vol. IX, issue 4, pp. 295–300, 1988.

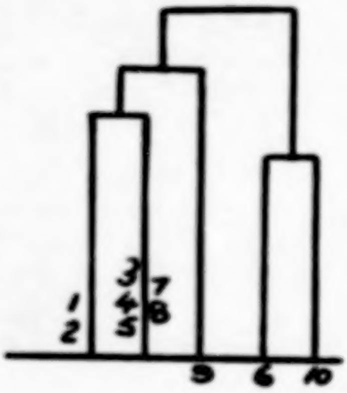

Fig 1. Dendrogram Analysis I

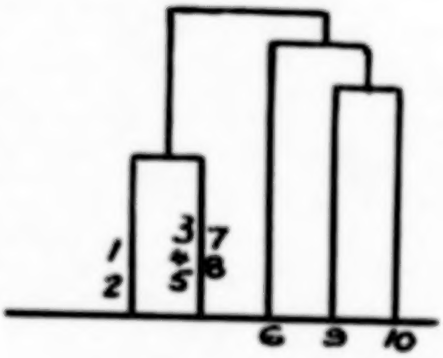

Fig 2. Dendrogram Analysis II

TABLE I RAW SYMPTOM SUMMARY

	RESPONDENT										KEY
PARAMETER	1	2	3	4	5	7	8	9	6	10	
Short Term Symptom	(Non Significant p < .05)										
Loss of Conc.	A	N	N	N	A	A	A	Y	A	N	A=Altered Conc. Y=Yes N=No
Ear Paraesthesia	+									++	
Pain		+								+++	
Tinnitus	+	+									
Burns Presence	Y			Y				Y			
Site	3			1				2			1=arm,leg,chin 2=mouth 3=singed hair
Arm Paraesthesia									++	++++	
Pain									++	++++	
Facial Swelling	+									++	
Nausea/Pain abdo		N						P	P		N=nausea P=pain
Tachycardia							++	+		+	
Haemoptysis								+			
Muscular Pain						1,3		2		3	1=Thorax 2=Back 3=Neck
Duration of initial Sympts	5	2	0	2	0	3	1	3	1	3	(Days)
Long Term Symptoms	(All significant p <.05)										
Nil	Y	Y	Y	Y	Y	Y	Y				
Duration								C	C	C	Currently Continuing
Psych. upset									+++	+	
Abdominal Pain								+	+		
Arm Pain/Paraes									+	+++	
Weakness										+++	
Headache									+		
Muscular Pain								+		+++	
Examination	In all cases, objectively normal										

TABLE 1 (continued)

	RESPONDENT										KEY
PARAMETER	1	2	3	4	5	7	8	9	6	10	
Telecom "Physical" Data			(*	significant p <.05				Analysis 1)			
(supplemented by teams data)			(+	significant p <.05				Analysis 2)			
Location	U	U	R	R	U	U	R	U	S	U	U=Urban S=Suburban R=Rural
Topography	F	H	F	U	F	F	H	F	H	U	U=undulating H-hilly F=flat
Distance to nearest hill		20		200			0		25		(metres)
Storm intensity	L	L	L	L	M	S	S	M	?	L	Light, Mod, Severe
Concurrent Lighting	N	M	O	O	M	N	F	F	?	O	Light, Occas, Mod, Freq
Strike Distance	400	N	N	N	N	200	N	250	25	N	Not known, Otherwise Metres
Local Storm History	M	M	L	?	L	M	M	L	M	M	Light, Moderate
Power System Feed	O	U	O	O	U	O	O	U	O	U	)Overhead, Underground
Retic	O	U	O	U	U	O	U	U	U	U	)
Damaged in Strike	N	N	N	N	N	N	N	N	Y	N	* +
Appliances Damaged	N	Y	N	N	N	N	N	N	N	Y	* +
Phone Feed	U	U	U	O	U	U	U	U	U	U	
Retic	U	U	U	O	U	U	U	U	U	U	
Phone Damage	1	3	0	1	1	0	0	4	0	3	Scale 0-4
Building Constr.	B	B	T	B	B	B	F	B	B	C	Fibro, Brick, Concrete
High/Low Set	L	L	H	L	L	L	L	L	L	H	
Roof	M	T	M	?	T	M	M	M	T	.	Metal, Tile, .=Not applicable
Building Frame	M	T	T	T	T	T	M	M	T	?	Metal, Tile, ?=Unknown
Floor Height	O	O	A	O	O	O	O	O	O	A	On/Above ground
Floor Material	C	C	T	C	C	T	C	C	T	C	Timber/Covered Concrete
Body Contact	O	O	O	G	O	P	P	P	P	G	Good/Poor/No Earth
Shoes	N	N	N	Y	N	Y	N	Y	Y	Y	+
Handset Thrown	Y	N	Y	Y	D	D	N	Y	N	Y	Yes/No/Dropped
Service made faulty	Y	Y	N	Y	Y	N	N	Y	N	Y	
Sparks seen	N	N	N	Y	Y	N	N	Y	Y	N	
Self Thrown	N	Y	N	N	N	N	N	Y	N	Y	+
Acoustic Shock	3	3	0	0	0	2	1	0	0	0	Scale 0-3

STEP VOLTAGE ANALYSIS FOR THE CATENOID LIGHTNING PROTECTION SYSTEM

J.C. Chai, R. Briët, D.L. Barker, and H.E. Eley

The Aerospace Corporation
P.O.Box 92957, M4/934
Los Angeles, CA 90009

ABSTRACT

The main objective of the Aerospace Corporation-proposed overhead Catenoid Lightning Protection System (CLPS) is personnel safety. To ensure working personnel's safety in lightning situations, it is necessary that the potential difference developed across a distance equal to a person's pace ('step voltage') does not exceed a separately established 'safe voltage' in order to avoid electrocution (ventricular fibrillation) of humans. Therefore the first stage of the analytical effort is to calculate the open-circuit step voltage. In this paper we develop an impedance model for this purpose, which takes into consideration the earth's complex impedance behavior and the transient nature of the lightning phenomenon. In the low frequency limit, this impedance model is shown to reduce to results similar to those predicted by the conventional resistor model in a DC analysis.

INTRODUCTION

Lightning presents a major *recurring* concern in space launch operations. Today's space launch requires a great deal of preparation, and any delay of launches due to adverse weather conditions, such as lightning, would result in considerable schedule and cost impact. For example, Range Safety requires that personnel be evacuated when a possible lightning storm is expected to occur within five nautical miles (9.25 km) of the launch complex when solid propellants are present. The result is, among other things, a significant loss of man-hours and many delayed launches. While all hazards from lightning cannot be completely eliminated, it is a fact that a system and working personnel can be made relatively immune to lightning effects by well-planned protection schemes. The Aerospace Corporation-proposed overhead Catenoid Lightning Protection System (CLPS)[1] as shown in Figure 1, which is designed to divide and divert lightning currents away from the work areas beyond the perimeters of the launch pad, is such an example. Since its main objective is personnel safety, one of the first questions to be answered is: what is the potential difference developed between a person's feet one meter apart (commonly known as the 'step voltage')[2] within the CLPS umbrella when a direct lightning attachment to the catenary wires or fuel vents occurs? This voltage, when compared to a separately established 'safe step voltage' to avoid ventricular fibrillation (electrocution) in humans, would define a safe zone for working personnel. MIL-STD-419A utilizes a 1000-volt maximum *safe* step voltage for humans in situations such as a lightning environment.

To predict the open-circuit step voltage, a resistor model for the soil is usually used in a DC analysis. In studying ground hazards due to lightning for the CLPS, The Aerospace Corporation first proposed a soil resistor model which consists of two different soil layers each with different resistivities. While this approach is consistent with available literature[3,4], it was felt that because of the transient nature of lightning and the complex impedance behavior of the medium (e.g. soil, water, etc.), a transient analysis of the situation, especially when personnel safety is at issue, is necessary. The need for a transient analysis becomes clearer when the adequacy of the DC analysis for lightning events is re-examined in terms of the skin depth [4] $\delta = \sqrt{2/\mu\omega\sigma}$, where $\mu = 4\pi \times 10^{-7} Henry/m$ is the permeability of the medium, $\omega = 2\pi f$ is the angular frequency of the lightning current, and $\sigma = 1/\rho$ is the conductivity with ρ as the resistivity of the medium. For a DC analysis to be valid, the skin depth has to be *large* (say, ten times larger) compared to the grounding system (in this case, the ground rod at the end of a catenary wire). For a nominal soil resistivity of 40Ω-m and a lightning frequency of 100kHz, the skin depth is approximately 10 meters which is about the same length as a typical ground rod. Therefore, an approach different from the conventional DC analysis has to be adopted. For this reason we propose to use an impedance model for the media and perform a simplified transient analysis to predict the step voltage.

---

[1] H. Hastings, & H.E. Wilson, Aerospace Corp., private communications.
[2] 'IEEE Guide for Safety in Substation Grounding', IEEE Std 80-1976.
[3] MIL-HDBK-419A, Volume I, Chapter 2, 20 December, 1987.
[4] A.P. S. Meliopoulos, 'Power System Grounding and Transients', Chapter 5, Marcel Dekker, Inc., 1988.

IMPEDANCES OF MEDIA AND INJECTION CURRENTS

In this paper we propose to model the ground as a two-layer medium with complex impedances (see Figure 2), and compare it with the two-layer resistor (DC) model. The upper layer represents the dry soil and the lower layer consists of the water-saturated earth below. In practice, the length of the ground rod is chosen to ensure that good contact is established with the more conductive lower layer for that location. The frequency dependence of the medium impedance is well known in problems related to electromagnetic propagation in media such as soil and water[5]. The intrinsic impedance of a medium for the electromagnetic wave propagation $Z(\omega)$[6] in ohms is given by

$$Z(\omega) = \sqrt{\frac{\mu_o}{\epsilon\left(1 + \frac{\sigma}{j\omega\epsilon}\right)}} \tag{1}$$

where μ_o is the permeability for non-ferromagnetic media such as free space, soil and water, and ϵ for the upper soil layer is taken to be twelve times the free space permittivity [6]. In this analysis the above impedance is assumed for the current wave propagation through the two-layer soil medium. The dependence of $Z(\omega)$ on the upper soil layer depth (L) has been introduced implicitly through the average soil resistivity, for example, at $L = 3$ meters. Based on our measurements of ρ at Launch Complex #41 at Cape Canaveral Air Force Station (LC41/CCAFS)[7], it is found that the general dependence of ρ on L is difficult to quantify. However, since our measurements show that beyond soil depth $L \sim 3$ meters, ρ has, in general, a value around $\leq 20\Omega \cdot m$ because of saturation with salty underground water, therefore $Z(\omega, L = 3 \text{ meters})$ is chosen in this analysis to illustrate the methodology. The transient source current $i(t)$ due to lightning is taken to be a double exponential waveform[8], although any other lightning waveforms can also be used:

$$i(t) = i_o \cdot \left(e^{-\alpha t} - e^{-\beta t}\right) \tag{2}$$

which has the complex form in the frequency domain by Fourier transformation:

$$I(\omega) = i_o \cdot \left(\frac{1}{\alpha + j\omega} - \frac{1}{\beta + j\omega}\right) \tag{3}$$

where $j = \sqrt{-1}$, α is equal to 1/25, β is equal to 1/1.5, time t is in μSec, and i_o is the current amplitude at the ground injection point. In case of a direct lightning attachment to the lightning rod on top of the catenary tower which is deemed to be most probable, the peak lightning current of 255kA is assumed to be equally divided among 10 catenary wires, resulting in a 25.5kA peak current on each catenary wire at the ground injection point. Note that for an asymmetric structure like the proposed Catenoid System, the simplistic way of dividing current equally is not true even for the DC case, let alone in the transient situation where cross couplings and re-radiations among all structures and wires are known to exist. However, as a *scoping* effort, we feel this current division is a reasonable simplification.

---

[5] K.S.H. Lee, Ed.,'EMP Interaction: Principles, Techniques and Reference Data', AFWL-TR-80-402, December 1980.

[6] Vance, 'Coupling to Shielded Cables', Wiley-Interscience, 1978.

[7] R. Babb & J.C. Choi, 'Additional Measurement Data on Soil Resistivities at LC41/CCAFS', Aerospace Memo #90(5217-JC)03, January 24, 1990.

[8] An approximate analytical form for the lightning waveform specified in 'Military Specification, Bonding, Electrical, and Lightning Protection for Aerospace Systems', MIL-B-5087B, 31 August, 1970.

A direct lightning attachment to the existing vent towers protruding outside of the catenary system can also occur, although with lower probability. The injection current at the vent tower will be larger due to fewer dividing wires (e.g. four wires in this case), which will result in a greater potential difference, also because of closer proximities to the work areas.

TRANSIENT ANALYSIS AND STEP VOLTAGES

The potential $E(z)$ due to a current flow I_s at z in a two-layer medium (Figure 2), according to the resistor (DC) model [3 and 4] is given by

$$E(z) = \frac{0.366\rho_s I_s}{L} \cdot \log_{10}\left[\frac{L}{z} + \sqrt{1 + \left(\frac{L}{z}\right)^2}\right] \tag{4}$$

where L is the upper soil layer depth of resistivity ρ_s, and I_s is the DC current flow through the upper soil layer which is explicitly dependent on L and can be found by the proportional DC current relation to ρ's and L's of the two soil layers[*]. The step voltage between z meters and $(z+1)$ meters from the current injection point predicted by the DC model is then

$$V_{DC_{step}}(z) = E(z) - E(z+1) \tag{5}$$

In our analysis a simplified approach is adopted to give an estimate of the *transient* effects. The total ground current $I(\omega, z) = I(\omega)e^{-\gamma(\omega)z}$ at a distance z from the ground injection point is divided, according to the current division rule in the AC circuit analysis, to yield the residual current flowing in the upper layer of soil:

$$I_s(\omega, z) = \frac{Z_w(\omega)}{Z_w(\omega) + Z_s(\omega)} \cdot I(\omega, z) \tag{6}$$

where $Z(\omega)$ is the complex impedance, and subscripts s and w represent upper layer soil and lower layer wet soil, respectively. The propagation constant $\gamma(\omega)$ which contains an attenuation factor and a phase factor is included in the model. The potential difference between a distance of z meters and $(z+1)$ meters from the current injection point in the surface soil layer, known as the step voltage, then follows directly

$$V_{step}(\omega, z) = [I_s(\omega, z) - I_s(\omega, z+1)]Z_s(\omega) \tag{7}$$

The Fourier transform of V_{step} to the time domain will yield the waveform of $v_{step}(t, z)$, whose maximum value is then picked as the step voltage for each distance z from the source of injection. For this analysis, the upper soil resistivities, ρ_s, used were 1500 and 100 $\Omega \cdot m$, which represent two typical values for the dry and wet upper soil layers at the launch site, while the lower layer starting at a depth of $L = 3$ meters is less influenced by weather and was taken to be a constant $\rho_w = 20\Omega \cdot m$. The calculations were repeated for various distances from the current injection point ranging $z = 3$ to 46 meters. The analysis can, of course, be carried out for other layer depths with different resistivities.

RESULTS

The step voltages with catenary wire current injection calculated using the impedance model are shown in Table I, which are also plotted in Figure 3 for easy visualisation. As expected, a more resistive upper soil layer (e.g. $\rho_s = 1500\Omega \cdot m$ vs. $\rho_s = 100\Omega \cdot m$) results in a larger step voltage. It shows that in order to keep the step voltage below a fixed voltage, say, one thousand volts, the distance from the injection point should be greater than 41 meters for $\rho_s = 1500\Omega \cdot m$, while for $\rho_s = 100\Omega \cdot m$ the distance is 18 meters.

A comparison of the impedance model results (injection by Catenary Wire) with those of the resistor model is shown in Figure 4 for $\rho_s = 100\Omega \cdot m$. It shows that in order to keep the step voltage below a fixed voltage, say, one thousand volts, the 'keep-out' distance is only 3.5 meters for $\rho_s = 100\Omega \cdot m$ by the resistor model prediction, while a 18-meter distance is required by the impedance model. However, in order to fairly assess the safety issue for humans in lightning situations, the *human body impedance*[10] and induced human body currents have to be included in the consideration to establish a safety standard. Very little is available in the open literature regarding the current level versus frequency required to produce ventricular fibrillation in humans, although it has been known[11] that higher currents can be tolerated at higher frequencies (or shorter durations).

---

[*] H.E. Eley, 'Step Potential with the Overhead Lightning Protection System', Aerospace Memo #3530.HEE.2251I, 9 March, 1990.

Calculations were also performed for two different current injection scenarios: catenary wire current injection and vent towers (oxidiser vent stack and fuel vent stack) current injections. Table II gives a comparison of the step voltages due to these two different current injection scenarios for the closest points in the work area. For illustration purposes, the work area is assumed to be a 30-meter square at the center of the launch pad (see Figure 1(b), Top View). Of course, there are other areas (e.g., near the vent towers) that may also be designated as work areas which can be considered using the same methodology. It can be seen from Table II that vent tower wire current injections result in much greater step voltages, thus posing greater risks for personnel safety if the lightning is to attach itself to the vent towers which protrude outside the protective region of the proposed catenary system.

Since the step voltage is crucial to personnel safety, a verification of this quantity is of utmost importance. Short of the actual measurements of the step voltage in a lightning environment, the impedance model can be checked to see if it can be reduced, in the *low frequency* limit, to the resistor model, i.e.,

$$\lim_{\omega \to 0} [V_{step}(Z(\omega))] = V_{DC_{step}}(R) \tag{8}$$

where $Z(\omega)$ is the complex impedance and R is the DC resistance of the upper soil. This was accomplished by using 8 kHz as the low frequency cut-off of the impedance model. It was found that at 10 meters and $\rho_s = 100\Omega \cdot m$, the low frequency approximation of the impedance model yields a step voltage of 177 volts, while the resistor model result is 168 volts. This lends some confidence to the analytical validity of the impedance model and the transient analysis.

CONCLUSIONS

The study of step voltage for the CLPS leads to the following observations:

- In comparison to the resistor model, the impedance model predicts:
  - A higher (~ 3x) step voltage at all distances. This could result in a larger 'keep-out' distance; however, the human body response as a function of the lightning frequency needs further investigation in order to establish a safety zone.
  - A similar attenuation of step voltages as the distance increases.
- The vent tower current injection scenario results in greater step voltages, and thus poses greater threat to personnel safety in the assumed work area. Some measures to reduce this threat may need to be addressed.
- At low frequencies, the impedance model can be reduced to yield similar results as the resistor model. This lends some *analytical* credibility to the model and analysis.

---

[10] For example, human body impedance as measured and calculated by A.W. Guy, 'Analysis of Time Domain Induced Current and Total Absorbed Energy in Humans Exposed to EMP Electric Fields', Bioelectromagnetics Research Laboratory, University of Washington, Final Report, June 30, 1989.

[11] T. Bernstein,'Effects of Electricity and Lightning on Man and Animals', Journals of Forensic Sciences, Vol. 18, No.1, January 1973, and 'Electrocution and Fires Involving 120/240-V Appliances', IEEE Transactions on Industry Applications, Vol. IA-19, No.2, March/April, 1983.

- It is of utmost importance to ensure personnel safety at launch sites in lightning situations. To fully verify the prediction of step voltages which concerns personnel safety (the major purpose of the CLPS), a well-conducted *dynamic test* in a simulated lightning environment is necessary.

ACKNOWLEDGEMENT

This study was conducted in support of the AF/SSD Titan IV Program. The authors would like to express their appreciation of H. A. Heritage and H.Z. Wilson for the valuable discussions of their design concepts of the catenoid system. Also, thanks are due to the ground supporting crews of the ETR for their help in obtaining the resistivity measurements at LC41/CCAFS.

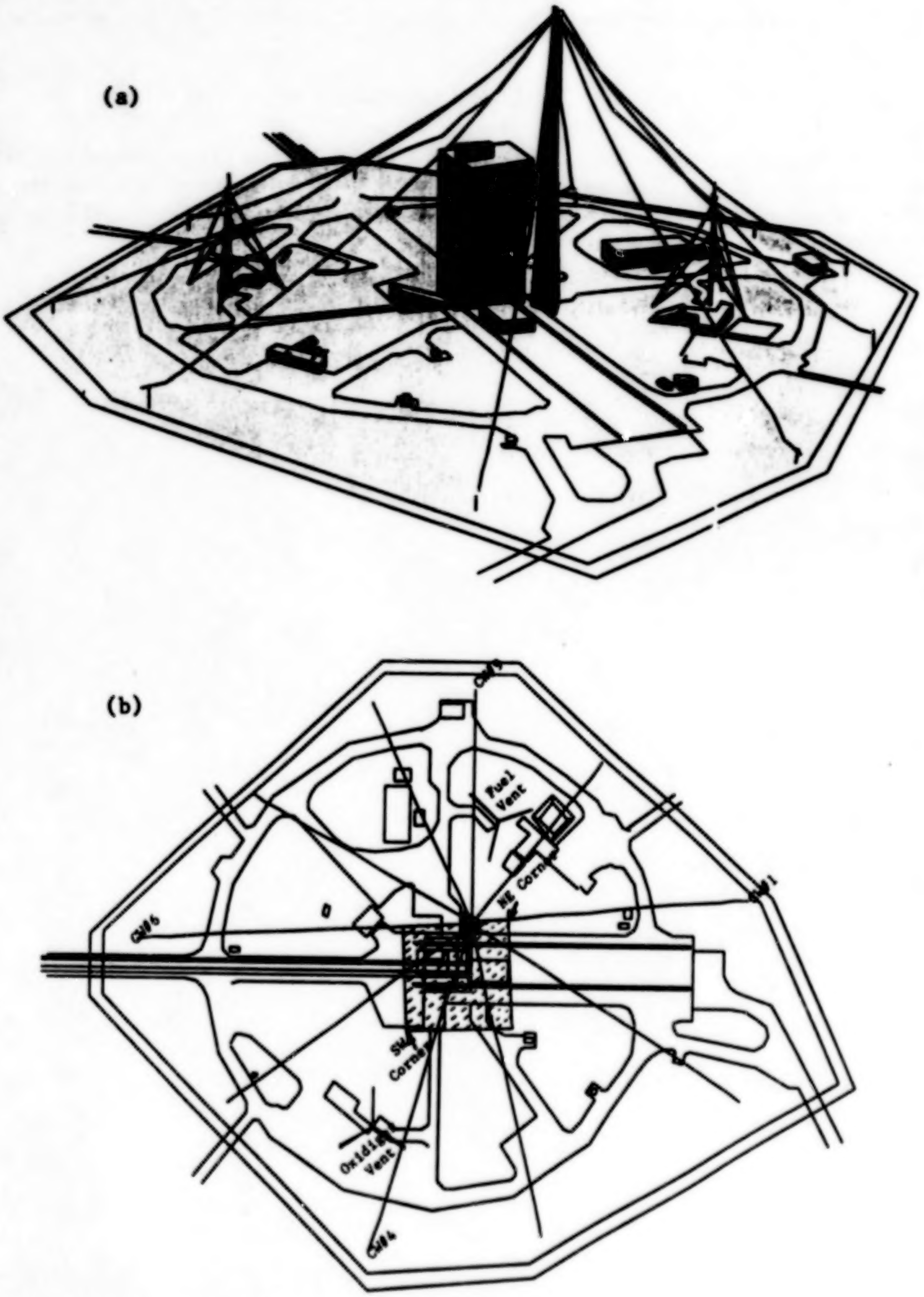
(a)
(b)
CW#6
CW#1
CW#4
Fuel Vent
NE Corner
SW Corner
Oxidizer Vent

Figure 1. Artist's Rendition of the Overhead Catenoid Lightning Protection System (CLPS) at Launch Complex #41 at Cape Canaveral Air Force Station: (a) Slant View. (b) Top View, shaded area is the assumed work pad.

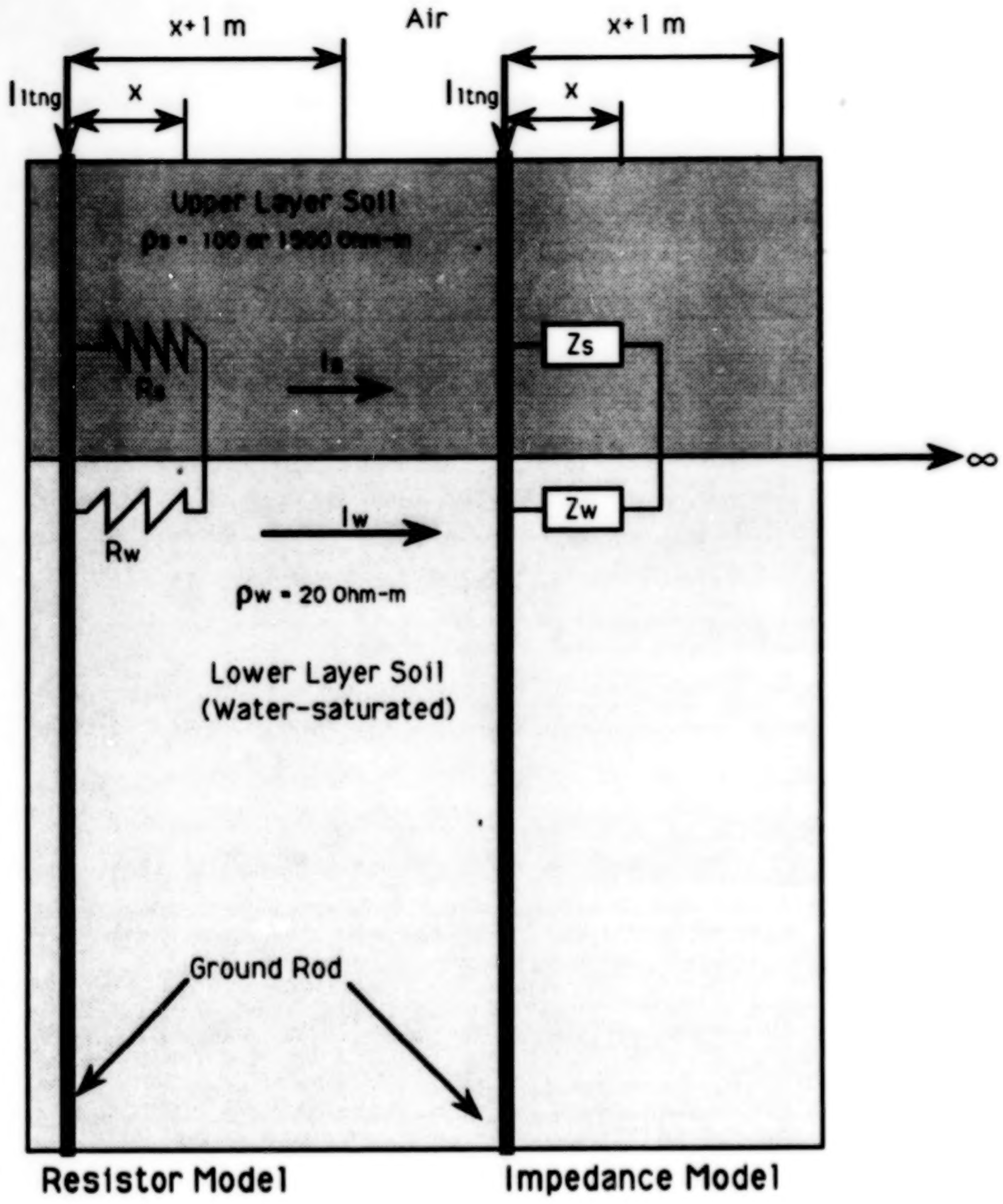
Air
x+1 m
x
I ltng
x+1 m
x
I ltng
Upper Layer Soil
ρs = 100 or 1500 Ohm-m
Rs
Is
Zs
Rw
Iw
Zw
∞
ρw = 20 Ohm-m
Lower Layer Soil
(Water-saturated)
Ground Rod
Resistor Model
Impedance Model

Figure 2. Resistor Model and Impedance Model for the Calculation of Step Voltages.

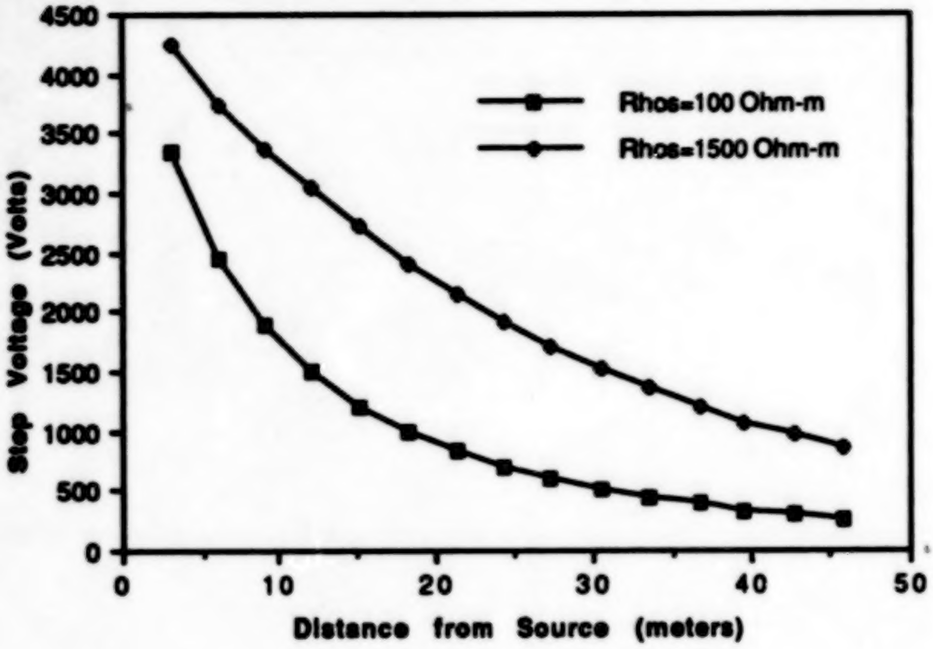

Figure 3. Comparison of Step Voltages by the Impedance Model for Different Upper Soil Resistivities $\rho_s = 1500\Omega \cdot m$ and $\rho_s = 100\Omega \cdot m$.

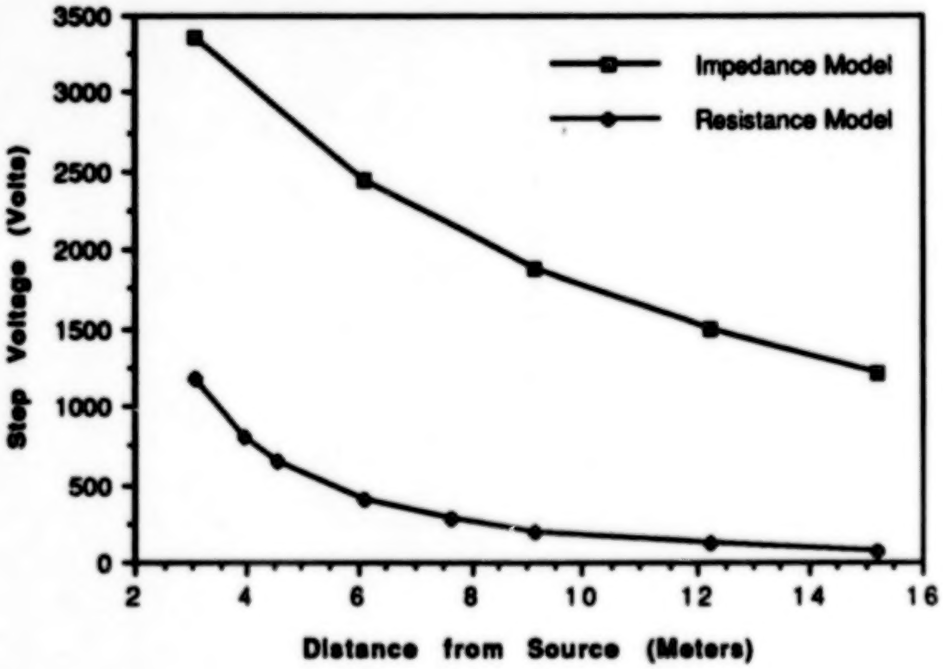

Figure 4. Comparison of the Impedance Model and the Resistor (DC) Model for $\rho_s = 100\Omega \cdot m$.

Table I. Step Voltages by Catenary Wire Current Injections
('Full Impedance Model' with $\rho_w = 20\Omega \cdot m$).

Source Distance		Step Voltages (volts)	
xft (feet)	x (meters)	$\rho_s = 1500\Omega \cdot m$	$\rho_s = 100\Omega \cdot m$
10	3.05	4245	3355
20	6.10	3740	2453
30	9.15	3370	1886
40	12.2	3047	1494
50	15.2	2714	1209
60	18.3	2401	995
70	21.3	2136	829
80	24.4	1909	698
90	27.4	1713	594
100	30.5	1527	509
110	33.5	1361	439
120	36.6	1205	382
130	39.6	1070	334
140	42.7	969	293
150	45.7	857	259

Table II. Step Voltages by Catenary and Vent Tower Wire Current Injections
for $\rho_s = 1500$ and $100\Omega \cdot m$ (Both with $\rho_w = 20\Omega \cdot m$)

Work Area	Current Injection Scenarios	Step Voltage (Volts) $\rho_s = 1500\Omega \cdot m$	Step Voltage (Volts) $\rho_s = 100\Omega \cdot m$
Southeast Corner	Oxidiser Vent	998	320
	CW #4	209	35.3
Northwest Corner	Fuel Vent	1214	417
	CW #9	169	29.1

HARDENING COMMUNICATION PORTS FOR SURVIVAL IN ELECTRICAL OVERSTRESS ENVIRONMENTS

O. Melville Clark
General Semiconductor Industries, Inc.
Tempe, Arizona

ABSTRACT

Greater attention is being focused on the protection of data I/O ports since both experience and laboratory tests have shown that components at these locations are extremely vulnerable to electrical overstress (EOS) in the form of transient voltages. Lightning and electrostatic discharge (ESD) are the major contributors to these failures; however, these losses can be prevented. Hardening against transient voltages at both the board level and system level has a proven record of improving reliability by orders of magnitude. This paper will review the EOS threats, typical failure modes and transient voltage mitigation techniques. Case histories will also be reviewed.

ORIGINS OF ELECTRICAL OVERSTRESS

Electronic systems transmit and receive vital information through sensitive communication ports. These vulnerable interfacing microcircuits are connected directly to signal lines which are often exposed to lightning to a varying degree. Electrical storms produce transient voltages on data lines which can range up to 300V or higher [1]. Failures of line drivers and line receivers occur at transient levels ranging from 40V to 90V [2], a level which is easily attained in long wire lengths which interconnect components of distributed systems.

Lightning discharges can produce high electromagnetic fields which can couple into signal lines. For example, Masters, et al, reported a voltage of 150kV induced on a 460m long open suspended wire caused by a lightning stroke 2.5km away [3]. This amounts to 325V induced for each meter of wire.

Lightning induced short circuit currents are another measure of electrical stress to which data I/O ports are subjected. After dielectric breakdown in the component, current produces excessive heat and damage. Data showing current levels induced into computer signal lines have not been reported; however peak currents induced into telephone subscriber loops have been reported by Bell Telephone Laboratories and are shown in figure 1 [4]. This graph indicates peak transient currents up to 50A can be expected on data lines with outdoor exposure.

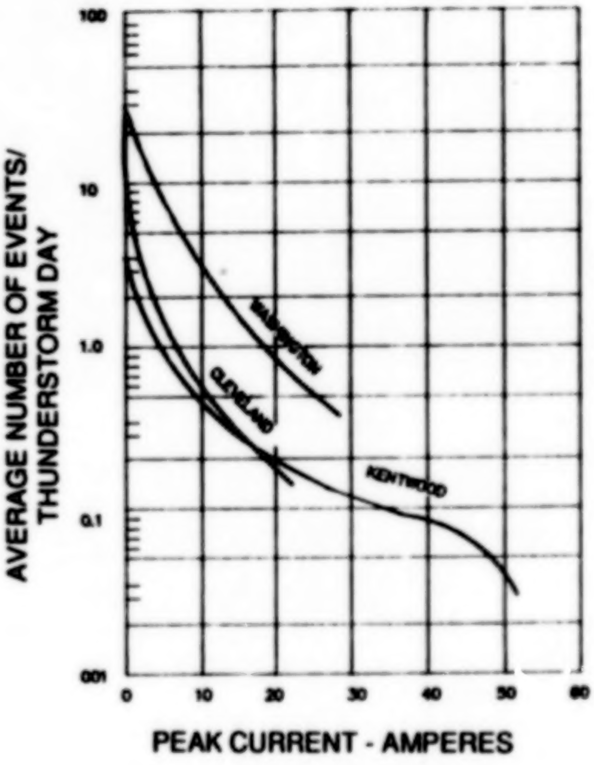

Figure 1. Peak Currents Induced Into Telephone Lines

ESD is also a major threat, producing an estimated 30% to 50% of all electronic equipment failures [5]. This is understandable, considering the low failure threshold levels of microchips reported by the Reliability Analysis Center [6]. ESD failure levels for

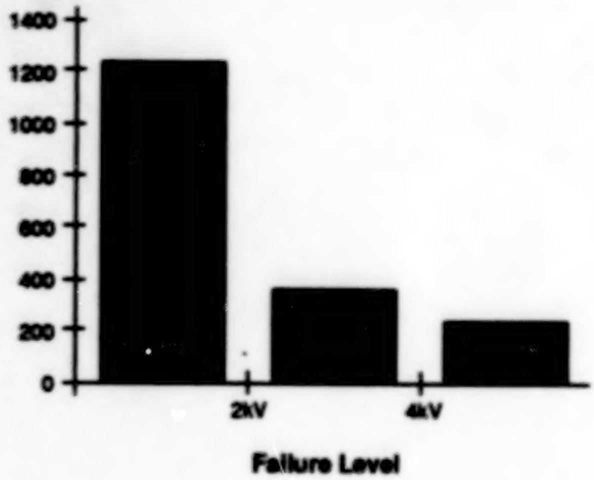

Figure 2. ESD Failure Levels For All Bipolar Devices

bipolar devices are shown in figure 2. In this graph, the vertical scale represents the number of parts which failed at a given level. CMOS structures fail at approximately the same stress levels. Since the fingertip can't feel ESD levels below 3000V, it is possible to kill a device without knowing it.

Line receivers are generally observed to have a higher failure threshold level than line drivers which can latch-up under transient conditions, subsequently producing excessive power dissipation in the device and eventual failure.

Increasing equipment losses have produced a growing sensitivity to data I/O port failures. Although industry is becoming more aware of protection needs, most computers and microprocessor based equipment in use have little or no built-in protection. Normally, only after the need has been established through excessive occurrence of field failures is corrective action taken.

TRANSIENT PATHS

Pathways to communication, or data I/O ports, are by electromagnetic coupling or direct injection into the data lines. Direct hits by lightning are rare, but injection of body generated ESD can happen while handling plugs and sockets of communication ports.

Direct strikes to buildings can also inductively coupled transient voltages into data lines from metal building framework. Since lightning typically has a current of 25kA peak, this is sufficient to produce currents of several kiloamperes through a given segment of building framework which can induce voltages into nearby conductors. In one reported case, the data port of an unprotected printer was damaged by lightning current through structural steel.

Nearby power wiring which runs parallel to data lines has been reported to cause computer system upset [7]. Radiation from the adjacent power lines, caused by load switching, can produce disturbances which corrupt data transmissions.

Transients on power lines have been reported to damage I/O ports of a printer shared with multiple PCs [8]. Failure was attributed to EOS caused by a ground loop since all components were not connected to the same ground window. Protection across the data I/O ports would have prevented this failure.

FAILURE MODES

The three basic failure modes include hard, upset and latent. Hard failures are those components which are permanently damaged and must be replaced to restore equipment to normal operation. Their appearance can be deceiving since microscopic damage cannot be seen from the exterior. An example of this type of failure is shown in figure 3. This is a transceiver chip which failed from induced lightning.

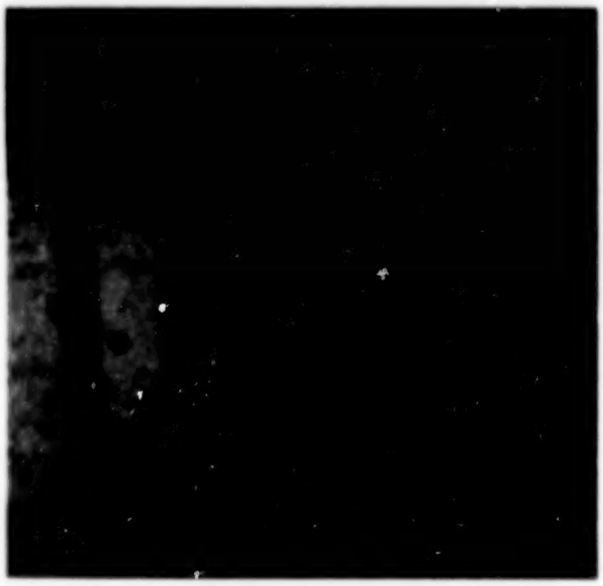

Figure 3. Failed Transceiver Chip

Line drivers which fail in a latch-up mode produce excessive heat and often results in charring of the component along with severe damage to the circuit board material. An example of latch-up failure of an RS-232 line driver is shown in figure 4. This type of failure could be a contributing factor to computer room fires which occur at the rate of 400 per year in the US [9]. Direct hits often cause components to explode or vaporize.

Figure 4. Line Driver Latch-Up Failure

Upset is a temporary malfunction which is usually associated with data loss or file corruption although the results may sometimes be catastrophic. In March 1987, an Atlas Centaur launch vehicle was struck, causing overwrite of the guidance control memory, resulting in destruction of the rocket and its payload [10].

Latent failures are the "walking wounded" which are zapped once but at an insufficient level to cause immediate failure but still causing degradation of the part without noticeable loss of performance. These devices eventually fail but some have survived up to a period of five years [11].

PROTECTIVE DEVICES

Transient voltage suppressor (TVS) devices protect data I/O ports by limiting voltage spikes to levels safely below component destruct thresholds. Suppressor devices also divert unwanted currents away from the protected components and in the process consume part of the transient energy. A properly selected TVS protects by limiting voltage spikes but does not interfere with circuit performance.

The three most commonly used TVS devices include gas discharge tubes, metal oxide varistors (MOVs) and silicon TVSs. For some telephone applications, the use of bilateral voltage triggered thyristors is growing.

Gas discharge tubes are characterized by multikiloampere capability. Impulse firing voltages usually start at 500V which is too high for microchip protection but adequate for nonsensitive circuits. Gas tubes are best suited for and frequently used in multistage protectors which are discussed later.

Metal oxide varistors (MOVs) are voltage dependent nonlinear resistors composed of zinc oxide granules in a matrix of bismuth oxide and other metal oxides. These devices are bilateral and electrically resemble two zener diodes back-to-back. Advantages of MOVs are low cost and high current handling on a limited basis. Their main disadvantage is high clamping voltage when compared to silicon TVS devices. MOVs are best suited for protection across ac power lines.

Silicon TVS devices use large area pn junctions mounted between metal heat sinks to dissipate the heat produced during suppressive action. These components are rated lower in peak current than gas tubes or MOVs; however, they consistently perform at rated levels with virtually no wearout. Silicon TVSs clamp at predictably lower levels than other TVS devices making them ideal for protecting sensitive microchips.

A comparison of clamping ability of both MOV and silicon TVS devices is illustrated in figure 5. Both parts were comparably rated for operating voltage and pulse current rating. Each device was surged with a 1.2/50us transient voltage spike (1.2us rise, 50us for decay to one-half peak value). Peak open circuit voltage is 1500V and peak current is 50A through each device. In this graph, the vertical scale is 5V per division and the horizontal scale is 10us per division.

Clamping under transient conditions is a qualitative measure of protective capability. Note that the MOV clamps at 19V but the silicon suppressor protects at a much lower level of 7V.

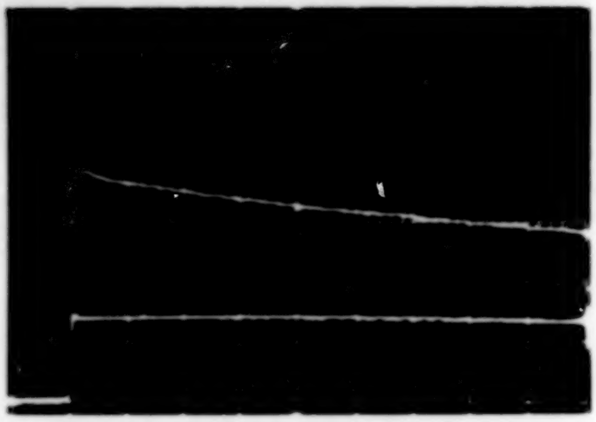

Figure 5. MOV and Silicon TVS Clamping

Some data/communication interfaces are interconnected with lines of one kilometer or more in length, which are exposed to harsh lightning environments. Protectors for these applications are usually multistage, using an up-front high current rated TVS such as a gas discharge tube. A low clamping voltage device such as a silicon TVS is often used in the second stage with an intervening impedance to develop sufficient voltage to fire the gas discharge tube. The topology for this circuit is shown in figure 6.

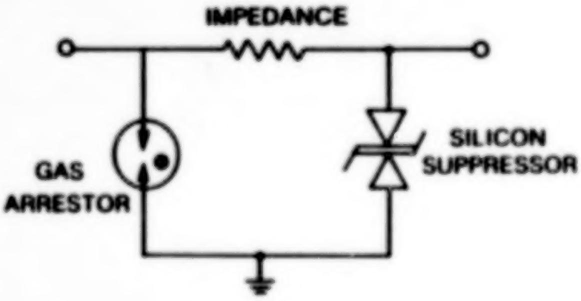

Figure 6. Multistage Suppressor Topology

Typical performance for an RS-232 signal transient voltage surge suppressor (TVSS) using a multistage suppressor containing an up-front gas tube followed by a silicon TVS is shown in figure 7. This illustrates the transient voltage reduction from 1500V down to an acceptable level below 40V, which is the failure threshold for these communication interfaces. The scale is 10V per division vertically and 5us per division horizontally.

During the first 37us of suppressor conduction, normal data flow is lost. The software should recognize this condition and ask for a retransmission.

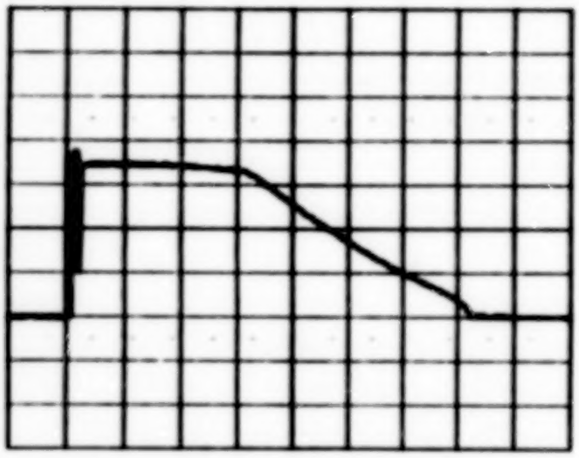

Figure 7. Multistage Suppressor Performance

GUIDELINES FOR TVS SELECTION

The main electrical parameters to be considered in selecting a TVS for I/O port protection are:

1. Maximum operating voltage (Vr)
2. Maximum clamping voltage (Vc)
3. Peak pulse current capability (Ipp)

The maximum operating voltage is the peak voltage, including high side of the tolerance, at which a device is designed to operate without drawing appreciable current. This level is typically ten percent below the minimum breakdown voltage, that voltage at which the device begins to conduct current.

Maximum clamping voltage is the highest voltage that will appear across the protected component under conditions of maximum rated peak pulse current. This is the protection level that is provided to the I/O port across which the device is connected.

Devices are available as unidirectional, for dc line protection and also as bidirectional for ac and other positive and negative going signals. Most data I/O ports use bidirectional devices. For high data transmission rates, the inherent capacitance in low voltage, large area silicon TVS may significantly attenuate signals. Specialized low capacitance TVSs are available for these applications.

These general guidelines for TVS selection apply for both board level and system level protection applications which are described in the following paragraphs.

BOARD LEVEL PROTECTION

Discrete components are available, with operating voltage levels over the range of 5V through 25V which includes most signal lines. These are also available for the higher voltage commercial telecom voltages.

Both through-hole axial lead and surface mount devices are available as industry standard components. Some devices are supplied as multiple components in 8 pin and 16 pin industry standard DIP packages for applications where space is limited.

Silicon TVSs are rated in terms of peak power capability, which is associated with the cross sectional area of the suppression element. The types normally used on PC boards for data I/O port protection are the 500W and 600W rated types. For example, an SMBG24CA surface mount silicon TVS would be a good selection for protecting RS-232 I/O ports as this device operates at +/- 25V and can handle pulse currents of 75A for 8/20us waveforms.

Placement of the protector is extremely important for optimum protection. The shunt current path through the protection circuit must be minimum for optimum protector performance [12]. Parasitic inductance in the suppressor leads contributes to L(dI/dt) effects which can be significant for fast rise-time transients originating from ESD and NEMP.

The protector should be placed as close as possible to the signal input terminations on the board to minimize radiation into other components on the board. The ground reference should likewise furnish a low impedance path between all suppressors as illustrated in figure 8.

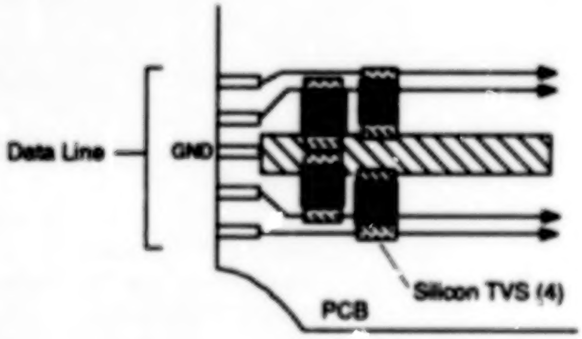

Figure 8. On-Board Suppressor Installation

A well designed protection scheme should protect I/O ports from body generated ESD and induced lighting into a system which is all contained within the same building structure. For distributed systems, which includes interconnected equipment in several separate buildings, additional higher current protection is required as described in the following section.

SYSTEM LEVEL PROTECTION

Networked and distributed systems usually have long interconnecting lines between equipment locations, often between several buildings. High voltage spikes produced by harsh lightning exposure should be suppressed at the point the signal lines enter the building as shown in figure 9. For these applications, multistage protectors, often called transient voltage surge suppressors (TVSSs) are required to handle these high current threats.

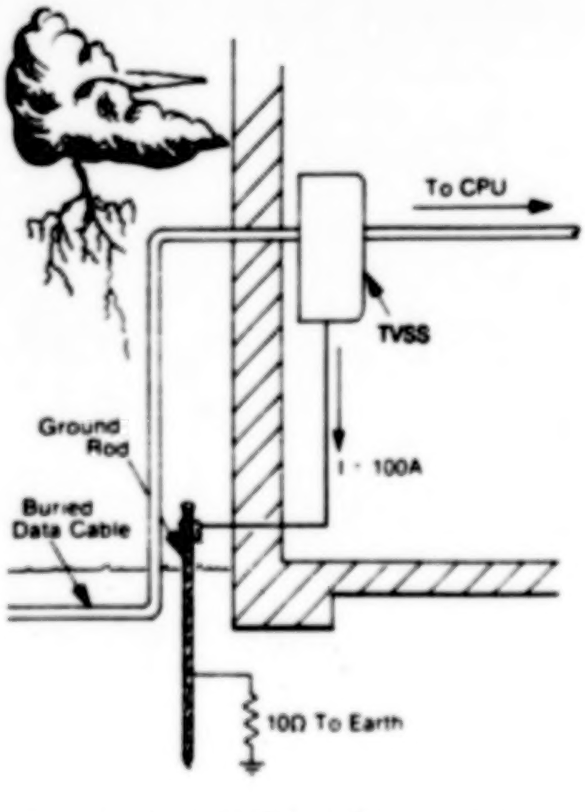

Figure 9. Transient Voltage Surge Protector for Signal Lines

If the TVSS is connected to a separate ground from the system, a common mode transient voltage will develop from current flowing through the ground resistance. This can be illustrated by a current of

100A flowing through a ground resistance of 10 Ohms producing a rise in voltage of 1000V above the user equipment frame ground. This is calculated using Ohms law as shown below:

$$V = iR$$

Where:

I = Instantaneous peak current of 100A
R = Resistance of 100 Ohms

Then:

$$V = 100A \times 10\Omega$$
$$V = 1000V$$

Without additional secondary protection at the equipment inputs to reduce the 1000V to a safe level of 40V or less, the communication interface chips will be destroyed.

The best alternative approach to high level surge protection is to have the TVSS ground connected through a short, low impedance bond to the frame ground of the user equipment. Then the entire system rides up in potential with ground current and the system is safe because it is all at the same potential. An illustration of this system is shown in figure 10.

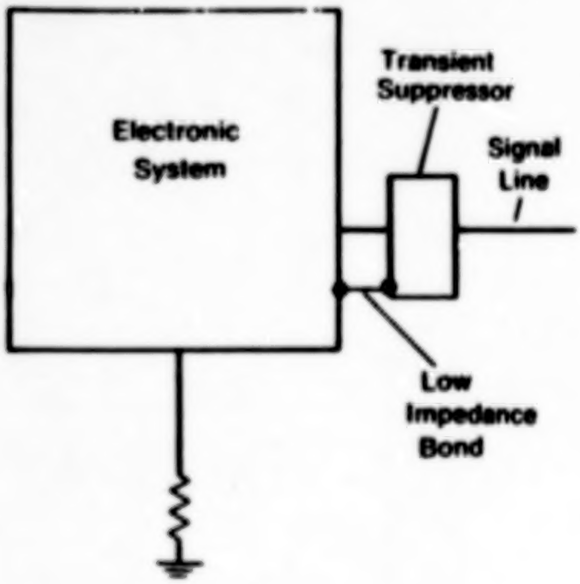

Figure 10. Low Impedance Bond

When the TVSS is located close to the equipment and some distance from the building wall, it is usually necessary to shield with metal conduit those data lines running from outside of the building. Otherwise, transients will be radiated inside the building and possibly coupled into other lines, increasing the risk factor for normally reliable equipment. For redundant high speed data lines, i.e., 1 MB and up, experience has shown that best performance is achieved with protectors attached directly to equipment frame ground.

Locating the position of the protector a significant distance from the user equipment can build up high voltages across the ground wire as shown in figure 11. Wires connecting protector grounds to frame grounds should not exceed 2 feet [13]. The self inductance of a straight wire is only 1.2uH/m, but this can result in high impedance of ground wires during high current fast rise-time transients. This develops high common mode voltages on the data lines similar to the condition previously described for high ground resistance paths.

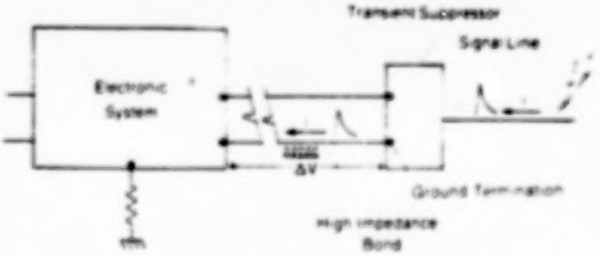

Figure 11. High Impedance Bond

For example, a potential of 3600V resulting from L(di/dt) effects will be developed across a 6m long straight wire carrying a transient current of 500A rising to peak in 1us.

Protection from infrequent strikes to buildings or near lightning hits is recommended for communication interfaces where indoor runs are longer than 10m. Although it rarely happens, all I/O ports in a single system have been destroyed by a single, nearby strike.

If protection is not built-in, it can be provided with add-on TVSSs which are readily available for RS-232 data systems using 25 pin "D" connectors. These add-on protectors are normally connected directly to the computer/peripheral at the I/O port.

Some TVSSs on the market combine protection for both the signal and power lines within the same enclosure. The advantage to this configuration is that the ground window, or ground potential reference, is common for both power and data which optimizes transient protection.

248

INSTALLATION PRECAUTIONS

Transient disturbances on ground and protector input wires produce radiating electromagnetic fields which are induced into nearby wiring and equipment. The results can cause upset or permanent damage. For this reason a few basic precautions must be taken during installation and routine maintenance of equipment.

Configure the wiring so that the protector output ("clean wires"), are routed away from the input and ground wires which carry the transient current. Surge currents flowing through input and ground wires will couple into the protector output if they are installed close and parallel to each other. Run them at right angles to minimize coupling. Also, keep noisy power lines away from data lines.

CASE HISTORIES

I. A manufacturer of high-end laser printers was having an unacceptable level of field failures which were traced to human body ESD events injected into RS-422 data I/O ports. Installing 500W rated silicon TVS devices at the board level provided the needed protection and eliminated the ESD caused failures.

II. A supplier of petrochemical tank level gauging systems was losing line drivers to lightning caused transient voltages. The transient caused latch-up and subsequent overheating which resulted in severe damage to the board. Adding on-board protection plus TVSS protectors for severe environments boosted reliability by orders of magnitude by virtually eliminating losses which normally occurred during electrical storms.

III. A high volume supplier of raw materials to the plastics industry converted its facility to total computer operation incorporating extensive use of TVSS protective devices to ward against induced lightning failure. A successful changeover was made during the winter months; however, when electrical storms began in late spring, equipment outages occurred.
System failures were attributed to improper routing of the data lines at the TVSS location. The protectors were installed with both field input wiring and the "clean" outputs to the computer in the same raceway for lengths of up to 8 feet. This allowed transients to couple into the TVSS outputs and subsequently to the computer I/O ports. Separating the input and ground transient conducting wires from the outputs eliminated this problem.

CONCLUSION

Signal I/O ports are easily destroyed by transient voltage spikes because of the inherently small geometries of microchips. Latch-up is also caused by voltage spikes resulting in damage and potential fire hazards. The major causes of this destructive electrical overstress are ESD and induced lightning; however, properly selected and installed protectors can virtually eliminate I/O port failures.

A broad range of off-the-shelf TVS protective components are available for board level protection while add-on TVSS assemblies can be installed by the user on unprotected ports. Depending on design and installation, some TVSS surge protectors can handle currents of more than 1 kiloamp on data lines exposed to harsh lightning conditions.

Location and installation of adequately rated protective devices must be optimum to provide effective system reliability under adverse transient voltage conditions.

REFERENCES

[1] M. Tetreault and F. Martzloff, "Characterization of Disturbing Waveforms on Computer Data Lines", Proceedings of Electromagnetic Compatibility, Zurich, March 1985, p. 426.

[2] M. Tetreault and F. Martzloff, p. 425.

[3] M. J. Master, et al, "Voltages Induced on an Overhead Line by the Lightning Stepped Leader", IEEE Transactions on EMC, Vol EMC-28, No. 3, August, 1986, pp. 168-171.

[4] "Bell Telephone Laboratory Journal", No. TR-EOP-000001, Issue 2, 1987 p. 9.

[5] M. Clarke, "DOD Raises Stakes in On-Chip ESD Tolerance", EDN, August 24, 1989, p. 70.

[6] W. Crowell, Electrostatic Discharge Susceptibility Data, VZAP-90, Reliability Analysis Center, Prepared under contract to Rome Air Development Center, 1990, p. 2-5.

[7] I. Hertzoff, "Electricians: a Net's Nemisis?",

Network World, November 5, 1990.

[8] F. Martzloff, "Coupling, Propagation and Side Effects of Surges in an Industrial Building Wiring System", IEEE/IAS Conference Proceedings, October 1988, pp. 1467.

[9] R. E. MacArthur, et al, "Fire Stats: Are EDP and Telecom Equipment Really Hazards?", Compliance Engineering, Vol. VII, Issue 4, Summer 1990, p. 36.

[10] R. J. Hanson, "Conducted Electromagnetic Transient-Induced Upset Mechanisms: Microprocessor and Subsystem Level Effects", Proceedings of EOS/ESD Symposium, EOS-9, 1987 p. 104.

[11] P. Gammill and J. Soden, "Latent Failures Due to Electrostatic Discharge in CMOS Integrated Circuits", Proceedings of EOS/ESD Symposium, EOS-8, 1986, pp. 78-79.

[12] O. M. Clark and J. J. Pizzicaroli, "Effect of Lead Wire Lengths on Protector Clamping Voltages", FAA/FIT Workshop on Grounding and Lightning Technology, Report No. FAA-RD-79-6, March 1979, p. 72.

[13] W. Lewis, Reported in Presentation at University of Wisconsin Program on Surge and Transient Immunity in Computer Systems, 1987.

Session 5B, Wednesday 8:00
Lightning Phenomenology
P-Static
Nanevicz, Chairman

P-Static Interference to Aircraft RF Receivers

by W. Devereux

No paper available.

Evaluation of the Observability of Electrostatically Charged Rotocraft

by P. McKenna, R. Dalke, R. Perala, and D. Steffen

No paper available.

CHARGE CONTROL EXPERIMENTS ON A CH-53E HELICOPTER IN A DUSTY ENVIRONMENT

C. B. Moore, J. J. Jones, S. J. Hunyady
Langmuir Laboratory for Atmospheric Research
New Mexico Institute of Mining and Technology
Socorro, NM 87801

ABSTRACT

Charge control tests were carried out on a ground-based, Marine Corps CH-53E helicopter at Davis-Monthan Air Force Base in Tucson, Arizona, during the week of March 19, 1990, to determine if control of the electric fields acting on the engine exhaust gases could be used to reduce the electrification of the helicopter when it operated in a dusty atmosphere.

The test aircraft was flown to a dusty, unpaved area of the base and was then isolated electrically from the earth. When the helicopter engines were operated at ground idle with the rotor locked, the isolated aircraft charged positively, just as had been observed in previous measurements in California. However, when the rotor brake was released in Tucson and the turning rotor created a downdraft that raised dust clouds, the aircraft always became charged more *positively*, to potentials ranging from +30 to +45 kV. (During the earlier tests in clean air in California, operation of the rotor caused the helicopter to charge to negative potentials exceeding −45 kV.)

The dust clouds raised by the rotor downwash in Tucson invariably carried negative space-charges with concentrations of up to -100 nC m^{-3} and caused surface electric fields with strengths of up to 10 kV m^{-1} immediately down wind of the aircraft. The natural charging of the helicopter operating in these dust clouds was successfully opposed by control of the electric fields acting on the hot, electrically-conductive exhaust gases. This control was achieved by placing electrostatic shields around the exhausts from #1 and #3 engines, coupled with the mounting of an isolated electrode inside the shield around #3 exhaust. Control voltages applied to this electrode created the electric fields required to export undesired airframe charges in the exhaust gases.

INTRODUCTION

Aircraft isolated from the earth often acquire electrical charges, which can be dangerous in some situations. For example, when a helicopter hovers near the ground, the charge that it acquires can give severe electrical shocks to ground personnel who come in contact with the aircraft. The cause of helicopter electrification has often been attributed to collisions between the rotor and dust particles in the surrounding air, but significant aircraft electrification has been observed in the absence of dust and other atmospheric particles.

We have been studying this phenomenon for some years and have found that a major cause of helicopter electrification is the flow of electrical currents in the hot, conductive, engine-exhaust gases under the influence of the local electric fields. As a result of these studies, we have been able to control the aircraft electrification by modifying the polarity and strength of the electric fields acting on the hot exhaust gases. The field modification has been accomplished by shielding the engine exhaust gases from the external electric fields with cylindrical wire mesh screens, then applying control voltages of the appropriate polarity to an electrode mounted within one of the shields in a manner that causes the export, on these gases, of the undesired charge residing at some given point on the helicopter.

This technique has been used effectively in experiments to minimize the charges on small helicopters and was successful even when they hovered in clouds of dust where electrification problems have been most severe. It has not been used in flight tests on large helicopters because the present apparatus is experimental and has not yet been engineered to be air-worthy. The current work, however, has been aimed at the development of apparatus that will be suitable for installation on a heavy-lift helicopter.

In some earlier studies at the Marine Corps Air Station in Tustin, California, we found that a ground-based CH-53E helicopter, isolated from the earth, tended to charge positively after the engines were started while the rotor was still stationary. Under low wind conditions, the aircraft sometimes attained potentials, relative to the earth, of about +1.5 kV. Immediately after the rotor brake was released and appreciable downdrafts were caused by the turning rotor, the helicopter potential reversed polarity quickly and voltages in excess of −35 kV were developed relative to the earth. This preference in Tustin for developing negative charge on the aircraft during strong downdrafts could be altered by "export" of negative ions in the exhaust gases when negative control voltages were applied to an electrode immersed in the engine exhaust [1].

Since helicopter electrification reportedly increases when the aircraft operates in a dusty atmosphere, it has been desirable that the charge control technique be tested in an environment with dusty air. Accordingly, arrangements were made with NAVAIR and Marine Corps Squadron HMH 465 for a series of ground-based tests in a dusty area of Davis-Monthan Air Force Base at Tucson, Arizona during March 1990 using a CH-53E helicopter flown in from the Marine Corps Air Station in Tustin, California.

FIELD STUDIES AT TUCSON: MARCH 19–21, 1990

On Monday, March 19, our Marine Corps pilot Captain David Cranford flew the test CH-53E helicopter (tail #YJ21, serial #161996) to an unpaved area on Davis-Monthan AFB in Tucson, Arizona. To isolate the aircraft from the earth, we rolled it up onto three polyethylene slabs, each of which was 1 m^2 and 5 cm thick.

INSTRUMENTATION

The equipment that we used in these studies included:

1. A potential-monitoring voltmeter with "infinite" input impedance patterned after a design by Douglas and Nanewicz [2]. It consists of an electric field mill facing a smooth, metal electrode to which the desired potential is applied. The output for the field mill is a linear function of the applied potential difference between the field mill and the electrode. Potentials (relative to the earth) of up to 80 kV can be measured with this device without any sustained flow of current.

2. Two Faraday cages, each equipped with a sensitive electric field mill, for the direct measurements of space-charges in the exhaust gases and in the atmosphere down wind of the helicopter. The walls of the Faraday cages were made of galvanised steel wire mesh with 1/2-inch openings. The field mill used to sense charge within the cage which was mounted beneath the #3 engine exhaust produced 1.0 V output for a calculated, mean charge concentration of 97 nC m^{-3} while the one mounted in the down-wind Faraday cage required 23 nC m^{-3} for 1.0 V output.

3. Two electric field mills, each mounted in an inverted fashion on a monopod at the height of 1.5 m above the ground for measurement of the atmospheric electric field near the earth's surface.

4. A video camera which was operated at a site about 70 m up wind of the helicopter to provide a record of the dust clouds raised by the rotor downwash.

ELECTROSTATIC SHIELDING AND CONTROL ARRANGEMENTS

The exhaust from #3 engine on the starboard (right) side of the aircraft was shielded electrostatically by an open-ended cylinder, 1 m in diameter and 0.9 m long, constructed from galvanised wire screen with 1/2-inch openings in the mesh. It was isolated both from the airframe and from earth to permit direct measurements of the electrical currents that flowed in the shield during the charge control experiments.

A similar screen cylinder was placed around the exhaust from #1 engine on the port side to shield its exhaust gases from the local electric fields. For comparison, no shielding was used around the exhaust from #2 engine.

A metal electrode was mounted on shielded, porcelain insulators inside the electrostatic shield around the exhaust stack on #3 engine such that the electrode was immersed in the exhaust gases when the engine operated. The electrode was constructed from 5-cm diameter steel tubing bent into a torus that had a diameter of 0.5 m. When high voltages were applied to the electrode, strong electric fields were created between the exhaust stack and the electrode. With this arrangement, ions of one polarity were collected from the emerging exhaust gases while ions having the same polarity as the voltage on the control electrode were exported in a controlled manner from the aircraft.

255

The voltages applied to the control electrode were supplied by a servo controller which contained two programmable power supplies, one furnishing variable positive high voltages of up to +32 kV, the other delivering up to −32 kV. The output of the supply which was energised at a given time was switched to the control electrode by an internally-selected, high-voltage relay. The servo output voltage was controlled either by the voltmeter that sensed the helicopter potential or manually, by the operator.

OPERATIONS

A total of 7 electrification tests were made on March 20 and 21 with the CH-53E helicopter isolated above the dry, bare earth. During this period, the ground surface was dry with a thin crust of salts where the surface was undisturbed. The ground was initially covered with fine dusty soil on the starboard (#3 engine) side of the aircraft while the port (#1 engine side) polyethylene slabs rested on a patch of weathered, poorly-consolidated asphalt. As dust was blown away by the rotor-induced downdrafts, we provided new dust between several of the runs by scoring and "plowing" the dry earth with tools.

In these studies, engine #3 was always started first and charge-control tests were carried out with this engine operating alone. After they were completed, engine #1 was usually fired up to determine if charge control with #3 engine could be maintained without an electrode inside the shield around #1 exhaust.

The behavior of the charge control system is shown in the data plotted in Figure 1. These were obtained on a cloudless, sunny morning, after #3 engine was started and while the rotor was not turning. The helicopter charged to about +1200 V on its own, presumably as the result of negative ion emission from the exhaust gases under the influence of the fine-weather atmospheric electric field of about −90 V m^{-1} at the earth's surface. At 0916:40 MST, we applied −29 kV to the electrode immersed in the exhaust. This caused the export of negative ions in the exhaust. Immediately afterward, the measurements from the Faraday cage mounted beneath #3 engine showed the presence of an intense, negative space-charge in the exhaust gases. This export of negative charge caused the isolated helicopter to become charged positively; it developed a potential of about +10 kV relative to the earth.

Five seconds later, the electric field at the closer field mill, 30 m down wind, reversed polarity and indicated the presence of negative charge passing overhead. About four seconds later, a similar indication of negative charge aloft began at the field mill at the 47-m distance. The surface wind at this time was about 4 m s^{-1} from the helicopter toward the instruments that were down wind, to the northwest.

At 0917 MST, we reversed the electrode voltage to +25 kV whereupon the sequence was repeated but now with inverted polarity: positive charge was exported, the airframe became charged negatively to about −9 kV, and, shortly afterward, positive space-charge passed over the field mills down wind. When the positive voltage was removed from the electrode, the helicopter was still charged negatively from the just-prior export of positive charge; as a result, negative charge was now exported by the exhaust gases until the aircraft was essentially charge-free, approaching its original condition.

These data illustrate how the charge on the helicopter can be modified by variation of the electric fields acting on the exhaust gases and how the exported charge can be detected down wind of the engines. We now present data from one of the charge control tests at Tucson. The six other tests gave similar results. These tests are described in our report [3] to the Office of Naval Research, copies of which are available from the authors.

CHARGE CONTROL TEST: 1237-1254 MST, MARCH 20, 1990 (WITH RING ELECTRODE 8 CM FROM #3 ENGINE EXHAUST STACK).

The weather conditions: The day was sunny with scattered, high-level alto-stratus clouds, the air temperature was about 27 °C, the relative humidity was estimated to be about 20%, and the surface wind was about 3 m s^{-1} from the southeast.

The results for this test are shown in Figure 2. Engine #3 was started at about 1239 MST and was then operated at ground idle for several minutes. The helicopter was ungrounded at 1240 MST whereupon the aircraft slowly acquired a positive charge. At 1241 MST, we applied −1550 V to the control electrode in the exhaust from #3 engine whereupon the aircraft charged more rapidly with the polarity still positive. The aircraft potential increased, reaching +1500 V at 1241:30 MST when the high voltage supply was turned off. Thereafter, the aircraft potential relaxed back toward zero with a 35-s time-constant.

The rotor began turning in flat pitch at 1242:30 MST and immediately raised a cloud of dust, whereupon the helicopter charged rapidly in the positive polarity and attained a potential of +35 kV within 30 s. This

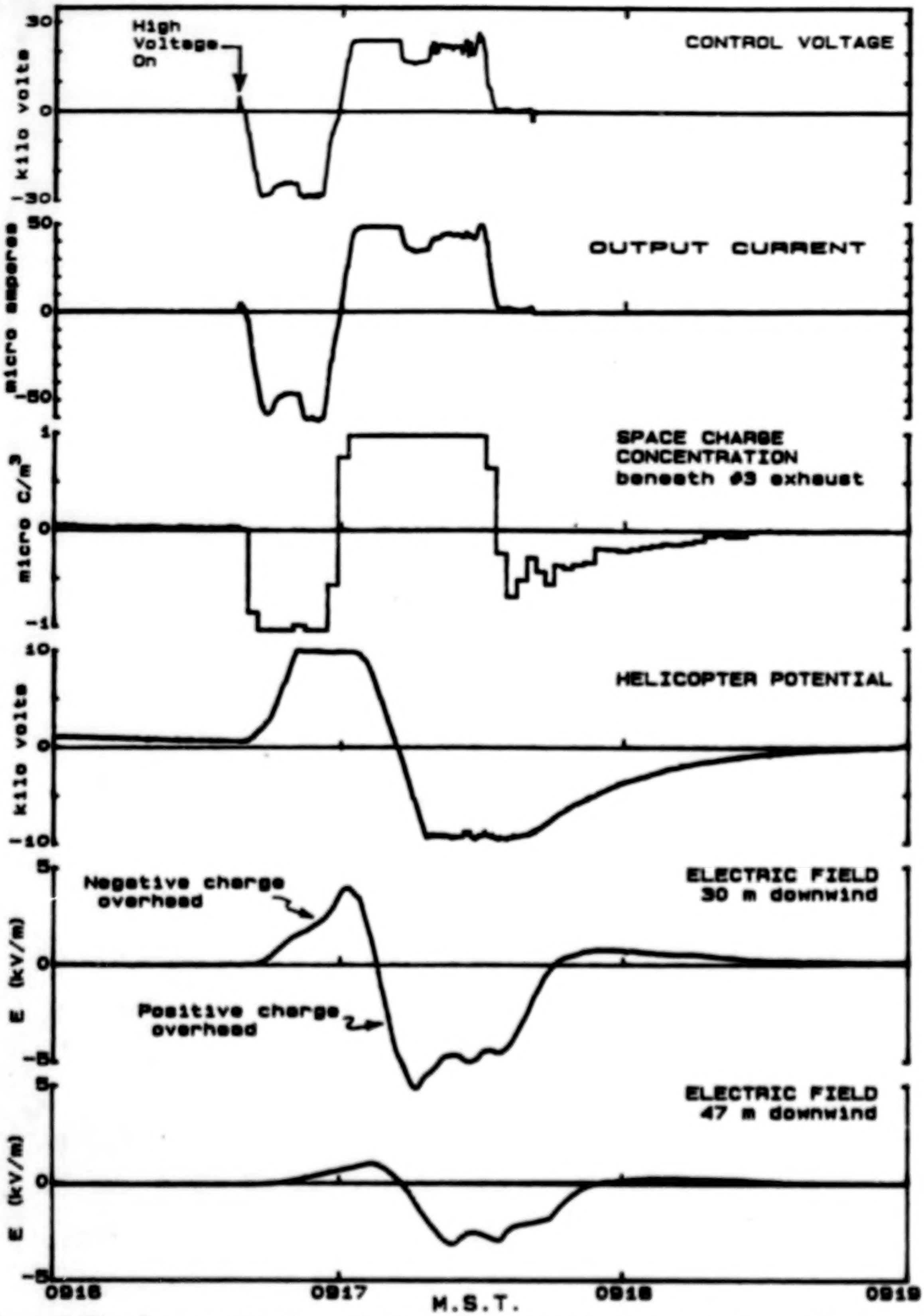

Figure 1: The effects produced by application of high voltages to an electrode immersed in the exhaust from #3 engine while the rotor was stationary (March 21, 1990).

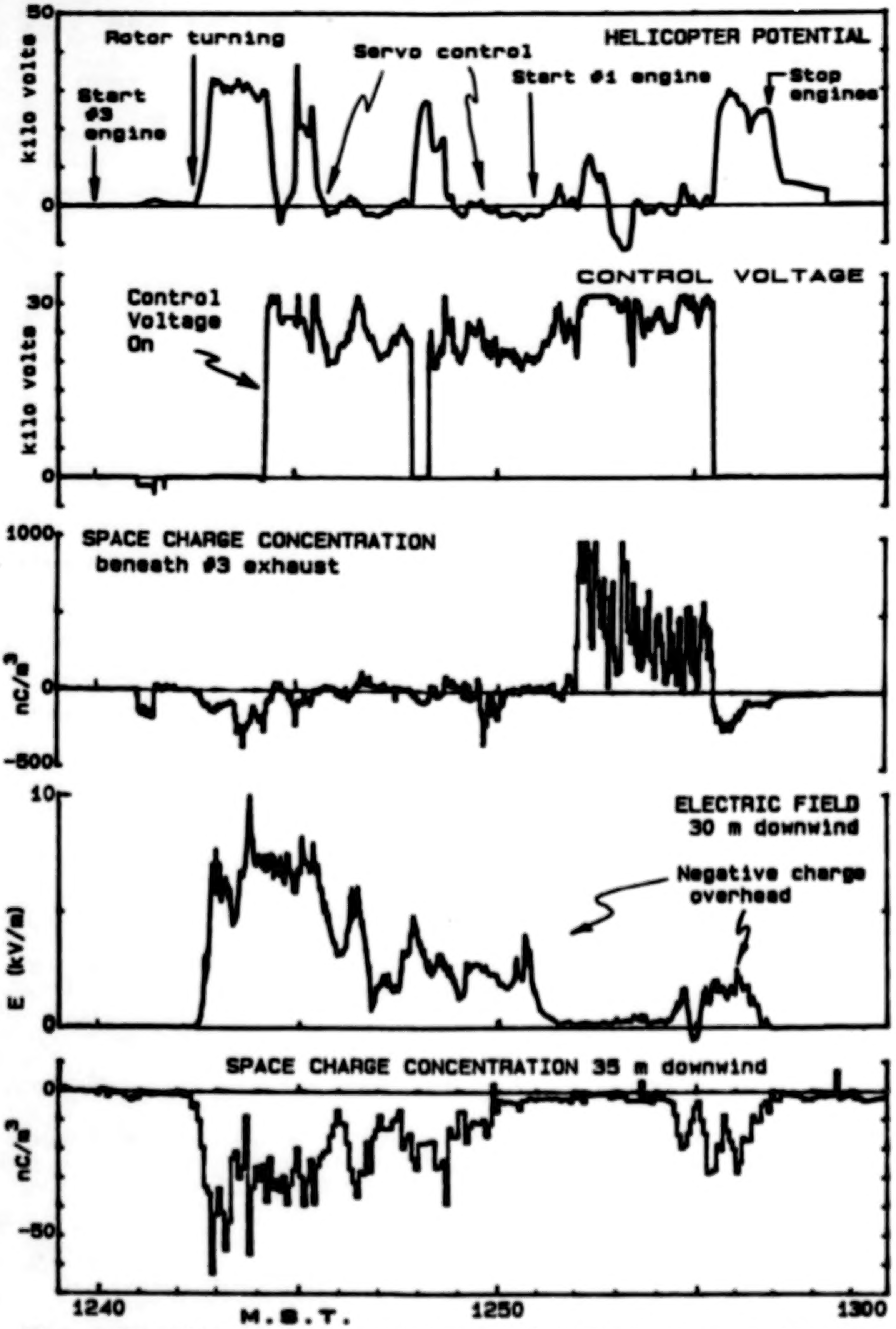

Figure 2: Test of the helicopter charge control system with the ring electrode mounted 8 cm from #3 engine exhaust stack (March 20, 1990).

positive charging in the cloud of dust particles was clearly a result of the rotor motion and did not involve our charge releases since our high voltage system was turned off during this period. Negative space-charges with concentrations of up to -250 nC m^{-3} were measured in the Faraday cage mounted beneath #3 exhaust during this initial, strong charging.

The Faraday cage located 35 m down wind of the rotor hub indicated that the dust clouds away from the aircraft were also negatively charged and carried varying charge concentrations of up to -40 nC m^{-3}. Similarly, the electric field mill 47 m down wind showed field strengths of up to 10 kV m^{-1} with positive polarity, indicating the presence of negative charge overhead.

At 1244:15 MST, we applied +32 kV to the control electrode; this caused positive charge to leave the aircraft and reduced its potential from the +32 kV level. After some adjustments, we were able to maintain the aircraft potential between -2500 V and $+1000$ V for more than 2 minutes by use of the servo control which varied the voltage on the electrode between +20 and +30 kV and caused the export of a current of about 50 μA in the exhaust. The control was turned off at 1248 MST whereupon the aircraft promptly recharged to +27 kV. We then reactivated the servo control which promptly reduced the helicopter potential to values varying around the zero level where it was maintained by the continued export of positive charges.

None of the positive charge carried away in the exhaust from #3 engine was ever detected by any of the down-wind instrumentation: during all of these tests, the negatively-charged dust clouds raised by the rotor downwash dominated the local atmospheric electricity down wind from the aircraft.

Since we appeared to have some control of the aircraft potential while #3 engine alone was operating, we asked the pilot to start #1 engine with its shielded exhaust. As engine #1 came up to speed, the servo voltage required to minimize aircraft potential increased and the control became less effective with initial excursions in helicopter potential of about 10 kV in both polarities. After the initial oscillation, the servo gained control and maintained the potential to within about 3 kV of zero for the next two minutes. The concentration of positive space-charge measured beneath #3 exhaust became very strong, exceeding +700 nC m^{-3} during this control effort. The servo was turned off at 1255 MST, whereupon the aircraft promptly charged positively again to about +30 kV with the export of up to -200 nC m^{-3} of negative charge recorded in the Faraday cage beneath #3 exhaust.

At 1257 MST, we asked the pilot to stop the engines so that we could change the electrode configuration. While we were able to control the helicopter charge about as expected, a major surprise to us from this test was the anomalous *positive* charging of the helicopter in the presence of the negatively charged dust.

DISCUSSION OF THE HELICOPTER CHARGE CONTROL EXPERIMENTS

The initial, positive charging of the helicopter to about +1 kV after the start of an engine but before the rotor turned (observed both at Tucson and at Tustin) appears to be caused by the fine-weather atmospheric electric field acting on the conductive exhaust gases emitted from the elevated exhaust stack. The strength of the undisturbed atmospheric field that we measured at Tucson was about -100 V m^{-1} and this would have caused negative ions in the exhaust plume to move upward while positive ions would have been driven downward. The effect would have been to cause the airframe to lose negative charge by conduction through the exhaust until it approached the potential of the air at the level reached by the buoyant plume of conductive exhaust gases. The top of the aircraft is at a height of about 7 m. The +1 kV developed by the airframe suggests that the buoyant exhaust gases coupled with the atmospheric potential at a height of about 10 m. This phenomenon provides continuing evidence that charges are transferred from aircraft through the exhaust gases.

A great surprise to us was the strong natural charging of the helicopter with *positive* polarity whenever the rotor caused a downdraft. This polarity of charging is opposite to that previously observed in the clean-air measurements at Tustin. The positive charging of the helicopter at Tucson was associated with the transport of *negative* charges away from the aircraft despite the negatively-charged dust cloud that always enveloped it when the rotor turned. One would normally expect that an isolated aircraft surrounded by a cloud of negatively-charged dust would acquire negative charge and become negatively charged itself. Among the processes that could transfer charge between an isolated helicopter and the surrounding air are the following:

1. Ingestion of space-charge in the combustion air drawn into the engine.

   An engine on the CH-53E helicopter operating at 23% capacity as in our tests at Tucson consumes about 400 kg hr^{-1} of hydrocarbon. To burn this fuel stoichiometrically requires about 1.4 m^3 s^{-1} of air. If the engine air contains the space-charge concentrations of up to −100 nC m^{-3} that we measured in the dust clouds around the helicopter, a charging current of around −0.14 μA would be arriving at the aircraft through each engine. Such currents are of the wrong polarity to charge the helicopter positively and they are too small to be significant in the charging processes encountered during these tests.

2. Collisions between the rotor and dust particles.

   Several different kinds of charge transfer can take place during collisions with dust particles. There can be charge transfers between the rotor blades and negatively-charged particles that leave some of the charges, initially carried by the dust, on the rotor surfaces from which they would be distributed over the entire airframe. Since this would make the aircraft carry a negative net charge, it obviously was not important in our Tucson measurements.

   Charge transfers can also occur during elastic collisions as a result of "contact electrification" which arises from a difference in the "work functions" of the two surfaces in contact. Elastic collisions between the rotor and dust certainly occurred in the tests at Tucson but, in our opinion, they were not the dominant cause of the electrification. One of our reasons for this opinion is that, in tests by Brook *et al.* [4], who caused similar collisions between road dust and an isolated rotor blade turning in the Whirl Tower at the Naval Air Repair Facility in San Diego, the maximum currents observed during intense dust injections were only 0.25 μA and their polarity fluctuated repeatedly during tests with dust of the same apparent composition. One might extrapolate from Brook's measurements to obtain a current of up to 2 μA for the seven rotor blades on the CH-53E helicopter but this is not large enough to explain the currents we encountered.

   Another reason for questioning this explanation is that the CH-53E helicopters used in similar, clean-air charging tests at Tustin charged just as vigorously as did CH-53E YJ21 in the dust in Tucson—but with the opposite, *negative* polarity. There is a common feature however: In Tucson, the atmospheric electric field acting on the helicopter in the negatively-charged dust clouds was upwardly-directed or, in our convention, the surface field under the dust was a "positive" one. In these positive fields, the helicopter always charged *positively* while the rotor was causing a downdraft. On the other hand, at Tustin the atmospheric electric field was always that observed in fine weather which is downwardly-directed and is termed a *negative* one. In such negative fields, all five of the CH-53E helicopters that we tested in Tustin charged *negatively*.

   This coupling between the polarity of the local electric field and that of the charge developed on the helicopter when the rotor creates a downdraft has occurred in all 24 tests that we have made with CH-53E helicopters with ambient electric fields of both polarities. In view of this evidence, it appears that there is a causal relationship involving the ambient electric field which determines the polarity of the helicopter charge.

3. Currents flowing in the exhaust gases.

   In earlier measurements of the electrical conductivity of the CH-53E engine exhaust gases at Tustin, we found that these gases emerge from the exhaust stacks with conductivities of up to 400 pS m^{-1} which indicates that a free charge immersed in such a gas would be essentially neutralised by conduction within 50 ms. After emergence, these gases entrain ambient air quickly. The resulting dilution of the gases and the ion loss by recombination and by attachment to aerosol particles cause the gas conductivities to decrease rapidly with distance from the exhaust stack: we found that the conductivity downstream from engine #1 decreased by e-fold in a distance of about 0.3 m when the rotor caused a downdraft.

   Appreciable electric currents will flow in such conductive gases under the influence of the local electric fields. In quiet air, the effect of such current flows would be to carry charges that act to neutralise the local fields. However, when the rotor causes a downdraft, the charges carried by the cooling exhaust gases can be transported downward and away such that they intensify the field and cause more charges to flow. It appears to us that this occurs regularly with CH-53E operation and results in a positive "feedback" process for charging the aircraft with charging time constants of about 7 s.

CONTROL OF THE CHARGES ON HELICOPTERS

These results clearly show that the residual charge on a helicopter can be reduced and controlled by applying appropriate electric fields to the exhaust gases at a point where they are still electrically conductive and *before* they get involved in the rotor-induced circulation. Despite the predictions and expectations of intense natural charging when the helicopter created a dust cloud, we found no problem in controlling the charging tendencies of a helicopter operating in fairly intense dust.

Our measurements suggest, however, that adequate control will require the use of this technique on the exhausts from all of the engines in operation. The need for this is shown by the experimental results given in Figure 2: During the period from 1246 to 1251 MST, the rotor was driven by #3 engine operating alone. When the servo applied control voltages to the electrode immersed in the #3 engine exhaust gases, it was able to maintain the helicopter potential (and therefore the helicopter charge) at low levels around zero with relatively low emissions of space charges in the exhaust. The application of variable control voltages of about +25 kV apparently was able to counteract the engine's natural tendency to release negative charges under the dusty conditions. (This natural tendency for charge emission when the servo control was not operating is demonstrated in the recordings of negative space charges carried by the exhaust from #3 engine for the times around 1243 MST and, again, after 1255 MST.)

On the other hand, after #1 engine was started around 1251 MST and joined #3 in driving the rotor, servo control voltages of up to +32 kV were required on the #3 exhaust to counteract the charging of the helicopter. Thereafter, high concentrations of positive space charges were detected in the Faraday cage beneath #3 exhaust; these indicate that emissions of high concentrations of positive space charges from #3 engine were needed to offset the releases of negative charges by the shielded, but uncontrolled, #1 engine exhaust. This sequence illustrates the desirability of controlling the electric fields acting on all of the engine exhaust gases if helicopter charges are to be reduced reliably to safe levels.

RECOMMENDATIONS

1. To overcome the natural charging tendencies of an isolated helicopter, we recommend that the exhaust gases be shielded electrostatically from external electric fields and that the fields within the shields be controlled by the application of an appropriate voltage with the same polarity as that of the undesired, residual charge on the aircraft.

2. To optimize this technique, more studies are needed with operating helicopters so that the minimum shielding necessary can be determined.

3. The shields and electrodes should be made airworthy so that the technique can be tested on a heavy-lift helicopter in flight.

4. An operational means of sensing the helicopter's charge or the electric field at some point such as the pendent hook should be investigated. If the servo provides a corrective field to the exhaust which results in making the field at the hook equal to zero, then by definition, the hook is at the potential of its surroundings. If this condition were maintained as a helicopter descended until the hook touched the earth, there would be no spark nor any signigicant charge transfer when contact was made because the hook would have been at ground potential. However, if a ground crewman were to grab the hook when it was hanging 2 m above earth in a dust cloud containing 100 nC of space charge per m^3 of air, the air at that level would be at a potential of about 23 kV relative to the earth and that would be the potential of the helicopter if the field at the hook were zero. A shock to a contacting ground crewman would be inevitable in this case.

   One solution for the avoidance of a shock, suggested by Marx Brook (private communication), would be to use a method similar to the technique for measuring the helicopter potential without drawing a sustained current. A weakly conducting, weighted line or rope could hang down from a potential sensor on the hook so that the line touches the earth or a crewman before he grabs the hook. The virtue of this approach is that it would not require good contact with the earth and is not aimed at direct discharge of the helicopter. Instead, the resulting signal from the sensor on the hook would be used to provide the necessary corrective voltages to the electrode in the exhaust to make the helicopter potential become that of the sensor. With this arrangement, there would be no sparks nor shocks to a ground crewman who contacted any part of the aircraft.

ACKNOWLEDGMENTS

This study was carried out under contract N00014-87-K-0783 with the Office of Naval Research. Drs. James Hughes and Paul Twitchell of ONR and Lt. Col. David Bloomer, PMA 261-2, NAVAIR, made these tests possible. We thank them and Lt. Col. Ron Johnston, Commander of HMH 465, for all of the support and assistance that they provided. We thank Capt. David Cranford, who was our pilot for these tests and we also thank our host, Major Thomas A. Linster, Deputy Commander for Maintenance, 71st Special Operations Squadron, USAF, for the use of the facilities at Davis-Monthan AFB. Finally, we thank S. M. Kieft and Professors Marx Brook and William Rison for their many contributions to this study.

REFERENCES

1. Moore, C. B., M. Brook and C. N. Richards, 1988: "Electrification of Hovering Helicopters," Proceedings of the 1988 International Aerospace and Ground Conference on Lightning and Static Electricity, Oklahoma City, OK, pp. 213–217.

2. Douglas, D. G. and J. E. Nanewicz, 1973: "Flight Evaluation of Helicopter Cargo-Handling Systems—Passive Electricity Drainage," Stanford Research Institute Report to the Boeing Company on SRI Project 2590, pp. 5–9.

3. Moore, C. B., J. J. Jones and S. J. Hunyady, 1990: "Studies of Helicopter Charging, Report #6, Charge Control Experiments on a CH-53E Helicopter In A Dusty Atmosphere, March 16–21, 1990," Contract N00014-87-K-0783, 40 pages.

4. Brook, M., C. B. Moore and C. N. Richards, 1986: "A Helicopter Electric Charge Control Study," Final Report under ONR Contract #N00014-84-K-0623, July 3, 1986, 67 pages.

RESULTS OF THE RECENT PRECIPITATION STATIC FLIGHT TEST PROGRAM ON THE NAVY P-3B ANTISUBMARINE AIRCRAFT

Mike Whitaker
Electromagnetic Pulse Section
Naval Air Test Center
Patuxent River, Maryland

ABSTRACT

The Naval Air Test Center's Electromagnetic Pulse Section recently investigated severe precipitation static problems affecting the communication equipment onboard the P-3B aircraft. This investigation was conducted at the request of Naval Air Systems Command after precipitation static created potential safety-of-flight problems on Naval Reserve aircraft. A specially designed flight test program was conducted in order to measure, record, analyze, and characterize potential precipitation static problem areas. The test program successfully characterized the precipitation static interference problems while the P-3B was flown in moderate to extreme precipitation conditions. Data up to 400 MHz were collected on the effects of engine charging, precipitation static, and extreme cross-fields. These data were collected using a computer-controlled acquisition system consisting of a signal generator, RF spectrum and audio analyzers, data recorder, and instrumented static dischargers.

This paper outlines this test program and describes in detail the computer-controlled data acquisition systems used during flight and ground testing. This paper also discusses the correlation of test results recorded during the flight test program and those measured during ground testing.

1. INTRODUCTION

For over 50 years, precipitation static (P-static), its causes, and cures have been examined in numerous reports and papers. These studies indicate that the U.S. Navy has been concerned about the effects of P-static on its aircraft for at least the past 45 years. After all this time and research, however, P-static remains somewhat of a mystery.

The biggest problem concerning P-static appears to be lack of awareness on the part of designers, users, and maintainers of aircraft, despite the abundance of technical literature on the phenomenon. The Naval Air Test Center's program, the focus of this paper, extensively utilized the research previously performed by the experts in the field of P-static. The aim of this paper is to provide some continuity between the information gathered in past P-static cleanup programs and in this more recent one.

P-static testing at the Naval Air Test Center is performed by the Electromagnetic Pulse (EMP) Section of the Electromagnetic Systems Department. The EMP Section also performs high-altitude EMP and lightning testing. Prior to 1986, P-static testing at the Test Center was conducted only on demand. Presently, however, all Navy aircraft being processed through the Test Center's shielded hangar for electromagnetic testing is also subjected to simulated P-static testing.

2. TEST AIRCRAFT BACKGROUND

P-static problems on aircraft can be attributed to several causes. The main causes historically have been the advanced age of the airframe, a new avionics installation, or unfamiliarity on the part of aircraft personnel with P-static. All three of these are factors with the P-3B aircraft (see figure 1). Specifically, the P-3B test program was initiated because the aircraft was being outfitted with a replacement communication receiver offering increased range, greater flexibility, and broadband. As a result of this new receiver's greater sensitivity (by 10 dB), P-static on the P-3B changed from a mere nuisance to a safety-of-flight issue.

The program described in the following pages was not the Navy's first attempt to clean up the P-3 airframe. An extenstive and successful effort was made 10 years earlier. As an outcome of this program, flight manuals were revised to include guidance on maintaining a clean airframe. But as often happens, no major problems were noted for years, so the requirement for periodic checks for P-static problems was eventually dropped.

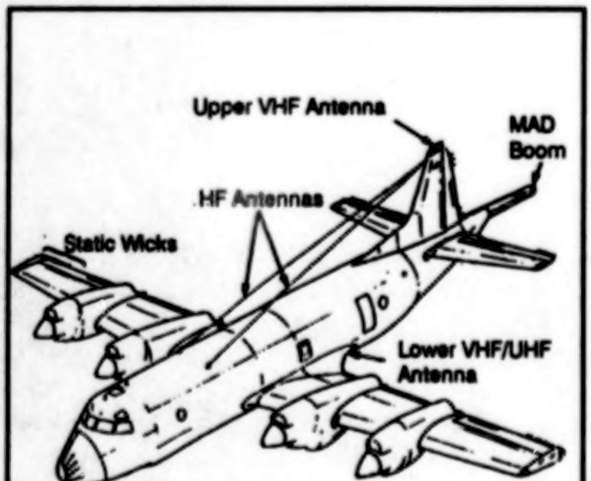

Figure 1. The Navy's P-3B Aircraft

Further compounding the Navy's problem was the lack of standard, acceptable test procedures for ground testing of aircraft. The EMP Section had a local test method, but not one that had been confirmed as adequate by a flight test program. Tasking for cleaning up the P-3B airframe came to the Test Center after six months had been expended by other, unsuccessful cleanup efforts.

To accomplish this task, a test program was developed jointly at the Test Center by the Force Warfare Test Directorate and the Systems Engineering Test Directorate's EMP Section. This collaboration resulted in a two-phase program. In Phase I, characteristics of the P-3B inflight environments were obtained, and the ground testing methods were modified as required. In Phase II of the program, other aircraft were tested for trends and common problems.

3. AIRCRAFT INSTRUMENTATION SUITE

In developing its P-3B flight instrumentation suite, the EMP Section thoroughly researched the technical literature outlining previously conducted P-static flight test programs. In particular, data from the aforementioned P-3 program that was conducted 10 years earlier provided excellent guidance. With this information, along with data gathered from related Boeing and Stanford Research Institute test programs, the Test Center designed its flight instrumentation suite. A block diagram of the P-3B instrumentation suite appears in figure 2.

One requirement for P-3B instrumentation was to record continuous P-static interference on all communication receivers and analyze the audio output of receivers. Since the charge levels for frontal areas had already been extensively documented, no data on these were gathered during this program. Three static dischargers were isolated from airframe and used as indicators for P-static conditions. Dischargers were sufficient to provide data on engine charging, P-static conditions, and crossfields.

The P-3B instrumentation suite (photo 1) provided a continuous recording capability, visual indicator meters to monitor outside conditions, and an in-flight hard copy printout capability. The PC controller saved interference events on disk for immediate or later processing.

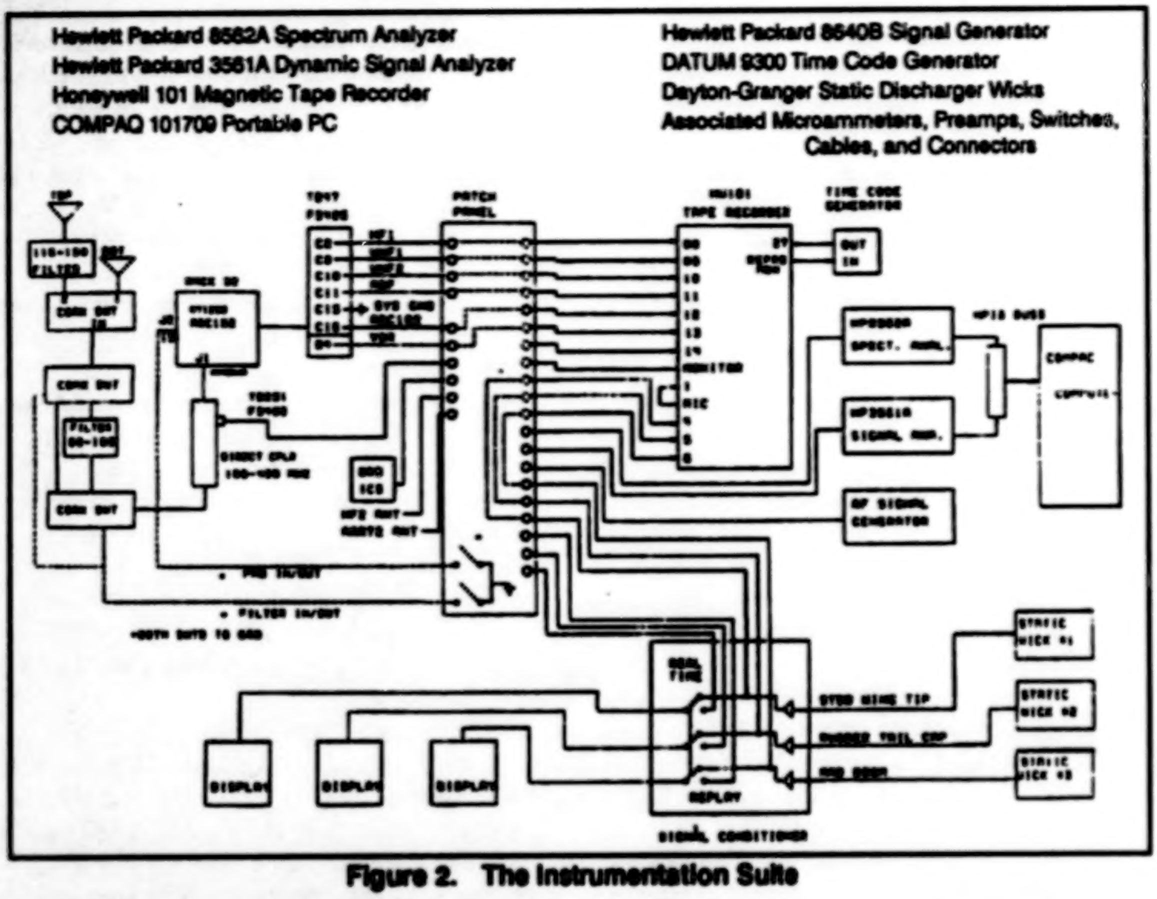
Hewlett Packard 8562A Spectrum Analyzer
Hewlett Packard 3561A Dynamic Signal Analyzer
Honeywell 101 Magnetic Tape Recorder
COMPAQ 101709 Portable PC
Hewlett Packard 8640B Signal Generator
DATUM 9300 Time Code Generator
Dayton-Granger Static Discharger Wicks
Associated Microammeters, Preamps, Switches, Cables, and Connectors
PATCH PANEL
TAPE RECORDER
TIME CODE GENERATOR
COMPAQ
DISPLAY
DISPLAY
DISPLAY
REAL TIME
REPLAY
SIGNAL CONDITIONER
STATIC WICK #1
STATIC WICK #2
STATIC WICK #3
RF SIGNAL GENERATOR

Figure 2. The Instrumentation Suite

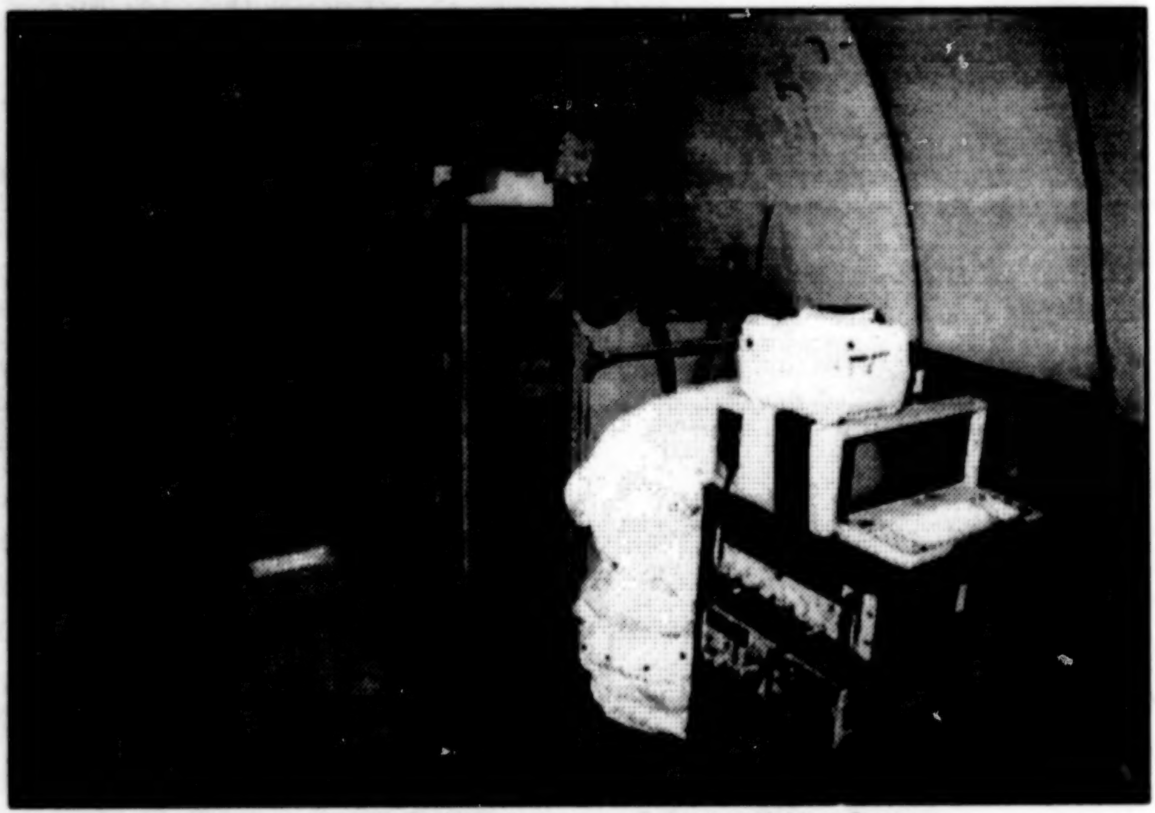

Photo 1. P-3B P-Static Interference Data Acquisition System

4. TEST FLIGHT PHASE

After extensive ground testing to confirm the operation of instrumentation and to characterize the P-static problem areas, the aircraft was ready to be flown in P-static conditions. The problem areas identified by ground testing were left uncorrected in order to obtain interference records reflecting an aircraft with known P-static problems.

By early January 1989, the aircraft, crew, and test team were ready to proceed with the test program. Initial flights were conducted from Glenview Naval Air Station north of Chicago, since weather forecasts indicated conditions were more favorable to encounter P-static in the midwest during this timeframe. Flying out of the Chicago area with the P-3B's range put the entire midwest within reach.

By consulting daily with weather forecasters at Glenview Naval Air Station, the test team could select an appropriate area for test flights. After a few flights, the test team became very successful at locating and documenting the P-static environment. A typical flight condition is described in table I.

Table I. Flight in Severe P-Static Conditions (Before Fixes)

- Altitude = 16,000 ft
- Outside Air Temperature = -16° C (actual)
- Airspeed = 235 Knots
- Discharge Current
  - — Mad Boom = 70 μA
  - — Wing Tip = 50 μA
  - — Fin Cap = 50 μA

Once team members were satisfied with the acquired data, their next step was to perform cleanup on the airframe. The following is a sampling of the types of cleanup necessary. Cleanup was required on the high-frequency antennas, MAD boom, and static wicks. The high frequency antenna parts were replaced to prevent corona discharge. The MAD boom had numerous isolated diverter strips which formed a Faraday cage. Rebonding the diverter strips and access door cleaned up this problem area. The worst problem, and the easiest to correct, was the static dischargers. The test aircraft's dischargers were measured open and were not effectively discharging any current. The static dischargers were replaced, and the isolated bases were grounded. Operating from a P-3 unit provided the personnel with the expertise needed to implement all corrective actions. Validity of these repairs was then confirmed by ground testing.

After ground testing of the fixes, the aircraft was flown once again to confirm that fixes were adequate to prevent the P-static interference that was documented during previous flights. Ideally in this situation, the environment must produce discharge currents on the instrumented static dischargers that are similar to those produced in the previous flight tests.

Unfortuantely, weather took a turn for the better, and the severe environmental conditions needed for testing could not be located in the midwest. The test team then decided to return to the Test Center and make the final flights from there. With patience, the test team eventually found conditions that were more severe than those encountered during flights with a "dirty" airframe. Interference-free aircraft communication receivers confirmed that corrective action had been successful in eliminating P-static interference. Typical before-and-after data plots are presented in figures 3 through 5.

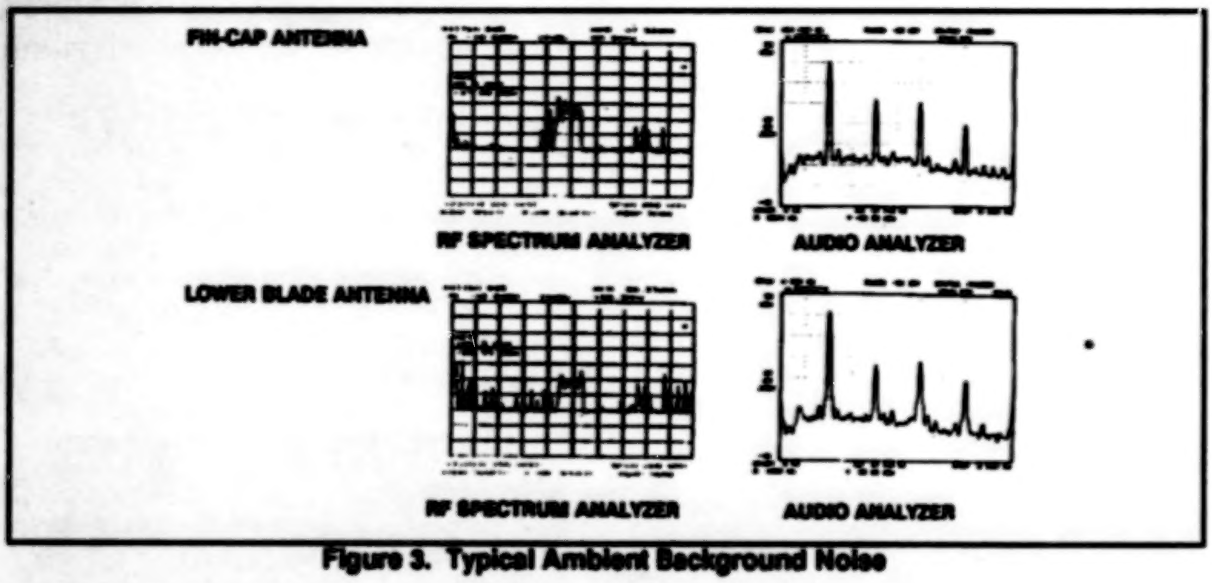

Figure 3. Typical Ambient Background Noise

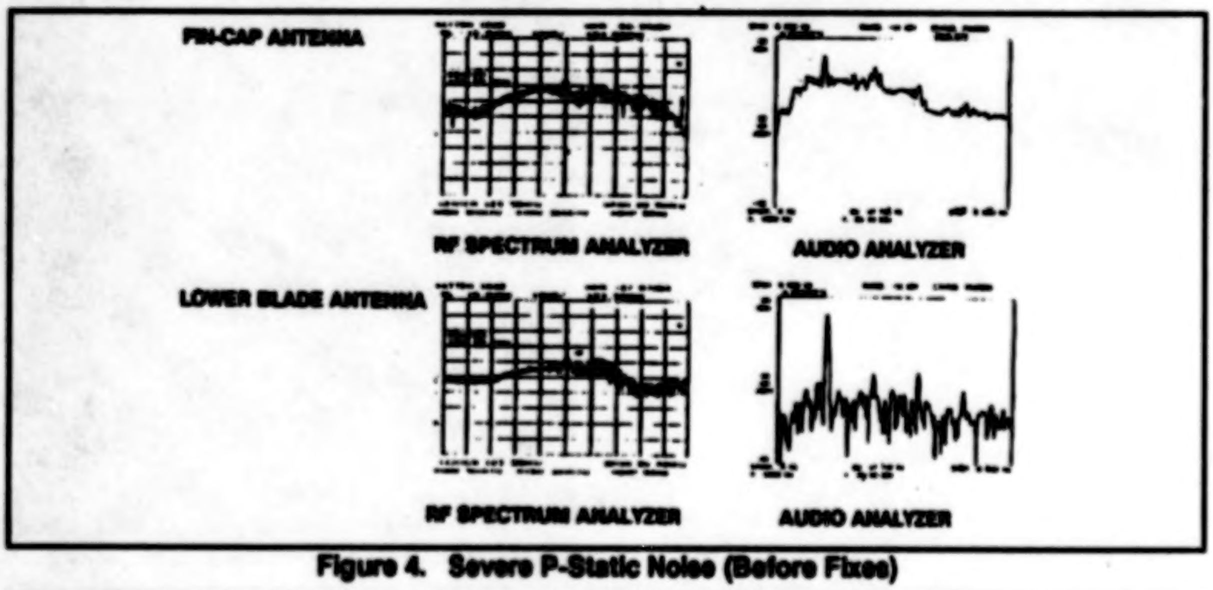

Figure 4. Severe P-Static Noise (Before Fixes)

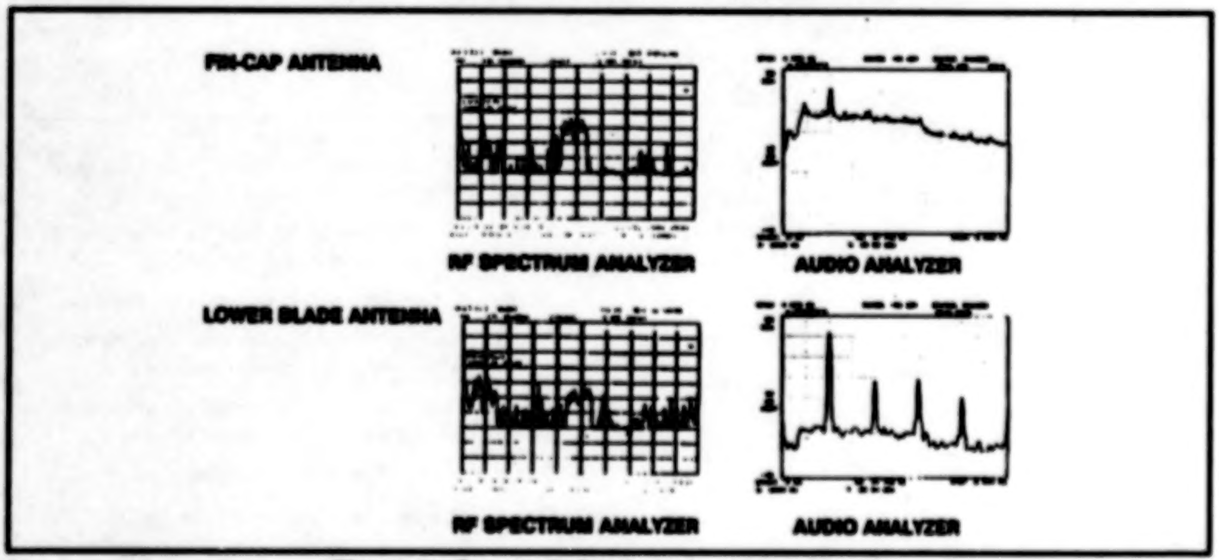

Figure 5. Severe P-Static Noise (After Fixes)

P-static conditions were similar during the different plots of figures 3 through 5. It should be noted that the audio analyzer plot for the fin-cap antenna of figure 5 was caused by improper bonding and was later corrected.

5. GROUND TEST CRITERIA

Preparations for this phase were made in parallel with preparations for the flight test program. This effort utilized a ground-based instrumentation suite similar to that used during flights (photo 2).

Photo 2. Ground Test Instrumentation Suite

In order to simulate the environment documented in the flight test phase, it was essential to first establish accurate guidelines. The high-voltage test set had to be a variable current source that could deposit charge onto a 1-foot-square area. According to applicable studies, the worst P-static conditions are established at 20 microamperes per square foot. In addition, the test team agreed upon a SINAD and signal-to-noise ratio. With the aircraft fully instrumented, it became very simple to determine which problem areas should be immediately repaired and which should be considered minor. Establishing these criteria resulted in a cost-effective corrective action program.

6. STANDARDIZED GROUND TEST METHOD

The method used by the Test Center for P-static testing is similar to the method employed by numerous aircraft manufacturers and repair facilities. This commonly used test method was simplified by Dayton-Granger, the manufacturer of the electrostatic test set used by most testers (photo 3). The Navy then adopted Dayton-Granger's testing method and refined it. Table II shows the main steps of a typical aircraft P-static evaluation.

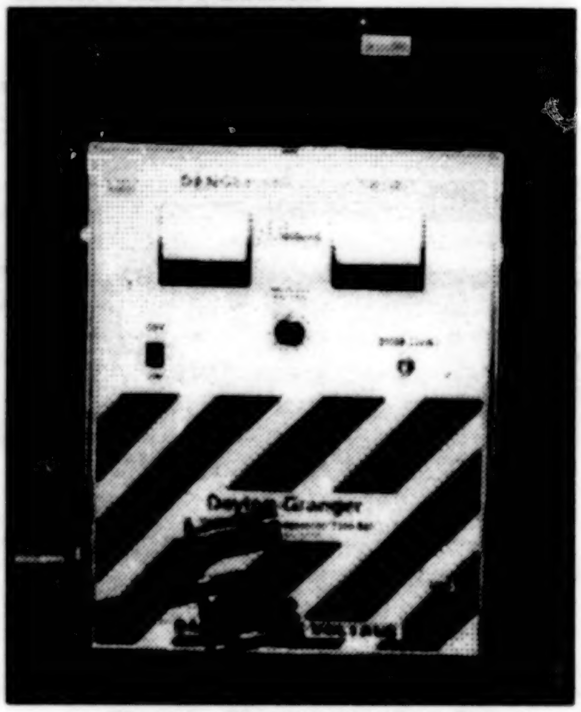

Photo 3. Electrostatic Test Set

Table II. Test Methods

Step 1	Deposit simulated P-static charge using an electrostatic test set.
Step 2	Monitor hand-held radios for noise generated by induced arcing.
Step 3	Document all problem areas for database.
Step 4	Monitor onboard radios and instrumentation while problem areas are resprayed.
Step 5	Record interference on the victim radio, both graphically and in data form.
Step 6	Incorporate fixes to problem areas.
Step 7	Evaluate fixes and record the results.

In ground testing, aircraft preparation is minimal. The test is performed on a grounded aircraft with fuel tanks topped off. The first sweep of the aircraft is made with applied ground power. Discharge capability of static wicks is confirmed by drawing current from wicks while monitoring a sensitive broadband receiver. Once instrumentation is installed (figure 6), the next step is to spray problem areas while monitoring receivers and recording data plots with the instrumentation system. Information collected is then entered into the P-Static Problem Area Tracking System (table III) for comparison with existing data and for further analysis. Aircraft deficiencies are then reported to the aircraft manufacturer and users through a variety of methods.

7. CONCLUSIONS

The preceding pages describe the process that the Naval Air Test Center uses to identify aircraft P-static problems and to correct them. Information has also been presented as recommended test levels for determining adequacy of aircraft's protection against the adverse effects of the P-static environment. Procedures discussed here are presently being used for verifying the specification compliance of Naval aircraft.

8. ACKNOWLEDGMENTS

This program could not have been performed effectively without the excellent documents produced by Stanford Research Institute, which are too numerous to be referenced here.

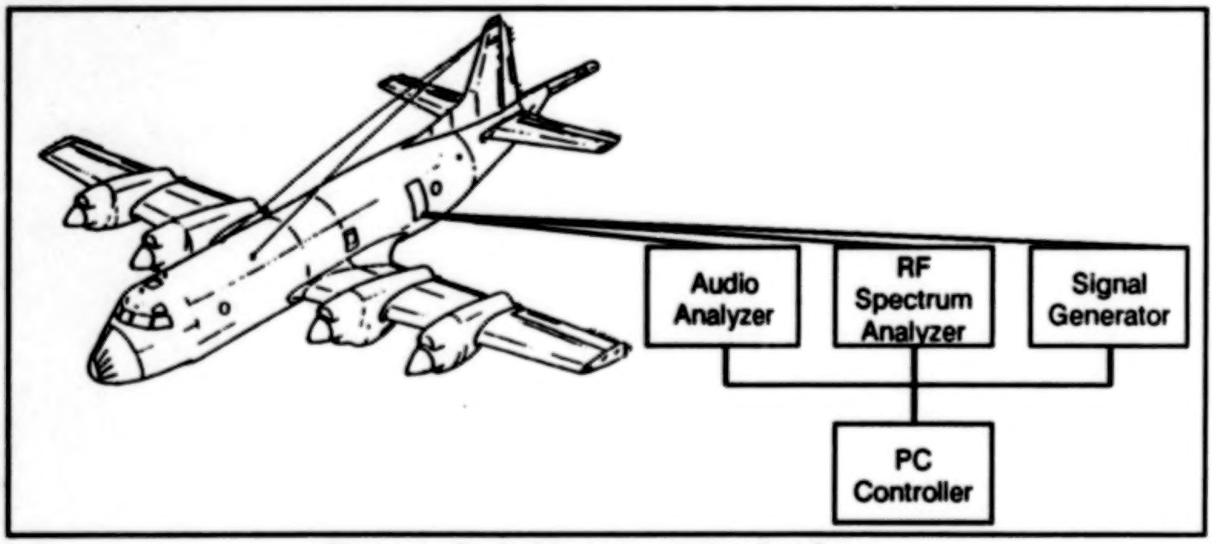

Figure 6. Typical Instrumentation Test Setup

Table III. P-Static Problem Area Tracking System

- Essentially a digital version of a traditional Microfiche cataloging system
- Hewlett Packard Scan Jet Plus replaces the camera
- Iomega 20 megabyte 1/4" cartridges replaces transparency films/fiches
- New generation graphical database Superbase 4 is the cataloging system
- Database allows direct on-screen preview of graphical data
- Intuitive VCR-like control panel allows easy database searching
- Key fields include:
  - A/C model
  - Bureau number
  - Problem area ID number
  - Problem area description
  - Work unit code
  - Category

Session 6A, Wednesday 10:15
Ground Protection 2
Rustan, Chairman

LAUNCH PAD LIGHTNING PROTECTION EFFECTIVENESS

James R. Stahmann
Boeing Aerospace Operations
Kennedy Space Center, FL 32899

ABSTRACT

Using the striking distance theory that lightning leaders will strike the nearest grounded point on their last jump to earth corresponding to the striking distance, the probability of striking a point on a structure in the presence of other points can be estimated. The lightning strokes are divided into deciles having an average peak current and striking distance. The striking distances are used as radii from the points to generate windows of approach through which the leader must pass to reach a designated point. The projections of the windows on a horizontal plane as they are rotated through all possible angles of approach define an area that can be multiplied by the decile stroke density to arrive at the probability of strokes with the window average striking distance. The sum of all decile probabilities gives the cumulative probability for all strokes.

The techniques can be applied to Kennedy Space Center (KSC) launch pad structures to estimate the lightning protection effectiveness for the crane, gaseous oxygen (GOX) vent arm, and other points. Streamers from sharp points on the structure provide protection for surfaces having large radii of curvature. The effects of nearby structures can also be estimated.

INTRODUCTION

The launch pads at KSC are protected by a 70-foot insulating fiber glass mast 5 feet in diameter located on the Fixed Service Structure with a lightning rod at the top of the mast. The rod is grounded 1,000 feet north and south of the tower by a 1/2-inch stainless steel cable called the catenary wire. The lightning protection system on Launch Pad 39A has been struck by lightning an average of three times per year since 1979. Probability calculations predicted about two strokes per year. The difference may be accounted for by the action of upward-going streamers that go out to meet the down-coming leader of the lightning stroke and meet it about 100 feet above the lightning rod. This effect increases the effective height of the mast and enhances its ability to attract strokes, especially the larger strokes. The probability of hitting the mast, without taking streamers into account, was calculated in a previous paper [1]. The probability of hitting selected points on the structure or the vehicle will now be considered using a similar technique to estimate the probability of hitting the selected point in the presence of other attracting points on the protection system, the structure, or the vehicle. This information can be used as a factor in a management decision, such as when to start fueling in relation to weather conditions.

Ignoring streamering effects and using the simple principle that lightning (in its last jump to earth at its striking distance) will hit the closest point on the mast, structure, vehicle, or ground, "windows" of approach through which the lightning must travel to reach the closest point are created by this assumption. The windows are largest in the most vulnerable direction of approach and then narrow and close as azimuth and stroke magnitude are changed. By calculating the projected area of these windows on the ground and multiplying by the stroke density for each stroke size increment (each direction increment) and summing all the increments, a cumulative probability for all strokes hitting a selected point can be determined. Launch Pad 39B at KSC is shown is figure 1.

Figure 1. Shuttle Vehicle on Launch Pad 39B With a Water Tower on the Right

CRANE WINDOWS OF APPROACH

To illustrate the probability calculation process, consider the calculation of the probability of hitting the tip of the crane boom, which is about 32.3 m (106 ft) from the lightning mast centerline and 30.5 m (100 ft) below the mast lightning rod tip, as shown in figure 2. Arcs of various striking distances from these two points intersect on the perpendicular bisector of the line joining the two points. The bisector is the upper boundary of "crane windows," which are sectors of approach where the lightning leaders are closer to the tip of the crane boom than to the mast lightning rod or the ground when the leader makes its last jump to earth. The lower boundary of the crane windows is a parabola with focus at the tip of the boom tip and the earth as directrix. This boundary is the locus of points equidistant from the boom and the earth. Below the parabola, all the strokes hit the earth and above it all hit the lightning mast. The crane windows close at the striking distance where the bisector intersects the parabola. For a mast height of 122 m (400 ft) and a boom height of 91.5 m (300 ft), this occurs at a striking distance of 390 m (1280 ft). The windows are also the locus of the center of a "rolling ball" (having the striking distance as radius) as it rolls over the tips of the boom and mast rod.

The technique used previously by Stahmann [1] for estimating the stroke probability divided all strokes into deciles (see table I) having average peak currents and striking distances. The attractive radius, R, was calculated from the striking distance S_d, and the height of the mast lightning rod, H, using the relationship:

$$R = \sqrt{2S_d\,H-H^2} \tag{1}$$

The attractive area was calculated and then multiplied by a relatively high stroke density of 20 strokes/km^2/yr or 2x10^{6} strokes/m^2/yr/decile to obtain the stroke probability. The lightning rod is exposed to all strokes from all directions all year. However, to hit points below the rod (such as the crane tip), the lightning leader must enter through the associated window to hit the point. The windows change with direction of approach. The windows for the direction the crane boom is pointing is shown in figure 2. In other directions, up to 90 degrees from the crane pointing direction, the crane and mast rod tips are no longer coplanar and the distance difference to the leader is reduced, becoming zero at 90 degrees. Therefore, in other directions, the crane windows become smaller and close at lower striking distances. To calculate the probability of striking the crane (see table II), the areas of the horizontal projections of the crane windows for the various deciles were calculated as the projections were rotated ±90 degrees from the pointing direction, assuming that the projection did not change. However, more detailed calculations indicated that this area is actually about one-half of that calculated because the windows and projections change as the direction of approach is rotated. The geometry of the window projected area calculations is discussed in the next section. The largest stroke deciles are listed first in tables II and III.

GOX VENT ARM AND SOLID ROCKET BOOSTER (SRB) WINDOWS OF APPROACH

Three possible strike points are shown in figure 3, the mast rod, the tip of a rod on the GOX vent arm, and the SRB nose below the vent arm. The geometry for calculating the probability of hitting the vent arm is shown in figure 4 where a fourth point is added, the tip of a lightning rod on the top of the nearby 87.2 m (286 ft) water tower 160 m (525 ft) from the lightning mast centerline in an easterly direction, 38 degrees from the north. Figure 3 shows the east-west plane. Lightning leaders must approach from the east to reach the vent arm or SRB tip.

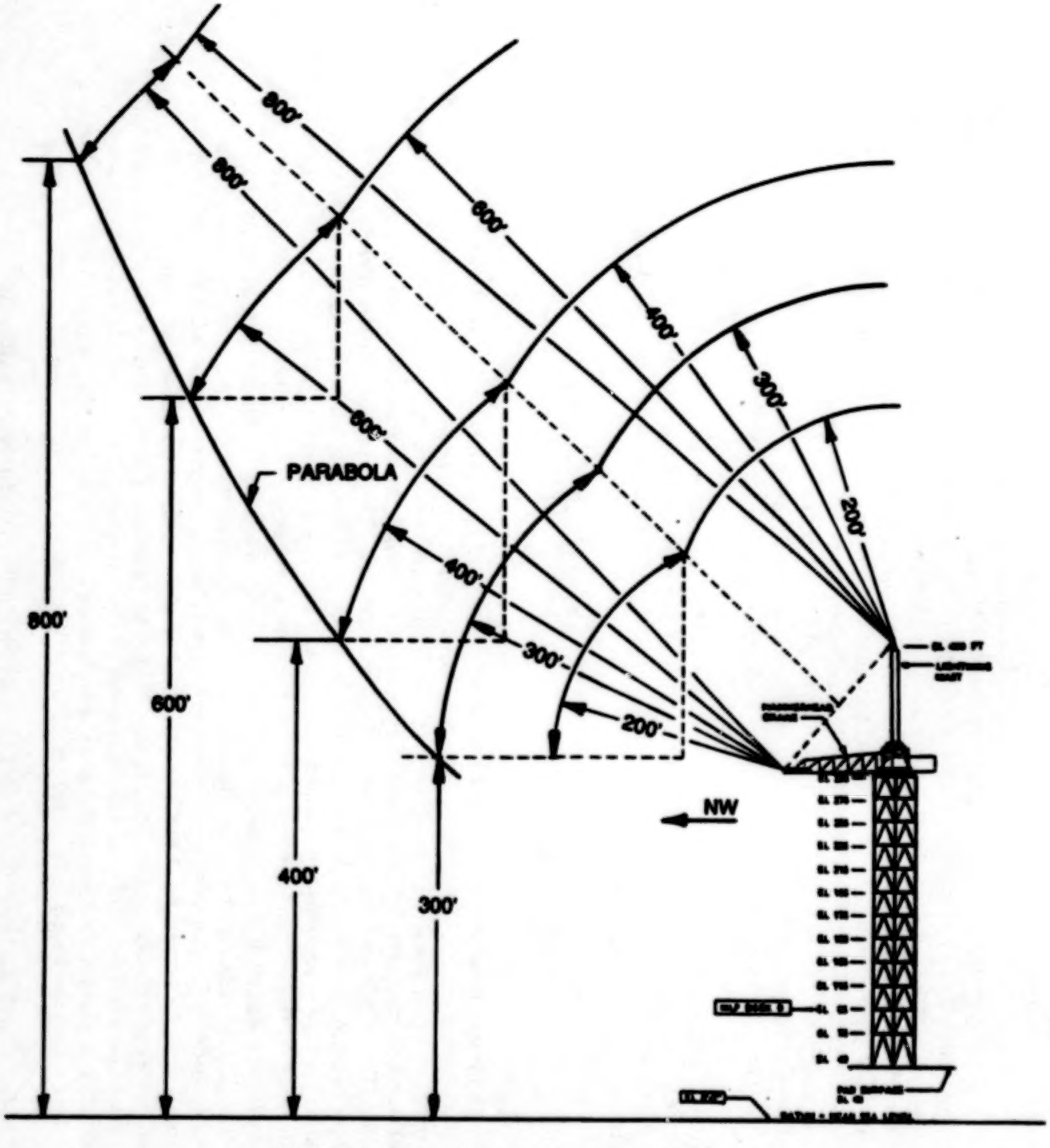
800'
800'
800'
600'
400'
300'
200'
800'
600'
400'
300'
200'
PARABOLA
800'
600'
400'
300'
NW
LIGHTNING MAST
HAMMERHEAD CRANE

Figure 2. Crane Windows of Approach

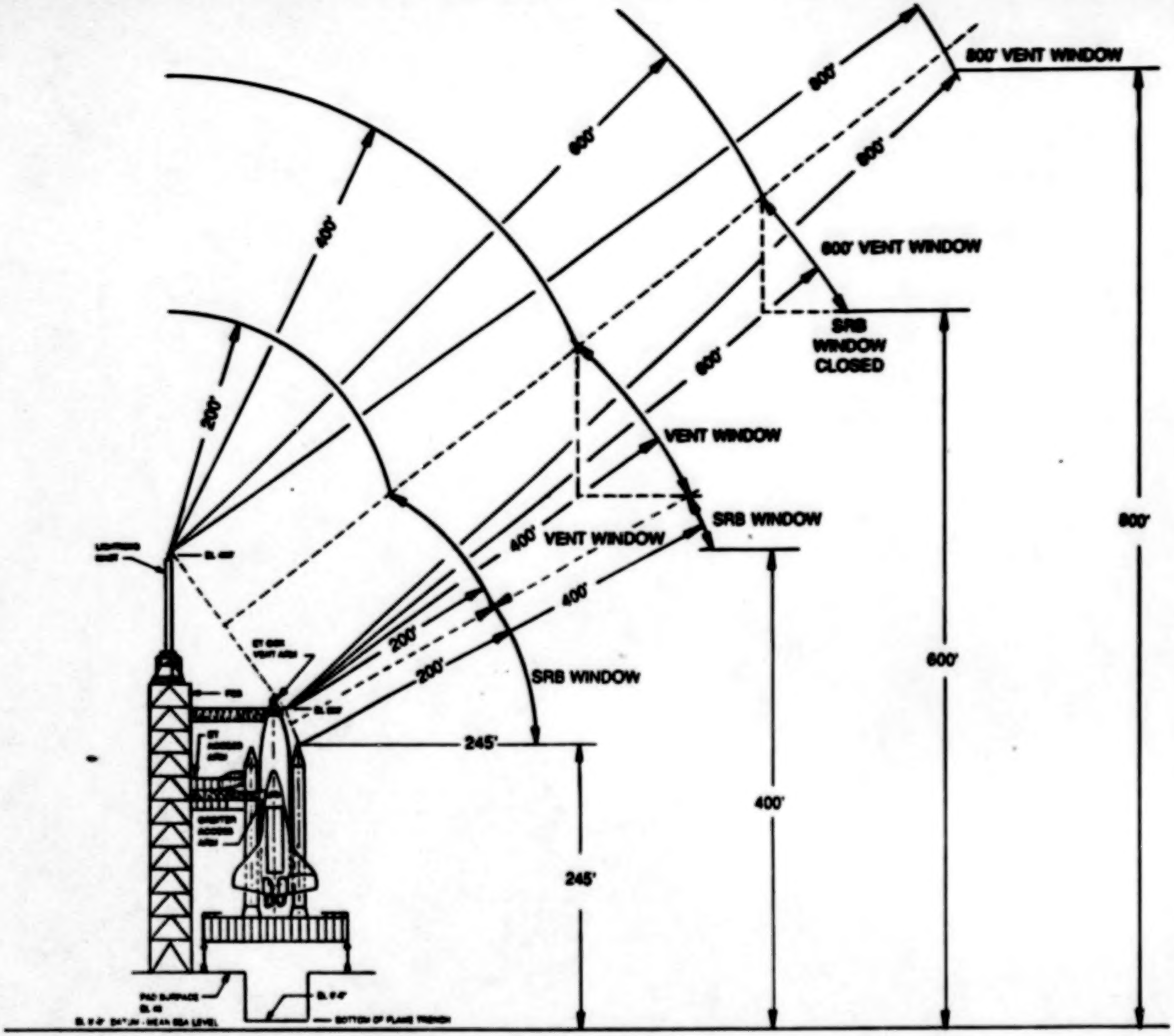
800' VENT WINDOW
800'
800'
800'
600'
400'
600' VENT WINDOW
SRB WINDOW CLOSED
600'
VENT WINDOW
200'
SRB WINDOW
400'
VENT WINDOW
400'
200'
200'
SRB WINDOW
LIGHTNING MAST
ET GOX VENT ARM
ORBITER ACCESS ARM
245'
245'
400'
600'
800'
PAD SURFACE
DATUM - MEAN SEA LEVEL
BOTTOM OF FLAME TRENCH

Figure 3. ET Vent Windows for Strokes Approaching Directly From the East

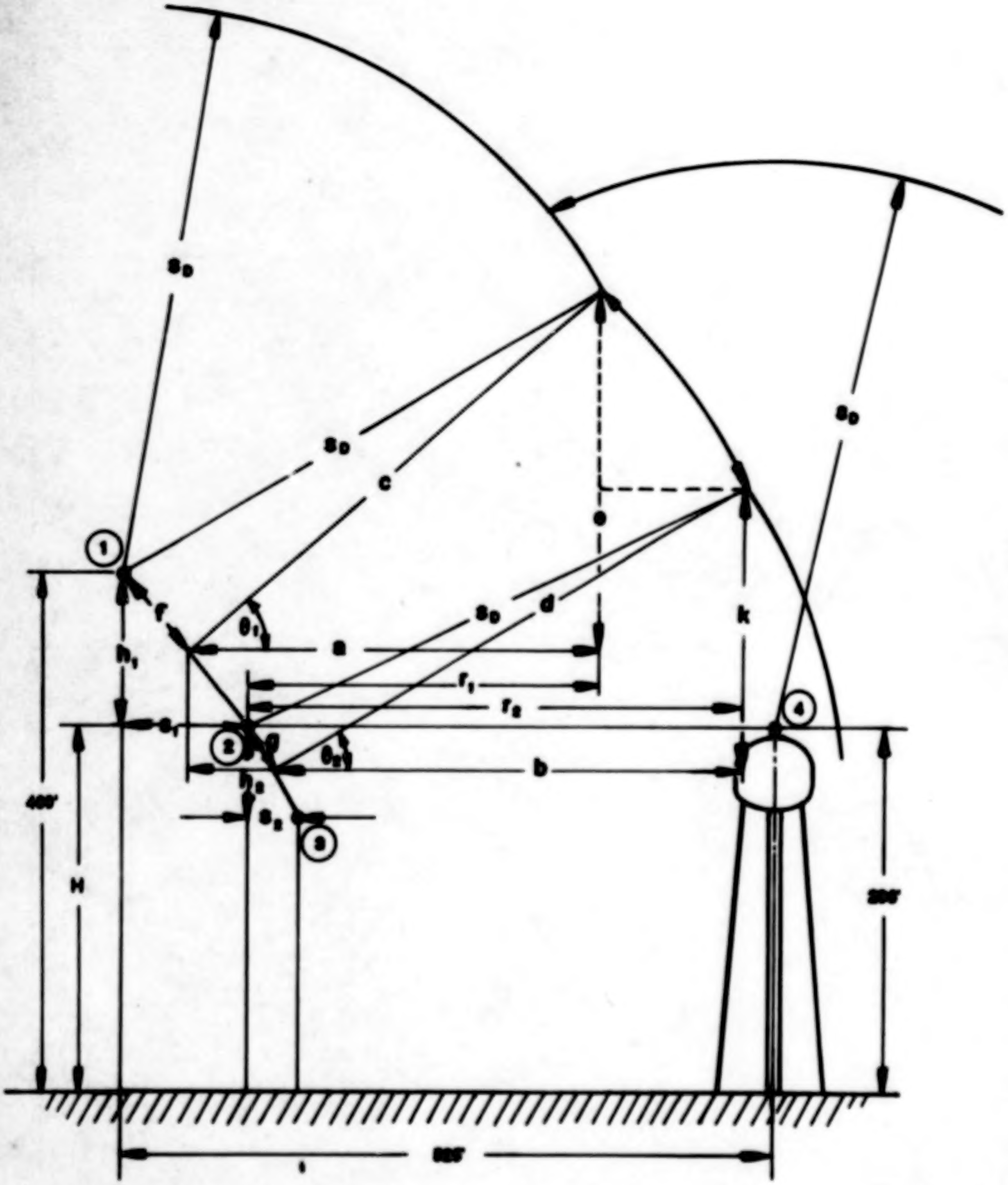
s_D
s_D
c
e
s_D
①
f
θ_1
s_D
d
k
h_1
a
r_1
r_2
④
s_1
②
θ
θ_2
b
h_2
s_2
③
400'
H
200'
825'

Figure 4. Geometry for Calculation of the ET Vent Window Projection on a Horizontal Plane

Table I. Probability of Striking a 122 m (400 ft) Tower

Decile	$\bar{i}_{pk}$	$\overline{S_d}$ (m)	$\bar{R}$ (m)	Area (m^2)	Decile Probability (Strokes/Year)	Cumulative Probability (Strokes/Year)	Years Per Strike
0-10	6.2 kA	46	46	6,648	0.01330	0.01330	75.2
10-20	12.9 kA	90	90	25,447	0.05089	0.06419	15.6
20-30	17.6 kA	115	115	41,548	0.08310	0.14729	6.8
30-40	22.7 kA	137	136	58,107	0.11621	0.2635	3.8
40-50	28.4 kA	161	156	76,454	0.15291	0.4164	2.4
50-60	35.2 kA	186	174	95,115	0.19023	0.6066	1.65
60-70	44.5 kA	217	195	119,459	0.23892	0.8455	1.18
70-80	57.0 kA	258	219	150,674	0.30135	1.1458	0.872
80-90	77.0 kA	318	250	196,350	0.39270	1.5395	0.65
90-100	112.0 kA	380	279	244,545	0.48909	2.0286	0.49

Table II. Probability of Striking the Crane

$\overline{S_d}$ (ft)	c (ft)	a (ft)	r_1 (ft)	r_2 (ft)	Area (m^2)	Decile Probability (Strokes/Year)	Cumulative Probability (Strokes/Year)
1246	1244	853	800	811	2,587	0.005174	0.005174
1043	1040	714	661	732	14,518	0.029036	0.03421
846	843	578	525	646	20,726	0.041452	0.07566
712	708	486	433	581	21,899	0.043798	0.11946
610	606	415	362	525	21,129	0.042258	0.16172
528	523	359	306	476	19,474	0.038948	0.20067
449	443	304	251	424	17,015	0.034030	0.23470
377	370	254	201	369	14,010	0.028020	0.26272
295	286	196	143	295*	9,721	0.019442	0.28216
151	132	91	37.7	151*	3,122	0.006244	0.28840**

* When $S_d < H$, $r_2 = S_d$

** Once every 3.46 years

Table III. Probability of Striking the GOX Vent Arm Lightning Rod

$\overline{S}_d$ (ft)	a (ft)	b (ft)	r_1 (ft)	r_2 (ft)	Area (m^2)	Decile Probability (Strokes/Year)	Cumulative Probability (Strokes/Year)
1043	772	**	717	711	Closed	--	--
846	625	**	571	629	10,181	0.020362	0.020362
712	525	**	471	566	14,424	0.028848	0.049210
610	449	**	394	513	15,716	0.031432	0.080642
528	387	**	333	466	15,540	0.031080	0.111722
449	328	**	273	416	14,362	0.028724	0.140446
377	243	**	219	364	12,374	0.024748	0.165194
295	210	344	156	295	8,691	0.017382	0.182576
151	95	204	40	150	3,036	0.006072	0.188648*

* Once every 5.3 years

** Ground stroke formula applies:

$$r_2 = \sqrt{2S_dH-H^2}$$

Windows are created for each of the three points. The SRB window starts to close at 74.7 m (245 ft) and closes at 164.9 m (541 ft) in this plane. The external tank (ET) vent windows close at about 313.7 m (1029 ft). The dimensions used are H=85.4 m (280 ft), h_1=36.6 m (120 ft), h_2=10.7 m (35 ft), s_1=33.1 m (108.5 ft), and s_2=2.7 m (9 ft). The formulas used for calculating the GOX vent arm window horizontal projected area are:

$$c = \sqrt{S_d^2 - f^2} \tag{2}$$

$$a = c \cos \theta_1 \tag{3}$$

$$d = \sqrt{S_d^2 - g^2} \tag{4}$$

$$b = d \cos \theta_2 + (s_1 + s_2)/2 \tag{5}$$

$$r_1 = a - s_1/2 \tag{6}$$

$$r_2 = r_1 + b - a \tag{7}$$

where r_1 and r_2 are the attractive radii of the upper and lower window boundaries, respectively. The maximum attraction area for each decile produced by rotating the windows through all easterly directions ±90 degrees from directly east is:

$$Area(m^2) < \pi/2 \ (r_2^2 - r_1^2)/3.28^2 \tag{8}$$

where r_1 and r_2 are in feet. As previously mentioned, this estimate of the area is a maximum since the windows close at shorter striking distances in other directions of approach other than directly east. The closure formulas are:

For the GOX vent arm, closure occurs at:

$$S_d = H + h_1/2 + e = \sqrt{c^2 + f^2} \qquad \text{Solve for e and } S_d \tag{9}$$

For the SRB, closure occurs at:

$$S_d = H - h_2/2 + k = \sqrt{d^2 + g^2} \qquad \text{Solve for k and } S_d \tag{10}$$

Of particular interest is the water tower shown in figure 4. This tower appears at first glance to offer little protection to the GOX vent arm. Actually, since the lightning leader must come in through the vent windows in order to reach the arm, it must pass within 85.4 m (280 ft) of the tower when approaching from a northeast direction (38 degrees). The water tower will then capture all strokes with striking distances greater than 85.4 m (280 ft) (80 percent of all strokes). From the south, the large rotating service structure (RSS) helps protect the ET so that the probability of hitting the ET is reduced in this direction. Table III gives a maximum cumulative probability of hitting the GOX vent arm with lightning rod once every 5.3 years. Considering window closure and other factors, the maximum probability is closer to once in 10 years.

The above assumes continuous exposure for a full year. Since the vehicle is not present at all times and the GOX vent arm is retracted most of the time, the probability must be multiplied by the exposure percentage per year. For example, if the exposure time is 10 percent per year, the probability is reduced to once in 100 years or less if the exposure is less.

STREAMERING EFFECTS

An important factor in protecting the pad structures is the formation of streamers from the sharp points on the structures. The most prominent sharp point is the tip of the rod on the lightning mast. As shown in figure 5, the streamers go out to greet the down-coming leaders and meet in the characteristic "knee" shown. Figure 6 shows that, while the ET ogive is protected since it is within the NFPA 78 zone of protection based on a 30 m (100 ft) striking distance, the ET ogive is further protected by streamers from the GOX vent arm and the tip of the SRB. These streamers form earlier and move farther than any streamers that may form on the ogive.

CONCLUDING DISCUSSION

The probability of lightning striking points on a structure beneath the highest point can be estimated. Often the protected points can be approached only from a limited range of directions and along paths that have a large horizontal component. In a particular case, such as hitting a vehicle in the presence of a nearby structure, the structure may be modified to better protect the vehicle by improving the protective geometry and by encouraging the formation of protective streamers that can intercept the stroke leader using diverters in the high field regions.

REFERENCES

1. J. R. Stahmann, "Inside the Cone of Protection," International Aerospace and Ground Conference on Lightning and Static Electricity, Fort Worth, Texas, June 21 to 23, 1983, pp. 27-1 to 27-7.

2. R. H. Golde, "Lightning Conductor," Lightning, Volume 2, Chapter 17, Academic Press, 1977, pp. 545 to 576.

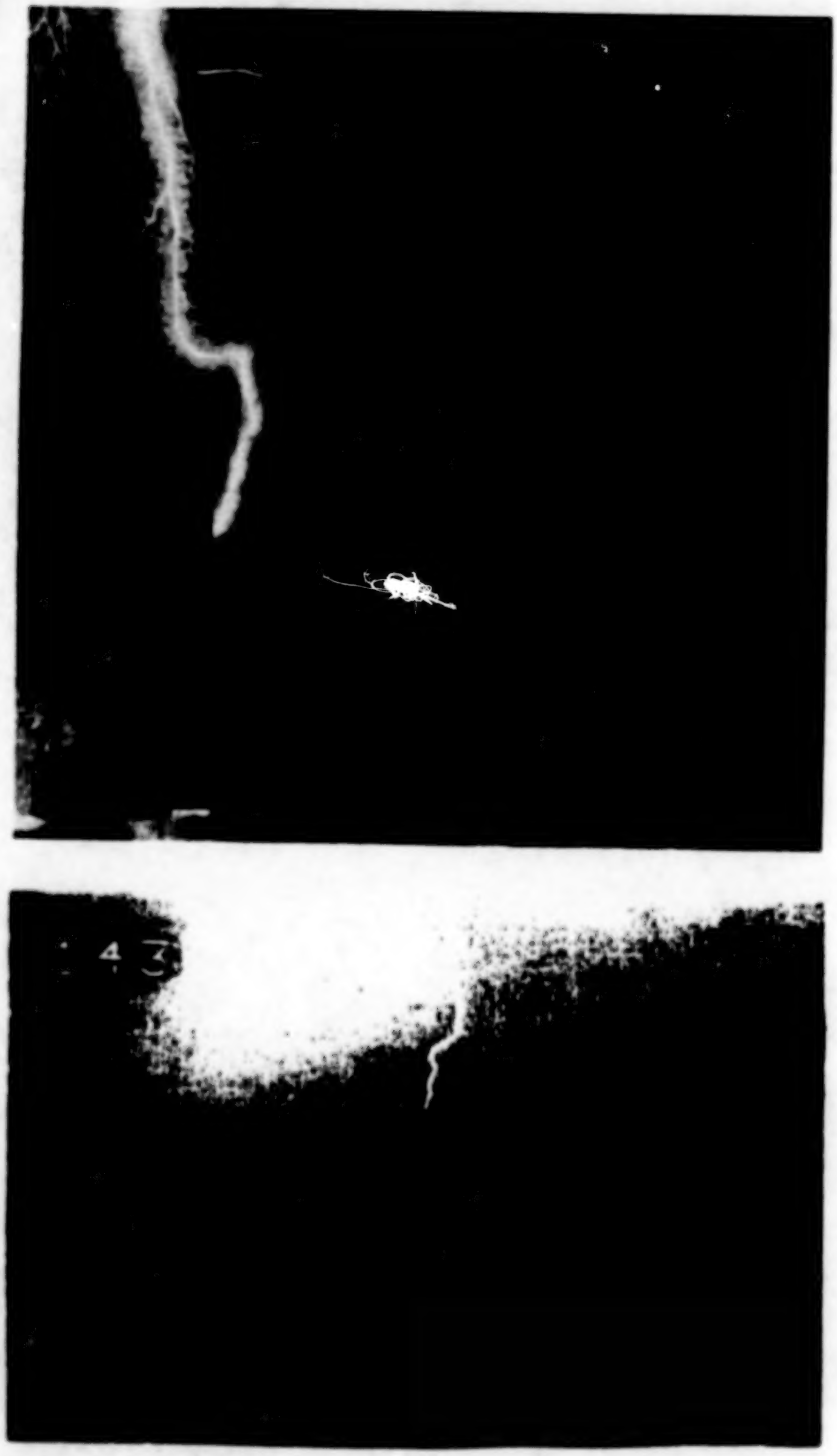

Figure 5. Two Strokes to the Pad Lightning Protection System Showing "Knee" Where an Upward-Going Streamer Meets a Down-Coming Leader

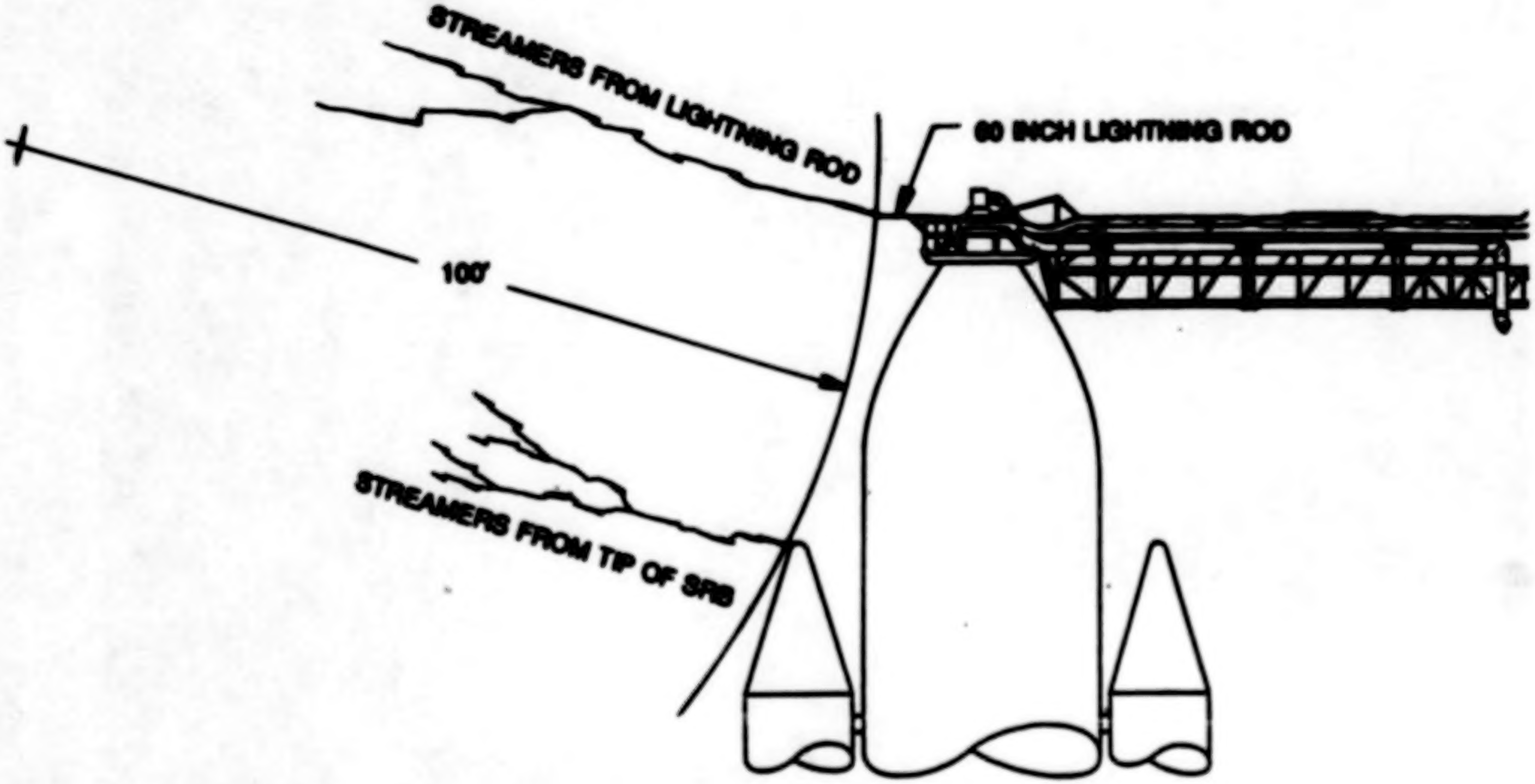
STREAMERS FROM LIGHTNING ROD
60 INCH LIGHTNING ROD
100'
STREAMERS FROM TIP OF SRB

Figure 6. With the lightning rod on the GOX vent arm, the ET ogive is protected against strokes with $S_d \geq 100$ feet (streamers provide additional protection).

ACTIVATION OF THE NAVY'S INDIRECT EFFECTS LIGHTNING SIMULATION LABORATORY

Mike Whitaker
Electromagnetic Pulse Section, Naval Air Test Center
Patuxent River, Maryland

ABSTRACT

The Naval Air Test Center is currently the Navy's lead laboratory for electromagnetic effects testing. As part of this charter, it has been performing lightning effects testing on Navy aircraft in support of specification compliance since 1973. This paper presents an overview of lightning test and evaluation efforts at the Naval Air Test Center, both past and present, as well as its plans for the future. The array of simulation capabilities presently operational are described, and a high-level look is given to the test methodology now being used.

The principal discussion of this paper centers on the results from the recent air-launched ordnance test and the testing of the Navy's A-6E all-weather attack aircraft. Particular attention is paid to the Naval Air Test Center's test approach, including details about coaxial return construction, aircraft preparation, and the test waveforms and data acquisition systems that were used.

1. INTRODUCTION

Electromagnetic effects testing for the Navy is the responsibility of the Naval Air Test Center's Electromagnetic Systems Department. The Navy's lightning simulation facility operated from 1973 through early 1986. In 1986, the old simulation equipment was dismantled due to equipment degradation and the concerns of the Occupational Safety and Health Administration about the insulation oil contained in the storage capacitors.

Almost immediately, the Naval Air Test Center began acquiring equipment to assume its role in the testing of naval aircraft. Studies were then conducted to evaluate the Navy's needs and to determine the equipment necessary to perform the testing required for qualifying Navy aircraft to operate in the lightning environment. It was determined that the primary thrust should initially be concentrated on full-scale testing for the indirect effects of lightning on aircraft and systems.

Equipment presently on hand at the Naval Air Test Center is described in table I. The Naval Air Test Center's in-house expertise provides the ability to construct simulators as required for testing in any of the disciplines.

SYSTEM	TYPE	OUTPUT	STATUS
LIGHTNING			
NAILS	SEVERE THREAT	UP TO 200 kA	DEPLOYED
NAPLES	PORTABLE MODERATE THREAT	UP TO 100 kA	DEPLOYED
LOW-LEVEL			
LLCW	LIGHTNING	UP TO 20 A, 10 kHz–10 MHz	UNDER DEVELOPMENT
DIRECT-DRIVE			
LIGHTNING	CIRCUIT/CABLE DIRECT-INJECT	MIL-STD-461 UP TO 30 A @ 100 kW	INITIAL PLANNING

Table 1. Major Lightning Simulators

2. TEST METHODOLOGY

The primary goals of electromagnetic transients testing at the Naval Air Test Center are to determine specification compliance and to quantify system survivability/vulnerability. Our mission is to provide cost-effective and timely test and evaluation services.

The Naval Air Test Center has developed a standardized, modular approach for all plans, procedures, and reports. Any of these can be modified to accommodate a user's requirement.

As shown in table I, the Naval Air Test Center has the simulators required for producing the waveforms for full-scale aircraft testing. Aircraft can be qualified either by full-threat testing or testing at a lower level. In addition, the Naval Air Test Center can extrapolate cable responses and perform current injection direct-drive testing at the threat level to determine the survivability/vulnerability of aircraft. Through cable injection, the aircraft can be tested to a moderate level without subjecting it to the unnecessary stresses of repeated injection of high currents into the airframe. This alternative provides the user with a non-destructive way to test to levels that are not obtainable or that are sometimes recommended for full-scale aircraft due to the unique construction of the airframe.

3. TEST WAVEFORMS AND SIMULATION

The Naval Air Test Center performs testing tailored to military standards and contractual requirements. Early on in the procurement cycle, the test waveforms are decided and agreed to by both the aircraft manufacturer and the Navy. The Navy can produce either the high threat severe waveform or waveforms of lower energy content to acquire large amounts of data without applying undo stresses to an operational aircraft.

During our recent testing on an air-launched torpedo and the composite-wing A-6E aircraft, a damped sinewave was used that met the amplitude and rate-of-rise requirements. Figures 1 and 2 identify the typical waveform injected into these test objects. The simulator used for testing (photo 1 and figure 3) is a modular generator with gas-operated switches. The simulator is portable, and each of its three stages can be operated separately or stacked for various loads and current requirements. Each stage can contain up to four parallel capacitors. Because each three-stage module is insulated with gas, the simulator has a low-inductance construction. The simulator can be triggered either electrically or by dumping the pressure on the first spark gap to cascade the Marx stack.

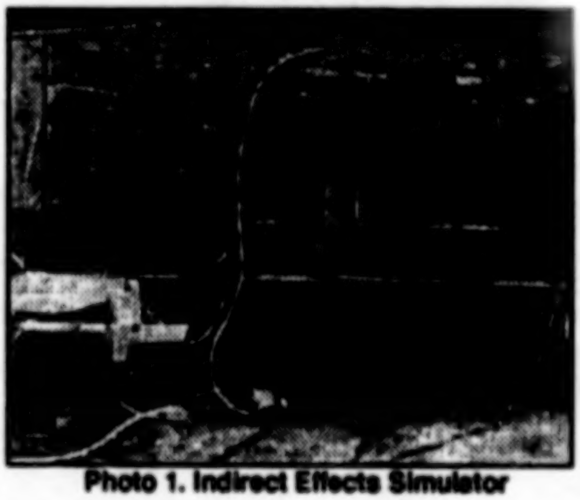

Photo 1. Indirect Effects Simulator

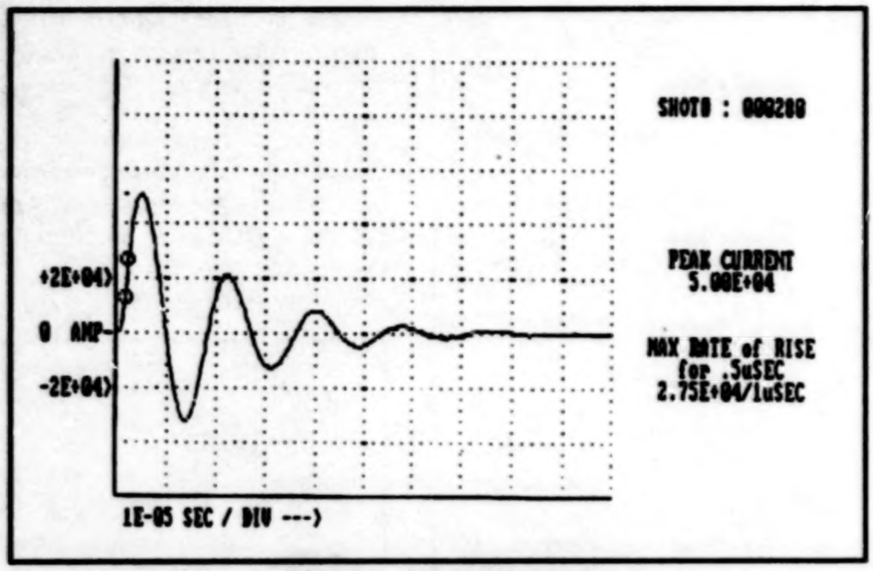

Figure 1. Input Waveform

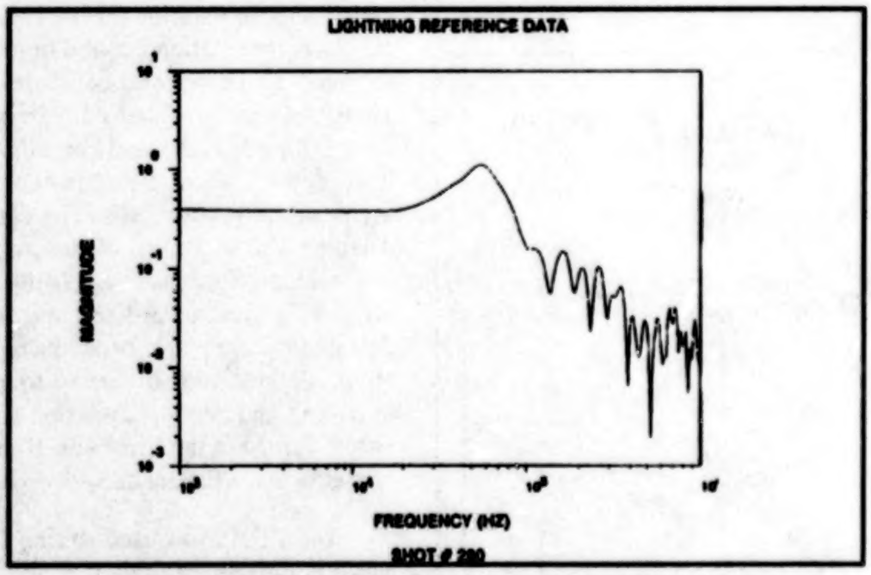

Figure 2. Frequency Spectrum of Input Waveform

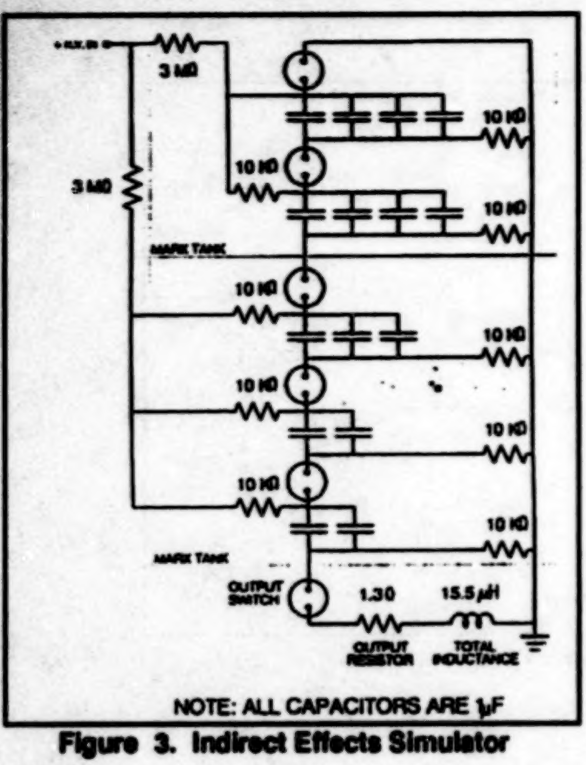
3 MΩ
3 MΩ
10 kΩ
MARX TANK
OUTPUT SWITCH
1.3Ω
15.5 μH
OUTPUT RESISTOR
TOTAL INDUCTANCE
NOTE: ALL CAPACITORS ARE 1μF

Figure 3. Indirect Effects Simulator

To gain a high level of confidence in the aircraft and systems during the composite-wing A-6E test, the Naval Air Test Center employed its Current Injection Direct-Drive System (figure 4) to increase the amplitudes at the cable level and performed this test with systems operating.

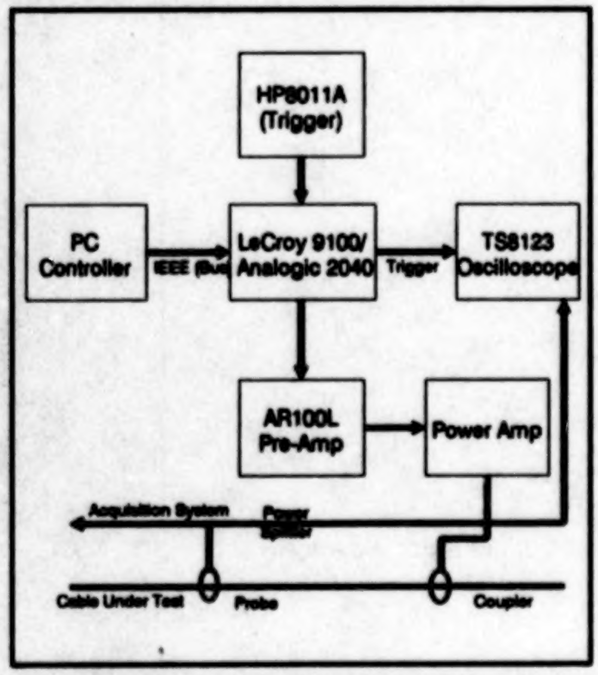
HP8011A (Trigger)
PC Controller
IEEE (Bus)
LeCroy 9100/ Analogic 2040
Trigger
TS8123 Oscilloscope
AR100L Pre-Amp
Power Amp
Acquisition System
Power Splitter
Cable Under Test
Probe
Coupler

Figure 4. Current Injection Direct-Drive System

4. DATA ACQUISITION SYSTEM

The portable data acquisition system (PDAS) is the primary system for lightning and direct-drive testing.

The data acquisition concept permits high-volume data throughout and immediate processing. All data are automatically maintained in a database. Data gathered from the simulators during testing are downloaded to a central laboratory (see figure 5).

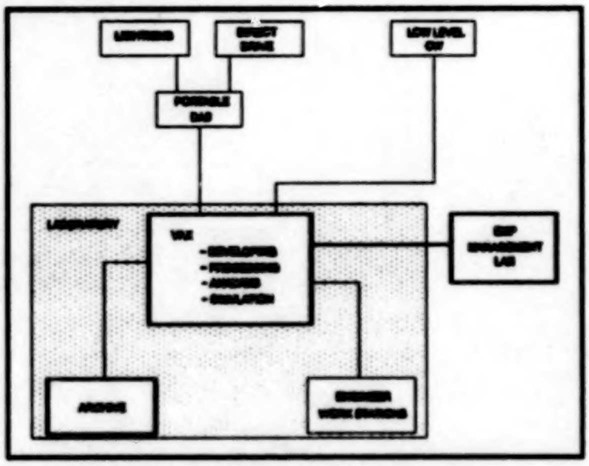
LIGHTNING
DIRECT DRIVE
LOW LEVEL CW
PORTABLE DAS
LABORATORY
VAX
EMP MANAGEMENT LAB
ARCHIVE
ENGINEER WORK STATIONS

Figure 5. The Instrumentation Suite

There, all data are maintained in a database and ultimately combined with other electromagnetic transient data for the user. Also avaiable are data presentation capabilities, such as histograms, bar charts, and comparison tables. These data are provided daily in hard copy form, along with other logs and records, as part of the final report. When testing is completed, the users can be provided with the data on a database and with most of the software necessary to continue offsite analysis. Most aspects of data acquisition are standardized and segmented. All data acquisition plans, procedures, and reports are predefined and structured to allow the user to outline and adequately scope his test. This system furnishes the user with high flexibility in cost-effective, efficient test environment.

The PDAS was used during recent testing, which is discussed in this paper. Figure 6 offers a brief block diagram overviewing the PDAS. In addition, sample outputs are shown in figures 7 and 8. Data from this test were acquired on test points from EG&G 91550-2 or Prodyn I-125-2C probes. Surface current measurements were made using MGL-5 probes.

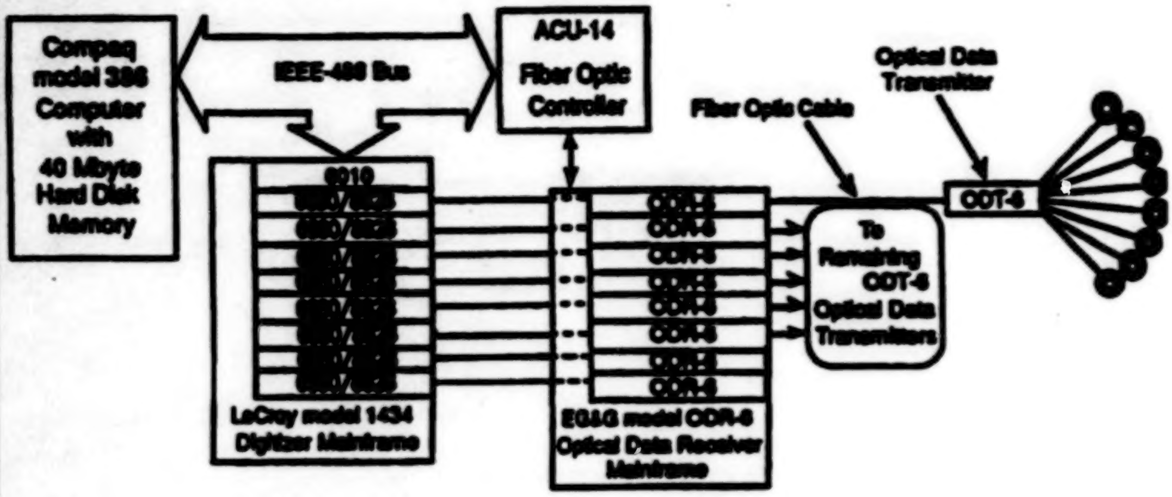
Compaq model 386 Computer with 40 Mbyte Hard Disk Memory
IEEE-488 Bus
ACU-14 Fiber Optic Controller
Optical Data Transmitter
Fiber Optic Cable
8010
ODT-8
ODR-8
To Remaining ODT-8 Optical Data Transmitters
LeCroy model 1434 Digitizer Mainframe
EG&G model ODR-8 Optical Data Receiver Mainframe

Figure 6. The Portable Data Acquisition System

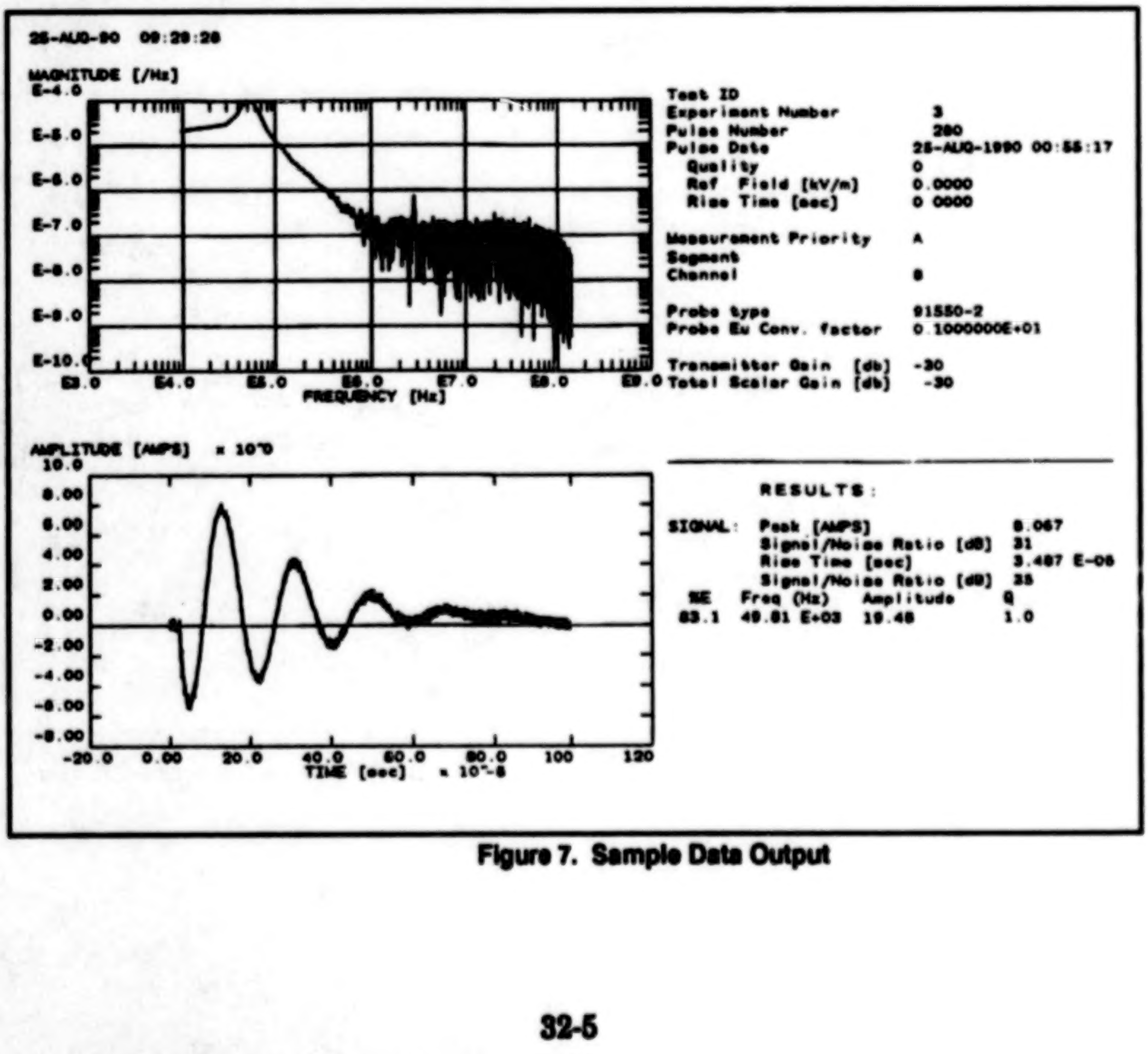

```
25-AUG-90   09:29:28

Test ID
Experiment Number            3
Pulse Number                 280
Pulse Date                   25-AUG-1990 00:55:17
   Quality                   0
   Ref  Field [kV/m]         0.0000
   Rise Time [sec]           0 0000

Measurement Priority         A
Segment
Channel                      8

Probe type                   91550-2
Probe Eu Conv. factor        0.1000000E+01

Transmitter Gain  [db]       -30
Total Scalar Gain [db]        -30

              RESULTS:

SIGNAL:  Peak [AMPS]                       8.067
         Signal/Noise Ratio [dB]           31
         Rise Time [sec]                   3.487 E-06
         Signal/Noise Ratio [dB]           35
  %E    Freq (Hz)    Amplitude        Q
 83.1   49.81 E+03   19.48            1.0
```

Figure 7. Sample Data Output

287

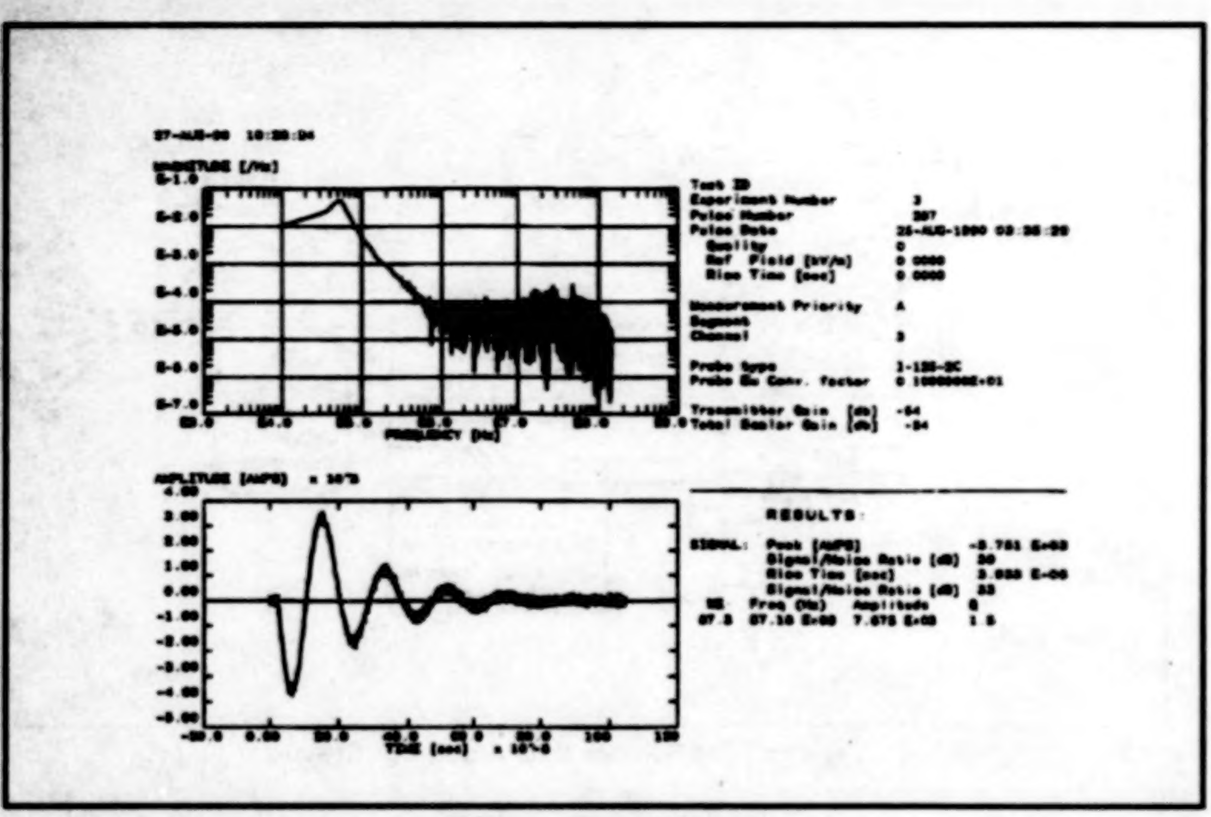

Figure 8. Sample Report

8. PREPARATION OF TEST FIXTURE

For the composite-wing A-6E test in summer of 1990, the aircraft was positioned within a coaxial return test fixture (figure 9). The aircraft was first hoisted onto isolation pads (photo 2). The second step of preparing the aircraft for test was to build a mechanically strong wooden frame around the aircraft to provide support and an adjustable coaxial return grid (see photo 3). The coaxial return consisted of 12 copper tubes, each one-quarter inch in diameter. Copper tubes were run both parallel and perpendicular to the aircraft. Tubing was soldered together, creating a 1-meter-square grid. Nylon ropes were used to control the 1-meter spacing from the aircraft skin. Use of the 1-meter grid and 1-meter spacing from the skin permitted easy access to equipment bays for changing instrumentation during the test. The calculated impedance of this 1-meter spacing ranged from 41.6 to 65.8 ohms. During testing of one configuration, the spacing from the aircraft skin was decreased to one-half meter, for an impedance range of 24.3 to 41.6 ohms.

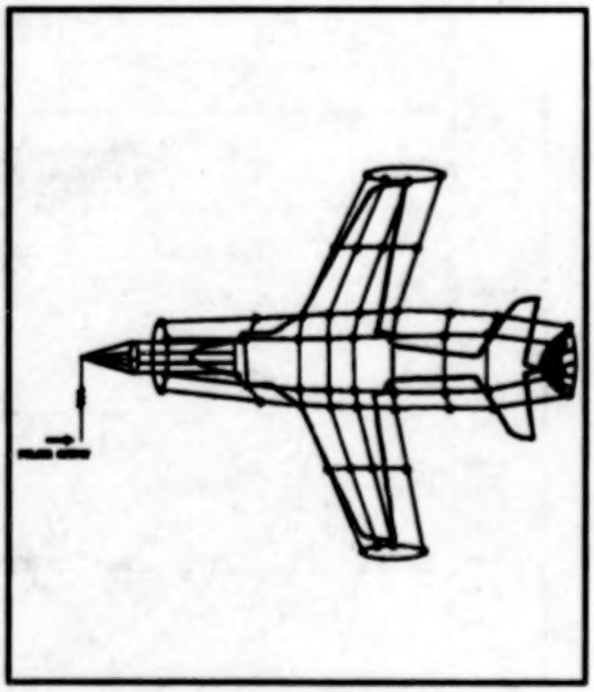

Figure 9. Coaxial Return Test Fixture

The construction of coaxial returns varies, depending on the size and shape of the test object. For smaller test objects, such as air-launched ordnance or missiles, styrofoam spacers are used to support the wire grid in place of wooden framework.

Constructing the coaxial return as a solid grid greatly facilitated changing from one test configuration to another, e.g., changing from nose-to-tail to wing-to-wing configuration. Very little test time was lost when relocating the simulator to vary the entry and exit points for injected current.

Photo 2. Isolation Pads

6. AIR-LAUNCHED ORDNANCE TEST

The Naval Air Test Center supported the Naval Surface Warfare Center in fall of 1989 by performing lightning and ESD tests on an air-launched torpedo. The test required 25 kV ESD, 300 kV ESD, and up to 50 KA injected current. ESD was injected in various test points. Lightning was injected into the major current paths that would exist if the torpedo or its host aircraft were hit by lightning. Due to the nature of the test object, there were no current probes mounted into the torpedo. After each amplitude, a functional checkout was performed to determine failures.

In response to numerous safety concerns, the test torpedo was mounted on a moveable stand, and the coaxial return was built around and supported by the test object itself. To remove the test object from the test area, as in cases of emergency, it would have been necessary only to release two bolts and tow the test object to a safe area.

This experience thoroughly exercised the Naval Air Test Center's procedures for conducting a potentially hazardous test, while causing little impact on other electromagnetic testing being performed within the shielded hangar.

Photo 3. Test Setup

7. COMPOSITE-WING A-6E TEST

During August and September of 1990, indirect effects lightning testing on the Navy's newly rewinged A-6E was performed. The new wing was constructed of graphite, titanium, and aluminum. Testing was required to assure the Navy that the new wing would not seriously degrade the inherent lightning protection offered by the old metal wing. Previous direct effects testing was performed by the new wing's manufacturer.

No lightning indirect effects testing was ever performed on the *metal* wing A-6E, although a substantial HEMP database had been developed on both the metal wing and the composite wing. This database proved invaluable in the development of the test points for the lightning test. The list of test points was narrowed to a minimum of 104 points. By acquiring data on these points, susceptibility of the safety-of-flight and mission essential equipment could be determined.

The test approach was to exercise all of the major current paths by injecting current from nose to tail, nose to wing, wing to wing, and wing to tail. A minimum of two current amplitudes was planned for each test configuration to aid in the extrapolation of data to the full-threat environment. Table II shows the allocation of test points and amplitudes. Table III presents the various experiments by aircraft location.

During this test, a total of 442 acceptable data responses on 104 test points was added to the A-6E database.

Of these 104 test points, the Naval Air Test Center used direct-drive test techniques to further drive 43 of the acquired responses to the full-threat level.

By using a moderate current followed by direct-drive testing, the Naval Air Test Center could evaluate the survivability of the A-6E with a high degree of confidence.

Table II. Allocation of Test Points and Amplitudes

Experiment ID Number	Configuration	Amplitude (in kA)	Number of Test Points	Number of Test Shots
1	Nose-to-Tail	20	104	95
2	Nose-to-Wing	35	71	51
3	Wing-to-Wing	50	53	26
4	Wing-to-Tail	50	53	26
5	Canceled	–	–	–
6	Wing-to-Wing (modified coaxial return)	50-72	22	20
10	Direct-Drive	N/A	43	43

Table III. Experiments by Aircraft Location

Aircraft Location	Experiment				
	1	2	3	4	6
Radome (RADOME)	X	X	–	–	–
Cockpit (CKPT)	X	X	–	–	–
Forward Fuselage (FWD)	X	X	–	–	–
Mid Fuselage (MID)	X	X	X	X	X
Main Wheelwell (MWWELL)	X	X	X	X	X
Aft Bay (AFTBAY)	X	–	–	X	–
Left Wing (LWING)	–	X	X	X	X

8. CONCLUSIONS

The Naval Air Test Center has a prominent role in the DoD as a Major Range Test Facility Base. It is the primary research, development, test, and evaluation laboratory for DoD aircraft. As such, it offers its users the highly sophisticated resources necessary to ensure specification compliance and mission survivability of aircraft systems in a lightning environment. And as plans for continued development of the facility's capabilities are implemented, the Naval Air Test Center will offer an even broader spectrum of services to support users.

9. ACKNOWLEDGMENTS

The Navy expresses its appreciation for the excellent support received from its contractual team: Ktech for its operation and maintenance of simulators and facilities, BDM for its operation and maintenance of the instrumentation, and UIE for its test engineering technical support.

CHARACTERIZATION OF VERTICAL ELECTRIC FIELDS AND ASSOCIATED VOLTAGES INDUCED ON A OVERHEAD POWER LINE FROM CLOSE ARTIFICIALLY INITIATED LIGHTNING

M. Rubinstein M.A. Uman E.M. Thomson P.J. Medelius

Department of Electrical Engineering
University of Florida, Gainesville 32611

ABSTRACT

We characterize measurements, obtained during the Summer of 1986 at the NASA Kennedy Space Center, of simultaneous vertical electric fields and voltages induced at both ends of a 448 m overhead power line from artificially-initiated lightning return strokes. The lightning discharges were about 20 m from one end of the line. The measured line voltages could be grouped into two categories, those in which multiple, similarly shaped, evenly spaced pulses were observed, which we call oscillatory, and those dominated by a principal pulse with subsidiary oscillations of much smaller amplitude, which we call impulsive. Voltage amplitudes range from tens of kilovolts for oscillatory voltages to hundreds of kilovolts for impulsive voltages.

INTRODUCTION AND EXPERIMENTAL SETUP

A top view of the experiment is shown in Fig. 1. Induced voltages from triggered lightning return strokes at 20 m were measured on a specially constructed unenergized three phase power distribution line spanning about 450 m. The measurements were made on the open circuited top phase of the line, that phase being approximately 10 m above the ground. The two remaining phases were also left open-circuited throughout the experiment. The voltage at either end of the top phase was sampled by means of a specially constructed noninductive voltage divider with a total resistance of about 10 kOhm, the "open circuit" termination impedance. Additionally, the vertical electric field was measured at a distance of about 500 m from the triggered return strokes.

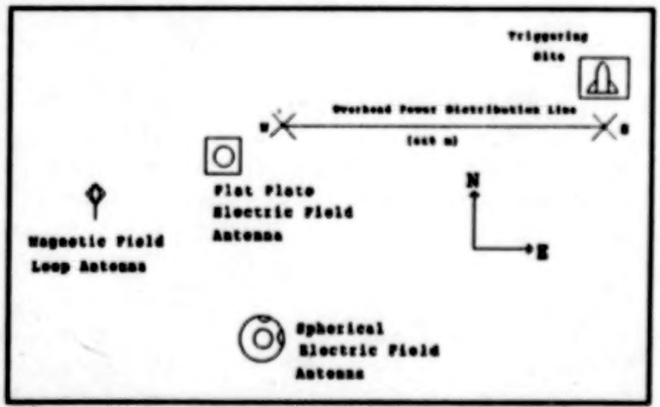
Triggering Site
Overhead Power Distribution Line
W
E
(448 m)
Flat Plate Electric Field Antenna
N
E
Magnetic Field Loop Antenna
Spherical Electric Field Antenna

Figure 1. Layout of the experiment site.

The signals out of the voltage dividers and the electric field antennas were amplified, transmitted through fiberoptics cables, and stored both on analog and on digital storage media. The digitization of the data was done in real time with a LeCroy high speed digitizer system. Simultaneously, the analog signals were recorded on direct and FM channels of a Honeywell 101 analog tape recorder. These analog data were later digitized with both a MassComp computer and an improved version of the LeCroy system. The voltage measurement system had a bandwidth of 750 kHz. The bandwidths of the direct and FM channels of the

Honeywell tape recorder are 400 Hz to 2 MHz and 0 Hz to 500 kHz, respectively, and they determined the bandwidth of the vertical electric field waveforms.

CHARACTERIZATION OF THE FIELDS

Examples of return stroke vertical electric field changes associated with a 7-stroke triggered lightning that occurred on day 232 in 1986, together with voltages measured at either end of the test line are shown in the top traces of Figures 2 and 3. To facilitate the characterization of the return stroke fields, a typical return stroke field has been sketched in Figure 4, in which all the parameters of interest (defined below) have been identified. The vertical electric field starts with a slow field change, presumably from the dart-leader. This slow change, which we label L for leader, precedes a fast positive field change termed R, for return stroke, which ends typically in a small glitch (not discernible in Figures 2 and 3). This fast change is followed by a slower change of the same polarity termed S in Figures 2 through 4. The overall S change, which typically exhibits a dip near its onset (which can be seen in Figures 2 and 3 and is not to be confused with the small glitch observed at the end of R), rises with constantly decreasing slope. The average amplitude of the R change is 878 V/m with a standard deviation of 445 V/m. The average 0 to 100% rise time of R is 803 nanoseconds with a standard deviation of 337 nanoseconds. The average time between the start of R and the bottom of the dip in the S field change is 2.5 μsec with a standard deviation of 0.87 μsec.

CHARACTERIZATION OF THE VOLTAGES

The voltages measured at either end of the test line can be grouped into two categories: (1) those in which a series of evenly spaced, similarly shaped pulses with decaying amplitudes can be observed, which we define as "oscillatory" voltages, of which six were recorded, and (2) those that present a clearly dominant pulse with subsidiary oscillations of much lower amplitude, which we call "impulsive" voltages, and of which five were recorded. Voltage waveforms corresponding to impulsive and oscillatory voltages are shown in figures 2 and 3, respectively. For the discussion that follows, refer to figures 5a and 5b where we have sketched typical impulsive and oscillatory voltages and where we have included the definitions of the parameters to be discussed. Both oscillatory and impulsive voltages were observed to occur for different strokes in the same 7-stroke flash recorded on day 232. The mean amplitude of the R electric field changes associated with oscillatory voltages on the line, 500 V/m, is less than half the mean amplitude of the R changes associated with impulsive voltages, 1.33 kV/m. As we shall see, the maximum induced oscillatory voltages are on average, a factor of 8 to 10 times less than the maximum impulsive voltages, indicating that there are other factors than the measured vertical field amplitude involved in the coupling.

Oscillatory Voltages

In the following characterization, all amplitudes are measured with respect to zero level, where zero is marked by the initial horizontal segment of the waveform. The oscillatory voltages measured at the end nearer to the triggering site (east end) start with a positive pulse whose front rises to peak in some 20 μsec. This pulse, which we term U_e, has a mean amplitude of 19 kilovolts with a standard deviation of 9 kilovolts. After this initial positive-going pulse a series of negative pulses ensues. We call the first three of these pulses T_o, subsidiary 1, and subsidiary 2, respectively. Typically, these pulses have monotonically decaying amplitudes although for the oscillatory voltages recorded on day 232 the second negative pulse is larger than the first. The mean amplitudes of the T_o, subsidiary 1, and subsidiary 2 pulses are −47, −43, and −29 kilovolts, respectively, with corresponding standard deviations 21, 10 and 5 kilovolts. The mean width at half amplitude maximum of T_o is 744 nanoseconds (standard deviation 149 nanoseconds). The average time between the peaks of the T_o and the subsidiary 1 pulses is 3.3 μs (standard deviation 0.3 μs), whereas between the peak of the two subsidiary pulses this time is 3.1 μs (standard deviation 0.2 μs).

The oscillatory voltages measured at the end farther from the triggering site (west end) exhibit features very similar to those described for the voltages measured at the near end: a slow positive pulse followed by a series of sharper negative pulses. We have labeled the positive pulse N_o and the first negative pulse M_o. As in the case of the oscillatory voltages at the east end, we call the two next negative pulses subsidiary 1 and subsidiary 2, respectively. At the west end, the voltages present monotonically decaying pulses in all the events recorded. The mean peak amplitude of N_o is 27 kilovolts (standard deviation 5 kilovolts). The mean peak amplitudes of the M_o, subsidiary 1, and subsidiary 2 pulses are −72, −53, and −39 kilovolts, respectively, with corresponding standard deviations 20, 10, and 3 kilovolts. The mean width at half amplitude maximum of M_o is 1.1 μsec with standard deviation 0.4 μsec. The average time between the peak of the M_o and the peak of the subsidiary 1 pulses is 3.3 μs (standard deviation 0.2 μs), and between the peaks of the subsidiary 1 and the subsidiary 2 pulses this time is also 3.3 μs (standard deviation 0.1 μs).

The main difference observed between typical voltages of the oscillatory type observed at the east and the west ends of the line is that the west end voltage is larger and the east end voltage has a higher negative offset on the voltage reflections.

Impulsive Voltages

Impulsive voltages at the end nearer to the rocket triggering site (east end) are now characterized. Recall that all amplitudes are defined with respect to the initial waveform level. The waveforms start with a slow positive pulse which rises to peak on a 10 to 20 μs time scale and which ends in finer structure, typically characterized by two positive-going peaks. The overall initial positive pulse is termed U_i. It has an average peak amplitude of 98 kilovolts (standard deviation 21 kilovolts). The mean width at half height of this pulse is 1.7 μsec (standard deviation 0.17 μsec). A large negative pulse, which we have labeled T_i in the figure, succeeds the positive pulse U_i. This pulse has a mean peak amplitude of −354 kilovolts and a standard deviation of 44 kilovolts. The mean width of T_i is 783 nanoseconds with standard deviation 123 nanoseconds. After this pulse has dropped to zero, or near zero, a smaller positive-going pulse occurs with mean amplitude 76 kilovolts (standard deviation 20 kilovolts), followed by a slow upward hump of some 25 μsec width.

We now characterize the impulsive voltages observed at the end farther from the triggering site (west end). These voltage waveforms start with a positive pulse which exhibits some structure much like the start of the impulsive voltages at the near end. We call this pulse N_i. The width at half amplitude maximum of this pulse has a mean value of 2.2 μsec and a standard deviation of 0.9 μsec. The end of this pulse is marked by a sharp positive peak. The peak amplitude of this pulse has a mean of 329 kilovolts with standard deviation 68 kilovolts. A large negative pulse which determines the maximum amplitude of the waveform follows with an average peak amplitude of -870 kilovolts (standard deviation 102 kilovolts). This large negative pulse, which we call M_1, exhibits a mean duration of 493 nanoseconds (standard deviation 86 nanoseconds). After this pulse has dropped to near zero, it is followed by a small negative pulse and a small positive pulse. The mean peak amplitudes of the negative and positive pulses are -149 kilovolts (standard deviation 35 kilovolts) and 128 kilovolts (standard deviation 39 kilovolts), respectively. A slow hump similar to that encountered in the east end ensues, lasting about 20 μsec. A series of small pulses is superimposed on this slow change.

Although the wave shapes for the east-end and west-end impulsive voltages are similar, the waveforms differ in that (1) the west end voltages have amplitudes that are about twice the amplitude of the voltages measured at the east end of the line, (2) the west end voltages exhibit two small pulses, one negative and one positive, after the main negative pulse, while the voltages at the east end of the line have only one small positive pulse, and (3) a series of oscillations, absent in the east end voltages, is observed to follow the second subsidiary pulse in the west end voltages.

DISCUSSION

Preliminary modeling of the experimental data presented above have been given in Rubinstein et al. [1] for the case of an oscillatory voltage (flash 1, day 232, event 2 shown in Figure 3 in this paper). Analysis is in progress to improve the modeling of the oscillatory voltages and to model the larger impulsive voltages for which it is thought that electrical flashover occurred at the voltage dividers at or during the voltage rise to peak, thereafter changing the voltage divider ratio and the termination impedance.

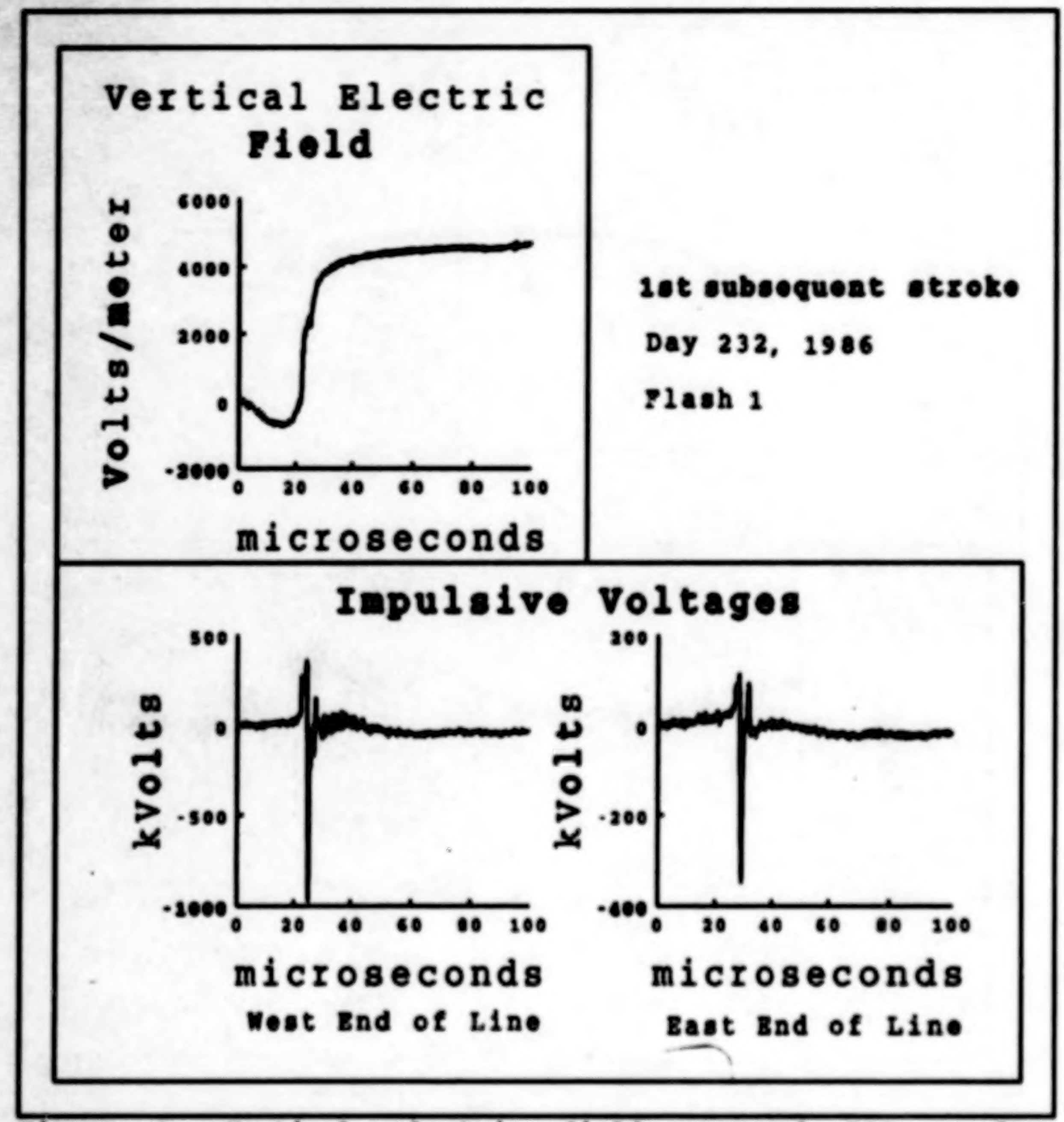

Figure 2. Vertical electric field measured 500 m from artificially initiated lightning return stroke and impulsive voltages at both ends of the test line for flash 1, stroke 1, on day 232, 1986, at KSC, Florida.

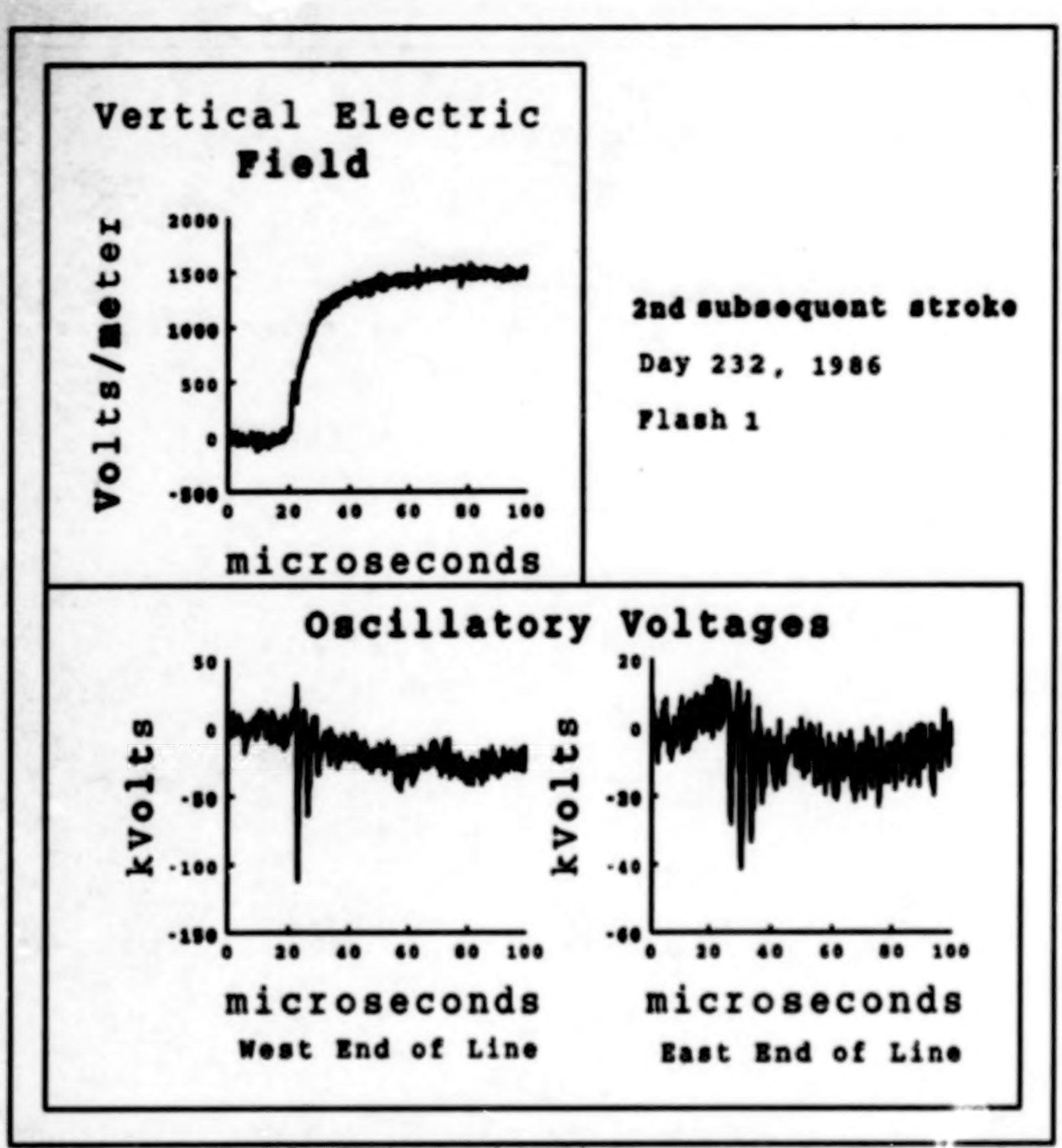

Figure 3. Vertical electric field measured 500 m from artificially initiated lightning return stroke and oscillatory voltages at both ends of the test line for flash 1, stroke 2, on day 232, 1986, at KSC, Florida.

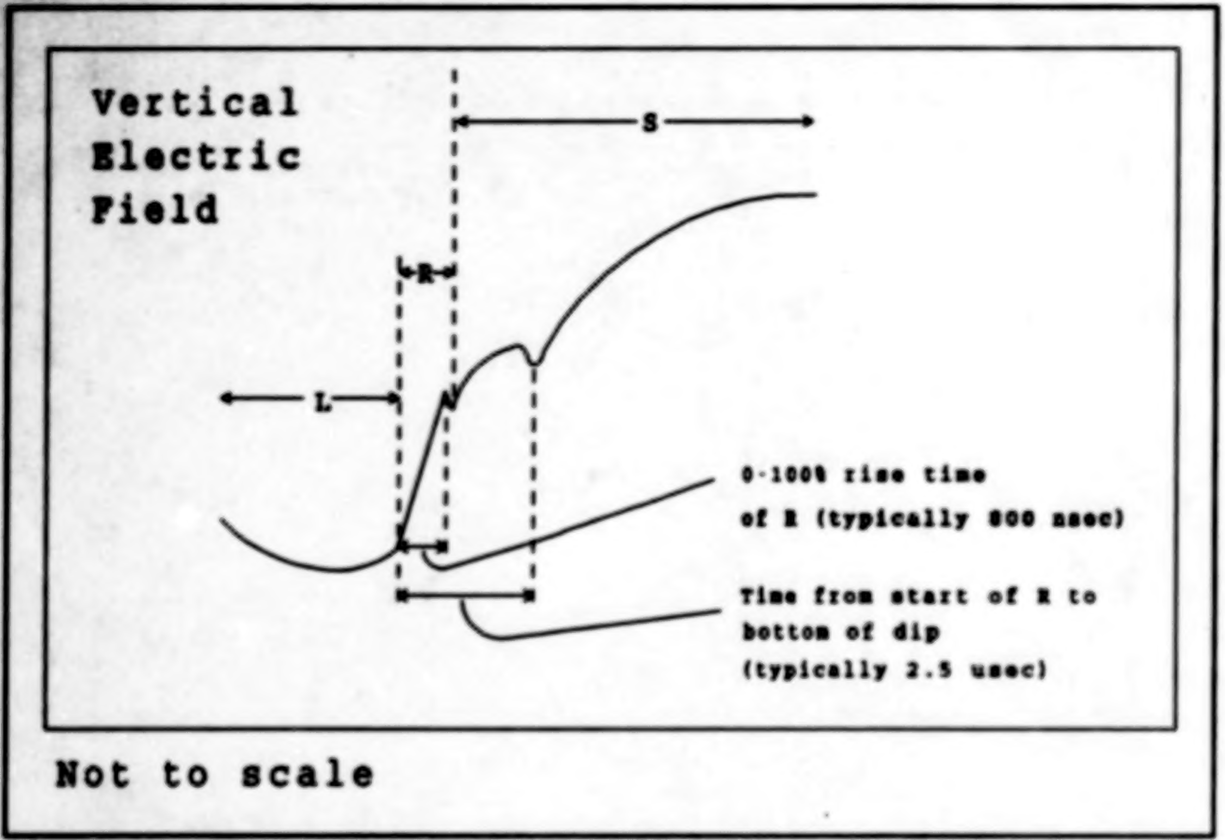
Vertical
Electric
Field
S
R
L
0-100% rise time
of R (typically 800 nsec)
Time from start of R to
bottom of dip
(typically 2.5 usec)
Not to scale

Figure 4. A sketch of the vertical electric field intensity showing definitions of some salient parameters. These parameters are defined in text.

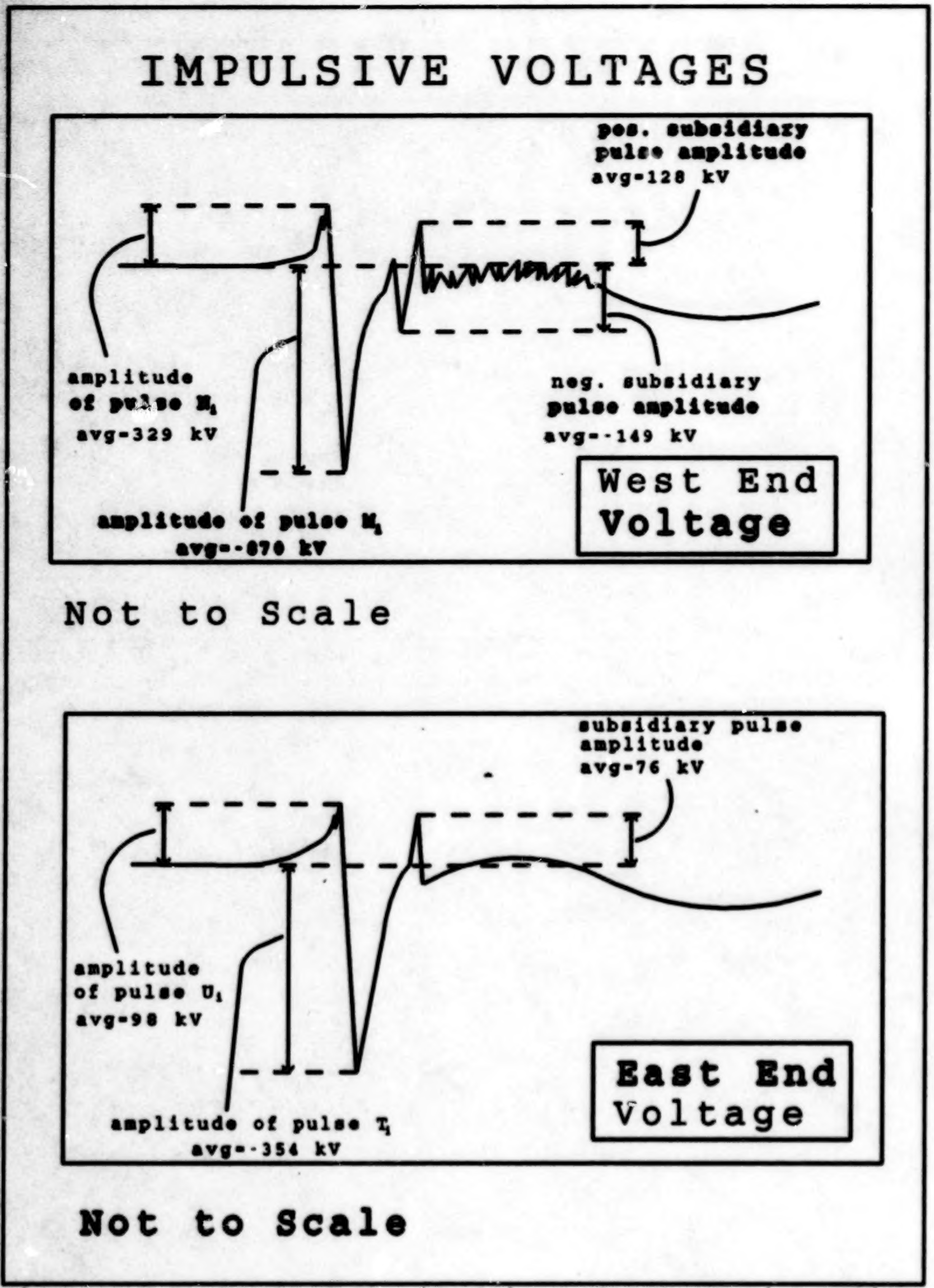
IMPULSIVE VOLTAGES
pos. subsidiary pulse amplitude
avg=128 kV
amplitude of pulse N_1
avg=329 kV
neg. subsidiary pulse amplitude
avg=-149 kV
West End Voltage
amplitude of pulse M_1
avg=-870 kV
Not to Scale
subsidiary pulse amplitude
avg=76 kV
amplitude of pulse U_1
avg=98 kV
East End Voltage
amplitude of pulse T_1
avg=-354 kV
Not to Scale

Figure 5a. A sketch of the impulsive voltages showing salient parameters. These parameters are defined in the text.

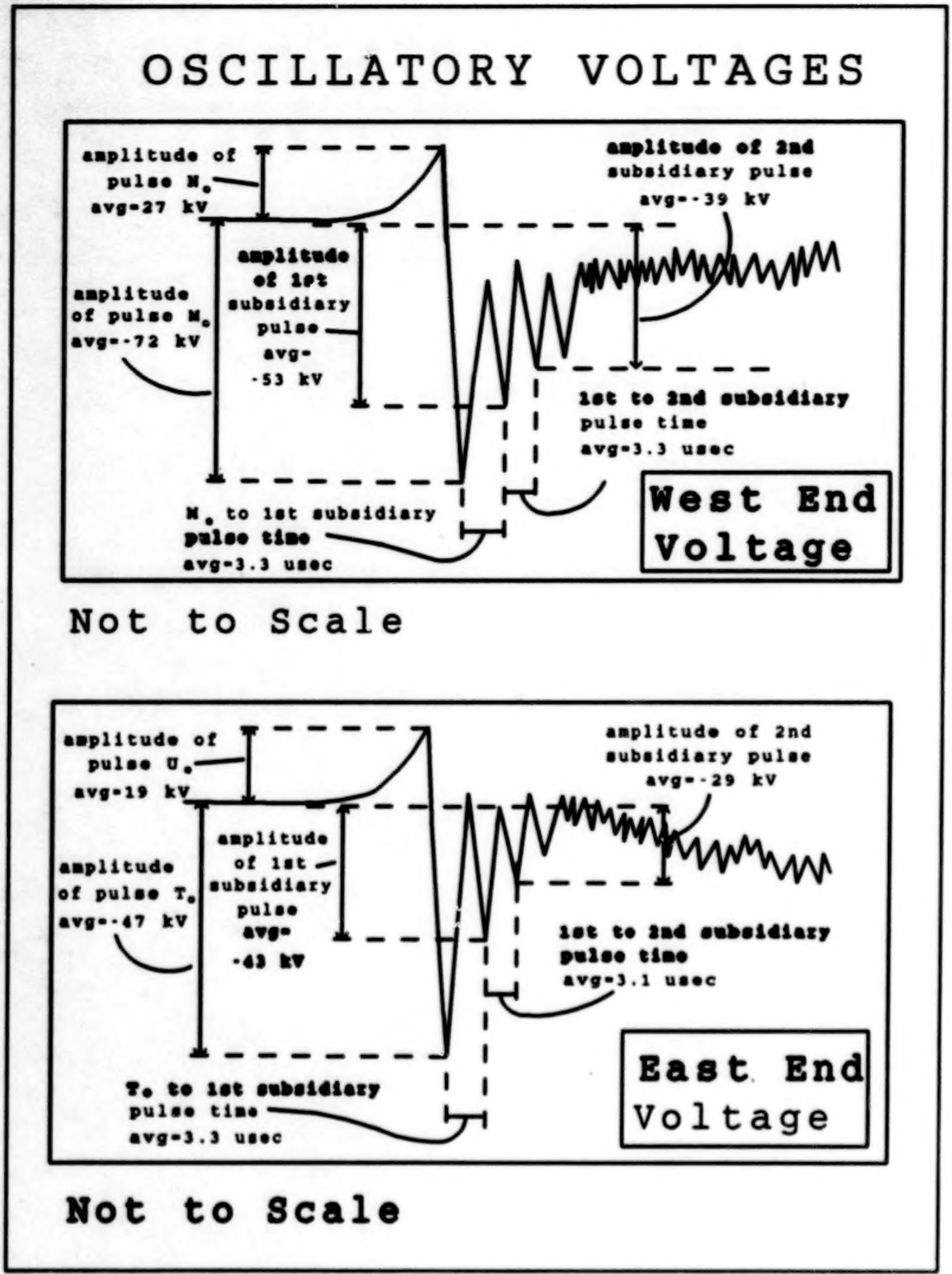
OSCILLATORY VOLTAGES
amplitude of pulse N$_o$ avg=27 kV
amplitude of pulse M$_o$ avg=-72 kV
amplitude of 1st subsidiary pulse avg= -53 kV
amplitude of 2nd subsidiary pulse avg=-39 kV
1st to 2nd subsidiary pulse time avg=3.3 usec
M$_o$ to 1st subsidiary pulse time avg=3.3 usec
West End Voltage
Not to Scale
amplitude of pulse U$_o$ avg=19 kV
amplitude of pulse T$_o$ avg=-47 kV
amplitude of 1st subsidiary pulse avg= -43 kV
amplitude of 2nd subsidiary pulse avg=-29 kV
1st to 2nd subsidiary pulse time avg=3.1 usec
T$_o$ to 1st subsidiary pulse time avg=3.3 usec
East End Voltage
Not to Scale

Figure 5b. A sketch of the oscillatory voltages showing salient parameters. These parameters are defined in the text.

REFERENCES

[1] M. Rubinstein, M.A. Uman, E.M. Thomson, and P.J. Medelius, Voltages Induced on a Test Distribution Line by Artificially Initiated Lightning at Close Range: Measurement and Theory, 20th International Conference on Lightning Protection, Interlaken, Switzerland, 1990.

ACKNOWLEDGEMENTS

Research sponsored by the U.S. Department of Energy, Office of Energy Management, under Contract No. DE-AC05-84OR21400 with Martin Marietta Energy Systems.

LIGHTNING PROTECTION FOR SHUTTLE PROPULSION ELEMENTS

Carolyn C. Goodloe
Systems Analysis And Integration Laboratory, EL-56
NASA/Marshall Space Flight Center
Huntsville, Alabama 35812
and
Robert J. Giudici
Sverdrup Technology, Inc.
620 Discovery Drive
Huntsville, Alabama 35806

ABSTRACT

The results of lightning protection analyses and tests are weighed against the present set of waivers to the NASA lightning protection specification. The significant analyses and tests are contrasted with the release of a new and more realistic lightning protection specification, in September 1990, that resulted in an inordinate number of waivers. After the first decade of Shuttle flight the Shuttle remains vulnerable to the effects of lightning. A variety of lightning protection analyses and tests of the Shuttle propulsion elements, the Solid Rocket Booster, the External Tank, and the Space Shuttle Main Engine, have been conducted. These tests range from the sensitivity of solid propellant during shipping to penetration of cryogenic tanks during flight.

The Shuttle propulsion elements have the capability to survive certain levels of lightning strikes at certain times during transportation, launch site operations and flight. Changes are being evaluated that may improve the odds of withstanding a major lightning strike. The Solid Rocket Booster is the most likely propulsion element to survive if systems tunnel bond straps are improved. An initial decision not to harden the Space Shuttle Main Engine to lightning has been reversed. Wiring improvements have already been incorporated and major lightning protection tests have been conducted. The External Tank remains vulnerable to burn-through penetration of its skin. Proposed design improvements include the use of a composite nose cone and conductive or laminated thermal protection system coatings.

INTRODUCTION

Lightning protection concerns and the resulting analyses, tests, design changes or waivers for the Shuttle propulsion elements are summarized from the perspective of the Systems Analysis And Integration Laboratory of the Marshall Space Flight Center (MSFC). Shuttle propulsion elements are the responsibility of MSFC and are differentiated from the Shuttle Orbiter which is the responsibility of the Johnson Space Center (JSC). There are three major Shuttle propulsion elements: (1) Solid Rocket Booster, (2) External Tank and (3) Space Shuttle Main Engine. The relationship of the Shuttle propulsion elements and the Shuttle Orbiter to the overall Space Shuttle is depicted in Fig.1.

All Space Shuttle elements, and the Kennedy Space Center (KSC) launch site, share a common lightning protection specification: NSTS 07636, Revision E. This revision was released in September 1990. The specification subdivides lightning characteristics to simulate the aspects of a major lightning strike: there is an initial component A, (200 kA peak, 500 µs); an intermediate component B, (4.2 kA peak, 10 coulombs); and a continuing component C, (400 A, 200 coulombs). Other lightning components defined by the specification account for restrikes and multiple bursts. Test equipment has been devised to simulate the various aspects of lightning protection.

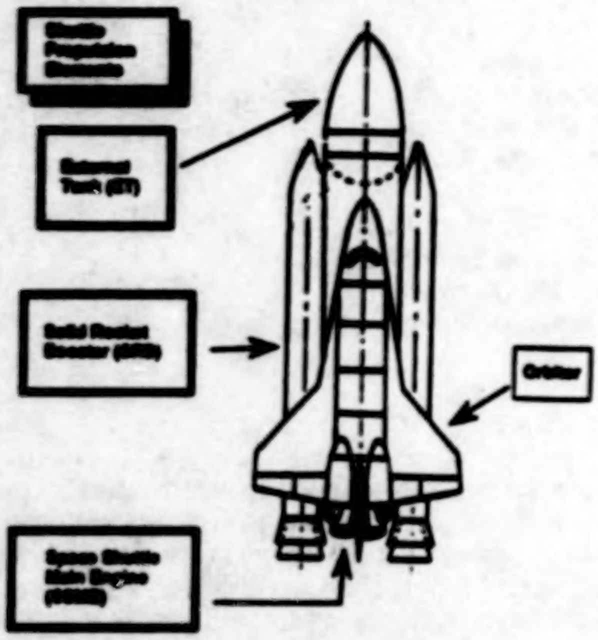
Shuttle Propulsion Elements
External Tank (ET)
Solid Rocket Booster (SRB)
Orbiter
Space Shuttle Main Engine (SSME)

Figure 1. Shuttle Propulsion Elements

EXTERNAL TANK

The External Tank (ET) is an aluminum vessel, 47 m (154 ft) in length and 8.4 m (28 ft) in diameter. A diagram identifying the major components is shown in Fig.2. Two Solid Rocket Boosters and the Orbiter are attached. The thickness of the 2219 aluminum skin varies from 2 to 3.6 mm (80 to 140 mils). Insulation, 1.9 to 3.8 cm (0.75 to 1.5 inches) thick, is required to minimize cryogenic boil-off and to provide protection against aerodynamic heating. The Tank has three main components: the Liquid Oxygen (LO2) tank, located under the forward ojive; the intertank section; and the aft liquid hydrogen (LH2) tank. External cable trays enclose fluid lines, pressurization gas lines, linear shaped charges, and electrical cables. Avionics are located in the nose cone and intertank areas.

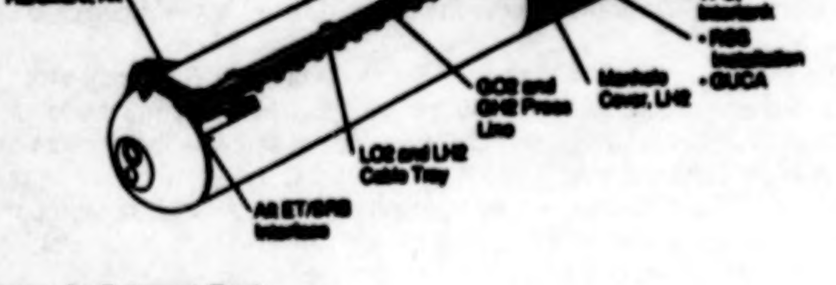
Manhole Cover, LO2
TPS, LO2
ET/Orbiter Attach Hardware Bipod
Intertank Joints
Nose Cone
LO2 Feedline
TPS, LH2
ET/Orbiter Attach Hardware, Aft
TPS, Intertank
• RSS Installation
• GUCA
GO2 and GH2 Press Line
Manhole Cover, LH2
LO2 and LH2 Cable Tray
Aft ET/SRB Interface

Figure 2. External Tank

External Tank Concerns

Burn-through of the External Tank is one of the most serious lightning threats to the Shuttle propulsion elements because the external tanks are prone to penetration of the skin that could result in hydrogen ignition or oxygen burning or loss of pressurization. During ascent of the Space Shuttle the External Tank is a potential attach point for lightning. The External Tank is protected by a catenary wire system while on the launch pad and is protected against launch into severe weather by strict launch commit criteria. However, there remains a possibility that prediction of triggered lightning strokes during boost may be beyond the capability of completely reliable weather prediction and therefore analyses, tests, and design changes continue with the objective of improving compliance with the lightning protection specification.

The External Tank can probably withstand a lightning strike to the lightning rod located at the forward most tip of the tank nose cone. The rod also functions aerodynamically to reduce thermal protection requirements. Tests [1] on a production nose cone demonstrated the capability of the lightning rod to distribute full lightning currents into the nose cone with no discernible damage. Analysis and tests verify that there would be no damage to the LO2 tank, the intertank, or the LH2 tank resulting from a lightning strike to the lightning rod.

Lightning can strike at any altitude but it is most likely to trigger a lightning strike at altitudes above 460 m (1500 ft). The lightning protection specification applies to a worst case major lightning strike. Practical considerations, though difficult to substantiate, suggest that the External Tank may realistically encounter less severe lightning strikes. When a lightning strike uses a moving space vehicle as part of its path from a cloud to ground or to another cloud, it establishes a step leader path for the first return stroke and return stroke currents usually continue for several milliseconds. If the whole surface is conductive, the attach point moves back in relatively smooth motion due to the forward motion of the vehicle, but if the surface is covered with insulation the lightning arcs through the insulation and attaches to the aluminum skin at one point. The initial lightning attach point clings to one spot and the

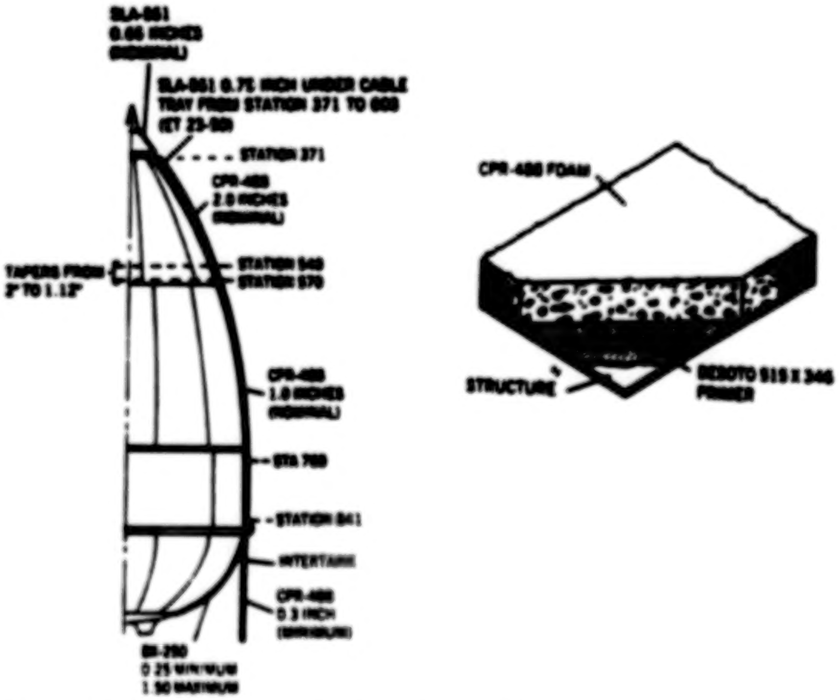
SLA-561
0.65 INCHES
(NOMINAL)
SLA-561 0.75 INCH UNDER CABLE
TRAY FROM STATION 371 TO 600
(ET 23-50)
STATION 371
CPR-488
2.0 INCHES
(NOMINAL)
TAPERS FROM
2" TO 1.12"
STATION 540
STATION 570
CPR-488
1.0 INCHES
(NOMINAL)
STA 760
STATION 841
INTERTANK
CPR-488
0.3 INCH
(MINIMUM)
BX-250
0.25 MINIMUM
1.50 MAXIMUM
CPR-488 FOAM
STRUCTURE
DESOTO 515X346
PRIMER

Figure 3. Typical Cross Section of the TPS

lightning channel bends along the insulated surface forming a heal just above the surface of the insulation. The lightning channel attaches to a new point further along the length of the vehicle when the heal is close enough and the voltage is high enough to arc through the insulation. Before this occurs, the dwell time at the initial attach point may be sufficient to burn through the underlying aluminum skin of the LO2 and LH2 tanks. Details of the flight vehicle insulation are shown in Fig.3.

Commercial aircraft typically survive two lightning strikes per year. The Saturn V, Apollo 12, mission survived two strikes during launch and went on to the second successful Lunar landing. The conductive skin of aircraft and the Saturn vehicle sweep the lightning channel along the surface without penetrating the skin whereas the insulated surface of the External Tank not only increases the dwell time but tends to narrowly focus the arc and enhance the potential to penetrate the walls.

The charge imparted to the skin of a vehicle by a swept stroke is the product of amperes and dwell time. Dwell time is highly dependant on insulation breakdown characteristics and is difficult to predict. There is a minimal data base on the effects of a swept strokes on thickly insulated surfaces, and testing is expensive and difficult to conduct. However, the charge imparted to the skin of the External Tank from a swept stroke can be less than the specified 200 coulomb level for a standing vehicle. Although amount of charge from a swept stroke may not be known, the amount of charge necessary to penetrate the skin of the External Tank can be determined through test and analysis.

A number of tests have been conducted to evaluate tank puncture and the effects of thick insulation. For example, elaborate coupon testing was performed using aluminum coupons covered with thermal insulation and stressed to flight pressures of 34,475 N/m^2 to 275,800 N/m^2 (5 to 40 psi) and liquid nitrogen (LN2) temperatures. A 2.5 mm (100 mil) panel marginally survived 31 coulombs. A 3.6 mm (140 mil) panel punctured but a 4 mm (160 mil) panel survived at a 75 coulomb level [2].

Designs for improving the capability to survive a server lightning strike are being evaluated. Overlaying the thermal protection insulation with laminated layers of thin aluminum and non-conductive adhesive, similar to the Solid Rocket Booster rail car covers, may offer solutions. An 2 mm (80 mil) panel covered with 6.4 mm (2.5 mil) aluminum tape and adhesive withstood 75 coulombs [2]. A normally nonconductive insulated panel required twice this thickness to withstand the same charge level. The outer foil separates from the surface being protected, probably due to the escaping adhesive gasses, and diverts the lightning arc. Painting the insulation with copper impregnated paint has also shown considerable promise and the incorporation of a composite nose cone is under consideration.

Launch Site Protection

The launch pad lightning protection system consists of three major systems: (1) a catenary wire instrumentation system that measures lightning wave form and peak current, (2) a system that measures induced voltage and current flow in the vehicle and ground support equipment, and (3) an optical system that determines the lightning attach point.

An updating of the ground based field mill network is scheduled to be operational by the summer of 1991. This system consists of 37 field mills covering all launch sites at the KSC. Data will be automatically collected in a central data facility.

External Tank Status

The LO2 and LH2 gas pressurization lines are important planned lightning attach points. The LO2 line runs the length of the vehicle and both lines are uninsulated. Lightning can sweep along the uninsulated lines when the vehicle is moving without dwelling long enough to burn through. The lines have the capability of surviving a swept stroke when vehicle velocity is above 20 m/s (64 fps). A waiver is in effect because the pressurization lines will puncture if the vehicle is stationary.

The cable trays were verified to withstand the direct effects of a 25 kA lightning strike derived from an earlier release of the lightning protection specification. The Rev E specification calls for 200 kA. Analyses of indirect effects, the coupling of undesired current and voltage into electrical cable harnesses from nearby structure or fluid and gas lines, must likewise be upgraded to the 200 kA level.

The major waivers to the External Tank involve tank penetration inclusive of the nose cone, LO2 tank, LH2 tank, and aft dome of the LH2 tank. A number of analyses and tests have been requested. One test, to evaluate the effects of a lightning strike to a simulated insulated liquid oxygen tank, may be performed at MSFC Huntsville in early 1991.

SPACE SHUTTLE MAIN ENGINE

The engine using the cryogenics from the External Tank is located in the Orbiter. The Space Shuttle Main Engine (SSME) is actually three engines having an engine controller mounted to each engine. The controllers contain digital computers necessary to process sensor signals, and issue control signals to hydraulic actuators and igniters. The existing controller is referred to as Block I but this version is scheduled to be replaced by a Block II controller in 1992. The controllers are wired to engine components and to Orbiter interface wiring. Features of the engine are shown in Fig.4. Note that the main engine is largely protected within the Orbiter boat tail but there remains concerns for cable shielding of the Block II engine controller and some concern for direct effects of a strike to the engine nozzle.

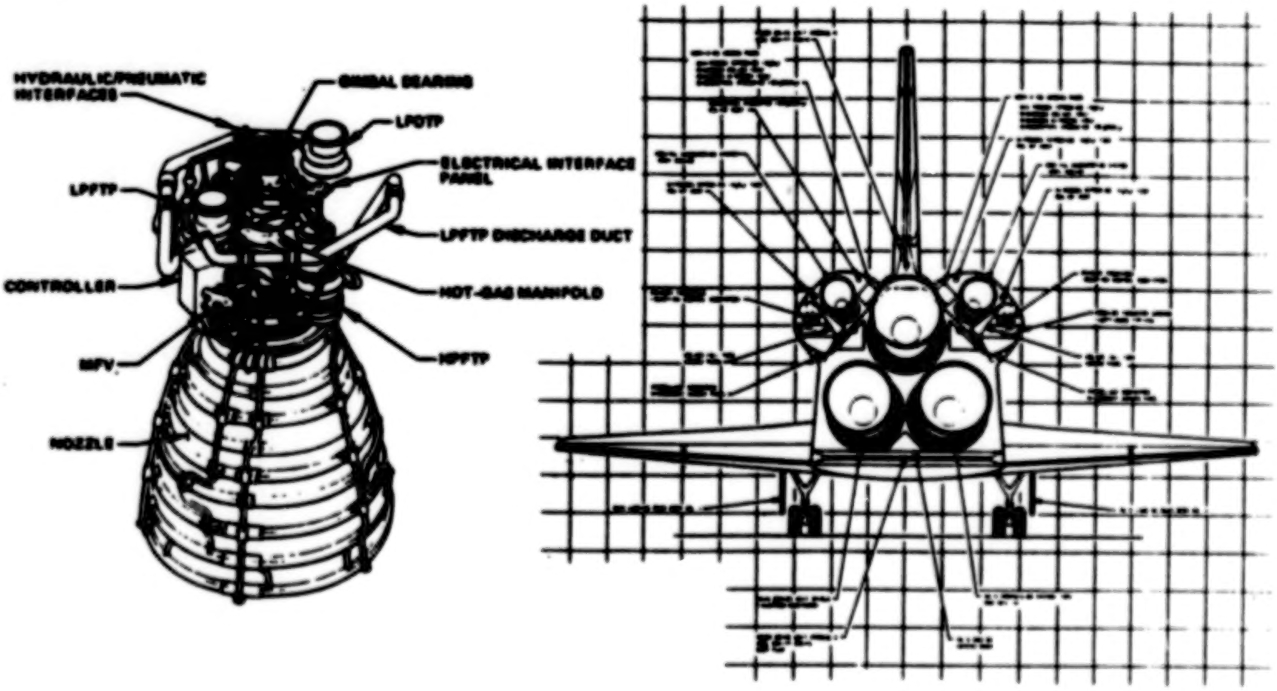

Figure 4. Space Shuttle Main Engine

Main Engine Concerns

A decision was made in 1975 that the main engine was not subject to direct effects of a lightning strike and it was believed that the added cost, weight and schedule of guarding against direct lightning strikes was not justified. Rationale included consideration that the engine was unlikely to be a primary lightning conductor during boost by virtue of protection afforded by the Orbiter structure and the booster plume and that the engine is not operational during landing and can, if struck by lightning, be repaired.

After the Atlas incident in 1987, it was discovered that certain shielding practices responsible for the Atlas accident were also utilized by the shuttle main engine. A direct lightning strike to the Atlas vehicle altered the core memory in a control unit causing the computer to issue an erroneous yaw command that resulted in destruction of the vehicle. The Space Shuttle Main Engine is a concern because the it contains 40 critical low inertia memory electronic circuits. Several changes were made to the wiring of the engine, e.g., braided cables were added for power, engine interface unit, and sensor interfaces. Shields were terminated on the outside of connector backshells to prevent lightning current from entering the chassis. However, unshielded cable was retained for actuators and this remains a waiver.

The engines are protected from direct lightning strikes by the Orbiter structure with the exception of the nozzles. The engines are not used during decent or landing but then they are more exposed and subject to expensive repair if struck by lightning. The nozzles are heavy steel that should diffuse lightning current away from the lightning attach point without burn through. Tests were conducted on a simulated nozzle section in 1973. The nozzle section withstood 100 kA, 3 ms, discharges provided the air velocity exceeded 40 m/s (90 mph), [3].

SSME Status

Previous analysis qualified the Block I engine controller to a 50 kA strike level derived from an earlier revision of the lightning protection specification. The analysis was for the indirect effects of coupling into cable harnesses by lightning current in the Orbiter skin. The new specification requires the Block II engine controller to be verified by test. Consideration of the direct effects to the nozzle during ascent and descent is also required.

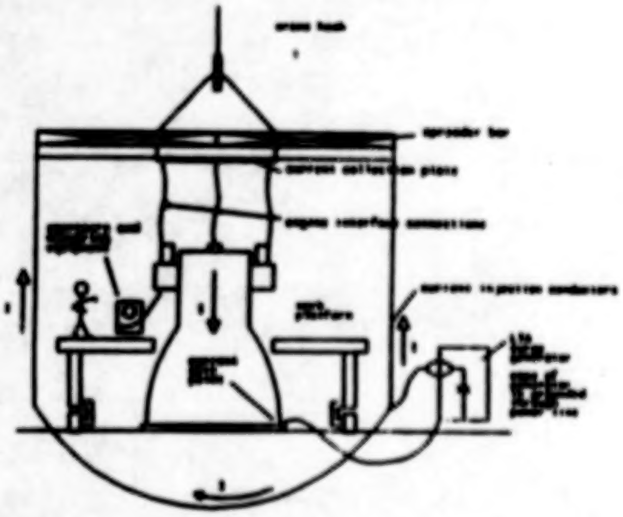

Figure 5. SSME Lightning Protection Test

Cable coupling must be readdressed and two tests are involved. The first series of tests injects relatively low level surge currents (approximately 1000 amps), representative of lightning currents, into the Nozzle as shown in Fig.5. Tests were conducted in December 1990 and January 1991 at Stennis Space Center (SSC) on a flight engine with the engine controller replaced by a dummy controller and flight cables connected. Input and output impedances were simulated and current and voltage measurements are taken. Measured values are extrapolated to determine the induced voltages and currents should a full amplitude lightning current enter the engine.

A second series of tests is performed with a flight engine controller. Tests are scheduled for April-May 1991. Currents and voltages (induced cable coupling levels determined by previous tests) are injected, by transformer coupling, into the cables of a functioning controller.

SOLID ROCKET BOOSTER

The Solid Rocket Booster (SRB) is illustrated in Fig.6. The length is 46 m (150 ft) and the diameter is 3.7 m (12.17 ft). Major elements of the booster include a nose cap, the solid propellant segments, engine nozzle, and the systems tunnel. Some of the booster segments are joined by factory joints and some are field joints assembled at the KSC launch site. The design for the initial segment joints were a major lightning protection concern because they are apertures that could couple electromagnetic energy into the solid propellant. The segment joints for the redesigned booster greatly reduce the potential to couple electric fields into the solid propellant. The steel case, approximately 1.3 cm (one-half inch) thick, eliminates the possibility of puncture due to lightning but does not completely eliminate all consideration for weakening the tank wall. The nose cap and other surface areas susceptible to aerodynamic heating are covered with insulation: typically 0.25 to 0.5 cm (one to two tenth inches) of cork. Vehicle electronics are located in the forward skirt, External Tank attach rings, and in the aft skirt. The major concern for electronics is induced coupling into the systems tunnel wiring that could cause upset or damage to any of 28 criticality I circuits.

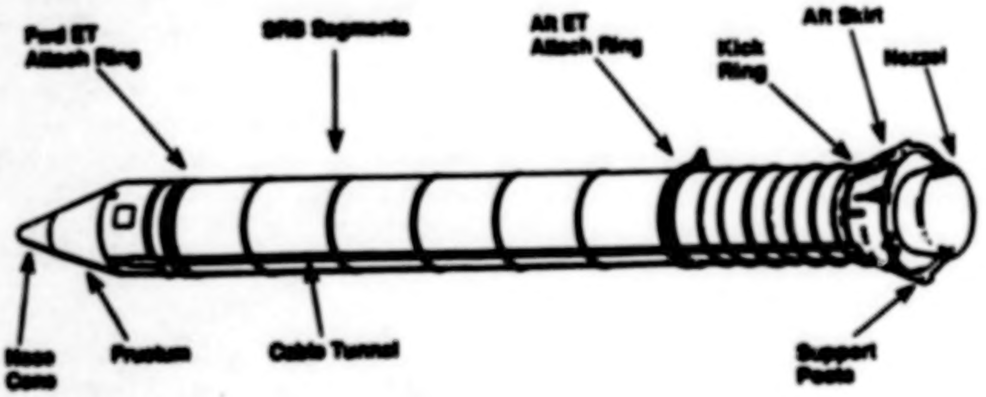

Figure 6. Solid Rocket Booster

Booster Concerns

Considerable activity within the lightning protection and electrostatic discharge community, both military and NASA, resulted from the accidental ignition of a Pershing II motor during assembly operation in West Germany in January, 1985. Electrostatic charging and subsequent internal breakdown within the solid propellent, resulting from removing the first stage motor from its shipping case container, was determined to be the cause. Pershing propellant is more sensitive than the Shuttle solid rocket booster propellant and has a kevlar composite case rather than a steel case as does the booster.

A simplified circuit for testing propellant sensitivity is shown in Fig.7. Test results for the 10 cm long samples indicated the booster propellant to be relatively insensitive at temperatures above -40 °C (-40°F). The booster propellant, TP-H1148, did not react at -23 to 24°C (-10 to +75°F) temperatures, for voltages up to 30 kV and therefore the resulting field level of 300 kV/m (30 kV/0.1 m) is considered to be safe for the booster propellant.

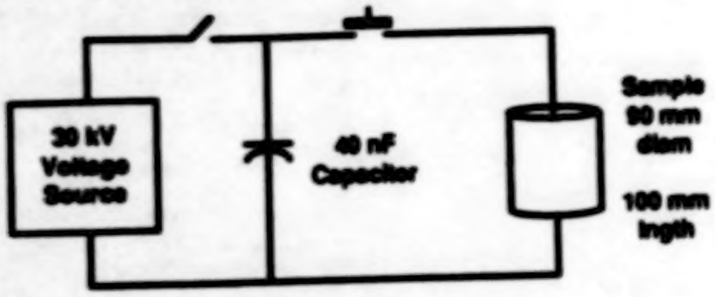

Figure 7. Propellant Sensitivity Test Circuit

Other tests and analyses evaluated induced electric fields from lightning and microwaves under various conditions for the booster [4]. The electric field from lightning current inside the propellant following through booster joints was determined to be 35 kV/m and well below the accepted 300 kV/m safe level. However, the safe level was exceeded when individual booster segments were being shipped from the manufacturing plant in Utah to the Florida launch site. Segments, shipped by rail car, were initially protected by a fiberglass rail car cover and a fiberglass end grain cover over both ends of the segment. Field levels were reduced from 480 kV/m for an unprotected booster segment to 0.06 V/m when the segment was protected by a laminated aluminum rail car and end grain covers. Electric fields resulting from microwaves were well below the safe level (e.g., a worst case microwave environment produced a field of only 80 V/m inside the propellant near the booster joints.)

The indirect effects of lightning were also analyzed and tested. Electrical cabling is routed external to the booster and protected by systems tunnel shown in Fig.8. A lightning strike to the systems tunnel

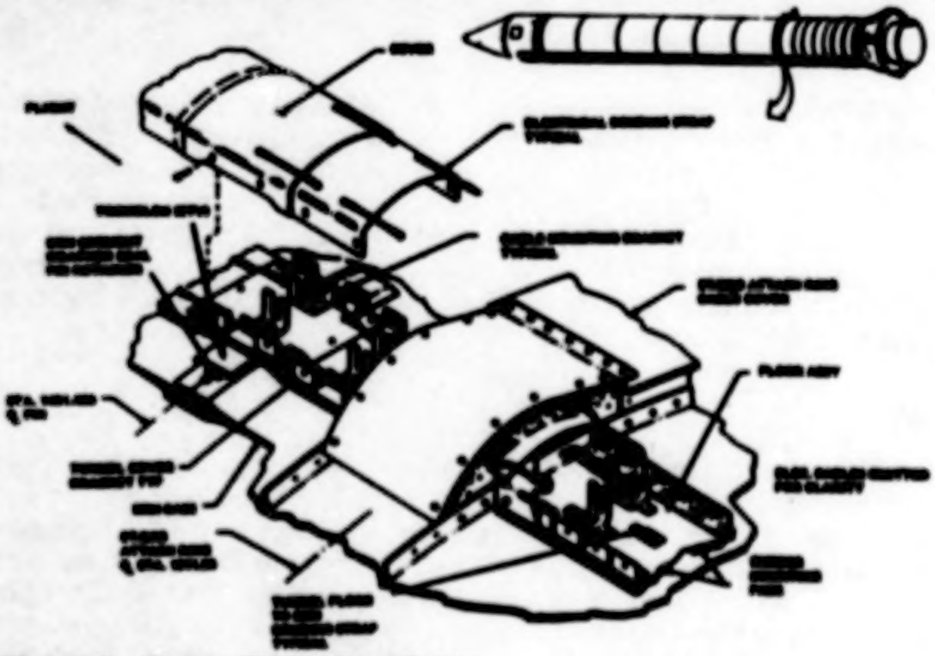

Figure 8. System Tunnel Bond Straps

cover must flow to the booster case through bond straps. The bond strap, shown in the figure, is located inside the systems tunnel. One end is bolted to the floor plate and the other end is attached to the steel case with adhesive. Lightning tests were conducted on full size motor segments at Wendover, Utah in 1989 to determine the adequacy of the bond straps [5]. Results from the tests proved that the internal bond straps were not adequate to survive full lightning currents. Excessive current and voltage was induced into the electrical cables and also caused the internal bond strap to separate at the case end and the loose end sprang straight up from its attachment at the floor. The loose end hit the linear shaped charge contained in the forward systems tunnel. This necessitated sensitivity testing of the linear shaped charge to verify that detonation does not occur.

A retest was conducted in 1990, also at Wendover, Utah. The internal bond strap was replaced by more substantial external cover-to-case bond straps. Cover-to-cover bond straps were also replaced with larger straps and all development flight instrumentation cables were removed. Test results are not available but all bond straps appear to have survived specified current and action interval limits and induced open circuit common mode voltages are reduced from 130 Volts to 30 to 60 Volts based on preliminary inhouse analysis.

A final lightning current path to be discussed is the lightning detach point. A likely detach point for lightning current is through the booster exhaust plume. However, current must transverse flex gimbals and the nozzle before reaching the exhaust plume. The flex joint is required because the engine must be gimballed to provide thrust vector control. Lightning current must flow through bond straps connecting the booster case to the nozzle. Bolts connecting to the bond straps to the nozzle extend through the nozzle and penetrate the inner carbon nozzle liner. The liner makes electrical contact with the plum. Another lightning current path for reaching the nozzle is though bond straps bypassing the engine actuators. Additional test and analysis sophistication considered the effect of bond strap failures that allow current to loop back toward the booster case near the propellant, and establish high electric fields.

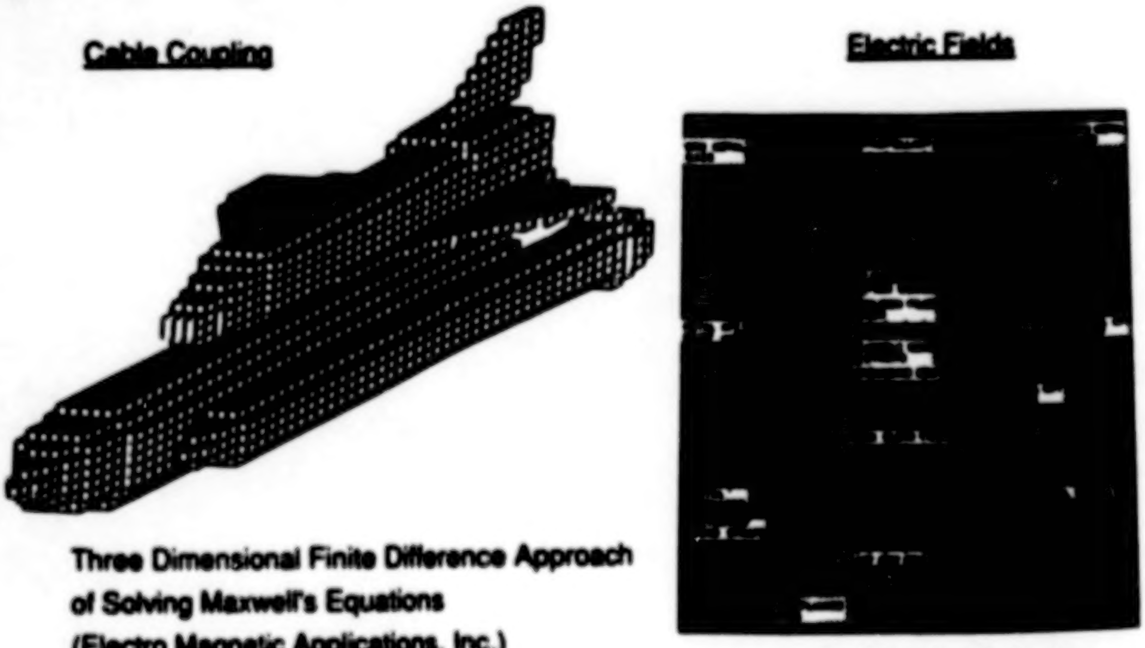

Three Dimensional Finite Difference Approach
of Solving Maxwell's Equations
(Electro Magnetic Applications, Inc.)

Two Dimensional Projection

Figure 9. Numerical Techniques

Testing of the lightning path from the booster case to the inside of the exit cone was performed at Wendover, Utah in 1988, [6]. This report is a noteworthy example of the analytical capability required for lightning protection analysis. Figure 9 is taken from the report to illustrate the numerical method of the finite difference technique of solving Maxwell's equations. The method is implemented by establishing a grid, without undue computer memory requirements, to create a smaller simulated structure capable of representing the pertinent aspects of the rocket motor.

Analysis and test results verified the capability to withstand 200 kA with minor pitting at the screw/carbon liner interface. The electric field strength within the propellant was 17 kV/m when all twelve case to nozzle bond straps and both actuator bond straps were in place. Bond straps were removed sequentially to simulate nozzle and actuator bond strap failures. The field strength increased to the extreme level of 430 kV/m for the limiting case when all nozzle and actuator straps were removed. Recall that the accepted safe level is 300 kV/m.

Solid Rocket Booster Status

Two engineering changes might correct the major lightning protection shortcomings of the booster. One change is being processed to replace the existing nose cap gasket with a conductive gasket. A second change is being evaluated to change the systems cable tunnel bond straps. The latest tests at Wendover, January 1991, evaluated cable coupling into NASA standard initiator circuits for the nozzle severance system. A main lightning path coupon test is contemplated to verify bond joints that must now be verified by analysis or test in accordance with Rev E to NSTS-07636.

CONCLUSION

Lightning protection for the Space Shuttle propulsion elements has been reviewed. Background information on the lightning specification, program history, and element descriptions provided a foundation for discussing design concerns and the status of the present test and analysis efforts. The propulsion elements can no doubt survive certain intensity lightning strikes attaching to less vulnerable vehicle locations during certain mission phases. The NASA lightning specification requires, as it should, that propulsion elements (and the Orbiter) withstand a very severe lightning model under all conditions. The Space Shuttle remains vulnerable in this respect and therefore efforts to improve the lightning protection design for the Space Shuttle continue after more than a decade of flight.

Acknowledgements

To fellow lightning protection engineers at MSFC-SAIL and to the Shuttle propulsion element contractors and subcontractors who have performed the majority of the lightning protection work.

REFERENCES

1. E. J. Lisk, and J. McCardle, Lightning Protection Design Features to Requirements of JSC 07636 Revision C, Lightning Protection Criteria Document, Martin Marietta, 826-2392, dated July 22, 1988.

2. F.A. Plumer and K. E. Crouch, Simulated Lightning Tests on ET Skin Panels, LT-88-480, dated August 1988.

3. Lightning and Transients Research Institute, Simulated Lightning Discharge Current Effects on Space Shuttle Exhaust Nozzle Coolant Tubing, Report No. 563, dated May 1973.

4. Rodney A. Perala, et. al, Electro Magnetic Applications, Inc., Evaluation and Mitigation of Lightning and Microwave Hazards to the SRB Propellant, EMA-87-R-63, dated June 1987.

5. United Technologies USBI, C. O. 191 Lightning Test Final Test Report, USBI-SYS-10-RPT-010, dated December 1989.

6. Morton Thiokol, Analysis of the Systems Tunnel Bond Straps, DFI Cables, and Lightning Test Configuration, TWR-17252, dated March 1990. This report is an introduction to EMA report EMA-88-R-50, dated August 1988.

Session 6B, Wednesday 10:15
Aerospace Vehicles
Test Criteria and Techniques 1
Moreau, Chairman

Photographic Spark Detection Sensitivity With Various Film Types and Utilizing Multiple Spark Sources

by D. Dodrill and D. Heidlebaugh

No paper available.

Lightning Transient Monitoring on the Titan

by D. Downs

No paper available.

INFLUENCE OF CONFIGURATION EFFECTS ON "MULTIPLE BURST" SIMULATION TESTING

J.L. EMANUELY - M. CANTALOUBE

CENTRE D'ESSAIS AERONAUTIQUE DE TOULOUSE
23, avenue Henri Guillaumet 31056 - TOULOUSE CEDEX

ABSTRACT

During the initial phasis of a lightning strike attachment on an aircraft, fast current pulses (rise time ≈ 100 ns, Imax ≈ few kA) have been measured, which can create equipment upsets or disturbances. This threat, made of repetitive pulses and usually called "multiple burst", can be reproduced at the equiment interfaces assuming that the transfer function of the structure was determined. The normalised waveform H (10kA - 100 ns rise time) is the reference for one of these pulses.
This paper emphasises the importance of the coaxial return path termination for the injection of the wave H. According to the constitutive materials of the test-bed, and the adaptation of the line, the natural oscillations of the structure and the internal coupling mechanism can be modified. As a conclusion, various test configurations in relation with the nature of the test-bed and the characteristics of the generator are detailed, for a more accurate ground simulation of the attachment phasis.

I - INTRODUCTION

The document SAE-AE 4L "ORANGE BOOK" suggests the following scenario for the attachment process : for each attachment or reattachment, a series of 20 pulses of current (waveform H) is flowing in the external structure with a repetition frequency between 20 and 100 kHz. It is mentioned that 24 bursts of 20 pulses (total of 480 pulses) can occur in a lightning event during a total duration time of 2 s.
The analysis of the results of "in flight measurements" (TRANSALL - CV 580) made by the ONERA ("Office National d'Etudes et de Recherches Aérospatiales" - FRANCE : in flight programme supported by the MOD/DGA) suggests another scenario [Ref. 1] : the multiple burst sequence could only appear 2 or 3 times maximum during the lightning flash, and Mr MAZUR explained in the ICOLSE 88 conference of OKLAHOMA that one attachment only was likely to occur for the stepped leaders.
We can however notice that there is a consensus about the characteristics of the waveform H, with the restriction that rise time of 60 ns have been recorded.
Whatever the number of pulses, it is clear that it will be impossible to drive n pulses of m bursts on a whole aircraft ! It would require n x m Marx generators from about 800 kv, sucessively triggered.
The demonstration method chosen by the C.E.A.T. consists in determining the tranfer function of the various bundles for a single excitation of a H pulse on the whole aircraft, and then to test the inside equipments at low level (2000 V.) with the repetition rate specified (arbitrary waveform synthesizer + pulse amplifier).

II - NATURAL RESONANCES

1°) When studying the data of in flight measurements, we can notice that natural resonances of the structure are excited. For exemple, on the F 106 [NASA-Ref 2] the measurements of dD/dt show oscillations at 7 MHz and 21 MHz ($L = \lambda/2 = 14\ m \rightarrow Fr = 10$ MHz) and the dB/dt leads to 7 MHz only. The oscillation at 21 MHz is preponderant on the nose current. On the TRANSALL [Ref 3]] the oscillation is about 5 MHz (very near to the fuselage resonance of the aircraft). Nevertheless, no information is given about the damping factor of these oscillations. A theoretical analysis with a 3 D code (Integral method) [Ref 4], on a model representing the central part of the fuselage with its 2 wings, shows the superposition of two main resonances $\lambda/2$ and $\lambda/4$ (lightning strike from one wing tip to the other wing tip).
In short :

Resonance	IN FLIGHT	3D MODELING
Wing	---	$\lambda/4$ - $\lambda/2$
Fuselage	$\lambda/2$ - $3\lambda/2$	---

Table I : strutural resonances

2°) Classical test set-up for the ground simulation :

A coaxial return path is built around the structure of the aircraft to ensure that the repartition of currents on the skin is the same as it would be in free space, during a lightning strike (Fig. 1)

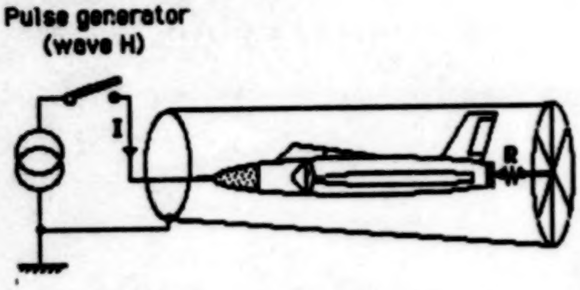

Figure 1. Usual test set-up

To prevent parasite reflections, the inductance (µH/m) of the transmision line will be as constant as possible. But the same question remains for the simulation : what appropriate mismatching must be recreated and how to reproduce the in flight oscillations ?
It is obvious that the induced effects on the internal wirings are strongly correlated to the possible oscillations and their damping factor. That's why 2 different values of load resistance R were choosen :

First case : R = 0 (short-circuit = usual test set-up configuration for very high current injections)
Travelling waves (f= c/4l) are going to pile on the bi-exponential current delivered by the generator. The frequency spectrum of the normalized wave H is strongly modified at the frequencies corresponding to $l = \lambda/4$ and $l = 3\lambda/4$

Second case : R = Zo (characteristic impedance of the coaxial return path)
Except some discontinuities of the aircraft geometry, the line is matched, and the natural structural oscillations are not excited. The frequency spectrum of the normalised wave H is not modified.

III COUPLING ON TYPICAL WIRES FOR BOTH CONFIGURATIONS (short circuit load and matched load)

To quantify the importance of the resistive load R, this paragraph summarises the results achieved on 3 different test-beds

III 1 - "ECUREUIL" helicopter :

In the frame of the joint venture programme AFARP 17 (Anglo French Aeronautical Research Programme), different tests (CW - High voltage test - High current injections) have been performed on the structure of a helicopter (with large dielectric parts). A view of the test set-up is given on fig. 2, for the high current injection phasis.

Figure 2. "ECUREUIL" Helicopter in the coaxial return path (Zo=60 Ω)

The comparison is performed for the single wire L4 located in the aluminium tail, between the rear rotor and the equipment bay (length = 10 m = 33 ft)
Table II. presents in time and frequency domains the characteristics of the induced levels (for I injected = 1 kA waveform H/10)

COAXIAL RETURN CONFIGUR.	OPEN CIRCUIT VOLTAGE L4 Voc		SHORT CIRCUIT CURRENT L4 Isc	
	Max Level	Main Fr.	Max Level	Main Fr.
Matched R = 60)	180 v	7,8Mhz 22 Mhz	1 A	6-12Mhz 22Mhz
Short Circuit (R = 0)	230 v	4,3Mhz 7,8Mhz 12 Mhz 22 Mhz	1,5 A	5,4Mhz 6,3Mhz 12 Mhz 22 Mhz

Table II. Induced levels on the line L4 (10m) for I injected = 1 kA (H/10)

- Resonances of the structure of the helicopter : (l = 16 m = 52 ft)
  λ/4 = 4.3 MHZ
  λ/2 = 8.6 MHZ
  3λ/4 = 12.5 MHZ

•Resonances of the wire L4 (l= 10m = 33 ft)

λ/4 = 7.8 MHZ
3λ/4 = 22. MHZ

In table 2 and fig. 6b we can notice that :

- The maximum levels are measured in the short-circuit coaxial return path (the ratio is however < 2)
- The energy at the frequency corresponding to λ/2 of the structure is very low (8,6 MHZ)
- Resonances at the quarterwave length and 3λ /4 of the structure are strong but the coupling on the line at these frequencies is only clear on the short circuit current.
- Same level of energy corresponding to λ/4 and 3λ /4 of the wire itself for both configurations. (we can notice that the capacitance of the line decreases the frequency of the resonance)
- The transfer fonctions Voc/Iinj are different according to the load R. (Fig.)
  - **Short circuit line** = extrema for λ/4 and 3λ/4 of the structure and, λ/4, 3λ/4 of the wire itself.
  - **Matched line** = extrema only for λ/4 and 3λ/4 of the wire itself

The source impedances Z_g= Voc/Icc of the generator equivalent to the cable are the same for both configurations (fig.6a).
It varies from 1Ω to 300Ω between 50 kHz and 20MHz, and can increase 10 kΩ for the resonances mentioned above. This parameter, dependent on the position of the wire in the structure, is not depending on the test condition [Remark : for F → 0, Z_g→ ohmic resistance of the wire]
In short, the frequency responses can be simplified as follow ;

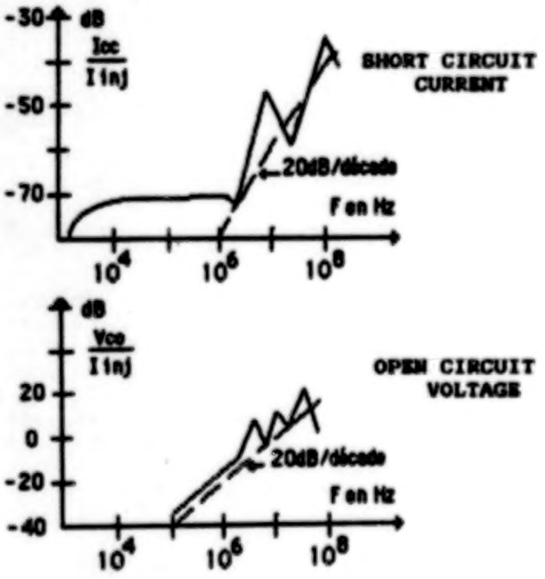

Figure 3. Transfer functions (short circuit current - open circuit voltage) for a wire in an aluminium structure

III 2 - CARBON FIBER WING "V.C.C."

III 2-1- : Without coating mesh :

Characteristics : L = 5m (16ft)
Zs= 20 mΩ.□
R total = 16 mΩ

Figure 4. Wing "VCC" in the coaxial return path

On a single wire located in the center part of the wing (E field not significant), the following levels have been measured for Iinj = 1kA (H/10)

COAXIAL RETURN CONFIGUR.	OPEN CIRCUIT VOLTAGE Voc		SHORT CIRCUIT CURRENT Isc	
R= 60Ω	Max Level 20 V peak 8,5 MHz		Max Level 13 A no oscill.	bi-expo.wave tm = 8 µs td =30 µs
R= 0Ω	29 V peak 8,5 MHz		13 A no oscill.	bi-expo.wave tm = 8 µs td =30 µs

Table III : Induced levels on a wire (L = 5m) located in the center part of the carbon fiber wing (without mesh) for Iinj=1kA (H/10)

We can notice here, that no excitation corresponding to the natural resonances of the structure (wing) is visible, contrary to the case of the helicopter part in aluminium. The only resonance measured is the one of the wire itself (8.5 MHz)
So, in this case, the test configuration has no influence on the induced levels, which are identical. (Fig.7b)
This result is fundamentally different from the previous one concerning the aluminium structure of the ECUREUIL (§ III 1)
It's important to look at the waveform of the induced short circuit current (Fig.5): the injected waveform is a 0.1/4µs wave and the induced wave is a 8/60µs wave. The carbon fiber skin acts as an integrator (1st order filter with fc < 10 kHz), which leads to an important delay between the two waveform peaks :

$$I_{cc} = K \int V_{oc} \cdot dt$$

The ratio of the extrema (Fig. 5) of the values of Voc and Icc has no physical meaning. Only the integral $1/4 \int Voc.Icc\, dt$ can be interpreted as the maximum energy that the wire will be able to deliver on a terminal load.

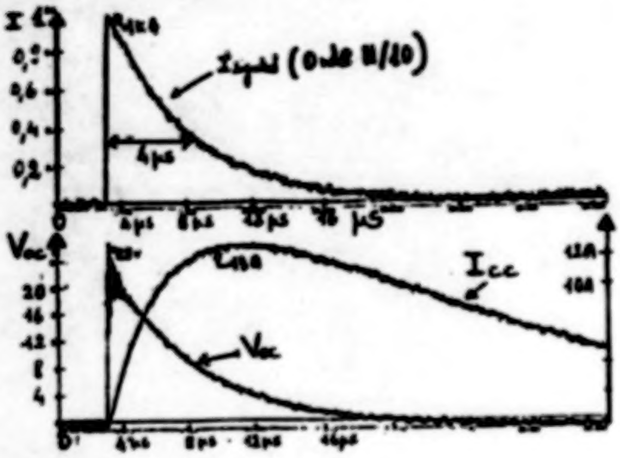

Figure 5. Iinjected current Icc and Voc waveforms

III 2-2- Carbon fiber wing covered by an aluminium mesh :

The same wing (as in & III.2.1.) was covered by a mesh : Zs = 3 mΩ.□
The total resistance of the wing Rt=7.8 mΩ

	OPEN CIRCUIT VOLTAGE Voc		SHORT CIRCUIT CURRENT Icc	
R= 60 Ω	Max Level 14 V Peak 0,5 Mhz	L.F.= 6 V H.F.= 8 V.	Max Level 4 A.	Long wave tm = 0µs td = 30µs
R= 0 Ω	2,9 V peak 0,5 Mhz	L.F.= 6 V. H.F.= 6 V.	3,5 A.	tm = 0µs td = 30µs

Table IV : Induced levels on a single wire (5m) in the center part of the wing covered by alumesh (wave H/10).

By comparison of the tables III, IV and Fig. 8 we notice the following important results :

- Same internal behaviour of the wing, whichever the coaxial return load is used. The transfer functions are given below : the shielding effect of the mesh is only evident below 1 MHz on the voltage transfer function (-10dB). We have to bear in mind that the main reason for the use of a mesh is the protection of the fuel tank against the direct effects (burning through) and not to achieve high attenuation levels.

A summary of the typical transfer functions on a wire in a carbon fiber structure is given below :

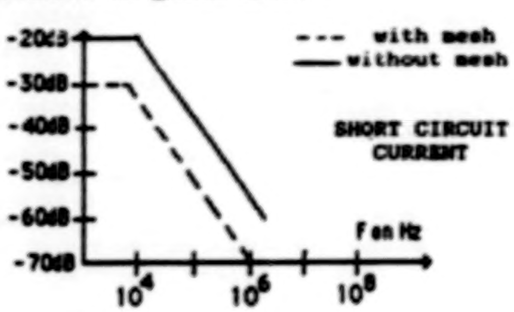

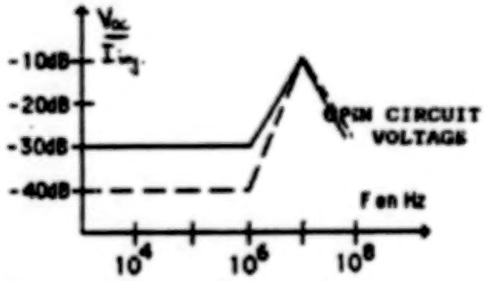

The shielding effect of the mesh is about -10 dB between 10 khz and 1 MHz (Fig. 9)

IV- INFLUENCE OF THE ELECTRIC FIELD ASSOCIATED TO THE CURRENT

A high voltage generator is necessary to inject the current waveform. So, an important electric fied raises in the coaxial return. The previous analyses were performed on wires located in areas where the electric field was insignificant, that means without any effect.

But, more generally, the extrapolation of the signals to the threat (D/10 → D and H/10 → H) requires a precise analysis to separate the electric coupling from the magnetic coupling. This is particularly true for the wirings exposed under open structures (dielectric fairings). The two test set-up above mentionned lead to a different electric coupling.

• matched coaxial return :

The values of E and dE/dt on the extrados of the wing are constant along the coaxial return. An idea of the levels is given below for H/10 wave - (1 kA)

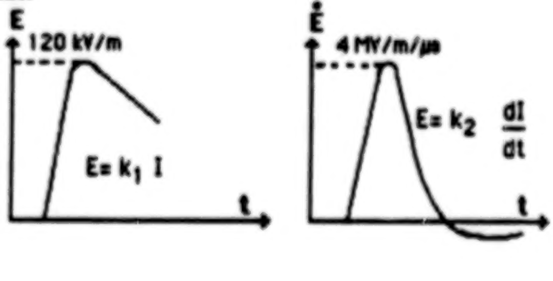

• Short-circuit coaxial return :

The values of E and dE/dt are not constant any more along the line : maximum at the entry and zero at the end of the line. The following diagrams show the waveforms recorded at the input of the transmission line (for H/10) ;

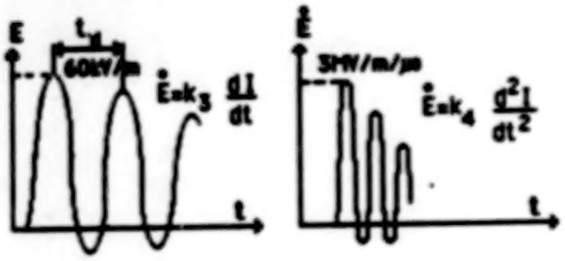

For a test at H level (10 kA), the order of magnitude of dE/dt is 10^{13} V/m/s, close to the values of in flight measurements (Ref.3) Although it is controlled by the current parameter, the simulation in a coaxial return gives a proper electrical excitation, by comparison with the levels encountered in free space (excitation not yet normalised)

REMARK : A test configuration can help, in some cases, to determine the type of coupling (E or I) and thus enables the extrapolation method : by creating a second arc channel at the end of the coaxial return, the electric field is maintained till the connection of this gap (few µs) and then a negative dE/dt is appearing, though I and DI/dt are positive. An inversion of polarity on the induced voltage, due to the subsequent effects of E and I is visible.

V - CONCLUSION

This paper reminds us of the influence of the type of return load used (matched or short circuit) on the levels and frequency spectrum of the induced transients. According to the nature of the structure, a test configuration is more suitable to recreate the real threat.

Nature	Structure	Resonance (In flight)	Test set-up Extrapolation method
Metal	wing	λ/4 3λ/4	-short circuit coaxial return. Wave H(10kA) -If excitation by an hypothetic reduced wave, extrapolation by scaling factor
	fuselage	λ/2	-matched coaxial return. Wave H(10KA) -For the extrapolation add to the spectrum of the wave H, an oscillation at f corresponding to λ/2.
Carbon (with or without mesh)	Wing	λ/4 3λ/4	- Short Circuit or matched coaxial return (indifferently) Extrapolation : see 1 st case
	Fuselage	λ/2	- Short Circuit or matched coaxial return (indifferently) Extrapolation : see 2nd case
Carbon + metal	Main Aircraft	See § II-1	- To analyse, according to the quantity and location of metal parts and convenient possibilities for the realisation of the test-bed.

The generator must be able to inject the normalised current waveform. That's why the C.E.A.T. has given the following specifications for its new facilities.

- Marx generator (8 stages of 100 kV) with low internal inductance L < 2 µH and a coaxial output Z = 60 Ω)
- Two biexponential waves will be possible :
  - -H : Imax=10 KA   tm = [60,100ns]
    t 1/2 = 4 µs
  - -D/2 : (with crowbar)
    Imax = 50 kA   tm= 1µs   t1/2 = 35 µs

The results of the V.C.C. (Voilure Composite Carbon = Carbon Composite Wing) come from a joint programme C.E.A.T. / AEROSPATIALE / DASSAULT AVIATION supported by DGAC and DGA/ DCAé/STTE

DGAC = Direction Générale de l'Aviation Civile
DGA/DCAé/STTE = Délégation Générale pour l'Armement . Direction des Constructions Aéronautiques. Service Technique des Télécommunications et Equipements Aéronautiques.

References :

1) Eurocae comments on the FAA NPRM number 89-15 lightning protection 25 august 1989.

2) Investigations into the triggered lightning response of the F106B Thunderstorm Research Aircraft (1980-1982 data) Nasa Report 3902 H. RUDOLPH, A. PERALA, P.B. KENNA, S.PARKER.

3) E and H fields measurements on the Transall C 160 Aircraft during lightning flashes (1984) J.P. MOREAU, J.C. ALLIOT, 10 th ICOLSE Paris Juin 1985

4) Rapport final sur l'étude théorique de la répartition des courants et charges instantanés sur une voilure composite carbone attaquée par une agression foudre. Université de Limoges IRCOM Convention n°87/22023 Février 1989

5) Draft Notes for EUROCAE WG subgroup (lightning Testing Standard) on pulse aspects of generator systems. J.C. HARDWICK, BJ BURROWS - CULHAM LABORATORY 26.9.88.

6) Anglo French Aeronautical Research Programme (N°17). Lightning Simulations on an helicopter test -bed CEAT E - 88/68 15 Juillet 89 J.L.EMANUELY C.DAVOISE.

7) Voilure Composite Carbone. Evaluations de niveaux induits sous foudroiement simulé. CEAT n°E89/409400 H.CANTALOUBE, F.ISSAC.

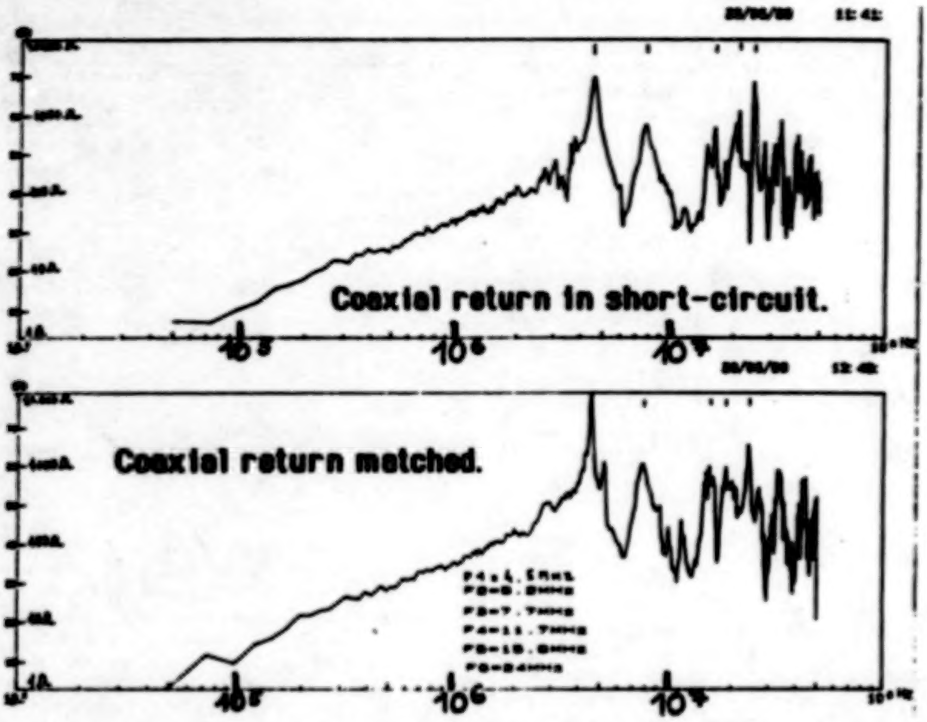

a) Source impedance Zg=Voc/Isc of the generator equivalent to the wire L4
(Coaxial return in short circuit or matched)

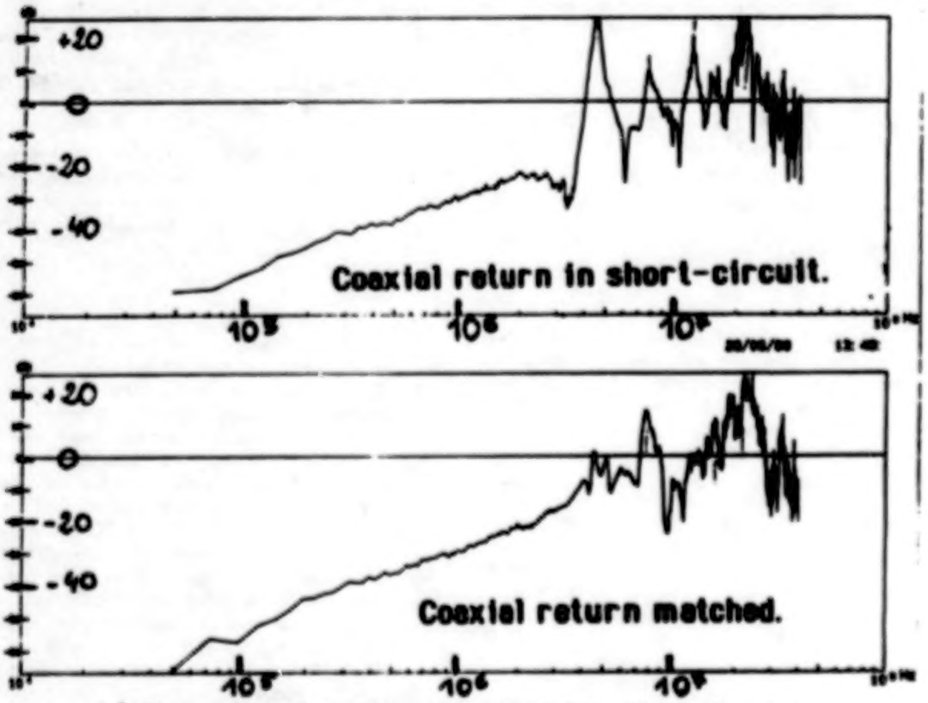

b) Transfer function Voc/Iinj for the wire L4
(2 different coaxial return loads).

FIGURE 6 : SINGLE WIRE BETWEEN THE TAIL ROTOR AND THE EQUIPMENT BAY OF THE HELICOPTER "ECUREUIL" FROM AEROSPATIALE (As 355).

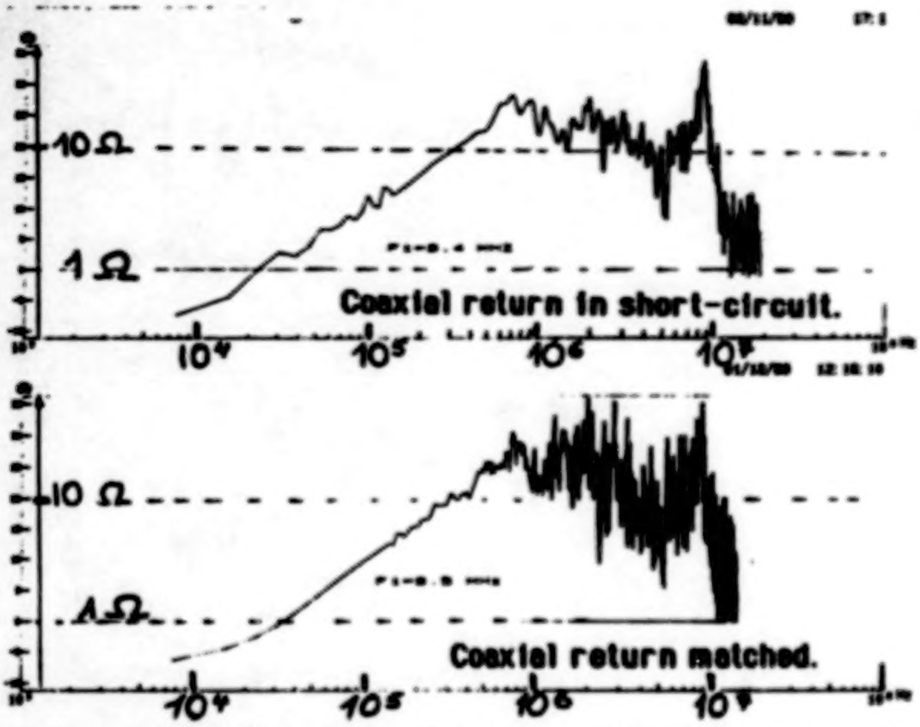

a)Source impedance Zg=Voc/Isc of the generator equivalent to the wire B2A
(Coaxial return in short-circuit or matched)

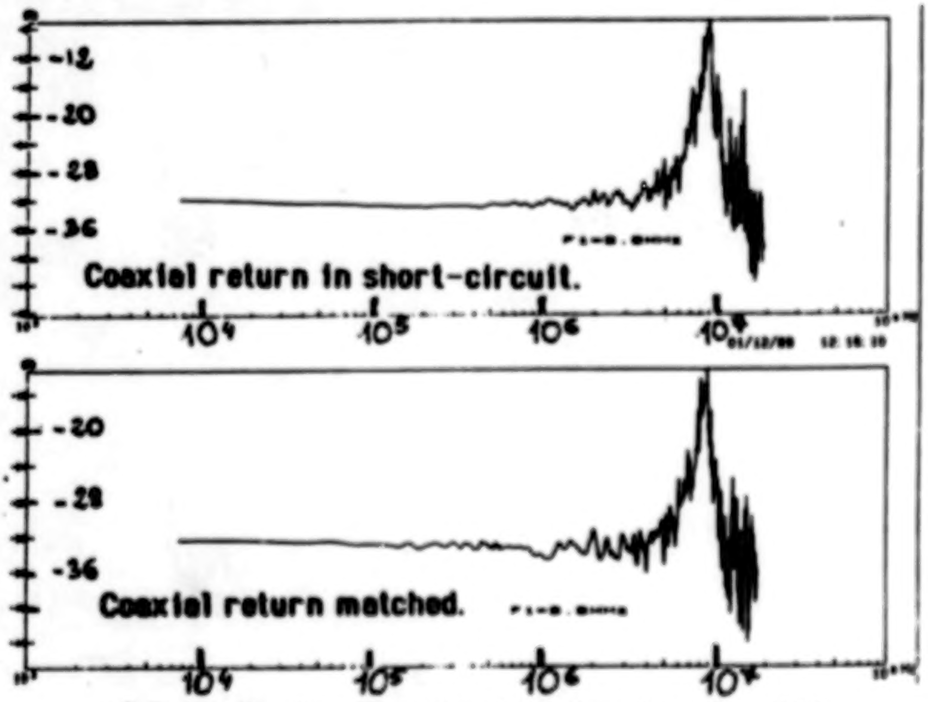

b) Transfer function Voc/Iinj for the wire B2A
(2 different coaxial return loads).

FIGURE 7 : COMPOSITE CARBON WING (VCC) WITHOUT MESH.

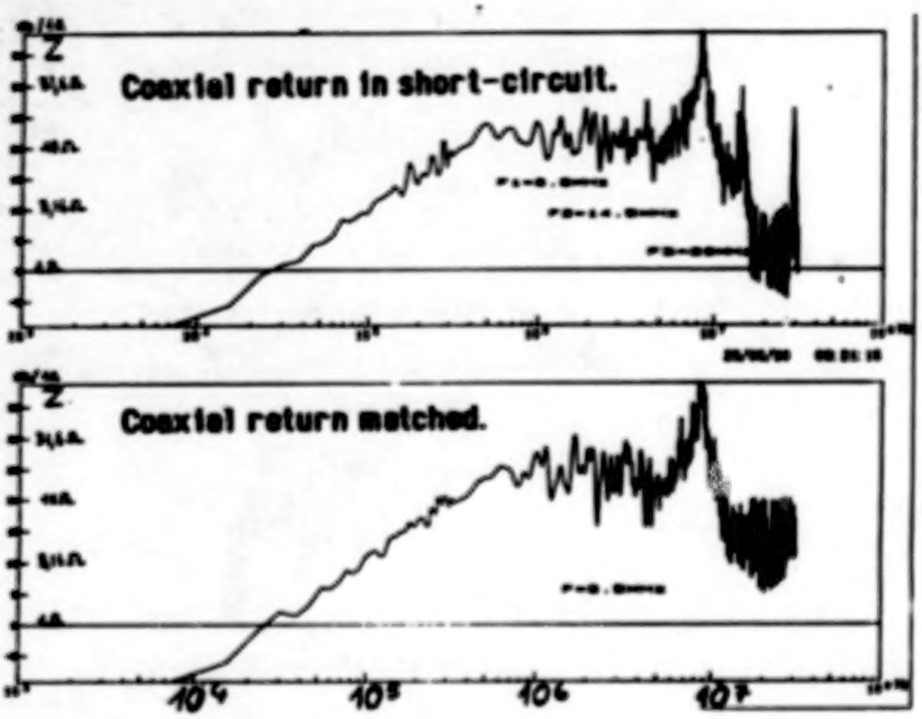

a)Source impedance Zg=Voc/Isc of the generator equivalent to the wire B2A
(Coaxial return in short-circuit or matched)

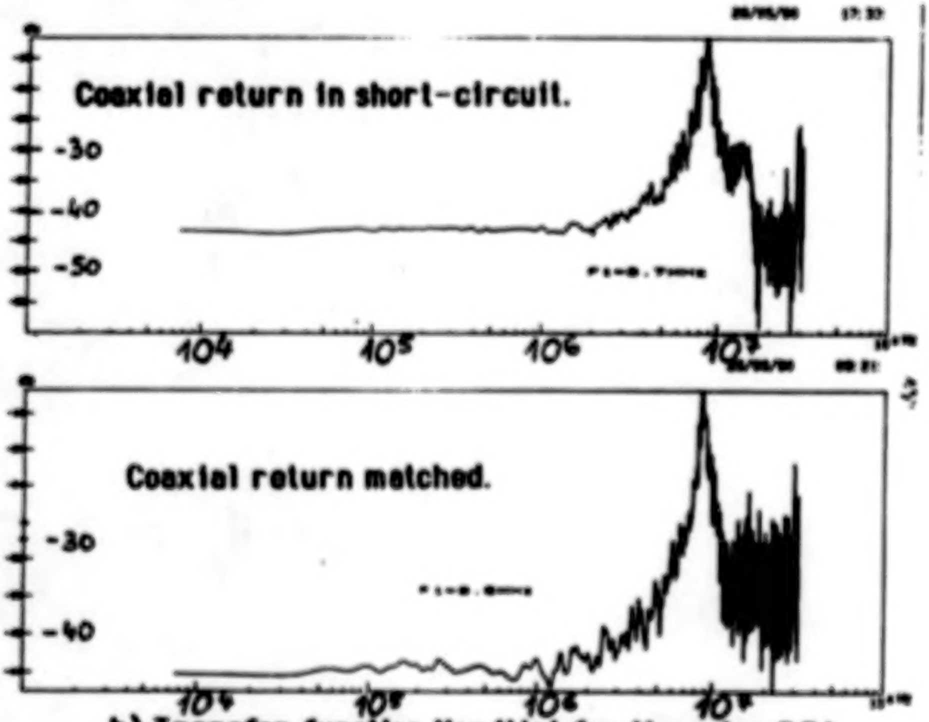

b) Transfer function Voc/Iinj for the wire B2A
(2 different coaxial return loads).

FIGURE 8 : COMPOSITE CARBON WING (VCC) WITH MESH.

342

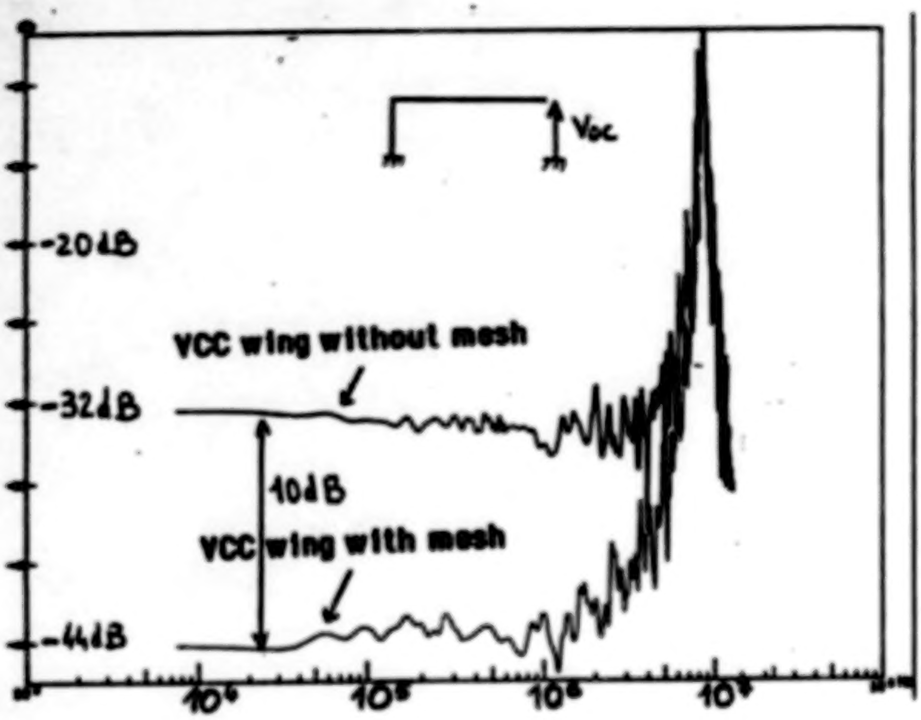

Coaxial return in short-circuit.

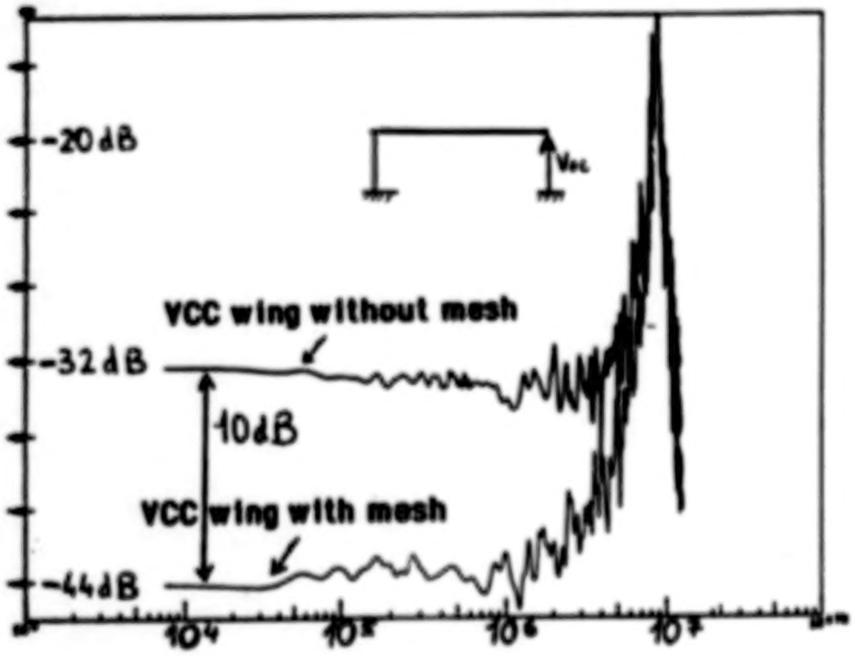

Coaxial return matched.

Transfer function Voc/Isc for the wire B2A of the carbone wing with and without mesh for both values of return load.

FIGURE 9

EVALUATION OF THE DAMAGES CAUSED BY LIGHTNING CURRENT FLOWING THROUGH BEARINGS

O. Celi, A. Pigini

High Voltage Division - CESI - Milano - Italy

and

E.Garbagnati

ENEL CREL - Milano - Italy

ABSTRACT

A laboratory for lightning current tests has been set up at CESI allowing the generation of the lightning currents foreseen by the Standards. Lightning tests are carried out on different objects, aircraft materials and components, evaluating the direct and indirect effects of lightning. Recently a research has been carried out to evaluate the effects of the lightning current flow through bearings with special reference to wind power generator applications.
For this purpose, lightning currents of different amplitude have been applied to bearings in different test conditions and the damages caused by the lightning current flow have been analysed.
The influence of the load acting on the bearing, the presence of lubricant and the bearing rotation have been studied.

INTRODUCTION

The peculiar structure of the wind power generators and often the weather conditions typical of the areas where the eolic plants are installed, increase the probability for a generator to be struck by a lightning flash. If a lightning flash happens to hit a wind power generator, the lightning current path to earth can involve the shaft and the bearing (Fig.1). Similar problems may arise, for example, if a lightning flash hits the blades of an helicopter.
The flow of the lightning current can damage bearing rolling elements and raceways, with a possible consequent reduction of the reliability of the structure where the bearing is installed.

The evaluation of the effects produced by the lightning current flow through bearings is important both to evaluate the efficiency of the structure and to identify possible protection systems. For this purpose, lightning currents of different amplitude have been applied to bearings in different test conditions and the damages caused by the lightning current flow have been analysed.

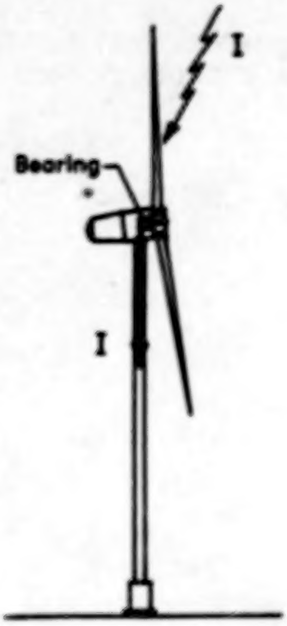

Fig. 1 - Schematic view of the lightning path in a wind power generator, with involvement of the generator bearings.

For the evaluation of the effects produced by the lightning current flow through bearings, the contact conditions among the rolling elements and the raceways are of special interest.
In the loaded zones of the bearings the rolling elements are in contact with the raceways, while in the unloaded zones the rolling elements are not in contact with the raceways and small gaps are formed.

The lightning current interests the contact areas between the rolling elements and the raceways.
The number of rolling elements in contact with the raceways is a function of the mechanical load (the number of rolling elements in contact increases when the mechanical load is increased); in the limit case only one rolling element can be in contact.
The extension of the contact area for each rolling element is also a function of the load.

The lightning current may interest the small gaps between the raceways and the rolling elements in the bearing zones not in contact. The electric strength of the gap depends on the kind and the characteristics of the insulating media.

The performance of the bearing under lightning can be finally influenced by its rotation.

It is evident that the phenomenon is very complex.
In order to try to understand the mechanism of damage, the tests were designed to analyse separately the influence of the parameters mentioned above.
In particular, the effect of the mechanical load and of the lightning current amplitude was analysed on a simplified configuration (single couple

of rollers), while the influence of rotation, lubrication and lightning current flow through the different rolling elements was analysed on complete bearings.

TEST OBJECT

The systematic research was performed on self-aligning roller bearings, with double order of rollers, having the following main characteristics: external diameter of 160 mm, internal diameter of 90 mm and dynamic load coefficient of 322 kN. The raceways and rollers of the bearings were made of high-chrome steel.
The following test configurations were examined, as shown in fig. 2:

a) simplified configuration with single couple of rollers (see fig. 2a) to analyse the effects of the lightning current flow through single rollers.
To this purpose all the rollers, except the two under investigation, were taken out from the bearing and substituted by an insulating ring having the function to maintain the bearing geometry. In this way the lightning current was forced to flow exclusively in the couple of rollers.
The bearing was tested in still condition, without lubricant.

b) complete bearings (see fig. 2b), to study their lightning performance in different conditions. Namely the bearings were tested without oil both in still and rotating conditions and finally in rotation with oil.
A rotation of 300 rpm was maintained through a motor mounted on the shaft. The lubricant was housed in a box under the bearing and transported through the rolling elements by the rotation itself.

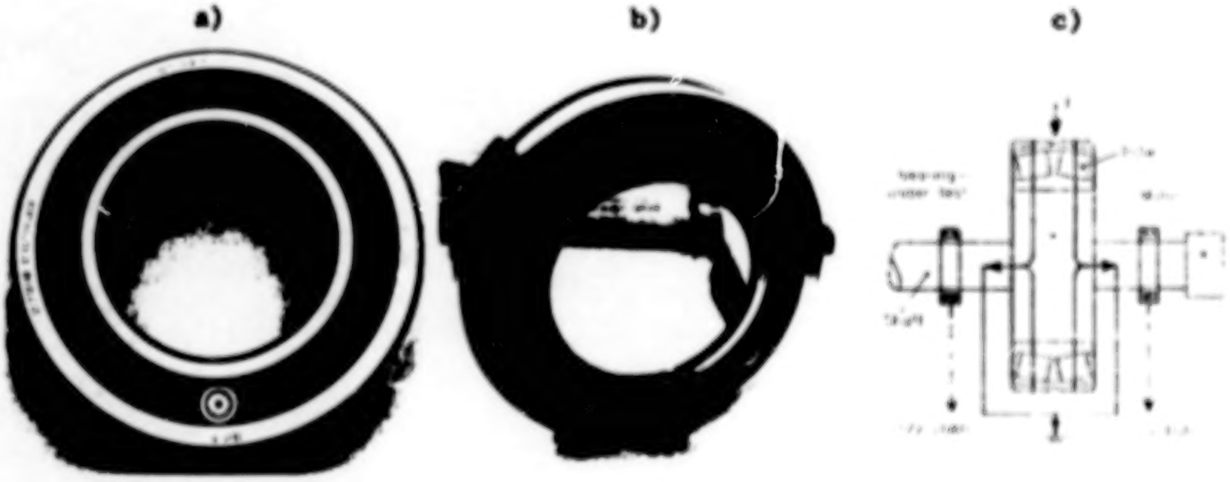

Fig. 2 - Test objects and test set up
a) picture of the simplified configuration (with single couple of roller)
b) picture of complete bearing
c) scheme of the test set up.

TEST CONDITIONS

MECHANICAL STRESSES

Radial mechanical loads were applied to the bearings under test; the load was applied symmetrically on the shaft (see fig. 2c).

The load was varied up to 10 kN in the tests on single couple of rollers to vary the contact area.
The relation between the contact areas on a single roller (S) (in the bearing under test, the contact areas are ellipses) and the load acting on the bearing is reported in Fig.3, where the curves relevant to inner and outer raceways are given [1].

A constant load of 5 kN was applied on the complete bearings. Mechanical calculations [1] indicate that in this case only 5 couples of rollers are in contact with the raceways. The calculation also permits to evaluate the load distribution among the different rollers and thus the contact areas. The extension of the single roller contact area results of 1.8 mm^2 for the most loaded rollers decreasing to 1.3 and 0.3 mm^2 for adiacent rollers (see fig. 8b).

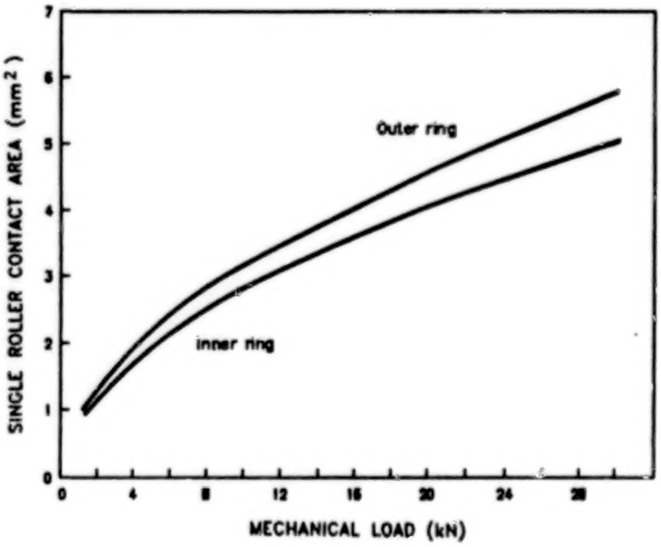

Fig. 3 - Mechanical calculations. Inner and outer ring contact areas of a single roller as a function of the mechanical load applied to the bearing simplified model, with only one couple of rollers.

CURRENT STRESSES

In all the above mentioned cases, the lightning current was injected in the outer ring of the bearing through an additional metallic ring externally clamped to the bearing itself.
The lightning current was flowing from the outer ring to the inner one through the rolling elements and then to earth through the shaft (see Fig.2 c).

327

The lightning current was generated by means of the test circuit shown in fig. 4; the circuit allows the generation of the current waveforms A,B,C and D foreseen by the Standards [2] both as single pulses and as a combined waveforms. It is composed by three current generators and a filter with blocking capacitors and inductances; the main characteristics of the current generators are described in the followings.

Fig. 4 - Test circuit to generate current components as in [2].

The A/D current generator consists of a 100 kV, 24 μF, 120 kJ capacitor bank; the capacitors can be charged in both positive and negative polarity. Damped oscillating waves with peak values up to 200 kA, action integral up to $2*10^6$ A^2*s and rise times between 8 μs and 20 μs can be achieved with load inductances up to some μH.
The B current generator is a 12 LC cell, 20 kV, 90 kJ generator. The cells can be charged both in positive and negative polarity. Currents with peak values up to 2.5 kA and duration of few ms can be generated.
The C current generator consists in a DC generator and a smoothing capacitor bank. Continuous currents up to 250 A with time durations up to 1 s can be generated.
Plasma gaps are used to switch the different lightning current components.

The systematic research was carried out injecting the A current component, while only few checks were made with B and C components.
The lower amplitude and rate of rise of the B & C lightning currents with respect to the A component, the longer time duration and the speed rotation of the bearing seem to be the most important parameters in determining the damage mechanism with this kind of current components. Further tests are foreseen in order to better analyse the influence of the different lightning components on the damage mechanism and extension.
In the following the results obtained with the A current component will be given.

Tests with current peak values in the range from 1 kA up to 100 kA and an action integral⁽¹⁾ in the range from 18 A^2*s up to $1.2*10^6$ A^2*s were applied to the simplified configuration with the single couple of rollers to determine the minimum current leading to damage (damage threshold) and study the relationship between current and damages.

A current impulse with a peak value of 100 kA and an action integral of $1.2*10^6$ A^2*s was applied to complete bearings under test.

TEST RESULTS

LIGHTNING TESTS ON SIMPLIFIED CONFIGURATIONS

Damages were observed both on the inner and the outer raceways and correspondingly on the rollers of the bearing.
The damage-threshold-peak-value of the injected current (Ipt) and the corresponding action integral (Et) are reported in fig. 5 as a function of the load acting on the couple of rollers: the threshold peak current increases when the load is increased.

By combining the data of fig. 3 and fig. 5, the threshold values of the current density Ipt/S and of the action integral density Et/S were determined. The damage-threshold peak current-density was found approximately constant (about 4 kA/mm^2) independently of the mechanical

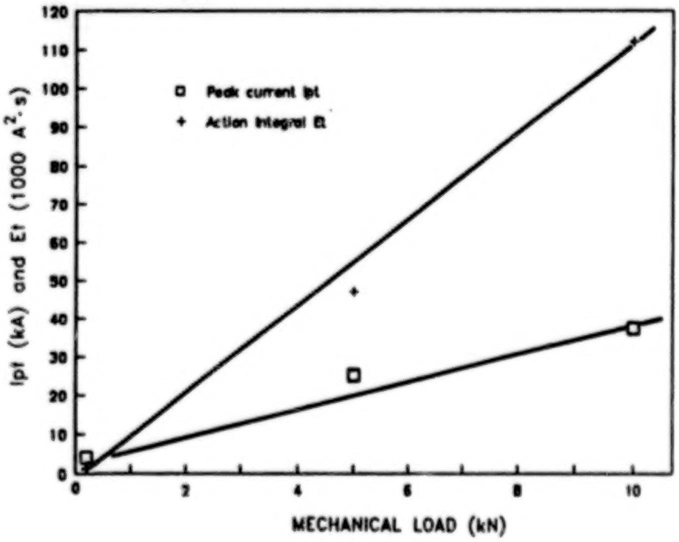

Fig. 5 - Tests on the simplified configuration with one single couple of rollers: damage- threshold current values as a function of the mechanical load applied to the bearing.
Ipt= peak current value
Et= action integral value

---

(1) The Action Integral E represents the energy per unit resistance transferred by the lightning current and is defined as: $E = \int_T i^2 * dt$, where T is the duration of the current waveshape.

load. The damage threshold action integral density varied from 190 A^2*s/mm^2 to 6.000 A^2*s/mm^2 when varying the mechanical load in the examined range.

The type and size of damage varied with current and mechanical load value. At low current values, craters (see fig. 6a) were observed when very low mechanical loads were applied, while flutes (as shown in Fig. 6b) were observed for higher loads.
For higher current values the type of damage remained similar. However, bigger surfaces of the rollers and raceways were damaged and melted materials appeared at the flute extremities.

The damages caused by the flow of the lightning current to the bearing rollers and raceways were estimated, in a preliminary way, by evaluating the extension of the damaged surface, independently of the damage type. Other more precise evaluation of damages in terms of depth, volume, type and so on are undergoing. Metallographic exams will be also made in order to detect possible changes of the metal characteristics in the damaged areas.

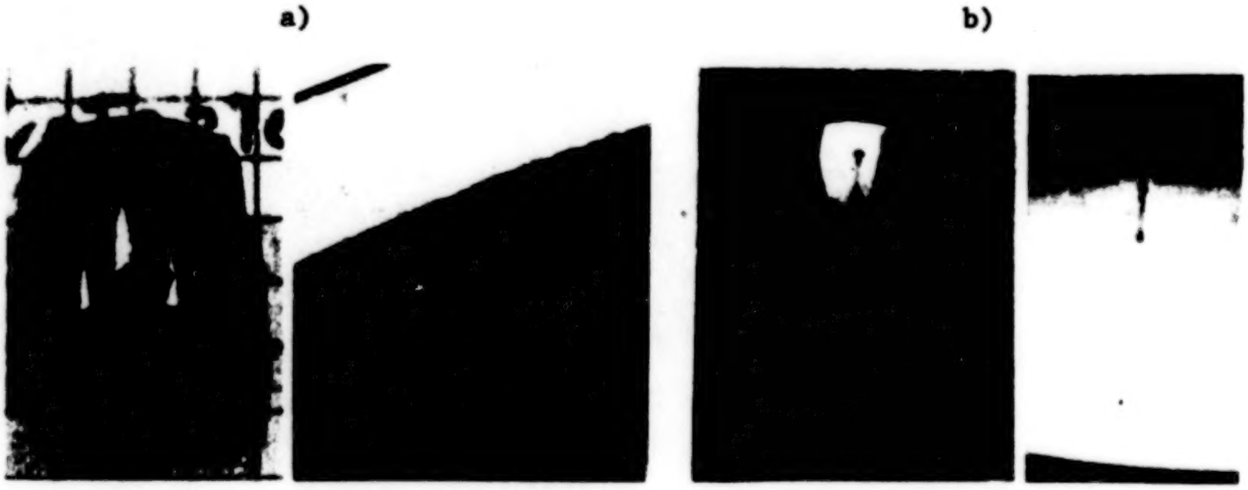

Fig. 6 - Tests on the simplified configuration with one single couple of rollers: damages observed:

a) craters
b) flutes

Fig. 7 reports the maximum values of the damaged area (independently of the type of damage), at one of the contact side of each roller, as a function of the peak value of the injected current for the three mechanical load conditions examined; the contact area of a single roller for the three different loads are also reported. The figure shows that the damage extension increases when the load is decreased and, for a given load, increases with the increase of the lightning current amplitude.
Comparing the damaged areas with the estimated contact areas, it appears clearly that while for low current values the damaged surface is close to the contact area size, for higher currents it is much larger.

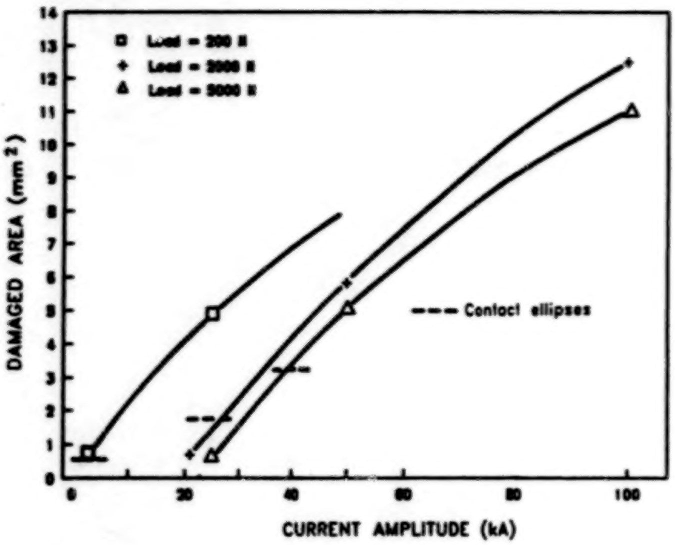

Fig. 7 - Tests on the simplified configuration with one single couple of rollers. Maximum values of the damaged surfaces as a function of the peak value of the lightning current for different load conditions.

TESTS ON COMPLETE BEARINGS

Also in the case of complete bearings, a rough estimation of the damages has been made. The damaged surfaces, independently of the damage type, are reported in Fig. 8 where the maximum values of the damaged areas are given in correspondence of each couple of rollers. For sake of simplicity only the cases of still bearing without lubricant and rotating bearing with lubricant are considered in the Figure.

A qualitative analysis of the damages observed on complete bearings was made.

In the case of bearings in still condition without oil, craters and burns were observed on the raceways and correspondingly on the rollers in the whole unloaded zone of the bearing, while very limited damages were observed in the loaded areas (small craters): a part of the lightning current had passed through the unloaded area, where air gaps were present.

For rotating bearings without lubricant, the damages were bigger than in the previous condition. Moreover abrasions were observed on the raceways. This may be explained considering that, owing to the rotations, the melted materials had been squashed around the damaged area and transported around the bearing causing abrasions on the bearing raceways.

In the case of rotating bearing with lubricant, craters were present in the unloaded zone only at the extremities of the loaded area, where the smallest gaps between rollers and raceways were present, while in the loaded zone, the size of the damages was higher than in the previous cases. Abrasions were more limited with respect to the case without lubricant.
This can be explained considering that the presence of lubricant, acting as

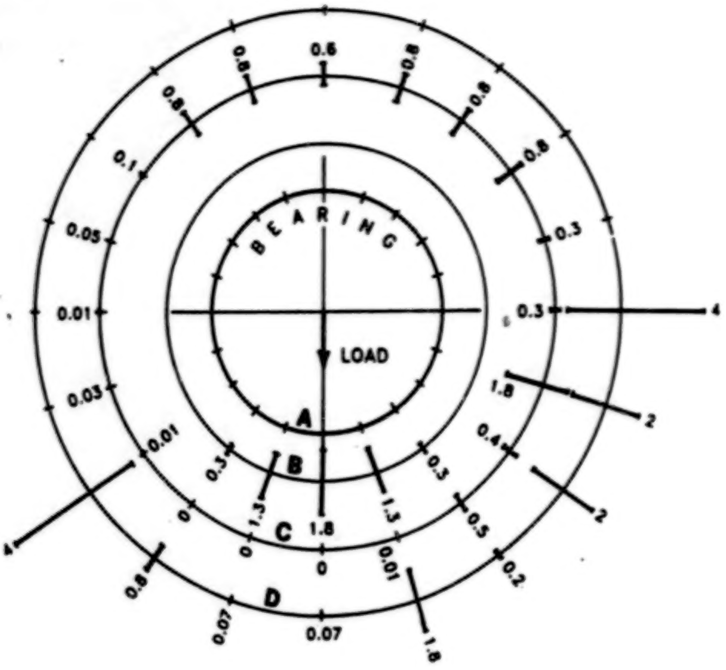

Fig. 8 - Tests on complete bearings. Contact areas and damage extension at each radial location (extension given in mm^2).

- A) Radial position of the rollers
- B) Contact areas
- C) Damages for bearing in still conditions without lubricant
- D) Damages for bearing in rotating condition with lubricant

a dielectric medium (with a higher dielectric strength than air), plays an important role in the prevention of the occurrence of localised discharge in the gaps and also in the reduction of the abrasions.

If the larger part of the lightning current would flow through the rollers in contact and it would distribute among them according to the contact areas, a theoretical peak current density of about 10 kA/mm^2 could be evaluated in the examined case of an injected peak current value of 100 kA. This value is more than twice the threshold value determined in the tests on the simplified configuration with one single couple of rollers and would imply damages of loaded zones. Actually the test results generally indicate a very limited damage in the loaded zone. This can imply that a large part of the current flows in the unloaded zone.

CONCLUSIONS

Lightning tests have been made on rolling bearings applying the A current component of the Standards and the damages caused by the lightning current flow have been analysed.
The damage mechanism and extension depend on current values and on the mechanical load condition, which determines the area of contact between roller and raceway.

When the lightning current flows through the contact areas, a consequent enhancement of the local temperature occurs. The high temperatures in the contact area can lead to local melting of the material, with a consequent formation of flutes.
The lightning current density (which is a function of the load and the current intensity) and the current energy content play an important role in this kind of damage mechanism.

Test in simplified conditions indicate that for areas in contact a peak current density of 4 kA/mm2 resulted sufficient to initiate the damage.

The lightning current may also interest the zone where rollers are not in contact with the raceways (unloaded zones). In fact, owing to the high di/dt associated with the A lightning current component, voltages are induced across the small gaps. These voltages can lead to the breakdown of the gaps; once the gap has been broken, the lightning current can flow through it and the resulting arc leads to the formation of craters and burns. The extension of the damages produced by the arc root can be bigger than that corresponding to the current conduction damages.

The research is going on and further tests will be made on bearings of different dimensions, with different lightning current components and in different test conditions, in order to better understand the ligthning performance of rolling bearings, obtain statistical data on the different kinds of damage and finally define an electrical-mechanical model able to describe the lightning behaviour of bearings in different operating conditions.

ACKNOWLEDGEMENTS

The authors wish to acknowledge Mr. Ballarin of CESI for the collaboration to the tests. Thanks are also due and to Dr. Orlandini and Dr. Beretta, from SKF, for mechanical advises and calculations.

REFERENCES

[1] Orlandini and Beretta-SKF-Torino-Italy. Private communication.

[2] SAE AE-4L "Lightning Tests Waveforms and Techniques for Aerospace Vehicles and Hardware" 1978.

Session 7A, Wednesday, 1:30
Ground Protection 3

Stahmann, Chairman

A TRANSPORTABLE 50 KA DUAL MODE LIGHTNING SIMULATOR[1]

K. Salisbury, S. Lloyd, Y.G. Chen
Maxwell Laboratories, Inc.

ABSTRACT

Maxwell Laboratories, Inc. has designed, built and tested a transportable lightning simulator capable of delivering more than 50 kA to an 8 μH test object. The simulator was designed to be a versatile device in the lightning laboratory while meeting the requirements of MIL-STD-1757A for component E current waveforms. The system is capable of operating in either a ringing mode with a Q greater than 5 and a nominal frequency of 160 kHz, or a unipolar mode with no hardware configuration changes.

The ringing mode is obtained by the LCR series circuit formed by the pulse generator and test object. The unipolar mode is obtained by closing an electrically triggered crowbar switch at peak current. The simulator exceeds the peak current requirement and rate of rise requirements for MIL-STD-1757A in both the ringing and unipolar modes. The pulse half width in the unipolar mode is in excess of 50 μs and the action is in excess of 10^5 A^2s.

The design, component values, and test results are presented.

SYSTEM DESCRIPTION

The 50 kA Transportable Lightning Simulator is a complete turn-key lightning simulation system including the pulse power generator, system output diagnostics, control and auxiliary systems. The simulator is rugged and compact, for easy transportability, and provides a highly reproducible output pulse over a wide operating range. The ability to change the operating mode of the simulator without hardware changes at the pulse generator is a key feature of this system that helps to maximize the operational availability of the system. A photograph of the simulator output connection and the control console is shown in Figure 1. A simplified block diagram of the system is shown in Figure 2.

The simulator provides peak current of more than 50 kA to an 8 μH load, with either a damped sinusoidal or unipolar waveform. The system was specified to produce peak current and current rate-of-rise performance to meet MIL-STD-1757A Waveform E, shown in Figure 3. The generator was tested into an 8.05 μH, 110 mΩ load at Maxwell Laboratories in San Diego in July 1990. Table I provides a listing of the demonstrated performance of the simulator, which meets or exceeds all customer specifications.

The simulator produces the damped sinusoidal waveform with an underdamped series RLC circuit consisting of the Marx generator and simulator inductance in series with the inductive load. This imposes a severe design constraint since the voltage across the crowbar switch and output bushing reverses to positive polarity and is present for a much longer time than in the crowbarred mode. The unipolar output pulse, with >50 μs FWHM, is produced by closing a crowbar switch which shorts the simulator output terminal to ground at near peak current to provide an L/R decay time dominated by the load inductance as in previous lightning simulator systems[2,3]. The modest voltage of the 50 kA simulator compared with full threat simulators[3] allows the use of an electrically triggered SF_6 insulated crowbar switch. The 50 kA simulator can be changed from unipolar to ringing mode by simply disabling the crowbar trigger and overpressurizing the crowbar switch, with no reconfiguration of hardware in the pulse generator tank.

---

[1] This system was developed for Boeing Advanced Systems under contract number B239503.

[2] R. A. White, "Lightning Simulator Circuit Parameters and Performance for Severe-Threat, High-Action-Integral Testing," International Aerospace and Ground Conference on Lightning and Static Electricity, Orlando, FL, June 26-28, 1984.

[3] J. L. Harrison, et.al., "A Severe Threat-Level Lightning Simulator," International Aerospace and Ground Conference on Lightning and Static Electricity, Dayton, OH, June 24-26, 1986.

PULSE GENERATOR

The compact pulse power system is housed in a steel tank (110" l x 66" w x 80" h) insulated with one atmosphere (absolute) SF_6 gas. High voltage power supplies, trigger generators and auxiliary systems are located at the back wall of the tank, opposite the HV output. The generator is mounted on casters and weighs approximately 5000 lbs. The controls are mounted in a single rack that can be located up to 75 ft. from the generator.

A simplified circuit model of the 50 kA simulator is shown in Figure 4. The Marx generator is an 8 stage unit, with 2 plastic case 0.4 µF capacitors per stage, arranged in a vertical column. The Marx stores about 18 kJ at full operational charge voltage. All Marx components are easily accessible for maintenance with charge and ground resistors mounted along the sides of the Marx and switches and trigger components mounted on the front. The Marx generator is assembled on an aluminum base plate and can be lifted from the pulse generator tank as a complete assembly.

The Marx generator is connected to the crowbar switch and output buswork through R_{series}, an assembly of 6 parallel water resistors. These protect the Marx generator in case of a short circuit fault and help damp out oscillations in the Marx/crowbar loop. The crowbar switch is located directly below the output buswork between the Marx and output bushing.

The crowbar switch is the same basic design as the laser triggered Sandia switch[4], except for the addition of a midplane trigger electrode and a reduced main electrode gap spacing for the much lower voltage operation of the 50 kA simulator. The crowbar switch is SF_6 insulated, with a typical pressure of 48 psig for a 50 kA shot. The overall envelope of the crowbar switch housing is comparable to previous full threat simulators due to the SF_6 insulation of the pulse generator instead of oil, and the requirement for the crowbar switch to withstand the voltage waveform of the ringing output mode.

The crowbar switch is triggered from a small 6 stage Marx generator located inside an EMI shielded enclosure in the main pulse generator tank, shown in Figure 5. The crowbar switch trigger Marx is shielded to prevent crosstalk between the main Marx and trigger Marx when the main Marx generator erects. The crowbar switch trigger Marx is isolated from the crowbar midplane with an SF_6 insulated isolation switch, pressurized to hold off the peak midplane voltage of about -250 kV and then close when the approximately -450 kV trigger pulse is applied.

The HV output connection of the pulse generator is insulated from the tank with a fiberglass reinforced polyester bushing mounted on the sloped front wall of the pulse generator tank. Connection rails on the front of the tank all around the output bushing allow the connection of wide planar current return conductors. This output configuration allows easy connection of the simulator to a wide variety of load configurations.

The output pulse is initiated when the Marx generator is triggered and the stored energy is transfered to the circuit inductors. Ideally the crowbar switch should close at peak current when there is no voltage accross the switch. Previous laser triggered crowbar systems have operated with the crowbar switch closing somewhat past the current peak, when the voltage on the switch is increasing. The initial design for the 50 kA simulator was based on the crowbar voltage increasing to +100 kV before closing, which would give acceptable pulse width and ripple while easing the electrical triggering of the switch. In practice the crowbar switch triggered more easily than expected giving increased pulse width and reduced ripple compared to our baseline design.

EXPERIMENTAL RESULTS

System diagnostic monitors provided with the 50 kA pulse generator include an output voltage probe and a Marx current probe inside the pulse generator tank. The voltage probe is a water resistor voltage probe, connected between the output buswork and ground, which provides the voltage across the crowbar switch. The Marx current is monitored with a Pearson 301X current transformer in the ground leg of the Marx. B-dot probes are provided to monitor the trigger Marx and crowbar switch currents.

For the purpose of acceptance tests the 301X current probe and a Rogowski belt, cross calibrated to the Pearson current transformer, were installed outside the tank to measure the actual load current and load dI/dt. A Pearson 1049 probe was used to monitor Marx current during some acceptance test shots.

Data for a typical damped sinusoidal output pulse is shown in Figure 6, for a Marx charge voltage of 73 kV per stage. Load current and dI/dt are shown in Figure 6a, with a peak load current of 51.2 kA and a peak dI/dt of 5.3×10^{10} A/s. Figure 6b shows the Marx voltage (top) and current (bottom), with a peak output voltage of 452 kV. The oscillation frequency is 156 kHz with reversal of 75%. This full current ringing output mode is the most severe for the Marx generator and the Marx components are generously derated to provide high reliability, long life operation even under these harsh operating conditions.

---

[4] M. J. Landry and W. P. Brigham, "UV Laser Triggering of Crowbars Used in the Sandia Lightning Simulator," International Aerospace and Ground Conference on Lightning and Static Electricity, Orlando, FL, June 26-28, 1984.

Lifetime of the Marx capacitors is given approximately by the formula,

$$L_x = L_{REF} \left\{ \frac{V_x}{V_{REF}} \right\}^{-7.5} \left\{ \frac{Q_x}{Q_{REF}} \right\}^{-1.6} \qquad (1)$$

The Marx capacitors have a design life $L_{ref} = 100{,}000$ shots at a reference voltage $V_{ref} = 85$ kV and $Q_{ref} = 0.976$. The full current ringing mode has values $V_x = 75$ kV and $Q_x = 5.5$ which gives an estimated Marx capacitor life of 18,730 shots. In actual operation many of the system shots will be at lower current or crowbarred, which will greatly extend the life of the capacitors. The Marx generator switches use tungsten-copper electrode material and have a design life of 10,000 shots at 100 kA and 0.5 C per shot, compared with the operation levels of 50 kA and 0.4 C per shot.

Typical unipolar output data is shown in Figure 7, for two different shots at 76 kV per stage charge. Figure 7a shows the Marx voltage and load current, Figure 7b shows the Marx current and load current. The peak voltage is -490 kV, with the voltage crossing through zero and increasing to about +65 kV before the crowbar switch closes. The peak load currents in Figure 7 are 51 kA and 50 kA, with ripple of 7.6% and 6%.

For the crowbarred mode the Marx voltage reversal is only 13%, compared to 75% for the ringing mode. Therefore the expected life of the Marx capacitors is 336,000 shots for full current unipolar operation. The charge transfer through the Marx switches is reduced to 0.165 C, from 0.4 C for the ringing mode.

Figure 8 shows the load current at long time scale for a crowbarred shot at 30 kV per stage charge. Peak load current is 19.6 kA and an exponential decay time of 92 µs. This gives crowbar switch charge transfer of 1.8 C and action integral of 1.77×10^3 A^2s. The maximum charge transfer and action demonstrated for the system are 4.4 C and 1.1×10^5 A^2s for a charge voltage of 76 kV per stage.

CONCLUSIONS

The 50 kA dual mode lightning simulator system described provides a versatile testing device for the lightning laboratory. The generator provides peak currents of more than 50 kA in a compact, lightweight system that is easily adapted to a wide variety of load configurations. The electrically triggered crowbar switch has proven to be reliable and effective, without the operational problems and safety hazards associated with laser triggered designs. The ability to change between two output modes with no hardware change provides maximum testing availability for the system.

Table I. Pulse Generator Electrical Performance

PARAMETER	MAXWELL DEMONSTRATED PERFORMANCE
Load	8.05 µH, 110 mΩ
Maximum Current	51.2 kA
Minimum Current	
Ringing	<15 kA
Unipolar	<15 kA
Frequency (ringing)	157 kHz
Pulse Width (unipolar)	60 µs
Circuit Q	5.3
Time to Current Peak	1.52 µs
Current Rate of Rise	$>5 \times 10^{10}$ A/s for >0.3 µs $>2.5 \times 10^{10}$ A/s for >1 µs
Ripple	7.7%
Peak Current Variation	<4.6%
Action	1.1×10^5 A^2-s
Pulse Repetition Rate	≥1 Pulse Every 2 Minutes for 5 Pulses

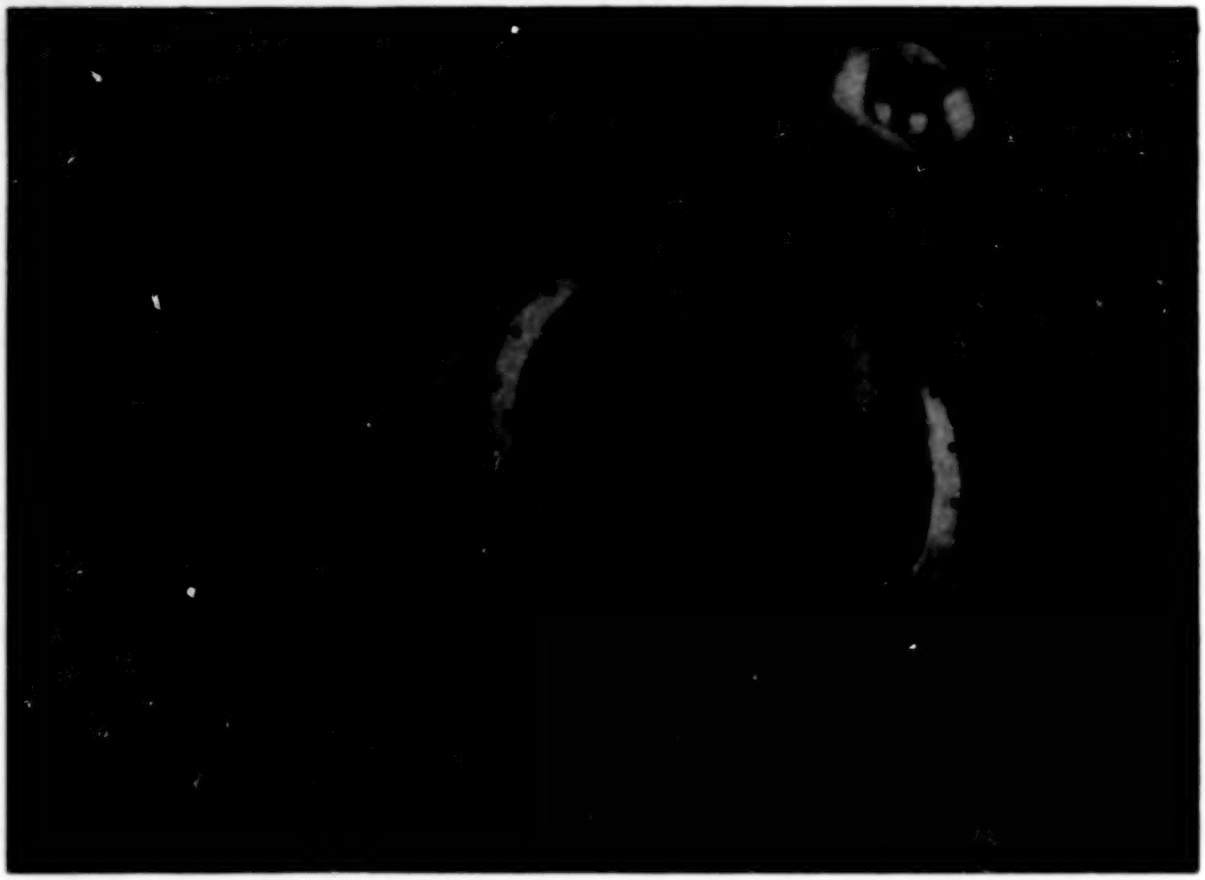

Fig. 1 - Output section and control console of the 50 kA lightning simulator

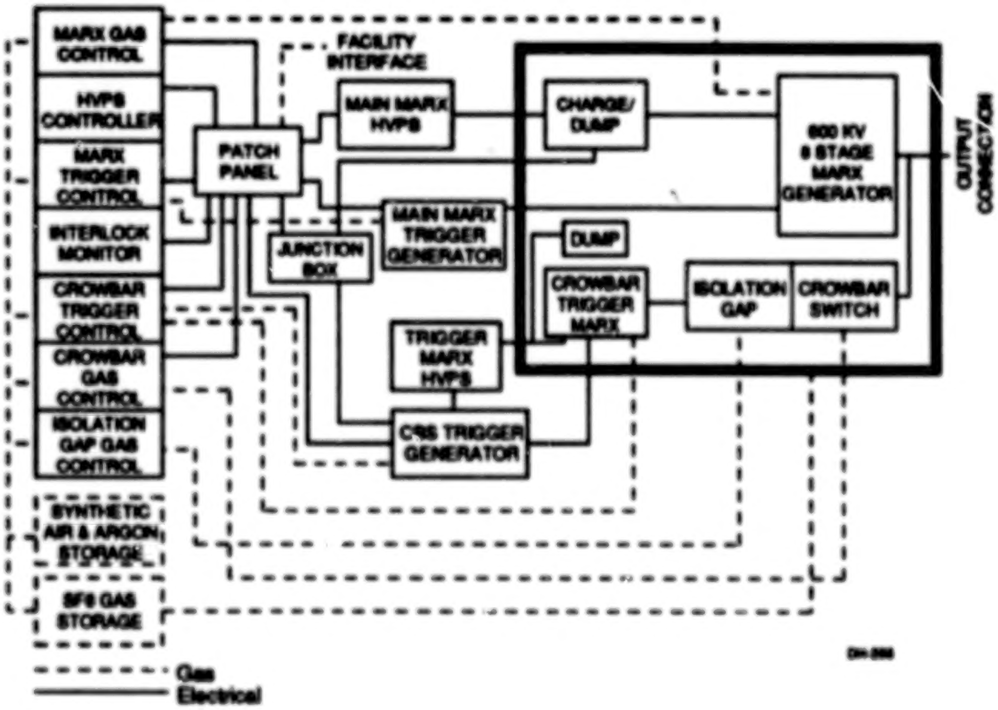
MARX GAS CONTROL
HVPS CONTROLLER
MARX TRIGGER CONTROL
INTERLOCK MONITOR
CROWBAR TRIGGER CONTROL
CROWBAR GAS CONTROL
ISOLATION GAP GAS CONTROL
SYNTHETIC AIR & ARGON STORAGE
SF6 GAS STORAGE
PATCH PANEL
FACILITY INTERFACE
JUNCTION BOX
MAIN MARX HVPS
MAIN MARX TRIGGER GENERATOR
TRIGGER MARX HVPS
CBS TRIGGER GENERATOR
CHARGE/ DUMP
DUMP
CROWBAR TRIGGER MARX
ISOLATION GAP
CROWBAR SWITCH
600 KV 8 STAGE MARX GENERATOR
OUTPUT CONNECTION
Gas
Electrical

Fig. 2 - System block diagram

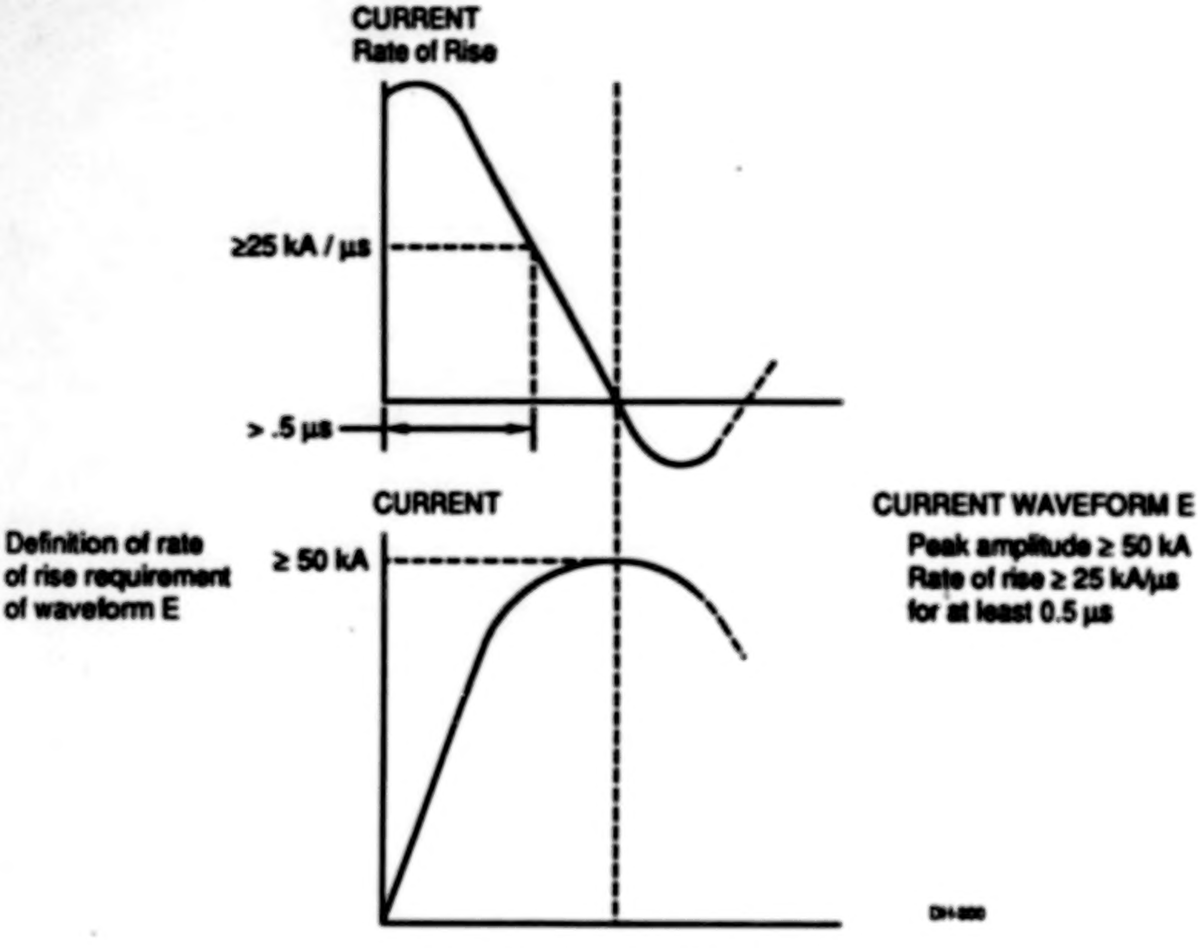

Fig. 3. - MIL-STD-1757A Current waveform E requirements

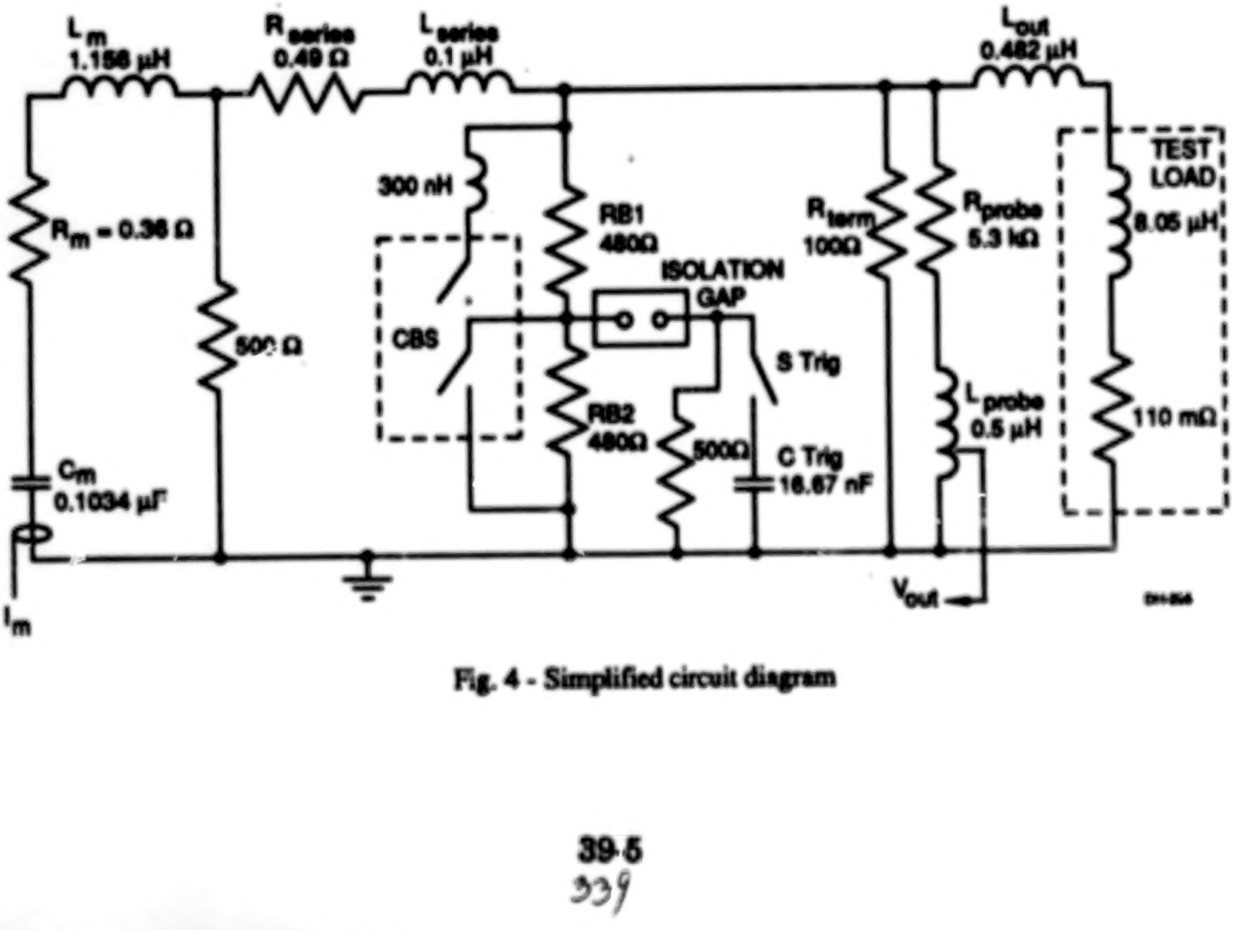
L_m
1.156 µH
R_series
0.49 Ω
L_series
0.1 µH
L_out
0.482 µH
300 nH
RB1
480Ω
R_m = 0.36 Ω
R_term
100Ω
R_probe
5.3 kΩ
TEST
LOAD
8.05 µH
ISOLATION
GAP
500 Ω
CBS
S Trig
RB2
480Ω
500Ω
C Trig
16.67 nF
L_probe
0.5 µH
110 mΩ
C_m
0.1034 µF
I_m
V_out
DH-804

Fig. 4 - Simplified circuit diagram

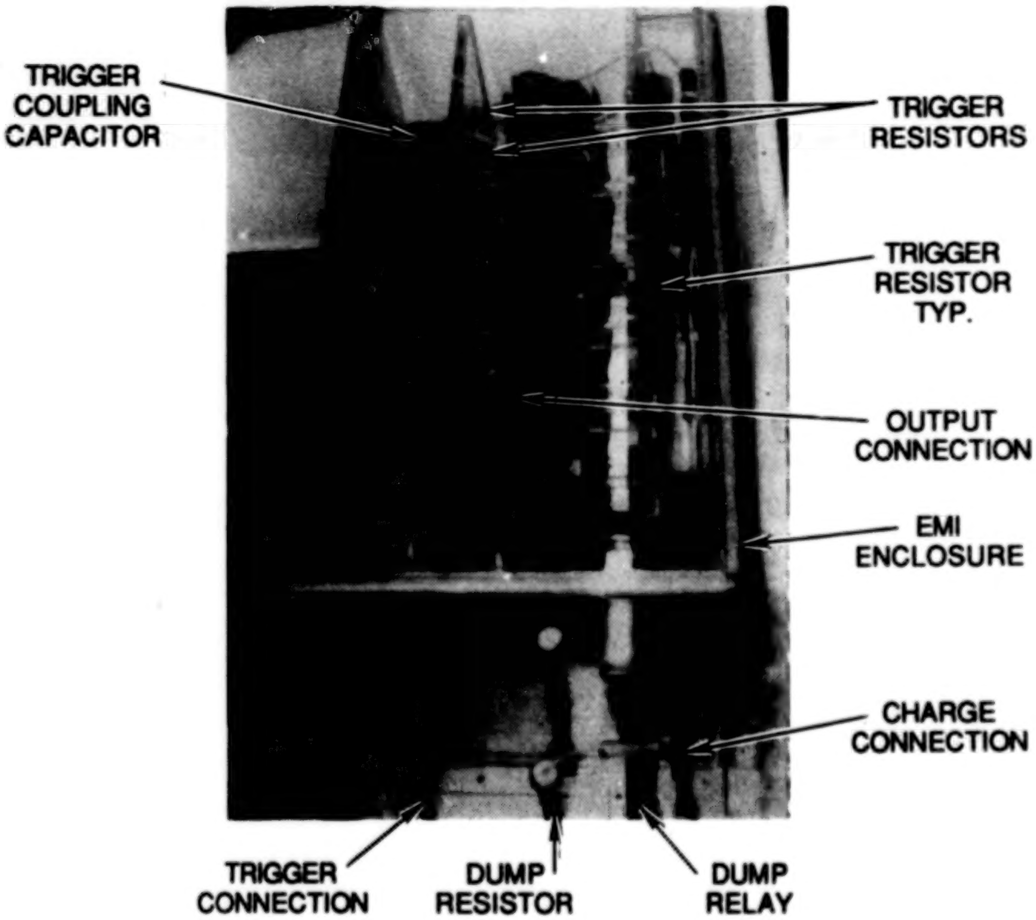
TRIGGER COUPLING CAPACITOR
TRIGGER RESISTORS
TRIGGER RESISTOR TYP.
OUTPUT CONNECTION
EMI ENCLOSURE
CHARGE CONNECTION
TRIGGER CONNECTION
DUMP RESISTOR
DUMP RELAY

Fig. 5 - Marx generator

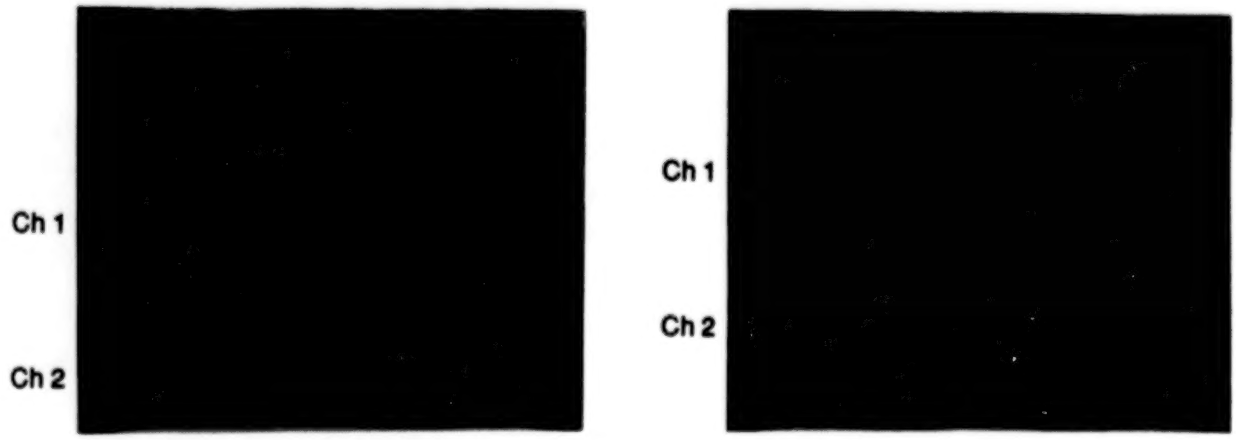

(A) Ch 1 - I_L (22.95 kA/Div)
Ch 2 - I-dot$_{Load}$ (16.83 x 10^{10} A/s/Div)

(B) Ch 1 - V_{Marx} (211.25 kV/Div)
Ch 2 - I_{Marx} (25 kA/Div)

Fig. 6 - Typical damped sinusoidal output pulse

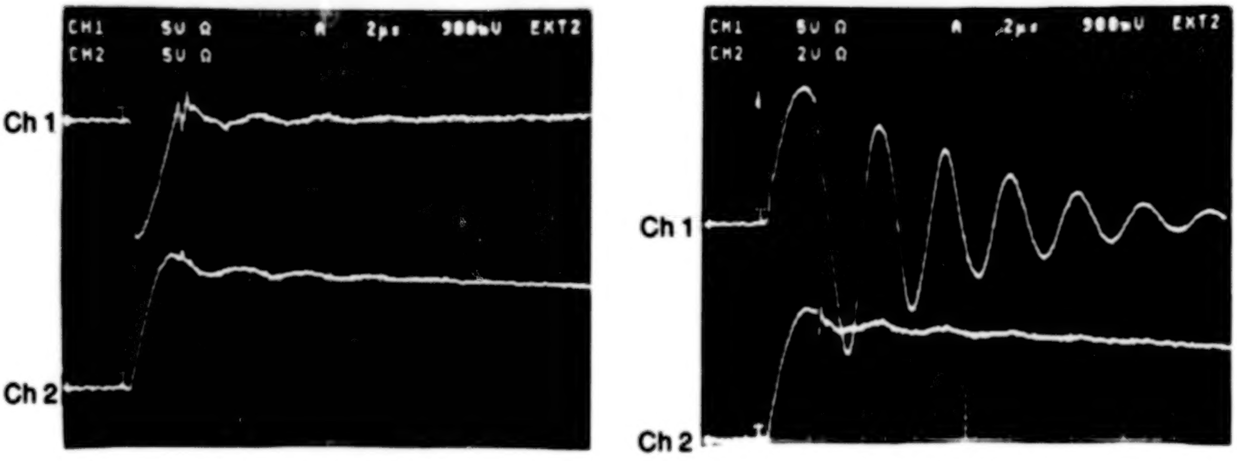

(A) Ch 1 - V_{Marx} (225 kV/Div)
Ch 2 - I_L (20.4 kA/Div)

(B) Ch 1 - I_{Marx} (20 kA/Div)
Ch 2 - I_L (20 kA/Div)

Fig. 7 - Typical unipolar output pulse

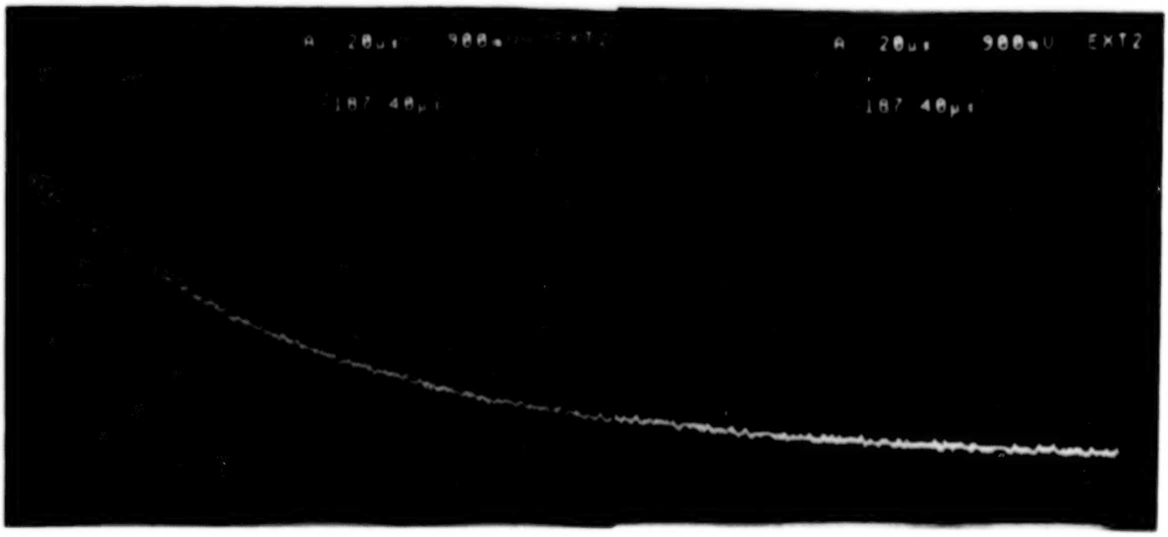

4.08 kA/Div

Fig. 8 - Load current

MATHEMATICAL MODELS FOR DETERMINING THE PROTECTED SPACES OF THE VERTICAL LIGHTNING ROD

Mladenović I., Vorgučić A.
University of Niš, 18000 Niš, Yugoslavia

ABSTRACT

This paper is concerned with two mathematical models for determining the protected spaces of the vertical lightning-rod. In the first model there was applied the circular approximation. Through the introduction of the modified striking distance in the second improved approximation there was obtained a new model for the protected space of the lightning-rod. The models are of general type, foreseen for the three-dimensional space and they are simply applied on solving the practical problems.

INTRODUCTION

The new theories about a greater number of protected spaces of one vertical lightning-rod depending on the maximum value of the stroke current impulse afford the possibility of a more precise evaluation of the lightning-rod's protective effect. The models to be set out in this paper start from the approach to the determination of protected spaces around the lightning-rod, depending on the amplitude of the stroke currents [1].

Namely, the degree of menace is evaluated on the basis of the determination of maximum stroke currents to which is exposed a structure of a smaller height or a device in the proximity of the vertical lightning-rod or of a structure playing a role of the lightning-rod. The procedure is based on the determination of protected space, which is a function of the well-known striking distance, the height of the lightning-rod, the height of the protected structure and their mutual distance. The length of the striking distance, for the purpose of the maximum stroke current, is determined by electrogeometrical method and numerically. In further elaboration there will be discussed two approximative approaches - the circular approximation of protected spaces and the elliptical approximation of protected spaces, constituting a more precise determination of the protected space, where was taken into consideration the impact of change in the electric field due to the presence of the lightning-rod. The above approximations are spaciously enlarged because of the more precise evaluation of the degree of menace, taking into account all the structure's dimensions. There are also given the corresponding mathematical models for both approximations.

CIRCULAR APPROXIMATION MODEL

When the leader of the atmospheric electrical discharge is approaching a very long vertical lightning-rod or a high structure, the site of striking will be a point on the structure nearest to the top of the coming leader, i.e. when the distance equals the striking distance. In Fig. 1 is shown an example when the critical electric field is equal in two points and the thunderbolt is possible on any of them.

In this model we start from the assumption that the generating line of "cone"[1] is the arc of circle of a radius approximately equalling the striking distance. Such an approximation is satisfactory in case when we have in view the fact that the striking distance depends exclusively on the stroke current, and when we neglect the other influential factors.

In this case the protected space is within the "cone", whose generating line is the arc of circle. The height of the cone is the height of the lightning-rod or of the high structure H, and the radius of the basis equals approximately the striking distance D.

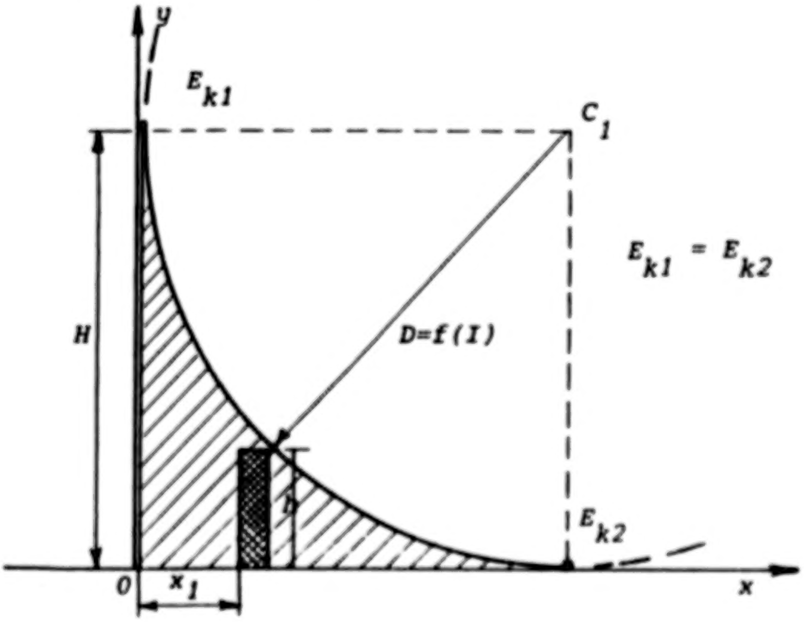

Fig. 1 The geometrical determination of the striking distance

The geometrical determination of the striking distance for this case is reduced to the construction of the circle attaining the protected structure and passing through the top of the lightning-rod. For numerical calculation of the striking distance we start from the following equation:

$$(x-D)^2 + (y-D)^2 = D^2 \qquad (1)$$

provided that $x \le D$ and $y \le H$.

The practical application of this model is presented in two examples when the height of the vertcal lightning-rod is smaller than the striking distance (H<D) and when the height of the vertical lightning-rod is greater than the striking distance (H>D).

The first case is illustrated in Fig. 2 and it practically refers to the small (low) lightning-rods of the height H in whose close proximity is, at the distance r, the structure of the height h (h>H).

Through the application of (1) we obtain:

---

[1] *The "cone" stands for a surface of revolution obtained by the revolution of the arc around the lightning-rod's axis to the curve of which corresponds the radius approximating the striking distance.*

$$D = \frac{H+h}{2(H-h)^2}\left[(H-h)^2+r^2\right] + \frac{Hr}{(H-h)^2}\sqrt{\frac{h}{H}\,[r^2+(H-h)^2]} \qquad (2)$$

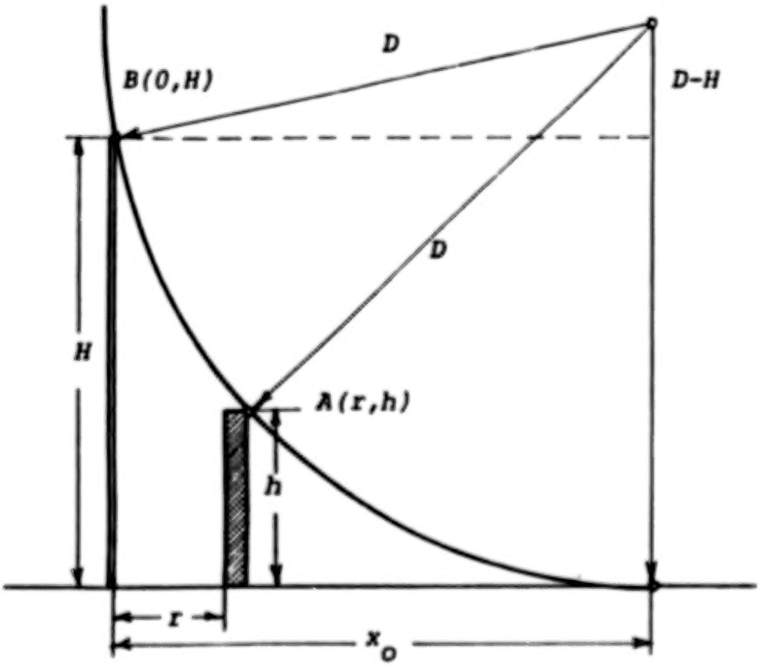

Fig. 2 The case H<D

In Fig. 3 is represented another case (H>D). This is the case of the very high lightning-rods of the height H, or of the high structure whose slenderness permits it to be considered a lightning-rod. Here we can notice a part of the inefficient height of the lightning-rod for the currents of lower intensity.

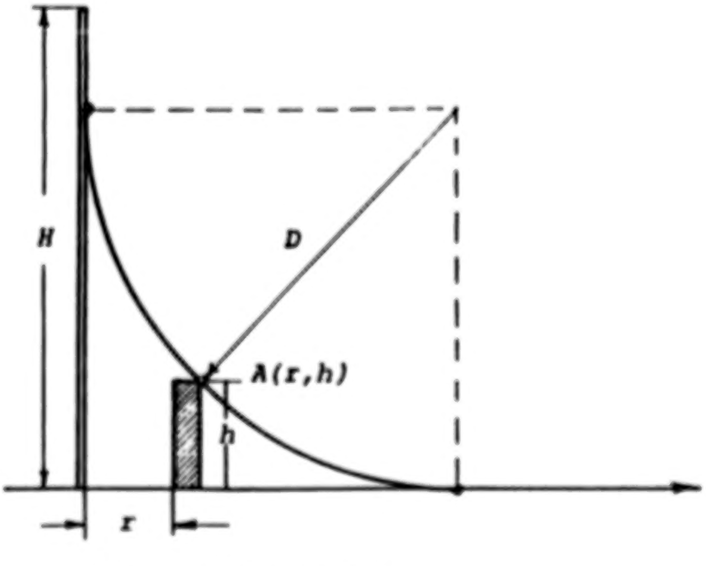

Fig. 3 The case H>D

According to (1), the striking distance D is given by the expression:

$$D = (r+h) \pm \sqrt{2rh} \qquad (3)$$

In addition to the above examples, this model may be also applied in the case when the other dimensions of the structure are taken into consideration [2].

ELLIPTICAL APPROXIMATION MODEL

The value of the striking distance, in addition to the maximum value of the stroke current (exerting the greatest influence), is influenced by the other parameters, too. In his research work Whitehead [3] found out that the height of the structure, i.e. the height of the lightning-rod because of the increased value of the electric field at the top, exerted the influence on the value of the striking distance. He introduced the modified striking distance (D^*) and gave the following functional dependence in relation to the reference striking distance towards the ground:

$$D^* = D\ [1+E_1 I_f^{\,2} \exp(-D/H)] \qquad (4)$$

where:

D^* - modified striking distance to a structure of height H,

E_1 - field intensification factor, which takes into account the structure the slenderness ratio,

I_f - factor which relates the prospective stroke current to the median of a reference current amplitude distribution,

D - reference striking distance to the ground, given by

$$D = 10\ I^{0.65} \qquad (5)$$

Having in view the modified striking distance which is, according to the expression (4), greater than the reference one, in this approximative approach we started from the fact that the protected space of the vertical lightning-rod (a high structure) of the height H is within the "cone with the elliptical generating line" - Fig. 4.

The basis of such an obtained "cone" is a circle, the radius of which equals approximately the length of the modified striking distance.

The case in Fig. 4 may be considered to be characteristic (a limit one) with the current I_1 and D=H. Observed in the xOy plane, this is an ellipse with semiaxes D^* and D, and the equation is:

$$\frac{(x-D^*)^2}{D^{*2}} + \frac{(y-D)^2}{D^2} = 1 \qquad (6)$$

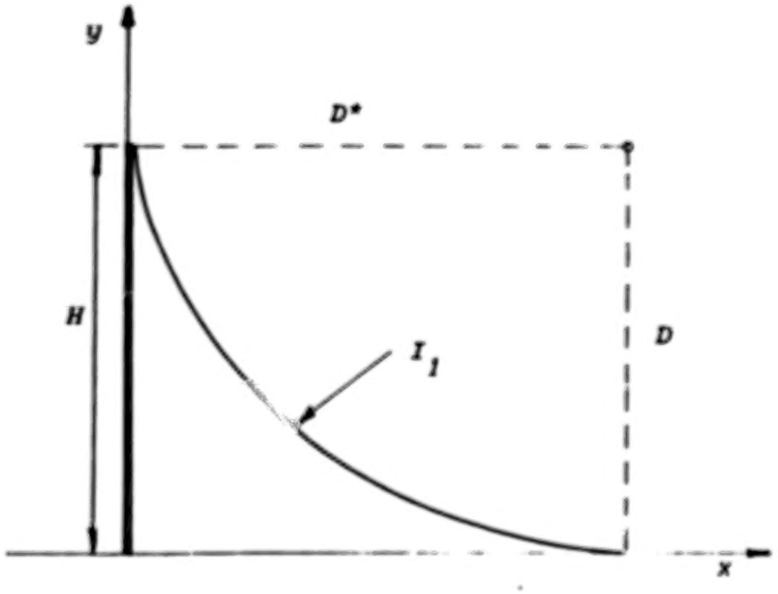

Fig.4 The protective zone with modified striking distance

As in the previous model, here too, we can discuss two cases. The first case refers to the protected spaces of those currents whose values are smaller than the values of the limit current I_1, i.e. $I_i' < I_1$. The graphic illustration of this case is displayed in Fig. 5, with the generating lines of "cone" within which are the protective zones, the arcs of ellipses:

$$\frac{(x-D_i^*)^2}{D_i^{*2}} + \frac{(y-D_i)^2}{D_i^2} = 1 \qquad i=1,2,3,\ldots \qquad (7)$$

where:

D_i^* and D_i are the modified and reference striking distances for the current less powerful than $I_1 (I_i < I_1)$.

The second case refers to the striking distances D^* and D greater than the height of the lightning-rod ($D^* > D > H$), i.e. for the currents more powerful than $I_1 (I_i > I_1)$. In Fig.6 is displayed the illustration of this case in the xOy plane. The equation of any curve from Fig.6, i.e. for any current $I_i (I_i > I_1)$ and the corresponding distances D_i^* and D_i reads as follows:

346

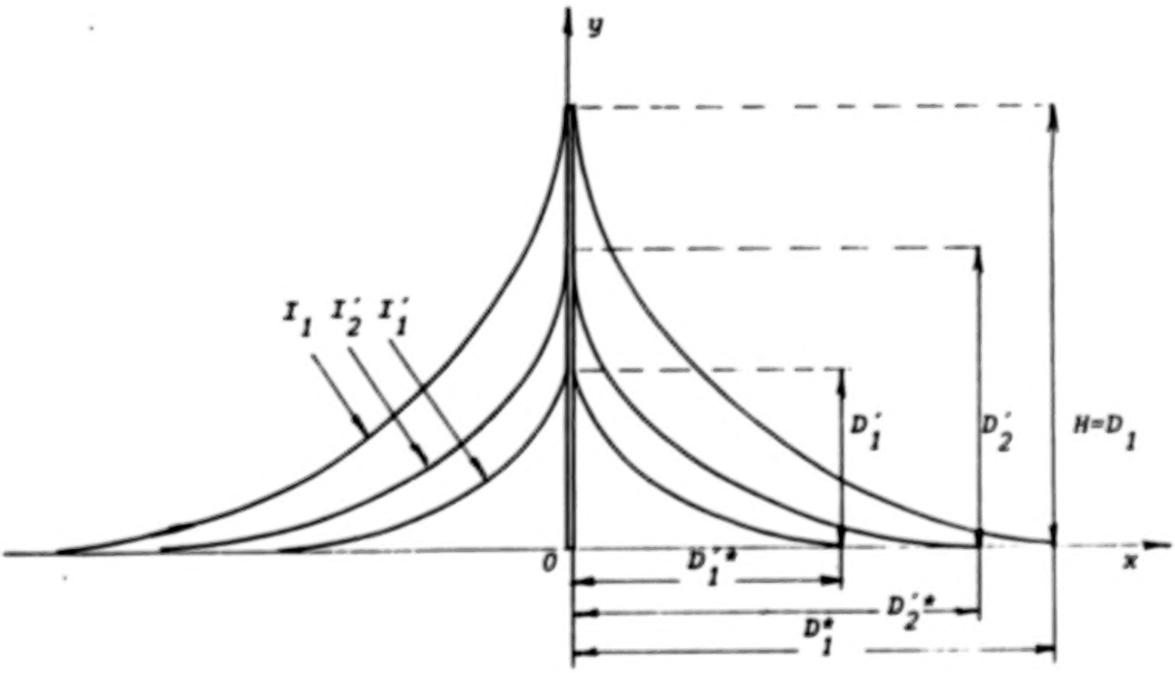
y
I_1
I'_2
I'_1
D'_1
D'_2
$H=D_1$
0
x
D'^{*}_1
D'^{*}_2
D^{*}_1

Fig.5 The protective zones for the case $H>D>D^{*}(I_1>I'_2>I'_1)$

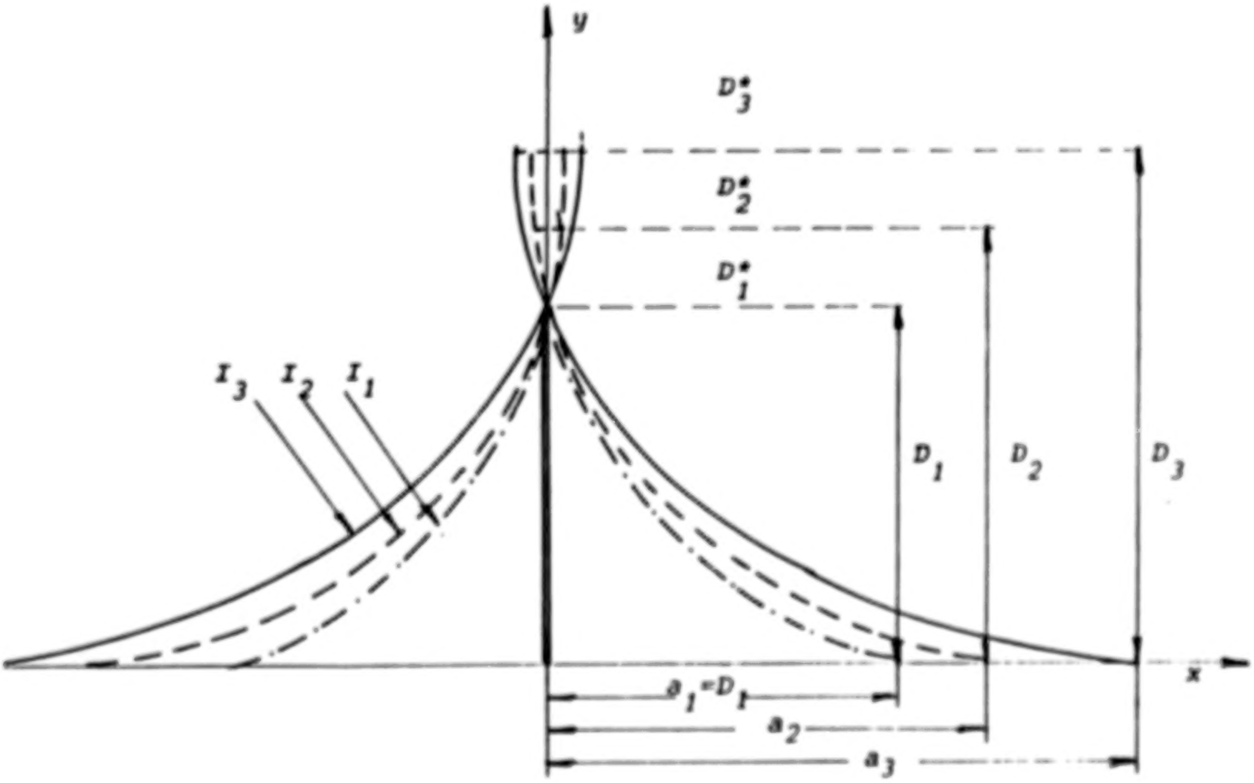
y
D^{*}_3
D^{*}_2
D^{*}_1
I_3
I_2
I_1
D_1
D_2
D_3
x
$a_1=D_1$
a_2
a_3

Fig.6 The case $D^{*}>D>H$ $(I_3>I_2>I_1)$

$$\frac{(x-a_1)^2}{D^{*2}} + \frac{(y-D_1)^2}{D_1^2} = 1 \tag{8}$$

where:

$$a_1 = \frac{D_1^*}{D_1}\sqrt{H(2D_1-H)} \tag{9}$$

provided that $D_1^* > D_1 > H$.

CONCLUSION

The mathematical models set out in this paper afford the possibility of electrogeometrical and analytical determination of the protective spaces of the vertical lightning-rod or of the high structure which may play the role of a lightning-rod.

By set out methods we can evaluate the degree of menace of a structure in the close proximity of the high structure or of the vertical lightning-rod. The reason for this is the fact that the analysis may be carried out within the space with the influence of all the dimensions of the protected structure and that through the modified striking distance are measured the influences of several parameters of lightning on the protective zone.

The purpose of this paper is to point to the new electrogeometrical method and to the corresponding mathematical models for as precise as possible determination of the striking distance. The application of the set out models within the space and to the practical examples is presented in [2].

REFERENCES

[1] Vorgučić A.: Condition for Evaluation of the Protective Zone of the Lightning Rod, FAA_RD_78_83, Atlanta (USA), pp. 115-129, 1978.

[2] Mladenović I.: Stepen ugroženosti od udara groma uredjaja i objekta u blizini vertikalnog gromobrana, Doctoral dissertation, Faculty of Electronic Engineering, Niš, (YU), pp. 60-81, 1988.

[3] Whitehead, E.R.: Analytical speculation on Improved Geometric Models of the Lightning Flash and Transmission Line Environment and Discussion, Private Communications, August 1976 and June 1977.

DESIGNS FOR SURGE IMMUNITY IN CRITICAL ELECTRONIC FACILITIES

Edward F. Roberts, Jr
FAA Southern Region
PO Box 20636 ASO-463
Atlanta, GA 30320

ABSTRACT

The Federal Aviation Administration is charged with maintaining a wide range of electronic facilities. These facilities range from pole mounted marker beacons, used as portions of an instrument landing system to Air Route Traffic Control Centers, responsible for thousands of cubic miles of air space. Because of the positioning and physical requirements of these facilities they are frequently subject to lightning related surges and transients as well as direct strikes. In recent years, FAA has embarked on a program replacing older tube type electronic equipment with newer solid state equipment. This replacement program has dramatically increased the susceptibility of FAA's facilities to lightning related damages.

This paper presents the author's proposal of techniques which may be employed to lessen the susceptibility of new FAA electronic facility designs to failures resulting from these causes. The general concept espoused is one of a consistent system approach employing both perimeter and internal protection. It compares the technique presently employed to reduce electronic noise with other techniques which reduce noise while lowering susceptibility to lightning related damage. It is anticipated that these techniques will be employed in the design of an ATCT in a high isokeraunic area. This facility would be subjected to rigorous monitoring over a multi-year period to provide quantitative data hopefully supporting the advantages of this design.

INTRODUCTION

Threat levels within FAA Southern Region facilities are characterized by a relatively low incidence of locally generated power line switching transients, unlike many industrial facilities. Typically the power line transients experienced at these facilities are from lightning generated surges, either locally or to the power distribution grid. Switching transients generated by the local power utility; or switching transients from industrial neighbors are far fewer and less likely to inflict damage on the facility. Lightning generated surges have been identified as the cause of the majority of the power line related surges which resulted in equipment failures. Direct strikes to FAA facilities are quite common and have been recorded on video tape on several occasions. FAA facilities on airports are interconnected with a web of signal, control and data cable which are also susceptible to lightning related transients.

Since the loss of FAA facilities may significantly impact the safety of the flying public, a stringent, rational as well as cost effective, approach to protection is warranted. The specious argument that protection should be implemented regardless of cost is totally unrealistic. Maintenance costs; facility and equipment purchase, and installation; and lightning protection all impact system reliability and thus flying safety while vying for the same budgetary dollar.

KEYS TO PROPER DESIGN

The scientist or engineer confined in a laboratory or office environment will find it difficult to identify all possible situations extant within the field environment. The complexities associated with the protection of a specific facility are extensive. Isokeraunic levels, thunderstorm strength, soil type, distribution system characteristics, relative and absolute elevation, soil moisture and composition, and equipment susceptibility levels are among the principal considerations. A rational approach to specific site design must examine these parameters and assign importance to each variable. This awareness of the impact of the environment is the first key to proper design.

Education is the second key to proper design. It is not possible to properly incorporate a given element of protection within a system of protection if the purpose and operation of that element is not understood. The impact of protective elements must be evaluated both during their normal operation and in a failure mode. A device connected in series with the power line which fails open is every bit as dangerous if not more dangerous than a surge which damages a component within the facility.

Regardless of the pains taken in designing an effective lightning protection system, all efforts are useless if the technicians charged with maintaining the system are unaware of the techniques employed.

Education is an ongoing process. Engineers charged with generating specific facility designs must have available support from engineers specializing in the application of lightning protection, grounding, bonding and shielding. For this reason, the educational process must flow in two directions. From the project engineer to the specialist engineer must flow information on the physical environment, regulatory environment, and constraints of purpose. From the specialist engineer to the project engineer must flow information on design goals, design techniques, device utilization and solutions to specific design problems. The accuracy of the data flowing in each direction will have a direct bearing on some elements of the data flowing in the opposite direction.

The third key to a proper design is a consistent review process. All facility designs, regardless of how simple, should be passed to the specialist engineer for review of the adequacy of design. Additionally, the review of these facility plans by field personnel prior to the letting of contracts will frequently prevent costly mistakes. Another source of loss of effectiveness is the failure to properly monitor the construction of the facility.

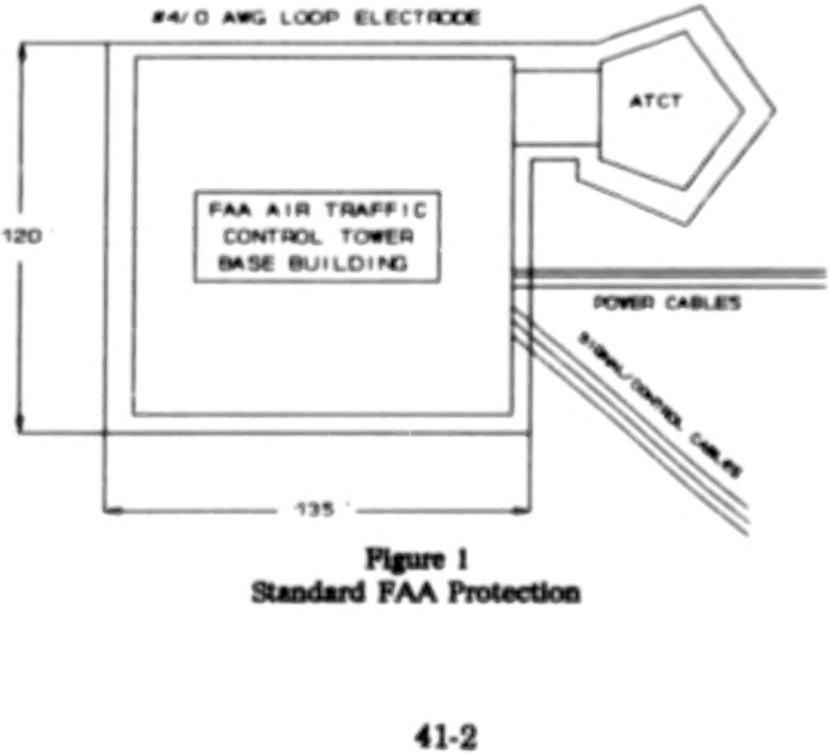

Figure 1
Standard FAA Protection

LIGHTNING PROTECTION

PRESENT FAA TECHNIQUES

FAA utilizes a system of lightning, surge, and transient protection based on the concept of creating an envelope of protection around the perimeter of the facility. This concept is mandated for all new construction or major modification by FAA-STD-019. This concept of protection is still valid but the lower threshold of susceptibility which is becoming apparent in recent procurements is such that improvements should be made.

The present system begins with the incorporation of integral, structural lightning protection. This protection is established to comply with NFPA-78, the Lightning Protection Code. The FAA system is designed to meet or exceed this code in all aspects. The system incorporates air terminals (lightning rods) which provide a zone of protection based on a 150' radius arc.

A loop electrode constructed of #4/0 AWG bare copper cable is buried 2 ft deep around the facility approximately 2 to 4 feet outside of the building foundation (or drip line). The typical grounding systems utilizes 10' by 3/4" copper clad ground rods spaced 20 feet apart around the counterpoise. These ground rods (earth electrodes) are exothermically welded to the 4/0 loop. All conductive paths entering the facility are bonded to this loop.

All power, control, or signal lines which penetrate the structural envelope should be equipped with surge/transient protection. This protection may include silicon avalanche suppressors (SAS), metal oxide varistors (MOV), or gas discharge devices. Carbon block type arresters are found in some telco equipment but are not commonly installed by the FAA. These devices are frequently incorporated into hybrid protection circuits installed at signal demarcs. Crowbar portions of these hybrid circuits are typically bonded directly to the external loop electrode. The clamp element is bonded to the internal multipoint grounding system.

The internal facility grounding system consists of three interconnecting grounds. The NEC required safety ground is incorporated as required for code compliance. All non-current carrying elements of the premises equipment are bonded to the grounding conductor. A second multipoint ground system is established which connects to the loop electrode with a 500 kcmil cable terminated at the main electronic ground plate. This plate serves as an interconnection point with the third, single-point, grounding system.

The multipoint grounding system utilizes building steel, where available and incorporates items such as ducts, cable trays, and conduits to create a grid of conductors. Where building steel is unavailable, 2000cmil/foot cables are utilized to interconnect the plates in this system. All racks and chassis are connected to this system.

The single-point ground system utilizes isolated plates and dedicated 500cmil/foot cables constructed in a star or tree pattern to ensure a single path to the main electronic ground plate. This system is designed to eliminate the system noise caused by loop currents.

PROTECTION FOR THE FUTURE

It began to become apparent in the late 1980's that the present FAA method of grounding was insufficient to provide the protection required for increasingly sophisticated facilities. A rethinking of the basic techniques was required which drew on numerous documents including FIPS PUB-94. A significant consideration for a new design was the ability to retrofit it to existing facilities and to establish it in facilities without significant amounts of building steel.

An additional problem appeared to result from the use of the single point ground system to minimize system noise. Constituent elements of systems which were directly connected to landlines were being protected while elements which were deeper in the system were receiving lightning related damage. It appeared that the poor bonding due to high frequency impedance inherent in a cable grounding system was allowing large voltage differentials to form between the elements. It was also apparent that a single compromise of a single point system resulted in a multipoint system with a single loop. This single loop system was found to be the noisiest possible ground.

New FAA air traffic control tower (ATCT) designs are on the drawing board. These new designs have tower shafts 300' tall. The direct strike risk associated with these towers mandates that we must assume that they will be struck on a regular basis when located in areas of even moderate isokeraunic activity. Protection for the electronics equipment located within these structures must be of a nature to prevent damage from this type of a strike.

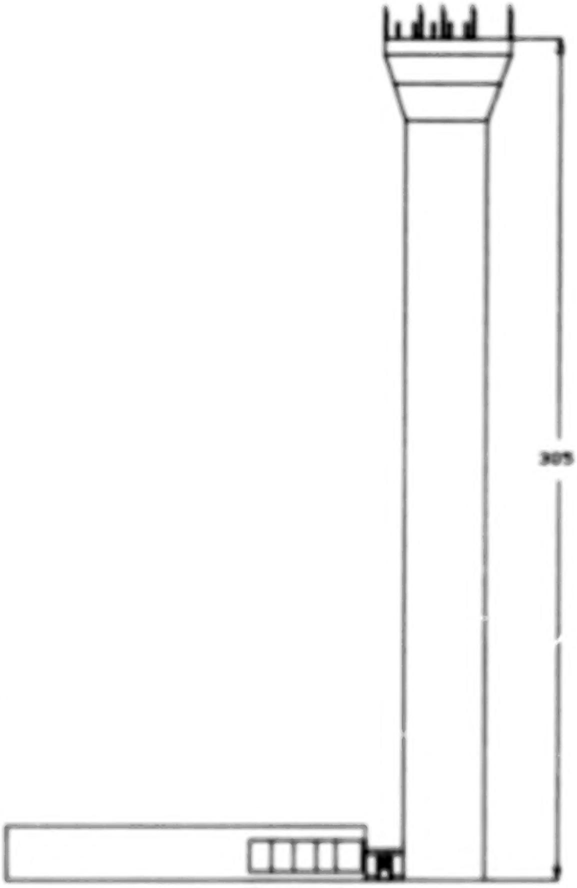

Figure 2
300' ATCT Design

In essence, these ATCTs incorporate two separate facilities within a single structure. These facilities are located over 300' apart. The first of these facilities is the terminal radar control and it's associated electronics located in the base building. The other facility is the ATCT cab and it's associated electronics located at or near the top of the tower shaft. The fact that this separation is primarily vertical enhances the voltage differential which is likely to be imposed upon them. Typically the tower shaft is constructed of precast, interlocking concrete modules. This construction technique reduces the vertical metallic elements to such items as metal staircases, cable trays, conduits and piping. External down conductors are utilized for the structural lightning protection.

PROTECTING THE TOWER TOP EQUIPMENT

Good design technique, for the reduction of electrical noise, locates signal and control wiring as far as possible from electrical wiring within the tower shaft. The utilization of fiber optic cabling between these facilities will minimize the threat of transients and noise coupled through the signal and control cabling. The power system is left as the single greatest threat other than a direct strike to the equipment located at the top of the tower shaft.

The first element of protection for the tower top facility is to establish a grounding grid or near equipotential plane for each level. These levels are interconnected with solid backed cable trays. These cable trays are supplemented with copper cabling to ensure the lowest possible impedance between these levels. These grids are connected to earth with a 500kcmil cable. The impedance of this cable is such that it cannot prevent differences in potential between the 2 facilities. The nature of this protection system is such that we recognize this effect but protect in a manner so as to render it inconsequential.

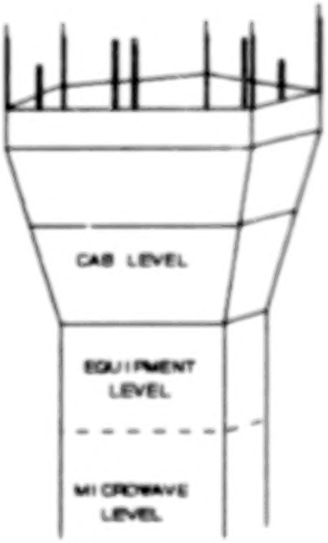

Figure 3
Tower Levels

The electrical power feed is brought into a service entrance at the microwave level. A secondary surge arrester is provided at this point. The grounded conductor (neutral) is bonded to the grounding electrode conductor and to the grounding conductor at this point. The normal mode surge arrester is connected between the phase conductors and the grounded conductor. The power ground and the grounding grid are interconnected at the microwave level through a main ground plate. The main ground plate functions as an interconnection point between the grounding grid and a single point ground system, if one is required[1]. The power feed for the levels is provided through a UPS system with critical power centers on each level. This minimizes stress between the power feed and signal and control elements.

Emergency communication equipment located within the tower cab is connected directly to antennas mounted on the tower roof. The coaxial cabling for these emergency transceivers is brought from the roof, where the shield is bonded to the structural lightning protection system, to the microwave level. At this point it is connected through a bulkhead plate utilizing a gas type surge protection device. The bulkhead plate is connected to the grounding grid on the microwave level. By connecting the bulkhead plate on the microwave level we minimize the differential between levels due to current flow from this source.

---

[1]. Some equipment manufacturers mandate that an isolated ground be established for their equipment.

The utilization of fiber optic cabling between the tower top equipment and the base building equipment obviates the need for transient protection for the signal and control wiring. If there is a metal sheath on the fiber optic cable for physical protection this is bonded to the grounding grid at the microwave level.

PROTECTING THE BASE BUILDING EQUIPMENT

Many of the techniques utilized in protecting the tower top environment are applied in the base building. The first element is the establishment of a grounding grid or near equipotential plane for all equipment areas. The base building electronics are typically located on a single level. A raised floor extending under equipment room and the operational area is equipped with a grounding grid bonded to a conductive, rigid or bolted stringer, raised flooring system. The floor system and grid are interconnected at every other stanchion. This floor is bonded as frequently as possible to the building steel if available or alternatively to the loop electrode with 500 kcmil cable at a minimum of four points. The building steel is bonded to the loop electrode at alternate columns with #2/0 AWG bare copper cabling.

The electrical power feed is brought into a service entrance located in an emergency engine generator and power distribution room. A secondary surge arrester is provided at this point. The grounded conductor (neutral) is bonded to the grounding electrode conductor at this point and is in turn bonded to the grounding conductor. The normal mode surge arrester is connected between the phase conductors and the grounded conductor. The power feed for the levels is provided through a UPS system with a critical power center, connected as a separately derived source, in the equipment room.

A single point of entry for signal, control, and power cabling is utilized to minimize differentials at the point where the cables enter the raised floor area. Fiber optic cabling is utilized to the maximum extent possible for the signal and control cabling. These fiber optics are not expected to be all inclusive, however. Primary transient protection for these cables is provided at the building entrance with gas discharge and MOV devices connected to the loop counterpoise. Secondary protection with silicon avalanche suppressors is provided at the entrance to the raised floor area. Protection at the equipment is also required to be included on equipment manufactured to FAA specifications. The near equipotential plane functions as a means of minimizing the differentials due to the protective devices firing.

Cable entrances to the facility are through rigid metal (ferrous) conduit. This conduit extends 10 feet beyond the loop electrode and is bonded to it. Cable armor is also bonded out to the loop electrode.

Emergency communication equipment located within the operational area is connected directly to antennas mounted on the tower roof. The coaxial cabling for these emergency transceivers is brought from the roof, where the shield is bonded to the structural lightning protection system, to the base building level. At this point it is connected through a bulkhead plate utilizing a gas type surge protection device. The bulkhead plate is directly connected to the loop conductor with a #2/0 AWG copper cable.

354

SUMMARY

The present FAA concept of an envelope of protection is valid but it is necessary to carry the process a step further. Widely separate areas within a single structure must each have their own envelope of protection. The areas so protected must have a grounding system which minimizes the differentials within the envelope. All cabling entering the envelope must be closely referenced to this grounding system.

Even the best design can be compromised by poorly trained installers or technicians responsible for maintaining the system. The training of these people is every bit as critical as the proper design for protection.

The best general concept will usually fail to include in consideration at least one weak point. Lightning will ultimately find this point and cause damage within the facility. At this point the engineer must perform an in depth analysis to determine the weak point and protect it. When protecting this weak point it is important to consider the affect that this new protection will have on the overall system so as not to just move the problem.

THE SANDIA TRANSPORTABLE TRIGGERED LIGHTNING INSTRUMENTATION FACILITY

George. H. Schnetzer and Richard J. Fisher
Sandia National Laboratories
Albuquerque, NM 87185

ABSTRACT

Development of the Sandia Transportable Triggered Lightning Instrumentation Facility (SATTLIF) was motivated by a requirement for the *in situ* testing of a munitions storage bunker. Transfer functions relating the incident flash currents to voltages, currents, and electromagnetic field values throughout the structure will be obtained for use in refining and validating a lightning response computer model of this type of structure. A preliminary shakedown trial of the facility under actual operational conditions was performed during the summer of 1990 at the Kennedy Space Center's (KSC) rocket-triggered lightning test site in Florida. A description is given of the SATTLIF, which is readily transportable on a single flatbed truck or by aircraft, and its instrumentation for measuring incident lightning channel currents and the responses of systems under test. Measurements of return-stroke current peaks obtained with the SATLLIF are presented. Agreement with data acquired on the same flashes with existing KSC instrumentation is, on average, to within ~7 percent. Continuing currents were measured with a resolution of ~2.5 A. This field trial demonstrated the practicality of using a transportable triggered lightning facility for specialized test applications.

INTRODUCTION

During 1990, the Sandia Transportable Triggered Lightning Instrumentation Facility (SATTLIF) was designed, built, and fielded at the Kennedy Space Center's (KSC) rocket-triggered lightning test site in Florida. Development of the facility was jointly sponsored by the U.S. Army and Sandia National Laboratories (SNL) to support the testing of a munitions storage bunker located at Ft. McClellan, Alabama. In that test, scheduled for the summer of 1991, lightning will be triggered to various points on the bunker's lightning protection system (Figure 1). Both the incident flash current and response voltages, currents, and electromagnetic fields within the structure and its grounding system will be simultaneously measured. The data will be used to improve and validate a detailed finite difference computer model of the structure developed for the Army by Electro Magnetic Applications, Inc. (EMA) [1].

Selection of the triggered lightning technique over the use of a conventional large-scale capacitive pulser as a test source for this application was based on at least two major technical considerations. First, the inductance inherent in a large test object and its connections to the test source would result in an inadequate rise rate of the test current that could be delivered by any practical pulser. Since rise rate is a dominant controlling factor in the coupling process, this represents a serious shortcoming. Second, of particular importance in the validation of the computerized response model is the proper simulation of the natural distribution of lightning current throughout the test object's structural members, grounding system, and surrounding earth. This distribution simply cannot be reproduced with a conventional test source. Given the present maturity of the triggered lightning technique, which circumvents the above technical issues, it was chosen for the bunker test application.

In preparation for the bunker test, the SATTLIF was fielded during the summer of 1990 at KSC. In this way, the facility and its basic instrumentation designs could be validated under actual field conditions prior to procurement of the multiple data channels that will be required for the 1991 test. A further benefit of the 1990 shakedown test was that added responsibility for rocket operations, range clearance, and other administrative requirements could be left to KSC. Finally, once in the field, the opportunity was taken to acquire direct-strike damage data on aluminum and steel

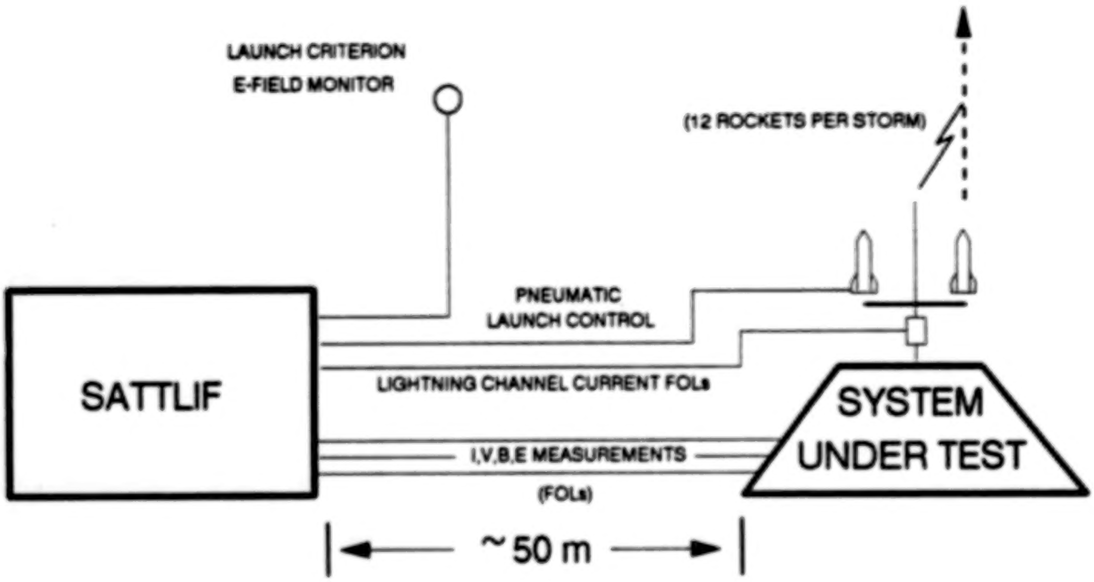

Figure 1. Munitions Storage Bunker Triggered Lightning Test Configuration

specimens produced by fully recorded lightning. These particular experiments are presented in a companion paper in these proceedings [2]. The remainder of this paper describes the SATTLIF and its performance.

GENERAL DESCRIPTION

The SATTLIF is housed in a 20'x8'x8' steel ocean cargo container that has been converted to an instrumentation shelter. This air-conditioned unit provides electromagnetic shielding as well as safety for the test personnel and instrumentation. A single window is provided to permit visual observation of the launch and test area and optical recording of the triggered lightning events. The facility subsystems include an ambient electric field monitor, video and cinematic photographic systems, data acquisition channels for measuring both test item response and the incident lightning (return-stroke and continuing-current components), data processing computer and plotter, pneumatic rocket launch control system, National Lightning Detection Network [3], test range radio communications, and an external power generator. The entire self-contained SATTLIF is readily transportable on a single flatbed truck or by aircraft and can be made operational within one or two days of its arrival at a test site. Figure 2 shows the SATTLIF deployed at KSC 80 feet from the strike tower.

Figure 3 is a diagram of the SATTLIF subsystems. Except for the short lines from the power generator and the antennas of the range communications and lightning detector systems, there are no penetrations into the shelter (dotted enclosure in the figure) by conductive lines. The lightning measurement signals are transmitted from the experiment over fiber optic links (FOLs), and rocket launch control is by pneumatic lines. Figure 4 shows the interior of the shelter.

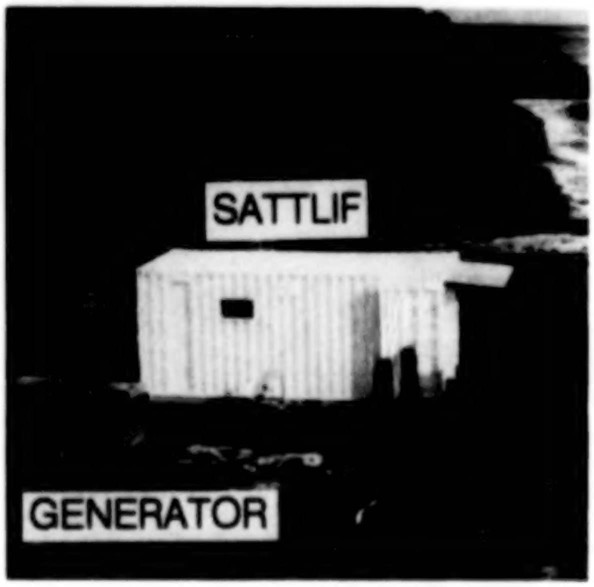

Figure 2. SATTLIF Deployed at KSC RTL Site

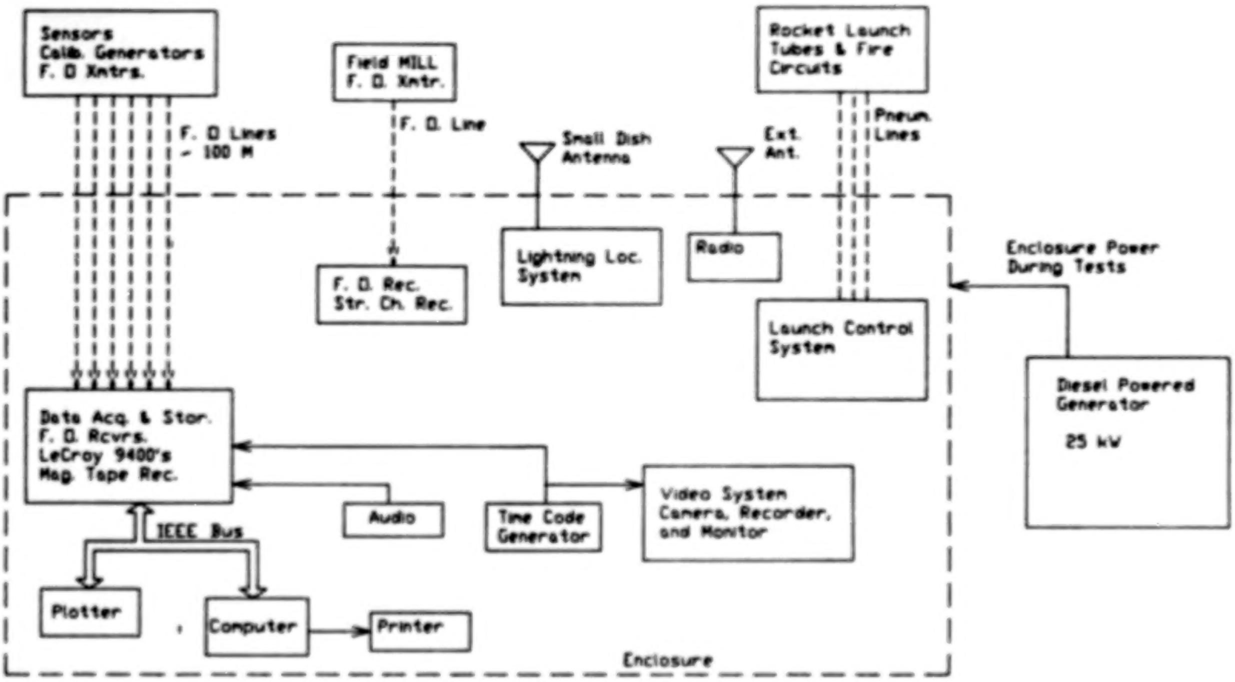
Sensors
Calib. Generators
F. O Xntrs.
F. O Lines
~ 100 M
Field MILL
F. O. Xntr.
F. O. Line
Small Dish
Antenna
Ext.
Ant.
Rocket Launch
Tubes & Fire
Circuits
Pneum.
Lines
F. O. Rec.
Str. Ch. Rec.
Lightning Loc.
System
Radio
Enclosure Power
During Tests
Launch Control
System
Diesel Powered
Generator
25 kW
Data Acq. & Stor.
F. O. Rcvrs.
LeCroy 9400's
Mag. Tape Rec.
Audio
Time Code
Generator
Video System
Camera, Recorder,
and Monitor
IEEE Bus
Plotter
Computer
Printer
Enclosure

Figure 3. Diagram of SATTLIF Subsystems

Figure 4. Interior Views of the SATTLIF

The ambient electric field is monitored by a Mission Instruments Model EFS 100 inverted field mill, which produces an analog output of 0 to ±10 V, corresponding to a ±20 kV/m field. This output is transmitted to the shelter via a dc to 10-kHz Dymec frequency modulated (FM) FOL and is there scaled as desired and displayed on a strip chart recorder. The field mill and its FO transmitter are powered from a rechargeable battery that provides for at least 8 hours of continuous operation per charge.

An IBM AT compatible computer with an IEEE 488 interface is used in the data acquisition system. Traces stored on LeCroy 9400A digitizing oscilloscopes are transferred via the IEEE 488 bus to the computer where they can then be analyzed, processed, and plotted. The data can also be plotted directly on an HP 7440 digital plotter.

The video recording system includes (1) a Pulnix TM 545 high-resolution CCD camera (disabled AGC and $\gamma=1$ options) with a Vivitar 70- to 210-mm macro zoom lens, (2) a JVC BR-S600U SVHS video cassette recorder, (3) FOR-A VTG-33 video timer, and (4) a Sony SSM-910 black and white monitor. The video camera lens was operated at f/22 with an additional eight-stop equivalent neutral density filter. An Action Master 500 high-speed 16-mm, cinematic camera with zoom lens was operated at 200 frames per second to provide a 5-ms time resolution.

A six station electro-pneumatic rocket launch controller was housed in a 10.5-in-high rack space adjacent to the observation window. Arming pressure is applied by activating any one of the six key switches. All are operated by a single, common key, thereby ensuring that only one rocket can be armed at a time. Panel lights indicate the status of each rocket: one light for the armed condition and a second, SPENT, light to indicate that the proper launch pressure has been applied to the selected rocket. All activated SPENT lights remain lit until panel power is interrupted, so that a continuous indication is given of which rockets have been fired. The pneumatic pressure source is located inside the shelter and consists of a small compressor with integral reservoir. The operating pressure is 95 psi.

The receiving end of the pneumatic control system (the Safing, Arming, and Firing box) is housed in an 8"x8"x4" steel box with snap-tight fasteners. The associated circuit is shown in Figure 5. The PREARM and SAFE shorting plugs are provided as additional positive operational safety features.

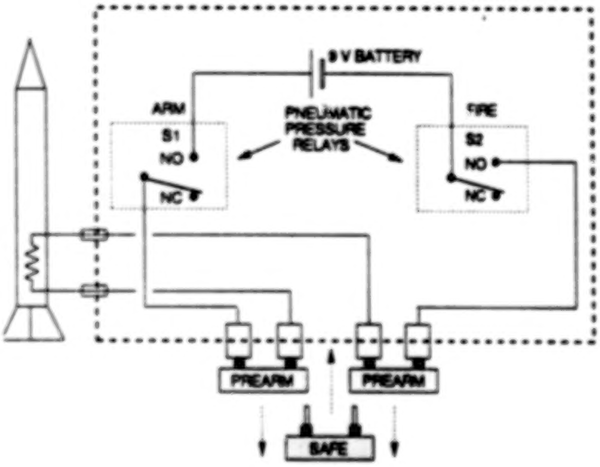

Figure 5. Rocket Launch Safing, Arming, and Firing Circuit

Actual firing of rockets from the SATTLIF was not part of the 1990 program. All rocket operations were provided at KSC by experimenters from the Centre D'Etudes Nucleaires de Grenoble (CENG) using their systems that are described elsewhere [e.g., 4]. However, the SNL launch control system was fully deployed and was successfully tested in all safety modes with both dummy and real initiator squibs.

The facility requires 208 V, 3-phase power. During triggering operations, or whenever a commercial source is not available, this power is provided by a 25-kW diesel generator. The generator is located within 25 feet of the shelter. For safety reasons, the connecting power cable is provided with a shield that is connected to both the generator and the shelter, as well as to a ground rod.

INSTRUMENTAION

A block diagram of the data acquisition instrumentation system is shown in Figure 6. In this configuration, there are two sensor packages: one for the incident flash current, and a second for measuring currents within some test item, which, in this case, was one of the down conductors of the grounding cable grid below the experiment platform.

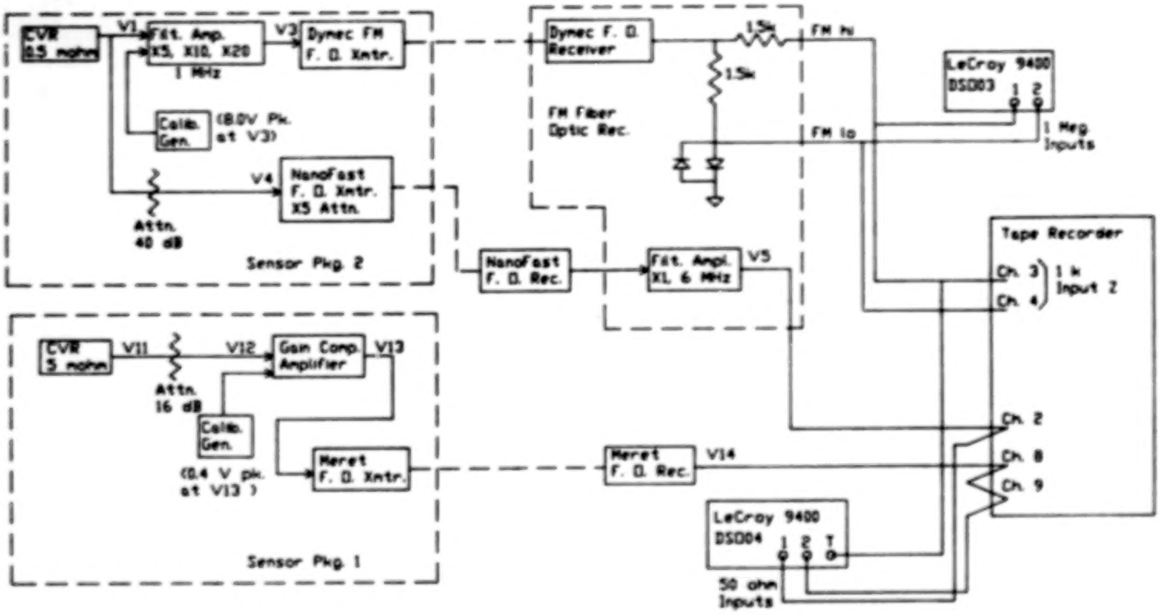
CVR
0.5 mohm
V1
Filt. Amp.
X5, X10, X20
1 MHz
V3
Dymec FM
F. O. Xmtr.
Calib.
Gen.
(8.0V Pk.
at V3)
V4
NanoFast
F. O. Xmtr.
X5 Attn.
Attn.
40 dB
Sensor Pkg. 2
Dymec F. O.
Receiver
1.5k
1.5k
FM hi
FM lo
FM Fiber
Optic Rec.
LeCroy 9400
DSO03
1
2
1 Meg
Inputs
NanoFast
F. O. Rec.
Filt. Ampl.
X1, 6 MHz
V5
Tape Recorder
Ch. 3
Ch. 4
1 k
Input Z
Ch. 2
Ch. 8
Ch. 9
CVR
5 mohm
V11
V12
Gain Comp.
Amplifier
V13
Attn.
16 dB
Calib.
Gen.
(0.4 V pk.
at V13)
Meret
F. O. Xmtr.
Meret
F. O. Rec.
V14
LeCroy 9400
DSO04
1
2
T
50 ohm
Inputs
Sensor Pkg. 1

Figure 6. SATTLIF Data Acquisition Instrumentation

Both sensor packages were housed in gasketed, EM-tight steel Hoffman boxes.

In order to record both return-stroke and continuing-current components faithfully, two separate transmission and recording channels were used. For the return stroke, the output of a 0.5-mΩ T&M R-14000-20N coaxial current viewing resistor (CVR) was transmitted to the shelter over a NanoFast 300-2A FOL. There the signal was recorded on a LeCroy 9400A digitizing oscilloscope channel and on a direct-record (1 MHz) channel of the Ampex 2300 tape recorder. Overall signal bandwidth was set by the 164-ns rise time of the CVR, which, in this case, was selected on the basis of its energy handling capacity rather than rise time. A 6-MHz filter was inserted as indicated in Figure 6 to improve signal-to-noise ratio. The LeCroy was operated in the segmented memory mode at an 80-ns sampling rate, thereby permitting the capture of the first 200 μs of up to eight individual return strokes per flash. A trigger level equivalent to 1000 A was selected.

Due to the long duration and relatively low amplitude of lightning continuing currents, a separate data channel was used to record these components of the flash. In this channel, the output from the CVR is amplified and clipped to pass only the signal equivalent of 1000 A or less. Diodes from the op amp input to ground clamp at ±0.5 V to limit saturation caused by the return-stroke portions of the signal. The output from this amplifier is transmitted via a Dymec Model 5717 FM FOL that has a bandwidth of dc to 1 MHz. During the 1990 trials, the signal was scaled and recorded on two LeCroy channels and on two 500-kHz FM Ampex tape channels. Use of two channels with sensitivities differing by a factor of ten increased the dynamic range of the measurement by 20 dB. As operated during the 1990 field trials, the selected attenuations yielded an overall measurement dynamic range from an approximate 2.5-A floor to the 1000-A saturation level.

Both channel types (return-stroke and continuing-current) are provided with end-to-end calibration features. The NanoFast system has a built-in calibration function that is activated via fiber optic link. A pneumatically activated calibration system was implemented in the Dymec channel (Figure 6) to inject a fixed-peak signal (clipped square wave) at the input of the FOL transmitter.

Table I summarizes the set of common data measured simultaneously by KSC and SNL. The comparison includes only return strokes, since the available KSC instrumentation does not record continuing current. The KSC peak currents in the table were read from a set of hard copy plotted on a 4-μs-per-division scale, which limited the accuracy with which those peaks could be established. The resulting differences between the two measurement sets has a mean of 7.4% and a standard deviation of 5.9%. For example comparison, Figure 7 shows the stroke currents of Flash 90-07 as measured by KSC and SNL. All the other data are similar. Figure 8 is a plot of the early portion of the first stroke of Flash 90-07 with the actual sampled data points indicated.

Table I. Comparison of Stroke Current Measurements

Shot No.	Stroke No.	Sandia Ip (kA)	KSC Ip (kA)
90-07	1	24.5	22.6
	2	18.0	17.2
	3	23.5	22.3
90-08	1	13.8	14.4
90-09	1	16.5	16.0
	2	4.1	4.2
90-12	1	3.9	3.9
	2	15.8	13.4
	3	27.5	22.4
90-14	1	17.0	15.0

An example of recorded continuing current is shown in Figure 9. Figure 10 is a similar example of Flash 90-03, a two-stroke flash with a single interstroke continuing current. Other examples are given in these proceedings (Ref. 2) and in Reference 5.

Except for the type of sensor employed, measurements of lightning responses of a system under test can generally be made with the same basic type of instrumentation channel. One issue always of particular concern, however, is achieving sufficient overall dynamic range for such measurements, which sometimes need to be performed on a one-shot basis and for which reliable predictions are often unavailable. In such cases, the penalty is the assignment of multiple recording channels of varying sensitivities to the same measurement point.

During the 1990 tests, a baseline channel was tested that incorporated an experimental feature that was hoped would improve achievable dynamic range. This feature was the insertion of a "gain compression" amplifier with an output function as indicated in Figure 11 (in effect, a crude approximation of a logarithmic function). In principle, improvement in dynamic range results from this response function because the lower and higher amplitude portions of the input are amplified by different factors. In practice, the design functioned basically properly but two problems were encountered. First, baseline drift of the amplifier corrupted the data in a complicated way, since the various portions of the input signal were affected by differing amounts. Recovery of the true waveform then required a generally unacceptable trial-and-error iteration in which the baseline of the raw digitized data was adjusted prior to the application of the unfolding algorithm. Second, digitization noise riding on the different portions of the waveform was artificially distorted in the unfolded data. Figure 12 is an example of one (unfolded) measurement of ground cable current obtained with this arrangement. No further pursuit of this technique is planned for the present. Nevertheless, with further development of a compensated amplifier with improved stability, the basic idea might still prove worthwhile for these types of tests.

CONCLUSIONS

The 1990 field trial of the SATTLIF demonstrated the general practicality of using a transportable triggered lightning facility for specialized test applications. These applications include, but are not limited to, cases in which test objects are either too large to be transported to a conventional test facility or cannot be driven adequately by such a facility. A further case involves the situation in which objectives require features in the test current that cannot be obtained from a conventional simulation source.

Lightning return-stroke and continuing-current components were recorded with high resolution by the SATTLIF, which was deployed 80 feet from the strike tower. The Dymec FM FO system used for the latter functioned well and reliably. Its stability proved so good that frequent calibration was found to be superfluous. The combination of

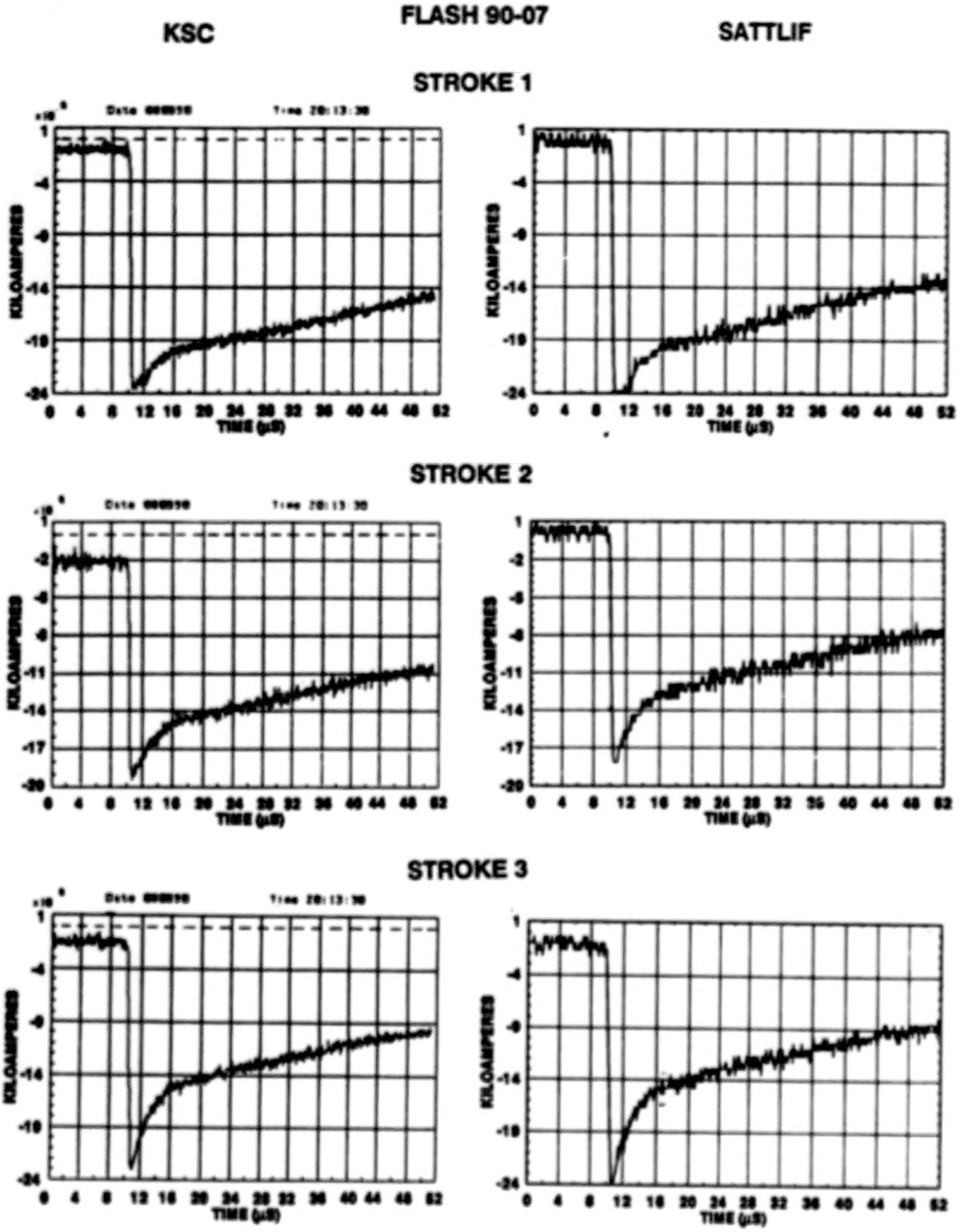

Figure 7. Stroke Currents of Flash 90-07 as Measured by KSC and SNL

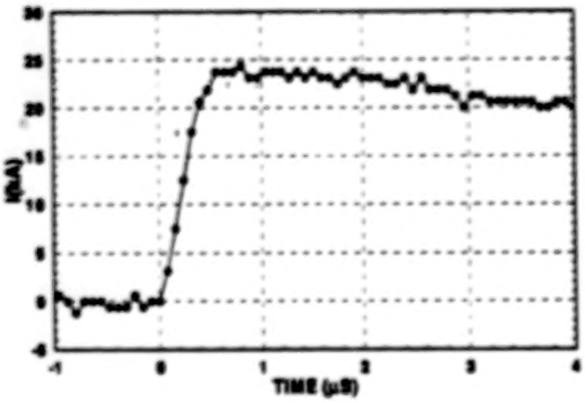

Figure 8. Early Portion of Stroke 1 Current, Flash 90-07. Dots Indicate Data Sample Points.

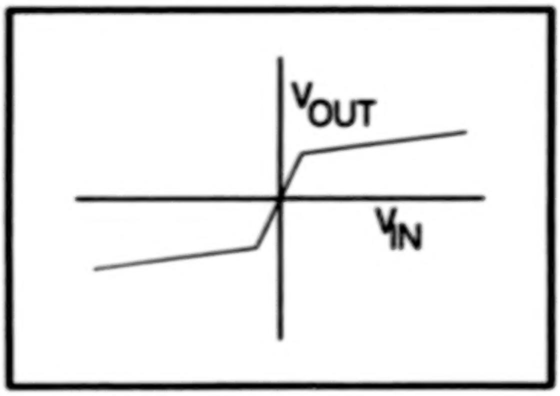

Figure 11. "Gain Compression" Amplifier Response Function

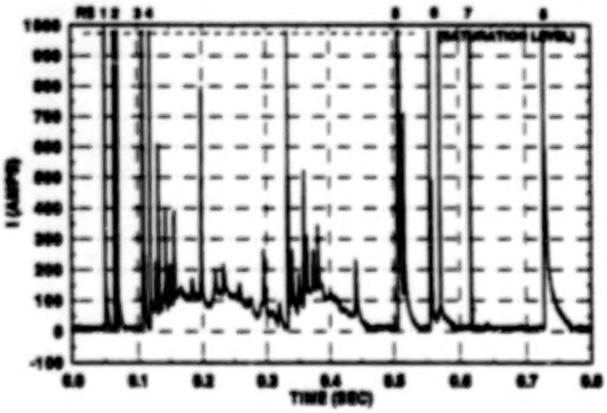

Figure 9. Flash 90-04 as Recorded by the SATTLIF Continuing-Current Instrumentation

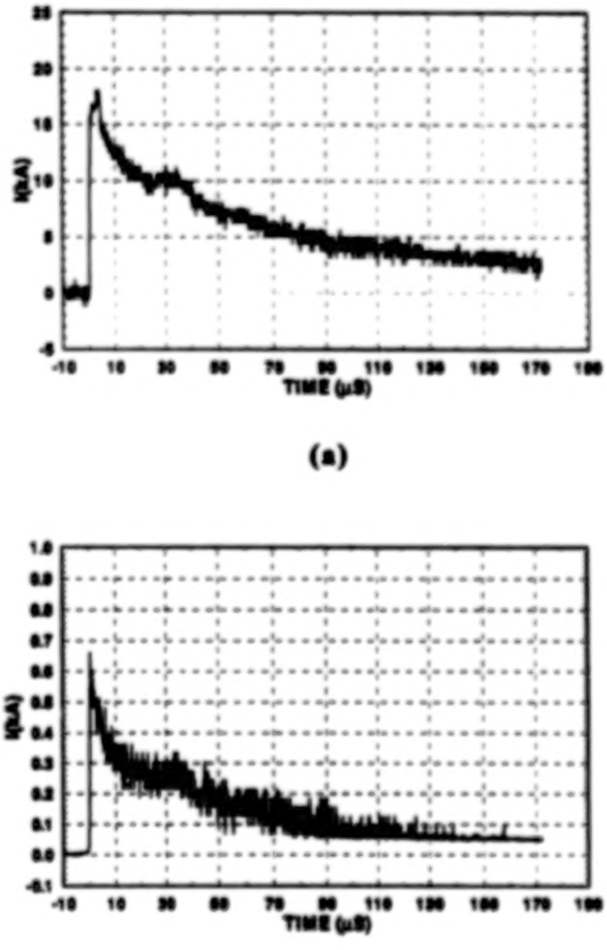

(a)

(b)

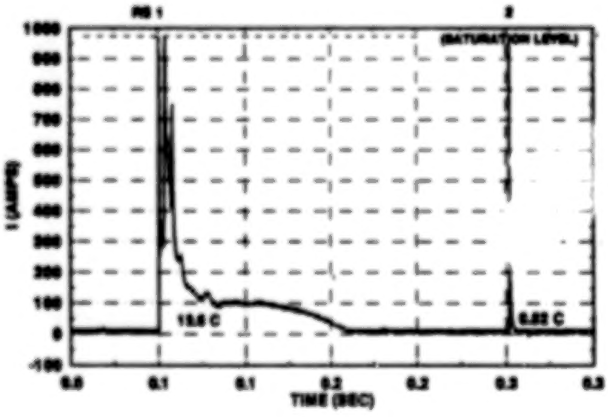

Figure 10. Flash 90-03 as Recorded by the SATTLIF Continuing-Current Instrumentation

Figure 12. a) Incident Flash Current and b) Corresponding Cable Current Obtained Using Experimental "Gain Compression" Amplifier

FM FOL and FM tape recording was so successful that, in future testing, digitizer channels will be reserved solely for the recording of faster phenomena.

Additional examples of data obtained with the SATTLIF during these trials are available in Reference 2, which appears in these proceedings. A fuller description of the facility and all the data acquired during 1990 is available in Reference 5.

ACKNOWLEDGEMENTS

The authors wish to express their appreciation to the Kennedy Space Center and Mr. William Jafferis for the opportunity to participate in their 1990 rocket-triggered lightning program. The considerable technical input of Dr. Larry D. Scott (SNL) and his contribution in setting up the LeCroy digitizer system software are acknowledged. The detailed design of the SATTLIF's rocket launch system and supervision of its fabrication was largely carried out by C. S. Chocas (SNL). Development of the SATTLIF was jointly funded by U.S. Department of Energy, the Project Managers' Office of the Department of the Army, and the U.S. Army Armament Research, Development, and Engineering Center (ARDEC).

REFERENCES

1. Collier, R. S., P. M. McKenna, and R. S. Perala, "Evaluating Lightning Hazards to Building Environments Using Explicit Numerical Solutions of Maxwell's Equations," *Proc. 1991 Int. Conf. on Lightning and Static Electricity*, April 1991.
2. Fisher, R. J., and G. H. Schnetzer, "Damage to Metallic Samples Produced by Measured Lightning Currents," *Proc. 1991 Int. Conf. on Lightning and Static Electricity*, April 1991.
3. Orville, R. E., R. B. Pyle, and R. W. Henderson, "The East Coast Lightning Detection Network," *IEEE Trans. on Power Systems*, PWRS-1, No. 4, November 1986.
4. Larouche, P., A. Eybert-Berard, and L. Barret, "Triggered Lightning Flash Characteristics," *Proc. 1985 Int. Conf. on Lightning and Static Electricity*, June 1985.
5. Fisher, R. J., and G. H. Schnetzer, *1990 Sandia Rocket-Triggered Lightning Field Tests at Kennedy Space Center, Florida*, SAND90-2926, February 1991.

Session 7B, Wednesday 1:30
Aerospace Vehicles
Test Criteria and Techniques 2
Burrows, Chairman

FD-TD CALCULATION WITH COMPOSITE MATERIALS.
APPLICATION TO C160 AIRCRAFT MEASUREMENTS.

J.C. Alliot*, J. Grando*, F. Issac* and X. Ferrières**

*Office National d'Etudes et de Recherches Aéropatiales,
B.P. 72, 9232 CHATILLON CEDEX, FRANCE

**SLX Informatique, 1 Place Charras, 92400 COURBEVOIE, FRANCE

ABSTRACT

In a frequency domain in which a material thickness is smaller than the skin depth, a formalism based on the sheet impedance concept has been developed and introduced in the FD-TD code ALICE. The predictive capabilities of the 3D code have been evaluated by comparison to analytical and experimental data.

1. INTRODUCTION

For large structures such as aircraft, the spatial resolution of 3D computer codes is insufficient to model thin surfaces such as lossy skins. There is therefore a need to accurately include their effects on the electromagnetic coupling paths and so, to define an approach whereby lossy surfaces can be treated in the time-domain. This can be achieved by defining a relationship between the surface electric and magnetic fields such that the details of the skin do not have to be directly modelled. In a frequency domain in which a material thickness is smaller than the skin depth, a formalism based on the sheet impedance concept has been developed and introduced in the FD-TD code ALICE [1]. The predictive capabilities of the 3D code have been evaluated by comparison to analytical results obtained by K.F. Casey [2] on a loaded aperture and by comparison to experimental data obtained during an in-flight experiment conducted in France to study lightning interaction with a vehicle [3].

2. LOW FREQUENCY ELECTROMAGNETIC PENETRATION OF LOADED APERTURES

In a frequency domain in which a material thickness is smaller than the skin depth, it can be shown [4] that a lossy material may be characterized by its sheet impedance defined as:

$$Z_s = \frac{\vec{E}}{\vec{J}_s} \qquad (1)$$

where $\vec{J}_s$ is the surface current density and $\vec{E}$ is the tangential electric field component.

For good conductors in which displacement currents are negligibly small compared with conduction currents for the frequency of interest ($\sigma \gg \varepsilon\omega$), equation (1) reduces to:

$$Z_s = \frac{1}{\sigma d} \tag{2}$$

where σ and d are the material conductivity and thickness respectively.

The Magnetic Shielding Effectiveness (MSE) of a structure is defined as:

$$MSE = \left|\frac{\vec{H}}{\vec{H_o}}\right| \tag{3}$$

where $\vec{H_o}$ is the field at a point chosen in the absence of the shield and $\vec{H}$ is the field at the same point with the shield in place.

K.F. Casey [2] has shown analytically that the MSE of a circular aperture (of radius a) loaded by a panel characterized by its sheet impedance Z_s is given, in the frequency domain, by:

$$MSE = F_1 \left\{ 1 + j \frac{F}{2F_{co}} \frac{2 - \frac{F_c}{F_{co}}}{\frac{F_c}{F_{co}}} F_1 \right\}^{-1} \tag{4}$$

with:

F: frequency in Hz

$$F_{co} = \frac{3\, Z_s}{8\, \mu_o\, a} \tag{5}$$

$$F_c = F_{co} \left[1 + \frac{RL}{Z_s\, a}\right] \tag{6}$$

R: the net resistance of the joint (length L) located around the panel.

F_1 is obtained by solving the linear system $F_m + \frac{\beta}{\pi} \sum K_{mn} F_n = \delta_{m,1}$ where $\beta = j \frac{3\pi}{8} \frac{F}{F_{co}}$ and K_{mn} is a combination of m and n index.

When the junction between the panel and the metallic plane is perfect (R = 0), equation (4) reduces to:

$$MSE = \frac{1}{1 + j\dfrac{F}{F_c}} \tag{7}$$

This expression corresponds to a first order filter function with a cut-off frequency $F_c = F_{co}$ for 3 dB attenuation.

3. FD-TD MODELLING

If we consider a composite sheet in the plane OXY of a unit cell (figure 1), it can be shown [5] that the current density $\vec{J}$ may be expressed as:

$$\vec{J} = \frac{1}{Z_s \Delta z} \vec{E} \tag{8}$$

With this expression for $\vec{J}$, equation (2) in reference [1] can be solved in finite difference form without taking into account the panel thickness.
Assuming that the contact resistance around a panel corresponds to a joint of width W, we can define a surface impedance of this joint as:

$$Z_J = \frac{RL}{W} \tag{9}$$

The expression (6) for F_c then becomes:

$$F_c = F_{co}\left[1 + \frac{W}{a}\frac{Z_J}{Z_s}\right] \tag{10}$$

In the FD-TD code, W will be the mesh size.
The joint surface impedance Z_J can be related to a conductivity σ_J and a thickness d_J so that $Z_J = (\sigma_J d_J)^{-1}$.

4. COMPARISON TO ANALYTICAL RESULTS

The structure used to study field penetration through a loaded aperture is a perfectly conducting cavity having a square aperture on the upper side (figure 2). The aperture dimensions are small compared to the cavity size. The box is connected to two thin wires of infinite extend in space. A current generator is located on one of them at 5.3 m from the cavity. The waveform of the injected current is of trapezoïdal shape with a rise time of 2 ns and a peak value of 1000 A. In a first step, the joint around the panel will be considered as perfect (R = 0).

Figure 3a shows the waveform of the magnetic field component H_o computed at a point P (figure 2) in the case of a free aperture.

The point P is located inside the cavity, 5 cm below the aperture. As indicated by the FFT of H_o shown in figure 3b, the high frequency content is mainly due to a $\lambda/4$ resonance of wire 1 (between the current generator and the box - F = 15 MHz) and to a $\lambda/2$ resonance of the cavity (F = 45 MHz).

Figures 4a and 5a show the temporal waveforms of the magnetic field component H computed at the point P when the aperture is loaded with a composite panel having a sheet impedance of 1 Ω and 0.1 Ω respectively. A low frequency content appears as a consequence of the panel filtering effect.

Figures 4b and 5b show the FFT ratios for the magnetic field components H and H_o corresponding to the previous results. The agreement with the theory presented in § 2 is excellent. The code has predicted:

- The same low frequency content for H_o and H.
- The cut-off frequency corresponding to a 3 dB attenuation (7),(5). An equivalent radius "a" of the square aperture can be calculated by comparison to a circular aperture having the same area. Using (5) with a = 0,3 m, we obtain F_c = 1 MHz for Z_s = 1 Ω and F_c = 0.1 MHz for Z_s = 0.1 Ω.
- The decrease of the spectrum with a slope of 20 dB/decade for $F \gg F_c$ as indicated by (7).

We consider, now, that there is a joint all around the panel. Two values Z_J = 2.5 Ω and Z_J = 22.5 Ω have been considered. These values have been chosen to satisfy F_c/F_{co} = 2 and F_c/F_{co} = 10. With the contact length L = 2 πa, the corresponding contact resistances are R = 0.16 Ω and R = 1.43 Ω respectively. From (5), the theoretical cut-off frequency for a loading material having a sheet impedance Z_s = 1 Ω is F_{co} = 1 MHz.

Figures 6 and 7 show the variation of the MSE given by (4) and (7) and also the variation of the MSE obtained with the FD-TD code using W = 0.12 m: H_o and H are the magnetic field components computed on the axis of the aperture, 15 cm inside the cavity, in the case of a free aperture and in the case of a loaded aperture with a joint, respectively. For R = 0.16 Ω, the approximate expression (7) is close to the exact value given by (4) and the FD-TD result is also in very good agreement with these results. For R = 1.43 Ω, the cut-off frequency (for 3 dB attenuation) is 6 MHz with the exact expression (4) and 10 MHz with the approximate expression (7). The FD-TD result gives a cut-off frequency of 7.8 MHz between the two previous values.

5. IN-FLIGHT EXPERIMENT MODELLING

In reference [1] when the current pulse simulating the negative leader mechanism is injected onto the aircraft by means the 3D computer code all the calculated fields are in good agreement with experimental results except the magnetic field computed in the fuselage, behind the carbon composite door.

The signal obtained (figure 8b) exhibits a first order low-pass filter response having a cut-off frequency of 9 kHz whereas the measured signal (figure 8a) exhibits a response with a 50 kHz cut-off frequency. It has been shown that the only possible path for this high frequency content is the joint located all around the door and used to pressure the aircraft: a joint of poor quality increases the penetration of electromagnetic energy and so increases the internal frequency content (see § 2). This joint resistance being unknown our purpose here is to calculate its value and then to introduce this value in the 3D code and compare the results to the experimental data.

When penetrating inside the fuselage the external magnetic field is:

- Attenuated by a geometrical effect. This attenuation (40 dB) has been evaluated using the 3D code and assuming the door is unloaded (figure 9).
- Filtered by the carbon composite material of the door. This filtering effect if given by the relations (4) and (6).

Knowing the values of F_c, a and Z_s, we can deduce from (6) the resistance R of the joint. In the case of the Transall experiment, we obtained $Z_s = 30$ mΩ, $a = 0.68$ m and $F_c = 50$ kHz, so $R = 12$ mΩ.
These values of Z_s and R have been introduced in the code "ALICE" and the result is shown in figure 10. This response is in very good agreement with the in-flight measurement.

6. CONCLUSION

The goal of this paper is to present a formalism based on the sheet impedance concept which has been introduced in a 3D FD-TD code in order to take into account electromagnetic coupling through lossy materials and through resistive joints. The predictive capabilities of the code have been evaluated by comparison to analytical results obtained by K.F. Casey. The numerical tool has been used to model the penetration of electromagnetic fields through a carbon composite door located on the fuselage of an aircraft struck by lightning during an in-flight experiment. A very good agreement with in-flight measurements can be obtained if one takes into account the coupling through the joint surrounding the door.

REFERENCES

[1] Alliot, J.C.; Grando, J.; Muller, J.D.; Ferrières, X.: FD-TD numerical simulation of an entire lightning strike on the C160 aircraft. International Aerospace and Ground Conference on Lightning and Static Electricity, Cocoa Beach, Florida (USA) (April 16-19 1991).

[2] Casey, K.F.: Low frequency electromagnetic penetration of loaded apertures. IEEE Trans. on EMC, Vol. 23, No 4, (November 1981).

[3] Moreau, J.P.; Jouan, J.Y.; Issac, F.: Transall 88 characterization program. Proceedings of ICOLSE Conference, Bath (UK) (Sept. 26-28 1989).

[4] Gobin, V.; Aparicio, J.P.; Grando, J.; Alliot, J.C.: The surface impedance: a pertinent parameter to describe finite conductivity materials in numerical codes. Paper proposed to EMC, Zurich (1991).

[5] Grando, J.; Issac, F.; Labaune, G.; Alliot J.C.; Ferrières, X.: Field penetration through composite material using FD-TD method. 1990 IEEE AP-S International Symposium and URSI National Radio Science Meeting, Dallas (Texas) (6-11 May 1990).

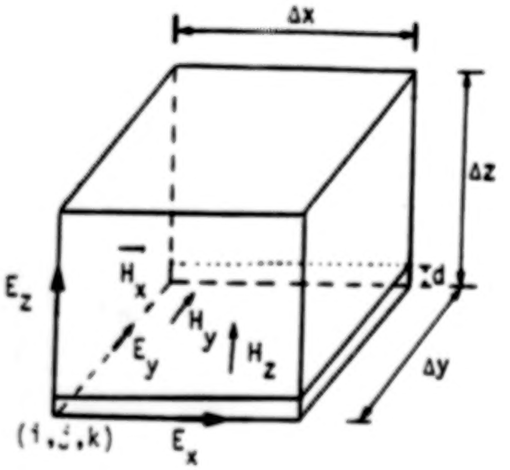
Δx
Δz
d
Δy
E_z
$\overline{H}_x$
H_y
E_y
H_z
(i,j,k)
E_x

Figure 1 : Elementary cell with a composite material (ε,σ,d).

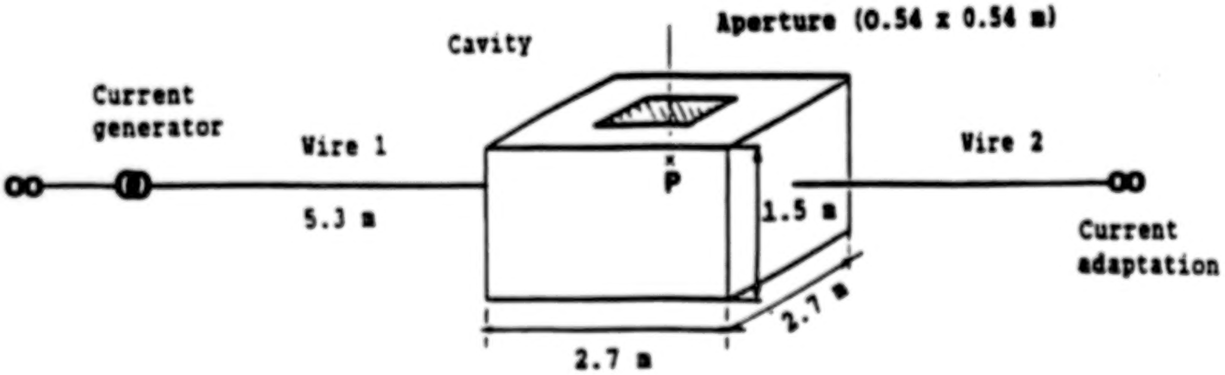
Cavity
Aperture (0.54 x 0.54 m)
Current generator
Wire 1
5.3 m
P
1.5 m
Wire 2
Current adaptation
2.7 m
2.7 m

Figure 2 : Structure used to calculate field penetration through a loaded aperture.

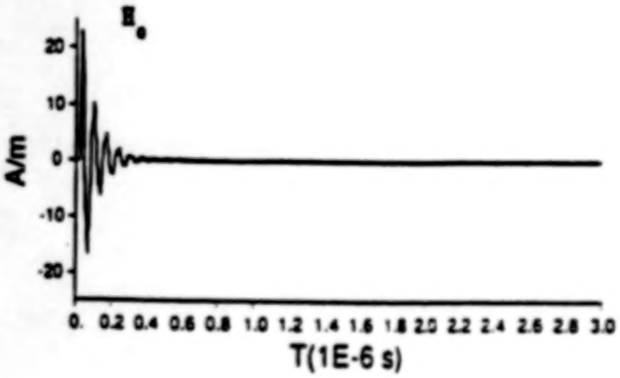

Figure 3a : Waveform of the magnetic component at point P. (free aperture)

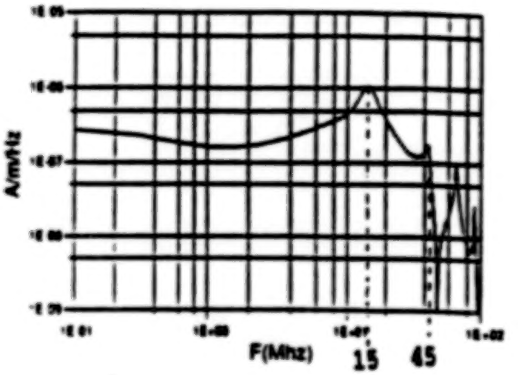

Figure 3b : FFT of H_o component.

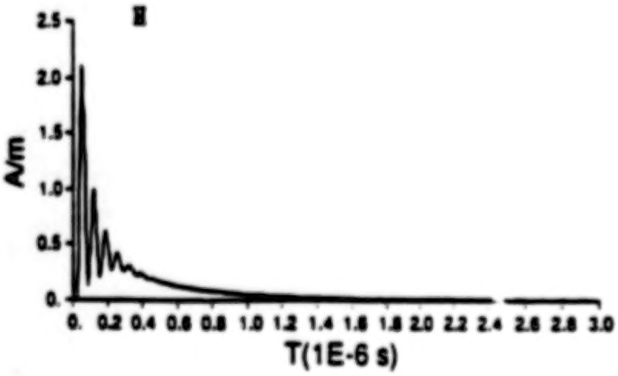

Figure 4a : Waveform of the magnetic component at point P. (loaded aperture Z_s = 1 Ω)

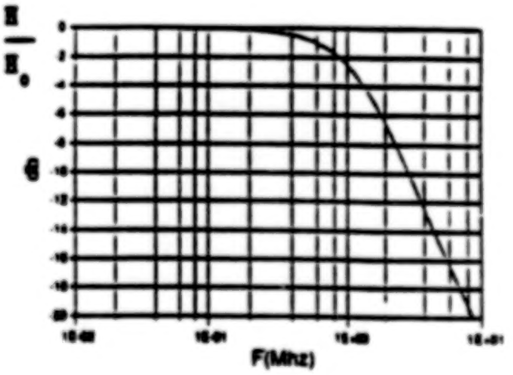

Figure 4b : H and H_o FFT ratio.

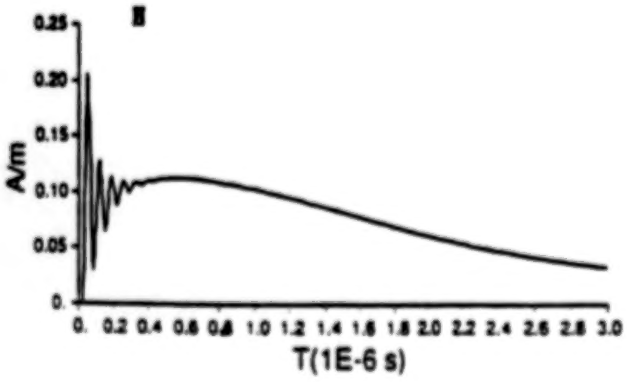

Figure 5a : Waveform of the magnetic component at point P. (loaded aperture Z_s = 0.1 Ω)

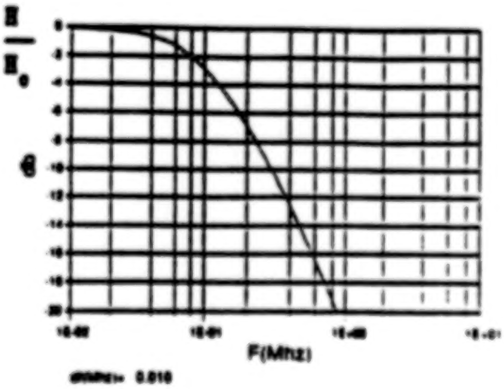

Figure 5b : H and H_o FFT ratio.

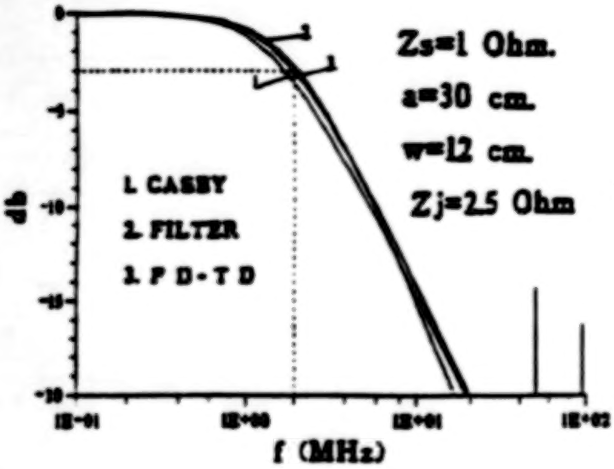

Figure 6 : Magnetic field attenuation for a composite panel (Z_s = 1 Ω) with a net contact resistance R = 0.16 Ω.

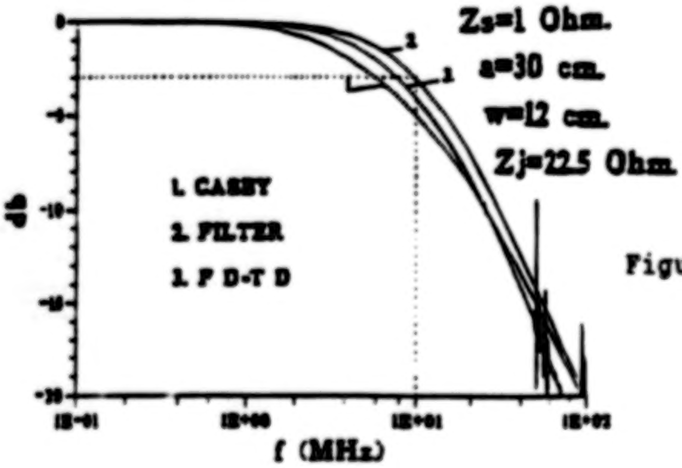

Figure 7 : Magnetic field attenuation for a composite panel (Z_s = 1 Ω) with a net contact resistance R = 1.43 Ω.

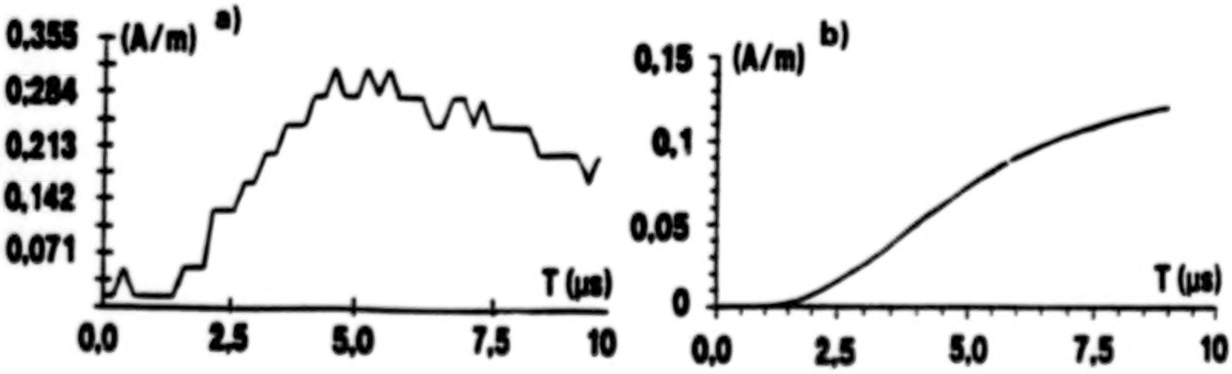

Figure 8 : Internal magnetic field.

a) Measured during in-flight experiment.
b) Calculated without taking into account the joint resistance.

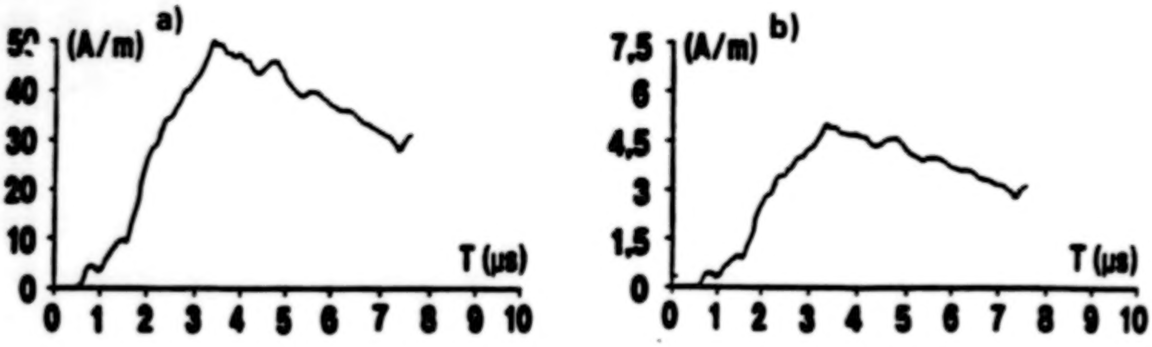

Figure 9 : Calculated magnetic fields.

a) On the external skin of the fuselage near the composite door.
b) Inside the fuselage assuming the door unloaded.

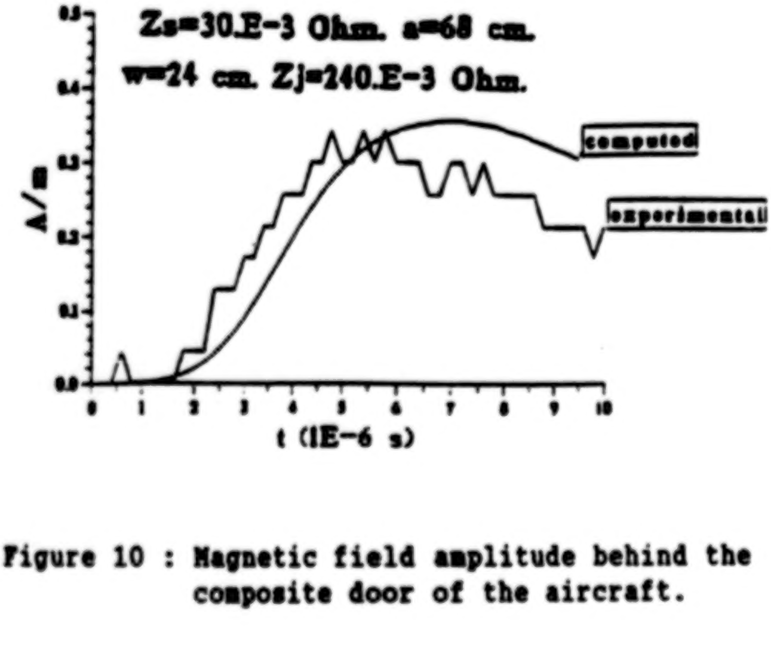

Figure 10 : Magnetic field amplitude behind the composite door of the aircraft.

Time Dependant Behavior of a Carbon Composite Case to Simulated Lightning

by M. Taylor

No paper available.

THE ELECTROMAGNETIC ENVIRONMENT IN CFC STRUCTURES

C J Hardwick and S J Haigh
Culham Lightning Test and Technology ,Abingdon, Oxford, UK, OX14 3DB

ABSTRACT

Extensive measurements of induced voltages and currents have been made using a CFC horizontal stabilizer from the A320 as a test bed .The work was done to investigate the efficacy of various protection schemes to reduce the magnitudes of the induced voltages and validate a computer program INDCAL.Results indicate that a good understanding of the various induced voltage mechanisms including the long wave effect due to current redistribution has been obtained

1 INTRODUCTION

The use of CFC in airframe construction produces indirect effects which have generated much interest in recent years. In particular, the relatively high resistivity of composite compared to aluminium leads to significant redistribution of current from the carbon fibre to any metallic components of the airframe during later times of the lightning waveform (References 1 and 2). This is because after the initial fast current rise, the di/dt magnitude decays and the current distribution is no longer inductively dominated.

In the latest FAA advisory circular AC20-136 (Reference 3), a long duration waveform, waveform 5 is specified for equipment tests to take account of the phenomenon. This current waveform, which will occur on conducting conduits or cable screens in hybrid structures (structures containing both metallic and CFC components) has a rise time of 50μs and time to $^1/_2$ height of 500μs. Peak amplitudes specified are from 3-20kA.

This waveform 5 is supplementary to waveforms 1 and 4 which are current and voltage waveforms respectively which have the same shape as a component A lightning strike, waveform 2 which is the derivative of waveform 1 and waveform 3 which is a damped sinwave.

Some measurements on induced voltages and currents in a CFC horizontal stabiliser box were reported in a previous paper of this conference series (Reference 4); no protection was installed on the box resulting in conduit currents of up to 17kA, of a waveform 5 type due to current redistribution.

This present paper covers work investigating the effects of various protection methods such as aluminium strips bonded to the box and of surface coatings of metallic foil. Induced voltages were measured on wires routed inside and outside of conducting conduits, as well as the current distribution around the structure.

Section 2 describes the experimental configuration, Section 3 presents the results and Section 4 presents some limited comparisons with INDCAL (Reference 5) computer predictions. Section 5 makes predictions for more general hybrid structures.

The work has been supported by the Culham Lightning Club.

2 EXPERIMENTAL CONFIGURATION

The basic experimental configuration is shown in Figure 1 and this is similar to that used in the previous work reported in Reference 4. A 1.5m long metallic braided conduit was installed inside the stabiliser and linked two aluminium boxes both of which were well bonded to the CFC; induced voltage diagnostics were installed in one of the boxes. The extent of the aluminium protection strips and foil are also indicated in the figure. Figure 2 indicates the wire circuits on which the induced voltage measurements were made. Each wire was shorted to the metallic box at one end and terminated in a high impedance at the other end. In addition to the unprotected structure (Figure 2a), data for three different protection configurations were measured; these were:

Al Strips

2.5cm wide, 2mm thick A1 strips bonded along their entire length with M4 screws using existing captive nuts. These nuts were present for attaching aluminium strips on the production aircraft (Figure 2b).

376

Foil

25μ thick aluminium foil of resistivity 2.5mΩ/□ was placed over the upper and lower skins and extended as far as the entire length of the strips. The foil was clamped near the leading and trailing edges by the aluminium strips. It was isolated from the CFC surface by a layer of polythene - this was in order to ensure the current paths to the foil were well defined (Figure 2c).

Thin aluminium strip was also used to sandwich the foil edges to the CFC at its furthest inboard and outboard extent, and held down with several self tapping screws. This was to enable current to pass straight from the CFC to the foil without having to deviate to the aluminium strips at the leading and trailing edges first.

External Conduit

The 1.5m, conduit used hitherto was joined by a 360° joint to a similar piece of conduit giving a 3m long conduit of total resistance of 9.6mΩ. The ends of this assembly were again bonded to the termination boxes A and B with 360° joints, but the cable was routed external to, and its centre 4cm away from the front spar of the stabiliser (Figure 2d).

3 RESULTS

The measurements are tabulated in Table 1 for the unprotected configuration, Table 2 for the "strip" configuration, Table 3 for the "foil and strip" and Table 4 for the "external conduit". The data values have been linearly extrapolated to 200kA peak current, but were generally obtained with a driving waveform of 12kA peak current, rise time 1.3μs, time to $^1/_2$height on falling tail, 12μs. For a Component A driving waveform, because of the longer decay time (70μs), larger redistribution currents would be obtained.

The capacitor bank voltage was 120kV, which with the 2.2μH inductance of the structure gave a peak value of di/dt of 53kA/μs. Hence the appropriate scaling factors to 200kA peak current and 140kA/μs peak di/dt are 18 and 2.64 respectively.

INDCAL calculations were made using the cross section of the structure shown in Figure 2e and comparisons with data in the different configurations are made in Figures 3-6. The agreement is very favourable (3dB). Aspects of these waveforms are discussed in Section 4.

TABLE 1

	VALUE of Peak Current/Voltage at 200kA	RISE TIME μs
Current at box corner	11.87 kA	1
Upper skin	7.85 kA	1.7
Lower skin	7.15 kA	2.0
Lower skin density * resistivity x 1.5m	1185 V	
ICORE current	17.25 kA	23
ICORE current x 3.8mΩ (ICORE resistance)	66 V	
Inner wire voltage	52 V	24
Outer wire voltage	109 V	2.6
Inner, ICORE disconnected	1500 V	2.5

TABLE 2
2.5cm A1 strips installed + ICORE

	VALUE AT 200kA	RISE TIME μs
Strip current	21 kA	4
Upper skin	7.3 kA	2
Lower skin	6.6 kA	2
Density x resistivity x 1.5	1110 V	
ICORE	11.8 kA	20
ICORE current x 3.8mΩ	44 V	
ViR inner	46 V	18
Difference dB	0.4	
ViR outer	90 V	2.5

TABLE 3
Strips and foil installed

	VALUE AT 200kA	RISE TIME, µs
Strip current	18 kA	
Upper skin	7.3 kA	2
Lower skin	6.2 kA	2
Density x resistivity x 1.5m	206 V	
ICORE	8.5 kA	30
ICORE current x 3.8mΩ	32 V	
ViR inner	33 V	26
ViR outer	54 V	4
ICORE current x 3.8mΩ	32 V	

TABLE 4
ICORE routed outside

	VALUE AT 200kA	RISE TIME, µs
Strips	16 kA	2.5
Upper skin	7.1 kA	2
ICORE	7.6 kA	2
ICORE current x 9.6mΩ	77 V	2.5
ViR inner	90 V	.8
ViR outer	94 (648)V⁺	~ .1
ViR outer ICORE disconnected	7.9 kV	

Notes:

+ Bracketed figure is figure that would be obtained by scaling di/dt by same factor as current
For waveforms with high HF content we have scaled to peak di/dt (factor 2.6) not current (x18) as the coupling mechanism is proportional to di/dt rather than current.

4 DISCUSSION

Measurements of voltages on wires in many different internal positions were made in addition to those illustrated in Figure 2, however space precludes their inclusion; details are available in the Culham Lightning Club reports (Reference 6). Nevertheless the agreement with INDCAL predictions for voltages was generally within about 6dB and the trend of values and waveshapes is shown in Figure 7. These trends can be understood in terms of the resistive voltage drop and diffusion flux penetration through the box walls.

Circuits using the box structure as a return path will have an induced voltage due to the sum of the resistive voltage drop along the structure itself plus a contribution from the rate of change of flux threading the circuit of wire and structural return. Well inside the CFC structure and away from any apertures this will be diffusion flux whose rate of change, roughly follows the current wave shape. Depending on direction of the flux it may add or subtract to the structural voltage. At conducting elements in the box, the structural/diffusion flux voltage will drive redistribution current into the conduit; this current will in turn reduce the total flux near to the conduit.

The relative screening offered by the different configurations have been summarised in Figure 8. The results have been derived from the peak voltage data from the tables normalised to 1A, or to 140kA/µs/200kA depending on the coupling mechanism, to give a screening figure of merit in dBΩ. Shown on the same graph are the AC20-136 threat levels. Computations show that with an AC20-136 component A driving waveform (longer than our experimental waveform) the values of induced voltage on wires inside the conduit which carry a redistribution current would be 7dB higher. Hence with a component A waveform, the ICORE routed inside gives a waveform 5 type of induced voltage 3dB below level 2 (redistribution will effect peak value and 7dB correction added). The externally routed ICORE would give a waveform 4 type of induced voltage, 3dB below level 2 (redistribution current will not effect peak value which occurs with the peak of the driving current and no correction made). For longer cables 6dB should be added for each doubling of length. Computer studies (see next section) have shown that provided the resistance per unit length of the conduit is not too high the current is largely determined by the CFC resistance and structure geometry which leads to the induced voltage developed being roughly proportional to conduit resistance. Differential voltages on two wire circuits of course would be some 20dB lower. Simple computations like these can thus be used to define the shapes and magnitudes of currents and voltages on circuits in the structure that will occur.

Detailed comparisons between data and predictions are now discussed:-

a) BASIC STRUCTURE

The current density at the corners of the wing box, near to the position of the aluminium strips is initially higher than elsewhere but decays more quickly than for example the current on the top skin. This is understood in terms of an initial inductive current distribution followed by resistive redistribution. The INDCAL/data comparison is made in Figure 4.

b) STRIPS

As expected the Aluminium strips drain current from the structure at late times so the strip current waveform is higher in amplitude and shows a much later zero crossing than the current measured in the carbon fibre at the same position before the strips were installed.

Moreover as the strips are more conductive than the ICORE current redistributes into them more readily and the ICORE current has a lower amplitude (-3dB) and decays earlier. Figure 5 shows that INDCAL is accurate to within 3dB.

Due to flux generated by redistribution current flowing in the conduit (whose rate of change is proportional to structure current) threading between the "outer" wire and the ICORE, the "outer" voltage is higher than the inner and has a shorter time to peak.

c) FOIL

Since the average resistivity of the skin has been reduced considerably the redistribution out of the skin and into the strips is not now so marked. Consequently the strip current is less and decays more quickly. The diffusion flux takes longer to penetrate the more conductive skin and hence. The current in the ICORE now has a longer rise time and its amplitude is reduced by a further 2dB compared to the "strips only" configuration. A comparison with INDCAL is made in Figure 6 and again agreement with INDCAL is good.

It was difficult to make a good joint between the foil and the CFC, and the joint resistance was substantial compared to the 2.5mΩ/□ foil resistance. Since the ICORE current is a sensitive function of the foil resistivity the computation includes a value of foil resistivity that takes account of the measured joint resistance. INDCAL predicted an ICORE current of 3% for an effective skin resistivity of 4mΩ/□, which is close to the observed value of about 4%.

The "outer" wire voltage has been reduced by a larger factor (6dB) by the addition of foil than by the addition of strips since the diffusion flux penetrating to the interior will be lower due to the lower effective skin resistance. Hence foil is very effective at reducing common mode resistive voltage that would occur on unscreened wires in CFC structures.

d) EXTERNAL CONDUIT

The flux driving the current into the conduit is mainly fast aperture flux threading between the ICORE and structure so the current waveform follows more nearly the driving waveform except it remains higher at late times due to current redistribution. INDCAL predictions are shown in Figure 7 together with measured values. The computation includes a reduced cross section for the conduit to give a 50% increase in the self inductance of the ICORE (The ICORE conduit is longer than the length of structure it spans). Because of the large amplitude of di/dt of the current in the conduit there is a big difference between inner and outer voltages.

5 COMPUTATIONAL STUDY

To find how the redistribution currents were affected by the variation of several parameters some computational studies were made. Table 5 shows the result of such a study on a box of similar cross section and make up to the experimental structure. As the resistivity of the structure and hence total resistance is lowered (a similar effect would result from increasing the size of the box) the peak current in the conduit takes a longer time to reach peak but the magnitude decreases rapidly. As the resistance of the conduit becomes lower, its current also increases as does the time to peak but it is limited eventually by its inductance and these are a range of values below which the conduit current does not vary greatly.

More studies of different structures indicated that in general the more important parameters, are the CFC resistivity as noted in this section and the relative proportion of CFC to metal as noted in Section 4b). A range of rise times and fall times for the long wave are possible and the 50µs/500µs is only one example of the form of redistribution currents, longer and shorter waveforms can occur. In particular if a substantial proportion of the structure is a poorly conducting metal such as would be found in a CFC covered titanium engine, very long pulses due to redistribution from the titanium to a good conducting conduit could be produced.

TABLE 5
Computational results for box with strips and foil

BOX RESISTIVITY MΩ/□	ICORE RESISTANCE mΩ	ICORE %	CURRENT RISE TIME µs
2	4.8	4.8	90
4	4.8	7.6	70
6	4.8	9.5	58
4	2.4	8.5	80
4	9.6	6.5	60
4	48	3.2	35

6 CONCLUSIONS

6.1 A resistive INDCAL analysis gives a good understanding of the induced voltage and current redistribution mechanism in hybrid structures. The agreement on the structure studied was within 3dB for currents in the structure and 6dB for voltages.

6.2 The most severe common mode voltages inside hybrid structures are of the order of the maximum resistive voltage drop and these occur for wires routed near the composite skin particularly skin with high curvative; for other wires the voltage will in general be lower especially those routed near to internal low resistance current carrying conductors.

Currents on internal conduits will have long rise times and the induced voltage waveform of a wire inside a 360° bonded conduit follows the current waveform precisely and has a magnitude equal to the conduit current x DC resistance.

6.3 Computational predictions show that the current carried by conduits or cable shields within a hybrid structure has a peak magnitude and a rise time-to-peak which is dependent on several factors relating to the geometry and resistivity of the skin and internal structure; the more important factors being the relative proportion of metal to CFC in the outer skin and the CFC resistivity.

7 REFERENCES

1. A Plummer et al. The Behaviour of Electric Currents in Graphite/Epoxy Structures. ICOLSE 1988, Oklahoma, USA.
2. C Jones. The Slow Equipment Test Waveform for Systems in CFC Structures. ICOLSE 1989, Bath, UK.
3. FAA AC20-136, Protection of Aircraft Electrical/Electomic Systems against the Indirect Effects of Lightning, 1991.
4. C Hardwick et al. Induced Effects Associated with Lightning Strikes to Hybrid Structures. ICOLSE 1989, Bath, UK.
5. C Hardwick et al. A Filamentary Method for calculating Induced Voltages within Resistive Structures in either the Frequency Doman or Time Domain. ICOLSE 1988, Oklahoma,USA.
6. C Hardwick et al. The Electromagnetic Environment Inside the CASA CFC Horizontal Stabilizer. Culham Lightning Club Report 6-13.

8 ACKNOWLEDGEMENTS

The authors would like to acknowledge financial suport from the Culham Lightning Club; comprising: British Aerospace, Rolls Royce, Westlands, CASA, SAAB, Shorts, CAA, DTI.

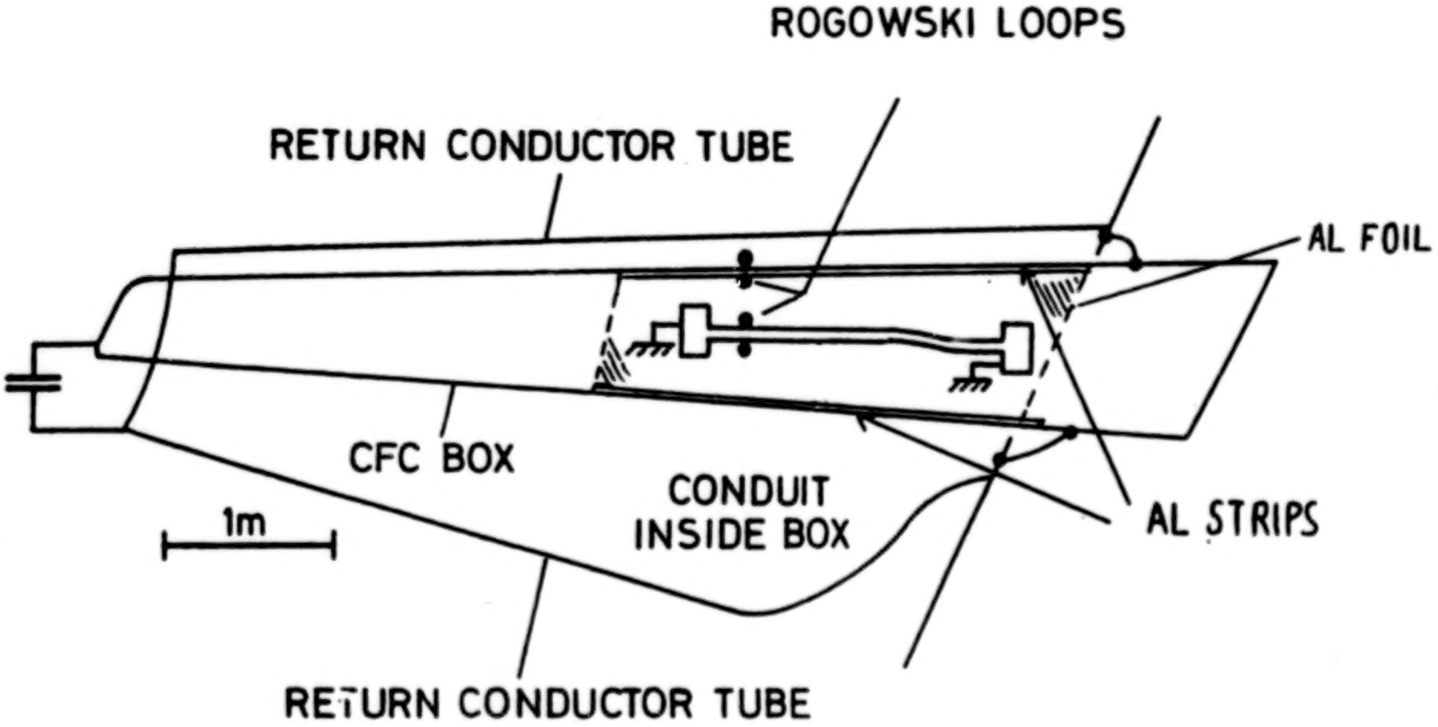
ROGOWSKI LOOPS
RETURN CONDUCTOR TUBE
AL FOIL
CFC BOX
CONDUIT INSIDE BOX
AL STRIPS
1m
RETURN CONDUCTOR TUBE

FIG 1 Plan view of A320 horizontal stabilizer central box section.

Figure 2: Different configurations whose results are plotted in figure 8

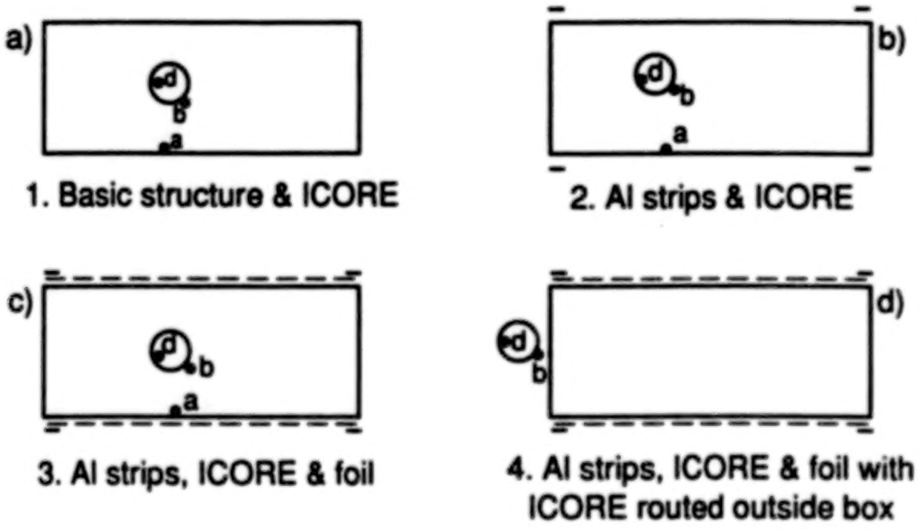

1. Basic structure & ICORE

2. Al strips & ICORE

3. Al strips, ICORE & foil

4. Al strips, ICORE & foil with ICORE routed outside box

Key : Wire a - Structural return
b - External to ICORE
d - Internal to ICORE

For configuration 4 datum for structural return plotted in figure 8 is for wire d with the ICORE disconnected

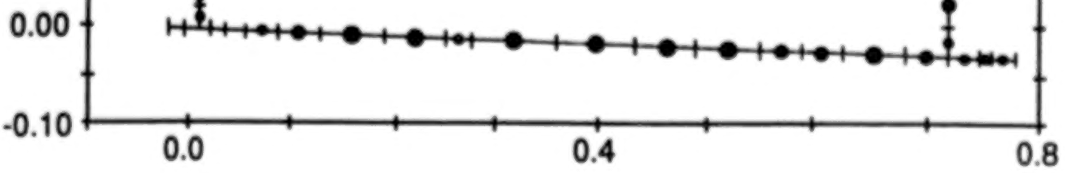

e) Typical filamentary representation for INDCAL

FIG 3 BASIC STRUCTURE RESULTS

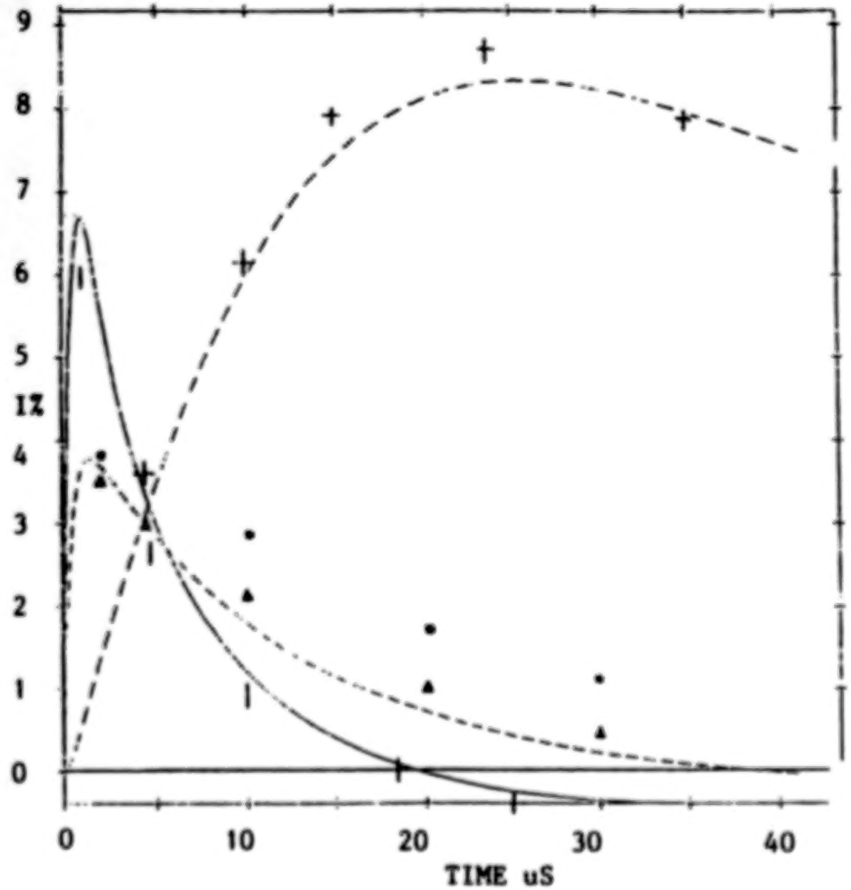

FIG 4 STRUCTURE WITH STRIPS RESULTS

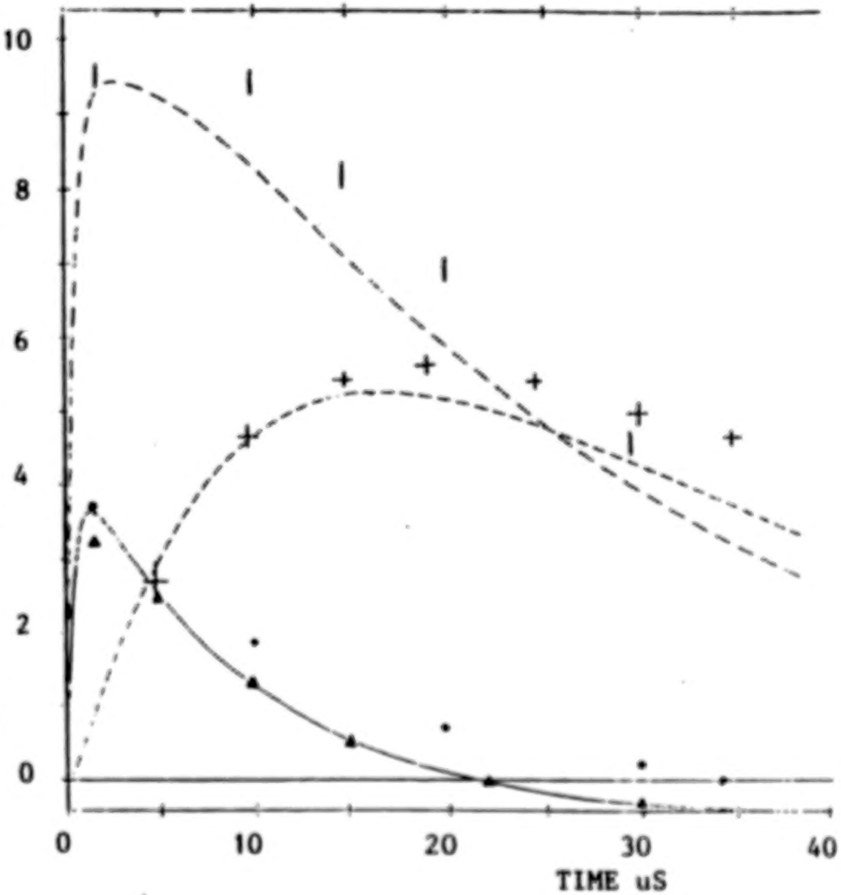

KEY FOR FIGS 3-6

Diagram opposite shows a section through the stabilizer box showing the positions of the current measurements.The data are plotted with the corresponding symbol and the INDCAL predictions are plotted as lines

1 CONDUIT	+
2 UPPER SKIN	•
3 LOWER SKIN	▲
4 BOX CORNER	/

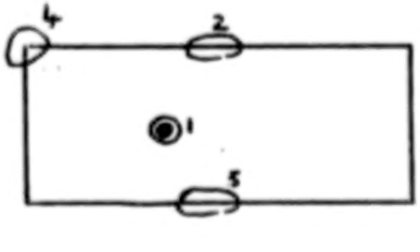

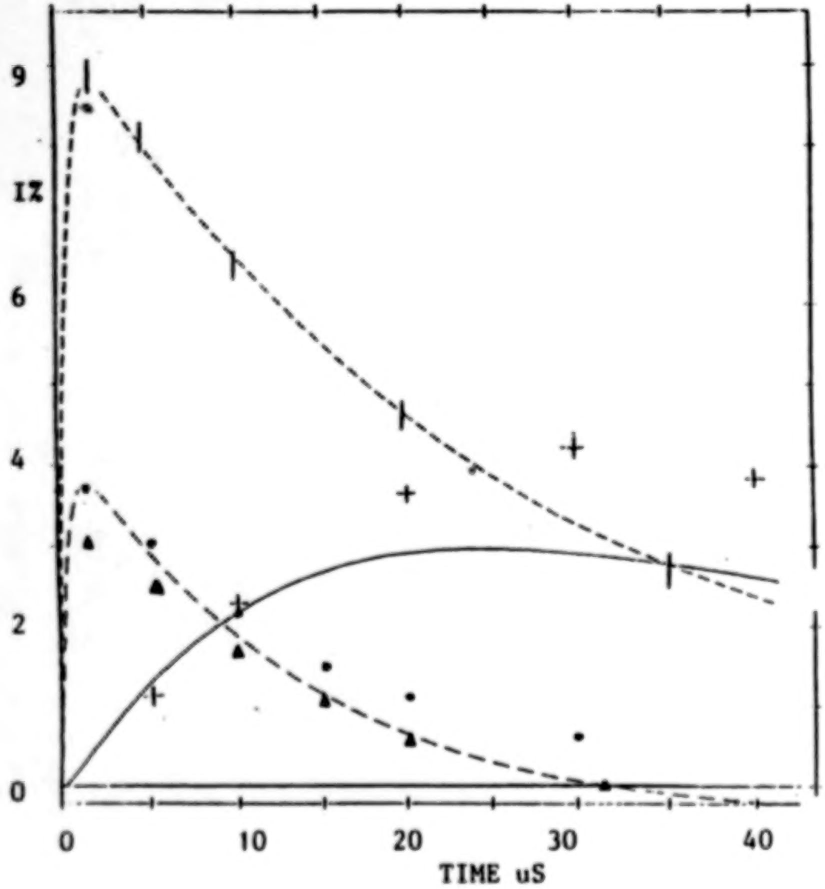

FIG 5 STRUCTURE WITH STRIPS & FOIL

KEY as FIGS 3 & 4

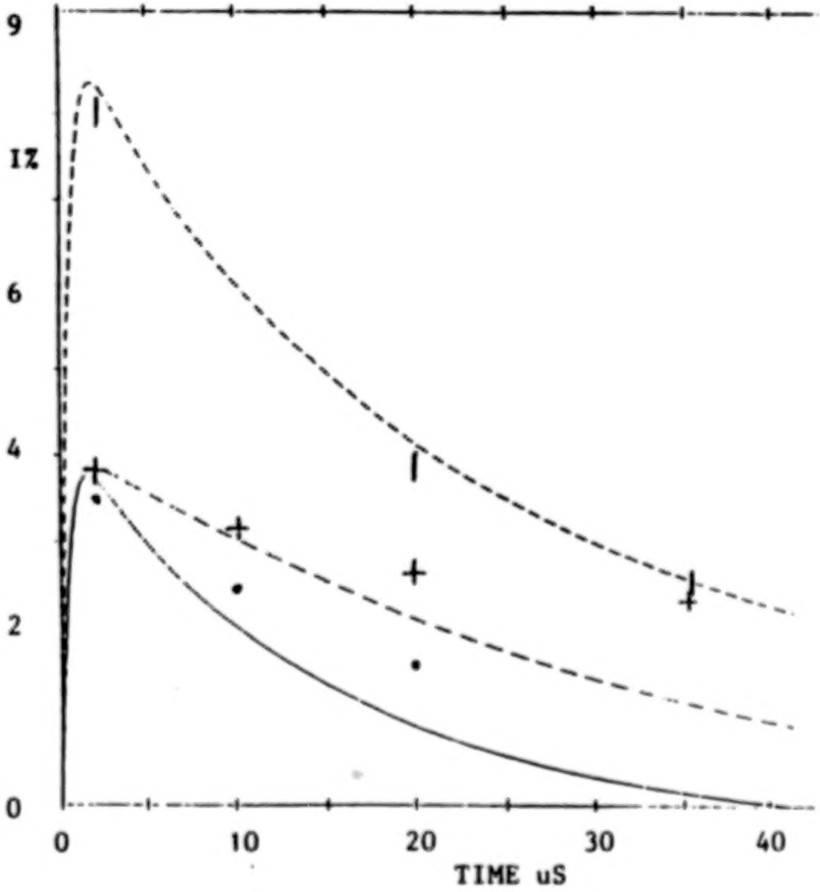

FIG 6 STRUCTURE WITH EXTERNAL CONDUIT

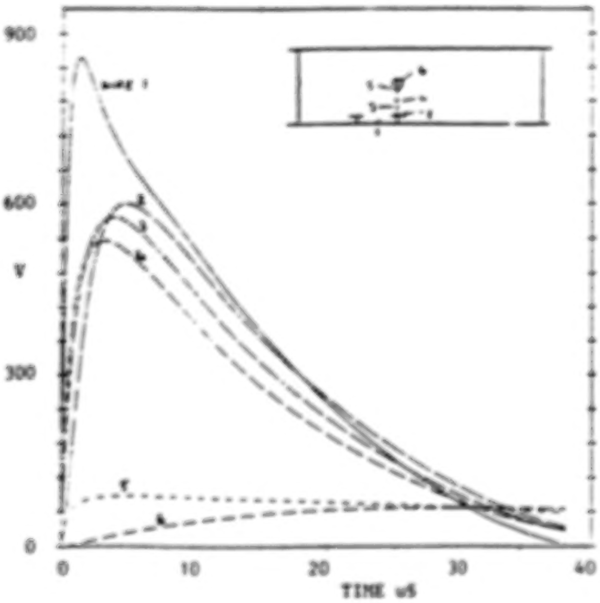

Figure 7: Voltage waveforms for wires at different positions as shown in insert. The longer rise times for the wires 2-4 are due to current taking time to penetrate to the internal structure

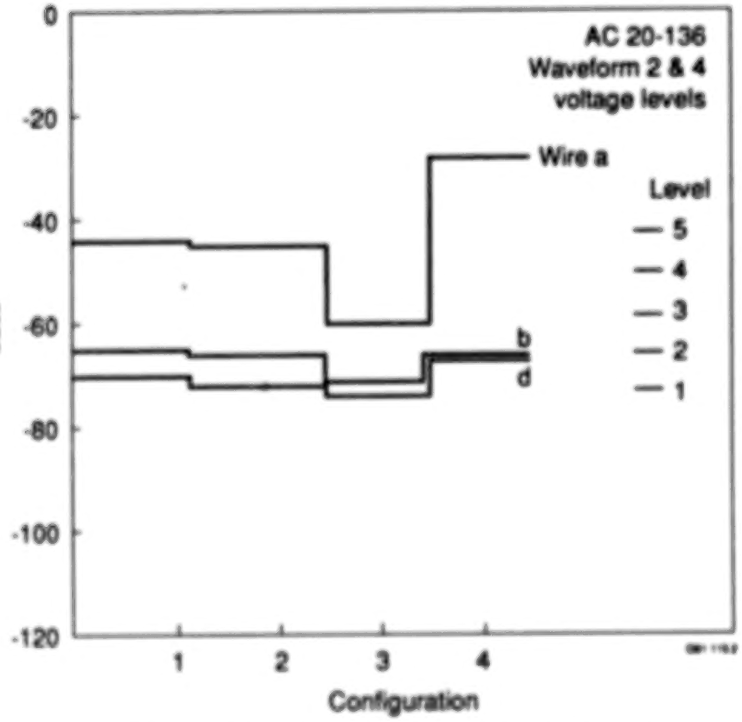

Figure 8: Time domain peak voltage data from tables 1 to 4 plotted relative to driving current in dBΩ

A NEW APPROACH TO EQUIPMENT TESTING

C J Hardwick, V P Dunkley, B J C Burrows, I Darney*

Culham Lightning Test and Technology, Abingdon, Oxford, UK, OX14 3DB
* BAe (Commercial Aircraft), Filton, Bristol, BS99 7AR

ABSTRACT

Considerable controversy has arisen during the recent discussions over the new version of the RTCA DO160C/ED 14C Section 22 document at the European Committee for Aviation Electronics. Section 22 is concerned with lightning waveform tests to equipment.Investigations of some of these controversies with circuit analysis and measurements indicate the impedance characteristics required of the transient generators and the possibility of testing to a voltage limit even for current waveforms.

1 INTRODUCTION

This paper is particularly concerned with calibration procedures and test methods for the lightning transient waveforms 1 and 2 for both bulk current injection and ground plane injection tests. Several of the working drafts have specified the source impedance of the generator, and its verification has been a requirement of the calibration procedure. The calibration procedure has also determined the generator charge level (power setting) required to produce a particular voltage level into a high impedance load. The ensuing test to the equipment/cable bundle assembly has required that the generator setting be increased until either the calibration setting is reached, or in the case of a bundle with a screen bonded at both ends to the aircraft structure, until a current limit is reached.

This paper discusses the relationship between the transients expected for such systems installed in aircraft and in equipment tests. It shows that the source impedance of any test generator should preferably be low (<<5Ω). It also notes a definite relationship between the voltage that would be measured in an aircraft test on a high impedance circuit and the current that would be measured if the circuit was a very low impedance and predominantly inductive thus defining the voltage and current limits for equipment tests.

A test method is proposed where either the power setting of the generator is increased until the voltage applied to the circuit reaches the test limit if the cable length and installation is unknown, thus giving an induced voltage on screened wires that is independent of cable length, or either a voltage or a current limit if the installation is known and the proper cable length is used.

These ideas are illustrated with data from both aircraft and equipment tests.

2 RELATIONSHIP BETWEEN A/C TEST AND EQUIPMENT TEST

2.1 Predictions

The aim of an equipment test is to subject an item of equipment to transients that are representative of those that the equipment will experience when installed in an aircraft that is struck by lightning. The test may be in the form of a pin test where voltages and currents are applied between the individual pin inputs of the unit and the unit case or where a current is injected into a loop formed by the cable bundle connecting the equipment under test (EUT) and another item of equipment forming part of an avionics system and to the current return formed by either the test bench or the airframe. This paper is concerned with cable tests on simple equipment configurations such as those addressed by DO160C where the EUT and other items of equipment are connected together by a single cable loom. Often cable looms will be quite complex and have branch points; the current distribution in the cable harnesses that will occur in a lightning strike to the aircraft will be quite different from the distribution obtained by injection into single branches of a system on a test bench. This problem is not addressed in the paper but is being investigated in a further program of research.

Initially we consider aperture coupled voltages. Figure 1 shows a schematic representation of the mechanism for inducing voltage on an open circuit loop exposed to aperture flux in an aircraft and the current in the same loop if it is shorted to the airframe. If the shorted loop consists of a cable screen which has a negligible resistance then there will be no net magnetic flux threading the loop. Using the principle of superposition we can represent the shorted loop configuration as a sum of the two circuits shown in Figure 2.

FIGURE 1

Schematic circuits for open circuit voltage and short circuit current measurements

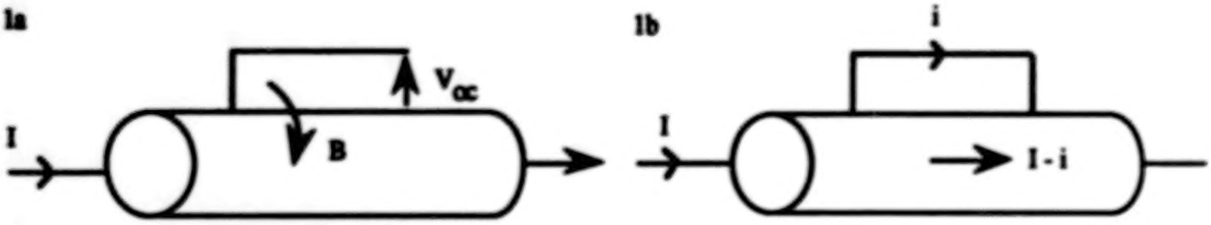

I is lightning current passing through airframe.
V is voltage measured across open circuit loop.
i_{oc} is current measured when the loop is shorted to the airframe.
B is the magnetic flux threading the loop

FIGURE 2

Representation of circuit 1b by sum of two circuit configurations

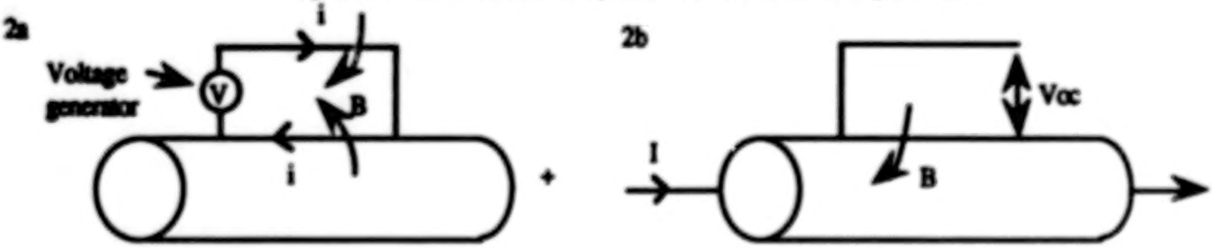

The second diagram is simply the lightning current flowing through the airframe when the cable loom is not connected. However the first diagram is a circuit that represents an equipment test where a voltage is injected into the loop formed by the EUT, the cable harness, another item of connected equipment and the airframe as a return conductor. In order that the net magnetic flux is zero and the current in the loop is i when the two configurations are summed, the voltage applied to circuit 2a will be equal to the Vo/c in 2b.

Hence an important parameter in an equipment test is the voltage applied across the loop under test which is equivalent to the Vo/c threat measured in an aircraft test or predicted by electromagnetic modelling.

Practically, for ground plane injection (GPI) tests the voltage can simply be measured by connecting a high impedance voltmeter across the loop under test and for cable injection tests by the voltage measured on a tightly wound monitor loop on the injection transformer.

What is the current flowing in the shorted loop in the equipment test or in the aircraft?

The open circuit voltage V_{OC} in Figure 2b, is given by:

$$V_{OC} = M_{TF} \frac{dI}{dt}$$

where M_{TF} is the mutual transfer inductance between the airframe and circuit.

Neglecting any resistance in the shorted loop, the voltage across the loop in Figure 2a causes a current to flow given by:

$$V = L \frac{di}{dt}$$

where L is the self inductance of the loop.

But we have already shown $V = V_{OC}$.

Therefore $$\frac{di}{dt} = \frac{M_{TF}}{L} \frac{dI}{dt}.$$

Integrating $$i = \frac{M_{TF} I}{L} = \frac{V_{oc} I}{L \, dI/_{dt}}. \qquad (1)$$

The differential and integral quantities in the equation can be mixed providing that each of the two differential and integral quantities are taken at the same time.

Hence the maximum current in the loop is defined by the waveform shape of the driving waveform, the $V_{o/c}$ and the inductance of the circuit loop. For the lightning current Component A waveform (see AC20-136 Reference 1) the maximum current I = 200kA (at t = 6µs) and the dI/dt = 140kA/µs (at t = 0+) hence the maximum loop current i is given by:

$$i = \frac{1.43\,\hat{V}}{L}$$ where $\hat{V}$ is the maximum induced o / c voltage measured at t = 0+.

where $\frac{I}{\frac{dI}{dt}}$ is 1.43µs and L is in µH. (For consistency of units M_{TF} is also in µH.)

Other factors will apply for other waveform shapes eg, Component D will have a factor of 0.71µs.

While for a particular geometry of cable installation there will be a fixed "voltage threat" which is due to the cables exposure to aperture flux, the "current threat" will depend also on the inductance and resistance of the cable harness/equipment loop.

Restricting the discussion to screened cables, the voltage at the equipment pin, which is what we are ultimately trying to achieve in the equipment test is given by:

$$V_{pin} = i Z_T$$

where Z_T is the total transfer impedance of the cable screen (strictly speaking this is a function of frequency but below about 1MHz is approximately equal to the screen resistance for coaxial screens).

Alternatively $V_{pin} = \frac{1.43\,\hat{V} Z_T}{L}$

But $Z_T = Z_0 \ell$

and $L = L_0 \ell$.

where Z_0 and L_0 are the transfer impedance (in ohms) and inductance (in µH) per unit length of the cable and ℓ is the total length through which current is flowing.

Therefore $V_{pin} = \frac{1.43\,Z_0}{L_0}\hat{V}$, which is independent of cable length. (2)

$= Z_o \ell i$, which is dependent on cable length. (3)

Hence if we do an equipment test and drive to a notional voltage limit, the voltage at the equipment pin is independent of cable length whereas, if the test is driven to a current limit the V_{pin} achieved is a function of length. It should be noted that in this analysis where the resistance of the cable is assumed negligible, the waveform of V will be the differential of the current waveform. These will follow waveforms 2 and 1 of AC20-136 respectively.

The magnitude of the pin voltage is simply related to current and the cable harness characteristics in equation 3 and thus driving to current limit represents an adequate method of achieving particular V_{pin} levels if the current flowing along the cable harness used in the test results in the same value of the product of current and cable length as in the aircraft.

The magnitude of maximum pin voltages can also be related to the maximum open circuit voltage using equation 2, this is independent of cable length but is dependent on cable inductance and as the pin voltage follows the cable screen current in form it is important that the voltage driving waveform in the equipment test follows waveform 2 well. The inductance of a cable above a return conductor is a logarithmic function and not very sensitive to separation above the conductor. However deviations from the waveform 2 shape have more important effects as will be shown in the next section.

2.2 Data

Measurements of $V_{o/c}$ and current in the shorted circuit were made using a 5m long cable installed in an aluminium fuselage with several apertures. A double exponential current waveform of 30kA was injected into the airframe. Using the same test set up, equipment tests were made using the GPI technique into the cable bundle. The set up is shown in Figure 3. The cable aircraft loop had a self inductance of about 3µH and a resistance of 37mΩ.

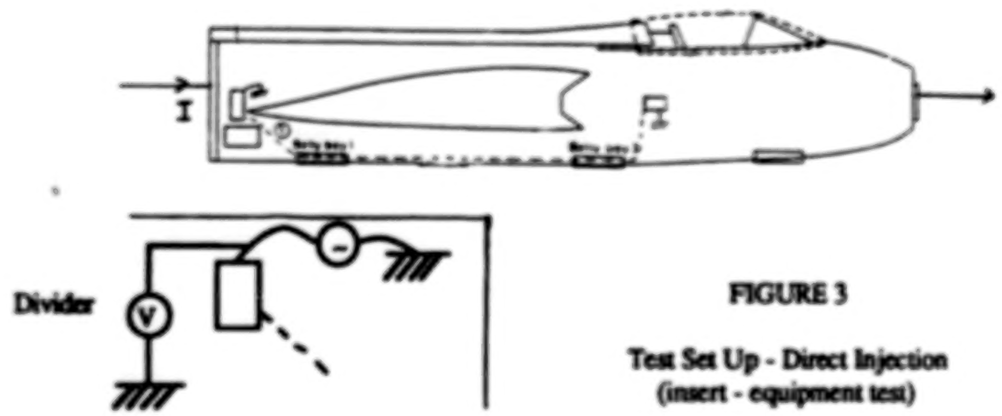

FIGURE 3

Test Set Up - Direct Injection
(insert - equipment test)

Waveforms of driving current and open circuit voltage for direct injection of current into the fuselage are shown in Figure 4. The open circuit voltage is complicated by air frame resonances, but the average value at time t=0+ can be evaluated. The open circuit voltage is 82 volts and the ratio of $I / \frac{dI}{dt}$ for the current waveform is 2.12µs.

The current when the loop was shorted was 37A and the shape was similar to the driving waveform (Figure 5). The maximum current occuring in the loop according to the prescription of equation 1 is 2.12 x 82/3 = 58A compared to 37A measured which is within 4dB.

We then performed an equipment test by disconnecting the EUT from the airframe and inserting our Waveform 1 current generator between the EUT and the airframe (see inset on Figure 1). The voltage is monitored on the high voltage potential divider and the current measurement used was the same current transformer as in the direct injection tests. The power level was increased until the monitored voltage value was near to 82V, the value obtained in the direct injection test. The waveforms of bundle current and monitored voltage waveforms are shown in Figure 6. For the same value of monitored voltage as open circuit voltage, the current is 85A (78.5 x 82/76). This value is considerably higher (7dB) than the value of 37A measured during the direct injection tests. As noted above we have to account for the different rise time of the voltage waveform of the equipment test. Reference to the Voc and monitored voltage waveforms in Figure 4b and 6 respectively reveals the voltage impulse of the equipment test is considerably slower. The rise times are about 100ns and 1000ns and zero cross times are about 7 and 12µs respectively. As the current is proportional to the integral of the voltage impulse we expect the equipment test to give a larger current for the same peak voltage. A circuit analysis program showed that the slower waveform of the equipment test gives a factor 2 larger current accounting for the observed difference between the peak current measured in aircraft and equipment test for the same open circuit voltage (Figure 7). Hence after the difference in voltage impulse shapes has been accounted for, the currents in both direct injection and equipment tests will be the same.

3 IMPLICATION ON GENERATORS FOR EQUIPMENT TESTS

The analysis of the configuration discussed above showed that the equipment test can be simulated by a voltage generator of zero source impedance (Figure 2a). This idealised generator will give either a voltage waveform 2 across a high impedance load or a waveform 1 current into a purely inductive load. For circuits with an L/R ratio intermediate between these two extremes an intermediate response will be obtained though in practice only for a small range of values of L/R = 1 will these intermediate responses be obtained. Generally the usual values of L/R give responses approximating either waveform 1 current or waveform 2 voltage.

Some of the earlier drafts of DO160C and indeed appendix IV of AC20-136 implies specific source impedances for the generator; 5Ω for waveform 2 and 4, and 25Ω for waveform 3. This section of the paper shows that these requirements are incompatible with the idealised response discussed above.

3.1 Waveforms 1, 2 and 3

One way of satisfying the 5Ω source impedance requirement is the generator indicated in the diagram below (Figure 8a):

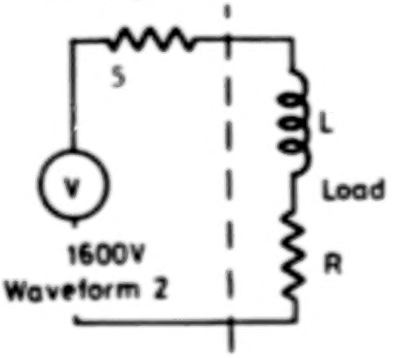

FIGURE 8a
Circuit diagram of 5Ω generator

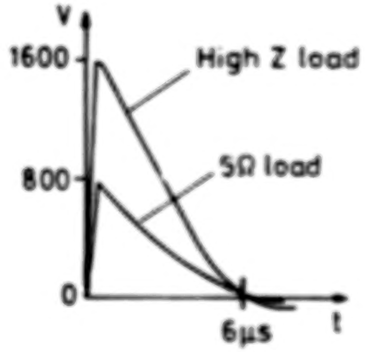

FIGURE 8b
Output response of circuit of Figure 8a on calibration loads

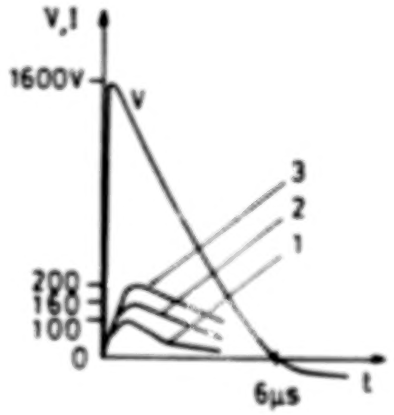

FIGURE 8c
Output of circuit of Figure 8a on a variety of loads

TABLE 1

			5Ω Generator			0Ω Generator		
R Ω	L μH	L/R μs	I Amps	t rise μs	Curve No. in Figure 8c	I Amps	t rise μs	Curve No. in Figure 9b
5	3	.6	100	0.8	1	200	1	1
1	3	3	160	1	2	400	2	2
37mΩ	3	81	200	1	3	760	6	3
37mΩ	1.5	41				1.54kA	6	4

The waveforms of the voltage obtained with such a generator across high impodance loads and a load of 5Ω are shown in Figure 8b. Using this generator into a variety of loads with different values of L/R gives responses as shown in Figure 8c. Corresponding waveforms that would be obtained with the ideal generator are shown in Figure 9 This does not satisfy the calibration requirement with a 5Ω load but gives the desired range of current waveforms, in the limit giving a waveform 1 current into a purely inductive load; on the other hand the 5Ω generator cannot achieve the correct waveshapes or levels for a particular value of monitored voltage. The magnitudes are compared in Table 1.

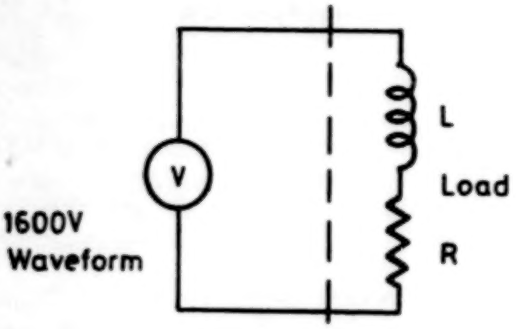

FIGURE 9a
Circuit diagram of 0Ω
source impedance generator

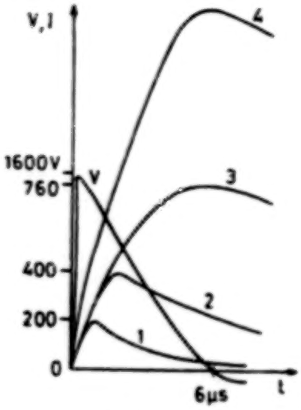

FIGURE 9b
Output of circuit of Figure 9a
on a variety of loads

While we do not address particular generator designs in this paper, we note that the generator design proposed in DO160C (published Reference 2) has a low source impedance and gives reasonable responses. The main point is that the waveform achieved into the load is the important consideration, not the generator source impedance. For example, a voltage waveform into 1000Ω impedance could be achieved with a generator with a source impedance of 50Ω.

At Culham for generating current waveforms, we have some particular generators with a high source impedance which drive the same shape current waveform regardless of the load impedance. For these generators, it is very important to monitor the voltage across the loop to prevent the loop being stressed too highly.

Waveform 3 which is also excited by aperture flux shows similar trends but the response is no longer purely inductive when the frequency is greater than or equal to the first cable resonance.

3.2 Waveform 4 and 5

For induced voltages in resistive structures such as those made from carbon fibre composite (CFC) the situation is complicated by current redistribution effects. In this case the driving voltage around a cable harness loop is due to resistive drop (waveform 4) generated in the CFC by lightning current flowing through the structure but this voltage will fall faster than the current as it redistributes from the resistive structure into the low resistance of the cable screen after peak dI/dt. The mathematical analysis is thus more complex but we can still use the same trick as in Section 2 by representing the configuration by the sum of two simpler ones as below in Figure 10.

FIGURE 10

Representation of resistive voltage mechanism by two circuits.

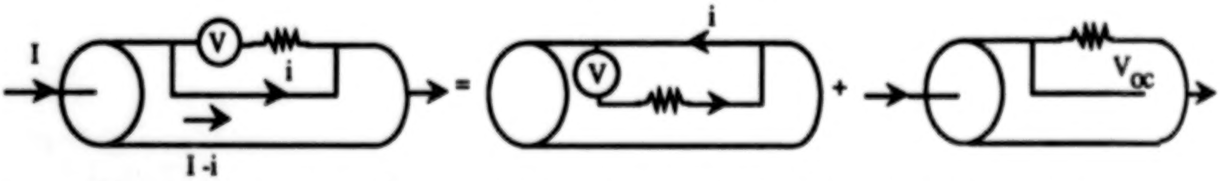

Hence the ideal waveform 4 generator will have a source impedance equal to the resistance of the structure between cable connection points. Typically this would be 10 →100mΩ. A circuit analysis program was used for a series of loads. Table 2 and Figure 11 show the results. We note that the characteristic waveform 5 shape is produced into a predominantly inductive load. A comparison of Table 1 and 2 and Figures 9b and 11 shows that for the same voltage level threat and same cable bundle, a waveform 4 voltage will produce a much larger waveform 5 current thanwaveform 2 voltage produces a waveform 1 current due to the relative width of the voltage impulse.

The current levels for waveform 1 and 5 chosen to correspond to the voltage levels of waveform 2 and 4 are indeterminate as they depend on cable inductance. The value will determine a value of inductance below which the current level will be reached first and above which the voltage level will be reached first.

TABLE 2

RΩ	I kA	t rise µs	Curve No.
1.5	1	6	1
150mΩ	8.4	40	2
37mΩ	23	60	3

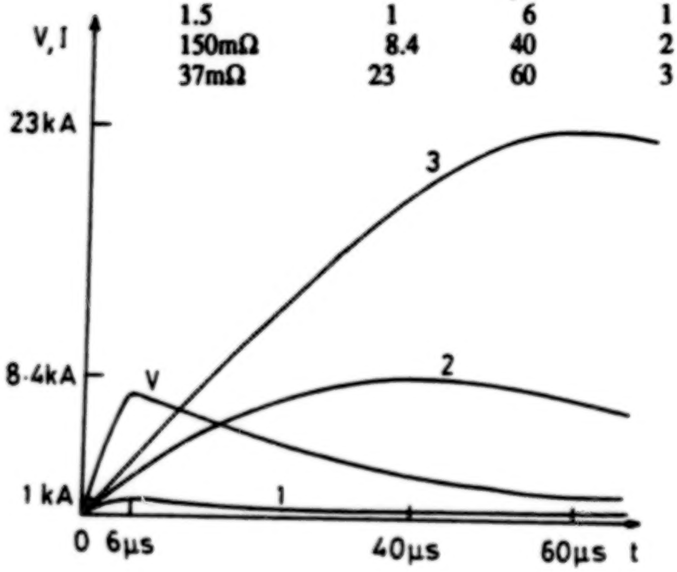

FIGURE 11
Response of a variety of circuits to a waveform 4 low source impedance generator

4 CONCLUSIONS

1. The open circuit voltage measured in an aircraft test is equivalent to the monitored voltage across the loop under test in an equipment test.
2. The current that would result in this loop when shorted to airframe return has a value which can be determined from the amplitude and shape of the driving waveform and the self inductance of the loop.
3. Circuit analysis has shown the impedance requirements of an ideal generator for achieving waveform 1/2 and 4/5 waveforms into any load. These requirements are not satisfied by the 5Ω values implicit to Appendix 4 of AC20-136. The current levels suggested by AC20-136 are thus also misleading. Actual current levels associated with the voltage levels are dependant on cable resistance and inductance.
4. For simple cable configurations adequate test levels at the equipment pin can be achieved with a test to a known Voc voltage limit if the monitored voltage waveform follows accurately the waveform 2 shape or with a test to a known current test level if the product of current and cable transfer impedance is the same as in the aircraft.

5 REFERENCES

1. FAA AC 20-136, Protection of Aircraft Electrical/Electronic Systems against the Indirect Effects of Lightning, 1991.
2. RTCA DO160C/ED 14C, Environmental Conditions and Test Procedures for Airborne Equipment, Section 22. 14th February 1990.

6 ACKNOWLEDGEMENTS

The authors would like to acknowledge financial suport from the Culham Lightning Club; comprising: British Aerospace, Rolls Royce, Westlands, CASA, SAAB, Shorts, CAA, DTI.

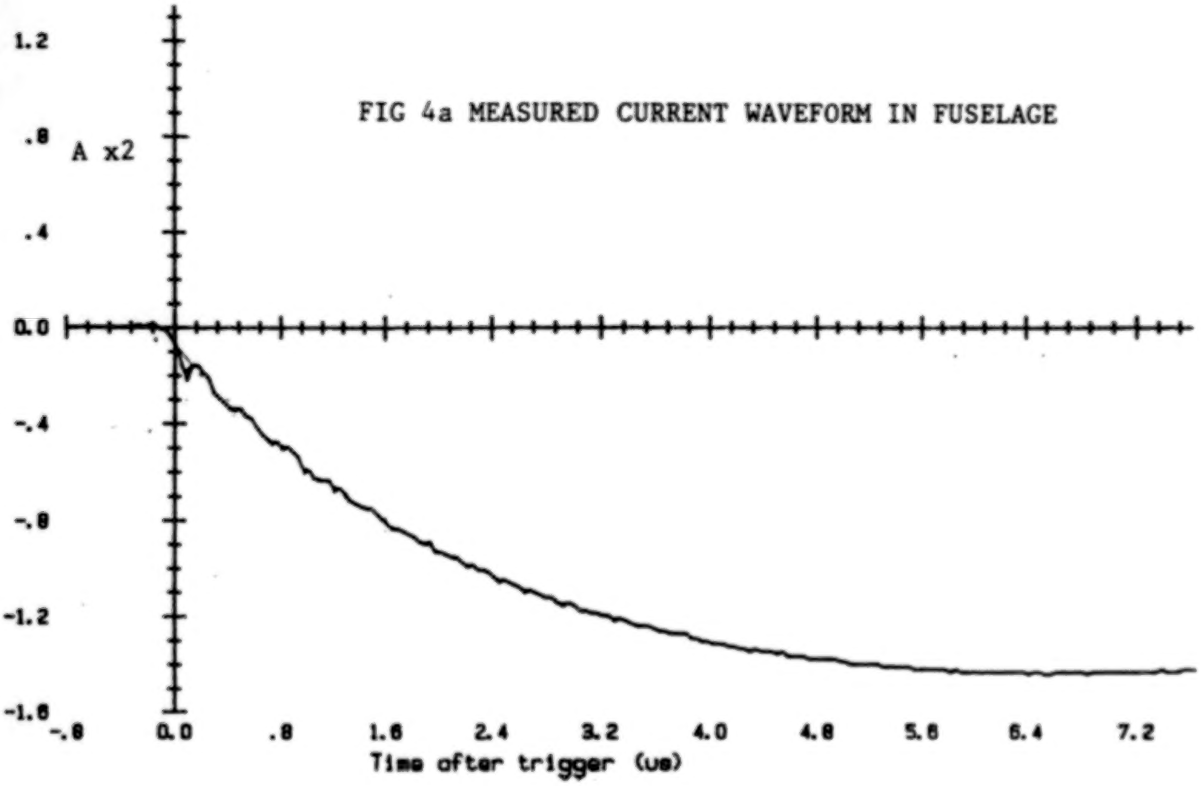
FIG 4a MEASURED CURRENT WAVEFORM IN FUSELAGE

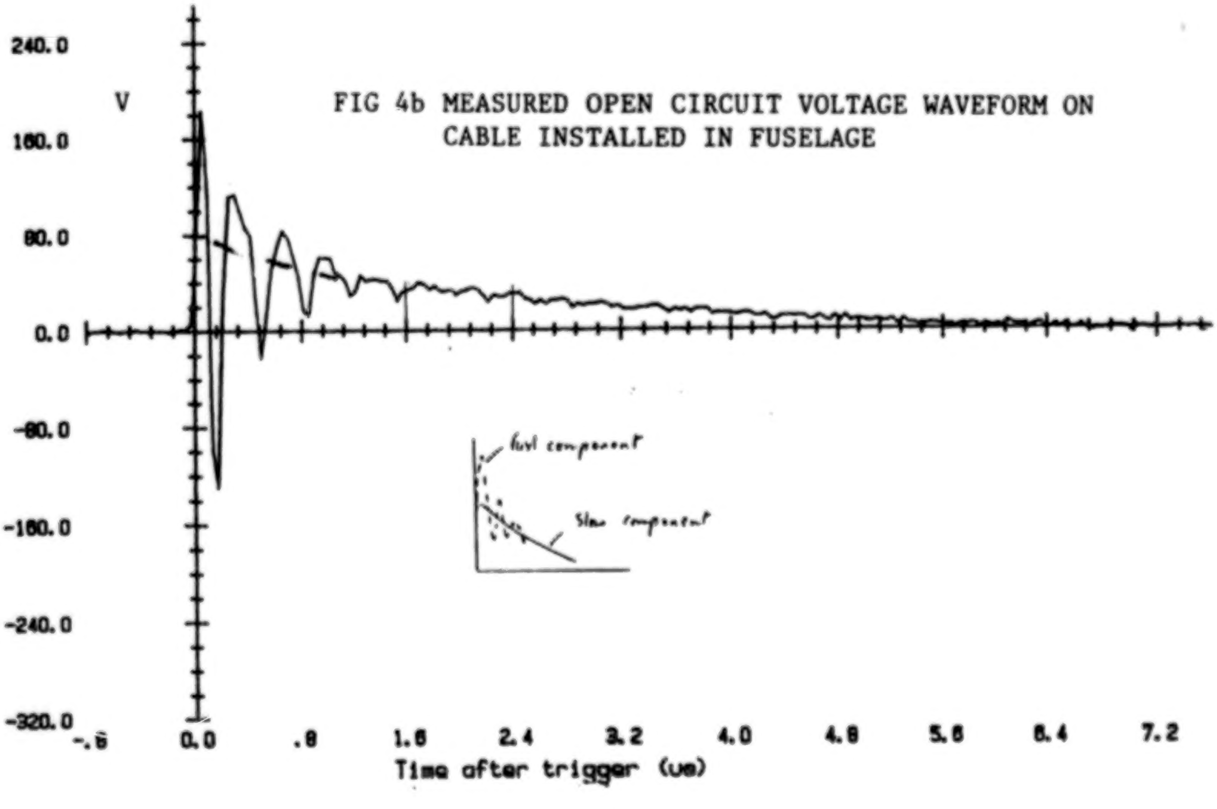
FIG 4b MEASURED OPEN CIRCUIT VOLTAGE WAVEFORM ON CABLE INSTALLED IN FUSELAGE

FIG 5

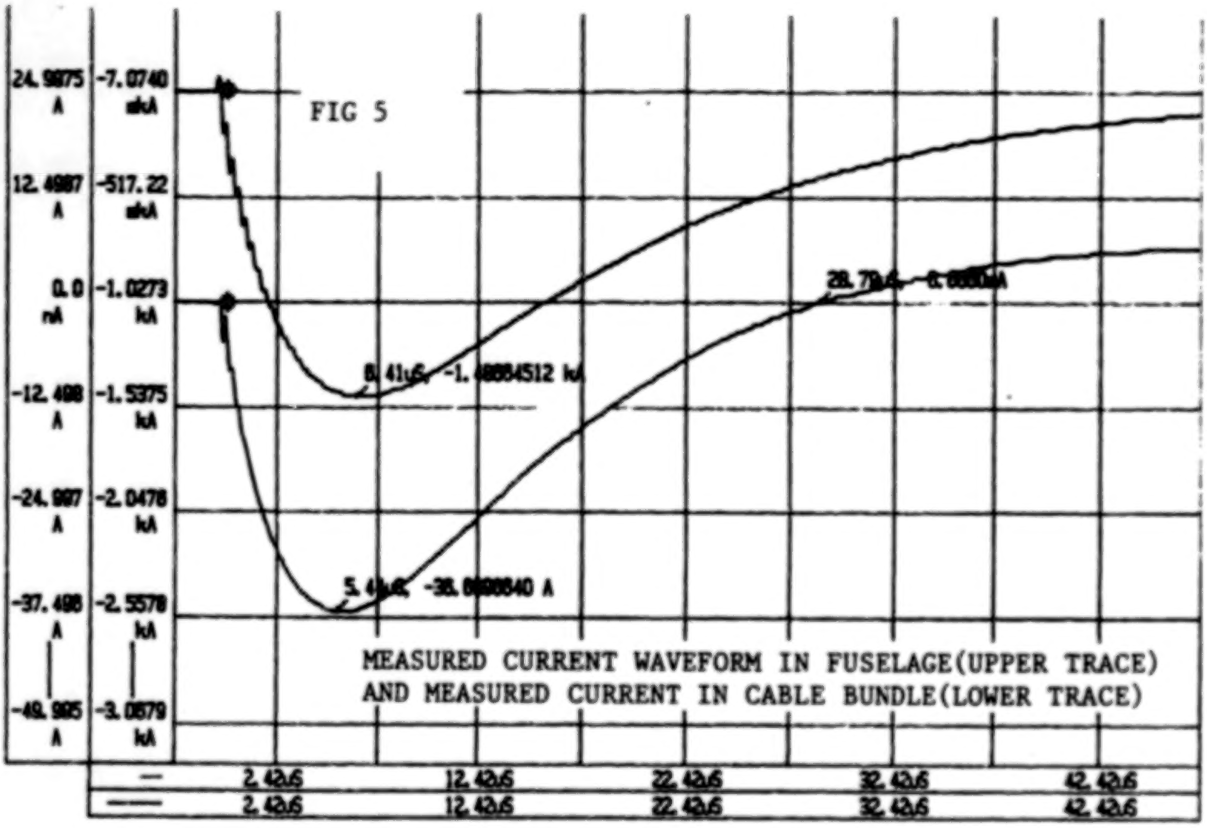

MEASURED CURRENT WAVEFORM IN FUSELAGE(UPPER TRACE)
AND MEASURED CURRENT IN CABLE BUNDLE(LOWER TRACE)

FIG 6

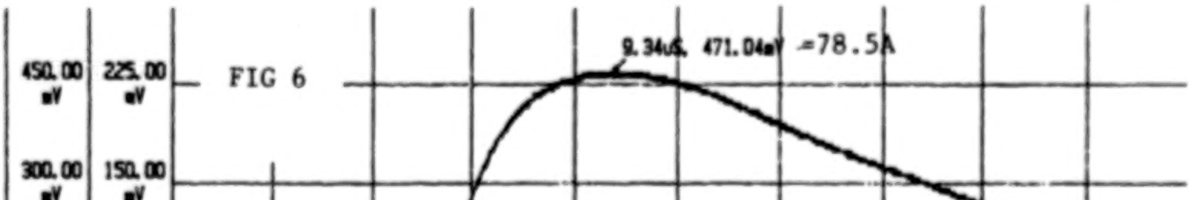

EQUIPMENT TEST WAVEFORMS:
BUNDLE CURRENT(UPPER)
DRIVING VOLTAGE(LOWER)

FIG 7 COMPUTER CIRCUIT ANALYSIS FOR CURRENT ASSOCIATED WITH PARTICULAR VOLTAGE WAVEFORMS ACROSS A LOOP CONSISTING OF A 37mΩ RESISTANCE & A 3μH INDUCTANCE

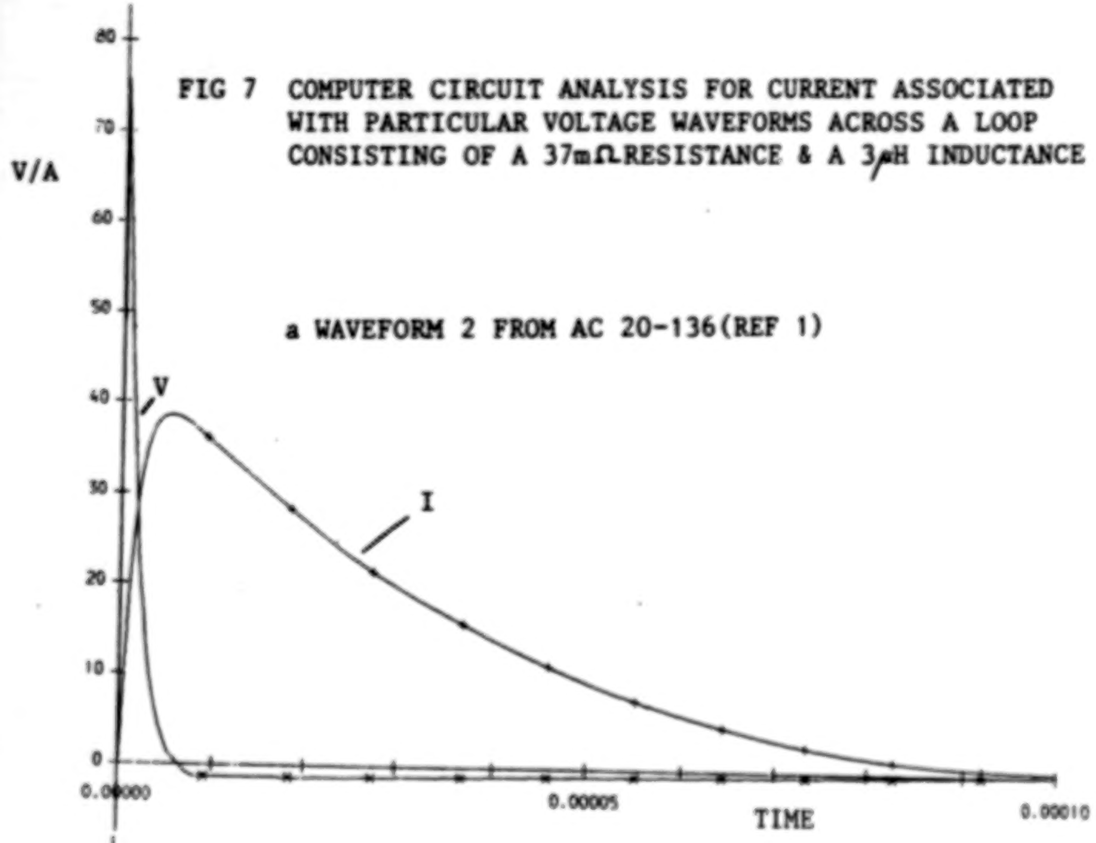

a WAVEFORM 2 FROM AC 20-136(REF 1)

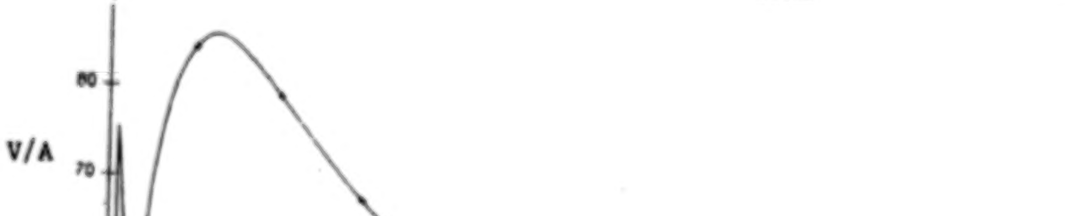

b EXPERIMENTAL WAVEFORM FROM EQUIPMENT TEST PULSER

Session 8A, Wednesday 3:45
Aerospace Vehicles
Structures and Materials 3
Walker, Chairman

DAMAGE TO METALLIC SAMPLES PRODUCED BY MEASURED LIGHTNING CURRENTS

Richard J. Fisher and George H. Schnetzer
Sandia National Laboratories
Albuquerque, NM 87185

ABSTRACT

A total of 10 sample disks of 2024-T3 aluminum and 4130 ferrous steel were exposed to rocket-triggered lightning currents at the Kennedy Space Center test site in Florida during the summer of 1990. The experimental configuration was arranged so that the samples were not exposed to the preliminary streamer, wire-burn, or following currents that are associated with an upward-initiated rocket-triggered flash but which are atypical of naturally initiated lightning. Return-stroke currents and continuing currents actually attaching to the sample were measured, augmented by close-up video recordings of approximately 3 feet of the channel above the sample and by 16-mm movies with 5-ms resolution. From these data it was possible to correlate individual damage spots with streamer, return-stroke, and continuing currents that produced them. Substantial penetration of 80-mil aluminum was produced by a continuing current of submedian amplitude and duration, and full penetration of a 35-mil steel sample occurred under an eightieth percentile continuing current. The primary purpose of the data acquired in these experiments is for use in improving and quantifying the fidelity of laboratory simulations of lightning burnthrough.

INTRODUCTION

Laboratory simulation of lightning arc effects has long been used in both engineering development studies and qualification testing. Such testing is widely employed throughout the aerospace industry, usually according to the SAE Committee AE4L lightning test specifications [1], MIL-STD-1757A [2], or some derivative thereof. In these documents, the components of the test currents to be applied are specified in considerable detail, and their physical correlation with corresponding components of natural lightning flash currents is established. However, when it comes to the details of test electrode geometry, spacing, and materials, these specifications are decidedly more vague and indicate no apparent basis for quantitative correspondence with actual lightning.

It is well known that erosion and penetration of metallic test materials during laboratory simulations is sensitive not only to the applied test current but equally so to the specifics of electrode geometry and materials. References 1 and 2, for example, include cautionary notes and qualitative guidance for mitigating against these sensitivities. In a series of preliminary burnthrough experiments performed during 1988 using the Sandia Lightning Simulator (SLS)[1], the sensitivity of test results to test configurational parameters was observed to be pronounced. That is, for the same applied simulated return-stroke/continuing-current composites, the damage that resulted on identical aluminum and steel test specimens varied significantly as functions of the electrode configuration and arc length. These results and a subsequent cursory look into the literature served to stimulate a more in-depth consideration of the general issues of what should constitute the "proper" simulation technique for penetration testing and how to quantify the fidelity of that technique *vis-a-vis* results produced by natural lightning.

An extensive literature review was undertaken to determine the present general understanding of arc-to-metal interactions, particularly as relevant to the transfer of energy to an electrode surface [4]. Specific attention was focused on arc physics, especially as related to atmospheric, high current, long duration arcs; lightning channel and attachment physics and phenomenology; lightning simulation technology; and welding technology. The survey succeeded in providing the desired overview; but the wherewithal, either theoretical or empirical, with which to reliably quantify simulation fidelity was not forthcoming.

---

[1] The SLS is described in detail in Reference 3.

One pragmatic and rather straightforward approach was suggested by an experiment conducted by Uman [5] in 1964. During the course of a summer, he exposed a set of copper disks to lightning by mounting them atop a TV tower. The resulting damage spots provided a qualitative indication of the diameter of the lightning attachment spot, but, unfortunately, there were no means available for measuring the incident current that produced the damage. It followed that acquisition of similar data points correlated to the incident current that caused them would provide a reliable data base against which to calibrate the laboratory simulation. Successful replication of the spots in the laboratory would then constitute a definitive validation of the test technique. Electrode parameters and other aspects of the test configuration could be systematically varied until the best duplication was achieved. Under each variation, the applied current, particularly the continuing current, which is primarily responsible for producing burnthrough, would be tailored to correspond to the measured natural lightning that caused the individual spot in question.

During the summer of 1990, such an experiment was performed at the Kennedy Space Center (KSC) rocket-triggered lightning test site in Florida. Disk samples of nominal 80-mil-thick 2024-T3 aluminum and 35-mil-thick 4130 ferrous steel were exposed to fully recorded return-stroke and continuing currents. The remainder of this paper describes the experiment and the data that were acquired.

INCIDENT LIGHTNING CURRENT

For these experiments, the rocket and wire dispensing assemblies developed by the Centre D'Etudes Nucleaires de Grenoble (CENG) in France were employed [6]. There are several variations of these systems. The one employed here, called LRSG (for lightning rocket system, grounded), incorporates a 2100-ft length of wire that is tied to earth ground at the bottom of its launch tube. The typical flash current that results from this system is illustrated schematically in Figure 1.

There are certain features of this current that depart from those of a naturally initiated flash, most notably the presence of the few hundred milliseconds of low-level initial continuous current (ICC) that precedes the first return stroke. A second, more subtle difference is that the first return stroke of the triggered flash is thought to be most often initiated by a dart, rather than stepped, leader and is otherwise typical of a subsequent return stroke of a purely natural flash [7]. From the viewpoint of the objectives of the present experiment, however, this latter issue is of no practical consequence. This is so because, in a metal of any appreciable thickness, virtually all penetration is due to the intermediate and continuing-current components of the flash current, which in triggered flashes fall well within the statistical envelopes of their counterparts in purely natural flashes.[2]

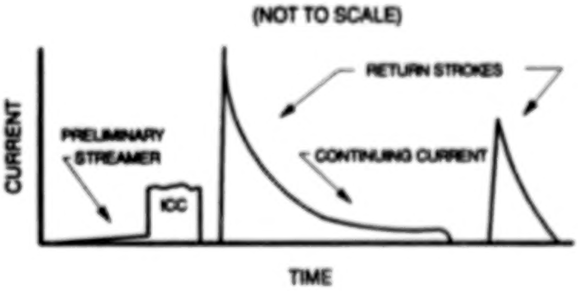

Figure 1. Typical Rocket-Triggered Lightning (RTL) Flash Current

---

[2] It is postulated that, in some instances, the shock wave associated with subsequent strokes following significant continuing currents may contribute to material erosion by splashing away molten material. However, since there are no significant differences between subsequent strokes of triggered and naturally initiated lightning, this effect should be faithfully represented in the present results.

The ICC flows in the channel prepared by the vaporized wire that terminates on the launcher tube. The tube is grounded to earth potential via an array of stranded steel wire cables. As indicated in Figure 2, it was arranged that this portion of the current would not be intercepted by the test specimens so that interpretational complications associated with this component of the triggered lightning flash were avoided. The typical sequence following cessation of the ICC was that one or more return strokes, often with intervening continuing currents, would jump from the ICC channel and attach to the top of the sample, evidently because this path to ground presented a lower impedance than the decayed original channel. In this way the desired data spots created by individual return strokes and return-stroke/continuing-current combinations were acquired.

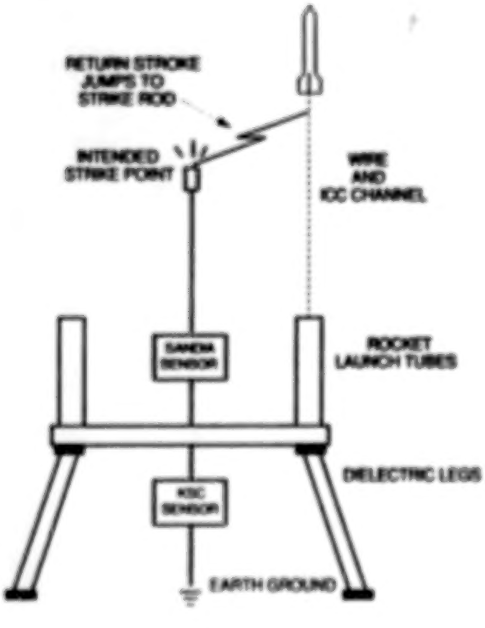

Figure 2. RTL Materials Damage Experiment Configuration

EXPERIMENT DESCRIPTION

Figure 3 shows the fixture in which the individual samples were held. The development of upward streamers from the edge of the brass fixture cup, which would lead to undesired attachments there, were suppressed by the presence of the dielectric sleeve of woven phenolic material. Two 0.5-in holes were provided in the dielectric shield to prevent the build-up of rain water over the surface of the sample. The entire arrangement was mounted on a 10-ft hollow aluminum pole, the bottom of which was tied by a 1.5-in braided ground strap to the input of a coaxial 0.5-mΩ current viewing resistor (CVR). In order to discourage the attachment of return strokes along its length, the pole was encased in PVC pipe of ~0.2-in wall thickness from just below the fixture cup to the bottom of the pole.

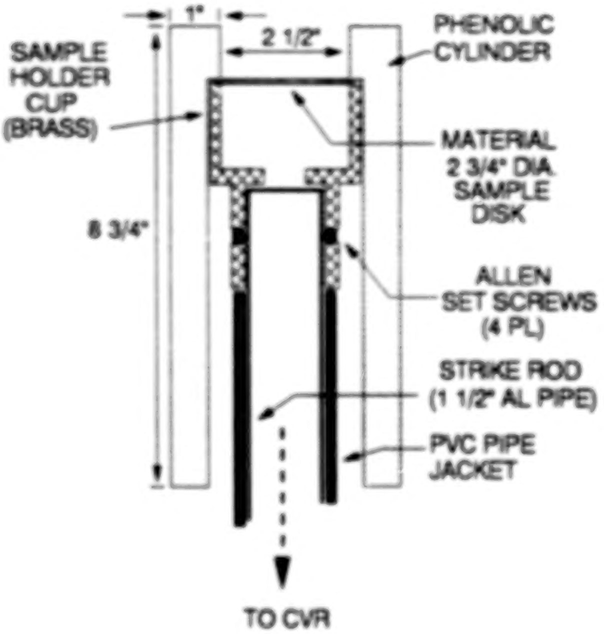
1"
2 1/2"
PHENOLIC CYLINDER
SAMPLE HOLDER CUP (BRASS)
MATERIAL 2 3/4" DIA SAMPLE DISK
8 3/4"
ALLEN SET SCREWS (4 PL)
STRIKE ROD (1 1/2" AL PIPE)
PVC PIPE JACKET
TO CVR

Figure 3. RTL Materials Damage Specimen Fixture

The potential data return during any triggering session was increased by arranging four identical poles and fixtures on a hinging mechanism so that they could be remotely raised and lowered sequentially during the course of a given storm. Figure 4 shows the hinging mechanism that was employed. A network of plastic ropes and metal pulleys led back to the instrumentation van to allow the raising and lowering of the samples. For safety reasons, two of the sets of pulleys over which the ropes passed were tied together and led to local grounds via braided strap. The eyebolts through which the ropes passed just outside the door of the instrumentation van were also electrically tied together and to the structure of the steel van so that the ends of the ropes were held at the same potential as the structure. The ropes were only operated between rocket launches, and only then after clearance from the rocket launch controller was received.

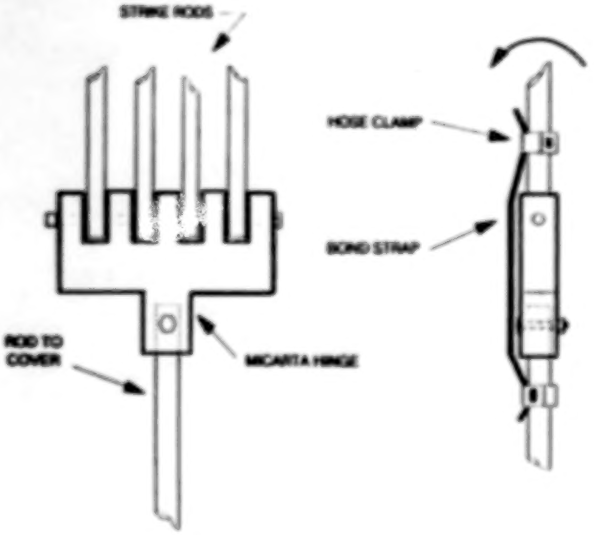

Figure 4. Hinging Mechanism for Raising and Lowering Test Specimens

INSTRUMENTATION

Measurement of the incident channel current was performed with the instrumentation provided by the Sandia Transportable Triggered Lightning Instrumentation Facility (SATTLIF), which is described in detail in a companion paper in these proceedings [8]. The voltage developed by the coaxial CVR described above was fed to two different fiber optic data links (FOLs) and transmitted to the SATTLIF for recording. In order to capture the return-stroke currents, one channel consisted of a NanoFast 300-2A FOL, followed by a 6-MHz filter and LeCroy 9400A digitizing oscilloscope. Overall bandwidth of the system was set by the 164-ns rise time of the CVR. The digitizer was operated in the segmented memory mode at an 80-ns sampling rate. This permitted the capture of the first 200 μs of up to eight individual return strokes per flash. A trigger threshold of 1000 A was chosen. The NanoFast FOL transmitter is provided with an internal calibration signal generator, and a cal record was recorded prior to each test event as part of the countdown checklist. The return-stroke signals were also backed-up on a 1-MHz direct-record magnetic tape recorder channel. Return-stroke measurements obtained with this instrumentation compared well with those made by KSC personnel with their own system, the sensor of which was in series with the Sandia CVR (Figure 2). A comparison of the common data is given in Reference 8.

More important to the objectives of these experiments was the measurement of the low-level, long-duration continuing currents. These were recorded via a second channel that consisted of a 1-MHz Dymec frequency modulated (FM) FOL playing into both a 500-kHz FM Ampex PR2300 magnetic tape recorder and two LeCroy 9400A digitizer channels. The sensitivities of the two digitizer channels were staggered, and a 2-A continuing-current resolution was achieved. The digitizer was operated in the single segment mode with a 40-μs sampling rate. The Dymec channel provided a dc to 500-kHz bandwidth and was found to perform extremely reliably throughout the course of the fielding period. A pneumatically actuated pulse calibration signal was provided at the input of the Dymec transmitter so that an end-to-end calibration signal could be recorded prior to each test event. The associated LeCroy channel was triggered at a level corresponding to 1000 A.

Two photographic systems were also employed. One was a Super VHS black and white video system that was zoomed to capture a 3-foot distance above and below the erected sample. The main function of this recording was to aid, immediately following the event, in determining whether or not the erected sample had been struck, so that a decision could be made as to whether or not to exchange it for a fresh one. The lens was operated at its minimum aperture (f/22), and neutral density filters were added to provide up to an equivalent of eight additional f-stops. These records are thought to represent the closest known photographs of lightning attachment points, and they reveal some interesting streamer behavior that is presently being analyzed in detail.

The time resolution of the video records is limited by the VCR framing rate to ~30 ms. In order to provide a resolution sufficient to separate individual return strokes within a flash, a 16-mm film cinematic framing camera was also operated. The field of view was adjusted to cover the entire experiment tower, and a framing rate of 200 fps was chosen, providing a 5-ms resolution. The records obtained with this camera were of critical importance in sorting out where each stroke terminated. Analysis on a frame-by-frame basis and comparison with the various current records ultimately enabled the correlation of individual damage spots on the samples with the specific return strokes and continuous currents that caused them.

DATA AND DISCUSSION

Data spots on a total of six aluminum and four steel samples were obtained during three separate storms occurring on August 8, 9, and 11. Several of the more interesting examples are presented below. A fuller presentation and discussion of the data are available in Reference 9.

Figure 5 shows a photograph of the aluminum sample exposed to Flash 90-02 and a plot of the corresponding flash current recorded by the 500-kHz Dymec channel. These data illustrate the importance of the cinematic films. The sample exhibits numerous small surface marks clustered near the center. These correspond to upward-going streamers, which were recorded during several events by the close-up video system. Aside from those, there is a single significant spot, identified as RS#8 in Figure 5a. In this case, the cinematic film clearly revealed that the wind carried the ICC channel across the fronts of three samples that were lying horizontal prior to being raised for exposure. As a result, the first seven strokes attached to one of the horizontal samples, while only the last stroke attached to the erected one, thereby creating the data spot shown in the figure.

The stroke that hit this sample had a peak current of 13 kA. A charge of 7.6 C was transferred by the continuing current, which lasted approximately 50 ms. The spot is a raised mound of crystalline material of 0.16-in diameter and 0.002-in height above the flat surface. There is a pinhole in the center of the mound with a depth of approximately 0.002 in below the flat surface. Such an isolated spot, caused by an unambiguously known current, represents precisely the sort of data that was sought.

The two most dramatic results are indicated in Figures 6 and 7. Flash 90-03 consisted of two strokes, both of which were confirmed photographically to have hit the top of the sample. The first stroke (I_p=13 kA) was followed by a continuing current that transferred ~13.6 C of charge at a sustained level of 100 A. The corresponding spot is evidently the large one (#1 in Figure 6a), which has a diameter of 0.3 in. Inside the spot is a 0.19-in-diameter raised mound of crystalline material of ~0.04-in height. This bead is surrounded by a crater of maximum depth of 0.001 in. There is no significant discoloration on the back side of the spot, but there is a 0.06-in-diameter round dot, very much like a single braille dot. Precise correlation of the other two major spots (#2 and #3) appearing in the photograph is more tenuous due to the clear photographic evidence that only two return strokes attached to the erected sample. Nevertheless, tentative correlation has been established based on a detailed examination of all the data and a rationale that is discussed in Reference 9.

Figure 7 corresponds to a 0.035-in thick steel sample. The three distinct overlapping spots have diameters of 0.33, 0.39, and 0.28 in, respectively, and the sample was fully penetrated at the center spot. Again, as confirmed by the film record, the first two strokes indicated in Figure 7b terminated on one of the horizontal samples. Only the current to the right of the indicated line attached to the top of the sample. The current consisted of a single return stroke and a rather severe continuing current. The large peak occurring at ~540 ms represents a large surge (peak of ~1500 A) riding on the established continuing current. Figure 8 shows the back side of the sample. The appearance of the melted material is different from that of the aluminum. It is not crystalline, and seems to have flowed smoothly. In several instances, the residue is silver and shiny, indicating some sort of chemical separation process of the alloy constituents.

Aside from their immediate utility in the process of quantifying simulation fidelity, the data offer additional points of interest. Consider Figure 7. The continuing current following the initial return stroke in Flash 90-03 had a duration of ~120 ms, a sustained current level of ~100 A, and a total charge transfer of 13.6 C. According, for example, to Cianos and Pierce [10], this amplitude and duration fall at approximately the thirtieth percentile points on their respective frequency distributions. The 13-C charge transfer falls at the twelfth percentile. That is, only the stated percentage of all continuing currents have smaller corresponding values. Thus, by any measure,

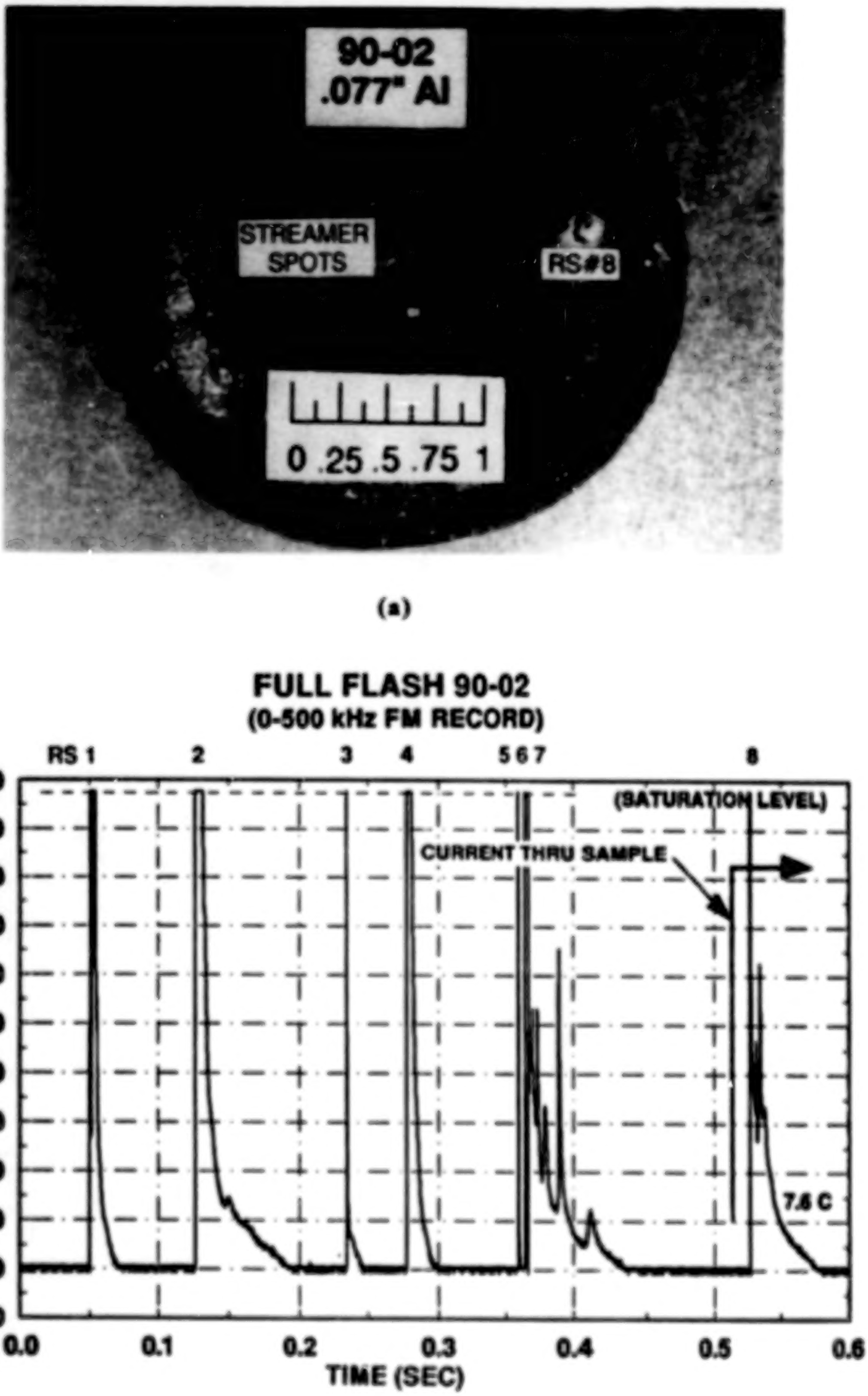

(a)

(b)

Figure 5. a) 80-mil-Thick Al Specimen Exposed on Flash 90-02 and b) Current Recorded on Same Flash

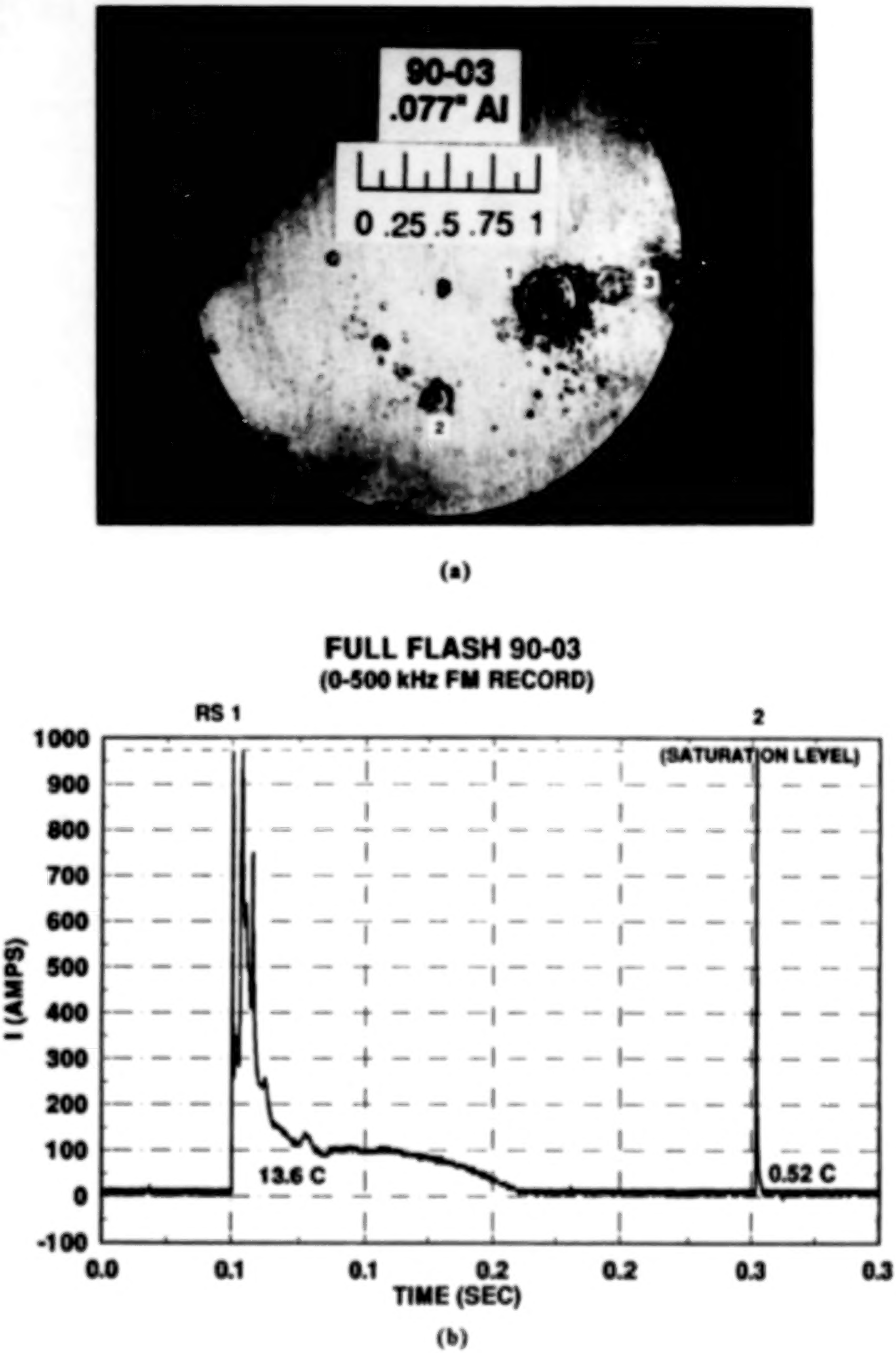

(a)

(b)

Figure 6. a) 80-mil-Thick Al Specimen Exposed of Flash 90-03 and b) Current Recorded on Same Flash

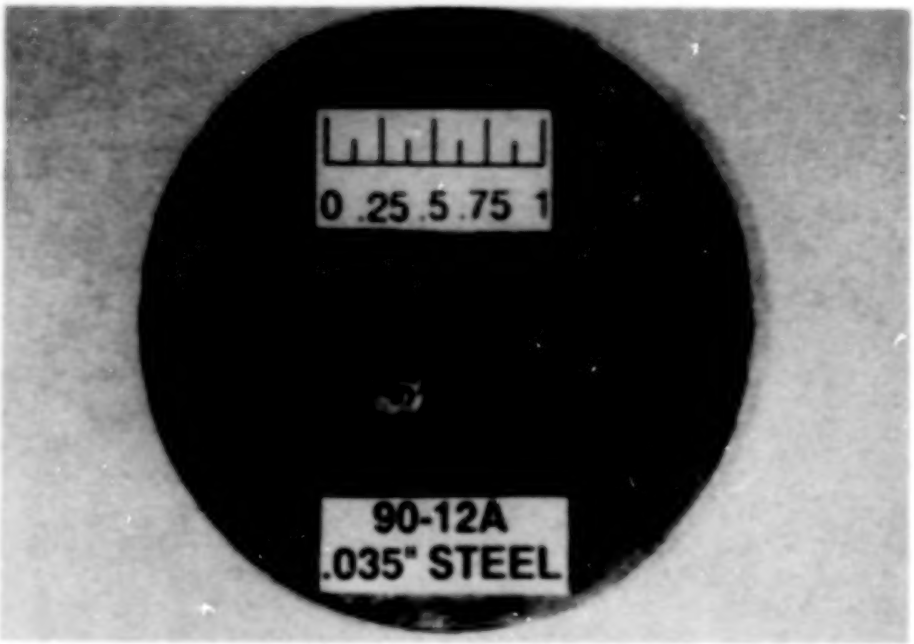
0 .25 .5 .75 1
90-12A
.035" STEEL

(a)

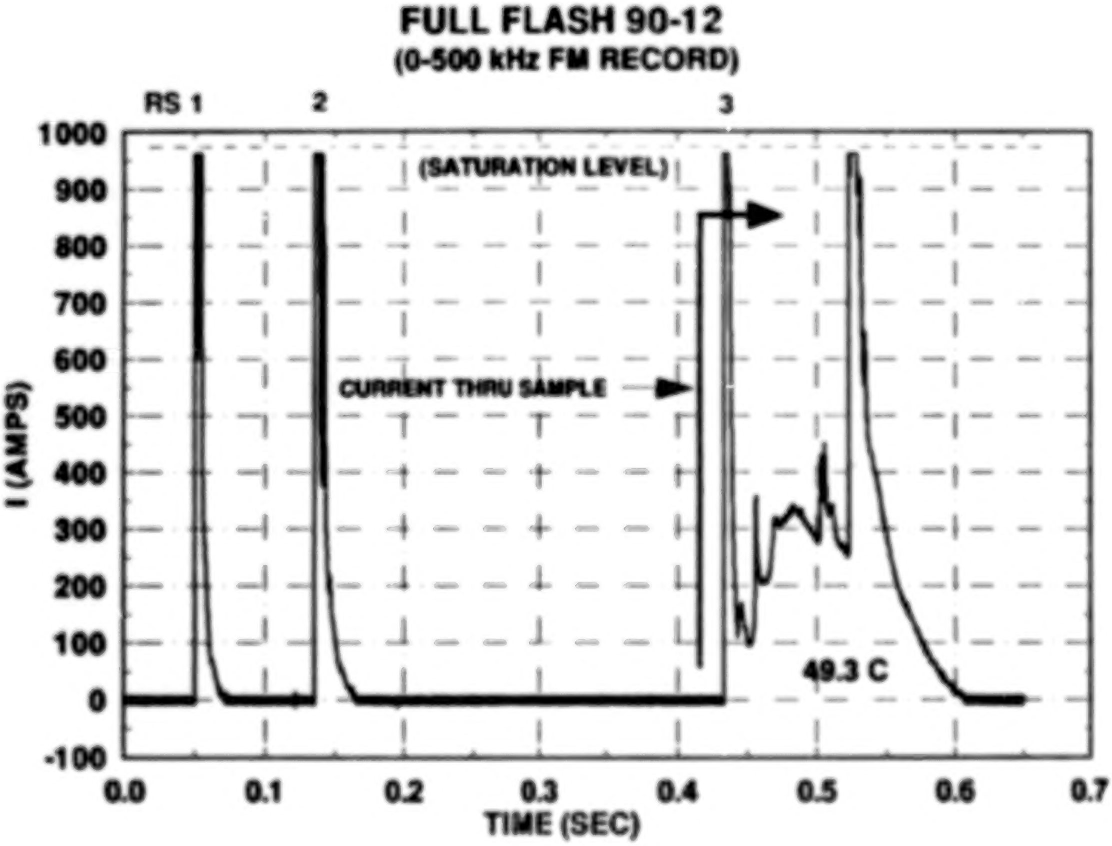

(b)

Figure 7. a) 35-mil-Thick Steel Specimen Exposed on Flash 90-12 and b) Current Recorded on Same Flash

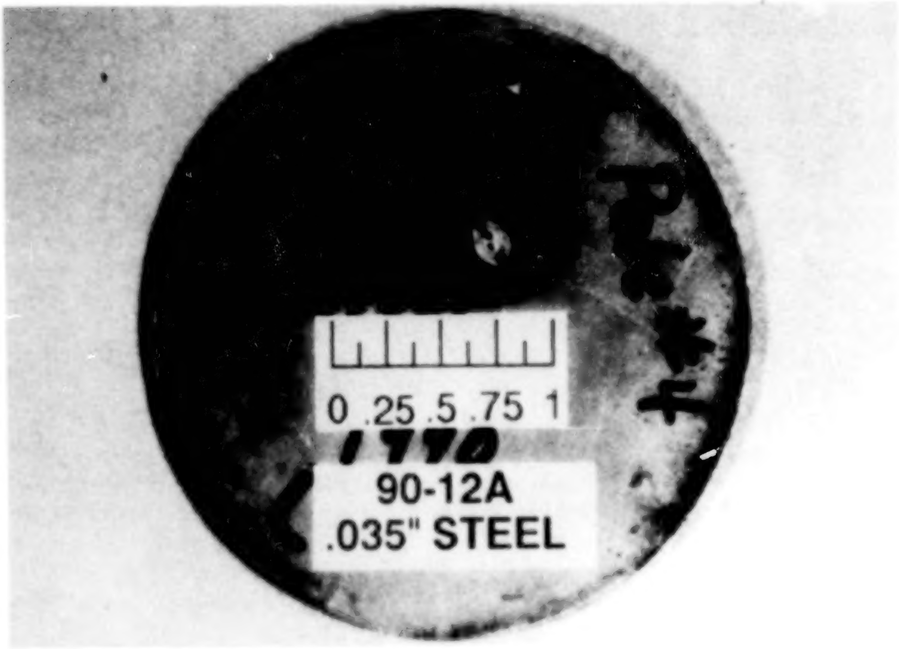

Figure 8. Back Side of 35-mil-Thick Specimen Exposed on Flash 90-12

90-03 represents a flash of very modest severity. It nevertheless produced significant damage on a material and thickness with wide practical aerospace applications, many with safety implications under nonflight conditions.

The 49-C charge transfer represented by the final stroke and continuing current indicated in Figure 7b corresponds to approximately the eightieth percentile level, according to the Cianos and Pierce model. It therefore ranks as a relatively severe, but by no means extreme, flash.

No destructive metrology on the samples is planned, at least until after the laboratory duplication efforts are completed.

CONCLUSIONS

Nine individual damage spots were acquired for which correlation with specific and measured return strokes or return-stroke/continuing-current combinations have been established with reasonable to excellent confidence. These data represent a reliable set of benchmarks against which the fidelity of laboratory simulation of lightning penetration can be improved and quantified, at least for aluminum and steel. This will be done by exposing identical samples in the SLS to the same currents as those that produced the benchmark spots. Simulator electrode and other test configurational parameters will be varied until the best replications are obtained. *Post-mortem* analysis of all the samples will then be used to quantify the achieved duplication in terms of erosion diameter and depth and relevant metallurgical factors. Additional benchmark data spots would be very valuable, both to augment the statistical base on the present materials and to widen coverage to other materials.

One particularly significant outcome of the present experiment is definitive confirmation of the possibility of burnthrough of aluminum of thickness in excess of 80 mil, under nonflight conditions, by continuing currents of median intensity or less.

ACKNOWLEDGEMENTS

The authors wish to express their appreciation to the Kennedy Space Center and Mr. William Jafferis for the opportunity to participate in their 1990 rocket-triggered lightning program. Particular thanks are due to Mr. Jafferis for his enthusiastic personal support of these experiments and to Messrs. Andre Eybert-Berard and Louis Barret of CENG for their cooperation in conducting the rocket operations. This work was jointly sponsored by the Department of Energy, by the Project Manager's Office of the Department of the Army, and by the U.S. Army Armament Research, Development, and Engineering Center (ARDEC).

REFERENCES

1. *Lightning Test Waveforms and Techniques for Aerospace Vehicles and Hardware*, Report of SAE Committee AE4L, June 20, 1978.
2. "Lightning Qualification Test Techniques for Aerospace Vehicles and Hardware," *MIL-STD-175A*, 20 July 1983.
3. White, R. A., "Full-System Tests Using the Sandia Lightning Simulator," *Proc. 1983 Int. Conf. on Lightning and Static Electricity*, April 1983.
4. Fisher, R. J., and M. A. Uman, *Simulation Fidelity in Lightning Penetration Studies*, SAND89-3051, February 1990.
5. Uman, M. A., *All About Lightning*, Dover (1986), pp 88-89.
6. Larouche, P., A. Eybert-Berard, and L. Barret, "Triggered Lightning Flash Characterization," *Proc. 1985 Int. Conference on Lightning and Static Electricity*, June 1985.
7. Uman, M. A., "Natural and Artificially-Initiated Lightning and Lightning Test Standards," *Proc. IEEE*, Vol. 76, No. 12, December 1988.
8. Schnetzer, G. H. and R. J. Fisher, "The Sandia Transportable Triggered Lightning Instrumentation Facility (SATTLIF)," *Proc. 1991 Int. Conf. on Lightning and Static Electricity*, April 1991.
9. Fisher, R. J., and G. H. Schnetzer, *1990 Sandia Rocket-Triggered Lightning Tests at Kennedy Space Center, Florida*, SAND90-2926, February 1991.
10. Cianos, N., and E. T. Pierce, *A Ground-Lightning Environment for Engineering Use*, SRI Report, Project 1843, August 1972.

AN ASSESSMENT OF TAILORING OF LIGHTNING PROTECTION DESIGN REQUIREMENTS FOR A COMPOSITE WING STRUCTURE ON A METALLIC AIRCRAFT

T. L. Harwood
Atlantic Research Corporation, Professional Services Group
Defense Systems Division, Arlington, Virginia

ABSTRACT

The Navy A-6E aircraft is presently being modified with a new wing which uses graphite/epoxy structures and substructures around a titanium load-bearing structure. The ability of the composites to conduct electricity is less than that of aluminum. This is cause for concern where the wing may be required to conduct large lightning currents. The manufacturer attempted to solve lightning protection issues by performing a risk assessment based on a statistical approach which allows relaxation of the wing lightning protection design levels over certain locations of the composite wing. This paper presents a sensitivity study designed to define the total risk of relaxation of the design levels.

INTRODUCTION

The new A-6 wing design uses graphite/epoxy structures in an effort to minimize weight while maximizing the strength and life of the wing (design life of 4400 hours). The flight control surfaces (i.e., slats and flaps) and aircraft fuselage are of metallic construction. The graphite/epoxy structures are connected to the inner wing by metal rivets. They are present in the wet wing area (fuel is contained behind these panels) as well as other areas which do not contain fuel. The composite panels do not conduct electricity as well as the aluminum they replace. This is cause for concern where the wing is required to conduct large lightning currents as a result of direct stroke attachment. Lightning channel attachment to the aircraft structure and/or wiring can result in damage to the aircraft surface and wiring. Traditional protection from direct attachment lightning effects consists of establishing a low impedance path between any two points where the lightning induced currents will flow. The Navy normally requires that aircraft meet the requirements of MIL-E-6051D and MIL-B-5087B when tested to the waveforms and specifications of MIL-STD-1757A. MIL-E-6051D outlines the overall requirements for systems electromagnetic compatibility (EMC). MIL-E-6051D stipulates that lightning protection be guided in accordance with direction given in MIL-B-5087B. MIL-B-5087B specifies that protection for lightning requires that bonding allow discharge current to be carried between the extremities of an aircraft without risk of damage to flight controls or producing sparking or voltages within the vehicle in excess of 500 volts. These requirements are based on a lightning current waveform of 200 kA peak, a pulse width of 5 to 10 microseconds and a rate of rise of 100 kA per microsecond. MIL-B-5087 also gives the following guidance for aircraft vehicle skin: "Vehicle skin shall be so designed that a uniform low-impedance skin is produced through inherent RF bonding during construction. RF bonding must be accomplished between all structural components comprising the vehicle". MIL-STD-1757A presents the standardized set of test waveforms and techniques to be used to qualify aerospace vehicles and hardware for lightning. The tests are designed to define the physical effects of lightning induced current and its interaction with fuel, structural and electrical hardware as well as indirect effects associated with strikes coupling to internal wiring and electronics. Lightning strike zones are defined dependent on attachment or transfer characteristics. Three major surface zones are identified. Zone 1 defines surfaces where there is a high probability of initial attachment. It is further broken down to Zone 1A and Zone 1B. Zone 1A is an initial attachment point with a low probability of flash hang-on (such as a leading edge). Zone 1B is an initial attachment point with a high probability of flash hang-on (such as a trailing edge). This zone should be designed to withstand direct strike lightning components up to 200 kA. Zone 2 defines surfaces for which there is a high probability of a lightning flash being swept by the airflow from a Zone 1 point of initial attachment. Zone 2 regions also subdivide into 2A and 2B, dependent on the probability of flash hang-on. Zone 3 surfaces are required to conduct the induced current between any two Zone 1 regions but are not subject to direct attachment effects. Figure 1 depicts the MIL-STD-1757A direct strike waveform components A, B, C, and D for required levels of protection, dependent on zoning. Another military standard (MIL-STD-1795A) also gives lightning design guidance for aerospace vehicles. It more clearly defines the concept of tailoring the lightning protection design requirements. It states that identification of zoning can be accomplished by use of analysis, attachment tests, similarity or any combination of these methods. It states that the direct effects waveform components A, B, C and D of MIL-STD-1757A should be used for design and verification purposes.

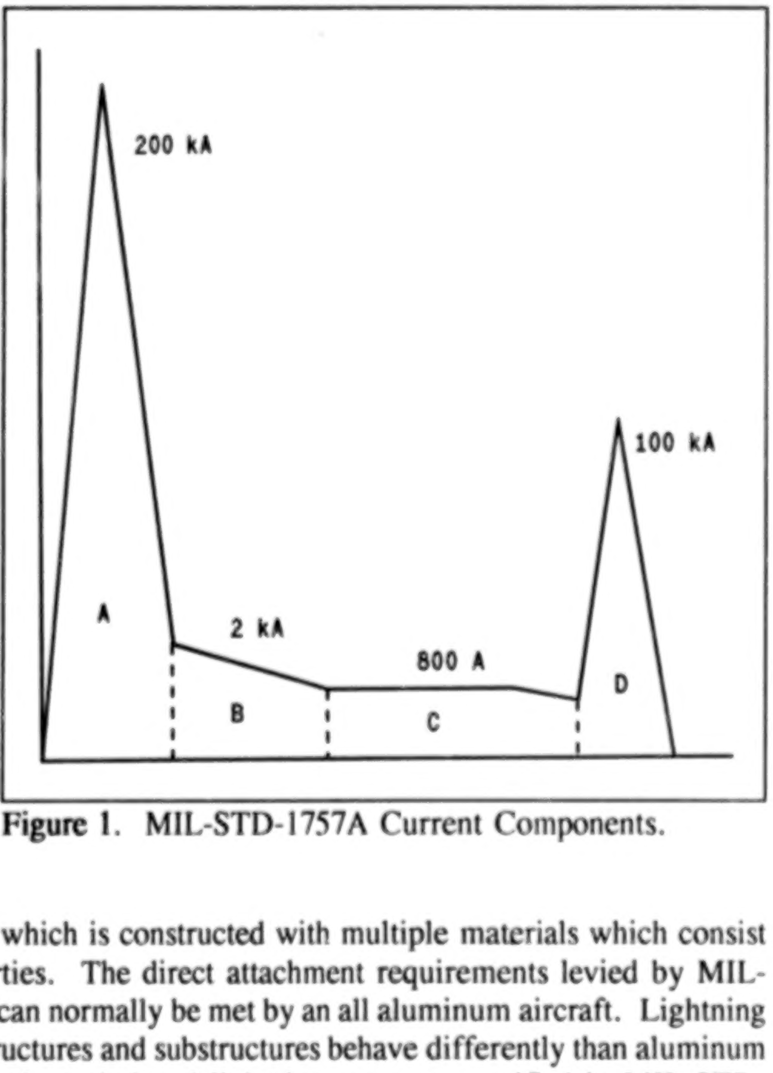

Figure 1. MIL-STD-1757A Current Components.

The uniform low-impedance requirement stated in MIL-B-5087B can normally be met by an all aluminum aircraft, but is much more difficult for one which is constructed with multiple materials which consist of many different electrical properties. The direct attachment requirements levied by MIL-STD-1757A and MIL-STD-1795A can normally be met by an all aluminum aircraft. Lightning testing has shown that composite structures and substructures behave differently than aluminum and indeed can be damaged by the large induced lightning currents specified in MIL-STD-1757A and MIL-STD-1795A. Herein lies the dichotomy of terms: The A-6 composite wings consist of high-impedance composite panels attached to a medium-impedance titanium spar with low-impedance metallic fasteners and in electrical contact with low-impedance aluminum flight control surfaces. A uniform low-impedance skin is not possible in this configuration. The manufacturer of the A-6 composite wing attempted to solve this dichotomy by applying a MIL-STD-1795A approach by performing a risk assessment based on analytical and statistical data. The methodology entailed definition of a probabilistic approach towards lightning design criteria as related to maximum lightning current amplitude and expected location of strike on the aircraft. The analysis considered wing surface zoning, scale model lightning strike lab studies, a computer simulation of lightning strike locations, lightning strike rates on tactical aircraft and lightning threat statistics.

THE ANALYSIS

The analysis was based on definition of risk measure factors to establish the lightning protection design requirements. The risk measure factors included the number of wings, the flight hours guaranteed for each wing, the number of lightning strikes expected per flight hour, the lightning threat statistics based on Cianos and Pierce [1] and the percentage of lightning strikes predicted to specific wing areas. The Cianos and Pierce lightning charts define two threats (severe and moderate) as shown in Figure 2. The severe threat (upper curve) was equated to a MIL-STD-1757A component A for definition of the Zone 1 threat. The moderate threat (lower curve) was equated to MIL-STD-1757A component D for definition of the Zone 2 threat. The number of wings times twice the total guaranteed flight hours per wing defines the total flight exposure (taking into account a safety factor of two). The total flight exposure times the lightning strikes per hour (the manufacturer used 1 in 64,000 flight hours as defined by Corbin [2]) defines the total strikes expected during the life of the wing. If the probability of the lightning strike distribution on the aircraft is known then the strike probability to individual aircraft areas can be defined. The lightning zone definition was accomplished by test of a 1/25 copper coated scale model at LTRI, Miami, Florida. The wing area definition is shown in Table I.

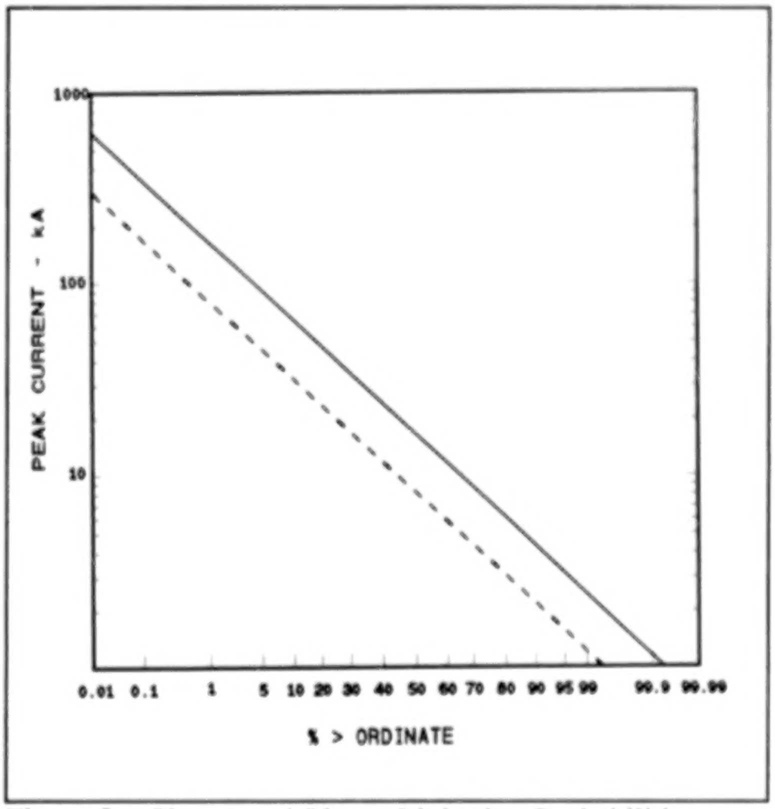

Figure 2. Cianos and Pierce Lightning Probabilities.

Table I. A-6E Wing Lightning Strike Category Definition.

WING AREA	CONFIGURATION	DESCRIPTION	ZONE
1	SLATS EXTENDED (10% of Flt)	OUTBOARD SLAT TIP WING AREA AFT OF SLAT TIP	ZONE 1 ZONE 2A
2	OUTBOARD FENCE UPPER WING	OUTBOARD FENCE 18" EITHER SIDE	ZONE 1 ZONE 2A
3	LARGEST STORES STATIONS L, 1, 2, 4, 5, R	FRONT TIPS STRUCK FROM SLIGHTLY ABOVE HORIZON 18" EITHER SIDE ON UPPER SURFACE	ZONE 3 (STORE/WING INTERFACE) ZONE 2A
4	LARGEST STORES STATIONS L, 1, 2, 4, 5, R	ALL POINTS ON WING STORES INCLUDING TIPS, EXCLUDING FROM SLIGHTLY ABOVE HORIZON	ZONE 3 (STORE/WING INTERFACE)
5	ALL CONFIGURATIONS	WING TIPS	ZONE 1

The probability model then used this test data in the following lightning strike probability model:

$$C(t,a) = L_o t \sum_{i=1}^{k} P_i Q(a_i) \qquad (1)$$

Where:

C = Risk Measure (the expected number of lightning strikes with amplitudes greater than the design value)
L_o = Lightning strikes per fleet flight hour
t = Hours exposed to lightning (number of A-6 wings times twice the guaranteed flight hours)
k = Number of wing areas (5)
P_i = Probability of strike to critical wing area
$Q(a_i)$ = Probability that strike exceeds design.

A risk factor was assigned to each wing area (1 - 5) such that the total number of strikes which would be allowed to the total wing in excess of the design level over twice the wing lifetime was 0.5. This risk factor was distributed evenly over the five wing areas. This allowed calculation of $q(a_i)$ at each of the wing areas. Using this value as the known variable one could then enter the Cianos and Pierce chart to identify the respective unknown design value for the lightning current. Table II presents the calculated lightning attachment design levels identified as a function of wing areas. The lightning design requirement included the protection for Zone 1 and Zone 3 regions to the full 200 kA requirement. Wing area 3 (Zone 2A) was specified at 40 kA, well in excess of the identified design level of 15 kA.

Table II. A-6 Calculated Wing Strike Probabilities and Threat Levels.

WING AREA	P_i (LAB DATA)	$q(a_i)$ X 100%	a_i		RISK FACTOR
			ZONE	CURRENT	
1	0.1 X 6/132 = 0.00455	4.0%	1 2A	25 kA 13 kA	0.1
2	2/330 = 0.00606	38%	1 2A	34 kA 17 kA	0.1
3	1/195 = 0.00505	36%	3 2A	30 kA 15 kA	0.1
4	9/198 = 0.0455	4.0%	3	110 kA	0.1
5	106/330 = 0.321	0.57%	1	220 kA	0.1
			TOTAL RISK FACTOR		0.5

This approach was accepted by the Navy. The strike rate was modified, however, to a rate of 1 in 3362. The strike rate chosen by the manufacturer was one of the least stressing strike rates reported by Corbin. The strike rates discussed in the Corbin data ranged from 1 in 2,000,000 to 1 in 2,500. All of these values were related to peace time civilian flight and were not considered as adequate for an all weather attack aircraft.

One concern associated with this statistical tailoring approach was the use of total exposure time as a variable. (i.e., if the number of wings procured decreased then this decreases the total exposure of the wing in the lightning environment which in turn can decrease the specification level). In an attempt to minimize the impact of number of wing sets on the statistical analyses the strike data was normalized to include only single wing events. This allowed calculation of a risk factor for each wing area using the 200 kA and 40 kA levels identified by analysis and the 200 kA and 100 kA levels specified by MIL-STD-1757A. These comparisons took into account restrikes as a result of swept strokes. Information presented by Fisher, etal. [3] indicates a restrike rate which can vary between 20 msec and 200 msec. The incorporation of restrikes in swept stroke regions (Zone 2) alters the P_i value in the wing areas 1 and 3. A comparison of the increased of strikes expected above the design criteria as a function of design level is shown in Figure 3.

Several mitigating factors were taken into account during the specification tailoring effort. These factors included: (1) The use of only cloud-to-ground lightning and peace time strike data for definition of the lightning threat variable; (2) The Navy's use of JP-5 fuel; (3) The data from previous composite direct attachment testing which indicated that lightning induced currents on composites usually resulted in low energy arcing from the composite material [4-7]; and, (4) The A-6 automatic Halon fire extinguisher. The mitigation factors are discussed in more detail below:

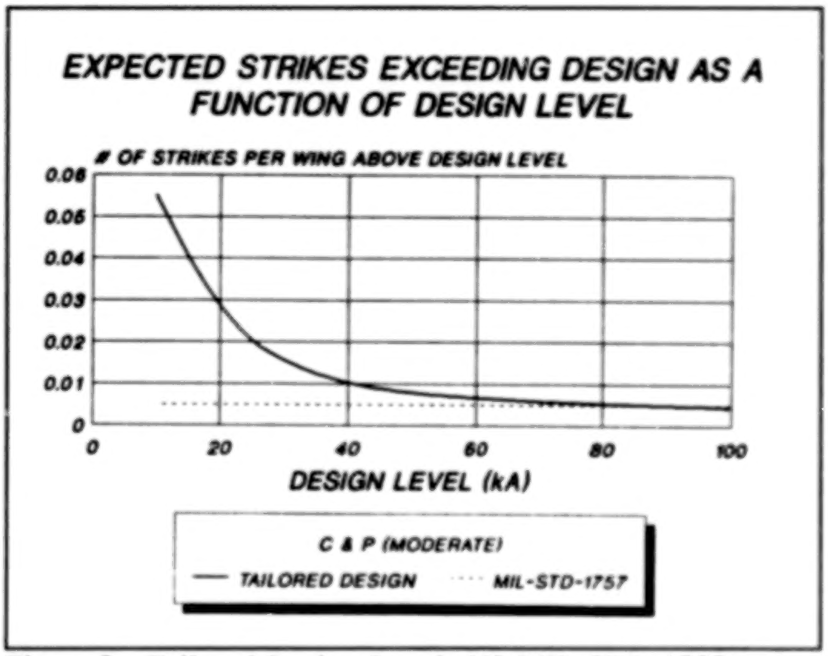

Figure 3. Tailored Design Levels VS MIL-STD-1757A.

Cloud-To-Ground Lightning Definition. A tactical aircraft will experience an airborne lightning environment which includes both cloud-to-ground and cloud-to-cloud lightning events. The Atmospheric Electricity Hazards Protection Program (AEHP) discussed by Beavin [9] was an attempt to measure the lightning threat to tactical aircraft. In the early stages of the program there were few lightning strikes for each thunderstorm penetration. The majority of penetrations were attempted at or below the freezing level (levels < 16,000 feet) as a result of previous observed lightning interactions with aircraft as reported by Corbin [2]. The rate of strikes at this altitude resulted in few direct lightning strikes. Using new procedures the NASA test aircraft encountered frequent strikes on penetrations in the vicinity of 20,000 feet. This would lead the reader to conclude that the cloud-to-cloud aircraft/lightning interaction is more probable. There are other factors, however, which reduce these cloud-to-cloud aircraft/lightning interaction probabilities. Aircraft flying above 20,000 feet have more latitude in their flight path and can more easily "see and avoid" the thunderstorm cells. Aircraft in a take-off, departure, penetration, approach or landing pattern (< 15,000 feet) are more confined in their flight path due to flight path restrictions imposed by FAA for aircraft separation and obstacle clearance requirements. As a result the "see and avoid" capability is often not possible, therefore exposing the aircraft to increased cloud-to-ground aircraft/lightning interactions. Additionally, most tactical aircraft have established procedures for thunderstorm penetration as directed in the aircraft type Naval Air Training and Operating Procedures Standardization (NATOPS) manuals. The direction given in these manuals is: "Unless the urgency of the mission precludes a deviation from course, intentional flight through thunderstorms should be avoided to preclude the high probability of damage to the airframe and components by impact of ice, hail and lightning ... If circumnavigation of the storm is impossible, penetrate the thunderstorm in the lower third of the storm cell..." The possibility of physical damage to the aircraft at the higher altitudes due to hail and ice result in procedures which enhance the cloud-to-ground aircraft/lightning interaction probabilities. The amount of mitigating effect to the actual aircraft by definition of threat using cloud-to-ground interactions is therefore reduced.

JP-5 Flammability. Flammable vapors can be ignited if the correct concentration of fuel-to-air mixture and temperature are present when introduced to a sufficient ignition source. A vapor/air mixture is too rich too burn if there is insufficient vapor space in the fuel tank, as is the case in a fully fueled wing. A vapor/air mixture is too lean to burn if the vapor space is too large. Ignition of JP-5 requires that very high temperatures (> 104 degrees Fahrenheit) be associated with altitudes below 10,000 feet. Any mixture of JP-5 and JP-4 significantly reduces this level of protection. The case of a fuel mixture occurs for Navy aircraft if joint Navy/Air Force operations are conducted and Navy aircraft are refueled in-flight by Air Force tankers (the Air Force uses JP-4 fuel). This mitigation effect is therefore reduced during joint operations.

Composite Material Low Energy Arcing. The source of ignition must be present at the same time the vapor/air mixture can sustain combustion. This source must produce sufficient energy to produce a minimum combustion flame to sustain ignition. Ignition can occur as a result of sparking or hot spot interaction with the fuel/vapor mixture. Numerous laboratory tests and analyses have been conducted to ascertain effects of lightning currents to composite material which enclose fuel tanks [4-7 and 16-19]. Tests comparing the hot spot time/temperature characteristics of carbon epoxy (C/E) and aluminum panels indicate that for swept stroke lightning the aluminum panels get hotter, but their peak temperatures and thermal dissipation occur two orders of magnitude faster than the C/E panels. The conclusions were that there is a considerable margin precluding hot spot ignition of fuel behind composite materials.

Fay Sealant At Wing Joints And Fasteners. The most significant lightning fuel ignition hazard was found to be interior sparking at the interface of adjacent materials or at fasteners. This can occur for both aluminum and composite materials. It is normally caused by poor conductivity between the interface materials as a result of gaps or voids between the main conduction channel (the fastener) and the adjacent material (the aluminum or composite panel). The spark shower which can occur for untreated adjacent materials or fasteners can be of sufficient magnitude to cause fuel ignition given the correct vapor/air mixture. The probability of arcing is higher for composite panels because of the poor conductivity as a result of interface surface irregularities. Additionally, in composite panels with fasteners, swept stroke testing has indicated that lightning has a tendency to attach to the fasteners regardless of panel material. [7] The composite wing incorporates a fay sealant internal to the fuel tank at these interface joints in order to mitigate these effects. This sealant provides the primary protection for high energy spark mitigation as a result of direct effects lightning induced currents in wing Zone 2 regions. The sealant is designed to prevent arcing by suppressing the heated matter away from the fuel.

Halon Fire Extinguishing System. The A-6E composite wing has an additional survivability feature designed into the aircraft to preclude fuel fed fire. The wing incorporates a Halon fire extinguisher system which may be activated in the anticipation of combat operations. When activated the vapor/fuel void is monitored for sufficient energy which would ignite the vapor/fuel mixture. Upon sensing auto-ignition of the fuel the system will discharge the halon into the void to extinguish the fire. This system can only be activated once in-flight and requires reset/recharge upon landing in the event it is activated but not used.

RESULTS

In order to more completely evaluate the effect of the multiple variables which were utilized for the statistical analysis a sensitivity study was accomplished where each variable utilized in the analysis was given an upper and lower bound. The lightning amplitude threat definition was varied, the restrike rate was varied and the strike rate was varied. The change to the design level as a result of altering each of these variables is addressed below.

The Threat Variable. Numerous studies have been accomplished to date regarding the lightning threat [8-14]. Melander and Axup reported [10 and 13] that measurements of lightning currents on towers could be suspect data. Berger and Garbagnati measurements were taken on towers in mountains of Switzerland and Italy. Uncertainties can arise with data due to the presence of tower on rocky mountain. Larger amplitude strokes are thought to strike tall towers. Also it is thought that positive strikes are more prevalent at higher altitudes where the towers were located. Recently Podgorski [15] completed a study of lightning strikes on a tall tower and reported that the peak current distributions of lightning in cloud-to-ground strikes indicate that the lightning measurements of Berger were accurate. These and the tall tower measurements were compared to the Lightning Positioning and Tracking System (LPATS) network measured data from Atmospheric Research System Inc. to define the low probability occurrence distribution of data. The probability distribution of peak lightning currents was also evaluated for the data from the Lightning Direction Finders (LDFs). A unified lightning threat was derived for aircraft near/on ground (within 1000 meters) and in-flight. The results of variation of the lightning threat show that slight divergences (an increase from 0.008 to 0.015 strikes per wing above design level) exist at the higher design levels (> 70 kA) to major divergences (an increase from 0.008 to 0.05 strikes per wing above design level) exist below design levels of 20 kA.

The Restrike (Swept Stroke) Variable. The aircraft speed and physical wing dimensions were driving factors. Three values (0, 4, and 10 restrikes) were chosen based on the calculated boundaries using information on restrike rates identified by Fisher [7]. The impact of variation of restrikes while holding all other variables constant is shown in Figure 4.

The Strike Rate. The strike rate data (1 in 3362) was Navy aircraft historical lightning strike rate data and considered only peacetime operations. A number of Navy pilots interviewed stated that it was their opinion that a number closer to 1 in 500 would be a more realistic strike rate. Although the historical Navy tactical aircraft strike data indicated a rate closer to 1 in 3362 the number of events may be understated. This seems to be borne out by the interviews. Since the strike rate was tied to more of "see and avoid" peace time operations the 1 in 500 number was established as the upper bound (i.e., wartime operations), the 1 in 3362 as the median (i.e., normal ship based operations), and 1 in 10,000 as the lower bound (i.e., shore based operations). Figure 5 shows the result of variation of the strike rate. The rate of 1 in 500 shows a significant deviation in the vicinity of 60 kA and diverges exponentially below the 40 kA design level.

The consequence of exceeding the lightning design protection can range from minor upset or damage of aircraft systems and subsystems to complete loss of aircraft due to fuel tank explosion. The worst case over-design strike could occur because the Zone 2 restrike region (wing area 3) can become Zone 1 due to migration of the Zone 1 initial attachment point onto the wing. The distance as related to the migration of the initial attachment position on the wing along the flight path are shown in Table III.

The dotted line in Table III indicates where the wing area 3, Zone 2 transition occurs. The region to the left of the line indicates the migration does not impact the composite panels on the top of the wing. The region to the right of the line indicates the initial attachment migration results in a Zone 1 threat of 200 kA can occur on the composite panels. The case of fuel ignition as a result of puncture or burn-through and direct interaction of the lightning current with the fuel is a possibility. Aluminum will exhibit burn-through in relation to the lightning dwell time. If the channel of 100 kA were to maintain the same relative position on the aircraft for a period of over 50 msec then burn-through is possible. The equivalent sized composite panel without fasteners does not exhibit burn-through. The composite panel with fasteners, however, exhibited burn-through at dwell times below 1 msec. The lightning threat dwell time for Zone 1A and 2A in accordance with MIL-STD-1757A is approximately 500 microseconds. This could be cause for concern.

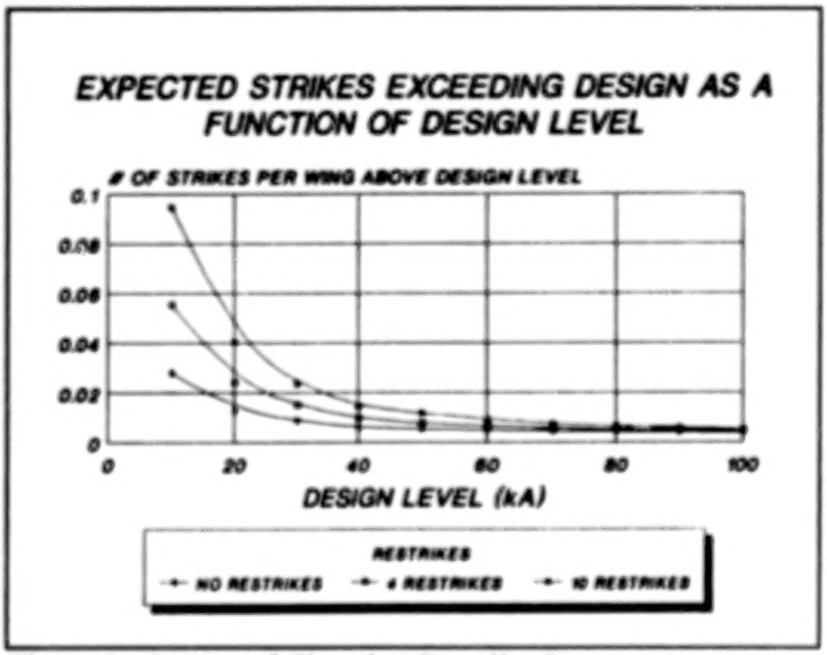

Figure 4. Impact of Changing Restrike Rate.

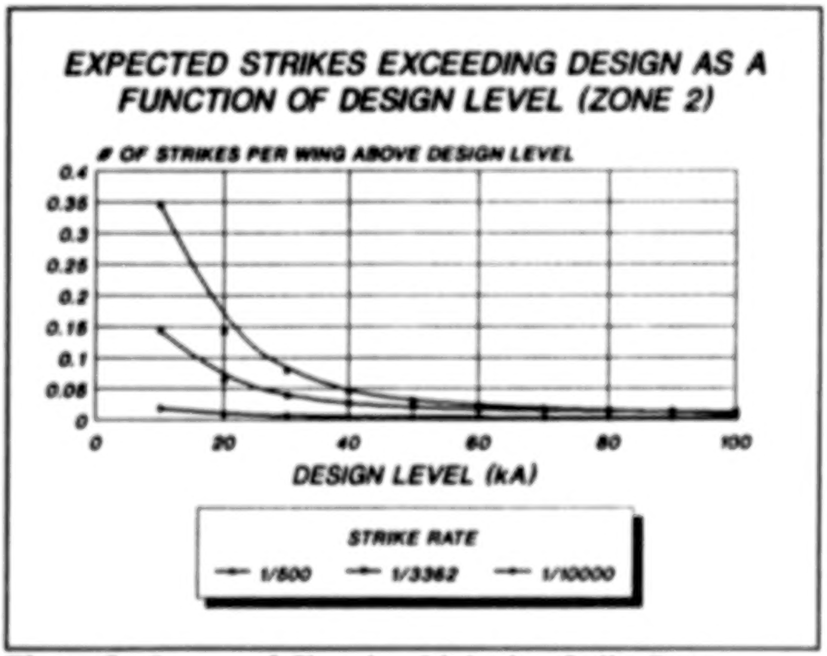

Figure 5. Impact of Changing Lightning Strike Rate.

CONCLUSIONS

The direct effects lightning test levels of MIL-STD-1757A appear to be highly conservative for lightning design guidance if areas on the aircraft structure exhibit a low probability of direct attachment. The tailoring of lightning design levels can be accomplished

Table III. Migration of Zone 1 Areas.

SPEED (KTS)	ALTITUDE (METERS) 500	1000	1500	2000	2500	3000	3500	4000
150	0.26	0.51	0.77	1.00	1.30	1.50	1.80	2.10
200	0.34	0.68	1.00	1.30	1.70	2.10	2.40	2.70
250	0.43	0.86	1.30	1.70	2.10	2.60	3.00	3.40
300	0.51	1.00	1.50	2.10	2.60	3.10	3.60	4.10
350	0.60	1.20	1.80	2.40	3.00	3.60	4.20	4.80
400	0.68	1.40	2.10	2.70	3.40	4.10	4.80	5.50
450	0.77	1.50	2.30	3.10	3.90	4.60	5.40	6.20
500	0.86	1.80	2.60	3.40	4.30	5.10	6.00	6.80

on a given platform if the dynamics of flight regime and threat remain relatively constant, however, this case history indicates that a relaxation of design levels below 60 kA for swept stroke regions can be hazardous. The manufacturer of the A-6 composite wing, using generally acceptable procedures outlined in MIL-STD-1795A, was able to justify a relaxation of MIL-STD-1757A swept stroke design levels from 100 kA to 40 kA for a portion of the wing surface. The disturbing finding of this study was that of the migration of the Zone 1 regions into the area of composite material which has shown inability to conduct these high currents without damage. Additionally, given the worst case scenarios by which all variables could be adversely affected simultaneously the mitigation factors become subordinate to the lightning protection deficiencies.

The A-6E composite wing lightning protection design appears sufficient for adequate protection to a reasonable lightning threat. The requirement for design levels for wing area 3, Zone 2 to be above 40 kA has been analyzed and found to be desirable but not absolutely necessary due to low probabilities of direct lightning interaction in these regions. The A-6 composite wing design features diminish, but do not eliminate the risk of catastrophic damage due to direct attachment of lightning to the composite structure.

REFERENCES

1. Cianos, N., Pierce, E. T., "A Ground Lightning Environment for Engineering Usage", SRI Technical Report 1, Project Number 1834, Aug 1972.

2. Corbin, J. C., "The Risk Factor in Aircraft Lightning Protection", Proc. of the 9th Intl. Aerospace and Ground Conf. on Lightning and Static Electricity, Orlando, Fl., Jun 1984.

3. Fisher, F. A., Plumer, J. A., and Perala, R. A., "Lightning Protection of Aircraft", Lightning Technologies Inc., Pittsfield, Ma., 1990.

4. Shulte, E. H., "Effects of Lightning Waveform Components on Graphite/Epoxy Material", Proc of the 23rd National Symposium, Society for the Advancement of Material and Process Engineering, 2-4 May 1978.

5. "Lightning Effects on Composite Material Fuel Tank", Report No. NADC-83106-20, Naval Air Development Center, Warminster, Pa., Aug 5, 1983.

6. Andersson, L., Lovstrsand, K., Olsson, B, Wahlgren, B., "Lightning Test of a CFC Aircraft Wing Tank Skin", Proc. of the 9th Intl. Aerospace and Ground Conf. on Lightning and Static Electricity, Orlando, Fl., Jun 1984.

7. Schulte, E. H., Walker W. T., "Rear Surface Temperature Measurement of Aircraft Materials Subjected to Zone 2A Lightning Strikes", Proc. of the 9th Intl. Aerospace and Ground Conf. on Lightning and Static Electricity, Orlando, Fl., Jun 1984.

8. Clifford, D. W., "Another Look at Aircraft-Triggered Lightning", FAA/NASA/FIT Symposium on Lightning Technology, 22-24 Apr 1980.

9. Beavin, R. C., Lippert, J. R., Lavoie, J. E., "Atmospheric Electricity Hazards Protection Program", Proc. of the 8th Intl. Aerospace and Ground Conf. on Lightning and Static Electricity, Fort Worth, Tx., Jun 1983.

10. Melander, B. G., "Atmospheric Electricity Threat Definition for Aircraft Lightning Protection", Proc. of 8th Intl. Aerospace and Ground Conf. on Lightning and Static Electricity, Fort Worth, Tx., Jun 1983.

11. Weinstock, G. L., "A Realistic Approach to Aircraft Lightning Protection", Proc. of the 8th Intl. Aerospace and Ground Conf. on Lightning and Static Electricity, Fort Worth, Tx., Jun 1983.

12. Ziegler, W., "Lightning Strikes to Aircraft of the German Federal Armed Forces", Proc. of the 8th Intl. Aerospace and Ground Conf. on Lightning and Static Electricity, Fort Worth, Tx., Jun 1983.

13. Axup, P. R., Rustan, P. L., "Analysis of Lightning Current Measurements", Proc. of the 9th Intl. Aerospace and Ground Conf. on Lightning and Static Electricity, Orlando, Fl., Jun 1984.

14. Podgorski, A. S., "Lightning Standards for Aircraft Protection", Proc. of the IEEE 1990 Intl. Symposium on EMC, Washington, D.C., Aug 1990.

15. Podgorski, A. S., "Composite Electromagnetic Pulse Threat", Proc. of the IEEE 1990 Intl. Symposium on EMC, Washington, D.C., Aug 1990.

16. Rasch, N., "User's Manual for AC-20-53A Protection of Airplane Fuel Systems Against Fuel Vapor Ignition Due to Lightning", DOT/FAA/CT-83/3, Oct 1984.

17. Robb, J. D., Chen, T., "Integral Fuel Skin Material Heating from Swept Simulated Lightning Discharges", IEEE Intl. Symposium on EMC, 1977.

18. Shulte, E. H., "Effects of Lightning Waveform Components on Graphite/Epoxy Material", Society for Advancement of Material and Process Engineering, 23rd National Symposium, Anaheim, California, May 1978.

19. Harshman, B., Heady, B., Schulte, E., Wooldridge, J., and Zeisel, K., "Lightning Effects on Composite Material Fuel Tanks", Naval Air Development Center, NADC-83106-20, Aug 1983.

LIGHTNING PROTECTION DESIGN AND TESTING OF AN ALL COMPOSITE WET WING FOR THE EGRETT

B J C Burrows, S J Haigh, C Chessum, V P Dunkley
Lightning Test and Technology, Culham Laboratory, Abingdon, Oxfordshire,
OX14 3DB, England

1 INTRODUCTION

The Egrett aircraft, made by Grob of Germany, has an all composite wing comprising CFC/Nomex sandwich skins, full length CFC main spar caps and GFRP main and auxiliary spar webs. It also has short inboard CFC auxiliary spar caps. It has fine aluminium wires woven into the surface for protection. It has an integral fuel tank using the CFC/nomex skins as the upper and lower tank walls, and lies between the forward auxiliary spar and the forward of the two main spar webs. The fuel tank is not 'bagged', ie it is in effect a wet wing tank. It has conventional capacitive type fuel gauging.

The aircraft has been cleared to IFR standards and so required full lightning protection and demonstration that it would survive the lightning environment. Grob Aircraft Company, with Culham Lightning Test and Technology as consultants, designed the lightning protection for the wing (and also for the remainder of the aircraft). An inner wing test sample (which included a part of the fuel tank) was tested at the Culham Lightning Simulation Laboratory as part of the proving programme. This paper describes the protection design, the testing process and indicates the intrinsic structural features that improve lightning protection design and which therefore minimise the weight and cost of any added lightning protection components.

The design and testing procedures must meet the requirements of AC20-53A(1) for fuel systems for aircraft.

2 BASIC WING DESIGN LIGHTNING CONSIDERATIONS

The wing cross section is shown in Figure 1, where the construction, comprising CFC/Nomex, CFC spar caps, and glass fibre reinforced plastic (GFRP) spar webs, is fully cocured and bonded, and virtually no fasteners are used. The only metallic components originally in the design were the fuel gauge wires (A), the aileron operating rod (B), a drive cable for the flaps (C), electric wires to the wing tip light, Pitot and other wing mounted electrical items (D), and fuel and vent pipes (E). Item (C) only runs a very short distance along the wing (there are only inboard flaps) and fuel gauge wiring ran only as far as the outer-most gauge, about half way along the wing. Apart from these, the main components of the wing which would carry lightning current would be the main spar caps which are solid 0° carbon lay up, and to a less extent the skins, but these were very thin. Inboard, the CFC spar caps of the auxiliary spars could in principle carry current. (The auxiliary spar caps were shown later on to be completely insulated from the rest of the wing and so played no part in lightning protection.)

The hazards from lightning can be divided into three main areas:

a) structural damage (excluding fuel explosions) to the wing affecting flight safety.
b) fuel vapour explosions in or around the tanks and pipes.
c) excessive induced voltages causing (b) or damaging the aircraft electrical system.

419

Apart from some tests on 'coupon' samples of the wing skins and fuel tank access doors, the remainder of the lightning protection design evolved by detailed consideration of the wing design, so making optimum use of the wing structure for protection.

3 PROTECTED WING DESIGN AS TESTED

3.1 Examination of the fuel tank design together with the results of the coupon tests suggested that the tank was unlikely to spark as a result of Zone 3 conduction currents or swept stroke 2A/2B attachment to the wing. However, because of the novel features of the design, a simple similarity argument could not be made, and there were also three possible sparks site zones which could only be qualified by test. Two of these are shown in Figure 2 and involved first, possible sparking at the inboard close-out of the tank, and secondly at a bonded panel in the undercarriage bay area of the tank. (The third one is associated with the fuel gauge systems and will be discussed later.) Sparking at the fuel tank access doors had already been shown to be absent from coupon tests to the door and its immediate surround, so this was not to be considered during the main tests. Camera and fibre optic light sensors were placed in the wing as shown in Figure 3 in order to specifically cover the identified sites, but to cover the whole tank as well.

The tests showed that with both Zone 3 and Zone 2A/2B tests, no sparking occurred in the tank area. This conclusion required very close attention to the test details since a lot of stray light leaked in through partially transparent GFRP in areas of the tank not covered by opaque sealant.

3.2 Fuel and vent pipes for tank. To avoid problems with these, low electrical conductivity "static dissipating" pipes were used to prevent the risk of current flow in them and so to prevent sparking at joints, etc.

3.3 Fuel gauge wiring. As previously discussed, the fuel gauges contribute a potential fuel ignition hazard owing to the possibility of sparking between the fuel gauges and the CFC skins locally. This depends upon the magnitude of the voltage generated by current flow in the wing material and the insulation level at the gauge. The magnitude of voltage generated in the fuel gauge wiring is determined critically by the position of the wires in relation to good conducting structure, in this case being the mass of 0° CFC comprising of the main spar caps (see Figure 1). Modifications to wiring positions were made both externally, where it was recommended that the wiring outside the wing was screened, and inside, where it was demonstrated that voltages could be brought low enough by careful positioning of the fuel gauge wires right in the corner of the spar cap/spar web as shown in Figure 1, where (a) shows the original position and (b) the improved position. The measurements shown in Table 1 demonstrated the advantage of careful use of structure and wiring location. The original configuration voltage (extrapolated to 'full threat') was 3440 resistive volts and 18kV inductively generated voltage, reducing to 2600 resistive and 4.6kV inductive after the modification. No added material was needed within the wing to secure this improvement, only repositioning of the wiring tight within the corner of the spar cap/web. The reduction in inductive voltage (ie, the component of voltage proportional to di/dt) is very marked, and suggests that di/dt coupling occurs along part of the wing internally; probably in the region between the undercarriage bay and the wing root where the skin is presumably insulated from the main spar caps as well as from the auxiliary spar caps. Evidence for this was the reduction in di/dt voltage when the skin was joined to the spar cap at the root by the add on copper sheets.

With adequate insulation at the fuel gauges, the induced voltages will be insufficient to cause sparking and therefore no fuel ignition.

3.4 Induced voltages in wing tip and Pitot wiring. The wiring runs from the wing tip light and from a Pitot tube well out on the wing to the wing root. Insulation is not practical for the system, and the risk of a very high current injection into the aircraft electrical system is very serious unless precautions are taken. The protection method is an aluminium tube running the full length of the wing in an electrically continuous length, bonded to the light surround at the outer edge and to the fuselage ground plane at the inner, with the wires inside. By this method, almost complete elimination of the induced voltage occurs except for a residual resistive voltage resulting from current flow in the tube. This was proved by the test in which the current along the tube, and the voltage inside were measured during a current pulse to the wing, and shown to be in Ohm's law agreement with the tube current and resistance, ie, the current pulse of 67k amps max produced a voltage of 200V in a tube of 3mΩ.

The presence of the tube has an effect on current flow in the wing, especially at late times during the pulse as shown in the following section.

3.5 Current sharing and current waveforms in wing bonding components. Table 2 shows the current distribution between the various connections to the wing at the root end, these tests were made mainly using oscillatory pulses of approximately 50kA peak. This table shows that the forward and rear auxiliary spars are not in electrical contact with the wing, so the lightning current is taken only by four components; upper spar, lower spar, aileron rod, and the lightning protection tube in the ratio of 30%, 39.5%, 17%, 13.5%. However tests with a unidirectional Component A pulse through the whole of the wing sample produced a current pulse in the tube like Figure 4 of 1280µs long compared with the Component A current pulse of approximately 460µs total length.

The tube current rose to 67kA at 216µs after the start of the pulse and had a very flat top, at which time the Component A current pulse was only 50kA; ie, the tube current was larger than the applied current pulse, since an eddy current had been established in the wing between the CFC and the metal.

This is a familiar phenomenon with CFC structures incorporating high conductivity components such as a metal tube.

4 COMMENTS ON DESIGN OF WING/FUEL TANK AFFECTING CERTIFICATION FOR LIGHTNING

In Section 2 of this paper, 3 types of potential hazard were mentioned as being specifically applicable to CFC structures. The first was structural damage affecting flight safety resulting from an attachment. Tests carried out prior to and during this test procedure (but not reported here) showed that the CFC/Nomex/CFC material, with aluminium wires in the outer ply is virtually unaffected by Zone 2A lightning attachments apart from minor tufting at the the arc attachment points. Owing to the absence of metal components there are no current concentration points to cause direct effects damage to the wing away from the arc attachment point either, so making it safe.

The second hazard was fuel vapour ignition from sparking within the tank. Tests on coupons had previously verified that Zone 2A attachments to the fuel tank access panels did not cause sparking within the tank, and tests at Culham prior to the main test using an infra-red camera had shown that Zone 2A attachments to the fuel tank upper or lower skin material gave a temperature rise in the inside tank wall of no more than 87°C, which is safe.

The tests reported here have shown that no sparking occurs within the tank from conduction tests (Zone 3) at 200kA or with Zone 2A attachments to the wing skin (near the undercarriage bay). The design features of special significance here are that there are no fasteners used in the tank region; it is a fully bonded structure with CFC/Nomex upper and lower skins and glass fibre forward and rearward walls. The CFC skins are unjointed in the tank region, since the forward GFRP auxiliary spar protects the tank from possible sparking at the upper skin/lower skin bond line at the leading edge shown as Point A in Figure 1.

Although some light was observed in the tests, careful exploratory work showed that it was light leaking through the semi transparent GFRP from minor sparking elsewhere, probably in the region *aft* of the main spar, and also at the root end, where external surface sparking occurred at the wing skin/spar joint prior to the addition of the copper sheet referred to in Section 3.3. Light leaks in the structure incorporating fibre-glass are a severe problem in achieving a satisfactory optical test for sparking. It would, in principle have been possible to use an ignitable gas test but the provision of adequate blow-out panels would have been very difficult in such a large volume, and the damage resulting from a mis-test would have stopped the test programme owing to a shattered test specimen.

The other principle problem concerning lightning in a CFC wet wing is excessive induced voltage either in the fuel gauge wiring causing sparking in the fuel tank or large induced or injected currents in other wiring which can damage aircraft power systems, etc. As discussed in Section 3.3 wiring can be protected by routing and insulation where all the wiring and the items to which it is connected are *totally inside* the structure and not subject to direct attachment, as indeed for the fuel gauge wiring. (The use of conduit inside a fuel tank is *very unsatisfactory* owing to the sparking problem at its bonding points, and the same problem applies to any other form of shielding. Conduit which is grounded one end only or which has an insulation break in it does not reduce the magnitude of the voltage available and therefore does not prevent over voltage sparks at the gauge units.) In the Egrett design, protection is obtained by optimum routing and adequate insulation at the gauge transmitters.

Wiring to Pitots, stall warning devices, navigation lights can not be protected in this same way since they risk a direct lightning attachment. For this the Egrett design uses an aluminium tube which is bonded to structure and to the light surround to carry the wiring all the way into the fuselage. This method minimises the voltage induced in the wiring, and reduces them to a tube resistive voltage only as explained above.

5 CONCLUSIONS

The Egrett wing design achieves lightning protection by a combination of aluminium wire skin protection in the outer ply of the CFC/Nomex/CFC structure, a no-fastener design including an all-bonded fuel tank structure, and low induced voltages by a) choice of locations of the fuel gauge wiring and b) by use of a light weight tube for the wing tip navigation light. A few bond straps are also required to complete the protection together with inboard wire screens for the wiring connection to fuselage items.

Lightning protection of composite aircraft can be achieved, and the aircraft certificated with minimum increase in weight if due care and attention is given to details. The assistance of experienced consultancy is essential well before certification is to take place, and preferably at the detailed design phase, so that low weight techniques can be incorporated to solve the lightning problems. Lightning is potentially a very severe environmental hazard to composite aircraft, but good design can minimise the weight and cost penalty of achieving protection.

ACKNOWLEDGEMENTS

The authors would like to acknowledge the support of Grob Aircraft Company of Mindelheim in Germany, and Messrs Fuller, Osbourn and Butler for their assistance in setting up the test system, the optical and electrical diagnostics and in preparation of photographs and oscillograms.

REFERENCES

1. FAA Adviser Circular AC20-53A. Protection of Airplane Fuel Systems against Fuel Vapour Ignition due to Lightning. 1985.

TABLE I
FUEL GAUGE VOLTAGE EXTRAPOLATED FROM ~50kA TO 200kA, 140kA/µs

SHOT NO.	PEAK TEST CURRENT kA	EXTRAPOLATED VOLTAGES		EXTRAPOLATED LESS EXTERNAL di/dt	COMMENTS
		∝ I	∝ di/dt		
1	50	3.4kV	22kV	18kV	Original route
2	50	3.4kV	22kV	18kV	Revised external route
3	50.5	2.96kV	11.9kV	7.9kV	Revised internal route
4	52	3.1kV	7.7kV	3.9kV	As 3) but copper added spar/skin (upper)
5	50	2.6kV	8.6kV	4.6kV	As 4) but copper added to spar/skin (lower)
6	48.5	3.1kV	10.7kV	6.7kV	Contact moved to 1L
7	47	2.4kV	9.0kV	5.0kV	Contact moved to 2U

TABLE II
CURRENT SHARING AT WING ROOT BONDING POINTS

BOND POSITION	MEASURED CURRENT kA	EXTRAPOLATED TO 200kA KA	%
Main Upper Spar	14.7	60.6	30
Main Lower Spar	20.0	80.2	39.5
Lightning Tube	6.95 67.6(1)	27.9 73.0(1)	13.76 *(1)
Aileron Bond	8.5	34.1	16.8
Forward Auxiliary Spar	0	0	0
Rear Auxiliary Spar	0	0	0

All tests at ~50kA oscillatory except (1) using a 200kA Component A unidirectional Pulse. The % current reached was 36.5% of the initial peak current, but it occurred 216µs after the initiation of the current pulse, at which time it was greater than the applied pulse.

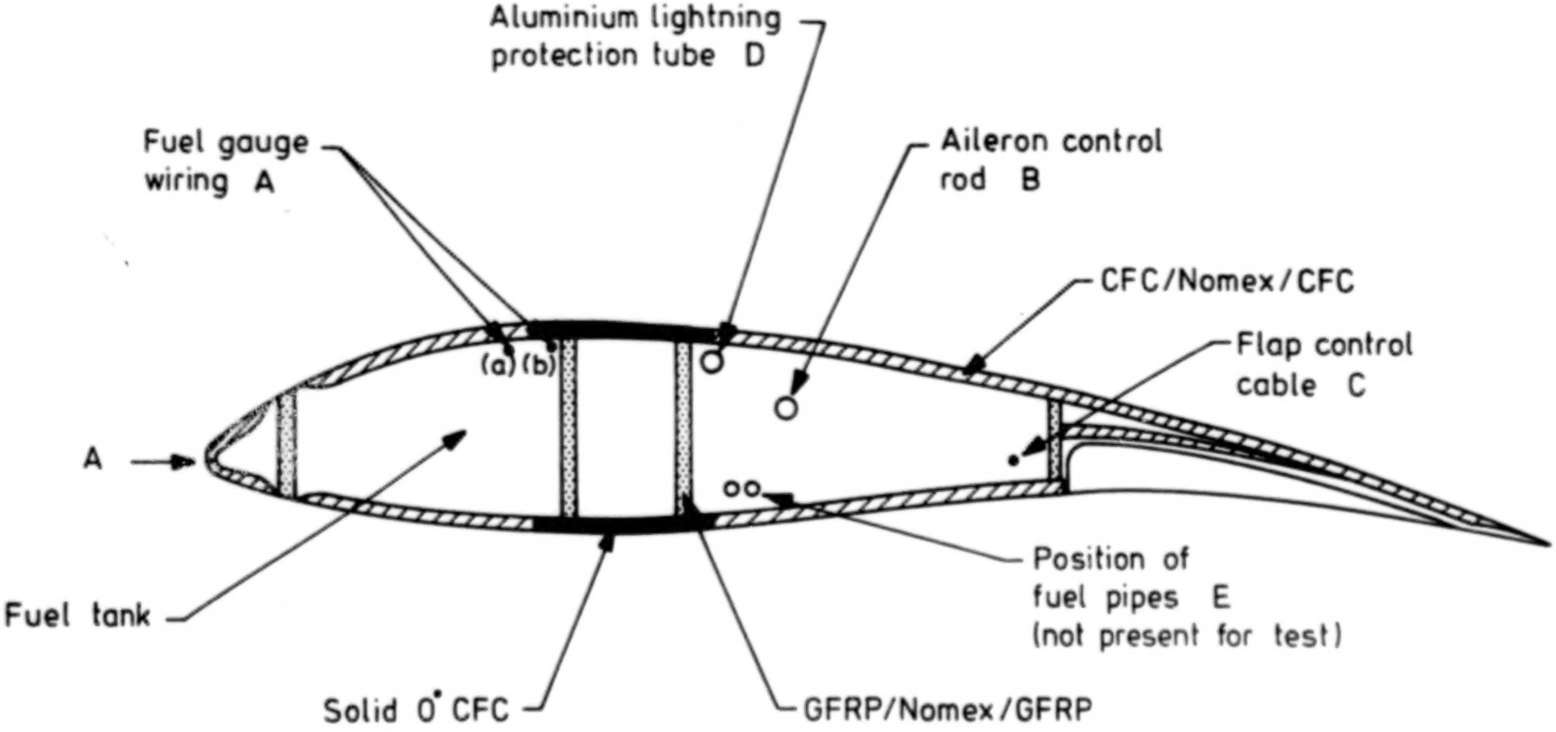
Aluminium lightning protection tube D
Fuel gauge wiring A
Aileron control rod B
CFC/Nomex/CFC
Flap control cable C
(a) (b)
A
Fuel tank
Position of fuel pipes E (not present for test)
Solid 0° CFC
GFRP/Nomex/GFRP

Fig 1 Cross section of wing tank test specimen

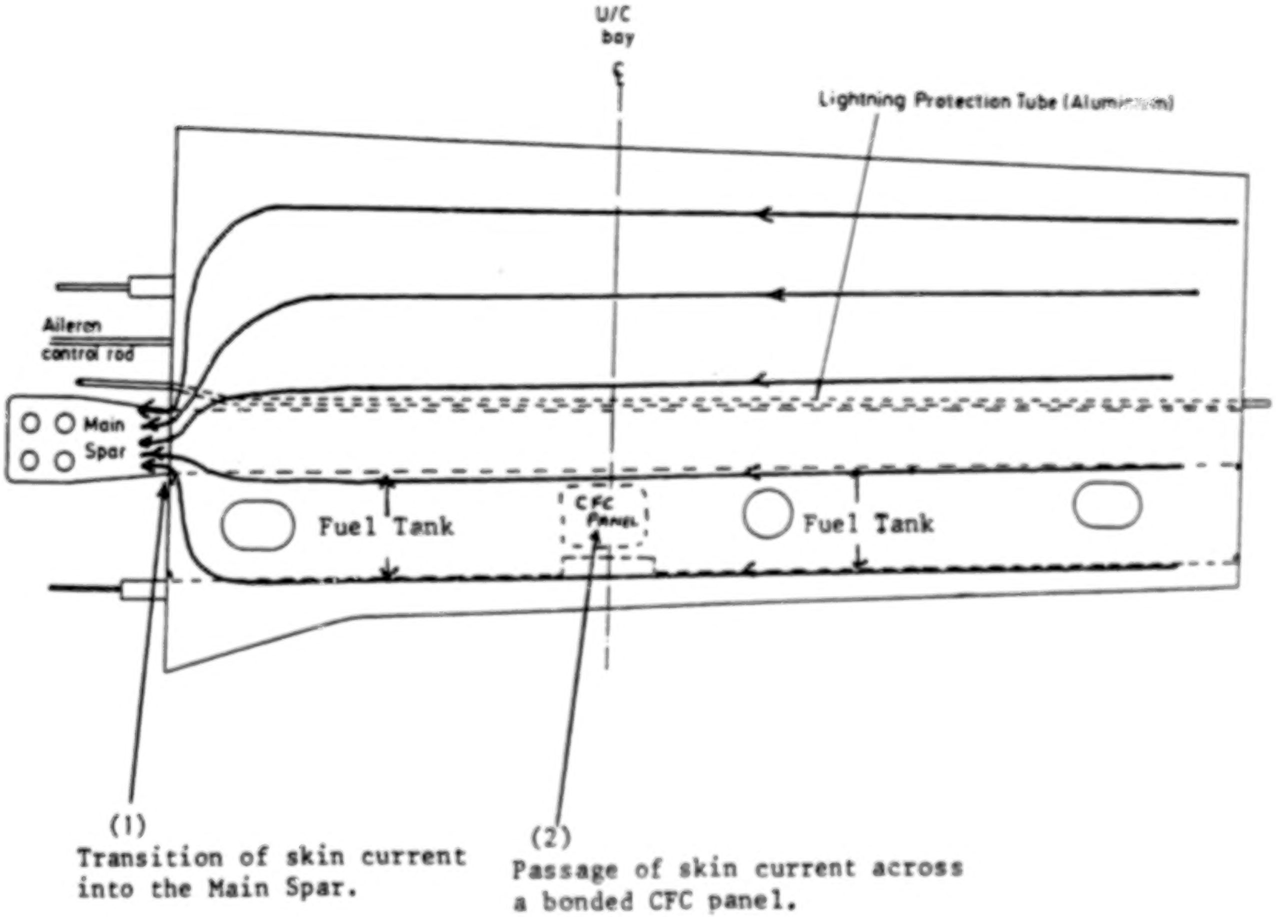
U/C
bay
℄
Lightning Protection Tube (Aluminium)
Aileron
control rod
Main
Spar
Fuel Tank
CFC
PANEL
Fuel Tank
(1)
Transition of skin current into the Main Spar.
(2)
Passage of skin current across a bonded CFC panel.

Fig 2 Top view of wing tank specimen showing possible sparking sites.

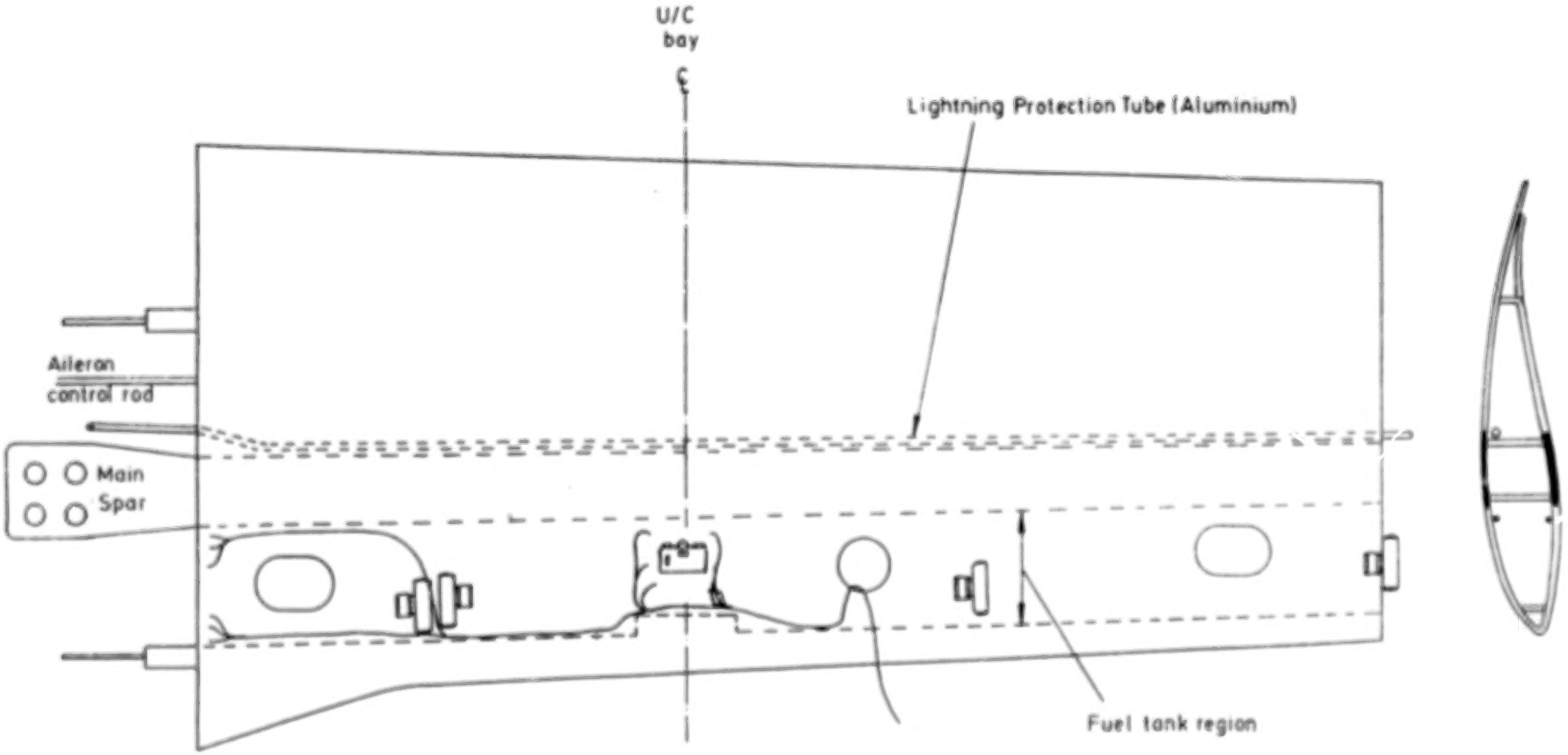
U/C bay
℄
Lightning Protection Tube (Aluminium)
Aileron control rod
Main Spar
Fuel tank region

Fig 3 Fibre optic and camera layout for sparking observations.

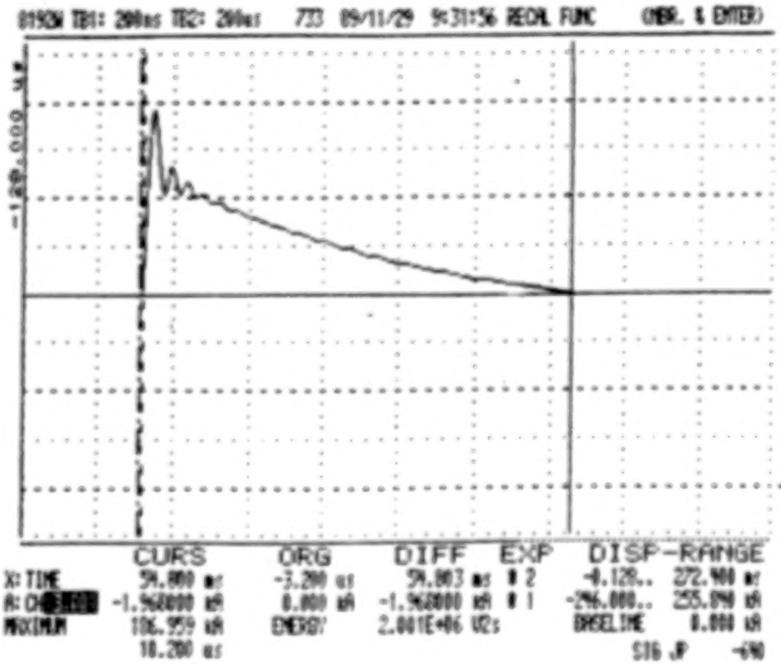

```
8192W TB1: 200ns TB2: 200us   733 09/11/29 9:31:56 RECAL FUNC   (NBR. & ENTER)
            CURS          ORG          DIFF       EXP   DISP-RANGE
X:TIME      59.800 us     -3.200 us    59.003 us  # 2   -8.120..  272.900 us
A:CH        -1.960000 kA  0.000 kA     -1.960000 kA # 1 -296.000.. 255.090 kA
MAXIMUM     186.959 kA    ENERGY       2.001E+06 A2s    BASELINE  0.000 kA
            18.200 us                                   SIG JP    -690
```

Component A current pulse

Î - 187kA, AI - 2 x 10⁶ A²s

H: 80µs/cm

V: 49.2kA/div

(Shot 4377)

1 division

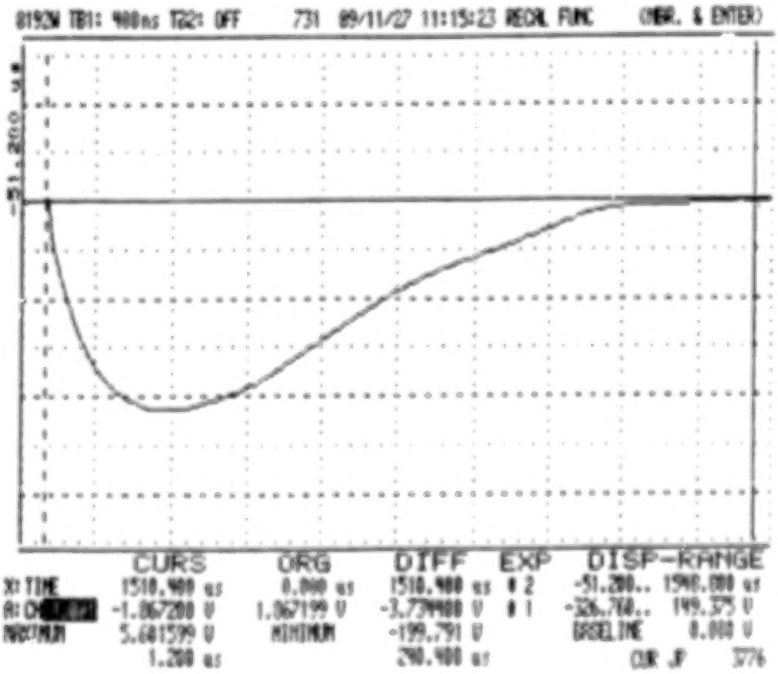

```
8192W TB1: 400ns TB2: OFF   731 09/11/27 11:15:23 RECAL FUNC   (NBR. & ENTER)
            CURS          ORG          DIFF       EXP   DISP-RANGE
X:TIME      1510.400 us   0.000 us     1510.400 us # 2  -51.200..  1598.000 us
A:CH        -1.067200 V   1.067199 V   -3.739400 V # 1  -326.700.. 199.375 V
MAXIMUM     5.681599 V    MINIMUM      -199.791 V       BASELINE   0.000 V
            1.200 us                   290.400 us       CUR JP     3776
```

Voltage induced in WLPT
(fuselage region screened)

Component A.

H: 160µs/cm

V: 46.7v/div

Fig 4 Total current in wing (upper) Current and voltage waveform in Lightning protection tube

Total pulse duration 460µs
Total pulse length 1280µs

Session 8B, Wednesday 3:45
Aerospace Vehicles
Test Criteria and Techniques 3
Wiles, Chairman

LIGHTNING PROTECTION OF FULL AUTHORITY DIGITAL ELECTRONIC SYSTEMS

David Crofts
Raychem Ltd, Swindon, UK.

ABSTRACT

Modern electronic systems are vulnerable to transient and they now provide safety critical functions such as full authority digital control units for fly by wire aircraft. There has been some confusion as to the precise specifications for these transients, however, within Europe there has been a preference for pin injection of the transient, line by line at the full threat. Given this the use of Transient Suppression Devices is essential, but with the magnitude of the threats these consume considerable volume and weight budgets.

Of the traditional suppression technologies available diodes have gained the widest acceptance, however, they lack the current handling capacity to meet existing threat levels. The development of high speed fold back devices where, at a specified voltage, the off state resistance switches to a very low on state one has provided the equivalent to a semi-conductor spark gap. The size of the technology enables it to be integrated into connectors or interconnection cables .

To illustrate the performance the technology has been developed to meet the Lightning Protection requirements for FADEC units within aeroengines. This calls for Level 5 transients to be handled on a pin by pin basis and at temperatures between -65°C and 125°C. For this application the technology was packed at 0.050" spacing within connectors inside the equipment. Results are given of the performance of the technology to the waveforms at Level 4 and 5.

Work was also carried out to study switching behaviour with the new waveform 5, the 500us, 10kAmp pulse applied to cable assemblies. This test enabled all the switches in a connector to be fired simultaneously.

INTRODUCTION

Modern electronic systems based on semi-conductor technology are very vulnerable to transient voltages or currents. As these devices are fabricated with smaller and smaller features with higher and higher densities then their vulnerability to external transients increases. Today with micron size features and millions of circuits per device, burn out levels can be lower than one milli joule of energy. Dielectric punch through

429

can occur with voltages of only a few hundred volts for nanosecond time periods.

These electronic systems now fulfil key rolls in modern aircraft, they often provide safety critical functions such as full authority digital control units in fly by wire aircraft. The number of these systems in each application is also increasing rapidly resulting in high packing densities which in turn leads to increased system to system interaction. Finally these systems are now being located in exposed regions of the aircraft outside of any Faraday cage where they are both more vulnerable to a strike and the resultant transient more severe.

The new draft Advisory Circular (SAE AE4L-87-3 Rev B 1989), Airbus Industries Specification ABD0007 and the RTCA/DO-160C Document on lightning protection of flight critical/essential electrical and avionic systems demonstrate the growing industry concern for aircraft safety as the airframe structures and electronic systems evolve. The airframe designer or system integrator must use whatever techniques of cable routing, shielding and grounding necessary to ensure that the actual transients induced in the aircraft wiring do not exceed transient control levels. The equipment designer has to ensure that the electronics can tolerate the assigned transient level.

Various suppression technologies have been used in the past and diodes have gained strong support because of their high speed, consistent performance and reliability. However, they lack the current handling capacity unless they are very large. The development of high speed fold back technology has lead to the equivalent of a semi-conductor spark gap. They still operate with the same very high speed of diodes but have a very low on-state resistance. The result of the combination of high speed and low on state resistance is that any overshoot is limited and that the current handling capability is very high. This occurs since the energy of the pulse is not dissipated within the device but into the ground. This enables very small devices to be fabricated which can be directly integrated into the interface connectors.

The application of this type of technology has lead to the development of connectors capable of protection electronics from the most severe transients directly applied to each interface line .

TRANSIENT THREAT LEVELS

There is still considerable confusion as to how these assigned transients should be applied to the equipment wiring interface. There are three basic techniques , ground injection, bulk cable injection and pin injection and these were reviewed by Wiles [1]. If one is developing a protection technology one cannot be anything but specific about the capability of the device. One has to assume the worst possible case unless each application is studied separately. This means that the technology should be capable of withstanding the most severe transient applied to the smallest possible cable i.e. one wire. It is not possible to make assumptions as to likely current sharing and coupling and hence assuming full threat by each waveform on each line is extremely conservative but essential given the large numbers of unknowns within a design.

This has been the stance taken by Airbus Industries in their specification where pin injection of both the long and short waveform as well as the oscillatory waveform are specified at the assigned threat level. A final aspect of the testing is that none of the specifications call for the testing to be carried out at anything other than room temperature. Given the extreme temperature sensitivity of most semi-conductor technology this is a major oversight.

To qualify transient protection devices it is necessary to test them with each of the waveforms at the maximum specified level, line by line and across the full specified temperature operating range. Further the number of operations that the device can withstand has to be substantially above the equipment specification. This is because given the number of lines in one FADEC (>450) and the required reliability one would have to specify at least one order of magnitude above the equipment specification. A further requirement would be to specify that any let through transient would have to have an energy content below the damage threshold of the equipment and the let through voltage spike was below any dielectric punch through level

A general specification for a FADEC unit in a critical zone for example in a engine could be summarized as follows:-

LIGHTNING TRANSIENT PROTECTION REQUIREMENTS

TRANSIENT	Wfm 2	Wfm 3	Wfm 4
WAVESHAPE	6 us	1-50 MHz	70 us
PEAK CURRENT	320	128	320
PEAK VOLTAGE	1600	3200	1600

TEMPERATURE RANGE	-65 TO 125° C
NUMBER OF OPERATIONS	100 BOTH POLARITIES
LET THROUGH ENERGY	< 1 milli JOULE
VOLTAGE SPIKE	< 500 VOLTS

A further factor that should always be considered is the other parts of the EMC specification that the equipment would have to meet. For example a military aircraft would also have to meet EMP requirements and civilian aircraft the latest HIRF requirements of RTCA/DO 160C Chpt. 20. It is certainly the trend for the airframe manufacturers to assume the aircraft wiring gives no protection against all these EMC threats and to place the total requirements on the equipment supplier. In which case the protection devices are almost certainly working in conjunction with filters.

PROTECTION TECHNOLOGIES

There are various basic technologies used in transient protection and they are characterized into two distinct families, voltage clamps and voltage foldback. The two types are shown, however, there are variations on these basic curves and the author discussed these in previous papers [2,3] Typical voltage clamps have been Zener diodes and Metal Oxide Varistors whilst fold back technologies have included Gas Discharge Tubes and Fold Back Diodes.

Each of these suppression technologies have been used in the past and diodes have been preferred because of their fast response time (< 1ns), consistent performance and high reliability. However, these acts as voltage clamps and they do not have the necessary current handling capability in an economically sized package. Fold back devices, because of their low on state resistance, have far higher current handling capabilities. The development of multi-layered thyristor technology provided the equivalent of a high speed semi conductor Gas Discharge Tube.

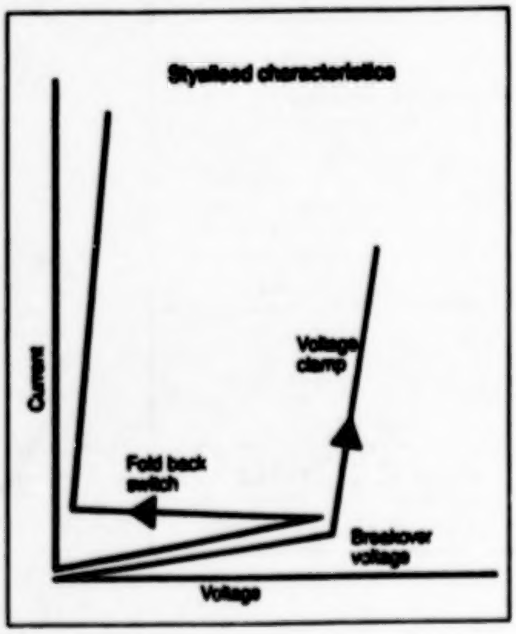

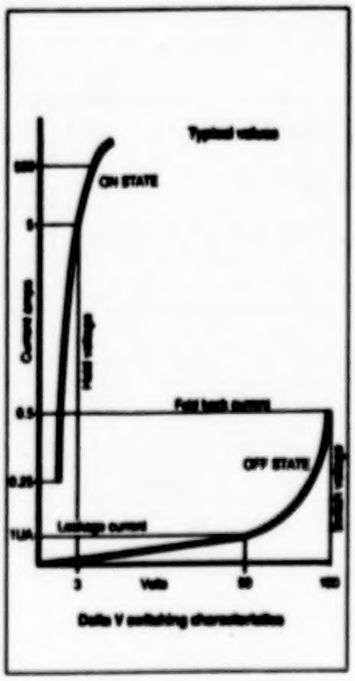

Protection Mechanism

The device under consideration is based on a four layer thyristor structure which gives a fold back crowbar type action which is voltage triggered. The switch has a high holding current which ensures reset after the transient has subsided. The initial action of the switch is the same as a Zener and hence one achieves a balance of their good points with those of a Gas Discharge Tube but without their disadvantages. The switch has the same rapid response as Zeners to fast voltage transients and at low currents acts as a similar voltage clamp. Higher currents initiates the fold back action and the voltage across the switch falls to a low level.

The switch acts as a shunt element which is voltage triggered and to ensure bidirectional operation, consists of two switching elements. The switch can sink very high levels of current in the low voltage "on" state. Because of this the active area is efficiently used enabling small devices to be made. A normal 100 volt Zener under 40 amps pulsed conditions might develop 4 kW whereas with a foldback switch the "on" voltage may only be 3 volts giving 120 W. This greatly reduces the heat that has to be dissipated and reduces the junction temperature. This also results in the power derating with temperature being much less than for Zeners.

Delta V 'off state' electrical properties

Parameter	Test conditions	Units	Minimum	Typical	Maximum
Leakage current I off	+/- 50V 25°C 125°C	micro amps	0.001 0.5	0.020 1.0	1.0 10.0
DC withstand voltage	I off <1uA	Volts	50	50	50
Capacitance coef	1Khz	pF	100	140	200

Delta V switching characteristics

Parameter	Test conditions	Unit	Minimum	Typical	Maximum
Switch voltage Vt	0.1/10 us pulse 500 V	Volts	80	100	100
Switch speed Tsw	As Above	nano-secs	0.5	1.0	2.0
Fold back time Tfb	As Above	nano-secs	100	250	500
Charge transfer Q	As Above	nano-C	200	500	1000
Fold back current Ifb	As Above	Amps	0.5	0.5	0.5
Hold current Ihld	As Above	Milli amps	150	250	400
Characteristics	Sine Wave	Bipolar			

LIGHTNING EVALUATION OF THE FADEC

Specification Levels

The testing and qualification of the electronic system was carried out in a series of steps. The system was a Full Authority Digital Electronic Control for an Aeroengine. As such the specified threat level was 5 except that for waveform 4 this was reduced to 4. Since this appears somewhat contradictory test were carried out at level 4 & 5 with waveform 4.

The basic procedure adopted was that of the Airbus Specification ABD007, i.e. pin injection. There is one serious drawback to this and that is only one line is tested at the same time whilst in the real world it would be assumed that the transients would appear on all the lines at approximately the same time period. Indeed the author reported in an earlier paper [4] that during whole aircraft testing that the waveform that appeared on each pin was a composite of all three waveshapes giving a combination of high frequency oscillatory components as well as a wide pulse. Because of this experiments were set up with more than one pulse generator to drive several lines simultaneously at the peak specified current.

A further test added was an evaluation with the new waveform 5 of the SAE advisory circular i.e. 500 us width at 10 kA. This was a ground injection test onto the screens of the cable and this test certainly excited all lines simultaneously.

All waveforms and test levels specified are those described in the SAE AE4L 87-3 Rev B 1989 advisory circular.

Test Methodology

The equipment was complicated with several input connectors with the number of protected lines > 500. The technology was packaged into two product forms, the Raychem MTC (Trade Mark) flat modular connector system and a Splice unit designed to be fitted into the interconnection from connectors to the electronics. There were also filters on most lines which were in the connectors interfacing directly with the aircraft wiring. Because of this the testing was carried out in separate blocks.

Component Test. This was the simplest test and involved testing individual connectors, pin by pin at the full threat of each waveform. In each case the voltage transient remaining on the line was recorded as well as the energy it dissipated into a 50 ohm system. These tests could also be carried out at a range of temperatures between -65 and + 125° C and also over a high number of operations.

Box Interconnection Test. Here the filter connector was in place and the protection switch fitted to the interconnections within the box. Each input line was tested with each transient at the full threat level. The tests were carried out at room

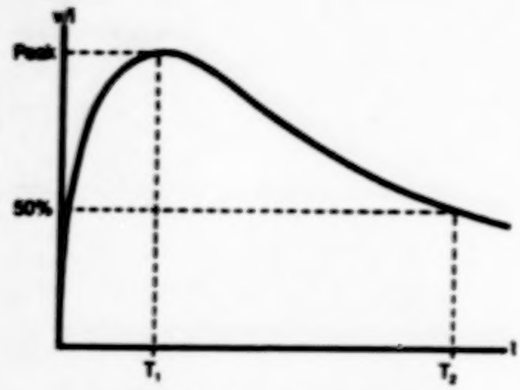

Current Waveform 1 — $T1 = 6.4\ us \pm 20\%$, $T2 = 70\ us \pm 20\%$

Voltage Waveform 4 — $T1 = 6.4\ us \pm 20\%$, $T2 = 70\ us \pm 20\%$

Current Waveform 5A — $T1 = 40\ us \pm 20\%$, $T2 = 120\ us \pm 20\%$

Current Waveform 5B — $T1 = 50\ us \pm 20\%$, $T2 = 500\ us \pm 20\%$

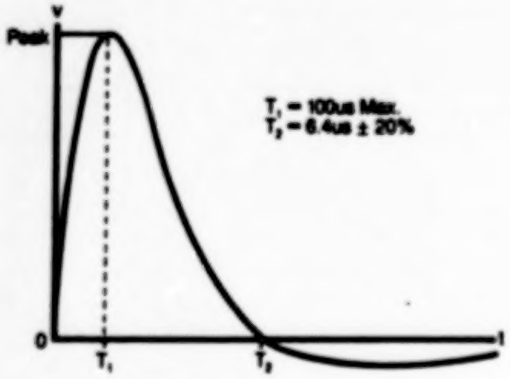

Voltage Waveform 2

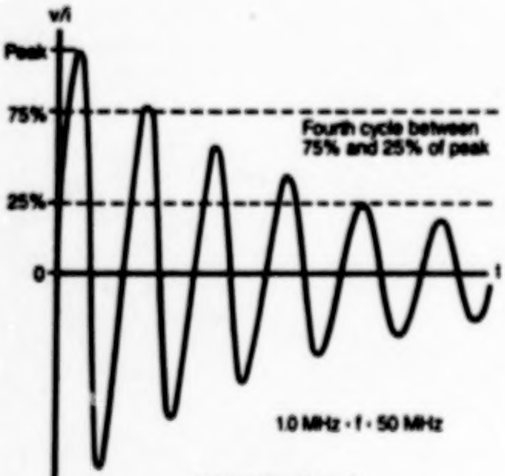

Voltage Waveform 3

Idealised induced voltage and current waveforms

Level	Waveforms 2 Vp/Ip	3 Vp/Ip	4 Vp/Ip	5 Vp/Ip
1	50/10	100/4	50/10	N/A
2	125/25	250/10	125/25	N/A
3	300/60	600/24	300/60	300/100
4	750/150	1500/60	750/150	750/1000
5	1600/320	3200/128	1600/320	1600/3000 to 20,000

Vp = Peak Open Circuit Voltage Line-to-Ground
Ip = Peak Short Circuit Current On A Line

Suggested ETDL Voltage and Current Levels

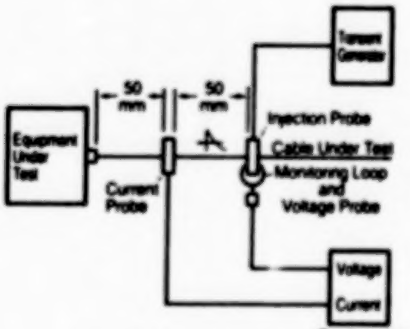
Transient Generator
50 mm
50 mm
Equipment Under Test
Injection Probe
Cable Under Test
Monitoring Loop and Voltage Probe
Current Probe
Voltage
Current
Oscilloscope

Bulk cable injection test setup

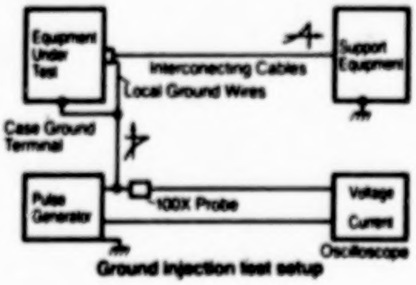
Equipment Under Test
Support Equipment
Interconnecting Cables
Local Ground Wires
Case Ground Terminal
Pulse Generator
100X Probe
Voltage
Current
Oscilloscope

Ground injection test setup

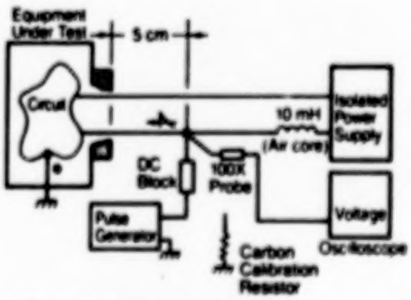
Equipment Under Test
5 cm
Circuit
10 mH
(Air core)
Isolated Power Supply
DC Block
100X Probe
Pulse Generator
Voltage
Oscilloscope
Carbon Calibration Resistor

• External equipment grounds should be tied to case for these tests

Pin injection test setup

temperature and the resulting voltage across each filter pin was monitored as well as at the board level. The functionality of the board mounted components were evaluated at the end of the tests for damage or degradation of performance.

In this series covering 37 input lines, tests were carried out using waveform 2 at level 5 on a total of 3 lines using three separate generators. The lines were chosen that interfaced with the same board area.

Waveform 5 Testing. This test did not represent part of the original specification. However, it was considered essential to demonstrate that the protected harness which consisted of individual screened twisted pairs should be tested. More details of the test and the method are given in a separate paper to be given by this author in this conference. Basically a current waveform of 500 us width and of 10 kA peak amplitude was ground injected into the protected cables and the resultant voltage transients on each pin monitored. A total of 10 twisted pairs were tested giving 20 lines which was one half of a hardened connector. The performance of each switch element was re-evaluated at the end of the test.

TEST RESULTS

Box Interconnection Test. The resulting waveshapes were distorted by the presence of the filters and the system LC parameters. During testing at component level there were high voltage transients (2 - 300 V) when the high frequency waveform 2 with its 100 ns rise time was used as well as with the 10MHz oscillatory waveform 3. With these tests the filter reduced these significantly and the most severe test was the waveform 4 the slow pulse. In all cases the voltage across the filter pins never exceeded 150 Volts. The transient let through energy was recorded and never exceeded 250 micro Joules. Since no damage occurred to any of the board mounted components it was concluded that these transients were below their susceptibility levels.

Waveform 5 Test. The result is shown with the other transients and it is interesting to note that the voltage induced without protection was 200 volts on each line which with a protected line caused the switch to fire at 100 volts and operate in the normal fashion. There was no other damage to the switches with this test.

DELTA V PROTECTION
LIGHTNING Wfm 2

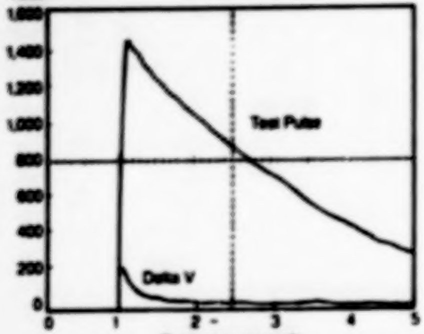

Test Pulse 1500 V 300 A
2 us Width
50 ns Rise

Delta V Pulse 230 V
Let Through Energy
into 50 Ohms 1 mJ

DELTA V PROTECTION
LIGHTNING Wfm 4

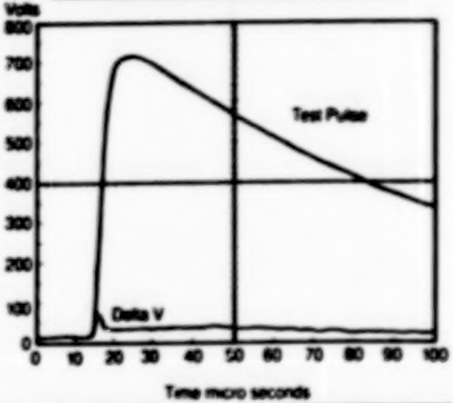

Test Pulse 750 V / 150 A
70 us Width
5 us Rise

Delta V Pulse 85 V
Let Through Energy
into 50 Ohms 1 mJ

DELTA V PROTECTION
LIGHTNING Wfm 3A

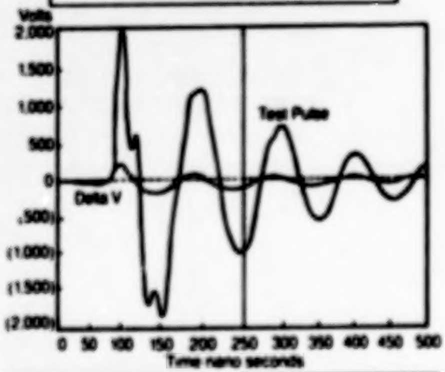

Test Pulse 2000 V 80 A
Damped Sinusoidal
10 MHz Frequency

Delta V Pulse 240 V
Let Through Energy
into 50 Ohms 0.3 mJ

DELTA V PROTECTION
LIGHTNING Wfm 4

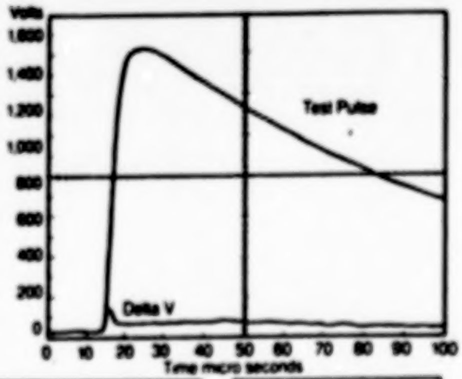

Test Pulse 1500 V 300 A
70 us Width
5 us Rise

Delta V Pulse 140 V
Let Through Energy
into 50 Ohms 1 mJ

DELTA V PROTECTION
LIGHTNING Wfm 3B

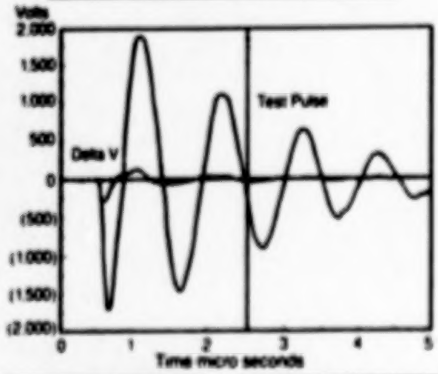

Test Pulse 2000 V 80 A
Damped Sinusoidal
1 MHz Frequency

Delta V Pulse 140 V
Let Through Energy
into 50 Ohms 0.1 mJ

DELTA V PROTECTION
LIGHTNING Wfm 5B
Ground Injection into Cable Shield

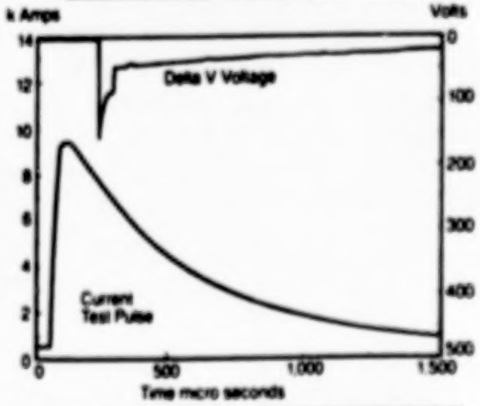

Test Pulse 10 kA Ground
Injected 500 us Width
Current in Cable Braid

Delta V Pulse 134 V
All conductors of Cable
Commoned. Short Drive End

Component Test. The results are graphically represented for each waveform at level 5 (waveform 4 is also given at level 4). The results represented are the 100th. shot on each line and at room temperature. To obtain clear performance data like this it is necessary to use very short test leads, when testing at elevated temperatures the longer test leads causes some difficulties in accurate measurements

In all cases the switches were able to perform to specification across the full temperature operating range.

CONCLUSIONS

This test programme demonstrated that it is possible to protect electronic equipment interfaces to the full threat currents of each waveform on a pin by pin basis.

It was demonstrated that current levels of 320 amps with a 70 us wide pulse could be handled even at 125° C for a number of operations an order of magnitude above the specified number of 10.

The performance of multiple firing of a number of switches was demonstrated including with the new proposed waveform 5.

It is recognized that this type of testing represents a very severe case and is applicable to component testing where the specific application is not known whilst for know systems bulk cable injection would be preferable to pin injection.

REFERENCES

[1] K.G. Wiles, Lightning Protection Verification of Full Authority Digital Electronic Control Systems. 1989 International Conference on Lightning and Static Electricity.
[2] D. Crofts & B.Z. Raisch, System Protection Against EMP Transients Using High Speed Fold Back Devices. 7th International Zurich Symposium on EMC.
[3] D. Crofts, Primary ESD Protection Technologies. Electromagnetic Compatibility & Micro processor based Equipment. ERA EMC 88 , London.
[4] D. Crofts & M. Wright, Protection of Aircraft Harnesses Against Lightning-Induced Voltages. 7th International Zurich Symposium on EMC.

Simulation and measurement of melting effects on metal sheets caused by direct lightning strikes

Alexander Kern

University of the Federal Armed Forces,

Munich Germany

Abstract

Direct lightning strikes melt metal parts of various systems, like fuel and propellant tanks of rockets and airplanes, at the point of strike. Responsible for this melting are the impulse current and, if occuring, the long duration current, both carrying a remarkable charge Q.

For studying these meltings the simulation in the laboratory has to be based on the parameters of natural lightnings. International standards exist defining certain threat levels of natural lightnings and giving possible generator circuits for the simulation.

The meltings caused by both types of lightning currents show different appearance. Their characteristics, their differences in melting and heating of metal sheets are investigated.

Nevertheless the simulation of lightning in the laboratory is imperfect. While natural lightning is a discharge without a counter electrode, the simulation always demands a close counter electrode. The influence of this counter electrode is studied.

1. Introduction

Metal sheets as parts of various systems can be exposed to direct lightning strikes, e.g. fuel and propellant tanks of rockets and airplanes.

Direct lightning strikes may cause melting effects on metal sheets up to burn throughs. But even if the metal is thick enough to withstand puncturing, the temperature rise at the opposite side of the metal sheet, i.e. the inner side of a tank, may be high enough to ignite explosive mixtures.

Responsible for this heating resp. melting effect is mostly the charge Q. From Q, multiplied by the nearly constant anode or cathode voltage drop, results the energy converted at the point of strike.

The two components of a natural lightning strike carrying a significant charge Q are the impulse current and, if it occurs, the long duration current. If one wants to simulate those heating or melting effects, the simulation has to be very close to natural lightning, i.e. the simulated impulse and long duration currents have to correspond to the components of natural lightnings as far as possible.

In the past years a lot of efforts were done from the International Electrotechnical Commission (IEC), to work out definitions for the threat of natural lightnings. At the October 1990 - meeting of the Technical Committee 81 (TC 81) of IEC the parameters have been finally concluded /1/. Now these definitions are accepted internationally, and they will be obligatory for standards for lightning protection.

In this paper generators are presented, which are able to fulfil the definitions given by IEC TC 81: an impulse current generator with a double-crowbar sparkgap and a long duration current generator. Both generators are realized at the High Voltage Laboratory of the University of the Federal Armed Forces in Munich, Germany.

With these generators experiments have been performed at different metal sheets made of copper, aluminium, brass and two kinds of steels. The differences in the meltings on these metal sheets caused by impulse currents and long duration currents are presented. The melting effects are discussed as a function of the kind of metal, the thickness of the sheets and the parameters Q (charge) and W/R (specific energy) of the lightning current.

Natural lightning is a discharge without a nearby counter electrode, while in the laboratory simulation there always has to be a rather close counter electrode. Therefore the influence of the distance between the test sample and the counter electrode and the geometrical form of the counter electrode are especially investigated.

If the metal sheet is thick enough to withstand puncturing by the lightning current, measurements of the heating at the opposite side of the sheet are conducted with infrared thermosensors. These measurements conclude the time slope and the maximum value of the temperature at the hottest point of the sheet's opposite side, i.e. directly behind the point of strike of the electric arc.

2. Natural lightnings

For analysis and for classification of lightning currents four threat parameters are defined characterizing specific effects of lightning:

- Peak current i_{max}, responsible for the ohmic voltage drops of stroken objects.
- Charge $Q = \int i dt$, leading to melting, vaporizing and welding by the electric arc at the point of strike. Because of the different effects the total charge Q_t has to be divided into the charge of the impulse current Q_i and the charge of the long duration current Q_l.
- Specific energy $W/R = \int i^2 dt$, also called the action integral, responsible for the heating and the electrodynamic forces of metal wires carrying the lightning current.
- Current rate-of-rise $\Delta i/\Delta t$ in the front of a lightning current, leading to electromagnetically induced voltages in installation circuits.

About ten years ago the measurements of natural lightning currents, which were available worldwide, were taken together. Then the data were statistically prepared, related to the four defined threat parameters. This work was conducted by the Working Group 33 of the International Conference On Large High Voltage Electric Systems (CIGRE WG 33) /2, 3/.

The basic results of that work are shown in fig. 1 to 4, seperated for negative first strokes, negative following strokes and positive flashes. The figures give the frequency distribution of the peak current i_{max}, the total charge Q_t, the impulse charge Q_i and the specific energy W/R, those threat parameters, which are necessary to define impulse and long duration currents for the laboratory simulation. The distribution of the current rate-of-rise $\Delta i/\Delta t$ is not shown in this paper, because this parameter does not have a remarkable influence on melting or heating effects.

3. Standards for the laboratory simulation

Standards for the simulation of lightning currents in the laboratory have to be based on the parameters of natural lightnings given in chapter 2. At first one has to define a certain protection level for the device under test. IEC TC 81 fixes four protection levels, which can be chosen /1/. The highest level, protection level "I", includes about 99% of all natural lightnings, i.e. only 1% of natural lightnings exceeds the defined current parameters.

The german military standard VG 96 901 Teil 4 /4/, valid for planning and construction of systems and equipment for the Bundeswehr, corresponds to the definitions of IEC. Two threat levels are determined here: threat level "high" also includes about 99% of natural lightnings, threat level "normal" about 95%.

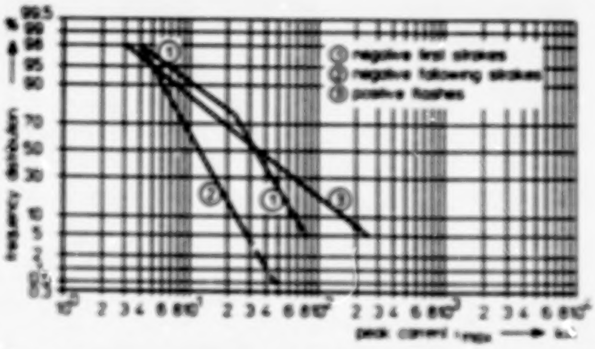

Fig. 1 Frequency distribution of the peak current i_{max}

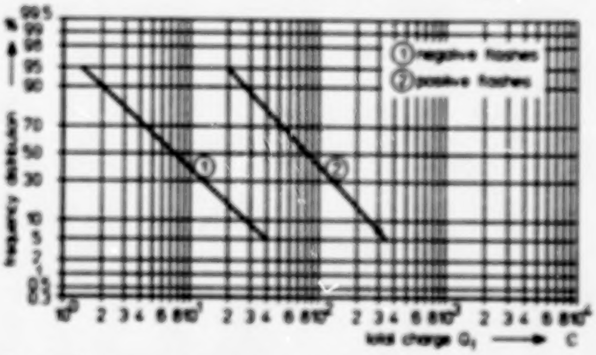

Fig. 2 Frequency distribution of the lightning total charge Q_t

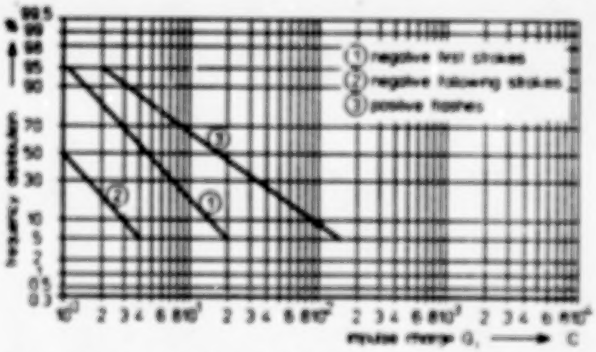

Fig. 3 Frequency distribution of the impulse charge Q_i

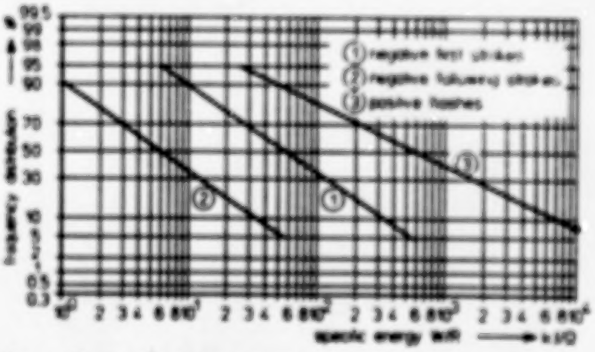

Fig. 4 Frequency distribution of the specific energy W/R

If the protection resp. threat level is fixed, one can go into the statistical data. There one gets the current parameters for the chosen level. It is important, that all parameters for a simulated lightning current are based on the same protection level. For example, if a impulse current for protection level "I" shall be simulated, all current parameters, in this case the peak current i_{max}, the impulse charge Q_i and the specific energy W/R, have to fulfil the 99%-value.

Furthermore for accurate reading of the current parameters in the statistical data it has to be taken into account, that about 10% of natural lightnings are positive flashes. So for the fixing of the current parameters the influence of these positive flashes must be included with appropriate importance.

Responsible for the heating resp. melting effects on metal sheets are two components of a natural lightning current, the impulse and the long duration current. Based on the above considerations the following parameters are fixed for protection level "I" of IEC /1/ resp. threat level "high" of VG 96 901 Teil 4 /4/:

- impulse current
  - peak current i_{max} = 200 kA ± 10%
  - charge Q_i = 100 C ± 20%
  - specific energy W/R = $\int i^2 dt$ = 10 MJ/Ω ± 35%
- long duration current
  - charge Q_l = 200 C ± 20%
  - time T_l = 0,5 s ± 10%

The experimental investigations published in this paper are conducted with currents fulfilling these parameters, which, as mentioned before, include about 99% of natural lightnings.

The aviation industry normally uses another standard for the simulation of lightning currents, the SAE AE4L /5/ resp. the MIL-STD 1757A /6/. These standards define a long duration current, which corresponds to the definitions of IEC, but the impulse current shows remarkable differences.

This impulse current has a peak current i_{max} of 200 kA, an impulse charge Q_i of 20 C, which is increased by an intermediate current up to 30 C, and a specific energy W/R of 2 MJ/Ω. Using the statistical data of chapter 2, the current parameters can be analyzed:

- The peak current i_{max} includes about 99% of natural lightnings, like required by IEC for protection level "I".
- The impulse charge Q_i corresponds only to the 90%-value of natural lightnings (95% of first negative strokes, 50% of positive flashes). If the charge of the intermediate current is added, it corresponds to the 94%-value.
- The specific energy W/R includes about 96% of natural lightnings. In fact the defined value of 2 MJ/Ω considers about 99% of the first negative strokes /7/, but only about 70% of the positive flashes, which absolutely may not be forgotten.

The impulse current fixed in SAE AE4L resp. MIL-STD 1757A shows parameters, which are not correlated in relation to the probability of appearance in the reality. It simulates natural lightnings only incompletely.

So if one wants to simulate the real threat of natural lightnings, the parameters given by IEC have to be taken. In the future it can be expected, that more and more national and international standards will be based on the definitions of IEC.

4. Laboratory equipment

4.1 Impulse current generator

For the simulation of impulse currents with peak currents in the range of some 100 kA mostly capacitive surge current generators are used. Especially for the simulation of extreme values of charge and specific energy, as demanded in /1, 4/, a capacitive surge current generator with a crowbar sparkgap is of great advantage. As shown in /8/, with the crowbar technique it is possible to achieve a charge transfer through the device under test, which is up to a factor of 40 greater than the stored charge in the capacitor bank. Thus the capacitor bank can be kept relatively small.

The costs of a surge current generator are dominated by the prize of the capacitor bank. Therefore the equipment should be used as efficient as possible. A further improvement of the efficient use of a given capacitor bank can be realized by seperating the whole test equipment into two identical parts, each with its own crowbar sparkgap. The two parts of the generator are only connected by the device under test, where their currents are summarized.

Compared with a single surge current generator of the same total surge capacitance and the same charging voltage the peak current i_{max} as well as the impulse charge Q_i achieved in such a twin arrangement are greater according to a factor $\sqrt{2}$, the specific energy W/R according to a factor 2 /9/.

The equivalent circuit of a twin arranged surge current generator is shown in fig. 5.

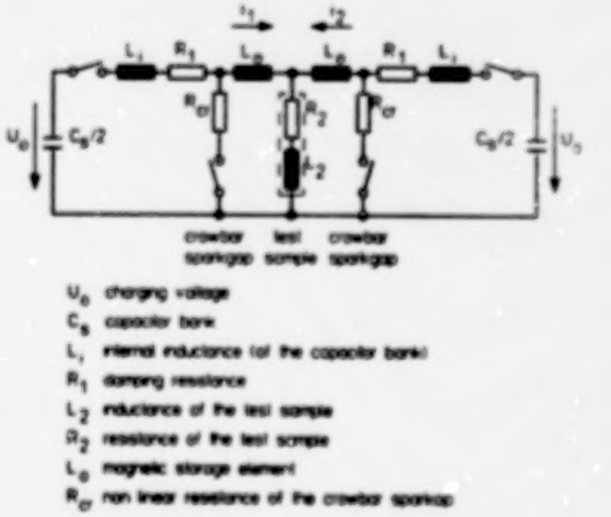

U_0 charging voltage
C_s capacitor bank
L_i internal inductance (of the capacitor bank)
R_1 damping resistance
L_2 inductance of the test sample
R_2 resistance of the test sample
L_0 magnetic storage element
R_{cr} non linear resistance of the crowbar sparkgap

Fig 5 Twin arrangement of a surge current generator

The decay time constant τ_1 of the exponential decay of the current is given by

$$\tau_1 = (L_0 + 2 \cdot L_2)/(R_{cr} + 2 \cdot R_2).$$

The parameters of the current can be calculated according to the following equations:

$$Q_i = i_{max} \cdot \tau_1 ; \quad W/R = i_{max}^2 \cdot \tau_1 / 2$$

$$i_{max} = U_0 \cdot \sqrt{\frac{C_s}{L}} \cdot \eta ; \quad \eta = \exp\left(- \frac{\mathrm{Atn}(\omega \cdot T)}{\omega \cdot T}\right)$$

$$L = \frac{L_0 + L_i}{2} + L_2;\ R = \frac{R_1}{2} + R_2$$

$$\tau = \frac{2L}{R};\quad \omega = \sqrt{\frac{1}{L \cdot C_s} - \frac{1}{\tau^2}}$$

The realization of a twin arranged surge current generator for the simulation of the impulse current according to /1, 4/ is shown in fig. 6. A typical current obtained with this equipment and a sparkgap with a spacing of 20 mm as test sample is given by fig. 7.

The use of a surge current generator in a twin arrangement has a further significant advantage, if melting or heating effects are to be studied. Because of the geometric symmetry the magnetic fields and the resulting magnetic forces of both generator parts are neutralised at the position of the test sample. Thus the arc in the test sample burns uninfluensed by the external magnetic fields caused by the leads to the test generator. This situation corresponds to the impact mechanism of a natural lightning strike to a metal sheet.

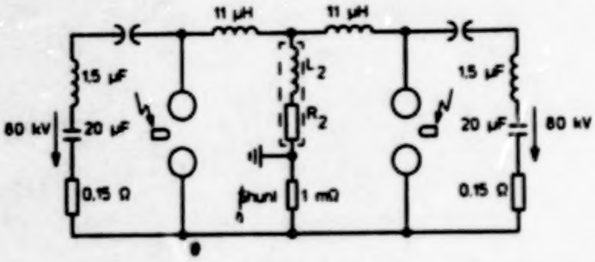

Fig 6: Twin arranged surge current generator with two crowbar sparkgaps

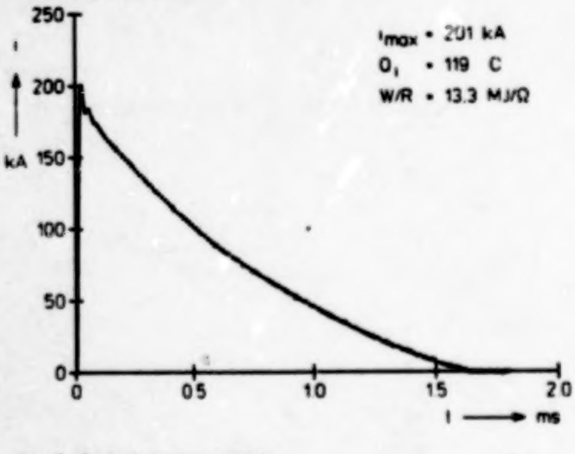

Fig 7: Typical impulse current

4.2 Long duration current generator

For the simulation of the long duration current another capacitor bank is used. The circuit is shown in fig. 8.

The control unit creates the triggering impulses for both thyristors V regulating the primary transformer current. On the secondary side of the transformer the voltage is demodulated by the d.c.-converter. The capacitor bank C is charged on this direct voltage.

After the long duration current has been triggered, the capacitor bank feeds in the test sample over an electric arc. While the current flows, the capacitor bank is permanently recharged by the transformer via the d.c.-converter. With this arrangement the long duration current of fig. 9 with nearly rectangular wave shape is generated.

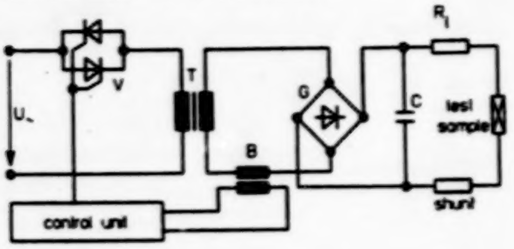

$U_\sim$ alternating voltage 220 V
V thyristors
T transformer 220/400 V
B current transformer
G d. c.- converter
C capacitor bank 41,3 mF
R_l loading resistor

Fig 8: Long duration current generator

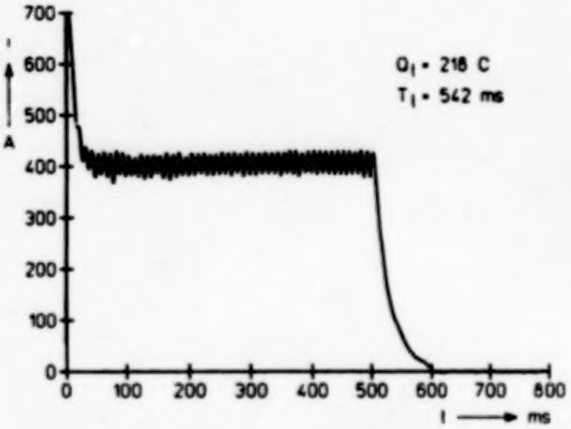

Fig 9: Typical long duration current

The current amplitude is fixed by the output voltage of the capacitance and the resistance in the circuit. The total resistance consists of the resistances of the test sample, the electric arc, the shunt and the loading resistor R_1. With this adjustable loading resistor different current amplitudes can be created at constant transformer resp. capacitance voltage.

The secondary 50 Hz-half waves behind the transformer are counted with the current transformer B. After a certain time duration, which has to be fixed at the control unit previously, no more triggering impulses for the thyristors are created. The primary and therefore also the secondary transformer current are blocked, and the capacitor bank is discharged exponentially via the test sample.

5. Melting effects

For the tests on metal sheets the following typical materials were selected:

- aluminium
- copper
- brass
- soft steel (St37)
- stainless steel (V2A)

5.1 Impulse currents

The melting effects on metal sheets caused by impulse currents have a typical appearance. The melted material is spread over a large area with diameters of several cm up to 10 cm. Some examples of melting caused by impulse currents are shown in fig. 18 and 19. The melted areas are surrounded by a zone of splashed material.

The radius of the melted area depends on the kind of material. Sheets of soft and stainless steel show the largest melted areas (typ. 8 cm), followed by aluminium sheets (typ. 6 cm), brass and copper (typ. 4 to 5 cm). The depth of those melted areas is very small. It ranges from 0.1 to 0.2 mm, for aluminium up to 0.4 mm.

The comparatively large melted areas result from the high specific energy (which is equal to $\int i^2 dt$) of the impulse current. This specific energy is responsible for the electrodynamic forces. The melted areas found at the tests with long duration currents, which have a considerably lower specific energy, are remarkably smaller (typ. 1..2 cm).

The spacing and the geometrical construction of the counter electrode does not affect the diameter of the melted area.

5.1.1 Test performance

The decay time constant τ_1 of the current and as a consequence the impulse charge Q_i are a function of the resistance in the circuit. If the distance between the counter electrode and the test sample increases, the resistance of the electric arc and therefore the total resistance in the circuit rises. The attitudes of the decay time constant τ_1 and the charge Q_i as a function of the spacing of the counter electrode are shown in Fig. 10 and 11. The charging voltage here was fixed at 80 kV.

The results allow a rough calculation of the arc's resistance. Comparing the different decay time constants τ_1 or the charges Q_i according to the equations of 4.1, the resistance of the electric arc related to it's length is approximately

$R' = 0{,}75$ mΩ/cm.

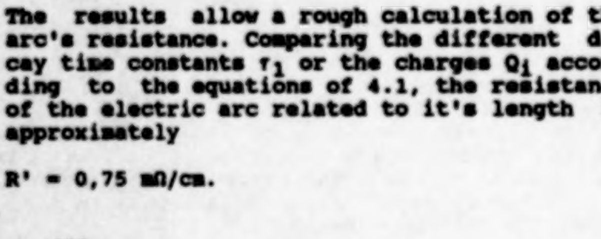

Fig. 10: Decay time constant τ_1 as a function of the spacing s of the counter electrode

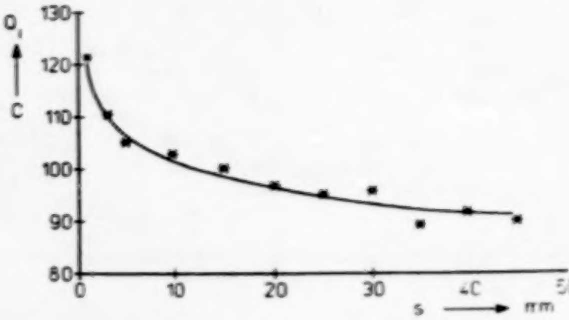

Fig. 11: Impulse charge Q_i as a function of the spacing s of the counter electrode

This relation is only valid for arcs of currents in the range of 200 kA. Furthermore the anode and cathode voltage drop is not considered in this relation. In the investigated case the value of this voltage can be estimated to $U_{A,K} \approx 30$ V.

To make comparable measurements the charging voltage was accommodated to the spacing of the counter electrode. The resulting charge Q_i could be kept constant within 5% ($Q_i = 100 \pm 5$ C).

To eliminate the remaining differences, the values were corrected linearly to $Q_i = 100$ C.

5.1.2 Test results

The spacing between the counter electrode and the test sample affects the melting loss in material. An increasing distance drags a decreasing value for the loss in volume.

Melted and splashed material is a result of the formation of plasma rays between the sheets and the counter electrode. The larger their spacing, the weaker the influence of the plasma rays at the surface of the sheets and the fewer their power to melt and to splash the material.

A simple way to eliminiate the power of those plasma rays as far as possible is the use of a so called insulating electrode (electrode II), like shown in fig. 12.

In contrast to the standard electrode (electrode I) this insulating electrode has a teflon cap at its top. With this the electric arc is forced to leave the electrode radially and to "curve" to the test device. The plasma rays also leave the electrode radially, and therefore they do not strike the test device with the same power as known from electrode I.

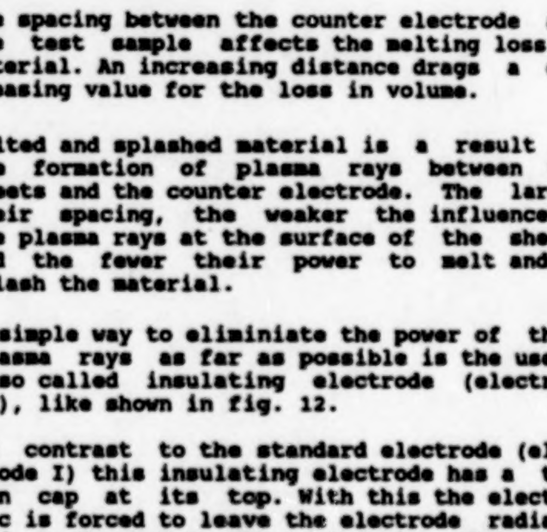

Fig. 12: Construction of two counter electrodes

The tests were conducted with the five chosen metals and for both electrodes. The losses in volume ΔV as a function of the spacing s of the electrode are shown in fig. 13 to 17.

Different materials show different values of the loss in volume. The specified losses of the different materials are a function of the melting and boiling temperatures and of the thermal capacities and conductivities. The higher the temperatures, the capacities and conductivities, the smaller the loss in volume.

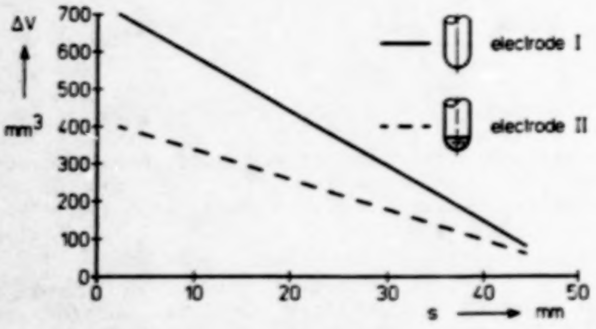

Fig. 13: Loss in volume ΔV of aluminum

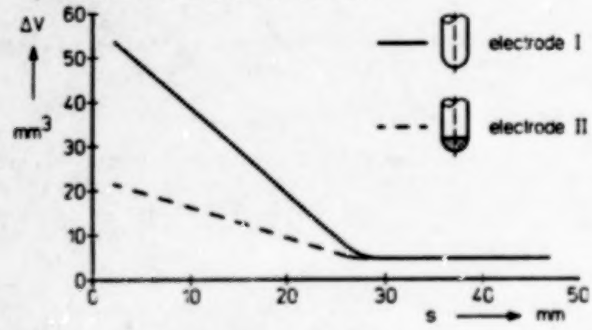

Fig. 14: Loss in volume ΔV of copper

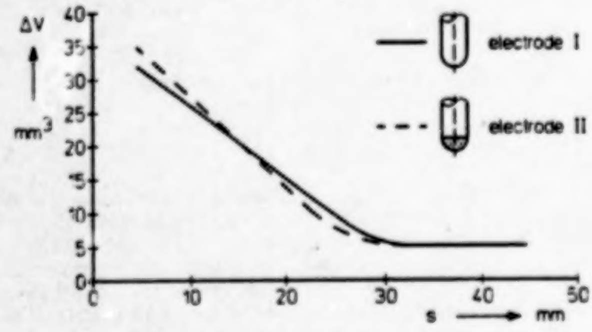

Fig. 15: Loss in volume ΔV of brass

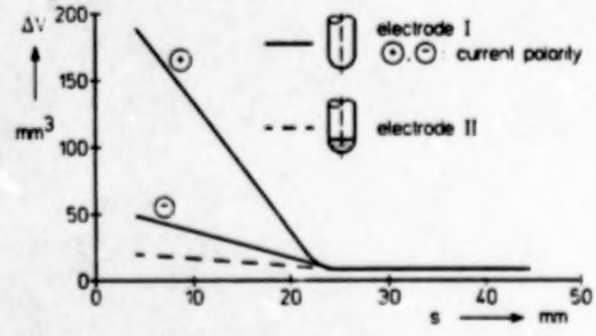

Fig. 16: Loss in volume ΔV of soft steel

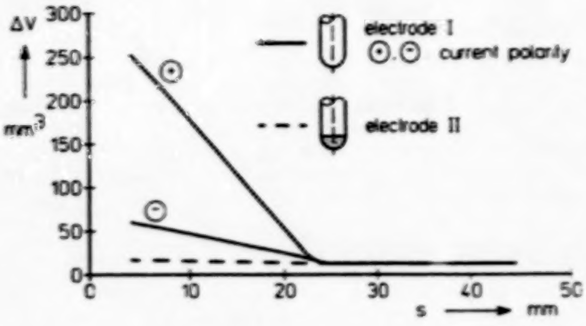

Fig. 17: Loss in volume ΔV of stainless steel

The loss in volume is independent of the impulse current's polarity, excepted steel sheets. For both steels the values for positive polarity are four times greater than for negative, if the standard electrode I is used. The loss in volume is dominant at the cathode. It can be assumed, that the plasma rays starting from the anode are "stronger" than those starting from the cathode. The same phenomenon occured at tests with safety gaps for overvoltage protection made of stainless steel /8/. Here meltings at the cathode were dominant, too. For electrode II there is no remarkable difference between anodic or cathodic meltings.

The losses in volume depend on the spacing of the counter electrode. The larger the spacing, the smaller the loss. This is valid up to a spacing of about 25 mm. Then a minimum value for the loss in volume of 5 to 10 mm^3 is reached, remaining constant for larger spacings. However, for aluminium this minimum value can only be seen for spacings of more than 45 mm. Reason for this is probably the softness of aluminium, which allows an easier splashing of melted material. The common minimum value for all investigated metals of not more than 10 mm^3 should be that part of the material vaporizing at the point of strike.

The comparison of the losses in volume for both electrodes leads to different results. For brass there is no significant influence; copper and aluminium show values for electrode II, which are only 40% to 60% of the values measured for electrode I. However, for the steels the reducing effect of electrode II is very high. The loss in volume is minimized to not more than 20 mm^3.

As mentioned before, the reason for this results is, that the influence of the plasma rays on the metal sheet is remarkably smaller for electrode II. The remaining differences between the investigated metals, especially for aluminium, are caused by their different softness.

The thickness d of the sheets affects their resistance. However, though the resistance of the circuit increases with thinner sheets, the influence on the decay time constant τ_1 and the impulse charge Q_i is unimportant. Also the loss in volume is not influenced by the thickness of the test samples.

5.1.3 Theoretical analysis

A theoretical description of the loss in volume as a function of charge and specific energy is given in /8/:

$$\Delta V = C_1 \cdot Q_i^{C_2} \cdot (W/R)^{C_3},$$

with C_1, C_2 and C_3 as parameters typical for the material, the impulse charge in C, the specific energy in J/Ω and the volume ΔV in mm^3. This equation was developed for safety gaps for overvoltage protection /8/, but the experimental results with metal sheets show a comparable relation.

The experimental results allow also an extension of this equation. The loss in volume decreases with increasing spacing of the counter electrode:

$$\Delta V \sim (1 - C_4 \cdot s).$$

This relation is verified for a spacing of 1 mm up to 25 mm (resp. 1 mm and 45 mm for aluminium). The complete equation for the description of the loss in volume can be written as

$$\Delta V = C_1 \cdot Q_i^{C_2} \cdot (W/R)^{C_3} \cdot (1 - C_4 \cdot s),$$

with the spacing s in mm. The parameters C_1 and C_4 depend on the different materials and the used electrode (table 1 and 2), whereas C_2 and C_3 are valid for all investigated materials:

$C_2 = 1{,}4$
$C_3 = 0{,}45.$

5.2 Long duration currents

The meltings caused by long duration currents show a typical appearance, too. The diameter of the melted area is smaller, the melting itself deeper than in the case of impulse currents. Examples of these meltings are shown in fig. 20 and 21.

Using the long duration currents carrying a charge Q_l = 200 C according to /1, 4/, the diameter of the melted area is larger for the steels and aluminium (typ. 2 cm) than for brass and copper (typ. 1 cm).

These relatively small melted areas result from the smaller specific energy (action integral $\int i^2 dt$) of the long duration current. This is also the reason, that a measurement of the loss in volume, comparable to the tests with impulse currents, is impossible. The material is melted at the base of the electric arc, but not splashed significantly. Therefore the melted material hardens again, if the current flow is over. The loss in volume is nearly equal to 0.

So the measurements concentrate on the investigation, which thickness of a metal sheet can withstand the long duration current without being punctured. International and national standards define minimum thicknesses of different materials, if direct lightning strikes are assumed. The CO paper of IEC TC 81 /10/ for instance fixes:

- aluminium: 7 mm
- copper: 5 mm
- steel: 4 mm.

C_1	$\cdot 10^{-6}$ mm^3/A$^{2.3}$ $\cdot$ s$^{1.85}$	
	electrode I	electrode II
aluminium	800	450
copper	70	30
brass	40	45
soft steel ⊙	250	25
soft steel ⊖	60	25
stainless steel ⊙	350	25
stainless steel ⊖	90	25

Table 1: Parameter C_1 for different metals.

C_4	mm^{-1}	
	electrode I	electrode II
aluminium	0,020	0,020
copper	0,033	0,030
brass	0,030	0,033
soft steel	0,035	0,020
stainless steel	0,037	0

Table 2: Parameter C_4 for different metals, valid up to a spacing of 25 mm (aluminium: 45 mm).

The experimental results show, that aluminium sheets can be punctured up to a thickness of 3 mm, the steels, brass and copper up to 2,5 mm, but for these thicknesses the occurence of puncturing is not sure. For example the 3 mm aluminium sheet is punctured only with a probability of 25%. The thicknesses of sheets, which are surely punctured, are given in table 3, together with the diameter of the occuring hole /11/. Sheets being 1 mm thicker than the values of table 3 are surely not punctured.

metal	d (mm)	h (mm)
aluminium	2.5	5 - 13
copper	2.0	4 - 10
brass	2.0	4 - 10
soft steel	2.0	6 - 12
stainless steel	2.0	6 - 12

Table 3: Thicknesses d and hole diameters h of metal sheets being surely punctured by a long duration current with Q_l = 200 C.

Both electrodes are used for these tests, and their spacing is varied. Nevertheless the appearence of the melted areas, the possibility of puncturing the metal sheets and the current parameters are not affected by the different spacing and the kind of electrode.

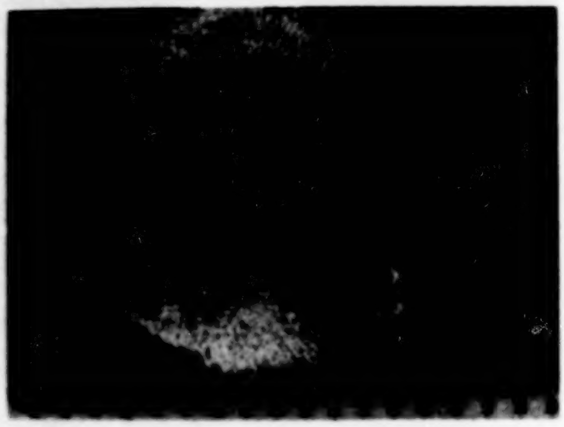

Fig. 18: Typical melting of aluminium sheet caused by impulse current (thickness d = 1,5 mm).

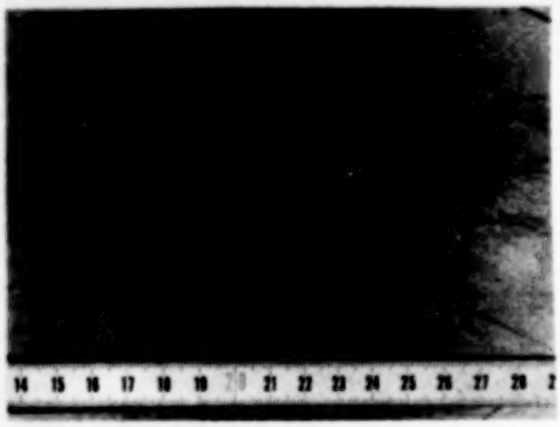

Fig. 19: Typical melting of stainless steel sheet caused by impulse current (d = 1,5 mm)

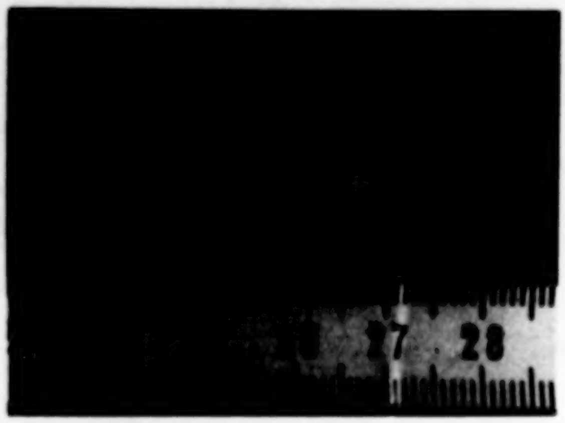

Fig. 20: Typical melting of aluminium sheet caused by long duration current (d = 2,0 mm)

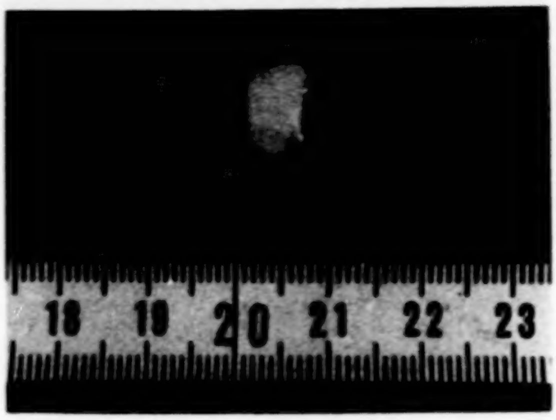

Fig. 21: Typical melting of stainless steel sheet caused by long duration current (d = 1,5 mm)

6. Temperature distributions

For metal sheets, which are thick enough that they can't be punctured, another thermal effect has to be investigated: the temperature rise at the interior surface. The temperatures occuring at the sheet opposite to the point of strike are high enough to decolorate the metal. These high temperatures can lead to an ignition of an explosive mixture inside a metal tank struck by lightning.

The time dependent temperatures at the interior surface of metal sheets are measured by two infrared thermosensors for different temperatur ranges with rise times of 250 ms resp. 550 ms. Therefore only relatively slow temperature rises can be measured exactly.

The test assembly is shown principly in fig. 22. The infrared thermosensor is adjusted to that point of the sheet opposite to the point of strike, i.e. in the axis of the counter electrode. At this point the highest temperatures occur.

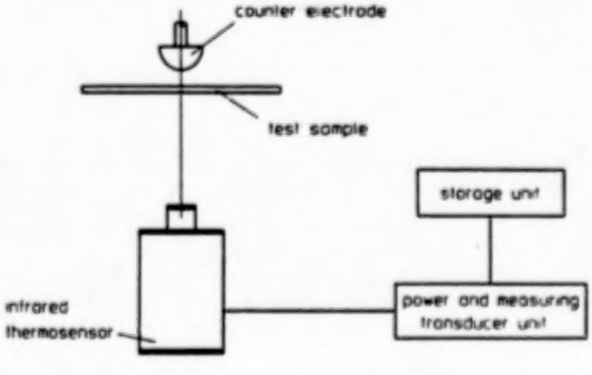

Fig. 22: Temperature measurement assembly

The radius of the detected area is proportional to the distance between thermosensor and the sheet. For thermosensor I the used distance of 30 cm corresponds to an area's radius of 10 mm; thermosensor II detects an area with the radius 3 mm. With this arrangement the integrated temperatures of two detected areas with the same center but different radius are recorded.

It has to be considered, that the temperatures in the middle of the detected area are normally still higher than the integrated temperatures. Based on the measurement results, however, a numerical model allows the calculation of the temperatures at each point of the metal sheet /11/.

The emission coefficient ε of the investigated metals is smaller than 1. Therefore the measured temperatures T_m in K have to be translated in the real temperatures T_r according to the equation

$$T_r^4 = \frac{T_m^4 - (1 - \varepsilon)\cdot T_o^4}{\varepsilon}$$

with T_o being the ambient temperature, usually 293 K.

The temperature rise of metal sheets caused by impulse currents is relatively fast, but after reaching the maximum temperature the tail of the curve is very even. Though the thermosensor isn't able to follow the front steepness exactly, the maximum temperature and the tail can be measured sufficiently. The maximum temperatures for sheets with a thickness of 2 mm are given in table 4.

metal	ϑ_{max} (°C)
aluminium	103
copper	68
brass	62
soft steel	94
stanless steel	105

Table 4: Maximum temperatures ϑ_{max} for 2 mm metal sheets caused by impulse currents

These temperatures were measured only with the thermosensor detecting an area with a radius of 10 mm, because the minimum temperature for the second thermosensor is 400°C. So the use of the second thermosensor was not possible, because of the relatively low temperatures of not more than about 100°C. The reason for those low temperatures are the large melted areas with only a small depth caused by the impulse currents.

The temperatures for sheets struck by long duration currents show a different time slope. The crest values are many times higher, and the tail is much shorter. So the thermosensors aren't able to follow the time dependent temperatures for all metals exactly. Only the steel sheets show temperature distributions, which are slow enough, to fulfil the measurement requirements, and so the investigations have to be limited to them.

The recorded temperatures with time constants for steel sheets with different thicknesses are shown in table 5. Both thermosensors were used and therefore the radius of the detected area is different. These relatively high temperatures are caused by the deep melted areas at the point of strike of long duration currents.

metal	z (mm)	r (mm)	ϑ_{max} (°C)	T_{cr} (s)	T_2 (s)
soft steel	3	3	1 120	0,7	2,7
		10	740	1,1	6,0
	4	3	950	1,0	--
		10	540	1,4	6,2
	5	3	750	1,4	--
		10	430	1,7	6,4
stanless steel	3	3	1 150	0,8	3,5
		10	550	1,0	10,5
	4	3	940	1,3	--
		10	400	1,8	10,0
	5	3	570	1,7	--
		10	270	2,7	13,4

z: thickness of sheet

r: radius of detected area

ϑ_{max}: maximum temperature

T_{cr} : time to crest

T_2 : decay time to half value

Table 5: Temperature distributions for metal sheets caused by long duration currents.

7. Conclusions

The simulation of lightning currents in the laboratory has to be based on the parameters of natural lightnings. The investigations of this paper are carried out with simulated lightning currents including about 99% of natural lightnings, as required by IEC /1/.

Meltings of metal sheets caused by impulse currents show a large melted area. The depth of the melting is small. The reason for this kind of melting is the high specific energy of the impulse current.

The loss in volume decreases with increasing spacing of the counter electrode due to the weaker influence of plasma rays on the metal sheet. If a so called insulating electrode is used, the influence of plasma rays and therefore also the loss in volume is reduced remarkably.

Meltings of metal sheets caused by long duration currents show a small, but deep melted area. Aluminium sheets can be punctured up to a thickness of 3 mm, stainless and soft steel, brass and copper up to 2,5 mm.

Metal sheets, which can't be punctured, can show high temperatures at their interior surface, i.e. opposite to the point of strike. Responsible for this are mainly long duration currents. They lead to maximum temperatures of more than 1.000°C, whereas the temperatures for impulse currents usually are below 100°C. Reason for these different temperatures are also the different melting processes of impulse and long duration currents.

Steel sheets show the most "dangerous" temperature distributions, because high temperatures occur at the interior surface of the sheets for a long time. The temperature decrease of sheets made of aluminium, copper and brass is faster.

In general it is a fact, that the thermal threat for metal sheets caused by long duration currents is dominant. They lead to deeper meltings and higher temperatures at the interior surface of the sheets than impulse currents.

References:

/1/ CEI/IEC 1024-1(1990-03): Lightning protection of structures. Part I: General principles.

/2/ Berger, K.; Anderson R.B.; Kröninger H.: Parameters of lightning flashes. Electra 41(1975), p. 23-37.

/3/ Anderson R.B.; Eriksson A.J.: Lightning parameters for engineering application. Electra 69(1980), p. 65-102.

/4/ VG 96 901 Teil 4/10.85: Schutz gegen Nuklear-Elektromagnetischen Impuls (NEMP) und Blitzschlag; Allgemeine Grundlagen, Bedrohungsdaten. Beuth Verlag, Köln.

/5/ SAE AE4L: Protection of aircraft electrical/electronic systems against the indirect effects of lightning. Committee report, 4. Feb. 1987.

/6/ MIL-STD 1757A: Lightning qualification test techniques for aerospace vehicles and hardware.

/7/ Melander B.G.: Atmospheric electricity threat definition for aircraft lightning protection. 8th. Int. Conf. on Lightning and Static Electricity, Fort Worth, Texas, 1983, Paper 36.

/8/ Zischank W.: Schutzfunkenstrecken zur Überspannungsbegrenzung bei direkten Blitzeinschlägen. Diss. Hochschule der Bundeswehr München, 1983.

/9/ Zischank W.: A surge current generator with a double-crowbar sparkgap for the simulation of direct lightning stroke effects. ISH Braunschweig, 1987, Paper No. 61.07.

/10/ IEC TC 81; CO paper 4/87: Standards for lightning protection of structures. Part I: General principles.

/11/ Kern A.: Theoretische und experimentelle Untersuchung der Erwärmung von Metallblechen bei Blitzeinschlag. Diss. Universität der Bundeswehr München, 1990.

Adress of author:

Dr.-Ing. A. Kern
Universität der Bundeswehr München
ET / 7
Werner-Heisenberg-Weg 39
D-8014 Neubiberg

Application of Designed Experiments Statistical Approach to Lightning Testing of Carbon Fiber Composites

by J. Ward and A. Booker

No paper available.

Session 9A, Thursday 8:00
Lightning Phenomenology
Modeling 1
Laroche, Chairman

A SURVEY OF LASER LIGHTNING ROD TECHNIQUES

Arnold A. Barnes, Jr. and Robert O. Berthel
Atmospheric Sciences Division
Geophysics Directorate
Phillips Laboratory (AFSC)
Hanscom AFB, MA 01731

ABSTRACT

The concept of using a laser to create an ionized path in the atmosphere to act as a lightning rod is not new. Over the past four decades since the invention of the laser, there have been many documented investigations into the ionization of atmospheric gasses with an eye towards creating a laser lightning rod (LLR). Initial experimental attempts using lasers operating in the IR were not successful. Although some ionization was attained, it was found that the laser beam was self-quenching so that distances of only tens of meters were obtained in the atmosphere near sea level.

With advances in both the power output of lasers and the tunability of the laser frequencies, researchers have been looking for sophisticated ways of avoiding the plasma quenching problem. The direct single photon ionization of atmospheric gasses would require operations in the UV part of the spectrum where there is overwhelming absorption by the atmospheric gasses. This, in concert with the quenching at the longer IR wavelengths, would suggest the use of intermediate wavelengths to produce ionization of atmospheric constituents by multiphoton capture.

This paper briefly reviews the work which has been done in trying to create a laser lightning rod and discusses some ongoing research which has potential for achieving an operational laser lightning rod for use in the protection of missile launch sites, launch vehicles, and other property.

BACKGROUND

Natural lightning occurs with the local breakdown of air inside a cloud which has an electrical field of critical potential. Physical objects, such as the leading edges of aircraft or noses of rockets, may artificially trigger lightning from subcritical charge centers. From the observed torturous track of

451

lightning (see the upper portion of the lightning in Figure 1.) and the research into step leaders, it is apparent that lightning is seeking and following the path of least resistance through the atmosphere. Rocket triggered lightning experiments have demonstrated that a conducting wire trailing from a rocket will provide such a path of least resistance as is shown in the lower section of the lightning stroke in Figure 1. If a sufficiently dense ionized column could be created in the atmosphere with a laser beam, such a column would provide a preferred path for lightning [1-3].

The laser evolved on the heels of the development of the maser in the mid 1950's. The intervening years brought investigations in the breakdown of air [4-6] and, more specifically, the possible use of lasers for triggering lightning [7-8]. An attempt was made during the Thunderstorm Research International Program 1978-1979 to trigger lightning using a long-wavelength, CO_2 laser with microsecond pulse where a laser-produced, clear-air breakdown was observed although no lightning could be attributed to the laser firings during thunderstorms. At that time the failure was thought to be the result of the scattering of radiation by raindrops and attenuation of the limited laser energy to below breakdown thresholds [9]. Self quenching of the laser beam is now identified as the major problem.

With advances in both the power output of lasers and the tunability of the laser frequencies, researchers have been looking for sophisticated ways of avoiding this plasma quenching problem. Direct single photon ionization of atmospheric gasses would require operation in the low-wavelength UV part of the spectrum where there is overwhelming absorption by the atmospheric gasses. This suggests the use of an intermediate wavelength between the IR and the UV for multiple photon ionization of air with minimal energy expenditure.

New technology, largely the result of research sponsored by the DoD Strategic Defense Initiative (SDI), has lead to the creation of increasingly powerful lasers. Powerful, short pulse lasers have such high densities of photons that multiple photon capture may easily raises electrons to excited states from which ionization readily occurs by absorption of yet another photon. This combined with advances in frequency "shifting" of the lasers output now presents the possibility of laser output being tuned to specific wavelengths so that specific atmospheric constituents may be selected for ionization. These new developments have now dramatically increased the possibility of creating a sufficiently long ionized column which could act as a preferred path for the discharge of electrified clouds, i.e., an LLR.

Another approach would be to choose a laser with a particular wavelength which would not ionize the clear atmosphere but which would ionize cloud droplets thereby leaving an elevated path similar to an exhaust plume from a rocket or to an "altitude" triggered lightning rocket. Recent studies [10] have indicated that absorption of laser beams by cloud droplets cause shattering and vaporization. Increases in the available power might create ionization which could be maintained by a second suitably tuned laser.

POSSIBLE APPLICATIONS

Since a marginally-charged cloud cannot be reliably determined from ground-based electric field measurements because of a possible space-charge screening layer, such a charged cloud presents a hazard to airborne operations.

Because of the ease with which a laser beam can be steered into any cloud overhead, an LLR could be used to ascertain if there exists enough charge in the clouds to discharge to ground as triggered lightning. This holds the possibility of using LLRs to test clouds prior to launching missiles through the clouds or prior to flying aircraft through the clouds. LLRs could also be used to probe and discharge clouds before or during any hazardous ground operations. Thus an operational LLR may be able to both detect such sub-critical electrical fields and effectively neutralize them.

One thing which LLRs probably will not be able to do in the near future is to discharge clouds or cloud systems which are actively producing lightning. In these cases the charges are being builtup so rapidly that a single LLR system would not be able to cover the whole sky quickly enough. On the other hand, there is a possibility that as we learn more about the morphology of lightning, a computer controlled bank of LLRs operating on data from ground based field mills, lightning mappers and other data sources might be able to discharge the energy from active thunderstorms and, perhaps, collect the energy for man's use.

CURRENT PROGRAMS

Two promising research efforts are currently being conducted using multiple photon ionization with each proposing vastly different solutions for the creation of an ionized path to trigger lightning.

The University of New Mexico's concept (Geophysics Directorate contract) will use a femtosecond pulsed KrF laser at 248 nm for ionization of oxygen by multiphoton absorption. To compensate for loss of energy in the beam, the laser pulse will be frequency swept which will produce pulse compression as the pulse propagates through the atmosphere. A second Nd:YAG laser at 1.06um will be used to maintain a conductive path by preventing the attachment of the multiphoton-absorption generated electrons to oxygen. Inter-cloud discharge triggering is separately addressed by using a third cloud clearing and waveguiding CO_2 laser at 10.6 um.

The Ophir Corporation [11] proposes a more energy efficient approach (NASA SBIR contracts) using a single laser to excite a minor atmospheric constituent. In this concept, it is proposed that a smaller number of photons at 314.5 nm will produce sufficient ionization of Argon. A tunable dye laser will be used in the laboratory feasibility experiments although atmospheric testing will require the further development of Raman excimer technology to shift the 308 nm wavelength of a XeCl laser.

CONCLUSIONS

The advantages of an efficient, reliable LLR are many. In the immediate future an LLR could be used to signify the presence of atmospheric electric fields that would be hazardous to rocket or shuttle launches and aircraft operations. Further into the future, banks of LLRs could be used to neutralize atmospheric corridors for airborne operations and also be utilized as a protective screen for sensitive ground facilities against lightning strikes. One might even peer into the distant future and envision a world-wide harvesting of atmospheric electricity for use by man as a power source.

The success of either or both of these studies will enhance the prospects of an operational LLR in the very near future. The failure of both on the other hand, would generate new ideas and alternate approaches through lessons learned and would not necessarily prove the impossibility of the LLR concept.

REFERENCES

1. Hagen, 1969: "Diffraction-limited high irradiance Nd-glass laser system, J. Appl. Phys., 40, 511-516.

2. Greig, J.R., D.W. Koopman, R.F. Fernsler, R.E. Pechacek, I.M. Vitovitsky, and A.W. Ali, 1978: "Electrical discharges guided by pulsed CO_2-laser radiation", Phy. Rev. Lett., 41,174.

3. Koopman, D.W. and T.D. Wilkerson, 1971: "Channeling of an ionizing electrical streamer by a laser beam", J. Appl. Phy. 42, 1883- 1886.

4. Tozer, A., 1965: "Theory of the ionization of gasses by laser beams",Phys. Rev., 137, A1665-A1667.

5. Smith, D.C., 1977: "Gas Breakdown Initiated by Laser Radiation Interaction with Aerosols and Solid Surfaces", J. Appl., 48, 2217.

6. Parfenov, V.A., et al., 1976: "Optical Breakdown of Atmosphere over Long Distances", Sov. Tech. Phys. Lett., 2, 286.

7. Schubert, C.N., Jr., 1977: "The laser lightning rod system: a feasibility study", Air Force Flight Dynamics Laboratory, Technical Report AFFDL-TR-78-60. AD A063 847.

8. Schubert, C.N., Jr. and J.R. Lippert, 1979: "Investigation into Triggering Lightning with a Pulsed Laser", Proceedings of the 2nd IEEE International Pulse Power Conference, Lubbock, Texas, 12-14 June 1979, pp. 132-135.

9. Lippert, J.R.,1978: "Laser-Induced Lightning Concept Experiment", Air Force Flight Dynamics Laboratory, Technical Report AFFDL-TR-78-191. AD A065 897.

10. Caramana, E.J., J.L. Kindel, R.L. Morse, G.P. Quigley, R.B. Webster and G.W. York, 1990: "Droplet Shattering, Vaporization and Recondensation in Cloud Clearing with Long Pulse Infrared Chemical Lasers", Proceedings of the Cloud Impacts on DoD Operations and Systems - 1989/90 Conference, 285-291.

11. Fetzer, G.J., J.J. Rocca, L.J. Radziemski, 1989: "Perturbation of the local charge concentrations in the atmosphere due to high irradiance laser beams", Proceedings of SPIE Symposium on Innovative Science and Technology for Government and Civilian Applications, O/E Lase Conference, Los Angeles, California.

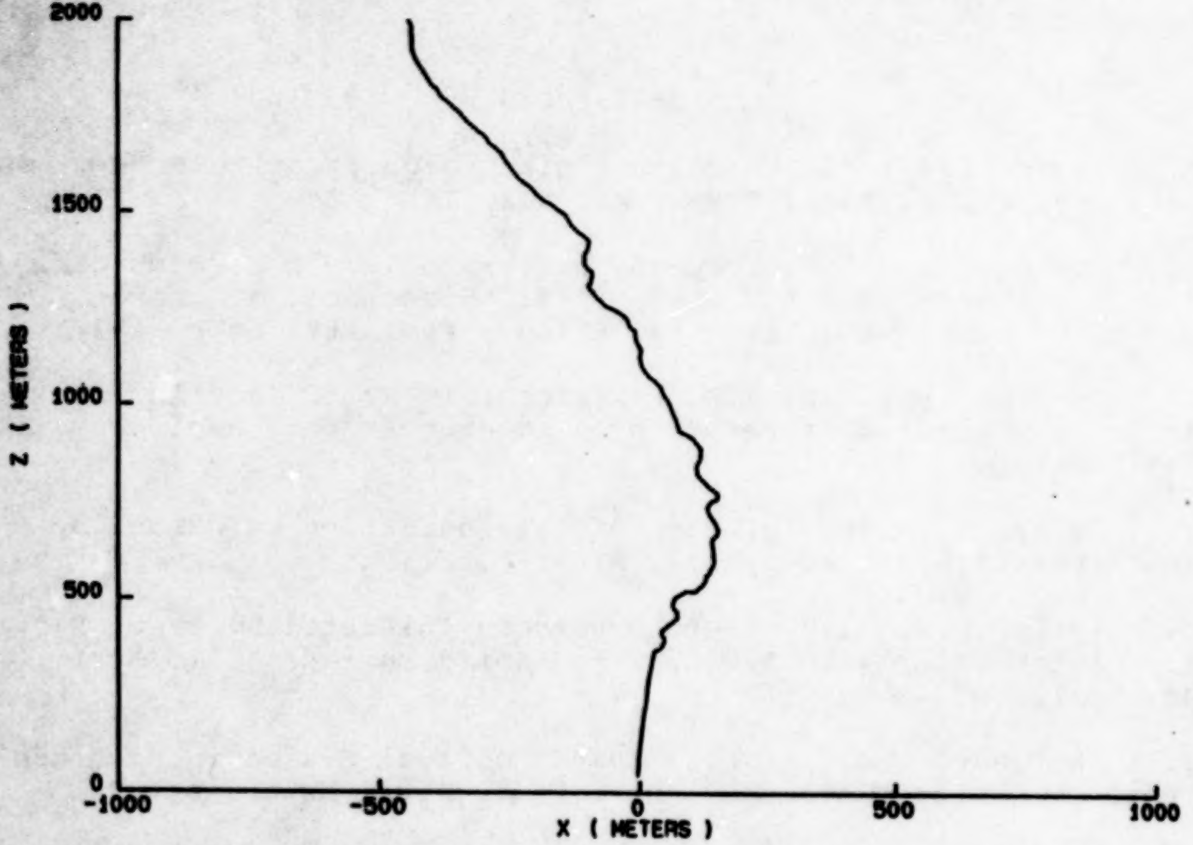

FIGURE 1. Computer reconstructed X-Z projection of a triggered lightning stroke. The straight channel from the ground is typical of "classical" triggering when the copper wire attached to the rocket is also electrically attached to the ground. The torturous path of the lightning channel higher up is typical of natural lightning.

456

PREDICTING CLOUD-TO-GROUND LIGHTNING WITH NEURAL NETWORKS

Arnold A. Barnes, Jr.
Atmospheric Sciences Division
Geophysics Directorate
Phillips Laboratory (AFSC)
Hanscom AFB, MA 01731

Donald Frankel and James Stark Draper
KTAADN, Inc.
Newton, MA 02159

ABSTRACT

Lightning is a hazard to ground operations, missile launch operations and recovery of the Space Shuttle at Cape Canaveral. The Air Force is responsible for providing the forecasts of lightning for these operations. In an effort to improve the forecasting of cloud-to-ground lightning, neural networks are being applied using the large data bases from the Cape Canaveral area which includes Cape Canaveral Air Force Station (CCAFS), Kennedy Space Center (KSC) and peripheral locations.

The initial study [1-3] employed the wind data from a number of different levels on 32 towers to predict lightning strikes in 16 blocks over Cape Canaveral for four time periods; 0-15 min., 15-30 min., 30-60 min. and 1-2 hours. The network was trained by backpropagation using the data from one day, 24 July 1988, and was verified on independent data from 25 July 1988. Comparisons were made with the convergence method of Watson et al [4] and were found to give similar results. The neural network results should improve with larger training sets and with the addition of more of the readily available meteorological data. Results of further training and the addition of ground based field mill data are discussed.

INTRODUCTION

ANS is a sub-discipline of artificial intelligence which deals with the relationships between sets of data. The excellent meteorological and field mill data sets from Cape Canaveral are being used as inputs and the lightning strike data from the Lightning Location and Prediction, Inc. (LLP) system are used as the output (predicted) data to train the networks. The objective is to predict lightning location and time from the meteorological and field mill data.

The purpose of this paper is to report on four additional extensions of the initial study. First, the training was expanded to include two days; second, the wind convergence values of Watson et al [4] were added as an input; third, five minute mean values from the ground-based electric field mills were added as input values; and forth, neural networks with two rather than one hidden layers were investigated.

ADDITIONAL TRAINING DAY

The initial study trained on just one day, 24 July 1988, and verified using independent data from 25 July 1988. Comparison with the Watson convergence was good as is shown in Table 1.

Table 1. Comparison of results

TYPE OF MEASURE	WATSON ET AL	INITIAL NETWORK
Probability of Detection	0.41	0.47
False Alarm Rate	0.57	0.56
Critical Skill Index	0.26	0.29

Two days, 21 and 23 July 1988, were added to the training base. This larger data base improved the results. (Limitations on the software and hardware of the MAC IIx restricted the training data files to just two days. We plan to overcome this restriction by connecting to large vax files through an ethernet.) Figure 1. shows the probability of detection (POD) on the independent data set, 24 July 1988. The hidden layer was run with 5, 6, 7 and 8 nodes, and the line WLHD shows the POD performance of the Watson convergence method. Note that there is substantial improvement at 1 hour for the networks with 6,7, or 8 nodes in the hidden layer.

DIVERGENCE AS AN INPUT

Watson et al [4] showed that convergence over the CCAFS/KSC area was a good predictor of lightning within 80-120 minutes, and this technique is presently available and being used by the Air Force forecaster. By adding these values as inputs to the neural networks, improvements were made in the POD as shown in Figure 2.

USE OF ELECTRIC FIELD MILL DATA

The success of the networks with the 1 hour predictions pointed out how poorly the predictions were for short lead times. We felt that data from the ground based electric field mills would help to improve the forecasts in the two shorter time period prediction epochs. Inspection showed that these field mill data were not very clean, so it was decided to take five minute averages which is the same time average used for the other data. Results of adding the electric field data are shown in Figure 3.

The results for the two shorter epochs were disappointing. This is attributed to the fact that the data are rather noisy and the impression that most of the information is in the rapid changes of the signals rather than in the five minute averages. This suggests that short term means and variances of the electric fields be used along with the LLP data to train a completely new ANS for short term forecasts of lightning employing just the ground based field mill data.

These electric field mill results are preliminary but it should be noted that one of the networks, the one shown with 10 nodes in the hidden layer in Figure 3, performed fairly well in the "NOW" time epoch.

USE OF TWO HIDDEN LAYERS

ANS with two hidden layers are more powerful than ANS with only one hidden layer. To quote from the DARPA Neural Network Study [5, pages 79-80] "The utility of the backpropagation algorithm stems from the surprising computational power of three-layer perceptrons with two hidden layers. These networks can form any desired decision region. ... They can thus emulate any traditional deterministic classifier by producing the decision region required by that classifier. Kolmogorov also proved a theorem described in Lorentz [6] which, in effect, demonstrates that a three-layer network can form any continuous nonlinear function of the inputs. This proof requires carefully specified nonlinearities with wide dynamic ranges. More recent theoretical work [7] has demonstrated that continuous nonlinear functions can be approximated to arbitrary precision using three-layer perceptron with sigmoidal non linearities. A three-layer perceptron can thus create any continuous likelihood function required in a classifier, given enough nodes."

Table 2. lists the steady state pass error for different training runs using wind data, convergence values, and field mill data from the 21st and 23rd of July 1988.

Table 2.

Nodes in 1st layer	Nodes in 2nd layer	Steady state pass average error
3	3	600
5	5	500
8	6	350
8	8	250
12	12	200

Since all these networks used the same data, the smaller value pass average errors show improvements with increasing numbers of nodes. Comparisons on independent data will be necessary to ascertain which of these networks is the best predictor. Those with the larger number of nodes are not necessarily the best predictors since they may be training specific and not have generalized.

Figures 4 and 5 are derived from exactly the same neural net program run on exactly the same data. The only differences are that they were run on two different MAC IIx at different times which meant that the initial weights, which were randomly chosen, were different. The training runs seem to be similar to about the 200th pass through the training data at which point the pass errors starts to fluctuate. These fluctuations in pass errors imply that both of these networks have wandered into rough-textured regions of the error surfaces near minima but not at minima. On the other hand, we do know that both are near minima because the pass errors dropped and flattened out before the fluctuations started. Since both runs exhibit the same characteristic, it would indicate that both are at the same minimum on the error surface which would suggest that they are near the global minimum. This could be further investigated by employing simulated annealing in the training.

CONCLUSIONS

Prediction of cloud-to-ground lightning using ANS improved with a second day's worth of data used in the training. The addition of the Watson convergence values improved predictions at 1 hour. Five minute averages of electric field data did not improve the short term predictions significantly, and perusal of the data suggests that short term electric field variations be used to improve the forecasting of lightning for periods up to one hour. Details are provided in [8] and [9]. In addition, ANS with two hidden layers were investigated and the results suggest that a global minimum is being approached on the error surface. Simulated annealing should be used in the training to test this.

REFERENCES

1. Frankel, D.S., I. Schiller and J.S. Draper, 1989: Evaluation of Correlations Between Meteorological Measurements and Observations of Lightning Activity Using Artificial Neural Systems. Final Report. 28 December 1989. GL-TR-89-0339. AD A222 659.

2. Barnes, A.A., 1989: Predicting Triggered Lightning, Proceedings of the 1989 International Conference on Lightning and Static Electricity, Bath, England, 25-28 September 1989, pages 9B.1.1-9B.1.6. GL-TR-90-0271. AD A228 621.

3. Barnes, A.A, and D.S. Frankel, 1990: Investigation of the Prediction of Lightning Strikes Using Neural Networks, AIAA 28th Aerospace Sciences Meeting, Reno, Nevada, 8-11 January 1990. GL-TR-90-0269. AD A229 042.

4. Watson, A.I., R.L. Holle, R.E. Lopez, R. Ortiz and J.R. Daugherty, 1989: Use of the Surface Wind as a Predictor of Thunderstorms and Cloud-to-Ground Lightning at Kennedy Space Center, Proceedings of the 1989 International Conference on Lightning and Static Electricity, Bath, England, 25-28 September 1989, pages 9B.2.1-9B.2.7.

5. Anon, 1988: DARPA Neural Network Study. AFCEA International Press, Fairfax, Virginia. xxx + 629.

6. Lorentz, G.G., 1976: "The 13th problem of Hilbert", in Mathematical Developments Arising from Hilbert Problems, (F.E. Browder, ed.), Providence, R.I.: American Mathematical Society.

7. Cybenko, G., 1988: Continuous valued neural networks with two hidden layers are sufficient", Technical Report Department of Computer Science, Tufts University, March 1988.

8. Frankel, D.S., I. Schiller, J.S. Draper and A.A. Barnes, 1990: Investigation of the Prediction of Lightning Strikes Using Neural Networks. Preprints of the 16th Conference on Severe Local Storms and the Conference on Atmospheric Electricity, Kananaskis Park, Alberta, Canada, 22-26 October 1990, pages 7-12.

9. Frankel, D.S., and J.S. Draper, 1990: Improved ANS Lightning Predictors Using Additional Surface Wind and Electric Field Data. Final Report. 31 December 1990. GL-TR-90-0361.

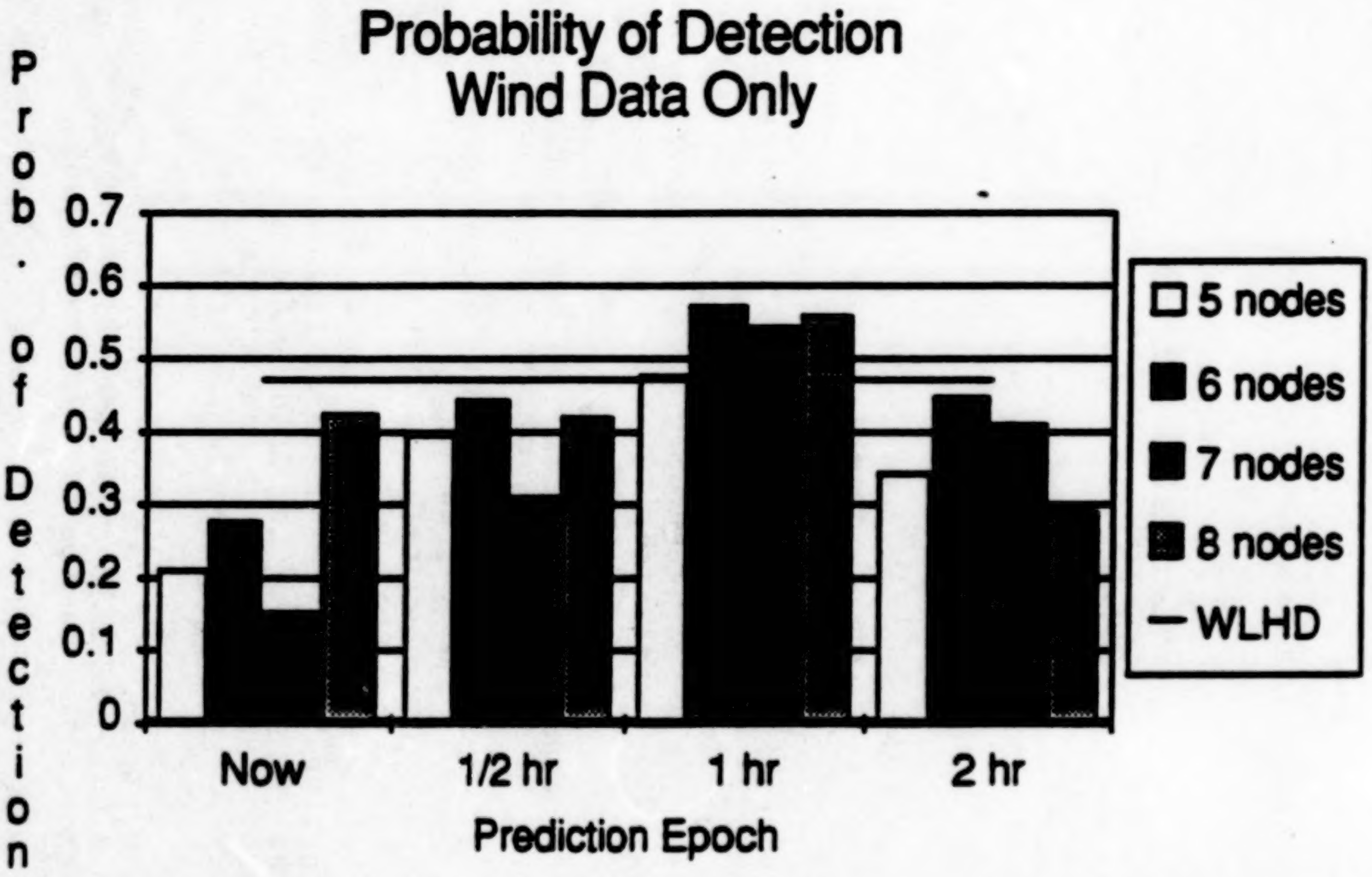

Figure 1 Probability of detection by time epoch of the ANS using two days of wind data as input. The horizontal line labeled WLHD is the level of performance of Watson et al. 1987 in predicting lightning for the entire KSC area at any time following a threshold crossing of the Total Area Divergence.

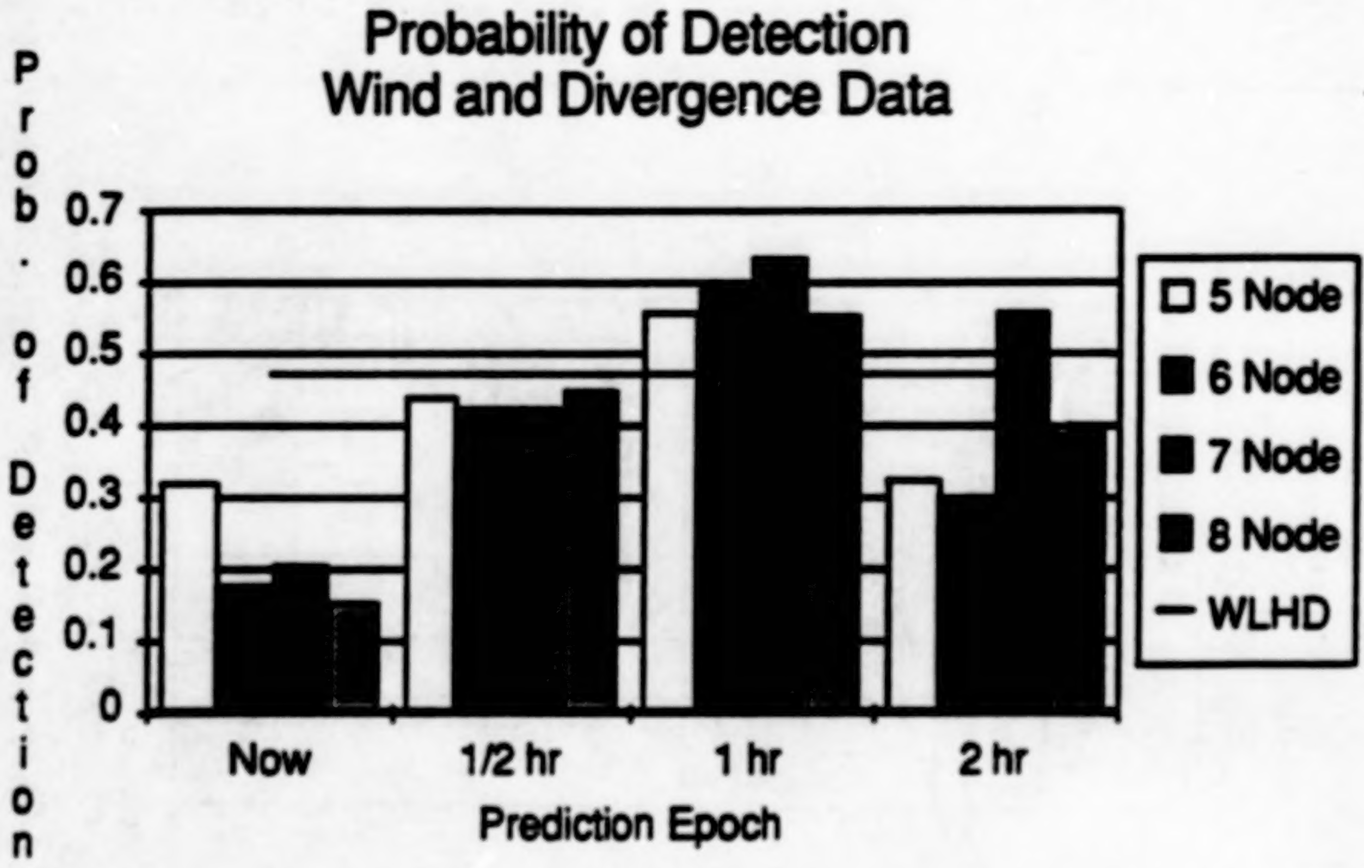

Figure 2. Probability of detection by time epoch of the ANS using two days of wind data and the Total Area Divergence as input. The horizontal line labeled WLHD is the level of performance of Watson et al. 1987 in predicting lightning for the entire KSC area at any time following a threshold crossing of the Total Area Divergence.

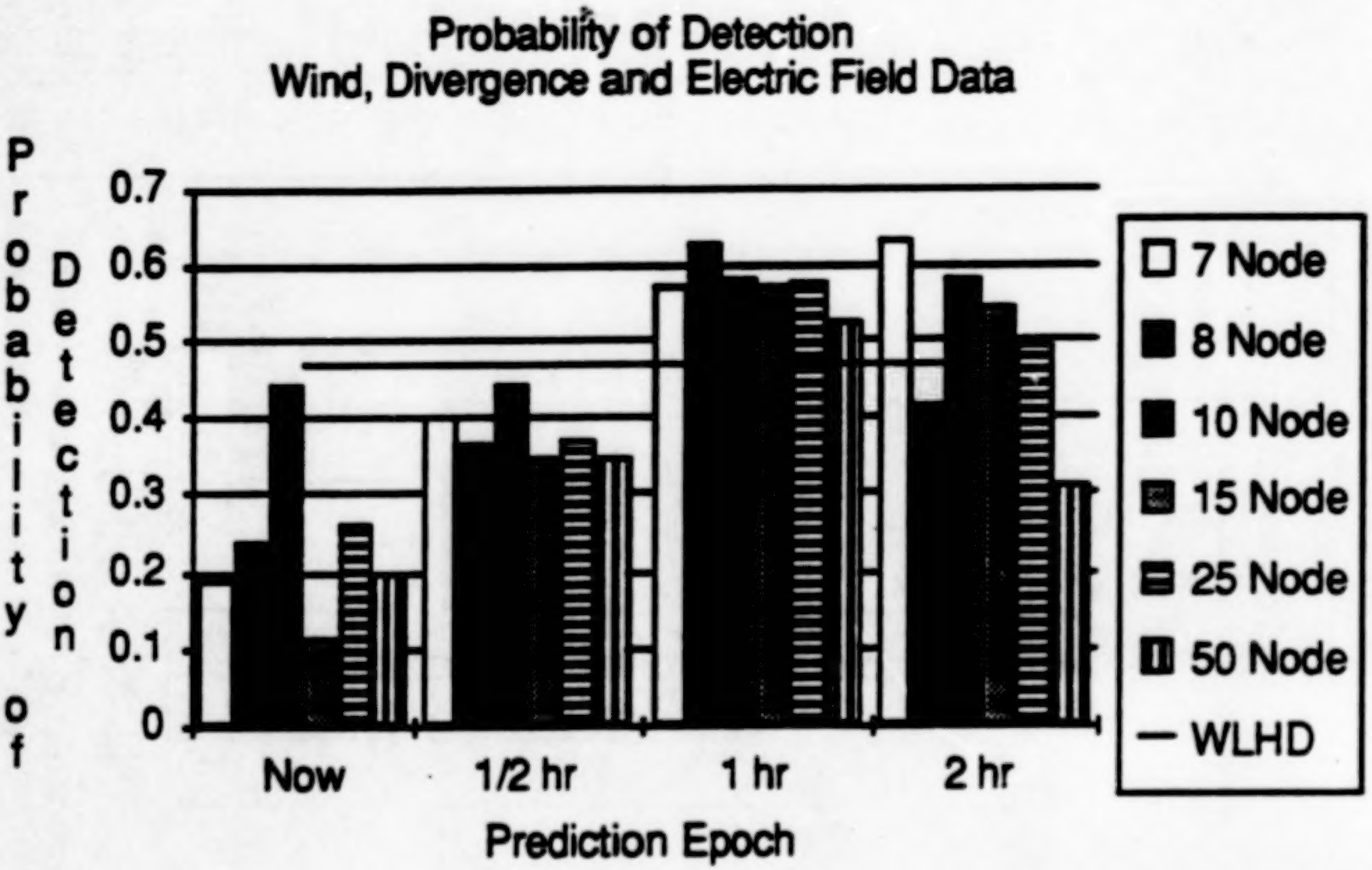

Figure 3 Probability of detection of the ANS using two days of wind data, the Total Area Divergence, and the electric field data as input. The horizontal line labeled WLHD is the level of performance of Watson et al. 1987.

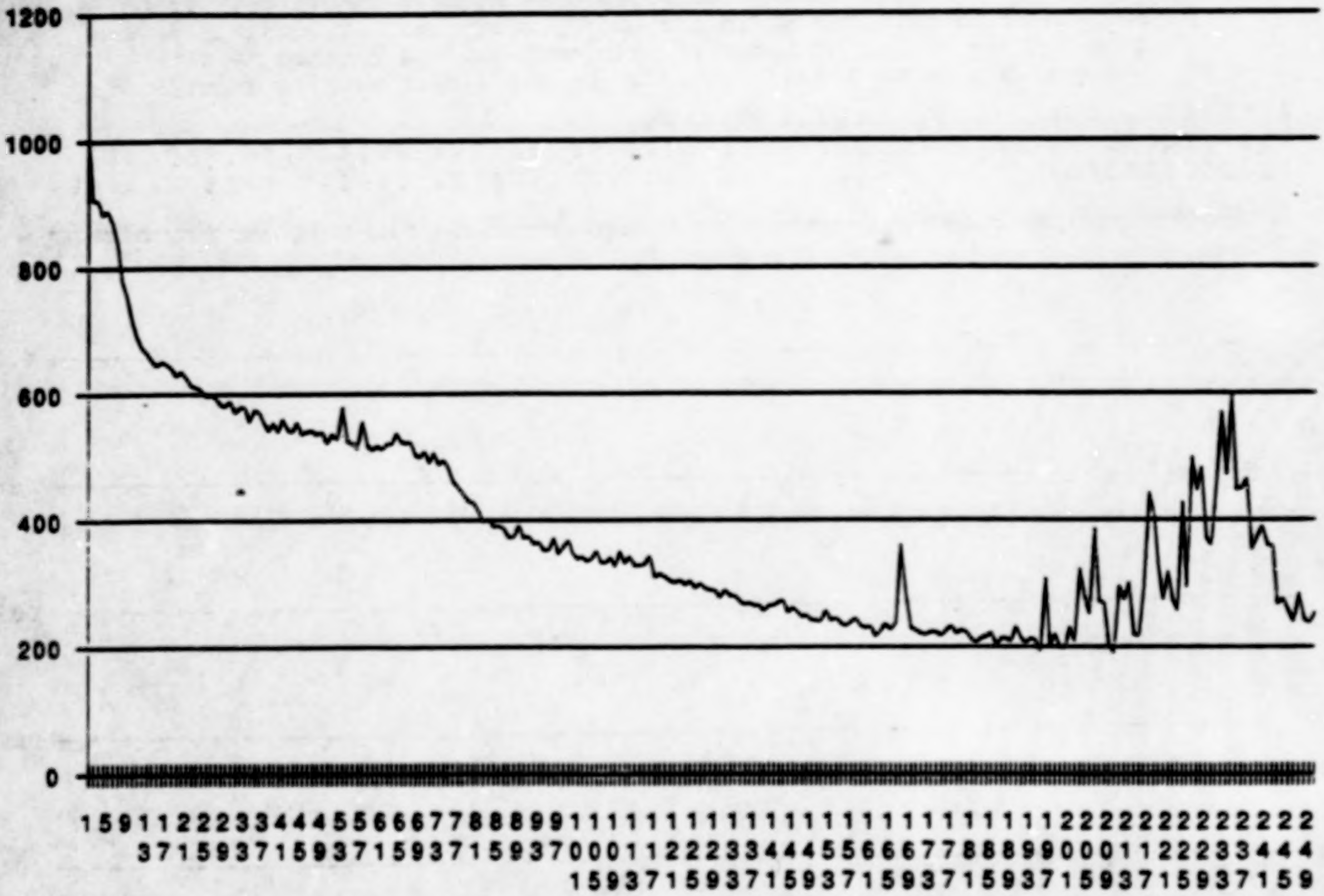

FIGURE 4. Pass errors for 249 training passes through the two hidden layer, 138x12x12x64 neural network using data from 21 and 23 July 1988 on the GP/CC MAC IIx.

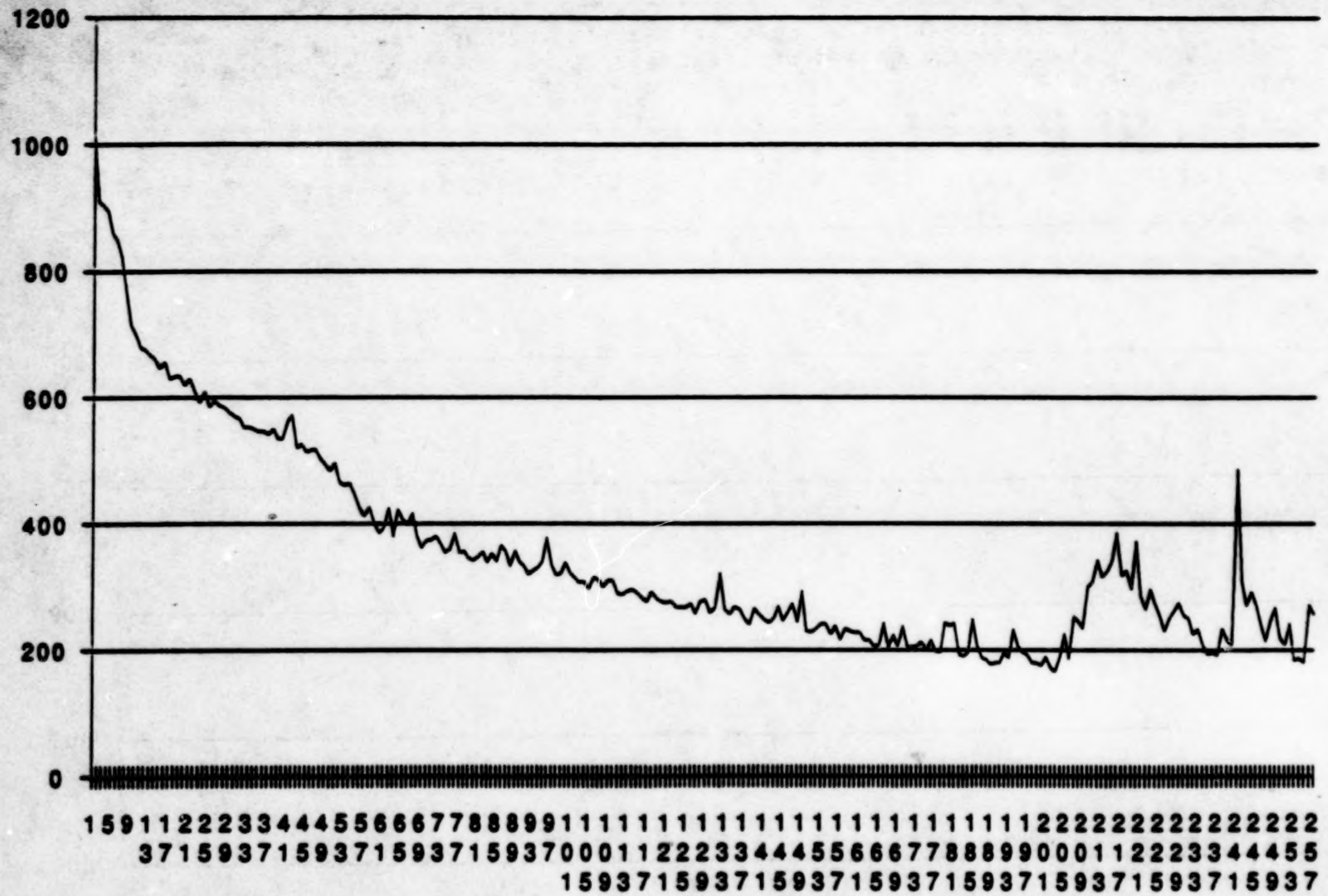

FIGURE 5. Pass errors for 257 training passes using the same neural network and the same data as shown in Figure 4. The only difference is that the MAC IIx from GP/PH was used therefore the initial random weights were different.

THE ELECTRIC FIELD CHANGE CAUSED BY A GROUND FLASH WITH MULTIPLE CHANNELS

Minoru NAKANO
Toyota College of Technology, Toyota, Japan

Nobuyuki TAKAGI, Izumi ARIMA
Gifu University, Gifu, Japan

Zen-Ichiro KAWASAKI
Osaka University, Suita, Japan

Tosio TAKEUTI
Aichi College of Technology, Gamagori, Japan

ABSTRACT

The electric field and the magnetic flux changes caused by a ground flash with multiple channels are measured near the electric power transmission lines during winter thunderstorms. Triggered lightning strokes and the following associated strokes to the transmission line towers produce characteristic waveforms of the field changes. A few examples of the waveforms and a brief discussion are given.

INTRODUCTION

In winter thunderstorms, lightning is often initiated upward almost simultaneouly from several transmission line towers which are distributed along the mountain ridge. This type of lightning is called as 'concurrent flashes', 'a ground flash with multiple channels', or 'a ground flash with multiple striking points'. Hereafter, 'concurrent flashes' is used in this paper. Takagi et al. [1] defined a stroke to the ground which occured within one second after the first return stroke as an associated stroke in concurrent flashes. They summarized the occurrence characteristics of the concurrent flashes. The occurrence rate is 55 % of the ground flashes, the average number of striking points is 5.1, the horizontal distance between striking points is 1.3 km, and the average time intervals between strokes is 6.7 ms for winter lightning. The largest numbers of the striking points are 4 in summer and 17 in winter. Hara et al. [2] also reported that the occurrence rate of the concurrent flashes was 43.3 % and the maximum distance between striking points was 4.7 km in winter.

The concurrent ground flashes may bring multi-conductor and double-circuit tripouts of the electric power transmission line which often occur when winter thunderstorms pass over the transmission lines.

Kawamata et al. [3] discussed the generation mechanism of triggered lightning with multiple striking points. A preceeded cloud flash triggers the first ground flash, and the electric field change caused by the first ground flash is possible to trigger the following ground flashes which strike to other transmission line towers.

we made observations of the electric field and the magnetic flux changes caused by lightning and also recorded lightning channels with video cameras during winter thunderstorms. In this paper, we present a few examples of the electric field changes due to the concurrent ground flashes and give a brief discussion on the characteristics of the field changes.

OBSERVATIONS

We used a fast antenna system and a single-turn loop antenna system for the detections of the electric field and the magnetic flux changes caused by lightning. The bandwidths of the systems are both ranged roughly from 200 Hz to 2 MHz. We set video camera systems at two stations to identify the location of the striking point. We used several video cameras to cover wide view angles at each station.

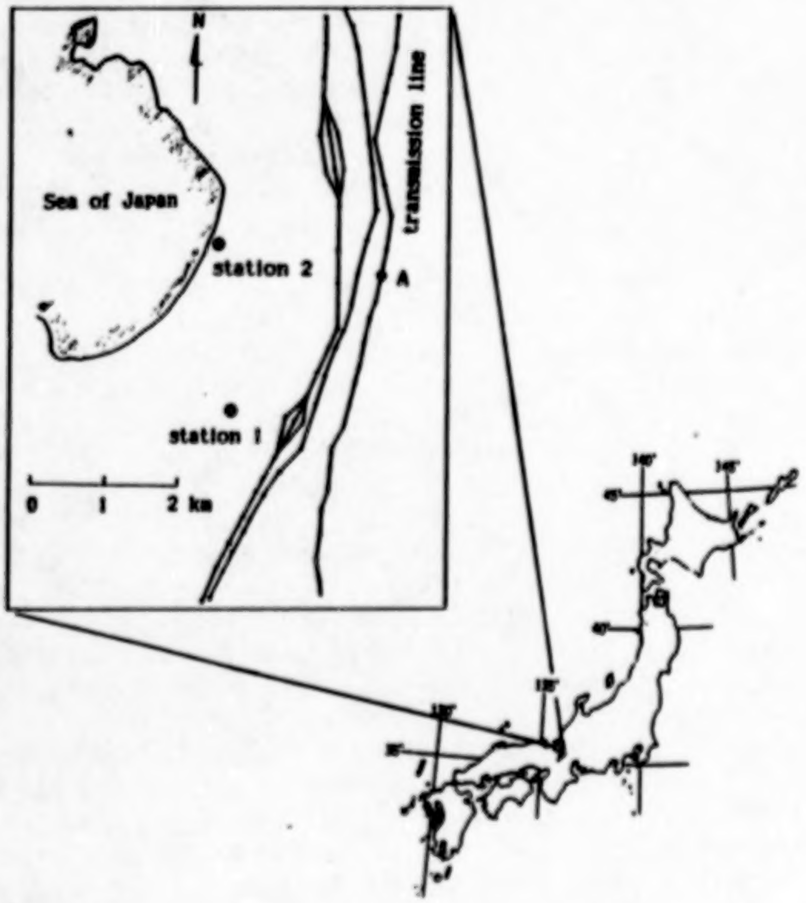

Fig.1. Observation site and transmission lines.

Fig. 1 shows the locations of observation stations where is very close to the electric power transmission lines. Three transmission lines are distributed along low mountain ridge. Small dots on the solid lines show the locations of transmission line towers. The transmission line tower A of 101.7 m height is located at the small peak where is 310 m high above sea level, and a lightning conductor of 4 m length is set on the top of the tower A. So upward streamers often start first from the tip of the lightning conductor.

Fig. 2 shows the electric field and the magnetic flux changes caused by the return stroke of the natural ground flash to a transmissin line tower. Here, 'natural' means that a ground flash starts with a downward streamer from the cloud to the ground. Two traces in Fig. 2 show the same waveforms due to the close return stroke as those in summer lightning. The horizontal distance to the tower struck is 2.1 km.

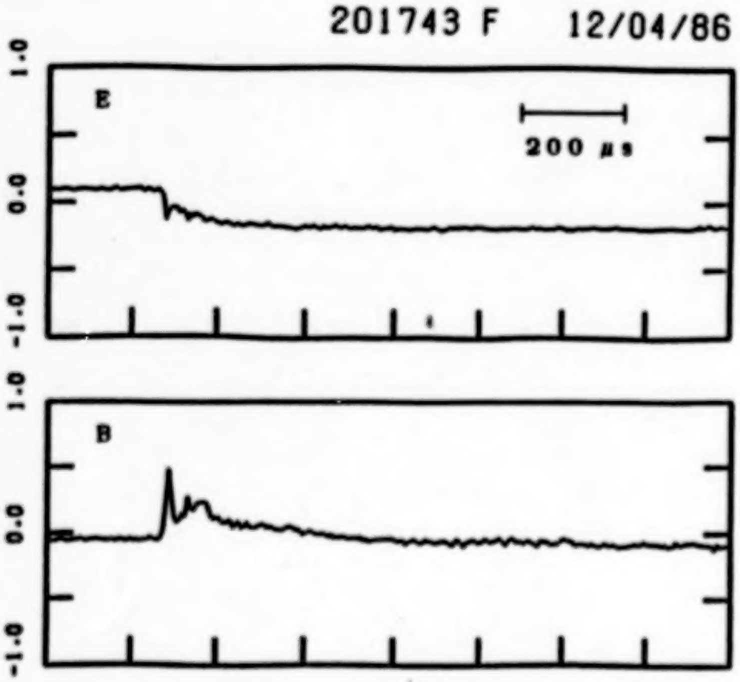

Fig.2. The electric field and the magnetic flux changes caused by a natural lightning to a transmission line tower.

Fig. 3 shows the electric field and the magnetic flux changes caused by triggered lightning flashes. Open circles on the transmission lines in Fig. 3 show the tower to which lightning struck. This was identified with video pictures at two stations. Fig. 4 shows the sketch of video picture of the same triggered flash as one in Fig. 3.

Fig. 5 shows another concurrent flash with several striking points near the tower A. Sketches of video pictures for the same flash are shown in Fig. 6 for different directions. Lightning channels corresponding to striking points given in Fig. 5 are shown in the top sketch in Fig. 6. Fig 7 and Fig. 8 show examples of concurrent flashes

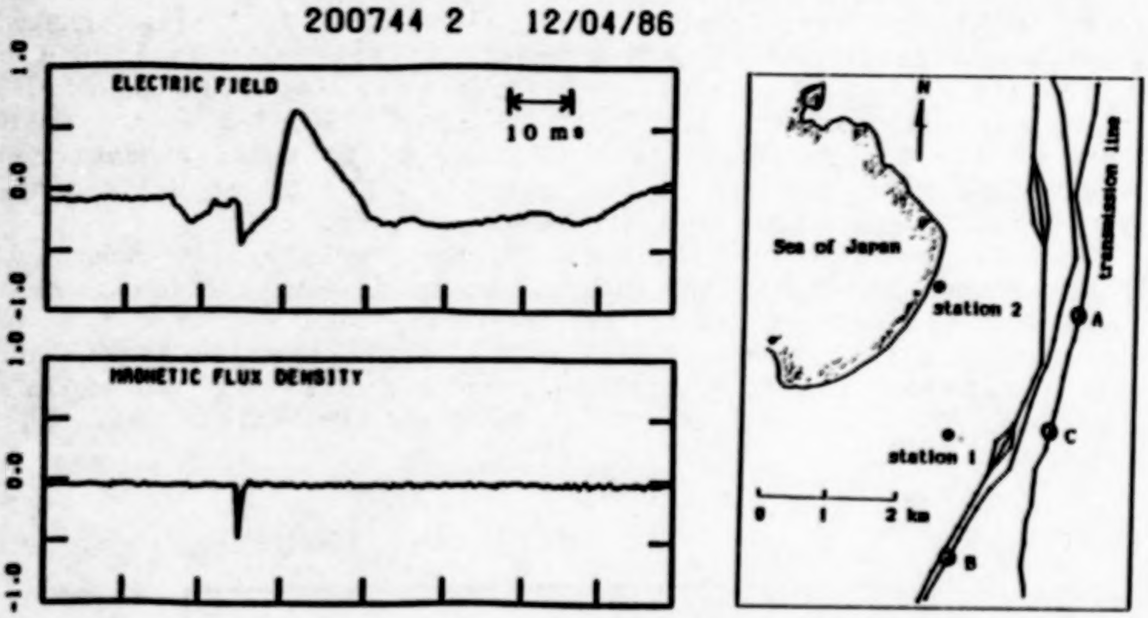

Fig.3. The electric field and the magnetic flux changes caused by a concurrent flash to transmission line towers. Open circles on transmission lines show the towers struck by lightning.

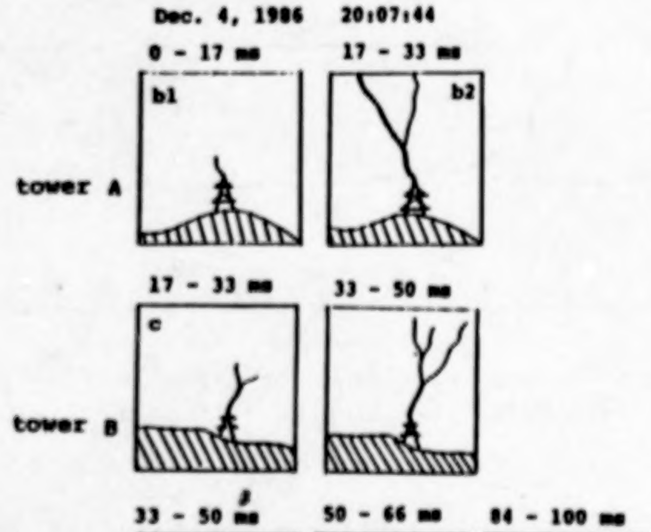
Dec. 4, 1986 20:07:44
0 - 17 ms
17 - 33 ms
b1
b2
tower A
17 - 33 ms
33 - 50 ms
c
tower B
33 - 50 ms
50 - 66 ms
84 - 100 ms
d1
d2
d3
tower C

Fig.4. Sketches of video pictures of concurrent flashes to three transmission line towers.

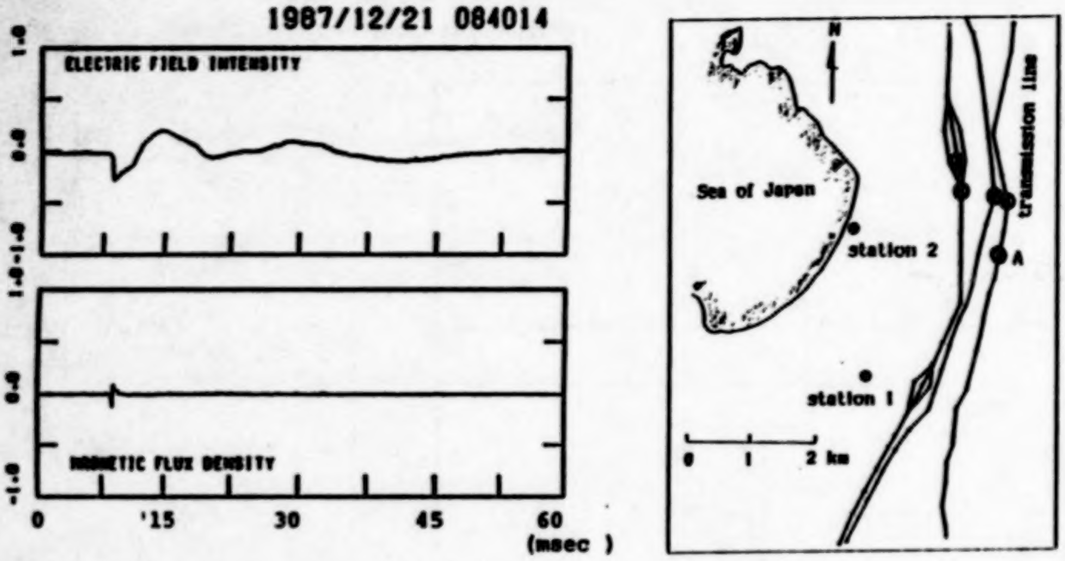

Fig.5. Same as Fig.3 except for date.

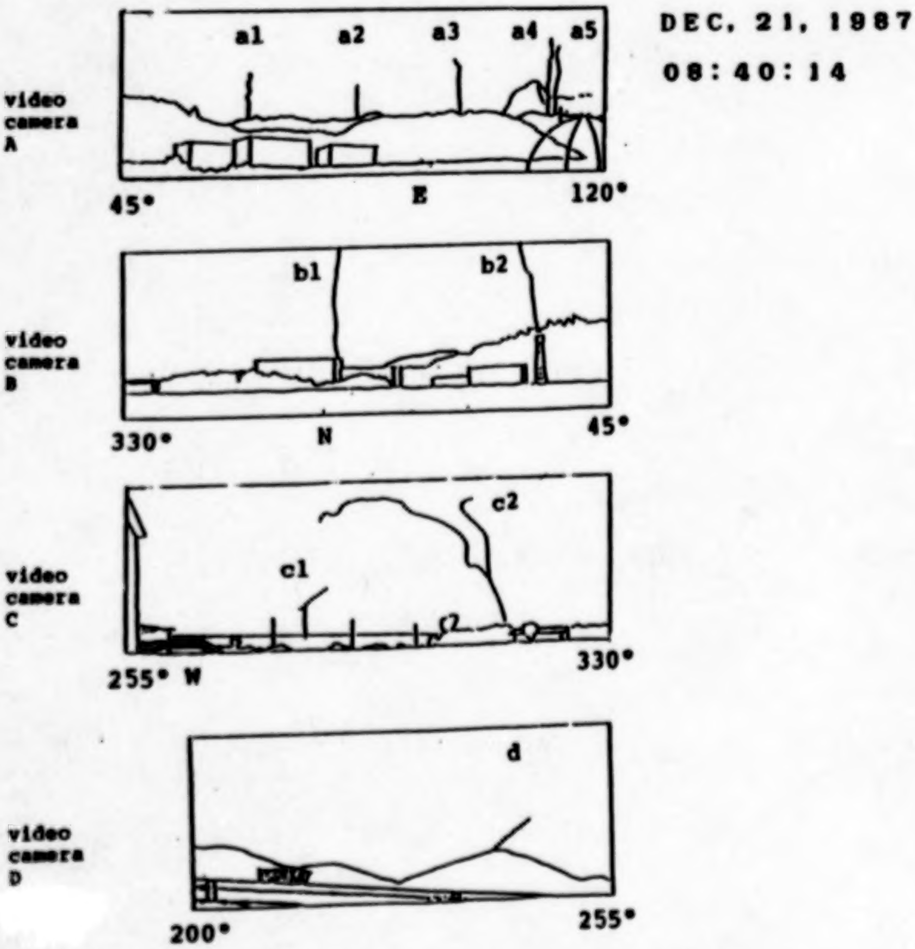
DEC. 21, 1987
08:40:14
a1
a2
a3
a4
a5
video camera A
45°
E
120°
b1
b2
video camera B
330°
N
45°
c1
c2
video camera C
255° W
330°
d
video camera D
200°
255°

Fig.6. Sketches of video pictures of concurrent flashes to transmission line towers and other structures for different directions. Direction angles show in each sketch.

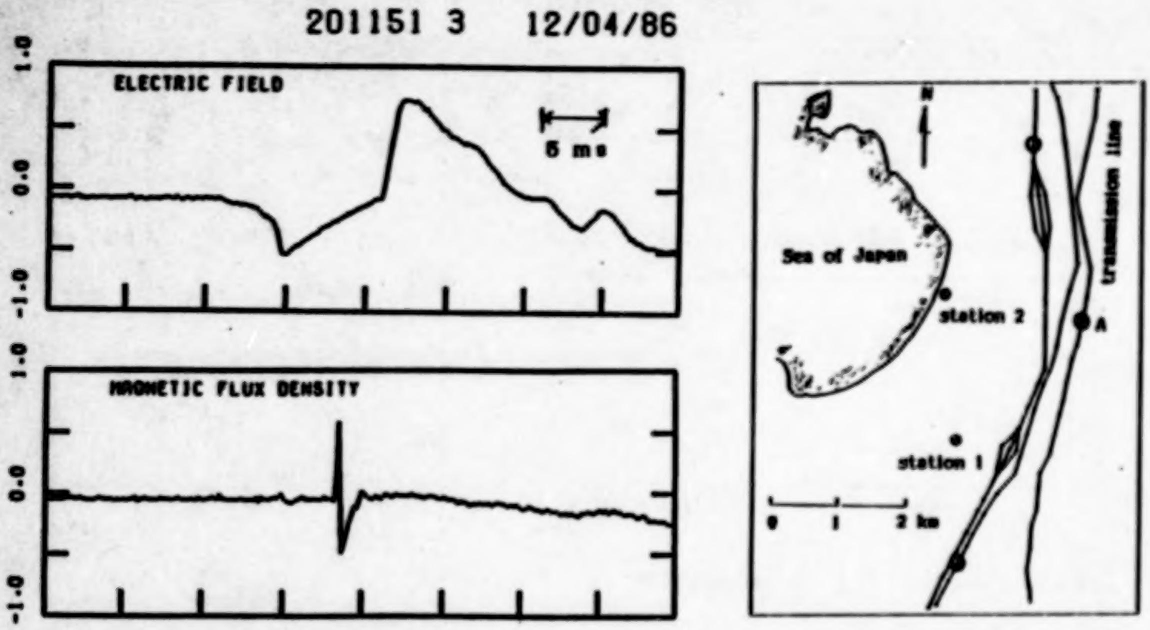

Fig.7. Same as Fig.3 except for date.

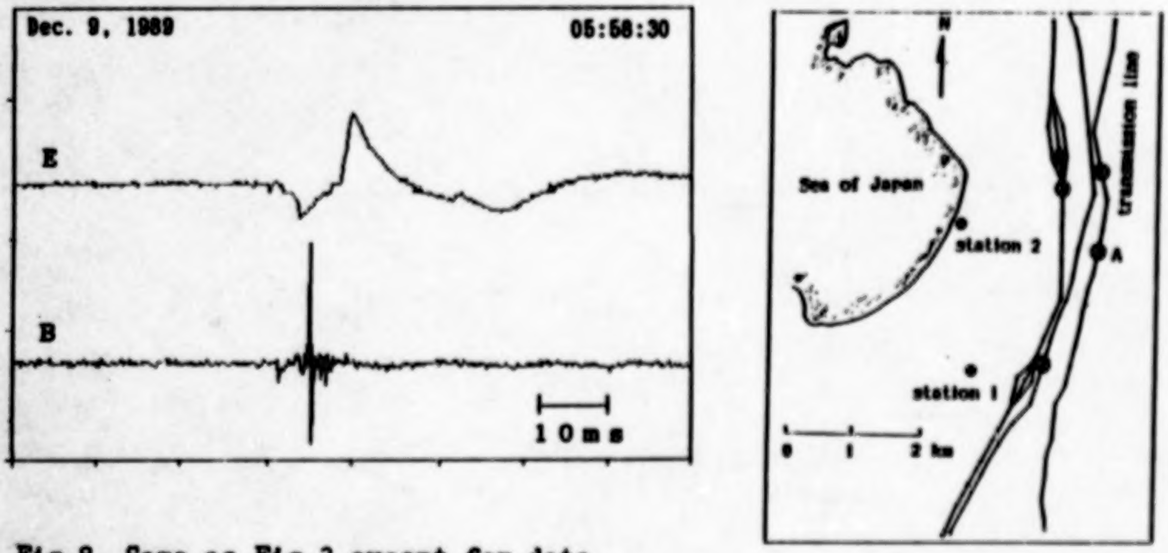

Fig.8. Same as Fig.3 except for date.

in which the magnetic flux changes are different from those in Fig. 3 and Fig. 5. In Fig. 3 and Fig. 5, the rapid changes of the electric field and the magnetic flux occur simultaneously, as well as the return stroke in summer lightning. On the other hand, in Fig. 7 and Fig. 8, the occurrence time of the large changes in the magnetic flux is not corresponding to the rapid changes in the electric fields. The horizontal extents of the striking points in the flashes shown in Fig. 3 to Fig. 8 are 4.1 km, 1.5 km, 6.3 km and 3.0 km respectively. All cases, upward streamers start from the lightning conductor at the top of the tower A, as shown in the figures.

RESULTS AND DISCUSSION

Continuing currents

Seven ground flashes which starts with upward developing streamers show very similar electric field changes to those shown in Fig. 3 to Fig. 8. The slow field change preceeds the negative rapid changes corresponding to return strokes or M-components. The slow field change may due to some electrical activities within clouds. Since the propagation direction of the electric current pulses was not measured, the electrical processes of the rapid field changes are not discussed further. After rapid changes, the electric fields vary almost linearly to the positive direction, and are followed by slow changes with large amplitudes. As the time constant of the input circuit is 1 ms, the response of the system to the slow field changes is rather poor. The electric field changes corresponding to the linear changes is actually increasing to the negative direction with time. Thus the field changes are interpreted as caused by the continuing currents. The electric field changes always show rapid changes which are followed by slow changes caused by the continuing currents flowing through the lightning channel to the ground.

Table 1 shows the time of the duration of the continuing currents and the horizontal extents of striking points. The horizontal extents of the electric charge in clouds may influence on above two parameters, and they correlate positively. Table 1 shows the tendency of positive correlation between two parameters. The electric field changes by the continuing currents, as well as first return stroke, may trigger lightning strokes to other transmission line towers, when the streamer develops into the deep clouds.

Magnetic flux change pulses

As mentioned previously, any rapid change of the electric field is not detected at the time when the rapid change of the magnetic flux is detected. Small changes of the magnetic flux are found at the time of the negative fast changes of the electric fields. We used a disk antenna for the electric field change meters and measured only the vertical electric field changes. Thus, horizontal lightning channel may responsible to the results that no rapid electric field changes are detected at the time corresponding to the large pulses of the magnetic

473

Table I Duration of the continuing current and the maximum distance between striking points.

Duration of C.C. (ms)	Maximum distance (km)
7.5	6.3
6.2	3.0
6.0	4.1
2.3	1.5
1.3	1.0

flux changes. In winter lightning, long horizontal channels often observed below the cloud base. Small current pulses which produce large changes of the magnetic flux may superimpose on the continuing currents through the horizontal channels.

Concluding remarks

The electric field changes caused by a concurrent lightning flash have continuing current components. The electric field changes due to the continuing currents is possible to trigger the associated strokes. Quantitative analysis of the data is remained as further study. Simultaneous measurements of the occurrence time of each lightning stroke to the tower and the electric field change are very important for the discussion on the mechanism of the concurrent lightning flash. We designed optical measuring system with 1 us time resolusion and 4 degrees spatial resolusion by using horizontal photodiode array to measure the time interval between stroke to different towers. Data obtained by new system will be helpful for further quantitative discussion on the mechanism of the concurrent lightning with multiple channels.

The observations were partly supported by Technical Research Center, Kansai Electric Power Co., Inc.. M. Nagatani and H. Nakada of Nagoya University are very helpful for the instrumentations and the observations.

REFERENCES

[1] Takagi, N., et al., Lightning flash with multiple strikes to the ground, Trans. IEE, Japan, 111-B, 93-98, 1991.
[2] Hara, T., Y. Takahashi and M. Yasui, Observation of winter lightning on a 500 kV line on the Japan Sea coast, Trans. IEE, Japan, 108-B, 289-296, 1988.
[3] Kawamata, Y., T. Takeuti, M. Nakano and Z-I Kawasaki, A case study on triggered lightning in winter, IEE Tech. Report, HV-89-50, 31-38, 1989.

Session 9B, Thursday 8:00
Aerospace Vehicles
Modeling and Coupling Analysis 1
Mazur, Chairman

FD-TD NUMERICAL SIMULATION OF AN ENTIRE LIGHTNING STRIKE ON THE C160 AIRCRAFT

J.C. Alliot*, J. Grando*, J.D. Muller* and X. Ferrières**

*Office National d'Etudes et de Recherches Aérospatiales,
B.P. 72, 92322 CHATILLON CEDEX, FRANCE

**SLX Informatique, 1 Place Charras, 92400 COURBEVOIE, FRANCE

ABSTRACT

Experimental transient electromagnetic fields measurements have been performed on a Transall C160 aircraft during in-flight lightning strikes. The data allow a test of the predictive capabilities of a three dimensional time-domain finite-difference code (ALICE) developed at ONERA in order to investigate lightning aircraft interactions. Using a transfer function technique in the 3D code it is shown that a bi-leader attached to an aircraft can be simulated by a linear model and so electromagnetic fields can be calculated everywhere on the vehicle. Comparison of experimental and numerical results have been made for several lightning strikes. Skin current density and electromagnetic fields distributions are discussed in detail.

1. INTRODUCTION

The electromagnetic pulses associated with a lightning threat can induce large charges and currents on the external skin of an aircraft in-flight that, in turn, couple into the interior of the vehicle where they can cause failures or temporary upsets in mission critical subsystems, if these subsystems are not sufficiently hardened. The recent introduction of advanced composite materials, sophisticated low level flights and mission critical electronics into aerospace vehicles has raised concerns that these may increase the vehicle's inherent susceptibility/vulnerability to transient electromagnetic fields.

Because of this concern, DRET (Direction des Recherches, Etudes et Techniques) has been sponsoring, for several years, a research program to investigate aircraft interaction with direct lightning strikes and to develop analytical and numerical tools necessary for a theoretical determination or prediction of lightning electromagnetic interactions with a vehicle.

The most recent in-flight program was conducted in France with an instrumented C160 Transall aircraft [1].

The data obtained allowed a test of the predictive capabilities of a three-dimensional finite-difference computer code set up at ONERA in order to calculate charge and current distributions on the external skin of an in-flight vehicle struck by lightning.

Magnetic field coupling through a carbon composite panel located on the fuselage has also been studied [2]. The experimental and numerical results are compared for several strikes.

476

2. IN-FLIGHT INSTRUMENTATION DESCRIPTION

During Summer 1988, ONERA has performed a complete airborne lightning characterization program, including sensors design, instrumentation lay out, extensive ground test of the whole aircraft set in a coaxial return path and in-flight measurements. The sensors were implemented on the aircraft as shown in figure 1. Four resistive current shunts (I) were mounted on the aircraft. One was fixed to the nose-boom, two were fixed to the wing tips and one was located at the base of the tail-boom. Two derivative current sensors (I-Dot) were also installed in the middle of the front and tail-booms. Seven locations were instrumented with electromagnetic sensors for E, H, E-Dot, H-Dot external fields measurements (noted EH1 to EH7 in figure 1). An internal magnetic field measurement has been achieved at the center of the fuselage, behind a carbon composite panel located on the left side of the aircraft. Seven video cameras were used to record the scene all around the aircraft. One of them was a 200 frames/second camera located under the right wing. A more detailed description of the instrumentation and of the sensors characteristics is given in [1].

3. NUMERICAL SIMULATION METHOD

The numerical code "ALICE" employed in this study can take into account lightning electromagnetic interactions with a vehicle (nearby and direct strikes, electromagnetic coupling through lossy structures, coupling through resistive and isotropic joints, ...).

3.1. FINITE-DIFFERENCE TIME-DOMAIN METHOD

The code is based on an explicite Finite-Difference Time-Domain (FD-TD) algorithm developed by K.S. Yee [3] in cartesian coordinates. The goal of the FD-TD method is to model the propagation of an electromagnetic wave into a volume of space containing a dielectric or conducting structure. The procedure produces a finite difference approximation to the solution of Maxwell's differential curl equations implemented on rectangular cross section-unit-cell space lattice.

The differential time domain form of Maxwell's equations in an isotropic medium is:

$$\nabla \times E = - \frac{\partial B}{\partial t} \qquad (1)$$

$$\nabla \times H = J + \frac{\partial D}{\partial t} \qquad (2)$$

with: $B = \mu_0 H$; $D = \epsilon_0 E$.

These equations are written in the code in a finite difference form. For a parallelepipedic cell space lattice, this procedure involves positioning the components of E and H about a unit cell of the lattice, as shown in figure 2, and evaluating E and H at alternate half time steps. In this manner, centered difference expressions can be used for both the space and time derivatives to attain second-order accuracy in the space and time increments. The size of the unit cell determines the time step Δt which, for numerical stability condition, must satisfy the criterion:

$$\Delta t^2 < \frac{\varepsilon_0 \mu_0}{1/\Delta x^2 + 1/\Delta y^2 + 1/\Delta z^2} \tag{3}$$

where Δx, Δy and Δz are the dimensions of a cell (figure 2).

3.2. LATTICE TRUNCATION CONDITIONS

To minimize computer storage, the lattice must be truncated as close as possible to the modelled structure. However, care must be exercised because this condition must not cause excessive spurious reflection of waves scattered outward by the structure.

The field components at the lattice truncation planes must be computed using an auxiliary radiative truncation condition. The method used in "ALICE" is achieved by using highly absorbing boundary conditions to simulate free space. This approximation is successful when the lattice is at least twice the largest vehicle dimension in each direction of space.

3.3. THIN WIRE FORMALISM

FD-TD codes cannot resolve coupling to wires of diameters less than a mesh size unless special features are added. The thin-strut formalism developed by R. Holland [4] allows such resolution and has been introduced in "ALICE". On a wire segment parallel to the x-axis (λ, μ coordinate location of the wire - figure 2). The current I and the charge Q per unit length are calculated by finite differencing the two following equations:

$$\frac{\partial Q}{\partial t} = - \frac{\partial I}{\partial x} \tag{4}$$

$$\frac{\partial I}{\partial t} = - C^2 \frac{\partial Q}{\partial x} + \frac{\langle E_x \rangle}{L_x} \tag{5}$$

where

C is the light velocity

$\langle E_x \rangle$ is the electric field component averaged over the cross section of the cell surrounding the wire.

L_x is the in-cell inductance, the inductance per unit length a thin wire would have with respect to an enclosing conductor half a mesh removed.

Thus, a cell with a wire running through it requires eight quantities (six fields components, the current I and the charge density Q) to be advanced each program cycle.

3.4. TRANSALL AIRCRAFT MODELLING

The Transall aircraft was modelled using three-dimensional rectangular cells having dimensions of $\Delta x = 45$ cm, $\Delta y = 90$ cm and $\Delta z = 45$ cm that were part of a total cell space of 121 x 70 x 79 cells. The relatively small cell size allows a reasonable condition of the aircraft geometry to be made as figure 3 reveals. The time step Δt employed is found from the condition (3) and has been chosen equal to 0.9 ns. For the external fields calculations a uniform mesh has been used inside a box that just encloses the modelled aircraft-extremities and slowly varying around it (adjacent cells differed in size by 20%). For the internal fields calculations, a varying mesh has been chosen on the aircraft in order to properly take into account the right composite door dimensions and a second one in space around the aircraft as in the previous meshing.

The metallic parts of the vehicle are modelled by the necessary condition:

$$\vec{n} \wedge \vec{E} = 0 \qquad (6)$$

on the structure, $\vec{n}$ is a unit vector perpendicular to the surface.

The connecting lightning channels are modelled using thin wire formalism describe in § 3.3.

A test of the predictive capabilities of the computer code "ALICE" has been performed, several years ago, by comparing experimental and numerical results obtained on an aircraft mock-up [5].

4. COMPARISON OF NUMERICAL PREDICTIONS AND IN-FLIGHT MEASUREMENTS

We give here the comparison of experimental and theoretical results obtained for a nose-wing lightning strike obtained during the 1988 in-flight experiment. For this event electromagnetic signatures on the sensors and photographic evidence from the on-board video cameras indicated that the aircraft initiated a bi-leader mechanism. The sequence of the phenomena is the following (figure 4a):

- at the beginning (between A and B) the aircraft is immersed in an ambiant electrostatic field,
- at the nose-boom, the electric field is high enough to initiate a positive leader which propagates towards ground (between B and C),
- at the right wing tip, a negative leader is initiated and propagates, by steps, towards the rear part of the fuselage (between C and E). The direction of propagation is parallel to the fuselage as shown in figure 3. It is to be noticed that the negative leader propagation generates current pulses which are superimposed on a slowly varying current component (figure 4b).

The numerical simulation of this event has been achieved for the phenomena occuring between points C and E in figure 4a. During this phase, the positive leader could be considered as having an infinite length and the negative leader could be considered as having a 30 m characteristic length corresponding to its first step [6].

The numerical calculations have been undertaken in two steps using a frequency domain transfer function technique.

4.1. ELEMENTARY PULSES MODELLING

The principle of the transfer function method is the following:

a) We assume the lightning aircraft interaction is a linear mechanism. So, for a given geometry of the vehicle attached to lightning channels (as shown in figure 3) one can put, in the 3-D code, a current generator in place of the negative leader tip and which injects a known current pulse $I_0(t)$ towards the aircraft. In one point p_0 of the vehicle (taken as a reference point) a magnetic field response $H_0(t)$ can be calculated and using a FFT of $H_0(t)$ and $I_0(t)$ one can then determine (in the frequency domain) a transfer function $T(F)$ between these two points:

$$T(F) = H_0(F)/I_0(F) \tag{7}$$

where F is the frequency and $H_0(F)$, $I_0(F)$ are the FFT of $H_0(t)$, $I_0(t)$ respectively.
We generally use a standard sine-squared pulse for $I_0(t)$:

$$I_0(t) = I_M \sin^2(\pi t/2\tau) \tag{8}$$

where τ is chosen in function of the frequency content of the in-flight measured responses.

b) If we consider the response $H_3(t)$ which has been obtained, at the same point P_0 on the aircraft, during in-flight experiment, its FFT $H_3(F)$ allows the calculation, in the frequency domain, of an equivalent current generator $I(F)$ located at the negative leader extremity and defined by:

$$I(F) = H_3(F)/T(F) \tag{9}$$

and in time domain:

$$I(t) = \mathrm{IFT}\,[I(F)] \tag{10}$$

c) This current waveform $I(t)$, simulating the negative leader mechanism, is introduced in the 3-D code and then the temporal responses at every instrumented points on the aircraft (figure 1) can be computed and compared to experimental data.
This technique is illustrated in figure 5 to 8, for the measurement current pulse noted "pulse n°7" in figure 4b. The pulse noted "pulse n°2" has been studied previously [5] using the same technique.

Figure 5 represents the comparison between magnetic field pulses measured and calculated on the left side (curves a), on the right side (curves b) and on the top (curves c) of the forward fuselage.

Figure 6 represents the comparison between magnetic field pulses measured and calculated inside the fuselage, behind the carbon composite door.

Figure 7 represents the comparison between electric field pulses measured and calculated on the top of the forward fuselage.

Figure 8 represents the comparison between the current pulses measured and calculated on the right wing tip (curves a) and on the nose boom (curves b). The magnetic field H_3 measured on the top of the fuselage has been used as reference to compute the transfer function T(F). The comparisons show a good agreement between measured and calculated waveforms at different locations on the aircraft, the magnitude discrepancy is better than 3 dB for all the fields and currents.

4.2. PULSE SERIES MODELLING

Knowing the entire strike response of a sensor in one point on the aircraft, we can calculate the responses everywhere on the aircraft using the transfer function technique described previously.

In the phase a) of § 4.1 we can calculate the transient response $H_o(t)$ at the reference point P_o but also the transient responses $H_i(t)$ at different points P_i of interest on the aircraft.
We can then determine (in the frequency domain) the transfer functions $T_i(F)$ beetween the points P_i and the reference point P_o, such as:

$$T_i(F) = H_i(F)/H_o(F) \tag{11}$$

where $H_i(F)$ and $H_o(F)$ are the FFT of $H_i(t)$ and $H_o(t)$ respectively.

If we consider the pulses series $H_3(t)$ (figure 9) which has been measured during in-flight experiment at point P_o on the top of the front fuselage (figure 1), its FFT $H_3(F)$ allows the calculation, in the frequency domain, of the responses $H_i(F)$ at each point P_i:

$$H_i(F) = T_i(F).H_3(F) \tag{12}$$

This technique is illustrated in figures 10 to 12.

Figure 10 represents the comparison between the magnetic fields measured (curve a) and calculated (curve b) on the left side of the forward fuselage.

Figure 11 represents the comparison between the magnetic fields measured (curve a) and calculated (curve b) inside the fuselage, behind the carbon composite door. The pulses of the measured field (curve a) are superimposed on a CW component due to an induced effect on the sensor of the aircraft power supply.

Figure 12 represents the comparison between the currents measured (curve a) and calculated (curve b) at the right wing tip. As explained in § 4, the measured current pulses are superimposed on a slowly varying current component. This low frequency component has not been measured by the magnetic field sensor H_3 (cut-off frequency of 100 Hz - figure 9) and so can not be calculated (figure 12b) using relation (12).

5. CONCLUSION

The goal of this paper is to present a 3-D FD-TD computer code developed at ONERA to model ligthning interaction with an aircraft. The predictive capabilities of the code have been quantified, a few years ago, by comparing experimental and computed results obtained on an aircraft mock-up and on an helicopter carbon composite fuselage.

We show in this paper that the code may be a powerful tool to analyse in-flight data. Using a transfer function technique, it has been shown that a bi-leader attached to an aircraft can be simulated by a linear model and so E.M. fields can be calculated everywhere on the vehicle.

Furthermore, knowing the entire strike response of a sensor in one point on the aircraft, we can calculate the responses everywhere on the aircraft.

REFERENCES

[1] Moreau, J.P.; Jouan, J.Y.; Issac, F.: Transall 88 characterization program. Proceedings of ICOLSE Conf., Bath (UK), (Sept. 26-28, 1989).

[2] Alliot, J.C.; Grando, J.; Issac, F; Ferrières, X.: FD-TD calculation with composite materials. Application to C160 aircraft measurements. International Aerospace and Ground Conference on Lightning and Static Electricity, Cocoa Beach, Florida (USA), (April 16-19 1991).

[3] Yee, K.S.: Numerical solution of initial boundary value problems involving Maxwell's equations in isotropic media. IEEE Trans. Ant. and Prop., Vol. AP 14, 302-307 (May 1966).

[4] Holland R.; Simpson L.: Finite-difference analysis of EMP coupling to thin struts and wires. IEEE Trans. on EMC, Vol. EMC 33, No 2, 88-97 (May 1981).

[5] Grando J.; Labaune G.; Alliot J.C.; Issac F.: Comparison of experimental and numerical results for transient electromagnetic fields induced on the C160 aircraft by current injection techniques. ICOLSE 1989, Bath (UK) (Sept.26-28 1989).

[6] Labaune G.; Richard P.; Bondiou A.: Electromagnetic properties of a lightning channel formation and propagation. Electro-magnetics, Vol. 7, No 3-4, 361-393 (1987).

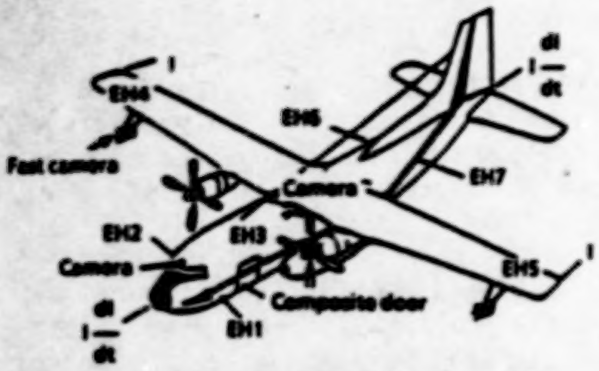
I
EH4
Fast camera
EH6
Camera
EH7
EH2
EH3
Camera
Composite door
EH5
I
EH1
I dI/dt
I dI/dt

Fig. 1 : Sensors locations on the aircraft.

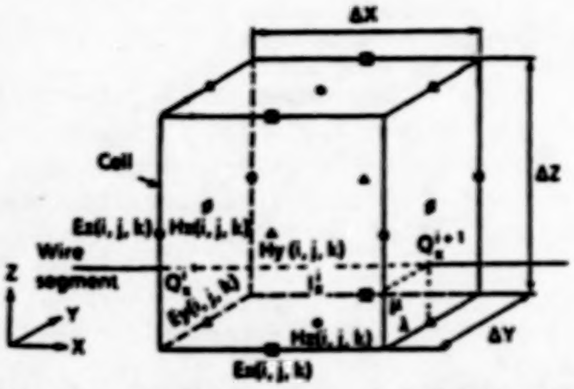
ΔX
Cell
ΔZ
Ex(i, j, k)
Hx(i, j, k)
Wire
Hy (i, j, k)
Q_x^{i+1}
Z
segment
Q_x^i
Ey(i, j, k)
I_x^i
Y
X
Hz(i, j, k)
ΔY
Ez(i, j, k)

Fig. 2 : Location of I, Q and the six field-evaluation points in a unit cell.

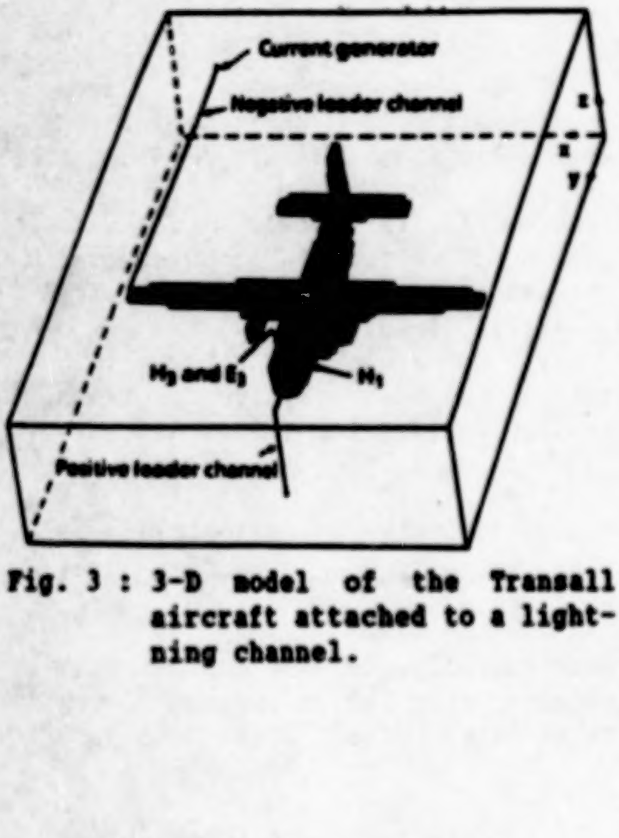
Current generator
Negative leader channel
Z
X
Y
H_3 and E_3
H_1
Positive leader channel

Fig. 3 : 3-D model of the Transall aircraft attached to a lightning channel.

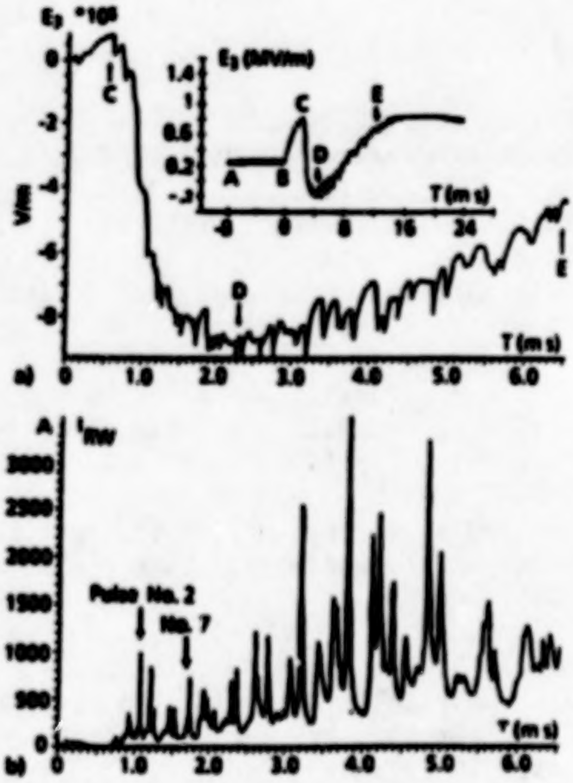

Fig. 4 : Typical experimental signatures of a bi-leader mechanism.

a) Electric field variations on two time scales.
b) Current waveform on the right wing-boom.

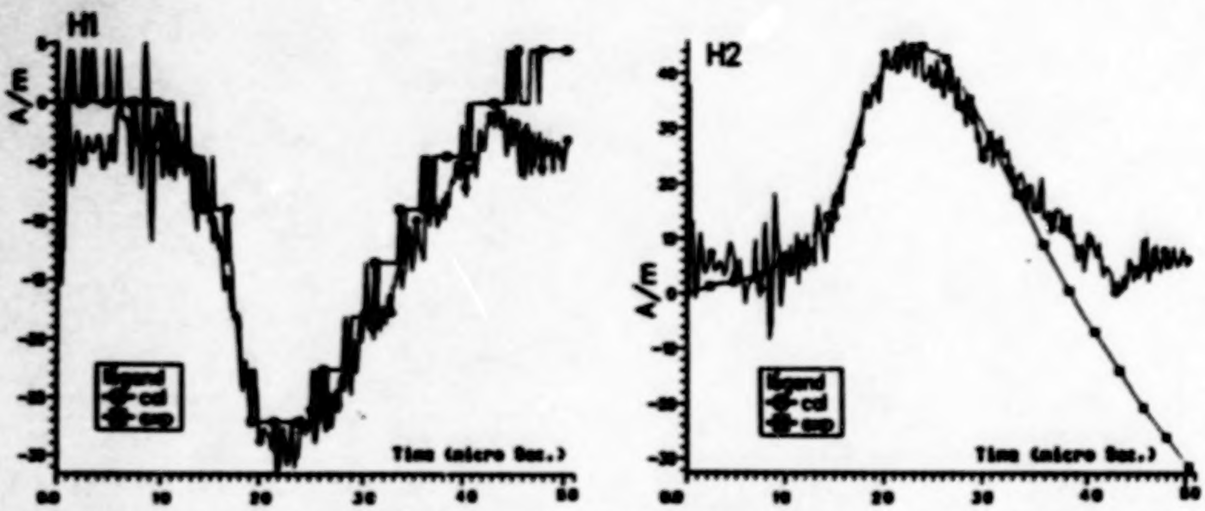

a) On the left side of the forward fuselage.

b) On the right side of the forward fuselage.

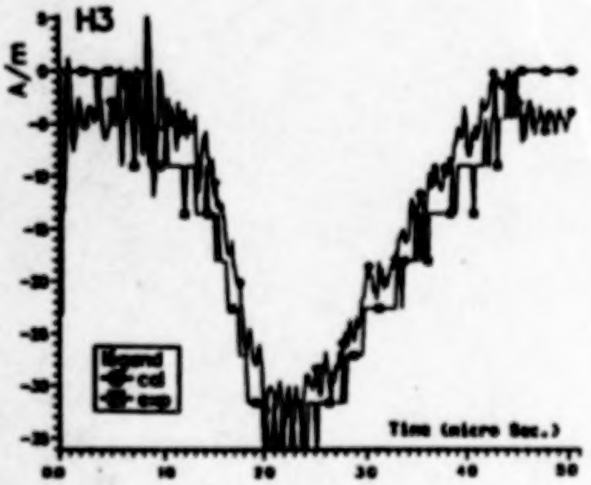

c) On the top of the forward fuselage.

Fig. 5 : Comparison of measured and calculated magnetic field pulses:

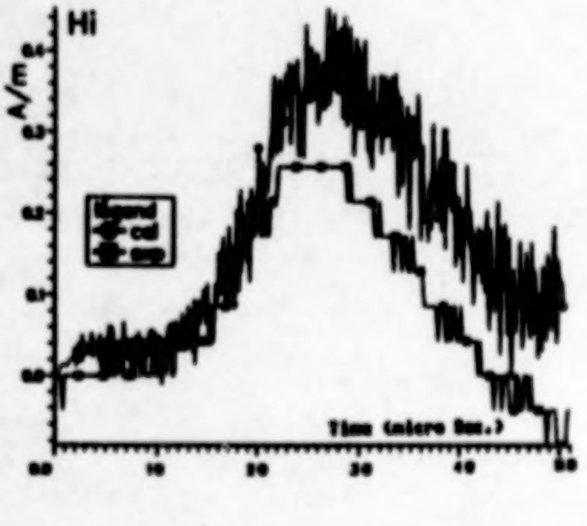

Fig. 6 : Comparison of the magnetic field pulses measured and calculated inside the fuselage behind the carbon composite door.

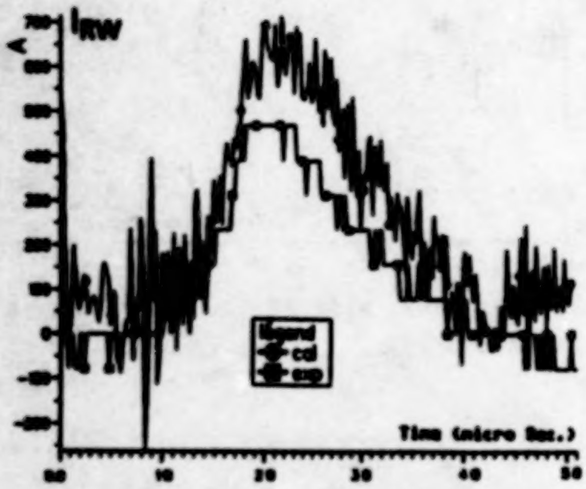

a) At the right wing tip.

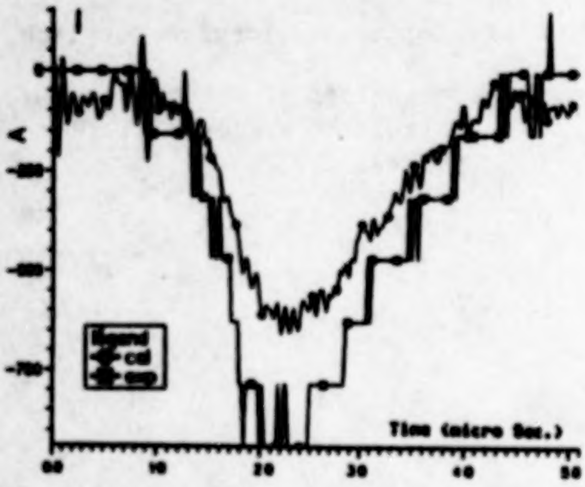

b) On the nose boom.

Fig. 8 : Comparison of measured and calculated current pulses:

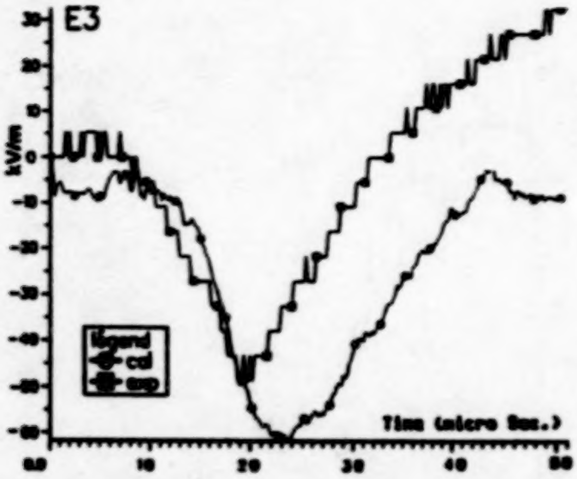

Fig. 7 : Comparison of the electric field pulses measured and calculated on the top of the forward fuselage.

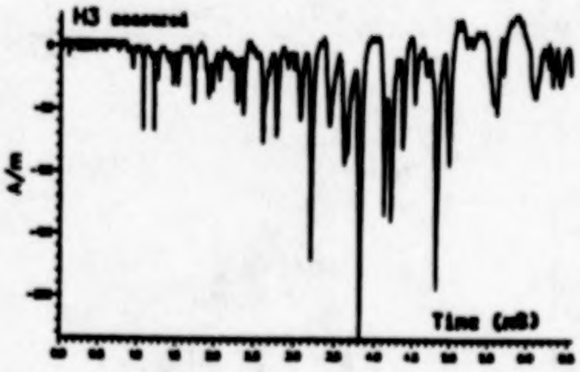

Fig. 9 : Magnetic field measured on the top of the forward fuselage.

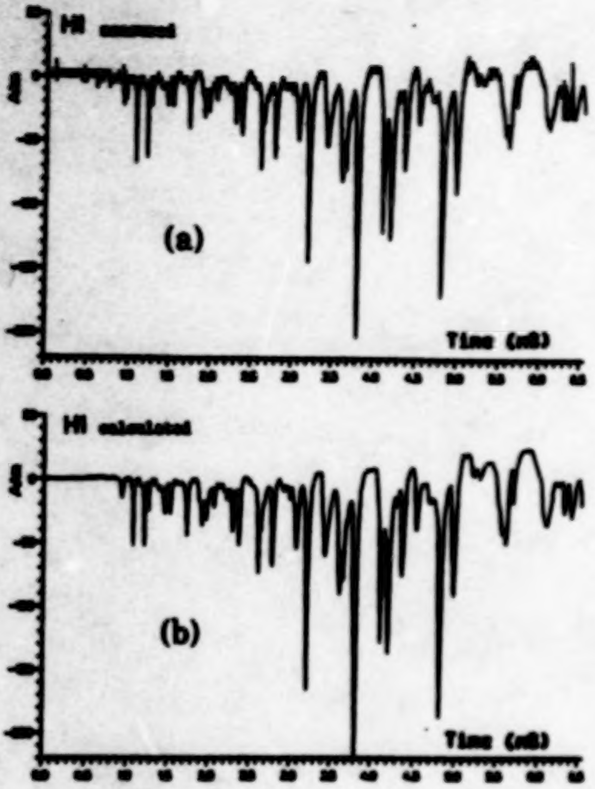

Fig. 10 : Comparison of the magnetic fields measured (a) and calculated (b) on the left side of the forward fuselage.

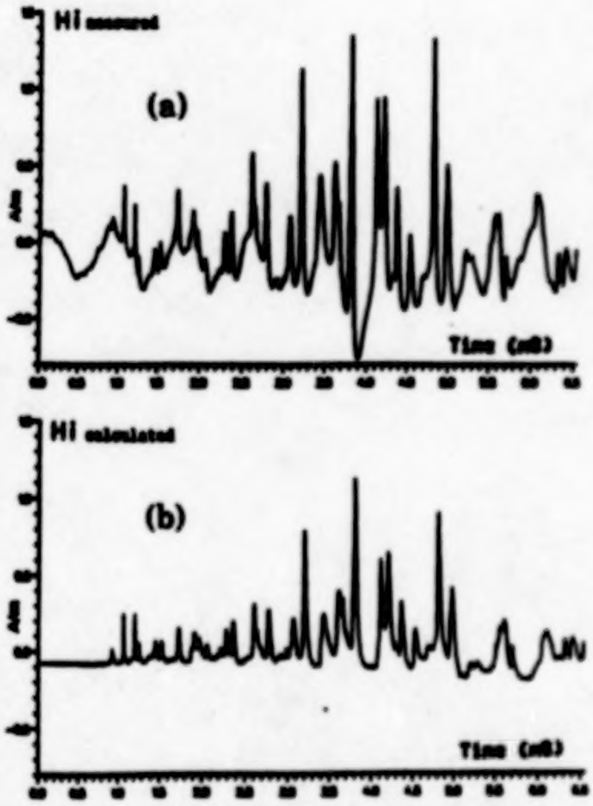

Fig. 11 : Comparison of the magnetic fields measured (a) and calculated (b) inside the fuselage behind the carbon composite door.

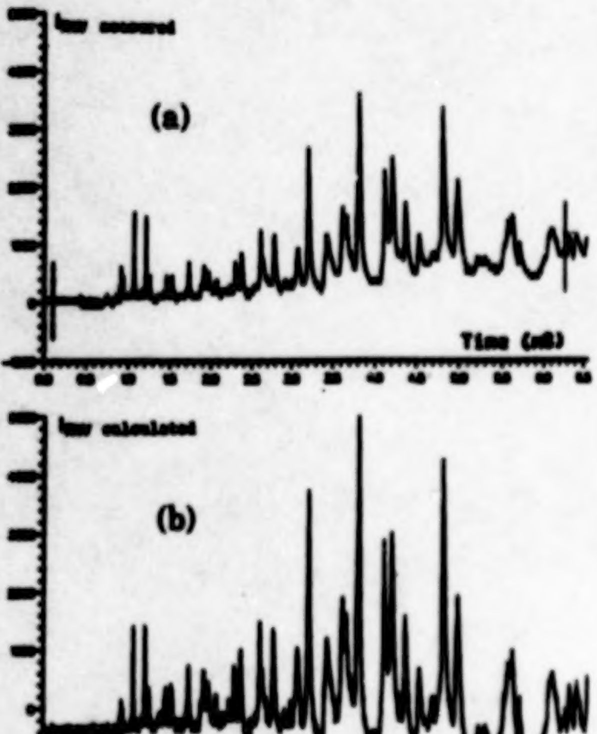

Fig. 12 : Comparison of the currents measured (a) and calculated (b) at the right wing tip.

OBSERVATIONS OF BI-DIRECTIONAL LEADER DEVELOPMENT IN A TRIGGERED LIGHTNING FLASH

P. Laroche*, V. Idone**, A. Eybert-Bérard***, L. Barret***

* Office National d'Etudes et de Recherches Aérospatiales,
Division "Environnement Electromagnétique",
B.P. 72, 92322 CHATILLON CEDEX, FRANCE.

** State University of New York at Albany,
Departement of Atmospheric Sciences,
12222 Albany, USA.

*** Centre d'Etudes Nucléaires de Grenoble,
Laboratoire d'Applications Spéciales de la Physique,
85 X, 38041 GRENOBLE CEDEX, FRANCE.

1. INTRODUCTION

Recent analyses of lightning strikes to aircraft indicate that such strikes are actually initiated by the aircraft itself [1], [2] through its interaction with the ambient electrostatic field configuration. The discharge process begins with the initiation from the aircraft of a net neutral bi-directional leader system: two simultaneously propagating but oppositely charged leaders moving in nearly opposite directions. Though the aircraft studies to date on this type of discharge have provided important new information, they have also necessarily involved the formidable difficulties and complexities of such in-flight experiments. Hence, a detailed analysis of the physical processes involved has not been possible.

A more detailed study of this type of discharge could be attempted in a laboratory setting using a long air-gap arrangement. Valuable physical insights would certainly be obtained, but it is also certain that the limited length of the laboratory discharge (ten meters, for example) would preclude a full representation of the physics involved. However, this crucial experimental restriction is removed (and other advantages are realized) if artificially triggered lightning is used as the experimental format.

Rocket triggered ligthning has been used for over a decade now to allow the close observation and detailed study of large scale electric discharges. The most recent experiments have been carried out at the Kennedy Space Center, Florida [3], under the auspices of NASA with the active participation of several french and american agencies and universities.

In this paper, a unique set of observations of a modified form of rocket triggered lightning will be described. This type of triggered lightning is termed "altitude triggering" and is relevant because it has much in common with the conditions of an aircraft triggered flash. The flash of interest was triggered during the summer of 1989. This event provided an unusually good set of observations which should provide important guidance in the modeling of the bi-directional discharge.

2. DESCRIPTION OF THE EXPERIMENT

2.1. THE TRIGGERED TECHNIQUE

The classic technique of artificially triggering lightning involves the launching of a small rocket which spools out a thin, grounded, conducting wire. The wire is connected to a current measuring device on the ground. The rocket is fired when the ambient electric field observed at ground exceeds a few kV/m. The maximum height of the rocket is typically limited to 1100 m. The two key factors that determine the triggering success are the strength of the field aloft and the rocket velocity. (The rocket velocity must be greater than the ion drift velocity so as to prevent electrostatic shielding of the top of the wire).

This basic technique has been modified to trigger flashes at altitude. This is done by making the initial run of wire trailed from the rocket a non-conducting length of kevlar thread that extends to a height above ground of between 50 m and 400 m. Subsequent to this initial kevlar section, a conducting wire section is trailed out and extended in the ambient electric field aloft. With sufficient extension of the conducting wire, a discharge begins. This situation mimics that which prevails in an aircraft triggered flash.

For the particular flash described here, a short conducting length of 50 m was trailed out initially, followed by 400 m of non-conducting kevlar. The short conducting segment near ground was used to "force" the attachment to ground and thereby allow measurement of the currents of the connecting leader (see figure 3).

2.2. OPTICAL OBSERVATIONS

As depicted in figure 1, still photographs and video records of this flash were obtained from station B, located 600 m west of the trigger site. Other optical recordings were made from station C, 2.2 km south of trigger site. These observations included two streak recordings, one obtained in the near-UV and the other obtained in the visible. The near-UV recording was made with a 51 mm lens while the visible recording was made with a 24 mm lens for a wider field of view. Both recordings used a writing rate of about 22 m/s.

2.3. DIRECT CURRENT MEASUREMENTS

The devices used for the current measurements have been described in previous papers. Basically, the current is measured by recording the output voltage of a coaxial non-inductive shunt. The smaller current of the leader discharge that precedes melting of the wire was measured with a shunt of 167 milliohm resistance. Data was transmitted from the trigger site to the transient recorders and analog DC-500 kHz magnetic recorder by fiber optic links (bandwidth of DC-1 MHz for lower range and a few hundred Hz to 100 MHz for the higher range).

2.4. ELECTRIC FIELD MEASUREMENT AT GROUND

Fast electric field variations at ground were measured with two capacitive antennas installed at 200 m and 600 m from the trigger site (points A and B in figure 1). The electric field variation between times t_1 and t_2 is a simple function of the sensor's output voltage V:

$$E(t_1) - E(t_2) = \frac{C_m}{\varepsilon_0\, S}\left[V + \int_{t_2}^{t_1} \frac{1}{DT}\, V\, dt\right]$$

with S the effective surface of the antenna, C_m the measured capacitance, and DT the decay time constant.
The time constants of antennas A and B were 470 µs and 47 µs, respectively. Thus, for signals with a duration much longer than either of these values, the voltage, V, is proportional to the time derivative of the field. On the figures presented here, we have simply displayed the variation versus time of the voltage V; so, the electric field values indicated hold only for fast signals. However, the relative variation of the field with time is the important aspect of these observations.

3. DESCRIPTION OF THE FLASH

3.1. GENERAL DESCRIPTION

That this flash was initiated by a bi-directional leader was mainly determined by the observations of the streak camera records. The recordings clearly show a negative downward propagating leader that was initiated from the bottom of the conducting wire section aloft and which later connected with an upward moving positive leader initiated from the lowest 50 m wire section at ground. After this initial phase, the sequence of events typical of a classic triggered lightning ensued: an upward moving, positive leader propagated for about 175 ms as inferred from a negative continuous current registered at ground for this duration. (This positive leader was not recorded on the streak record). About 200 ms after the leader onset, the first return stroke occurred and was followed by 11 subsequent strokes. The overall flash duration was 0.64 s. The multiplicity of this flash was more than twice that of two earlier flashes (each had 5 strokes) triggered minutes before in the same field conditions of about 7 kV/m. The sequence of current pulses is shown in figure 2 from the records of the fast electric-field antenna A and the low frequency logarithmic current measurement. Note that the low gain channel of antenna A was sensitive to fast field variations; this record shows that there was no strong high-frequency radiation during the continuous current phase except at the end of this period when two abrupt signals were recorded corresponding to light pulses from the channel (see signals "a" and "b" in figure 2). Further details on the sequence of events in this flash from initiation of the discharge until the first return stroke are presented below.

3.2. OPTICAL OBSERVATIONS

The downward branching of the discharge channel is evidenced in the video recording from station B (see figure 3; the channel depicted was actually realized from the combination of two separate video images). The characteristics of this particular triggering technique are evident in the recording: the straight section of channel indicates the wire section aloft prior to melting. This section of wire had reached a length of 160 m at the time of flash initiation.

The dual leader propagation presumed in a bi-directional discharge was not verified in the streak camera recording; only the downward, negative leader was imaged. Nonetheless, the existence of a positive leader, initiated from the top of the wire aloft, and starting well prior to inception of the negative leader is supported by the electric field variations recorded at ground (see figure 5a). In past experiments of this kind [5], the positive leader has invariably initiated the discharge as inferred from electric field recordings.

The onset of the downward propagation of the negative stepped leader from the bottom of the wire aloft was recorded by the near-UV streak camera and the electric field antenna B; both records are presented with a common time scale in figure 4a. Propagation of the initial leader continued for about 120 µs reaching a distance of about 20 m below the wire. At this point, the leader branched with continued simultaneous propagation of both branches toward ground. The mean step interval was 18 µs for the first 26 steps of the primary branch; the mean step interval for the branch was essentially the same, 19 µs. The typical step length was about 3 m, with a range of 1-4 m. The 2-D propagation speed for the initial leader was $2.5x10^5$m/s and $3x10^5$m/s for the branch.

Unfortunately, the field of view of the near-UV camera restricted imaging to levels above a height of 320 m. Below this level, however, both leaders were well imaged on the visible streak-camera record as shown in figure 4b. This record indicates that both leaders accelerated as they approached ground: speeds for the main and branch leader reached $3.1x10^5$m/s and $3.8x10^5$m/s, respectively. The lowest level imaged for the leaders is about 20 m above the 50 m section of conducting wire. (Recall that the purpose of this lowest section of conducting wire was to force attachment to the current measurement arrangement at ground).

The first return stroke imaged in the streak records consisted of two distinct events separated by only 5 µs (see enlarged view in figure 4c). The first of these events was a weak illumination of the main channel between the wire sections at ground and aloft. The wire was not melted at this time. The next event was a stronger illumination of the channel that involved both branches and which also initiated a fast upward propagation along the wire section aloft (speed of $1.3x10^7$m/s) for which melting is not apparent.

3.3. ELECTRIC FIELD VARIATIONS AT GROUND

The electric field variation at station B (figure 5a) indicates that an upward propagating positive leader preceded the negative leader onset by nearly a full 6 ms. Presumably, the positive leader emerged from the top of the wire section aloft. For an assumed speed of 10^5m/s, this leader would have propagated for abour 600 m and reached a height of roughly 1200 m at the time of negative leader initiation. As the decay time for antenna B is 47 µs, the record in figure 5a is actually a record of dE/dt. The overvall field change due to the positive leader is about 1500 V/m.

In figure 5b, the electric field recordings of antennas A and B are presented on a common time scale along with the near-UV streak record of the negative leader. The step pulses measured by antenna B (600 m distant) show strong damped oscillatory structure, indicating that the field variation was primarily due to potential variations of the wire. The effect of the space charge associated with each step is more evident in the record from the closer antenna, A (200 m distant), for which the step oscillations are much reduced. The overall duration of propagation for the negative leader was 1.13 ms as indicated in both the streak and electric field records (see figure 6a). Note that the field derivative in both antenna records was modified by inception of the branch leader: the mean dE/dt value returned to near zero but then steadily increased until connection with ground.

3.4. CURRENT MEASUREMENTS

As the negative leader approached ground, a positive leader emerged from the top of the 50 m wire section as part of the attachment process. This component of the discharge is inferred from the negative current measured by the low current channel. This current lasted for 230 µs and was pulse modulated with an interval of about 25 µs, somewhat longer than the typical negative leader step interval of 19 µs noted previously. The typical magnitude of the current pulses was about 10 A. This suggests that the pulsing of this leader was determined by the mean electrostatic conditions around the attachment wire rather than the field pulses produced by the approaching negative leader.
The current waveform for the first return stroke event also evidenced the dual pulse structure recorded in the streak images. This record is shown in figure 7 and clearly indicates an initial negative current peak of 15.8 kA with a time to peak of 2 µs and a decay to zero of only 0.78 µs. The next current pulse occurred only 4.7 µs later, reaching a peak value of 36 kA with a risetime of 0.48 µs.

The combination of current and photographic recordings indicate that the initial current pulse corresponded to melting of the wires aloft and at ground. This melting then abruptly separated the lower charged channels from the upper channel created by the leader aloft.

4. DISCUSSION

Our data reduction to date is not complete and we will continue to analyse the data to try to determine the electrostatic characteristics of the negative leader. This will entail an attempt to apply a simple electrostatic model of the leader guided by the total set of measurements as contained in the current, electric field and photographic recordings.
The consistent set of observations obtained in this case illustrate the potential for study of this important type of discharge in this experimental format. Consider the following:

1. The close observation of natural lightning negative leaders is extremely difficult for obvious reasons. A limited number of distant observations have been made, providing basic information on step lengths, step intervals and step peak currents [6]. Clearly, the conditions of observation of a triggered leader are superior to those of a natural leader. Granted, the triggered leader may not be completely developed as indicated by the shorter step lengths observed here (3 m versus 20 m). This is probably due to the limited voltage obtained by the wire in an ambient field of about 30 kV/m. On the other hand, the step interval observed here compares quite favorably with that of natural negative leaders near ground (about 20 µs).

2. The type of triggering arrangement described here reproduces much of the conditions present in a natural triggered flash initiated through the presence of an aircraft or rocket. From previous experiments, we have shown that the essential behavior is the same: the discharge is initiated by a positive leader from one end of the conductor which propagates alone for several milliseconds until the field at the opposite end of the conductor becomes large enough to launch a negative leader. The specific mechanisms of the bi-directional discharge remain to be quantitatively studied and modelled.

3. The technique of altitude triggering provides a more realistic format to study the attachment process. Accepting that a scaling factor may be involved with respect to natural flash leaders, such experiments could provide the basis for the formulation and testing of models that better describe the physics of the attachment process than can be achieved within the severe limitations of laboratory gap experiments.
Regardless of the specific objective of such triggered experiments, it is clear that a critical piece of information required for most model studies is specification of the vertical profile of electric field, from which the discharge draws its energy. Hence, for future studies two new experimental configurations must be attempted:

a) detailed studies of triggered discharges initiated at altitude for relatively low altitudes (500 m or less) concurrent with atmospheric field profiles up to 1000 m or so;
b) attempts at triggering at altitude to heights of several kilometers as suggested by electric field profiles obtained to heights up to 8 km.

These two experiments will form the basis of an experimental program we intend to conduct in the future with NASA, AFGL, and various associated US and french universities.

References

[1] J.P. Moreau, J.C. Alliot, "Analysis of the first milliseconds of aircraft lightning attachement", ICOLSE, Paris, june 1985.

[2] V. Mazur, "A physical model of lightning initiation on aircraft in thunderstorms", JGR Vol. 94, n° D3, march 1989.

[3] P. Laroche, A. Bondiou, A. Eybert-Bérard, L. Barret, J.P. Berlandis, G. Terrier and W. Jafferis, "Lightning flashes triggered in altitude by the rocket and wire technic", ICOLSE, Bath, sept. 1989.

[4] V.P. Idone, "Length bounds for connecting discharges in triggered lightning subsequent strokes", JGR, Vol. 95, n° D12, nov. 1990.

[5] P. Laroche, A. Eybert-Bérard, L. Barret and J.P. Berlandis, "Observation of preliminary discharges initiating flashes triggered by the rocket and wire technic", 8th Int. Conf. on Atmos. Electricity, Uppsala, june 1988.

[6] E.P. Krider and G.J. Radda, "Radiation field wave forms produced by lightning stepped leaders", JGR. Vol. 80, N° 18, june 1975.

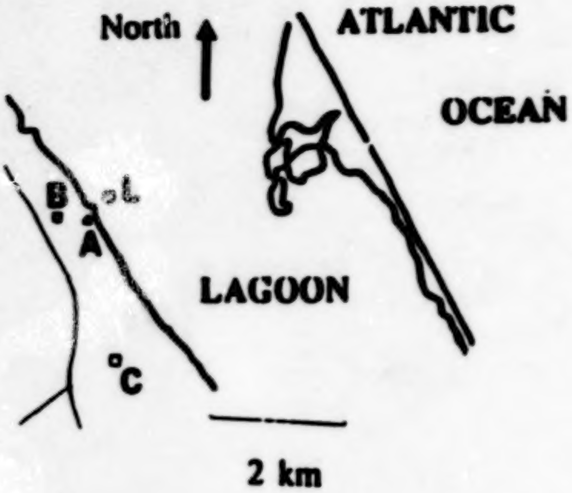
North
ATLANTIC
OCEAN
B
L
A
LAGOON
C
2 km

L Launching pad on water.
A Current measurements.
Fast electric field.
B Optical measurements.
Fast electric field.
C Optical measurement.

Figure 1: 1989 experiment site at KSC.

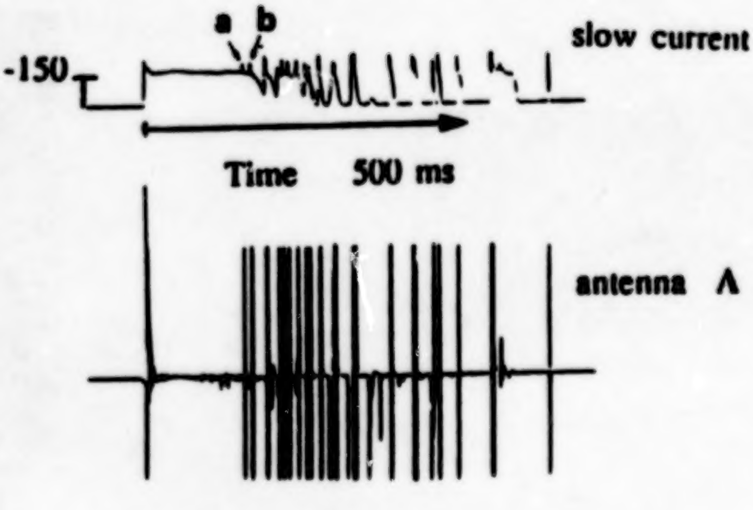

Figure 2: Timing of the flash.

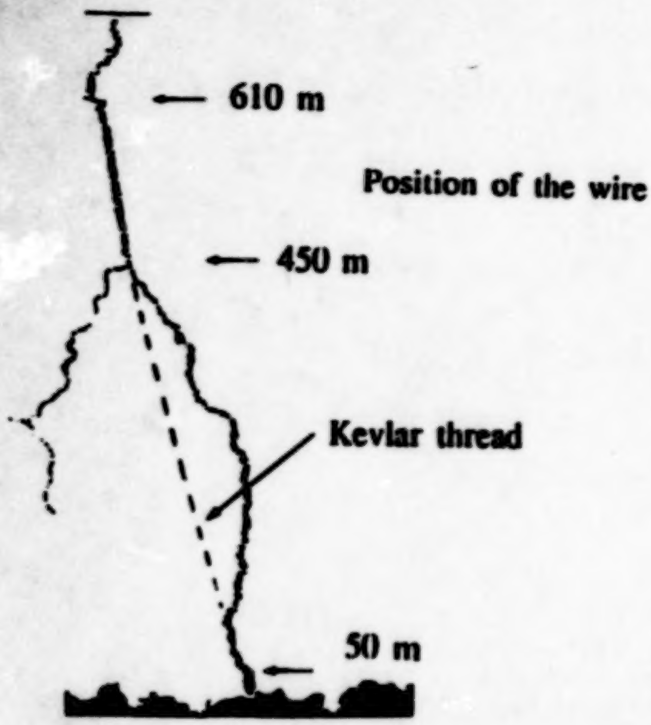
610 m
Position of the wire
450 m
Kevlar thread
50 m

Figure 3: Component video picture from station B.

4b visible streak picture

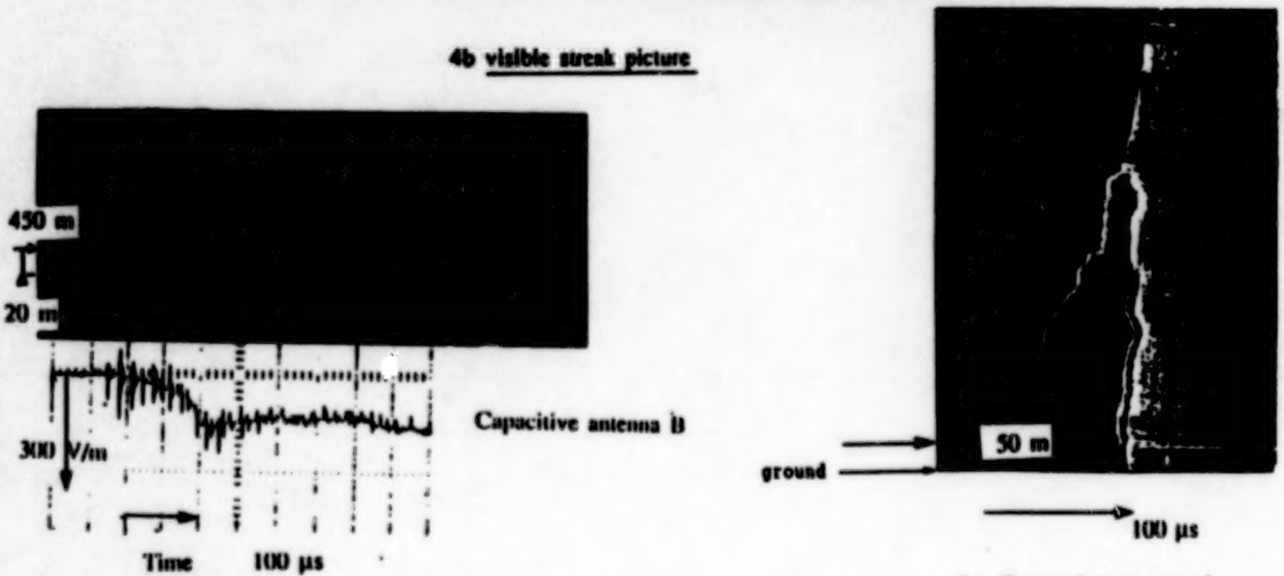

4a near UV streak picture

4c Connection to ground: visible streak picture

Figure 4: Streak picture of the downward negative leader.

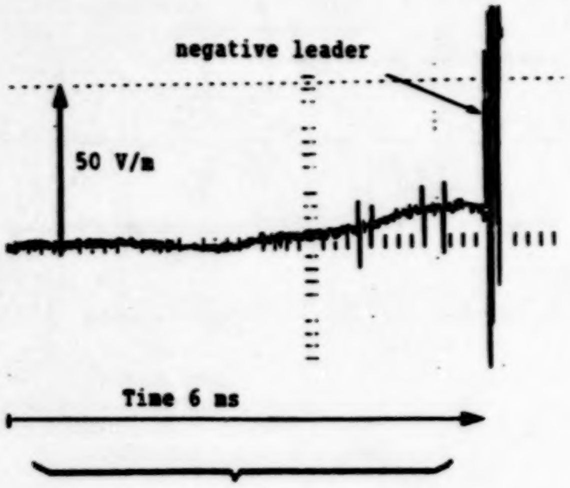

5a positive leader onset

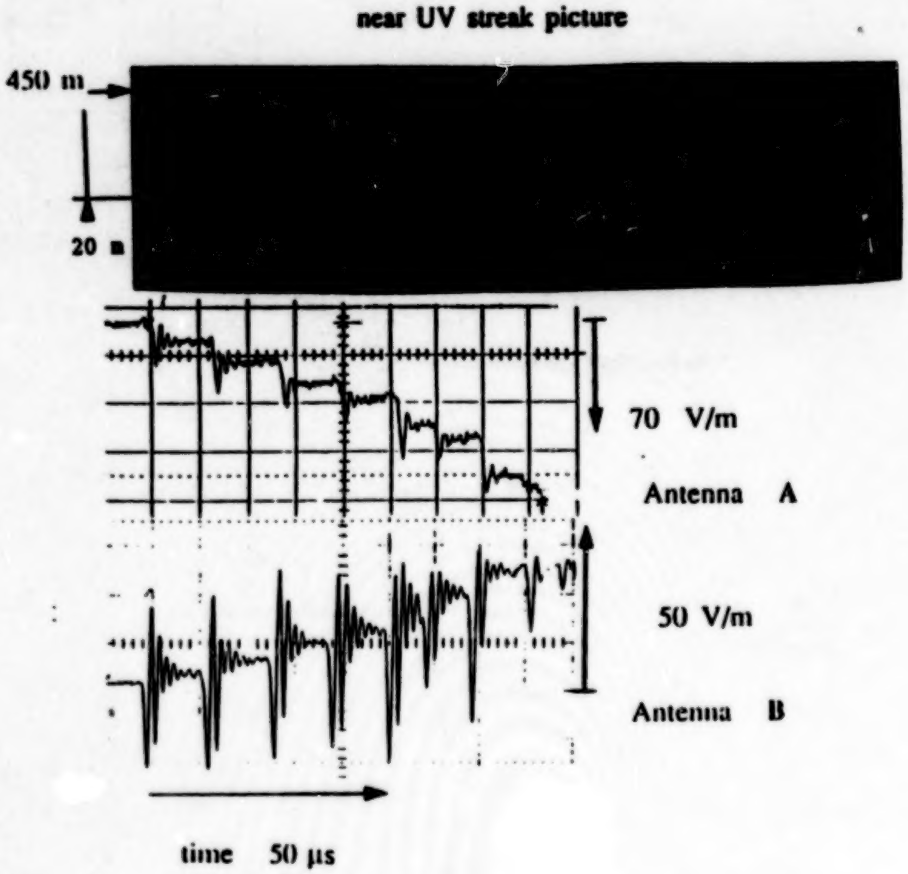

5b negative leader ons

Figure 5: Onset of positive a gative leader.

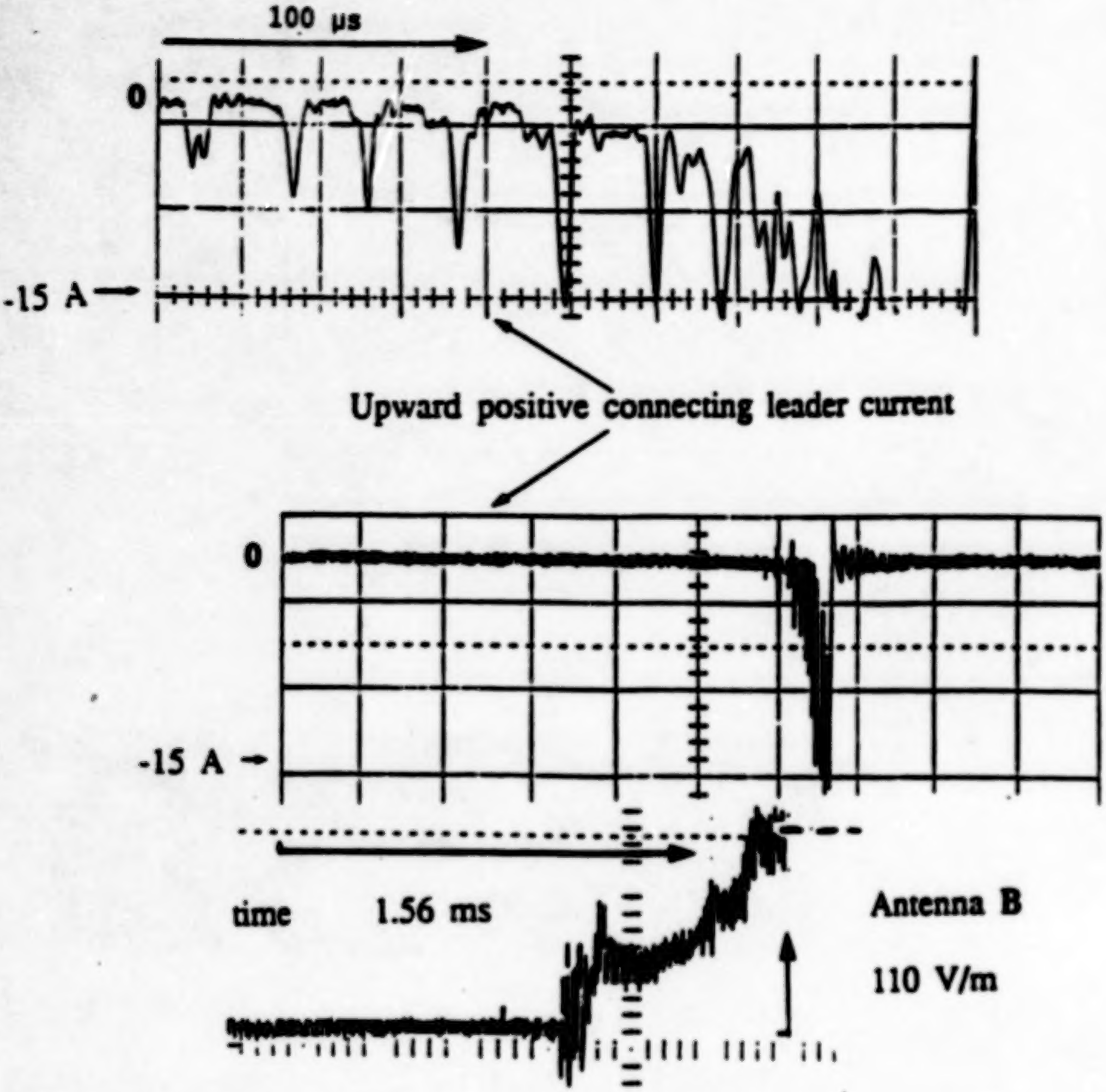

Figure 6: Connection to ground.

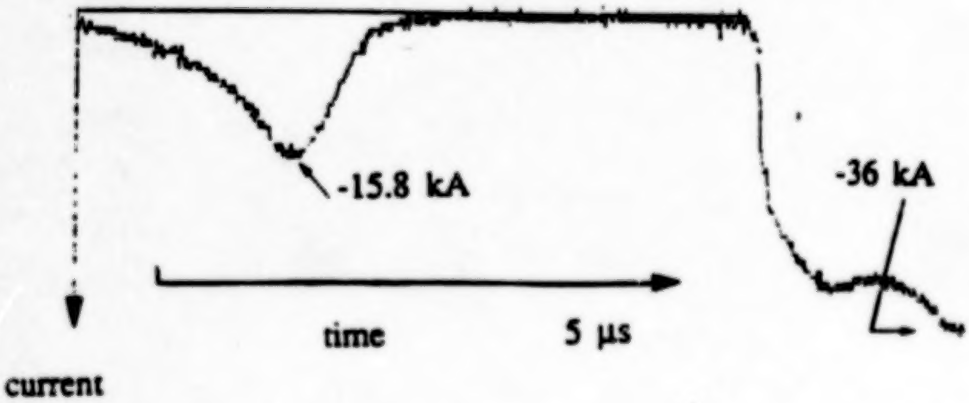

Figure 7: Current of the first return stroke.

APPLICATION OF SURFACE ELECTRICAL DISCHARGES TO THE STUDY OF LIGHTNING STRIKES ON AIRCRAFT

J.L. Boulay, S. Larigaldie

OFFICE NATIONAL D'ETUDES ET DE RECHERCHES AEROSPATIALES
B.P. 72 - 92322 CHATILLON CEDEX - FRANCE

1. INTRODUCTION

For a number of years, aircraft carrying instruments have enabled a large quantity of information to be obtained on the characteristics of in-flight lightning strikes. Whether we consider the NASA programme on the F106 aircraft, [1] the US Air Force programme on the CV580 aircraft [2] or the French programme involving the Transal 04, [3] [4] the results of all three are unquestionably comparable. The main readings taken were recordings of discharge currents in one or several points, and recordings of the electrical and magnetic components of the resulting electromagnetic field. Wherever possible, readings were taken of the current or electromagnetic field within the structures of the aircraft. We now know that a lightning strike phenomenon on an aircraft involves extremely varied discharges, the intrinsic properties of which are very different from one another. Several characteristic phases are observed when an aircraft is struck by lightning.

a) The first is a preparatory phase, which lasts approximately 10 seconds just before the actual strike occurs. The aircraft flies through a high atmospheric field during this phase, and the emission of positive or negative corona discharges can occur in different places around the structure. The balance between these positive and negative corona currents contributes to the evolution of the global potential of the aircraft. During this initial phase, the discharges that act on the aircraft involve very low currents, i.e. in the region of a hundred microamperes.

b) The next is the attachment phase, in which we know that the aircraft simultaneously emits positive and negative streamer and leader systems. This phase is important, as it produces repeated high amplitude pulses on the structure of the aircraft, with an extremely short rise time. The discharges corresponding to this phase are of the streamer or leader type (or both together), and correspond to currents of between a few amperes and several hundred amperes.

c) If the aircraft is flying close to the ground, return current phenomena can be expected ; under these conditions, this will correspond to a very high current pulse since peak values of 100,000 amperes can be reached. Note that this return current phase is rare, and in any case has never been recorded on an aircraft.

d) In most cases, after the attachment phase, a discharge phase occurs between two cloud zones with charges of opposite polarities ; this corresponds to discharges known as junction phenomena. These discharges

497

involve high currents, which can reach 50,000 amperes with rise times as short as a few nanoseconds.

It is clear that such aircraft programmes will be very difficult to repeat, partly because of the experimental difficulties involved, but mostly because of the financial costs of such programmes. For this reason, and before considering the possibilities of creating models of lightning strikes on aircraft in flight, it would be interesting if we could use electrical discharges capable of simulating the actual in-flight phenomenon in a much more accessible manner. [5] [6]

It is obvious that the corona discharges occurring during the preparation phase are very easily accessible under laboratory conditions, since they involve low amplitude currents and discharges with only a small extension. It has recently been discovered that the attachment phase, which corresponds to the streamer or leader type discharges, can be simulated under laboratory conditions by using pulse generators with peak voltages of several megavolts, capable therefore of simulating electrical discharges of up to 15 metres in length. Note that, using such facilities, the first bileader type discharge was produced in the EDF Renardières laboratory in 1989. [7]

There is also the technique of triggered lightning strikes [8]. This technique, which consists in launching small rockets from the ground, towing an electric wire, enables real lightning strikes to be produced. This technique has an extremely interesting future, since we are already taking steps to use it to trigger lightning strikes at an altitude ; these strikes will therefore be similar to those observed on aircraft. The purpose of this document is to consider the characterisation of surface discharges which, as they are easy to produce under laboratory conditions, provide a facility which is fully complementary to that of artificially triggering lightning, in an attempt to understand the mechanisms involved in lightning strikes on aircraft. These discharges are very small in size. As we will see below, they enable a very precise instrumental record to be obtained, and provide access to the very detailed intrinsic characteristics of these discharges ; we also know that these discharges have properties which are fundamentally very similar to those involved in aircraft lightning strikes, particularly with respect to propagation speed, intrinsic internal field and current involved. ONERA has been using this technique for over ten years, and this has enabled us to make an immense amount of progress in the field of basic understanding of the phenomenology of discharges. [5] [6]

2. GENERAL CHARACTERISTICS OF A SIMPLIFIED SURFACE DISCHARGE

2.1. IMPLEMENTATION PRINCIPLES

Experimentation in the field of electrical discharges is certainly not a new field of investigation, since Toepler was responsible for such work at the beginning of the century. Referring to Figure 1, we consider the main properties of these surface discharges.

The experiment carried out by Toepler consisted in using a thin dielectric plate, beneath which was placed a grounded metal electrode. By means of an electrode located above the dielectric plate, a high voltage is applied

with a variable value VO. We know that as long as VO remains below a critical value, a perfectly isotropic streamer discharge becomes established, in the form of a circle with the electrode as its centre.
If the voltage applied exceeds this peak value, the configuration of the surface electrical discharge changes, and sparks are generated ; these sparks take the form of a propagated channel, with a limited streamer zone in front of it.

Under these conditions, the most simple diagram that can be provided is that of a discharge, which therefore consists of a filament A, preceded by a streamer zone which can be of varying lengths, bearing in mind that the complete unit can propagate either continuously or discontinuously. The same experiment can be repeated, not using a polarised electrode to initiate the process this time, but instead using a method which consists in depositing either positive or negative electrical charges on the dielectric plate, and placing a grounded initiation electrode in front of it.
Figure 2, obtained at ONERA by S. LARIGALDIE, shows the appearance of a surface discharge obtained using a very thin dielectric (a few hundred microns). The discharge structure that appears is highly arborescent, which reveals a large number of spark channels ; the mean distance between these spark channels appears as a constant value. We now know that this mean distance between channels is a direct property of the thickness of the material and of its intrinsic properties. However, it is easily understandable that the study of such a discharge is particularly difficult, due to its complexity and to the non-conservation of the current in the discharges. At ONERA, we had the idea of simplifying the method in order to be able to create an elementary discharge that was as linear as possible, so as to be able to determine its basic characteristic.
The diagram in Figure 3 shows the principle of this type of experiment. The dielectric plate used is again one whose thickness can vary between a few hundred microns and a few millimetres, with a metal strip on one side to enable the propagation of the discharge.
The positive or negative polarity electrical discharges are added on the other face of the dielectric, using a metal comb made up of corona emitting points ; this comb can be connected to a variable high voltage supply.
When the electrostatic charging process of the plate has been completed, the metal comb is removed, and it is merely necessary to earth a floating electrode which is also used to measure the current. It is clear that, under these conditions, it is extremely easy to measure this type of discharge since, in addition to the possibility of easily connecting a current sensing probe in the earth return circuit, it is also possible to add facilities for electromagnetic detection and cinematographic recording at different frequencies, in the close environment of the discharge. This method has been in use for several years at ONERA.

2.2. CURRENT WAVEFORM

The discharge current is directly connected to the generation voltage used to charge the dielectric plate. As soon as the floating electrode is earthed, a breakdown current is established with a waveform as shown in Figure 4.

499

Curve 1 shows the evolution of the current of an undisturbed electrical discharge, i.e. which propagates from the floating electrode to the end of the electrical strip. Three distinct phases are identified. First, there is a current build-up phase, in which the current starts at zero and finally reaches a peak value (80 amperes on the figure), in a time which is often far shorter than a few tens of nanoseconds. The next phase involves a very slight decrease in the current during the actual propagation of the electrical discharge. Finally, after a period of a few hundred nanoseconds, the current decreases more rapidly during the phase consisting of the relaxation of the charges deposited on the electrical plate.

The waveforms corresponding to curves 2 and 3 are related to disturbances imposed on the path followed by the discharge. In the case of curve N° 2, a dielectric object has been placed in the channel of propagation, and the current pulse corresponds to the by-passing of this dielectric object by the discharge. Conversely, if the path of the discharge is disturbed by a conductive object (curve 3), a secondary pulse is observed that can reach extremely high current values in very short rise times. This secondary pulse obviously corresponds to the discharge of the polarised conductor specimen.

2.3. CONSTITUTION OF A SURFACE DISCHARGE

Through the use of electronic image converters, it has been possible rapidly to obtain a fairly precise idea of the general shape of this discharge. The two photographs in Figure 5 show a recording obtained with this type of image converter. It is perfectly clear that the discharge consists firstly of a filament zone, and secondly of a more widely spread header zone. When considered in detail, this discharge can be structured into several different zones, one of which (defined by AB) corresponds to a 'streamer' zone. This zone AB is followed by a 'transition' zone, which extends to point C and which then appears between two other zones, firstly CD, and secondly DE.

The diagram of Figure 5 constitutes the basis for a more accurate description of these different zones. The evolution of the drop in potential V along this discharge has been plotted. It is clear that the streamer zone AB corresponds to an initial plasma zone in which the electrical field is in the region of 1.1×10^6 volts per metre. The electron density of the medium is approximately 10^{15} electrons per cubic centimetre, and the electron temperature is approximately 20,000 K.
Point B corresponds to a zone in which the mean gas temperature exceeds 1 500 K. The result is an explosion of electrons around this discharge, and the generation of a transition zone between point B and point C, which corresponds to a very sharp increase in the electron density (N_e = approximately 10^{18} electrons per cubic centimetre), and in which the internal electrical field is also high, since its value is approximately 4×10^6 volts per metre.
Point C corresponds to the beginning of the thermalisation rating, in which the gas temperature approaches the electron temperature, and in which the number of ions will reach 10^{18} per square centimetre. This thermalisation zone concludes with the emergence of the actual channel of sparks which

will connect this leader zone to the initiating electrode. This entire system can therefore propagate at speeds on the order of 2 x 10^6 metres per second, either discontinuously in the case of negative polarity discharges, or continuously for positive polarity discharges.

3. APPLICATION TO THE STUDY OF AIRCRAFT LIGHTNING STRIKES

Thanks to these surface discharges, it has been possible to experimentally show a complete series of typical discharges that can occur during the general process of aircraft lightning strikes.
In reality, modifications made to the experimental apparatus make it possible to successively consider the establishment of leader or streamer type discharges, return-stroke type discharges, two-directional type leader discharges, and also recoil-streamer type discharges.

3.1. REPRESENTATION OF THE LEADER-STREAMER PHASE

In reality, this leader-streamer phase is perfectly represented by the study of surface discharges such as those shown in paragraph 2.
Among the phenomena demonstrated, we have shown that the propagation speed of such discharges could be variable according to the voltage applied to the dielectric, but would nevertheless always be between some 10^5 metres per second and some 10^6 metres per second - these values are absolutely identical to those known to be reached by lightning leaders.
The most important point obtained during these experiments concerns the rise time of the current wave. We have indeed been able to experimentally show that the electromagnetic radiation threshold that is detectable in presence of such discharges exists only at the beginning and end of the surface discharge. Consequently, this means that the electromagnetic radiation could only be associated with the rapid rise time of the current obtained either at the beginning or at the end of the surface discharge.
This point is of paramount importance, since it has made it possible to understand the electromagnetic radiation properties of lightning discharges in a natural environment. This concept of a rapid rise time has been in particular used to create an electromagnetic interferometer, capable of following the propagation of discharges between clouds in both time and space. [9]
In particular, and as demonstrated elsewhere, we now know that the initiation of a discharge between clouds occurs according to the two-directional leader model recorded during aircraft lightning strikes. [10] [11]

3.2. REPRESENTATION OF THE RETURN-STROKE PHASE

A relatively simple modification of the original surface discharge experiment enabled us to produce a laboratory representation of a return-stroke type discharge phase. It was merely necessary to complete the previous experimental set-up (described in paragraph 2) by adding an electrode connected to a high energy capacitor, in turn connected to the earth. The experiment therefore consisted, as explained in paragraph 2, in triggering a leader type discharge by means of the spark gap at the top ; once the leader discharge had reached the lower electrode, a return wave was immediately initiated, therefore causing the discharge of the capacitor which had been charged in the channel of the preceding leader. Under these conditions, it was possible to produce an extremely high energy electrical discharge, with properties which were sully similar to the return stroke of natural lightning.

As an example, we have included two curves in Figure 6 to show the evolution of the electrical currents measured on the capacitor and the floating electrodes. In the capacitor current pulse, the emergence of a very fast pulse can be seen, with an over-oscillation which subsequently tends to become identical to the current wave observed on the floating electrode. In the same way, it was possible to use small capacitive antennae, located along the path of the return-stroke, to show the potential variation laws in several points along the discharge channel.

These evolutions of potential are shown by the different curves in Figure 7. It can therefore be seen that this potential, which starts when the leader touches the capacitor electrode, with a field distribution related to the leader phases, will therefore lead to the establishment of a field curve with a higher value, and show the superimposition of an oscillating value of the electrical field. This experimental set-up has also made it possible to directly observe the geometry of the discharge channel. In particular, we have been able to use an interferometric holography technique at ONERA to enable channel diameter fluctuations to be observed over extremely short periods of time. As an example, we have provided an idea of the evolution of this channel in Figure 8, for build-up times of between 50 and 500 nanoseconds as from the instant when the return-stroke is established. It is particularly clear that, during this phase of some 500 nanoseconds, the diameter of the channel has changed from approximately one millimetre to three millimetres.

All of these measurements, current, potential, holography and also spectroscopy of the discharge, have enabled us to record the intrinsic parameters necessary to produce a theoretical model. This theoretical model was able to be assessed by numerical calculation.

3.3. APPLICATION TO THE TWO-DIMENSIONAL DISCHARGE PHASE

In the same way, the experimental set-up used for the surface discharges was easily modified to enable the generation of two-dimensional discharges, identical to those recorded during lightning strikes on aircraft. The method consists in using two dielectrics, charged to different potentials.

The installation of a floating conductor between the two dielectric plates makes it possible to generate a surface discharge which initiates from each side of the interface, showing the dual propagation of a positive leader and a negative leader.

The photograph in Figure 9 gives an idea of the type of two-directional discharge produced in this way. A complete study is currently in progress in order to acquire the most accurate knowledge possible of the properties connected with these types of propagation.

The use of surface electrical discharges can also be extrapolated to the examination of recoil-streamer type discharges that occur on aircraft.

In this case, the experimental equipment concerned comprises three dielectrics separated from each other, and the middle dielectric has its conductive plate connected to the earth : the zones on either side are

charged with potentials of positive and negative voltages. The obtainment of recoil-streamer type discharges can be considered in the following manner :
the two dielectrics on either side are charged, and when a state of equilibrium of the charges is reached, the two generation devices are removed and a discharge is initiated on one of the interfaces. The result is the propagation of a two-directional discharge, as specified earlier, with, for example, a negative discharge propagating on the left-hand electrode and a positive discharge on the middle electrode. When this positive discharge reaches the extreme right-hand zone, a recoil-streamer type process will be able to be established. We are currently in the process of providing instrumentation for this experiment. The objective is to establish a viable mechanism which could explain the readings obtained on lightning-struck aircraft.

4. CONCLUSION

We have just demonstrated that the laboratory studies carried out on surface discharges have proven to be extremely profitable to the increase of our knowledge on aircraft lightning strike phenomena. The preliminary phase consisted in creating surface discharges with properties that are absolutely identical to those of the streamer or leader type discharges that occur during the phase leading up to natural lightning or aircraft lightning strikes.

The fact that the initiation times of these discharges could be perfectly controlled, and most of all the ability to pre-determine the path followed by the discharge channels, meant that it was possible to produce a highly dedicated high-performance instrumentation system.

Simultaneous measurement of the electric current, the electric field, and spectroscopics of the discharge channel made it possible to create reliable theoretical models. More particularly, we were able to obtain and demonstrate a very thorough knowledge of the electromagnetic radiation mechanisms involved in a discharge.

We now know that simple modifications can be made to the basic set-up, in order to obtain electrical discharges of different types. An additional study has already been carried out, with the aim of examining the return stroke type process. At ONERA, we are currently in the process of making a third type of modification to this equipment, with the objective of carrying out a detailed study, firstly of two-dimensional leader type discharges, which correspond to the attachment phase of the lightning strike on the aircraft, and subsequently of the recoil-streamer type discharge phases, which are extremely important for the study of the electromagnetic disturbances that can occur on aircraft.

REFERENCES

[1] F.L. Pitts et al. - F106 data summary and model results relative to threat criteria and protection design analysis - 11th ICOLSE, Dayton, June 1986.

[2] P.L. Rustan and J.P. Moreau - Aircraft lightning attachment at low altitudes - 10th ICOLSE, Paris, June 1985.

[3] J.P. Moreau and J.C. Alliot - E and H field measurements on the Transall C160 aircraft during lightning flashes - 10th ICOLSE, Paris, June 1985.

[4] J.L. Boulay et al. - Analysis of recent in flight lightning measurements on different aircraft, ICOLSE 88, Oklahoma city 19, 21 Avril 1988.

[5] S. Larigaldie - "The spark propagation mechanism in ambient air at the surface of a charged dielectric: I - Experimental: the main stages of the discharge" - J. Appl. Phys., 61, 90, 1987a.

[6] S. Larigaldie - "The spark propagation mechanism in ambient air at the surface of a charged dielectric: II - Theoretical modeling" - J. Appl. Phys., 61, 102, 1987b.

[7] B. Hutzler, I. Taudière - Attachment process of lightning on aircraft in the light of laboratory simulations. ICOLSE 89, bath, 26-28 september 1989.

[8] P. Laroche, A. Eybert-Berard, L. Barret and J.P. Berlandis, "Observations of preliminary discharges initiating flashes triggered by the rocket and wire technique", 8th Int. Conf. on Atmospheric Electricity. Uppsala, june 1988.

[9] P. Richard, G. Auffray : "VHF-UHF interferometric measurements, application to lightning discharge mapping", Radio Science, 20 (2), 171-192, (1985).

[10] V. Mazur, "A physical model of lightning initiation on aircraft in thunderstorms", J.G.R., Vol. 94, n°D3, March 1989.

[11] J.P. Moreau, S. Larigaldie - at this conference.

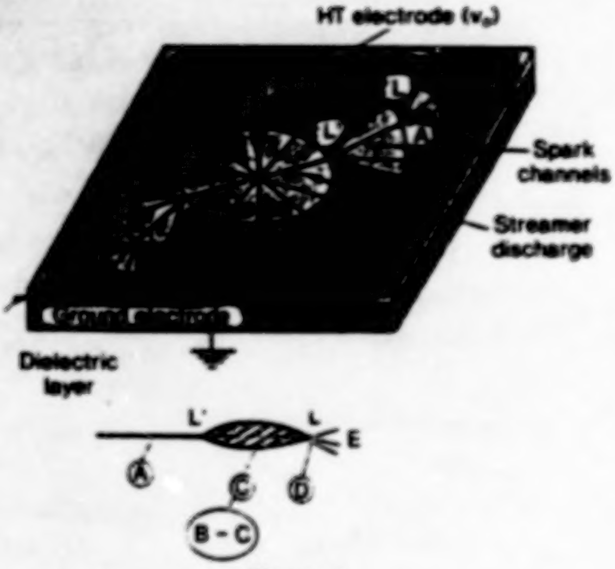
HT electrode (v0)
Spark channels
Streamer discharge
Ground electrode
Dielectric layer
L
L'
A
B
L'
L
E
A
C
D
B - C

Figure 1
Surface discharge propagation.

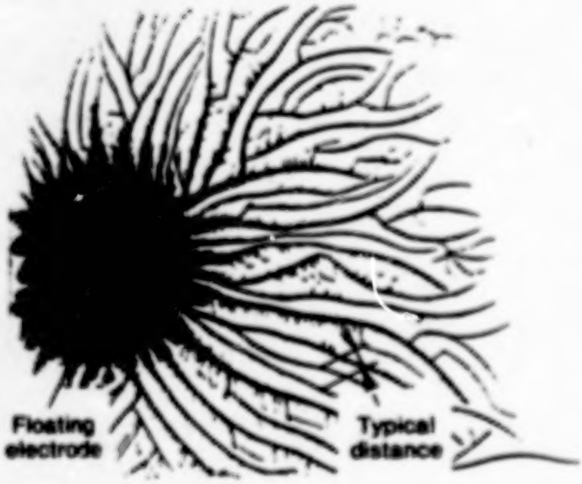
Floating electrode
Typical distance

Figure 2
Photography of an electrical surface discharge.

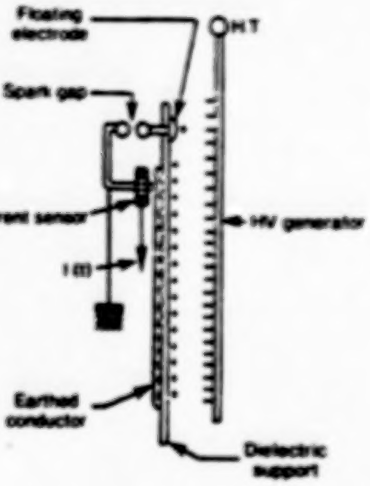
Floating electrode
HT
Spark gap
Current sensor
HV generator
I (t)
Earthed conductor
Dielectric support

Figure 3
Surface discharge experiment.

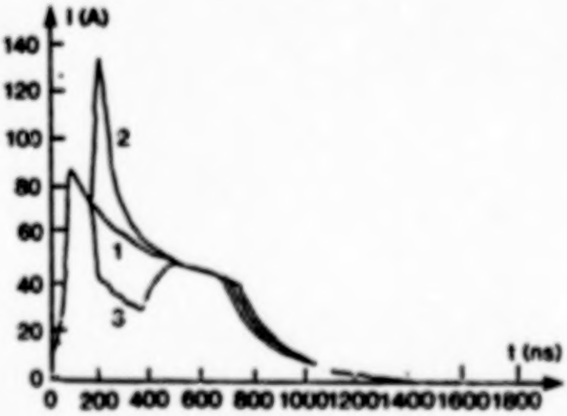

Figure 4
Current waveforms.
1) Normal. 2) Conductive obstacle.
3) Dielectric obstacle.

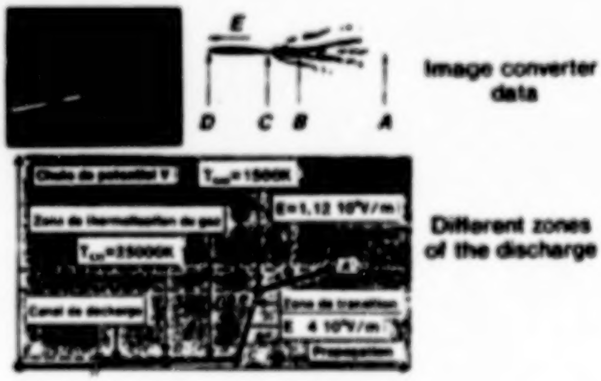
E
D
C
B
A
Image converter data
Chute de potentiel V
T_max = 15000K
E = 1,12 10^6 V/m
Zone de thermalisation du gaz
T_ch = 25000K
Canal de décharge
Zone de transition
E 4 10^6 V/m
Propagation
Different zones of the discharge

Figure 5
Surface discharge structure.

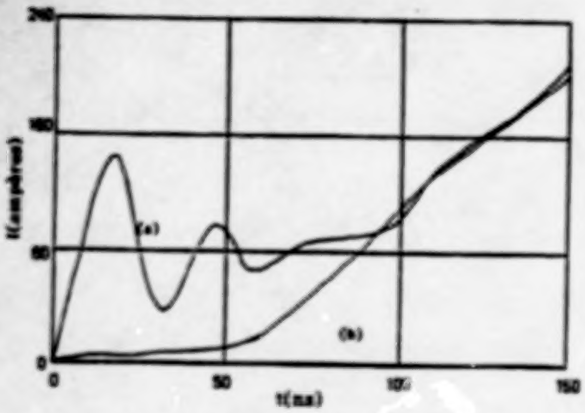

Figure 6
Discharge currents.
a) At the capacitor level.
b) At the upper electrode level.

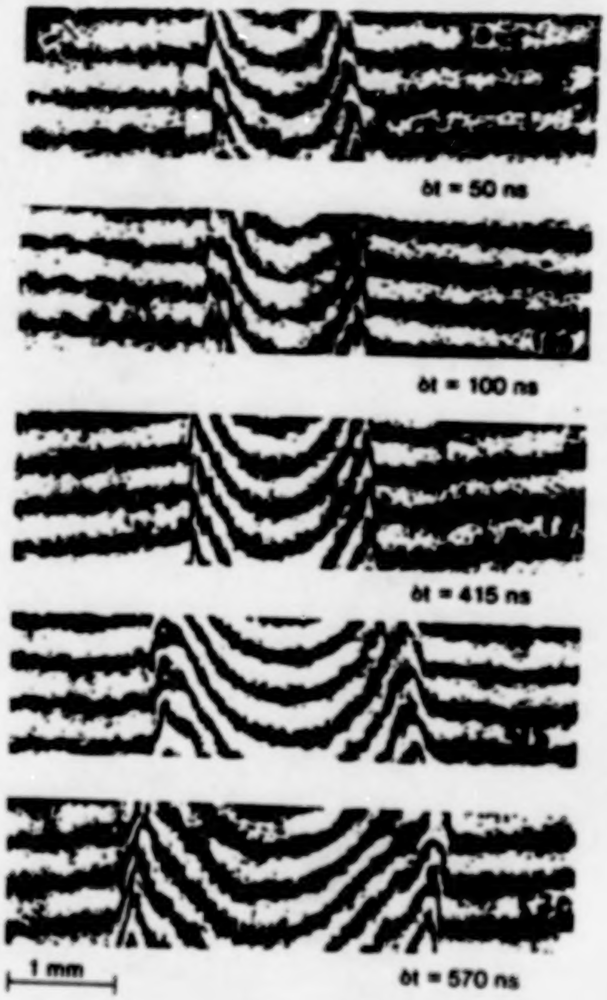
δt = 50 ns
δt = 100 ns
δt = 415 ns
1 mm
δt = 570 ns

Figure 8
Return-stroke channel observed by holography.

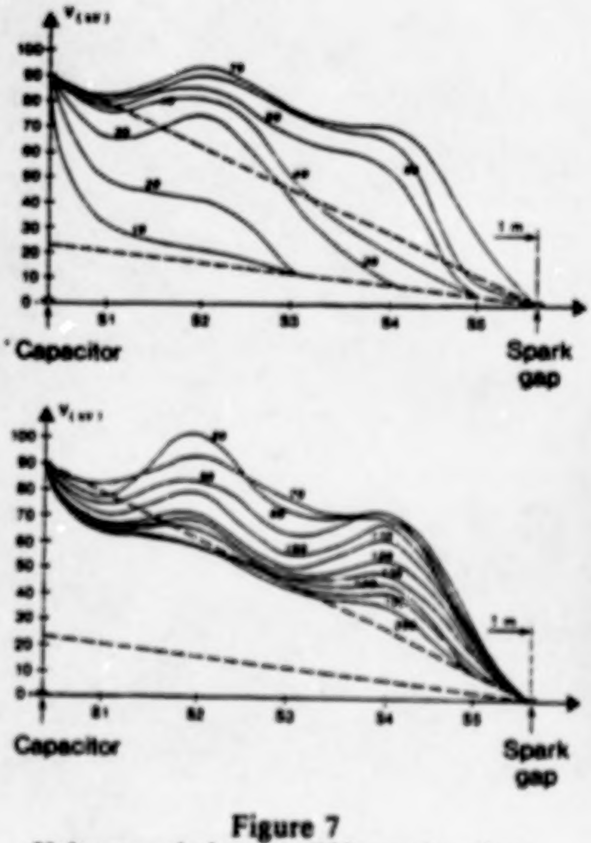

Figure 7
Voltage variations at different locations.
Voltage: 90 kV. e: 2 mm.

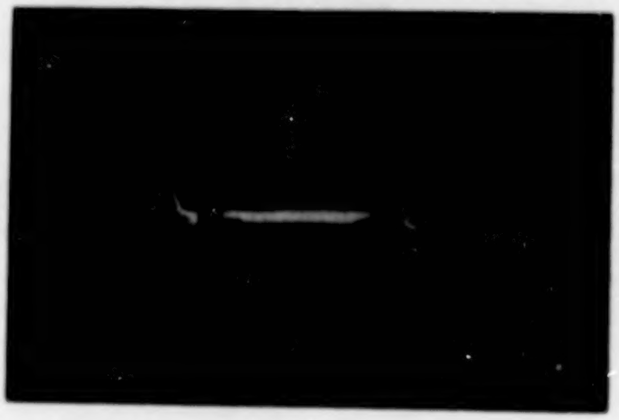

Figure 9
Example of a bidirectionnal leader obtained on a dielectric support.

SCALE-MODEL CHARGE-TRANSFER TECHNIQUE FOR MEASURING ENHANCEMENT FACTORS

J. Kositsky and J.E. Nanevicz
SRI International, Menlo Park, California

ABSTRACT

Determination of aircraft electric-field enhancement factors is crucial when using airborne field mill (ABFM) systems to accurately measure electric fields aloft. SRI used the scale-model charge-transfer technique to determine enhancement factors of several canonical shapes and a scale model Learjet 36A. The measured values for the canonical shapes agreed with known analytic solutions within about 6%. The laboratory-determined enhancement factors for the aircraft were compared with those derived from in-flight data gathered by a Learjet 36A outfitted with eight field mills. The values agreed to within experimental error (~15%).

INTRODUCTION

Aerial measurements of atmospheric electric fields can provide data that are essential for accurately assessing the danger of triggered lightning to space-launch vehicles. A properly instrumented aircraft can resolve the ambient vector electric field aloft in real time and can telemeter critical data to ground personnel during a prelaunch countdown sequence. In addition, postflight analyses of stored electric-field and meteorological data can be used to study the fundamental processes of cloud electrification.

To successfully measure the ambient electric fields aloft, it is crucial to accurately quantify the perturbation of the fields by the aircraft itself. In general, an electrostatic field is perturbed by the presence of a conducting body so that the field lines terminate normal to the object's surface. The factor by which the ambient field is modified at a given point on the surface is referred to as the "enhancement" or "form" factor of that object at that point.

Several methods of determining enhancement factors have been used historically. The method described here, the scale-model charge-transfer technique, has been used with varying degrees of success since the time of Maxwell [1]. Studies at SRI International [2,3] have shown that, for various canonical shapes (spheres and prolate spheroids) with analytic solutions in closed form, this technique, when carefully performed, can provide accurate enhancement factors. The technique was also used to determine the enhancement factors of a Learjet 36A. During the latter part of July 1989, SRI modified and updated an existing ABFM system for integration with the Aeromet Learjet 36A High-Altitude Reconnaissance Platform (HARP) that had also been used for meteorological support of rocket launch and reentry tests in the Pacific. Flight experiments were performed using aircraft maneuvers with the HARP under specific field conditions near the Kennedy Space Center. These data were used to independently compute the enhancement factors at the field meter locations and verify the scale-model charge-transfer measurements.

SCALE-MODEL CHARGE-TRANSFER TECHNIQUE

The scale-model charge-transfer technique is performed in an artificially produced uniform electric field. A conductive model of an object, for which the enhancement factors are required, is suspended in this field, distorting the otherwise uniform field in the same manner as the full-scale object would distort a uniform ambient field.

The charge density at any point, *i*, on a conductor's surface is proportional to the electric field magnitude, E_i, at that point. In the scale-model charge-transfer technique, the electric field at the points where the enhancement factors are required is measured by sampling the charge density at those points. This is accomplished by touching a small metal probe to the points of interest and measuring the charge that transfers from the model to the probe. Since the magnitude of this charge, q_i is proportional to the field at the point probed, the enhancement factor, a_i, can be determined by dividing by the charge q_o acquired by the same probe at a reference plate where the field is maintained at the uniform field value E_o.

$$a_i = \frac{E_i}{E_o} = \frac{q_i}{q_o} \tag{1}$$

The charge on the probe is measured by bringing the charged probe into contact with the inside surface of a shielded Faraday "bucket" charge receptacle. A Cary 31 vibrating-reed electrometer, capable of measuring charges of 5×10^{-16} C, is connected to the receptacle to measure this deposited charge.

The uniform electric field was created in an electrostatic cage that consists of two large (152 cm per side) square aluminum parallel plates held 152 cm apart by a wooden frame (Figure 1). The edges of the plates are rolled over and taped to mitigate corona production. The whole frame rests on two wooden sawhorses, placed parallel to the end plates.

Electric-field fringing is minimized by a system of 15 equally spaced, insulated guard-ring wire loops held by the wooden frame parallel to the aluminum end plates. Each loop is maintained at the correct voltage to give a linear variation of potential between the plates by connecting it to a resistance voltage divider that spans the full cage voltage. Although the electric field has some fine structure near the guard wires, the field is essentially uniform over most of the cage volume.

The voltage source is an FRP-200 capable of providing 40 kV. For safety reasons, a 15 MΩ resistor is connected in series with each leg of the high-voltage supply. The voltage divider consists of fourteen 3.6 MΩ resistors, one between each pair of wire loops in the guard ring, and two 1.8 MΩ resistors for the half-width sections between the end loops and the end plates.

The high-voltage supply to the cage end plates is activated by an operator foot switch through a pair of high-voltage vacuum relays. In operation, the probe tip is touched to the correct spot on the suspended model, the relay is activated, the probe is removed from contact with the model, the relay is deactivated, and the charge on the probe is placed in the electrometer Faraday bucket.

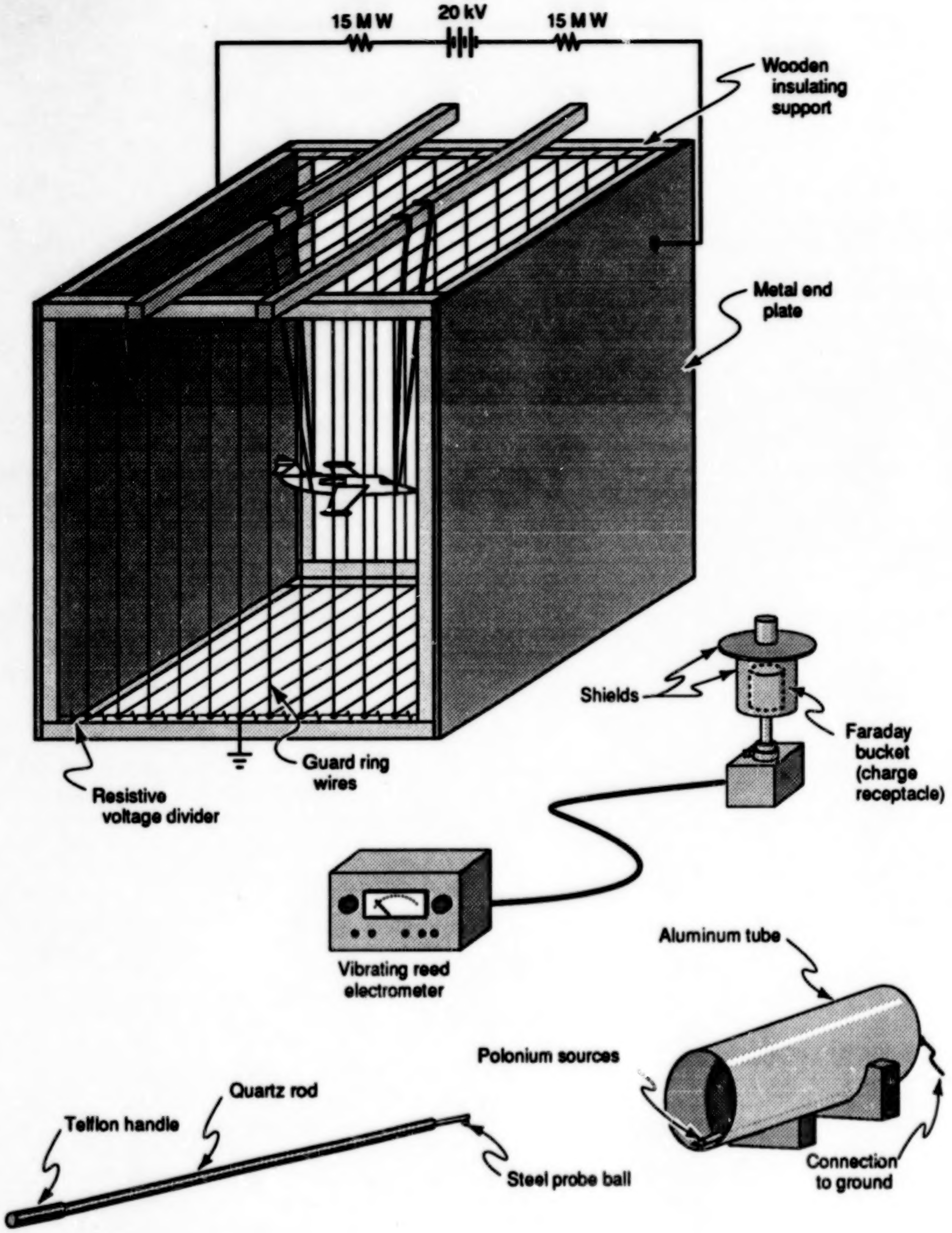
15 M W
20 kV
15 M W
Wooden insulating support
Metal end plate
Shields
Faraday bucket (charge receptacle)
Guard ring wires
Resistive voltage divider
Vibrating reed electrometer
Aluminum tube
Polonium sources
Connection to ground
Quartz rod
Telflon handle
Steel probe ball
p91-003/f1

Figure 1 ELECTROSTATIC CAGE SCALE-MODEL CHARGE-TRANSFER APPARATUS

The probe is a 3 mm (1/8 inch) diameter steel ball fastened to the tapered end of a 50 mm (2 inches) long Teflon rod. The Teflon rod, which is about 3 mm (1/8 inch) in diameter, is inserted into one end of a hollow quartz rod about 1 m (40 inches) in length that is insulated from the experimenter by a 15 cm (6 inches) Teflon handle (Figure 1).

Experiments were performed with the probes to check for charge buildup and leakage by varying the time between probing the model and depositing the charge in the Faraday bucket. No leakage or buildup effects were noted for delay times of up to 5 minutes. Typically, only 5 to 10 seconds are needed to transfer the charge to the electrometer bucket.

Several 500 µCi polonium sources were placed inside a 15 cm (6 inches) diameter metal grounded tube, thus producing a field-free ionized region. Before taking a measurement, stray charges that might collect on the probe's dielectric surfaces are neutralized by passing the probe over the polonium sources.

An accurate conductive scale model of the aircraft (or other object) is suspended near the center of the cage by waxed nylon thread tied to wooden slats placed on top of the frame parallel to the equipotentials. The thread, as well as the insulated guard rings, are neutralized by passing polonium sources along their lengths. The model is oriented in turn with its x, y, and z axes parallel to the applied electric field. This allows the enhancement factors a_x, a_y and a_z, due to electric-field components E_x, E_y and E_z respectively, to be measured independently. The model is momentarily grounded before the measurements to ensure that it is electrically neutral.

The field enhancement at the points where field mills are located is determined by measuring a quantity proportional to the charge density, and therefore the electric field, at these points using the small metal probe, as outlined above. The electrostatic cage end plates are then similarly sampled to obtain a quantity proportional to the ambient field in the cage. The enhancement factors are equal to the ratio of these measurements as shown in Eq. 1.

This procedure is repeated with the aircraft model suspended in the cage in three orthogonal positions relative to the applied electric field to obtain the enhancement factors, a_{ix}, a_{iy}, and a_{iz}. To obtain the coefficients, a_{iv}, quantities analogous to enhancement factors that give the field at point *i* due to charge buildup on the airframe, a similar procedure is followed with the model suspended in a field-free region ($E_x = E_y = E_z = 0$). The model is charged to a known potential and probed at the same field mill sites. In this case, however, the results must be divided by the scaling factor of the scale model to obtain a_{iv}.

CANONICAL SHAPE EXPERIMENTS

Several solids have shapes that allow the enhancement factors to be computed in closed form directly from Maxwell's equations. Experiments with several of these shapes (spheres and various prolate spheroids) were performed to test the experimentally derived enhancement factors against the theoretical values. The results of these experiments (described below) show that the absolute uncertainty of the enhancement factors calculated from the scale-model charge-transfer technique data are within approximately 6% (including systematic errors).

A 130 mm (5 inches) diameter aluminum sphere and two aluminum prolate spheroids with axis ratios of 2 and 5 and major axes of 200 mm and 300 mm, respectively, were machined. Each solid was carefully marked to divide the semimajor axis into ten equal segments. A freshly cleaned 6 mm (1/4 inch) dot punched from copper tape was centered on the marks. These dots acted as targets for the experimenter to probe and also nullified most of the contact potential effect, since the Faraday bucket was also made of copper.

The results of the experiments (plotted points) and theoretical curves (lines) for the sphere and the prolate spheroids of axis ratio $c/b = 2$ with major axis aligned perpendicular to the field are shown in **Figures 2a**. **Figure 2b** shows the results for the prolate spheroids of axis ratios $c/b = 2$ and $c/b = 5$ with major axes parallel to the field. In these figures, the models are assumed to be at the center of a rectangular coordinate system. The enhancement factors are shown for points on the model surface as a function of relative position in the z-direction, though (except for the end point) not on the z-axis itself. Even at the spheroid tips, which have small radii of curvature (a place field mills are not normally located), the experimental results presented in all the curves are in close agreement with theory.

Field-free measurements ($E = 0$) were taken on the prolate spheroid of axis ratio 5 raised to a potential of 1300 V by means of a suspending wire. Image charge problems were minimized by suspending the model about 1.5 m (5 ft) from any other object. As shown in **Figure 3**, the agreement between the measured and the theoretically calculated values is better in the lower half of the prolate and diminishes as points approach the wire. This is to be expected, since the wire, being of the same polarity as the model, causes like charge to migrate from proximal to distal regions on the suspended model. The perturbation effect observed is, of course, greater at points closer to the perturbation source, the wire. Nonetheless, the results indicate that, as long as the wire to the model is kept on the side opposite the points probed, the results (including systematic errors) are typically within 6%.

Figures 2 and 3 show that almost all the experimentally derived values are less (by about 6%) than the theoretical values, which indicates a small systematic error in the technique. A similar systematic error was reported by Rudolph et al. [4]. Even with this error, the agreement between the measured and the theoretical values of the enhancement factors, indicative of the absolute accuracy of this technique, is excellent.

LEARJET 36A MODEL MEASUREMENTS

A 1:36 scale model of a Learjet 36A was spray-painted with silver conductive paint. After testing the conductivity with an ohmmeter, the locations of the field mills were carefully marked. The model was suspended at the center of the electrostatic cage and aligned in turn to each of the three Cartesian coordinates defined by the cage axes. After determining the enhancement factors, a_{ix}, a_{iy}, and a_{iz}, the model was suspended in a field-free region and raised to a potential of 1300 V to obtain the a_{iv}.

Eight electric field mills were installed on a Learjet 36A at locations corresponding to the points probed on the scale model. The in-flight data from 18 deployments at Kennedy Space Center during August and September 1989 were used to check the laboratory-derived enhancement factors. The results from two of the many techniques that were used to verify the enhancement factors [3] are presented here.

a. Sphere and prolate spheroid (c/b = 2) with major axis perpendicular to field

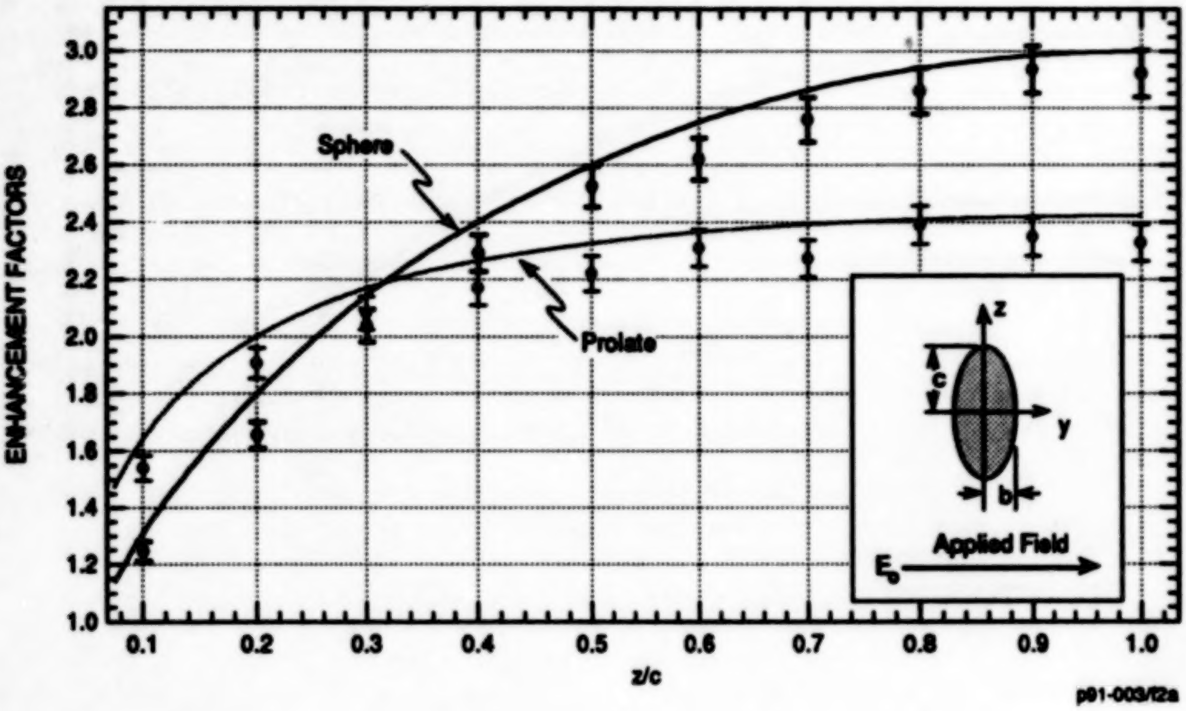

b. Prolate spheroids (c/b = 2, c/b = 5) with major axes parallel to field

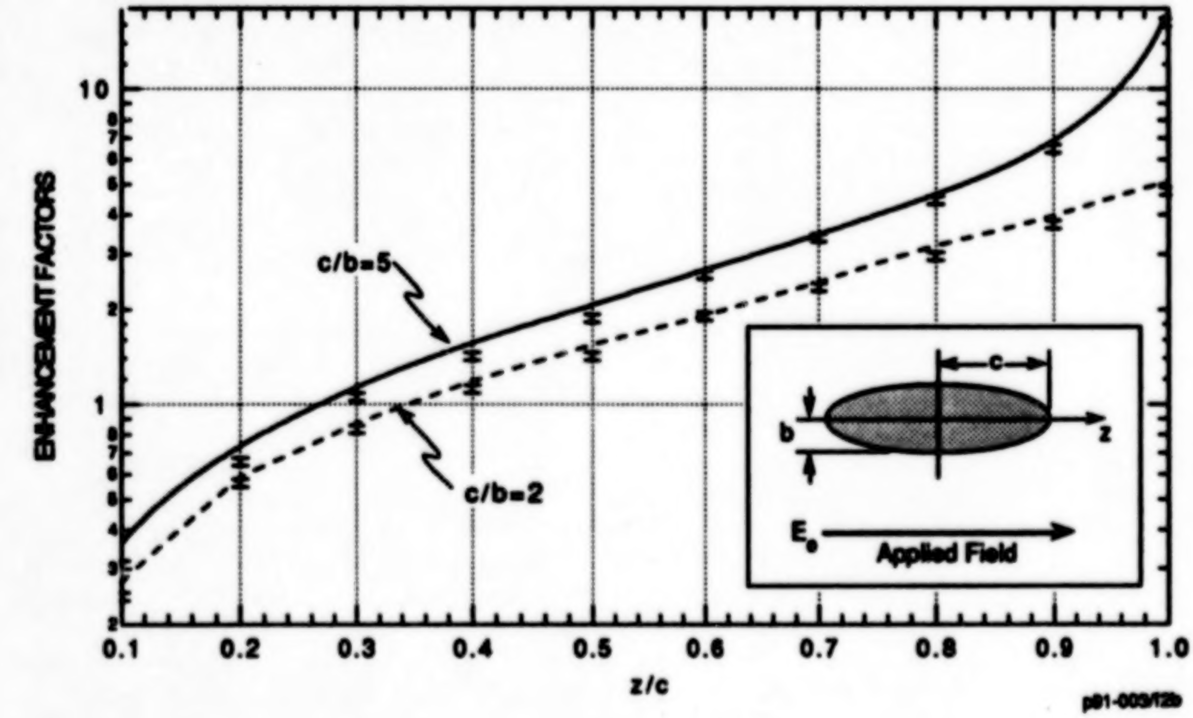

Figure 2 THEORETICAL CURVES AND EXPERIMENTAL DATA OF ENHANCEMENT FACTORS

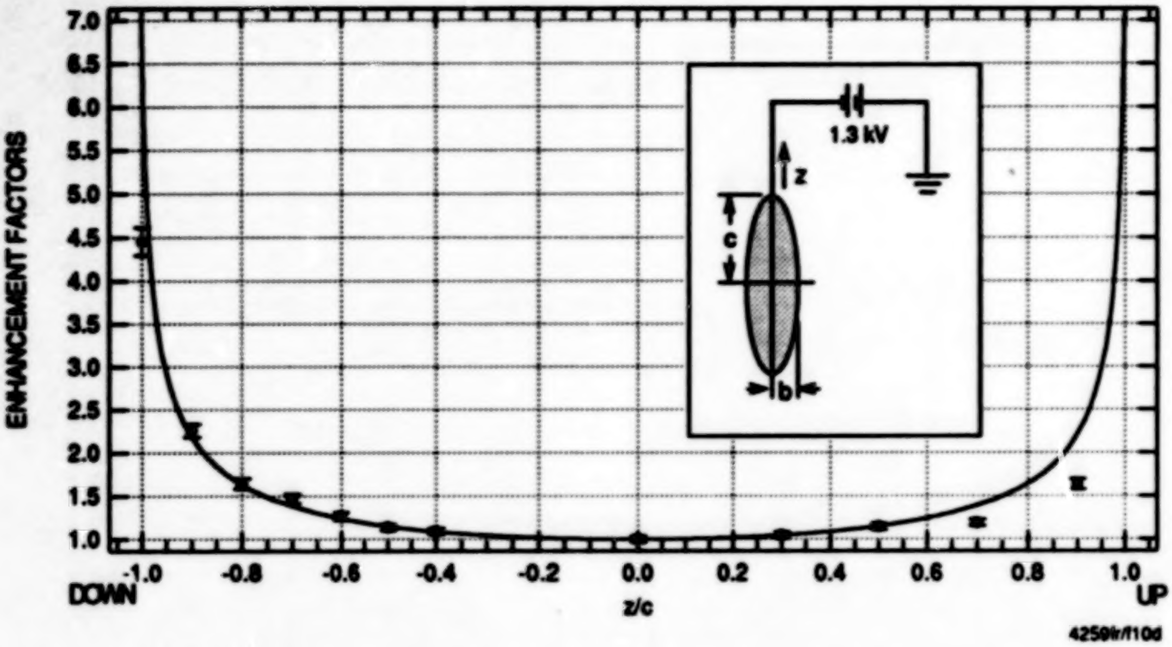

Figure 3 THEORETICAL CURVE AND EXPERIMENTAL DATA OF ENHANCEMENT FACTORS FOR A CHARGED PROLATE SPHEROID c / b = 5, SUSPENDED BY A WIRE IN A FIELD-FREE REGION

During fair weather (very low ambient field conditions), the aircraft was artificially charged to high potentials via a corona discharge point. The field-mill output data due to this self-charging were used to calculate the ratios of the electric potential enhancement factors, a_{iv}. The results from experiments performed on six different days show excellent agreement between the laboratory-measured and the in-flight-data-derived enhancement factors. Table I shows that the results are well within experimental error, with an average difference of only 1%.

Table I

COMPARISON OF LABORATORY AND IN-FLIGHT-DATA-DERIVED ENHANCEMENT FACTORS DURING ARTIFICIAL CHARGING EXPERIMENTS IN CLEAR AIR

Enhancement Factor Ratio	Laboratory-Derived Ratio	In-Flight Data-Derived Ratio	Difference
a_{1v}/a_{3v}	1.08 ±0.03	1.07 ±0.02	1%
a_{2v}/a_{3v}	1.01 ±0.03	1.01 ±0.03	0%
a_{4v}/a_{3v}	1.00 ±0.03	1.01 ±0.02	1%
a_{5v}/a_{3v}	0.62 ±0.02	0.61 ±0.01	2%
a_{6v}/a_{3v}	0.93 ±0.03	0.93 ±0.03	0%
a_{7v}/a_{3v}	0.62 ±0.02	0.62 ±0.02	0%

Data were collected during aircraft roll and pitch maneuvers during periods of strong vertical fields (at low altitudes over the ocean under a large thunderstorm system). These data were used to calculate several enhancement factor ratios, which are compared with the laboratory-derived enhancement factors in Tables II and III.

Table II

COMPARISON OF Z-COMPONENT ENHANCEMENT FACTORS FROM SCALE-MODEL CHARGE-TRANSFER MEASUREMENTS AND IN-FLIGHT DATA DURING ROLL MANEUVERS

Enhancement Factor Ratios	Charge-Transfer	In-Flight Data	Difference
a_{1z}/a_{3y}	1.47 ±0.03	1.73 ±0.17	18%
a_{2z}/a_{3y}	-1.47 ±0.03	-1.21 ±0.13	18%
a_{5z}/a_{3y}	1.16 ±0.03	1.13 ±0.10	3%
a_{6z}/a_{3y}	-1.37 ±0.03	-1.46 ±0.15	7%

Two pairs of ratios in Table II agree within one error bar, while the remaining two pairs of ratios agree to within two error bars. The agreement is not as good as it might be because uncertainties in the in-flight ratios were underestimated. These uncertainties were calculated while ignoring the errors introduced by the assumptions of a purely vertical field and perfectly performed maneuvers (i.e., roll maneuvers with zero pitch and vice versa). Even with these underestimated uncertainties (median of 10%) in the in-flight ratios, the ratios from the scale-model charge-transfer technique have even smaller computed uncertainties (median of 2%).

Table III

COMPARISON OF X-COMPONENT ENHANCEMENT FACTORS FROM SCALE-MODEL CHARGE-TRANSFER MEASUREMENTS AND IN-FLIGHT DATA DURING PITCH MANEUVERS

Enhancement Factor Ratios	Charge-Transfer	In-Flight Data	Difference
a_{1x}/a_{3x}	1.00 ±0.03	0.89 ±0.10	11%
a_{2x}/a_{3x}	0.93 ±0.03	0.81 ±0.12	13%
a_{4x}/a_{3x}	1.00 ±0.03	1.01 ±0.09	1%
a_{5x}/a_{3x}	-0.01 ±0.02	-0.27 ±0.15	-
a_{6x}/a_{3x}	-0.62 ±0.02	-0.37 ±0.08	40%
a_{7x}/a_{3x}	0.46 ±0.02	0.47 ±0.05	2%

Four of the six pairs of ratios in Table III agree within one error bar, and one pair agrees within two error bars. As in Table II, the uncertainties in the in-flight ratios (median of 19%) are underestimates, but still larger than the uncertainties in the ratios from the scale-model charge-transfer technique (median of 3%). The large percent standard deviations for the ratio a_{3z}/a_{3x} are due to the small absolute values of the ratios themselves. Because the percent standard deviations in this ratio themselves are so large, the percent difference is not a meaningful quantity and was omitted.

The uncertainties shown for the in-flight data potential ratios (Table I) are much smaller than the errors shown for ratios computed during maneuvers (Tables II and III). For several reasons, measurements made during aircraft maneuvers are inherently more difficult and less accurate. The uncertainties in enhancement factors calculated by the scale-model charge-transfer technique are generally several times smaller than the uncertainties in the in-flight data-derived enhancement factors.

SYSTEMATIC ERRORS

Although the scale-model charge-transfer technique is excellent for measuring enhancement factors, care must be taken in designing and performing the experiments. Many details, if overlooked, can lead to errors that substantially degrade the results. Some of these concerns are discussed below.

Contact potential errors can result from the use of dissimilar metals for the model, probe, and charge receptacle. To counteract contact potential effects, three strategies are simultaneously adopted: (a) The spots on the cage end-plate and the model that are to be probed are marked by copper tape to match the copper Faraday bucket of the electrometer; (b) the polarity of the field is reversed and the results averaged; and (c) the highest voltages possible (without producing corona) are selected to increase the induced charge on the model and thus decrease the ratio of contact potential effect to induced charge effect.

The electrically polarized model in the electrostatic cage will cause a redistribution of charge on the cage end plates. The resulting **image charging** will affect the magnitude and uniformity of the field within the cage. A given level of acceptable image charge perturbation constrains the size of the model that can be used in a given electrostatic cage. A detailed calculation of the image charge effect for our setup indicated a very small image charge effect (< 1%) on the field in the cage.

Probe perturbation errors result from the finite-sized spherical probe interacting with the model in the electric field. An analytic solution was found for the problem of two uncharged, touching conducting spheres of different radii in a uniform electric field [5]. This solution gives the correction factors by which the raw data need to be divided to account for probe perturbation on a sphere. These correction factors are can also be used to estimate the probe interaction with more complex shapes, as long as the probe is small and the point probed is convex. This is accomplished by estimating the "radius of curvature" of the model at the points probed. This method gives good results, since the correction terms are a weak function of the radius of curvature of the surface probed and, except for "sharp" spots on the model, typically range between 0.95 and 0.99.

CONCLUSIONS

When carefully performed with a small probe, the scale-model charge-transfer technique accurately determines enhancement factors. Comparisons with analytic solutions for spheres and prolate spheroids show the high accuracy of the charge-transfer technique for simple canonical shapes. Comparisons with the results from methods of determining and testing enhancement factors from in-flight data (more of which can be found in [3]), also demonstrate the high accuracy of this technique on complex bodies.

ACKNOWLEDGMENTS

Part of the work reported here was supported by the Air Force Space Systems Division under contract F04701-90-C-0023.

The authors would like to thank Major M. Jeane and Captain M. Johnson, as well as Dr. K. Moe, Major J. Bassi, Dr. S. Book, J. Brinkley and H. Heritage for their helpful input and management. R. Harris-Hobbs, L. Rose and many others at Aeromet, Inc. were indispensable partners in the Learjet experiments. K. Giori, R. Maffione, and P. Sechi were among the many people at SRI who have contributed heavily in the continuing work on electric field measurements aloft.

REFERENCES

1 J. C. Maxwell, *A Treatise on Electricity and Magnetism*, Vol. 1, Article 175, Dover Publications, Inc., New York, 1891.

2 R. A. Maffione, J. Kositsky, K. L. Giori, and J. S. Thayer, "Aerial Measurements of Electric Fields Aloft: Flight Report, System Calibration and Accuracy," Final Report, Project 4259, SRI International, Menlo Park, California, 1989.

3 J. Kositsky, K. L. Giori, R. A. Maffione, D. H. Cronin, and J. E. Nanevicz, "Airborne Field Mill (ABFM) System Calibration Report," Task A, Final Report, Project 1449, SRI International, Menlo Park, California, January 1991.

4 T. H. Rudolph, J. Horenbala, F. J. Eriksen, H. W. Weigel, J. R. Elliott, S. L. Parker, and R. A. Perala, "Interpretation of F106B and CV580 In-Flight Lightning Data nd Form Factor Determination," NASA Contractor Report 4250, Contract NAS1-17748, September 1989.

5 J. Latham and B. J. Mason, "Electrical Charging of Hail Pellets in a Polarizing Electric Field," Proc. Roy. Soc., London, A266, pp. 387-401, 1962.

Session 10A, Thursday 10:15
Lightning Phenomenology
Modeling 2
Willett, Chairman

The Electric Field Changes and UHF Radiations Caused by the Triggered Lightning in Japan

Zen-Ichiro KAWASAKI, Tadashi KANAO, Kenji MATSUURA
(Osaka University)

Minoru NAKANO, Kenji HORII
(Toyota College of Technology)

Koh-Ichi NAKAMURA
(Nagoya Institute of Technology)

1. Introduction

A rocket-triggered lightning experiment has a merit that it allows the direct measurement of a lightning current which is one of the important parameters for protection against lightning. It also has a merit that tests on a variety of electric and electronic equipment and arresters can be made by using actual lightning currents. Because of such merits rocket-triggered lightning experiments have been carried out actively in and out of Japan with significant results. Lightning parameters that have been given much attention in such experiments include, in addition to lightning current, the velocity of propagation of the lightning return stroke, lightning channel configuration , and corona currents; many parameters are directly related to lightning and are normally measured at a relatively short distance.

On the other hand, the lightning current and the associated electromagnetic field changes are theoretically related with each other by Maxwell's equations. Just like the cases of natural lightning, electromagnetic field changes are considered to be important indirect or remote sensing measurement parameters for rocket-triggered lightning. In addition to it, as exemplified by the success of SAFIR (1) by the ONERA group of France, the UHF radiation is one measurement parameter worthy of attention for the realization of an interferometeric system for the localization of lightning discharge position. In other words, the use of UHF radiation will allow us to know the state of propagation of lightning discharge with higher space and temporal resolutions(1). Furthermore it will enable us to quickly know the conditions just before the initiation of a lightning stroke. Thus the combination of observation of electric and magnetic fields that have been practiced extensively over many years and observation of UHF radiation has a high possibility of providing an effective measure of protecting an electric power system against lightning.

With such views in mind, we conducted rocket-triggered lightning experiments (at Okushishiku Kogen) in fiscal 1989, and measured the electromagnetic field changes and the UHF radiation intensity accompanying triggered lightning, by means of a slow antenna, a fast antenna, a loop antenna, and a discone antenna, at a base camp 2.5 km away from the rocket launching site. This paper presents the results of the observation, and discusses the rocket-triggered lightning from the view points of electromagnetic field changes and the UHF radiation.

2. Observation System

The observation system used in the rocket-triggered lightning experiments of fiscal 1989 will be outlined below, in two parts; the sensor block and the recording block, respectively.

(Sensor Block)

(a) Measurement of electric field changes at the ground level

To grasp the state of lightning discharge, the electric field changes were measured with two disc antennas. A disc antenna was a combination of an electrostatic antenna and an amplifier. The electrostatic antenna was a metal disc of several tens of centimeters in diameter placed horizontally at a level of several tens of centimeters above the ground. One disc antenna was the fast antenna with a time constant of 1 ms and a frequency band ranging from several hundreds Hz to 2 MHz, that was designed to cover rapid changes of electric fields associated with return strokes of lightning. The other disc antenna was the slow antenna with a time constant of 5 s and a frequency band ranging from 0.1 Hz to 1 kHz, that was designed to cover relatively slow changes of electric fields before and after a lightning discharge(2).

(b) Measurement of changes of magnetic fields

Magnetic field changes associated with lightning discharges were measured with a single loop antenna. This antenna output was also used as a trigger signal of the recording system (4 ch

1991 INTERNATIONAL AEROSPACE AND GROUND 7 OF 7
CONFERENCE ON LIGHTNING & STATIC ELECTRICITY 24X
NAS 1.55:3106/V.1 ... NASA CONFERENCE PUBLICATION 3106, VOL. I SUPTDOCS/GPO
... N.A.S.A. ... APRIL 16-19, 1991 P.0520-0601

digital memory) that will be explained later.

(c) Measurement of UHF radiation

UHF waves (327 MHz) radiated in the early stage of the discharge were measured by means of the discone antenna. We used the discone antenna (4) because it has the following merits:
(1) As the antenna has a wide band, it is convenient for selecting, during measurement, a frequency range with less background noises such as radio broadcasting waves;
(2) As the antenna is nondirectional, it is capable of receiving atmospherics from any direction; and
(3) It does not give corona discharge even in strong electric fields.

(Recording Block)

The outputs of the fast antenna, slow antenna, and discone antenna were recorded by a 4-ch digital memory unit (System 1) in which one word comprises 12 bits to have a wide dynamic range. The sampling frequency was 1 MHz, and the total capacity of the temporary storage was 64 kilowords for each channel, and the working record length was 64 milli-seconds. Measurement of electric field changes by means of the long-time waveform recorder described in reference (5) was also made simultaneously. Although detailed description is omitted here, the recorder is indicated as System 2 in this report. The configuration of the total system is shown in Fig. 1.

3. Electromagnetic Field Changes and Rocket-triggered Lightning

Rocket-triggered lightning is a method of triggering a lightning by launching a small rocket of about 20 cm in length, to which a steel wire of 0.2 mm in diameter is connected, under thundercloud. When the rocket ascends, an electric field is concentrated at the top end of the rocket, and a leader will initiate towards the thundercloud, and lightning will be triggered along this weakly ionized channel. In a rocket-triggered lightning experiment, two kinds of rocket-triggered lightning tests, rocket-triggered lightning to the ground, and rocket-triggered lightning to the tower, are normally made under different conditions. The rocket-triggered lightning to the ground is a system in which the wire connected to a rocket is extended to the ground. On the other hand, the rocket-triggered lightning to the tower means that the rocket itself is isolated to the ground. A nylon thread is paid out up to a height of about 100 m above the ground, and then from that point a steel wire is paid out. As the rocket assembly is insulated up to 100 m above the ground, a downward-moving leader can be initiated from the lower end of the wire to a power transmission tower of 60 m high(3),(8) .

The rocket-triggered lightning experiment of fiscal 1989 was conducted by using the test transmission line and a tower on the top of Mount Okushishiku (930 m above the sea) from November 6, 1989 to December 5, 1989. The observational results of the individual rocket-triggered lightning experiments are summarized in Table 1. Marks ○ × − denote successful collection of data, failure in data collection, and no observation, respectively. Examples of actual observed waveforms are shown below, one each for the lightning to the tower and the lightning to the ground. Ez and B of the diagrams indicate the vertical electric field strength on the ground and the interlinkage magnetic flux density, respectively. Their intensities are relative ones.

Fig. 2 shows waveforms of electromagnetic field changes for the experiment number 89-07 (rocket-triggered lightning to tower). Fig. 2-a shows of electric field change for a portion of 512 micro-seconds which is considered to correspond to the initiation of triggered lightning, out of the whole record length of 64 milli-seconds. Fig. 2-b shows magnetic field change for the same time period. Fig. 2-c shows electric field change triggered by this rocket-triggered lightning experiment for 262 milli-seconds; the data of the entire triggered-lightning experiment were recorded by the long-period waveform recorder. On the other hand, Fig. 3-a, b, c show the electromagnetic field changes of the portion corresponding to the initiation of the triggered lightning and the whole signature of lightning of the experiment number 89-11 (rocket-triggered lightning to ground). Although not shown here because of the limited space, all of the other results of observation were similar to those shown in Fig. 2 and Fig. 3. In the electromagnetic field changes of rocket-triggered lightning, we found no rapid changes corresponding to return stroke of natural lightning. Moreover, the relatively slow changes, as shown in the traces, were superimposed with impulse-like waveforms. The phenomenon of superimposing with many impulses was similar to the result obtained by Yoda et al.(7) for the direct measurement of lightning stroke current.

Next, we will compare the waveforms of the electromagnetic fields obtained in the rocket-triggered lightning to tower and those of the rocket-triggered lightning to ground to identify discrepancy between the two methods. In the case of rocket-triggered lightning to the tower, as shown in Fig. 2-a and b, a bipolar pulse of a relatively large amplitude is present in the portion corresponding to the initiation of triggered lightning. In contrast, as shown in Fig. 3-a and b, in the case of the rocket-triggered lightning to ground, there is no bipolar pulse with a relatively large amplitude at the initiation of triggered lightning, and the amplitude of the impulses tends to get larger gradually. Such differences of waveforms of electromagnetic fields between the two triggered-lightning methods were not confined to the particular cases shown above, but common to all of the results of observation during this experiment.

From the results of observation of the past rocket-triggered lightning experiments, it is known that, in the case of rocket-triggered lightning to tower, as the rocket and the wire connected to it are insulated from the ground, leaders of different polarities propagate upward from the lightning inducing point of the rocket and downward from the lower end of the wire, respectively, to eventually trigger a lightning, whereas, in the case of rocket-triggered lightning to ground, as the rocket is grounded by the wire, the leader propagates only upward from the lightning inducing point of the rocket.(8) The differences of the waveforms of electromagnetic fields at the initiation of triggered lightning between the triggered-lightning to tower and the triggered-lightning to ground and the presence of bipolar impulse of a large amplitude of the present results were attributed to the differences between the lightning triggering mechanisms of both the methods as described above. We are now examining the causes in detail.

4. Preceding UHF Pulses

In this section we will discuss the relationship between electromagnetic field changes during a rocket-triggered lightning and accompanying UHF electromagnetic radiation.

Fig. 4 shows magnetic field changes before and after the initiation of the triggered lightning of the experiment number 89-04 (triggered lightning to the tower) and the accompanying UHF electromagnetic radiation. As discussed in the preceding section, the magnetic field waveform has a bipolar pulse, which is a feature of the rocket-triggered lightning to the tower, at the initiation of the triggered lightning. On the other hand, as clearly shown by the diagram, the UHF electromagnetic radiation preceded the bipolar pulse of the changes of magnetic field corresponding to the initiation of the discharge. Pulses were isolated each other before the bipolar pulse, but after the bipolar pulse the radiation intensity increased suddenly and the state of radiation was like a burst. Such a sudden change of the UHF radiation intensity was similar to the states of UHF radiation before and after a return stroke of natural lightning shown in Fig. 5.

The burst-like change of UHF radiation of natural lightning is attributed to the net-shaped propagation of the return stroke in the cloud after it reaches the bottom of the cloud.(9) If the change of UHF radiation observed in rocket-triggered lightning were generated by the same cause with natural lightning, the isolated UHF pulses of Fig. 4 could be attributed to leaders moving upward from the rocket or leaders moving downward from the lower end of the wire. The mean time intervals of the isolated pulses of Fig. 4 is about 27 micro-seconds which is close to the statistical values ranging from 29 to 52 micro-seconds for time intervals of stepped leaders.(16)

The distributions of time intervals of isolated UHF pulses observed in the experiment numbers 89-04 and 89-7 (triggered lightning to the tower) are shown in Fig. 6. The transitions of time intervals of these pulses are shown in Fig. 7. The pulse number of Fig. 7 indicates the numbers given to the isolated pulses initiation from the first pulse. Thus Fig. 7 shows that the time interval between two consecutive pulses get shorter with the passage of time. This feature is similar to that observed in stepped leaders of natural lightning.(11)

We have described the magnetic field changes and UHF radiation of the rocket-triggered lightning to tower. Similar phenomena were observed in the rocket-triggered lightning to the ground although there were some differences. Fig. 8 shows the changes of magnetic field and UHF electromagnetic radiation of the experiment number 89-11 (rocket-triggered lightning to the ground). The UHF radiation showed isolated pulses preceding the first magnetic field change. The changes from isolated pulses to burst-like pulses, however, were not so rapid as those observed in the rocket-triggered lightning to the tower.

Some statistics of the UHF isolated pulses preceding the magnetic field changes observed during the rocket-triggered lightning to the tower and to the ground are shown in Table 2; the number of pulses, pulse intervals, and the time duration up to the changes of magnetic field. In the table the polarity indicates the polarity of the lightning stroke current measured at the launching point of the rocket.(12) For those to which this datum is not available, the polarity of the point corona current at the time of launching of the rocket is shown in parentheses.(13) When the number of pulses and the polarity of induced lightning were examined for the rocket-triggered lightning to tower according to the statistics, the positive rocket-triggered lightning tended to have smaller number of pulses than those of negative polarity. On the other hand, in cases of the rocket-triggered lightning to the ground, the relationship between the number of pulses and the polarity was not as clear as that of the rocket-triggered lightning to tower. When we examined the number of pulses and the time duration from rocket launching to triggering (13), the lightning, both to the tower and to the ground, having longer time duration up to triggering tended to have a greater number of pulses.

5. Concluding Remarks

In the rocket-triggered lightning experiment of fiscal 1989, we observed electromagnetic field changes and UHF electromagnetic radiation accompanying rocket-triggered lightning. The findings were as follows:

(1) No rapid changes corresponding to the return stroke of natural lightning were observed in the electric field changes accompanying rocket-triggered lightning. Continuous currents, however, were present.

(2) In the case of the rocket-triggered lightning to the tower, in electromagnetic field changes corresponding to the initiation of triggered lightning showed a bipolar pulse of a relatively large amplitude. In contrast, the rocket triggered lightning to the ground did not have such a bipolar pulse.

(3) The UHF radiation accompanying the rocket-triggered lightning preceded the waveform portions corresponding to the first changes in electromagnetic fields. In particular, in the case of the rocket-triggered lighting to the tower, the UHF radiation showed a change from isolated pulses to burst-like pulses of larger amplitude across a bipolar pulse of a relatively large amplitude in magnetic field.

(4) The number of isolated pulses in the UHF radiation showed a

correlation with the time duration from rocket launching up to triggered lightning. The time interval between consecutive isolated pulses tended to get shorter with the passage of time just like the stepped leaders of natural lightning.

Physical interpretation of the above-mentioned features of the rocket-triggered lightning of the present experiment is a future task, and is expected to contribute much to the understanding of winter lightning of Japan.

To be more specific, the feature of (1) above differs from that of the electric field changes observed in the rocket-triggered lightning experiment at the U.S. Kennedy Space Center indicated in reference (14) in that the changes in electric field of the latter showed a rapid change corresponding to return stroke. The difference is attributed to that our experiment was conducted in a mountainous area while the U.S. experiment was conducted in a place of the sea level. In other words, their experimental condition was close to an ordinary lightning stroke with the bottom of the cloud being fairly high above the ground, whereas our experiment was made in the thundercloud, and the triggering conditions were similar to those of intracloud discharge. It should be noted that the transmission towers erected in the mountainous areas of Hokuriku District tend to be covered by thunderclouds in winter. As their environment is comparative to that of our experiment, the result of our experiment discussed in Section 3 or relatively slow changes overlapped by many pulses is attributed to propagation of negative leaders from the top of the rocket to the interior of the cloud. This, in turn, is expected to be of some help in understanding the mechanism of the "triggered lightning" that is started by an upward-moving leader from a transmission tower.

One possible cause of (2) may reflection of current. It, however, is difficult to make a conclusion on the basis of the present experiment alone. Nevertheless, as clearly shown in reference (15), the results of our measurement and the results of the direct measurement of current conducted by the Chubu Electric Power Co., Inc. agree well with each other. This agreement suggests our method of observation can be applied to lightning strokes to transmission towers to which the direct measurement is not applicable.

With regard to (3) and (4), it is indicated in reference (1) as well as in reference (16) that VHF radiation waves are used in the interferometoric system to understand the discharge inception mechanism; nevertheless, such research efforts are not present at all in Japan. We will try to utilize our results in development of techniques for measuring inside thunderclouds by means of UHF or VHF.

To the best of our knowledge, the significant difference between the discharge inception portion of the rocket-triggered lightning to the ground and that of the rocket-triggered lightning to the tower have not been reported up to now. This may provide, if we repeat experiments and continue theoretical investigation, a clue to the discovery of the "discharge inception mechanism." Furthermore, the UHF isolated pulses preceding to the discharge inception portion suggest a possibility of prediction of lightning stroke although the time allowance is very short. It will mark a step forward towards the ultimate objective of elimination of lightning.

We would like to acknowledge that this research received a scientific research grant from the Ministry of Education (Experimental Research Program No. 63850055).

References

(1)P. Richard and G. Auffray :" VHF-UHF interferometric measurements application to lightning discharge mapping". Radio Science, Vol.20, No.2, PP.171-192 (March-April 1985)

(2)Edited by Lightning Observation Committee of IEE Japan :" On the recent research of lightning physics", Technical Report of IEE Japan No.278, PP.41-43, (Aug. 1988)

(3)ditto , P. 49

(4)Edited by Radio Telecommunication committee of IECE Japan :" Handbook on Radio Telecommunication Engineering", OHM Press, Tokyo, PP.17-21,(1964)

(5)Z-I. Kawasaki et al.,:"Design of the transient memory of extremely large size for electric field changes due to the lightning discharge and observation results during summer and winter thunderstorms", Trans. IEE. Japan (B), Vol. 111, in printing (May 1991)

(6)A. Wada and K. Horii :" Discussion on the rocket triggered lightning experiment during winter in Japan", Technical Report of IEE Japan HV89-78 (Oct. 1989)

(7)M. Yoda et al., :" On the direct lightning current measurement during rocket triggered lightning experiment", Annual meting of IEE Japan, 1133, (April 1990)

(8)S. Sumi et al., :" Observation of rocket triggered lightning to the power transmission tower by a streak camera", Technical Report of IEE Japan HV88-63 (Oct. 1988)

(9)T. Shirai et al., :" On the measurement of UHF-VHF radiations and Electric field change caused by lighting return stroke", Technical Report of IEE Japan HV88-63 (Oct. 1988)

(10)M. Uman :" The Lightning Discharge", Academic Press, New York, P. 84 (1985)

(11)ditto, PP.34-85

(12)A. Wada et al., :"On the triggered lightning by a two stage rocket and the current measurement in the space", Annual meeting of IEE Japan, 1138, (April 1990)

(13)K. Horii et al.,:" On the Rocket Triggered Lightning Experiment during winter in Japan in 1989", Annual meeting of IEE Japan, 1140, (April 1990)

(14)J. C. Willet et al., :"Submicro second intercomparison of radiation fields and currents in triggered lightning return strokes based on the transmission line model", J. Geophys. Res., 94, D11, PP. 13275-13286, (Oct. 1989)

(15)T. Katuragi et al., :" On the relation between the rocket triggered lightning current and the magnetic fields", Technical Report of IEE Japan HV90-23, (Oct. 1990)

(16)C. Rhodes et al., :" Interferometric observations of a single stroke cloud-to-ground flash", Geophys. Res. Lett., 16, 10, PP. 1169-1172 (1989)

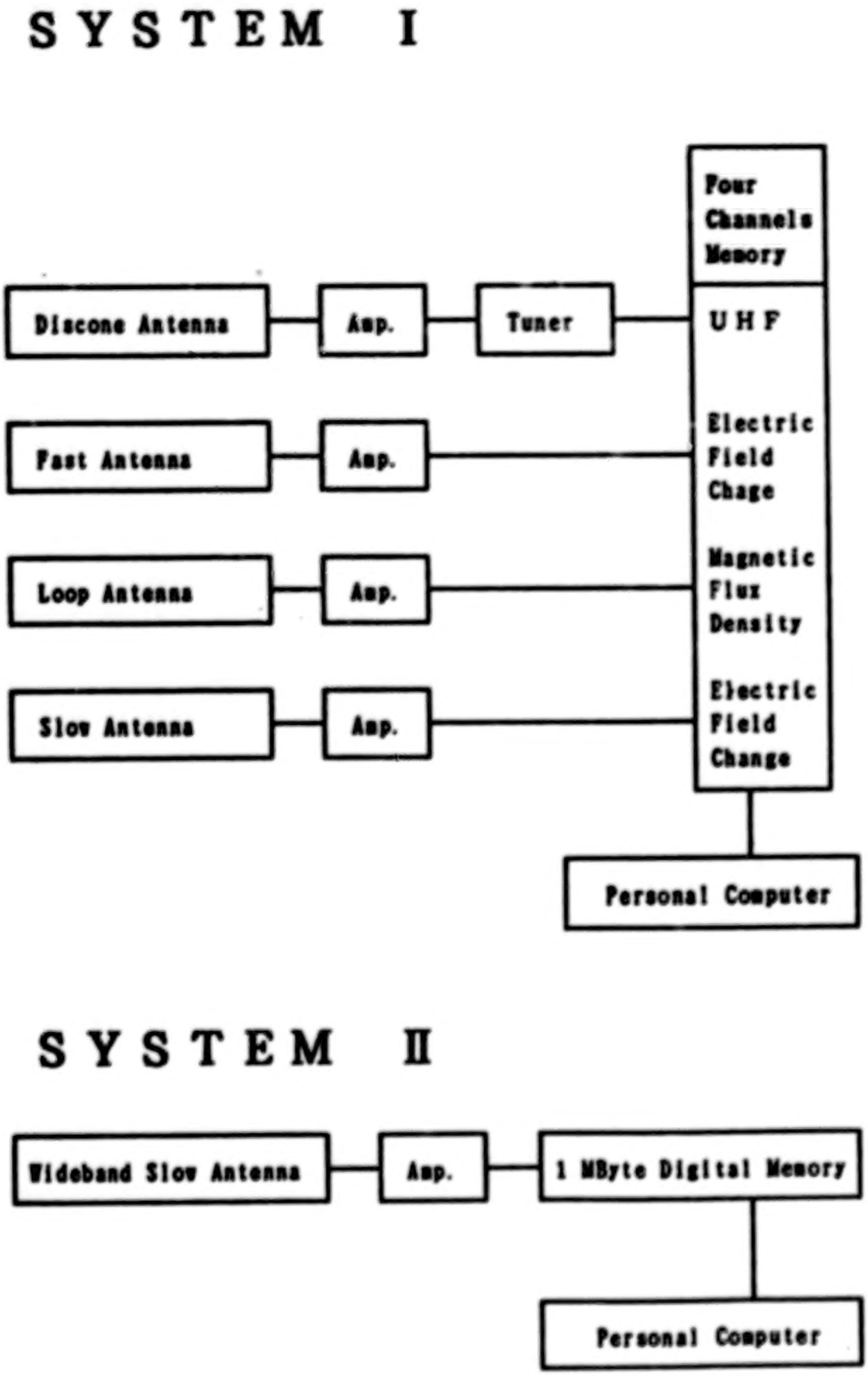
SYSTEM I

SYSTEM II

Four Channels Memory
Discone Antenna
Amp.
Tuner
UHF
Fast Antenna
Amp.
Electric Field Chage
Loop Antenna
Amp.
Magnetic Flux Density
Slow Antenna
Amp.
Electric Field Change
Personal Computer
Wideband Slow Antenna
Amp.
1 MByte Digital Memory
Personal Computer

Fig. 1 A schematic of the observation system

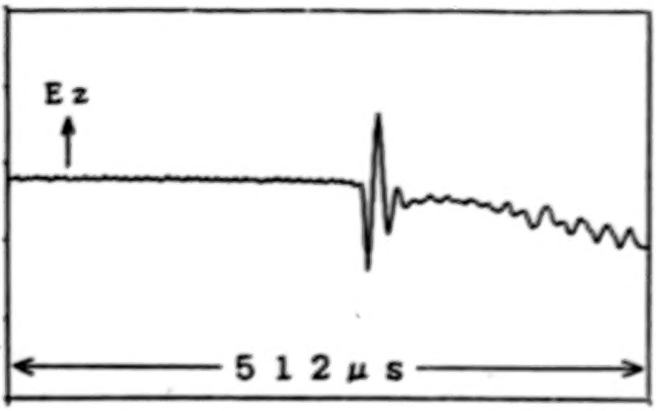

Fig. 2-a The initiation of an electric field change caused by the rocket triggered lightning to the power transmission tower

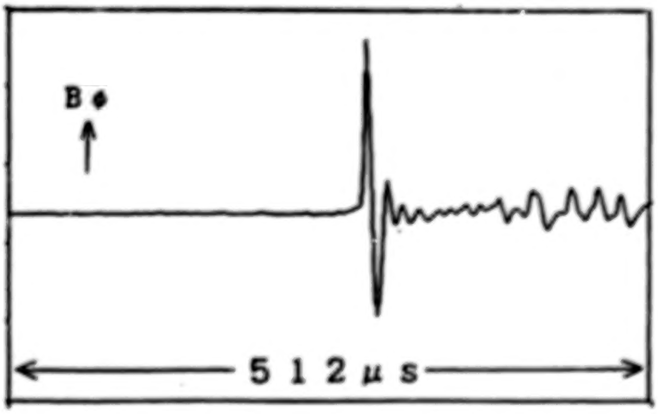

Fig. 2-b The initiation of a magnetic field change caused by the rocket triggered lightning to the power transmission tower

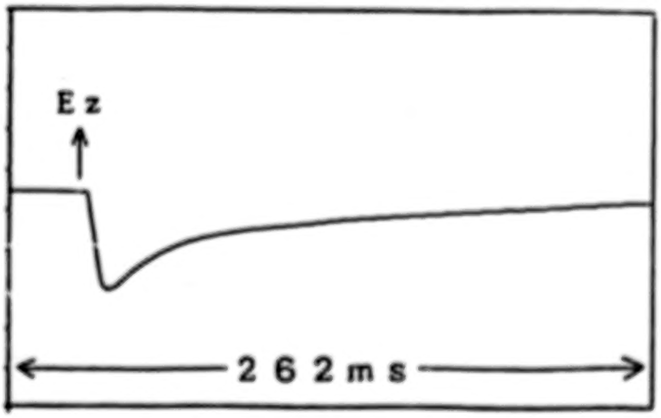

Fig. 2-c The whole signature of an electric field change caused by the rocket triggered lightning to the power transmission tower

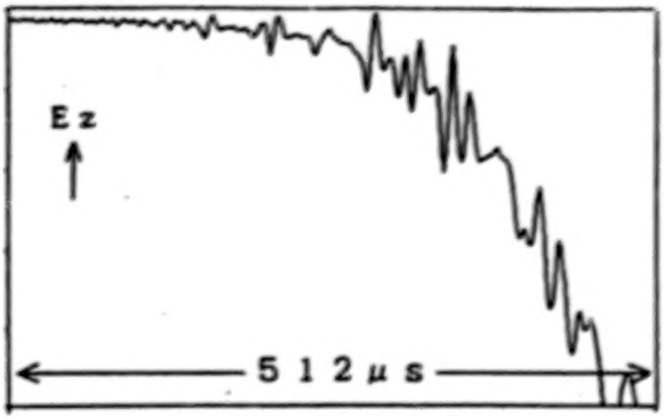

Fig. 3-a The initiation of an electric field change caused by the rocket triggered lightning to the ground

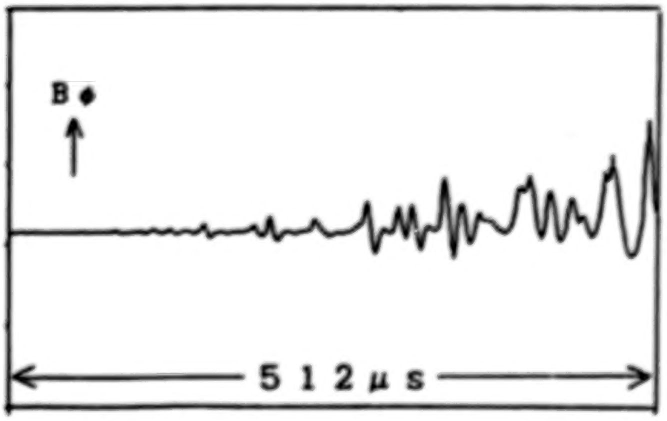

Fig. 3-b The initiation of a magnetic field change caused by the rocket triggered lightning to the ground

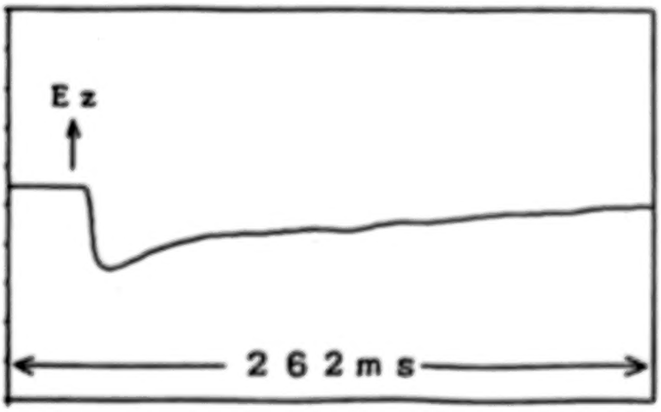

Fig 3-c The whole signature of an electric field change caused by the rocket triggered lightning to the ground

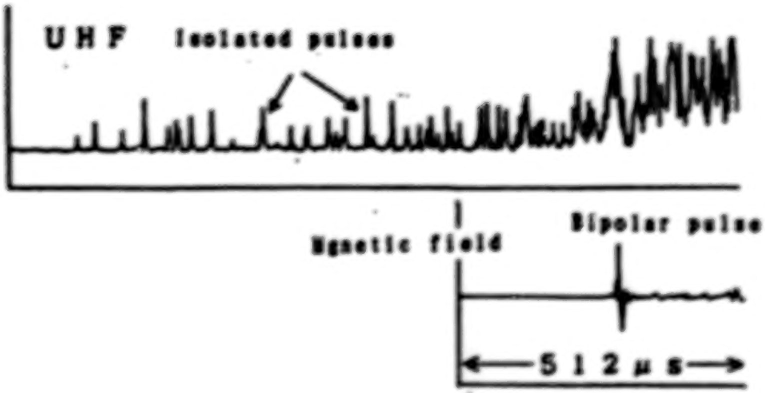

Fig. 4 The preceding UHF isolated pulses of the rocket triggered lightning to the power transmission tower

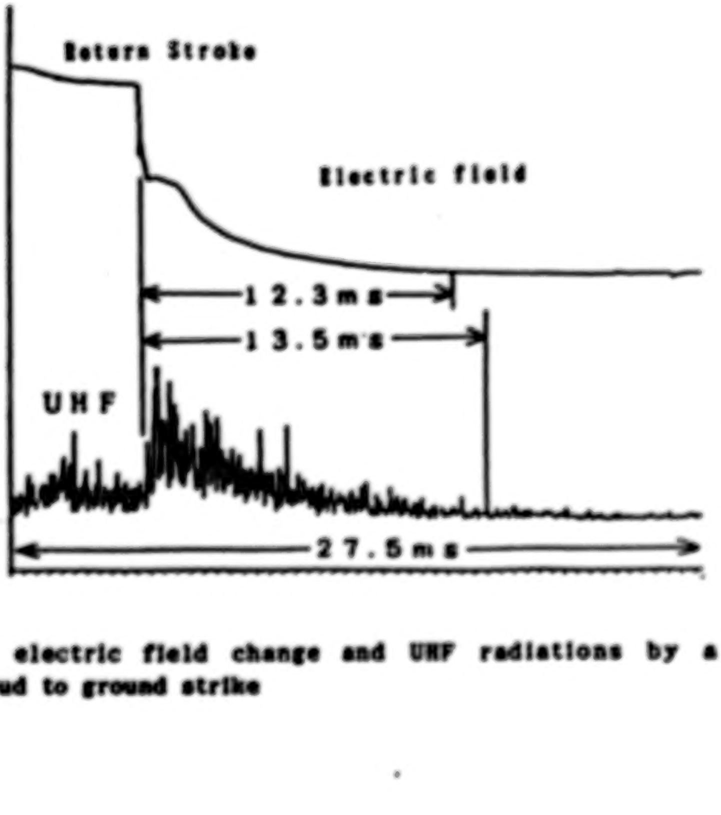

Fig. 5 The electric field change and UHF radiations by a natural positive cloud to ground strike

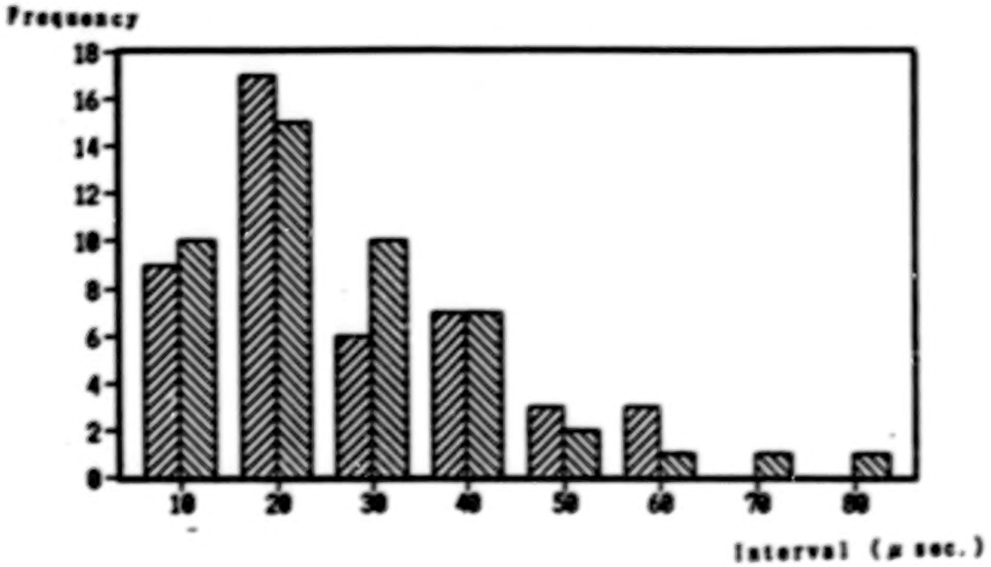

Fig. 6 The statistics of time intervals for UHF isolated pulses preceding the triggered lightning to the power transmission tower

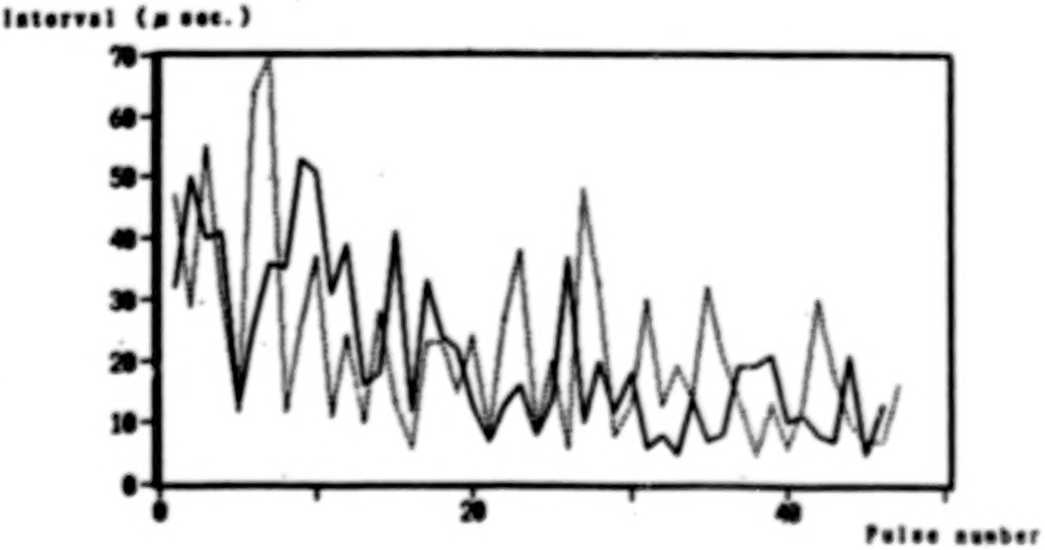

Fig. 7 The transitions of time intervals for UHF isolated pulses preceding the triggered lightning to the power transmission tower

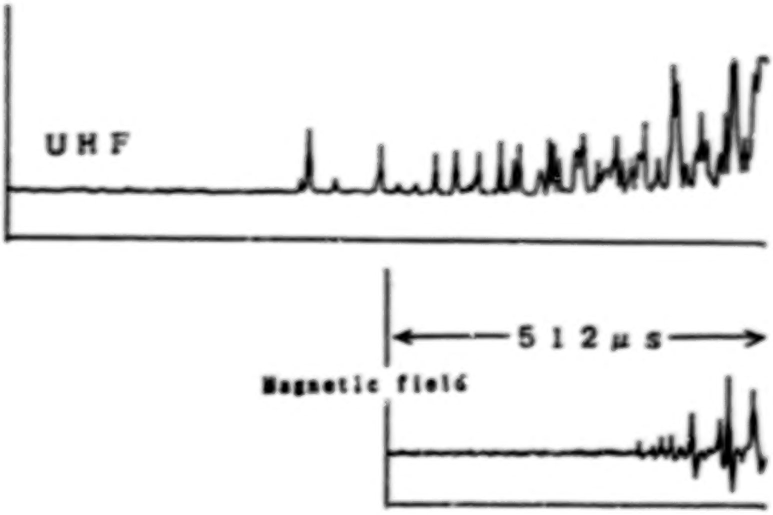

Fig. 8 The preceding UHF isolated pulses of the rocket triggered lightning to the ground

Table 1 The results of the measurement during the rocket triggered lightning experiment

Rocket No.	SYSTEM I				SYSTEM II
	UHF	FAST	SLOW	LOOP	WIDEBAND SLOW
89-04	○	○	○	○	○
89-05	○	○	○	○	○
89-06	○	○	○	○	○
89-07	○	○	○	○	○
89-08	○	○	○	○	○
89-09	○	○	○	○	×
89-10	○	○	○	○	○
89-11	○	○	○	○	○
89-12	○	–	–	○	×
89-13	–	–	–	–	–
89-14	○	–	–	○	○
89-15	–	–	–	–	–
89-16	○	–	–	○	○
89-17	○	–	–	○	○
89-18	○	–	–	○	○
89-19	×	×	×	×	×
89-20	×	×	×	×	×
89-21	×	×	×	×	○
89-22	○	–	–	○	○

○ denotes data can be recorded.
× denotes no data can be recorded.
– denotes no measurement.

Table 2 The statistics of the UHF isolated pulses of the rocket triggered lightning

	Rocket No.	Frequency of pulses	Pulse intervals AV. & SD. (μ sec.)		Durations (μ sec.)	Pola-rity
Tower	89-04	46	21.2	13.8	951	−
	89-05	63	26.7	39.8	1695	
	89-07	47	22.1	15.2	1036	
	89-09	8	28.1	10.0	221	
	89-10	10	29.2	34.5	197	
	89-16	34	31.6	20.8	1075	−
Ground	89-06	13	41.5	61.8	557	−
	89-11	17	22.1	13.3	385	−
	89-14	2	312		312	
	89-18	0				+
	89-22	1			53	−

THE DETECTION OF THE ELECTRIC FIELD VERTICAL DISTRIBUTION UNDERNEATH THUNDERCLOUD : PRINCIPLE AND APPLICATIONS

Serge Soula and Serge Chauzy

Laboratoire d'Aérologie, Toulouse, France

ABSTRACT

During the Florida 89 experiment at Kennedy Space Center a new system was used in order to obtain the vertical distribution of the electric field underneath thunderstorm. It consists of a standard shutter field mill at ground level and five other field sensors suspended from a cable fastened to a tethered balloon located at the altitude of about 1,000 m. It also includes a reception station for telemetered information transmitted by the sensors in altitude and a processing system in order to store data and real time display on a screen the simultaneous field variations at each level and the instantaneous electric field profile. The first results obtained show the great importance of the knowledge of the electric field vertical distribution. The field detected at a height of 600 m reaches 65 kV/m while that at the surface does not exceed 5 kV/m. The field intensity in altitude is a better criterion in determining the right moment to launch a rocket devoted to flash triggering. Using Gauss's law the simultaneous field variations at several levels are used in order to evaluate charge densities. Average values close to 1 nC.m^{-3} are calculated in layers up to 600 meters. The calculation of different average charge densities leads to characterize the layer between cloud and ground just before the leader propagation in the case of a cloud-to-ground flash.

1. INTRODUCTION

The electric field largely varies with altitude below a thundercloud. It has been suggested by Wilson [1] that the field increases with altitude because of corona ions produced at the surface. Field measurements above ground using free balloons [2 and 3], tethered balloons [4] and insulating cables [5] show a greater intensity (and sometimes even of opposite polarity) than at the surface. At ground level the field intensity is larger also above water which leads to conclude that the charge layer created by ground coronae has a great influence on the surface electric field [6, 4, 2 and 5]. The only way to detect evaluate and avoid this influence is to measure the field intensity above and across this layer.

On one hand, the vertical electric field distribution provides a good information on the evolution of corona ions from the ground. According to Vonnegut [6], these ions carried up by convective currents can markedly participate in cloud electrification. Unfortunately, no measuring system has been run yet in order to continuously detect the electric field within the first hundreds of meters. On the other hand, the rapid variations of the instantaneous electric field profile are a very useful element for the interpretation of the characteristics of the leader propagation, like channel geometry, velocity. As a matter of fact, Idone and Orville [7] reported a speed increase and a reduction of the channel tortuosity with height for the upward leader and they suggested that this observation might be related to larger fields in altitude.

Furthermore, since the surface field intensity alone is not always the best instantaneous indicator of cloud electrification [5], a permanent monitoring of the vertical field profile brings a helpful contribution for the purpose of lightning flash warning and triggering.

In order to help to solve these problems we have developed a system conceived to measure the electric field at the surface and at five levels above it. The sensors aloft are designed to be suspended from a tethered balloon and to transmit the data by telemetry. The whole system has been built to be used during the Florida 89 experiment at Kennedy Space Center. It can display in real time the six superimposed field variations renewed every minute and the vertical field profile renewed every second.

Some of the results obtained from the Florida 89 experiment on August 10 1989 are reported in this paper. In the late afternoon of August 10 a thunderstorm was advected from the West and developed over the site propagating easterly. Due to the long duration of the event, the lifetime of sensors batteries did not allow us to record data during the whole thunderstorm. During this event several lightning flashes were triggered by rockets from the ground and from the Lightning Strike Object (L. S. O., described in the next section) located 150 m above ground. The electric field data processing leads to a satisfactory description of the charge layer evolution during the thunderstorm lifecycle and up to 600 m. The electric field is considered positive in the layer above ground when it is created by a negatively charged cloud.

2. THE MEASUREMENT SYSTEM

2.1 THE SYSTEM CONFIGURATION

The tethered balloon where the sensors were suspended during the Florida 89 experiment was carried out by the American company L. T. A. (Ligher Than Air) of Florida. This stream-lined 570-m^3 helium balloon is maintained in a convenient orientation in relation to the wind even when it lies on a mooring system at the ground. The figure 1 shows the whole system in the exact configuration of the experiment mentioned before. It is important to note that in this display the scale is respected for the distances between each element but not for their size. The main tether is exclusively used to sustain the balloon. A kevlar tripod, made of three tethers attached to the ground, is hung up on the balloon by a secondary cable. At the top of the tripod, 160 m high, a metal cylinder is suspended, the L. S. O. (Lightning Strike Object), designed to be hit by triggered lightning flashes. The sensors devoted to electric field measurement aloft are hooked up on the secondary tether between ground level and the maximum height, roughly 200 m below the altitude of the balloon, so the latter does not influence the upper sensor.

2.2 THE ELECTRIC FIELD SENSORS

The instruments used to detect the local electric field are displayed on figure 2. A standard shutter field mill, flush with the ground, measures the surface field. It delivers a 1000-Hz voltage whose amplitude is modulated by the electric field. A fast amplitude detection provides a DC voltage proportional to the field. An in situ calibration is performed to relate the output voltage to the applied electric field, by using an electrode parallel to the instrument ground plane and connected to a high voltage generator.

The other sensors shown on figure 2 are devoted to ambient electric field measurement in altitude. The requirements taken into account for a correct design are of several types: (1) Self-contained unit working by telemetry, (2) Shape producing a local field enhancement as weak as possible, (3) Compensation system for the electric field created by the net charge on the apparatus.

__The geometry and general configuration:__ According to various authors and specially Clarke [8], Rust and Moore [9], Few et al. [10], the instrument housing is made to be close to a conductive sphere in order to obtain the most uniform curvature possible and to minimize the emission of space charge. Thus the conducting sphere, 0.25 m in diameter, contains the whole system assembly: electronic circuits, rotation motor, batteries. On the other hand, since it has been decided to measure only the vertical component of the electric field, a double field mill configuration is adopted (fig. 3). Thus two identical field mills are symmetrically located at the top and the bottom of the sphere with a common rotation axle driven by a small electric motor. As it has been previously described [2], the combination of the signals provided by the two field mills achieves the elimination of the field component created by the net charge on the instrument. The principle of this elimination is schematized on figure 3. The vertical component of the ambient field creates, at the top and the bottom of the spherical sensor, equally enhanced fields of the same polarity, E_a. On the other hand, the net charge on the instrument generates, at the same places, fields of opposite polarity whose common intensity is E_n. So the upper field mill measures $E_n + E_a$, while the lower one measures $E_n - E_a$. Making the difference between the signals delivered by both mills eliminates E_n. This procedure is achieved by the electronic circuit and requires the adjustment of the amplification during calibration.

Rotors and stators of each field mill are divided into ten sectors, which provides a signal frequency (500 Hz) equal to ten times the rotation frequency (50 Hz). The transmission antenna is a dipole, made of the two half-spheres that constitute the sensor housing. The sphere is mechanically coupled to the suspension system of the tether using a Cardan coupling device that provides two degrees of freedom and the weight balance of the whole instrument keeps it in the vertical position.

__The electronic circuitry:__ The modulation circuit is designed to provide an AC voltage whose frequency is modulated by the electric field signal. This voltage itself modulates in frequency a commercial transmitter built by C.E.A.F. (Construction Electronique André Fortier), whose frequency is crystal stabilized between 400 MHz and 406 MHz and power limited to 50 mW.

The modulation block diagram is indicated on figure 4. It uses a synchronous detection device whose reference signal is provided by a Light Emitting Diode/Photo Transistor system coupled with a rotating screen identical to and synchronous with the field mill rotors. Each field mill is associated with an independant circuit, both signals being combined at the end of the processing. As Winn and Moore [11] did with their instrumented rocket, we use first, in both circuit associated to each field mill, a charge amplifier that provides an output voltage proportional to the induced charge on the electrode. After DC elimination and variable gain amplification, a double fast peak detector samples both positive and negative peaks. After summing, the signal is applied to a double sample hold circuit triggered by the reference signal for synchronous detection. A difference amplifier finally provides the peak to peak value proportional to the electric field, including its polarity. This final signal is combined, in a difference amplifier, with that provided by the circuit originated from the other field mill, in order to eliminate the field component created by the net charge on the apparatus. The output voltage, proportional to the ambient field, is converted into frequency, thanks to a V.C.O. (Voltage Controlled Oscillator) whose output signal modulates the FM transmitter already mentioned. The V.C.O. central frequency is 15 kHz and the corresponding bandwith 10 kHz. Three different sensitivities have been chosen for each sensor: +/- 150 kV/m, +/- 100 kV/m and +/- 50 kV/m. The calibration of each sensor in real conditions (telemetry) is performed at the laboratory.

2.3 THE RECEPTION SYSTEM

The ground station (fig. 5) is designed to receive five simultaneous channels transmitting within the frequency range: 400-406 MHz. The directional antenna is connected to a wideband UHF preamplifier. It is followed by a frequency converter whose local oscillator frequency is such that the output signals frequencies fall within the range of a commercial FM tuner. Each of the five tuners whose input are connected in parallel, delivers a frequency modulated signal corresponding to a given altitude. A P.L.L. (Phase Locked Loop) restores the voltage proportional to the electric field detected by each sensor. Finally the reception system provides five simultaneous field variations with a response time of about 2 ms. The surface field evolution detected by the standard field mill located by the ground station is digitized in the processing system along with the variations aloft: its response time is 1 ms. The six simultaneous evolutions are numerically processed in order to provide clear and simple real time display as well as delayed treatments. In parallel with the numerical data processing, an analog tape recorder is used to record the multilevel simultaneous field data at 1 ms time resolution. This analog recording carries out the storage of the data at the shortest time resolution of the sensors, while the digitizer and numerical data processing is performed with a 10-ms time resolution.

2.4 THE DATA PROCESSING

The whole numerical processing is performed using a Hewlett-Packard 1000/A600 minicomputer and a Vectra ES Hewlett-Packard microcomputer in the terminal configuration. The system digitizes the six channels data with a 12-bit resolution and a rate of 100 samples per second and achieves two kinds of procedures renewed every second: a real time display and a relevant storage (53 Megabytes hard disk capacity) for subsequent utilization.

The real time procedure consists in fact in displaying the six values of the field intensity at a reduced rate of one instantaneous value per second, at the end of each acquisition sequence. This is performed on the color screen of the Vectra microcomputer and presented under three different formats (fig. 6): (1) instantaneous numerical values of the field at all levels (upper left), (2) simultaneous time evolution of multilevel field intensities (lower left), (3) profile evolution (right). These three different modes of representation provide complementary information about the electric field distribution within the first hundreds of meters, about the structure of the charge layer above ground and about the electric field evolution at each level.

3. EXAMPLES OF APPLICATIONS

3.1 LIGHTNING FLASH TRIGGERING

In agreement with previous results, it has been observed during Florida 89 experiment that the electric field is usually much higher in altitude than at the ground. Figure 7 shows the simultaneous variations of the electric field at ground level and at 603 m recorded during the thunderstorm of August 10 between 23:30 and 00:30 (Universal Time). During this event the electric field was measured at several levels up to 603 m. After the balloon rising the electrical activity was detected on the site at about 23:00. The recording presented on figure 7 stops at 00:30 when the last sensor stopped functioning (because of normal power supply failure), but the thunderstorm activity was not finished. Both available field variations undergo discontinuities corresponding to several lightning flashes, five of them being triggered by rockets (23:47, 23:53, 23:58, 00:04 and 00:30). The sign convention corresponds to a positive intensity when the field vector is upward. The observation of such a graph calls for some remarks:

(i) The field intensity detected at 603 m is always positive whereas the one measured at the ground can reverse after a lightning flash.

(ii) The surface field intensity does not exceed about 5 kV/m while that at 603 m reaches 65 kV/m (23:58). This large difference is the result of stabilizations of the surface field intensity for a few minutes during which the field continues to increase at 603 m.

(iii) When the surface field intensity reaches large values after a lightning flash it decreases very quickly. Generally after the same discontinuities the field at 603 m does not undergo this sort of decrease, its intensity varies little during the minute following the lightning flash responsible for the discontinuity. Many examples illustrate this observation: each triggered flash and some natural flashes at 23:34, 23:46, 23:52 and 00:09.

(iv) The field discontinuities corresponding to lightning flashes are larger in altitude specially when the intensity of the field at ground level becomes important.

All these remarks can be interpreted in terms of corona ions production at ground level. During the development of the thunderstorm activity, these ions progressively build up a charge layer that keeps the surface field from reaching high intensities. Consequently, its value is no longer directly related to the thunderstorm activity. For example at the beginning of this recording, at 23:30, the field intensity is close to 2 kV/m at ground level and reaches 15 kV/m at 603 m. At this moment the difference between the two levels can be attributed to corona ions previously released. At the end of this recording, just before 00:30, the difference is much larger, since the field intensity is again close to 2 kV/m at the surface, whereas it exceeds 50 kV/m at 603 m. As a matter of fact, the field intensity measured at ground level is the sum of two components, one related to cloud charges and the other due to the whole charge layer between the ground and the cloud [4 and 5]. The value of this intensity is generally used in order to evaluate the proximity of the thunderstorm or its development stage. In the case of lightning flash triggering for example the surface field intensity is considered as the criterion to launch a rocket [12]. According to figure 7 the fifth flash (00:30) was triggered with a surface field intensity very close to 2 kV/m. However the one detected at 603 m reached 50 kV/m which means good conditions to produce a flash. This case shows that a flash can be triggered even if the field is low at ground level. We can suppose that a triggering could be successfully attempted with a surface field intensity close to zero or even slightly negative. Such conditions appear on the variation of figure 7 at 00:07, 00:14 and 00:19. At such moments there is a discrepancy between the surface field intensity and the real thunderstorm electrification better accounted for by the altitude electric field. The detection of the electric field at several hundreds of meters above ground is therefore helpful for lightning flash triggering. Until now, thanks to the good experience of specialists, the success rate in lightning flash triggering reaches the satisfactory value of 70 % (percentage of technically successful launches that trigger lightning) [12]. However with the new information constituted by the field values aloft more numerous favorable occasions could be considered specially at the end of thunderstorms when the surface field component due to the charge layer is important. As a matter of fact the number of flashes triggered during a thunderstorm could probably be greater.

3.2 VERTICAL ELECTRIC FIELD DISTRIBUTION

The measurement system provides electric field variations during a thunderstorm at six levels including the ground. The data obtained can be displayed in two different ways, in terms of simultaneous electric field variations at several levels or in terms of evolution of the electric field profile. In the present paper we choose to point out the second aspect, the first one needing a more extensive development and the display of several graphs in order to provide reasonable legibility and clearness.

The vertical electric field profile is therefore available at any instant during the thunderstorm. It permits to clearly visualize the vertical electric field distribution. It is a way to characterize the electrical conditions of the medium where the lightning leader propagates. The time resolution of these profiles corresponds to that of our sensors i. e. 2 ms. Consequently it is possible to study the evolution of the profile at any time resolution larger than 2 ms. This kind of study will be interesting to develop during a very brief phenomenon like a lightning flash. Figure 8 displays an example of field profile evolution corresponding to a natural flash during the thunderstorm of August 10. Five levels are used and the time separating two consecutive profiles is 10 ms. This graph shows for example that the electric field varies during a longer period of time in altitude than at ground level. This observation can be explained again by corona ions generation during the field change produced by the flash [13]. The evolution of the vertical field profile can be studied during other periods of the thunderstorm: regeneration after a lightning flash or the whole thunderstorm lifetime.

Figure 9 displays two evolutions of this profile beginning at 23:10 on August 10. Unfortunately in this case the resolution of a given profile is limited by the number of working levels available and consequently decreases during the thunderstorm (while sensors stop functioning because of power supply failure). As a matter of fact the evolution 9A that lasts 23 minutes uses five-level profiles and the evolution 9B that lasts 48 minutes uses only three levels.

In figure 9A it clearly appears that only the lower part of the profile (below 436 m) evolves in such a way that the vertical gradient of the electric field increases during this period. In contrast, this gradient stays close to zero within the upper part. In the case of the second evolution (fig. 9B) the steepening of the vertical field profile indicates a strong increase of the electric field vertical gradient due to the building up of the charge layer. Although the global evolution of the profile corresponds to an increasing slope, some anomalous profiles (for example n° 7) are observed. They only denote the occurrence of a lightning flash that suddenly reduces the electric field everywhere. It is easy to check that the development of the charge layer keeps the field intensity at the surface and at 80 m from reaching high values. As a matter of fact, at these levels it does not exceed respectively 5 and 10 kV/m. Furthermore, by the end of the period displayed on figure 9B (after profile 6), a field difference appears and increases between the two upper levels. This phenomenon indicates that corona ions from the charge layer probably reach the 436-m level.

3.3 THE SPACE CHARGE DEVELOPMENT AND EVOLUTION

The multilevel electric field distribution can be used in order to describe the evolution of charge layer above ground. However special conditions must be fulfilled and some hypotheses about charge motions must be formulated to make it possible to deduce charge and current densities from electric field measurements.

The calculation of charge density using Gauss's law requires an essential condition on the surface producing corona ions. This surface must be homogeneous and its dimensions large compared to the height where the calculation is performed. A recent study about this experiment [14] shows that the local wind and vertical drift of the ions lead to this condition fulfilment. On the other hand a calculation of a possible "distance effect" influence indicates that this effect can be neglected in a first approximation.

This procedure has been utilized to compute the average charge density evolution within the various layers defined by the multilevel measurements. We essentially consider the layers whose lower limit is the ground. In order to smooth the evolution of the charge density within the above defined layers, we plot its variation averaged over periods of 350 seconds, versus time, during the most active stage of the thunderstorm (50 minutes duration). This procedure reduces the fluctuations due to the field changes caused by flashes and provides a better observation of the slow evolution of the charge layer. Figure 10 displays four diagrams corresponding to the three layers limited by the ground and the upper layer 436-603 m. The charge density within the lower layer (0-80 m) fluctuates around a rather stable value of about 0.3 nC m^{-3} (fig. 10A). This stationary behavior indicates that, during this period, the upper charge outflow (conduction and/or convection current density) roughly compensates for the lower charge inflow (ground corona current density). Within the layers 0-436 m and 0-603 m, the charge density progressively increases and tends to 1 nC m^{-3} (fig. 10B and 10C). It logically stabilizes first within the 0-436-m layer, which seems to show that a substantial current crosses the 436-m level and penetrates the upper layer. The variation of the average charge density between 436 m and 603 m shown on Figure 10D confirms this fact. Until 23:38 no charge appears above 436 m. Subsequently the density rapidly increases and exceeds 0.5 nC m^{-3} by the end of the period. This observation does not give any information about the nature of the electric current that flows through the 436-m level, conduction or convection, but it clearly reveals its presence.

The present dynamical analysis shows that the charge layer that develops above ground during thunderstorms does not always stay confined close to the ground. Previous papers by Standler and Winn [4] and by Chauzy and Raizonville [2] reported layer depths ranging about 150 to 200 m. Standler and Winn evaluated average charge densities from 0.5 to 1 nC m^{-3}, quite close to those estimated here. Chauzy and Raizonville measured local maximum charge densities ranging from 3 to 6 nC m^{-3}, that are consistent with the average densities computed over deeper layers.

4. CONCLUSION

The system described here was especially designed to be used for research purposes. It was tested during the FLORIDA 89 experiment at Kennedy Space Center and successfully detected the time evolution of the vertical electric field profile above ground during thunderstorms. Such a measurement technique makes it possible to study the formation and development of the space charge layer created at the ground by corona effect. It also provides the characteristics of the field structure in which a cloud to ground lightning flash propagates. In a near future, it is intended to function as main tool of an experimental program on the evaluation of electric currents between cloud and ground. It will be interesting to establish the balance of the various components of the slow exchange of electric charges between cloud and ground, this exchange being part of the thundercell electrification: displacement current, corona current, conduction current, convection current, and precipitation current.

This equipment could also be of some help associated with a thunderstorm warning system. As it has been extensively observed [5 and 14] the raw intensity of the surface electric field is a good indicator of a thunderstorm approach or development, but it is not quite able to evaluate the imminent risk for a given site to be stroken by lightning. The evolution of field intensity aloft provides a useful complementary information about this risk.

Acknowledgments: We are grateful to the Direction des Recherches Etudes et Techniques for supporting our participation in Florida 89 experiment. We appreciate the support and the help of W. Jafferis in the organization of the experiment at NASA Kennedy Space Center. We also wish to thank the members of ONERA and CENG groups whose participation was very helpful.

543

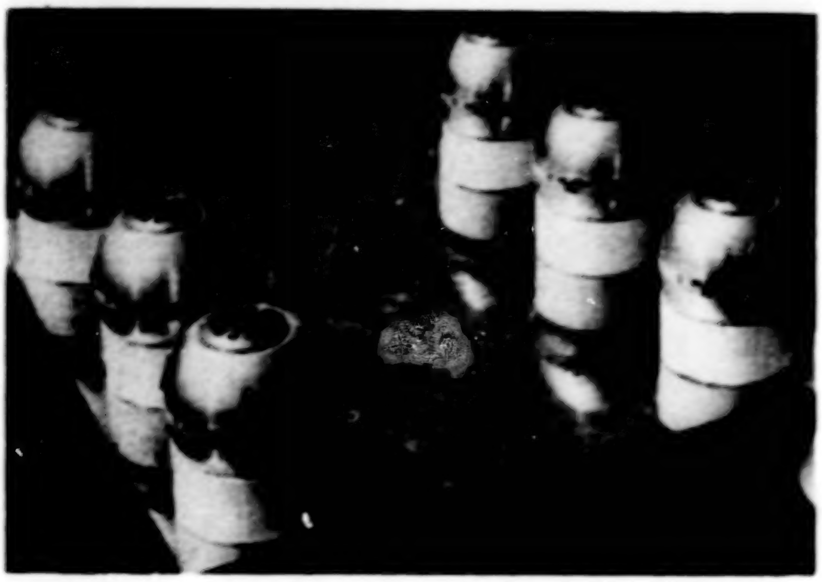

Fig. 2 : The six electric field sensors designed to be suspended from the balloon and the standard field-mill (center) flush with the ground.

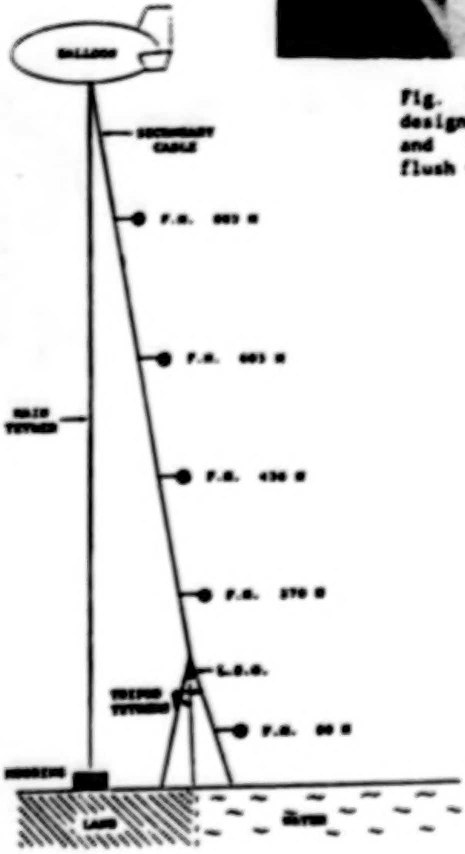
BALLOON
SECONDARY CABLE
F.M. 803 M
F.M. 603 M
MAIN TETHER
F.M. 436 M
F.M. 270 M
L.E.O.
TRIPOD TETHERS
F.M. 80 M
MOORING
LAND
WATER

Fig. 1 : Sketch of the sensors (F.M.) distribution along the tether when the system is in the measurement position.

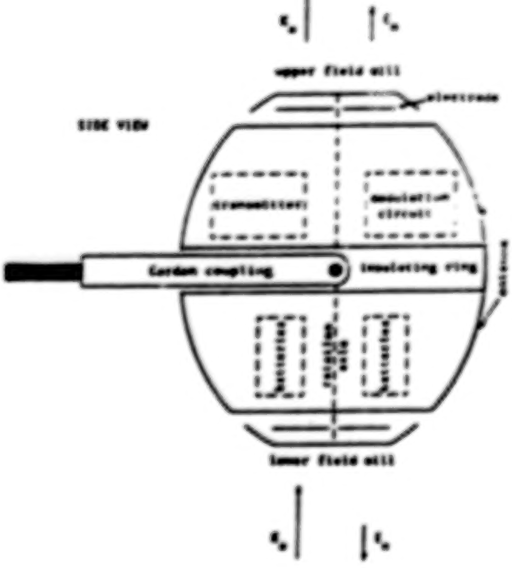
E_u
E_u
upper field mill
electrode
SIDE VIEW
transmitter
modulation circuit
Cardan coupling
insulating ring
antenna
batteries
rotation axis
batteries
lower field mill
E_o
E_o

Fig. 3 : Diagram of each electric field sensor geometry.

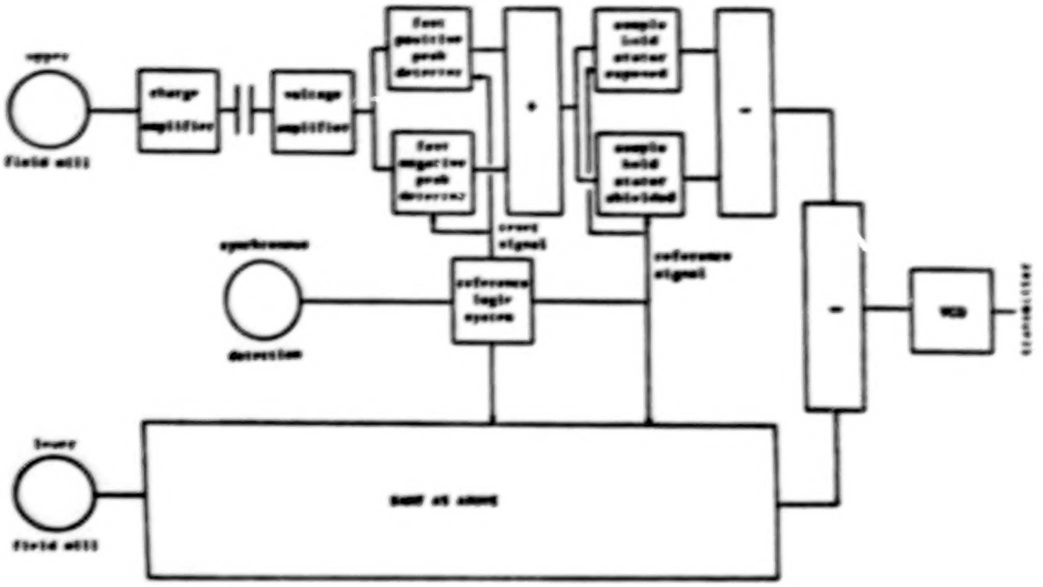
upper
field mill
charge
amplifier
voltage
amplifier
fast
positive
peak
detector
fast
negative
peak
detector
+
sample
hold
stator
exposed
sample
hold
stator
shielded
−
cross
signal
synchronous
detection
reference
logic
system
reference
signal
−
VCO
transmitter
lower
field mill
same as above

Fig. 4 : Block diagram of the modulation circuit of each electric field sensor.

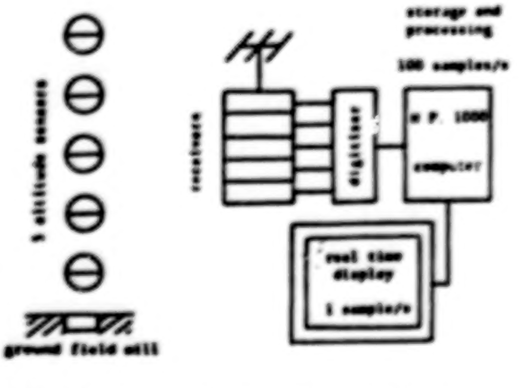
storage and
processing
100 samples/s
H.P. 1000
computer
receivers
digitizer
real time
display
1 sample/s
5 altitude sensors
ground field mill

Fig. 5 : Ground reception station sketch-plan.

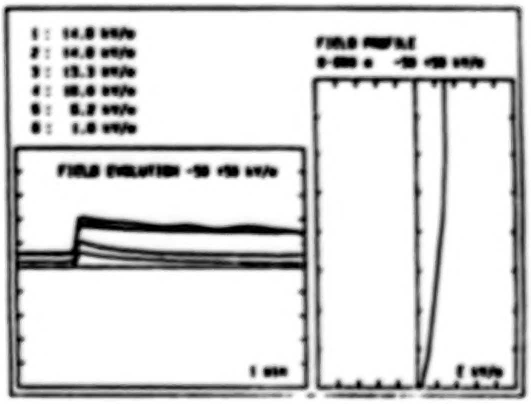

Fig. 6 : A simulation of the computer screen during the experiment at Kennedy Space Center. Upper left: the six instantaneous values. Lower left: the evolution of the electric field at six levels during one minute. Right: the instantaneous vertical profile.

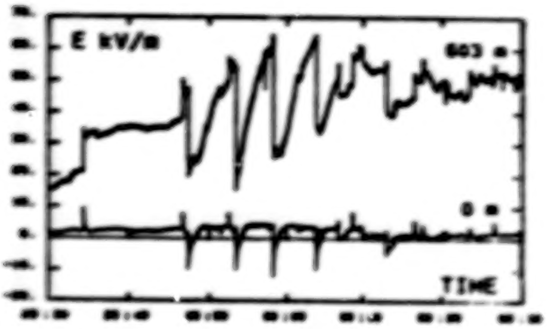

Fig. 7 : Electric field variations measured at ground level and at 603 m beneath a thunderstorm on August 10, versus universal time. During this period five lightning flashes (89-10, 89-11, 89-12, 89-13 and 89-14) were triggered at respectively 23:47, 23:53, 23:58, 00:04 and 00:30.

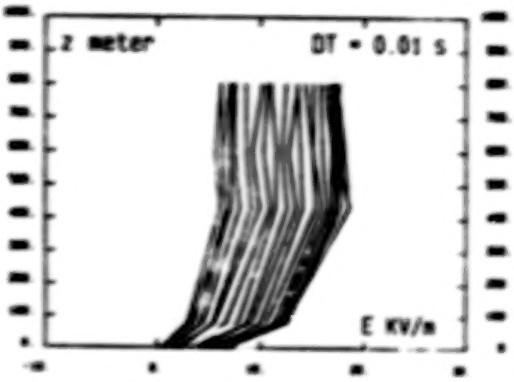

Fig. 8 : Evolution of the electric field profile composed using five level data during a natural lightning flash. The time interval between two consecutive profiles is 1 ms.

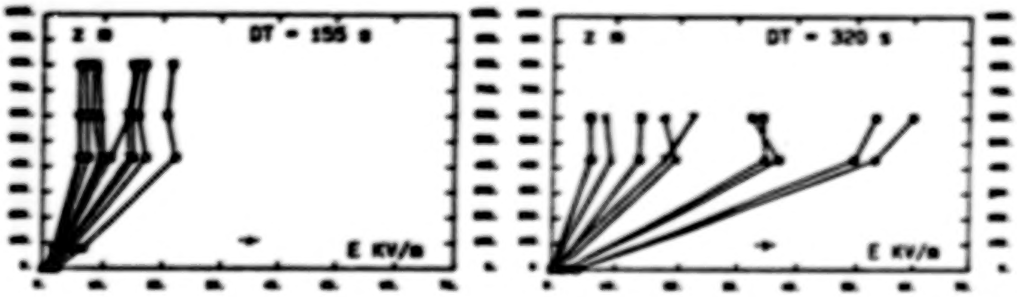

Fig. 9 : Evolution of the electric field profile constructed with five levels and during 23 minutes (case A between 23:10 and 23:33) and with three levels and during 48 minutes (case B between 23:10 and 23:58).

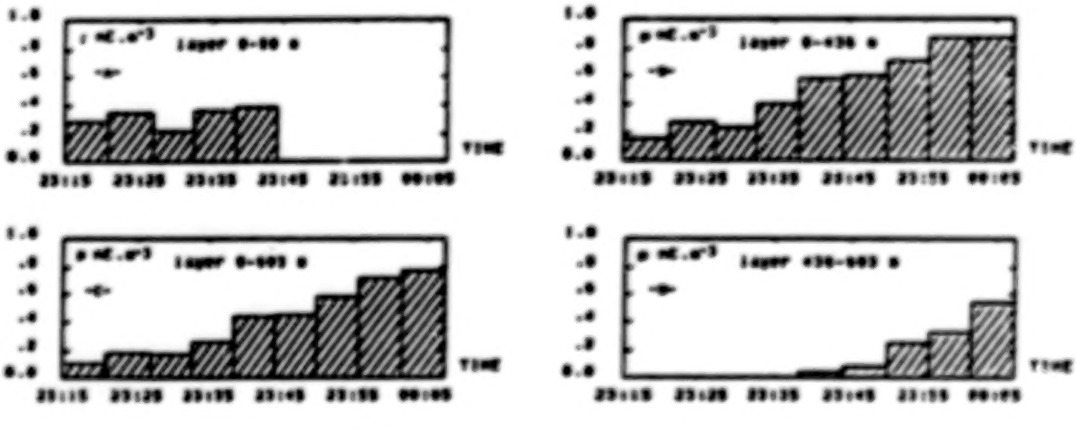

Fig. 10 : Evolution of the average charge density versus universal time during the thunderstorm within four layers: A : 0-80 m, B : 0-436 m, C : 0-603 m and D: 436-603 m. The average charge density is calculated for equal time intervals.

REFERENCES

[1] Wilson, C. T. R., The electric field of a thundercloud and some of its effects, Proc. Phys. Soc. London, 37, 32D-37D, 1925.

[2] Chauzy, S. and P. Raizonville, Space charge layers created by coronae at ground level below thunderclouds: measurements and modeling, J. Geophys. Res., 87(C4), 3143-3148, 1982.

[3] Rust, W. D., Utilization of a mobile laboratory for storm electricity measurements, J. Geophys. Res., 94 D11, 13305-13311, 1989.

[4] Standler, R. B. and W. P. Winn, Effects of coronae on electric fields beneath thunderstorms, Quart. J. R. Met. Soc., 105, 285-302, 1979.

[5] Chauzy, S. and S. Soula, General interpretation of surface electric field variations between lightning flashes, J. Geophys. Res., Vol. 92, D5, 5676-5684, 1987.

[6] Vonnegut, B., Some facts and speculations concerning the origin and role of thunderstorm electricity, Meteorological Monographs, Vol. 5, N° 27, 224-241, 1963.

[7] Idone, V. P. and R. E. Orville, Channel tortuosity variation in Florida triggered lightning, Geophys. Res. Letters, 15, 7, 1988.

[8] Clark, D., Balloon-borne electric field mills for use in thunderclouds, Thesis presented to the Faculty of the New-Mexico Institute of Mining and Technology, 1970.

[9] Rust, W. D. and C. B. Moore, Electrical conditions near the base of thunderclouds over New Mexico, Quart. J. R. Met. Soc., 100, 450-468, 1974.

[10] Few, A. A., M. E. Weber and H. J. Christian, Vector electric field structure in thunderstorms, Conf. Cloud Physics and Atmospheric Electricity, Issaquah, Wash. A. M. S., 601-604, 1978.

[11] Winn, W.P., and C.B. Moore, Electric field measurements in thunderclouds using instrumented rockets, J. Geophys. Res., 76, 21, 5003-5017, 1971.

[12] Saint-Privat-d'Allier Research Group, Eight years of lightning experiments at Saint-Privat-d'Allier, Revue Générale de l'Electricité, 9, 1982.

[13] Soula, S. and S. Chauzy, The effects of ground coronae during lightning flashes, Annales Geophysicae, 4B, 6, 613-624, 1986.

[14] Soula, S. and S. Chauzy, Multilevel measurement of the electric field underneath a thundercloud; Part 2: Dynamical evolution of a ground space charge layer, J. Geophys. Res., submitted.

DISCUSSIONS ON A LONG GAP DISCHARGE TO AN EHV TRANSMISSION TOWER BY A ROCKET TRIGGERED LIGHTNING EXPERIMENT

Koichi NAKAMURA
Nagoya Institute of Technology, Nagoya, Japan

Atsushi WADA
Nagoya University, Nagoya, Japan

Kenji HORII
Toyoda College of Technology

ABSTRACT

The triggered lightning experiments using a rocket have been carried out on a winter mountain in Japan since 1986. The lightning stuck, nineteen times, the EHV test transmission line and tower. This paper emphasizes the methodology for triggering lightning to the transmission system and presents the record of experiments carried out. Based on the results of these experiments, the failure of lightning protection and the striking distance of lightning have been discussed.

INTRODUCTION

The rocket triggered lightning experiments have been carried out in the several countries [1,2,3,4]. In Japan such experiments have been performed in the northern region for the winter thunderclouds since 1977 [5,6,7]. From 1986, the experiment site was shifted to mountainous range of about 1000 m altitude [8]. The lightning struck, nineteen times, the EHV test transmission line and tower. The artificial method for triggering lightning involves a rocket and a bobbin fixed together. The bottom of the rocket system is connected to a 200 m long steel wire which in turn is connected to a 70 - 120 m long nylon line. Both steel wire and nylon line are wounded on a bobbin. The free end on the nylon line is held to the ground and thus acts as a insulator for a rocket steel wire. During the shooting operation of the rocket, the nylon line gets unwound first, followed by unwinding of the steel wire.

Most of the lightning strokes occurred on the ground wire and the peak or the arm end of tower. However, a few lightning strokes occurred on the phase conductors. This indicates the inadequate lightning protection for the transmission line.

The current was measured by a Rogowski coil unit placed on the tower. The sampling time and memory capacity of the unit were one micro-seconds and 256 kilo-words respectively. The peak current was measured by a magnetic tape placed on the top of rocket.

In order to obtain the triggered lightning discharge on a high tower artificially but similar to the natural one, a two-stage rocket was used to initiate lightning as well as to carry the current measuring system (Rogowski coil - for the measurement of lightning discharge in the air).

The striking distance was estimated from the photograph or the reconstructed channel by an acoustic analysis method. In the measurement of the acoustic analysis, three microphones were used, each separated by a 10 m distance amongst them. This analysis was quite useful to estimate the discharge channel within the cloud or under the invisible condition such as snowfall, etc. This analysis method and its accuracy have been discussed in the literature [9,10]. The striking distance versus the peak current characteristics were thus obtained. The results were comparatively close to the characteristics reported by Golde and Chan [11,12].

This paper primarily emphasizes the methodology for triggering lightning to the transmission system and presents the record of experiments carried out in the four years. Finally, based on the results of these experiments, the failure of lightning protection and the striking distance of lightning have been discussed.

TRIGGERING METHOD

The experiment site was chosen on the peak of the Okushishiku mountain with the altitude of 930 m above sea level and IKL(Iso Keraunics Level) of about forty. A test transmission line of 275 kV of about 2 km length running over seven transmission towers is located near the site. Fig. 1 indicates

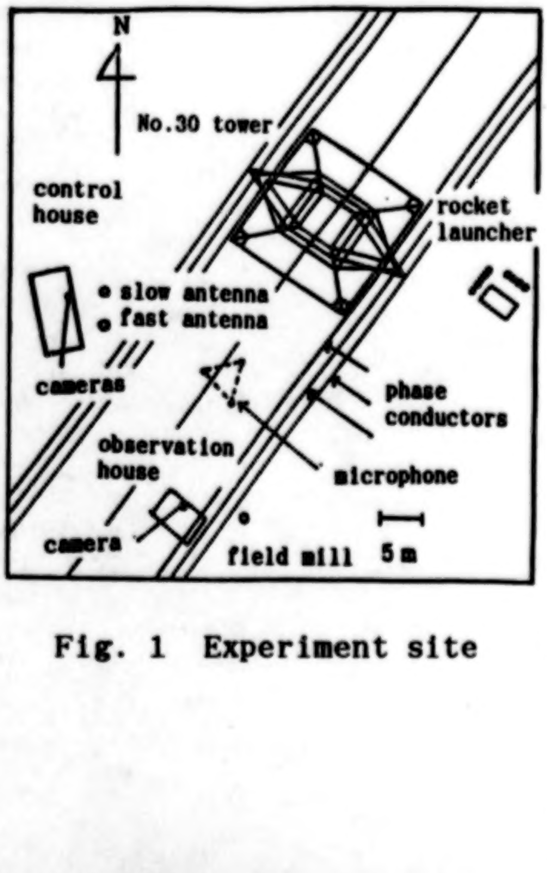
N
No.30 tower
control house
rocket launcher
• slow antenna
• fast antenna
cameras
phase conductors
observation house
microphone
camera
field mill
5 m

Fig. 1 Experiment site

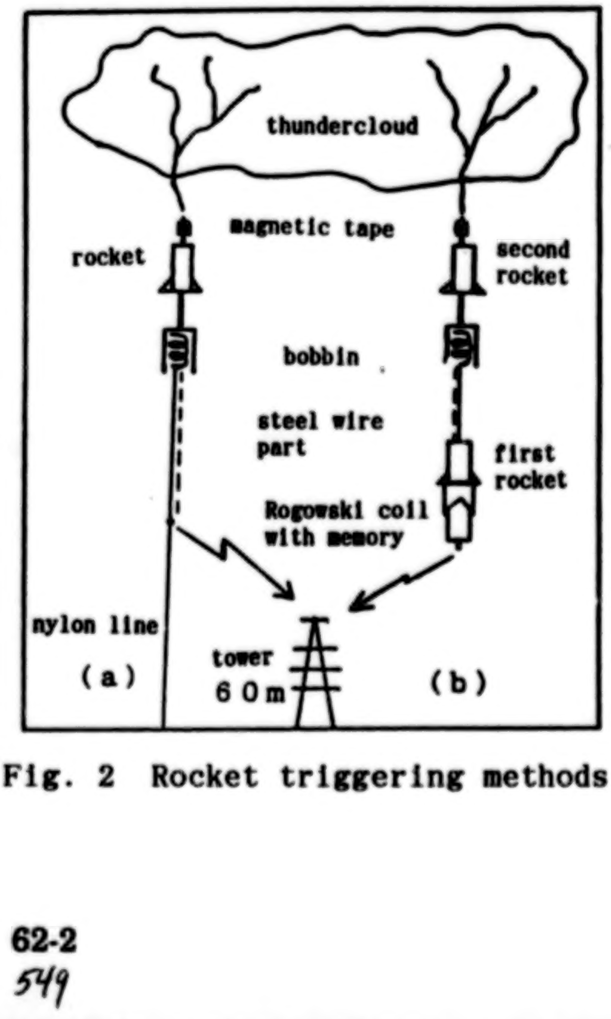
thundercloud
magnetic tape
rocket
second rocket
bobbin
steel wire part
first rocket
Rogowski coil with memory
nylon line
(a)
tower
60m
(b)

Fig. 2 Rocket triggering methods

the arrangement of the site. The height of one of the towers, tower No. 30, is about 60 m. The rocket launchers were placed at a distance of 10 - 15 m from the tower. In order to get the lightning on the towers one-stage and two-stage rocket methods were applied.

One-stage rocket system

This method has been applied since 1986. One of the rockets launched employing this method is shown in Fig. 2(a). The length, the diameter and the weight of rocket were 170 mm, 40 mm and 0.5 kg respectively. During launching of rocket, initially the nylon line was pulled out by about 70 to 120 m from the ground followed by unwinding of the steel wire of 0.2 mm diameter. With such a long nylon line, the steel wire gets well insulated from the ground. This paves the way for triggering of the lightning discharge to the nearest transmission line and tower making a long gap discharge of length 10 - 60 m. Hence the change in the starting point of the downward leader, (i.e. the distance from the ground), can be achieved simply by selecting the different lengths of nylon line. Fig. 3 shows one example of the triggered lightning to the top of tower.

Two-stage rocket system

In the one-stage rocket system the comparatively long partial discharges were often observed along the surface of the nylon line in the beginning of triggering of the lighting discharge [8]; To eliminate these discharges, the two-stage rocket system was then developed completely dispensing with the nylon line.

As shown in Fig. 2(b), the two-stage rocket was launched by firing the first rocket and within two seconds the second rocket got automatically fired to separate each other in the air and then the steel wire was unreeled connecting them. On the top of the second rocket a magnetic tape and on the bottom side of the first rocket a compact Rogowski coil with a memory unit were equipped to measure the lightning current peak and waveform respectively. The diameter of Rogowski coil was 70 mm. The current signal was directly written into a compact memory card with memory of 256 kilo-words. As the magnetic tape used was pre-magnetized with 1 kHz signal and so the peak current was estimated from the demagnetized distance on the tape. The triggered lightning by the two-stage rocket system was obtained two times in 1989, but unfortunately the current measurement could not be successfully recorded.

EXPERIMENTED RESULTS

General

The table 1 depicts the results of the triggered lightning strokes occurred on the ground wire, phase conductors and tower. In the table, the nylon length indicated is that of the nylon line wound on the bobbin for the one-stage rocket system. The results shown against the experiment No.89-16 and No.89-21 have been evaluated using the two-stage rocket system. The striking points were estimated either using the camera photograph or the lightning channel reconstruction by an acoustic analyzing method. Several points were identified and confirmed through the visual inspection after the end of experiment as well as other measurements such as the induced voltage on the insulator strings. The peak currents were obtained by Rogowski coil measurement except in case of experiment No.89-16 and 89-21 in which relevant observation were taken by the magnetic tape measurement. The triggering time means the time lapse after the rocket launching till the occurrence of lightning.

Striking distance here is defined as the distance between the striking point on the transmission system and the nearest bending point of the channel. According to the streak photograph, the downward leader began from the tip of the partial discharge appeared along the surface of the nylon line, and propagated towards the transmission system. The local return stroke run up from the transmission system to meet the leader within several hundred microseconds before the vaporization of wire. The main discharge occurred after the upward leader reached the nearest cloud [8].

Table 1 Experimental Results

No.	nylon length	striking points	current peak(kA)	remarks (protection)
86-11	70 m	upper arm end of tower	>+50	
86-13	70	ground		
87-05	100	peak of tower	+23.0	
87-07	100	upper arm end of tower	-8.5	
87-08	100	ground wire	-11.0	
87-10	100	rocket launcher	negative	
87-18	100	upper arm end of tower	+14.0	
87-21	100	middle phase conductor	negative	failure
87-22	100	upper arm end of tower	(-5.5)	
88-12	100	ground wire	-	
88-04	120	upper phase conductor	-	failure
88-16	120	ground wire	-	
89-04	120	peak of tower	+25.6	
89-05	120	upper phase conductor	positive	failure
89-07	120	upper phase conductor	positive	failure
89-09	120	peak of tower	-18.1	
89-10	120	ground wire	-4.3	
89-16	•	ground wire	+13.0	(two-stage)
89-21	•	middle arm end of towe	+5.0	(two-stage)

Lightning Discharges

The length of nylon line applied in the 1986 was 70 m. The experiment No. 86-11 in Fig. 3 shows the sketch of the triggered lightning to the tower, obtained by the three dimensional analysis of photograph. In this case, the lightning discharge propagated 23 m from the junction point of the steel wire and the nylon line to strike the upper arm end of tower with the angle of 50 degrees. According to the current measurement, the peak value was estimated to be +50 kA [8].

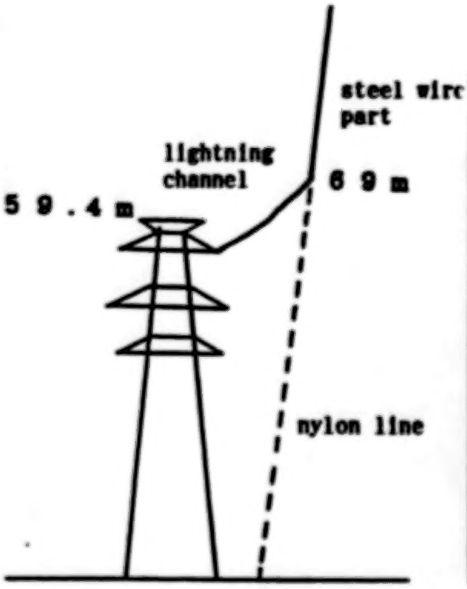

Fig. 3 Lightning flash 86-11(sketch)

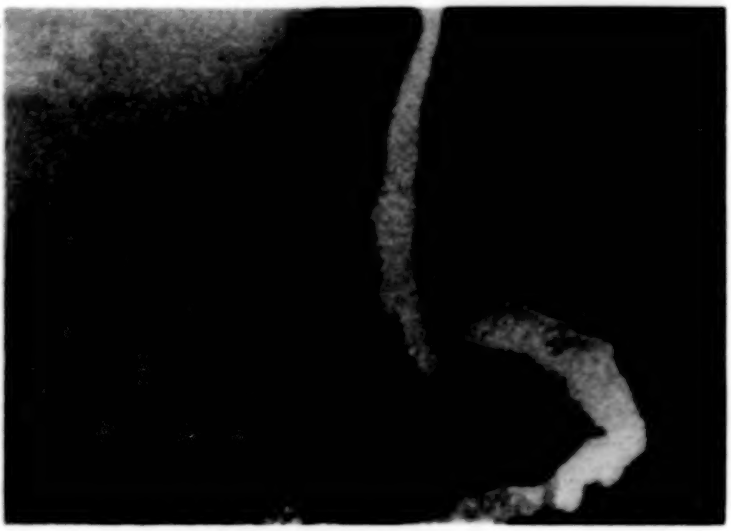

Fig. 4 Lightning flash 87-10

The length of nylon line used in this experiments conducted during 1987 was 100 m. Rocket launcher was placed 12 m distant from the tower with an elevation of 87 degrees. As described in Table 1, six lightning occurred on the transmission tower, the ground wire and directly on the ground. One of the lightning struck the phase conductor which indicates the inadequacy of lightning protection.

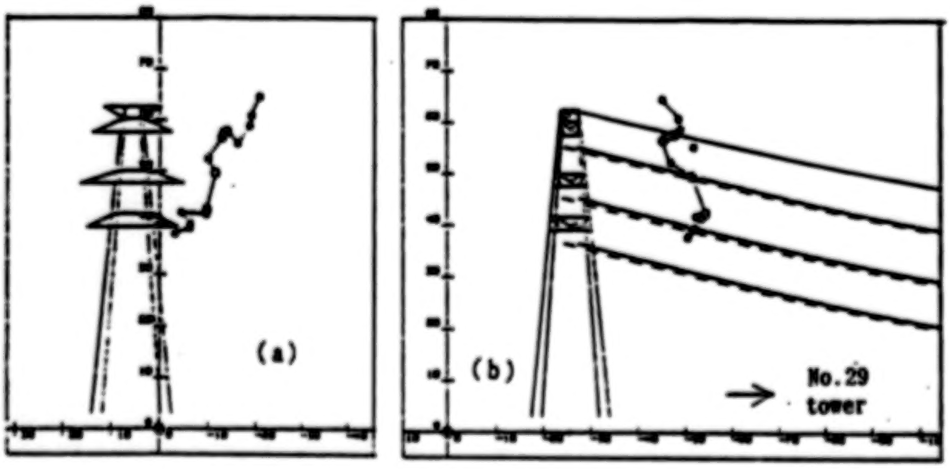

Fig. 5 Reconstruction of lightning flash 87-21 (middle phase)

Fig. 4 shows the lightning flash of experiment No.87-10 on the launcher. The lightning discharge came down straight from the air, and jumped to one of the six launchers on the ground after flashing over along the nylon surface for about 20 m length. Fig. 5 shows the reconstruction of the lightning experiment No.87-21. The striking point was estimated to be on the middle phase conductor 20 m at a distance from the tower.

Fig. 6 shows a photograph and a current through the ground wire measured by a Rogowski coil unit in the lightning experiment No.87-08. The lightning experiments viz, No.87-21 and No.87-10 was the negatively charged clouds.

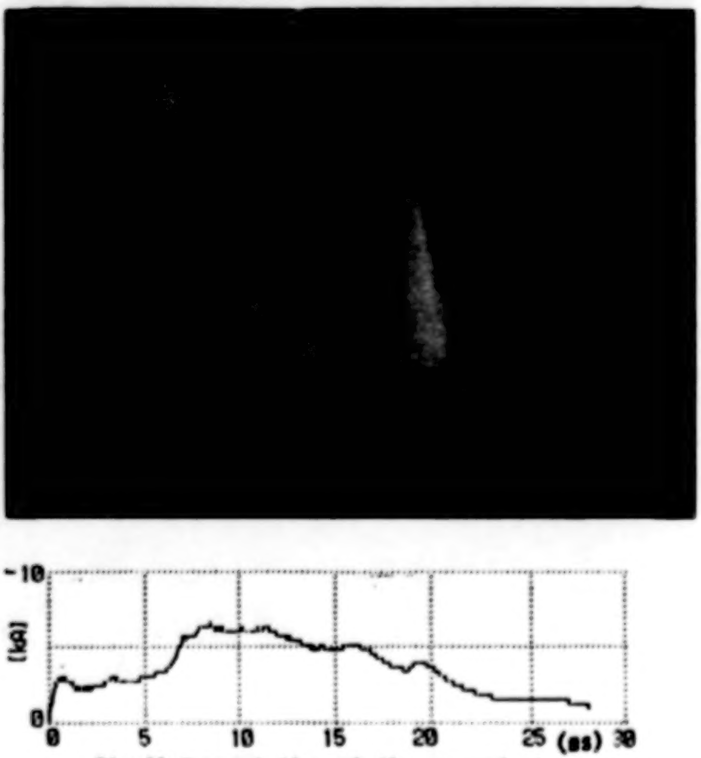

Fig.11 Current through the ground wire

Fig. 6 Lightning flash and current through the ground wire 87-08

In case of experiments conducted during 1988, two nylon lines of 100 m and 120 m length were applied. Two lightning occurred on the ground wire and one occurred on the upper phase conductor. Fig. 7 shows the reconstruction of the lightning flash of 88-04. Fig. 7-a , 7-b and 7-c are the front, the side and the plane views, respectively. The striking point were estimated to be 60 m away from the tower.

In the year 1989, such experiments were conducted using nylon line of length 120 m. Seven triggered lightning including the two initiated by the two-stage rocket system were obtained. The triggering lightning strokes as recorded in the experiments No.89-05 and No.89-07 occurred directly on the upper phase conductor which indicates the insufficient shielding against lightning. Clear photographs could not be obtained for any of lightning discharges because of the heavy snowfall. Fig. 8

indicates the seven striking points of the lightning estimated by the reconstruction method. The locations of these points were evaluated by another methods and found to be in good agreement.

DISCUSSIONS

As shown in Table 1, two lightning strokes occurred separately on the tower or the ground without the failure of shielding against lightning in the case of 70 m nylon line. However, out of seven lightning strokes triggered using nylon line of 100 m length, only one struck the middle phases conductor, whereas one of same number of strokes triggered using nylon line of 120 m length, three struck the upper phase conductor. On evaluating of this date, it was observed that the failure rate of the lightning protection was 14 % in the case of 100 m nylon line and 43 % in the case of 120 m nylon line.

These results suggest that the longer the nylon line, the higher is the failure rate of the protection as well as the striking point of the lightning. It was also observed that in the event of triggered lightning striking the tower, the downward leader began near the junction of the nylon line and the steel wire [8]. Thus the starting location of the leader may depend on the length of nylon line. If the length of the nylon line is small so as to make the starting point of the leader within the attracting

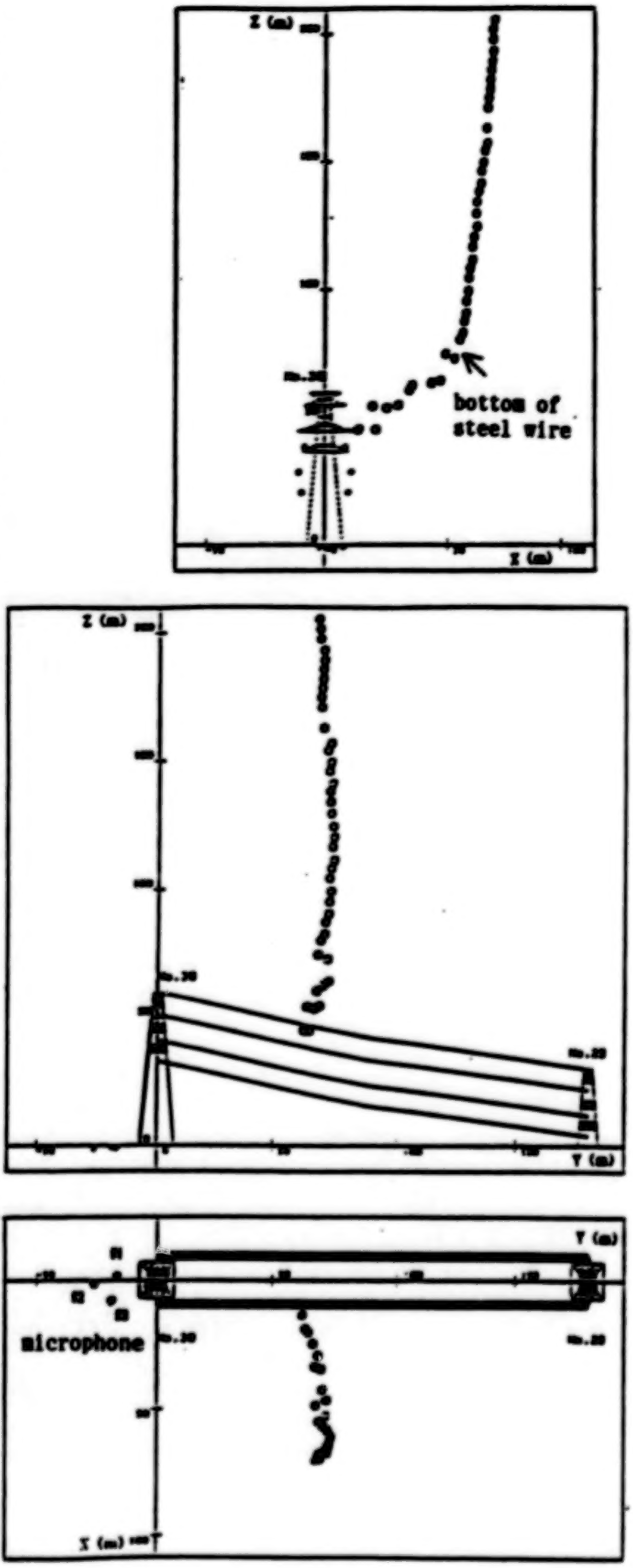

Fig. 7 Lightning reconstruction (88-04)

area of the tower, the lightning can occur on the tower. If the length of the nylon line is comparatively long, the leader can begin outside from the attracting area and then the lightning can take place on somewhere the nearest point from the leader.

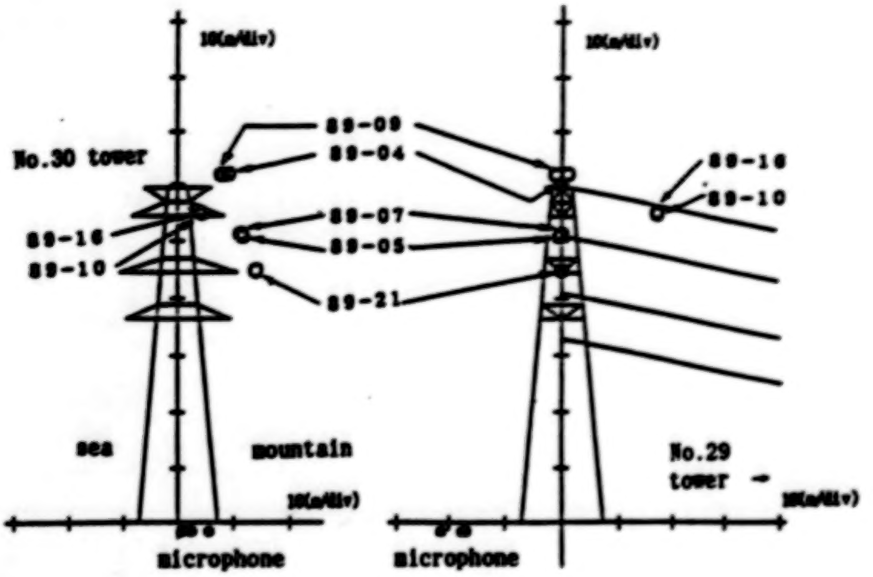
10(m/div)
10(m/div)
No.30 tower
89-09
89-04
89-16
89-10
89-07
89-05
89-21
89-16
89-10
sea
mountain
No.29
tower
10(m/div)
10(m/div)
microphone
microphone

Fig.8 Striking points identified by the reconstruction

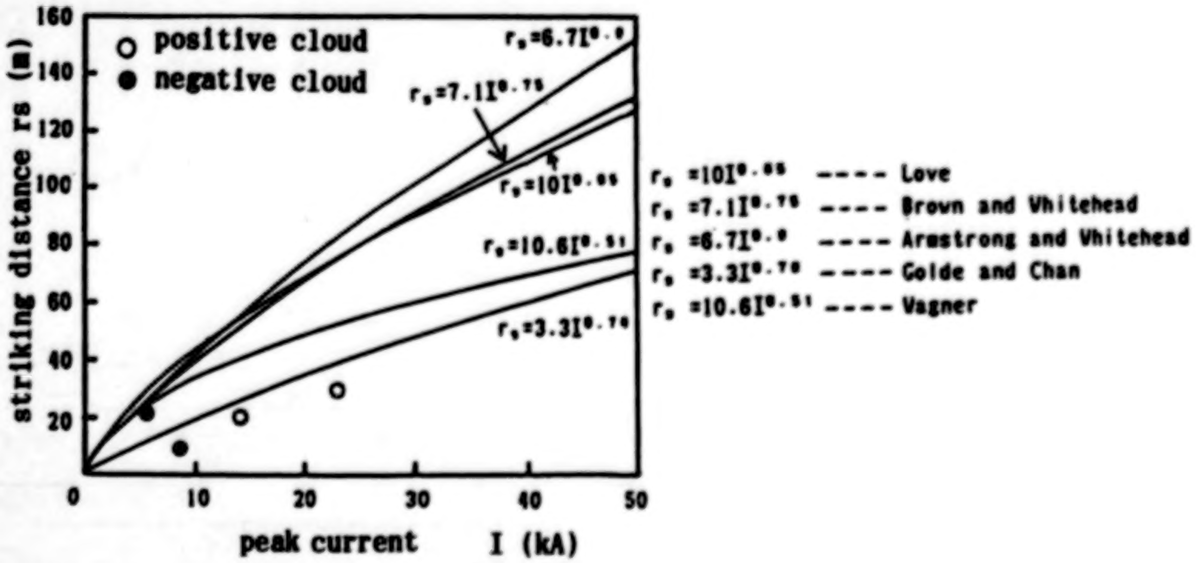

Fig. 9 Striking distance and peak current

Fig. 9 shows the characteristics of thestriking distance versus the current peak. Several theoretical curves are documented together. The characteristics curve of the triggered lightning becomes close to or comparatively below the curve reported by Golde and Chan. According to the theory, the larger the total charge of the downward leader, the longer is the striking distance or the final jump because of the higher potential of the leader. And the return stroke current must be larger enough to cancel the corresponding charge the leader left behind.

On the other hand, the downward leader was forced to start from the bottom of wire and propagated only several tens meters towards the transmission system in the triggered lightning. Then the return stroke did not reach the cloud at a dash, but ceased in the way. For this reason we named it as a partial return stroke. Within a few hundred microseconds the upward leader subsequently began to move towards the cloud to initiate the main lightning discharge. The peak current in Fig. 9 is not corresponding to the partial return stroke current, but the main discharge current. Therefore, the comparatively large currents were obtained corresponding to the same striking distance. If the current during the partial return stroke can be measured by using the two-stage rocket, the more reasonable characteristics may be obtained.

CONCLUSIONS

The results and the discussions on the triggered lightning experiments to the transmission line for four years from 1986 to 1989 are summarized as follows.

(1) Thirty nine rockets were launched and nineteen triggered lightning strokes were obtained on the transmission line and tower, and on the ground. The rate of success was 50 %. Four times lightning strokes occurred on the phase conductor which meant the failure of lightning protection, and the twice struck the ground.

(2) The nylon lines of 70 - 120 m length were used for the insulation of the steel wire. The longer the nylon line, the higher was the failure rate of the protection.

(3) The characteristics of the striking distance was close to or comparatively below the curve reported by Golde and Chan.

(4) The lightning using the two-stage rocket was successfully triggered. Unfortunately, the measurement of the discharge current could not be done successfully.

The authors would like to thank the members involved in conducting the experiments and the students for their great help and assistance. The authors would also like to thank Hokuriku Electric Power Company and Chubu Electric Company for their great co-operation. We also gratefully acknowledge the financial support of the Ministry of Education, Science and Culture of Japan.

REFERENCES

[1] M.M.Newman et al., "Triggered Lightning Strokes at Very Close Range", Journal of Geophysical Research, vol.72,pp.4761-4764, 1967.

[2] R.P.Fieux et al., "Research on Artificially Triggered Lightning in France", IEEE Transaction on Power Apparatus and Systems, vol.PAS-97,pp.725-733, 1978.

[3] W.Boeck et al., "Aktuelle Aufgaben und Methoden der

Blitzforschung", etz-a Bd.99,pp.652-654, 1978.

[4] K.Horii et al., "Experiment of Rocket-Triggered Lightning in Indonesia", T.IEE Japan, vol.110-B,No.12,pp.1068-1069, 1990.

[5] K.Horii et al., "Experiment of Long Gap Discharge by Artificially Triggered Lightning with Rocket", 3rd International Symposium on High Voltage Engineering, vol.51.10, 1979.

[6] I.Miyachi et al., "Five Years' Experiences on Artificially Triggered Lightning in Japan", 7th International Conference on Gas Discharge and their Applications, pp.468-471, 1982.

[7] K.Horii et al., "Observation of Final Jump of the Discharge in the Experiment of Artificially Triggered Lightning", IEEE Transactions of Power Apparatus and Systems, vol.PAS-104, No.10, pp.2910-2917, 1985.

[8] K.Nakamura et al., "Artificially Triggered Lightning Experiments to an EHV Transmission Line",IEEE/PES Summer Meeting, 90 SM 360-0 PWRD, 1990.

[9] H.Akiyama et al., "Channel Reconstruction of Triggered Lightning Flashes with Bipolar Currents from Thunder Measurements", J. of Geophysical Research, vol.90,No.D6,pp.10674-10680, 1985.

[10] M.Wakamatsu and K.Horii, "Rocket-Triggered Lightning to Power Transmission Line Tower and Estimation of the Lightning Channel by Computer Graphics", Research Letters on Atmospheric Electricity, Vol.7,pp.17-20, 1987.

[11] G.W.Brown and E.R.Whitehead, IEEE Transactions on Power Apparatus and Systems, vol.PAS-88,No.5, 1969.

[12] M.A.Uman, "The Lightning Discharge", pp.101, Academic Press, New York, 1987.

Correlation Between Some Current Parameters and Optical Radiation Generated by 280 mm Long Laboratory Sparks

Dan Windmar, Vernon Cooray and Viktor Scuka
Institute of High Voltage Research
A Department at Uppsala University
S-755 92 Uppsala
Sweden

ABSTRACT

In remote sensing of lightning and other discharge phenomena it is of interest to know the relationship between optical radiation and the current parameters. Unfortunately, little information is available in the literature on these relationships. In this paper we have studied, therefore, the optical radiation generated by 280 mm long laboratory discharges and its relationship to the current flowing in the discharge channel. In the experiment the optical radiation generated by the discharges was measured at wavelengths 777 nm (bandwidth 10 nm) due to O I(1), and 500 nm (bandwidth 5 nm) due to N II(19), and the broadband optical radiation between the wavelengths 400 - 1100 nm. The shape of the current waveform, which had a rise time of 0.1 µs and a decay time of 5 µs, remained the same with increasing peak value. The experiment was conducted with peak current amplitudes in the range of 1 - 4 kA. In order to test the effect of current rise time on the optical radiation we have also conducted studies with a current waveform having a 5 µs rise time. The main observations are the following: (a) The peak amplitude of the optical radiation pulse at the wavelengths mentioned above is proportional to the peak amplitude of the current flowing through the discharge channel. (b) The rise time of the optical radiation pulse at a given wavelength does not depend significantly on the peak amplitude of the current waveform. (c) The rise time of the optical radiation pulse decreases with decreasing wavelength. (d) A slight increase in the decay time of the optical pulse, at a given wavelength, is observed with increasing peak amplitude of the current waveform. (e) The results show that the rise time of the optical radiation pulse increases with the increasing rise time of the current waveform. The relationship between peak current, peak optical power and peak electrical power is studied. Also the relationship between peak current, optical energy (400 - 1100 and 777 nm) and electrical energy is discussed.

INTRODUCTION

The study of optical radiation generated by long sparks is of interest in two respects. First, in the use of geostationary satellites to detect lightning, one of the demands on the space based detector is the ability to detect lightning during full daylight [1]. Goodman et al. [2] suggested that this could be realized by detecting either the spectral line of oxygen (O I(1)) at 777 nm or the spectral line of nitrogen (N I(1)) at 868.3 nm. From various observations, done at ground level and above clouds [2-3], the oxygen line at 777 nm appears to be a strong, narrow and stable spectral line in the spectrum of lightning flashes. By recording a strong and narrow spectral line,

556

the background noise may be suppressed so that the recording can be performed even during the day time. The absorption in clouds, in the near infrared region of the spectra, is negligible which is also one of the reasons that we have chosen the O I(1) spectral line.

Second, in the remote sensing of lightning return stroke through the optical radiation it is important to know the relationship between return stroke current parameters and the characteristics of the optical radiation. For example, if the knowledge is available it is possible to estimate how the characteristics of the lightning current is changing along the return stroke channel by analysing the optical radiation.

A lot of work has been done on the optical radiation from lightning [3-7] but there is very little work done on optical radiation from laboratory sparks under controlled atmospheric conditions. For example, by extrapolating the data obtained from laboratory discharges, Krider et al. [6] and Uman et al. [8] have estimated the electric power and electric energy dissipated in lightning flashes. To increase our knowledge of the correlation between the optical and some electrical parameters of the discharge channel, we have started to investigate the appearance of the O I(1) and the N II(19) spectral lines and the broad band optical radiation between the wavelengths 300 and 1100 nm from long laboratory sparks to increase our knowledge of the correlation between the optical and some electrical parameters of the discharge channel.

EXPERIMENTAL SYSTEM

The light output from the discharge channel was measured with an optical detector, especially designed for this purpose [9] (figure 1). The optical detector consist of a light collecting and a collimating lens system, an optical interference filter and a photodiode with electronics.Some characteristics of the optical detector: rise time < 0.4 µs, fall time < 10 µs, transmission 64%. A typical optical pulse waveshape from a 280 mm long laboratory discharge can be seen together with current in figure 2.

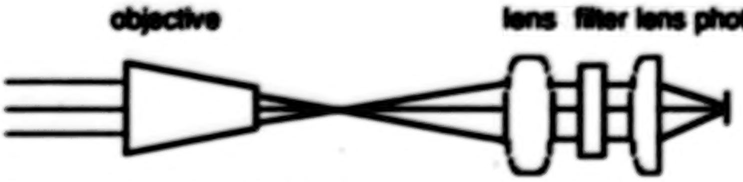

Figure 1 The optical detector

The current was measured with a Rogowski coil. The coil used was a Singer Current Probe, model 94456-4, which is designed to measure current pulses with durations up to 500 µs and peak current levels of up to 6000 A. The frequency range of the probe is 10 kHz to 100 MHz. The current probe is placed around the rod to which the discharge takes place, as can be seen in figure 2. The output from the optical detector and the current probe were recorded and displayed on a Hewlett Packard 54111D Digitizing Oscilloscope. The displayed waveforms were then transferred via a HPIB bus to a portable IBM Personal Computer for post processing. The recording system was placed in a screening cage, see figure 3. The electrode configuration is sphere-rod and a negative impulse voltage is applied to the sphere. The shape of the voltage impulse is 1.2;50 µs. The shape of the current waveform generated by the impulse generator has 0.1 µs rise time and 5 µs decay time. The distance between the electrodes in the spark gap is 0.28 m. The distance between the optical detector and the discharge channel was 6 meter. Measurements have shown that for distances larger then 6 meters, the discharge channel can be regarded as a point light source, i.e. the radiated flux density is decaying as $1/r^2$ [9].

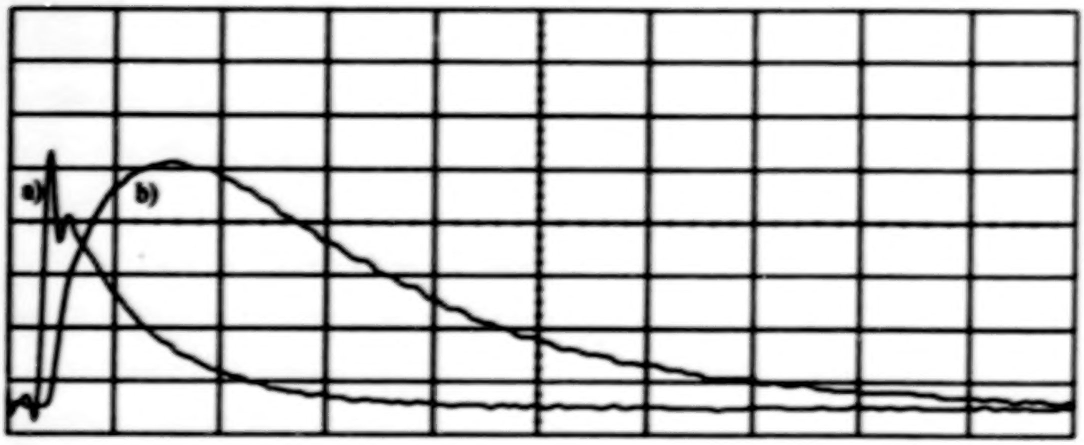

Figure 2 Typical optical and current waveforms obtained from 280 mm long laboratory discharges, a) current waveform, b) optical waveform, time base 5 µs/div

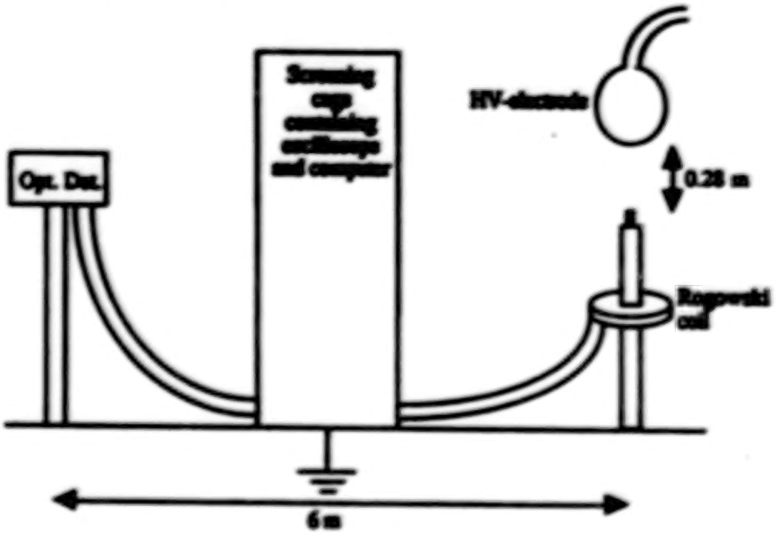

Figure 3 Experimental set-up in high voltage hall

The O I(1) spectral line is a triplet with three lines of almost equal intensity, separated 0.34 nm, and the N II(19) spectral line is a doublet with two lines separated with 0.03 nm. Therefore, the light detected from the discharge channel at this wavelengths is due to the a sum all the components in the spectral line. The light signal received by the optical detector is basically a superposition of the geometrical growth of the discharge channel and other luminous effects happening when a discharge takes place.

RESULTS

PEAK LIGHT OUTPUT VERSUS PEAK CURRENT

Measurements show that there is a nonlinear relationship between the peak output of the optical radiation at 777 nm, 500 nm, 400 - 1100 nm and the peak current. The results for the 777 nm spectral line is shown in figure 4. The following curve can approximate the data to a high accuracy (correlation coefficient 0.991):

$$P_{o,777} = 1.76 \times I_p^{1.37} \qquad (1)$$

where P_o is in 10^3 W/m and I_p in kA. The peak power generated by 3 kA peak current is 7.92×10^3 W/m.

The results for the broad band optical radiation is shown in figure 5. The following curve can approximate the data to a high accuracy (correlation coefficient 0.988):

$$P_{o,400\text{-}1100} = 0.68 \times I_p^{1.40} \qquad (2)$$

where P_o is in 10^5 W/m and I_p in kA. The peak power generated by 3 kA peak current is 3.16×10^5 W/m.

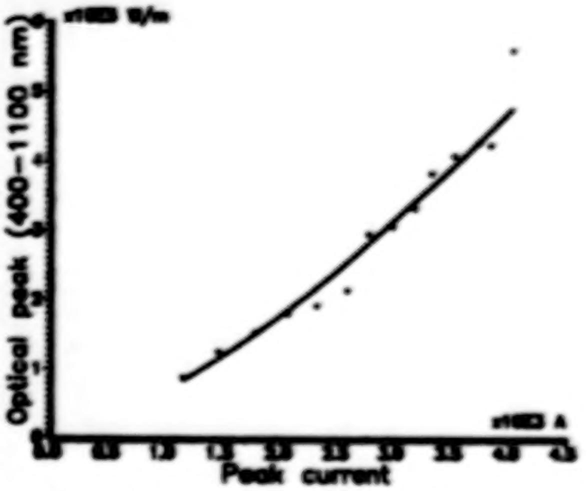

Figure 4 Peak light (400 - 1100 nm) peak current

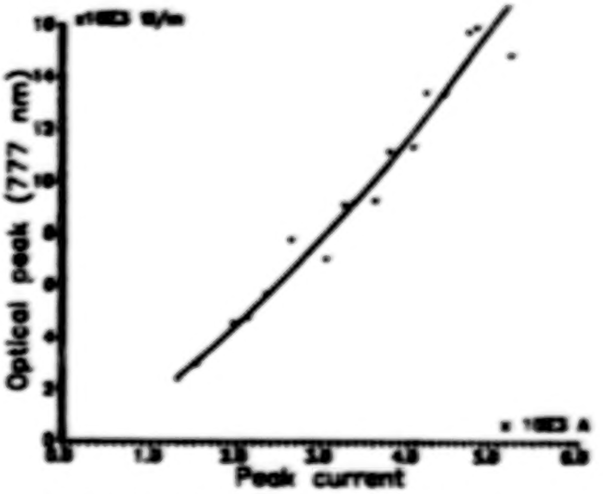

Figure 5 Peak light (777 nm) versus versus peak current

It is of interest for us to compare our results with those obtained from lightning. Recently, Idone and Orville [10] measured the optical radiation (spectral range 300 - 670 nm) generated by a short segment of lightning channel situated at 50 meters from ground level and the peak current in the return stroke channel. They found that there is a linear relationship between the peak light intensity and the peak current for subsequent strokes in triggered lightning. Unfortunately, Idone and Orville did not give the optical power in absolute units so that we can investigate whether the laboratory results can be extrapolated to lightning conditions. Baker et al. [7] have measured the peak optical power and the peak current from triggered lightning. For a 17 kA current they have measured a peak optical power of 3.7×10^6 W/m. They have also calculated the peak optical power for a 17 kA current to be 10.9×10^6 W/m. If we assume that our measurements can be extended to lightning we get for a 17 kA current a peak optical power of 3.5×10^6 W/m which is in good agreement with the measured results.

THE RISE AND DECAY TIME OF THE OPTICAL PULSE

The results shows that the rise time of the optical radiation pulse at a given wavelength does not depend significantly on the peak amplitude of the current waveform (figure 6). We have also found that the rise time of the optical radiation pulse decreases with decreasing wavelength. We measured the mean rise time τ_{mean} to be 2.32 µs for the O I(1) (777 nm) spectral line and 0.48 µs for the N II(19) (500 nm) spectral line. This result is, in principal, in good agreement with measurements done by Lundquist and Scuka [11]. They have measured the time characteristics of the spectral line H_α (655.5 nm) and the channel continuum at wavelength 390.5 nm from lightning discharges and have found that there is an decrease in rise time with decreasing wavelength as in our case.

There is a slight increase in the decay time (the time it takes for the peak light output, I_p to fall to half the peak light, $0.5I_p$) of the optical pulse at a given wavelength with increasing peak current (figure 7).

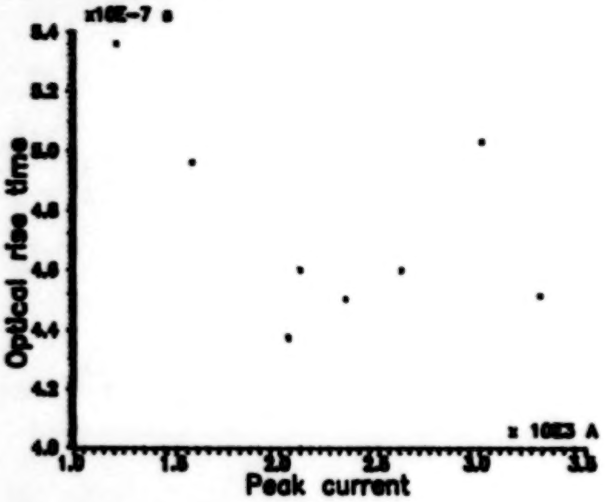

Figure 6 Optical rise time (400 - nm) versus peak current

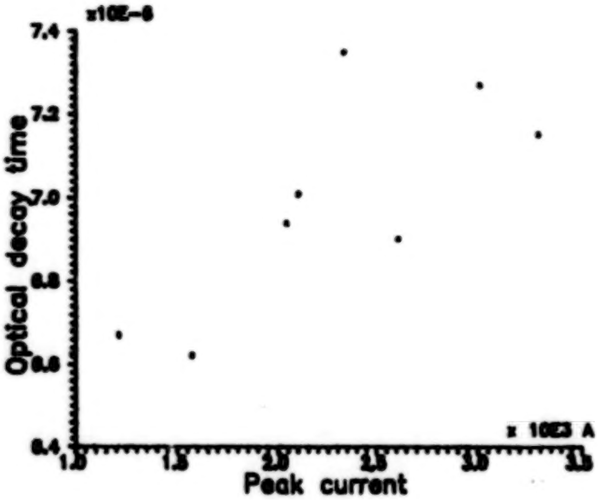

Figure 7 Optical decay time (400 -1100 1100 nm) versus peak current

In order to test the effect of the current rise time on the optical radiation we have conducted studies with a current waveform having 5 µs rise time and 25 µs decay time. The result is that the rise time of the optical radiation pulse increases with increasing rise time of the current waveform (figure 8).

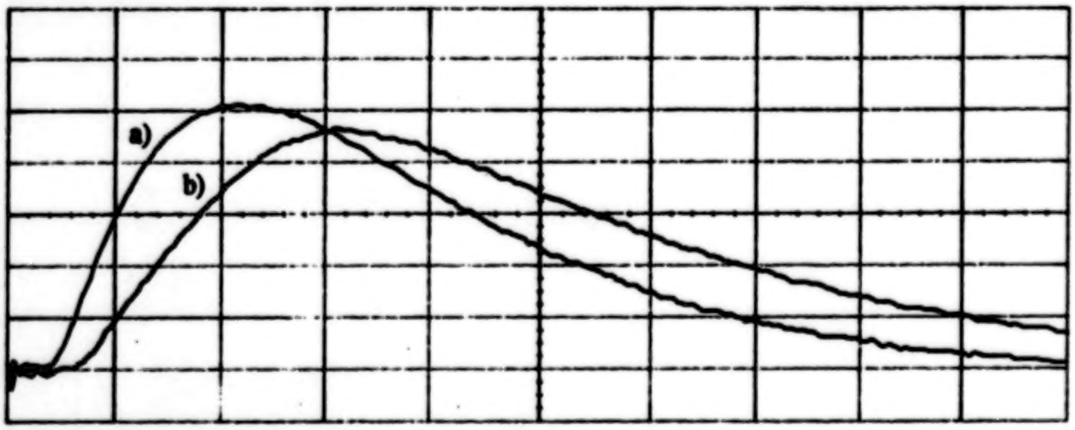

Figure 8 The effect of increasing current rise time on the optical pulse, a) current waveform, b) optical waveform, time base 5 µs/div

For lightning it has been observed that the rise time of the optical radiation is increasing with increasing height. This indicates, according to our results, that the current rise time is increasing with increasing height. A similar result is predicted by a new return stroke model introduced by Cooray [12-13]. A thorough investigation of the relationship between the current rise time and the optical rise time will be carried out in the near future at the Institute of High Voltage Research.

POWER MEASUREMENTS

We have measured the electrical power dissipated in the discharge channel by measuring the voltage V and the current I. The results of this investigation together with peak optical power is given in table I.

Table I Results of the power measurements

Current (A)	Peak electrical power P_{el} (10^9 W/m)	Peak optical power P_o (10^5 W/m)
-1157	0.87	0.83
-1564	1.33	1.27
-1919	2.05	1.69
-2214	2.66	2.07

According to this results the relationship between the peak electrical power P_{el} and the peak current I_p can be represented by

$$P_{el} = 0.65 \times I_p^{1.75} \qquad (3)$$

where P_{el} is in 10^9 W/m and I_p in kA. This agrees very well with calculations done by Cooray [14] for the lightning return stroke. According to these calculations the relationship between the peak electrical power P_{el} and the peak current I_p is given by $P_{el} = k \times I_p^{1.7}$ where k is a constant.

According to table I, the relationship between the peak optical power P_o and the peak electrical power P_{el} can be represented by

$$P_o = 0.96 \times P_{el}^{0.80} \qquad (4)$$

where P_o is in 10^5 W/m and P_{el} is in 10^9 W/m. Jordan et al. [15] have measured that the optical radiation generated by lightning decreases with a factor of two within the first 100 meters of the return stroke. On the other hand, Cooray [14] have calculated that over this length the electrical power in the channel decreases with a factor of three. If we assume that relationship 3 is also valid for lightning then the results obtained by Cooray indicate that the peak optical power decreases by a factor of two over the first 100 meters. This in agreement with the results obtained by Jordan et al.

ENERGY MEASUREMENTS

By integrating the power curve obtained in the measurements mentioned above we get the electrical energy in the channel and the energy emitted as optical radiation (400 - 1100 nm and 777 nm). The results of this investigation is given in table II.

Table II Results of the energy measurements

Current (A)	Electrical energy E_{el} (J/m)	Optical energy $E_{o,400\text{-}1100\ nm}$ (J/m)	Optical energy $E_{o,777\ nm}$ (J/m)
-1157	35	0.68	0.05
-1564	53	1.74	0.12
-1919	78	2.99	0.21
-2214	92	4.52	0.34

The ratio between the electrical energy and the energy going into optical radiation (400 - 1100 nm) is varying from 1.9% to 4.8%. The relationship between the electrical energy and the energy emitted as optical radiation (400 - 1100 nm) is

$$E_o = 9.34\text{x}10^{-4} \text{ x } E_{el}^{1.87} \tag{5}$$

where E_o and E_{el} is in J/m.

According to table II, the relationship between the electrical energy E_{el} and the peak current I_p can be represented by

$$E_{el} = 27 \text{ x } I_p^{1.6} \tag{6}$$

where E_{el} is in J/m and I_p is in kA. This agrees well with calculations done by Cooray [14] for the lightning return stroke. According to these calculations the relationship between the electrical energy E_{el} and the peak current I_p is given by $E_{el} = k \text{ x } I_p^{1.9}$ where k is a constant.

The ratio between the amount of energy going into optical radiation (400 - 1100 nm) and O I(1) is measured to be 7%. In case of lightning, Goodman et al. [2] and Wolfe et al. [16] have observed that 5 - 15% of the total optical energy goes into the O I(1) spectral line. Of course, this percentages may be influenced by the spectral sensitivity of the photodiode.

CONCLUSIONS

The results obtained show that the relationship between peak optical output (at 500 nm, 777 nm, 400 - 1100 nm) and the peak current can be represented by $P_o = k \text{ x } I_p^{1.40}$. The decay time of the optical pulse is increasing with increasing peak current. An increase in the rise time of the current leads to an increase in the rise time of the optical radiation. The relationship between these two parameters will be investigated in the near future. The ratio between the amount of electrical energy in the discharge and the energy emitted as optical radiation (400 - 1100 nm) is measured to be between 1.9 - 4.8%. This ratio have a tendency to increase with increasing electrical energy. The energy associated with the O I(1) spectral line is approximately 7% of the total optical energy (400 - 1100 nm). The relationships between the electrical energy E_{el} and the peak current I_p, the peak electrical power P_{el} and the peak current I_p can be represented by $E_{el} = 27 \text{ x } I_p^{1.6}$ and $P_{el} = 0.65 \text{ x } I_p^{1.75}$

ACKNOWLEDGEMENTS

We would like to thank the Swedish Natural Science Research Council for their financial support, contract number G-GU 2789-303 and E-EG 1448-301.

LIST OF REFERENCES

[1] Hoekstra, R. and Scuka, V., Lightning Flash Detector for Second Generation Meteosat Satellite, *Int. Conf. Atm. El.*, 737-742, 1988

[2] Goodman, S. J., Christian, H. J. and Rust, W. D., A Comparison of the Optical Pulse Characteristics of Intra-Cloud and Cloud-to-Ground Lightning as Observed Above Clouds, *J. Appl. Meteorology*, 1369-1381, 1988

[3] Orville, R .E. and Henderson, R .W, Absolute Spectral Irradiance of Lightning from 375 to 880 nm, *J. Atmos. Sci.*, 41, 21, 3180-3187, 1984

[4] Guo, C. and Krider, E .P, The Optical Power Radiated by Lightning Return Strokes, *J. Geophys. Res.*, 88, C13, 8621-8622, 1983

[5] Guo, C. and Krider, E .P, The Optical and Radiation Field Signatures Produced by Lightning Return Strokes, *J. Geophys. Res.*, 87, C11, 8913-8922, 1982

[6] Krider, E .P., Dawson, G .A. and Uman, M .A., Peak Power and Energy Dissipation in a Single-Stroke Lightning Flash, *J. Geophys. Res.*, 73, 10, 3335-3339, 1968

[7] Baker, L., Gardner, R. L., Paxton, A. H., Baum, C. E. and Rison, W., Simultaneous Measurement of Current, Electromagnetic Fields and Optical Emission from Lightning, Lightning Electromagnetics, edited by Robert L. Gardner, 365-374, 1990

[8] Uman, M .A., Orville, R .E., Sletten A .M. and Krider, E .P, Four-Meter Sparks in Air, *J. Appl. Phys.*, 39, 11, 5162-5168, 1968

[9] Jansson, M., Design, Construction and Calibration of an Optical Instrument for Measuring of Infrared Radiation from Long Laboratory Sparks and Discharges of Lightning, UURIE 225-89, Inst. of High Voltage Research, Uppsala University, 1989

[10] Idone, V. P. and Orville, R. E., Correlated Peak Relative Intensity and Peak Current in Triggered Lightning Subsequent Return Strokes, *J. Geophys. Res.*, D4, 90, 6159-6164, 1985

[11] Lundquist, S, and Scuka, V., Some Time Correlated Measurements of Optical and Electromagnetic Radiation from Lightning Flashes, *Arkiv för Geofysik*, Band 5, Nr. 39, 585-593, 1970

[12] Cooray, V., A Return Stroke Model, *Proceedings of the 1989 International Conference on Lightning and Static Electricity*, 1A.31-1A.39, University of Bath, United Kingdom, September 1989

[13] Cooray, V., Relationship between different return stroke parameters as predicted by a new return stroke model, *Proceedings of the International Conference on Lightning Protection*, 2.11P/1-2.11P/7, Interlaken, Switzerland, September 1990

[14] Cooray, V., Power and Energy Dissipation in Subsequent Return Strokes as Predicted by a New Return Stroke Model, published in this conference

[15] Jordan, D. M., Uman, M .A.,Idone, V. P. and Orville, R. E., Evidence that M-component Propagates Downwards, *Paper presented at the Fall Meeting of the American Geophysical Union, San Fransisco*, 1988

[16] Wolfe, W .L. and Nagler, M., *Conceptual Design of a Spaceborn Lightning Sensor, Contemporary Infrared Sensors an Instruments*, 246, 22-32, 1980

Session 10B, Thursday 10:15
Aerospace Vehicles
Modeling and Coupling Analysis 2
Boulay, Chairman

Modeling Structural Joint Lightning Currents for Direct Effects Evaluation

by J. Carter and J. Sutton

No paper available.

THE EFFECTS OF THE EXHAUST PLUME ON THE LIGHTNING TRIGGERING CONDITIONS FOR LAUNCH VEHICLES

By

Frederick J. Eriksen, Terence H. Rudolph and Rodney A. Perala

Electro Magnetic Applications, Inc.
12567 West Cedar Drive, Suite 250
Lakewood, Colorado 80228-2091
U.S.A.
(303) 980-0070

ABSTRACT

Apollo 12 and Atlas Centaur 67 are two launch vehicles which have experienced triggered lighting strikes. Serious consequences resulted from the events, especially with AC-67, for which the vehicle and payload were lost. These events indicate that it is necessary to develop launch rules which would prevent such occurrences.

In order to develop valid lightning related launch rules, it is necessary to understand the effects of the plume. Some have assumed that the plume can be treated as a perfect conductor, and have computed electric field enhancement factors on that basis. We have looked at the plume, and believe that these models are not correct, because they ignore the fluid motion of the conducting particles. We have developed a model which includes this flow character.

In our model the external field is excluded from the plume as it would be for any good conductor, but in addition the charge must distribute so that the charge density is zero at some location in the exhaust. When this condition is included in the calculation of triggering enhancement factors, they can be 2 to 3 times larger than calculated by other methods which include a conductive plume but don't include the correct boundary conditions.

In our paper we review the relevant features of rocket exhausts for the triggered lighting problem, present an approach for including flowing conductive gases, and present preliminary calculations to demonstrate the effect that the plume has on enhancement factors.

1.0 INTRODUCTION

Rocket exhausts are of interest electromagnetically in several areas. They have the potential of altering the coupling of high frequency fields to rockets [1-3]. The exhaust is also of interest in the development of advanced weapons. The plume will attenuate and scatter laser light or high power microwave energy for example. Another area of interest is the radar reflectivity of the plume, for which both measurements and calculations have been performed [4-6].

Regarding the effect of exhaust conductivity on the local electric fields around a rocket during ascent through a thunderstorm region, there is less work. Some of the first work on enhancement factors was performed by Kasemir [7]. Perala et al., [8] have included the plume in calculations of triggered lightning threshold electric fields in the analysis of the Atlas Centaur AC-67 failure. Other work in this area has been done by Krider et al. [9] who made measurements of the optical emissions of a Saturn V plume and inferred the electrical conductivity.

The temporal conditions in the triggered lightning case are somewhat different from other rocket/plume electromagnetic problems because the external field in this case changes slowly, on the time scale of 1-10 sec, and in other cases the time scale of the external fields is relatively short (microseconds or nanoseconds). When the time scale is long, the velocities of the rocket and the exhaust gases become important. The objective of the work reported here is to suggest a model which can be used to determine the electric field enhancement factor of a rocket exhaust system.

In this paper we describe the significant features of the rocket exhaust, its chemistry, and how the exhaust responds to a dc or slowly varying electric field environment such as occurs in a thunderstorm. We then describe a model which can be used to obtain the triggering conditions on a rocket.

2.0 GENERAL DESCRIPTION OF THE ROCKET EXHAUST

Figure 1 is a schematic diagram showing three regions of the exhaust material expelled by the rocket motor. The three areas of the exhaust that have been identified are denoted by the terms plume, corona, and trail. The term 'exhaust', will denote everything that leaves the rocket, i.e., the combination of the plume, the corona, and the trail. Because the scope of this work is limited to the triggering of lightning and this occurs at altitudes below 20 km, consideration has been given only to the exhaust structure in the lower atmosphere (< 20 km).

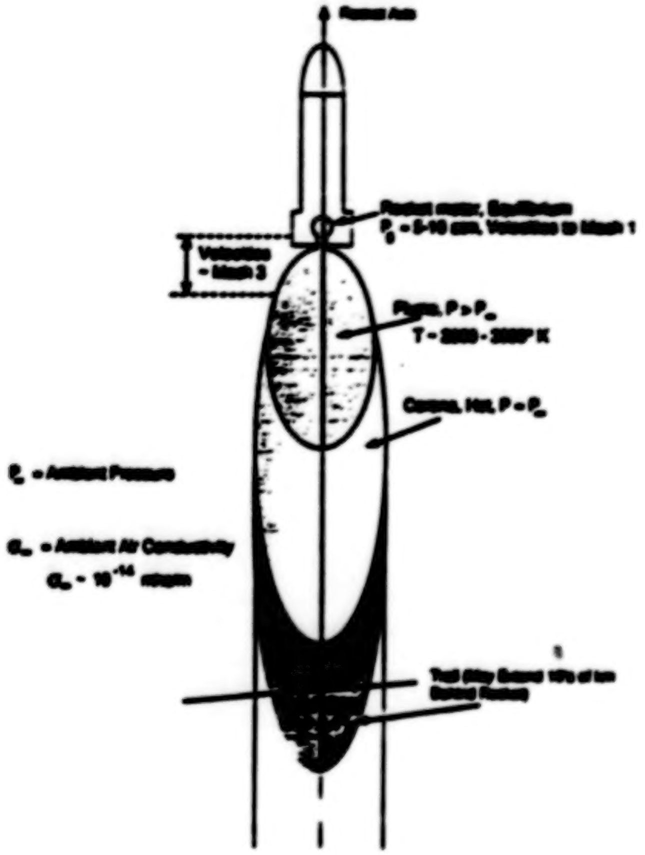
Rocket Axis
Rocket motor, Equilibrium
P_0 = 5-10 atm, Velocities to Mach 1
Velocities ~ Mach 3
Plume, $P > P_\infty$
T ~ 2000 - 2500° K
Corona, Hot, $P = P_\infty$
P_∞ = Ambient Pressure
σ_∞ = Ambient Air Conductivity
$\sigma_\infty \sim 10^{-14}$ mhos/m
Trail (May Extend 10's of km
Behind Rocket)

Figure 1 General Features of a Generic Rocket Exhaust (No External Fields)

The plume is the region where the temperature is the highest and where there is a strong blackbody luminosity in the visible regime [9]. The high temperature is due in part to afterburning (CO and H_2 with O_2 in the Saturn V, [9]) . It is usually one to two times the size of the rocket, and has the largest conductivity [1]. The pressure in this region varies from several atmospheres near the nozzle to nearly ambient pressure at the downstream end of the plume. The flow of gas at the outer edge of the plume is very turbulent.

Gases in the corona are cooler than in the plume but still substantially hotter than the surrounding air. The pressure in the corona is probably within a factor of two of the surrounding air. Some optical emissions still occur, but there is no visible blackbody radiation, only line radiation [9].

The region denoted trail has remnant chemical species of the motor, and may contain a large amount of other material (now condensed) that is expelled by the rocket motor. This region is cool, and is at nearly ambient temperature.

The ambient air around the exhaust has a pressure (denoted P_{inf}) that depends on the altitude of the rocket and the atmospheric conditions. The conductivity of the ambient air, σ_{inf}, is taken to be 10^{-14} mhos/m.

On an atomic scale, the plume contains predominantly neutral atomic and molecular species, but more importantly it contains free ions of both charge states and free electrons. The density of positive and negative ions is about equal, and the density of the electrons is about 1/1000 of the ions. The charged species stream out of the rocket nozzle with a fluid velocity that can be on the order of 1000 m/s. In the absence of external electric or magnetic fields, the regions of the plume, corona and trail are electrically neutral: there is no net charge and no net current density. At the downstream end of the plume, and at the beginning of the corona, the gas cools rapidly and recombination processes drastically reduce the number of free charges, and hence the conductivity.

From the point of view of calculating threshold fields for triggering of lightning, the most significant region is the plume because it has the largest conductivity. Typically the maximum conductivity is 0.1 to 1.0 mhos/m in the hottest part of the plume and falls rapidly to 10^{-5} mhos/m or less at the downstream edge of the plume. The time constant (ε_o/s) in the most conductive part of the plume is very small, ~0.1 nsec. In the cooler, less conducting parts of the corona, the time constant is still fairly short, 1 µsec or less. The conductivity of the surrounding air is on the order of 10^{-14} mhos/m with a time constant of 1000 sec or so.

Because of their low conductivity, the parts of the corona near the trail, and the entire trail have little effect on the triggering electrostatic fields of the rocket, and so are not explicitly included in this analysis. They may however affect the location of the eventual lightning channel if a strike occurs. For example, the particulate matter in the trail could enhance the formation of a leader channel, and so cause the main channel to develop in the exhaust path or partly in the exhaust path.

3.0 PHYSICAL MODELING OF PLUME ELECTRICAL PROPERTIES

One of the most extensive pieces of work on the electrical properties of plumes was done by Nordgard and Smith [1] and Smith et al. [2]. Their objective was to determine the effect of the plume on the VHF field response of a REDEYE rocket. They performed calculations of the coupling of the fields to the rocket, reported data on the conductivity of the plume from results of several large computer codes, constructed a full scale static model of the rocket and the plume, and performed electrical measurements of the coupling of sinusoidal fields to the static model, with and without the plume.

One of the important results of the Nordgard and Smith work is the conductivity as a function of position in the plume for the Redeye rocket. This rocket is a small tactical rocket (~2 m long, ~10 cm in diameter) with a solid fuel propellant. Figure 2 shows a plot of the maximum conductivity as a function of the axial position. Figure 3 shows a contour plot of the conductivity as a function of the axial and radial positions normalized to the rocket length and nozzle diameter, respectively.

The data presented in Figures 2 and 3 are calculated data. The code that was used to determine this data was the Low Altitude Plume Program (LAPP). Note that the conductivity in Figure 2 falls by four orders of magnitude in about five rocket lengths.

The results showed that the plume did not have a large effect on the coupling of VHF radiation to the rocket. Measurements made of the coupled signals to a wire in a small aperture forward in the rocket were compared to the coupled signals determined analytically. The measured signals were smaller than the theoretically predicted signals, and in both cases the coupled energy was not changed a great deal by the plume. The difference in the coupled energy between plume and no plume conditions was about 2-3 dB.

Note that the modeling done by Nordgard and Smith does not treat the fluid velocity of the plume, but instead takes the point of view that the conductive part of the plume behaves like a stationary conductor. This is appropriate because the time scale of the VHF radiation, < 1 microsec, is short compared to the travel time of particles in the plume (~10 msec).

Also Nordgard and Smith assumed a perfectly conducting connection between the plume and the rocket. This might not be the real circumstance. Their reasoning for this choice was that the perfect connection would give the worst case difference in the VHF coupling.

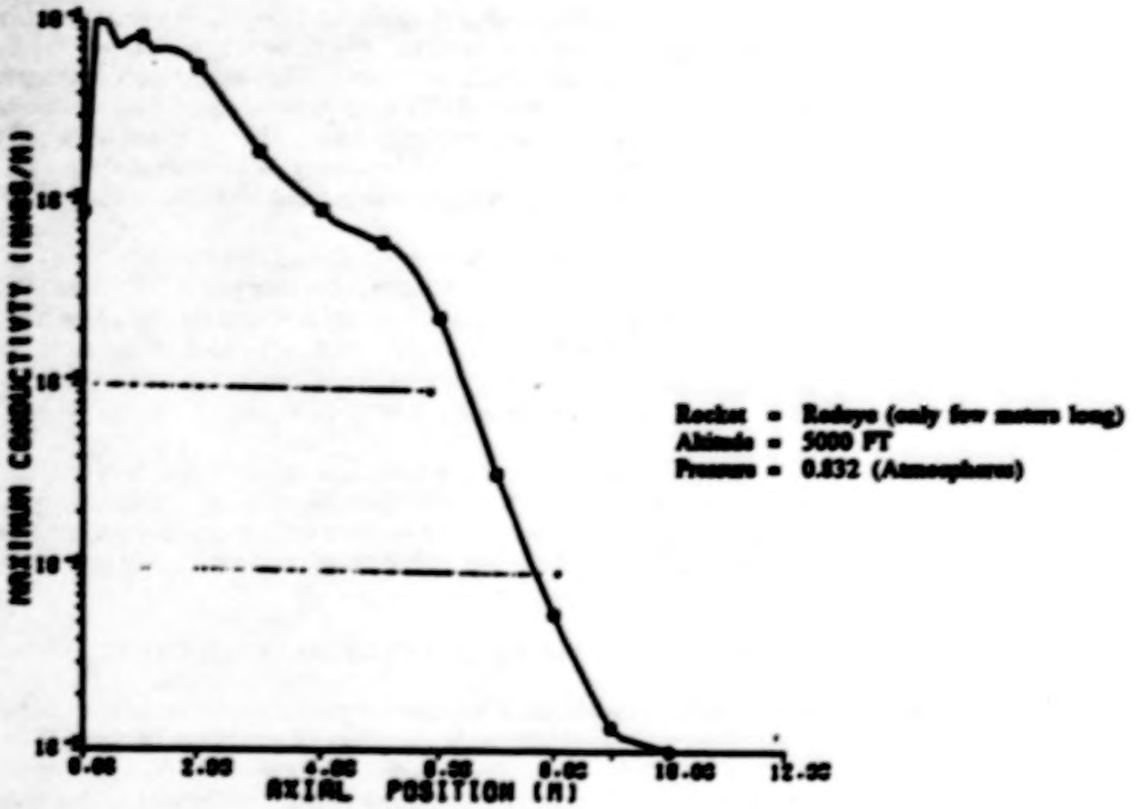

Figure 2 Maximum Conductivity as a Function of Axial Position for the REDEYE Rocket from the LAPP Code [1]

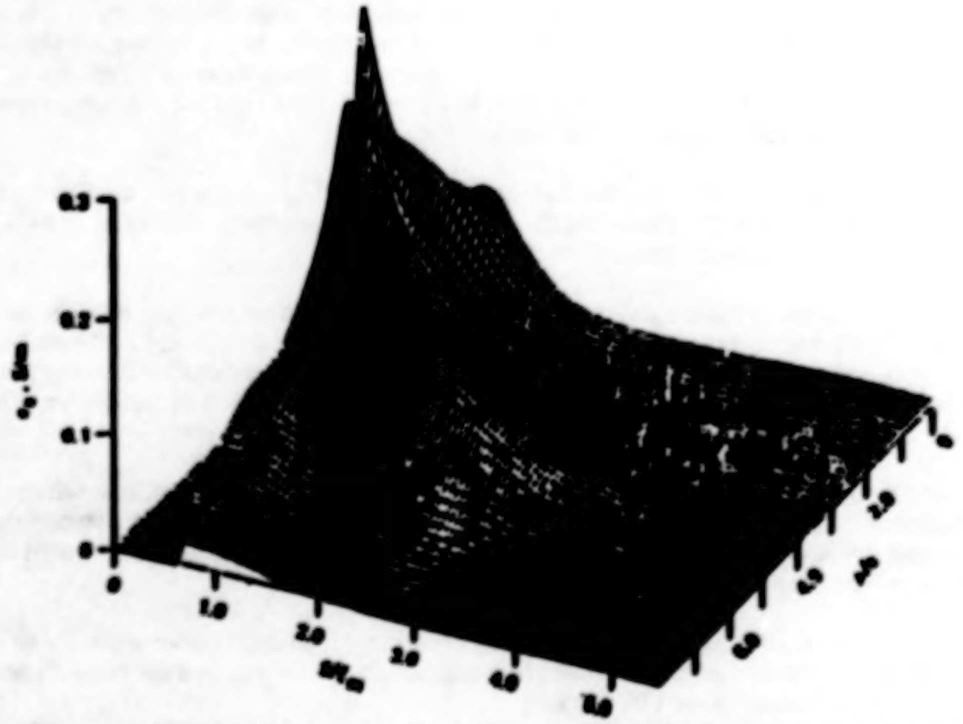

Figure 3 Effective Electron Conductivity as a Function of Normalized Axial and Radial Positions. Axial Position Normalized to Rocket Length and Radial Position Normalized to Nozzle Radius [2]

4.0 PLUME CHEMISTRY

The chemical composition of the exhaust gases has a large effect on the plume conductivity. The propellant for the Space Shuttle Main Engine (SSME) is LOX and H_2, and (except for unintentional impurities) there will be very few metal atoms naturally in the plasma. In practice though, some alkali metal atoms do appear in the exhaust [10] and they will impact the electron concentration. Impurity species are being used, for example, as the basis for a diagnostic tool to monitor the health of the engine. The Saturn V first stage (S-1C) is also a liquid propellant rocket but with LOX and kerosene as the fuel.

Solid rockets can have a larger proportion of metal ions in the exhaust and the plume might therefore have a higher conductivity. For example the shuttle SRB propellant has a large proportion of aluminum (as a propellant filler and in the propellant itself) and this Al is in relatively large proportion in the exhaust. The exhaust analyzed by Nordgard and Smith [1-3] was from a solid rocket also, although Al was not in the propellant.

The temperature and chemical composition varies throughout the exhaust. In the nozzle region the temperature and pressure are lower than in the motor chamber or in the plume. Because of the reduced temperature in the nozzle region, the conductivity there is also reduced. The temperature in the plume can be quite high (~2500° K for the Saturn V [9]) because of afterburning, and it is in the plume that the largest conductivity occurs. In the Saturn V, afterburning is the result of CO and H_2 ignition with ambient O_2.

There are a number of large computer codes which endeavor to calculate exhaust gas properties such as chemical composition, ion density, temperature, pressure and flow velocity. For the present purposes, the important parameters are the density of charged species and the collision frequency which enable a calculation of the conductivity. Among the various codes, the Low Altitude Plume Program (LAPP), the Rocket Exhaust Program (REP), the Naval Weapons Center (NWC) code, and the JANAAF Standard Plume Flowfield (SPF) code are ones that we know have been applied to the solution of electromagnetic problems. The codes take into account (to various degrees) the fluid dynamics and chemical reactions that occur in the plume.

A key feature of the exhaust is the variation in conductivity at the downstream end of the plume, and in particular the distance from the nozzle to the location where the conductivity gets below 10^{-5} to 10^{-6} mhos/m.

5.0 ELECTROMAGNETIC MODEL OF EXHAUST

The goal here is to develop a model that will enable the effect of the plume on electric field enhancement factors to be calculated. To calculate this directly, one needs to understand in detail the processes within the plume; this includes the dynamical balance between the electric field forces, the chemical reactions that are taking place which change the number of free charge carriers, and the fluid flow which is changing the speed and temperature of the plasma. The equations governing this problem are complicated and include the Navier-Stokes equations for the compressible fluid flow, Maxwell's equations for the electromagnetic phenomena, and the Boltzmann equation with chemical rate equations to account for the thermal and chemical distribution of ion, atomic and molecular species.

Some simplification in these coupled equations is possible. Applied electric fields of 100 kV/m or less do not change the flow profile (there are mostly neutral species in the exhaust), and the applied fields do not affect the temperature significantly. Therefore, the fluid flow and chemistry/thermodynamics are to first order independent of the electromagnetics. The remainder of this section will describe some general characteristics of the model and then some details of the charge distribution predicted by the model when the rocket/plume is placed in an external field.

5.1 GENERAL FEATURES

The velocity of the exhaust gases plays an important role in determining how the plume reacts to an external field. On the average the fluid velocity of the gas atoms and ions in the plume is much larger (as large as 2-3 x 10^3 m/s) than any drift velocity induced by an external electric field. For this reason the flow is always away from the rocket motor. Thus charge builds up on parts of the rocket/plume when there is a differential flow rate between the positive and negative charges.

The temperature in the plume is about 2500° K so the thermal velocity of electrons is about 10^5 m/s. The density of neutral atoms and molecules is about 7×10^{25} m^{-3}. The fluid velocity is 2-3 x 10^3 m/s. So the mean time between collisions (< 1 ns) of the electrons with the surrounding atoms/molecules is shorter than the flight time of a particle through the plume (millisecs), and the Drude model of conductivity with a collision frequency can be used to describe the conducting plume.

There are roughly equal positive and negative ion densities in the plume, and about 1/1000 this density of free electrons. But the mobilities of the ions are about 1000 times smaller than the electrons so the three charged species carry about equal currents under the influence of an external field. The total conductivity is therefore about three times the electron conductivity and the plume will be viewed as being composed of three conducting species.

The results of calculations of Nordgard and Smith using LAPP will be used for the exhaust physical size and conductivity. It is convenient to discuss the plume axial dimensions scaled to the length of the rocket. The conductivity in the model is three times the electron conductivity given in Figure 3, and the coordinates for any solid propellant rocket will be interpreted with the appropriate scale factors l_{rocket} and d_{noz} which are the length of the rocket and the diameter of the rocket nozzle, respectively.

5.2 RESPONSE TO EXTERNAL ELECTRIC FIELDS

To show the effect of the exhaust on the field enhancement of the rocket in an atmospheric external electric field, it is necessary to have a model of how the charge in the plume reacts to the external field. As discussed previously, the motion of the charge carriers and the fact that there are chemical and physical scattering processes occurring in the plume make the interpretation complicated, and a calculation from first principles is difficult. The effect has been interpreted simply in terms of acceleration or deceleration of individual streams of charged particles and there should be an approximate solution that will represent the steady state. It will be required that:

1. The E-field inside the plume (and probably part of the corona) is zero, and,
2. Charges that would tend build up at the bottom of the E=0 region in the absence of the plasma flow will stay with the plasma and move in the trail downstream away from the rocket.

Consider a one dimensional (in the key spatial range) model of the exhaust which includes an exponential variation in conductivity. This variation is not too different from the axial dependence found by Smith and Nordgard [1]. The exhaust will be exposed to a step increase in uniform field, and suppose for the moment that the fluid velocity is very small. Figure 4 shows the physical geometry.

When the external field changes, a volume distribution of positive charge is generated inside the material which has a peak whose position is time dependent. The peak moves downstream in the exhaust toward smaller conductivity. This model gives a picture for how the charge distributes in the exhaust of the rocket for some rapid change in the external field.

Figures 5 shows the sequence of peaks in the volume distribution of charge in this static model. In the real rocket exhaust, the charge will be swept away at some point downstream.

Occurring simultaneously with this charge build up, there is a fluid flow. There is a critical position z_{crit} beyond which the charges will be swept downstream. Therefore, in steady state, the field distribution around the rocket is qualitatively like Figure 6. The total field (E_{tot}) is zero in the plume up to some distance z_{crit} and the field rises again to E_o downstream of z_{crit}. The field changes back to E_o in some distance Δ. The charges at z_{crit} are no longer able to adjust their position in the plume to keep up with the rocket motion and are swept downstream. The condition defining z_{crit} in the steady state is that the relaxation time at z_{crit} be equal to the time (roughly Δ/V_{rocket}) necessary to maintain the spatial field distribution; therefore z_{crit} is defined by

$$\frac{\varepsilon_0}{\sigma(z_{crit})} = \frac{\Delta(z_{crit})}{V_{rocket}} \tag{1}$$

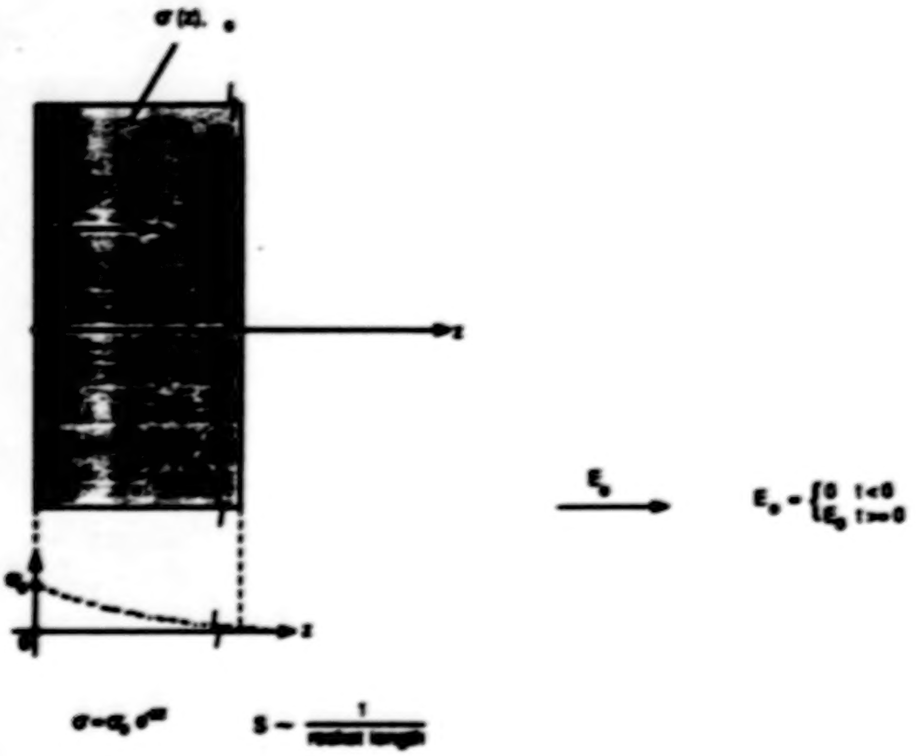
σ(z), ε
z
E_0
$E_0 = \begin{cases} 0 & t<0 \\ E_0 & t>=0 \end{cases}$
σ_0
0
l
z
$\sigma = \sigma_0 e^{-\delta z}$
$S \sim \frac{1}{\text{radial length}}$

Figure 4 Example of a Semi-Infinite Material With Varying Conductivity σ (z) Like a Typical Rocket Exhaust, Without Flow

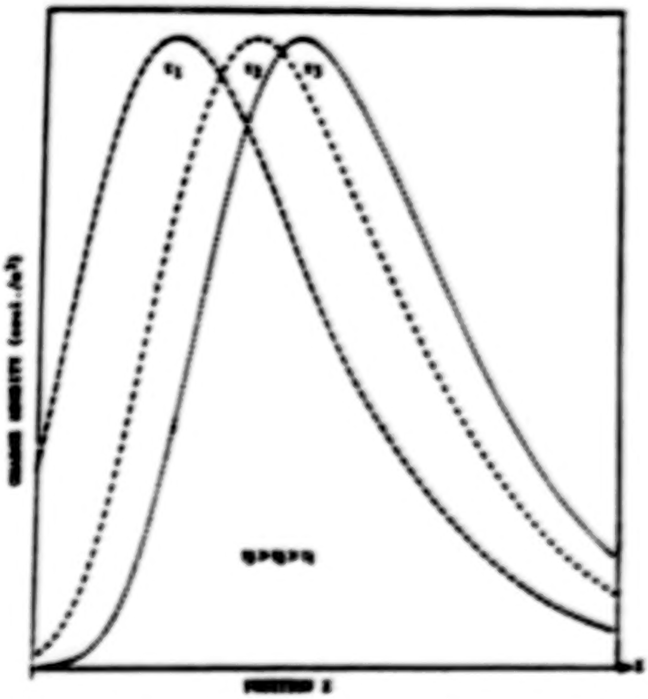

Figure 5 Qualitative Dependence of the Peaks in the Charge Distribution of a One Dimensional Varying Conductivity

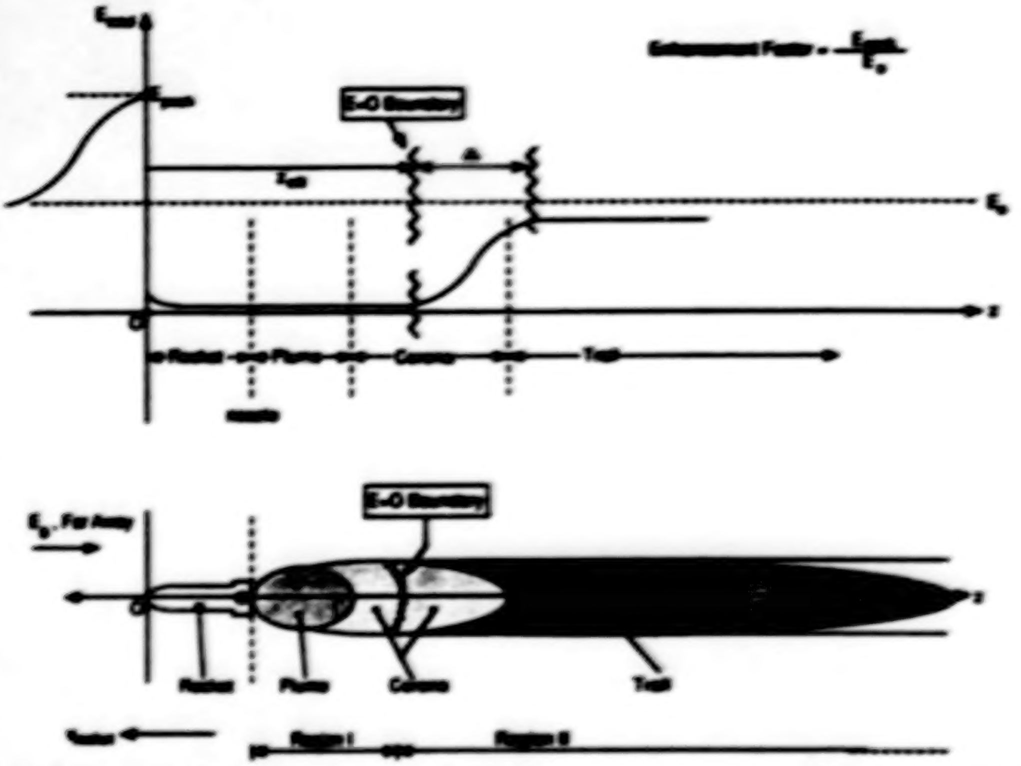

Figure 6 Qualitative Representation of Fields/Charges Around a Rocket System in an External Field

The functional dependence of σ can be obtained from code calculations or possibly measurements. Note that Δ depends on z_{crit} so Eq. 1 must be solved implicitly for the parameter z_{crit}. Therefore the size of Region I (E = 0) defined in Figure 6 behind the rocket is dependent on rocket velocity, and the faster the rocket moves, the smaller z_{crit} is. Δ is a slowly varying function of z_{crit}. Note that if Δ is on the order of a rocket dimension (60 m for the Saturn V), then σ is

$$\sigma\,(z_{crit}) = \frac{\varepsilon_0 V_{rocket}}{\Delta(z_{crit})} = \frac{8.8 \times 10^{-12} \times 1000}{60} = 10^{-10}\,\frac{\text{mhos}}{\text{m}} \quad . \tag{2}$$

This is a very small conductivity and its position is almost certainly out of the plume and in the hottest part of the corona. This corresponds to an effective electrical size of the exhaust which is bigger than one would expect on the basis of higher frequency scattering processes.

Figure 7 shows a schematic representation of the positions of a rocket during launch. At launch and during the time the plume is still in contact with the ground (t_1), negative polarization charge accumulates on the rocket. As the rocket rises, it encounters changing E-fields, and the polarization charge changes. The E-field may change because the rocket gets nearer to the atmospheric sources or because the sources are changing.

Suppose the field is increasing at the site of the rocket, then as the polarization charge grows to keep E=0 in Region I, negative charge will increase on the rocket and positive charge will be left behind in the trail. In principle, the fields near the rocket need to be calculated in a time varying environment. For example, the charge left in the trail will be moving downstream and it will have a time varying effect on the enhancement factor. It is assumed that the time variation effects are small so a steady state condition exists.

This picture for the charge distribution in the exhaust with an external field allows an equivalent electrostatics problem to be developed to calculate the rocket-exhaust field enhancement factor. The equivalent problem ignores the actual time dependence of the fields, and it assumes that the charge left in the trail doesn't affect the fields around the rocket very much. The prescription for setting up and solving the equivalent problem is as follows:

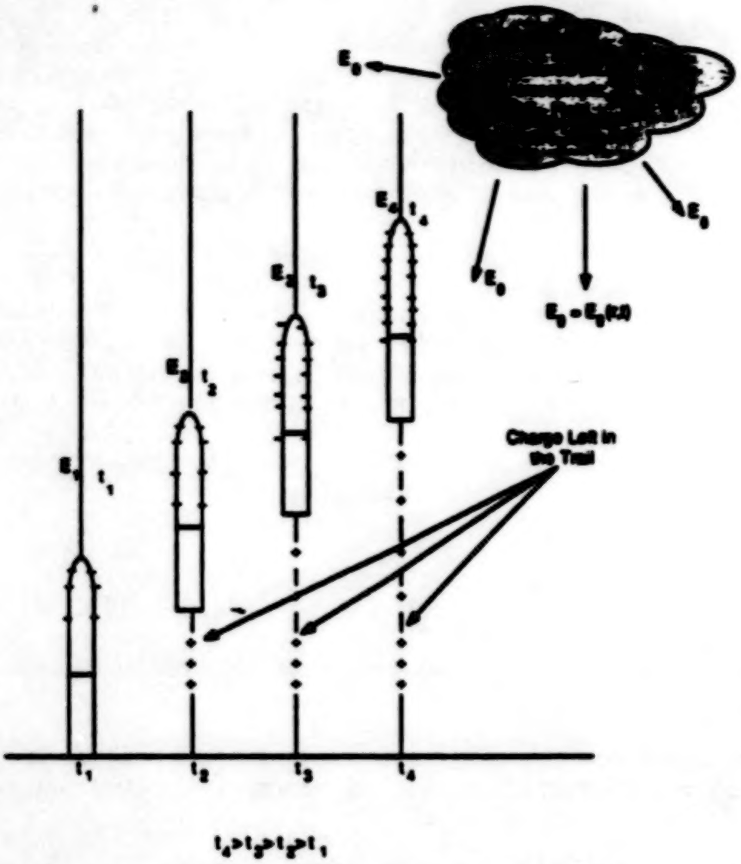

Figure 7 Schematic Diagram of Charge/Field Build-Up as Rocket Ascends

1. Choose a speed for the rocket. Take the parameter Δ_{hyp} to be 1.5 rocket lengths, and calculate the σ_{crit}.
2. From the conductivity as a function of position calculated from a code or by measurement, determine the parameter z_{crit} and the size of Region I.
3. Solve for the electric field around a perfect conductor C whose size and physical shape are identical to the rocket plus Region I. Use the following boundary conditions:
   a. The surface of the conductor C is an equipotential
   b. The charge density at the most downstream point of the conductor C is zero (E=0 at this point)

4. Find the field as a function of position on the cylindrical axis from the critical point (z_{crit}) downward. Estimate Δ from the field variation, i.e. from the 10% to 90% values of E(z).
5. If Δ differs from the initial Δ_{hyp} by more than x %, change Δ_{hyp} accordingly in step (1). Use the new Δ_{hyp} and repeat steps (1), (2), (3) and (4). x determines the accuracy of the solution.
6. If Δ is consistent with the original Δ_{hyp}, then use the fields around the rocket to get the enhancement factor.

The equivalent problem used to model the exhaust differs conceptually only slightly from the previous model developed by Perala and Rudolph [8], although the added size of Region I can make a substantial difference in the numerical value of the enhancement factor. The difference is caused by the location of the 'zero charge' boundary condition. In the previous model the condition was imposed at the bottom of the rocket, i.e., at the nozzle. In the current model it is imposed at a position that is at the end of Region I.

There is a complication introduced here because the end of Region I is not easy to define. The critical distance z_{crit} must be calculated using Eq. 1. The result will be that the exhaust has more of an effect on the enhancement factor than previously calculated. If z_{crit} is large, i.e., several rocket lengths, then the enhancement factor may be increased by factors of 2 or 3 over those calculated with the old boundary condition.

There is an interesting property of this model that was recognized by Perala and Rudolph [85] which has to do with the effect of charging the rocket. Regardless of the charging process (precipitation, dust, triboelectrification, or plume charging), the boundary condition E = 0 (step 3b above) will cause the charge distribution on the rocket to be the same (provided there is a sufficiently large charge source) as would occur in the polarization case/external E-field. Therefore the one model addresses all rocket charging effects.

6.0 SUMMARY

There has been a distinct evolution of the model for taking into account the rocket exhaust. Early work by Kasemir [7] and Perala and Rudolph [85] had the size of the equivalent conductor only as big as the rocket. Other work by Krider et al. [9] had the equivalent conductor large enough but didn't recognize the effect of the fluid flow on the downstream boundary condition. The present model takes into account all the exhaust effects.

In order to illustrate the importance of the plume model we have calculated the ambient triggering field for an SRB-like rocket by itself for different plume assumptions [11]:

• Rocket/No Plume:	50 KV/m
• Rocket and Perfectly Conducting Plume:	31 KV/m
• Rocket Plume with a Zero Net Charge Boundary Condition:	15 KV/m

The results show a factor of 3 variation indicating a substantial need to understand how the plume affects the triggering conditions.

Because the issue of how the plume behaves in an electric field is so important to field enhancements and the prediction of triggered lightning, it is vital that both theoretical and experimental confirmation of the new plume electrical model be obtained.

7.0 REFERENCES

1. Nordgard, J. D. and G. S. Smith, "A Plasma Model of Missile Exhaust Plumes", RADC-TR-77-144, Griffiss Air Force Base, NY, April 1977.
2. Smith, G. S., J. D. Nordgard, W. A. Holm, and H. L. Bassett, "Electromagnetic Simulation of Missile Exhaust Plumes, Construction and Testing of a Physical Plume Simulator and the Predicted Results of a Theoretical 'Thin Wire' Rocket/Plume Model", RADC-TR-81-8, Griffiss Air Force Base, NY, March 1981.
3. Smith, G. S., J. D. Nordgard and J. Edwards, "The Alteration of the Surface Current on a Missile by the Presence of an Exhaust Plume," IEEE Trans. EMC, 19-30, November 1977.
4. Draper, J.S. and R.F. Sperlein, "Analysis of Radar Returns from a Rocket Plume," AIAA Journal, Vol. 18, June 1980, p. 712-713.
5. Balwanz, W.W., "Rocket Exhausts and Their Interaction with Electromagnetic Waves," in "Fluid Dynamic Aspects of Space Flight," Proceedings of the AGARD-NATO Specialists Meeting, Marseille, France, April 1964.
6. Albrecht, G.H., "A Comparison of RF Energy Absorption Made Statically and in Rocket Flight on the Exhaust from a Certain Solid Propellant," Proceedings of the AGARD-NATO Specialists Meeting, Marseille, France, April 1964, p. 331.
7. Kasemir, H.W., "Basic Theory and Pilot Experiments to the Problem of Triggering Lightning Discharges by Rockets," NOAA Technical Memorandum, ERL APCL-12, Boulder, Colorado, April 1971.
8. Perala, R. A., R. S. Collier, and T. Rudolph, "An Analysis of Atlas-Centaur Triggered Lightning Conditions," EMA-87-R-49, Denver, CO, May 1987.
9. Krider, E. P., R. C. Noggle, M. A. Uman, and R. E. Orville, "Lightning and the Apollo 17/Saturn V Exhaust Plume", Jour. of Spacecraft and Rockets, Vol 11, no 2, 72-75, February 1974.
10. Price, M. L., E. B. Mann, W. M. Druen, W. R. Zimmerman, C. J. Rives, and R. W. McCullough, "EMP/Plume Coupling of Sprint Motors," EMA-84-R-44, Huntsville, AL, June 1984.
11. Perala, R.A., T. Rudolph, F.J. Eriksen, M. C. Erie and G.J. Rigden, "Investigation of the Triggering of Lightning by Launch Vehicles During Ascent," EMA-89-R-61, August 1989.

POWER AND ENERGY DISSIPATION IN SUBSEQUENT RETURN STROKES AS PREDICTED BY A NEW RETURN STROKE MODEL

Vernon Cooray
Institute of High Voltage Research
(A department at Uppsala University)
Uppsala, Sweden

ABSTRACT

Recently, Cooray [1] introduced a new return stroke model which is capable of predicting the temporal behaviour of the return stroke current and the return stroke velocity as a function of height along the return stroke channel. We have employed this model to calculate the power and energy dissipation in subsequent return strokes. The results of these calculations are presented in this paper. The main conclusions of this paper are the following. (a) A large fraction of the total energy available for the dart leader-subsequent stroke process is dissipated in the dart leader stage. (b) The peak power per unit length dissipated in a subsequent stroke channel element decreases with increasing height of that channel element from ground level. For a given channel element the peak power dissipation increases with increasing current in that channel element. (c) The peak electrical power dissipation in a typical subsequent return stroke is about 1.5×10^{11} W. (d) The energy dissipation in a subsequent stroke increases with increasing current in the return stroke channel and for a typical subsequent stroke the energy dissipation per unit length is about 5.0×10^3 J/m.

INTRODUCTION

Recently Cooray [1] introduced a new return stroke model which is capable of predicting the temporal behaviour of the return stroke current and the return stroke velocity as a function of height along the return stroke channel. The basic concepts used in this return stroke model are the following. The dart leader current travels along the central core of the channel depositing charge along the channel. Due to the high lateral field, this charge expands outward giving rise to a corona sheath. At the point of contact with ground all the charge is concentrated on the central core and, due to the development of the corona sheath, the charge on the core decreases rapidly upwards. As the return stroke propagates up, the charge on the central core and corona sheath discharge into the channel. This gives rise to current components which subsequently travel along the highly conducting return stroke channel to ground. The total current at any height is due to the sum of sheath current and core current from levels above that height. The amplitude of the core current decreases rapidly upwards and the duration of the sheath current is assumed to be equal to the time for the streamers to propagate into the space charge region. The velocity of the return stroke along the channel is calculated as a function of current parameters and channel temperature. Most of the predictions of this model concerning the radiated electromagnetic fields and the variation of return stroke velocity, current risetime, peak current amplitude, and peak current derivative along the return stroke channel are substantiated by recent experimental observations.

In the study reported in this paper we have employed this return stroke model to calculate the power and energy dissipation during subsequent return strokes. First, from the charge and current distribution along the return stroke channel the electric field inside the channel as a function of time is calculated. This was combined with the current waveform along the channel to calculate the power and energy dissipation during subsequent return strokes. In this paper we will present results to show how the power dissipation along the channel is changing as a function of height from ground level and the variation of power and energy dissipation as a function of peak current at ground level.

POWER DISSIPATION ALONG THE CHANNEL

The current in the return stroke channel at a point situated 10 m from ground level is shown in figure 1(a). The current waveform rises to it's peak value, which is about 10 kA, in about 0.3 μs. The axial electric field, caused by the current and charge distribution along the return stroke channel, in the same channel element as a function of time is shown in figure 1(b). The method of calculation of the axial field in the channel element is similar to that described by Cooray et al. [2]. In calculating this axial field the radius of the return stroke channel was assumed to be 0.001 m. The value of 0.001 m may be a good approximation for the radius of the return stroke channel at the initial stages of the discharge but at later times the channel radius may be of the order of 0.01 m. Note that the electric field in the channel has a peak value of about 3.5×10^5 V/m and it decreases to 4×10^3 V/m in about 3.0 μs. This low value of the electric field is probably associated with the arc phase of the discharge. For example, an arc channel in air with a current of 10 kA has a electric field in the range of about 10^3 V/m [3]. Our calculations show that the resistance of the channel decreases with time reaching a minimum value of 0.5 ohm/m in about 3.0 microsecond.

The power dissipation in the channel element as a function of time is shown in figure 1(c). Note that the peak power dissipation in this channel element is about 2.0×10^9 W/m. After the initial peak the power decreases to about 5×10^7 W/m. Our calculations show that the return stroke can maintain this low level of power dissipation for several tens of microseconds. This low level of power dissipation is probably associated with the arc phase of the discharge. A similar procedure can be applied to calculate the power dissipation in channel elements situated at different heights along the channel. For example figure 2 shows the power dissipation, as a function of time, in channel elements situated at 10 m, 100 m and 500 m from ground level. Note that the width of the of the initial peak in the power curve increases and the peak power decreases with increasing height from ground level. The peak power generated by channel elements as a function of their height from ground level is shown in figure 3 for three peak values of current, i.e. 10 kA, 20 kA, and 30 kA , at ground level. Note that over the first 100 m from ground the peak power dissipation in channel elements decreases by almost a factor of three. This decrease in peak power is caused by the decrease in current amplitude and the increase in current risetime with increasing height from ground level.

As can be seen from the data in figure 3, the peak power dissipation in a channel element at a given height increases with increasing peak value of the current amplitude at ground level. The relationship between these two parameters for a channel element at ground level is shown in figure 4. This relationship can be represented approximately by the formula

$$Pp = 4.0\times10^{7}\ Ip^{1.7} \qquad (1)$$

where Ip is the peak current in kA at ground level and Pp is the peak power in W/m generated by the channel element. The relationship given in (1) is drawn in figure 4 by a dashed line. Of course it is possible that the relationship between these two quantities is not the same at other heights along the channel since the shape of the current and the velocity of the return stroke is changing along the channel.

The data given above correspond to the power dissipation in a single channel element situated at a given point along the channel. However, the return stroke is composed of large number of channel elements and the number of channel elements contributing to the power dissipation increases with increasing time due to the geometrical growth of the return stroke channel. Therefore, the total power dissipation in the return stroke is a function of the geometrical growth of the return stroke channel and the time development of the power in each individual segment of the channel. The total power dissipation in the return stroke channel as a function of time for a 10 kA current at ground level is shown in figure 5. The peak power dissipation in this return stroke is about 9×10^{10} W. Note that the power reaches its peak value in about 7.5 µs and our calculations show that the height of the return stroke channel when the power reaches its peak value is about 1 km. Figure 6 shows the variation of peak power dissipation in return strokes as a function of peak current. Again observe that the peak power dissipation in subsequent return strokes increases with increasing peak current.

ENERGY DISSIPATION IN RETURN STROKES

The temporal variation of the power dissipation can be integrated to calculate the energy dissipation along the return stroke channel as a function of time. Figure 7 shows the energy dissipation, as a function of time, in a channel element situated at 10 m from ground level. Note that the energy dissipation along in the channel element increases rapidly initially which is followed by a slow increase. The peak energy dissipation in the channel element (not shown in the diagram) is about 4.0×10^3 J/m. We have also calculated the energy dissipation in channel elements close to ground as a function of peak return stroke current. The results are shown in figure 8. Note that the energy dissipation in the return stroke channel increases with peak current . For a 30 kA peak current the energy dissipation in the return stroke channel is about 2.8×10^4 J/m and for a 50 kA current it is about 8.0×10^4 J/m. The relationship between the total energy dissipation, per unit length, in channel elements close to ground and the peak current at ground level can be represented approximately by the formula

$$E = 43.2 I_p^{1.9} \qquad (2)$$

where E is the total energy, in J/m, dissipated in the channel and I_p is the peak current, in kA, in the channel.This formula is depicted in figure 8 by a dashed line.Note that the energy dissipation in the return stroke channel increases approximately as the square of the peak current.

DISTRIBUTION OF POWER AND ENERGY DISSIPATION IN SUBSEQUENT RETURN STROKES

As we have shown above the energy and the power that will dissipate in a return stroke depend on the peak current in the return stroke channel. On the other hand as shown by Cooray [4] the return stroke model predicts an approximate linear relationship between the peak return stroke current and the peak return stroke radiation field. Therefore, if the distribution of peak radiation fields generated by subsequent return strokes are known, the relationships given in the earlier section can be used to obtain the distribution of power and energy dissipation in subsequent return strokes. The best data set available at present on the distribution of peak radiation fields from subsequent strokes was obtained by Master et al. [5]. We have used this distribution to calculate the distribution of energy and power dissipation in return strokes. The results are shown in figure 9(a) and 9(b). Note that the 50% values of the energy and power dissipation in subsequent return strokes are 5.0×10^{3} J/m and 1.5×10^{11} W/m respectively.

DISCUSSION

Several theoretical simulations of the energy dissipation in lightning return strokes have been made by several researchers [6,7,8,9,10]. In an investigation conducted by Hill [6] power and energy dissipation due to a 21 kA current was estimated. The risetime of the current waveform was 8.5 μs. The peak power dissipation in the channel was calculated to be 1.5×10^{9} W/m and the total energy dissipation in the channel was estimated to be about 1.5×10^{4} J/m. Plooster [7] estimated that a 20 kA current with a 5 μs risetime will dissipate about 2.5×10^{3} J/m of energy in the return stroke channel. More recently Paxton et al.[10] estimated that a 20 kA return stroke current with a 5 μs risetime will dissipate about 4.0×10^{3} J/m of energy in the return stroke channel. Our analysis show that the peak power dissipation in return strokes depends on the risetime of the current waveform. The results in figure 3 show that the peak power dissipation in a return stroke channel element close to ground with a 20 kA peak current is about 7×10^{9} W/m. Furthermore, the risetime of the current waveform close to ground level is about 0.3μs. However, the risetime of the current waveform increases with height and at heights of about 500m from ground level the risetime of the current waveform is about 5 μs. Calculations show that the peak power dissipation caused by a 21 kA current at this level is about 1.0×10^{9} W/m. This value agrees with the peak power estimated by Hill [6]. Furthermore, our estimates of energy dissipation are in general agreement with the values reported in the literature.

To the best of our knowledge no experimental observations of electrical energy dissipation in subsequent return strokes are available in the literature. In the case of first return strokes the only available information is due to Krider et al. [11]. In that investigation the energy dissipated in a single stroke flash was estimated to be 2.3×10^{5} J/m. The current in the return stroke was unknown. On the other hand several researchers have attempted to calculate the energy dissipation in return strokes by electrostatic considerations [11,12,13,14]. According to these electrostatic considerations the potential of the cloud is of the order of 10^{8} - 10^{9} V. Now, according to the return stroke model of Cooray [1] the total charge brought down by a 10 kA subsequent return stroke is about 0.5 C. If we assume that the length of the return stroke channel is about 7 km and the potential of the cloud is about 5×10^{8} V then the energy per unit length available for the return stroke process would be of the order of 3.5×10^{4} J/m. However, the calculated value of 4.0×10^{3} J/m is about an order of magnitude less than this expected value. If the calculated value is correct then some of the energy available for the return stroke-dart leader process must dissipate in a process other than the return stroke. It is possible that some of this energy will dissipate in the dart leader stage but, unfortunately, no information is available in the literature concerning the energy dissipation in the dart leader stage. In order to investigate this apparent discrepancy we have used the following simplified model to estimate the energy dissipation in the two stages i.e. dart leader and return stroke. The two charge centers, i.e. negative and positive, in the cloud were assumed to be spherical in shape and each charge center was assumed to carry 40 C of charge. The radius of the charge center was calculated by assuming that the outer boundary of the charge center is at breakdown electric field. Now, due to the decrease in pressure at cloud height the breakdown field may be a factor of 2 lower than that at atmospheric pressure and due to the presence of water drops the breakdown field may decrease further by a factor of about 3 [15]. Therefore, the radius of the charge centers will be of the order of 1 km. The height of the center of negative charge was assumed to be at 8 km and the height of the positive charge center was assumed to be at 12 km. The situation is shown in figure 10(a). Now, according to the return stroke model, just before the return stroke all the charge that will be neutralised in the return stroke is distributed over the dart leader channel. The charge density (denoted by ρ) along the channel was assumed to decreases exponentially with height with a decay height constant of 5000 km. The diameter of the dart leader channel was calculated by assuming that the outer boundary of the charge cylinder is at breakdown electric field. The situation is shown in figure 10(b). The total charge on the leader channel is 0.5 C which is the value corresponding to a 10 kA peak current. During the return stroke the charge stored on the leader channel is brought to ground and at the end of the return stroke the situation is similar to that depicted in figure 10(c). Using this configuration we have calculated the energy dissipation during the dart leader stage i.e. the energy difference in the situations 10(a) and 10(b) and the energy dissipation during the return stroke stage i.e. the energy difference in the situations 10(b) and 10(c). In these calculations the effect of the earth was taken into account by the method of images. The results show that the energy dissipation during the dart leader stage is about 2.0×10^4 J/m and the energy dissipation during the return stroke is about 2.6×10^3 J/m. This shows that about 90% of the energy available for the dart leader- return stroke process will dissipate in the dart leader stage. The value calculated for the energy dissipation in the return stroke i.e. 2.6×10^3 J/m is similar to that calculated by using the return stroke model. Now, the total energy dissipation in bringing down 0.5 C of charge to ground is about 2.3×10^4 J/m and since the length of the leader channel is 7.5 km the total energy dissipation during the dart leader-return stroke process is 1.7×10^8 J. This energy value corresponds to a discharge to ground of 0.5 C from an initial potential difference of 3.5×10^8 V. This value agrees with the estimations of cloud potential obtained by other researchers.

CONCLUSIONS

In this paper we have calculated the energy and power dissipation in subsequent return strokes by using a recently introduced return stroke model. For a given return stroke current the highest power is dissipated in channel elements close to ground and the peak power dissipation in a given channel element decreases with increasing height of that channel element from ground level. For example, our results show that, for a 10 kA peak current, the peak power dissipation in a channel element at ground level is about 2.0×10^9 W/m and the peak power dissipation in a channel element at 100 m from ground level is about 6×10^8 W/m. The total power dissipation in the overall return stroke channel reaches its peak when the length of the return stroke channel is about a kilometer and for a typical subsequent stroke peak total power dissipation is about 1.5×10^{11} W. The energy dissipation in a typical subsequent return stroke is about 5.0×10^3 J/m. Both the energy and the power dissipation in the return strokes increase with increasing peak current. The calculations presented in this paper show that most of the energy available for the dart leader-return stroke process is dissipated in the dart leader stage.

ACKNOWLEDGEMENTS

The research work reported here was supported by a grant (No. E-EG 1448-303) to the author from the Swedish Natural Science Research Council.

REFERENCES

[1] Cooray, V., A return stroke model, Proceedings of the 1989 International Conference on Lightning and Static Electricity, pp. 1A.31-1A.39, University of Bath, United Kingdom, September, 1989.

[2] Cooray, V., V. P. Idone and R. E. Orville, Velocity of self propagating discharge as a function of current parameters with special attention to return strokes and dart leaders, UURIE: 207-88, Institute of High Voltage Research, University of Uppsala, Sweden.

[3] King, L. A., The voltage gradient of the free burning arc in air or nitrogen, Proceedings of the International Conference on Ionization Phenomena in Gases, pp. 871-877, Munich, 1961.

[4] Cooray, V., Relationship between different return stroke parameters as predicted by a new return stroke model, Proceedings of the International Conference on Lightning Protection, 2.11P/1-2.11P/7, Interlaken, Switzerland, 1990.

[5] Master, M. J., M. A. Uman, W. H. Beasley and M. Darveniza, Lightning induced voltages on power lines: Experiment, IEEE Trans. PAS, PAS-103, 2519-2529,1984.

[6] Hill, R. D., Channel heating in return stroke lightning, J. Geophys. Res., 76, pp. 637-645, 1971.

[7] Plooster, M. N., Numerical model of the return stroke of the lightning discharge, Phys. Fluids, 14, pp. 2124-2133, 1971.

[8] Hill, R. D., Energy dissipation in lightning, J. Geophys. Res., 82, pp. 4967-4968, 1977.

[9] Hill, R. D., A survey of lightning energy estimates, Reviews of Geophys. and Space Phys., 17, pp. 155-164, 1979.

[10] Paxton, A. H., R. L. Gardner and L. Baker, Lightning return stroke. A numerical calculation of the optical radiation, Phys. Fluids, 29, pp. 2736-2741, 1986.

[11] Krider, E. P., G. A. Dawson and M. A. Uman, Peak power and energy dissipation in a single-stroke lightning flash, J. Geophys. Res., 73, pp. 3335-3339, 1968.

[12] Wilson, C. T. R., Investigations on lightning discharges and on the electric field of thunderstorms, Phil. Trans. Roy. Soc. London. Ser. A. 221, pp. 73-115, 1920.

[13] Malan, D. J., Physics of Lightning, pp. 75, English University Press, London, 1963.

[14] Connor, T. R., The 1965 ARPA-AEC joint lightning study at Los Alamos, Rep. LA-3754, vol. 1, Los Alamos Sci. Lab., Los Alamos, New Mexico, 1967.

[15] Uman, M. A., Lightning, McGraw-Hill, New York, 1969.

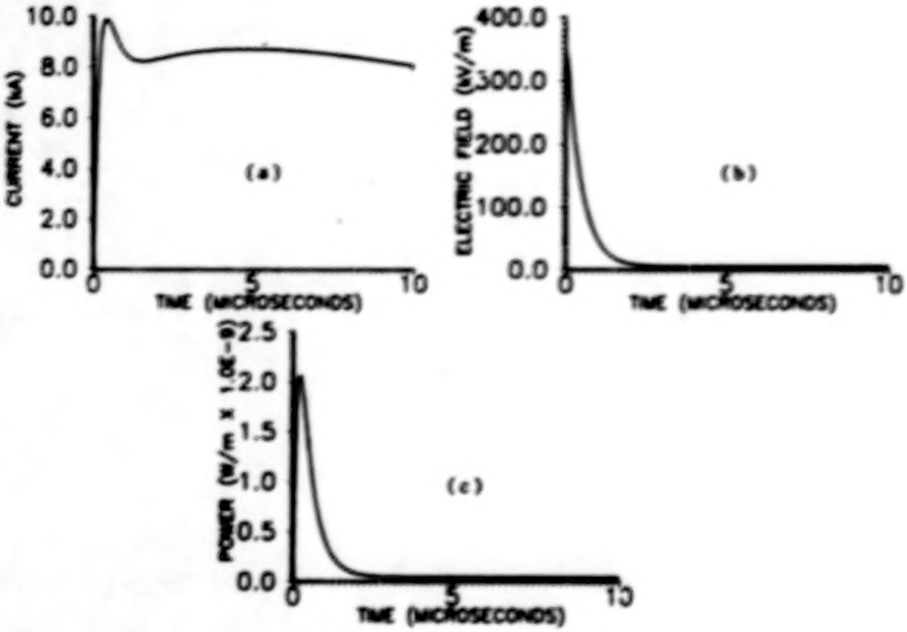

Fig.1 (a) The current, (b) the axial electric field and (c) the power dissipation as a function of time in a subsequent stroke channel element situated at 10 m from ground level. The peak current in the return stroke channel is 10 kA. The time is measured from the beginning of the current waveform in the channel element.

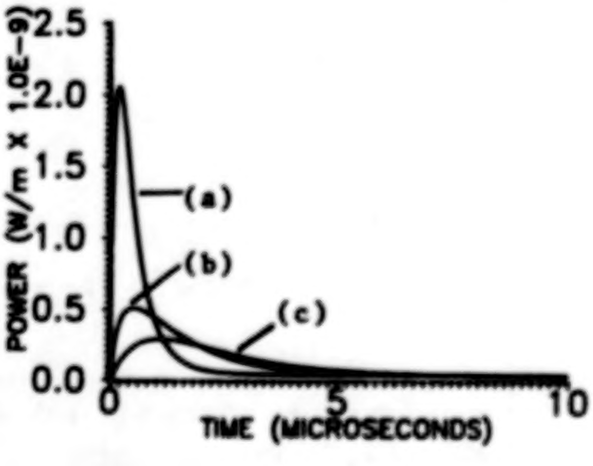

Fig.2 Power dissipation, per unit length, as a function of time in channel elements situated at (a) 10 m, (b) 100 m, and (c) 500 m from ground level. The peak current in the subsequent return stroke is 10 kA. Note that the time delay between the initiation of power dissipation in different channel elements is not shown in the diagram.

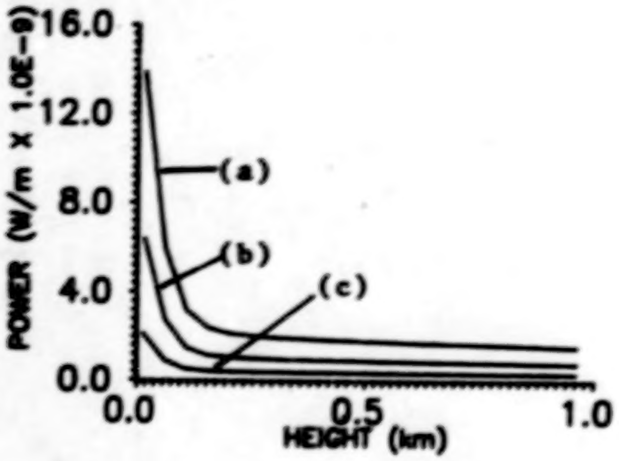

Fig.3 Peak power dissipation, per unit length, in a channel element as a function of it's height from ground level. The peak current in the return stroke channel is (a) 30 kA, (b) 20 kA, and (c) 10 kA.

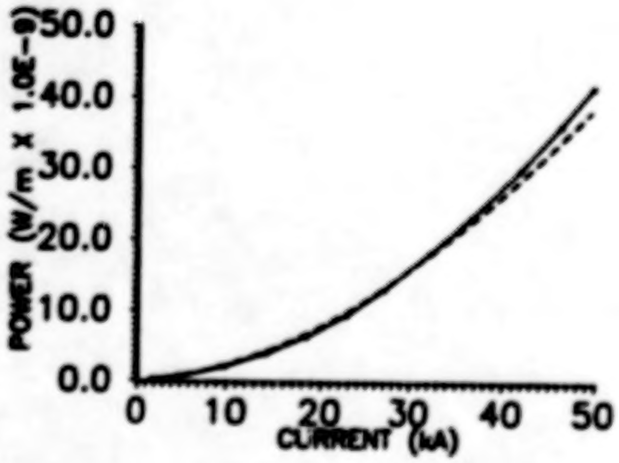

Fig.4 Peak power dissipation, per unit length, in a channel element at ground level as a function of the peak current (solid line). The relationship between these two parameters can be approximated (dashed line) by the equation $Pp = 4.0 \times 10^{7}\ Ip^{1.7}$ where Ip is the peak current in kA at ground level and Pp is the peak power generated by the channel element.

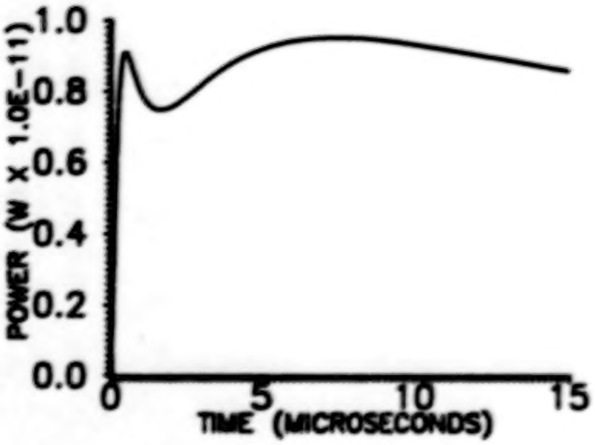

Fig.5 The total power dissipation as a function of time in a return stroke with a 10 kA peak current at ground level.

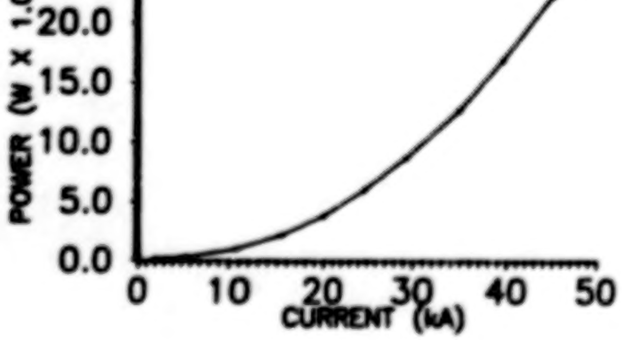

Fig.6 Peak total power dissipation in subsequent return strokes as a function of peak current at ground level.

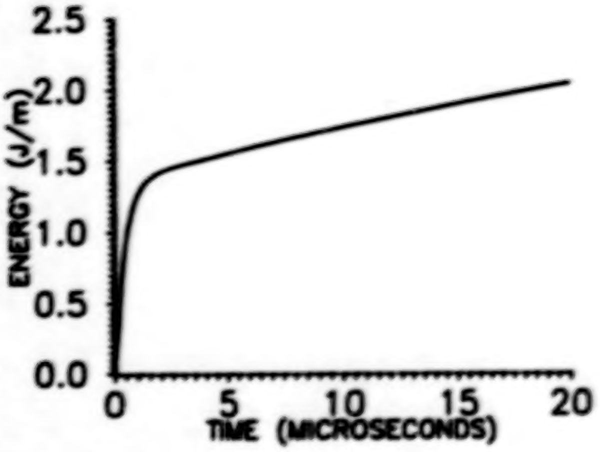

Fig.7 Energy dissipation, per unit length, in a channel element at 10 m from ground level as a function of time. The peak current in the return stroke channel is 10 kA.

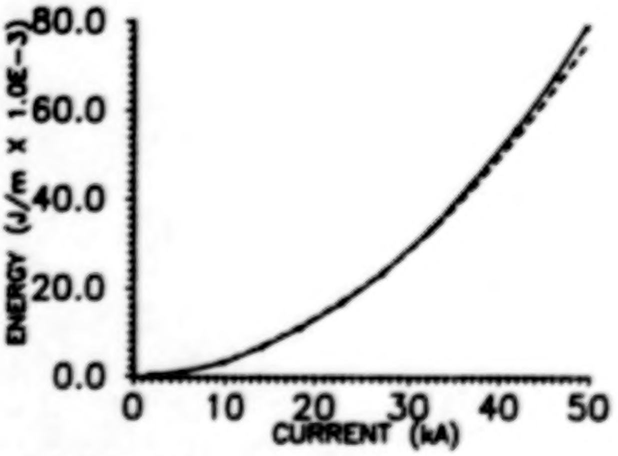

Fig.8 The total energy dissipation, per unit length, in channel elements close to ground as a function of return stroke peak current (solid line). The relationship between these two parameters can be approximated (dashed line) by the equation $E = 43.2 \times Ip^{1.9}$ where Ip is the peak current in kA at ground level and E is the peak power generated by the channel element.

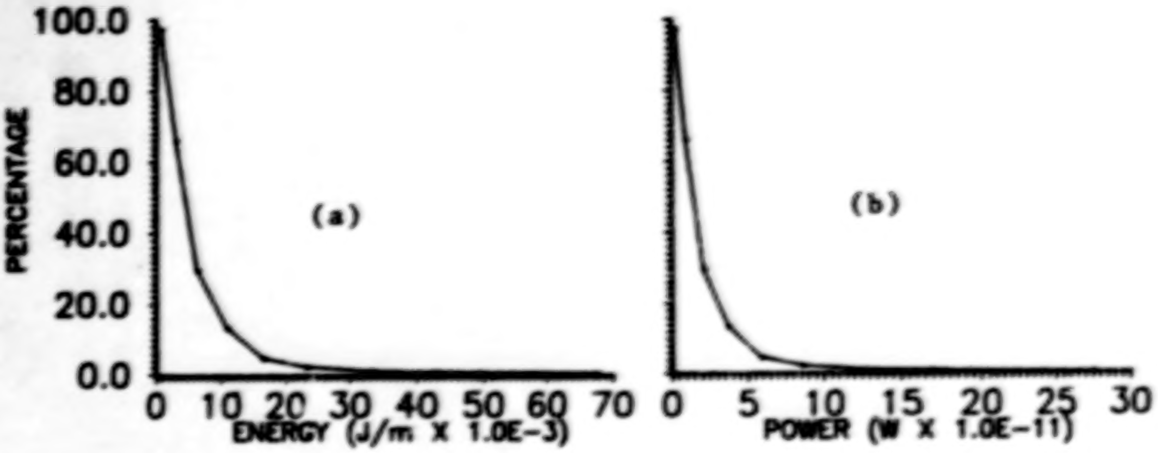

Fig.9 (a) Distribution of the energy dissipation in subsequent return strokes and (b) distribution of the total power dissipation in subsequent return strokes derived from the distribution of peak electric radiation fields.

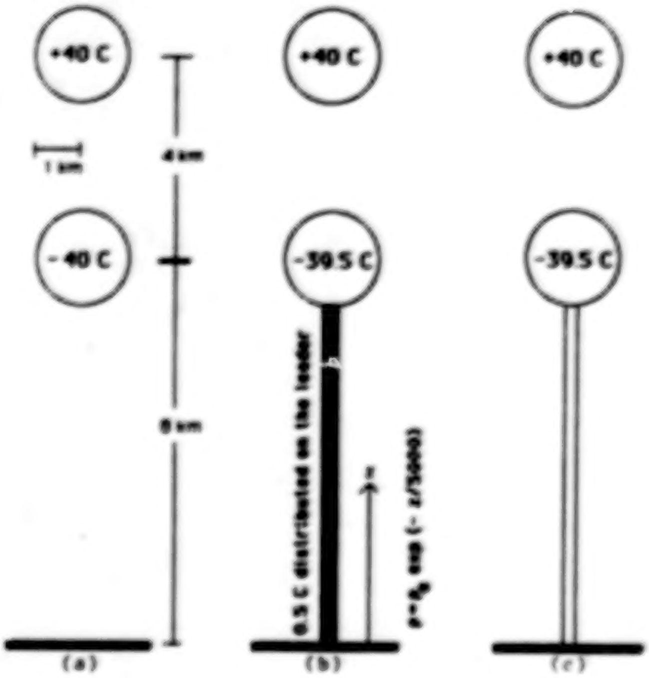
+40 C
+40 C
+40 C
1 km
4 km
- 40 C
-39.5 C
-39.5 C
8 km
0.5 C distributed on the leader
z
ρ=ρ0 exp (- z/5000)
(a)
(b)
(c)

Fig.10 Analysis of the energy dissipation in return strokes by using a simplified model of the thunder cloud. (a) Situation just before the initiation of dart leader. (b) Situation just before the initiation of return stroke. (c) Situation just after the end of return stroke.

HORIZONTAL FIELDS GENERATED BY RETURN STROKES

Vernon Cooray
Institute of High Voltage Research
(A department at Uppsala University)
Uppsala, Sweden

ABSTRACT

Horizontal fields generated by return strokes play an important role in the interaction of lightning generated electromagnetic fields with overhead power lines. In many of the recent investigations on the interaction of lightning electromagnetic fields with power lines, the horizontal field was calculated by employing the expression for the tilt of the electric field of a plane wave propagating over finitely conducting earth. In this paper we show that the horizontal field generated by return strokes over finitely conducting ground can be obtained to a high accuracy by using the expression for the surface impedance of the finitely conducting earth. The method is suitable to calculate horizontal fields generated by return strokes at distances as close as 200 m. At these close ranges the use of the wavetilt expression can cause large errors.

INTRODUCTION

Recent experimental investigations indicate that the electric field component parallel to the ground plane i.e. horizontal field, plays a dominant role in the interaction of lightning generated electromagnetic fields with over head power lines [1,2,3]. The accuracy of the induced voltage calculations depends, therefore, on the accuracy to which the horizontal field generated by lightning return strokes can be calculated. These calculations require the knowledge concerning the electromagnetic fields generated by dipoles over finitely conducting earth. The pioneering work on the electromagnetic fields generated by dipoles over finitely conducting ground was done by Sommerfeld [4]. He presented the solutions to the problem in integral form. The horizontal fields generated by lightning return strokes over finitely conducting earth can be written in terms of these integrals and the results can be obtained by solving these equations numerically. However, this method of calculation is not practical because of the limitations on the computational time. To overcome these problems many researchers have used different approximations to calculate the horizontal fields generated by lightning return strokes.

One of the approximations used frequently in the literature, to calculate the horizontal fields generated by lightning, is the method of "Wavetilt". When a plane electromagnetic wave propagates over finitely conducting ground the electric field at the surface is tilted towards the ground (in the case of perfectly conducting earth the electric field is perpendicular to the earth's surface). That is, at the surface of the ground the electric field component parallel to the ground surface is not zero. The magnitude of the tilt, and hence the amplitude of the horizontal electric field, depends on the conductivity and dielectric constant of the ground. According to the wavetilt expression the ratio between the electric field component perpendicular to the ground, Ez, and the electric field component parallel to the ground, Eh, in frequency domain is given by

$$E_h(j\omega) / E_z(j\omega) = 1/(\varepsilon + \sigma/j\omega\varepsilon_o)^{0.5} \qquad (1)$$

where ε is the relative dielectric constant, σ is the conductivity, ε_o is the permittivity of free space and ω is the angular frequency. In most of the studies mentioned earlier the above relationship was used to calculate the horizontal filed from either the measured or the calculated vertical electric field. However, the above relationship is valid under two conditions, namely, (a) the fields are radiation and (b) the angle of incidence is near grazing. Unfortunately, very close to the lightning return stroke channel, both these conditions could be violated and the horizontal field calculated from the wavetilt expression could be in error. On the other hand, the horizontal field can be related to the horizontal magnetic field, $B_h(j\omega)$, through the expression for the surface impedance of the earth (the earth is assumed to be flat and homogeneous) as follows :

$$E_h(j\omega) / B_h(j\omega) = c/(\varepsilon + \sigma/j\omega\varepsilon_0)^{0.5} \tag{2}$$

where c is the speed of light in free space. In this paper we will show that this relationship can be used to calculate the horizontal fields generated by lightning at close ranges to a higher accuracy than is possible from the wavetilt formula. We will also investigate the errors caused by the use of wavetilt expression to calculate horizontal fields when the lightning return strokes are within about 2 km from the point of observation.

FIELDS GENERATED BY A VERTICAL DIPOLE OVER FINITELY CONDUCTING EARTH

As we have mentioned earlier many approximate solutions are available for the fields generated by vertical dipoles over finitely conducting ground [5,6,7,8]. In this paper we will consider the solutions given by Bannister [8]. Recently these solutions were compared with the exact integrations of Sommerfeld integrals by Zaddam and Degauque [9]. Their results show that the equations given by Bannister [8] can be used to calculate fields to an accuracy higher than 5%.

Let us consider the geometry shown in figure 1. The dipole is at a height h from ground level and the current in the dipole is directed in the direction of z axis. The ground is assumed to be flat and homogeneous and is associated with the constants ε and σ. According to Bannister [8] the electromagnetic field components at point P are given by (see figure 1 and the 'glossary of symbols' for the definition of parameters used in these equations)

$$\begin{aligned} E_h(j\omega) = \frac{M}{4\pi\varepsilon_0 j\omega} \Big\{ & (3 + 3\gamma_0 R_0 + \gamma_0^2 R_0^{\,2}) \sin\psi_0 \cos\psi_0 \frac{e^{-\gamma_0 R_0}}{R_0^{\,3}} \\ & + (3 + 3\gamma_0 R_1 + \rho\gamma_0^2 R_1^{\,2}) \sin\psi_1 \cos\psi_1 \frac{e^{-\gamma_0 R_1}}{R_1^{\,3}} \\ & - \frac{2}{n^2} (3 + 3\gamma_0 R_1 + \gamma_0^2 R_1^{\,2}) \sin\psi_1 \cos\psi_1 \frac{e^{-\gamma_0 R_1}}{R_1^{\,3}} \\ & + \gamma_0^2 \Big[\frac{\cos\psi_2 \, e^{-\gamma_0 R_2}}{R_2 + d + z + h} - \frac{\cos\psi_1 \, e^{-\gamma_0 R_1}}{R_1 + z + h} (1 + \gamma_0 d) \Big] \\ & + 2\Delta \Big[1 - \Big(\frac{1-\rho}{2}\Big) F(\omega) \Big] \cos\psi_1 \, \gamma_0^2 R_1^{\,2} \frac{e^{-\gamma_0 R_1}}{R_1^{\,3}} \Big\} \end{aligned} \tag{3}$$

$$E_z(j\omega) = -\frac{M}{4\pi\varepsilon_0 j\omega}\left\{\left[(1-3\sin^2\psi_0)(1+\gamma_0 R_0)+\gamma_0^2 R_0^2\cos^2\psi_0\right]\frac{e^{-\gamma_0 R_0}}{R_0^3}\right.$$

$$+\left[(1-3\sin^2\psi_1)(1+\gamma_0 R_1)+\rho\,\gamma_0^2 R_1^2\cos^2\psi_1\right]\frac{e^{-\gamma_0 R_1}}{R_1^3}$$

$$\left.+(1-\rho)\,F(\omega)\cos^2\psi_1\,(\gamma_0^2 R_1^2)\frac{e^{-\gamma_0 R_1}}{R_1^3}\right\} \qquad (4)$$

$$B_p(j\omega) = \frac{M\mu_0}{4\pi}\left\{(1+\gamma_0 R_0)\cos\psi_0\frac{e^{-\gamma_0 R_0}}{R_0^2}+(1+\rho\,\gamma_0 R_1)\cos\psi_1\frac{e^{-\gamma_0 R_1}}{R_1^2}\right.$$

$$\left.+(1-\rho)\,F(\omega)\cos\psi_1\,(\gamma_0 R_1)\frac{e^{-\gamma_0 R_1}}{R_1^2}\right\} \qquad (5)$$

According to Bannister [8] these equations are valid at any point on the earth provided that $n^2 >> 1$. Now, the dominant angular frequencies in the lightning generated electromagnetic fields lie in the range of 10^4 to 10^7 rad/s and the conductivity and the dielectric constant of typical soils are distributed in the range of 0.01 to 0.001 S/m and 3 to 10 respectively. Calculations show that $n^2 >> 1$ for the values of frequencies, conductivity and dielectric constants in the above ranges. Therefore we conclude that the above equations could be used to calculate the fields generated by lightning over finitely conducting ground.

COMPARISON OF THE HORIZONTAL FIELDS CALCULATED FROM WAVETILT AND SURFACE IMPEDANCE WITH THE EXACT EXPRESSION

Let $E_{hw}(j\omega)$ represents the horizontal field at ground level as calculated by using the wavetilt expression (i.e. equation 1), $E_{hs}(j\omega)$ represents the horizontal field at ground level as calculated by using the surface impedance expression (i.e. equation 2) and $E_h(j\omega)$ represents the exact value of the horizontal field at ground level as given by equation (3). We have calculated these field components over a large range of frequencies, heights of the dipole and distances. From these calculations we have estimated the ratio $|E_{hw}/E_h|$ and $|E_{hs}/E_h|$. The variation of these ratios as a function of distance, conductivity, height of the dipole from ground level and frequency are shown in figures 2 through 4. In each figure the solid line represents the ratio $|E_{hs}/E_h|$ and the dashed line represents the ratio $|E_{hw}/E_h|$. Figure 2 shows how these ratios vary as a function of frequency and conductivity when the dipole is at ground level. Figures 3 and 4 correspond to dipoles at heights 500 m and 1000 m respectively.

Let us consider the results in figure 2. These results show that for distances greater than about 200 m from the dipole the ratio $|E_{hs}/E_h|$ is equal to unity. Figures 3 and 4 show that this is also true for dipoles at heights 500 m and 1000m from ground level. That is for distances greater than 200 m and for dipoles situated at heights between 0 to 1000m the horizontal field calculated by using the surface impedance expression is an accurate representation of the horizontal field component at ground level i.e. $E_{hs}(j\omega) = E_h(j\omega)$.

On the other hand the ratio $| E_{hw}/E_h |$ is far from unity, specially at small distances and low frequencies. However, with increasing distance and frequency the results obtained from the wavetilt expression approaches that obtained by using the exact expression. The reason for this is that with increasing distance the radiation field becomes the dominant component in the electric field, which enhance the validity of the wavetilt expression. However, as one can see from these figures, the horizontal fields calculated by using the wavetilt expression would be in error even at distances as large as 5000 m when the frequencies of interest are in the range of 10^5 rad/s.

In the calculation of lightning generated induced voltages in power lines it is the first few microseconds, i.e. up to about 10 μs, of the horizontal field which is mainly of interest. During this time the length of the return stroke channel is not more than 1000 meters. Furthermore, the frequencies which will contribute to the electric field during this time interval are distributed in the range of 10^7 to 10^5 rad/s. From the results given in figures 2 through 4 we can conclude, therefore, that the surface impedance expression can be used to calculate the horizontal fields generated by return strokes to a high accuracy and for distances larger than or equal to 200 m the results are almost identical to those calculated by more exact formulation. In the next chapter we will use the surface impedance expression to calculate the horizontal fields generated by lightning return strokes in time domain and, since these are almost identical to the results given by exact formulation, it is reasonable to assume that they are a faithful representation of the horizontal fields generated by lightning.

HORIZONTAL FIELDS GENERATED BY RETURN STROKES

Let $B_p(t)$ and $E_h(t)$ are the horizontal magnetic field and the horizontal electric field generated by a lightning return stroke over finitely conducting earth. Let $B_p(jw)$ and $E_h(jw)$ are the corresponding field components in the frequency domain. Then, according to the surface impedance expression

$$E_h(j\omega)/B_p(j\omega) = c/(\varepsilon + \sigma/j\omega\varepsilon_o)^{0.5} \tag{6}$$

Performing the inverse Laplace transformation of the above equation, the horizontal field in time domain can be written as

$$E_h(t) = \int_0^t B_p(t - \tau)\, S(\tau)\, d\tau \tag{7}$$

where

$$S(t) = (c/\varepsilon^{0.5})\, \zeta\, e^{-\zeta t}\, [\, I \quad [illegible] \quad I_0(\zeta t)] \tag{8}$$

and $\zeta = \varepsilon_0\varepsilon/\sigma$. Furthern [illegible] $_0(\zeta t)$ and $I_1(\zeta t)$ are the modified Bessel functions of order zero and one respectively [illegible] rgument ζt. A similar procedure can be used to calculate the horizontal field from th [illegible] ilt expression.

In order to calculate the horizontal field from the above equation it is necessary to know the magnetic field generated by return strokes at a given distance over finitely conducting ground. This in turn requires the knowledge concerning the temporal and spatial variation of the return stroke current along the return stroke channel. Recently, Cooray [10] introduced a new return stroke model which is capable of generating the temporal and spatial variation of the return stroke current along the return stroke channel. The model calculations are in good agreement with the hitherto known properties of the temporal and spatial variation of the return stroke current, spatial variation of the return stroke velocity and the lightning generated electromagnetic fields. In the results to be presented below the electric and magnetic fields generated by lightning return strokes at a given point are calculated by using the model of Cooray [10]. The calculations are performed for a return stroke with a peak current of 10 kA at ground level.

The first 5 μs of the vertical electric field and the horizontal magnetic field at different distances, when the ground is perfectly conducting are shown in figure 5. The resulting field components when the ground is finitely conducting are shown in figure 6. Let us denote these field components (i.e. those calculated over finitely conducting ground) as $E_z(t)$ and $B_p(t)$ respectively. In these calculations the effects of the finitely conducting ground on the electromagnetic fields were incorporated as described in Cooray and Lundquist [11] and Cooray [12]. Note how the risetime of the field components increases with increasing distance. The reason for this is the attenuation of the high frequency components in the electromagnetic fields when they propagate along the finitely conducting earth. The horizontal electric field was then calculated by inserting $B_p(t)$ in equation (7). The results of the calculations are presented in figures 7 and 8 (solid line). As we have mentioned earlier, it is reasonable to assume that they are a faithful representation of the horizontal fields generated by lightning. For comparison purposes the horizontal field calculated by using the wavetilt expression is also given in each figure (dashed line).

First, note that the peak value of the horizontal field, for $\rho = 0.001$ S/m, falls off much faster with distance than that of the inverse distance dependence (figure 8). The reason for this is the attenuation of the high frequency components in the magnetic field due to propagation over finitely conducting earth. This also shows the importance of including the propagation effects in the magnetic field which is used to calculate the horizontal field. For example, if we use the magnetic field calculated over perfectly conducting earth (i.e. figure 5) in (7) to calculate the horizontal field the resulting peak amplitude of the horizontal field would be significantly larger than the correct value. For example, in the case of $D = 2000$ m and $\rho = 0.001$ S/m the difference will be about 100%. Second, observe the narrow initial peak in the horizontal fields. The higher the conductivity the narrower the initial peak. For example at 200 m and for 0.01 S/m the half width of the initial peak of the horizontal field is about 0.3μs (figure 7). As shown by Cooray and DeLa Rosa [2] these narrow initial peaks are responsible for the narrow initial peaks measured in induced voltages in power lines. Third, observe that, for a given distance, the peak amplitude of the horizontal field increases with decreasing conductivity. Now let us compare these waveforms with the horizontal fields calculated by using the wavetilt expression. Note that the difference between the two waveforms is larger at small distances than at long distances. For a given distance and conductivity the the error associated with the horizontal field calculated from the wavetilt expression increases with increasing time. For example at 200 m and for conductivity 0.01 the difference is about 200 % at 5 μs. Note that even at 1000 m from the lightning return stroke the horizontal field calculated by the wavetilt expression could be in error by about 50%.

CONCLUSIONS

The results presented in this paper show that the horizontal field generated by return strokes over finitely conducting earth can be calculated to a high accuracy by using either the measured or the calculated horizontal magnetic field in the expression for the surface impedance . The method is suitable to calculate horizontal fields for distances down to about 200 m from the return strokes. The use of wavetilt expression to calculate the horizontal field can result in large errors specially when the return stroke is within about a kilometer from the point of observation.

ACKNOWLEDGEMENTS

The research work reported here was supported by a grant (No. E-EG 1448-303) to the author from the Swedish Natural Science Research Council.

REFERENCES

[1] Master, M. J. and M. A. Uman, Lightning-induced voltages on power line: Theory, IEEE Trans., PAS-103, pp. 2502-2518, September, 1984.

[2] Cooary, V. and De La Rosa, F., Shapes and amplitudes of the initial peaks of lightning induced voltage in power lines over finitely conducting earth: Theory and comparison with experiment, IEEE Trans., vol. AP. 34, pp. 88-92, January, 1986.

[3] Rubinstein, M., M. A. Uman, E. M. Thomson and Pedro Medelius, Voltages induced on a test line by artificially initiated lightning at close range: Measurements and Theory, Proceedings of the International Conference on Lightning Protection, Interlaken, Switzerland, 1990.

[4] Sommerfeld, Uber die Ausbreitung der Wellen in der drahtlosen Telegraphie, Ann. Phys. 28, 665, 1909.

[5] Norton, K, A., Propagation of radio waves over the surface of the earth and in the upper atmosphere, II, Proc. IEEE, 25, pp. 1203-1236, 1937.

[6] Banos, A., Dipole radiation in the presence of a conducting half-space, Pergamon press, 1966.

[7] Sakar, T. K., Analysis of radiation by arrays of vertical wire antennas over imperfect ground (reflection coefficient method), IEEE Trans., vol. AP.23, September, 1975.

[8] Bannister, P. R., Extension of finitely conducting Earth-image-theory results to any range, Technical Report 6885, Naval Under Water Systems Center, January, 1984.

[9] Zeddam, Z. and P. Degauque, Current and Voltage induced on telecommunication cables by a lightning stroke, Electromagnetics, vol. 8, pp. 171-211, 1988.

[10] Cooray, V., A return stroke model, Proceedings of the 1989 International Conference on Lightning and Static Electricity, 1A.3.1-1A.3.9, University of Bath, United Kingdom, September, 1989.

[11] Cooray, V., and S. Lundquist, Effects of propagation on the risetimes and the initial peaks of the radiation fields from return strokes, Radio Sci., vol. 18, pp. 409-415, 1983.

[12] Cooray, V., Effects of propagation on the return stroke radiation fields, Radio Sci., vol. 22, pp. 752-768, 1987.

GLOSSARY OF SYMBOLS

R_0	$[D^2 + (z - h)^2]^{0.5}$ (meters)
R_1	$[D^2 + (z + h)^2]^{0.5}$ (meters)
R_2	$[D^2 + (d + z - h)^2]^{0.5}$ (meters)
Ψ_0	$\tan^{-1}(\frac{z - h}{D})$
Ψ_1	$\tan^{-1}(\frac{z + h}{D})$
Ψ_2	$\tan^{-1}(\frac{d + z - h}{D})$
z	Height of the point of observation with respect to earth's surface
D	Horizontal distance between the dipole and the point of observation
h	Height of the dipole with respect to earth's surface
σ	Conductivity of the earth
ε	Relative dielectric constant of the earth
ε_0	Permittivity of free space
μ_0	Permeability of free space
ω	Angular frequency (radians/s)
j	$(-1)^{0.5}$
γ_0	$j\omega / c$
γ_1	$[j\omega\mu_0\sigma - \omega^2\mu_0\varepsilon\varepsilon_0]^{0.5}$
d	$2 / \gamma_1$
Δ	γ_0 / γ_1
n	$1/\Delta$
F	Sommerfeld attenuation function
M	Electric current moment of the dipole
c	Velocity of light in free space
$E_z(j\omega)$	Vertical electric field component in frequency domain
$E_h(j\omega)$	Horizontal electric field component in frequency domain
$B_p(j\omega)$	Horizontal magnetic field component in frequency domain
E_{hw}	Horizontal electric field component calculated from the wavetilt
E_{hs}	Horizontal electric field component calculated from the surface impedance
$\mathcal{E}_h(t)$	Horizontal electric field in time domain generated by lightning stroke
$\mathcal{B}_p(t)$	Horizontal magnetic field in time domain generated by lightning stroke

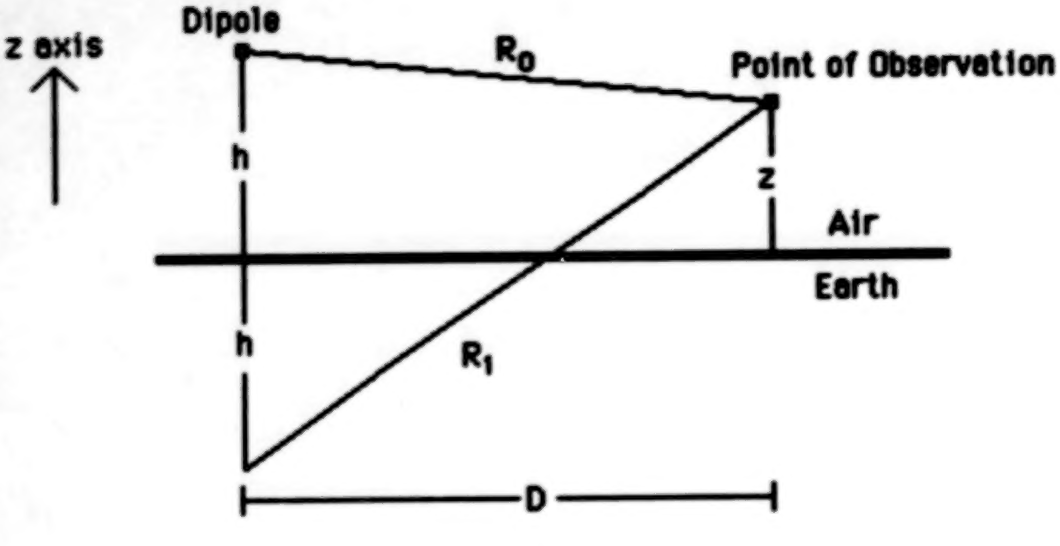

z axis
Dipole
R0
Point of Observation
h
z
Air
Earth
h
R1
D

Fig.1 Geometry relevant to the problem under consideration.

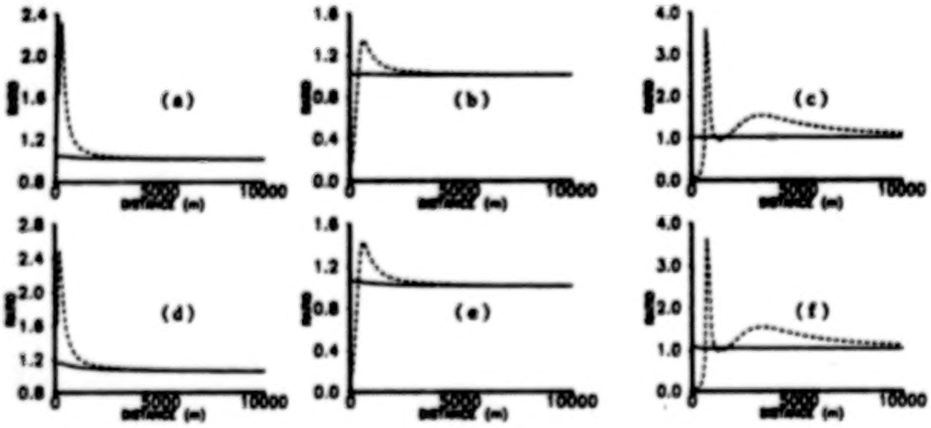

Fig.2 The variation of the ratios $|E_{hs}/E_h|$ (solid line) and $|E_{hw}/E_h|$ (dashed line) as a function of distance for (a) $\omega = 10^7$ rad/s and $\sigma = 0.01$ S/m (b) $\omega = 10^6$ rad/s and $\sigma = 0.01$ S/m (c) $\omega = 10^5$ rad/s and $\sigma = 0.01$ S/m (d) $\omega = 10^7$ rad/s and $\sigma = 0.001$ S/m (e) $\omega = 10^6$ rad/s and $\sigma = 0.001$ S/m and (f) $\omega = 10^5$ rad/s and $s = 0.001$ S/m. The dipole is situated at ground level i.e. $h = 0$.

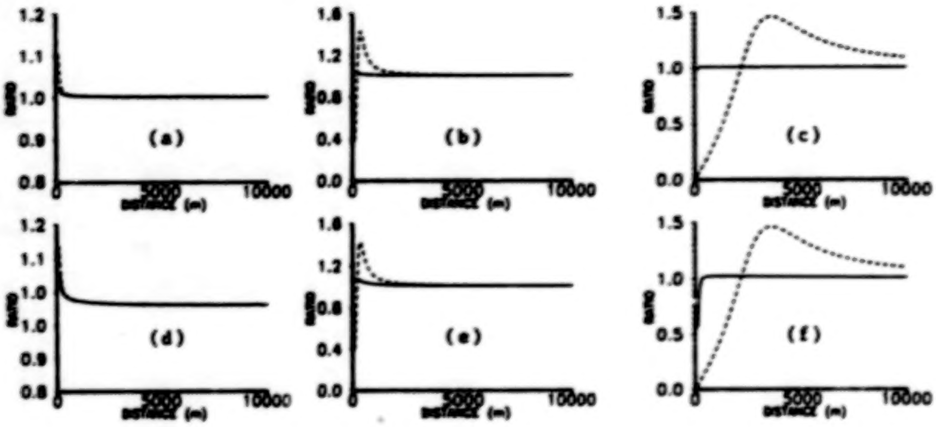

Fig.3 Same as in figure 2 except that the dipole is at 500 m from ground level.

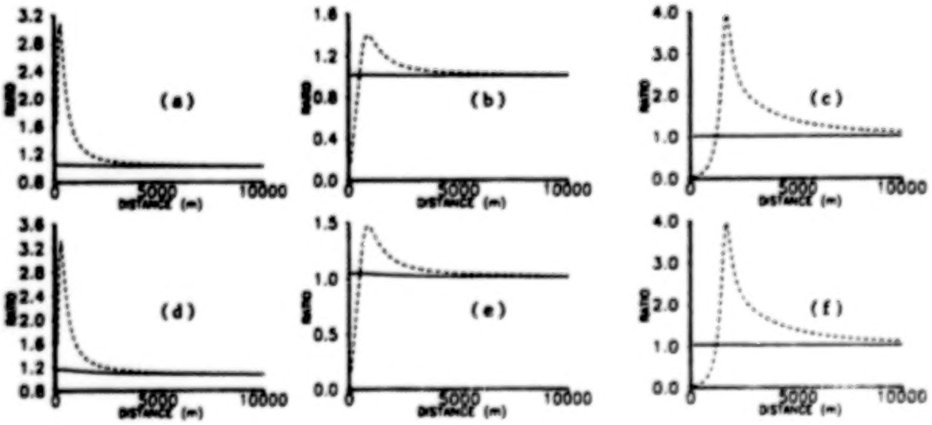

Fig.4 Same as in figure 2 except that the dipole is at 1000 m from ground level.

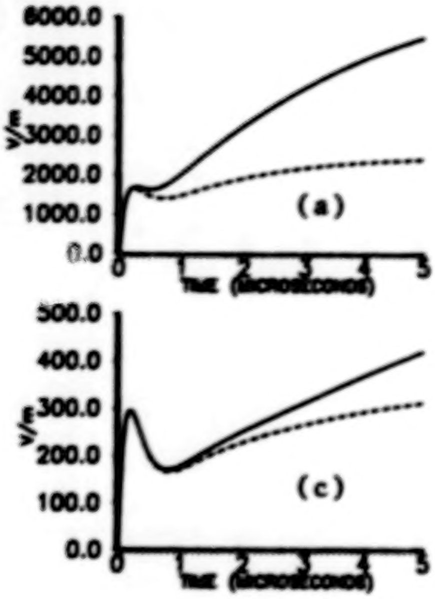

Fig.5 Vertical electric field (solid line) and the horizontal magnetic field x c (dashed line) generated by a return stroke over perfectly conducting ground, as calculated by using the model of Cooray (1989). The peak current in the return stroke is 10 kA. The distances to the point of observations are the following: (a) 200 m, (b) 500 m, (c) 1000 m and (d) 2000 m.

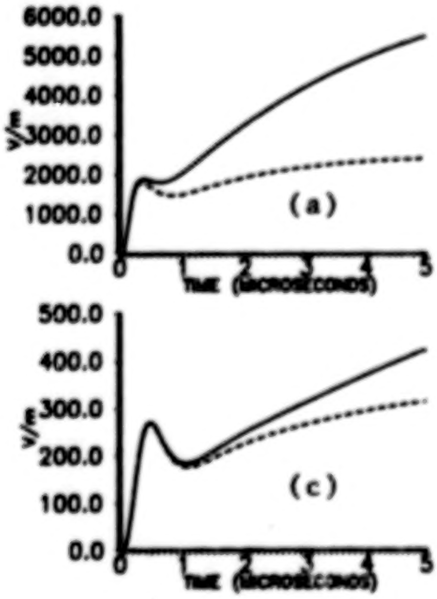

Fig.6 Same as in figure 5 except that the conductivity of the ground (i.e. σ) is 0.001 S/m.

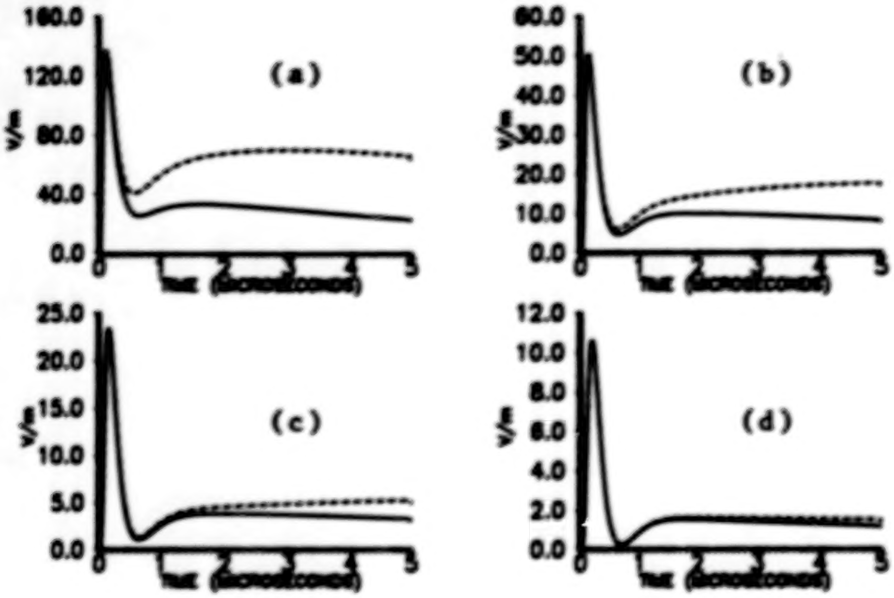

Fig.7 Horizontal field generated by a return stroke at different distances when the conductivity of the ground is 0.01 S/m (solid line). The peak current in the return stroke is 10 kA. The distances to the point of observations are the following: (a) 200 m, (b) 500 m, (c) 1000 m and (d) 2000 m. The horizontal fields calculated by using the wavetilt expression are drawn by dashed lines.

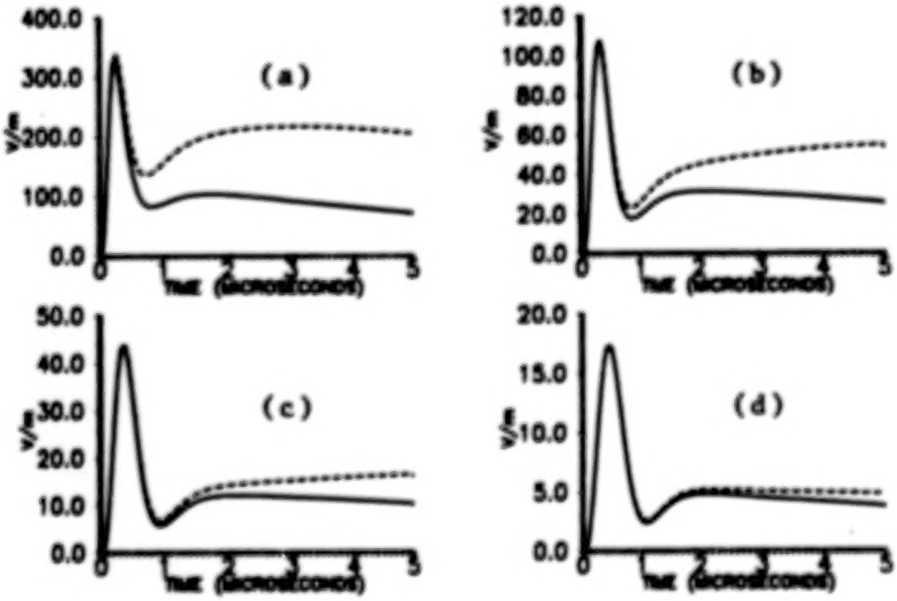

Fig.8 Same as in figure 7 except that the conductivity of the ground is 0.001 S/m.

NASA
National Aeronautics and Space Administration

Report Documentation Page

1. Report No. NASA CP-3106, Vol. I

2. Government Accession No.

3. Recipient's Catalog No.

4. Title and Subtitle
1991 International Aerospace and Ground
Conference on Lightning and Static Electricity

5. Report Date August 1991

6. Performing Organization Code

7. Author(s)

8. Performing Organization Report No.

10. Work Unit No.

9. Performing Organization Name and Address
John F. Kennedy Space Center
Kennedy Space Center, FL 32899

11. Contract or Grant No.

13. Type of Report and Period Covered Conference Publication

12. Sponsoring Agency Name and Address
National Aeronautics and Space Administration
Washington, D.C. 20546

14. Sponsoring Agency Code

15. Supplementary Notes

This publication supersedes NASA CP-10058, Volume I

16. Abstract

The proceedings of the 1991 International Aerospace and Ground Conference on Lightning and Static Electricity, which was held at the Howard Johnson Plaza Hotel, Cocoa Beach, Florida, on April 16 to 19, 1991, are reported. The conference was sponsored by Kennedy Space Center and the National Interagency Coordination Group (NICG), which consists of research experts from the National Aeronautics and Space Administration, the Federal Aviation Administration, Department of Defense, the National Oceanic and Atmospheric Administration, in concert with the Florida Institute of Technology.

17. Key Words (Suggested by Author(s))

Aerospace Vehicles
Electrostatics
Meteorological
Electromagnetic
Specifications
Lightning
Mapping
Modeling
Coupling
P-static
Standards

18. Distribution Statement
Unclassified - Unlimited

Subject Category 47

19. Security Classif. (of this report)	**20. Security Classif. (of this page)**	**21. No. of pages**	**22. Price**
Unclassified	Unclassified	676	A99

NASA FORM 1626 OCT 86

600

NASA
National Aeronautics and
Space Administration
Washington, D.C.
20546

SPECIAL FOURTH CLASS MAIL
BOOK

Postage and Fees Paid
National Aeronautics and
Space Administration
NASA-451

Official Business
Penalty for Private Use $300

L1 001 CP-3106-V1910801S002378D
GOVERNMENT PRINTING OFFICE
LIBRARY PROGRAMS SERVICE/SLIA
ACQUISITIONS SECTION
WASHINGTON DC 20401